THE UNIVERSITY of ADELAIDE

The Stenian-Cambrian Tectonic Evolution of Central Madagascar

Donnelly Brian Archibald

Department of Earth Sciences

School of Physical Sciences

The University of Adelaide

May 2016

Table of Contents

Abstract

Madagascar occupies an important location in many Proterozoic plate reconstructions. It lies within the East African Orogen, which involves a collage of Proterozoic microcontinents and arc terranes wedged between older cratonic units during Gondwana assembly. Oceanic crust is an important component of palaeogeographic reconstructions that is often overlooked because exposures of in situ oceanic crust older than ~200 Myr do not exist. Therefore, studies of ancient oceanic crust require proxies such as analysing the products of magmatic arcs. The Malagasy basement preserves five magmatic suites emplaced consecutively from ~1100-500 Ma. During this time, the Rodinia supercontinent amalgamated then dispersed and the Gondwana supercontinent formed. This whole-rock geochemical and zircon isotopic study attempts to unravel the Proterozoic tectonic history of central Madagascar using the tectonic setting and duration of various Stenian to Cambrian magmatic episodes. These magmatic suites are the ~1080-980 Ma (Dabolava Suite), ~850-750 Ma (Imorona-Itsindro Suite) and ~650-520 Ma (Kiangara, Ambalavao and Maevarano Suites). Gabbroic and granitoid rocks of the Dabolava Suite combined with the coeval Ikalamavony Group represent a magmatic arc and volcano-sedimentary sequence deposited in an oceanic-arc environment based on isotopic and geochemical characteristics. The Imorona-Itsindro Suite represents contemporaneous emplacement of various lithologies from gabbro to granitoids and syenite. Oxygen and hafnium isotope data have a broad inverse relationship with apparent magmatic cycles occurring on the scale of ~15-40 Ma that emphasize periods of significant supracrustal assimilation evolving to "mantle-like" (or below) signatures. The spatial distribution of isotopic data indicates that the isotopic character of Tonian-aged zircon replicates the basement domain into which the magmas intruded. Samples intruding the Ikalamavony Domain exhibit a less evolved $\varepsilon_{Hf}(t)$ isotopic signature than Tonian-aged rocks intruding the domains to the east, implying melting of different source material. The zircon isotopic dataset emphasises the age range and composition of the Tonian lithosphere beneath central Madagascar. Geochemically, mid-Tonian rocks are calc-alkaline with trace-element characteristics consistent with a continental arc genesis. Radiogenic isotope data show evolved Sr and Nd signatures. Changes in subduction zone dynamics, crustal anatexis and crustal assimilation of the diverse basement domains into ascending magmas contributed to geochemical variations. Prolonged subduction (>100 Myr) provided sufficient time for the arc to mature and a shallow (<100km), metasomatised spinel lherzolite mantle source is preferred. The isotopic and geochemical characteristics of the Imorona-Itsindro Suite argue for a collective genesis in a supra-subduction zone tectonic setting with the Neoproterozoic suture located west of the Ikalamavony Domain. The Ediacaran to Cambrian Kiangara, Ambalavao and Maevarano Suites are post-collisional, mainly granitoid suites emplaced during the final assembly of Gondwana. Magmas incorporated crustal material and isotopic signatures reflect the basement unit in which samples intrude and these rocks are related spatially and temporally with major late-Neoproterozoic deformation episodes. Collectively, these data identify a previously unrecognised and long-lived (~500 Ma) active continental margin correlative to the present-day Pacific Ocean margin. Understanding this large dataset is critical for understanding Madagascar's tectonic evolution during the Stenian to Cambrian.

List of Figures

List of Tables

Chapter 5

Chapter 6

Appendices

Supplementary Appendices

Declaration

I certify that this work contains no material which has been accepted for the award of any other degree or diploma in my name, in any university or other tertiary institution and, to the best of my knowledge and belief, contains no material previously published or written by another person, except where due reference has been made in the text. In addition, I certify that no part of this work will, in the future, be used in a submission in my name, for any other degree or diploma in any university or other tertiary institution without the prior approval of the University of Adelaide and where applicable, any partner institution responsible for the joint-award of this degree.

I give consent to this copy of my thesis when deposited in the University Library, being made available for loan and photocopying, subject to the provisions of the Copyright Act 1968.

The author acknowledges that copyright of published works contained within this thesis resides with the copyright holder(s) of those works.

I also give permission for the digital version of my thesis to be made available on the web, via the University's digital research repository, the Library Search and also through web search engines, unless permission has been granted by the University to restrict access for a period of time.

_____

Donnelly B. Archibald

Journal Articles

Archibald, D.B., Collins, A.S., Foden, J.D., Payne, J.L., Taylor, R., Holden, P., Razakamanana, T., Clark, C., 2015. Towards unravelling the Mozambique Ocean conundrum using a triumvirate of zircon isotopic proxies on the Ambatolampy Group, central Madagascar. Tectonophysics 662, 167-182.

Archibald, D.B., Collins, A.S., Foden, J.D., Payne, J.L., Holden, P., Razakamanana, T., De Waele, B., Pitfield, P.E.J., Thomas, R.J., 2016. Genesis of the Tonian Imorona-Itsindro Magmatic Suite in central Madagascar: Insights from U-Pb, oxygen and hafnium isotopes in zircon. Precambrian Research 281, 312-337.

Archibald, D.B., Collins, A.S., Foden, J.D., Razakamanana, T. under review. Petrogenesis of the Tonian Imorona-Itsindro Suite. Journal of Geology.

Archibald, D.B., Collins, A.S., Foden, J.D., Payne, J.L., Holden, P., Razakamanana, T. under review. Tectonics and chemistry of late to post tectonic magmatism in the Malagasy Mozambique Belt. Lithos

Acknowledgements

I would like to extend my gratitude to Prof Alan Collins for his guidance and encouragement during the course of my PhD. Most of all, I would like to thank him for the opportunities to experience exotic cultures in new countries while completing my project. These opportunities have made me a better geologist and scientist by providing me with the opportunity to travel around Australia and the world. I would also like to thank my co-supervisor Emeritus Prof John Foden for his insight, guidance and support especially when trying to understand and interpret geochemical and isotopic data.

This project would not have been possible if not for Prof Theodore Razakamanana from the University of Toliara, Madagascar. His upbeat personality, knowledge of the Madagascan geology and technical assistance in the field made for two enjoyable field seasons.

The Razafinjoelina family, in particular Auguste and Berthieu are thanked for providing transportation, assistance in the field, and their hospitality during fieldwork in Madagascar.

I would like to thank my co-authors, Dr. Justin Payne for his assistance acquiring hafnium isotopic data and for careful manuscript editing. David Bruce is recognised for his assistance acquiring Sr and Nd-Sm isotopic data and Dr. Peter Holden for his assistance acquiring oxygen isotopic data. Dr. Richard Taylor and Dr. Chris Clark are thanked for their assistance acquiring SHRIMP U-Pb data.

I would also like to thank several members of the PGRM project including Bert De Waele, Bob Thomas and Peter Pitfield for providing samples and for providing alternative interpretations on the geology of central Madagascar. The staff at Adelaide Microscopy, in particular, Dr. Ben Wade, Ms. Aoife McFadden, and Mr. Angus Netting are acknowledged for their technical assistance when acquiring analytical data. Dr. Diana Plavsa is recognised for her assistance helping me get this project started.

I would like to acknowledge the University of Adelaide geology faculty for their support over the past three years. I would especially like to thank Dr. Rosalind King, Dr. Stijn Glorie, Dr. Dave Kelsey, Dr. Katie Howard and Dr. Graham Heinson for allowing me to learn and develop my teaching skills while demonstrating undergraduate practicals.

My “officemates” Katherine and Morgan made walking into Mawson everyday entertaining. I would not have made it to Australia if it were not for Bonnie Henderson visiting Canada and convincing me Adelaide was worth moving half-way around the world. I thank Lachlan for giving me a place to live when I arrived and for not kicking me out for almost 2 years! Funny and Stijn moved to Australia at the same time as I did and they made the transition a lot easier. Funny’s cooking made my early days feel like home. Finally, I would like to thank Francesco and the rest of the PhD cohort at Adelaide (both new and old) for their friendship and support over the past 3+ years.

Last and certainly not least, finishing this project would not have been possible without the love and support of my Canadian Family and my new Australian Family. It was difficult to move to Adelaide but Maggie, Brian, Daniel, Amanda and the rest of my friends and family supported me every step of the way. My second family (Kath, Steve, Annie, Bruce, Joan and Theo) in Australia made being away from home easier and fun. Eliza, for being there with me during all of the fun times and difficult times I am forever grateful to you. Hopefully, we will have many more adventures together as we begin our next chapter in Canada.

Chapter 1

Introduction and Geology of Madagascar

1.1 Introduction

Ancient tectonic plate reconstructions are essential for understanding controls on past climates, the distribution of ancient ecosystems and the tectonic setting of petroleum or mineral systems. Madagascar occupies an important location in Proterozoic supercontinent reconstructions of Rodinia and Gondwana (Fig. 1.1). Proterozoic (~2500-541 Ma) rocks are notoriously difficult to study especially if they experienced more recent metamorphic events. Fortunately, the mineral zircon is an incredibly robust mineral that preserves its original isotopic abundances over a wide range of lithospheric temperatures and pressures. The ubiquity and chemical durability of zircon make it a particularly useful tool for studying these old rocks, especially if they experienced post-crystallization metamorphism or alteration. This PhD research project examines the tectonic setting and palaeogeography of the lithotectonic domains that comprise central Madagascar from Stenian to Cambrian time (~1100-500 Ma). This is an important period in Earth's history. During this time, the Rodinia supercontinent amalgamated then dispersed, the Gondwana supercontinent formed, and the Ediacaran fauna appeared, the first multicellular organisms on Earth. Unfortunately, many of the published continental reconstructions fail to incorporate oceanic crust since exposures of *in situ* oceanic crust older than ~200 Myr do not exist. Therefore, studies of ancient oceanic crust require proxies such as analysing the products of magmatic arcs. Central Madagascar contains two magmatic arc rock suites named the Dabolava Suite (~1080-980 Ma) and the Imorona-Itsindro Suite (~850-750 Ma) and the post-collisional Kiangara, Ambalavao and Maevarano Suites (~630-520 Ma) that form the basis for the proxies employed in this study. In addition, Proterozoic supracrustal sequences are studied in order to constrain the timing of sediment deposition, to infer possible sediment source regions and to relate Malagasy supracrustal sequences to contemporaneous sequences elsewhere.

The main objective of this PhD research project is to assemble a large geochemical and isotopic dataset and to integrate these data with field knowledge to develop a tectonic model for the mid- to late-Proterozoic development of central Madagascar. The timing of sediment deposition and the tectonic setting of the magmatic suites form the basis of the model. The duration of magmatism for each system is obtained along with the potential source components involved during magma genesis. This model is then integrated into plate reconstructions of Rodinia and Gondwana to infer the proximity of Madagascar to other continental blocks. A number of studies have undertaken this method for Phanerozoic accretionary systems (Kemp et al., 2006; Kemp et al., 2007; Kemp et al., 2009) but no study has considered an ancient subduction zone system and attempted to link the nature of Proterozoic accretionary orogens to plate reconstructions. Furthermore, this project has broad scientific relevance in that it represents the examination of a tectonically active region during the ~ 500 Myr preceding the origin of multicellular life.

1.2 Geology of Madagascar

Madagascar contains several Precambrian to earliest Palaeozoic 'basement' units overlain by Phanerozoic sedimentary and volcanic rocks (Roig et al., 2012). The oldest rocks are located along Madagascar's east coast in the Palaeoarchaean to Palaeoproterozoic Antongil and Masora Domains (Fig. 1.2). These units are considered remnants of the Dharwar Craton of southern India that were separated from the craton during the Mesozoic break-up of Gondwana (Tucker et al., 1999b; Collins and Windley, 2002; Collins et al., 2003c; Collins, 2006; Schofield et al., 2010; Tucker et al., 2011a; Tucker et al., 2011b; Tucker et al., 2014). The Antongil Craton consists primarily of ~3300-3100 Ma gneiss of the Nosy Boraha Suite,

~2550-2520 Ma granitoids of the Masoala Suite and Mesoarchaean supracrustal rocks (~3176-2597 Ma) of the Mananara Group (Schofield et al., 2010; Key et al., 2011; Tucker et al., 2014). Neoproterozoic to Cambrian intrusions are not recognised in the Antongil Domain, which is only marginally affected by Ediacaran-Cambrian deformation events (Collins, 2006; Key et al., 2011). The Masora Domain contains a core of Nosy Boraha Suite orthogneiss interlayered with meta-volcanosedimentary rocks of the Mesoarchaean Vohilava Group (BGS-USGS-GLW, 2008; Key et al., 2011). These rocks are overlain by the metasedimentary Maha Group which has a maximum depositional age of ~1740 Ma (De Waele et al., 2011). Unlike the Antongil Domain, older lithologies in the Masora Domain were intruded by the Tonian-aged magmatic rocks and all rocks experienced Ediacaran-Cambrian orogenesis (Key et al., 2011).

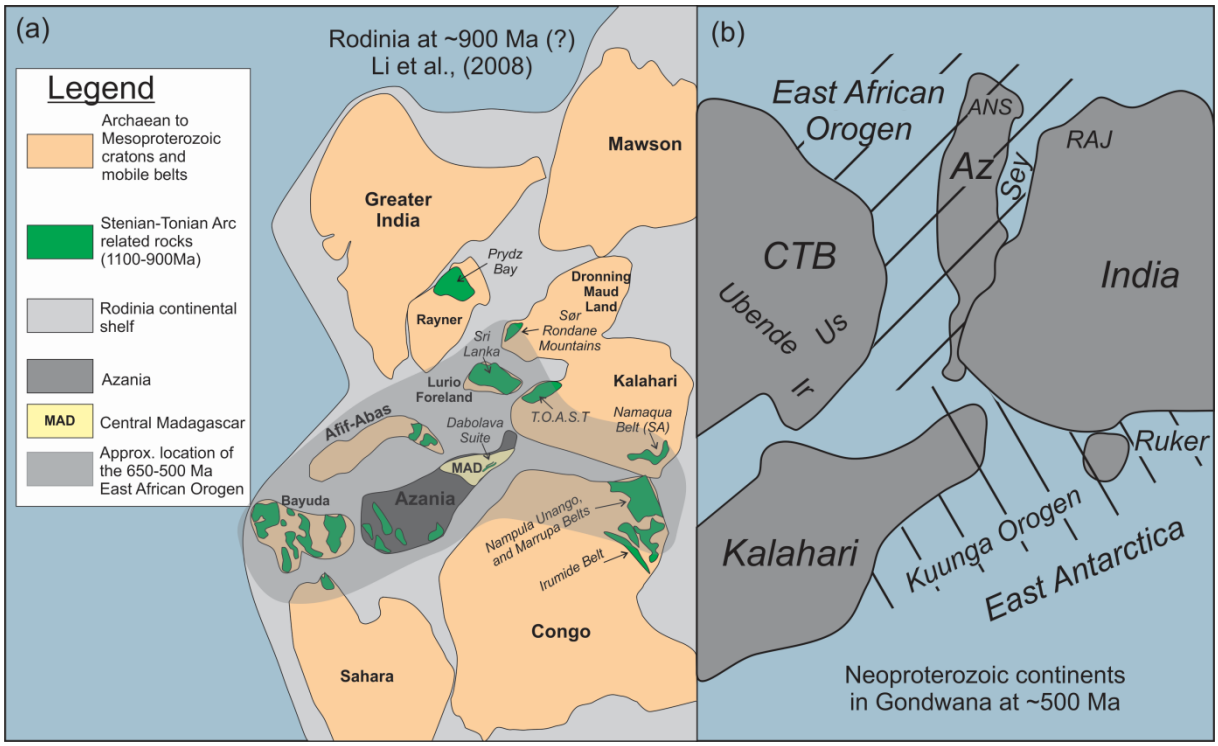

Fig. 1.1 (a) Simplified palaeogeographic reconstruction of the Rodinia Supercontinent at ~900 Ma after Li et al. (2008). The locations of several of the late-Mesoproterozoic to early Neoproterozoic magmatic arc suites discussed in Chapter Six are indicated. Also shown is the inferred extent of rocks involved in the ~650-500 Ma East African Orogen. (b) Simplified palaeogeographic reconstruction of the Neoproterozoic continents in Gondwana (after Collins and Pisarevsky, 2005). Madagascar is considered to have been part of the Azania microcontinent (Az). Abbreviations: Az = Azania; Sey = Seychelles; Ir = Irumide Belt; Ruker = Ruker Terrane, East Antarctica; CTB = Congo Tanzania Bangweulu Block; ANS = Arabian Nubian Shield; Ubende = Ubende Belt; RAJ = Rajasthan; and Us = Usagaran orogen.

The largest component in Madagascar, the Antananarivo Block (or Domain), underlies the central highlands and comprises granulite- to upper-amphibolite facies orthogneiss and paragneiss (Kröner et al., 2000; Collins et al., 2003a; Collins, 2006; Roig et al., 2012). The orthogneiss consist of ~2550–2500 Ma granitoids (the Betsiboka Suite) that are tectonically interlayered with paragneiss of the Meso- to Neoarchaean Sofia and Vondrozo Groups (Fig. 1.2). The entire Antananarivo Domain was thermally and structurally reworked between ~850 and 500 Ma with pre-existing rocks being metamorphosed to granulite-facies coinciding with the development of shallow dipping gneissic fabrics that pre-date intrusion of the Ediacaran-Cambrian magmatic rocks and later, discrete shear zones that

are syn-to post- Ediacaran magmatism (Collins et al., 2003c; BGS-USGS-GLW, 2008; Moine et al., 2014). Some of these later shear zones have been interpreted as related to orogenic extensional collapse (Collins et al., 2000).

To the west of the Antananarivo Domain is the Itremo Domain (Fig. 1.2). The Itremo Group consists primarily of quartzite, mica schist and dolomitic marble. Detrital zircon studies show significant U-Pb age populations at ~ 2500 Ma and ~1800 Ma (Cox et al., 2004; Fitzsimons and Hulscher, 2005; De Waele et al., 2011). The precise depositional age of these rocks is poorly constrained to younger than ~1700 Ma based on the youngest detrital zircon (Collins et al., 2003c; Cox et al., 2004; De Waele et al., 2011). The minimum depositional age (~850 Ma) is constrained by intrusion of the Imorona-Itsindro Suite (e.g. Handke et al., 1999) or by late Ediacaran-Cambrian metamorphism and intrusion of the Ambalavao Suite (e.g. Key et al., 2011). The protolith sediments were deposited on a continental shelf or passive margin sometime after ~1700 Ma (Fernandez et al., 2003; Cox et al., 2004) with their interpreted sediment source in East Africa (Cox et al., 1998; Cox et al., 2004; Fitzsimons and Hulscher, 2005) or locally from the Archaean to Proterozoic basement of Madagascar (Tucker et al., 2011b). The nature of the relationship of metasedimentary units to the Archaean gneisses of the Antananarivo Domain and the relationship of the Neoproterozoic intrusive rocks in the Itremo Domain is controversial (Tucker et al., 2007). Moine (1967) considered metaigneous rocks to be the crystalline basement to the Itremo Group because many plutons are strongly foliated and have concordant contacts with neighbouring stratified rocks. Cox et al. (1998) suggested the plutons in the Itremo region were relatively undeformed and interpreted the period of pluton emplacement (~833 Ma) as the time of regional metamorphism and deformation. Collins et al. (2003b) demonstrated that Tonian plutons were emplaced into the already intensely folded and translated Itremo Group and hence, the intrusions postdate the isoclinal folds and thrusts of the region. Fernandez et al. (2003) recognized the general concordance between the orthogneiss and the Itremo Group, but they considered the contact to be a thrust that was subsequently folded and metamorphosed during Cambrian time. Tucker et al. (2007) posited that the Neoproterozoic (~1000–720 Ma) plutons were emplaced into the Itremo Group and Archaean basement, and all that all rocks were affected by younger metamorphic events. Itremo Group lithologies generally increase in metamorphic grade from east to west (Tucker et al., 2007) with the lowest-grade rocks (lower greenschist facies) preserved in the hanging-wall of the Betsileo Shear Zone (Moine, 1974; Collins et al., 2000). Recently, the Itremo Group was correlated with the Maha Group that structurally overlies the Masora Domain in south-east Madagascar (Fig. 1.2), the Sambirano-Sahantaha Group from the southern Bemarivo Domain (De Waele et al., 2011), the Ambatolampy Group (Archibald et al., 2015) and similar-aged metasedimentary rocks in southern India (Plavsa et al., 2014).

The Ambatolampy Group is a granulite-facies metasedimentary group that lies within the Antananarivo Domain (Fig. 1.2) that was previously assumed to be a corollary of the Itremo Group (Collins et al., 2000). The group is characterised by abundant mica schists and quartzites that increase in metamorphic grade towards the east into gneisses and migmatitic rocks (BGS-USGS-GLW, 2008). The schist consists of biotite, sillimanite, garnet ± corundum, and graphite. Other sequences found within the Ambatolampy Group include metre-scale quartzite beds, and thin meta-carbonate and calc-silicate rock units that are intercalated with the mica schists (BGS-USGS-GLW, 2008). Detrital zircon U-Pb analyses undertaken as part of a regional mapping programme (BGS-USGS-GLW, 2008; Tucker et al., 2011b; Tucker et al., 2014), reported largely Neoarchaean and Palaeoproterozoic detritus, similar to that from the Itremo Group, but with 12 near-concordant analyses at ~1100- 1000 Ma from one of the three analysed samples. The interpreted maximum and minimum depositional ages were constrained to 1001 ± 44 Ma by the youngest detrital zircon (De Waele et al., 2011) and ~560 Ma by intrusion of the Ambalavao Suite (BGS-USGS-GLW, 2008).

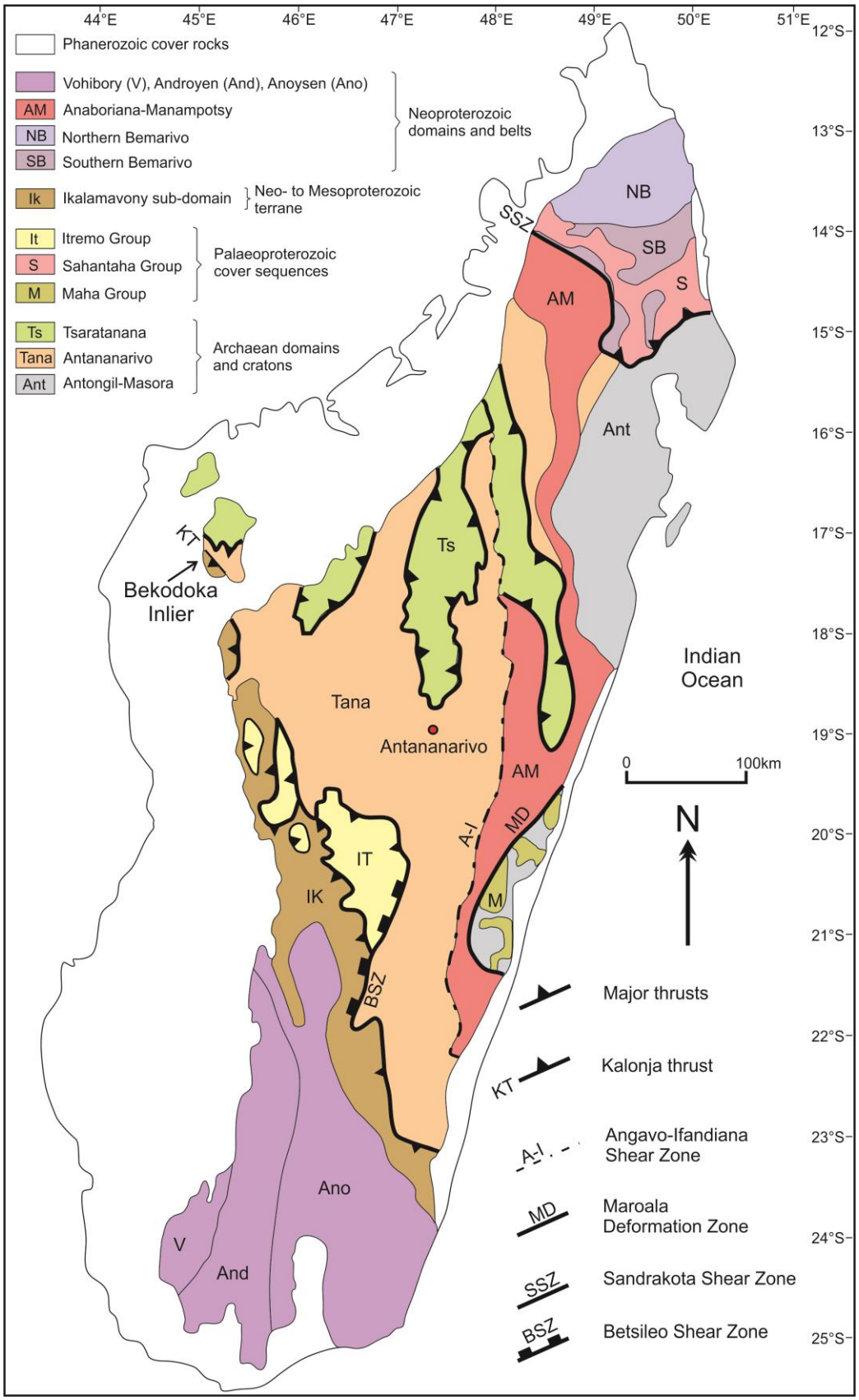

Fig. 1.2 Simplified basement geology of Madagascar showing the pre-Neoproterozoic tectonic elements (after Collins, 2006 and De Waele et al., 2011). The locations of the metasedimentary unit or magmatic suite (s) discussed in subsequent chapters are indicated in each chapter.

The Ikalamavony Domain defines a narrow north-northwest trending unit that is traced from the southeast to the central west of Madagascar (Fig. 1.2). In contrast to the Itremo region, the Ikalamavony Domain contains metavolcanic and metasedimentary rocks of mainly intermediate and mafic composition of a probable oceanic origin. The Ikalamavony Group (formerly known at the Amborompotsy Group; Besairie, 1964; Tucker et al., 2007) consists of inferred ocean floor basalts (now metamorphosed to tholeiitic amphibolite), thick sequences of calcium and magnesium rich paragneiss (now metamorphosed to biotite hornblende gneisses), calc-silicates, and locally marble and quartzite (CGS, 2009a). The precise age of the Ikalamavony Group is unknown but U-Pb zircon crystallisation ages from the Dabolava Suite provide a maximum depositional age of ~1035 Ma (Rakotoarimanana, 2001; Tucker et al., 2007; CGS, 2009a; Tucker et al., 2011b). Regardless of their earlier tectonic history, the Ikalamavony and Itremo Domains amalgamated prior to ~850 Ma and were subsequently intruded by mid-Tonian magmas (CGS, 2009a).

The poorly understood Molo Group lies west of the Itremo Domain (Roig et al., 2012) (Fig. 1.2). Cox et al. (2004) identified the group and it was demonstrated that deposition occurred between ~620- 560 Ma and sourced from Neoarchaean, late Mesoproterozoic (~1100-1000 Ma) and Cryogenian rocks (Cox et al., 2004; Tucker et al., 2007; André-Mayer et al., 2014). The late Mesoproterozoic source was interpreted to be the Irumide Belt of Zambia, but subsequently the Dabolava Suite of western Madagascar was demonstrated to have crystallised at this time and could represent a local source (Tucker et al., 2011b; Tucker et al., 2014).

Successive emplacement of the Dabolava, Imorona-Itsindro, Kiangara, Ambalavao and Maevarano magmatic suites occurred during the Stenian to Cambrian (Fig. 1.2). Gabbroic and granitoid rocks of the Stenian-Tonian (~1080- 980 Ma) Dabolava Suite are only recognised in the Ikalamavony Domain west of the boundary with the Antananarivo Domain (GAF-BGR, 2008e; CGS, 2009a). Dabolava Suite rocks are of similar age to both the tholeiitic amphibolite and the sediments into which they intrude (CGS, 2009a). Geochemical data point to a supra-subduction zone, oceanic arc origin for the Dabolava Suite (Rakotoarimanana, 2001; CGS, 2009a). The Tonian-aged (~850-750 Ma) Imorona-Itsindro Suite consists primarily of granitoids and gabbro that intruded into most central Madagascar Precambrian units. Two opposing views of the tectonic setting of the suite have been proposed on the basis of whole-rock geochemistry: in a supra-subduction zone setting (Handke et al., 1999; Kröner et al., 2000; Key et al., 2011; Boger et al., 2015) or above a mantle plume (Tucker et al., 2011b; Yang et al., 2014; Zhou, 2015; Zhou et al., 2015b). Boger et al. (2014) proposed present-day eastward directed subduction beneath central Madagascar and India with the Neoproterozoic suture located west in the present-day Mozambique Channel (Boger et al., 2014). Previous studies by Handke et al. (1999) and Bybee et al. (2010) also advocated eastward directed subduction on the eastern edge of the Mozambique Ocean beneath Madagascar, India and the Seychelles. Eastward subduction resulted in continental arc-magmatism throughout all of Madagascar between ~850-700 Ma(including the Bemarivo Domain) and within-plate potassic magmatism manifested in the distal back-arc in the Malani Basin of Rajasthan (Boger et al., 2014). Alternatively, mid-Tonian subduction polarity has been suggested to be westward beneath central Madagascar with the Betsimisaraka Domain marking the Neoproterozoic suture zone (Kröner et al., 2000; Collins and Windley, 2002; Collins, 2006). Younger intrusive rock suites are represented by the ~630 Ma Kiangara Suite (Guyonnaud, 1951; Nédélec et al., 1994), the ~575-540 Ma Ambalavao Suite (Meert et al., 2001a; BGS-USGS-GLW, 2008) and the ~537-522 Ma Maevarano Suite (Goodenough et al., 2010; Zhou et al., 2015a). The Kiangara Suite was previously been interpreted to have formed at ~ 630 Ma using ID-TIMS U-Pb geochronology (Paquette and Nédélec, 1998). However, Nédélec et al. (2015) re-evaluated this age using micro-beam techniques and obtained a Tonian age (~791 Ma) as opposed to the published Ediacaran ages. The authors concluded

that the Ediacaran ID-TIMS ages were a result of analysing multiple zircon domains within heterogeneous grains and therefore may represent a later phase of the Imorona-Itsindro Suite and late-Cryogenian to early Ediacaran magmatism may not be present in central Madagascar at all.

The Bemarivo Domain is a distinct terrane in northern Madagascar (Fig. 1.2) that consists of Mesoproterozoic metasedimentary rocks (Sambirano-Sahantaha Group) and juvenile Tonian-Cryogenian calc-alkaline metaigneous rocks of the Antsirabe Nord (~760 Ma) and Manambato (~720 Ma) Suites (Thomas et al., 2009). Based on the depleted isotopic character of its metaigneous rocks (Tucker et al., 1999b), Archaean and Palaeoproterozoic rocks are thought to be absent in this domain. Thomas et al. (2009) proposed that the northern and southern sub-domains formed as coalesced magmatic arcs, predominantly at ~760 Ma in the south and ~720 Ma in the north (Table 1). These domains were translated southward over the Sambirano-Sahantaha Group and the combined Antananarivo-Antongil domains during late Ediacaran to early Cambrian time (ca. 540-520 Ma). This period of Tonian-Cryogenian igneous activity in northern Madagascar was correlated with extensive magmatism of the same age in the Seychelles and Rajasthan (Torsvik et al., 2001; Meert et al., 2013).

Southern Madagascar contains three domains divided by high-strain zones that are separated from central Madagascar by the Ranotsara Shear Zone (Fig. 1.2). The westernmost domain is the Vohibory Domain and is composed mainly of mafic and felsic orthogneiss intercalated with mafic paragneiss and marble (GAF-BGR, 2008c; Jöns and Schenk, 2008). The mafic rocks are thought to represent a combination of mid-ocean, back-arc and island arc basalts with inferred extrusion ages between ~850 – 700 Ma (Jöns and Schenk, 2008). Detrital zircon U-Pb studies of the sedimentary rocks yield a near unimodal population with ages ~900 Ma (Collins et al., 2012). Collectively, rocks from the Vohibory Domain resemble an island-arc (GAF-BGR, 2008c). The Androyen Domain contains mostly paragneiss, orthogneiss and ~940-900 Ma anorthosite-leuconorite, olivine gabbro/peridotite and alkali-granites of the Ankiliabo Suite (GAF-BGR, 2008a). Recent work dates the protoliths of this Androyen domain to ~2120–1770 Ma (Tucker et al., 2011b; JICA, 2012). The Anoysen Domain is the most extensive and contains primarily paragneissic rocks of the Iakora Group (~2400–1600 Ma detrital zircon ages) and the inferred Tonian-aged volcano-sedimentary rocks of the Horombe Group (Boger et al., 2014). The inferred felsic volcanic rocks of the Horombe Group are metaluminous and peraluminous, have a similar geochemistry and are the same age as the Imorona–Itsindro Suite (Boger et al., 2014). These metasedimentary packages are suggested to be deposited in the Tonian to Cryogenian based on the inferred absence of the Ankiliabo, Dabolava, and Imorona–Itsindro Suites (GAF-BGR, 2008b; Boger et al., 2014). Deformation and high-temperature metamorphism occurred in two pulses in southern Madagascar. The earliest phase was between 620 – 600 Ma in the Androyen and Vohibory Domains and later at 580 – 520 Ma in the Androyen and Anosyen Domains (Markl et al., 2000; de Wit et al., 2001; Jöns and Schenk, 2011).

The Neoproterozoic Anaboriana-Manampotsy Belt (Fig. 1.2) forms the boundary between the Antongil-Masora and Antananarivo Domains (Key et al., 2011; Roig et al., 2012). The belt consists of mid-Tonian supracrustal sediments that were deposited on the continental shelf of the Antananarivo Domain (Key et al., 2011). There are also minor occurrences of tectonic pods of mafic-ultramafic rocks (Collins, 2006). The belt corresponds spatially with the Betsimisaraka Domain or Betsimisaraka Suture Zone (Collins and Windley, 2002; Collins, 2006). Metamorphic fabrics in the Tonian-aged magmatic rocks and metasedimentary rocks are strongly overprinted by Ediacaran to Cambrian events in both domains (Key et al., 2011). Key et al. (2011) suggested the Manampotsy Belt (southern Betsimisaraka Domain; Collins, 2006) developed as a pre-Kiangara Suite (>630 Ma) collisional/suture zone between the Antananarivo and Masora Domains (Key et al., 2011).

Alternatively, Tucker et al. (2014) suggested the Manampotsy Group was deposited in a long, narrow depositional basin that opened during a period of continental extension and magmatism in the mid-Tonian. The depositional age of the Manampotsy Group is approximately 840-780 Ma, based on the age of the youngest detrital zircon, inferred syn-depositional volcanic rocks (De Waele et al., 2008; Tucker et al., 2011a), and the age of the igneous rocks (Imorona-Itsindro Suite) that intrude the sediments (BGS-USGS-GLW, 2008). Manampotsy Group lithologies are strongly deformed and the main rock types are migmatitic quartzofeldspathic paragneiss, graphitic gneiss, quartzite, marble, calc-silicate gneiss and biotite gneiss (BGS-USGS-GLW, 2008). Near the end of the East African Orogen, the amalgamated Antananarivo-Masora Craton collided with the Antongil Domain (Key et al., 2011) prior to later thrusting of the Bemarivo Belt southwards over the older terranes (Thomas et al., 2009). The Anaboriana Belt (northern Betsimisaraka Domain; Collins, 2006) represents the suture between the Bemarivo Belt and the Antongil-Antananarivo Craton (Key et al., 2011). Granitoid rocks of the Maevarano Suite comprise much of the Anaboriana Belt (~70% of the surface area) and the remaining 30% is high-grade supracrustal gneisses and migmatite of the Bealanana Group (BGS-USGS-GLW, 2008).

1.3 Proterozoic tectonic context

The late-Palaeoproterozoic to mid-Mesoproterozoic was a tectonically quiet time in Madagascar (Key et al., 2011; Tucker et al., 2014) with the Archaean shield of Madagascar flanked to the south by the Palaeoproterozoic Androyen-Anosyen Domain (Tucker et al., 2014). To the north and west of the stable craton lay an open ocean and continental shelf (Tucker et al., 2014). Two alternative hypotheses exist for the origin of the cratonic units, the ocean or passive margins that bounded the remaining peripheries of central Madagascar during Proterozoic time.

The “Out of Africa” hypothesis suggests that the basement of central Madagascar was originally part of the East African Congo-Tanzania-Bangweulu Block (Fitzsimons and Hulscher, 2005). This idea was largely based on the similarities in detrital zircon age spectra from the Muva Supergroup and the Itremo Group (Cox et al., 1998; Collins et al., 2003c; Cox et al., 2004; Fitzsimons and Hulscher, 2005). It was later argued that central Madagascar rifted from the Congo-Tanzania-Bangweulu Block to form a microcontinent named Azania (Collins and Windley, 2002) that was later wedged between the African and Indian plates in the Neoproterozoic (Collins and Pisarevsky, 2005) along the Betsimisaraka Suture (Collins and Windley, 2002).Central Madagascar along with fragments of southern India (the Madurai Block, Plavsa et al., 2014; Collins et al., 2014), East Africa, Yemen and Saudi Arabia (Collins and Windley, 2002), were isolated from both Neoproterozoic India and the Congo-Tanzania-Bangweulu Block by oceanic crust. The Betsimisaraka Suture was later correlated with the Palghat-Cauvery Shear Zone in southern India (Collins et al., 2007; Plavsa et al., 2014; Plavsa et al., 2015). Key et al. (2011) agreed that central Madagascar was likely an isolated microcontinent during the Neoproterozoic but noted that the Betsimisaraka Suture zone as defined by Collins (2006) could not exist given the similar early Neoproterozoic histories of the Antananarivo and Masora Domains on either side of the of the structure. They renamed the Betsimisaraka Suture Zone as the Anaboriana-Manampotsy Belt (Fig. 1.2) and suggested the Manampotsy developed as a pre-630 Ma collisional/suture zone between the Antananarivo and Masora Domains (Key et al., 2011). Near the end of the EAO, the amalgamated Antananarivo-Masora Craton collided with the Antongil Domain (Key et al., 2011) prior to later thrusting of the Bemarivo Belt southwards over the older terranes (Thomas et al., 2009). The Anaboriana Belt represents the suture between the Bemarivo Belt and the Antongil-Antananarivo Craton (Key et al., 2011).

Alternatively, to the east of central Madagascar during the Proterozoic was the Dharwar Craton of India in the "Greater Dharwar Craton" model (Tucker et al., 2011a). Tucker et al. (2014) advocated that during the Proterozoic the Archaean Shield of central Madagascar formed part of a larger continent based on inconsistencies in the "Out-of-Africa" hypothesis. These discrepancies included: (1) the presence of Neoarchaean rocks on both sides of the Betsimisaraka Suture in the Antananarivo, Masora, and Antongil Domains in Madagascar and in the northern Madurai Block and Dharwar craton in India (Schofield et al., 2010; Tucker et al., 2011a), (2) the presence of Tonian-aged plutonic rocks and similar aged metamorphism on both sides of the suture (Schofield et al., 2010; Tucker et al., 2011a), and (3) similar aged detrital zircon arrays exposed on both sides of the suture (De Waele et al., 2011). In this model, the margins of the Malagasy Shield had a Mesoproterozoic oceanic arc to the present day west (Ikalamavony Domain), a Palaeoproterozoic continental terrane to the south (South Madagascar-India-Wanni-Highland Province; SMIWH; Tucker et al., 2011b) and the northern margin was partially covered by Palaeoproterozoic- to Mesoproterozoic clastic and chemical sedimentary rocks of the Andrarona and Sambirano-Sahantaha groups (Tucker et al., 2014). To the west and far north of the Greater Dharwar Craton lay the Mozambique Ocean (Tucker et al., 2014). Tucker et al. (2011b) proposed the SMIWH and that the Androyen-Anosyen Domain together with the Indian Trivandrum Block and the Wanni and Highland Complexes in Sri Lanka represent a continuous Palaeoproterozoic terrane. This Palaeoproterozoic terrane represented a potential source for enigmatic zircon (2200-1800 Ma) detrital zircon found in the Itremo Group which are not common in East Africa (Tucker et al., 2011b).

During Mesoproterozoic time, several predominantly clastic dominated sedimentary sequences were deposited in Madagascar. The Andrarona and Sambirano-Sahantaha Groups were deposited along the north and east margins of the craton and were suggested as correlatives to the Aravalli and Delhi Supergroups of India in the Greater Dharwar model (Tucker et al., 2014). Other metasedimentary sequences namely the Itremo, Ambatolampy, Maha, Tranomaro, Imaloto, and Mangoky Groups were also deposited on the central, southern and western regions of the Malagasy shield (Key et al., 2011; Tucker et al., 2012). Following this period of sediment deposition at around 1100 Ma, an active magmatic arc and marginal depositional basin developed outboard to the west of the Antananarivo Domain (Tucker et al., 2014). Magmatic suites are represented by the Dabolava Suite (1035-982 Ma) in the Ikalamavony Domain and Ankiliabo Suite (930-910 Ma) in the Androyen Domain (Rakotoarimanana, 2001; GAF-BGR, 2008e, a; CGS, 2009a, b; Tucker et al., 2011b). Arc magmatism was likely related to the amalgamation of Rodinia, a supercontinent that formed between 1300 Ma and 900 Ma with virtually all cratonic blocks existing at that time being involved (Li et al., 2008; Li et al., 2013). Rodinia existed for ~150 Myr before extensional basins opened and widespread continental rifting occurred between ca. 825 Ma and 740 Ma, with episodic plume events at ca. 825 Ma, ca. 780 Ma and ca. 750 Ma (Li et al., 2008; Li et al., 2013). At the same time (~850-750 Ma), central Madagascar was situated in an active continental arc as shown by intrusion of the calc-alkaline Imorona-Itsindro Suite (Handke et al., 1999; Kröner et al., 2000) and the Antsirabe-Nord (~760-750 Ma) and Manambato Suites (~720-700 Ma) in northern Madagascar (Thomas et al., 2009). Some authors have questioned the presence of a widespread Tonian Andean-like arc in Madagascar and favour intracontinental rifting environment to fit the Rodinia model (Tucker et al., 2011a; Yang et al., 2014; Zhou, 2015; Zhou et al., 2015a). However, recent studies demonstrate geochemical and isotopic data for Tonian-aged rocks are more compatible with supra-subduction zone processes (Boger et al., 2014, 2015).

The reshuffling of continental blocks throughout the mid-Neoproterozoic eventually culminated in multiple collisions of smaller crustal plates between ~650 Ma and 500 Ma along the East African Orogen (Stern, 1994; Meert, 2003; Collins and Pisarevsky, 2005; Viola

et al., 2008; Bingen et al., 2009; Torsvik and Cocks, 2013). Madagascar occupies an important location within the East African Orogen (EAO; Fig. 1.1b), one of the largest of orogens that formed during the Ediacaran/Cambrian amalgamation of Gondwana (Stern, 1994; Stern, 2002; Meert, 2003; Collins and Pisarevsky, 2005; Johnson et al., 2011; Fritz et al., 2013). This relationship is expressed in the Mozambique Belt (see Fritz et al. 2014 for a recent summary), where the EAO separated Neoproterozoic India from the African Congo-Tanzania-Bangweulu Block (Fig. 1.1b). To the north, in the Arabian-Nubian Shield, the EAO consists of fragments of pre-Neoproterozoic continental crust in Saudi Arabia, Yemen and the Horn of Africa (e.g. the Afif Terrane), interlayered with Neoproterozoic oceanic-arc like terranes (Johnson et al., 2011; Robinson et al., 2014; Blades et al., 2015) with final amalgamation occurring during the Ediacaran to Cambrian (Doebrich et al., 2007; Cox et al., 2012). The pre-Gondwana ocean that separated these landmasses is referred to the Mozambique Ocean. The Arabian-Nubian Shield preserves many oceanic suture zones recording accretion of the shield but as the orogen is traced south, the identification of potential sutures becomes equivocal. This led Shackleton (1996) to review the various suggested traces of the Mozambique Ocean suture. He concluded that, unlike many Phanerozoic orogens that involve accretion of multiple terranes (e.g. the Appalachians of eastern North America), the Mozambique Ocean closed as a single suture; and this lay within East Africa.

Collins and Windley (2002) proposed that this single-suture model was an over-simplification, and suggested a wide band of pelitic gneiss, with Neoproterozoic depositional ages (Collins et al., 2003c) and associated pod-like peridotite bodies, gabbro and emerald mineralisation represented another Mozambique Ocean suture zone (named the 'Betsimisaraka Suture'), that separated central Madagascar from India. The accretion of Azania to the Dharwar Craton along the Betsimisaraka Suture was accompanied by voluminous arc-magmatism in central Madagascar (Collins, 2006) – interpreted to result from Andean-style subduction. Alternatively, the Greater Dharwar Craton hypothesis incorporates all of eastern and most of central Madagascar on the margin of Neoproterozoic India (Tucker et al., 2011b; Tucker et al., 2014) thus, reverting to a single suture hypothesis for the Mozambique Ocean. However, unlike the Dharwar Craton of India, the Archaean rocks of Madagascar were extensively reworked by multiple Proterozoic tectonothermal events (Tucker et al., 2014).

1.4 Project aims and hypotheses

This PhD research project will attempt to resolve a number of controversies regarding the Proterozoic geology of central Madagascar. The specific details associated with each controversy are defined in the introduction and discussion of each chapter. Below is a brief outline of the major research questions tackled by this project and a brief introduction as to how each topic was addressed.

What are the maximum and minimum depositional ages and where are potential source regions for Proterozoic metasedimentary rocks?

Although there are abundant U-Pb ages for detrital zircons on several metasedimentary sequences in Madagascar, there are unresolved issues regarding the depositional age and the source regions for these sediments. The Ambatolampy Group is one of these enigmatic sedimentary sequences. Recent mapping (Roig et al., 2012) showed the unit to be extensive and preliminary U-Pb (zircon) data indicated a Neoproterozoic depositional age (BGS-USGS-GLW, 2008). This result had important tectonic implications causing a paradigm shift for the Neoproterozoic tectonic evolution of Madagascar and was part of the reason why the Greater Dharwar hypothesis was proposed. To determine the

depositional age of the Ambatolampy Group, new U-Pb detrital zircon age data was collected. Hafnium and oxygen isotope data were collected were collected to constrain possible source regions. Additionally, a compilation of all of the available U-Pb detrital zircon data from the Precambrian metasedimentary units in Madagascar permitted a re-evaluation and re-interpretation of the relationships of the depositional basins in Madagascar. Finally, this large dataset aided in determining relationships of metasedimentary units in Madagascar to contemporaneous sequences in India and East Africa.

What is the nature of mid-Tonian magmatism?

The voluminous Imorona-Itsindro Suite is an enigmatic magmatic suite emplaced in central Madagascar between ~850-750 Ma. Traditionally, the suite was thought to be emplaced in an Andean-type subduction zone environment. However, recent studies have questioned the presence of an extensive continental arc- system in Madagascar and favoured an intracontinental rifting event related to plume magmatism. Two chapters, one focusing on the zircon isotope signatures (Chapter 3) and the other on whole-rock geochemical characteristics including radiogenic isotope data (Chapter 4) attempt to resolve the conundrum of the nature of magmatism. In addition, these data are used to determine the subduction polarity provided that these rocks were most likely emplaced in a supra-subduction zone environment during closure of the Mozambique Ocean.

What is the significance of the Dabolava Suite?

Prior to the recognition of the Stenian-Tonian Dabolava Suite, magmatism of this age was not recognised in Madagascar. The recently identified metaigneous rocks are only found in the Ikalamavony Domain. The tectonic setting for these rocks and their relationship to other units in Madagascar is unclear. New U-Pb (zircon) age data, oxygen and hafnium isotope data from zircon with complimentary whole-rock geochemical data provide insight on the nature of magmatism. These data are integrated into the genesis of the Ikalamavony Domain and incorporated into the broader picture of the amalgamation of Rodinia (Fig. 1.1a).

What is the nature of Ediacaran-Cambrian magmatism?

The waning stages of Gondwana assembly were accompanied by emplacement of three magmatic suites in the central Madagascar. The Ediacaran to Cambrian was also the time of regional high-temperature/low pressure metamorphism and the development of transcurrent and transpressive shear zones. Emplacement of the Ambalavao and Maevarano Suites were related spatially to extensive shear zones and temporally with major deformational episodes. However, the nature of magmatism was poorly understood and understudied since most work over the past ~30 years focussed on the Ediacaran-Cambrian deformation and metamorphism. New U-Pb (zircon) age data, oxygen and hafnium isotope data from zircon with complimentary whole-rock geochemical data provide insight on the nature of Ediacaran to Cambrian magmatism. The timing and nature of magmatism combined with the deformation data are then placed in a regional context to test the hypothesis related to the Neoproterozoic history of Madagascar and the amalgamation of Gondwana (Azania microcontinent versus Greater Dharwar Craton).

Examination of Proterozoic metasedimentary rocks and three Mesoproterozoic to Neoproterozoic plutonic rock suites provide insight into the tectonic evolution of central Madagascar. The main objectives of the research project are: (1) to compile all previously published isotopic and geochemical data from Proterozoic rock units in Madagascar; (2) use the detrital zircon dataset to determine the timing and duration of sediment deposition; (3) use the isotopic and geochemical data from plutonic rocks to understand the processes involved in

magma genesis and relate these to possible tectonic settings; and (4) to better understand the overall geologic evolution and tectonic history of Proterozoic Madagascar.

1.5 Thesis outline

This PhD thesis is divided into six chapters each focusing on a different aspect related to the Meso- to Neoproterozoic tectonic development of central Madagascar. The following chapters constitute a published paper, manuscripts under review, submitted manuscripts or manuscripts prepared for submission. Therefore, there is unavoidable repetition of background information in the introduction, methodology and discussion sections of each chapter.

Chapter two attempts to constrain the depositional age and source region of Proterozoic sedimentary rocks (the Ambatolampy Group) using zircon isotopic proxies and compares Malagasy rocks with contemporaneous rocks in India and East Africa. Three isotope systems in zircon provide information regarding the age and nature of magmatism from which the detrital zircons were derived and/or younger metamorphic events including U-Pb, hafnium and oxygen isotopes. U-Pb data constrains the age of zircons whereas Hf and O isotope data provide insight into the nature of the magma from which zircon crystallized. Together, these data represent three independent variables for comparing detrital zircon populations. Correlatives of the Ambatolampy Group are found elsewhere in Madagascar including the Itremo, Maha, and Sambirano-Sahantaha Groups, and imply a large, interconnected sedimentary basin covered vast regions of Madagascar during the Palaeo- to Mesoproterozoic.

The third and fourth chapters involve two related studies investigating the Tonian-aged Imorona-Itsindro Suite. These chapters represent the first comprehensive studies devoted to the enigmatic plutonic suite. Chapter three focuses on the age (U-Pb zircon), oxygen, and hafnium isotope characteristics of Tonian-aged zircon. Emplacement of the suite occurred continuously over ~100 Myr. Oxygen and hafnium isotope data show involvement of both the crust and depleted mantle during magma genesis. Isotopic data reflect the diversity of the basement lithologies present in central Madagascar. Chapter four focuses on the petrography, mineral chemistry and whole-rock geochemistry of the magmatic suite to further characterize the petrogenesis of the suite. Data show plate margin processes explain the genesis of the suite more appropriately than intracratonic processes. The suite correlates with the eastward directed subduction of the Mozambique Ocean beneath central Madagascar.

Chapter five focusses on the Ediacaran to Cambrian Ambalavao and Maevarano Suites. Emplacement of these magmatic suites coincided with the final stages of Gondwana amalgamation. U-Pb, oxygen, and hafnium isotopic data in zircon with complementary whole-rock geochemical data show magma genesis occurred in a post-collisional tectonic setting. Emplacement corresponds with Cambrian regional high-temperature/low pressure metamorphism and simultaneous deformation episodes. These post-tectonic intrusions are often associated with major shear zones. Melting occurred during lithospheric delamination or lithospheric underplating following collision or accompanied the extensional collapse of the EAO in Madagascar.

Chapter six examines the Stenian-Tonian Dabolava Suite, a recently recognized magmatic suite that consists primarily of intermediate to felsic plutonic rocks with juvenile geochemical and isotopic characteristics. It was suggested that the coeval volcano-sedimentary Ikalamavony Group and the Dabolava Suite represent a marginal magmatic arc and basin environment possibly correlating with the amalgamation of Rodinia. U-Pb, oxygen, and hafnium isotopic data in zircon with complementary whole-rock geochemical data show

the Ikalamavony Domain developed as a juvenile, oceanic arc terrane in the Mozambique Ocean. Melting of new crust resulted in the emplacement of the Dabolava Suite.

Finally, chapter seven summarises this study of Stenian to Cambrian rocks in Madagascar and attempts to relate the studied rocks into a unified story for the tectonic development of central Madagascar. These data indicate a prolonged (~500 Ma) plate margin microcontinent in the Mozambique Ocean (Azania), Neoproterozoic India (Greater Dharwar Craton) or East Africa (Congo-Tanzania-Bangweulu Block) during this time remains equivocal but our data suggests it was likely a microcontinent. This project represents an important contribution to the understanding of the geologic history of Madagascar, our perception of Proterozoic tectonic geography, and the evolution of the Mozambique Ocean.

Chapter 2

The Ambatolampy Group

Published as:

Archibald, D. B., Collins, A. S., Foden, J. D., Payne, J. L., Taylor, R., Holden, P., Razakamanana, T., Clark, C. (2015). Towards unravelling the Mozambique Ocean conundrum using a triumvirate of zircon isotopic proxies on the Ambatolampy Group, central Madagascar. Tectonophysics 662, 167-182.

Statement of Authorship

Title of Paper	Towards unravelling the Mozambique Ocean conundrum using a triumvirate of zircon isotopic proxies on the Ambatolampy Group, central Madagascar
Publication Status	_X_ Published __ Accepted for Publication __ Submitted for Publication __ Publication Style
Publication Details	Archibald, D.B., Collins, A.S., Foden, J.D., Payne, J.L., Taylor, R., Holden, P., Razakamanana, T., Clark, C., 2015. Towards unravelling the Mozambique Ocean conundrum using a triumvirate of zircon isotopic proxies on the Ambatolampy Group, central Madagascar. Tectonophysics 662, 167-182.

Author Contributions

By signing the Statement of Authorship, each author certifies that their stated contribution to the publication is accurate and that permission is granted for the publication to be included in the candidate's thesis.

Name of Principal Author (Candidate) Contribution to the paper Conceptualisation of the work It's realisation Documentation and write-up Development of ideas and conclusions	Donnelly B. Archibald Prepared samples, carried out analyses and interpretation of the data, wrote manuscript, acted as the corresponding author		
Signature		Date	9/7/2016

Name of Co-Author Contribution to the paper	Prof Alan S. Collins Supervised work, help with data interpretation and manuscript revision		
Signature		Date	9/7/2016

Name of Co-Author Contribution to the paper	Prof John D. Foden Helped with manuscript revision		
Signature		Date	11/7/2017

Name of Co-Author Contribution to the paper	Dr. Justin L. Payne (University of South Australia) Helped with hafnium isotope data collection		
Signature		Date	7/4/2016

Name of Co-Author Contribution to the paper	Dr. Richard J.M. Taylor (Curtin University) Helped with U-Pb isotope data collection and interpretation		
Signature		Date	7/4/2016

Name of Co-Author Contribution to the paper	Dr. Chris Clark (Curtin University) Helped with U-Pb isotope data collection		
Signature		Date	10/7/2016

Name of Co-Author Contribution to the paper	Dr. Peter Holden (The Australian National University) Helped with oxygen isotope data collection and interpretation		
Signature		Date	28/04/2016

Name of Co-Author Contribution to the paper	Dr. Theodore Razakamanana (University of Toliara, Madagascar) Assistance in the field, sample logistics, manuscript editing		
Signature		Date	8/4/2016

Abstract

Madagascar occupies an important location within the East African Orogen (EAO), which involves a collection of Neoproterozoic microcontinents and arc terranes lodged between older cratonic units during the final assembly of the supercontinent Gondwana. The detrital zircon record of Proterozoic metasedimentary rock packages within the Antananarivo Domain (the Ambatolampy, Manampotsy, Vondrozo, Itremo and Ikalamavony Groups) are used to identify pre-orogenic tectonic affiliations of the region—affiliations that control interpretations of the evolution of the Mozambique Ocean and the formation of this part of central Gondwana. Here we focus on the Ambatolampy Group, a previously poorly known group of high-grade siliciclastic metasedimentary rocks, and compare these data to similar data from the other sedimentary packages in central Madagascar (the Vondrozo, Sofia, Manampotsy, Itremo, Molo, Ikalamavony, Androyen, Ambodiriana, Iakora and Maha Groups). New U-Pb (SHRIMP) zircon data for the Ambatolampy Group yield detrital age maxima of ~3000 Ma, ~2800-2700 Ma, ~2500 Ma, ~2200- 2100 Ma and ~1800 Ma. The youngest near-concordant detrital zircon age is 1836 ± 25 Ma, which we suggest represents the maximum depositional age of the Ambatolampy Group, in contrast to younger ages reported elsewhere. The detrital spectra are very similar to those from the Itremo Group and we suggest that they correlate with each other. Metamorphic zircon and zircon rims constrain the minimum depositional age to be ~540 Ma; the interpreted age of metamorphism. New $\delta^{18}O$ data and hafnium isotopic data complement the U-Pb data and provide new constraints on the age, geochemistry and provenance of the metasedimentary rocks. We suggest that Madagascar contained a Mesoproterozoic (to possibly Tonian) siliciclastic sedimentary basin, within which the Ambatolampy Group, and the Itremo and Maha (and possibly part of the Iakora Groups) were deposited. Younger sedimentary systems are represented by the Ikalamavony, Ambodiriana, Manampotsy and Molo Groups.

2.1 Introduction

The East African Orogen is one of the largest orogens that formed during the Ediacaran/Cambrian amalgamation of Gondwana (Stern, 1994; Stern, 2002; Meert, 2003; Collins and Pisarevsky, 2005; Johnson et al., 2011; Fritz et al., 2013). To the present-day north, in the Arabian-Nubian Shield, the East African Orogen consists of a pre-Neoproterozoic continental terrane (the Afif Terrane), surrounded by many Neoproterozoic oceanic-arc like terranes (Johnson et al., 2011; Robinson et al., 2014; Robinson et al., in press) that sutured together as late as the Ediacaran (Doebrich et al., 2007; Cox et al., 2012). To the south, in the Mozambique Belt (see Fritz et al. 2014 for a recent summary), the East African Orogen separated Neoproterozoic India from the African Congo-Tanzania-Bangweulu Block (Fig. 2.1a). The pre-Gondwana ocean that separated these landmasses is known as the Mozambique Ocean. In the Arabian-Nubian Shield many oceanic suture zones tie together the various terranes. However, as you trace the orogen south, the sites of these sutures becomes more enigmatic, leading Shackleton (1996) to posit the question as to where the Mozambique Ocean suture lay. He suggested that, unlike Phanerozoic orogens, the Mozambique Ocean closed to form one single suture; and this lay within East Africa.

Collins and Windley (2002), proposed that this single-suture model was an over-simplification, and that a wide band of pelitic gneisses, with Neoproterozoic depositional ages (Collins et al., 2003c) and associated pod-like peridotite bodies, gabbro and emerald mineralisation represents another Mozambique Ocean suture zone (termed the Betsimisaraka Suture), which separates central Madagascar from India (Collins and Windley, 2002). Several authors (Collins and Windley, 2002; Cox et al., 2004; Fitzsimons and Hulscher, 2005; Collins, 2006) have suggested that central Madagascar formed a Neoproterozoic continent, which, along with parts of southern India (the Madurai Block, Plavsa et al., 2014; Collins et

al., 2014), East Africa, Yemen and Saudi Arabia (Collins and Windley, 2002), was isolated from both Neoproterozoic India and the Congo-Tanzania-Bangweulu Block by oceanic crust. Collins and Pisarevsky (2005) called this continent 'Azania'. Recently, the existence of Azania has been challenged, and an alternative 'Greater Dharwar' continent has been proposed (Tucker et al., 2011b; Boger et al., 2014; Tucker et al., 2014) that incorporates all of eastern and most of central Madagascar on the periphery of Neoproterozoic India.

The provenance of Neoproterozoic (meta-) sedimentary rocks has long been known to form a possible test to the tectonic affiliation of central Madagascar, particularly as the pre-Neoproterozoic crust in southern India and eastern Africa contain very different-aged exposed rocks. Cox et al. (1998; 2004) pioneered using detrital zircons to test the tectonic geography of pre-Gondwana Madagascar by focussing on the prominent metasedimentary rocks of central Madagascar. These authors suggested an African source for this area, which was supported by Fitzsimons and Hulscher (2005). Collins et al. (2003c) examined detrital zircons in pelitic rocks from eastern Madagascar and constrained these rocks to be also deposited in the Neoproterozoic, but in contrast to the Malagasy examples, they had detritus more consistent with an Indian source. Supporters of the Greater Dharwar hypothesis point out that there are Proterozoic basins in southern India, that contain some formations with Palaeoproterozoic detritus, similar to those in Madagascar (Amarasinghe et al., 2015; Collins et al., 2015).

Zircon is an attractive provenance proxy because of its durability and chemical stability over a wide range of lithospheric pressures, temperatures, and fluid/melt compositions (e.g. Cherniak et al., 1997) . Analysis of individual zircon grains using micro-beam techniques is invaluable when zircons are chemically altered during metamorphism or old grains are rimmed by younger metamorphic zircon overgrowths. In this manuscript, we present new U-Pb SHRIMP II (sensitive high-resolution ion microprobe) data with complimentary SHRIMP SI (stable isotope) oxygen isotope data and multicollector LA-ICP-MS (laser ablation inductive coupled plasma mass spectroscopy) hafnium isotope data for detrital zircons from metasedimentary rocks in central Madagascar. These data allow us to constrain the depositional age of protoliths, to characterise the geochemical nature of zircon sources, and data assists in correlation with other major metasedimentary sequences in Madagascar and elsewhere in the EAO.

2.2 Regional geology of Madagascar

Madagascar contains a number of Precambrian to earliest Palaeozoic 'basement' units. The oldest of these are the Palaeoarchaean to Palaeoproterozoic Antongil and Masora blocks (Fig. 2.1b). These units crop out on the island's east coast and are considered to be parts of the Dharwar Craton of southern India (Tucker et al., 1999b; Collins and Windley, 2002; Collins et al., 2003c; Collins, 2006; Schofield et al., 2010; Tucker et al., 2011a; Tucker et al., 2011b; Tucker et al., 2014).

The largest unit in Madagascar, the Antananarivo Block (or Domain), underlies the central highlands and comprises granulite- to upper-amphibolite facies orthogneiss and paragneiss (Kröner et al., 2000; Collins et al., 2003a; Collins, 2006; Roig et al., 2012). The orthogneiss consist of ~2550–2500 Ma granitoids (the Betsiboka Suite) that are tectonically interlayered with paragneiss of the Ambatolampy Group (Besairie, 1968-1971) and intersheared with, and intruded by, voluminous ~ 820–760 Ma granitoids, syenites and gabbroic rocks of the Imorona-Itsindro Suite. This Cryogenian suite has traditionally been considered to have supra-subduction zone geochemical affinities (Handke et al., 1999; Kröner et al., 2000; Key et al., 2011) but recent studies have challenged this hypothesis and suggested

a within-plate or mantle plume tectonic setting (McMillan et al., 2003; Yang et al., 2014; Zhou et al., 2015b).

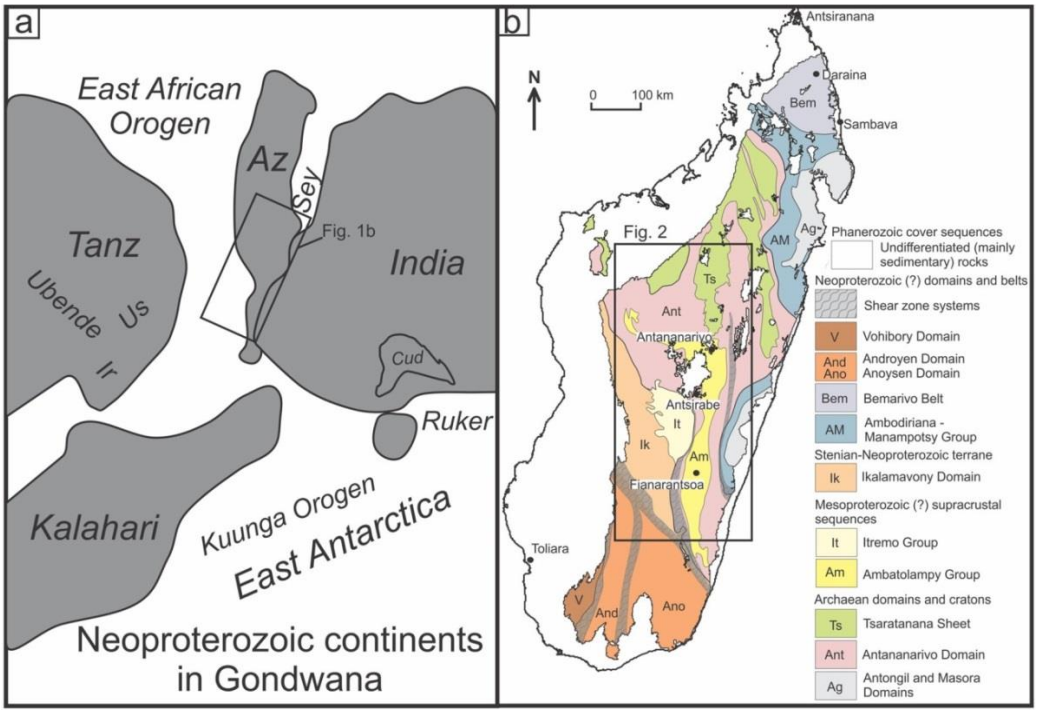

Fig. 2.1 a) Palaeogeographic reconstruction of the Neoproterozoic continents in Gondwana showing the location of the present study (after Collins and Pisarevsky, 2005). Abbreviations: Az = Azania; Sey = Seychelles; Ir = Irumide Belt; Cud = Cuddapah Basin; Ruker = Ruker Terrane, East Antarctica; Tanz = Tanzanian craton; Ubende = Ubende Belt; and Us = Usagaran orogen. b) Simplified basement geology of Madagascar (after Collins, 2006 and De Waele et al., 2011).

Older units are intruded by the sheet-like ~630 Ma Kiangara Suite A-type granitoids (Nédélec et al., 1994) and the post-tectonic Ediacaran to Cambrian (~560-540) granitoids of the Ambalavao and Maevarano Suites (Goodenough et al., 2010). The entire Antananarivo Domain was thermally and structurally reworked at ~850 Ma (Moine et al., 2014) and between ~700 - 500 Ma with pre-existing rocks being metamorphosed to granulite-facies and with the development of gneissic fabrics (Collins et al., 2003c; BGS-USGS-GLW, 2008).

Structurally overlying the Antananarivo Domain are several Proterozoic metasedimentary units. The Itremo Group (Cox et al., 1998; Cox et al., 2004) consists of quartzite, conglomerate and dolomitic marble (previously known as the 'Schisto-Quartzo-Calcaire' Besairie, 1968-1971; or 'Schisto-Quartzo-Dolomitique, Moine, 1974). The Itremo Group is characterized by significant detrital zircon peaks at ca. 2500 Ma and 1800 Ma (Cox et al., 2004; Fitzsimons and Hulscher, 2005; De Waele et al., 2011). Rocks of the Itremo Group increase in metamorphic grade from east to west with its lowest-grade rocks (lower greenschist facies) preserved in the hanging-wall of the Betsileo shear zone (Moine, 1974; Collins et al., 2000). The protolith sediments were deposited after ~1700 Ma (Fernandez et al., 2003; Cox et al., 2004) and have been interpreted to be derived from East Africa (Cox et al., 1998; Cox et al., 2004; Fitzsimons and Hulscher, 2005). Recently, the Itremo Group has been correlated with the Maha Group that structurally overlies the Masora Domain (Fig. 2.2) in south-east central Madagascar, and the Sambirano-Sahantaha Group from the southern Bemarivo Domain (De Waele et al., 2011), which is thrust over the Antongil Domain (Thomas et al., 2009; Schofield et al., 2010).

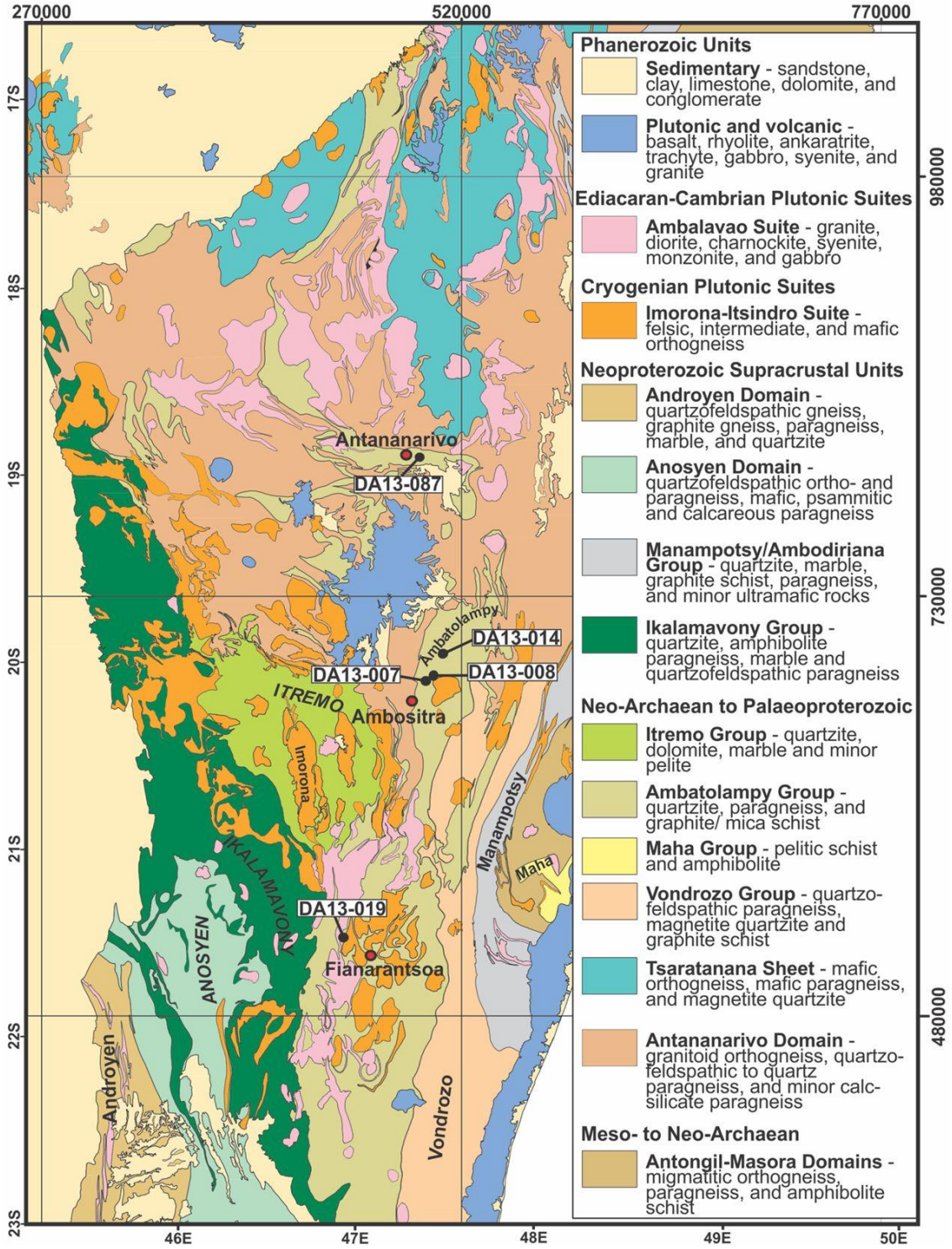

Fig. 2.2 Geologic map of central Madagascar showing the distribution of the Ambatolampy Group, other central Malagasy metasedimentary units and sample locations (modified after Roig et al., 2012). Note that Ediacaran to Cambrian plutonic rocks are undivided and given the name Ambalavao Suite (Roig et al., 2012).

The poorly understood Ikalamavony and Molo Groups lie west of the Itremo Group (Roig et al., 2012). Cox et al. (2004) identified and named the latter group and demonstrated that it was deposited between ~620 Ma and ~560 Ma and sourced from Neoarchaean, late Mesoproterozoic (~1100-1000 Ma) and Cryogenian rocks. The late Mesoproterozoic source was interpreted to be the Irumide Belt of Zambia, but subsequently the Dabolava Suite of western Madagascar has been demonstrated to have crystallised at this time and could be a source (Tucker et al., 2011b; Tucker et al., 2014). Little is known of the provenance or age of

the Ikalamavony Group, and its distinction from the Molo Group is also unclear as some rocks used in the definition of the Molo Group (Cox et al., 2004) have been recently assigned as being part of the Ikalamavony Group (Tucker et al., 2011b; Roig et al., 2012; Tucker et al., 2014).

The Ambatolampy Group forms the focus of this paper. It is a granulite-facies metasedimentary group that lies within the Antananarivo Domain and has previously been postulated to be a corollary of the Itremo Group (Collins et al., 2000). Recent detrital zircon U-Pb analyses undertaken as part of a World Bank funded mapping programme (BGS-USGS-GLW, 2008; Tucker et al., 2011b; Tucker et al., 2014), reported largely Neoarchaean and Palaeoproterozoic detritus, similar to that from the Itremo Group, but with 12 near-concordant analyses at ~1000-1100 Ma from one of the three samples they analysed. Here we report the results of a more extensive U-Pb detrital zircon study, and couple it with hafnium and oxygen isotope analyses from the same dated zircons to develop a multiproxy provenance database to better compare with data recently published from India (Teale et al., 2011; Plavsa et al., 2012; Sarma et al., 2012; Glorie et al., 2014; Mohan et al., 2014; Collins et al., 2015).

2.3 The Ambatolampy Group

2.3.1 Group Description

The Ambatolampy Group, formerly termed the "Séries d'Ambatolampy" (Hottin, 1964), is named after the town of Ambatolampy located approximately 70 km south of Antananarivo (Fig. 2.2). Recent work (BGS-USGS-GLW, 2008) defines the Ambatolampy Group and describes field relationships with other units. The group is a supracrustal package patchily preserved on the highland plateau west of the Angavo-Ifanadiana Shear Zone and Ankay-Alaotra rift. The group consists of tightly folded metasedimentary sequences characterised by graphite-bearing sillimanite ± garnet mica schist and paragneiss with abundant quartzite beds (BGS-USGS-GLW, 2008). The entire region is intensely weathered and fresh outcrops are rare.

The Ambatolampy Group is one of a number of metasedimentary units that were originally distinguished on metamorphic character or subtle differences in lithology (Besairie, 1968-1971). These include the Vondrozo and Manampotsy Groups (Fig. 2.2; BGS-USGS-GLW, 2008). The distinction of these different metasedimentary units has been upheld in the new mapping programme (BGS-USGS-GLW, 2008; Roig et al., 2012). The Ambatolampy and Vondrozo Groups are separated on the basis of interpreted age relationships (BGS-USGS-GLW, 2008). The Vondrozo Group is intermixed with, and presumably host to, Neoarchaean orthogneiss whereas a sample mapped as the Ambatolampy Group yielded 12 >90% concordant late Mesoproterozoic U-Pb detrital zircons (BGS-USGS-GLW, 2008). Lithologically, the Ambatolampy Group is distinguished from the Vondrozo Group by the common occurrence of graphitic units, mafic-ultramafic lenses, and a rarity of magnetite bearing quartzites in the former. However, this distinction is not robust as ferruginous rocks occur in the Ambatolampy Group and there are occurrences of graphite-bearing lithologies in the Vondrozo Group (BGS-USGS-GLW, 2008). Both groups comprise high-grade amphibolite facies (sillimanite-garnet-tourmaline) assemblages and host granitoid intrusions. The Perinet paragneiss of the Manampotsy Group are also difficult to distinguish from the Ambatolampy Group (BGS-USGS-GLW, 2008). Prior to the recent World Bank funded mapping programme, the units were distinguished by the extent of migmatisation. Recent mapping suggests that the Ambatolampy Group is primarily juxtaposed against the Vondrozo Group and orthogneiss of the Mangoro Complex (Antananarivo Domain) rather than the Manampotsy Complex (BGS-USGS-GLW, 2008). Previous workers interpreted the depositional age of the Manampotsy Group to be approximately 840 - 780 Ma, based on the

age of its youngest detrital zircons (De Waele et al., 2008; Tucker et al., 2011a) and interpreted syn-depositional volcanic rocks (Tucker et al., 2014). However, coeval plutonic rocks of the Imorona-Itsindro Suite are also reported to intrude the group (BGS-USGS-GLW, 2008; Roig et al., 2012) and thus part of the group could be older than ~800 Ma. Tucker et al. (2014) concluded that diachronous deposition of the Manampotsy Group occurred in a long, narrow basin that formed during a brief period of continental extension and magmatism in Cryogenian times.

2.3.2 Lithologies and stratigraphy

Overall, the Ambatolampy Group is characterised by abundant mica schists and quartzites that increase in metamorphic grade towards the east into gneisses and migmatitic rocks (BGS-USGS-GLW, 2008). The schists consist of biotite, sillimanite, garnet ± corundum, and graphite. Related pelitic paragneiss are biotite-rich, are variably schistose, and commonly contain sillimanite and garnet. Quartzites, ranging from metre-bedded ridge-forming units to fine cm-scale interbeds, preserve relic bedding transposed into the tectonic foliation. They preserve varying amounts of garnet, sillimanite, pyroxene, tourmaline, graphite and magnetite. Small metre- and decametre-sized bodies of pyroxenite, pyroxene-amphibolite, amphibolite ± garnet, pyroxene gneiss, garnet and graphite schist are also reported in this unit (BGS-USGS-GLW, 2008). Thin metacarbonate and calc-silicate rock units are intercalated with the mica schists and are generally associated with graphitic zones and skarn (BGS-USGS-GLW, 2008).

Quartzites are mostly coarsely recrystallised, massive bedded, centimetre to decametre scale units alternating with pelitic rocks. Thicker units (>1 metre) normally contain pelitic to semipelitic interbeds. Beds contain feldspar (up to 25%), small magnetite grains and other accessory phases. Graphite is also found disseminated in quartzite beds but is more commonly found near contacts with the mica schists (BGS-USGS-GLW, 2008).

2.3.3 Previous work and interpretation

Previous U-Pb geochronology for Ambatolampy Group detrital zircons indicate a maximum depositional age of 1001 ± 44 Ma (BGS-USGS-GLW, 2008; De Waele et al., 2011) based on 12 <10% discordant data from one sample. Detrital zircon ages vary from ~2740 to ~1001 Ma, consistent with derivation from the Antananarivo Domain basement and from the Dabolava Suite in the Ikalamavony Domain (BGS-USGS-GLW, 2008). Tucker et al. (2014) suggests an even younger maximum deposition age of less than ~ 650 Ma based on unpublished data and unspecified locations of Cryogenian detritus. In addition, there are no reports of the igneous rocks of the Imorona-Itsindro Suite (850-760 Ma) intruding the Ambatolampy Group, but "*lit-par-lit"* relationships with the suite have been noted (CGS, 2009a, b). The minimum age of deposition (~560 Ma) is well constrained by the age of metamorphic zircon and monazite within the group along with the Ediacaran granitoids (Ambalavao Suite) that intrude the group (Tucker et al. 2014).

2.4 Analytical methods

2.4.1 Zircon separation and imaging

Approximately 2.5 to 3 kg of each sample was collected for thin sectioning and zircon separation. After sample crushing, zircons were separated by conventional sieving, magnetic and heavy liquid techniques. Zircon grains were mounted in epoxy resin, polished, and imaged under reflected light. To investigate the internal structure of the zircon grains and to select target sites for U–Pb, hafnium, and oxygen isotopic analyses, cathodoluminescence

(CL) imaging was carried out using a Phillips XL40 Scanning Electron Microscope equipped with a tungsten filament electron source and a Gatan CL detector attached for high-resolution imaging at Adelaide Microscopy. Zircon grains were imaged using ~15mm working distance and accelerating voltage of 12 kV.

2.4.2 Zircon U-Pb Geochronology

Zircon U–Pb–Th isotopic data were collected using the Sensitive High Resolution Ion Microprobe Mass Spectrometer (SHRIMP II) based in the John de Laeter Centre of Mass Spectrometry, Perth, Western Australia. The sensitivity for Pb isotopes in zircon using SHRIMP II was 21 cps/ppm/nA, the primary beam current was 2.5–3.0 nA and mass resolution was ≥ 5000. Correction of measured isotopic ratios for common Pb was based on the measured ^{204}Pb in each sample and often represented a <1% correction to the ^{206}Pb counts (see % common ^{206}Pb in Appendix 2.1). Pb/U isotopic ratios were corrected for instrumental inter-element discrimination using the observed covariation between Pb+/U+ and UO+/U+ (Hinthorne et al., 1979; Compston et al., 1984) determined from interspersed analyses of the zircon standard BR266. BR266 is a zircon from Sri Lanka with an age of 559 ± 0.3 Ma, a ^{206}Pb/^{238}U = 0.09059, with U and Th contents of 909 and 201 respectively (Stern, 2001). Thirty four analyses of BR266 yielded an age of 557.7 ± 1.4 Ma (MSWD = 1.5; Table 2.1). The standard Temora II was used as a secondary standard and 44 analyses yielded an age of 414.3 ± 2.6 Ma (MSWD = 1.3; Table 2.1) which is comparable to the published age of 416.8 ± 0.33 Ma (Black et al., 2004). Ages of individual analyses and weighted means are quoted at the 2 standard deviation level unless otherwise stated.

2.4.3 Zircon Oxygen Isotope Analysis

Oxygen isotopes were collected from the same samples that were U-Pb dated. The U-Pb mounts were repolished and oxygen isotope spots were placed on the same zircon sites as those used in the U-Pb determination. Analyses were undertaken using the SHRIMP SI at the Research School for Earth Sciences in the Australian National University, Canberra. A 10 kV, ~3 nA Cs^+ primary ion beam was focused to a ~30 μm diameter spot on an Al-coated sample. Each analysis consisted of a pre-burn of about 2 min to allow the secondary ion isotopic composition to stabilise and remove the Al-coat prior to the analysis, followed by 5, ~10 second estimates of the ^{18}O/^{16}O ratio. A standard (Temora II) was analysed first, then again after 6 unknown samples. Sample $\delta^{18}O_{(zircon)}$ values were determined by difference relative to the mean $\delta^{18}O_{(zircon)}$ measured on standards following normalisation for long-term drift in its measured composition. The $\delta^{18}O_{(zircon)}$ values for the Temora II standard analysed in this study are 8.19 ± 0.20 ‰ (n=38; Table 2.1). These values are comparable with published $\delta^{18}O_{(zircon)}$ value of 8.20 ± 0.01 ‰ (Valley et al., 2005).

2.4.4 Zircon Lu-Hf isotope analyses

In situ LA-MC-ICPMS hafnium isotope analyses were carried out at the University of Adelaide facility using a New Wave Research 193 nm Excimer laser attached to a Neptune multi-collector ICP-MS system as per Payne et al. (2013). Only grains with U–Pb ages having ≤ 10% discordance were analysed for Lu–Hf isotope composition. Analysis locations were in the same spot as concordant U–Pb and O SHRIMP spots. The bulk of analyses were carried out using a beam diameter of ~50 μm for large and a minimum of ~25 μm for smaller grains. Typical ablation times were 40 –100 seconds using 5 Hz repetition rate, 4 ns pulse rate, and an intensity of ~10 J/cm^2. Zircons were ablated in a helium atmosphere, which was then mixed with argon upstream of the ablation cell.

Analyses used a dynamic measurement routine with ten 0.524 s integrations on ^{171}Yb, ^{173}Yb, ^{175}Lu, ^{176}Hf (+Lu + Yb), ^{177}Hf, ^{178}Hf, ^{179}Hf and ^{180}Hf, one 0.524 s integration on ^{160}Gd, ^{163}Dy, ^{164}Dy, ^{165}Ho, ^{166}Er, ^{167}Er, ^{168}Er, ^{170}Yb and ^{171}Yb, and one 0.524 s integration of Hf oxides with masses ranging from 187 to 196 amu. An idle time of 1.5 s was included between each mass change to allow for magnet settling and to negate any possible effects of signal decay. The measurement cycle was repeated 15 times providing a total maximum measurement time of 3.75 min including an off-peak baseline measurement. Hf oxide formation rates for all analytical sessions in this study were in the range 0.1–0.07%. Hf mass bias was corrected using an exponential fractionation law with a stable ^{179}Hf/^{177}Hf ratio of 0.7325. Yb and Lu isobaric interferences on ^{176}Hf were corrected for following the methods of Woodhead et al. (2004). ^{176}Yb interference on ^{176}Hf was corrected for by direct measurement of Yb fractionation using measured ^{171}Yb/^{173}Yb with the Yb isotopic values of Segal et al. (2003). The applicability of these values were verified by analysing JMC 475 Hf solutions doped with varying levels of Yb with interferences up to ^{176}Yb/^{177}Hf = ~0.5. Lu isobaric interference on ^{176}Hf was corrected using a ^{176}Lu/^{175}Lu ratio of 0.02655 (Vervoort et al., 2004) assuming the same mass bias behaviour as Yb. Confirmation of accuracy of the technique was monitored using the Plešovice (Sláma et al., 2008), Mudtank (Woodhead and Hergt, 2005) and Temora II (Woodhead and Hergt, 2005) zircon standards. Mean ^{176}Hf/^{177}Hf values for each standard along with the published values are given in Table 2.1. $\varepsilon_{Hf}(t)$, and T_{DM}c crustal were calculated using ^{176}Lu decay constant after Scherer et al. (2001). T_{DM} crustal was calculated using the methods of Griffin et al. (2002) with an average crustal composition of ^{176}Lu/^{177}Hf = 0.015.

Table 2.1 Summary of standard data collected for each method in this study. SHRIMP II = Sensitive High-Resolution Ion Microprobe II; SHRIMP SI = Sensitive High-Resolution Ion Microprobe Stable Isotope; MC-ICPMS = Multicollector Inductively Coupled Mass Spectroscopy.

Standard	Method	n	Measured Value	Reference Value	Reference
U-Pb isotopes (Age)					
BR266	SHRIMP II	34	557.7 ± 1.4 Ma	559.0 ± 0.3 Ma	Stern, 2001
Temora II	SHRIMP II	44	414.3 ± 2.6 Ma	416.78 ± 0.33 Ma	Black et al., 2004
Oxygen isotopes ($\delta^{18}O$)					
Temora II	SHRIMP SI	38	8.19 ± 0.20 ‰	8.20 ± 0.01 ‰	Valley et al., 2005
Hafnium isotopes ($^{177}Hf/^{176}Hf$)					
Mudtank	MC-ICPMS	17	0.282512 ± 0.000019	0.282507 ± 0.000006	Woodhead and Hergt, 2005
Plešovice	MC-ICPMS	7	0.282473 ± 0.000030	0.282482 ± 0.000013	Sláma et al., 2008
Temora II	MC-ICPMS	12	0.282671 ± 0.000031	0.282686 ± 0.000008	Woodhead and Hergt, 2005

2.5 Sample information and results

Sample DA13-007 was collected at the junction of Route National (RN) 41 and RN7 near the town of Ambositra (Fig. 2.2). The sample is a quartzite containing recrystallised quartz, alkali-feldspar, biotite, Fe-oxides, zircon and secondary muscovite (Table 2.2). The quartzite is intruded by granite and dolerite dykes. These dykes are extremely weathered and their absolute age was not determined. Zircon is predominantly rounded to sub-rounded prisms and their broken equivalents varying in colour from clear and colourless to pale yellow (Table 2.3). Grain size length varies from ~50 to 300 μm with aspect ratios of 1:1 – 3:1 (length versus width). Most zircon show clear magmatic oscillatory zoning, minor sector zoning, and narrow, dark metamorphic overgrowths (Fig. 2.3).

Sixty-seven analyses of zircon cores and rims were randomly selected for U–Pb (SHRIMP II) analysis, of which 29 analyses yielded ages ≤ 10% discordant (Appendix 2.1). A Tera-Wasserburg concordia diagram shows the discordant nature of the majority of analyses (Fig. 2.4a). $^{207}Pb/^{206}Pb$ ages of near-concordant analyses vary from 2466 ± 24 to 2957 ± 13 Ma and the majority of ages are between 2500 and 2700 Ma. Probability density plots (PDPs) show age peaks at ~2500 Ma and ~2650 - 2760 Ma (Fig. 2.5a). None of the metamorphic overgrowth analyses yielded concordant ages.

Sample DA13-007 has $\delta^{18}O$ ratios between +3.94 and +8.34 ‰ (Fig. 2.6) and an average of +6.18 ‰ (Appendix 2.2). No metamorphic overgrowths were analysed for their $\delta^{18}O$ ratios during this study. $\varepsilon_{Hf}(t)$ values vary between +7.27 and -12.76 with an average value of +0.93 (Fig. 2.7). Initial $^{176}Hf/^{177}Hf$ ratios range between 0.280807 and 0.281259 (Appendix 2.3).

Sample DA13-008 is also quartzite and was collected approximately 200m from sample DA13-007 (Fig. 2.2). The sample is similar and DA13-008 contains recrystallised quartz, alkali-feldspar, biotite, Fe-oxides, zircon and secondary muscovite and sillimanite (Table 2.2), indicating these rocks were metamorphosed at high temperatures. The quartzite is intruded by granitic dykes but they are very weathered and their absolute age was not determined. Zircon is predominantly rounded to sub-rounded prisms and their broken equivalents varying in colour from clear and colourless to pale yellow (Table 2.3). Grain size length varies from ~50 to 400 μm with aspect ratios of 1:1 – 3:1. Most zircon show clear magmatic oscillatory zoning, minor sector zoning, and dark overgrowths (Fig. 2.3).

Fifty-five analyses of zircon cores and rims were randomly selected for U–Pb analysis of which 30 analyses yielded ages ≤ 10% discordant (Appendix 2.1). A Tera-Wasserburg concordia plot shows the discordancy of many analyses (Fig. 2.4b). Concordant ages vary over 300 Ma between 2495 ± 8 to 2815 ± 15 Ma. PDPs show age peaks at ~2500 Ma and ~2650-2700 Ma (Fig. 2.5b). Three analyses of metamorphic overgrowths yielded an age of approximately 530 Ma.

Neoarchaean to Palaeoproterozoic zircons from sample DA13-008 have $\delta^{18}O$ ratios between +4.07 and +7.41 ‰ with an average of +5.90 ‰ (Appendix 2.2). Similar to sample DA13-007, many zircons have $\delta^{18}O$ values higher than what is expected for juvenile zircons (Fig. 2.6). Metamorphic rims have varied $\delta^{18}O$ values encompassing the range of values seen in the cores. $\varepsilon_{Hf}(t)$ values are between +5.33 and -12.71 (mean = 1.83) for Neoarchaean to Palaeoproterozoic zircons in sample DA13-008 and -34.45 to -38.05 for metamorphic rims (Fig. 2.7). Initial $^{176}Hf/^{177}Hf$ ratios are between 0.280795 and 0.281307 for the old zircons and average 0.281432 for rims metamorphic rims (Appendix 2.3).

Sample DA13-014 is a quartzite and was collected 5.5 km east of Ambositra along Route 41 toward the village of Fandriana (Fig. 2.2). The sample contains recrystallised quartz, biotite, alkali-feldspar, magnetite, zircon, and secondary muscovite (Table 2.2). Zircons are predominantly rounded to sub-rounded prisms and their broken equivalents ranging in colour from clear and colourless to pale yellow/brown (Table 2.3). Grain size length varies from ~50 to 250 μm with aspect ratios of 1:1 – 3:1. The majority of zircons show clear magmatic oscillatory zoning, minor sector zoning, and dark metamorphic overgrowths (Fig. 2.3).

Ninety-one analyses of zircon cores and rims were randomly selected for U-Pb geochronology, of which 50 analyses are ≤ 10% discordant. Construction of a Tera-Wasserburg concordia diagram shows the distribution of ages (Fig. 2.4c). Concordant ages

vary from 1836 ± 25 to 3005 ± 8 Ma. PDPs show age peaks at ~1850 Ma, ~2300 Ma, ~2500 Ma and ~2700 Ma (Fig. 2.5c).

Neoarchaean to Palaeoproterozoic zircons from sample DA13-014 have $\delta^{18}O$ ratios between +3.95 and +9.38 ‰ with an average of +6.64 ‰ (Fig. 2.6), slightly higher than the other samples. Only one analysis of metamorphic zircon was undertaken and this yielded a $\delta^{18}O$ value of +11.11 ‰, indicating significant crustal recycling or hydrothermal involvement during metamorphism. Hafnium isotope analyses occupy a similar range to the other samples (Fig. 2.7) with $\varepsilon_{Hf}(t)$ values varying between +6.66 and -10.38 (mean = -0.45) for Neoarchaean to Palaeoproterozoic zircons and low negative values for metamorphic overgrowths (-35.95 to -42.11). Initial $^{176}Hf/^{177}Hf$ ratios are between 0.280767 and 0.281416 (Appendix 2.3).

Table 2.2 Summary of sample locations, rock characteristics, and mineralogy. Abbreviations: qtz = quartz; af = alkali-feldspar; bt = biotite; py = pyrite; he = haematite; mag = magnetite; zr = zircon; ms = muscovite; and sil = sillimanite. Coordinates are given using the Laborde (1928) projection.

	Location Information				Sample Information			
Sample	Latitude	Longitude	Easting	Northing	Lithology	Grain Size	Texture	Mineralogy
DA13-007	20° 29' 01.6"	47° 15' 23.9"	485446	624477	quartzite	<4mm	recrystallised	qtz+af+bt+mag+py+he+zr+ms+sil
DA13-008	20° 29' 05.2"	47° 15' 28.0"	485627	624461	quartzite	<4mm	recrystallised	qtz+af+bt+mag+py+he+zr+ms+sil
DA13-014	20° 26' 55.0"	47° 16' 15.2"	486944	628367	quartzite	<5mm	recrystallised	qtz+af+bt+mag+zr+ms
DA13-019	21° 15' 20.2"	46° 48' 25.0"	438337	539238	quartzite	<2mm	recrystallised	qtz+af+bt+mag+zr+ms
DA13-087	18° 54' 56.0"	47° 32' 57.9"	517097	797864	quartzite	<2mm	recrystallised	qtz+af+bt+mag+zr+ms

Sample DA13-019 is a quartzite from a road cutting near Manavandra Village ~50 km northwest of the town of Fianarantsoa (Fig. 2.2). The sample contains recrystallised quartz, biotite, alkali-feldspar, magnetite, zircon, and secondary muscovite (Table 2.2). The quartzite is intruded by highly weathered granitic dykes. No sample was collected but a similar granitic sample was gathered approximately 100m southeast. This sample yielded a U-Pb zircon (LA-ICP-MS) age of 577 ± 8.2 Ma (MSWD = 3.4; D. Archibald unpublished data) consistent with previous observations (BGS-USGS-GLW, 2008; Tucker et al., 2014). Zircons are predominantly well-rounded to sub-rounded grains and their broken equivalents ranging in colour from clear and colourless to pale brown/yellow. Grain size length varies from ~50 to 200μm with aspect ratios of 1:1 – 3:1. Zircons show magmatic oscillatory zoning and dark metamorphic overgrowths (Fig. 2.3).

Random selection of seventy-eight analyses of zircon cores and rims yielded only nine ≤ 10% discordant results (Appendix 2.1). A Tera-Wasserburg concordia diagram shows the discordancy of many analyses as well as the variability in ages (Fig. 2.4d). Concordant detrital ages are between 1867 ± 15 and ~3078 ± 13 Ma (Fig. 2.5d).

Because of the limited concordant zircons in sample DA13-019, few $\delta^{18}O$ data were collected. The few that were analysed yield $\delta^{18}O$ ratios between +5.24 and +6.40 ‰ (Fig. 2. 6). Hf isotopic data were also limited. $\varepsilon_{Hf}(t)$ values vary between +3.16 and -11.68 (Fig. 2.6; mean = -4.75) with initial $^{176}Hf/^{177}Hf$ ratios between 0.281241 and 0.280722. One overgrowth yielded an $\varepsilon_{Hf}(t)$ value of -31.23.

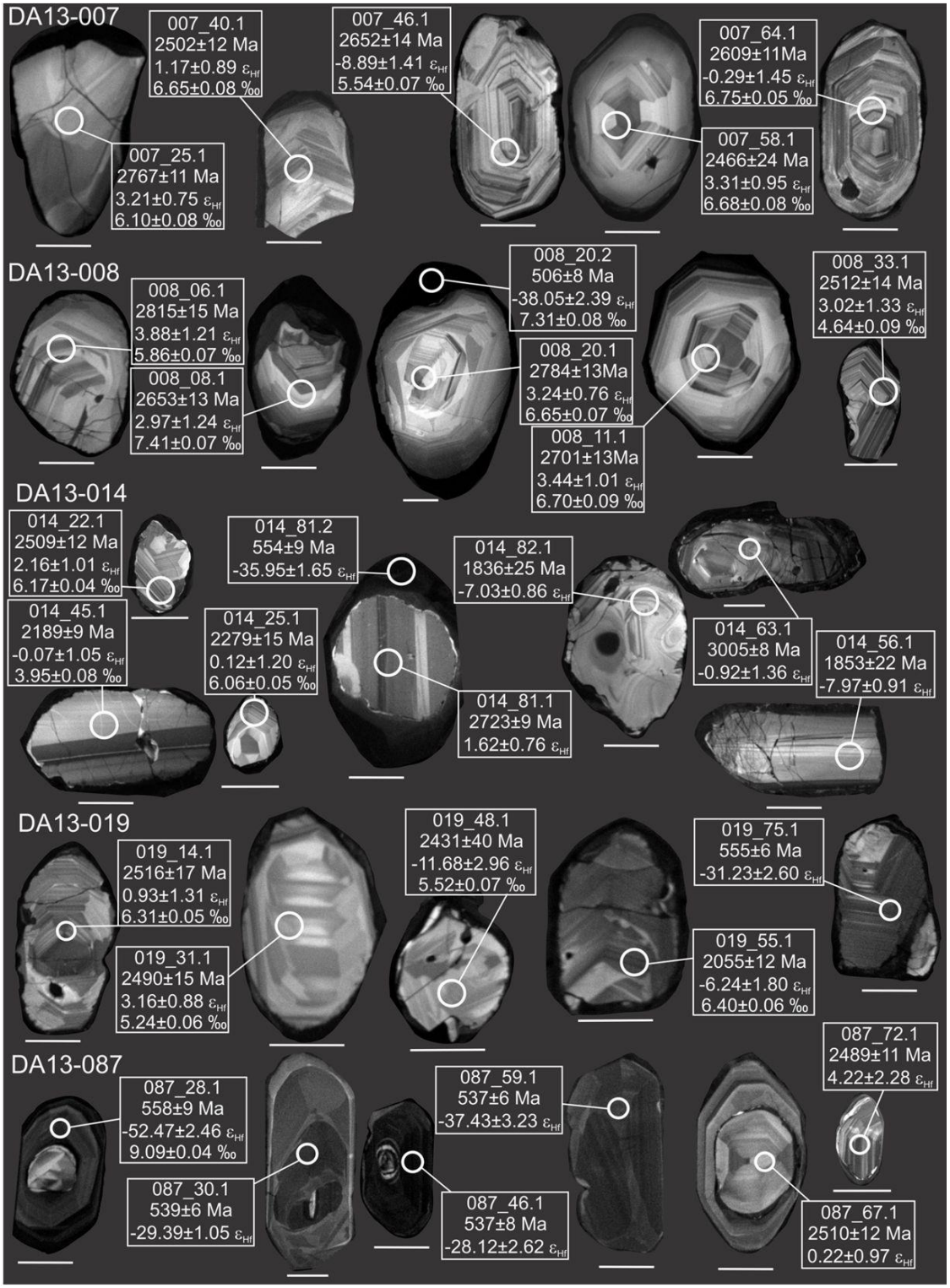

Fig. 2.3 Cathodoluminescence (CL) images for representative zircons (≤10% discordant) from the Ambatolampy Group. Spot names, $^{207}Pb/^{206}Pb$ ages with one standard deviation error, $\varepsilon_{Hf}(t)$ values with one standard deviation error and $\delta^{18}O$ values with one standard deviation errors are listed with the images.

Table 2.3 Physical and optical characteristics of zircons from Ambatolampy Group samples.

Sample	Colour	Size (mm)	Aspect ratio	Morphology	Internal zoning	Interpretation
DA13-007	Colourless, clear, pale yellow, slightly turbid	50-300	1:1 – 3:1	Rounded to sub-rounded	Magmatic, minor sector zoning, dark rims	Detrital zircons with metamorphic overgrowths
DA13-008	Colourless, clear, pale yellow, slightly turbid	50-400	1:1 – 3:1	Rounded to sub-rounded	Magmatic, minor sector zoning, dark rims	Detrital zircons with metamorphic overgrowths
DA13-014	Colourless, clear, pale yellow/brown	50-250	1:1 – 3:1	Rounded to sub-rounded	Magmatic, minor sector zoning, dark rims	Detrital zircons with metamorphic overgrowths
DA13-019	Colourless, clear, pale yellow/brown	50-200	1:1 – 3:1	Well-rounded to sub-rounded	Faint magmatic zoning, dark rims	Detrital zircons with metamorphic overgrowths
DA13-087	Water-clear to pale brown/yellow	75-300	1:1 – 3:1	Rounded to sub-rounded	Xenocrystic cores with magmatic zoning, dark overgrowths	Detrital zircons; reset overgrowths

Sample DA13-087 is a quartzite from an outcrop near the Université d'Antananarivo (Fig. 2.2). The sample contains recrystallised quartz, biotite, alkali-feldspar, magnetite, zircon, and secondary muscovite (Table 2.2). Zircons are predominantly rounded to sub-rounded grains and their broken equivalents varying in colour from water-clear to pale brown/yellow (Table 2.3). Grain length varies from 75-300 μm with aspect ratios of 1:1 – 3:1. Cathodoluminescence imaging shows zircons have xenocrystic cores with magmatic zoning with dark metamorphic overgrowths (Fig. 2.3).

Eighty-four analyses of randomly selected zircon cores and rims yielded only 20 ages that are near concordant (Appendix 2.1). Three near <10% discordant analyses yielded $^{207}Pb/^{206}Pb$ ages of ~2500 Ma (Fig. 2.4e) with the youngest age being 2489 ± 11 Ma. This matches a broad discordia with an upper intercept of 2596 ± 25 Ma and a lower intercept of 542 ± 12 Ma. This sample contains 17 domains that yielded near-concordant Ediacaran-Cambrian ages that are interpreted to represent metamorphic growth or resetting (Fig. 2.5e). The weighted average $^{206}Pb/^{238}U$ age of these metamorphic overgrowths and reset zircon domains is 540 ± 18 Ma (MSWD = 0.04).

Limited $\delta^{18}O$ data were collected due to the scarcity of near concordant data. Data were collected from a single detrital zircon that had a value of +6.74 ‰ (Appendix 2.2). $\delta^{18}O$ ratios for reset domains or metamorphic rims varied between +6.68 and +9.38 ‰, significantly higher than values expected for juvenile zircons (Valley et al., 2005) indicating that the oxygen values probably reflect the age of the host zircon and that the rims developed by in-situ recrystallization (Hoskin and Black, 2000). $\varepsilon_{Hf}(t)$ values for ~2500 Ma zircon are between +0.22 and +4.22 (Fig. 2.7). Reset domains or metamorphic overgrowths yielded low negative values varying from -22.49 and -52.47 (Fig. 7), again demonstrating the recycled nature of the rims (e.g. Kröner et al. 2014). Initial $^{176}Hf/^{177}Hf$ ratios vary between 0.281307 - 0.281181 for ~2500 Ma zircon and 0.281813 to 0.280965 for reset domains (Appendix 2.3).

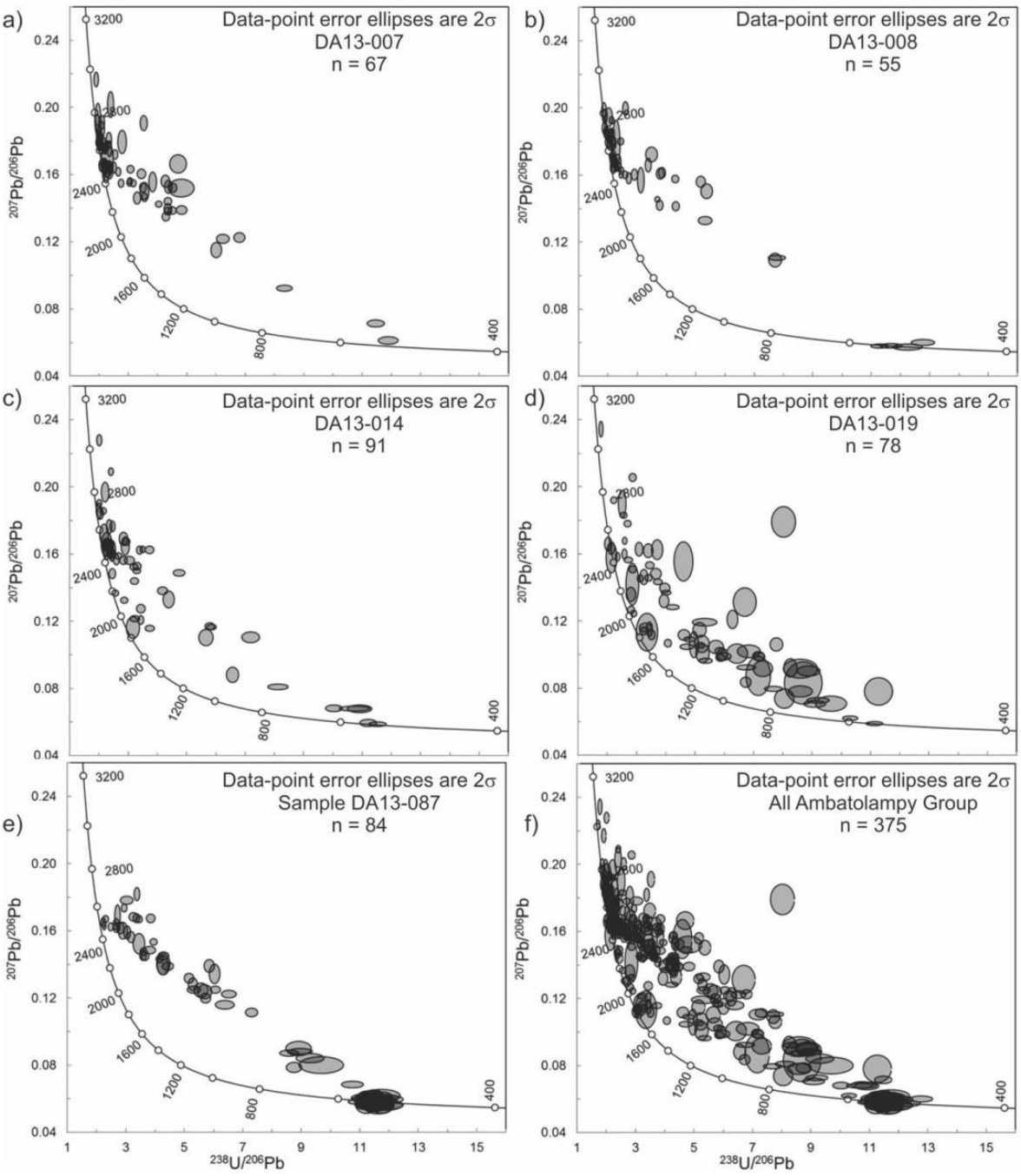

Fig. 2.4 Tera-Wasserburg concordia diagrams for Ambatolampy Group samples analysed in this study. a) DA13-007; b) DA13-008; c) DA13-014; d) DA13-019; e) DA13-087; and f) all Ambatolampy Group samples. Error ellipses are at drawn at the two standard deviation level. Ages on the concordia are in Ma.

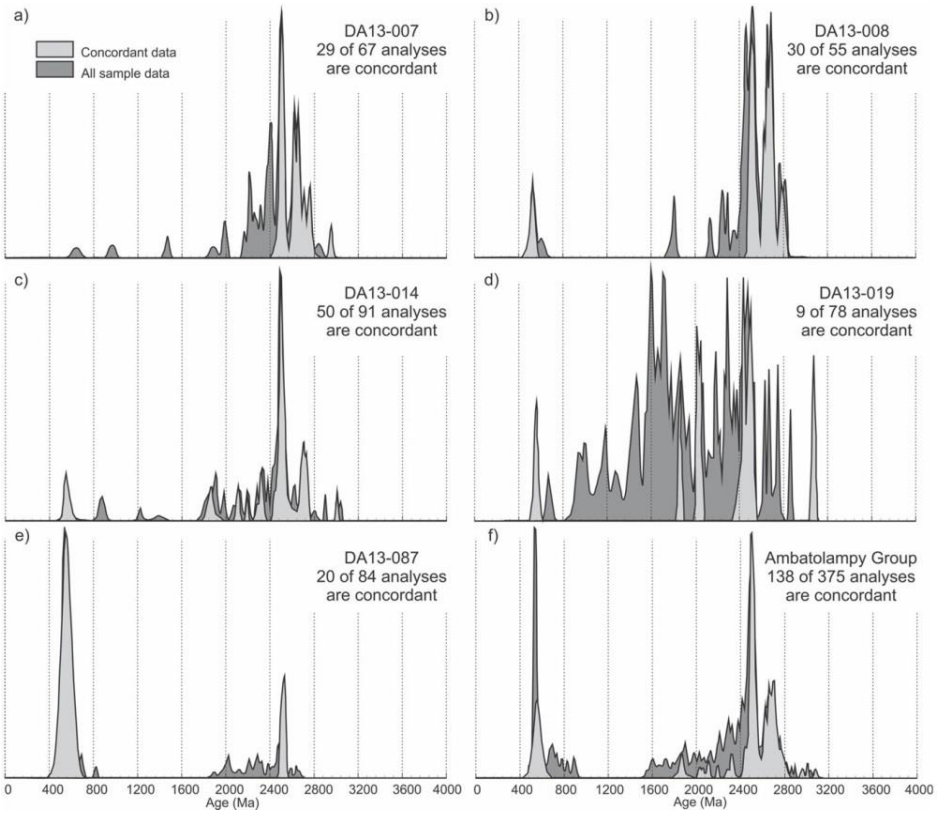

Fig. 2.5 Probability density plots for detrital zircons from the Ambatolampy Group. a) DA13-007; b) DA13-008; c) DA13-014; d) DA13-019; e) DA13-087; and f) all samples. 'Age' is quoted as the $^{207}Pb/^{206}Pb$ age for analyses over 1000 Ma and the $^{206}Pb/^{238}U$ age for younger analyses.

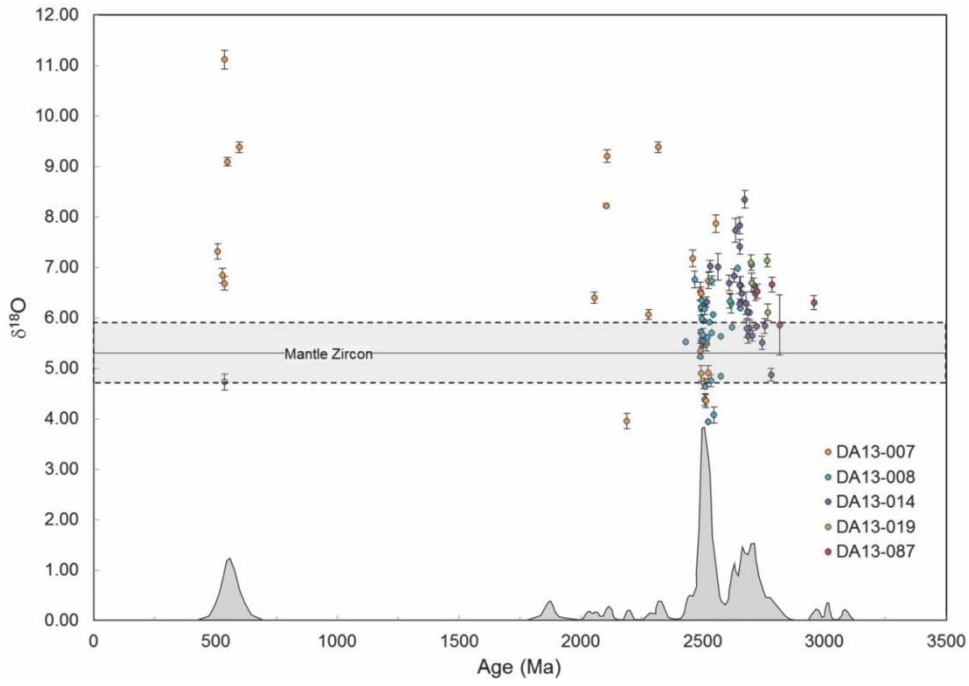

Fig. 2.6 Plot of $^{207}Pb/^{206}Pb$ (zircon) age versus $\delta^{18}O$ (zircon) for five samples from the Ambatolampy Group. Error bars are 1σ. Range of mantle derived $\delta^{18}O$ (zircon) values are 5.3 ± 0.6 ‰ (Valley et al., 2005). A reproduction of the Ambatolampy Group probability density diagram is shown below the $\delta^{18}O$ data.

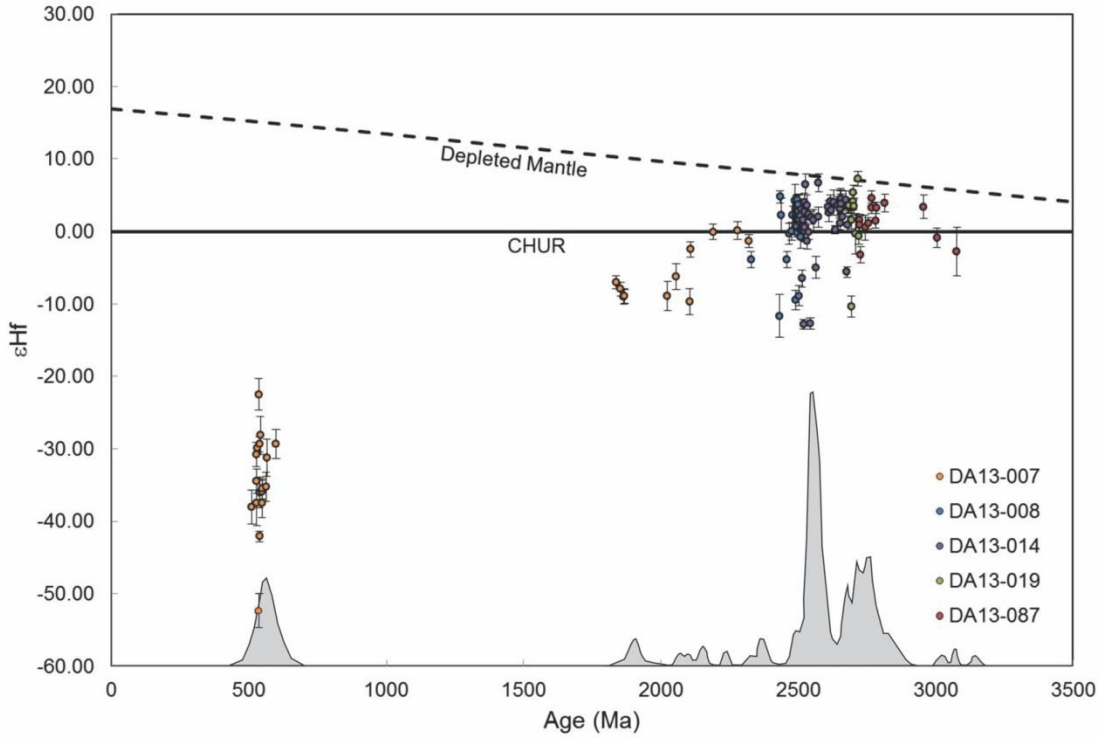

Fig. 2.7 $\varepsilon_{Hf}(t)$ plotted against $^{207}Pb/^{206}Pb$ (zircon) age for five samples of the Ambatolampy Group. Error bars are 1σ. A reproduction of the Ambatolampy Group probability density diagram is shown below the $\varepsilon_{Hf}(t)$ data.

2.6 Discussion

2.6.1 Depositional age constraints of the Ambatolampy Group protoliths: maximum depositional age and age of metamorphic zircon.

The youngest ≤ 10% discordant analyses of samples DA13-007, DA13-008, DA13-014, DA13-019 and DA13-087 yielded $^{207}Pb/^{206}Pb$ ages of 2466 ± 24 Ma, 2495 ± 8 Ma, 1836 ± 25 Ma, 1867 ± 15 Ma, 2489 ± 11 Ma respectively. The youngest concordant detrital zircon age of 1836 ± 25 Ma (1σ uncertainty) is considerably older than data reported from a sample collected near Fandriana during the World Bank funded mapping campaign. The youngest concordant detrital zircon from this sample yielded a $^{207}Pb/^{206}Pb$ age of 1001 ± 44 Ma (BGS-USGS-GLW, 2008). Including these previously reported data, seven samples, reported as belonging to the Ambatolampy Group, have now yielded >1700 Ma detrital zircon ages (this study and BGS-USGS-GLW, 2008). Only one sample has yielded a significant number of near concordant 1000-1100 Ma ages, in addition to these older grains. Whether this one sample truly represents a significant source variation in rocks originally deposited in the same basin, at broadly the same time, or whether this sample represents sediment deposited in a different, considerably younger, depositional system, is unknown. Because of this detrital age difference, here we suggest that the outlier sample is a tectonically interleaved sample of the younger (Neoproterozoic) Manampotsy Group. This emphasizes the uncertainly in assigning formal 'Groups' to these highly deformed and metamorphosed rock units.

Definitive intrusive contacts between the ~850-750 Ma Imorona-Itsindro Suite intrusive rocks and the Ambatolampy Group are absent. Therefore, the age of metamorphism provides the best estimate of the minimum age of deposition. Dark cathodoluminescent rims observed mantling many detrital zircon cores are interpreted as metamorphic overgrowths (Fig. 2.3). When all ≥ 90% concordant metamorphic rim ages are combined, they yield a weighted mean $^{238}U/^{206}Pb$ age of 541.0 ± 4.4 Ma (MSWD = 2.4; n = 24). This age is

interpreted as the age of high-grade metamorphism of these rocks (as evidenced by the presence of sillimanite in many samples) and the minimum constraint on the age of deposition. Previous authors report high-U zircon metamorphic rim ages of 548 ± 17 Ma, 543 ± 1 Ma and 559 ± 4 Ma (BGS-USGS-GLW, 2008) all nearly or within error of our data.

It is often difficult to determine metamorphic from magmatic domains in zircon from CL imaging alone. Consequently, the Th/U ratio in zircon is an additional tool used when differentiating metamorphic from magmatic zircon (e.g. Rubatto, 2002). Low Th/U ratios commonly indicate metamorphic domains while higher ratios indicate zircons of magmatic origin (Rubatto, 2002). Ediacaran to Cambrian analyses have Th/U ratios less than 0.10 in all samples except sample DA13-087 (Appendix A). In this sample, values are slightly higher (up to 0.40) but considerably lower than those from Archaean-Palaeoproterozic detrital cores, supporting metamorphic partial resetting.

2.6.2 $\delta^{18}O$ in the Ambatolampy Group

The zircon $\delta^{18}O$ record is generally preserved even after rocks experience high-grade metamorphism or intense hydrothermal alteration when other minerals are reset (Valley, 2003). Crustal recycling can be differentiated from magmatic $\delta^{18}O$ values in zircons (Valley et al., 2005), therefore making $\delta^{18}O$ a valuable geochemical signature. The majority of Neoarchaean to Palaeoproterozoic zircons from the Ambatolampy Group have $\delta^{18}O$ values varying between 3.94‰ and 9.38‰ (mean = 6.15; Appendix 2.2). This range exceeds the expected ratios for zircon derived from the mantle (5.3‰ ± 0.6‰; Valley et al., 2005). The limited data from Palaeoproterozoic detritus appears to show a further excursion to higher positive $\delta^{18}O$ values than the Neoarchaean grains. Metamorphic zircon overgrowths and reset domains in detrital zircons show a similar range of values to those in the magmatic cores, but also show a weak trend toward more positive values (Fig. 2.6; Appendix 2.2). Therefore, the majority of detrital zircons are interpreted to be derived from Neoarchaean to Palaeoproterozoic magmas that were contaminated by upper crustal rocks with heavier oxygen isotope values than that of the mantle. Heavy metamorphic zircon values suggest partial isotopic equilibration with metamorphic fluids—a phenomena reported elsewhere by Martin et al. (2008). Unfortunately, published detrital zircon $\delta^{18}O$ data is absent from elsewhere in Madagascar or elsewhere in the EAO for that matter. The collection of comparable data from elsewhere in central Gondwana should now be a priority to allow correlation and determine source terranes.

2.6.3 Relationship to metasedimentary units in central Madagascar

The basement of central Madagascar (between the parallels of 16˚S and 22˚S) contains a number of metasedimentary successions receiving variable scientific attention over the previous decades. These sequences are the Itremo Group, the Manampotsy Group, the Sofia Group, the Vondrozo Group, the Ambodiriana Group, the Mananara Group, the Fenoarivo Group, the Maha Group, the Ikalamavony Group, the Molo Group, and sequences in the Anosyen Domain (Iakora Group) and Androyen Domain (Fig. 2.2). Here we summarise what is known about the provenance and age of these sequences and compare them to the Ambatolampy Group.

The Ambatolampy Group detrital zircon population is remarkably similar to the Itremo Group (Figs. 2.8 a-c). In particular, the dual Neoarchaean peaks at ~2700 Ma and ~2500 Ma are distinctive. The youngest reported detrital zircon U-Pb age in the Itremo Group is 1722 ± 80 Ma (Cox et al., 2004), which broadly compares with the maximum depositional age of 1836 ± 25 Ma (1σ uncertainty) for the Ambatolampy Group reported here. The Itremo Group lies directly west of the exposed Ambatolampy Group and is separated from it by the

Betsileo Shear Zone (Collins et al., 2000); an extensional detachment that marks a distinct metamorphic jump with the sillimanite-bearing Ambatolampy quartzites in the footwall and the greenschist-facies Itremo Group lying in the hanging wall.

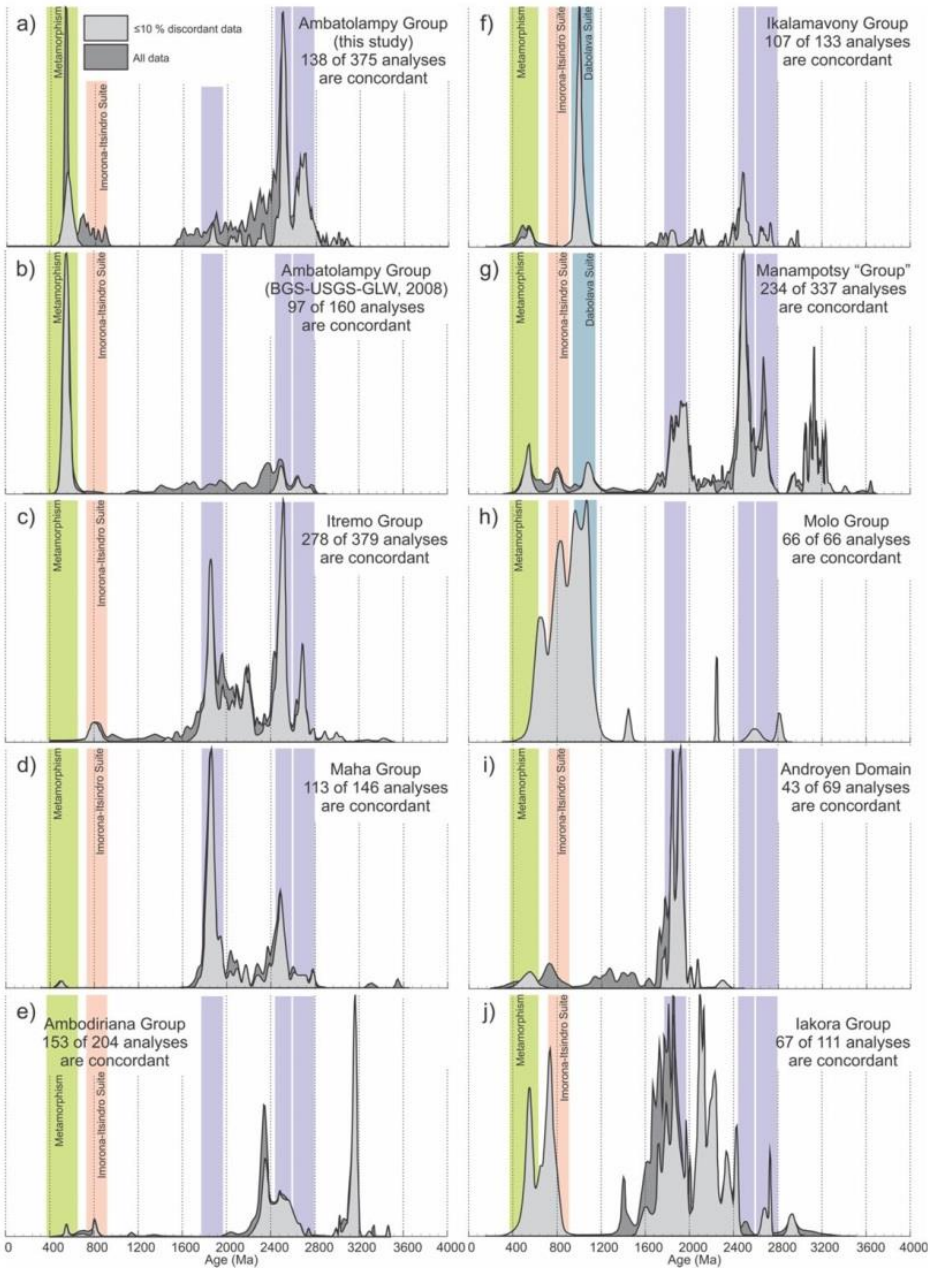

Fig. 2.8 Comparative U-Pb age of detrital zircon probability density diagrams for (meta) sedimentary units in Central Madagascar. Blue bars show the most prominent peaks present in the Ambatolampy Group. Sources for other U-Pb detrital zircon data are: Ambatolampy Group (BGS-USGS-GLW, 2008); Itremo Group (Cox et al., 1998; Cox et al., 2004; Fitzsimons and Hulscher, 2005; De Waele et al., 2011); Maha Group (De Waele et al., 2011); Ambodiriana Group including the Mananara Group, Fenoarivo Group, and Andrarona Group (Collins et al., 2003c; BGS-USGS-GLW, 2008; Schofield et al., 2010); Ikalamavony Group (Tucker et al., 2011b); Manampotsy "Group" including the young sample from BGS-USGS-GLW (2008) included, by them, in the Ambatolampy Group and the Ampasary Group (BGS-USGS-GLW, 2008; Tucker et al., 2011a); Molo Group (Cox et al., 2004); Androyen Domain (Collins et al., 2012); and the Iakora Group in the Anosyen Domain (Boger et al., 2014). No detrital zircon data are available for the Vondrozo and Sofia Groups.

The Manampotsy Group is a poorly defined Neoproterozoic metasedimentary group that crops out generally east of the Ambatolampy Group and contains similar lithologies to the Ambatolampy Group (BGS-USGS-GLW, 2008; Tucker et al., 2011a). Some samples attributed to being part of the Manampotsy Group contain Cryogenian detritus, whereas others are interpreted to be intruded by the ~800 Ma Imorona-Itsindro Suite (BGS-USGS-GLW, 2008). This led to the suggestion that the group may be diachronous (Tucker et al., 2011a). Some samples contain only late Mesoproterozoic-Neoproterozoic detritus (BGS-USGS-GLW, 2008), whilst others contain considerable Palaeoproterozoic and Neoarchaean zircons (Tucker et al., 2011a). We note that (a) no intrusive relationships are directly reported with the Imorona-Itsindro Suite, and, (b) the only common feature of samples of the Manampotsy Group is that the protoliths are interpreted to be Neoproterozoic. As such, we suggest that the term 'Group' be treated with caution as it may well include a number of separate-aged protolith successions. We suggest that the term be restricted to metasedimentary rocks with a Stenian-Neoproterozoic protolith depositional age that lie within the Antananarivo Domain. The outlier sample of 'Ambatolampy Group' reported in the BGS-USGS-GLW (2008) report that contained appreciable Mesoproterozoic detritus fits this tentative 'Manampotsy Group' classification.

Two poorly known and understudied metasedimentary packages lie to the north and south of the Ambatolampy/Manampotsy Groups. These are the Sofia and Vondrozo Groups respectively. Both successions are undated, but Tucker et al. (2014) suggest that they are Neoarchaean based on their map association with the intrusive Neoarchaean Betsiboka Suite.
To the east of the Vondrozo and Manampotsy Groups lies the Masora Block, an Archaean orthogneiss-rich block with greenschist-facies metavolcanics of the Vohilava Group. To the east of the Vondrozo and Manampotsy Groups lies the Masora Block, an Archaean orthogneiss-rich block with greenschist-facies metavolcanics of the Vohilava Group.

Tectonically interlayered with the margins of this terrane are siliciclastic metasedimentary rocks of the Maha Group that preserve detrital zircon U-Pb ages similar to the Ambatolampy Group (this paper) and the Itremo Group (Fig. 2.8d; Cox et al., 1998; 2004; De Waele et al. 2011). These rocks lie along the eastern margin of the proposed Betsimisaraka Suture (Collins and Windley, 2002; Collins, 2006) and have been interpreted to show that the suture does not exist (Tucker et al., 2011a; Tucker et al., 2014). However, as pointed out by De Waele et al. (2011), no stratigraphic contact between the Maha Group and the underlying Masora Block is known. Therefore, it is possible that the Maha Group is allochthonous, and a correlative of the Ambatolampy Group.

The poorly exposed and poorly defined Ambodiriana Group and Mananara Group lie to the east of the Manampotsy Group (Schofield et al., 2010). The best exposed region of these rocks lies along the coast between the towns of Fenoarivo and Soanierano Ivongo where metapelitic rocks yielded Palaeoarchaean, Mesoarchaean and Neoarchaean detrital zircons along with significant number of Cryogenian grains (Collins et al., 2003c). The data were used to demonstrate a ~710 Ma maximum depositional age, and as such, the sequence may be considered an equivalent to the Manampotsy Group as discussed above (Fig. 2.8e). Recently, Schofield et al. (2010) argued that the Fenoarivo and Soanierano Ivongo metasedimentary rocks are not Neoproterozoic, but instead were deposited in the Mesoarchaean or Neoarchaean with a minimum depositional age being constrained by the upper intercept age of an array of mainly discordant zircon cores and rims from a foliation parallel granitoid. This age was quoted despite the discordant array yielding a Neoproterozoic lower intercept allowing a permissive interpretation that the granite crystallised in the Neoproterozoic, with the upper intercept representing partially reset zircon inherited from the surrounding metasedimentary rocks. Tucker et al. (2011a) went further and suggested that they dated a metarhyolite that constrained the age of deposition (and extrusion) at 3320 ± 14 Ma. The

dated rock was a quartzofeldspathic layer in metasedimentary gneiss that yielded a near unimodal zircon age population. Interpreting the protolith of rocks of this type is notoriously difficult and unimodal age populations are certainly not unique to metavolcanic rocks. A crosscutting leucosome contains discordant zircons with Neoarchaean upper intercept ages and Neoproterozoic lower intercept ages (similar to the data presented in Schofield et al., 2010) and a late crosscutting dyke contains Neoarchaean zircons. Both samples from Tucker et al. (2011a) and Schofield et al. (2010) contain near-concordant Tonian/Cryogenian zircon that are dismissed as due to an undefined hydrothermal event (for which no other evidence is provided). Instead, we interpret the reported zircons in these intrusions as being inherited from the metasedimentary rocks they crosscut. Maxwell et al. (2014) recently reported U-Pb monazite and xenotime data that demonstrate that the high-grade metamorphism that affected these outcrops was Cambrian. The unmetamorphosed intrusions must therefore be Cambrian or younger, supporting the interpretation that their entrained zircons are inherited. This questions the separation of the Fenoarivo Group from the Ambodiriana Group (as proposed by Tucker et al. 2011a) and challenges the assignment of the Mananara and Ambodiriana Groups to the Archaean (as presented in Roig et al. 2012).

The Ikalamavony Group lies within the Itremo-Ikalamavony Domain (Tucker et al., 2011a; Tucker et al., 2011b), or the Ikalamavony Domain (Roig et al., 2012; Tucker et al., 2012; Tucker et al., 2014). The recent publication of the 1:1,000,000 map of Madagascar (Roig et al., 2012) and its accompanying report (Tucker et al. 2012; see also Tucker et al. 2014) has created some confusion as to the definition of the Ikalamavony Group by assigning all pre-Cryogenian metasedimentary rocks in the Ikalamavony Domain to the Ikalamavony Group. This has resulted in the unsatisfactory situation where we have a 'lower' Palaeoproterozoic/ early Mesoproterozoic Ikalamavony Group, directly correlative with the Itremo Group, and an 'upper' late Mesoproterozoic-early Neoproterozoic Ikalamavony Group (Roig et al., 2012). We see no reason for splitting the 'lower' Ikalamavony Group from the Itremo Group due to their lithological and geochronologic similarities (Cox et al., 1998; Cox et al., 2004; Tucker et al., 2011b). In contrast, two metasedimentary rocks from the 'upper' Ikalamavony Group contain detrital zircons that range from ~1070-1010 Ma (Tucker et al., 2011b). These overlap with crystallisation ages from a metarhyolite and intrusive rocks of the Dabolava suite (Fig. 2.8f; Tucker et al., 2011b).

The Molo Group (Cox et al., 2004) is an Ediacaran metasedimentary succession that lies within the Ikalamavony Domain. It postdates the voluminous Cryogenian Imorona-Itsindro Suite and contains considerable Cryogenian-Ediacaran detrital zircon (Fig. 2.8h).

The Androyen-Anosyen Domain lies west of the Ikalamavony Domain and is dominated by supracrustal gneisses that have been interpreted to have both sedimentary (Iakora Group) and volcanic (Horombe Group) protoliths (Boger et al., 2014). The Iakora Group siliciclastic rocks detritus are dominated by Palaeoproterozoic detrital zircons (Figs. 2.8i, j; Boger et al., 2014; Collins et al., 2012). Boger et al. (2014) reports Cryogenian rocks in the Anosyen Domain and posited whether the Anosyen Domain is actually Neoproterozoic.

In summary, central Madagascar contains a number of spatially distinct sedimentary successions, a number of which display notable similarities in their detrital zircon provenance profiles. In particular, the Ambatolampy Group, the Itremo Group (including the lower Ikalamavony Group; Roig et al. 2012), the Iakora Group, and the Maha Group are all dominated by Palaeoproterozoic detritus and have late Palaeoproterozoic-early Mesoproterozoic maximum depositional ages. These appear to represent an originally contiguous Mesoproterozoic sedimentary basin across central Madagascar. In contrast to these successions, the latest Mesoproterozoic to Neoproterozoic formations are much more heterogeneous. The (upper) Ikalamavony Group exclusively contains late Mesoproterozoic

detritus and may have been deposited at that time, or in the early Tonian. The imprecise definition of the Manampotsy Group means that some components of it could be coeval with the Ediacaran Molo Group—some samples show distinct provenance similarities. In contrast, the Ambodiriana Group preserves a distinctive detrital profile with zircons limited to the Archaean and Cryogenian.

2.6.4 Provenance and potential source regions for the Ambatolampy Group

The Ambatolampy Group has prominent detrital U-Pb age populations at ~2700 Ma and ~2500 Ma and fewer data between 2350-1800 Ma and between 3100-2900 Ma (Fig. 2.5f). Older populations (>2500 Ma) could be sourced from magmatic rocks located in Madagascar. Approximately 3200-3000 Ma igneous rocks are present in the Madagascan Antongil and Masora Domains (e.g. Schofield et al., 2010; Tucker et al., 1999; Tucker et al., 2014) and are a potential source for Mesoarchaean to Neoarchaean detritus in the Ambatolampy Group. 2700-2450 Ma igneous rocks are widespread in the Antananarivo Domain (Tucker et al., 1999b; Kröner et al., 2000; Kabete et al., 2006; Tucker et al., 2007; BGS-USGS-GLW, 2008) and could provide a local source for Neoarchaean to earliest Palaeoproterozoic detrital zircons. However, the sources of the ~2350 - 1800 Ma zircons are not apparent in Madagascar—a conundrum that led Cox et al. (1998; 2004) and Fitzsimons and Hulscher (2005) to suggest that similar-aged detritus in the Itremo Group was sourced from East Africa. This also led Collins et al. (2003b) to suggest the existence of a 'provenance front' within Madagascar separating 'African-derived' Neoproterozoic detritus in the centre and west, from 'Dharwar-derived' detritus in the east of the island. Tucker et al. (2011a; 2011b) opined that, instead of an African source, these enigmatic grains may correlate with the fill of the Proterozoic Purana basins in central and east India (e.g. the Cuddapah, Chhattisgarh and Indravati Basins; see Saha and Patranabis-Deb, 2014 for recent review). In a stratigraphically controlled analysis of 21 detrital zircon samples from the Cuddapah Basin, Collins et al. (in press) demonstrated that the fill of the lower and west part of this 46,000 km^2 basin is devoid of Palaeoproterozoic detritus, but is instead sourced from the Archaean Dharwar Craton to the west. However, they demonstrated that the tectonically-juxtaposed Nallamalai Group, in the east of the basin, does contain considerable Palaeoproterozoic detritus of a similar age range to that described here in the Ambatolampy Group and also in the Itremo Group. They interpreted this to correlate with the ~1620 Ma Somanpalli Group of the Pranhita-Godavari Basin (Amarasinghe et al., 2015) and form a foreland basin to the ~1680-1590 Ma Krishna Orogen of the southern Eastern Ghats (Henderson et al., 2014; Sarkar et al., in press). No outliers of the Nallamalai Group are known from the central or western Dharwar Craton, or from the Proterozoic Bhima and Kaladgi basins that lie nearer the Gondwana position of Madagascar. However, based on U-Pb ages alone, it cannot be ruled out that corollaries of this formation were deposited over the breadth of the Dharwar Craton and that the voluminous Palaeoproterozoic detritus in Madagascar are sourced from here.

Determining ancient tectonic geography using U-Pb age detrital provenance alone can lead to considerable problems. For example, the present-day Pacific Ocean is surrounded by contemporaneous magmatism: trying to distinguish tectonic affiliation of suspect terranes in a hypothetical post-Pacific orogen will be impossible using the age of presently-forming zircon. Ancient examples of erroneous interpretations based on U-Pb detritus include the Palaeoproterozoic of South Australia, where Howard et al. (2011) used hafnium isotopes to complement U-Pb ages of detritus in metasedimentary rocks. Here we used both hafnium and oxygen isotopes from detrital zircons to produce three complementary data series to better interrogate the conundrum of the tectonic affiliation of the Malagasy suspect terranes.

Neoarchaean to Palaeoproterozoic zircons from all analysed samples of the Ambatolampy Group display a wide range of εHf values between -12.86 and 7.27 with a

mean εHf value of 0.34. These values are diverse and suggest that the source region contained magmas derived from a mixture of mantle melts and crustal recycling. Metamorphic overgrowths and reset domains in detrital zircons have significantly lower values varying between -22.49 and -52.47 (mean = -34.47). These values support an interpretation that these rims are developed by metamorphic near solid-state recrystallization of pre-existing zircon (Hoskin and Black, 2000) rather than being crystallised from a melt.

Data from the Neoarchaean of the Dharwar Craton (Sarma et al., 2012; Glorie et al., 2014; Mohan et al., 2014) and from ancient sedimentary sequences interpreted to be sourced from the Dharwar Craton (Collins et al., in press) show a similar range in $\varepsilon_{Hf}(t)$ values. This appears to suggest a source fingerprint. However, at present, there are very limited Hf data to compare with in East Africa. For example, no data are available from the Muva Supergroup in East Africa, which was suggested as a corollary to the Itremo Group (Cox et al., 2004). In fact, data from modern rivers draining the Tanzania Craton and surrounding orogens, also yield similar $\varepsilon_{Hf}(t)$ values for Neoarchaean zircons (Brick, 2011), suggesting that hafnium isotopes for the Neoarchaean detritus may not be distinctive from both possible source areas. Palaeoproterozoic granitoids are not found on the Dharwar Craton (see Peucat et al., 2013 for a recent review). The Palaeoproterozoic detritus in the east Cuddapah Basin's Nallamalai Group, though, does overlap in εHf values with those from the Ambatolampy Group (Collins et al., 2015). However, due to the lack of intervening outliers, the local source of the Nallamalai Group, and the observed decrease in Palaeoproterozoic detritus away from the Krishna Orogen in the Cuddapah Basin (Collins et al. in press), we suggest that it is unlikely that the Nallamallai Group is a corollary of the Ambatolampy Group. Again, the limited data available from eastern Africa suggests that Africa is still the likely source for the central Malagasy Palaeoproterozoic detritus. However, this hypothesis cannot be fully tested until comparable Hf and O isotope data from Africa become available.

Detrital zircon U-Pb and Hf isotopic results have also been recently published from the Madurai Block in southern India a terrane often correlated with central Madagascar as a part of Azania (Collins and Windley, 2002; Collins et al., 2007; Plavsa et al., 2012; Collins et al., 2014). Plavsa et al. (2012; 2014) separated the Madurai Block into a northern and southern domain, the southern domain containing juvenile Neoproterozoic rocks (see also Tomson et al., 2013) and many Mesoproterozoic and Neoproterozoic detrital zircons. Crystallisation-age corrected $\varepsilon_{Hf}(t)$ values for the Neoarchaean detritus from the Northern Madurai Block (and for the Salem Block directly to its north) yield positive values, similar to many of the similar-aged Ambatolampy Group results (Fig. 2.7). Palaeoproterozoic detritus yields slightly more negative values that overlap with the Ambatolampy Group detritus. These similarities support the correlation between the Madurai Block and central Madagascar.

2.7 Summary and conclusions

New detrital zircon U-Pb data with complementary $\delta^{18}O$ and $\varepsilon_{Hf}(t)$ isotopic data from five samples of the Ambatolampy Group demonstrate the following conclusions.

1) The youngest concordant detrital zircon age of 1836 ± 25 Ma is interpreted to represent the maximum depositional age for the Ambatolampy Group. This age is considerably older than data collected during the BGS-USGS mapping campaign ($^{207}Pb/^{206}Pb$ age of 1001 ± 44 Ma) and the distribution of detrital zircon ages is comparable to the Paleoproterozoic Itremo Group. The minimum age of deposition is constrained by the age of metamorphic overgrowths at 541.0 ± 4.4 Ma and the intrusive age of the Ambalavao Suite.

2) Neoarchaean to Palaeoproterozoic zircons from the Ambatolampy Group have $\delta^{18}O$ values varying between 3.94‰ and 9.38‰ (mean = 6.15). These values exceed the expected ratios for zircon derived from the mantle (5.3‰ ± 0.6‰; Valley et al., 2005). Metamorphic zircon overgrowths and reset domains in detrital zircons show a similar range of values to those in the magmatic cores, but show a trend toward more positive values. These values coupled with low Th/U ratios support our interpretation that rims are developed by metamorphic recrystallization of pre-existing zircon. Therefore, detrital zircons are interpreted to be derived from Neoarchaean to Palaeoproterozoic magmas that were contaminated by upper crustal rocks with heavier oxygen isotope values than that of the mantle. This study represents the first documentation of $\delta^{18}O$ concentrations in detrital zircon in the region and provides a base for comparison during future studies.

3) Neoarchaean to Palaeoproterozoic zircons from the Ambatolampy Group $\varepsilon_{Hf}(t)$ values vary between -12.86 and +7.27 (mean = +0.34). These diverse values suggest the source region contained magmas derived from a mixture of mantle melts and pre-existing crust. Metamorphic overgrowths and reset domains in detrital zircons have significantly lower values between -22.49 and -52.47 (mean = -34.47). These values support our interpretation that rims are developed by metamorphic recrystallization of pre-existing zircon rather than crystallisation of new zircon. Data from the Neoarchaean of the Dharwar Craton in India (Glorie et al., 2014; Mohan et al., 2014; Sarma et al., 2012) and from ancient sedimentary sequences interpreted to be sourced from the Dharwar Craton (Collins et al., in press) show a similar range in $\varepsilon_{Hf}(t)$ values. However, comparable data from Africa are not yet available, so a possible source comparison cannot be undertaken.

4) Central Madagascar contains a number of spatially distinct sedimentary successions. However, many of these units display remarkable similarities in their detrital zircon provenance profiles. In particular, the Ambatolampy, the Itremo (including the lower Ikalamavony Group), the Iakora, and the Maha groups are all dominated by Palaeoproterozoic detritus and have late Palaeoproterozoic to early Mesoproterozoic maximum depositional ages. Taken together, they appear to represent an originally contiguous Mesoproterozoic basin in Madagascar.

5) This study is the first to present three independent zircon-hosted isotopic datasets from central Gondwana. These data do not prove or disprove the existence of Azania (Collins and Pisarevsky, 2005). Likewise, these results do not confirm or reject the Greater Dharwar hypothesis (Tucker et al., 2011b; Tucker et al., 2014). Instead these data challenge researchers to collect comparable data from India and Africa to test these palaeogeographic models.

2.8 Acknowledgements

Brian Windley has been instrumental in developing new concepts to the understanding of the Precambrian. In particular, his application of plate tectonic concepts to Precambrian orogens, such as the East African Orogen, has transformed how we view the evolution of ancient plate tectonics. We acknowledge Brian's contribution to supporting the second author (ASC) in his early post-doctoral work in Madagascar and are indebted to his generous sharing of ideas, thoughts and to his friendship. The Razafinjoelina family, in particular Auguste and Berthieu are thanked for providing transportation, assistance in the field, and hospitality during fieldwork in Madagascar. Ms. Aoife McFadden (Adelaide Microscopy) is also thanked for assistance obtaining CL images. Dr Diana Plavsa is acknowledged for providing a compilation of all the available detrital zircon data across the East African Orogen. This paper forms TRAX Record 323 and is an output of ARC Future Fellowship grant FT120100340.

Chapter 3

The Imorona-Itsindro Suite zircon isotopic characteristics

Published as:

Archibald, Donnelly B., Collins, Alan S., Foden, John D., Payne, Justin L., Holden, Peter, Razakamanana, Théodore, De Waele, Bert, Thomas, Robert J. and Pitfield, Peter, E. J. 2016. Genesis of the Tonian Imorona-Itsindro Magmatic Suite in central Madagascar: Insights from U-Pb, oxygen and hafnium isotopes in zircon. Precambrian Research, 281, 312-327.

Statement of Authorship

Title of Paper	Genesis of the Tonian Imorona-Itsindro Suite in central Madagascar: Insights from U-Pb, oxygen and hafnium isotopes in zircon
Publication Status	X Published __ Accepted for Publication __ Submitted for Publication __ Publication Style
Publication Details	Archibald, D.B., Collins, A.S., Foden, J.D., Payne, J.L., Holden, P., Razakamanana, T., De Waele, B., Pitfield, P.E.J., Thomas, R.J., 2016. Genesis of the Tonian Imorona-Itsindro Magmatic Suite in central Madagascar: Insights from U-Pb, oxygen and hafnium isotopes in zircon. Precambrian Research. 281, 312-327.

Author Contributions

By signing the Statement of Authorship, each author certifies that their stated contribution to the publication is accurate and that permission is granted for the publication to be included in the candidate's thesis.

Name of Principal Author (Candidate) Contribution to the paper Conceptualisation of the work It's realisation Documentation and write-up Development of ideas and conclusions	Donnelly B. Archibald Prepared samples, carried out analyses and interpretation of the data, organised manuscript and data, wrote manuscript, acted as the corresponding author		
Signature		Date	9/7/2016

Name of Co-Author Contribution to the paper	Prof Alan S. Collins (University of Adelaide) Supervised work, assisted with data interpretation and manuscript revision		
Signature		Date	9/7/2016

Name of Co-Author Contribution to the paper	Prof John D. Foden (University of Adelaide) Assisted with manuscript revision		
Signature		Date	11/7/2017

Name of Co-Author Contribution to the paper	Dr. Justin L. Payne (University of South Australia) Assisted with hafnium isotope data collection, manuscript revision		
Signature		Date	7/4/2016

Name of Co-Author Contribution to the paper	Dr. Peter Holden (The Australian National University) Assisted with oxygen isotope data collection and interpretation		
Signature		Date	28/04/2016

Name of Co-Author Contribution to the paper	Dr. Theodore Razakamanana (University of Toliara, Madagascar) Assistance in the field, sample logistics, manuscript editing		
Signature		Date	8/4/2016

Name of Co-Author Contribution to the paper	Dr. Bert De Waele (SRK Consulting) Collected U-Pb SHRIMP data, provided zircon mounts for O and Hf isotope analysis and manuscript editing		
Signature		Date	13/04/2016

Name of Co-Author Contribution to the paper	Dr. Robert J. Thomas (Council for Geoscience) Provided mounts for O and Hf isotope analysis and manuscript editing		
Signature		Date	6/4/2016

Name of Co-Author Contribution to the paper	Dr. Peter E.J. Pitfield (IGS Consultants) PGRM Project leader in central Madagascar, manuscript editing, and provided zircon mounts for O and Hf isotope analysis		
Signature		Date	07/04/2016

Abstract

Madagascar occupies an important location within the East African Orogen (EAO). The EAO comprises an assemblage of Neoproterozoic microcontinents and arc terranes lodged between older cratonic blocks during the final assembly of the supercontinent Gondwana. The Imorona-Itsindro Suite of central Madagascar represents voluminous Tonian-aged (850-750 Ma) magmatism with controversial petrogenesis. Early work proposed arc magma generation coinciding with oceanic plate subduction during closure of the Mozambique Ocean along the 'Betsimisaraka Suture' in eastern Madagascar. Recently, others have questioned the existence of such a suture in Madagascar and rather suggest extension related emplacement into the middle and upper crust through a system of pre-existing structures. New U-Pb (zircon) geochronological data coupled with in-situ oxygen and hafnium isotopic analyses demonstrate that the Imorona-Itsindro Suite had several source components. Most of the Tonian-aged magmatic rocks were derived by mixing between ancient crust and mantle derived melts. $\delta^{18}O$ values show variation that indicates significant involvement of crustal material and hydrothermal fluids. Predominantly low negative $\varepsilon_{Hf}(t)$ values are also variable and indicate significant crustal involvement in the genesis of the Tonian magmas. A compilation of all available geochronological data shows magmatism was essentially continuous for ~100 Myr but with periods of increased activity at ~800 Ma, ~791 Ma and ~784 Ma. Temporal analysis shows magmatic cycles of enrichment and depletion on the scale of 15-40 Ma. Spatial variations in isotope compositions reflect the heterogeneity of probable crustal source rocks present in the Ikalamavony, Itremo, Antananarivo and Masora Domains. A tectonic model is proposed for the Imorona-Itsindro Suite as a long-lived Andean-like arc on the margin of the Mozambique Ocean. The longevity and temporal isotopic trends are interpreted as reflecting cycles of arc advance and retreat.

3.1 Introduction

The East African Orogen (EAO) is one of the largest of orogens formed during the Ediacaran/Cambrian amalgamation of Gondwana (Stern, 1994; Stern, 2002; Meert, 2003; Collins and Pisarevsky, 2005; Johnson et al., 2011; Fritz et al., 2013). This relationship is expressed in the Mozambique Belt (see Fritz et al. 2014 for a recent summary), where the EAO separates Neoproterozoic India from the African Congo-Tanzania-Bangweulu Block (Fig. 3.1a). To the north, in the Arabian-Nubian Shield, the EAO consists of fragments of pre-Neoproterozoic continental crust in Saudi Arabia, Yemen and the Horn of Africa (e.g. the Afif Terrane), interleaved with Neoproterozoic oceanic-arc like terranes (Johnson et al., 2011; Robinson et al., 2014; Blades et al., 2015) with final amalgamation in the Ediacaran (Doebrich et al., 2007; Cox et al., 2012). The pre-Gondwana ocean that separated these landmasses is referred to the Mozambique Ocean. Although the Arabian-Nubian Shield preserves many oceanic suture zones recording accretion of the shield but as the orogen is traced south, the identification of potential sutures becomes less clear. This led Shackleton (1996) to review the various suggested traces of the Mozambique Ocean suture. He concluded that, unlike many Phanerozoic orogens that involve accretion of multiple terranes, the Mozambique Ocean closed as a single suture; and this lay within East Africa.

Collins and Windley (2002) proposed that this single-suture model was an over-simplification, and suggested a wide band of pelitic gneiss, with Neoproterozoic depositional ages (Collins et al., 2003c) and associated pod-like peridotite bodies, gabbro and emerald mineralisation represented another Mozambique Ocean suture zone (termed the 'Betsimisaraka Suture'), which separated central Madagascar from India. Several authors (Collins and Windley, 2002; Cox et al., 2004; Fitzsimons and Hulscher, 2005; Collins, 2006) have suggested that central Madagascar formed a Neoproterozoic microcontinent, which, along with parts of southern India (the Madurai Block, Plavsa et al., 2014; Collins et al.,

2014), East Africa, Yemen and Saudi Arabia (Collins and Windley, 2002), was isolated from both Neoproterozoic India and the Congo-Tanzania-Bangweulu Block in East Africa by oceanic crust. Collins and Pisarevsky (2005) called this continent 'Azania' (Fig. 3.1a). The accretion of Azania to the Dharwar Craton along the Betsimisaraka Suture was accompanied by voluminous magmatism in central Madagascar (Collins, 2006) – interpreted to result from Andean-style subduction. Recently, the existence of Azania has been challenged, and an alternative 'Greater Dharwar' continent has been proposed (Tucker et al., 2011b; Boger et al., 2014; Tucker et al., 2014) that incorporates all of eastern and most of central Madagascar on the margin of Neoproterozoic India – reverting to a single suture hypothesis for the Mozambique Ocean. According to Tucker et al. (2014), during Tonian times (recently redefined as ca.1000-720 Ma; Cohen et al. 2015), to the west and north of central Madagascar lay an open ocean – the Mozambique Ocean – the subduction of which resulted in widespread magmatism in central Madagascar (Handke et al., 1999) implying a major magmatic event ~300-200 Myr prior to the final amalgamation of Gondwana.

Although the age of the Imorona-Itsindro Suite is well documented, (see Tucker et al., 2014 for a recent summary), the interpretation of the geochemistry of the suite as a whole is controversial. Traditionally, the suite was likened to a continental arc (Handke et al., 1997; Handke et al., 1999; Tucker et al., 1999b; Kröner et al., 2000). However, recent work proposed the suite may have formed during crustal extension, possibly involving a putative mantle plume (Tucker et al., 2014; Yang et al., 2014; Zhou et al., 2015b). This new model was based on: (1) the general bi-modal felsic-mafic nature of the suite (McMillan et al., 2003), (2) the nested geometry of the complexes and apparent emplacement of the suite into a series of pre-existing fractures (Moine, 1974), (3) the presence of similar lithologies with a common Proterozoic history on both sides of the Betsimisaraka Suture Zone (Tucker et al., 2011a) and (4) geochemical characteristics of some Tonian rocks (Yang et al., 2014; Zhou, 2015; Zhou et al., 2015a). To try and clarify this conundrum, the current investigation presents an age, provenance, source study of the entire Imorona-Itsindro Suite using isotopic information preserved in zircon. Zircon is a powerful tool in this context because of its durability and chemical stability over a wide range of lithospheric pressures, temperatures, and fluid/melt compositions (e.g. Cherniak et al., 1997). Analysis of individual zircon grains using micro-beam techniques is imperative because Tonian zircon grains in Madagascar frequently show evidence of Ediacaran to Cambrian metamorphism resulting in lead-loss or new zircon overgrowths. New U-Pb (zircon), oxygen and hafnium isotopic data allow us to better determine the components involved in sourcing the Imorona-Itsindro Suite. We also discuss the presence of spatial and temporal isotopic variations in the suite across the various tectonic domains in central Madagascar and determine the tectonic implications of these variations.

3.2 Regional geology of Madagascar

Madagascar contains several Precambrian to earliest Palaeozoic basement units. The oldest of these are the Palaeoarchaean to Palaeoproterozoic Antongil and Masora domains (Table 3.1), which crop out along Madagascar's east coast (Fig. 3.1b). These units are considered to be parts of the Dharwar Craton of southern India left behind following the break-up of Gondwana (e.g. Schofield et al., 2010; Tucker et al., 2014). The origin of the Masora Domain is enigmatic but it must have accreted to the Antananarivo Domain before ~850 Ma since the Imorona-Itsindro Suite intrudes both domains (BGS-USGS-GLW, 2008). Therefore, if the Betsimisaraka Suture exists, the Neoproterozoic suture must lie to the east of the Masora Domain.

The largest component in Madagascar, the Antananarivo Block (or Domain), underlies the central highlands and comprises granulite- to upper-amphibolite facies

orthogneiss and paragneiss (Kröner et al., 2000; Collins et al., 2003a; Collins, 2006; Roig et al., 2012). The orthogneiss consist of ~2550–2500 Ma granitoids (the Betsiboka Suite) that are tectonically interlayered with paragneiss of the Sofia and Vondrozo groups (Fig. 3.2; Table 3.1). The entire Antananarivo Domain was thermally and structurally reworked between ~850 and 500 Ma with pre-existing rocks being metamorphosed to granulite-facies coincident with the development of gneissic fabrics (Collins et al., 2003c; Moine et al., 2014).

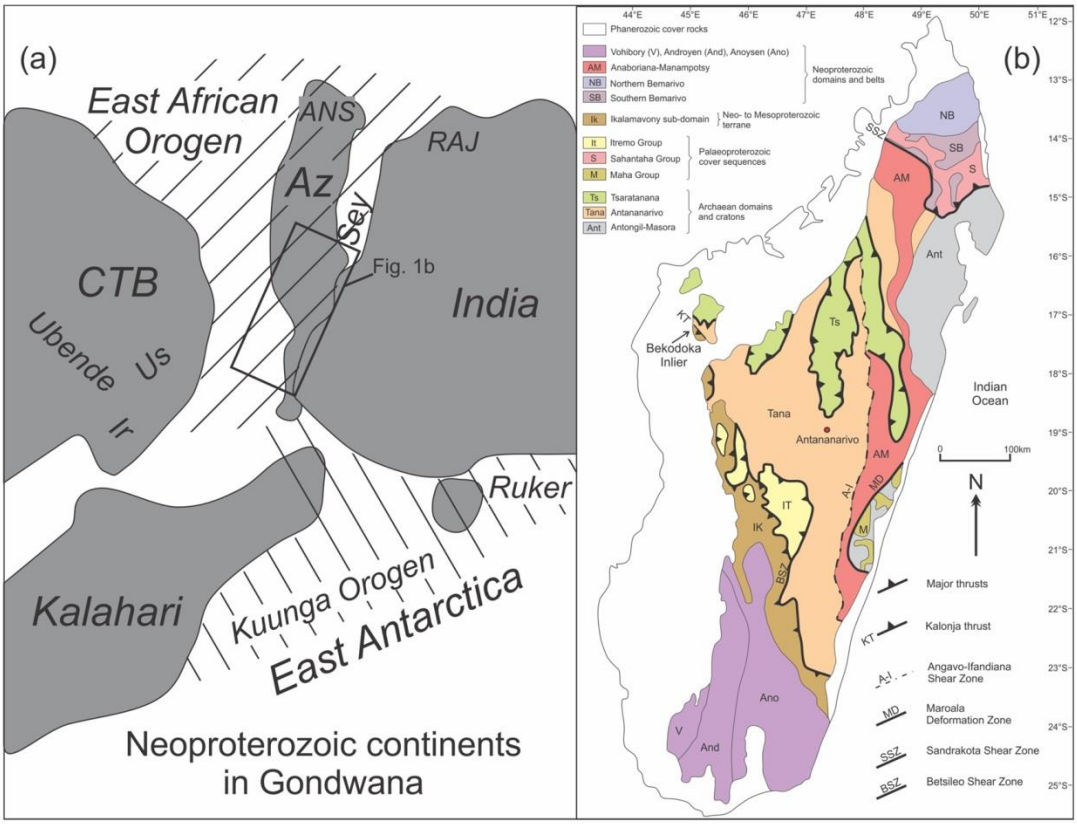

Fig. 3.1 a) Palaeogeographic reconstruction of the Neoproterozoic continents in Gondwana showing the location of the present study (after Collins and Pisarevsky, 2005). Abbreviations: Az = Azania; ANS = Arabian Nubian Shield; Sey = Seychelles; Ir = Irumide Belt; Ruker = Ruker Terrane, East Antarctica; CTB = Congo-Tanzania-Bangweulu Block; Ubende = Ubende Belt; and Us = Usagaran orogen. b) Simplified basement geology of Madagascar (after Collins, 2006 and De Waele et al., 2011).

Overlying the Antananarivo Domain are several Proterozoic metasedimentary rock units including the Itremo and Ambatolampy Groups. The Itremo Group consists of quartzite, conglomerate and dolomitic marble that increase in metamorphic grade from east to west with its lowest-grade rocks (lower greenschist facies) preserved in the hanging-wall of the Betsileo shear zone (Moine, 1974; Collins et al., 2000). Detrital zircon populations at ca. 2500 Ma and 1800 Ma characterise the metasedimentary package (Cox et al., 2004; Fitzsimons and Hulscher, 2005; De Waele et al., 2011). The protolith sediments were deposited after ~1700 Ma (Fernandez et al., 2003; Cox et al., 2004) and have been interpreted to be derived from East Africa (Cox et al., 1998; Cox et al., 2004; Fitzsimons and Hulscher, 2005). More recently, the Itremo Group has been correlated with the Maha Group that structurally overlies the Masora Domain in south-east Madagascar, the Sambirano-Sahantaha Group from the southern Bemarivo Domain (De Waele et al., 2011) and the Ambatolampy Group (Archibald et al., 2015). The understudied Ikalamavony and Molo Groups lie west of the Itremo Domain (Roig et al., 2012) and their depositional age is thought to be Neoproterozoic (Table 3.1; Cox et al., 2004; Tucker et al., 2007).

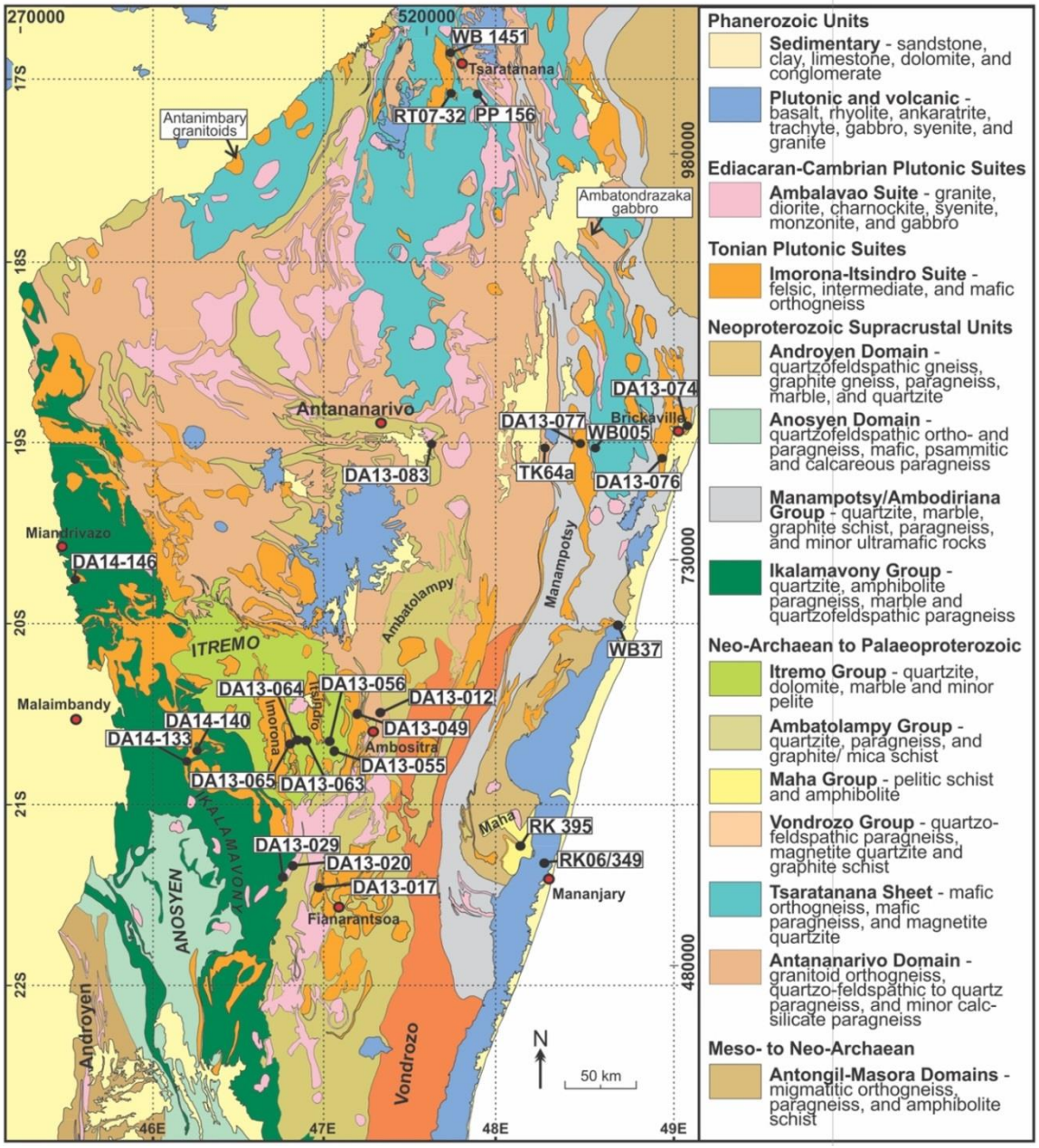

Fig. 3.2 Geological map of central Madagascar (modified after Roig et al., 2012) showing the extent of Tonian-aged magmatism sampled in this study. Samples with a "DA" prefix were collected as part of this study. Other samples are from BGS-USGS-GLW (2008). Also shown are the locations of the Ambatondrazaka Gabbro (Zhou et al., 2015b) and the Antanimbary Granitoid (Yang et al., 2014). Note that Ediacaran to Cambrian plutonic rocks are undivided and given the name Ambalavao Suite (Roig et al., 2012).

Successive emplacement of the Dabolava, Imorona-Itsindro, Kiangara, Ambalavao and Maevarano magmatic suites occurred during the latest Mesoproterozoic to Cambrian (Fig. 3.2; Table 3.1). Gabbroic and granitoid rocks of the Stenian-Tonian (~1080- 980 Ma) Dabolava Suite with the similarly aged volcanic and metasedimentary rocks of the Ikalamavony Group were interpreted to represent a magmatic arc and marginal volcano-sedimentary sequence within a continental back-arc tectonic setting outboard of the Antananarivo Domain (CGS, 2009a). The Tonian (~850-750 Ma) Imorona-Itsindro Suite consists primarily of granitoids and gabbro that intruded into most central Madagascar Precambrian units. As noted above, two opposing views of the tectonic setting of the suite have been proposed on the basis of whole-rock geochemistry: in a supra-subduction zone

setting (Handke et al., 1999; Kröner et al., 2000; Key et al., 2011; Boger et al., 2015) or above a mantle plume (Tucker et al., 2011b; Yang et al., 2014; Zhou, 2015; Zhou et al., 2015b).Younger intrusive rock suites are represented by the ~630 Ma Kiangara Suite A-type granitoids (Guyonnaud, 1951; Nédélec et al., 1994), the post-tectonic granitoids of the ~575-540 Ma Ambalavao Suite (Meert et al., 2001a; BGS-USGS-GLW, 2008; Archibald et al., submitted-b) and the ~537-522 Ma Maevarano Suite (Goodenough et al., 2010; Zhou et al., 2015a; Archibald et al., submitted-b). The Kiangara Suite has previously been interpreted to have formed at ca. 630 Ma using ID-TIMS U-Pb geochronology (Paquette and Nédélec, 1998). However, Nédélec et al. (2015) recently re-evaluated this age using micro-beam techniques and obtained a Tonian age (~791 Ma) as opposed to the published Ediacaran ages. The authors concluded that the Ediacaran ID-TIMS ages were a result of analysing multiple zircon domains within heterogeneous grains and therefore may represent a later phase of the Imorona-Itsindro Suite and late-Cryogenian to early Ediacaran magmatism may not be present in central Madagascar at all.

Table 3.1 Summary of the major tectonic elements of central and northern Madagascar with the approximate age range for each sedimentary unit or magmatic suite. Unit descriptions are from Roig et al., (2012) and Tucker et al., (2012). Age ranges are from the compilation of Tucker et al., (2014), BGS-USGS-GLW (2008), Key et al. (2011) and unpublished data for the Dabolava Suite (D.B. Archibald unpublished; Chapter 6).

Basement Domain	Group or Suite Name	Description	Crystallisation Age (Ma)	Depositional Age (Ma)
Antongil-Masora	Masoala Suite	granodiorite orthogneiss	~2600-2450	
	Mananara Group	quartzofeldspathic orthogneiss		~2600-2400
	Vohilava/Nosivolo Group	amphibolite, schist		~2800-2500
	Fenoarivo Group	paragneiss		~3200-2500
	Nosy Boraha Suite	migmatitic orthogneiss	~3300-3100	
Antananarivo	Manampotsy Group	quartzite, paragneiss, schist, ultramafic rocks		>840
	Molo Group	quartzite, pelitic gneiss		~850-650
	Ambatolampy Group	quartzite, graphitic schist		~1750-580
	Betsiboka Suite	mainly felsic orthogneiss	~2520-2480	
	Sofia Group	quartzite, paragneiss, schist		~2800-2700
	Vondrozo Group	graphitic schist, paragneiss		~3000-2800
Tsaratanana	Tsaratanana Complex	quartzite, mafic para- and orthogneiss	~2500	
Itremo	Itremo Group	marble, quartzite, psammitic schist		~1780-850
Ikalamavony	Dabolava Suite	intermediate, felsic, mafic orthogneiss	~1080-980	
	Ikalamavony Group	amphibolite gneiss, paragneiss, quartzite		~1800-1080
Bemarivo	Manambato Suite	granite	~720-700	
	Antsirabe Nord Suite	intermediate-felsic orthogneiss	~760-740	
	Daraina and Milanoa Groups	felsic volcanic, quartzite, amphibolite		~800-650
	Sambirano-Sahantaha Group	quartzite, paragneiss, schist		~1750-760

The Bemarivo Domain is a distinct terrane in northern Madagascar that consists of Mesoproterozoic metasedimentary rocks (Sambirano-Sahantaha Group) and juvenile Tonian-Cryogenian calc-alkaline metaigneous rocks (Thomas et al., 2009). Based on the depleted isotopic character of its metaigneous rocks (Tucker et al., 1999b), Archaean and Palaeoproterozoic rocks are thought to be absent in this domain. Thomas et al. (2009) proposed that the northern and southern sub-domains formed as coalesced magmatic arcs, predominantly at ~760 Ma in the south and ~720 Ma in the north (Table 3.1). These domains

were translated southward over the Sambirano-Sahantaha Group and the combined Antananarivo-Antongil domains during late Ediacaran to early Cambrian time (ca. 540-520 Ma). This period of Tonian-Cryogenian igneous activity in northern Madagascar is correlated with extensive magmatism of the same age in the Seychelles and Rajasthan (Torsvik et al., 2001; Meert et al., 2013).

3.3 The Imorona-Itsindro Suite

3.3.1 Suite description and contact relationships

The Imorona-Itsindro Suite is named after the Imorona and Itsindro massifs located near Ambatofinadrahana village (Moine, 1968) approximately 120 km west of Ambositra (Fig. 3.2). Imorona-type intrusions consist primarily of granitoid rocks while the Itsindro intrusions are primarily gabbroic. Recent work subdivided the suite into several sub-suites in addition to the Imorona and Itsindro-type lithologies that intrude the Antananarivo and Itremo Domains in the core of central Madagascar (BGS-USGS-GLW, 2008). These sub-suites include the Brickaville, Isinko, Angavo-Ankazobe, Ankaranando, Ambodilafa, Andohalobe, Ankera, and Kamoro subsuites (BGS-USGS-GLW, 2008). Significant geochemical or temporal grounds for distinction among the sub-suites are unclear and are based mainly on geographical distribution. For the purposes of this paper, we base our subdivisions of the Imorona-Itsindro Suite on the basement domains that the Tonian rocks intrude (Fig. 3.2).

The suite crops out as numerous dykes and sills typically associated with large intrusive igneous massifs or plutons of granitoid, gabbro, and syenite lithologies (Fig. 3.3a-c). Remarkably, unequivocally Tonian volcanic rocks have yet to be identified, despite claims that some the metasedimentary rocks of the Itremo Group were near surface in Tonian time (Moine, 1967; Moine, 1974). Potential Tonian volcanic rocks have been suggested to form part of the Manampotsy Group (BGS-USGS-GLW, 2008) and the Horombe Group (Boger et al., 2014). However, convincing petrologic evidence remains elusive due to the extent of Ediacaran to Cambrian metamorphism and deformation of these rocks. Intrusions have predominantly felsic compositions with fewer intermediate and mafic rocks. The felsic end-members consist of metaluminous to weakly peraluminous granitoids (rarely peralkaline; Archibald et al., submitted-b; Boger et al., 2015), intermediate rocks are quartz-monzodiorite to granodiorite (Archibald et al., submitted-b) and mafic rocks are typically high-alkali gabbro (McMillan et al., 2003; Kabete et al., 2006; Bybee et al., 2010). Mafic and felsic lithologies are commonly mingled at outcrop scale with abundant xenoliths and enclaves (Fig. 3.3d-f), or form nested intrusions on a regional scale (McMillan et al., 2003).

The Imorona-Itsindro Suite has clear intrusive relationships with older lithologies in the Antananarivo, Tsaratanana, Ikalamavony, and Itremo Domains and are inferred, but not observed, in the Masora Domain (BGS-USGS-GLW, 2008). Convincing contact relationships with the Antongil Domain lithologies (BGS-USGS-GLW, 2008; Schofield et al., 2010) and Ambatolampy Group (BGS-USGS-GLW, 2008; Archibald et al., 2015) remain elusive. BGS-USGS-GLW (2008) suggested deposition of the Ambatolampy Group occurred at the same time as intrusion of the Imorona-Itsindro Suite based on limited Meso- to Neoproterozoic detritus in the former. However, a more recent study of the Ambatolampy Group reassigned the samples with Meso- to Neoproterozoic detritus identified by BGS-USGS-GLW (2008) to the Manampotsy Group (Archibald et al., 2015). These authors concluded that detrital zircon age populations in the Ambatolampy Group are more comparable to the Itremo Group demonstrating the presence of a much larger Mesoproterozoic basin in central Madagascar than hitherto thought.

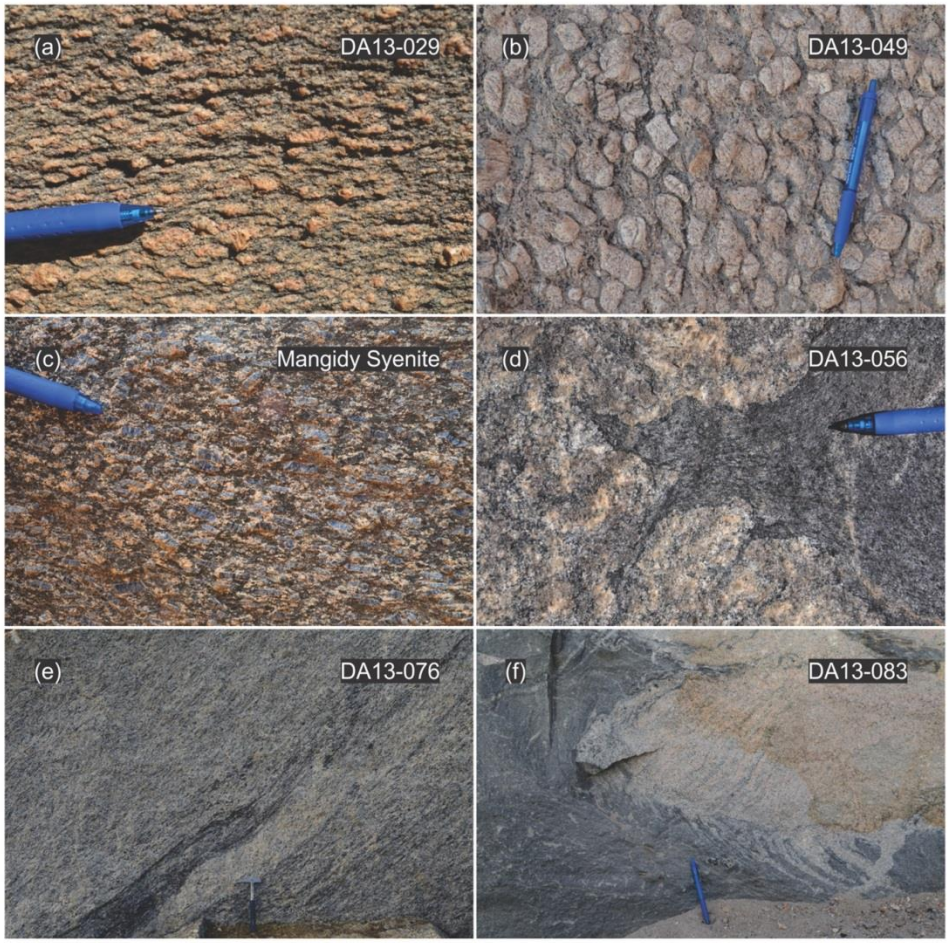

Fig. 3.3 Representative field photographs of the Imorona-Itsindro Suite: (a) granite orthogneiss sample DA12-029; (b) porphyritic alkali-feldspar granite (Ilaka Granite) sample DA13-049; (c) the Mangidy syenite; (d) magma mingling textures observed at the sampling location of DA13-056; (e) metasedimentary 'restite' in the Brickaville orthogneiss at the sampling locality of DA13-076; and (f) complex magma mingling relationships in the Ambatomara Quarry (sampling locality of DA13-083).

3.3.2 Previous isotopic work

Voluminous magmatism has long been recognised as a major component of central Madagascar (Besairie, 1968-1971). The Imorona-Itsindro Suite is the most extensively dated unit in Madagascar with more than 150 U-Pb and ^{207}Pb-^{206}Pb zircon ages collected over the past two decades (Guerrot et al., 1991; Handke et al., 1997; Handke et al., 1999; Tucker et al., 1999b; de Wit, 2003; Kabete et al., 2006; Tucker et al., 2007; BGS-USGS-GLW, 2008; Key et al., 2011; Yang et al., 2014; Zhou et al., 2015b). Early work studied intrusions in the Antananarivo and Itremo Domains and yielded ages between ~820 and 780 Ma (Handke et al., 1999; Tucker et al., 1999b). More recent work extended the duration of Tonian magmatism to between ~850 Ma to 740 Ma (see Tucker et al., 2014 compilation) or to 700 Ma if the Tonian magmatism in the Bemarivo Domain is considered to have a similar genesis as the rest of the Imorona-Itsindro Suite in central Madagascar (Boger et al., 2014).

Currently, no oxygen isotope data is published from Tonian rocks in Madagascar. Limited hafnium isotope data is available for the Ambatondrazaka gabbro (Zhou et al., 2015b) and the Antanimbary granitoid (Yang et al., 2014). Gabbroic rocks in the Ambatondrazaka area (Fig. 3.2) have $\varepsilon_{Hf}(t)$ values between -6.84 and -3.08, interpreted to represent significant involvement of an enriched component during magma emplacement or

mantle melting processes (Zhou et al., 2015b). ε_{Hf} (t) values for the Antanimbary granitoid (Fig. 3.2) are between -18.2 and -15.1 (Yang et al., 2014). The narrow range of ε_{Hf}(t) values and corresponding T_{DMc} model ages (2.06–1.94 Ga) were interpreted to result from mixing of both primary Tonian mantle and inherited Neoarchaean crustal sources initiated by underplating of mantle plume-derived magmas that subsequently triggered partial melting of thinned lower crust (Yang et al., 2014).

3.4 Analytical methods

A complete description of the methods employed in this study is available in online supplementary Appendix A. Sample collection focused on obtaining a representative sample set including Tonian lithologies from all tectonic domains in central Madagascar (Fig. 3.2). To complement our sample suite, seven Tonian samples collected as part of the World Bank funded mapping program (BGS-USGS-GLW, 2008) were added. The BGS-USGS-GLW (2008) samples are from areas not covered during our 2013 and 2014 field seasons (i.e. Masora Domain and Northern Antananarivo Domain). Lithological descriptions and zircon characteristics for all samples are provided in Table 3.2 and Table 3.3. LA-ICP-MS (laser-ablation inductively-coupled mass spectroscopy) U-Pb analyses were conducted at Adelaide Microscopy in Adelaide, Australia. Zircon standard reference material GJ (Jackson et al., 2004) was used as a primary standard and internal accuracy was monitored using the Plešovice zircon reference material ($^{206}Pb/^{238}U$ age of 337.1 ± 0.37 Ma; 2σ; Sláma et al., 2008). Plešovice analyses yield a weighted-mean $^{206}Pb/^{238}U$ age of 337.4 ± 1.3 (2σ; MSWD = 1.3; n = 80). The 5 or 10 % concordance level (based on the number of concordant analyses) is used to calculate the age because of common Pb [($^{204}Pb/$ ($^{204}Pb+^{206}Pb$)] x 100 (Appendix A) and Pb loss. Individual zircon ages are quoted at a 1σ level and weighted-mean ages are at a 2σ level. SHRIMP II (sensitive high resolution ion microprobe) geochronological data (BGS-USGS-GLW, 2008) were re-evaluated using the same procedures as the new LA-ICP-MS data to ensure consistency in our interpretations and to ensure deduction of a representative crystallisation age. Differences in age interpretations between BGS-USGS-GLW (2008) and this study are found in Table 3.4. Complete sample descriptions and age interpretations for SHRIMP II data can be found in BGS-USGS-GLW (2008; Appendix A). Oxygen isotope analyses were conducted at the Australian National University, Canberra, Australia using the SHRIMP SI (sensitive high-resolution ion microprobe stable isotope) or SHRIMP II instrument. The SHRIMP SI method involved a 10 kV, ~3 nA Cs^+ primary ion beam focused to a ~30 μm diameter spot size. Procedures for the SHRIMP II follow the methods of Ickert et al. (2008). Long term instrument drift was corrected using the Mudtank zircon reference material ($\delta^{18}O$ = 5.03 ± 0.10 ‰; Valley, 2003) and Temora II zircon ($\delta^{18}O$ = 8.20 ± 0.01 ‰; Valley, 2003). Standard results are found in Appendix 3.1 (Table A.3.1). In situ LA-MC-ICP-MS (laser-ablation multi-collector inductively-coupled mass spectroscopy) Hf isotope analyses were conducted at the University of Adelaide Waite Campus facility using a New Wave Research 193 nm Excimer laser attached to a Neptune multi-collector ICP-MS system as per Payne et al. (2013). Analysis locations were in the same cathodoluminescence domains as concordant U–Pb laser spots and in the same site as SHRIMP oxygen spots (Fig. 3.4). Procedural accuracy was monitored using the Plešovice, Mudtank and Temora II zircon standards. Mean $^{176}Hf/^{177}Hf$ ratios for each standard along with the literature values are presented in the supplementary Appendix 3.1 (Table A.3.1). ε_{Hf}(t) and $T_{DM}c$ were calculated using ^{176}Lu decay constant after Scherer et al. (2001). $T_{DM}c$ two stage crustal model ages were calculated using the methods of Griffin et al. (2002) with an average crustal composition of $^{176}Lu/^{177}Hf$ = 0.015.

Table 3.2 Summary of sample names, lithology, locations and mineralogy for samples of the Imorona-Itsindro Suite.

		WGS 84 (ddºmm'ss.s")					
Sample	Domain	Latitude	Longitude	Lithology	Grain size	Textures	Mineralogy
DA14-133	Ikal	20° 32' 58.4"	45° 52' 21.6"	granite	mg-cg inequigranular	foliated	af (50-60), pl (10-15), qtz (30-40), bt (2-5), zrc (<1), all (<1), op (<1), pyr (<1)
DA14-140	Ikal	20° 31' 06.0"	45° 53' 36.8"	granite	mg-cg inequigranular	-	af (60-70), pl (10-15), qtz (20-30), amph (2-5), bt (5-10), zrc (<1), all (<1), op (<1)
DA14-146	Ikal	19° 47' 39.3"	45° 32' 08.5"	granite	mg-cg inequigranular	granophyric	af (40-50), pl (20-30), qtz (30-40), bt (5-10), zrc (<1), all (<1), op (<1)
DA13-055	Itremo	20° 37' 40.9"	47° 02' 09.0"	qtz monzodiorite	fg-mg inequigranular	-	af (20-25), pl (50-60), qtz (5-10), amph (5-10), bt (5-10), zrc (<1), op (<1)
DA13-056	Itremo	20° 33' 41.9"	47° 00' 09.2"	granite	cg inequigranular	porphyritic	af (60-70), pl (10-15), qtz (20-30), bt (2-5), zrc (<1), op (<1)
DA13-063	Itremo	20° 33' 34.8"	46° 45' 12.2"	quartz syenite	fg-mg matrix	porphyritic	af (60-70), pl (10-15), qtz (15-20), amph (5-10), bt (2-5), zrc (<1), op (<1)
DA13-064	Itremo	20° 33' 11.3"	46° 43' 51.5"	granite	fg-mg matrix	porphyritic	af (55-65), pl (10-15), qtz (20-30), amph (10-15), bt (2-5), zrc (<1), op (<1)
DA13-065	Itremo	20° 34' 31.8"	46° 42' 47.3"	granite	fg-mg matrix	porphyritic foliated	af (50-60), pl (10-15), qtz (20-30), amph (10-15), zrc (<1), op (<1)
DA13-012	C. Ant	20° 22' 16.5"	47° 17' 29.3"	granodiorite	cg inequigranular	-	af (10-15), pl (40-50), qtz (30-40), amph (5-10), bt (2-5), zrc (<1), op (<1)
DA13-017	C. Ant	21° 20' 46.1"	46° 58' 38.9"	granodiorite	mg-cg inequigranular	-	af (15-20), pl (40-50), qtz (20-30), amph (5-10), bt (2-5), zrc (<1), op (<1)
DA13-020	C. Ant	21° 15' 29.8"	46° 46' 10.5"	granite gneiss	mg-cg inequigranular	porphyritic foliated	af (60-70), pl (10-15), qtz (20-25), bt (2-5), zrc (<1), op (<1)
DA13-029	C. Ant	21° 17' 46.9"	46° 43' 13.3"	granite	mg-cg inequigranular	porphyritic	af (25-35), pl (30-40), qtz (30-40), bt (2-5), zrc (<1), op (<1)
DA13-049	C. Ant	20° 22' 51.7"	47° 08' 44.0"	granite	mg-cg matrix	porphyritic	af (50-60), pl (15-20), qtz (25-30), amph (2-5), bt (2-5), zrc (<1), op (<1), ti (<1)
DA13-077	C. Ant	18° 54' 00.4"	48° 25' 53.1"	granite gneiss	fg-cg inequigranular	foliated	af (50-60), pl (20-30), qtz (20-30), amph (2-5), bt (5-10), zrc (<1), all (<1), op (<1)
DA13-083	C. Ant	18° 54' 51.6"	47° 33' 52.2"	granite	mg-cg inequigranular	-	af (50-60), pl (10-15), qtz (25-35), amph (2-5), bt (5-10), zrc (<1), all (<1), op (<1)
BGS-TK64a	C. Ant	18° 55' 34.5"	48° 11' 58.9"	granite gneiss	mg-cg inequigranular	foliated	af (15-20), pl (30-40), qtz (30-35), amph (2-5), bt (10-15), op (2-5), zrc
BGS-WB005	C. Ant	18° 58' 19.0"	48° 33' 20.1"	granite	mg inequigranular	foliated	af, pl, qtz, bt, amph, zrc
BGS-WB1451	N. Ant	16° 35' 09.1"	47° 36' 14.4"	granite gneiss	-	foliated	af, pl, qtz, bt (minor), zrc
BGS-PP156	N. Ant	17° 04' 00.1"	47° 57' 34.0"	granite gneiss	fg-mg	foliated	mineralogy not descibed in BGS-USGS-GLW (2008)
BGS-RT07-032	N. Ant	17° 03' 39.7"	47° 11' 17.6"	granite gneiss	fg equigranular	foliated	mineralogy not descibed in BGS-USGS-GLW (2008)
DA13-074	E. Ant	18° 49' 21.8"	49° 04' 34.8"	granite	mg-cg inequigranular	-	af (50-60), pl (10-15), qtz (20-30), amph (5-10), bt (5-10), gt (1-2), musc (2-5), zrc (<1), op (<1)
DA13-076	E. Ant	18° 54' 27.7"	48° 58' 34.2"	granite	mg-cg inequigranular	foliated	af (40-50), pl (20-25), qtz (20-25), amph (10-15), bt (2-5), gt (2-5), musc (2-5), zrc (<1), op (<1)
BGS-WB37	Masora	19° 55' 06.2"	48° 51' 01.2"	granodiorite	fg-mg inequigranular	foliated	pl, qtz, af (minor), bt, gt, tit, zrc
BGS-RK395	Masora	21° 04' 43.2"	48° 14' 48.6"	granodiorite	mg-cg	foliated	af (30), pl (20), qtz (25-35), bt (5-10), op (1-3), zrc, musc, ap, ep, mn,chl
BGS-RK06/349	Masora	21° 10' 22.5"	48° 21' 30.5"	granite gneiss	mg	foliated	mineralogy not descibed in BGS-USGS-GLW (2008)

Note: Samples with a DA prefix are part of this study and samples with a BGS prefix are from BGS-USGS-GLW, (2008). Abbreviations: Ikal=Ikalamavony, C. Ant=Central Antananarivo, N. Ant=Northern Antananarivo, E. Ant=Eastern Antananarivo, fg=fine-grained, mg=medium-grained, cg=coarse-grained, vcg=very coarse-grained, af=alkali-feldspar, pl=plagioclase, qtz=quartz, am=amphibole, bt=biotite, zrc=zircon, op=Fe-Ti oxide opaque minerals, pyr=pyrite, gt=garnet, all=allanite, ap=apatite, ep=epidote, mn=monazite, musc=muscovite, chl=chlorite.

Table 3.3 Physical and optical characteristics of zircon from the Imorona-Itsindro Suite.

Sample	Colour	Size (mm)	Aspect ratio (L:W)	Morphology	Internal zoning
DA14-133	colourless, pale yellow/brown	75-200	2:1 - 3:1	euhedral to mostly subhedral	magmatic oscillatory zoning, minor broad and faint zoning, and dark, narrow rims
DA14-140	colourless, pale yellow/brown	75-250	2:1 - 4:1	euhedral to mostly subhedral	bright domains have faint magmatic oscillatory zoning; dark domains are unzoned
DA14-146	colourless, pale yellow/brown	50-300	1:1 - 4:1	mostly euhedral to subhedral	bright domains have faint magmatic oscillatory zoning; dark domains are unzoned
DA13-055	clear, pale yellow	50-400	3:1 - 5:1	mostly euhedral	dark inclusions; broad magmatic oscillatory zoning
DA13-056	colourless, pale brown	50-300	2:1 - 3:1	euhedral to subhedral	partially metamict, faint broad zoning
DA13-063	colourless, pale brown	50-300	1:1 - 3:1	subhedral to anhedral	oscillatory zoned xenocrystic cores surrounded by clear, narrow magmatic oscillatory zoned rims
DA13-064	clear, pale brown	50-375	1:1 - 3:1	euhedral to subhedral	oscillatory zoned xenocrystic cores surrounded by clear, narrow magmatic oscillatory zoned rims
DA13-065	clear, colourless	50-150	1:1 - 2:1	mostly subhedral	dark or broadly zoned cores; moderate to narrow magmatic oscillatory zoned overgrowths
DA13-012	clear, colourless	50-375	2:1 - 3:1	mostly euhedral to subhedral	xenocrystic cores, magmatic oscillatory zoned overgrowths, narrow dark outer rims
DA13-017	clear, colourless	50-375	2:1 - 3:1	mostly euhedral to subhedral	xenocrystic cores, magmatic oscillatory zoned overgrowths, narrow dark outer rims
DA13-020	colourless, clear	100-375	2:1 - 4:1	mostly subhedral to euhedral	magmatic oscillatory zoning
DA13-029	water clear, colourless	50-250	1:1 - 3:1	mostly subhedral to euhedral	unzoned, broad zoning, magmatic oscillatory zoned, narrow dark outer rims
DA13-049	clear, colourless	50-250	1:1 - 3:1	euhedral to subhedral	dark, xenocrystic cores; magmatic oscillatory zoned overgrowths; minor narrow, dark coloured outer rims
DA13-077	clear, pale yellow/brown	50-550	2:1 - 4:1	mostly euhedral to subhedral	broad zoned interiors (both bright and dark); magmatic oscillatory zoned overgrowths
DA13-083	colourless, pale brown	50-500	1:1 - 4:1	mostly euhedral to subhedral	magmatic oscillatory zoning; dark, narrow rims
BGS-TK64a	clear, colourless	50-400	1:1 - 4:1	sub- to euhedral	faint internal zoning with embayment regrowth and minor rims
BGS-WB005	colourless, transparent to almost opaque	50-300	1:1 - 3:1	anhedral and rounded to euhedral	majority have magmatic oscillatory zoning
BGS-WB1451	yellow to pale brown	50-200	1:1 - 2:1	sub- to euhedral	oscillatory and sector zoning
BGS-PP156	clear, colourless, pink, yellow	50-200	1:1 - 4:1	subhedral to euhedral	bright core domains overgrown by broad, faint or unzoned rims
BGS-RT07-032	colourless to pale brown	50-150	1:1 - 2:1	mostly subhedral to euhedral	fuzzy concentric zoning: dark, narrow homogeneous rims
DA13-074	clear, colourless	50-1200	2:1 - 5:1	mostly euhedral to subhedral	complex zoning: unzoned to faint zoning; broad zoning; narrow, magmatic oscillatory zoning; and convolute zoning; dark, narrow rims
DA13-076	clear, colourless	50-700	2:1 - 4:1	mostly euhedral to subhedral	complex zoning: unzoned to faint zoning; broad zoning; narrow, magmatic oscillatory zoning; and convolute zoning; dark, narrow rims
BGS-WB37	clear	100-200	2:1 - 3:1	euhedral	oscillatory zoned
BGS-RK395	colourless	100-350	1:1 - 6:1	euhedral	oscillatory zoned cores with dark rims
BGS-RK06/349	turbid	50-200	1:1 - 3:1	mostly euhedral	dark cores with oscillatory zoned rims

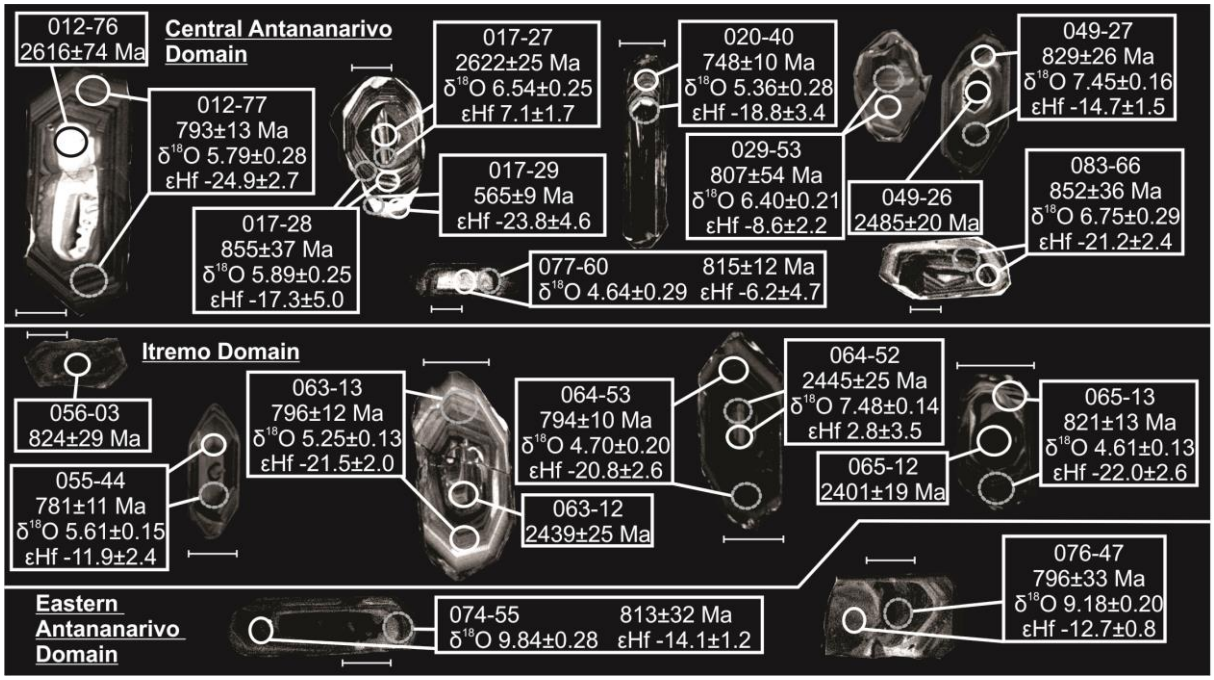

Fig. 3.4 Selected cathodoluminescence (CL) images for representative zircon from the Imorona-Itsindro Suite. Spot names, appropriate U-Pb ages with one standard deviation error, $\delta^{18}O$ values with two standard deviation error and $\varepsilon_{Hf}(t)$ values with two standard deviation error are listed alongside each image. Solid circles represent U-Pb analysis spots and broken circles represent the location of oxygen and hafnium isotope analyses. White scale bars adjacent to each image are ~50 μm.

3.5 Results

3.5.1 Sample description and U-Pb zircon results

Twenty-five samples of the Imorona-Itsindro Suite were selected for zircon U-Pb, oxygen and hafnium isotope analysis. The present study includes samples from the Ikalamavony (3), Itremo (5), Central Antananarivo (9), Northern Antananarivo (3), Eastern Antananarivo (2) and Masora (3) Domains. All of the analysed samples have intermediate to felsic compositions. Supposed Tonian gabbroic rocks were also collected but unfortunately these samples did not yield zircon. The U-Pb dated samples were also analysed for O and Hf isotope data collection, except sample DA13-056 for which O and Hf data were not collected. Cathodoluminescence images for representative zircon are presented in Fig. 3.4. Geochronology results and age deductions are summarised in Table 3.5 and U-Pb data are listed in Appendix 3.2. Concordia diagrams for all samples are presented in Figs. 3.5 to 3. 7.

3.5.1.1 Ikalamavony Domain

Three samples of granite from the Imorona-Itsindro Suite were collected from the Ikalamavony Domain for analysis.

Sample DA14-133 was collected ~45km east of Malaimbandy (Fig. 3.2), from an outcrop of foliated granite cross-cut by abundant acid veins, pegmatite dykes and quartz veins. The sample is homogenous, alkali-feldspar + quartz + plagioclase + biotite bearing, fine to medium-grained and well-foliated. It intrudes the Ikalamavony Group quartzite. The sample yielded a $^{207}Pb/^{206}Pb$ crystallisation age of 824 ± 23 Ma (Table 3.5; Fig. 3.5a).

Sample DA14-140 was collected ~50 km east of Malaimbandy near the top of a hill with prominent, well-foliated granite outcrops (Fig. 3.2). The coarse-grained biotite granite orthogneiss is cross-cut by low-angle granite veins and intrudes into the Ikalamavony Group quartzite. The sample has a $^{207}Pb/^{206}Pb$ crystallisation age of 770 ± 21 Ma (Table 3.5; Fig. 3.5b).

Sample DA14-146 was collected north of the Mania River Bridge between Malaimbandy and Miandrivazo (Fig. 3.2). It is a coarse-grained granite orthogneiss with mineral lineations defined by quartz, perthitic alkali-feldspar, plagioclase, and biotite. The granite is cross-cut by pegmatite veins but contact relationships with older lithologies are absent. The sample has a $^{207}Pb/^{206}Pb$ crystallisation age of 774 ± 11 Ma (Table 3.5; Fig. 3.5c).

3.5.1.2 Itremo Domain

Five samples of the Imorona-Itsindro Suite were collected from the Itremo Domain for analysis. The included samples from the type location of the more felsic lithologies in the suite from the Imorona massif are DA13-064 and DA13-065.

Sample DA13-055 is a quartz monzonite sample that outcrops alongside a more felsic lithology by a road. Both lithologies appear mingled on the outcrop scale, with the more felsic rocks in the outcrop being more altered. The sample was collected near the Itsindro massif, the type location for the Itsindro-gabbro (Fig. 3.2). The sample yielded a concordia age of 780 ± 7 Ma (Table 3.5; Fig. 3.5d).

Sample DA13-056, porphyritic granite, was collected ~10 km west of the sampling location for DA13-055 (Fig. 3.2). The granite intrudes mafic orthogneiss. The granite also demonstrates a mingling relationship with gabbro (Fig. 3d). The sample yielded a $^{207}Pb/^{206}Pb$ crystallisation age of 822 ± 28 Ma (Table 3.5; Fig. 3.5e).

Sample DA13-063 is porphyritic granite containing large (up to 10cm) phenocrysts of quartz and alkali-feldspar. It was collected from a roadside outcrop between the Itsindro and Imorona massifs (Fig. 3.2). The sample yielded a $^{206}Pb/^{238}U$ crystallisation age of 798 ± 8 Ma (Table 3.5; Fig. 3.5f).

Sample DA13-064 is granite collected ~3km west of sample DA13-063 (Fig. 3.2). It is porphyritic, weathered and contains large (up to 5cm) phenocrysts of quartz and alkali-feldspar and is cross-cut by ~1m wide plagioclase-rich diorite dykes. The sample yielded a $^{207}Pb/^{206}Pb$ crystallisation age of 819 ± 19 Ma (Table 3.5; Fig. 3.5g).

Sample DA13-065 was collected ~4km west of DA13-064 from part of the Imorona massif (Fig. 3.2). It is porphyritic granite containing large (up to 2cm) phenocrysts of quartz and alkali-feldspar. It is less weathered than DA13-064 and has an east-dipping foliation. The sample yielded a $^{206}Pb/^{238}U$ crystallisation age of 791 ± 17 Ma (Table 3.5; Fig. 3.5h).

3.5.1.3 Central Antananarivo Domain

A total of 14 samples of the Imorona-Itsindro Suite from the Antananarivo Domain were analysed. Nine of these samples are from the Central Antananarivo Domain. Samples that intrude the northern Antananarivo Domain and the Brickaville orthogneiss located in the easternmost Antananarivo Domain will be discussed in separate sections because of their spatial distribution or unique geochemical characteristics.

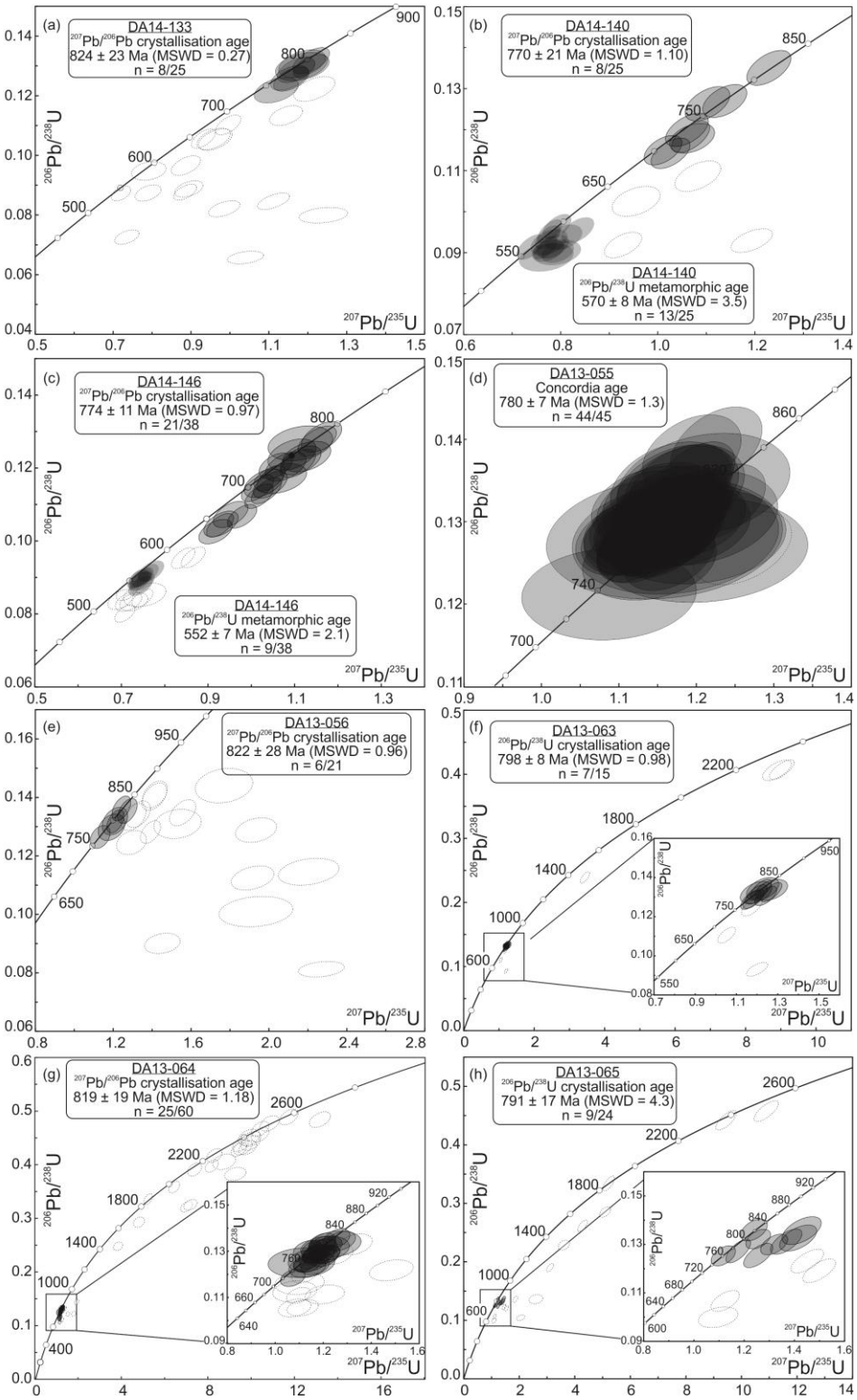

Fig. 3.5 Concordia diagrams showing zircon analyses from the Imorona-Itsindro Suite intruding the Ikalamavony Domain: (a) DA14-133; (b) DA14-140; (c) DA14-146 and the Itremo Domain (d) DA13-055; (e) DA13-056; (f) DA13-063; (g) DA13-064; and (h) DA13-065. U-Pb data are reported in Appendix 3.2. Data point error ellipses are 2σ. The interpreted age of each sample is summarised in Table 3.6. Shaded ellipses with a solid border were used in Tonian weighted-mean age calculations, shaded ellipses with a broken border were used in Ediacaran age calculations and open ellipses were rejected.

Sample DA13-012 comes from ~18 km north of Ambositra (Fig. 3.2). It is a strongly foliated and lineated leucocratic granodiorite that is cross-cut by undeformed pegmatite dykes. The sample has a $^{207}Pb/^{206}Pb$ crystallisation age of 849 ± 17 Ma (Table 3.5; Fig. 3.6a).

Sample DA13-017 is a strongly foliated granodiorite and is cross-cut by alkali-feldspar and biotite bearing pegmatite dykes. It was collected from a small roadside quarry ~20km north of Fianarantsoa (Fig. 3.2). The sample yielded a $^{207}Pb/^{206}Pb$ crystallisation age of 814 ± 19 Ma (Table 3.5; Fig. 3.6b).

Sample DA13-020 was collected near the boundary of the Ikalamavony and Antananarivo Domains (Fig. 3.2). It is a strongly foliated, lineated and porphyritic granitic orthogneiss which intrudes into paragneiss of the Sofia Group or possibly the Ambatolampy Group which crops out less than 2km to the east (Fig. 3.2). Small (2-5cm) granite dykes cross-cut the foliation and are themselves foliated but not lineated like their host. The sample yielded a $^{206}Pb/^{238}U$ crystallisation age of 758 ± 10 Ma (Table 3.5; Fig. 3.6c).

Sample DA13-029 was collected at the boundary between the Ikalamavony and Antananarivo Domains (Fig. 3.2). The sample is porphyritic granite with quartz phenocrysts up to 0.5cm in diameter. It is weakly foliated and intrudes amphibolite gneiss with calc-silicate nodules forming boudins. Whether the amphibolite gneiss is part of the Ambatolampy Group or the Ikalamavony Group was not resolved. The outcrop is cross-cut by younger aplitic and pegmatite dykes. The sample yielded a $^{207}Pb/^{206}Pb$ crystallisation age of 828 ± 14 Ma (Table 3.5; Fig. 3.6d).

Sample DA13-049 is weakly foliated granite porphyry containing quartz and alkali-feldspar phenocrysts which is remarkably similar to the porphyritic samples from the Itremo Domain (e.g. DA13-064). It was collected ~20km north of Ambositra along RN7 (Fig. 3.2). The granite is cross-cut by small (<3cm) aplite dykes that are probably related to the Ambalavao Suite. The sample has a $^{207}Pb/^{206}Pb$ age of 827 ± 16 Ma (Table 3.5; Fig. 3.6e).

Sample DA13-077 was taken from a river outcrop west of Antananarivo (Fig. 3.2). It is an intensely foliated granite orthogneiss with large alkali-feldspar phenocrysts. The sample yielded a $^{207}Pb/^{206}Pb$ crystallisation age of 837 ± 15 Ma (Table 3.5; Fig. 3.6f).

Sample DA13-083 was collected from the large Ambatomara quarry west of Antananarivo (Fig. 3.2). The foliated granite shows dark allanite with radiation alteration halos. The main fabric in the granite is cross-cut by a network of mafic dykes and felsic pegmatite and aplite dykes (Fig. 3.3f). The sample yielded a $^{207}Pb/^{206}Pb$ crystallisation age of 795 ± 13 Ma (Table 3.5; Fig. 3.6g).

Sample BGS-TK64a was collected west of Antananarivo (Fig. 3.2). It is a biotite-orthogneiss interlayered with mafic gneiss and cut by younger granitic sheets of the Kiangara Suite. The outcrop contains mafic enclaves and the granite gneiss is tightly folded with NE-striking and plunging fold hinges. The sample yielded a $^{207}Pb/^{206}Pb$ crystallisation age of 764 ± 16 Ma (Table 3.5; Fig. 3.6h).

Sample BGS-WB005 is granite gneiss collected west of Antananarivo (Fig. 3.2), which displays a similar gneissic fabric to sample DA13-077. The rocks in the quarry are slightly migmatitic with some areas showing charnockitisation as evidenced by recrystallised greasy green feldspars and orthopyroxene as a mafic phase. The sample was taken from a finely banded part of the gneiss which bore no evidence of charnockitisation or migmatisation. A $^{206}Pb/^{238}U$ crystallisation age of 793 ± 7 Ma (Table 3.5; Fig. 3.6i) was obtained.

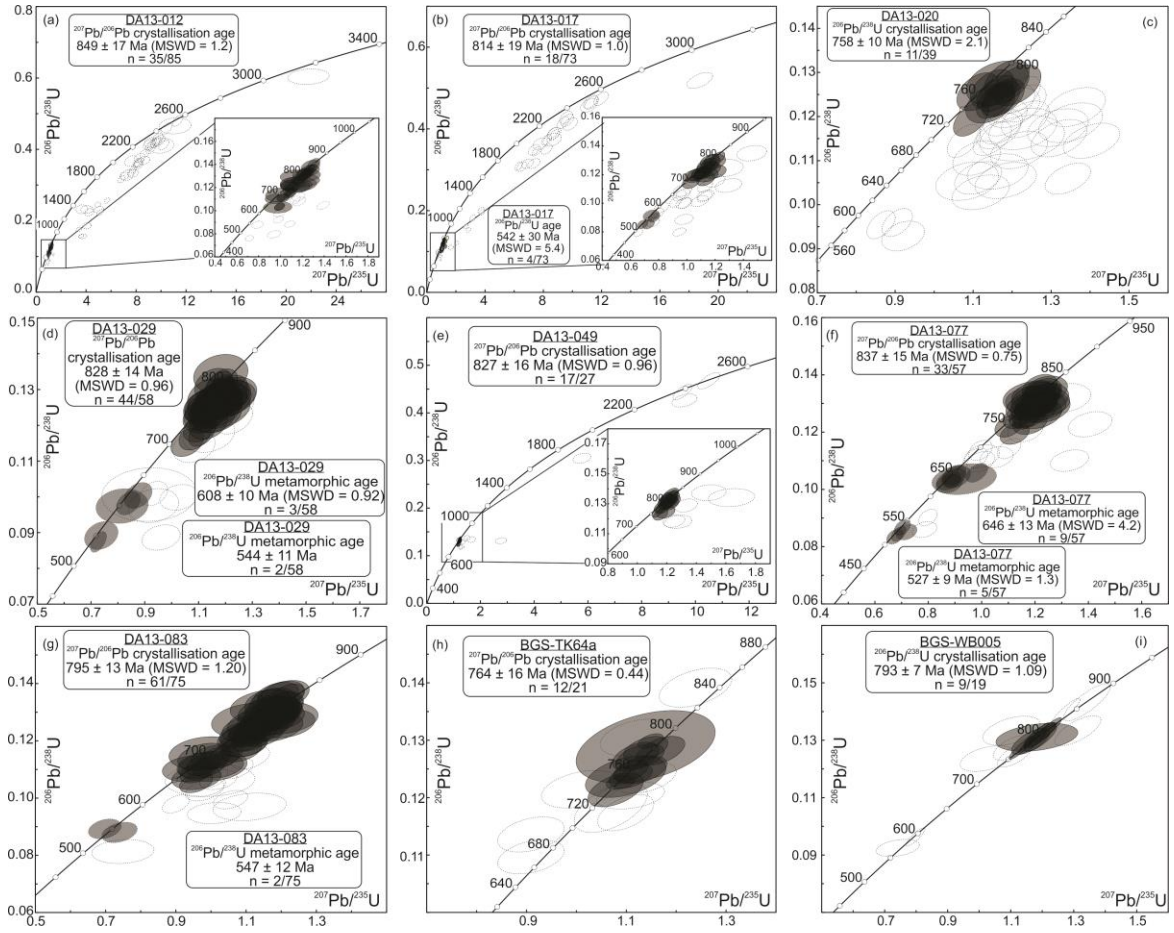

Fig. 3.6 Concordia diagrams showing zircon analyses from the Imorona-Itsindro suite intruding the Antananarivo Domain: (a) DA13-012; (b) DA13-017; (c) DA13-020; (d) DA13-029; (e) DA13-049; (f) DA13-077; (g) DA13-083; (h) BGS-TK64a; and (i) BGS-WB005. U-Pb data is reported in Appendix 3.2. Data point error ellipses are 2σ. The interpreted age of each sample is summarised in Table 3.6. Shaded ellipses with a solid border were used in Tonian weighted-mean age calculations, shaded ellipses with a broken border were used in Ediacaran weighted-mean age calculations and open ellipses were rejected.

3.5.1.4 Northern Antananarivo Domain

Geochronology data for the following three samples were collected as part of the BGS-USGS mapping program in the Northern Antananarivo Domain (Fig. 3.2)

Sample BGS-WB 1451was collected ~25km northwest of Tsaratanana in the Antananarivo Domain near the basal thrust of the Andriamena Unit (Fig. 3.2). It is a granite from the Kamoro Subsuite (BGS-USGS-GLW, 2008) and displays a weak foliation due to a dearth of mica. Locally, there are decimetre-long schlieren of incompletely molten xenoliths that are more aluminous and silicic in composition than the host granite. The sample has a $^{207}Pb/^{206}Pb$ crystallisation age of 774 ± 16 Ma (Table 3.5; Fig. 3.7a).

Sample BGS-PP 156 was taken from a streambed outcrop south of Tsaratanana (Fig. 3.2). It is a quartzofeldspathic leucogneiss that is interfolded with migmatitic hornblende ± biotite gneiss. These units are up to 500m (typically 10-15metres) thick and in places contain folded rafts of the associated amphibolite and hornblende gneisses. The leucogneiss are

weakly migmatitic with sub-concordant pegmatite dykes. The sample yielded a $^{207}Pb/^{206}Pb$ crystallisation age of 819 ± 23 Ma (Table 3.5; Fig. 3.7b).

Sample BGS-RT07-032 was taken from the summit of Manovasora Mountain in the Northern Antananarivo Domain (Fig. 3.2) near the crest of a major northeast-plunging antiform. The mineralogy (alkali-feldspar granite) and aplitic texture resembles nearby sills and minor injections of pink aplite into the overlying schist, paragneiss, and quartzofeldspathic gneiss (Betsiboka Suite). The sample has a $^{207}Pb/^{206}Pb$ crystallisation age of 768 ± 8 Ma (Table 3.5; Fig. 3.7c).

3.5.1.5 Eastern Antananarivo Domain (Brickaville orthogneiss)

Two samples of the Brickaville orthogneiss were collected east of the Angavo-Ifandiana Shear zone intruding into the Manampotsy Group or the Antananarivo Domain (BGS-USGS-GLW, 2008; Roig et al., 2012). These samples are geochemically distinguished from other Tonian-aged intrusions from the Antananarivo Domain by the presence of garnet and muscovite.

Sample DA13-074 was collected from a small quarry east of Brickaville (Fig. 3.2). It is granite with large garnet crystals (up to 1cm) and muscovite. The granite is cross-cut by pyrite-bearing mafic dykes and contains metasedimentary rafts with graphite and biotite, presumably from the Manampotsy Group. The sample yielded a $^{207}Pb/^{206}Pb$ crystallisation age of 821 ± 11 Ma (Table 3.5; Fig. 3.7d).

Sample DA13-076 is a strongly foliated granite orthogneiss that was collected from a quarry ~18 km west of Brickaville (Fig. 3.2). It contains large garnets up to 1cm in diameter. The outcrop contains abundant graphite-bearing metasedimentary xenoliths and rafts (Fig. 3e). Felsic dykes are concordant to the deformation fabric (Fig. 3.3e). The sample yielded a $^{207}Pb/^{206}Pb$ crystallisation age of 813 ± 10 Ma (Table 3.5; Fig. 3.7e).

Table 3.4 Summary of U-Pb data collected by BGS-USGS-GLW (2008) re-examined in this study.

Sample	Domain	Inheritance Age (Ma)		Crystallisation Age (Ma)		Metamorphism Age (Ma)	
		BGS-USGS-GLW (2008)	This study	BGS-USGS-GLW (2008)	This study	BGS-USGS-GLW (2008)	This study
BGS-TK 64a	C. Ant	-	-	762 ± 17	764 ± 16	-	-
BGS-WB 005	C. Ant	-	-	790 ± 7	793 ± 11	~600	~600
BGS-WB 1451	N. Ant	-	-	776 ± 8	774 ± 16	-	-
BGS-PP 156	N. Ant	2485 ± 13	2485 ± 13	819 ± 23	819 ± 23	-	-
BGS-RT07-032	N. Ant	-	-	768 ± 8	768 ± 8	-	-
BGS-WB 37	Masora	-	-	830 ± 27	843 ± 15	-	-
BGS-RK 395	Masora	-	-	815 ± 30	814 ± 30	516 ± 4	516 ± 4
BGS-RK06/349	Masora	-	-	784 ± 9	796 ± 33	-	-

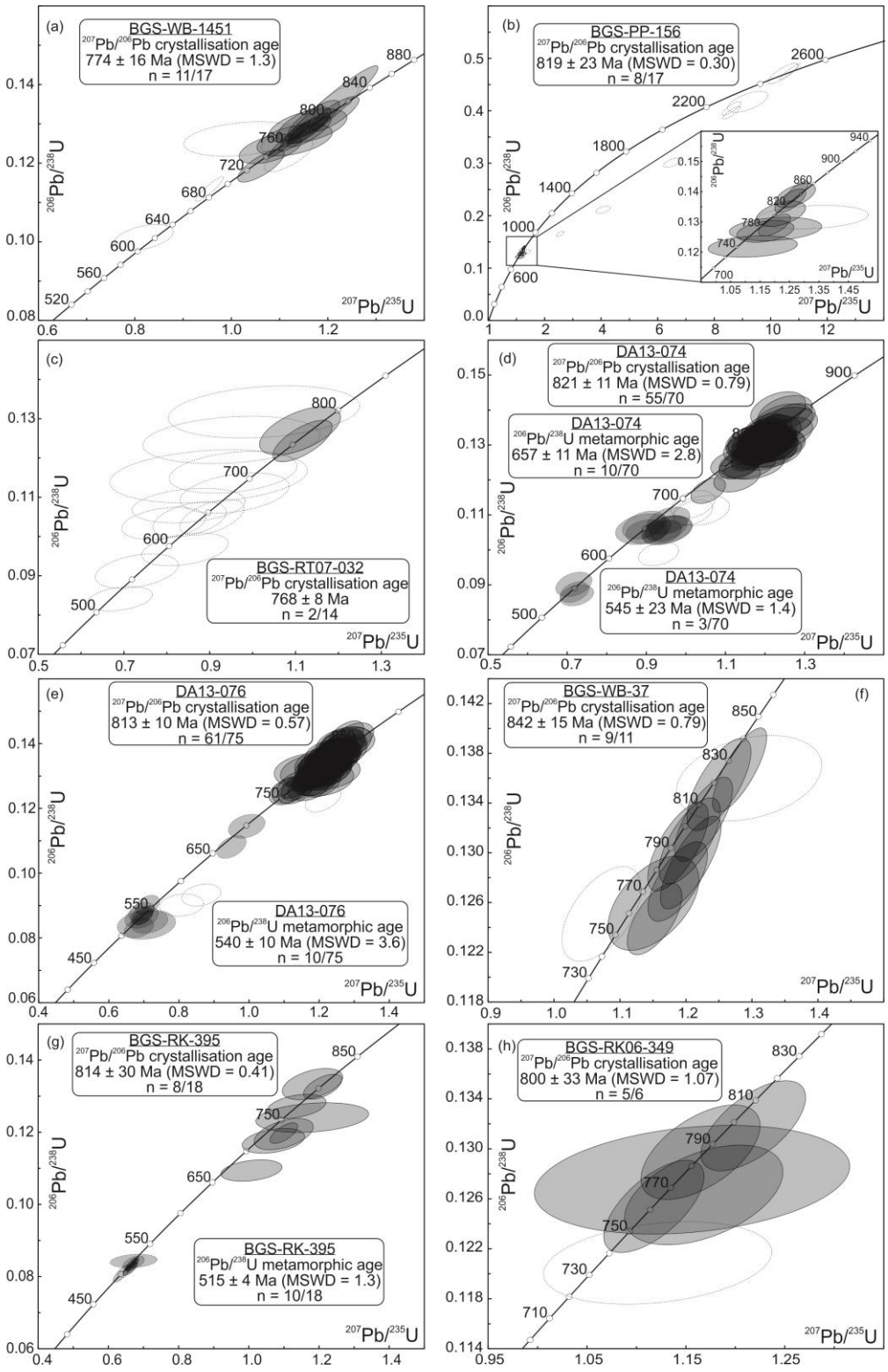

Fig. 3.7 Concordia diagrams showing zircon analyses from the Imorona-Itsindro Suite intruding the northern Antananarivo Domain: (a) BGS-WB1451; (b) BGS-PP156; (c) BGS-RT07-032, the Brickaville orthogneiss: (d) DA13-074; (e) DA13-076, and in the Masora Domain: (f) BGS-WB37; (g) BGS-RK395; and (h) BGS-RK06-349. U-Pb data are reported in Appendix 3.2. Data point error ellipses are 2σ. The interpreted age of each sample is summarised in Table 3.6. Shaded ellipses with a solid border were used in Tonian weighted-mean age calculations, shaded ellipses with a broken border were used in Ediacaran weighted-mean age calculations and open ellipses were rejected.

Table 3.5 Summary of U-Pb data and age deductions for Tonian rocks in central Madagascar.

Sample	n	n (≥95%)	Pb_c (%)	Remarks	Age (Ma)
DA14-133 (Ikal)	25	13	0.00-0.65	A cluster of concordant analyses between ~740-800 Ma yield a weighted-mean $^{207}Pb/^{206}Pb$ age of 824 ± 23 Ma (MSWD = 0.27; n=8). The weighted-mean $^{206}Pb/^{238}U$ age of the same analyses is 776 ± 16 Ma (MSWD = 3.4; n=8). Data ellipses plot slightly below concordia, consistent with lead loss. Younger concordant and discordant grains are presumably a result of Pb loss (Fig. 3.5a).	824 ± 23
DA14-140 (Ikal)	25	19	0.00-0.25	An older group of concordant data yield a weighted-mean $^{207}Pb/^{206}Pb$ age of 770 ± 21 Ma (Fig. 3.5b; MSWD = 1.10; n=8). The same analyses provide a $^{206}Pb/^{238}U$ age of 737 ± 33 Ma (MSWD = 19; n=8). In this case, the $^{207}Pb/^{206}Pb$ age is more precise and is also more reliable due to Pb loss. The cluster of younger ages yield a $^{206}Pb/^{238}U$ age of 570 ± 8 Ma (MSWD = 3.5; n=11), interpreted as the age of metamorphism.	770 ± 21
DA14-146 (Ikal)	38	32	0.00-0.36	Zircon cores and single grain analyses of similar CL domains yield a weighted-mean $^{207}Pb/^{206}Pb$ age of 774 ± 11 Ma (Fig. 3.5c; MSWD = 0.97; n=21). The same analyses yield a concordia upper intercept age of 790 ± 30 Ma (MSWD = 0.87; n=21) and a near zero lower intercept. This age is within uncertainty of the $^{207}Pb/^{206}Pb$ age. The weighted-mean $^{206}Pb/^{238}U$ age has a large MSWD (27) and uncertainty (± 21Ma) due to Pb loss. Younger concordant ages yield a weighted-mean $^{206}Pb/^{238}U$ age of 552 ± 7 Ma (MSWD = 2.1; n=9), inferred as a metamorphic age.	774 ± 11
DA13-055 (Itremo)	45	44	0.00-0.77	Analysis of concordant grains yields a $^{207}Pb/^{206}Pb$ age of 769 ± 18 Ma (Fig. 3.5d; MSWD = 1.5; n=45), a $^{206}Pb/^{238}U$ age 789 ± 7 Ma (MSWD = 2.7; n=45), and a concordia age of 780 ± 7 Ma (MSWD = 1.3; n=45). Since all 3 ages are within error, we interpret the crystallisation age to be the concordia age of 780 ± 7 Ma because it has the lowest MSWD and it lies between the $^{207}Pb/^{206}Pb$ and $^{206}Pb/^{238}U$ ages.	780 ± 7
DA13-056 (Itremo)	22	6	0.00-1.18	Weighted-mean age calculations provide $^{207}Pb/^{206}Pb$ and $^{206}Pb/^{238}U$ ages of 822 ± 28 Ma (MSWD = 0.96; n=6) and 799 ± 22 Ma (MSWD = 4.6; n=6) respectively. The $^{207}Pb/^{206}Pb$ age of 822 ± 28 Ma is more representative of the crystallisation age because of Pb loss (Fig. 3.5e).	822 ± 28
DA13-063 (Itremo)	15	11	0.00-0.24	Two Palaeoproterozoic cores analysed have $^{207}Pb/^{206}Pb$ ages of 2461 ± 25 Ma and 2439 ± 25 Ma (Fig. 3.5f). Analysis of zircon rims and Tonian grains provides a $^{206}Pb/^{238}U$ age of 798 ± 8 Ma (MSWD = 0.98; n=7) calculated with youngest concordant ages omitted from the age calculation because of inferred Pb loss. The $^{207}Pb/^{206}Pb$ age using the same data gives an age of 843 ± 38 Ma (MSWD = 2.4; n=7), The $^{207}Pb/^{206}Pb$ age has a higher MSWD so we consider the $^{206}Pb/^{238}U$ age to best representation of the crystallisation age.	798 ± 8
DA13-064 (Itremo)	60	43	0.00-0.36	Eighteen analyses of cores yielded near concordant $^{207}Pb/^{206}Pb$ ages between 2799 ± 24 and 1836 ± 26 Ma (Fig. 3.5g). The Neoarchaean to Palaeoproterozoic ages are similar to the detrital zircon ages derived from the metasedimentary Itremo Group (Cox et al., 2004) that the porphyritic granite intrudes (Fig. 3.2). Zircon rim domains and younger grains have a weighted average $^{207}Pb/^{206}Pb$ age of 819 ± 19 (MSWD = 1.18; n=25) and a $^{206}Pb/^{238}U$ age of 780 ± 10 Ma (MSWD = 5.6; n=25).	819 ± 19
DA13-065 (Itremo)	23	12 (>90%)	0.00-0.47	The >90% concordant data is used because of the limited number of zircon grains that are less than 5% discordant. Three analyses of cores yielded concordant $^{207}Pb/^{206}Pb$ ages of 2582 ± 20 Ma, 2401 ± 19 Ma, and 1853 ± 21 Ma (Fig. 3.5h). The Neoarchaean to Palaeoproterozoic ages are suggestive of detrital zircon ages derived from the metasedimentary Itremo Group (Cox et al., 2004). Zircon rim domains and younger grains have a $^{206}Pb/^{238}U$ age of 791 ± 17 Ma (MSWD = 4.3; n=9). The high discordance of many analyses results in the $^{207}Pb/^{206}Pb$ age having a large error, large analytical scatter (MSWD=17), and is unreliable.	791 ± 17
DA13-012 (C. Ant)	89	54	0.00-2.11	Xenocrystic zircon cores yield a weighted-mean $^{207}Pb/^{206}Pb$ age of 2491 ± 25 Ma (Fig. 3.6a; MSWD = 5.6; n=17). The same data yield a discordia upper intercept of 2516 ± 32 Ma (MSWD = 4.7; n=17) and a lower intercept near zero. These ages are inferred to represent inherited domains from the Betsiboka Suite. One Mesoarchaean core is also assumed to be inherited. Concordant ages of zircon rims or single grain analyses yield a weighted-mean $^{207}Pb/^{206}Pb$ age of 849 ± 17 Ma (MSWD = 1.19; n=35) and a discordia upper intercept of 843± 24 Ma (MSWD = 1.16; n=35) with a lower intercept of zero. Concordant ages between 750-850 Ma yield a $^{206}Pb/^{238}U$ age of 799 ±12 Ma (MSWD = 4.7; n=17). Including a wider age range decreases the age and increases uncertainty. Younger ages not included in age calculations are assumed to represent recrystallization during late-Neoproterozoic metamorphism or modern Pb loss. The $^{207}Pb/^{206}Pb$ age and intercept age are similar and the $^{206}Pb/^{238}U$ age has a large MSWD.	849 ± 17

Table 3.5 Summary of U-Pb data and age deductions for Tonian rocks in central Madagascar continued…

Sample	n	n (≥95%)	Pb_c (%)	Remarks	Age (Ma)
DA13-017 (C. Ant)	73	34	0.00-0.37	Five older grains vary in age between 2477 ± 29 Ma and 2681 ± 25 Ma ($^{207}Pb/^{206}Pb$ age; Fig. 3.6b). The 95% concordant data gives a $^{206}Pb/^{238}U$ age of 754 ± 11 Ma (MSWD = 4.3; n=18) and a $^{207}Pb/^{206}Pb$ age of 814 ± 19 Ma (MSWD = 1.01; n=18). The $^{207}Pb/^{206}Pb$ age is interpreted as the best estimate of the age of crystallisation. Younger concordant grains around ~550 Ma yield an imprecise $^{206}Pb/^{238}U$ age of 542 ± 30 Ma (MSWD = 5.4; n=4), interpreted to approximate the age of metamorphism. Other >95% concordant grains (n=7) not included in these age calculations are interpreted to represent Pb loss from the older populations.	814 ± 19
DA13-020 (C. Ant)	39	11	0.00-0.27	Data yield a weighted-mean $^{207}Pb/^{206}Pb$ age of 844 ± 29 Ma (MSWD = 1.4; n=11) and a $^{206}Pb/^{238}U$ age of 758 ± 10 Ma (MSWD = 2.1; n=11). Although the $^{207}Pb/^{206}Pb$ age has a lower MSWD, we interpret the $^{206}Pb/^{238}U$ age to more accurately represent the crystallisation age because concordant data cluster near concordia rather than plotting along a Pb loss trend (Fig. 3.6c).	758 ± 10
DA13-029 (C. Ant)	57	49	0.00-0.56	The oldest grains yield a $^{207}Pb/^{206}Pb$ age of 828 ± 14 Ma (Fig. 3.6d; MSWD = 0.96; n=44) and a $^{206}Pb/^{238}U$ age of 765 ± 7 Ma (MSWD = 4.9; n=44). The $^{207}Pb/^{206}Pb$ age has a lower MSWD than the $^{206}Pb/^{238}U$ age and is interpreted to best represent the crystallisation age. Two groups of younger ages give $^{206}Pb/^{238}U$ ages of 608 ± 10 Ma (MSWD = 0.92; n=3) and 544 ± 11 Ma (n=2) respectively and are inferred to represent Ediacaran reworking. Th/U ratios for the ~608 Ma analyses are between 0.17- 0.22 but the ~544 Ma have lower Th/U ratios of 0.02 and 0.07. The lower values are indicative of metamorphism (e.g. Rubatto, 2002).	828 ± 14
DA13-049 (C. Ant)	27	20	0.00-1.81	Three concordant analyses of zircon cores yield Palaeoproterozoic ages (Fig. 3.6e), interpreted to represent inheritance of Antananarivo basement material. Analysis of younger grains yields a $^{207}Pb/^{206}Pb$ age of 827 ± 16 Ma (MSWD = 0.96; n=17) and a $^{206}Pb/^{238}U$ age of 790 ± 10 Ma (MSWD = 4.4; n=17). The $^{207}Pb/^{206}Pb$ age of 827 ± 16 Ma is considered to be the best estimate of the crystallisation age.	827 ± 16
DA13-077 (C. Ant)	57	47	0.00-0.41	Data spread along concordia between ~850-750 Ma, between ~700-640 Ma and in a small cluster at ~550 Ma (Fig. 3.6f). The oldest population yield a weighted-mean $^{207}Pb/^{206}Pb$ age of 837 ± 15 Ma (MSWD = 0.75; n=33) and a $^{206}Pb/^{238}U$ age of 781.0 ± 7.6 Ma (MSWD = 4.3; n=33). The $^{207}Pb/^{206}Pb$ age is interpreted to be the most reliable. Concordant data distributed between ~700 Ma and 640 Ma yield a weighted-mean $^{206}Pb/^{238}U$ age of 658 ± 18 (MSWD = 7.3; n=9) and a $^{207}Pb/^{206}Pb$ age of 732 ± 44 (MSWD = 2.2; n=9). These data may represent zircon recrystallisation at approximately 650 Ma, or post-crystallisation Pb loss from older grains. Metamorphic rims analysed yield a $^{206}Pb/^{238}U$ age of 527 ± 9 Ma (MSWD = 1.3; n=5). Hence, we interpret the crystallisation age to be 837 ± 15 Ma with Cambrian metamorphism at 527 ± 9 Ma but the significance of the ~650 Ma grains is unclear.	837 ± 15
DA13-083 (C. Ant)	75	63	0.00-0.52	Data spread along concordia between ~825-750 Ma, between ~710- 650 Ma and in a small cluster at ~550 Ma (Fig. 3.6g). The oldest population has a weighted-mean $^{207}Pb/^{206}Pb$ age of 802 ± 12 Ma (MSWD = 1.14; n=49) and a $^{206}Pb/^{238}U$ age of 769.2 ± 7.7 Ma (MSWD = 6.5; n=49). A younger data cluster between ~710 Ma and 650 Ma give a weighted-mean $^{206}Pb/^{238}U$ age of 677 ± 11 Ma (MSWD = 3.2; n=12) and a $^{207}Pb/^{206}Pb$ age of 751 ± 30 Ma (MSWD = 0.69; n=12). The weighted-mean $^{207}Pb/^{206}Pb$ age of all concordant data is 795 ± 13 Ma (MSWD = 1.20; n=61). Because of the spread in ages, the $^{206}Pb/^{238}U$ age for all concordant data is unreliable. Th/U ratios for all concordant data between ~825-650 Ma are indistinguishable and therefore, the combined age is considered the most reliable and the analytical spread is a result of Pb loss. Two metamorphic rims analysed yield a $^{206}Pb/^{238}U$ age of 547 ± 12 Ma.	795 ± 13
BGS-TK64A (C. Ant)	21	12	0.00-0.53	Twenty-one analyses conducted on 21 zircon yielded 12 ≥ 95% concordant analyses. The data cluster around concordia (Fig. 3.6h). The weighted-mean $^{207}Pb/^{206}Pb$ age is 764 ± 16 Ma (MSWD = 0.44; n=12) and the $^{206}Pb/^{238}U$ age is 763 ± 11 Ma (MSWD = 13; n=12). We interpret the $^{207}Pb/^{206}Pb$ age of 764 ± 16 Ma to best represent the crystallisation age.	764 ± 16
BGS-WB005 (C. Ant)	19	13	0.06-4.34	Common Pb values are typically below 1% and the highest value is 4.34%. Data spread along concordia between ~875-750 Ma and two concordant ages plot at ~600 Ma (Fig. 3.6i). The oldest concordant data yield a weighted-mean $^{207}Pb/^{206}Pb$ age of 794 ± 15 Ma (MSWD = 2.1; n=12) and a weighted-mean $^{206}Pb/^{238}U$ age of 797 ± 16 Ma (MSWD = 6.1; n=12). Two concordant analyses plot above the main cluster but it is unclear whether geological meaning can be ascribed to these analyses based on CL imagery and chemistry alone. By excluding these analyses, the main cluster of concordant data yield a $^{207}Pb/^{206}Pb$ age of 789 ± 15 Ma (MSWD = 1.6; n=9). The weighted-mean $^{206}Pb/^{238}U$ age is 793 ± 7 Ma (MSWD = 1.09; n=9) and is interpreted to represent the crystallisation age. Two younger concordant ages record new zircon growth or metamorphism at ~600 Ma, analogous to other samples collected east of the Angavo-Ifandriana Shear Zone (e.g. DA13-074).	793 ± 7

Table 3.5 Summary of U-Pb data and age deductions for Tonian rocks in central Madagascar continued…

Sample	n	n (≥95%)	Pb_c (%)	Remarks	Age (Ma)
BGS-WB1451 (N. Ant)	21	11	0.00-4.28	Results show low common Pb values (<2%) except for 4 analyses. Analyses with >2% common Pb are not plotted on Fig. 3.7a. The majority of analyses define a cluster of data at ~ 775 Ma. Eleven concordant analyses yield a weighted-mean $^{207}Pb/^{206}Pb$ age of 774 ± 16 Ma (MSWD = 1.3; n=11) and a $^{206}Pb/^{238}U$ age of 773 ± 15 Ma (MSWD = 4.8; n=11). We interpret that Pb loss adequately explains the spread in data and that the $^{207}Pb/^{206}Pb$ age of 774 ± 16 Ma provides the best estimate for the crystallisation age.	774 ± 16
BGS- PP156 (N. Ant)	19	8	0.00-35.85	The data record consistently higher U and common Pb for rim domains (0.35-38.85%) compared to cores (0.01-3.44%). Two analyses on rims are not plotted in Fig. 3.7b because of their high common Pb contents. Nine analyses of zircon cores define a wide range of $^{207}Pb/^{206}Pb$ and $^{206}Pb/^{238}U$ ratios but typically show notable Pb loss. Two Palaeoproterozoic ages plot on concordia defining an age of 2485 ± 13 Ma (n=2), taken to represent inheritance. Concordant (>90%) rim data plot in a cluster near concordia (Fig. 3.7b) and yield a weighted-mean $^{207}Pb/^{206}Pb$ age of 819 ± 23 Ma (MSWD = 0.30; n=6) and a weighted-mean $^{206}Pb/^{238}U$ age of 795 ± 31 (MSWD = 17; n=6). We interpret the age of Tonian zircon growth to be represented by the $^{207}Pb/^{206}Pb$ age of 819 ± 23 Ma.	819 ± 23
BGS-RT07-032 (N. Ant)	14	2 (>90%)	0.25-1.68	Analyses indicate low common Pb with the highest values related to the lowest U zircon. Data plot over a relatively wide range of $^{206}Pb/^{238}U$ ratios and narrower range of $^{207}Pb/^{206}Pb$ ratios indicating recent Pb loss (Fig. 3.7c). Six data points (spots 3b, 5, 6, 7, 9, 10) represent the most concordant data (>90%) but four of these analyses either contain the highest common Pb (resulting in an overcorrection of these data points or appear much younger due to Pb loss. The remaining analyses (3b and 9) yield a $^{206}Pb/^{238}U$ age of 762 ± 18 Ma.	762 ± 18
DA13-074 (E. Ant)	70	68	0.00-0.34	Data show a spread of ages between ~850-700 Ma and clusters at ~650 Ma and ~550 Ma (Fig. 3.7d). The oldest population has a weighted-mean $^{207}Pb/^{206}Pb$ age of 821 ± 11 Ma (MSWD = 0.79; n=55) and a $^{206}Pb/^{238}U$ age of 788.8 ± 6.3 Ma (MSWD = 5.0; n=55).The $^{207}Pb/^{206}Pb$ age is considered the most reliable because it has a lower analytical spread. The data spread is interpreted to be caused by Pb loss. The cluster at ~650 Ma yields a $^{206}Pb/^{238}U$ age of 657 ± 11 Ma (MSWD = 2.8; n=10). The youngest group yields a $^{206}Pb/^{238}U$ age of 545 ± 23 Ma (MSWD = 1.4; n=3) and is interpreted as the age of metamorphism.	821 ± 11
DA13-076 (E. Ant)	75	72	0.00-0.49	Data show a spread of ages between ~850-750 Ma and a cluster at ~550 Ma (Fig. 3.7e). The oldest population has a weighted-mean $^{207}Pb/^{206}Pb$ age of 813 ± 10 Ma (MSWD = 0.59; n=61) and a weighted-mean $^{206}Pb/^{238}U$ age of 804 ± 6 Ma (MSWD = 5.1; n=61). Post-crystallisation Pb-loss is interpreted to be the reason that the $^{207}Pb/^{206}Pb$ age is more reliable. Two near-concordant data points plot at approximately 675 Ma and could represent older grains pulled along a discordia during Cambrian metamorphism. Rims yield a $^{206}Pb/^{238}U$ age of 540 ± 10 Ma (MSWD = 3.6; n=10), interpreted as the age of metamorphism.	813 ± 10
BGS- WB37 (Masora)	11	10 (>90%)	0.00-1.06	The >90% concordant data are used because only four analyses have >95% concordance. Common Pb values vary up to 1.06%. The $^{207}Pb/^{206}Pb$ age using only the 90% concordant data is 842 ± 15 Ma (Fig. 3.7f; MSWD = 0.79; n=10). Using the same 10 analyses, the $^{206}Pb/^{238}U$ age is 792 ± 18 Ma (MSWD = 9.6; n=10). We interpret the $^{207}Pb/^{206}Pb$ age to represent the crystallisation age because of Pb loss.	843 ± 15
BGS- RK395 (Masora)	18	3 (>90%)	0.00-20.17	Common Pb values vary up to 1.67% in concordant grains. The data form two distinct clusters (Fig. 3.7g). All zircon core data (up to 19%) discordant yield a weighted-mean $^{207}Pb/^{206}Pb$ age of 814 ± 30 Ma (MSWD = 0.41; n=8). Calculating the $^{207}Pb/^{206}Pb$ age using only the 90% concordant data (because of limited >95% concordant data) gives an imprecise age of 793 ± 49 Ma (MSWD = 0.59; n=3). The $^{206}Pb/^{238}U$ age calculated using only the 90% concordant data is 792 ± 49 Ma (MSWD = 5.3; n=3). Therefore, the weighted-mean $^{207}Pb/^{206}Pb$ age of ~814 Ma is inferred to be the more reliable estimate of the crystallisation age given the evidence for Pb loss and the large errors and higher MSWD associated with the >90% concordant data. The rim data define a cluster with a narrow range of $^{206}Pb/^{238}U$ ratios yielding a weighted-mean age of 515 ± 4 Ma (MSWD = 1.3; n=10). A concordia age of 516 ± 4 Ma can be calculated for the rims which we take to best represent the age of metamorphism.	814 ± 30
BGS- RK06-349 (Masora)	22	5	0.10-34.18	Many analyses show high common Pb values (0.10-34.18%). Data with the highest common Pb plot well away from concordia and are not included in Fig. 3.7h. Data with common Pb < 2% (n=6) define a narrow range of imprecise $^{207}Pb/^{206}Pb$ ratios. Using only the >95% concordant data, we obtain a $^{207}Pb/^{206}Pb$ age of 800 ± 33 Ma (MSWD = 1.07; n=5). The same data yield a $^{206}Pb/^{238}U$ age of 778 ± 19 Ma (MSWD = 3.0; n=5).	800 ± 33

3.5.1.6 Masora Domain

Geochronology data for the following three samples from the Andohalode subsuite were collected as part of the BGS-USGS mapping program. Masora Domain rocks sampled intrude the Palaeoarchaean Befody orthogneiss and undifferentiated Mesoarchaean schist and amphibolite of the Vohilava-Nosivolo Group (BGS-USGS-GLW, 2008; Roig et al., 2012).

Sample BGS-WB37 was collected north of Mananjary (Fig. 3.2). It is a granodiorite orthogneiss which intrudes the Nosivolo Formation of the Maha Group (which occur as xenoliths), in the Masora Domain. A gneissosity is poorly developed due to low mica content. The sample has a $^{207}Pb/^{206}Pb$ crystallisation age of 842 ± 15 Ma (Table 3.5; Fig. 3.7f).

Sample BGS-RK395 was collected ~30km northwest of Mananjary (Fig. 3.2). It is a massive granodiorite which weathers to large, rounded boulders. It is locally foliated and cut by quartz veins. The granodiorite post-dates much of the deformation and metamorphism in the host paragneiss of the Vohilava Group. The sample yielded a $^{207}Pb/^{206}Pb$ crystallisation age of 814 ± 30 Ma (Table 3.5; Fig. 3.7g).

Sample BGS-RK06/349 is biotite-granite gneiss collected ~7km north of Mananjary near the east coast (Fig. 3.2). It is a sheet-like body which intrudes the supracrustal rocks of the Vohilava Group. The sample has a $^{207}Pb/^{206}Pb$ crystallisation age of 800 ± 33 Ma (Table 3.5; Fig. 3.7h).

3.5.2 Oxygen and hafnium isotope results

3.5.2.1 Ikalamavony Domain

Thirty-five oxygen isotope analyses were carried out on three granite samples (DA14-133, DA14-140, DA14-146) intruding the Ikalamavony Domain including 23 Tonian-aged and 12 Ediacaran-aged concordant zircon grains. Results for Tonian-aged zircon domains vary between 5.16 ± 0.55 ‰ to a maximum value of 10.24 ± 0.55 ‰ (Appendix C). Although several analyses plot within the mantle range, the majority of analyses have $\delta^{18}O$ values higher than mantle-derived zircon (Valley et al., 1998; Fig. 3.8a). Analyses of Ediacaran metamorphic zircon have a similar mean $\delta^{18}O$ value of 6.57 ± 1.71 ‰ (2σ; n=12). Two sigma error values (Fig. 3.8a; Appendix 3.3) are higher for these three samples because O isotope data were collected using a SHRIMP II rather than the SHRIMP SI. The SHRIMP SI (used for all other samples) is designed for collecting stable isotope data and generates more precise data.

Seventeen $^{177}Hf/^{176}Hf$ ratios analyses included 14 analyses of Tonian zircon and three analyses of Ediacaran zircon. $\varepsilon_{Hf}(t)$ values vary between -4.2 ± 4.2 and +14.0 ± 3.6 (Fig. 3.9a). These samples have significantly larger 1σ uncertainties than zircon grains analysed from other samples. Large uncertainties are attributed to high REE concentrations, thus creating additional uncertainty due to the extent of the ^{176}Yb interference on ^{176}Hf measurements (Appendix D) and very short analysis time due to the thin nature of the analysed zircon grains after mounting and polishing. $T_{DM}c$ model ages vary from 0.8Ga and 1.9 Ga (Appendix 3.4).

3.5.2.2 Itremo Domain

Thirty-one O isotope analyses were conducted on concordant zircon from one intermediate sample (DA13-055) and three porphyritic granite samples (DA13-063, DA13-064 and DA13-065). Of these analyses, 27 are from Tonian-aged zircon domains and four are

from inherited Palaeoproterozoic zircon cores. $\delta^{18}O$ values form a narrow range (4.38 ± 0.33 ‰ to 5.85 ± 0.16 ‰) for the intermediate sample with an average of 5.43 ± 0.82 ‰ (2σ; n=9; Appendix 3.3). These $\delta^{18}O$ values are within the range of mantle derived zircon (Valley et al., 1998; Fig. 3.8b). Twenty-two analyses on felsic samples included four analyses of Palaeoproterozoic zircon cores. Core values are between 5.75 ± 0.18 ‰ and 7.48 ± 0.14 ‰ (1σ; n=4). Tonian-aged zircon have values between 1.91 ± 0.20 ‰ and 5.95 ± 0.15 ‰ (Fig. 3.8b).

Thirty-one analyses of $^{177}Hf/^{176}Hf$ ratios in zircon were conducted on four samples of Tonian-aged rocks from the Itremo Domain (Fig. 3.9b). Nine analyses on one intermediate sample (DA13-055) give a mean $\varepsilon_{Hf}(t)$ value of -11.6 ± 0.8 and $T_{DM}c$ model ages between 2.3 Ga and 2.4 Ga (Appendix 3.4). The remaining twenty-two analyses on three porphyritic granite samples include eighteen analyses of Tonian domains and four analyses of Palaeoproterozoic cores. Inherited core domains have less evolved $\varepsilon_{Hf}(t)$ values between +2.8 ± 1.8 and +12.9 ± 1.4 while Tonian-aged zircon domains vary between -37.3 ± 1.9 and -15.2 ± 1.3 (Fig. 3.9b). $T_{DM}c$ model ages are older than those observed in the Ikalamavony Domain (2.6 - 4.0 Ga).

3.5.2.3 Central Antananarivo Domain

Ninety-nine O isotope analyses were performed on concordant zircon from nine granitoid samples intruding the Antananarivo Domain. Eight analyses of Neoarchaean to Palaeoproterozoic inherited cores in sample DA13-017 yield $\delta^{18}O$ values between 3.58 ± 0.25 ‰ and 6.94 ± 0.25 ‰. Tonian-aged zircon from all nine samples has $\delta^{18}O$ values between 2.75 ± 0.23 ‰ and 8.33 ± 0.25 ‰. Individual samples show minor variation in $\delta^{18}O$ values while other samples behave coherently (Appendix 3.3). Coherent samples DA13-012, DA13-029, DA13-049, DA13-083 and BGS-TK64a all have values that plot within or slightly above mantle values (Fig. 3.8c). DA13-020 (4.92 ± 0.50 ‰; 2σ; n=14), DA13-077 (4.21 ± 1.10 ‰; 2σ; n=8) and BGS-WB005 (3.64 ± 0.88 ‰; 2σ; n=6) have $\delta^{18}O$ values near the lower extent or below values expected for mantle derived zircon (Valley et al., 1998). Analyses of Tonian-aged domains in DA13-017 are highly variable (4.46 ± 0.25 to 8.33 ± 0.25 ‰). This sample likely experienced open system behaviour during Ediacaran/Cambrian time as shown by the presence of metamorphic overgrowths (Fig. 3.4). The younger thermal and hydrothermal events seemingly modified the original $\delta^{18}O$ values. Data for metamorphic domains in 3 samples are between 0.61 ± 0.27 ‰ and 8.03 ± 0.25 ‰ (n=14).

Ninety-seven $^{177}Hf/^{176}Hf$ ratios were collected from nine samples from the Central Antananarivo Domain. Analyses included seven Neoarchaean to Palaeoproterozoic core domains, 82 analyses of Tonian-aged zircon, and eight measurements of metamorphic zircon (Appendix D). The Neoarchaean to Palaeoproterozoic cores have $\varepsilon_{Hf}(t)$ values between +2.4 ± 1.9 and +15.2 ± 2.2 (Fig. 3.9c). Tonian zircon demonstrates a wide range of $\varepsilon_{Hf}(t)$ values varying between -24.9 ± 1.3 to a maximum value of -5.1 ± 1.8 (Fig. 3.9c). $T_{DM}c$ model ages for Tonian-aged zircon vary from 2.0 Ga and 3.2 Ga and resemble the measured ages of units within the Antananarivo Domain (Table 3.1). Metamorphic zircon have $\varepsilon_{Hf}(t)$ values between -27.5 ± 4.0 and-13.7 ± 1.3.

5.2.4 Northern Antananarivo Domain

Thirteen O isotope analyses were conducted on concordant zircon from three samples of Tonian age including one analysis of a Palaeoproterozoic zircon core from the Northern Antananarivo Domain (Fig. 3.8d). The Palaeoproterozoic core has a $\delta^{18}O$ value of 4.32 ± 0.35.Tonian-aged zircon display a wide range in values between 1.69 ± 0.13 ‰ and 9.43 ±

0.36 ‰ (Appendix 3.3). Two samples have $\delta^{18}O$ values higher than expected for mantle derived zircon (mean = 7.77 ± 2.40 ‰; 2σ; n=6) and the third sample has considerably lower values (mean = 3.86 ± 2.16 ‰; 2σ; n=6).

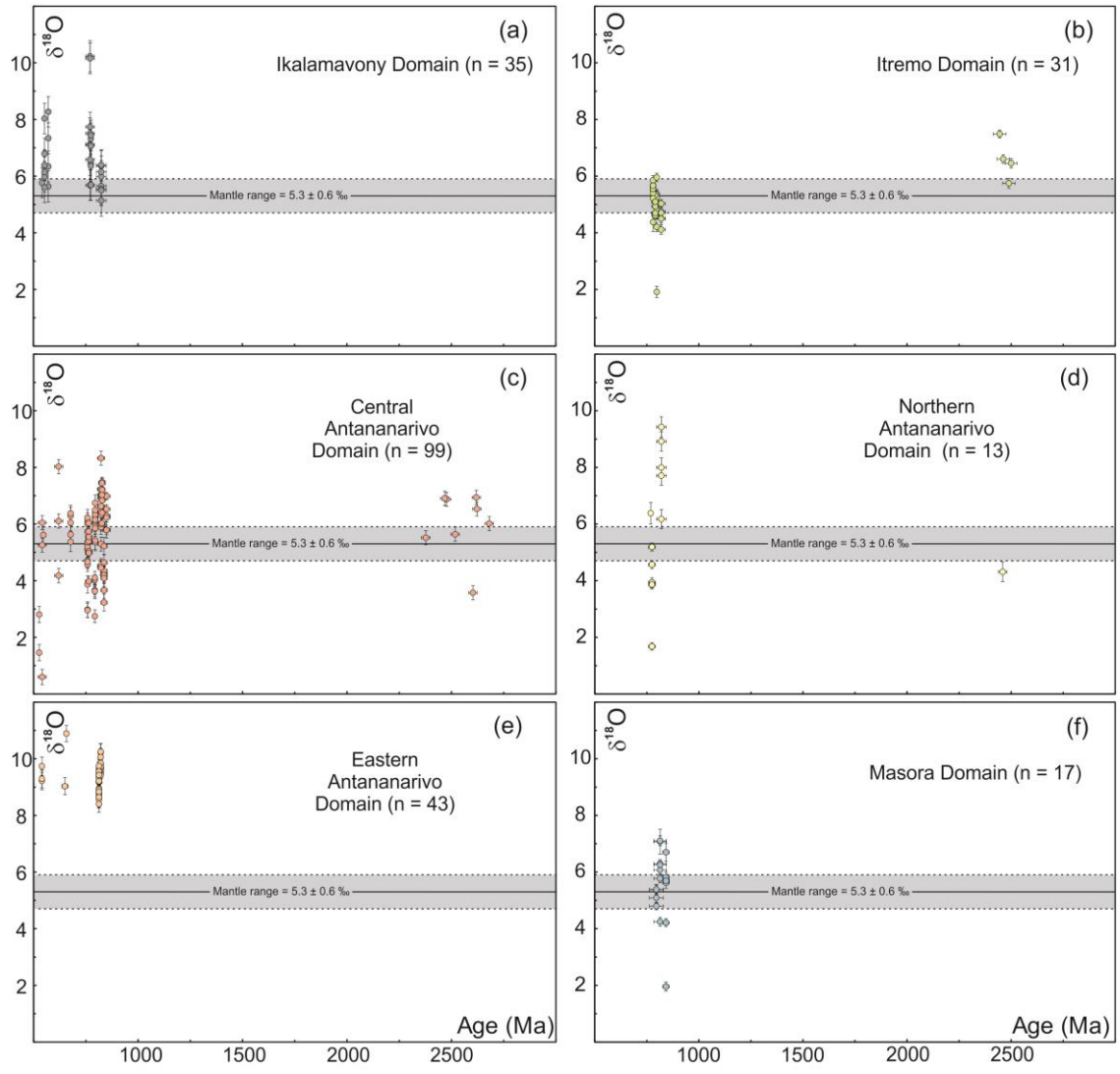

Fig. 3.8 $\delta^{18}O$ plotted against the interpreted crystallisation age for analyses of Imorona-Itsindro Suite samples: (a) Ikalamavony; (b) Itremo; (c) Central Antananarivo; (d) Northern Antananarivo; (e) Eastern Antananarivo; and (f) Masora Domains. Error bars are 2σ. Range of mantle derived $\delta^{18}O$ (zircon) values are 5.3 ± 0.6 ‰ (2σ; Valley et al., 1998).

Fifteen analyses of $^{177}Hf/^{176}Hf$ ratios on Tonian-aged zircon and one Palaeoproterozoic core analysis were performed on three samples of the Imorona-Itsindro Suite intruding the Northern Antananarivo Domain (Fig. 3.9d).The Palaeoproterozoic core has a $\varepsilon_{Hf}(t)$ value of +4.1 ± 0.9. $\varepsilon_{Hf}(t)$ values for Tonian-aged zircon range from -24.2 ± 1.9 to -9.5 ± 1.2. $T_{DM}c$ model ages (2.3 to 3.1 Ga) resemble the measured ages of units within the Antananarivo Domain (Table 3.1).

3.5.2.5 Eastern Antananarivo Domain (Brickaville Orthogneiss)

Forty-three O isotope analyses were conducted on concordant zircon from two samples of the Brickaville orthogneiss including five analyses of metamorphic zircon. Results vary between 8.40 ± 0.29 ‰ to a maximum value of 10.24 ± 0.29 ‰ (Appendix 3.3). These values on average are higher than other analyses on Tonian-aged zircon in Madagascar. All

analyses plot above the range expected for mantle derived zircon (Fig. 3.8e). The mean $\delta^{18}O$ value is 9.38 ± 0.88‰ (2σ; n=38). Five metamorphic zircon domains have $\delta^{18}O$ values between 9.03 ± 0.30 ‰ and 10.88 ± 0.29 ‰.

Twenty-nine analyses of $^{177}Hf/^{176}Hf$ ratios in Tonian-aged zircon yield $\varepsilon_{Hf}(t)$ values between -6.1 ± 0.9 and -12.3 ± 0.4 (Fig. 3.9e). Tonian zircon has $T_{DM}c$ model ages between 2.4 Ga and 2.7 Ga. Two analyses of metamorphic zircon yield negative $\varepsilon_{Hf}(t)$ values of -16.6 ± 0.7 and -19.6 ± 0.4.

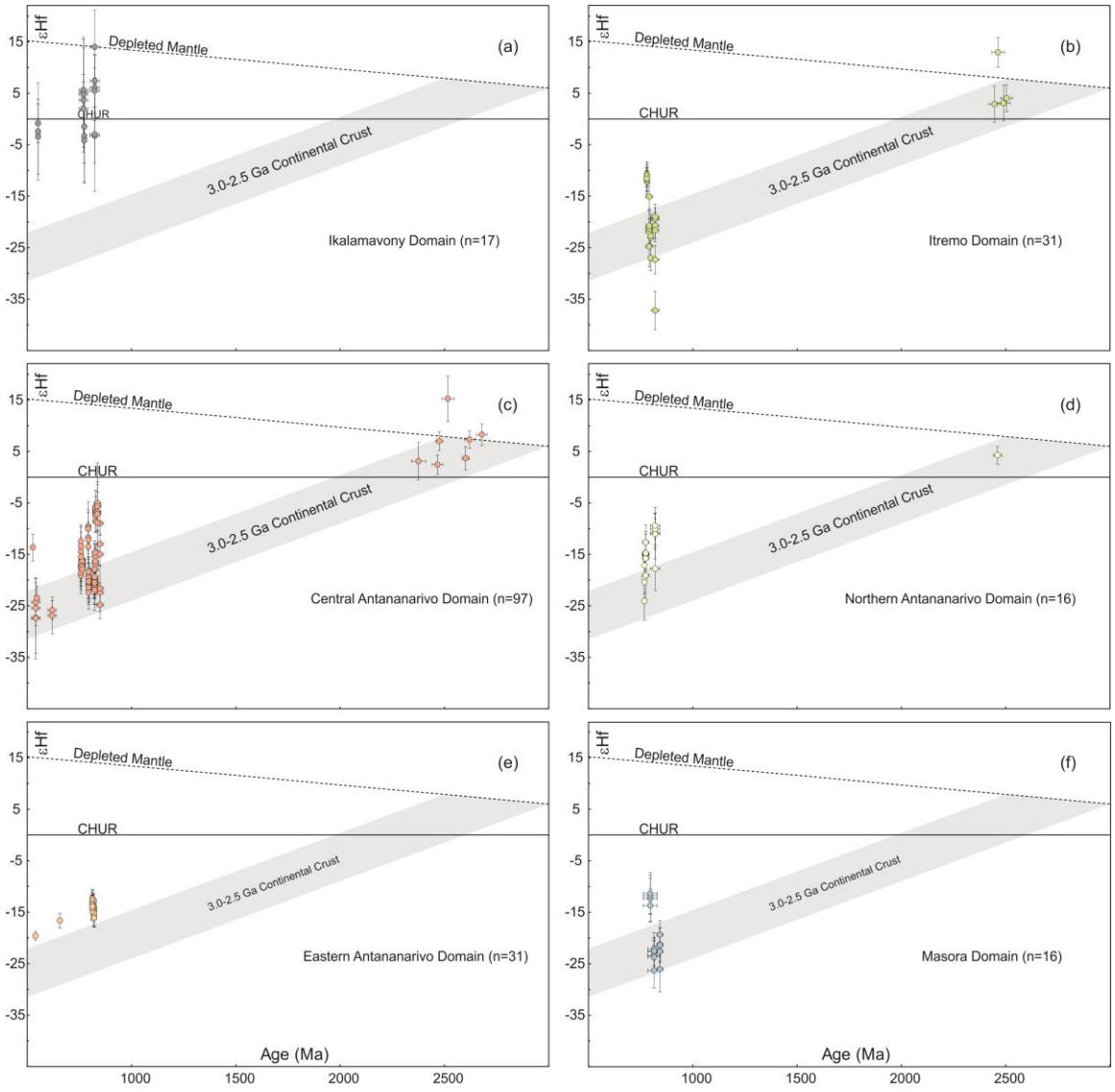

Fig. 3.9 $\varepsilon_{Hf}(t)$ plotted against the interpreted crystallisation age for analyses of Imorona-Itsindro Suite samples: (a) Ikalamavony; (b) Itremo; (c) Central Antananarivo; (d) Northern Antananarivo; (e) Eastern Antananarivo; and (f) Masora Domains. Error bars are 2σ. The $T_{DM}c$ Hf evolution field of 3.0 – 2.5 Ga crust is based on a $^{176}Lu/^{177}Hf$ ratio of 0.015 (Griffin et al., 2004). DM - depleted mantle. CHUR - chondrite uniform reservoir.

3.5.2.6 Masora Domain

Seventeen O isotope analyses were collected on concordant zircon from three Tonian-aged samples intruding the Masora Domain (Fig. 3.8f). Results vary between 1.95 ± 0.16 ‰ and 7.10 ± 0.18 ‰ (Appendix 3.3). Most analyses plot within or slightly higher than mantle derived zircon (Valley et al., 1998; Fig. 3.8f).

Sixteen analyses of $^{177}Hf/^{176}Hf$ ratios on Tonian zircon were performed on three samples from the Masora Domain (Fig. 3.9f). $\varepsilon_{Hf}(t)$ values are highly variable between -26.3 ± 1.7 to -11.3 ± 2.0. $T_{DM}c$ model ages are between 2.4 Ga and 3.3 Ga, comparable to ages found in the Masora Domain basement (Table 3.1).

Table 3.6 Summary of all Imorona-Itsindro Suite zircon U-Pb, $\delta^{18}O$, and $\varepsilon_{Hf}(t)$ isotopic data.

	U-Pb Age Data (Ma)			Isotope Data		
Sample Number	Inheritance	Crystallisation	Metamorphism	$\delta^{18}O$ (‰; 1s)	$\varepsilon_{Hf}(t)$ (1σ)	T_{DM} (Ga)
DA14-133	-	824 ± 23	-	5.88 ± 0.42	+4.4 ± 6.0	1.4 ± 0.4
DA14-140	-	770 ± 21	570 ± 8	6.97 ± 0.67	+4.2 ± 1.3	1.4 ± 0.1
DA14-146	-	774 ± 11	552 ± 7	6.69 ± 0.58	-3.0 ± 1.1	1.8 ± 0.1
DA13-055	-	780 ± 7	-	5.43 ± 0.41	-11.6 ± 0.4	2.4 ± 0.1
DA13-056	-	822 ± 28	-	-	-	-
DA13-063	Palaeoproterozoic	798 ± 8	-	5.15 ± 0.54	-22.2 ± 0.9	3.0 ± 0.1
DA13-064	Neoarchaean to Palaeoproterozoic	819 ± 19	-	4.60 ± 0.28	-21.7 ± 3.0	3.0 ± 0.2
DA13-065	Neoarchaean to Palaeoproterozoic	791 ± 17	-	4.93 ± 0.26	-20.8 ± 3.2	2.9 ± 0.2
DA13-012	Archaean	849 ± 17	-	6.27 ± 0.42	-19.5 ± 4.6	2.9 ± 0.3
DA13-017	Neoarchaean to Palaeoproterozoic	814 ± 19	542 ± 30	6.34 ± 1.06	-20.5 ± 1.2	3.0 ± 0.1
DA13-020	-	758 ± 10	-	4.92 ± 1.01	-16.6 ± 1.8	2.7 ± 0.1
DA13-029	-	828 ± 14	610 ± 8 & 544 ± 11	6.98 ± 0.33	-7.1 ± 0.8	2.1 ± 0.1
DA13-049	-	827 ± 16	-	6.89 ± 0.52	-15.9 ± 0.9	2.7 ± 0.1
DA13-077	-	837 ± 15	646 ± 13 & 527 ± 9	4.21 ± 0.56	-6.6 ± 1.3	2.1 ± 0.1
DA13-083	-	795 ± 13	547 ± 12	6.12 ± 0.38	-20.4 ± 1.0	2.9 ± 0.1
BGS-TK 64a	-	764 ± 16	-	5.46 ± 0.37	-19.9 ± 0.6	2.7 ± 0.1
BGS-WB 005	-	793 ± 7	~600	3.64 ± 0.44	-11.2 ± 1.4	2.4 ± 0.1
BGS-WB 1451	-	774 ± 16	-	3.86 ± 1.08	-15.5 ± 1.9	2.6 ± 0.1
BGS-PP 156	2485 ± 13	819 ± 23	-	8.05 ± 1.12	-10.5 ± 0.6	2.3 ± 0.1
BGS-RT07-032	-	762 ± 18	-	6.39 ± 0.38	-20.4 ± 2.5	2.9 ± 0.2
DA13-074	-	821 ± 11	657 ± 11 & 545 ± 23	9.75 ± 0.24	-14.7 ± 0.9	2.6 ± 0.1
DA13-076	-	813 ± 10	~675 & 540 ± 10	9.14 ± 0.37	-13.6 ± 0.7	2.5 ± 0.1
BGS-WB 37	-	843 ± 15	-	5.60 ± 0.80	-22.1 ± 2.2	3.1 ± 0.1
BGS-RK 395	-	814 ± 30	516 ± 4	6.11 ± 0.89	-23.4 ± 1.3	3.1 ± 0.1
BGS-RK06/349	-	800 ± 33	-	5.15 ± 0.24	-12.3 ± 0.9	2.4 ± 0.1

3.6 Discussion

3.6.1 Zircon U-Pb geochronological data for the Imorona-Itsindro Suite

Voluminous Tonian magmatic rocks are preserved in central Madagascar represented by the Imorona-Itsindro Suite. The suite comprises a range of lithologies including various granitoids, gabbro, and syenite with varying isotopic signatures characterizes this complex suite. New zircon U-Pb age data presented here agree with geochronological data previously reported by several authors (Handke et al., 1999; Tucker et al., 1999a; Tucker et al., 1999b; Kröner et al., 2000; Tucker et al., 2007; BGS-USGS-GLW, 2008; CGS, 2009a; Tucker et al., 2014; Yang et al., 2014; Zhou et al., 2015b). These earlier age data were collected using a variety of methods including isotope dilution, SHRIMP, LA-ICP-MS, and $^{207}Pb/^{206}Pb$ evaporation. $^{207}Pb/^{206}Pb$ evaporation ages (Guerrot et al., 1991; Kröner et al., 1999b; Kröner et al., 2000) are not considered further because these ages only provide a minimum emplacement age (e.g. Paquette et al., 2003). Furthermore, recent work demonstrates that some isotope dilution ages may be also be unreliable due complex growth zoning in some zircon grains (Nedelec et al., 2015). They demonstrate that previously reported ID-TIMS ages for the ~630 Ma Kiangara Suite (Nédélec et al., 1994; Paquette and Nédélec, 1998) may in

fact result from Tonian, ~790 Ma magmatic cores with Ediacaran to Cambrian metamorphic overprints (Nedelec et al., 2015). Consequently, the extent of the Imorona-Itsindro Suite may be significantly greater than previously reported (Besairie, 1964; Besairie, 1968-1971; BGS-USGS-GLW, 2008; Roig et al., 2012; Tucker et al., 2014). These findings highlight the importance of using micro-beam analytical methods when studying complicated zircon such as those found in this study. However, since isotope dilution age data represent a major component (42 ages) of the geochronological database for the Imorona-Itsindro Suite; these ages are included in the following discussion.

The oldest rocks classified as part of the Imorona-Itsindro Suite are 852 ± 6 Ma (Ikalamavony Domain; CGS, 2009), while the youngest age of 727 ± 8 Ma is found in the Tsaratanana Domain (Yang et al., 2014). Tonian magmatism was essentially continuous from ~850-750 Ma (n=106; Fig. 3.10), but there were several pulses of increased activity, particularly at ~800 Ma, ~791 Ma and ~784 Ma (Fig. 3.10). The majority of the preserved Tonian-aged magmatic rocks are in the core of the Antananarivo, Itremo and Ikalamavony Domains with ages between ca. 810 Ma and 770 Ma (Fig. 3.10). Although there are many exceptions, moving to the north and west in central Madagascar, the rocks become younger (Figs. 2 and 10). The youngest Imorona-Itsindro Suite rocks occur in the Tsaratanana Domain and are coeval with those collected in the Bemarivo Belt (Fig. 3.1b). The youngest sample dated in the Bemarivo Domain is 705 ± 6 Ma (Thomas et al., 2009) and because no rocks older than ~760 Ma are reported it is probable that this region represents a separate terrane with a different Proterozoic history (Thomas et al., 2009; Goodenough et al., 2010). Thomas et al. (2009) suggested that the Bemarivo Domain developed as a juvenile Neoproterozoic arc that combined with the Antananarivo/Antongil Craton during the Cryogenian to Ediacaran. These rocks are not part of the Imorona-Itsindro Suite as suggested by Boger et al., (2014) and are excluded from the foregoing discussion, which is restricted to rocks with crystallisation ages between ~850 Ma and ~750 Ma.

3.6.2 Oxygen and hafnium isotopes in the Imorona-Itsindro Suite

Mantle-derived magmas and those sourced by partial melting of crustal rocks are well discriminated by O isotopes (Taylor Jr, 1980; Valley et al., 1994). Zircon in equilibrium with mantle-derived melts have a restricted range of $\delta^{18}O$ (5.3 ± 0.6 ‰; Valley et al., 1998) and this value is insensitive to magmatic differentiation (Valley et al., 2005). Sedimentary rocks and derived gneisses tend to have heavy $\delta^{18}O$ values (> +8), while meteoric water is relatively light (e.g. Valley et al., 2005). The origin of low $\delta^{18}O$ values are often attributed to hydrothermal cycling of meteoric water into shallow intrusions or by the alteration of rocks by meteoric fluids (Valley et al., 2005). Hf isotope systematics applied to petrogenetic studies of igneous rocks is another powerful tool in determining the source components of magmas (Belousova et al., 2006; Kemp et al., 2007; Belousova et al., 2010).

Tonian-aged zircon extracted from rocks in central Madagascar varies in their $\delta^{18}O$ and $\varepsilon_{Hf}(t)$ values across all lithotectonic domains (Fig. 3.11). $\delta^{18}O$ values in the Ikalamavony Domain are on average higher than mantle values (Fig. 3.11a) indicating partial melting of sedimentary material or crustal assimilation in magma genesis. Tonian-aged samples typically have negative $\varepsilon_{Hf}(t)$ values with the exception of those intruding the Ikalamavony Domain (Fig. 3.11b). These samples have considerably higher $\varepsilon_{Hf}(t)$ values (-3.5 to +14.0) than recorded in Tonian-aged samples analysed from the other tectonic domains (Table 3.6; Fig. 3.11b). The Ikalamavony Domain basement consists of a Mesoproterozoic volcanic and metasedimentary sequence (Ikalamavony Group) in association with possible coeval gabbroic and granitoid orthogneiss of the Dabolava Suite (Table 3.1; CGS, 2009a). Dabolava Suite intrusions were originally classified as part of the Imorona-Itsindro Suite (Moine, 1963;

Besairie, 1968-1971, 1969-1971), but recent work has shown some of them to be Stenian to early Tonian in age (~1080-980 Ma; D.B Archibald, unpublished; CGS, 2009a; Tucker et al., 2007; Rakotoarimanana, 2001). $\varepsilon_{Hf}(t)$ data for the Dabolava Suite shows positive $\varepsilon_{Hf}(t)$ values between +7 and +16 indicating a more depleted mantle-like source with some contamination for these rocks (D.B. Archibald, unpublished). Dabolava Suite Hf data recalculated to800 Ma give $\varepsilon_{Hf}(t)$ values between +2.7 and +10.1, values that are consistent with those recorded in Tonian-aged samples. We therefore suggest melting of less evolved Ikalamavony Domain crustal material as the possible source of the Tonian-aged rocks in the Ikalamavony Domain.

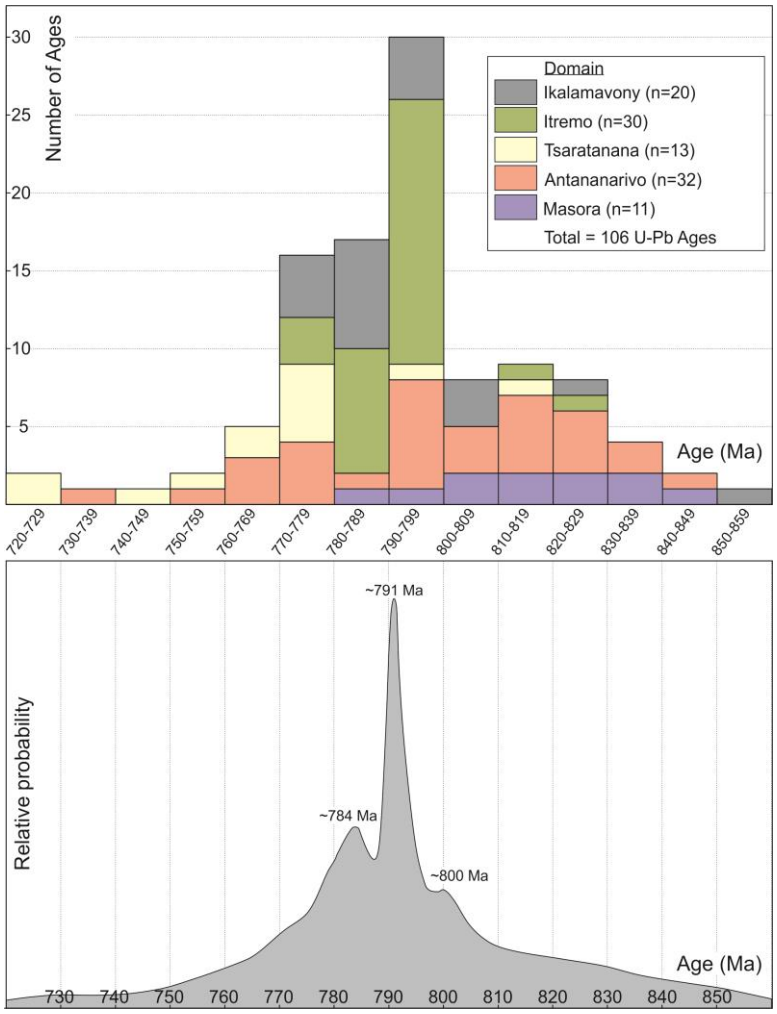

Fig. 3.10 Histogram and probability density plot of all reliable (as indicated in the text) magmatic crystallisation ages for the Imorona-Itsindro Suite intruding the Masora, Antananarivo, Tsaratanana, Itremo, and Ikalamavony Domains in Madagascar (Raoelison, 1997; Handke et al., 1999; Tucker et al., 1999a; Tucker et al., 1999b; Kröner et al., 2000; Collins et al., 2003c; Kabete et al., 2006; Tucker et al., 2007; BGS-USGS-GLW, 2008; CGS, 2009a, b; Tucker et al., 2011a; Tucker et al., 2011b; Yang et al., 2014; Zhou et al., 2015b). Also included are the new data presented in this study.

$\delta^{18}O$ values in the Itremo Domain all plot within or slightly below, the mantle range (Fig. 3.11a). These light values are surprising and noteworthy because, as evidenced by metasedimentary xenoliths and inherited zircon cores, it is clear that Tonian magmas digested what may be expected to be relatively high $\delta^{18}O$ (heavy) crustal material of the Itremo Group (i.e. samples DA13-063, DA13-064, DA13-065). We suggest shallow hydrothermal cycling of meteoric fluids reduced higher $\delta^{18}O$ values. This view is supported by suggestions that the

metasedimentary rocks of the Itremo Group were near surface during the emplacement of Tonian magmas (Moine, 1967; Moine, 1974). Itremo Domain samples yield negative $\varepsilon_{Hf}(t)$ values (Fig. 3.11b) consistent with Tonian-aged magmas assimilating considerable amounts of the metasedimentary Itremo Group (Table 3.1).

The diversity of $\delta^{18}O$ and $\varepsilon_{Hf}(t)$ values from Tonian-aged zircon from the Antananarivo Domain (including the Northern Antananarivo Domain) emphasizes the heterogeneity of potential source materials (Table 3.1). The Neoarchaean to Palaeoproterozoic basement of the Antananarivo Domain primarily consists of quartzofeldspathic paragneiss and graphitic schist (Vondrozo Group), quartzite, schist and quartz-rich paragneiss (Sofia Group) and the mainly felsic orthogneiss of the Betsiboka Suite (Besairie, 1968-1971; BGS-USGS-GLW, 2008; Roig et al., 2012; Tucker et al., 2014). Low $\delta^{18}O$ values (<4.21± 0.56 ‰) recorded from three samples (DA13-077, BGS-WB005, BGS-WB1451) indicate shallow, sub-volcanic intrusions where there was convection of meteoric fluids. Further investigation into the origin of low $\delta^{18}O$ values in central Madagascar is required to resolve their significance. Average $\varepsilon_{Hf}(t)$ values for each sample vary from -20.5 ± 1.2 (DA13-017) to -6.6 ± 1.3 (DA13-077). The most evolved values are from a sample that possibly intrudes the Ambatolampy Group although a clear contact relationship has yet to be observed (Archibald et al., 2015). This data suggests that some Tonian-aged magmas incorporated considerable Archaean to Palaeoproterozoic crust. This hypothesis is supported by Nd isotopic data and zircon inheritance from other Tonian-aged samples from the Antananarivo Domain from Kröner et al. (2000), who suggested the rocks were generated by subduction beneath an the Archaean to early Proterozoic block. The highest values obtained are from samples located near the suggested location of the Betsimisaraka Suture (Collins and Windley, 2002; Collins, 2006) or the intracontinental rift suggested by Tucker et al. (2011a) in which the Manampotsy Group was deposited (Fig. 3.1b).

Considerably higher $\delta^{18}O$ values (>8.4‰; Appendix 3.3) recorded in the Brickaville orthogneiss in eastern Madagascar clearly show that these intrusions had a sedimentary protolith. This protolith is presumed to be the nearby Manampotsy Group (Table 3.1) which has a similar maximum depositional age to the crystallisation age of the Brickaville orthogneiss (BGS-USGS-GLW, 2008). Geochronological data for the Manampotsy Group show a near unimodal distribution of ages between ~837-791 Ma which led the BGS-USGS-GLW (2008) to infer deposition as felsic volcanic rocks. The absence of zircon older than 840 Ma suggests isolated deposition, distal to older crustal sources such as the Antongil, Masora and Antananarivo Domains (Key et al., 2011). The lack of older inherited zircon grains and the similarity in maximum depositional age of the likely source to the Brickaville orthogneiss with its crystallisation age suggesting an origin within a volcanic arc, either an oceanic arc, or, possibly more likely, a fore-arc depositionally isolated from the more mature continental arc to the east. Metasedimentary bands and xenoliths within the Brickaville orthogneiss are common and are interpreted as ‘restites’ of the country rocks (this study; BGS-USGS-GLW, 2008). $\varepsilon_{Hf}(t)$ values between -14.7 ± 0.9 and -13.6 ± 0.7 are indistinguishable from $\varepsilon_{Nd}(t)$ data (-16.2 and -14.4) for Brickaville orthogneiss samples (BGS-USGS-GLW, 2008). These Hf and Nd isotopic data support the O isotope data indicating crustal involvement during genesis of the Brickaville orthogneiss.

$\delta^{18}O$ values for Tonian-aged zircon in the Masora Domain all plot within the mantle range (Valley et al., 1998) indicating hydrothermal alteration similar to that proposed for some Antananarivo and Itremo Domain intruding samples. These samples have $\varepsilon_{Hf}(t)$ values between -12.3 ± 0.9 and -23.4 ± 1.3 (Appendix 3.3). The contrasting $\delta^{18}O$ values and $\varepsilon_{Hf}(t)$ values in the Masora Domain are explained by the infiltration of meteoric fluids into crystallising magmas resulting in lower than expected $\delta^{18}O$ values.

3.6.3 Temporal and spatial distribution of U-Pb, O and Hf isotopic data

When the O and Hf isotope data are plotted against age for the same zircon grains, they reveal discrete trends that can be interpreted to indicate changing magma source/assimilation characteristics that in turn are interpreted to relate to changing tectonic conditions (Fig. 3.11). The O isotope against time trend for samples east of the Ikalamavony Domain demonstrate a decrease in $\delta^{18}O$ values from heavier than mantle values at ~850 Ma to near mantle values at ~840 Ma. A sharp increase in $\delta^{18}O$ values then occurs, reaching a maximum at ~820-810 Ma returning to near mantle values from ~ 800 to 775 Ma (Fig. 3.11a). A third spike to supra-mantle values occurs at ~770 Ma decreasing to ~760 Ma. These cycles suggest episodes of supracrustal assimilation evolving to "mantle-like" signatures and even to below mantle values in some samples. Contemporaneous patterns in Hf isotopic data broadly mirror the O isotopic changes, especially between ~850-820 Ma where lower $\varepsilon_{Hf}(t)$ values reflect higher $\delta^{18}O$ values, although trends are less pronounced because variations in some individual samples are high (Fig. 3.11b). Variations within a single sample are explained by open system processes capable of shifting the $^{176}Hf/^{177}Hf$ ratio of the melt from which the zircon crystallised (Kemp et al., 2007). An inverse relationship between $\varepsilon_{Hf}(t)$ and $\delta^{18}O$ temporal trends are expected because significant involvement of supracrustal material results in high $\delta^{18}O$ values and involvement of all crustal material results in negative $\varepsilon_{Hf}(t)$ values. In contrast, increased depleted-mantle input results in low $\delta^{18}O$ values and less evolved $\varepsilon_{Hf}(t)$ values. The evolutionary trends shown on the O diagram (Fig. 3.11a) are broadly similar to their inverse trends on the Hf diagram (Fig. 3.11b). Ikalamavony Domain samples (dark grey symbols) are not included in these evolutionary trends because these rocks were almost certainly incorporated different crustal material compared to the other samples.

Often spatial variations in isotopic data are overlooked in lieu of more conventional time-based plots. However, analysing the spatial distribution of isotopic data can provide valuable information especially when dealing with a complex dataset such as that of the Imorona-Itsindro Suite. Spatial variations in isotopic data are discussed focussing on longitudinal variations (Fig. 3.12) because of the general N-S strike of geological units in Madagascar (Figs. 3.1b and 3.2), and the proposition that the Imorona-Itsindro Suite is a product of plate margin processes, either due to westward-directed subduction (Collins and Windley, 2002; Collins, 2006) or eastward-directed subduction (Tucker et al., 2011b; Boger et al., 2014, 2015). Readily discernible spatial trends in U-Pb geochronological data are ambiguous to non-existent (Fig. 3.12a). Broadly, however, the rocks decrease in age from east to west even though the oldest age obtained comes from the Ikalamavony Domain in western Madagascar (CGS, 2009b). A large cluster of data between 800-780 Ma is recorded in the Itremo region (~ 46 to 47° E) but whether this represents a geologically meaningful feature or is an artefact of data availability remains unclear.

Spatial variations in $\delta^{18}O$ values are more apparent (Fig. 3.12b). In the easternmost part of central Madagascar, the Brickaville orthogneiss clearly had a sedimentary protolith as indicated by the high $\delta^{18}O$ values. Moving west, Tonian intrusive samples in the Antananarivo and Masora Domains yield mantle to below mantle values, implying cycling of meteoric fluids in shallow intrusions in such volumes as to decrease in $\delta^{18}O$ values for magmas derived from crustal material. Continuing west from approximately 48° 00' to 46° 42' E, $\delta^{18}O$ values initially plot within the mantle range then 'fan out' to values both above and below the mantle range (Fig. 3.12b). Looking at only samples in the Antananarivo Domain, but including the Brickaville orthogneiss (shaded area), a clearer evolution path emerges. Values are initially high in the east then drop to below mantle values (48°25'; DA13-077) before rising steadily to ~47° east then decreasing again to mantle values.

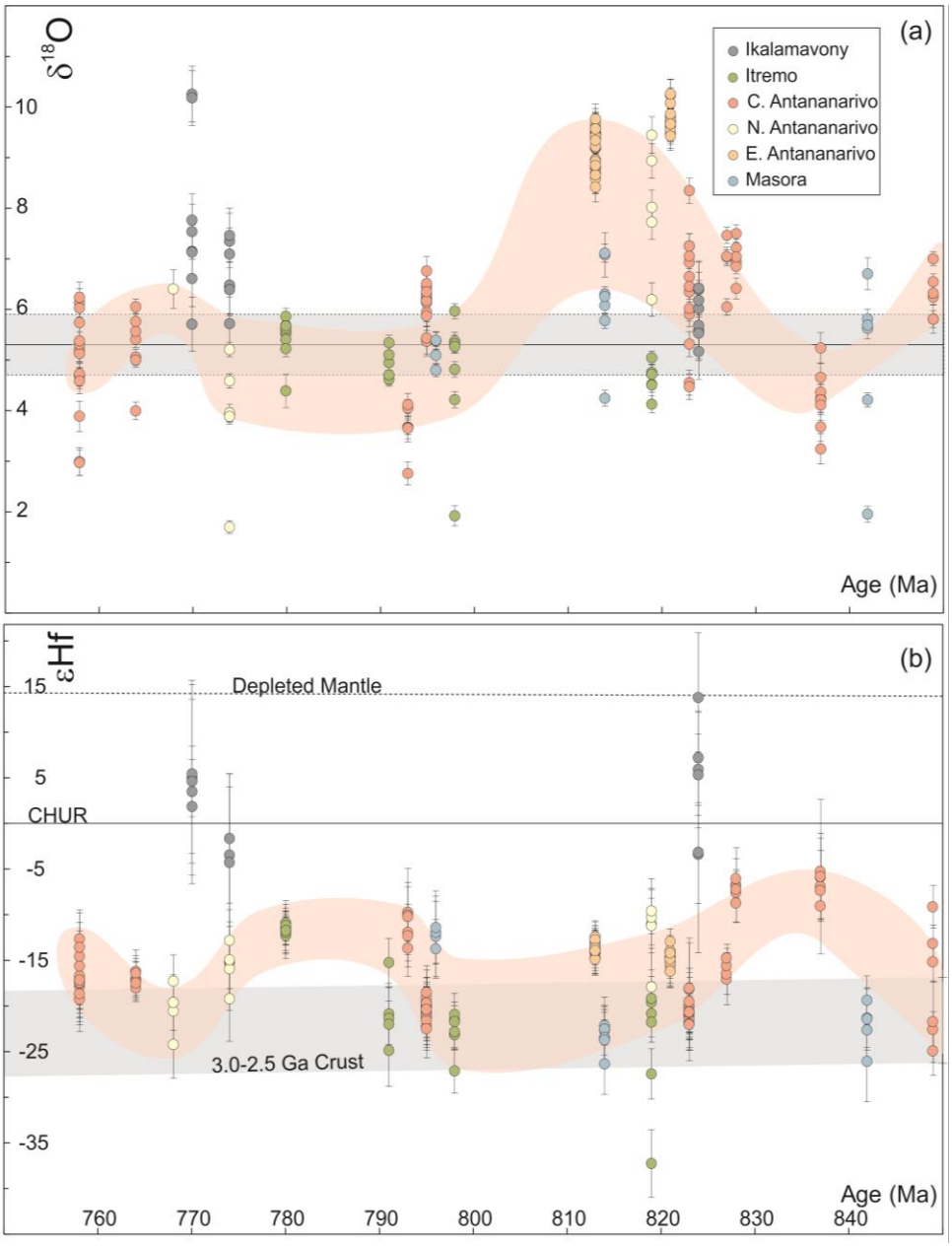

Fig. 3.11 Plot of (a) $\delta^{18}O$ and (b) $\varepsilon_{Hf}(t)$ plotted against the interpreted crystallisation age for all Tonian zircon analysed in this study. Error bars are 2σ. Range of mantle derived $\delta^{18}O$ (zircon) values in (a) are 5.3 ± 0.6 ‰ (Valley et al., 1998). The T_{DM} (crustal) Hf evolution field is based on a $^{176}Lu/^{177}Hf$ ratio of 0.015 (Griffin et al., 2004). The orange shaded field represents the general change in O and Hf isotopic data with time. DM - depleted mantle. CHUR - chondrite uniform reservoir.

Eastern $\varepsilon_{Hf}(t)$ values approximately show an inverse relationship with respect to the $\delta^{18}O$ values (Fig. 3.12c). Data changes from a crustal signature in the easternmost sample to less evolved Hf signatures at 48° 25' with the exception of one sample from the Masora Domain (Fig. 3.12c). Moving west between 48° 00' to 46° 42' east, $\varepsilon_{Hf}(t)$ values show a pattern analogous to the $\delta^{18}O$ data in that the data seems to 'fan out' towards the west. Focusing on only the Antananarivo and Brickaville samples, the same pattern emerges (shaded area, Fig. 3.12c), although the trend becomes less obvious further west. A prominent feature indicative of significant mantle input and/or hydrothermal activity at ~48° 25'E exists where the low $\delta^{18}O$ values and high $\varepsilon_{Hf}(t)$ values coincide (Figs. 3.12b, c). This region is the suggested location of the Betsimisaraka Suture Zone (Collins and Windley, 2002; Collins,

2006) or the intracontinental rift, in which deposition of the Manampotsy Group occurred (Tucker et al. (2011a). The isotopic data presented here do not clearly differentiate between these hypotheses, but they do indicate that the rocks here were isotopically altered by meteoric fluids, a process that could occur in either setting.

To the far west, samples of rocks intruding the Ikalamavony Domain lithologies clearly have a less evolved $\varepsilon_{Hf}(t)$ signature (Fig. 3.12c). Most samples plot in the Ikalamavony/Dabolava crust field and all samples overlap within uncertainty of each other (Fig. 3.12c). Geochronological and Hf isotopic data show little indication of crust older than the Mesoproterozoic. This contrasts with the Antananarivo, Itremo, and Masora Domains, which certainly contain substantial Mesoarchaean to Palaeoproterozoic components. The less evolved $\varepsilon_{Hf}(t)$ values recorded in Tonian-aged samples in the Ikalamavony Domain are a result of incorporation of the less evolved crust from the Ikalamavony Group and Dabolava Suite.

Mixing between ancient crust and mantle derived melts during genesis of the Imorona-Itsindro Suite is further supported plotting $\varepsilon_{Hf}(t)$ values against $\delta^{18}O$ values in a similar way to Kemp et al. (2007). Only zircon with both oxygen and hafnium data are plotted (Fig. 3.13). Unfortunately, no data are available for the Manampotsy Group or from the basement in the Masora Domain. Tonian zircon from the Antananarivo and Itremo Domains are not derived directly from the crustal components that they intrude, nor were the samples derived directly from the depleted mantle (Fig. 3.13). There was likely a mixture of sources causing data to plot to the right or left of the appropriate field. Ikalamavony Domain samples do, however, plot within the range of the Dabolava Suite. This supports the hypothesis that Tonian intrusive rocks intruded into and assimilated different basement rocks than their counterparts to the east.

3.6.4 Tectonic implications

Tucker et al. (2014) advocate that during the Proterozoic, the Archaean Shield of central Madagascar formed part of a larger continent termed the Greater Dharwar Craton. In this model, during Tonian time, the margins of the Malagasy Shield had a Mesoproterozoic arc to the present day west (Ikalamavony Domain), a Palaeoproterozoic continental terrane to the south (Androyen-Anoysen Domains) and the northern margin was partially covered by Palaeoproterozoic- to Mesoproterozoic clastic and chemical sedimentary rocks of the Andrarona and Sambirano-Sahantaha Groups (Tucker et al., 2014). To the far west and north lay the Mozambique Ocean (Tucker et al., 2014). Alternatively, others suggest central Madagascar was proximal to East Africa and that a strand of the Mozambique Ocean lay to the east between Madagascar and India (Collins and Pisarevsky, 2005; Collins, 2006). The Malagasy basement then amalgamated with Neoproterozoic India (including the Dharwar Craton and its Malagasy extension, the Antongil and Masora Domains) as a result of present-day ‘westward’ directed subduction of Mozambique oceanic crust beneath central Madagascar. This Neoproterozoic subduction event was interpreted to have generated the Imorona-Itsindro Suite in an Andean-style continental arc (Collins and Windley, 2002; Collins and Pisarevsky, 2005; Collins, 2006). Handke et al. (1999) proposed that the magmatic suite represented the root of a continental arc emplaced slightly before or during the break-up of the supercontinent Rodinia. Kröner et al. (2000) postulated that the suite formed by extensive remelting of Archaean to Palaeoproterozoic crust based on whole-rock Nd isotopic data and the presence of abundant inherited zircon xenocrysts in many Tonian samples. Kröner et al. (2000) proposed three mechanisms for the generation of Tonian magmatism in central Madagascar; (1) magmatic underplating following plume generation; (2) subcrustal mantle delamination during the breakup of Rodinia; or (3) continental arc magmatism related to the subduction of oceanic crust beneath Madagascar while the

continental block was adjacent to East Africa or formed a microcontinent in the Mozambique Ocean. They favoured a continental arc model based on the absence of the characteristic geochemical signatures of mantle plumes and the paucity of basic intrusions in central Madagascar (Kröner et al., 2000).

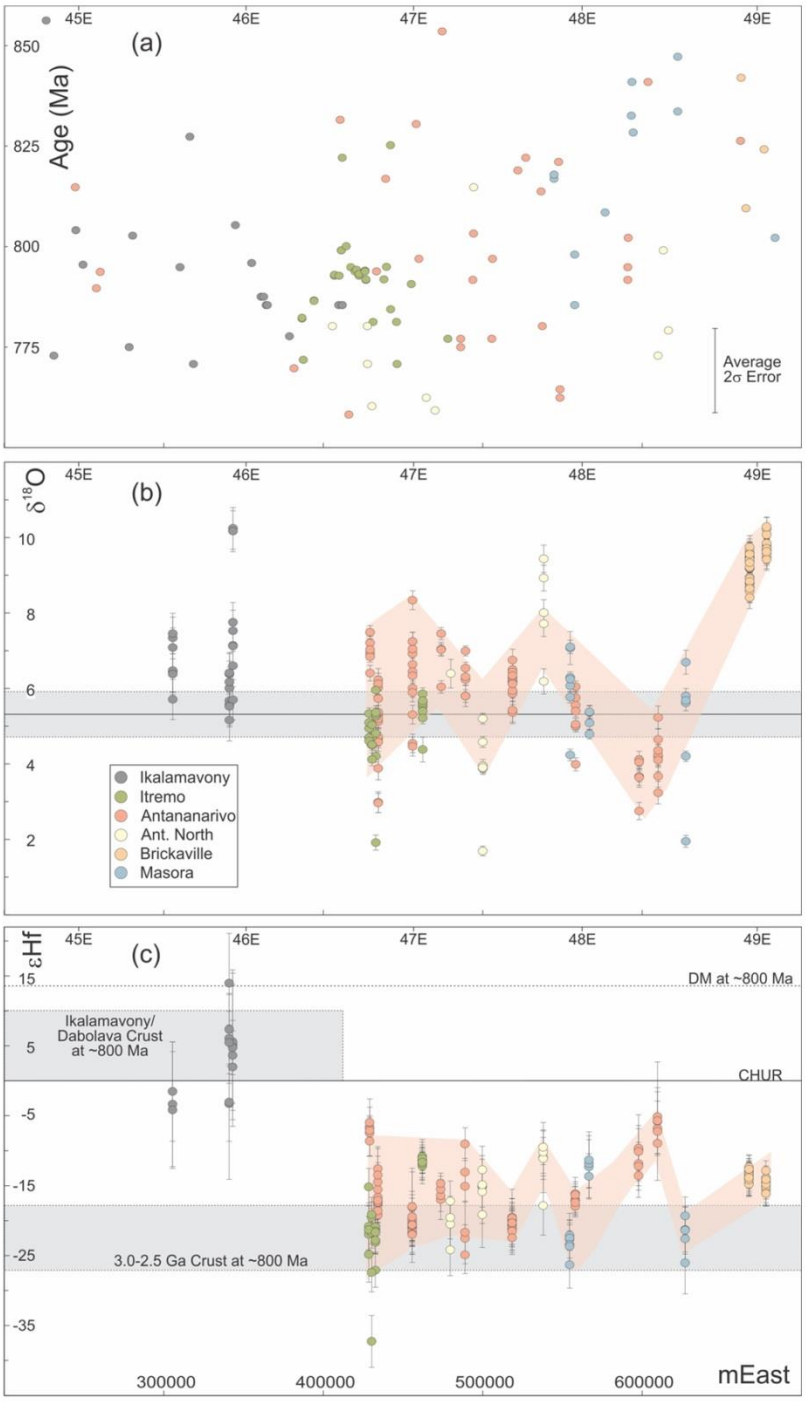

Fig. 3.12 Longitudinal coordinates plotted against (a) Interpreted crystallisation age, (b) $\delta^{18}O$, and (c) $\varepsilon_{Hf}(t)$ for all zircon in central Madagascar with Tonian crystallisation ages between ~850 and 750 Ma. Crystallisation age data includes all available data from references shown in Fig. 3.10. Error bars on $\delta^{18}O$ and $\varepsilon_{Hf}(t)$ plots are 2σ. Range of mantle derived $\delta^{18}O$ (zircon) values in (b) are 5.3 ± 0.6 ‰ (Valley et al., 1998). The orange shaded field represents the general change in O and Hf isotopic data spatially. $\delta^{18}O$ and $\varepsilon_{Hf}(t)$ data are only available for samples analysed in this study. Longitudinal coordinates are given using both conventional degrees and Laborde coordinate using the Laborde (1928) projection.

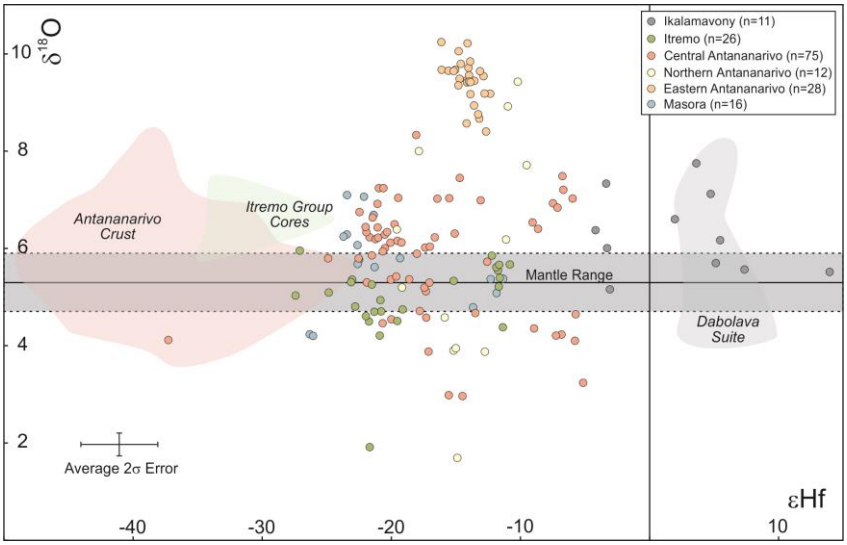

Fig. 3.13 Plot of $\delta^{18}O$ versus $\varepsilon_{Hf}(t)$ for all zircon analysed in this study. Range of mantle derived $\delta^{18}O$ (zircon) values are 5.3 ± 0.6 ‰ (Valley et al., 1998). Data for the shaded "Antananarivo Crust" field are from inherited cores (DA13-017, this study), Ambatolampy Group detrital zircon interpreted to have been derived from the Antananarivo Domain basement (Archibald et al., 2015) and from four samples of the Betsiboka Suite (D.B. Archibald, unpublished). Data for the shaded "Itremo Group Cores" field are from this study. Data for the "Dabolava Suite" are from unpublished data from five samples (D.B. Archibald, unpublished; Chapter 6). The fields on the diagram are from Hf data age corrected to 800 Ma using the methods of Griffin et al. (2002) with an average $^{176}Lu/^{177}Hf$ decay constant of 0.015.

More recent studies have challenged the subduction-continental arc theory and suggest continental rifting as the predominant magma generator (Kabete et al., 2006; Tucker et al., 2011b; Yang et al., 2014; Zhou, 2015; Zhou et al., 2015b). Although they did not collect any geochronological data, McMillan et al. (2003) studied the Ranomandry Complex, a nested intrusion allegedly part of the Imorona-Itsindro Suite that comprises a gabbroic core and a coeval peraluminous granite ring intruding pelitic metasedimentary rocks of the Itremo Group. They considered the complex to reflect melting of an enriched subcontinental mantle that generated gabbroic magmas which in turn caused advective heating and anatexis at the base of thickened continental crust (McMillan et al., 2003). Kabete et al. (2006) suggested that ca. 820-785 Ma rifting of the Andriamena basement produced mafic–ultramafic complexes and consequent high-temperature/low pressure granulite-facies metamorphism. However, it seems that this model is inconsistent with the continental arc origin for the Imorona-Itsindro Suite supported by data in this study. Yang et al. (2014) investigated Tonian intrusions in a restricted area in north central Madagascar (Antanimbary granitoids; Fig. 3.2). Based on geochronological, isotopic and whole-rock geochemical data, they also suggested a major rifting event proposed to have separated the Antananarivo and Antongil Domains prior to ~750 Ma followed by the onset of continental arc magmatism prior to ~730 Ma. The ~730 Ma continental arc magmatism proposed is preserved in the Bemarivo Domain (Thomas et al., 2009). The older magmas are thought to be a result of partial melting of thinned lower crust triggered by underplating of mantle plume-derived magmas (Yang et al., 2014). The plume theory was suggested again after investigation of the ~797–772 Ma Ambatondrazaka gabbroic rocks in east central Madagascar (Fig. 3.2; Zhou et al., 2015b). They concluded gabbroic rocks are more Fe-rich (ferroan) than typical arc basalts and felsic rocks have comparatively high FeO^T/MgO, Ga/Al, Zr and Zr + Nb + Ce + Y values that are typical of A-type granitoids. They challenged the theory of an extensive Neoproterozoic Andean-type arc along the northwest margin of Madagascar (Zhou, 2015; Zhou et al., 2015b) and favour

Neoproterozoic intraplate magmatism as central Madagascar was part of the Greater Dharwar Craton (Tucker et al., 2011a).

The drawback of these recent studies proposing an intra-plate origin for the Imorona-Itsindro Suite is that the investigations fail to incorporate the lithological and geochemical diversity of entire suite, and are focussed on very small sample suites. The presence of both intra-plate and continental-arc geochemical signatures highlight the importance of examining the entire suite. Boger et al. (2014) revived the continental-arc model after examining supposed Tonian volcanic rocks in the Horombe Group in the Anoysen Domain and again after re-examining all of the available whole-rock geochemical data from the entire Imorona-Itsindro Suite (Boger et al., 2015). In this discussion, Boger et al. (2015) noted that Tonian magmatic rocks in Madagascar do not yield irrefutable arc-like geochemical characteristics, nor, however, do they have convincing intra-plate signatures and that the suite required further investigation. They suggest the geochemical diversity of igneous rock compositions observed in Madagascar is more readily explained by means of plate margin processes (Boger et al., 2014, 2015). Their tectonic model proposed present-day eastward directed subduction beneath central Madagascar and India as both landmasses were part of the Greater Dharwar Craton with the Neoproterozoic suture located in the present-day Mozambique Channel.

New whole-rock geochemical data and a re-evaluation of all published data (Archibald et al., submitted-c) are strongly indicative of a continental arc tectonic setting, especially for mafic rocks. When incompatible trace elements and their ratios are plotted against reference datasets from the GEOROC database for contrasting tectonic settings (the Andes and the East African Rift), the Imorona- Itsindro Suite samples are more analogous to Andean rocks (Archibald et al., submitted-c). When coupled with the ~100 million year longevity of magmatism, the relative paucity of mafic magmatism and the scarcity of depleted-mantle isotopic signatures, the geochemical and isotopic evidence suggests plate margin, crustal incorporation processes rather than deep mantle sources strongly supports a continental-arc origin for the Imorona-Itsindro Suite. We therefore uphold the statement of Boger et al. (2015) that the genesis of the Imorona-Itsindro Suite is best explained via plate margin processes as the Mozambique Ocean was subducted beneath central Madagascar rather than intracratonic rifting.

The broad inverse correlation and cyclic patterns observed in $\delta^{18}O$ and $\varepsilon_{Hf}(t)$ data were reported from the long-lived accretionary system of eastern Australia (Kemp et al., 2006; Kemp et al., 2007). Here, these variations are interpreted to track the progressive interaction between basalt derived liquids and crustal melts in the source of the granites (Kemp et al., 2007). These interactions could be either mixing and hybridization of crustal partial melts or assimilation of supracrustal rocks with high $\delta^{18}O$ into magmas with a lower $\delta^{18}O$ (Kemp et al., 2007). We suggest that the times of increased $\varepsilon_{Hf}(t)$ values and decreased $\delta^{18}O$ in the Imorona-Itsindro Suite, reflect times of subduction-zone rollback allowing greater crustal penetration by mantle-derived magmatism along normal faults, and/or higher degrees of partial melting of the mantle wedge due to extension-derived uplift and exhumation.

3.7 Summary and conclusions

The Imorona-Itsindro Suite represents significant magmatism in Madagascar throughout the much of the Tonian. Our isotopic study of zircon from the suite contributes important isotopic information regarding the Neoproterozoic history of Madagascar during the closure of the Mozambique Ocean which can be summarised as follows:

1) New U-Pb (zircon) data from 25 samples combined with previous geochronological data, shows essentially continuous magmatism over the entire age range between ~ 850-750 Ma with periods of increased magmatic activity at approximately 800 Ma, 791 Ma, and 784 Ma.

2) Isotopic data for Tonian-aged zircon domains vary in their $\delta^{18}O$ and $\varepsilon_{Hf}(t)$ signatures across all lithotectonic domains in central Madagascar. When plotted against age, oxygen and hafnium isotope data have a broad inverse relationship with apparent magmatic cycles occurring on the scale of ~15-40 Ma. These cycles suggest times of significant supracrustal assimilation evolving to "mantle-like" (or below) signatures. Contemporaneous patterns in Hf isotopic data broadly mirror the observed O isotopic changes, especially between ~850-820 Ma where lower $\varepsilon_{Hf}(t)$ values reflect higher $\delta^{18}O$ values.

3) The spatial distribution of data indicates that the isotopic character of Tonian zircon reflects the basement domain into which the magmas intruded. Spatial trends in $\delta^{18}O$ values are more apparent than $\varepsilon_{Hf}(t)$ values but both isotope systems display a broadly inverse pattern moving from east to west. To the far west, samples intruding the Ikalamavony Domain clearly have a less evolved $\varepsilon_{Hf}(t)$ signature than any rocks intruding the other tectonic domains, implying melting of different source material.

4) A prominent geological feature suggestive of significant mantle input and hydrothermal alternation by meteoric fluids at 48° 25' E occurs where the sub-mantle $\delta^{18}O$ values and the highest $\varepsilon_{Hf}(t)$ values coincide in the Antananarivo Domain. This region is the suggested location of the Betsimisaraka Suture (Collins and Windley, 2002; Collins, 2006) or the intracontinental rift, in which deposition of the Manampotsy Group occurred (Tucker et al., 2011a), but our data alone cannot distinguish between these two models.

5) Altogether, this large isotopic dataset emphasises the large range in age and composition of the various source regions present in the Ikalamavony, Itremo, Antananarivo, and Masora domains into which the Tonian Imorona-Itsindro Suite were intruded. It also demonstrates the need to examine many samples from a broad region to understand the tectonic setting and evolution of complex magmatic suites. Furthermore, the dataset highlights the importance of interpreting isotopic data spatially (especially across strike) in addition to the more conventional temporal analysis.

3.8 Acknowledgements

Ms. Aoife McFadden and Dr. Benjamin Wade (Adelaide Microscopy) are acknowledged for assistance obtaining CL images and acquiring LA-ICP-MS U-Pb data. The Razafinjoelina family, in particular Auguste and Berthieu are thanked for providing transportation, assistance in the field, and hospitality during fieldwork in Madagascar. An especially thorough, insightful and helpful review from Dr. N. Wodicka significantly improved the quality of the manuscript. This paper forms TRaX Record 353 and is an output of ARC Future Fellowship grant FT120100340. This paper forms a contribution to IGCP projects #628 (Gondwana Map) and #648 (Supercontinent Cycles and Global Geodynamics).

Chapter 4

Geochemistry of the Imorona-Itsindro Suite

Submitted for publication:

Archibald, D. B., Collins, A. S., Foden, J. D., and Razakamanana, T. Tonian Arc Magmatism in Central Madagascar: Petrogenesis of the Imorona-Itsindro Suite. Journal of Geology

Statement of Authorship

Title of Paper	Petrogenesis of the Tonian Imorona-Itsindro Suite
Publication Status	__ Published __ Accepted for Publication X Submitted for Publication __ Publication Style
Publication Details	Archibald, D.B., Collins, A.S., Foden, J.D., Razakamanana, T. submitted. Petrogenesis of the Tonian Imorona-Itsindro Suite. Journal of Petrology.

Author Contributions

By signing the Statement of Authorship, each author certifies that their stated contribution to the publication is accurate and that permission is granted for the publication to be included in the candidate's thesis.

Name of Principal Author (Candidate) Contribution to the paper Conceptualisation of the work It's realisation Documentation and write-up Development of ideas and conclusions	Donnelly B. Archibald Prepared samples, carried out analyses and interpretation of the data, organised manuscript and data, wrote manuscript, acted as the corresponding author		
Signature		Date	9/7/2016

Name of Co-Author Contribution to the paper	Prof Alan S. Collins (University of Adelaide) Supervised work and manuscript revision		
Signature		Date	9/7/2016

Name of Co-Author Contribution to the paper	Prof John D. Foden (University of Adelaide) Assisted with manuscript revision and data interpretation		
Signature		Date	11/7/2017

Name of Co-Author Contribution to the paper	Dr. Theodore Razakamanana (University of Toliara, Madagascar) Assistance in the field, sample logistics, manuscript editing		
Signature		Date	8/4/2016

Abstract

The East African Orogen (EAO) is one of the largest orogens that formed during the Ediacaran to Cambrian amalgamation of Gondwana. In the Mozambique Belt, the EAO represents the amalgamation of Neoproterozoic India with the Congo-Tanzania-Bangweulu Block. In the Arabian-Nubian Shield, the EAO consists of a pre-Neoproterozoic continental terrane surrounded by Neoproterozoic juvenile oceanic-arc like terranes. A large ocean, the Mozambique Ocean divided these Neoproterozoic landmasses. Many oceanic sutures tie together the various terranes in the northern EAO but the location of potential sutures become less obvious moving south. A band of pelitic gneisses in Madagascar with Neoproterozoic depositional ages and pod-like peridotite bodies, gabbro and emerald mineralisation was suggested to represent a Mozambique Ocean suture (the Betsimisaraka Suture). This suture zone separated central Madagascar (in the microcontinent Azania) from India. Recently, the existence of Azania has been challenged in favour of an alternative 'Greater Dharwar' continent incorporating most of central Madagascar on the margin of Neoproterozoic India. The ~100 Myr duration of subduction of the Mozambique Ocean resulted in voluminous magmatism in Madagascar named the Imorona-Itsindro Suite. Our understanding of the petrogenesis of this suite is critical for developing Neoproterozoic palaeogeographic plate reconstructions. The age of the Tonian Imorona-Itsindro Suite is well documented but the geochemistry of the suite provides ambiguous evidence for the tectonic setting. Geochemically, these rocks are predominantly calc-alkaline with characteristics consistent with emplacement within a volcanic or continental arc. The suite has variable but mostly high $^{87}Sr/^{86}Sr$ and low $^{143}Nd/^{144}Nd$ signatures indicating significant crustal involvement. Changes in subduction zone dynamics accompanied by variable crustal anatexis and assimilation contributed to geochemical ambiguities and have prompting some authors to suggest an active rift as an appropriate tectonic model. We suggest that a prolonged history of subduction (>100 Myr) provided sufficient time for the continental Andean-style arc to mature and for the development of shallow mantle source metasomatism.

4.1 Introduction

The East African Orogen is one of the largest orogens that formed during the Ediacaran to Cambrian amalgamation of the supercontinent Gondwana (Stern, 1994; Stern, 2002; Meert, 2003; Collins and Pisarevsky, 2005; Johnson et al., 2011; Fritz et al., 2013). In the Mozambique Belt (see Fritz et al. 2013 for a recent summary), the East African Orogen is thought to represent the amalgamation of Neoproterozoic India to the East African Congo-Tanzania-Bangweulu Block (Fig. 4.1a). In the Arabian-Nubian Shield and Ethiopia, the East African Orogen consists of a pre-Neoproterozoic continental terrane (the Afif Terrane), surrounded by many Neoproterozoic juvenile oceanic-arc like terranes (Johnson et al., 2011; Robinson et al., 2014; Blades et al., 2015) that sutured together in the Ediacaran (Doebrich et al., 2007; Cox et al., 2012). The large ocean that divided these landmasses is known as the Mozambique Ocean. Many oceanic sutures tie together the various terranes in the northern EAO. However, the location of potential sutures becomes equivocal to the south, which led Shackleton (1996) to question the position of the Mozambique Ocean suture. He suggested that, unlike many Phanerozoic orogens that typically involve accretion of multiple terranes, the Mozambique Ocean closed to form one single suture located in present day East Africa.

Collins and Windley (2002), suggested this single-suture model was an over-simplification, and that a wide band of pelitic gneisses with Neoproterozoic depositional ages (Collins et al., 2003c) and associated pod-like peridotite bodies, gabbro and emerald mineralisation represented another Mozambique Ocean suture zone in Madagascar. This suture was termed the Betsimisaraka Suture (labelled as the Anaboriana-Manampotsy Group in Figs. 4.1b and 4.2) and it separated central Madagascar from India (Collins and Windley, 2002). Several authors (Collins and Windley, 2002; Cox et al., 2004; Fitzsimons and

Hulscher, 2005; Collins, 2006) have suggested that central Madagascar formed a Neoproterozoic microcontinent named Azania (Fig. 4.1a) by Collins and Pisarevsky (2005). Central Madagascar along with fragments of southern India (the Madurai Block, Plavsa et al., 2014; Collins et al., 2014), East Africa, Yemen and Saudi Arabia (Collins and Windley, 2002), were isolated from both Neoproterozoic India and the Congo-Tanzania-Bangweulu Block by oceanic crust. The suturing of Azania with the Dharwar Craton along the Betsimisaraka Suture was accompanied by continental arc magmatism in central Madagascar (Handke et al., 1999; Kröner et al., 2000; Boger et al., 2014, 2015). Recently, the existence of Azania has been challenged, and an alternative 'Greater Dharwar' continent proposed (Tucker et al., 2011b; Boger et al., 2014; Tucker et al., 2014) that incorporates all of eastern and most of central Madagascar on the margin of Neoproterozoic India, thus, reverting to a single suture hypothesis for the Mozambique Ocean. According to Tucker et al. (2014), during Tonian times, to the west and north of central Madagascar lay the Mozambique Ocean. The ~100 Myr subduction of this ocean resulted in voluminous Tonian magmatism in central Madagascar with arc-like geochemical and isotopic affinities suggesting a major tectonic event ~300-200 Myr prior to the final amalgamation of Gondwana (Handke et al., 1999; Kröner et al., 2000; Boger et al., 2014, 2015; Archibald et al., 2016).

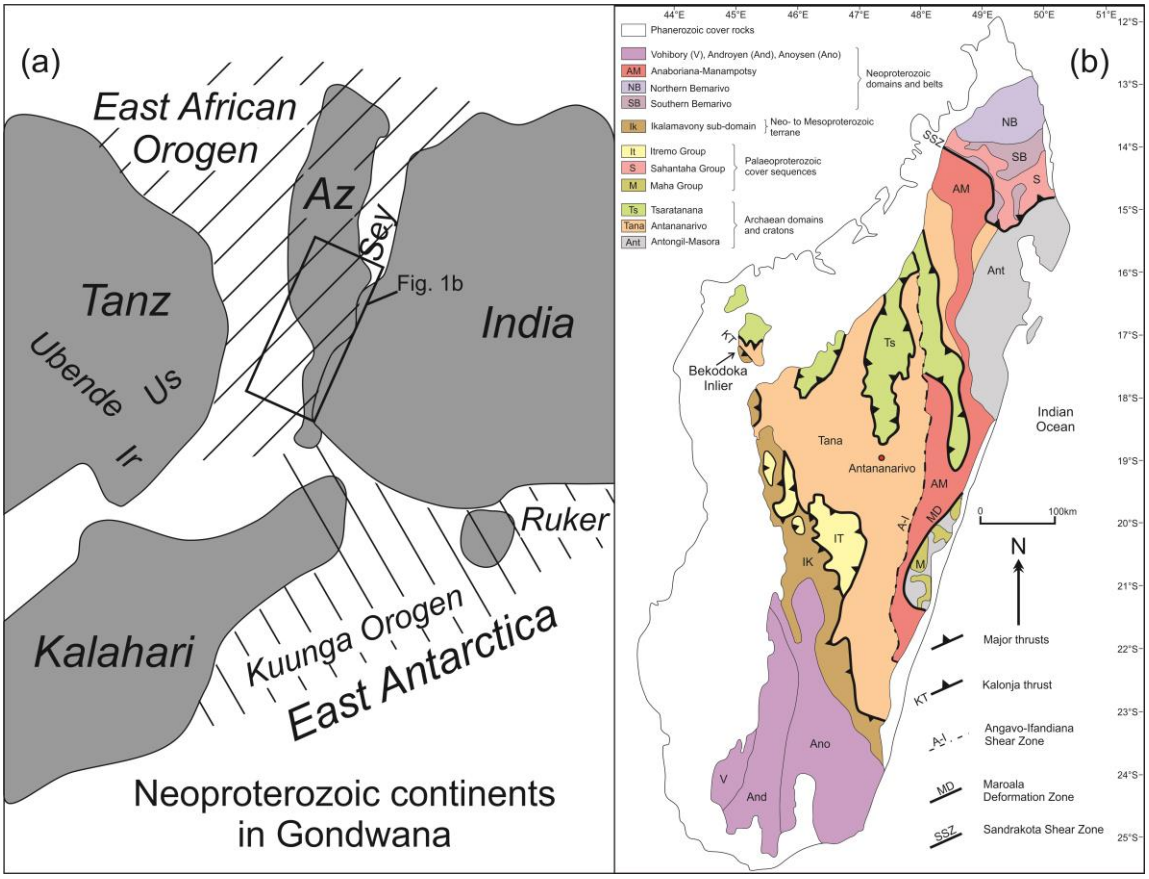

Fig. 4.1 (a) Palaeogeographic reconstruction of the Neoproterozoic continents in Gondwana showing the location of the present study (after Collins and Pisarevsky, 2005). Abbreviations: Az = Azania; Sey = Seychelles; Ir = Irumide Belt; Ruker = Ruker Terrane, East Antarctica; Tanz = Tanzanian craton; Ubende = Ubende Belt; and Us = Usagaran orogen. (b) Simplified basement geology of Madagascar (modified after Collins, 2006 and De Waele et al., 2011).

Previous work on the Imorona-Itsindro Suite has focused on the age of the suite intruding the Antananarivo Domain (Handke et al., 1997; Handke et al., 1999; Tucker et al., 1999a; Tucker et al., 1999b; Kröner et al., 2000; Archibald et al., 2016). These studies obtained Neoproterozoic crystallisation ages between ~850 Ma and 750 Ma. Although the age of the Imorona-Itsindro Suite is well documented, (see Tucker et al. 2014 and Archibald et al., in review for recent summaries) the geochemistry of the suite overall is poorly documented, and no study has attempted an entire-suite analysis. Traditionally, the suite has been interpreted to have been generated in a continental arc (Handke et al., 1997; Handke et al., 1999; Tucker et al., 1999b; Kröner et al., 2000). However, recent publications have proposed magma emplacement during crustal dilation, possible due to central Madagascar being situated above a mantle plume (Tucker et al., 2014; Zhou et al., 2015b). Here we present petrographic, mineralogical and whole-rock geochemical data that allow us to better determine the components involved during genesis of the Imorona-Itsindro Suite. In addition, we discuss the broader implications for the plutonic suite's tectono-geographic relevance during the consumption of the Mozambique Ocean and the transition from the supercontinent Rodinia to Gondwana.

4.2 Regional geology of Madagascar

Madagascar contains several Precambrian to earliest Palaeozoic 'basement' units overlain by Phanerozoic sedimentary and volcanic rocks (Roig et al., 2012). The oldest rocks are located along Madagascar's east coast in the Palaeoarchaean to Palaeoproterozoic Antongil and Masora Domains (Fig. 4.1b). These units are considered remnants of the Dharwar Craton of southern India that were separated from the craton during the Mesozoic break-up of Gondwana (Collins et al., 2003c; Collins, 2006; Schofield et al., 2010; Tucker et al., 2011a; Tucker et al., 2011b; Tucker et al., 2014), although exact correlation with terranes in India is controversial (Rekha et al., 2014; Ratheesh-Kumar et al., 2015; Ishwar-Kumar et al., in press).

The Antananarivo Domain (including the Tsaratanana Domain) represents the largest Precambrian unit and underlies much of central Madagascar. The domain is characterised by granulite- to upper-amphibolite facies orthogneiss and paragneiss (Kröner et al., 2000; Collins et al., 2003a; Collins, 2006; Roig et al., 2012). The orthogneiss is ~2550 – 2500 Ma granitoids (the Betsiboka Suite) tectonically interlayered with paragneiss of the Sofia, Ambatolampy and Vondrozo Groups (Besairie, 1968-1971; BGS-USGS-GLW, 2008; Roig et al., 2012). The entire Antananarivo Domain was thermally and structurally reworked between ~850 and 500 Ma with pre-existing rocks being metamorphosed to granulite-facies conditions, coincident with the development of gneissic fabrics (Collins et al., 2003c; BGS-USGS-GLW, 2008; Moine et al., 2014).

Overlying the Antananarivo Domain are Proterozoic metasedimentary rocks (quartzite, conglomerate and dolomitic marble) of the Itremo Group. Recently, based on common detrital zircon populations at ~ 2500 Ma and ~1800 Ma (Cox et al., 2004; Fitzsimons and Hulscher, 2005; De Waele et al., 2011), the Itremo Group was correlated with the Maha Group in the Masora Domain, the Sambirano-Sahantaha Group in the southern Bemarivo Domain (De Waele et al., 2011), the Ambatolampy Group (Archibald et al., 2015) and metasedimentary rocks in southern India (Plavsa et al., 2014). The poorly studied Ikalamavony and Molo Groups outcrop west of the Itremo Group (Roig et al., 2012) and their depositional ages are assumed to be late Mesoproterozoic to early Neoproterozoic (Cox et al., 2004; Tucker et al., 2007; André-Mayer et al., 2014).

In central Madagascar (Fig. 4.2), successive emplacement of the Dabolava, Imorona-Itsindro, Kiangara, Ambalavao and Maevarano magmatic suites occurred during the latest

Mesoproterozoic to Cambrian. Gabbroic and granitoid rocks of the Stenian-Tonian (~1080-980 Ma) Dabolava Suite with coeval volcanic and metasedimentary rocks of the Ikalamavony Group were interpreted to represent a magmatic arc and marginal volcano-sedimentary sequence within a continental back-arc tectonic setting (CGS, 2009). The Tonian (~850-750 Ma) Imorona-Itsindro Suite consists primarily of granitoids and gabbro that intruded into most central Madagascar Precambrian units, including the Masora, Antananarivo and Ikalamavony Domains (CGS, 2009a; Key et al., 2011; Tucker et al., 2012). Intrusive contact relationships are inferred with the Ambatolampy Group but have not been observed (Archibald et al., 2015). Younger intrusive rock suites are represented by the ~630 Ma Kiangara Suite A-type granitoids (Guyonnaud, 1951; Nédélec *et al*., 1994), the ~575-540 Ma Ambalavao Suite (Meert et al., 2001a; BGS-USGS-GLW, 2008; Archibald et al., submitted-b) and the ~537-522 Ma Maevarano Suite (Goodenough et al., 2010; Zhou et al., 2015a; Archibald et al., submitted-b).

Southern Madagascar contains three domains divided by high-strain zones and is separated from central Madagascar by the Ranotsara Shear Zone (Fig. 4.1b). The westernmost domain is the Vohibory Domain and is composed mainly of mafic and felsic orthogneiss intercalated with paragneiss and marble (GAF-BGR, 2008c; Jöns and Schenk, 2008). The mafic rocks are thought to represent a combination of mid-ocean, back-arc and island arc basalts with inferred extrusion ages between ~850 – 700 Ma (Jöns and Schenk, 2008). Detrital zircon from quartzite within the Vohibory Domain show single-aged Tonian sources (Collins et al., 2012). The Androyen Domain contains mostly paragneiss, orthogneiss and the ~930 – 900 Ma Ankiliabo Suite (GAF-BGR, 2008a). The Anoysen Domain is the most extensive and contains primarily paragneissic rocks of the Iakora Group (with detrital zircon U-Pb ages of ~2400–1600 Ma) and volcano-sedimentary rocks of the Horombe Group (Boger et al., 2014). Boger et al. (2014) suggested that the Horombe Group protoliths are extrusive equivalents of the Imorona-Itsindro Suite, based on similar interpreted extrusion ages and geochemistry.

The Bemarivo Domain is an exotic terrane in north Madagascar (Fig. 4.1b) consisting of Mesoproterozoic metasedimentary rocks (Sambirano-Sahantaha Group) and juvenile Tonian to Cryogenian calc-alkaline igneous rocks (Thomas et al., 2009). Based on the juvenile character of its igneous rocks (Tucker et al., 1999b), Archaean and Palaeoproterozoic rocks are assumed to be absent in this domain. Thomas et al. (2009) proposed that the northern and southern sub-domains formed as magmatic arcs, at ~760 Ma (Antsirabe Nord Suite) in the south and ~720 Ma (Manambato Suite) in the north, that were thrust southward over the Sambirano-Sahantaha Group and the combined Antananarivo-Antongil domains during late Ediacaran to early Cambrian times (ca. 540-520 Ma).

The Neoproterozoic Anaboriana-Manampotsy Belt contains supracrustal rocks with tectonic pods of mafic-ultramafic rocks that follow the boundary between the Antongil-Masora and Antananarivo Domains (Key et al., 2011; Roig et al., 2012). The belt broadly corresponds spatially with the Betsimisaraka Domain or Betsimisaraka Suture Zone (Collins and Windley, 2002; Collins, 2006). Manampotsy Group lithologies are highly deformed migmatitic quartzofeldspathic paragneiss, graphitic gneiss, quartzite, marble, calc-silicate gneiss and biotite gneiss (BGS-USGS-GLW, 2008). The Anaboriana Belt is a continuation of the Manampotsy Belt into a wedge-shaped block along the boundary with the Bemarivo Domain (Roig et al., 2012). Granitoid rocks of the Maevarano Suite comprise much of the Anaboriana Belt (~70% of the surface area) and the remaining 30% is high-grade supracrustal gneisses and migmatite of the Bealanana Group (BGS-USGS-GLW, 2008).

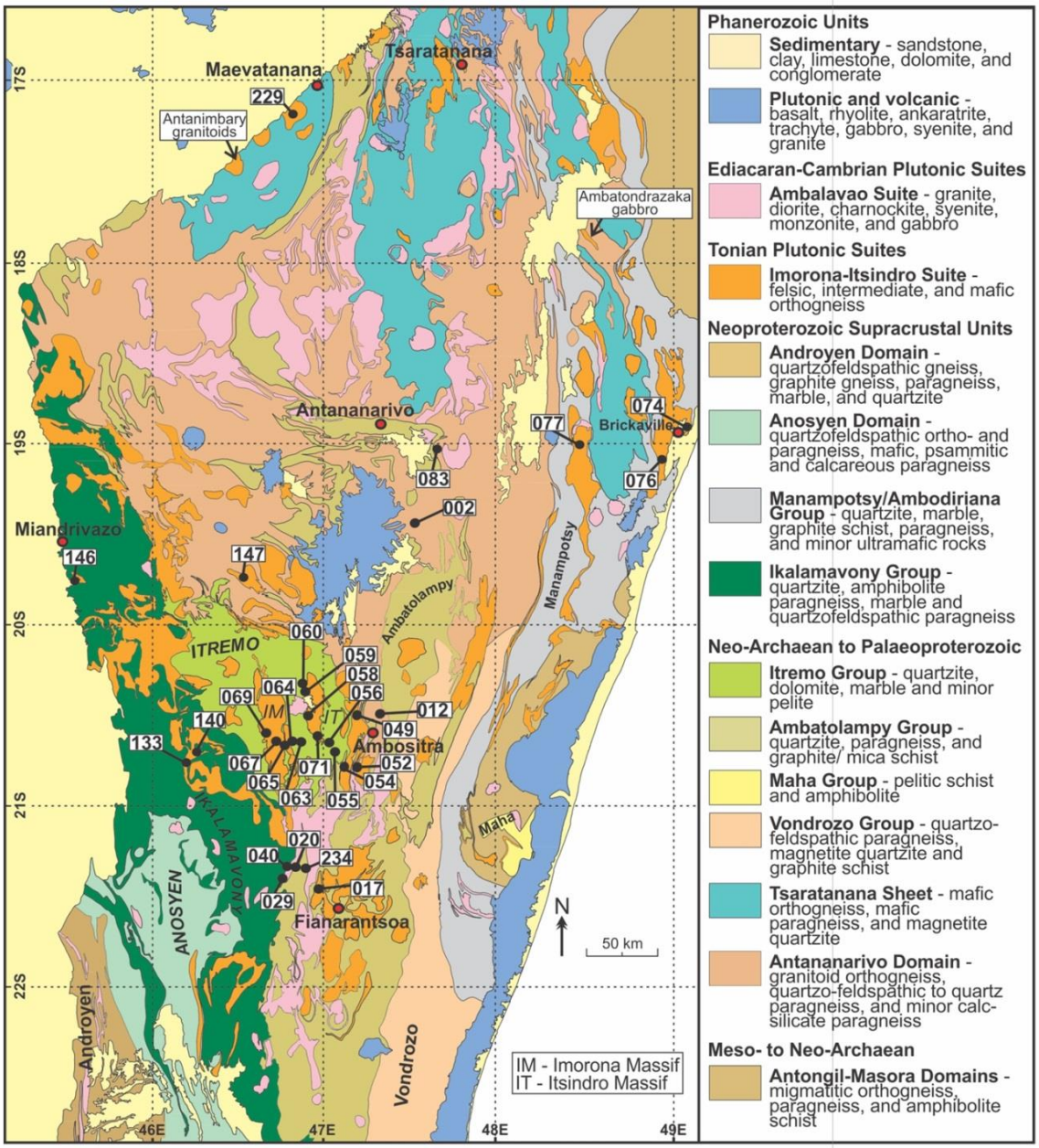

Fig. 4.2 Geologic map of central Madagascar (modified after Roig et al., 2012) showing the extent of Tonian magmatism sampled in this study. Note that Ediacaran to Cambrian plutonic rocks are undivided and given the name Ambalavao Suite (Roig et al., 2012).

4.3 Analytical methods

A complete description of the methods employed in this study is available in supplementary Appendix 4.1. Thirty polished thin-sections were examined under transmitted and reflected light to determine mineralogy, textures, and to select sites for mineral analysis. Mineral analyses were obtained at Adelaide Microscopy using a Cameca SX-Five Electron Probe with five wavelength dispersive spectrometers attached. Iron concentrations were measured as total iron (FeO^T = $FeO+Fe_2O_3$). All mineral formula calculations and ionic species recalculations were completed using Microsoft Excel spreadsheets modified after Tindle (2015) and Preston (2015). Fractions of the same thirty samples were selected for whole-rock geochemical analyses for major, minor and trace elements at ACME Labs in Vancouver, Canada. In addition, 20 samples, 14 of which had previously been dated by U-Pb geochronology and analysed for hafnium and oxygen isotopes in zircon (Archibald et al.,

2016) were selected for Nd-Sm and Sr isotopic analysis. The chosen samples are considered to represent the assortment of lithologies present in the Imorona-Itsindro Suite.

4.4 Results

4.4.1 Field description and contact relationships

Occurring to the west of the proposed Betsimisaraka Suture, the Imorona-Itsindro Suite is named for the Imorona and Itsindro massifs located near Ambatofinadrahana village (Moine, 1968) approximately 120km west of Ambositra (Fig. 4.2). Imorona-type intrusions are primarily granitoid compositions while the Itsindro-type intrusions are primarily gabbroic. Recent work by BGS-USGS-GLW (2008) subdivided the suite into nine sub-suites in addition to the Imorona and Itsindro-type lithologies intruding mainly the Antananarivo and Itremo Domains. These sub-suites include the Brickaville, Isinko, Angavo-Ankazobe, Ankaranando, Ambodilafa, Andohalobe, Ankera, and Kamoro subsuites (BGS-USGS-GLW, 2008). Except for geographical distribution, significant geochemical or temporal grounds for distinction between the sub-suites are unclear. Because of this, subdivisions of the Imorona-Itsindro Suite based on lithology or the basement domain that the Tonian rocks intrude (Fig. 4.2; Table 4.1).

The plutonic suite crops out as abundant dykes and sills often in association with intrusive batholiths (Handke et al., 1999) and plutons. Many exposures of Tonian rocks are cross-cut by Ediacaran-Cambrian veins and dykes of the Ambalavao and Maevarano Suites (Goodenough et al., 2010; Archibald et al., submitted-b). Remarkably, irrefutable exposures of Tonian volcanic rocks are absent, despite suggestions of epizonal magma emplacement into the Itremo Group (Moine, 1967; Moine, 1974). Potential Tonian volcanic rocks have been proposed within the Manampotsy Group (BGS-USGS-GLW, 2008) and in the Horombe Group of the Anosyen Domain (Boger et al., 2014). However, petrographic and petrologic evidence is ambiguous because of late Neoproterozoic metamorphism and deformation (Nédélec et al., 2000; Fitzsimons, 2016). Intrusive rocks are dominantly felsic with less common mafic and intermediate rocks (Fig. 4.3). Samples vary from gabbro to porphyritic granitoids and also include nepheline-bearing porphyritic syenitic rocks (Fig. 4.4). End-member rock types are commonly co-magmatic and mingled at outcrop scale (Fig. 4.4b) with abundant enclaves and xenoliths (Fig. 4.4d), or form nested intrusions on a regional scale (McMillan et al., 2003). The suite intrudes older lithologies in the Antananarivo, Tsaratanana, Ikalamavony and Itremo Domains and contact relationships are inferred, but not observed, in the Masora Domain (BGS-USGS-GLW, 2008). Conclusive contact relationships in the Antongil Domain (Schofield et al., 2010) and with the Ambatolampy Group (Archibald et al., 2015) are not recognised.

4.4.2 Petrography and mineral chemistry

Lithologies are assigned to samples based on the modal percentages of major rock forming minerals recorded in petrographic thin sections (Fig. 4.3). The lithological subdivisions used are felsic (granitoid and quartz syenite), intermediate (tonalite, granodiorite and quartz monzo-diorite), mafic (gabbro) and syenite (syenite and nepheline syenite). Summaries of petrographic studies are found in Table 4.2. Mineral chemistry data are found in Tables 4.3-4.8 and in Appendix 4.2.

Felsic Rocks

Seventeen samples analysed in this study have felsic compositions of mainly granite and quartz syenite (Fig. 4.3). These rocks display a variety of textures, the most common being porphyritic texture (Fig. 4.4a). Phenocrysts in porphyritic rocks are up to 10 cm in size and are composed of perthitic alkali-feldspar and quartz. Other common igneous textures

include granophyric and myrmeckite. Individual mineral grains in the matrix of porphyritic and in non-porphyritic samples are medium- to coarse-grained, inequigranular and mostly subhedral to anhedral.

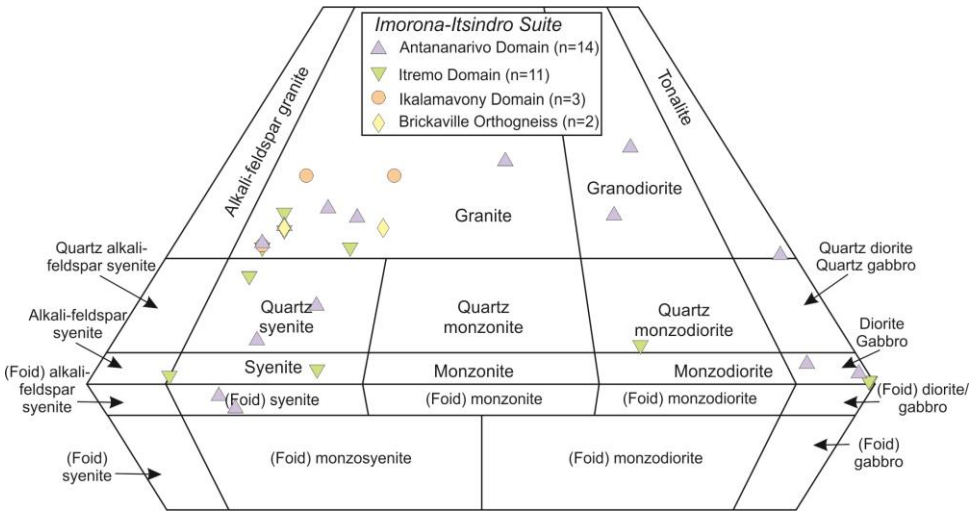

Fig. 4.3 Plutonic rock classification diagram (Streckeisen, 1976) plotting samples of the Imorona-Itsindro Suite collected in this study using modal mineralogy.

Alkali-feldspars (30-70%) display tartan and Carlsbad twinning (Figs. 4.5a, b). Crystals are predominantly subhedral and compose parts of both the matrix and phenocrysts in porphyritic samples. Mineral analyses show orthoclase compositions between $Or_{82}Ab_{17}An_1$ and $Or_{94}Ab_6An_0$ (Fig. 4.6a; Table 4.3). Most alkali-feldspar grains show varying degrees of sericitisation and commonly display perthitic textures. Exsolution lamellae have Na-rich compositions between $Ab_{84}An_{15}Or_1$ and $Ab_{97}An_2Or_1$ (Fig. 4.6a; Table 4.5). Plagioclase feldspars (10-40%) show albite and pericline twinning. Grains are mainly subhedral to euhedral and show varying degrees of saussuritisation. Mineral analyses show oligoclase to albite compositions between $Ab_{74}An_{24}Or_2$ and $Ab_{91}An_8Or_1$ (Fig. 4.6a; Table 4.4). Quartz (10-40%) typically displays undulatory extinction and is present in both the matrix and as phenocrysts in porphyritic lithologies.

Biotite (2-10%) exhibits characteristic birds-eye texture. Grains are mainly subhedral to euhedral, pale-yellow to brown, pleochroic and many biotite grains are partially altered to chlorite. Two clusters of mineral analyses show Fe-rich compositions of 0.79-0.90 ($Fe^{2+}/Fe^{2+}+Mg$) in samples from east-central Madagascar and more Mg-rich compositions of 0.38-0.46 to the west (Fig. 4.6b; Table 4.6). Amphiboles (0-15%) are subhedral to euhedral, dark blue/green and pleochroic. Using the classification scheme of Hawthorne et al. (2012), mineral analyses show calcium amphibole compositions of edenite and pargasite (Fig. 4.6c; Table 4.7). Garnet was identified in two samples of the Brickaville orthogneiss intruding into the Manampotsy Group (Fig. 4.2). Garnet crystals (1-5%) are mainly euhedral to subhedral and dark-red in hand-specimen. Mineral analyses reveal Fe-rich compositions of $Al_{67}And_3Gr_{21}Py_3Sp_6$ and $Al_{68}And_2Gr_{24}Py_4Sp_2$ (Table 4.8).The same samples containing garnet also contain muscovite (2-5%). Other accessory minerals identified in felsic samples include zircon (<1%), allanite (<1%), titanite (<1%), opaque minerals (<1%) and Fe-oxides (<1%).

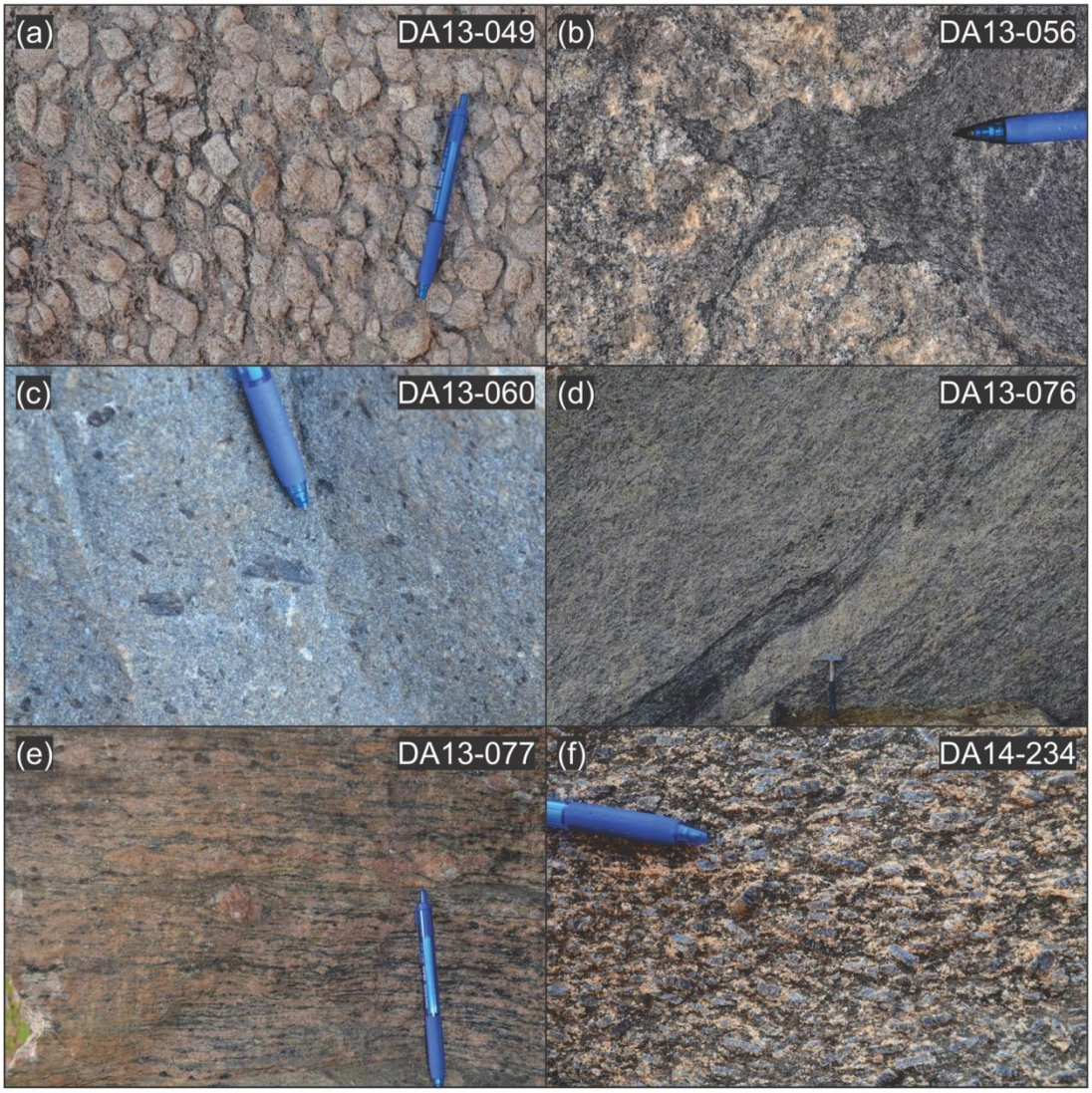

Fig. 4.4 Representative outcrop photographs of the Imorona-Itsindro Suite: (a) porphyritic granite sample DA13-049; (b) magma mingling textures at the sampling locality for DA13-056; (c) gabbro sample DA13-060; (d) metasedimentary restite at the sampling locality for DA13-076; (e) sample DA13-077showing gneissic texture; and (f) nepheline-syenite sample DA13-234.

Intermediate Rocks

Four intermediate samples have compositions of tonalite, quartz-monzodiorite and granodiorite (Fig. 4.3). Mineral grains are mainly subhedral-anhedral, fine- to coarse-grained, and inequigranular. Three samples display myrmeckite texture.

Intermediate lithologies contain a similar mineralogy to the felsic samples but vary in the relative proportions (Table 4.2). Mineral chemistry was only collected from one sample of quartz monzodiorite (DA13-055). Alkali-feldspar (2-20%) typically exhibits tartan twinning and mineral analyses demonstrate an orthoclase composition of $Or_{82}Ab_{17}An_1$ (Fig. 4.6a; Table 4.3). Grains show variable alteration to sericite and perthitic texture (Fig. 4.5c, d). Exsolution lamellae were not analysed. Plagioclase crystals are euhedral to mainly subhedral and exhibit albite and Carlsbad twinning. Some grains in sample DA13-017 also show deformation of albite twins. Mineral analyses reveal oligoclase compositions of $Ab_{71}An_{28}Or_1$ (Fig. 4.6a; Table 4.4). Quartz (5-40%) displays undulatory extinction.

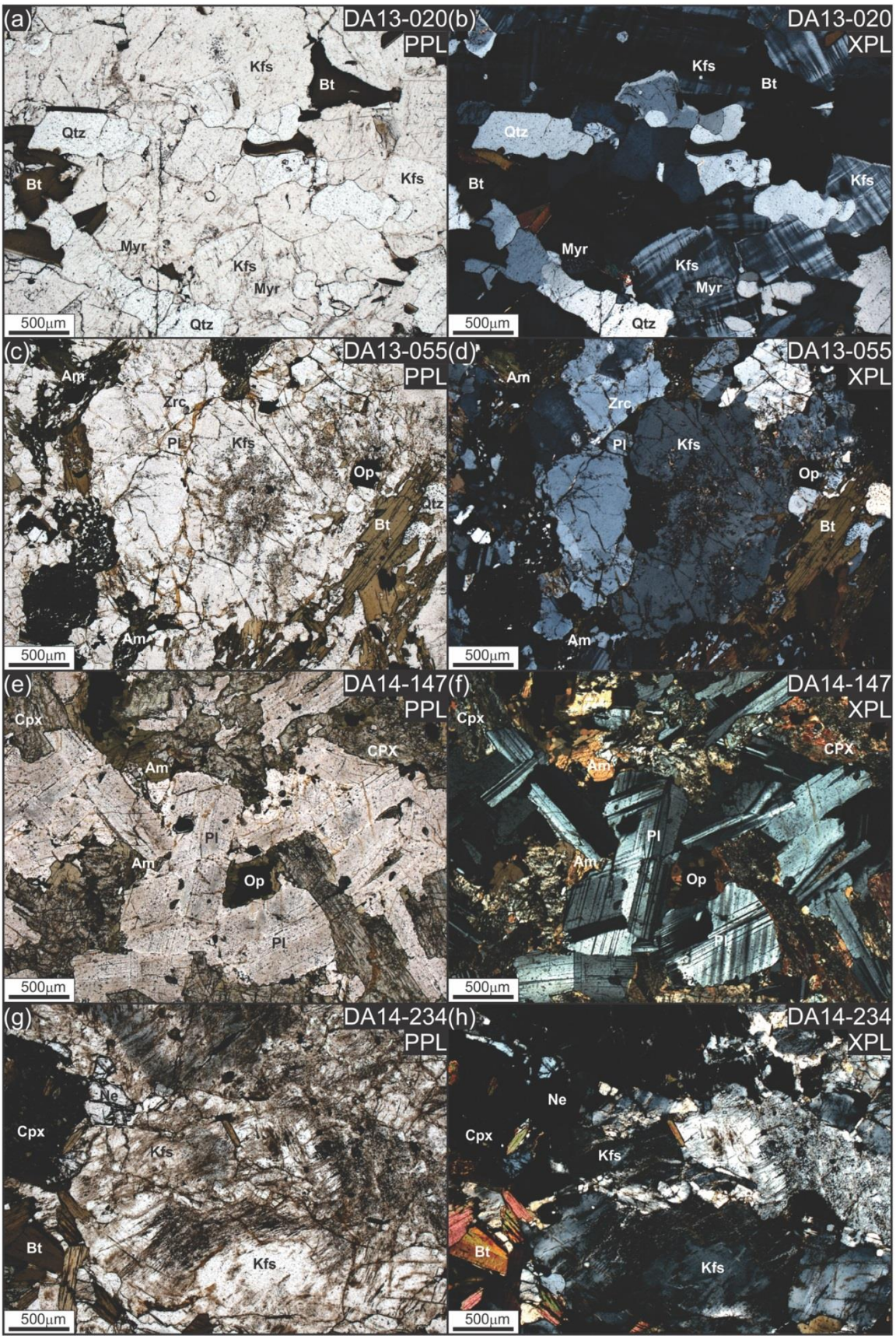

Fig. 4.5 Representative photomicrographs for samples of the Imorona-Itsindro Suite. (a-b) felsic sample DA13-020; (c-d) intermediate sample DA13-055; (e-f) mafic sample DA14-147; and (g-h) nepheline-syenite sample DA14-234.

Biotite (2-25%) exhibits characteristic birds-eye texture. Grains are mainly subhedral to euhedral, pale-yellow to brown, pleochroic, and many grains are partially altered to chlorite. Mineral analyses of biotite have a Fe/Fe+Mg ratio of 0.60 (Fig. 4.6b; Table 4.6). Amphiboles (5-15%) are subhedral to euhedral, dark blue/green in plane-polarised light and are pleochroic. Mineral analyses show calcium amphibole compositions of edenite (Fig. 4.6c; Table 4.7). Other accessory minerals identified in intermediate samples include zircon (<1%) and opaque minerals (<1%).

Table 4.1 Summary of sample names, lithology, locations and geographical reference for samples of the Imorona-Itsindro Suite. Abbreviations: ANT=Antananarivo, BRICK= Brickaville, IKAL=Ikalamavony. Note that the 4 samples at the bottom of the list are duplicates. DA14-347=DA14-147, DA14-355=DA13-055, DA14-364=DA13-064 and DA14-374=DA13-074.

	WGS 84 (dd°mm'ss.s")		Laborde (m)			
Sample	Latitude	Longitude	East	South	Geographical Reference	Domain
DA13-002	19° 22' 08.9"	47° 27' 25.3"	507095	747721	Quarry ~4km north of Ambatolampy	ANT
DA13-012	20° 22' 16.5"	47° 17' 29.3"	489183	636963	~18 km south of Fandriana on RN41	ANT
DA13-017	21° 20' 46.1"	46° 58' 38.9"	456004	529153	~20km north of Fianarantsoa on RN42	ANT
DA13-020	21° 15' 29.8"	46° 46' 10.5"	434465	538937	Near Milandroa Village on RN42	ANT
DA13-029	21° 17' 46.9"	46° 43' 13.3"	429355	534733	~10 km south of RN42 toward Solila	ANT
DA13-040	21° 15' 49.4"	46° 45' 56.6"	434060	434060	~3.5km west of Mangidy village	ANT
DA13-049	20° 22' 51.7"	47° 08' 44.0"	473912	635904	~20km north of Ambositra on RN7	ANT
DA13-052	20° 40' 11.7"	47° 08' 08.1"	472731	603979	~10km west of Ivato on RN35	ANT
DA13-054	20° 38' 43.1"	47° 03' 20.2"	464404	606574	~7 km west of Tsarafandry on RN35	ANT
DA13-055	20° 37' 40.9"	47° 02' 09.0"	462357	608608	Near Ankadilanana Village on RN35	ITREMO
DA13-056	20° 33' 41.9"	47° 00' 09.2"	458918	615973	Near Ampanetoana Village on RN35	ITREMO
DA13-058	20° 30' 39.7"	46° 56' 53.0"	453163	621811	~8km north of Ampanetoana Village	ITREMO
DA13-059	20° 28' 09.0"	46° 56' 11.5"	452079	626230	~13km north of Ampanetoana Village	ITREMO
DA13-060	20° 28' 13.5"	46° 56' 07.5"	451948	626089	~13km north of Ampanetoana Village	ITREMO
DA13-063	20° 33' 34.8"	46° 45' 12.2"	432912	616281	~6km west of Ambatofinadrahana	ITREMO
DA13-064	20° 33' 11.3"	46° 43' 51.5"	430607	617027	~8km west of Ambatofinadrahana	ITREMO
DA13-065	20° 34' 31.8"	46° 42' 47.3"	428779	614495	~12km west of Ambatofinadrahana	ITREMO
DA13-067	20° 33' 18.9"	46° 41' 15.8"	426106	616768	~20km west of Ambatofinadrahana	ITREMO
DA13-069	20° 33' 20.9"	46° 39' 59.4"	423850	616726	~23km west of Ambatofinadrahana	ITREMO
DA13-071	20° 33' 12.2"	46° 58' 24.3"	455885	616896	~1km west of Ampanetoana Village	ITREMO
DA13-074	18° 49' 21.8"	49° 04' 34.8"	678061	806305	Quarry east of Brickaville on RN2	BRICK
DA13-076	18° 54' 27.7"	48° 58' 34.2"	667414	797191	Loharano Quarry ~1 km east of RN2	BRICK
DA13-077	18° 54' 00.4"	48° 25' 53.1"	610002	796926	Near Perinet Village on RN2	ANT
DA13-083	18° 54' 51.6"	47° 33' 52.2"	518701	797984	Ambatomara quarry in Ankatso	ANT
DA14-133	20° 32' 58.4"	45° 52' 21.6"	341146	617323	~45km east of Malaimbandy on RN35	IKAL
DA14-140	20° 31' 06.0"	45° 53' 36.8"	343312	620786	~50km east of Malaimbandy on RN35	IKAL
DA14-146	19° 47' 39.3"	45° 32' 08.5"	305577	700750	Near Mania River bridge on RN34	IKAL
DA14-147	19° 36' 33.3"	46° 28' 07.5"	403304	721469	~25 km east of Mandoto on RN34	ANT
DA14-229	17° 00' 45.4"	46° 48' 19.2"	439190	1008702	~8km south of Maevatanana	ANT
DA14-234	21° 15' 13.5"	46° 47' 43.0"	437129	539430	Near Mangidy village	ANT
DA14-347	19° 36' 33.3"	46° 28' 07.5"	403304	721469	~25 km east of Mandoto on RN34	ANT
DA14-355	20° 37' 40.9"	47° 02' 09.0"	462357	608608	Near Ankadilanana Village on RN35	ANT
DA14-364	20° 33' 11.3"	46° 43' 51.5"	430607	617027	~8km west of Ambatofinadrahana	ITREMO
DA14-374	18° 49' 21.8"	49° 04' 34.8"	678061	806305	Quarry east of Brickaville on RN2	BRICK

Table 4.2 Petrographic summary of samples from the Imorona-Itsindro Suite. Abbreviations: fg=fine-grained; mg=medium-grained; cg=coarse-grained; vcg=very coarse-grained; Or=orthoclase; Ab=Albite; An=Anorthite; Ann=Annite; Phl=Phlogopite; opx=orthopyroxene; cpx=clinopyroxene; Al=Almandine; And=Andradite; Gr=Grossular; Py=Pyrope; Sp=Spessartine

Sample	Lithology	Grain Size	Textures	Alkali-Feldspar	Plagioclase	Quartz	Amphibole	Biotite	Pyroxene	Other Minerals
DA13-002	gabbro	cg equigranular	myrmeckite	5-10	60-70	2-5	10-15	5-10	15-20 (cpx)	zircon (<1), opaque minerals (<1)
DA13-012	granodiorite	cg inequigranular	myrmeckite	10-15	40-50	30-40	5-10	2-5	-	zircon (<1), opaque minerals (<1)
DA13-017	granodiorite	mg-cg inequigranular	myrmeckite	15-20	40-50	20-30	5-10	2-5	-	zircon (<1), opaque minerals (<1), secondary muscovite and chlorite (<1)
DA13-020	granite	mg-vcg inequigranular	myrmeckite, porphyritic	60-70	10-15	20-25	-	2-5	-	zircon (<1), opaque minerals (<1), secondary muscovite and chlorite (<1)
DA13-029	granite	mg-cg inequigranular	myrmeckite, porphyritic	25-35 ($Or_{94}Ab_{6}An_{0}$)	30-40 ($Ab_{91}An_{8}Or_{1}$)	30-40	-	2-5 ($Ann_{46}Phl_{54}$)	-	zircon (<1), opaque minerals (<1)
DA13-040	nepheline syenite	mg-cg inequigranular	porphyritic	60-70 ($Or_{83}Ab_{17}An_{0}$)	15-25 ($Ab_{99}An_{0}Or_{1}$)	-	-	5-10 ($Ann_{23}Phl_{77}$)	5-10 (aegirine-augute)	nepheline (2-5), allanite (<1), titanite (<1)
DA13-049	granite	mg-cg matrix	porphyritic	50-60 ($Or_{93}Ab_{7}An_{0}$)	15-20 ($Ab_{84}An_{15}Or_{1}$)	25-30	2-5 (pargasite)	2-5 ($Ann_{46}Phl_{54}$)	-	zircon (<1), opaque minerals (<1), titanite (<1)
DA13-052	quartz syenite	cg inequigranular	myrmeckite	60-70	15-20	10-20	-	2-5	-	zircon (<1), opaque minerals (<1), Fe-oxides (<1)
DA13-054	quartz syenite	cg inequigranular	myrmeckite	55-65	20-25	10-15	-	2-5	-	zircon (<1), opaque minerals (<1), magnetite (<1)
DA13-055	quartz monzodiorite	fg-mg inequigranular	myrmeckite	20-25 ($Or_{82}Ab_{17}An_{1}$)	50-60 ($Ab_{71}An_{28}Or_{1}$)	5-10	5-10 (edenite)	5-10 ($Ann_{60}Phl_{40}$)	-	zircon (<1), opaque minerals (<1)
DA13-056	granite	cg inequigranular	porphyritic, myrmeckite, granophyric	60-70	10-15	20-30	-	2-5	-	zircon (<1), opaque minerals (<1)
DA13-058	gabbro	mg-cg inequigranular	-	-	70-80	-	-	<1 (secondary)	5-10 (opx) 10-15 (cpx)	olivine (2-5), opaque minerals (<1)
DA13-059	syenite	fg-mg inequigranular	myrmeckite	50-60	5-10	10-20	-	20-25	<1 (cpx)	zircon (<1), secondary chlorite (2-5), allanite (<1),
DA13-060	gabbro	mg-cg inequigranular	-	-	65-75	-	-	2-5	5-10 (opx) 15-20 (cpx)	opaque minerals (<1)
DA13-063	quartz syenite	fg-mg matrix	porphyritic, myrmeckite	60-70	10-15	15-20	5-10	2-5	-	zircon (<1), opaque minerals (<1),
DA13-064	granite	fg-mg matrix	porphyritic	55-65 ($Or_{90}Ab_{10}An_{0}$)	10-15 ($Ab_{82}An_{17}Or_{1}$)	20-30	10-15 (edenite)	2-5 ($Ann_{42}Phl_{58}$)	-	zircon (<1), opaque minerals (<1), Fe-oxides (<1)
DA13-065	granite	fg-mg matrix	porphyritic	50-60	10-15	20-30	10-15	-	-	zircon (<1), opaque minerals (<1), Fe-oxides (<1)
DA13-067	syenite	mg-cg inequigranular	-	50-60	20-25	2-5	10-15	15-20	-	zircon (<1), allanite (<1), opaque minerals (<1)

Table 4.2 continued...

Sample	Lithology	Grain Size	Textures	Alkali-Feldspar	Plagioclase	Quartz	Amphibole	Biotite	Pyroxene	Other Minerals
DA13-069	granite	fg-mg matrix	porphyritic	50-60 ($Or_{92}Ab_8An_0$)	20-30 ($Ab_{88}An_{10}Or_2$)	20-30	5-10 (edenite)	2-5 ($Ann_{43}Phl_{57}$)	-	zircon (<1), allanite (<1), opaque minerals (<1), titanite (<1)
DA13-071	gabbro	cg inequigranular	porphyritic	-	65-75	-	-	<1 (secondary)	5-10 (opx) 20-25 (cpx)	olivine (2-5), opaque minerals (<1)
DA13-074	granite	mg-cg inequigranular	myrmeckite	50-60 ($Or_{87}Ab_{13}An_0$)	10-15 ($Ab_{74}An_{24}Or_2$)	20-30	5-10 (edenite)	5-10 ($Ann_{79}Phl_{21}$)	-	zircon (<1), garnet (1-2; $Al_{67}And_3Gr_{21}Py_3Sp_6$), opaque minerals (<1), muscovite (2-5)
DA13-076	granite	mg-cg inequigranular	myrmeckite, foliated	40-50 ($Or_{82}Ab_{17}An_1$)	20-25 ($Ab_{75}An_{23}Or_2$)	20-25	10-15 (edenite)	2-5 ($Ann_{80}Phl_{20}$)	-	zircon (<1), garnet (2-5; $Al_{68}And_2Gr_{24}Py_4Sp_2$), opaque minerals (<1), muscovite (2-5)
DA13-077	granite	fg-cg inequigranular	myrmeckite, foliated	50-60 ($Or_{90}Ab_{10}An_0$)	20-30 ($Ab_{83}An_{16}Or_1$)	20-30	2-5 (edenite)	5-10 ($Ann_{90}Phl_{10}$)	-	zircon (<1), allanite (<1), opaque minerals (<1)
DA13-083	granite	mg-cg inequigranular	myrmeckite	50-60 ($Or_{87}Ab_{13}An_0$)	10-15 ($Ab_{80}An_{18}Or_2$)	20-30	2-5 (edenite)	5-10 ($Ann_{38}Phl_{62}$)	-	zircon (<1), allanite (<1), opaque minerals (<1)
DA14-133	granite	mg-cg equigranular	myrmeckite, foliated	50-60	10-15	30-40	-	2-5	-	zircon (<1), allanite (<1), opaque minerals (<1)
DA14-140	granite	mg-cg inequigranular	-	60-70	10-15	20-30	2-5	5-10	-	zircon (<1), allanite (<1), opaque minerals (<1)
DA14-146	granite	mg-cg inequigranular	granophyric	40-50	20-30	30-40	-	2-5	-	zircon (<1), allanite (<1), opaque minerals (<1)
DA14-147	gabbro	mg-cg inequigranular	-	-	60-70	-	2-5	5-10	15-20 (cpx)	opaque minerals (2-5), Fe-oxides
DA14-229	tonalite	mg-cg inequigranular	-	2-5	60-70	15-25	10-15	15-25	-	zircon (<1), opaque minerals (<1)
DA14-234	nepheline syenite	mg-cg inequigranular	porphyritic	60-70	10-20	-	5-10	10-15	-	nepheline (2-5), allanite (<1), apatite (<1)

Table 4.3 Representative mineral chemistry (in wt. %) for alkali-feldspar from the Imorona-Itsindro Suite

Domain	Antananarivo					Brickaville		Itremo		
Sample	DA13-029	DA13-040	DA13-049	DA13-077	DA13-083	DA13-074	DA13-076	DA13-055	DA13-064	DA13-069
Lithology	granite	monzo-syenite	granite	granite	granite	granite	granite	monzo-diorite	granite	granite
	n=21	n=20	n=20	n=15	n=22	n=20	n=28	n=20	n=20	n=20
SiO_2	64.66	63.88	64.37	64.92	64.20	64.61	64.86	64.68	64.65	64.16
TiO_2	0.01	0.04	0.01	0.01	0.01	0.01	0.01	0.05	0.01	0.01
Al_2O_3	17.81	18.66	17.89	18.08	17.92	17.98	18.17	18.80	18.15	17.95
Cr_2O_3	0.01	0.01	0.01	0.01	0.01	0.01	0.01	0.03	0.01	0.00
FeO	0.07	0.29	0.03	0.01	0.04	0.01	0.03	0.08	0.03	0.03
MnO	0.00	0.00	0.01	0.01	0.01	0.01	0.01	0.01	0.01	0.01
MgO	0.01	0.00	0.00	0.00	0.00	0.00	0.01	0.01	0.00	0.01
BaO	0.18	2.65	0.65	0.21	0.29	0.53	0.50	1.06	0.95	0.99
CaO	0.00	0.00	0.00	0.03	0.06	0.06	0.11	0.13	0.00	0.00
Na_2O	0.65	1.71	0.74	1.07	1.45	1.43	1.88	1.89	1.12	0.84
K_2O	15.68	13.10	15.26	15.00	14.28	14.42	13.75	13.39	14.75	15.12
Total	99.07	100.33	98.97	99.36	98.27	99.07	99.34	99.03	98.71	98.11
Si	11.82	11.68	11.77	11.87	11.74	11.81	11.86	11.83	11.82	11.73
Ti	0.00	0.00	0.00	0.00	0.00	0.00	0.00	0.01	0.00	0.00
Al	3.84	4.02	3.85	3.90	3.86	3.87	3.91	4.05	3.91	3.87
Fe^{2+}	0.01	0.04	0.01	0.00	0.01	0.00	0.00	0.01	0.00	0.00
Ca	0.00	0.00	0.00	0.01	0.01	0.01	0.02	0.03	0.00	0.00
Na	0.23	0.61	0.26	0.38	0.51	0.51	0.67	0.67	0.40	0.30
K	3.66	3.05	3.56	3.50	3.33	3.36	3.21	3.12	3.44	3.53
Total	19.56	19.41	19.45	19.65	19.46	19.57	19.67	19.71	19.57	19.43
An	0.00	0.00	0.00	0.14	0.32	0.30	0.55	0.66	0.00	0.00
Ab	5.93	16.69	6.89	9.78	13.28	13.07	17.11	17.36	10.30	7.80
Or	94.06	83.31	93.11	90.08	86.40	86.64	82.34	81.98	89.70	92.19
Total	100	100	100	100	100	100	100	100.00	100.00	100.00

Mafic Rocks

Five samples of mafic rocks have gabbroic compositions (Fig. 4.3). Grains are medium- to very coarse-grained; euhedral to mainly-subhedral-anhedral, inequigranular, and one sample is porphyritic (DA13-071). Mineral analyses were not performed on any of the mafic samples.

Alkali-feldspar (5-10%) was identified in one sample (DA13-002). Grains show faint tartan and Carlsbad twinning and minor myrmeckite texture at grain boundaries. Plagioclase feldspars (60-80%) show albite twinning and some grains display deformed albite twins (Fig. 4.5e, f). Quartz (0-5%) was only identified in DA13-002.

Clinopyroxene (10-25%) is the most common mafic mineral in mafic rocks. Grains are pale-green, mainly subhedral to euhedral, and some grains exhibit simple twinning. Clinopyroxene is commonly secondary in more altered samples and forms coronas around opaque minerals, especially in sample DA14-147. Clinopyroxene mineral chemistry was collected by Zhou et al. (2015b) in gabbroic rocks from the Ambatodrazaka region and identified diopside compositions. Orthopyroxene (5-10%) was identified in three samples but is intensely altered. Relict grains are brown and yellow and euhedral. Amphibole (0-15%) is dark green, pleochroic, and mainly euhedral. Biotite (<1-10%) is present in all mafic samples

but is inferred secondary in DA13-058 and DA13-071. The least altered grains demonstrate birds-eye texture, brown/yellow pleochroism, partial replacement by chlorite, and are often found associated with opaque minerals. Olivine (2-5%) is found in two samples. Relict grains are euhedral and intensely altered to iddingsite and serpentine. Other common accessory minerals identified in mafic samples include opaque minerals (<1-5%), zircon (0- <1%) and Fe-oxides (<1%).

Table 4.4 Representative mineral chemistry (in wt. %) for plagioclase from the Imorona-Itsindro Suite.

Domain	Antananarivo					Brickaville		Itremo		
Sample	DA13-029	DA13-040	DA13-049	DA13-077	DA13-083	DA13-074	DA13-076	DA13-055	DA13-064	DA13-069
Lithology	granite	monzo-syenite	granite	granite	granite	granite	granite	monzo-diorite	granite	granite
	n=20	n=20	n=25	n=15	n=22	n=25	n=21	n=15	n=15	n=25
SiO_2	66.86	68.39	64.57	64.90	63.66	61.99	61.55	61.50	64.48	67.90
TiO_2	0.00	0.00	0.00	0.00	0.01	0.00	0.01	0.01	0.00	0.02
Al_2O_3	20.84	20.64	21.68	22.14	22.07	22.82	22.56	24.24	22.25	20.33
Cr_2O_3	0.01	0.01	0.01	0.01	0.01	0.01	0.02	0.01	0.01	0.01
FeO	0.18	0.22	0.08	0.05	0.07	0.06	0.06	0.08	0.08	0.15
MnO	0.01	0.01	0.01	0.01	0.01	0.00	0.01	0.01	0.01	0.01
MgO	0.01	0.02	0.00	0.00	0.01	0.00	0.00	0.01	0.00	0.01
BaO	0.02	0.01	0.01	0.00	0.01	0.01	0.02	0.03	0.01	0.02
CaO	1.80	0.08	3.14	3.45	3.86	5.03	4.87	5.96	3.57	1.78
Na_2O	10.75	11.47	10.00	9.77	9.58	8.78	8.74	8.23	9.67	10.11
K_2O	0.18	0.18	0.20	0.26	0.29	0.36	0.33	0.15	0.22	0.13
Total	100.61	101.01	99.68	100.57	99.54	99.05	98.11	100.16	100.28	100.42
Si	12.22	13.13	11.80	11.86	11.64	11.33	11.25	11.24	11.79	12.41
Ti	0.00	0.00	0.00	0.00	0.00	0.00	0.00	0.00	0.00	0.00
Al	4.49	4.45	4.67	4.77	4.76	4.92	4.86	5.22	4.79	4.38
Fe^{2+}	0.03	0.03	0.01	0.01	0.01	0.01	0.01	0.01	0.01	0.02
Ca	0.35	0.02	0.61	0.68	0.76	0.99	0.95	1.17	0.70	0.35
Na	3.81	4.06	3.54	3.46	3.40	3.11	3.10	2.92	3.43	3.58
K	0.04	0.04	0.05	0.06	0.07	0.08	0.08	0.03	0.05	0.03
Total	20.95	21.73	20.70	20.84	20.62	20.44	20.25	20.60	20.77	20.78
An	8.40	0.38	14.61	16.12	17.90	23.57	23.13	28.34	16.75	9.64
Ab	90.59	98.62	84.26	82.46	80.49	74.43	75.01	70.82	82.02	88.36
Or	1.01	1.00	1.13	1.42	1.61	2.00	1.86	0.84	1.23	2.00
Total	100	100	100	100	100	100	100	100.00	100.00	100.00

Syenite and nepheline-syenite

Four samples of syenite and silica-undersaturated syenite are fine- to very coarse-grained. Geochronological data is not available for these samples and the assigned a medial-Tonian age is based on field relationships. Two of these samples are porphyritic (DA13-040 and DA14-234; Fig. 4.3f) and one sample displays myrmeckite texture (DA13-059). Mineral analyses were performed on DA13-040.

Alkali-feldspar (50-70%) typically displays tartan twinning, Carlsbad twinning, and forms phenocrysts in porphyritic samples. Mineral analyses show orthoclase compositions of $Or_{83}Ab_{17}An_0$ (Fig. 4.6a; Table 4.3). Grains normally show variable sericitisation and perthitic texture (Fig. 4.5g, h). Exsolution lamellae are nearly pure albite ($Ab_{99}An_0Or_1$; Fig. 4.6a; Table 4.5). Plagioclase (10-25%) grains are euhedral to mainly subhedral and display albite

twinning. Mineral analyses reveal nearly pure albite compositions ($Ab_{99}An_0Or_1$; Fig. 4.6a; Table 4.4). Quartz (0-15%) displays undulatory extinction.

Biotite (5-25%) is partially replaced by chlorite. Unaltered grains are brown and display birds-eye texture and pleochroism. Compositions are more Mg-rich than the biotite compositions recorded in other lithologies (Fig. 4.6b; Fe/Fe+Mg = 0.23). Amphibole (0-15%) was identified in one sample and is intensely altered. Relict grains are dark brown or green and subhedral. Clinopyroxene (0-10%) is found in three samples and is intensely altered. Relict grains are subhedral and pale green. Mineral analyses on unaltered grains reveal aegirine-augite compositions (Fig. 4.6d; Table 4.8). Nepheline (0-5%) was identified in two samples. Grains are subhedral to euhedral and altered. Other minerals present in syenitic samples include allanite (<1%), zircon (<1%), titanite (<1%), apatite (<1%), and opaque minerals (<1%).

Table 4.5 Representative mineral chemistry (in wt. %) for feldspar exsolution lamellae from the Imorona-Itsindro Suite.

Domain	Antananarivo					Itremo
Sample	DA13-029	DA13-040	DA13-049	DA13-077	DA13-083	DA13-069
Lithology	granite	monzo-syenite	granite	granite	granite	granite
	n=10	n=9	n=5	n=10	n=20	n=15
SiO_2	69.58	70.36	69.74	70.44	64.92	67.41
TiO_2	0.00	0.01	0.00	0.01	0.01	0.00
Al_2O_3	19.98	20.03	20.24	20.21	21.94	20.88
FeO	0.04	0.24	0.05	0.03	0.06	0.04
Cr_2O_3	0.01	0.01	0.01	0.01	0.01	0.01
MnO	0.01	0.00	0.01	0.01	0.01	0.00
MgO	0.01	0.02	0.00	0.01	0.01	0.01
BaO	0.01	0.01	0.01	0.03	0.01	0.01
CaO	0.35	0.06	0.43	0.12	3.26	1.53
Na_2O	11.74	11.37	11.73	11.58	10.04	10.75
K_2O	0.18	0.11	0.11	0.57	0.14	0.22
Total	101.91	102.22	102.34	103.00	100.41	100.87
Si	12.72	13.13	12.75	12.88	11.87	12.32
Ti	0.00	0.00	0.00	0.00	0.00	0.00
Al	4.31	4.32	4.36	4.35	4.73	4.50
Fe^{2+}	0.01	0.04	0.01	0.00	0.01	0.01
Ca	0.07	0.01	0.08	0.02	0.64	0.30
Na	4.16	4.03	4.16	4.10	3.56	3.81
K	0.04	0.03	0.03	0.13	0.03	0.05
Total	21.30	21.55	21.39	21.50	20.84	20.99
An	1.59	0.31	1.98	0.54	15.12	7.20
Ab	97.43	99.05	97.40	96.43	84.11	91.57
Or	0.98	0.63	0.62	3.03	0.76	1.23
Total	100	100	100	100	100	100

4.4.3 Whole-rock geochemistry

Thirty-four samples were selected for whole-rock geochemical analysis including four duplicates. All major and trace element data are found in Table 4.9. Sm-Nd and Sr isotope data are found in Table 4.10. Samples are divided into five groups on whole-rock geochemical plots based on the lithologies identified from petrographic analyses (Fig. 4.3).

Table 4.6 Representative mineral chemistry (in wt. %) for amphibole from the Imorona-Itsindro Suite. Abbreviations: Ed=Edenite, Prg=Pargasite (Hawthorne et al., 2012).

Domain	Antananarivo			Brickaville		Itremo		
Sample	DA13-049	DA13-077	DA13-083	DA13-074	DA13-076	DA13-055	DA13-064	DA13-069
Lithology	granite	granite	granite	granite	granite	monzo-diorite	granite	granite
	n=22	n=20	n=20	n=24	n=23	n=20	n=20	n=30
SiO_2	40.42	44.28	45.88	39.64	40.92	43.93	43.79	45.18
TiO_2	1.48	0.56	1.60	1.78	2.02	1.30	0.47	0.52
Al_2O_3	10.22	9.45	8.65	11.22	11.18	10.02	10.13	8.70
Cr_2O_3	0.01	0.01	0.01	0.03	0.00	0.01	0.01	0.01
FeO	29.90	20.22	16.38	26.83	27.19	21.57	20.25	19.85
MnO	0.62	1.18	0.83	0.32	0.14	0.52	1.10	0.36
MgO	1.41	8.74	11.24	3.03	2.82	7.41	8.64	9.55
CaO	10.19	11.04	10.69	10.59	10.55	11.17	11.08	10.97
Na_2O	1.82	1.57	1.92	1.74	1.73	1.33	1.56	1.67
K_2O	1.79	1.39	1.14	1.87	1.82	1.27	1.45	1.34
TOTAL	97.87	98.44	98.32	97.05	98.38	98.53	98.49	98.15
Si	6.52	6.73	6.82	6.36	6.48	6.69	6.66	6.84
Al	1.48	1.27	1.18	1.64	1.52	1.31	1.34	1.16
Sum T	8.00	8.00	8.00	8.00	8.00	8.00	8.00	8.00
Al	0.46	0.42	0.34	0.49	0.54	0.48	0.47	0.39
Fe^{3+}	0.00	0.00	0.00	0.00	0.00	0.00	0.00	0.00
Cr	0.18	0.06	0.18	0.21	0.23	0.15	0.05	0.06
Ti	0.00	0.00	0.00	0.00	0.00	0.00	0.00	0.00
Fe^{2+}	4.03	2.57	2.04	3.60	3.61	2.74	2.57	2.51
Mn	0.08	0.15	0.10	0.04	0.02	0.07	0.14	0.05
Mg	0.24	1.79	2.34	0.65	0.60	1.56	1.76	1.99
Sum C	5.00	5.00	5.00	5.00	5.00	5.00	5.00	5.00
Mg, Mn, Fe	0.10	0.19	0.15	0.07	0.04	0.13	0.20	0.17
Ca	1.76	1.80	1.70	1.82	1.78	1.82	1.80	1.78
Na	0.14	0.01	0.15	0.10	0.18	0.05	0.00	0.05
Sum B	2.00	2.00	2.00	2.00	2.00	2.00	2.00	2.00
Ca	0.00	0.00	0.00	0.00	0.00	0.00	0.01	0.00
Na	0.43	0.45	0.41	0.44	0.33	0.34	0.46	0.44
K	0.37	0.27	0.22	0.38	0.37	0.25	0.28	0.26
Sum A	0.80	0.72	0.62	0.82	0.70	0.59	0.75	0.70
TOTAL	15.80	15.72	15.62	15.82	15.70	15.59	15.75	15.70
Classification	Ed	Ed	Ed	Ed	Prg	Ed	Ed	Ed

Major elements

Imorona-Itsindro Suite samples have SiO_2 concentrations between 66.00-77.40 wt. % in felsic samples and 44.70-49.98 wt. % in mafic samples (Fig. 4.7; Table 4.9). Intermediate and syenite samples have intermediary SiO_2 contents. MgO concentrations are between 0.02-15.15 wt. % (Fig. 4.7a) and have corresponding Mg numbers ($Mg/Mg+Fe^T$) between 8 and 84 (Table 4.9). TiO_2 contents are low (<1.5 wt. %; Fig. 4.7b) and $Fe_2O_3^T$ ($FeO + Fe_2O_3$) contents vary between 0.94 and 11.85 wt. % (Fig. 4.7c). MgO, TiO_2 and $Fe_2O_3^T$ negatively correlate with increasing SiO_2. CaO also exhibits a trend of decreasing values with increasing SiO_2 (0.45-12.47 wt. %; Fig. 4.7d). Na_2O (1.31 – 5.16 wt. %) and K_2O (0.23 - 10.78 wt. %) contents vary across variable SiO_2 but both elements illustrate a broad positive correlation with SiO_2 (Figs. 4.7e, f). Al_2O_3 increases then decreases (11.82-18.40 wt. %; Fig. 4.7g) corresponding with a constant decrease in CaO. Together these trends suggest the removal of clinopyroxene early during fractionation by removing Ca but not Al followed by plagioclase crystallisation removing both Ca and Al (Fig. 4.7). MnO (0.02-0.21 wt. %) and P_2O_5 (0.02-1.00 wt. %) contents are low and exhibit a negative correlation with SiO_2 (Fig. 4.7h, i).

Table 4.7 Representative mineral chemistry (in wt. %) for biotite from the Imorona-Itsindro Suite. Note: *H_2O calculations after (Tindle and Webb, 1990).

Domain	Antananarivo					Brickaville		Itremo		
Sample	DA13-029	DA13-040	DA13-049	DA13-077	DA13-083	DA13-074	DA13-076	DA13-055	DA13-064	DA13-069
Lithology	granite	monzo-syenite	granite	granite	granite	granite	granite	monzo-diorite	granite	granite
	n=20	n=20	n=20	n=22	n=21	n=27	n=6	n=15	n=14	n=20
SiO_2	39.09	42.55	38.92	35.89	39.46	36.48	35.46	37.46	40.22	39.64
TiO_2	2.53	1.71	1.08	4.17	3.43	4.41	3.98	3.92	0.95	1.24
Al_2O_3	15.89	11.39	14.71	12.70	13.46	13.33	13.42	13.93	15.68	13.18
FeO	16.92	10.57	17.80	31.33	15.52	29.02	30.10	23.07	15.78	18.27
MnO	0.62	0.16	0.82	0.38	0.30	0.18	0.07	0.28	0.85	0.24
MgO	10.94	20.32	11.71	1.98	14.40	4.32	4.34	8.62	12.44	13.58
CaO	0.00	0.01	0.13	0.01	0.03	0.08	0.07	0.03	0.06	0.02
Na_2O	0.12	0.10	0.08	0.15	0.10	0.11	0.09	0.10	0.07	0.09
K_2O	9.21	9.72	8.49	8.84	9.50	8.55	7.93	9.22	8.51	9.41
BaO	0.05	0.36	0.08	0.17	0.11	0.31	0.21	0.35	0.07	0.13
ZnO	0.19	0.06	0.14	0.21	0.08	0.11	0.16	0.08	0.17	0.03
F	2.35	2.66	1.91	1.53	1.38	2.01	1.82	0.16	1.86	2.13
Cl	0.15	0.05	0.01	0.34	0.09	0.16	0.15	0.06	0.03	0.11
H_2O*	2.86	2.91	3.02	2.90	3.38	2.82	2.85	3.83	3.14	2.95
Subtotal	100.92	102.64	98.93	100.59	101.26	101.89	100.66	101.11	99.84	101.06
O=F,Cl	1.02	1.13	0.81	0.72	0.60	0.88	0.80	0.08	0.79	0.92
Total	99.89	101.51	98.12	99.87	100.66	101.01	99.86	101.03	99.05	100.14
Si	5.84	6.09	5.93	5.81	5.83	5.74	5.66	5.72	5.99	5.96
Al (iv)	2.16	1.91	2.07	2.19	2.17	2.26	2.34	2.28	2.01	2.04
Total	8.00	8.00	8.00	8.00	8.00	8.00	8.00	8.00	8.00	8.00
Al (vi)	0.64	0.02	0.58	0.23	0.17	0.21	0.19	0.23	0.73	0.29
Ti	0.28	0.18	0.12	0.51	0.38	0.52	0.48	0.45	0.11	0.14
Fe^{2+}	2.12	1.27	2.27	4.24	1.92	3.82	4.02	2.95	1.97	2.30
Mn	0.08	0.02	0.11	0.05	0.04	0.02	0.01	0.04	0.11	0.03
Mg	2.44	4.34	2.66	0.48	3.17	1.01	1.03	1.96	2.77	3.04
Zn	0.02	0.01	0.02	0.02	0.01	0.01	0.02	0.01	0.02	0.00
Total	5.58	5.83	5.75	5.53	5.69	5.60	5.75	5.64	5.70	5.80
Ca	0.00	0.00	0.02	0.00	0.01	0.01	0.01	0.00	0.01	0.00
Na	0.03	0.03	0.03	0.05	0.03	0.03	0.03	0.03	0.02	0.03
K	1.75	1.78	1.65	1.82	1.79	1.71	1.61	1.80	1.62	1.80
Total	1.79	1.80	1.70	1.87	1.82	1.76	1.65	1.83	1.65	1.83
OH*	2.85	2.78	3.08	3.12	3.33	2.96	3.04	3.91	3.11	2.96
F	1.11	1.21	0.92	0.78	0.64	1.00	0.92	0.08	0.88	1.01
Cl	0.04	0.01	0.00	0.09	0.02	0.04	0.04	0.02	0.01	0.03
Total	19.37	19.63	19.45	19.40	19.52	19.36	19.40	19.46	19.35	19.64
Fe/Fe+Mg	0.46	0.23	0.46	0.90	0.38	0.79	0.80	0.60	0.42	0.43

Trace elements

Chondrite-normalised rare-earth element (REE) diagrams demonstrate the differences in REE profiles between lithologies. Felsic samples are plotted on two diagrams based on the magnitude of the Eu anomaly. Samples plotted on Fig. 4.8a have negative Eu anomalies < 0.70 and samples on Fig. 4.8b exhibit Eu anomalies ≥ 0.70. All of the samples shown on Fig. 8b are porphyritic except for quartz-syenite samples DA13-052 and DA13-054. Eleven felsic samples have Eu/Eu* values between 0.22-0.69 (Fig. 4.8a) implying a significant role for plagioclase fractionation and eight samples have Eu/Eu* values between 0.70-1.05 (Fig. 4.8b). Light rare-earth element (LREE) slopes for felsic rocks are steep with La/Sm_N ratios between 2.73 and 9.18. Heavy rare-earth element (HREE) slopes for felsic rocks are

shallower than LREE slopes having Tb/Yb_N ratios between 0.97 and 3.12. Intermediate samples have Eu/Eu* ratios between 0.91 and 1.84 implying accumulation of plagioclase in some samples (Fig. 4.8c). La/Sm_N ratios are between 3.45 and 7.25 and Tb/Yb_N ratios are between 1.02 and 1.63. Mafic rocks have Eu/Eu* ratios between 0.81 and 1.55 (Fig. 8d). LREE (1.65-2.51) and HREE (1.16-1.70) slopes are shallower than felsic or intermediate samples. Eu/Eu* ratios syenite and nepheline-syenite samples are (0.88-1.32; Figs. 4.8e, f). LREE slopes are steep (3.97-5.89) and HREE slopes (2.47-4.16) are similar to other rock-types.

Table 4.8 Representative mineral chemistry (in wt. %) for garnet, pyroxene and titanite from the Imorona-Itsindro Suite.

Mineral	Garnet			Pyroxene		Titanite		
Domain	Brickaville			Antananarivo		Antananarivo		Itremo
Sample	DA13-074	DA13-076	Sample	DA13-040	Sample	DA13-040	DA13-049	DA13-069
Lithology	granite	granite	Lithology	monzo-syenite	Lithology	monzo-syenite	granite	granite
	n=32	n=12		n=25		n=15	n=18	n=15
SiO_2 (wt%)	36.96	37.31	SiO_2 (wt%)	53.61	SiO_2 (wt%)	31.64	32.04	31.96
TiO_2	0.04	0.06	TiO_2	0.13	TiO_2	36.36	34.81	34.62
Al_2O_3	19.69	20.26	Al_2O_3	0.86	Al_2O_3	0.57	1.79	1.71
Cr_2O_3	0.01	0.01	Cr_2O_3	0.11	Cr_2O_3	0.05	0.01	0.01
FeO	30.47	31.18	FeO	10.36	FeO	1.57	1.37	1.50
MnO	2.64	0.83	MnO	0.28	MnO	0.06	0.17	0.05
MgO	0.73	0.88	MgO	12.12	MgO	0.01	0.01	0.03
CaO	7.99	8.86	CaO	18.71	CaO	26.55	27.12	27.17
Na_2O	0.02	0.01	Na_2O	3.14	Na_2O	0.11	0.05	0.04
K_2O	0.01	0.00	K_2O	0.01	K_2O	0.02	0.01	0.04
BaO	0.01	0.01	Total	99.32	Total	96.94	97.39	97.13
ZnO	0.03	0.03						
F	0.08	0.06						
Total	98.69	99.49						
Si	3.03	3.02	Si+Ti	1.99	Si	1.06	1.07	1.07
Al (iv)	0.00	0.00	Al (iv)	0.01	Ti	0.92	0.87	0.87
					Al	0.02	0.07	0.07
Al (vi)	1.90	1.93	Al (vi)	0.03	Cr	0.00	0.00	0.00
Ti	0.00	0.00	Fe^{3+}+Fe^{2+}+Mn	0.33	Fe^{3+}	0.00	0.00	0.00
Cr	0.00	0.00	Mg	0.64	Fe^{2+}	0.04	0.04	0.04
Fe^{3+}	0.06	0.04			Mn	0.00	0.00	0.00
			Mg	0.03	Mg	0.00	0.00	0.00
Fe^{2+}	2.03	2.07	Ca	0.74	Ca	0.95	0.97	0.97
Mn	0.18	0.06	Na	0.23	Na	0.01	0.00	0.00
Mg	0.09	0.11	Cations	4.00	K	0.00	0.00	0.00
Ni	0.00	0.00			Cations	3.01	3.03	3.03
Zn	0.00	0.00	Wo	48.57				
Ca	0.70	0.77	En	43.76				
Total	8.00	8.00	Fs	7.67				
Almandine	66.87	68.51	Aegerine	21.02				
Andradite	2.96	2.06	Jadeite	2.27				
Grossular	20.85	23.89	Diopside	76.71				
Pyrope	3.04	3.60						
Spessartine	6.24	1.92						
Uvarovite	0.04	0.02						
% cations	98.06	98.59						

Table 4.9 Major and trace element geochemical data collected in this study from the Imorona-Itsindro Suite. Eu/Eu*, La_N/Sm_N and Tb_N/Lu_N ratios were calculated using chondrite normalising values from Sun and McDonough (1989).

Sample	DA13-002	DA13-012	DA13-017	DA13-020	DA13-029	DA13-040	DA13-049	DA13-052	DA13-054
SiO_2 (wt%)	48.72	70.14	67.20	69.83	67.82	55.99	69.10	73.56	71.48
Al_2O_3	13.51	16.04	16.11	14.93	15.04	13.51	15.84	14.41	14.44
Fe_2O_3	14.05	1.60	3.27	2.59	4.84	5.96	2.44	0.95	1.89
MgO	6.33	0.46	0.91	0.78	0.10	6.24	0.50	0.11	0.39
CaO	9.26	2.19	3.58	1.70	0.47	4.34	2.07	1.00	1.23
Na_2O	3.15	5.16	4.47	3.69	3.62	3.10	4.41	4.29	2.94
K_2O	2.78	3.46	3.06	5.53	7.15	7.81	4.46	5.00	6.70
TiO_2	1.06	0.16	0.29	0.40	0.16	0.94	0.21	0.08	0.31
P_2O_5	0.09	0.08	0.14	0.14	0.02	0.33	0.07	0.02	0.09
MnO	0.19	0.05	0.07	0.04	0.04	0.08	0.07	0.02	0.02
Cr_2O_3	0.019	<0.002	<0.002	<0.002	<0.002	0.038	<0.002	<0.002	<0.002
LOI	0.5	0.3	0.5	0.1	0.4	0.5	0.5	0.5	0.3
Total	99.68	99.64	99.60	99.73	99.68	98.81	99.70	99.90	99.78
Ba (ppm)	615	1511	1924	1145	1093	6415	1271	324	857
Rb	99.9	136.9	80.6	194.1	191.3	321.2	101.0	291.9	222.1
Sr	379.3	1202.0	803.5	390.7	191.1	1791.4	946.8	172.9	209.3
Co	62.8	16.3	39.7	23.8	23.9	39.3	19.7	16.9	16.4
Cs	0.9	2.3	1.3	1.7	7.2	13.3	0.6	3.6	8.7
Ga	18.4	18.9	18.3	16.4	20.9	16.7	18.5	23.1	15.9
Hf	2.8	3.1	3.7	6.0	13.2	13.4	3.8	3.5	8.2
Nb	5.3	5.2	7.2	8.8	37.4	10.6	6.6	8.5	9.7
Ta	0.3	0.3	0.4	0.6	2.9	0.6	0.3	0.8	0.6
Th	3.5	4.0	5.4	20.2	33.2	10.9	6.3	30.2	34.4
U	0.8	3.4	0.9	2.2	7.0	2.8	1.3	3.0	7.0
V	296	14	46	33	<8	155	21	<8	26
W	54.6	113.2	251.4	136.3	165.0	114.8	99.7	139.8	110.8
Zr	107.3	120.0	144.1	232.9	470.4	539.4	141.3	96.7	298.6
Y	26.2	7.9	15.5	11.4	93.2	15.8	8.5	5.6	5.5
La	13.0	17.3	31.8	61.3	137.2	60.4	10.6	12.5	75.6
Ce	26.0	32.9	60.4	96.0	206.3	122.8	37.2	23.4	142.8
Pr	3.20	3.73	6.63	9.54	28.37	14.36	2.83	2.42	13.86
Nd	13.9	14.7	24.9	29.6	105.2	55.6	11.5	8.7	45.3
Sm	3.35	2.51	4.40	4.31	20.76	9.82	2.51	1.99	5.69
Eu	1.02	0.69	1.22	0.99	2.68	2.55	0.80	0.49	1.02
Gd	4.38	1.89	3.54	3.35	20.97	6.58	2.04	1.79	2.78
Tb	0.74	0.24	0.47	0.44	3.25	0.77	0.32	0.23	0.27
Dy	4.85	1.25	2.74	2.37	17.99	3.54	1.76	1.02	1.00
Ho	1.01	0.22	0.53	0.43	3.50	0.51	0.34	0.17	0.15
Er	2.97	0.70	1.63	1.17	9.73	1.35	0.99	0.48	0.49
Tm	0.44	0.10	0.26	0.16	1.42	0.19	0.15	0.06	0.07
Yb	2.79	0.78	1.51	0.93	9.00	1.20	1.21	0.41	0.51
Lu	0.42	0.10	0.22	0.15	1.28	0.17	0.17	0.05	0.08
Mo	0.6	<0.1	<0.1	0.3	0.4	0.2	<0.1	0.1	0.2
Cu	91.1	0.9	1.5	5.4	4.3	4.9	0.4	0.3	19.7
Pb	0.9	1.4	1.4	3.2	5.8	16.3	3.3	4.3	5.0
Zn	41	23	29	37	48	57	21	27	33
Ni	44.5	1.7	4.7	4.0	3.4	114.1	1.5	0.2	1.7
Be	1	1	2	6	2	4	5	7	<1
Au	1.2	2.0	1.0	1.2	2.2	0.7	0.8	1.0	1.3
Sn	1	<1	1	1	2	2	<1	1	2
Tl	0.3	<0.1	0.1	0.3	<0.1	0.4	<0.1	0.2	0.3
Sc	35	2	5	2	<1	11	3	<1	2
TOT/C	0.05	0.03	0.08	0.05	<0.02	<0.02	0.03	<0.02	<0.02
TOT/S	0.09	<0.02	0.02	<0.02	<0.02	<0.02	<0.02	<0.02	<0.02
Mg#	64	53	52	54	8	81	45	31	45
Eu/Eu*	0.81	0.93	0.91	0.77	0.39	0.91	1.05	0.78	0.70
La/Sm_N	2.51	4.45	4.67	9.18	4.27	3.97	2.73	4.06	8.58
Tb/Yb_N	1.20	1.63	1.45	1.99	1.72	3.08	1.28	3.12	2.29

Table 4.9 continued…

Sample	DA13-055	DA13-056	DA13-058	DA13-059	DA13-060	DA13-063	DA13-064	DA13-065	DA13-067
SiO_2 (wt%)	58.12	68.32	48.49	51.21	44.70	66.16	64.67	70.54	50.40
Al_2O_3	18.40	15.81	15.04	18.25	15.27	16.83	17.47	15.27	18.11
Fe_2O_3	6.32	3.11	10.85	5.74	11.31	3.19	2.63	1.97	9.24
MgO	1.15	0.83	8.79	1.30	15.15	0.58	0.52	0.27	4.37
CaO	3.65	2.34	12.23	3.89	10.24	2.56	2.02	1.27	6.46
Na_2O	4.06	4.03	2.00	4.80	1.31	4.47	3.73	4.27	4.47
K_2O	5.49	4.20	0.28	10.78	0.23	4.34	4.57	4.87	2.72
TiO_2	1.03	0.39	0.83	0.34	0.23	0.29	0.26	0.16	1.33
P_2O_5	0.35	0.11	0.07	0.59	<0.01	0.07	0.07	0.04	0.46
MnO	0.09	0.05	0.16	0.13	0.15	0.08	0.07	0.04	0.12
Cr_2O_3	<0.002	<0.002	0.048	<0.002	0.013	<0.002	<0.002	<0.002	<0.002
LOI	0.6	0.6	0.9	1.4	1.0	1.0	3.5	0.9	1.7
Total	99.28	99.77	99.75	98.40	99.66	99.53	99.52	99.64	99.43
Ba (ppm)	4081	938	79	6469	67	2046	2231	1683	2224
Rb	70.1	166.6	1.6	223.8	1.9	98.7	97.6	93.0	78.0
Sr	452.3	292.9	251.4	4321.1	342.5	1478.9	1374.4	1056.8	1521.8
Co	20.6	27.8	60.6	15.9	98.9	16.2	13.8	15.2	33.5
Cs	0.5	4.8	<0.1	5.9	<0.1	1.3	1.1	0.5	1.8
Ga	17.4	18.3	15.5	22.8	10.4	17.6	17.8	18.1	21.0
Hf	22.1	5.3	1.1	26.3	0.3	4.2	4.7	3.7	0.6
Nb	13.9	11.9	2.4	30.3	0.3	7.4	7.5	6.9	6.2
Ta	0.6	1.4	0.1	1.3	<0.1	0.5	0.5	0.4	0.4
Th	1.2	12.9	<0.2	48.5	<0.2	4.7	4.2	3.8	1.7
U	1.1	3.3	<0.1	8.7	<0.1	1.5	0.9	1.1	0.4
V	39	29	200	61	66	40	33	24	201
W	78.5	172.5	58.1	65.8	48.0	96.4	70.5	99.1	38.4
Zr	1150.5	177.7	35.1	1282.1	11.4	174.6	186.7	141.3	14.2
Y	23.7	29.7	13.4	33.0	4.8	16.1	14.0	6.1	9.7
La	18.4	42.4	5.3	245.4	2.0	31.9	35.9	14.8	37.4
Ce	33.3	58.6	11.7	477.8	4.3	75.6	60.5	38.3	62.5
Pr	4.14	7.48	1.66	51.92	0.61	7.73	7.77	3.48	6.58
Nd	17.0	26.4	8.0	180.5	3.1	28.1	27.8	12.6	25.9
Sm	3.44	5.02	2.07	26.96	0.67	5.00	4.76	2.45	4.10
Eu	2.16	1.02	0.77	7.05	0.38	1.36	1.35	0.67	1.62
Gd	3.92	5.63	2.61	16.09	0.84	4.08	3.65	1.87	3.19
Tb	0.57	0.92	0.44	1.80	0.13	0.54	0.50	0.26	0.40
Dy	3.19	5.18	2.53	7.48	0.85	2.91	2.78	1.22	2.03
Ho	0.76	1.04	0.56	1.13	0.17	0.56	0.52	0.24	0.36
Er	2.19	2.92	1.46	2.81	0.47	1.57	1.60	0.66	0.95
Tm	0.31	0.41	0.22	0.40	0.07	0.24	0.26	0.10	0.11
Yb	2.07	2.68	1.31	2.42	0.44	1.68	1.75	0.73	0.71
Lu	0.37	0.37	0.21	0.35	0.07	0.25	0.24	0.11	0.11
Mo	0.5	<0.1	<0.1	<0.1	<0.1	<0.1	<0.1	<0.1	0.4
Cu	11.9	5.7	99.2	3.5	70.8	0.9	0.4	0.4	61.3
Pb	1.0	7.5	0.5	150.1	0.4	1.8	4.3	7.6	2.5
Zn	62	49	9	71	27	10	20	11	67
Ni	1.3	3.9	61.3	4.5	298.5	0.2	0.8	0.5	10.5
Be	<1	1	<1	9	<1	1	3	<1	4
Au	1.7	2.1	1.0	0.7	1.2	0.9	1.3	0.6	1.4
Sn	<1	2	<1	2	<1	1	1	<1	<1
Tl	0.2	0.5	<0.1	1.3	<0.1	<0.1	<0.1	<0.1	0.5
Sc	9	7	32	4	16	5	4	2	16
TOT/C	0.06	0.07	0.11	0.13	0.19	<0.02	0.04	<0.02	0.14
TOT/S	<0.02	<0.02	0.10	0.22	0.04	<0.02	<0.02	<0.02	0.10
Mg#	42	51	76	47	84	42	44	35	65
Eu/Eu*	1.79	0.58	1.01	0.96	1.55	0.89	0.95	0.92	1.32
La/Sm_N	3.45	5.45	1.65	5.88	1.93	4.12	4.87	3.90	5.89
Tb/Yb_N	1.05	1.69	1.42	3.49	1.26	1.47	1.41	1.61	2.47

Table 4.9 continued…

Sample	DA13-069	DA13-071	DA13-074	DA13-076	DA13-077	DA13-083	DA14-133	DA14-140	DA14-146
SiO_2 (wt%)	68.35	48.03	66.57	66.54	69.93	75.50	73.83	73.77	77.40
Al_2O_3	15.36	14.96	14.33	14.95	13.96	11.82	13.37	13.31	12.06
Fe_2O_3	2.47	10.68	5.64	5.44	3.80	2.00	1.67	2.00	0.65
MgO	1.07	9.15	0.60	0.33	0.18	0.49	0.24	0.09	0.02
CaO	1.73	12.47	2.77	3.17	1.36	0.99	0.92	0.90	0.45
Na_2O	4.74	2.00	2.97	2.94	3.23	2.81	3.50	4.17	2.96
K_2O	4.84	0.45	4.99	5.16	6.03	5.04	5.27	4.95	5.61
TiO_2	0.25	0.79	0.77	0.67	0.39	0.38	0.19	0.16	0.16
P_2O_5	0.17	0.03	0.23	0.18	0.06	0.07	0.04	0.02	<0.01
MnO	0.03	0.15	0.06	0.06	0.05	0.03	0.03	0.04	<0.01
Cr_2O_3	0.002	0.017	<0.002	<0.002	<0.002	0.012	<0.002	<0.002	<0.002
LOI	0.5	1.0	0.7	0.2	0.7	0.6	0.8	0.4	0.5
Total	99.53	99.71	99.68	99.66	99.67	99.77	99.82	99.84	99.85
Ba (ppm)	2192	152	1340	1276	679	813	546	309	401
Rb	94.4	10.2	214.7	177.3	243.1	104.3	185.5	218.5	188.9
Sr	1240.0	411.5	204.8	219.6	86.6	167.2	114.7	76.3	93.6
Co	20.9	69.8	20.1	25.0	39.0	27.0	23.6	27.9	36.8
Cs	0.3	1.4	2.4	1.7	4.2	0.2	1.9	1.1	0.3
Ga	18.5	13.3	24.6	25.1	29.2	12.4	15.9	20.4	17.3
Hf	2.7	1.0	9.9	15.8	15.3	8.6	5.7	9.9	8.3
Nb	3.2	1.2	31.1	25.6	43.4	11.1	8.4	23.3	10.7
Ta	0.2	<0.1	2.2	1.7	2.6	0.8	0.4	2.4	0.4
Th	1.4	0.6	19.3	15.0	26.1	15.4	25.8	32.6	20.4
U	0.8	0.2	3.3	3.0	4.8	0.6	3.7	8.6	3.0
V	40	247	16	<8	<8	19	<8	<8	<8
W	122.3	51.5	120.3	166.7	289.1	190.6	192.1	220.1	280.8
Zr	96.7	34.2	410.5	635.4	579.8	325.6	178.9	345.3	248.9
Y	7.4	9.8	55.3	47.1	118.9	27.9	105.2	55.9	36.9
La	33.6	5.2	96.9	69.3	123.4	76.6	149.6	63.5	39.3
Ce	57.7	10.6	180.4	139.2	272.5	153.6	95.4	121.2	77.6
Pr	6.69	1.41	19.62	15.73	32.68	16.59	21.53	12.21	8.65
Nd	24.2	7.2	71.3	59.4	121.6	57.3	83.5	39.5	31.1
Sm	3.88	1.67	12.08	11.34	25.95	10.36	15.77	7.81	6.23
Eu	1.09	0.81	2.26	2.49	1.81	1.16	2.15	0.74	0.71
Gd	2.71	2.10	11.35	10.44	24.24	8.08	22.38	7.07	6.20
Tb	0.29	0.35	1.72	1.64	4.10	1.17	3.14	1.30	1.08
Dy	1.47	2.11	9.93	9.02	22.76	6.02	16.86	8.11	6.73
Ho	0.28	0.42	2.00	1.75	4.49	1.11	3.37	1.80	1.36
Er	0.63	1.04	5.92	4.97	12.92	2.74	8.54	5.52	3.88
Tm	0.09	0.15	0.83	0.72	1.90	0.38	1.12	0.94	0.59
Yb	0.59	1.00	5.63	4.54	11.46	2.23	6.29	6.12	3.49
Lu	0.09	0.14	0.85	0.71	1.67	0.30	0.99	0.91	0.52
Mo	<0.1	<0.1	1.7	1.8	1.2	<0.1	0.1	1.3	0.2
Cu	108.7	60.2	6.3	6.3	2.8	0.8	0.8	2.7	0.3
Pb	3.6	0.6	2.4	1.5	4.5	0.9	3.1	3.1	1.5
Zn	15	11	81	36	127	27	29	18	9
Ni	6.5	65.7	0.4	0.2	0.4	1.2	0.5	0.3	0.2
Be	<1	<1	4	3	6	2	2	8	3
Au	1.5	1.3	0.9	1.1	0.7	<0.5	1.1	<0.5	1.5
Sn	1	<1	2	2	7	1	2	7	1
Tl	0.2	<0.1	0.5	<0.1	0.5	0.1	0.2	0.2	<0.1
Sc	4	32	8	6	6	2	2	<1	1
TOT/C	<0.02	0.09	0.07	0.07	<0.02	0.03	0.03	0.03	<0.02
TOT/S	<0.02	0.17	0.02	<0.02	<0.02	<0.02	<0.02	<0.02	<0.02
Mg#	63	77	30	19	16	49	36	15	11
Eu/Eu*	0.98	1.32	0.58	0.69	0.22	0.37	0.35	0.30	0.35
La/Sm_N	5.59	2.01	5.18	3.95	3.07	4.77	6.12	5.25	4.07
Tb/Yb_N	2.19	1.70	1.37	1.57	1.67	2.65	2.15	0.97	1.41

Table 4.9 continued…

Sample	DA14-147	DA14-229	DA14-234	DA14-347	DA14-355	DA14-364	DA14-374
SiO_2 (wt%)	49.98	60.77	54.02	49.83	58.03	64.39	66.00
Al_2O_3	13.41	18.06	12.64	13.45	18.31	17.49	14.56
Fe_2O_3	14.43	4.93	6.24	14.26	6.34	2.52	5.64
MgO	7.32	2.35	7.61	7.38	1.16	0.54	0.61
CaO	10.61	4.78	5.70	10.56	3.63	2.01	2.77
Na_2O	2.02	5.16	2.28	2.01	3.97	3.74	2.96
K_2O	0.29	1.92	6.65	0.26	5.46	4.62	5.13
TiO_2	1.21	0.65	0.85	1.21	0.95	0.27	0.79
P_2O_5	0.09	0.28	1.00	0.10	0.35	0.08	0.22
MnO	0.21	0.06	0.11	0.21	0.09	0.07	0.06
Cr_2O_3	0.017	0.004	0.049	0.016	<0.002	<0.002	<0.002
LOI	0.1	0.6	1.3	0.4	1.0	3.8	0.9
Total	99.73	99.55	98.49	99.72	99.29	99.52	99.66
Ba (ppm)	275	1640	8225	290	4070	2278	1336
Rb	7.0	25.2	331.9	7.5	65.1	93.5	210.9
Sr	138.0	1405.9	2620.3	146.8	434.6	1360.6	208.0
Co	68.4	22.1	42.3	75.1	19.6	13.9	19.3
Cs	0.2	0.3	15.0	<0.1	0.4	1.1	2.6
Ga	14.8	17.2	14.1	14.4	16.8	17.3	23.2
Hf	2.1	4.7	7.1	2.2	21.1	4.0	12.4
Nb	6.3	4.3	3.5	6.2	13.1	8.3	31.4
Ta	0.3	0.2	0.2	0.3	0.7	0.5	2.5
Th	1.1	1.0	8.6	0.9	1.2	8.2	21.3
U	0.2	0.2	4.0	0.2	1.2	1.0	4.1
V	337	74	84	333	40	29	15
W	85.1	86.0	62.2	92.5	80.2	68.9	115.0
Zr	74.3	211.4	219.5	78.3	1077.0	165.3	482.1
Y	24.0	9.2	26.6	24.3	23.3	14.5	53.0
La	8.8	35.5	182.7	9.3	18.9	37.8	97.6
Ce	17.2	60.9	343.8	19.1	34.3	58.3	188.0
Pr	2.36	6.46	37.75	2.52	4.15	7.98	20.54
Nd	11.1	23.6	135.9	10.8	17.1	29.9	71.3
Sm	3.04	3.16	20.30	3.08	3.42	4.97	12.27
Eu	1.00	1.31	4.98	1.05	2.19	1.42	2.19
Gd	3.66	2.59	12.99	4.00	3.84	3.78	11.17
Tb	0.67	0.34	1.41	0.70	0.54	0.52	1.69
Dy	3.91	1.90	6.15	4.43	3.31	2.93	9.15
Ho	0.88	0.32	0.81	0.94	0.68	0.54	1.92
Er	2.49	0.87	2.00	2.68	1.93	1.63	5.30
Tm	0.38	0.13	0.25	0.39	0.31	0.24	0.81
Yb	2.41	0.76	1.53	2.50	2.00	1.60	5.38
Lu	0.36	0.12	0.23	0.41	0.36	0.25	0.78
Mo	0.1	<0.1	<0.1	0.1	0.4	<0.1	2.2
Cu	97.7	16.8	1.2	97.9	10.8	0.4	6.0
Pb	0.3	0.6	8.3	0.3	0.9	4.4	2.5
Zn	15	46	52	15	58	20	83
Ni	58.8	23.8	124.8	61.5	1.1	0.8	0.3
Be	<1	1	3	1	3	3	4
Au	<0.5	<0.5	0.5	<0.5	<0.5	<0.5	0.8
Sn	<1	<1	2	<1	<1	1	3
Tl	<0.1	0.1	0.8	<0.1	0.2	<0.1	0.5
Sc	43	8	13	43	10	4	8
TOT/C	<0.02	0.02	0.02	0.02	0.06	0.04	0.08
TOT/S	0.06	<0.02	<0.02	0.06	<0.02	<0.02	<0.02
Mg#	67	65	83	67	42	46	30
Eu/Eu*	0.92	1.36	0.88	0.91	1.84	0.96	0.56
La/Sm_N	1.87	7.25	5.81	1.95	3.57	4.91	5.14
Tb/Yb_N	1.26	1.92	4.16	1.16	1.02	1.41	1.47

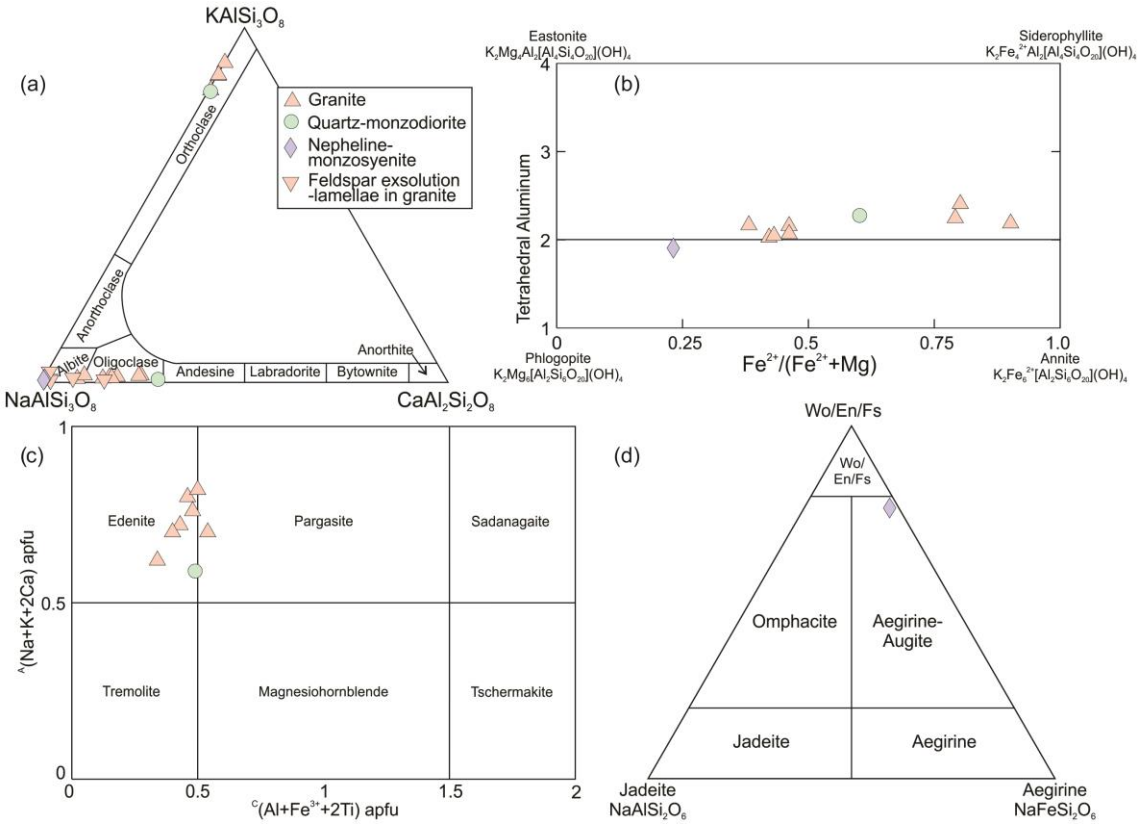

Fig. 4.6 Mineral compositions from EPMA analyses for: (a) alkali-feldspar, plagioclase and plagioclase exsolution-lamellae in perthite; (b) biotite (Rieder et al., 1998; Deer et al., 2013); (c) calcium amphibole (Hawthorne et al., 2012); and (d) sodium pyroxene (Morimoto, 1988).

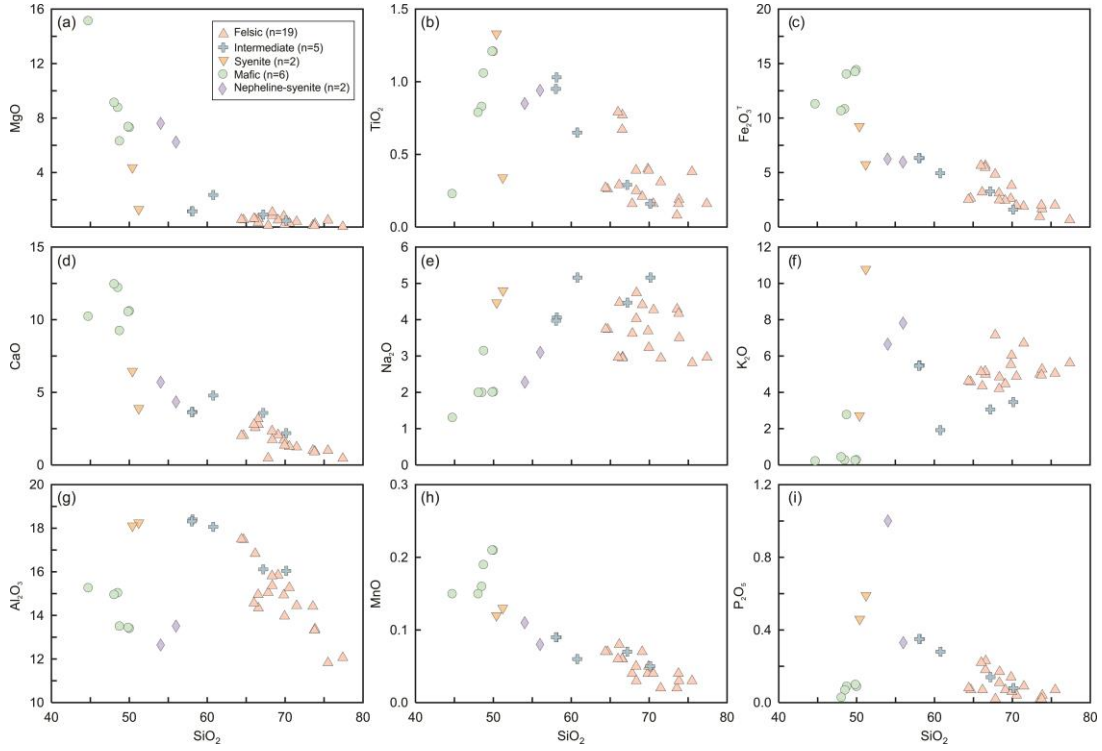

Fig. 4.7 Harker major element variation diagrams for major element oxides, showing the extent of fractionation in the Imorona-Itsindro Suite. Assigned symbols are based on the modal mineralogy shown in Table 4.2 and Fig. 4.3.

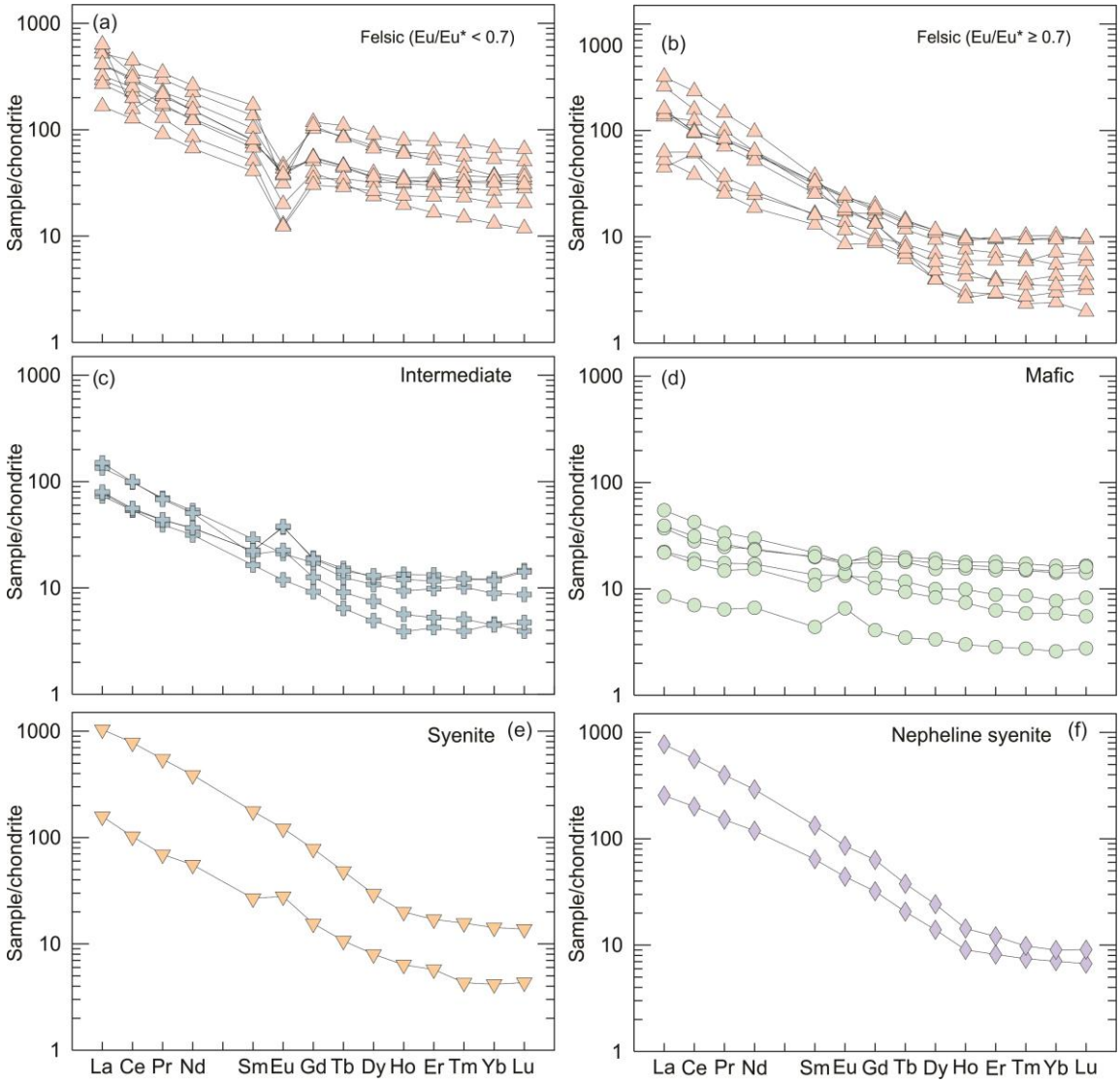

Fig. 4.8 Chondrite-normalized REE diagrams: (a) felsic samples with Eu/Eu* <0.70; (b) felsic samples with Eu/Eu* ≥ 0.70; (c) intermediate; (d) gabbro; (e) syenite; and (f) nepheline syenite. Data are from Table 4.9. Chondrite-normalizing values are from Sun and McDonough (1989). Symbols are the same as Fig. 4.7.

The same subdivisions used in Fig. 4.8 are used for trace-element spider diagrams (Fig. 4.9). MORB normalised spider diagrams (Pearce et al., 1981; Pearce, 1983) for felsic samples indicate enrichment in the large-ion-lithophile elements (LILEs) and depletions in Ta-Nb, P, and Ti (Figs. 9a, b). Intermediate samples exhibit a similar pattern to the felsic samples but the magnitude of negative Ta-Nb, P, and Ti anomalies is less (Fig. 4.9c). Mafic samples show a different pattern of moderate enrichment in LILEs and negative Nb and Ta anomalies are moderate in mafic rocks compared to felsic and intermediate samples (Fig. 4.9d). High-field strength elements (HFSEs) exhibit a relatively flat pattern. Syenite and nepheline-syenite samples demonstrate a comparable pattern to intermediate and felsic samples (Figs. 4.9e, f).

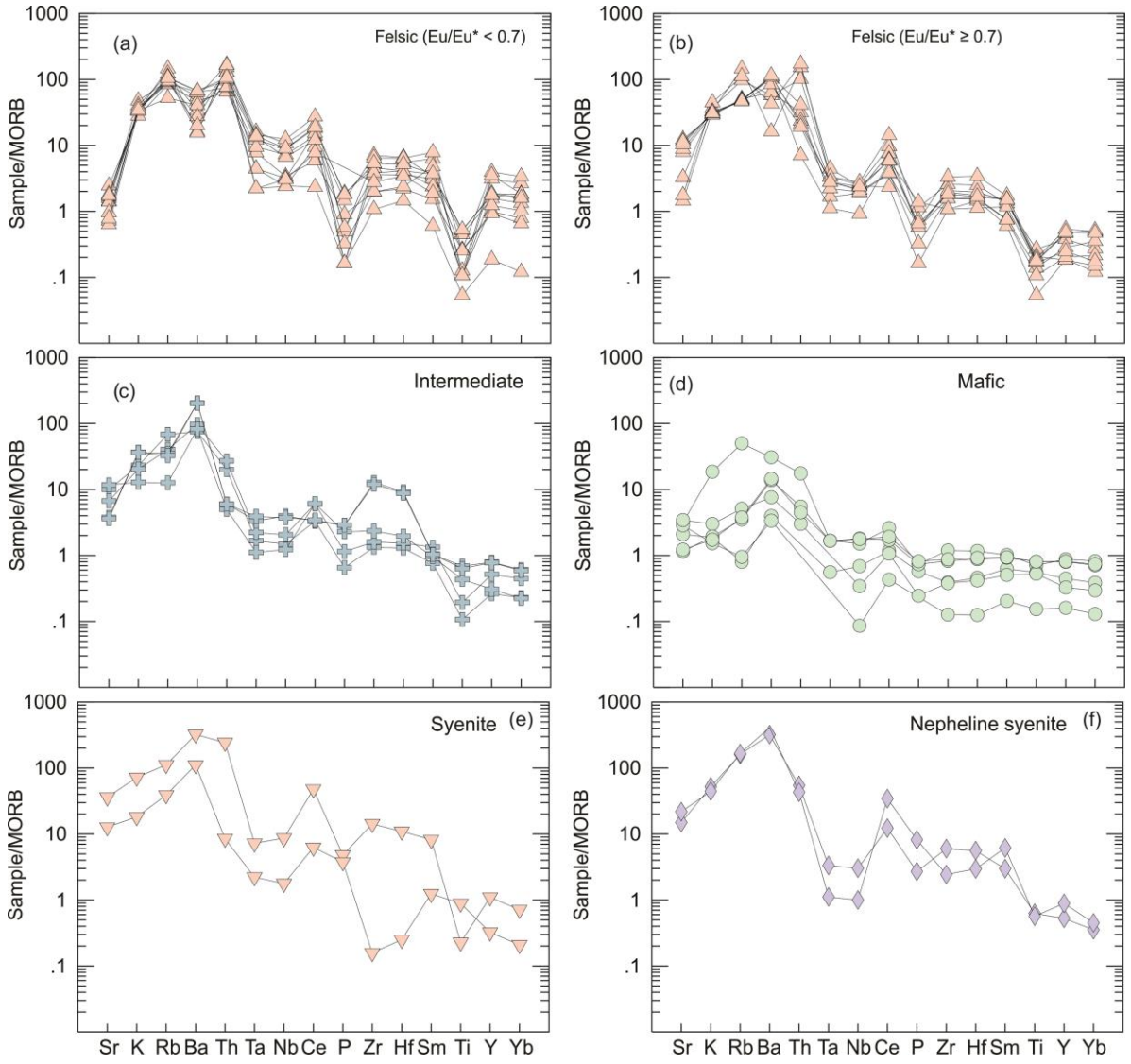

Fig. 4.9 MORB normalised trace-element spider diagrams (Pearce, 1983; Pearce et al., 1981) for samples of the Imorona-Itsindro Suite: (a) felsic samples with Eu/Eu* <0.70; (b) felsic samples with Eu/Eu* ≥ 0.70; (c) intermediate; (d) gabbro; (e) syenite; and (f) nepheline syenite. Data are from Table 4.9. Symbols are the same as Fig. 4.7.

Sm-Nd-Sr isotopes

Twenty-one samples including one duplicate (DA14-374) were selected for Sm-Nd and Sr isotopic analyses (Table 4.10). Thirteen felsic samples have $^{87}Sr/^{86}Sr(t)$ ratios between 0.70563 and 0.72522 (average = 0.71263; n=13). $^{143}Nd/^{144}Nd(t)$ ratios are between 0.51080 and 0.51156 (average = 0.51103; n=13). $\varepsilon_{Nd}(t)$ values vary from evolved values of -15.86 to near chondritic values of -0.23 (average = -11.07; n=15) and corresponding $T_{DM}c$ model ages are between 1.52 and 2.98 Ga. The least evolved $\varepsilon_{Nd}(t)$ values correspond to samples that intrude into the Ikalamavony Domain. Intermediate samples have $^{87}Sr/^{86}Sr(t)$ ratios between 0.70927 and 0.71257 (average = 0.70852; n=3). $^{143}Nd/^{144}Nd(t)$ ratios are between 0.51083 and 0.51106 (average = 0.51094; n=3). $\varepsilon_{Nd}(t)$ values are evolved (-14.80 to -11.18; average = -12.63; n=3) and corresponding $T_{DM}c$ model ages are between 2.30 and 2.57 Ga. Syenite and nepheline syenite samples have $^{87}Sr/^{86}Sr(t)$ ratios between 0.70592 and 0.72639 (average = 0.71280; n=3). $^{143}Nd/^{144}Nd(t)$ ratios are between 0.51106 and 0.51121 (average = 0.51115; n=3). Syenitic samples have less evolved $\varepsilon_{Nd}(t)$ values between -7.74 to -10.66 (average = -9.03; n=3) and corresponding $T_{DM}c$ model ages are between 1.84 and 2.10 Ga. Two gabbroic

samples have $^{87}Sr/^{86}Sr(t)$ ratios of 0.72072 and 0.70643. $^{143}Nd/^{144}Nd(t)$ ratios are 0.51102 and 0.51141. Gabbroic samples have $\varepsilon_{Nd}(t)$ values of -15.22 and -6.63 providing corresponding $T_{DM}c$ model ages are 3.58 and 2.83 Ga.

4.5 Discussion

4.5.1 Petrogenesis of the Imorona-Itsindro Suite

Voluminous Tonian magmatism is represented by the Imorona-Itsindro Suite in central Madagascar and demonstrates broad geochemical variation in both space and time. Previous work on the age of the suite show emplacement occurred between ~850 and 750 Ma (Handke et al., 1997; Handke et al., 1999; Tucker et al., 1999b; Kröner et al., 2000; BGS-USGS-GLW, 2008; Tucker et al., 2014; Archibald et al., 2016). Slightly younger (~ 750-700 Ma) plutonic and volcanic rocks in the Bemarivo Domain are represented by the Antsirabe-Nord and Manambato plutonic suites and the Daraina and Milanoa volcano-sedimentary groups (Thomas et al., 2009). Positive $\varepsilon_{Nd}(t)$ values (Tucker et al., 1999a) and an absence of older xenocrystic zircons demonstrated that Tonian-aged magmas in the Bemarivo Domain were largely uncontaminated by continental crust (Thomas et al., 2009) in contrast to the slightly older Tonian rocks in central Madagascar (this study; Archibald et al., in review; Tucker et al., 1999b; Kroner *et al*., 2000). Therefore, Thomas et al. (2009) concluded that the Antsiribe-Nord and Manambato Suites were sourced from the depleted-mantle into juvenile crust above a subduction zone. Because of the potentially dissimilar Neoproterozoic histories for the Bemarivo Domain and the rest of Madagascar, this discussion is restricted to plutonic rocks emplaced between ~850 Ma and 750 Ma in central and southern Madagascar.

An important feature of the Imorona-Itsindro Suite is the wide range of magma compositions emplaced simultaneously into the Malagasy basement. Some authors have suggested the suite is essentially bi-modal consisting mainly of granite and gabbro (e.g. Tucker et al., 2014). However, considering the continuous SiO_2 variation from mafic to felsic and the occurrence of lithologies varying in composition from ultramafic (McMillan et al., 2003) to granite to silica-undersaturated rocks (Fig. 4.10) the suite cannot be considered bi-modal. The normative mineralogy calculated using whole-rock geochemical data demonstrates the overall abundances of mafic, intermediate and felsic intrusions with fewer occurrences of ultramafic rocks and feldspathoid-bearing lithologies (Fig. 4.10). The AFM diagram (Irvine and Baragar, 1971) shows that the mafic samples are predominantly tholeiitic, whereas intermediate to felsic lithologies are calc-alkaline (Fig. 4.11a). Intermediate and felsic rocks are primarily calc-alkaline reflecting lower FeO^T/MgO ratios during melt evolution (Fig. 4.11a). The intermediate to felsic lithologies consist almost exclusively of metaluminous to weakly peraluminous granitoids (Fig. 4.11b). Only four samples are peralkaline. Tectonic discrimination diagrams (Pearce et al., 1984) demonstrate that Imorona-Itsindro Suite samples have geochemical features typical of volcanic-arc or syn-collisional granitoids (Figs. 4.11 c, d). The slightly higher rare-earth element concentrations observed in some of the more geochemically evolved samples (e.g. DA13-074) results in some samples plotting in the within-plate granite fields but, nevertheless, the majority of samples plot in the volcanic-arc fields. Tectonic discrimination diagrams for mafic rocks indicate a similar tectonic setting (Figs. 4.11e, f). Samples plot predominantly in the calc-alkaline and continental-arc fields on both diagrams (Figs. 4.11e, f).

Table 4.10 Nd-Sm, and Sr isotope data determined by Thermal Ionisation Mass Spectroscopy (TIMS). *Age assigned based on field relationships.

Sample	Age	± 2σ	Sm (ppm)	Nd (ppm)	$^{147}Sm/^{144}Nd$	$^{143}Nd/^{144}Nd$ (t)	± 2σ (x10^{-6})	ε_{Nd} (0)	ε_{Nd} (t)	T_{DM} (Ma)	Rb (ppm)	Sr (ppm)	$^{87}Sr/^{86}Sr$	± 2σ (x10^{-6})	$^{87}Sr/^{86}Sr$ (t)
DA13-002	*800		13.7	3.6	0.1600	0.511019	2	-15.22	-11.49	3582	99.9	379.3	0.729441	3	0.720716
DA13-012	849	17	14.0	2.5	0.1079	0.510934	2	-21.51	-11.90	2299	136.9	1202.0	0.709274	3	0.705276
DA13-017	814	19	24.1	4.5	0.1132	0.510831	3	-23.46	-14.80	2565	80.6	803.5	0.711099	3	0.707724
DA13-020	758	10	29.0	4.4	0.0907	0.510981	2	-23.53	-13.29	2107	194.1	390.7	0.730323	3	0.714734
DA13-029	828	14	96.2	19.5	0.1225	0.511259	2	-13.93	-6.09	2024	191.3	191.1	0.743516	3	0.709141
DA13-040	*800		60.8	11.2	0.1116	0.511162	2	-17.38	-8.70	2070	321.2	1791.4	0.71185	3	0.705921
DA13-049	827	16	12.6	2.9	0.1395	0.510918	2	-18.79	-12.78	2979	101.0	946.8	0.710852	3	0.707205
DA13-055	780	7	17.7	3.8	0.1289	0.511061	1	-17.91	-11.18	2533	70.1	452.3	0.717569	3	0.71257
DA13-063	798	8	31.3	5.7	0.1100	0.510900	2	-22.68	-13.87	2432	98.7	1478.9	0.709419	3	0.707219
DA13-064	819	19	26.9	4.9	0.1095	0.510913	4	-22.18	-13.08	2383	97.6	1374.4	0.709487	3	0.707083
DA13-067	*800		26.6	4.5	0.1020	0.511061	2	-20.31	-10.66	2098	78.0	1521.8	0.707775	3	0.706081
DA13-069	*800		25.8	4.3	0.0997	0.510845	2	-24.77	-14.89	2356	94.4	1240.0	0.708489	3	0.705909
DA13-074	821	11	75.5	13.9	0.1112	0.510900	2	-22.23	-13.29	2425	214.7	204.8	0.760975	4	0.725222
DA13-074 (dup)	821	11	73.2	13.6	0.1125	0.510914	2	-21.82	-13.02	2426	177.3	219.6	0.747944	3	0.720915
DA13-076	807	9	60.1	12.6	0.1269	0.510921	2	-20.39	-13.22	2693	243.1	86.6	0.80999	3	0.711911
DA13-077	837	15	133.1	28.6	0.1298	0.511119	2	-15.73	-8.60	2362	104.3	167.2	0.732778	4	0.712238
DA13-083	795	13	60.7	12.2	0.1217	0.510802	2	-23.45	-15.86	2798	185.5	114.7	0.768223	3	0.712825
DA14-133	824	23	91.8	18.4	0.1210	0.511564	1	-8.20	-0.23	1517	188.9	93.6	0.789208	4	0.724164
DA14-146	774	11	34.3	7.3	0.1278	0.511346	2	-12.54	-5.75	2024	7.0	138.0	0.707269	3	0.705634
DA14-147	*800		11.4	3.2	0.1688	0.511412	2	-6.63	-3.80	2828	331.9	2620.3	0.710617	3	0.706429
DA14-234	*800		142.3	22.6	0.0959	0.511211	2	-18.02	-7.74	1841	210.9	208.0	0.760973	3	0.726393

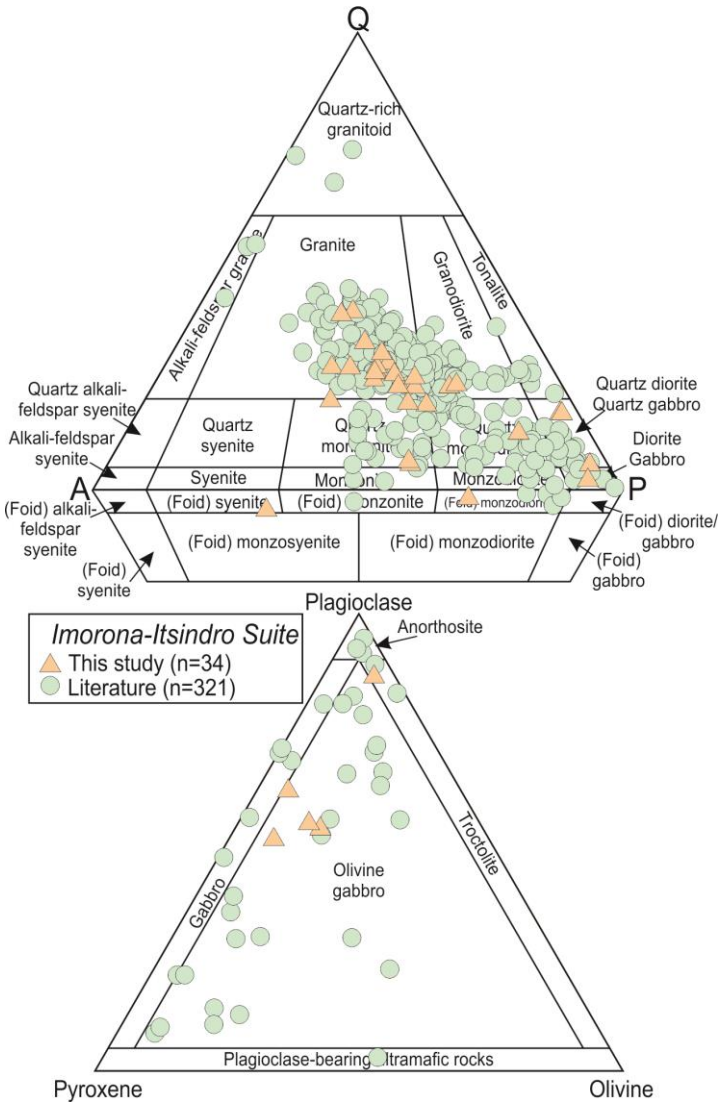

Fig. 4.10 Plutonic rock classification diagrams (Streckeisen, 1976) using normative mineralogy for all Imorona-Itsindro Suite samples (n=355). Whole-rock geochemical data are from this study, BGS-USGS-GLW (2008), CGS (2009a), GAF-BGR (2008e), Zhou et al. (2015b), Yang et al. (2014), Bybee et al. (2010), Boger et al. (2014), McMillan et al. (2003), Kröner et al. (2000), and Kröner et al. (1999a).

Water plays an important role in arc magma genesis. The negative Ti-anomaly in arc magmas reflects an increase in Ti compatibility in the solid residue during partial melting of water-bearing peridotite (Elburg, 2010). Water also influences which minerals are involved in crystal fractionation processes. The low-Fe (calc-alkaline) fractionation trend can be produced by lowering the temperature at which silicate minerals begin crystallising without influencing the crystallisation temperature of iron-oxides (Elburg, 2010). Fractionation of Fe-Ti oxides impedes the FeO^T/MgO ratio causing a depletion of iron in the residual magma. Water can delay plagioclase crystallisation meaning arc magmas commonly show early olivine and pyroxene crystallisation before plagioclase (Elburg, 2010). Major element bivariate diagrams (Fig. 4.7d, g) indicates early crystallisation of pyroxene removes Ca but not Al then both Al and Ca fractionate following the onset of plagioclase crystallisation. Myrmeckite, perthite and granophyric textures are common throughout the suggesting emplacement of some intrusions under shallow, undercooled and water-rich conditions. Flat HREE profiles imply a shallow (<100km) spinel lherzolite mantle source for these mantle derived melts rather than a deeper (>100km) garnet lherzolite source (Fig. 4.8). However, mantle melting is not the only process involved in generating the Imorona-Itsindro Suite as demonstrated by incorporation of crustal

material into evolving magmas (Fig. 4.4d). Mixing of mantle-derived melts (mafic end-member) with crustally-derived melts (felsic end-member) can produce intermediate compositions and calc-alkaline trends (Grove et al., 2004). Field evidence from the Itremo Domain shows magma mixing and mingling textures are common (Fig. 4.4b). Gabbroic rocks in the Ambatondrazaka area were inferred to represent involvement of an enriched component during magma emplacement (Zhou et al., 2015b). The narrow range of $\varepsilon_{Hf}(t)$ values and corresponding TDMc model ages (2.06–1.94 Ga) were interpreted to result from mixing of both primary Tonian mantle and inherited Neoarchaean crustal sources initiated by underplating of mantle derived magmas that subsequently triggered partial melting of thinned lower crust (Zhou et al., 2015b). We propose a combination of mantle-derived melts mixing with crustal melts or assimilation of crustally derived material followed by subsequent fractional crystallisation.

Sr and Nd isotopic compositions reflect mixing between different sources with contrasting high and low $^{143}Nd/^{144}Nd$ ratios. All $\varepsilon_{Nd}(t)$ data collected for the Imorona-Itsindro Suite over the past two decades have negative values and most have $\varepsilon_{Nd}(t)$ values lower than -5 (Fig. 4.12a). These $\varepsilon_{Nd}(t)$ data combined with previous studies demonstrating inheritance of xenocrystic zircon domains, evolved $\varepsilon_{Hf}(t)$ values in zircon, and crustal $\delta^{18}O$ ratios (Archibald et al., 2016) also support significant crustal involvement during magma genesis. $\varepsilon_{Nd}(t)$ data plotted against $\varepsilon_{Hf}(t)$ data from zircon from the same samples show a positive linear correlation evolving from the most depleted samples intruding into the Ikalamavony Domain and the Ambatondrazaka Gabbro (Zhou et al., 2015a) to more evolved isotopic signatures for samples intruding the Itremo and Antananarivo Domain crust (Fig. 4.12b). Hafnium isotope data in zircon (Nd data unavailable) for the Antanimbary granitoid near Maevatanana are evolved between -18.2 and -15.1 (Yang et al., 2014). Significant crustal involvement is also shown on a plot of $^{143}Nd/^{144}Nd(t)$ versus $^{87}Sr/^{86}Sr(t)$ where data plots below CHUR (chondrite uniform reservoir) in the evolved, crustal field (Fig. 4.12c). $^{87}Sr/^{86}Sr(t)$ values in this study vary between 0.70592 and 0.72639 but are as high as 0.82044 in granite samples from the Ranomandry Complex (McMillan et al., 2003). These values are much higher than values expected for MORB (Saunders et al., 1988) or plume generated magmas such as those in the East African Rift (e.g. Rogers *et al*., 2000). Elevated $^{87}Sr/^{86}Sr(t)$ values are typically found in ancient cratons (Windrim and McCulloch, 1986) or in rocks generated by melting of a metasedimentary protolith (McCulloch and Chappell, 1982).

The heterogeneity of basement rocks in central Madagascar provides the variety of crustal sources required to form the diverse geochemical signatures recorded in Tonian samples. Partial melting of the metasedimentary Manampotsy Group resulted in the Brickaville Orthogneiss (BGS-USGS-GLW, 2008), intrusions that contain magmatic muscovite and garnet. Most of the Imorona-Itsindro Suite samples intrude the Antananarivo and Itremo Domains (Fig. 2). Previous authors showed that the Antananarivo Domain crust originated by mixing between Neoarchaean depleted mantle and Mesoarchaean crust based on juvenile $\varepsilon_{Nd}(t)$ signatures and corresponding Mesoarchaean to Neoarchaean Nd model ages (Tucker et al., 1999b; Kröner et al., 2000; Tucker et al., 2014). Tonian rocks also intrude into the Ikalamavony Domain which consists of a juvenile Mesoproterozoic oceanic arc and marginal volcano-sedimentary sequence (CGS, 2009a; Tucker et al., 2014). Isotope data for Tonian samples from the Ikalamavony Domain reflect the juvenile nature of these basement rocks (this study; Archibald *et al.*, in review-a). The rare samples of silica-undersaturated melts are from a restricted area near boundary between the Itremo and Ikalamavony Domains and the Antananarivo Domain (Roig et al., 2012). Silica-undersaturated rocks are uncommon in arc tectonic settings. Neoproterozoic nepheline syenites in Malawi show similar trace element and REE profiles to the Tonian-aged nepheline syenite in Madagascar (Eby et al., 1998). REE patterns show moderate LREE enrichment and a flattening HREE trend. None of

the syenite samples display a Eu anomaly suggesting plagioclase fractionation did not play a significant role during the evolution of these magmas (Fig. 4.8). The authors suggested that the syenitic lithologies in Malawi were generated by high-pressure fractionation of an ocean-island basalt (OIB-like) source derived from the metasomatised lithosphere (Eby et al., 1998).

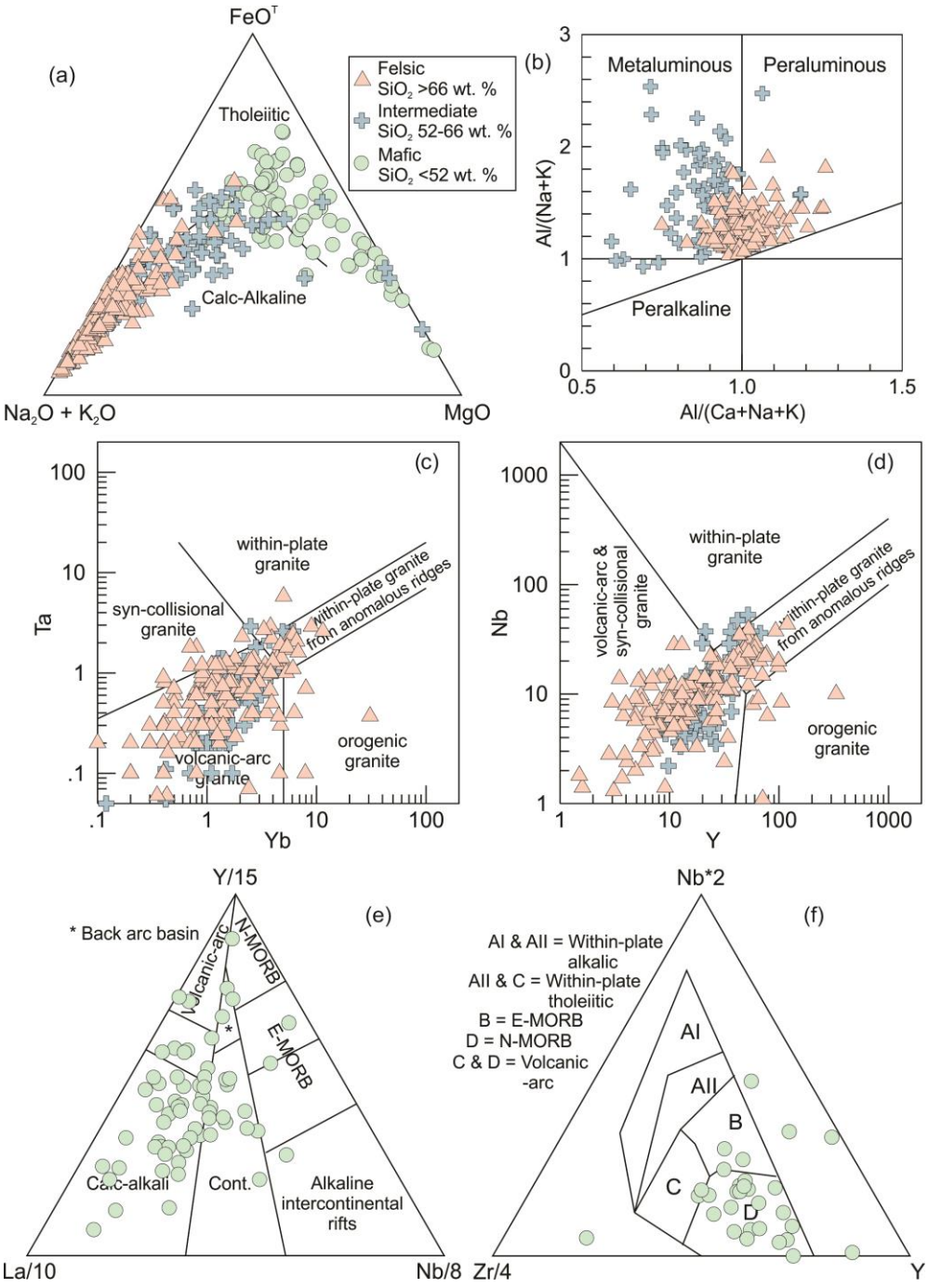

Fig. 4.11 Tectonic setting and classification diagrams for samples of the Imorona-Itsindro Suite: (a) AFM ($A=Na_2O+K_2O$; $F=FeO+Fe_2O_3$; $M=MgO$) diagram showing the boundary between calc-alkaline and tholeiitic trends (Irvine and Baragar, 1971); (b) Plot of A/NK = molar $Al_2O_3/(Na_2O+K_2O)$ versus A/CNK = molar $Al_2O_3/(CaO + Na_2O + K_2O)$; (c-d) Tectonic discrimination diagrams for intermediate and felsic rocks after Pearce et al. (1984); (e-f) Tectonic discrimination diagrams for mafic rocks. (e) La/10 v. Y/15 v. Nb/8 (Cabanis and Lecolle, 1989) and (f) Zr/4 v. Nb*2 v. Y (Meschede, 1986). Data are from Table 4.9 and the references listed in Fig. 4.10.

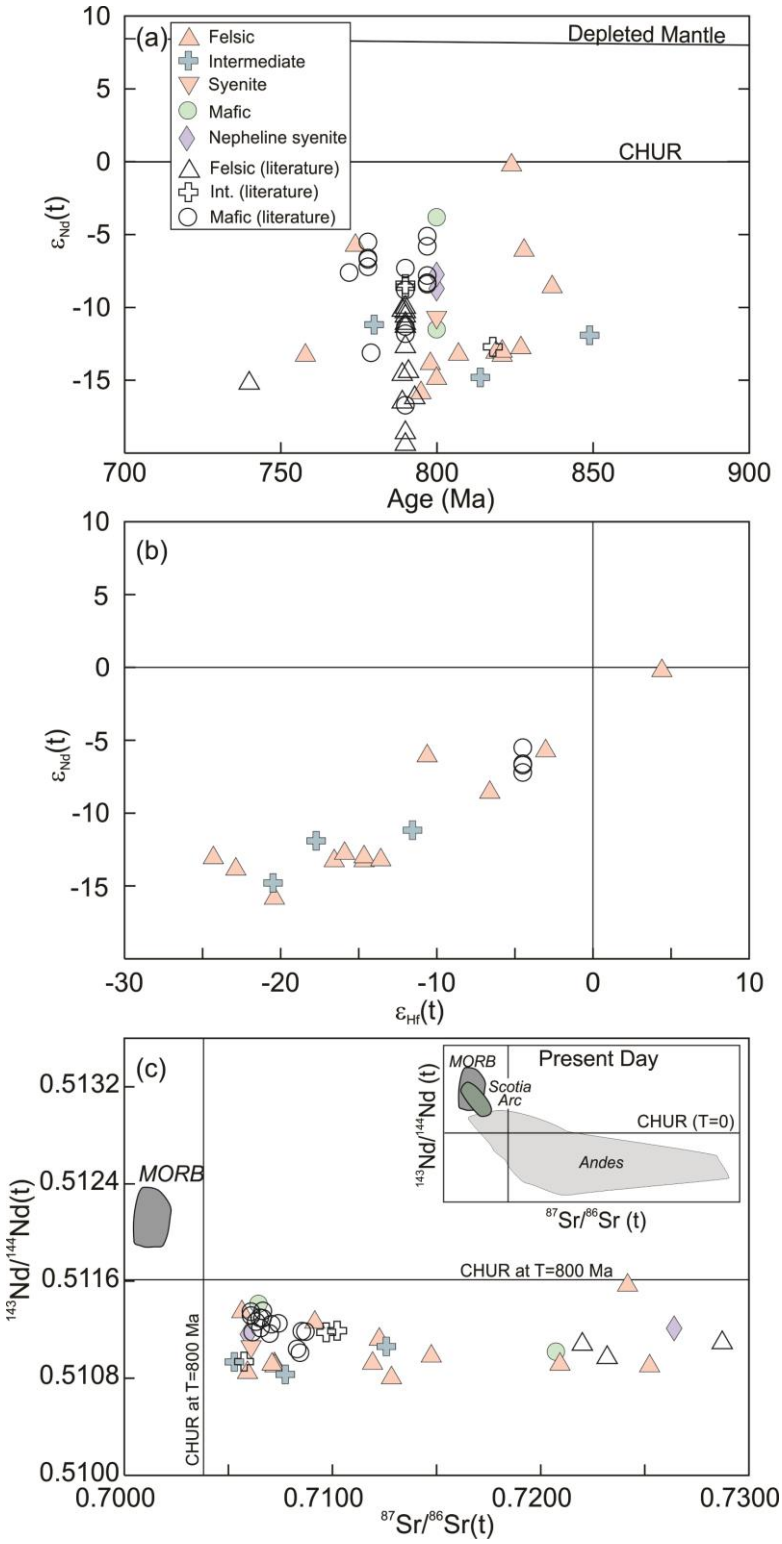

Fig. 4.12 Isotope plots for samples of the Imorona-Itsindro Suite: (a) Plot of Age (Ma) versus $\varepsilon_{Nd}(t)$. (b) Plot of $\varepsilon_{Nd}(t)$ versus $\varepsilon_{Hf}(t)$. $\varepsilon_{Hf}(t)$ data are mean ratios from zircon analyses (Zhou et al., 2015b; Archibald et al., 2016). (c) Plot of $^{87}Sr/^{86}Sr(t)$ versus $^{143}Nd/^{144}Nd(t)$. High $^{87}Sr/^{86}Sr(t)$ ratios (>0.73) from McMillan et al. (2003) are not shown. Inset box shows present day Andes, MORB, and oceanic arc data referenced to CHUR. Imorona-Itsindro Suite literature values are from Tucker et al. (1999b), Kröner et al. (2000), Zhou et al. (2015b), and McMillan et al. (2003). Andes and Scotia Arc data are from the GEOROC database and MORB data are from Saunders et al. (1988).

Large-ion-lithophile elements (LILs; Rb, Ba, K, Cs, and Sr) and high-field-strength elements (HFSs; Th, U, Zr, Nb, Y, and REE) have contrasting behaviours in water-rich solutions such as arc-derived magmas in that HFSs are insoluble and LILs are soluble in water. Thus, the behaviours of these groups of elements can be important for understanding the petrogenesis of arc-derived magmas (e.g. Pearce, 1996). Imorona-Itsindro Suite samples have similar Ba/Nb and Nb/Y ratios to Andean samples but higher Ba/Nb and lower Nb/Y ratios than East African Rift samples (Fig. 4.13a, b). Nb contents are comparable to Andean samples and similar but lower overall than East African Rift samples (Fig. 4.13c). Ba/Y ratios are higher in both Imorona-Itsindro Suite and Andean samples but lower in East African Rift samples (Fig. 4.13d). These discrimination plots demonstrate that although some Imorona-Itsindro Suite samples have within-plate features such as higher Nb/Y ratios and lower Ba/Y ratios, the vast majority of samples demonstrate geochemical similarities more comparable to an Andean rocks.

4.5.2 Tectonic implications

Two opposing views for the tectonic setting of the Imorona-Itsindro Suite have been suggested on the basis of whole-rock and isotope geochemistry: in a supra-subduction zone setting (Handke et al., 1999; Kröner et al., 2000; Key et al., 2011; Boger et al., 2014, 2015; Archibald et al., 2016) or above a mantle plume (Tucker et al., 2011a; Yang et al., 2014; Zhou, 2015; Zhou et al., 2015b). Tucker et al. (2014) advocate that during the Proterozoic the Archaean shield of central Madagascar formed part of a larger continent termed the Greater Dharwar Craton. In this model, the margins of the Malagasy Shield had a Mesoproterozoic oceanic arc to the present day west (Ikalamavony Domain), a Palaeoproterozoic continental terrane to the south (Androyen-Anoysen Domains) and the northern margin was partially covered by Palaeoproterozoic- to Mesoproterozoic clastic and chemical sedimentary rocks of the Andrarona and Sambirano-Sahantaha groups (Tucker et al., 2014). To the far west and north lay the Mozambique Ocean (Tucker et al., 2014).

Alternatively, other authors support a model in which central Madagascar originated from rifting off East Africa and that the Mozambique Ocean lay to the east between Madagascar and India (Collins and Pisarevsky, 2005; Collins, 2006). Collins and Windley (2002) proposed that the basement of central Madagascar was part of a microcontinent named ‘Azania’ that existed between India and East Africa during the Neoproterozoic. In this model, Azania collided with Neoproterozoic India (including the Dharwar Craton and its Malagasy extension, the Antongil and Masora Domains) after a period of westward directed subduction of Mozambique Ocean crust beneath central Madagascar. This is the subduction that is interpreted to have generated the Imorona-Itsindro Suite as a Neoproterozoic continental arc (Collins and Windley, 2002; Collins and Pisarevsky, 2005; Collins, 2006).

The Imorona-Itsindro Suite has long been thought of as being situated in an Andean-like continental margin. Handke et al. (1999) proposed that the suite represented the root of a continental magmatic arc emplaced before or during the break-up of Rodinia. They suggested rifting of eastern Gondwana from Laurentia may have been accompanied by subduction of Mozambique oceanic lithosphere under west-central Madagascar by convergence of oceanic lithosphere in an eastward directed subduction zone (Handke et al., 1999). Kröner et al. (2000) suggested that the suite formed by extensive remelting of Archaean to Palaeoproterozoic crust based on whole-rock neodymium isotopic data and the presence of abundant inherited xenocrystic zircon domains but these authors hedged their bets by suggesting three possible mechanisms for the generation of the magmatism; (1) magmatic underplating following plume generation; (2) subcrustal mantle delamination during the breakup of Rodinia; or (3) continental arc magmatism related to the subduction of oceanic crust beneath Madagascar while the continental block was adjacent to East Africa or formed a

microcontinent in the Mozambique Ocean. McMillan et al. (2003) studied the Ranomandry Complex, a Neoproterozoic, nested intrusion composed of a gabbroic core within a coeval peraluminous granite ring intruding pelitic metasediments of the Itremo Group. They concluded that the complex formed by melting of enriched subcontinental mantle that generated gabbroic magmas, which in turn caused advective heating and anatexis at the base of thickened continental crust which formed the granitoids (McMillan et al., 2003). Bybee et al. (2010) studied gabbroic and ultramafic rocks in the Andriamena region and concluded the hydrous mineralogy; platinum group and trace-element concentrations were consistent with modern-day continental arcs. They suggested that Madagascar was as a terrane outboard of Rodinia near India and the Seychelles and that the western margin of Rodinia was occupied by a continental Andean-like arc during the mid-Neoproterozoic (Bybee et al., 2010).

Other recent studies challenge the "continental arc" theory and suggest continental rifting as the predominant magma generator (Kabete et al., 2006; Tucker et al., 2011b; Yang et al., 2014; Zhou, 2015; Zhou et al., 2015b). Kabete et al. (2006) assessed the economic viability of the Ankisatra-Besakay District in the Andriamena unit of the Tsaratanana Domain using whole-rock geochemistry and geochronology. They proposed a ca. 820-785 Ma rifting event in the Andriamena basement produced mafic-ultramafic complexes and consequent high-temperature/low pressure granulite-facies metamorphism. Yang et al. (2014) focussed on slightly younger intrusions in a restricted area in north central Madagascar. They also suggested a major rifting event that temporarily separated the Antananarivo and Antongil domains prior to ~750 Ma that was subsequently followed by the onset of continental arc magmatism in the Bemarivo Domain (Thomas et al., 2009) prior to ~730 Ma based on geochronological, isotopic and whole-rock geochemical data (Yang et al., 2014). The older magmas are thought to be a result of partial melting of thinned lower crust triggered by underplating of mantle plume-derived magmas (Yang et al., 2014). More recently still, Zhou et al. (2015b) investigated the ~797–772 Ma Ambatondrazaka gabbroic rocks, one pluton within the Imorona-Itsindro Suite. These authors interpreted their whole-rock geochemical and isotopic data to favour an intra-plate tectonic environment (Zhou, 2015; Zhou et al., 2015b). They claimed these gabbroic rocks are more ferroan than typical arc basalts and have other geochemical characteristics supporting an A-type tectonic affinity. They concluded the Malagasy Shield and the Dharwar Craton of India were parts the Greater Dharwar Craton (Tucker et al., 2011a) and argue the geochemical signatures are better explained by melting of enriched sub-continental lithospheric mantle under extension.

Unfortunately, these recent studies proposing an intra-plate rifting origin for the Imorona-Itsindro Suite focus on small datasets in geographically restricted areas and fail to incorporate the lithological and geochemical diversity of entire suite. Zhou (2015) based their discussion arguing for an intra-plate tectonic setting on a restricted subset of only 66 of the 306 (including Bemarivo Domain samples) whole-rock geochemical analyses conducted on the Imorona-Itsindro Suite at the time. Their analysis was limited to samples with >57 wt. % SiO_2 and only samples with positive Eu anomalies (Eu/Eu*>1) to minimize the effect of plagioclase accumulation. However, as stated by Boger et al. (2015) felsic cumulate rocks are difficult to recognise and are not common in granitoid suites (Chappell and Wyborn, 2004). Therefore, we must consider all Tonian igneous rocks from central Madagascar in our discussion to accurately determine the origin of the suite. Boger et al. (2014) rejuvenated the continental-arc model after examining supposed Tonian volcanic rocks in the Horombe Group in the Anoysen domain and again after re-examining published whole-rock geochemical data (Boger et al., 2015). In this discussion, Boger et al. (2015) observed that Tonian magmatic rocks in Madagascar do not yield irrefutable arc-like geochemical characteristics, nor, however, do they have convincing intra-plate signatures. They suggested the geochemical diversity of igneous rock compositions observed in Madagascar is more effectively explained by means of plate margin processes (Boger et al., 2014, 2015). Their tectonic model proposed

present-day eastward directed subduction beneath central Madagascar and India as both landmasses were part of the Greater Dharwar Craton with the Neoproterozoic suture located west in the present-day Mozambique Channel.

Our data and analysis supports the second model (Boger et al., 2014, 2015) in which the Imorona-Itsindro Suite was emplaced above a subduction zone. Some of these rocks have some geochemical features generally attributed to intracratonic tectonic settings but the vast majority of data support an arc-setting. Additionally, the so-called "within-plate" signatures identified by Zhou et al. (2015b) and (Zhou, 2015) are recognised in plate margin environments. Zhou (2015) argues using the $FeO^T/(FeO^T+MgO)$ tholeiitic versus calc-alkaline diagram (Miyashiro, 1974) demonstrates that the Imorona-Itsindro Suite is predominantly tholeiitic. They neglect the AFM diagram (Fig. 4.11a) because of potential alkali mobility. However, alkalis have little effect on tholeiitic versus calc-alkaline trends because these trends are controlled by FeO^T/MgO fractionation (Miyashiro, 1974; Murphy, 2007). Some samples exhibit a tholeiitic trend (mainly mafic samples) but most demonstrate a calc-alkaline affinity (Fig. 4.11a). Second, Zhou (2015) contends that Imorona-Itsindro Suite rocks are A-type based on FeO^T/MgO, Ga/Al, Zr, Nb, Ce and Y contents. The included samples (Fig. 4.2; Zhou, 2015) are predominantly A-type but plot as a continuum from the S-, I- and M-type field into the A-type field. Similar diagrams presented in this study and that of Boger et al. (2015) demonstrate this same continuum but with significantly more samples plotting in the volcanic-arc field (Fig. 4.11c, d) again highlighting the importance of reviewing the entire dataset. Next, Zhou (2015) suggests the intra-plate tectonic affinity is further supported by the general bi-modal nature of the suite, the spatial extent of the suite, the nested geometry of some complexes, and the small nature of most intrusions allowing for emplacement through pre-existing fractures in an active rift system. Figs. 4.10 and 4.13 illustrate that when looked as in its entirety, the suite is not bi-modal, but forms a continuum of compositions. During prolonged subduction events, subduction dip angle and direction, the locus of subduction, and rate of subduction can change causing intermittent switching from compressional to extensional environments (Murphy, 2006) accounting for the other arguments presented by (Zhou, 2015). Changes in subduction dynamics was suggested by Archibald et al. (2016) to account for variations in age versus zircon isotopic (oxygen and hafnium) trends displayed by the Imorona-Itsindro Suite.

Further evidence against a plume origin is provided by field evidence and isotope data. Plumes are considered buoyant upwellings of primarily ultramafic-mafic melts that transport hot material from the deep-mantle into the upper crust often resulting in large igneous provinces or hot-spot tracks and crustal anatexis or assimilation (Davies and Davies, 2009). Two-thirds of all Tonian samples analysed have greater than 57 wt. % SiO_2 (Fig. 4.13a). Regardless of whether this reflects sampling bias, one would expect more voluminous mafic magmatism in central Madagascar if the Imorona-Itsindro Suite originated from a mantle plume. Extensive mafic magmatism at depth is also unlikely as shown by regional geophysical surveys (BGS-USGS-GLW, 2008; Ratheesh-Kumar et al., 2015). Evolved Sr, Nd and Hf (Archibald et al., 2016) isotopic signatures suggest significant Archaean to Palaeoproterozoic crustal involvement during magma genesis. Nd isotopic data for Neoproterozoic gabbro allegedly related to widespread Neoproterozoic plume magmatism associated with the break-up of Rodinia in Australia (Zhao et al., 1994), the Arabian-Nubian Shield (Stein and Goldstein, 1996; Teklay et al., 2002), and South China (Li et al., 2003) all demonstrate significantly higher $^{143}Nd/^{144}Nd(t)$ ratios and lower $^{87}Sr/^{86}Sr(t)$ ratios than Tonian rocks in Madagascar.

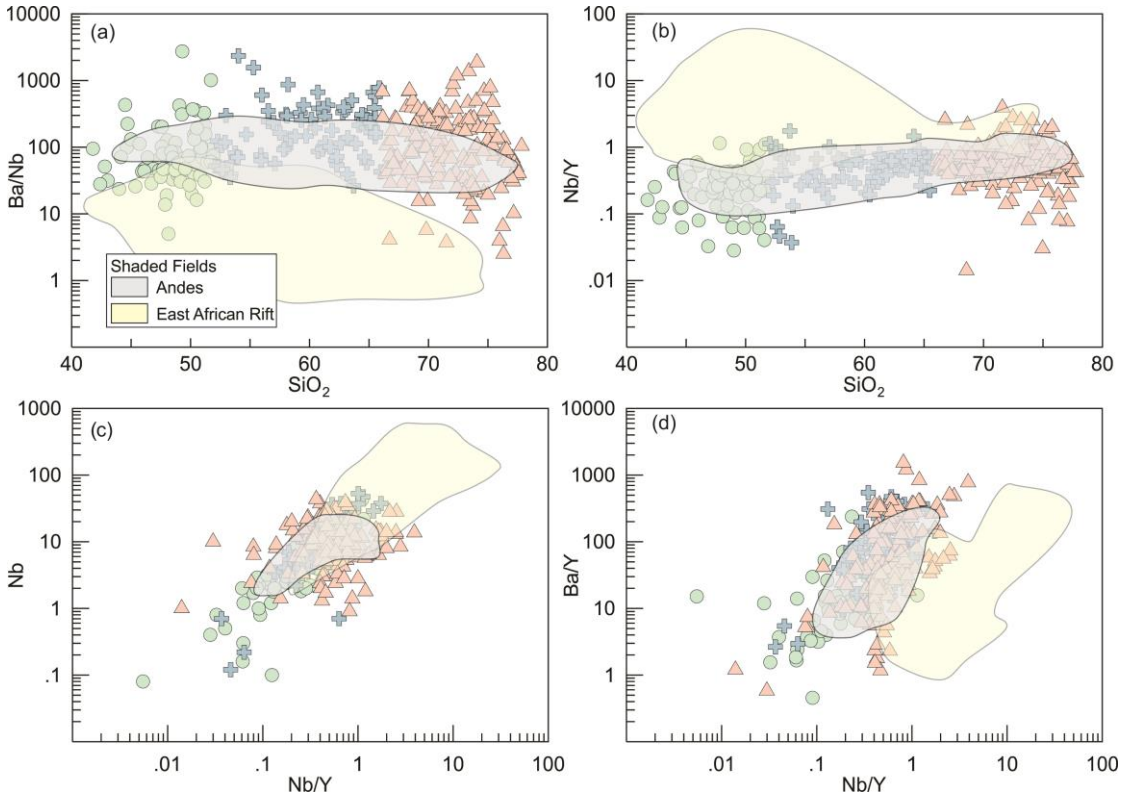

Fig. 4.13 Major and trace-element data for the Imorona-Itsindro Suite plotted against reference datasets from the GEOROC Database for the Andes and the East African Rift. (a) SiO_2 versus Ba/Nb; (b) SiO_2 versus Nb/Y; (c) Nb/Y versus Nb; and (d) Nb/Y versus Ba/Y. Reference datasets were initially filtered to include only plutonic rock samples with between 40 and 80 wt. % SiO_2. Fields for the Andes (n=169) and East African Rift (n=210) reflect inclusion of > 95% of all filtered data. Symbols for Imorona-Itsindro Suite samples are the same as in Fig. 4.11.

4.5.3 Implications for the tectonic development of central Madagascar

Three alternative propositions exist for the Proterozoic tectonic development of central Madagascar. The "Out of Africa" hypothesis suggests that the basement of central Madagascar was originally part of the Congo-Tanzania-Bangweulu Block of East Africa (Fitzsimons and Hulscher, 2005). This idea was largely based on the similarities in detrital zircon age spectra from the Muva Supergroup and the Itremo Group (Cox et al., 1998; Collins et al., 2003c; Cox et al., 2004; Fitzsimons and Hulscher, 2005). It was later argued that central Madagascar rifted from the Congo-Tanzania-Bangweulu Block forming a microcontinent named Azania (Collins and Windley, 2002) that was later wedged between the African and Indian plates in the Neoproterozoic (Collins and Pisarevsky, 2005). The Neoproterozoic suture between Azania and India (Betsimisaraka Suture) was then correlated with the Palghat-Cauvery Shear Zone in southern India (Collins et al., 2007; Plavsa et al., 2014; Plavsa et al., 2015). Present-day westward directed subduction of the Mozambique Ocean along the Betsimisaraka Suture resulted in Andean-type arc magmatism across Azania to the west of the Masora and Antongil Domains (Kröner et al., 2000; Collins, 2006).

The South Madagascar-India-Wanni-Highland Province (SMIWH) presented an alternative model based on apparent inconsistencies in the "Out of Africa" hypothesis (Tucker et al., 2011b). These discrepancies include: (1) the presence of Neoarchaean rocks on both sides of the Betsimisaraka Suture in the Antananarivo, Masora, and Antongil Domains in Madagascar and in the northern Madurai Block and Dharwar craton in India (Schofield et al.,

2010; Tucker et al., 2011a), (2) the presence of Tonian plutonic rocks and similar-aged metamorphism on both sides of the suture (Schofield et al., 2010; Tucker et al., 2011a), and (3) similar aged detrital zircon arrays exposed on both sides of the suture (De Waele et al., 2011). Tucker et al. (2011b) proposed that western India and north-central Madagascar were part of a contiguous Proterozoic craton and that the Androyen-Anosyen Domain together with the Trivandrum Block and the Wanni and Highland Complexes in Sri Lanka represent a continuous Palaeoproterozoic terrane. This led Tucker et al. (2011a) to propose deep crustal anatexis consistent with crustal dilation and pressure-reduced melting compatible with plume generation or lithospheric mantle delamination during continental break-up resulted in Imorona-Itsindro Suite magmatism. However, the authors were circumspect in acknowledging the ambiguity of geochemical data and proposed that if the Imorona-Itsindro Suite were derived from continental-arc magmatism, the active convergent margin was likely to the present-day west of the Antananarivo Domain (Tucker et al., 2011a).

Boger et al. (2014) agreed that the latter proposition complemented the field and geochemical data better than a plume origin for the Imorona-Itsindro Suite. Their tectonic model included the Greater Dharwar hypothesis and proposed present-day eastward directed subduction beneath central Madagascar and India with the Neoproterozoic suture located west in the present-day Mozambique Channel (Boger et al., 2014). Previous studies by Handke et al. (1999) and Bybee et al. (2010) also advocated eastward directed subduction on the eastern edge of the Mozambique Ocean beneath Madagascar, India and the Seychelles. Eastward subduction resulted in continental arc-magmatism throughout all of Madagascar between ~850-700 (including the Bemarivo Domain) and within-plate potassic magmatism manifested in the distal back-arc in the Malani Basin (Boger et al., 2014).

Spatial variations in isotopic data are discussed focussing on longitudinal variations (Fig. 4.14) because of the general N-S strike of geological units in Madagascar (Figs. 4.1b and 4.2), and the proposition that the Imorona-Itsindro Suite is a product of plate margin processes, either due to westward-directed subduction (Collins and Windley, 2002; Collins, 2006) or eastward-directed subduction (Handke et al., 1999; Bybee et al., 2010; Tucker et al., 2011b; Boger et al., 2014, 2015).

A range of studies suggest that at least in some arcs, there is a geochemical reflection of the polarity of subduction. These trends include the well-known K_h relationship demonstrated by increased magma K_2O content away from the subduction trench, which is thought to reflect increased depth of magma generation (Dickinson, 1975). The positive correlation between K_2O concentration and depth to slab may also be shown by other incompatible elements including the LIL, HFS and LRE elements (Shibata and Nakamura, 1997; Haschke et al., 2006; Mamani et al., 2009). Given that various differentiation processes including fractional crystallisation and accessory phase saturation may impose geochemical variation independent of the primary variation reflecting slab depth, the examination of spatial variation trends has been made excluding the felsic samples (Fig. 4.14). Similarly, as most of the mafic rocks in the sampled suites are intrusive gabbro, which are at least in part influenced by pyroxene-plagioclase accumulation, these have also been discounted and our spatial geochemical analysis has focussed on the intermediate samples with SiO_2 contents between 52 and 66 wt. % (Fig. 4.14). In general, K_2O concentrations in intermediate rocks increase from west to east (Fig. 4.14a), until 47°30'E. East of 48° E, data are few, but available K_2O concentrations are low (Fig. 4.14a). Most incompatible elements also show similar variations (e.g. Zr, Fig 4.14b) as do such critical ratios, such as Nb/La (Fig. 4.14c) and La/Yb (Fig. 4.14d). These trends are compatible with eastward directed subduction of the Mozambique Ocean beneath central Madagascar as suggested previously by Boger et al. (2014), Handke et al. (1999), and Bybee et al. (2010), perhaps implying eastward transition towards a continental interior (deeper subduction) and/or smaller degrees of primary melting

in the sub-arc mantle wedge. Fig. 4.14 also highlights the presence of a prominent geological discontinuity between 47°30'E and 48°30' E. This same area was noted by Archibald et al. (2016) as an area with more juvenile oxygen and hafnium isotope signatures. This is also near the location of the Betsimisaraka Suture Zone (Collins and Windley, 2002) or an alternatively posited intracratonic rift (Tucker et al., 2011a; Tucker et al., 2014). Our data are unable to distinguish between these two hypotheses, but it does highlight the presence of a prominent geologic feature in this region. These trends and interpretations are treated with caution because Tonian-aged samples intruded into different basement domains (Fig. 4.1b) and different lithologies (Fig. 4.2) that may have affected geochemical variation. For example, the Tonian-aged rocks east of ~46°E intruded through, and incorporated, older, predominantly felsic, continental crust than those west of ~46°E (Archibald et al., 2016). In addition, these trends ignore temporal variation and the arc system could have evolved through time and experienced periods of increased or decreased crustal melting /assimilation or mantle input.

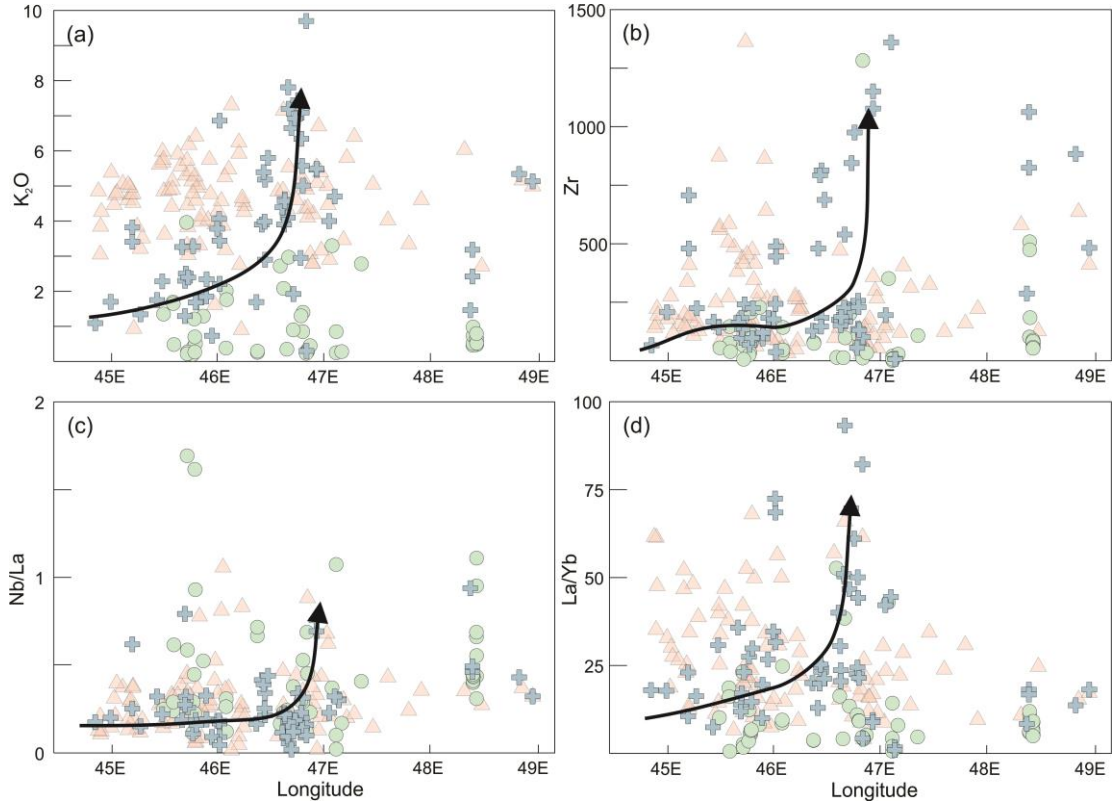

Fig. 4.14 (a) K_2O, (b) La/Yb, (c) Nb/La and (d) Zr plotted against longitudinal coordinates for samples of the Imorona-Itsindro Suite. Arrow represents the average trend for intermediate samples. Data are from the sources listed in Fig. 4.10. Symbols for Imorona-Itsindro Suite samples are the same as in Fig. 4.11.

4.6 Summary and conclusions

The Tonian Imorona-Itsindro Suite of Madagascar is a voluminous, dominantly calc-alkaline magmatic suite formed during an important time in Earth's history. Understanding of the petrogenesis of this suite is critical for developing Neoproterozoic palaeogeographic plate reconstructions. Field observations, petrography, and whole rock geochemical data favour magma generation at an Andean-style subduction margin. Intrusions vary in size from cm-sized dykes to large batholiths, and petrological analysis demonstrates a variety of lithologies from ultramafic rocks to granite to syenite. Mineralogical data shows an abundance of hydrous minerals including calcium amphiboles and biotite. Geochemically, these rocks are

predominantly calc-alkaline with characteristics consistent with emplacement within a volcanic or continental arc. Isotope data have evolved Sr and Nd signatures and indicate crustal assimilation during magma genesis. Changes in subduction zone dynamics, crustal anatexis and crustal assimilation contributed to geochemical discrepancies contrasting a continental-arc origin. Prolonged subduction (>100 Myr) provided sufficient time for the continental arc to mature and HREE arrays imply a shallow (<100km), metasomatised spinel lherzolite mantle source. Ascending mantle derived melts assimilated crustal material and the associated heat resulted in crustal anatexis. Discrimination plots demonstrate that although some Imorona-Itsindro Suite samples have some within-plate characteristics such as higher Nb/Y ratios and lower Ba/Y ratios, the vast majority of samples demonstrate geochemical similarities more comparable to Andean rocks. Overall, the geochemical characteristics of the diverse suite of lithologies argue for their collective genesis in a supra-subduction zone tectonic setting with proposed eastward directed subduction of the Mozambique Ocean beneath central Madagascar.

4.7 Acknowledgements

David Bruce (University of Adelaide) is acknowledged for his assistance acquiring isotope data. Dr. Benjamin Wade (Adelaide Microscopy) is recognized for assistance acquiring EMPA data. The Razafinjoelina family, in particular Auguste and Berthieu are thanked for providing transportation, assistance in the field, and hospitality during fieldwork in Madagascar. This paper forms TRaX Record ###. This paper is a contribution to IGCP projects #628 (Gondwana Map) and #648 (Supercontinent Cycles and Global Geodynamics). This work was financially supported by an Australian Research Council (ARC) Future Fellowship grant FT120100340.

Chapter 5

The Ambalavao-Maevarano Suite

Submitted for publication:

Archibald, D. B., Collins, A. S., Foden, J. D., Payne, J. L., Holden, P., Razakamanana, T., (submitted). Chemistry and Tectonic Setting of Late- to Post-Tectonic Magmatism in the Malagasy Mozambique Belt. Lithos.

Statement of Authorship

Title of Paper	Tectonics and chemistry of late to post tectonic magmatism in the Malagasy Mozambique Belt
Publication Status	__ Published __ Accepted for Publication X Submitted for Publication __ Publication Style
Publication Details	Archibald, D.B., Collins, A.S., Foden, J.D., Payne, J.L., Holden, P., Razakamanana, T. submitted. Tectonics and chemistry of late to post tectonic magmatism in the Malagasy Mozambique Belt. Lithos.

Author Contributions

By signing the Statement of Authorship, each author certifies that their stated contribution to the publication is accurate and that permission is granted for the publication to be included in the candidate's thesis.

Name of Principal Author (Candidate) Contribution to the paper Conceptualisation of the work It's realisation Documentation and write-up Development of ideas and conclusions	Donnelly B. Archibald Prepared samples, carried out analyses and interpretation of the data, organised manuscript and data, wrote manuscript, acted as the corresponding author		
Signature		Date	9/7/2016

Name of Co-Author Contribution to the paper	Prof Alan S. Collins (University of Adelaide) Supervised work, assisted with data interpretation and manuscript revision		
Signature		Date	9/7/2016

Name of Co-Author Contribution to the paper	Prof John D. Foden (University of Adelaide) Assisted with manuscript revision		
Signature		Date	11/7/2017

Name of Co-Author Contribution to the paper	Dr. Justin L. Payne (University of South Australia) Assisted with hafnium isotope data collection, manuscript revision		
Signature		Date	7/4/2016

Name of Co-Author Contribution to the paper	Dr. Peter Holden (The Australian National University) Assisted with oxygen isotope data collection and interpretation		
Signature		Date	28/04/2016

Name of Co-Author Contribution to the paper	Dr. Theodore Razakamanana (University of Toliara, Madagascar) Assistance in the field, sample logistics, manuscript editing		
Signature		Date	8/4/2016

Abstract

Ediacaran to Cambrian post-collisional granitoid suites are common throughout the East African Orogen. This extensive orogen involves a collage of Proterozoic microcontinents and arc terranes that became wedged between older cratonic units during the final assembly of the supercontinent Gondwana. The Ambalavao and Maevarano Suites of central Madagascar are weakly to undeformed magmatic suites emplaced during the waning stages of the amalgamation of Gondwana. The Ediacaran (~575 – 540 Ma) Ambalavao Suite and the Cambrian (~537 – 522 Ma) Maevarano Suite are composed mainly of porphyritic granitoids but also contain minor intrusions of gabbro, diorite and charnockite. New magmatic zircon oxygen and hafnium isotope data and whole rock geochemical data were collected to determine the source components involved in the genesis of these magmatic suites. Oxygen and hafnium isotope data are consistent with melting of an ancient continental crustal source. These isotopic data also demonstrate the isotopic variation of basement source components present in the Malagasy crust highlighted by the hafnium isotope character of the Ikalamavony Domain compared to contemporaneous rocks in the Antananarivo and Itremo Domains. Samples from both suites typically display HFSE, LILE and REE enrichments, high Ga/Al ratios, and have moderately negative Eu anomalies, consistent with emplacement in a post-collisional tectonic setting as A-type (anorogenic) suites. Together, the isotopic character and whole-rock geochemical signature of the Ambalavao and Maevarano Suites reflects lithospheric delamination melting interpreted to be coeval with the polyphase deformation in Madagascar during the East African Orogen.

5.1 Introduction

Formed during the Ediacaran to Cambrian amalgamation of the supercontinent Gondwana, the East African Orogen (EAO) is one of the planet's largest orogens (Stern, 1994; Stern, 2002; Meert, 2003; Collins and Pisarevsky, 2005; Johnson et al., 2011; Fritz et al., 2013). The northern part of the EAO (the Arabian-Nubian Shield) consists of a pre-Neoproterozoic continental terrane (the Afif Terrane), surrounded by many Neoproterozoic oceanic-arc terranes (Johnson et al., 2011; Robinson et al., 2014) that finally sutured together in the Ediacaran (Doebrich et al., 2007; Cox et al., 2012). The pre-Gondwana ocean that separated these landmasses is known as the Mozambique Ocean. In the Arabian-Nubian Shield many oceanic suture zones tie together the various terranes (Robinson et al., 2014; Blades et al., 2015; Robinson et al., 2015a). To the south, in the Mozambique Belt (see Fritz et al. 2013 for a recent summary), the EAO is thought to represent the amalgamation of Neoproterozoic India to the east African Congo-Tanzania-Bangweulu Block (Fig. 5.1a). However, as the EAO is traced south, the location of potential sutures become more complicated, which led Shackleton (1996) to question the position of the Mozambique Ocean suture. He suggested that, unlike many Phanerozoic orogens that typically involve accretion of multiple terranes (e.g. the Appalachians of eastern North America), the Mozambique Ocean closed to form one single suture lying within East Africa. Collins and Windley (2002) thought a single-suture model was an over-simplification, and that a wide band of pelitic gneisses with Neoproterozoic depositional ages (Collins et al., 2003c) represented another Mozambique Ocean suture zone in Madagascar. This suture was called the Betsimisaraka Suture and it separated central Madagascar from India (Collins and Windley, 2002). Elucidating the tectonic setting of central Madagascar during the Ediacaran to Cambrian is, therefore, critical to understanding the geography of the formation of central Gondwana.

During the waning stages of Gondwana assembly, the emplacement of voluminous Cryogenian to Cambrian magmatic suites occurred in central Madagascar and throughout the East African Orogen. As well as central Madagascar (this study; Goodenough et al, 2010; Tucker et al., 2014), such suites are located in East Antarctica (Jacobs et al., 2008),

Mozambique (Jacobs et al., 2008; Bingen et al., 2009), Sudan, Ethiopia and Somalia (Küster and Harms, 1998), Israel and Egypt (Be'eri-Shlevin et al., 2009), and Saudi Arabia (Robinson et al., 2014; Robinson et al., 2015b). Goodenough et al. (2010) noted that many of these post-collisional granitoids suites in the EAO are associated both spatially and temporally with major extensional shear zone systems such as the ~550 Ma Angavo Shear Zone in central Madagascar (Grégoire et al., 2009), the Betsileo Shear Zone (Collins et al., 2000), the Lurio Belt in Mozambique (Bingen et al., 2009) and in the Palghat-Cauvery shear zone in Southern India (Santosh et al., 2005; Plavsa et al., 2015). Here we focus on the geochemistry of these intrusions as elsewhere they have been used to constrain the late orogenic tectonic setting (Jacobs et al., 2008; Bingen et al., 2009; Goodenough et al., 2010).

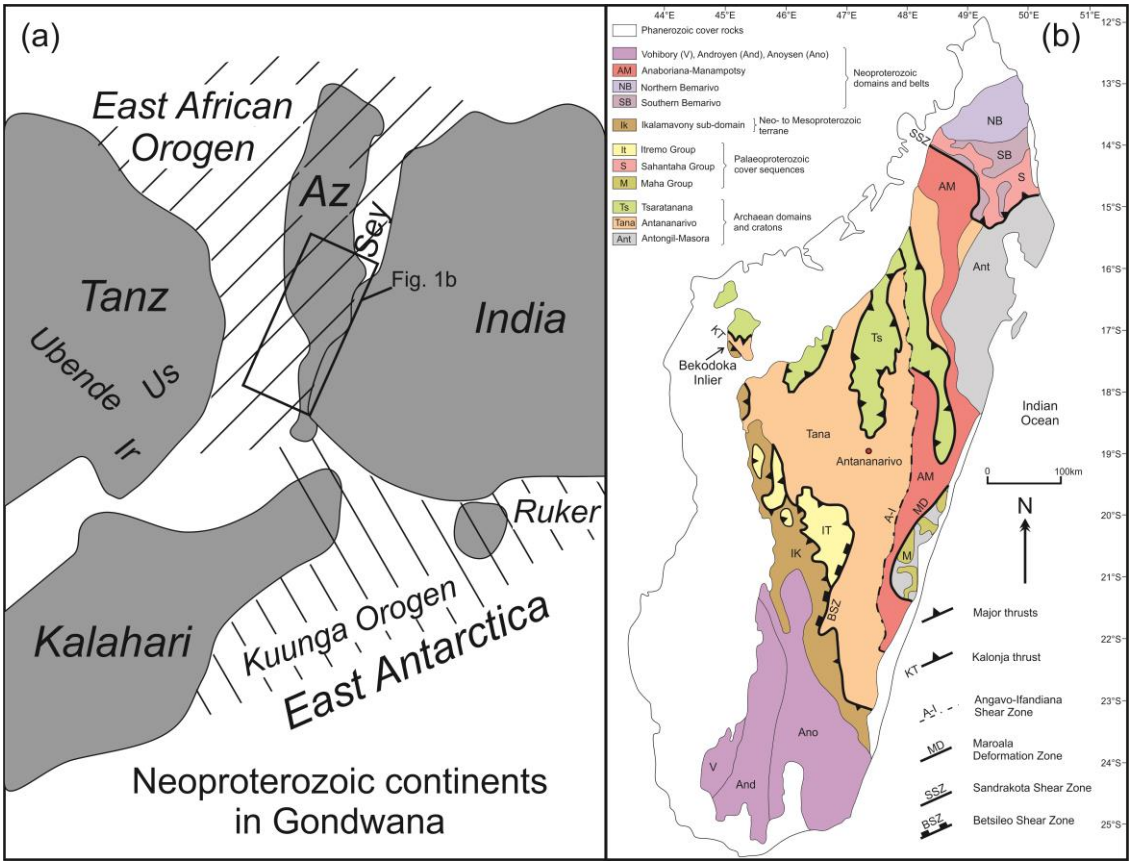

Fig. 5.1 (a) Palaeogeographic reconstruction of the Neoproterozoic continents in Gondwana showing the location of the present study (after Collins and Pisarevsky, 2005). Abbreviations: Az = Azania; Sey = Seychelles; Ir = Irumide Belt; Ruker = Ruker Terrane, East Antarctica; Tanz = Tanzanian craton; Ubende = Ubende Belt; and Us = Usagaran orogen. (b) Simplified basement geology of Madagascar (after Collins, 2006 and De Waele et al., 2011).

In Madagascar, peak prograde metamorphism occurred between ~ 570 – 520 Ma (Markl et al., 2000; Buchwaldt et al., 2003; Jöns et al., 2006; Jöns et al., 2009; Giese et al., 2011) and many post-collisional plutons were emplaced during the same time period (Paquette and Nédélec, 1998; Kröner et al., 2000; Meert et al., 2001b; Goodenough et al., 2010; Tucker et al., 2014). Previous geochemical data for the Ambalavao and Maevarano Suites are limited to studies by Meert et al. (2001a), BGS-USGS-GLW (2008), CGS (2009), Goodenough et al. (2010) and Zhou et al. (2015a) with isotopic data only available from Zhou et al. (2015a). The goal of this study was to establish the crystallization age of the Ambalavao and Maevarano Suites, and to determine the isotopic character to constrain the nature of the magma source components. New zircon U-Pb geochronology and Hf-O isotope data coupled with whole rock geochemical data to provide new insight into the petrogenesis of the

Ambalavao and Maevarano Suites. These data are then used to resolve the lithospheric processes associated with the waning stages of the formation of the Malagasy Mozambique Belt in central Madagascar.

5.2 Regional tectonic context

The literature is dominated by two competing hypotheses for the Proterozoic evolution of central Madagascar. The "Out of Africa" hypothesis is largely based on the similarities in detrital zircon age spectra from the Muva Supergroup in Zambia and the Itremo Group in central Madagascar (Cox et al., 1998; Collins et al., 2003c; Cox et al., 2004; Fitzsimons and Hulscher, 2005). In this model, the basement of central Madagascar was originally part of the Congo-Tanzania-Bangweulu Block of East Africa (Fitzsimons and Hulscher, 2005). Central Madagascar then rifted away in the Palaeoproterozoic to form a microcontinent named Azania (Collins and Windley, 2002). The microcontinent was later wedged between the African and Indian plates in the Neoproterozoic following subduction of the Mozambique Ocean along the Betsimisaraka Suture (Collins and Pisarevsky, 2005). Key et al. (2011) agreed that central Madagascar was likely an isolated microcontinent during the Proterozoic but noted that the Betsimisaraka Suture zone as defined by Collins (2006) could not exist given the similar early Neoproterozoic histories of the Antananarivo and Masora Domains on either side of the of the structure. They suggested that the southern Betsimisaraka Domain (Manampotsy Belt; described in section 5.3.1) represented a pre-630 Ma collisional zone between the Masora and Antananarivo Domains and the northern Betsimisaraka Domain (Anaboriana Belt; described in section 5.3.1) represented another suture between the amalgamated Antananarivo/Masora Domains and the Antongil Domain (Key et al., 2011).

Alternatively, the Archaean rocks of Madagascar including the Antongil, Masora, and Antananarivo Domains were suggested to be part of the Indian Greater Dharwar Craton from nearly 3.0 Ga to continental break-up around 100 Myr (Tucker et al., 2011b; Tucker et al., 2014). Tucker et al. (2011b) also proposed a Palaeoproterozoic South Madagascar–India, and the Wanni and Highland provinces of Sri Lanka (SMIWH) terrane that was sutured to the Greater Dharwar Craton at ~1800 Ma. They suggested that the enigmatic zircon of the Itremo Group (2200–1800 Ma) and other similar metasedimentary sequences in Madagascar, were derived from the SMIWH terrane (Tucker et al., 2011b). At the core of this controversy is the genesis of the voluminous Tonian-aged Imorona-Itsindro Suite with the main issues being the nature of magmatism and subduction polarity. The magmatic suite is the focus of a number of recent papers (Boger et al., 2014, 2015; Zhou, 2015; Zhou et al., 2015b; Archibald et al., 2016; Archibald et al., submitted-c) and a detailed discussion regarding the genesis of the enigmatic suite is beyond the scope of this paper. However, the genesis favoured by our research group as to the type of magmatism is that Tonian-aged magmas were emplaced in a supra-subduction zone environment (Key et al., 2011; Boger et al., 2014, 2015; Archibald et al., 2016; Archibald et al., submitted-c) rather than as plume derived magmas (Tucker et al., 2014; Zhou, 2015; Zhou et al., 2015b). Subduction polarity is equivocal, but geochemical variations point towards an east-dipping slab, with the oceanic suture located west of the Ikalamavony Domain (Boger et al., 2014, 2015; Archibald et al., submitted-c).

5.3 Geology of Madagascar

5.3.1 Lithotectonic domains and unit descriptions

Madagascar contains several Precambrian to earliest Palaeozoic 'basement' units overlain by Phanerozoic sedimentary and volcanic rocks (Roig et al., 2012). The oldest rocks are located along Madagascar's east coast in the Palaeoarchaean to Palaeoproterozoic Antongil and Masora Domains (Figs. 5.1b, 5.2). These units are considered remnants of the

Dharwar Craton of southern India that were separated from the craton during the Mesozoic break-up of Gondwana (Collins, 2006; Schofield et al., 2010; Tucker et al., 2011a; Tucker et al., 2014). However, unlike the Dharwar craton of India, the Archaean rocks of Madagascar were extensively reworked by multiple Proterozoic tectonothermal events (Tucker et al., 2014).

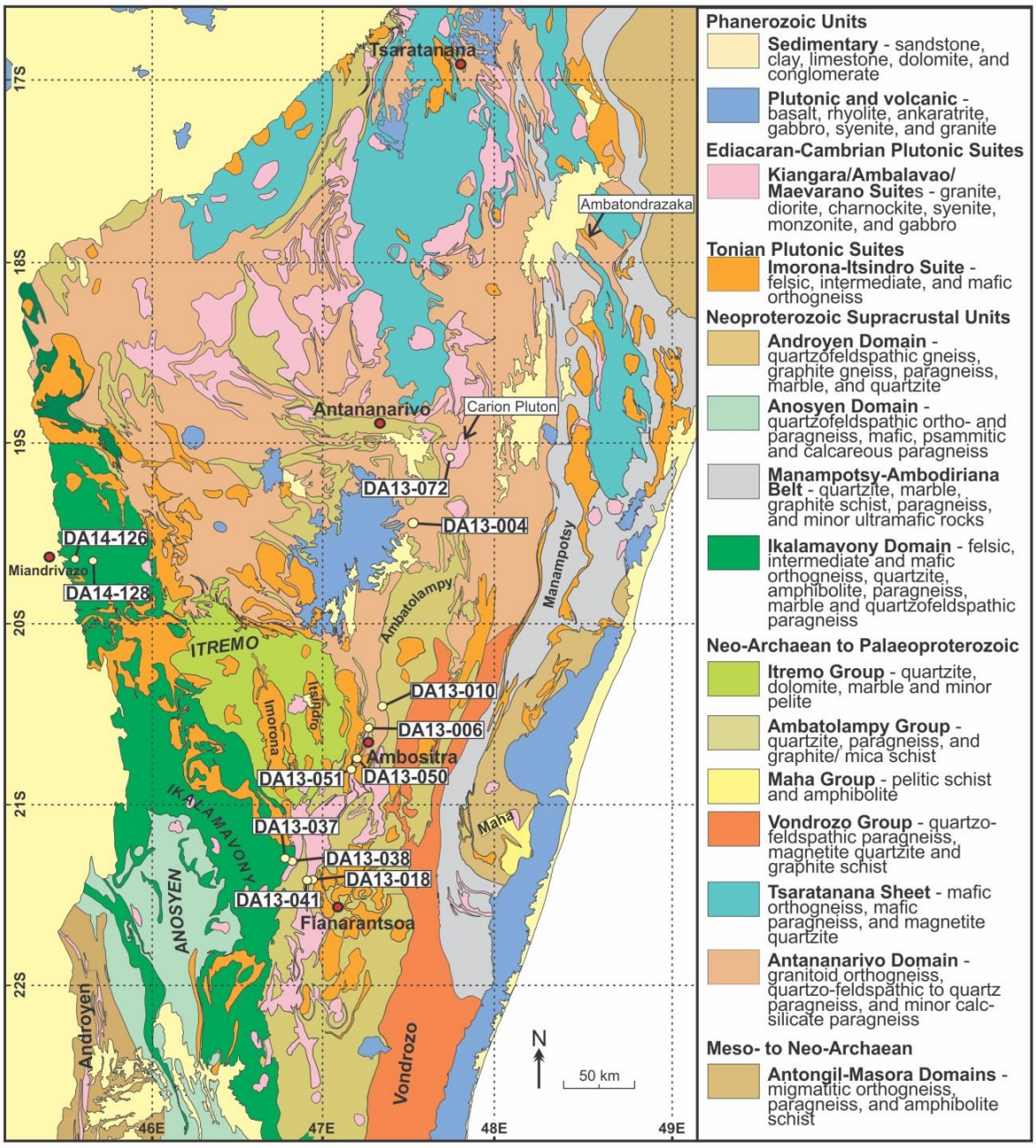

Fig. 5.2 Geologic map of central Madagascar (modified after Roig et al., 2012) showing the extent of Ediacaran to Cambrian magmatism sampled in this study. Note that Ediacaran to Cambrian plutonic rocks are undivided on this regional map and given the name Ambalavao Suite (Roig et al., 2012).

The Antananarivo Domain (including the Tsaratanana Domain) represents the largest Precambrian unit and underlies much of central Madagascar. Granulite- to upper-amphibolite facies orthogneiss and paragneiss characterise the domain (Kröner et al., 2000; Collins et al., 2003a; Collins, 2006; Roig et al., 2012). The orthogneiss consists of ~2550 – 2500 Ma granitoids (the Betsiboka Suite) that are tectonically interlayered with paragneiss of the Sofia,

Ambatolampy and Vondrozo Groups (Besairie, 1968-1971; BGS-USGS-GLW, 2008; Roig et al., 2012). The entire Antananarivo Domain was thermally and structurally reworked between ~850 and 500 Ma with pre-existing rocks being metamorphosed to granulite-facies coinciding with the development of shallow dipping gneissic fabrics that pre-date intrusion of the Ambalavao and Maevarano Suites and later, discrete shear zones that are syn-to post-Ambalavao and Maevarano Suite magmatism (Collins et al., 2003c; BGS-USGS-GLW, 2008; Moine et al., 2014). Some of these later shear zones have been interpreted as related to orogenic extensional collapse (Collins et al., 2000).

Overlying the Antananarivo Domain are Proterozoic metasedimentary rocks of the Itremo Group. The Itremo Group consists of quartzite, conglomerate and dolomitic marble and is characterized by significant detrital zircon populations at ~ 2500 Ma and ~1800 Ma (Cox et al., 2004; Fitzsimons and Hulscher, 2005; De Waele et al., 2011). The protolith sediments were deposited on a continental shelf or passive margin sometime after ~1700 Ma (Fernandez et al., 2003; Cox et al., 2004) with their interpreted sediment source in East Africa (Cox et al., 1998; Cox et al., 2004; Fitzsimons and Hulscher, 2005) or locally from the Archaean to Proterozoic basement of Madagascar (Tucker et al., 2011b). However, the precise nature of the relationship of metasedimentary units to the Archaean gneisses of the Antananarivo Domain and the relationship of the Neoproterozoic intrusive rocks in the Itremo Domain is controversial (Tucker et al., 2007; Moine et al., 2014). Cox et al. (1998) suggested that the plutons in the Itremo region were relatively undeformed and interpreted the period of pluton emplacement (~833 Ma) as the time of regional metamorphism and deformation. Collins et al. (2003b) described Tonian-aged plutons with contact metamorphic aureoles cutting already intensely folded and translated Itremo Group rocks. Fernandez et al. (2003) recognized the general concordance between the orthogneiss and the Itremo Group, but they considered the contact to be a thrust that was subsequently folded and metamorphosed during Cambrian time. Tucker et al. (2007) posited that Neoproterozoic (~1000–720 Ma) plutons were emplaced into the Itremo Group and Archaean basement, and all that all rocks were affected by younger deformation events. Itremo Group lithologies generally increase in metamorphic grade from east to west (Tucker et al., 2007) with the lowest-grade rocks (lower greenschist facies) preserved in the hanging-wall of the Betsileo Shear Zone (Moine, 1974; Collins et al., 2000). Moine et al. (2014) suggested polyphase mid-Tonian deformation of the Itremo Domain that could be extrapolated to the rest of central Madagascar and subsequent overprinting by polyphase Ediacaran-Cambrian deformation related to the amalgamation of Gondwana. Recently, the Itremo Group was correlated with the Maha Group that structurally overlies the Masora Domain, the Sambirano-Sahantaha Group from the southern Bemarivo Domain (De Waele et al., 2011), the Ambatolampy Group (Archibald et al., 2015) and similar-aged metasedimentary rocks in southern India (Plavsa et al., 2014).

The Ikalamavony Domain is more extensive than the Itremo Domain and constitutes a north-northwest trending unit that is traced from southeast to central west Madagascar (Figs. 5.1b and 5.2). The Ikalamavony Group (formerly known as the Amborompotsy Group; Besairie, 1964; Tucker et al., 2007) consists of tholeiitic amphibolite, thick sequences of biotite hornblende gneisses, calc-silicates, and locally marble and quartzite (GAF-BGR, 2008e; CGS, 2009a; Archibald et al., submitted-a). The ~1080-980 Ma Dabolava Suite has been reported as intruding into the Ikalamavony Group (Rakotoarimanana, 2001; CGS, 2009a; Archibald et al., submitted-a). Yet, where detrital zircon data has been obtained from Ikalamavony Group rock, data are characterised by the presence of Stenian-Tonian detritus (CGS, 2009a). Regardless of their earlier tectonic history, the Ikalamavony and Itremo Domains amalgamated prior to ~850 Ma and were subsequently intruded by the Imorona-Itsindro Suite (CGS, 2009a; Archibald et al., submitted-a).

Magmatic rocks of the Dabolava, Imorona-Itsindro, Kiangara, Ambalavao and Maevarano Suites were emplaced during late Mesoproterozoic to Cambrian times in central Madagascar (Fig. 2). Gabbroic and granitoid rocks of the Stenian-Tonian (~1080-980 Ma) Dabolava Suite are only recognised in the Ikalamavony Domain west of the boundary with the Antananarivo Domain (GAF-BGR, 2008e; CGS, 2009a). Isotopic and geochemical data point to a supra-subduction zone origin for the Dabolava Suite in the Mozambique Ocean on the periphery of Rodinia (Archibald et al., submitted-a). The Tonian (~850-750 Ma) Imorona-Itsindro Suite consists of various granitoids and gabbro that intruded into and are tectonically interlayered with most central Madagascar lithotectonic units except in the Antongil Domain (see Archibald et al., in review and Tucker et al., 2014 for recent summaries). Intrusive contact relationships are inferred with the Ambatolampy Group but have not been observed (Archibald et al., 2015). Two opposing views of the tectonic setting of the suite were proposed on the basis of whole-rock and isotope geochemistry: in a supra-subduction zone setting (Handke et al., 1999; Kröner et al., 2000; Bybee et al., 2010; Key et al., 2011; Boger et al., 2014, 2015; Archibald et al., 2016; Archibald et al., submitted-c) or above a mantle plume (Tucker et al., 2011a; Yang et al., 2014; Zhou, 2015; Zhou et al., 2015b). Younger intrusive rock suites are represented by the ~630 Ma Kiangara Suite A-type granitoids (Guyonnaud, 1951; Nédélec et al., 1994), the ~575-540 Ma Ambalavao Suite (Meert et al., 2001a; BGS-USGS-GLW, 2008) and the ~537-522 Ma Maevarano Suite (Goodenough et al., 2010; Zhou et al., 2015a). The Ambalavao Suite intrudes into the Antananarivo, Itremo, Ikalamavony, and Bemarivo Domains while the Maevarano Suite is recognised only in the Anaboriana-Manampotsy Belt and in the western Antananarivo Domain (Goodenough et al., 2010; Roig et al., 2012). Many intrusions of the Kiangara and Ambalavao Suites form "sill-like" bodies and emplacement during crustal extension was inferred based on whole-rock geochemistry and magmatic fabrics (Emberger, 1958; Windley et al., 1994; Nédélec et al., 1995; BGS-USGS-GLW, 2008).

The Bemarivo Domain is an exotic terrane in north Madagascar consisting of Mesoproterozoic metasedimentary rocks (Sambirano-Sahantaha Group) and juvenile Tonian-Cryogenian calc-alkaline igneous rocks (Thomas et al., 2009). Based on the juvenile character of its igneous rocks (Tucker et al., 1999b), Archaean and Palaeoproterozoic rocks are assumed to be absent in this domain. Thomas et al. (2009) proposed that the northern and southern sub-domains formed as coalesced magmatic arcs, at ~760 Ma (Antsirabe Nord Suite) in the south and ~720 Ma (Manambato Suite) in the north, that were thrust southward over the Sambirano-Sahantaha Group and the combined Antananarivo-Antongil domains during late Ediacaran to early Cambrian times (ca. 540-520 Ma).

The Neoproterozoic Anaboriana-Manampotsy Belt forms the boundary between the Antongil-Masora and Antananarivo Domains (Key et al., 2011; Roig et al., 2012). The belt consists of mid-Tonian supracrustal sediments that were deposited on the continental shelf of the Antananarivo Domain (Key et al., 2011). There are also minor occurrences of tectonic pods of mafic-ultramafic rocks (Collins, 2006). The belt corresponds spatially with the Betsimisaraka Domain or Betsimisaraka Suture Zone (Collins and Windley, 2002; Collins, 2006). Key et al. (2011) suggested the Manampotsy Belt (southern Betsimisaraka Domain; Collins, 2006) developed as a pre-Kiangara Suite (>630 Ma) collisional/suture zone between the Antananarivo and Masora Domains (Key et al., 2011). Metamorphic fabrics in the Tonian-aged magmatic rocks and metasedimentary rocks are strongly overprinted by Ediacaran to Cambrian events in both domains (Key et al., 2011). Alternatively, Tucker et al. (2014) suggested the Manampotsy Group was deposited in a long, narrow depositional basin that opened during a period of continental extension and magmatism in the mid-Tonian but this theory required the Imorona-Itsindro Suite. The depositional age of the Manampotsy Group is approximately 840-780 Ma, based on the age of the youngest detrital zircon, inferred syn-depositional volcanic rocks (De Waele et al., 2008; Tucker et al., 2011a), and the age of the

igneous rocks (Imorona-Itsindro Suite) that intrude the sediments (BGS-USGS-GLW, 2008; Archibald et al., 2016). Manampotsy Group lithologies are strongly deformed and the main rock types are migmatitic quartzofeldspathic paragneiss, graphitic gneiss, quartzite, marble, calc-silicate gneiss and biotite gneiss (BGS-USGS-GLW, 2008). Near the end of the East African Orogen, the amalgamated Antananarivo-Masora Craton collided with the Antongil Domain (Key et al., 2011) prior to later thrusting of the Bemarivo Belt southwards over the older terranes (Thomas et al., 2009). The Anaboriana Belt (northern Betsimisaraka Domain; Collins, 2006) represents the suture between the Bemarivo Belt and the Antongil-Antananarivo Craton (Key et al., 2011). Granitoid rocks of the Maevarano Suite comprise much of the Anaboriana Belt (~70% of the surface area) and the remaining 30% is high-grade supracrustal gneisses and migmatite of the Bealanana Group (BGS-USGS-GLW, 2008).

5.3.2 Structural and metamorphic context

The Ediacaran to Cambrian structural context in central Madagascar is not the focus of this paper but a general overview is provided below. The structural and metamorphic context have important implications for the possible timing of collision of the tectonic elements in Madagascar during the Ediacaran to Cambrian (Key et al., 2011). All the deformation events described post-date the intrusion of the Imorona-Itsindro Suite in the mid-Tonian. Nédélec et al. (2000) described D1 as a WSW-directed flat-lying foliation attributed to extension contemporaneous with the emplacement of the ~630 Ma Kiangara Suite (Nédélec et al., 1994). The period of extension is also manifested as an extensional detachment (Betsileo Shear Zone; Fig. 1b) where lower greenschist facies rocks of the Itremo Group are juxtaposed against upper-amphibolite facies rocks of the Antananarivo Domain basement (Collins et al., 2000). This extensional event was suggested to be post-collisional and was interpreted to link central Madagascar with East Africa in Gondwana before 650 Ma (Nédélec et al., 2000). D2 corresponds to a major east-west transpressive flexural zone (the Antananarivo virgation zone) that developed between ~630 and 560 Ma (Nédélec et al., 2000). Grégoire et al. (2009) suggested transcurrent movement along the Angavo Shear Zone was related to D2 and a U-Pb monazite age of 550 ± 11 Ma dated this D2 event. During D2 (and possibly post-D2), the Angavo Shear Zone was the locus of intense heat flow up to 60km from the main shear zone due to magma and fluids ascending from depth and the thermal event lasted until ~515 Ma (Grégoire et al., 2009). Nédélec et al. (2000) separated this younger thermal event (D3) and suggested it was related to transcurrent movement along the Angavo Shear Zone. Martelat et al. (2000) suggested a similar, but younger D3 event (~530-500 Ma) in southern Madagascar. In the Ikalamavony Domain, the nature and timing of deformation is slightly different. Ambalavao Suite granite cross-cuts the penetrative regional S_1 fabric that developed after the main D_1 (~620 Ma) orogenic episode (CGS, 2009a). The Dabolava Shear Zone was interpreted as an accommodation structure (northwest-southeast trending sinistral shearing) associated with major sub-horizontal folding during the main phase (D2; ~550 Ma) of EAO deformation in western Madagascar (CGS, 2009a). The authors noted the close temporal relationship between regional high-temperature/low-pressure metamorphism and emplacement of the Ambalavao Suite. They suggested that magmatism and metamorphism were probably associated with post-collisional lithospheric thinning, magmatic underplating and extensional relaxation (CGS, 2009a).

The following sections focus on the chemistry and age of samples of the Ambalavao and Maevarano Suites in order to determine the tectonic significance of these major magmatic systems.

5.4 Field Relationships and previous work

5.4.1 Ambalavao Suite

The Ediacaran to Cambrian (~575-540 Ma) Ambalavao Suite is named for the town of Ambalavao located ~50 km south of Fianarantsoa where these intrusions are common (BGS-USGS-GLW, 2008). It should be noted that the Ambalavao Suite does not represent a single, co-genetic magma but is a term used to signify a major post-collisional magmatic episode across Madagascar (BGS-USGS-GLW, 2008; CGS, 2009a).The oldest age reported as being part of the Ambalavao Suite is 575 ± 16 Ma (BGS-USGS-GLW, 2008) while the Andringitra granite from Itremo region denotes the youngest age of 539 ± 2 Ma (Tucker et al., 2007). Texturally, intrusions vary from fine-grained equigranular to porphyritic and often pegmatitic (Fig. 5.3). The suite varies in composition from syenite, granite, granodiorite, gabbro (Fig. 5.4) with minor occurrences of anorthosite, orthopyroxenite and charnockite (BGS-USGS-GLW, 2008). Porphyritic and non-porphyritic granitoid intrusions are grouped into the "Carion Subsuite" (BGS-USGS-GLW, 2008). Vohombohitra Subsuite intrusions are less common and are found in the northwest Antananarivo Domain (BGS-USGS-GLW, 2008).

Fig. 5.3 Representative field photographs of the Ambalavao and Maevarano Suites: (a) Maevarano granite sample DA12-004; (b) weakly foliated Ambalavao granite sample DA13-050; (c) pegmatite dyke cross-cutting Ambalavao granite sample DA13-010; and (d) porphyritic granite sample DA14-128.

Ambalavao Suite samples from this study belong to the Carion Subsuite including the Carion Pluton located approximately 25 km east of Antananarivo (Fig. 5.2). The subsuite is characterised by porphyritic syenogranite, quartz-syenite and granite with minor intrusions of

non-porphyritic granitoids (BGS-USGS-GLW, 2008). Pegmatite dykes and pods are commonly associated with Ambalavao Suite intrusions (Fig. 5.3a). Many intrusions (including some of those analysed in this study) are situated structurally below a major extensional detachment that separates the supracrustal Itremo Group to the west from the highly deformed Antananarivo Domain basement to the east (Betsileo Shear Zone; Collins et al., 2000; Figs. 5.1b and 5.2). Weakly foliated intrusive granitoids belonging to the Carion subsuite also contain mafic enclaves and/or xenoliths. Previous geochronological data for the Carion Pluton yielded U-Pb (SHRIMP) and ^{207}Pb-^{206}Pb evaporation ages of 532.1 ± 5.2 Ma (Meert et al., 2001b), 540 ± 5 Ma (BGS-USGS-GLW, 2008) and 537.6 ± 1.0 Ma (Kröner et al., 2000). Metamorphism of nearby host rocks was dated at 546 ± 5 Ma (BGS-USGS-GLW, 2008) and this prograde charnockitisation was attributed to carbonic fluid transfer along Neoproterozoic-Cambrian shear zones (Nédélec et al., 2014). Carion Subsuite intrusions are suggested to be emplaced near the end of late Neoproterozoic to lower Cambrian deformation affecting the Antananarivo Domain, although many of these intrusions (including the Carion Pluton) show varying degrees of deformation from the margin to the interior of plutons (Collins et al., 2003a; Razanatseheno et al., 2009). A zircon ^{207}Pb-^{206}Pb evaporation age of 537.6 ± 1.0 Ma was originally interpreted to date emplacement of the granite and signify the minimum age of Ediacaran-Cambrian deformation and metamorphism in central Madagascar (Kröner et al., 2000). However, more recent studies indicate that some intrusions were locally deformed at their margins by east-west shortening syn- or post emplacement (Nédélec et al., 2000; Collins et al., 2003b; Razanatseheno et al., 2009).

5.4.2 Maevarano Suite

The Cambrian (~ 537 - 522 Ma) Maevarano Suite is named after the Maevarano River where the phases of the suite are best exposed (BGS-USGS-GLW, 2008). Numerous batholiths and plutons of the Maevarano Suite intrude into the Anaboriana-Manampotsy Belt and also into the northern Antananarivo Domain and the Bemarivo Belt (BGS-USGS-GLW, 2008; Goodenough et al., 2010; Zhou et al., 2015a). Maevarano Suite rocks are distinguished in the field from older intrusive rocks because they are typically weakly foliated to unfoliated. Coeval pegmatite dykes and pods are widespread within the intrusions. Goodenough et al. (2010) subdivided the Maevarano Suite into three main phases of magmatism based on whole-rock geochemistry and field relationships. The earliest phase of magmatism includes the most mafic and most pervasively foliated intrusions. Lithologies vary in composition from granodiorite, monzonite, and monzodiorite to diorite and gabbro (Fig. 5.4). Gabbroic intrusions are often associated with, and cross-cut by, younger intrusions of porphyritic granite (Goodenough et al., 2010). The second, main phase is typically exposed as porphyritic granitoids with microperthitic potassium feldspar phenocrysts up to 2.5 cm in size (Goodenough et al., 2010). There are also minor charnockite intrusions with up to 20 modal percent orthopyroxene (BGS-USGS-GLW, 2008; Goodenough et al., 2010). The youngest phase is characterised by medium-grained granitoids and pegmatite and aplite veins.

The Maevarano Suite is distinguished from the Ambalavao Suite by its younger ages (~537-522 Ma) and the geographical distribution of the suite to only the northern Antananarivo Domain, the Bemarivo Domain and the Anaboriana Belt. Based on field relationships alone, the Maevarano Suite samples under study could not be assigned to the magmatic phases suggested by Goodenough et al. (2010). However, U-Pb data shows that the two samples of the Maevarano Suite (DA13-004 and DA13-006) belong to the earliest phase emplaced between ~ 537-531 Ma (Goodenough et al., 2010).

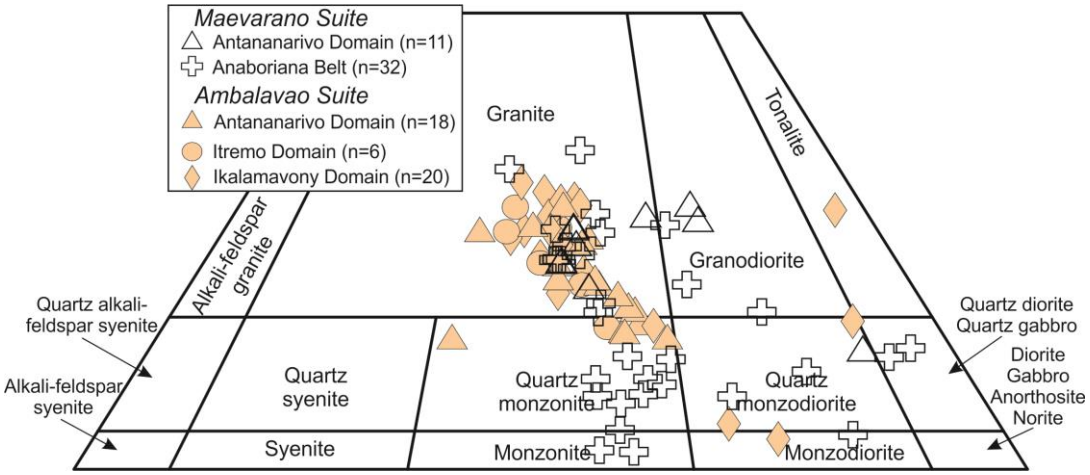

Fig. 5.4 Quartz-Alkali-feldspar-Plagioclase (QAP) diagram for the Ambalavao and Maevarano Suites using the normative mineralogy. Data for the Ambalavao Suite are from this study, Meert et al. (2001a), BGS-USGS-GLW (2008) and CGS (2009). Data for the Maevarano Suite are from this study, Goodenough et al. (2010) and Zhou et al. (2015). Thirty Maevarano Suite samples were collected by BGS-USGS-GLW (2008) and subsequently published in Goodenough et al. (2010).

5.5 Analytical methods

A complete description of the methods employed in this study is available in online supplementary Appendix 5.1. Sample collection focused on obtaining a representative sample set including Ediacaran-Cambrian lithologies from the Antananarivo, Itremo and Ikalamavony domains in central Madagascar (Fig. 5.2). The chosen samples are considered to represent the Ambalavao and Maevarano Suites. Lithological descriptions and zircon characteristics are provided in Tables 5.1 and 5.2. LA-ICP-MS (laser-ablation inductively-coupled mass spectroscopy) U-Pb analyses were conducted at Adelaide Microscopy in Adelaide, Australia. Zircon standard reference material GJ (Jackson et al., 2004) was used as a primary standard and internal accuracy was monitored using the Plešovice zircon reference material ($^{206}Pb/^{238}U$ age of 337.1 ± 0.37 Ma; 2σ; Sláma et al., 2008). Plešovice analyses yield a weighted-mean $^{206}Pb/^{238}U$ age 338.2 ± 1.8 Ma (2σ; MSWD = 2.6; n = 63). The 5 or 10 % concordance level (based on the number of concordant analyses) is used to calculate crystallisation ages because of common Pb [($^{204}Pb/$ ($^{204}Pb+^{206}Pb$)] x 100 (Appendix 5.2) and radiogenic Pb loss. Age deduction notes are summarised in Table 3. Individual zircon ages are quoted at a 1σ level and weighted-mean ages are at a 2σ level. Oxygen isotope analyses were conducted at the Australian National University, Canberra, Australia using the SHRIMP SI (sensitive high-resolution ion microprobe stable isotope) or SHRIMP II instrument. The SHRIMP SI method involved a 10 kV, ~3 nA Cs^+ primary ion beam focused to a ~30 μm diameter spot size. Procedures for the SHRIMP II follow the methods of Ickert et al. (2008). Long term instrument drift was corrected using the Mudtank zircon reference material ($\delta^{18}O$ = 5.03 ± 0.10 ‰; Valley, 2003) and Temora II zircon ($\delta^{18}O$ = 8.20 ± 0.01 ‰; Valley, 2003). Standard results are found in Appendix 5.1 (Table A.5.1). In situ LA-MC-ICP-MS (laser-ablation multi-collector inductively-coupled mass spectroscopy) Hf isotope analyses were conducted at the University of Adelaide Waite Campus facility using a New Wave Research 193 nm Excimer laser attached to a Neptune multi-collector ICP-MS system as per Payne et al. (2013). Analysis locations were in the same cathodoluminescence domains as concordant U–Pb laser spots and in the same site as SHRIMP oxygen spots (Fig. 5.5). Procedural accuracy was monitored using the Plešovice, Mudtank and Temora II zircon standards. Mean $^{176}Hf/^{177}Hf$ ratios for each standard along with the literature values are presented in the online supplementary Appendix 5.1 (Table A.5.1). $\varepsilon_{Hf}(t)$ and $T_{DM}c$ were calculated using ^{176}Lu decay

constant after Scherer et al. (2001). $T_{DM}c$ two stage crustal model ages were calculated using the methods of Griffin et al. (2002) with an average crustal composition of $^{176}Lu/^{177}Hf$ = 0.015. Fractions of twelve samples were selected for whole-rock geochemical analyses for major, minor and trace elements at ACME Labs in Vancouver, Canada.

5.6 Results

5.6.1 Sample descriptions and U-Pb zircon geochronology

5.6.1.1 Ambalavao Suite in the Antananarivo Domain

Sample DA13-010 was collected from a hillside exposure approximately 30km north of Ambositra (Table 5.1; Fig. 5.2). The pink, homogeneous granite is medium- to coarse-grained and undeformed. Coeval pegmatite leucosomes and lenses are common (Fig. 5.3a) but definitive contact relationships with older units are absent. The sample yielded a $^{206}Pb/^{238}U$ crystallisation age of 544 ± 5 Ma (Table 5.4; Fig. 5.6a).

Sample DA13-018 was collected from a water-washed stream-bed exposure approximately 42 km west of Fianarantsoa (Table 5.1; Fig. 5.2). The outcrop is massive and contact relationships with older units are absent. The Ambatolampy Group crops out 100m northwest and this sample was collected to try to constrain the depositional age of the metasediments (Archibald et al., 2015). Coeval, randomly oriented pegmatite dykes and granite veins are also present. The sample of pink, homogeneous granite is fine- to medium-grained and undeformed. The sample yielded a $^{206}Pb/^{238}U$ crystallisation age of 580 ± 8 Ma (Table 5.4; Fig. 5.6b).

Table 5.1 Summary of sample names, lithology, locations and geographical reference for samples of the Ambalavao and Maevarano Suites.

Sample	Domain	Latitude	Longitude	Lithology	Textures	Mineralogy
Maevarano Suite						
DA13-004	Antananarivo	19° 22' 08.7"	47° 27' 25.8"	Granite	fg massive	af+qtz+pl+bt+cpx+am+op+zrc+all
DA13-006	Antananarivo	20° 30' 28.0"	47° 14' 55.2"	Granodiorite	mg-cg massive	af+qtz+pl+bt+cpx+am+op+zrc+all+tit
Ambalavao Suite						
DA13-010	Antananarivo	20° 18' 13.8"	47° 18' 47.3"	Granite	mg-cg massive	af+qtz+pl+bt+cpx+am+op+zrc+all
DA13-018	Antananarivo	21° 15' 40.4"	46° 49' 31.3"	Monzogranite	fg-mg massive	af+qtz+pl+bt+cpx+am+op+zrc+all
DA13-037	Antananarivo	21° 15' 18.1"	46° 43' 03.1"	Granite	weakly foliated	af+qtz+pl+bt+op+zrc
DA13-038	Antananarivo	21° 15' 14.7"	46° 43' 58.3"	Granite	weakly foliated	af+qtz+pl+bt+op+zrc+all
DA13-041	Antananarivo	21° 15' 49.7"	46° 45' 56.7"	Granite	fg-mg massive	af+qtz+pl+bt+cpx+am+op+zrc+all
DA13-050	Itremo	20° 39' 13.8"	47° 09' 54.8"	Granite	mg-cg weakly foliated	af+qtz+pl+bt+op+zrc+all
DA13-051	Itremo	20° 40' 04.1"	47° 09' 01.6"	Granite	mg-cg porphyritic	af+qtz+pl+bt+op+zrc+all+tit
DA13-072	Antananarivo	18° 54' 05.9"	47° 41' 28.6"	Syenogranite	porphyritic	af+qtz+pl+bt+am+op+zrc
DA14-126	Ikalamavony	19° 32' 53.2"	45° 28' 09.0"	Granite	mg-cg porphyritic foliated	af+qtz+pl+bt+op+zrc+all
DA14-128	Ikalamavony	19° 34' 10.3"	45° 29' 28.7"	Granite	mg-cg porphyritic	af+qtz+pl+bt+op+zrc+all

Table 5.2 Physical and optical characteristics of zircon from the Ambalavao and Maevarano Suites.

Sample	Colour	Size (mm)	Aspect ratio (L:W)	Morphology	Internal zoning
DA13-004	clear, pale yellow	50-350	2:1 - 4:1	mostly euhedral to subhedral	xenocrystic cores; dark magmatic oscillatory zoning; some grains contain inclusions of unknown mineral
DA13-006	clear, pale yellow	100-400	2:1 - 5:1	mostly euhedral to subhedral	bright magmatic oscillatory zoning; some grains contain inclusions of unknown mineral
DA13-010	clear, colourless	50-250	2:1 - 4:1	mostly subhedral to euhedral	bright cores with magmatic oscillatory zoning; dark outer rims, dark inclusions
DA13-018	clear, colourless	50-250	1:1 - 3:1	mostly subhedral to euhedral	dark unzoned; faint magmatic oscillatory zoning
DA13-037	clear, pale brown	50-350	2:1 - 4:1	mostly subhedral	bright magmatic oscillatory zoning; narrow, dark overgrowths
DA13-038	clear, pale yellow	50-200	2:1 - 4:1	mostly subhedral	bright magmatic oscillatory zoning; narrow, dark overgrowths; some grains contain inclusions of unknown mineral
DA13-041	clear, colourless	50-300	1:1 - 4:1	mostly subhedral	bright, broad magmatic oscillatory zoning
DA13-050	colourless, clear	50-325	2:1 - 5:1	euhedral to subhedral	magmatic oscillatory zoning and narrow, dark coloured overgrowths
DA13-051	clear, pale yellow	50-325	2:1 - 5:1	euhedral to subhedral	small, dark core domains, bright magmatic oscillatory zoning, minor sector zoning
DA13-072	clear	100-400	2:1 - 3:1	mostly subhedral to euhedral	dark mineral inclusions; bright, unzoned domains, magmatic oscillatory zoning; some grains have irregular zoning and dark, narrow overgrowths
DA14-126	colourless, pale brown	150-600	2:1 - 4:1	mostly subhedral to euhedral	dark, unzoned cores; faint, bright, broadly zoned overgrowths; abundant cracks and inclusions
DA14-128	colourless, pale brown	75-500	1:1 - 3:1	mostly euhedral to subhedral	dark, unzoned cores; faint, bright, broadly zoned overgrowths; abundant cracks and inclusions

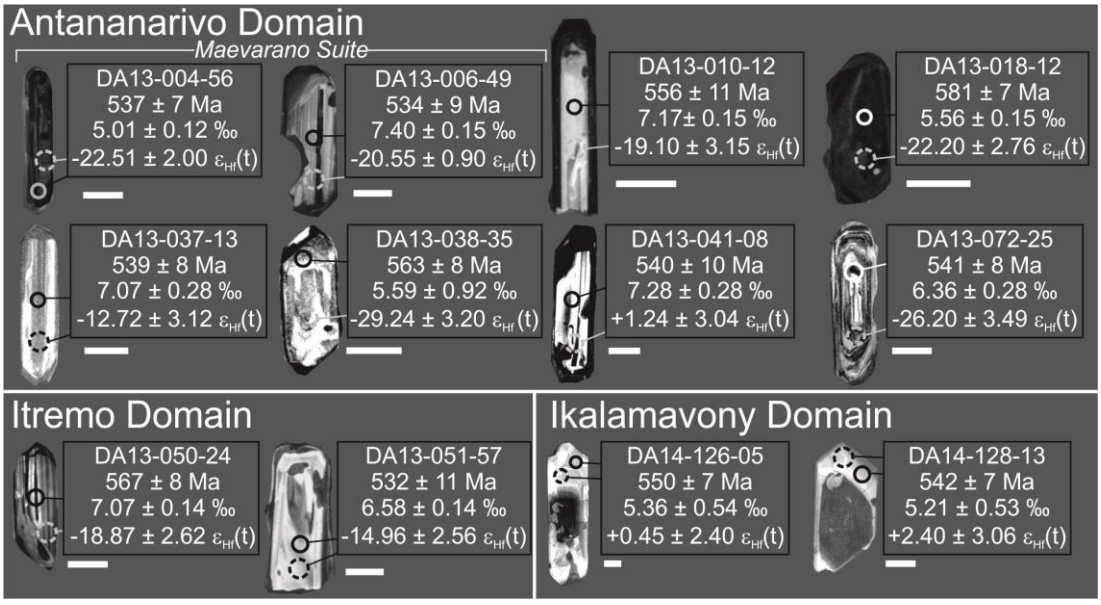

Fig. 5.5 Cathodoluminescence (CL) images for representative zircon from the Ambalavao and Maevarano Suites. Analysis names, appropriate U-Pb ages with one standard deviation error, $\delta^{18}O$ values with two standard deviation error and $\varepsilon_{Hf}(t)$ values with two standard deviation error are listed alongside each image. Solid circles represent U-Pb analysis spots and broken circles represent the location of oxygen and hafnium isotope analyses. White scale bars adjacent to each image are ~50 μm.

Sample DA13-037 was collected from a hillside exposure approximately 55 km west of Fianarantsoa (Table 5.1; Fig. 5.2). The outcrop contains numerous pegmatite dykes as well as enclaves and xenoliths of older lithologies. The granite intrudes into intensely deformed and recrystallised quartzite and schist of the Ambatolampy Group. The granite is fine- to medium- grained and displays variable foliation intensity on the outcrop scale. Syn-emplacement foliation variability may represent strain partitioning within the granite. The sample yielded a $^{206}Pb/^{238}U$ crystallisation age of 549 ± 9 Ma (Table 5.4; Fig. 5.6c).

Sample DA13-038 was collected from a hillside outcrop approximately 52 km west of Fianarantsoa (Table 5.1; Fig. 5.2). The outcrop contains numerous pegmatite, dykes and lenses. The fine- to medium- grained granite displays a variable foliation on the outcrop scale similar to sample DA13-037.Quartzite of the Ambatolampy Group (?) is observed overlying the weakly-foliated granite. The sample has a $^{206}Pb/^{238}U$ crystallisation age of 544 ± 7 Ma (Table 5.4; Fig. 5.6d).

Sample DA13-041 was collected from a stream-bed outcrop approximately 48 km west of Fianarantsoa (Table 5.1; Fig. 5.2). The relatively unaltered granite dyke (1-50cm in width) in which sample DA13-041 was collected cross-cuts weathered syenite of the Imorona-Itsindro Suite. Abundant felsic dykes, mafic dykes and pegmatite lenses are also present cross-cutting the main Tonian-aged body. U-Pb (zircon) analyses showed no evidence of inheritance of Tonian-aged zircon (Fig. 6e). The sample has a $^{206}Pb/^{238}U$ crystallisation age of 550 ± 8 Ma (Table 5.4; Fig. 5.6e).

Sample DA13-072 was collected from a roadside outcrop of the Carion Pluton approximately 25 km east of Antananarivo along RN2 (Table 5.1; Fig. 5.2). The Carion Pluton is porphyritic syenogranite with amphibole, biotite, quartz, and alkali-feldspar phenocrysts. The matrix consists of fine-grained alkali-feldspar, quartz, plagioclase, amphibole, biotite, opaque minerals, Fe-oxides, and zircon. The sample yielded a $^{206}Pb/^{238}U$ crystallisation age of 544 ± 4 Ma (Table 5.4; Fig. 5.6f). This age agrees with previous geochronological data from this pluton that yielded a ^{207}Pb-^{206}Pb age of 537.6 ± 1.0 Ma (Kröner et al., 2000) and U-Pb ages of 532.1 ± 5.2 Ma (Meert et al., 2001b) and 540 ± 5 Ma (BGS-USGS-GLW, 2008).

5.6.1.2 Ambalavao Suite in the Itremo Domain

Sample DA13-050 was collected from a hillside outcrop approximately 17 km south of Ambositra along RN 35 (Table 5.1; Fig. 5.2). The granite contains biotite rich mafic enclaves. The rock is weakly foliated and the foliation is defined by the flattened enclaves. Overall, the main granite body is massive, weakly foliated (Fig. 5.3b) with cross-cutting pegmatite dykes and lenses. The sample yielded a $^{206}Pb/^{238}U$ crystallisation age of 570 ± 8 Ma (Table 5.4; Fig. 75.a).

Sample DA13-051 was collected from a hillside outcrop approximately 20 km south of Ambositra along RN 35 (Table 5.1; Fig. 5.2). The granite body has a strong foliation and the outcrop displays abundant pegmatite dykes and pods. Given the strong foliation and that Carion Subsuite intrusions are intensely foliated only at their margins (BGS-USGS-GLW, 2008), we interpret this sample to be from the margin of a larger intrusion and that the foliation formed syn-emplacement. The sample yielded an imprecise $^{207}Pb/^{206}Pb$ crystallisation age of 581 ± 33 Ma (Table 5.4; Fig. 5.7b).

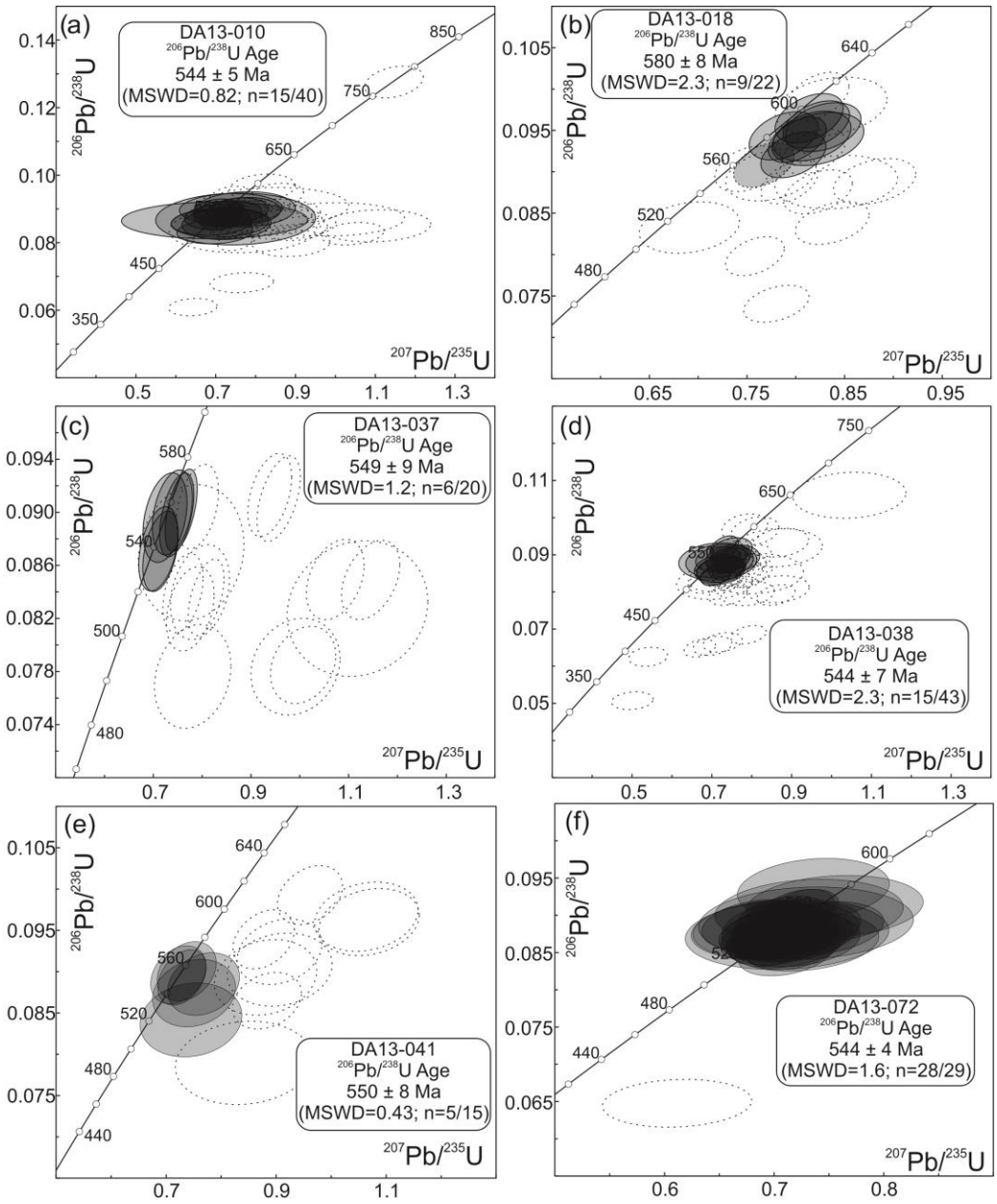

Fig. 5.6 Concordia diagrams showing zircon analyses from the Ambalavao Suite from the Antananarivo Domain: (a) DA13-010; (b) DA13-018; (c) DA13-037; (d) DA13-038; (e) DA13-041; and (f) DA13-072. U-Pb data are reported in Appendix 5.2. Data point error ellipses are 2σ. Shaded ellipses were used in the weighted mean age calculation and open ellipses were rejected. The interpreted age of each sample is summarised in Table 5.4.

5.6.1.3 Ambalavao Suite in the Ikalamavony Domain

Sample DA14-126 was collected from a small roadside quarry outcrop approximately 2 km east of Miandrivazo along RN34 (Table 5.1; Fig. 5.2). The porphyritic granite is observed in contact with highly-weathered schist of the Ikalamavony Group (Fig. 5.8a). There is also a small deformation zone in this exposure that mirrors the regional structure of the Dabolava Shear Zone (CGS, 2009a). The porphyritic granite becomes less deformed moving away from the contact zone into rocks that are essentially undeformed. This supports the idea the Carion sub-suite intrusions are intensely deformed on their margins. Structural measurements on the deformed granite provide a mineral lineation of 48° →284° and a foliation of 63°/335° (Fig 5.8b). The deformation in the underlying schist mirrors the deformation observed in the granite. However, cross-cutting relationships with the underlying

Ikalamavony Group (e.g. xenoliths) are not recognised suggesting this is probably a thrust rather than a pluton margin. We interpret these structures as S-C fabrics that indicate E-W (top to the west) thrusting of the Ambalavao granite over the Ikalamavony Group. Thrusting likely occurred late-syn to early-post emplacement of the granite during the regional D2 deformation event in the Ikalamavony Domain (CGS, 2009a). Small (cm-scale) pegmatite dykes cross-cut the granite, schist and the deformation zone (Fig. 5.8a). The medium- to coarse-grained porphyritic granite has phenocrysts (~1-2cm) of quartz and alkali-feldspar. The sample yielded a ^{206}Pb-^{238}U age of 559 ± 10 Ma (Table 5.4; Fig. 5.7c).

Sample DA14-128 was collected from a small roadside outcrop approximately 5 km east of Miandrivazo along RN34 (Table 5.1; Fig. 5.2). Contact relationships between the coarse-grained porphyritic granite and older units are not observed at this locality (Fig. 5.3c). Compared to sample DA14-126, this porphyritic granite is undeformed. The sample contains phenocrysts (~1-2cm) of quartz and alkali-feldspar. The sample yielded a ^{206}Pb-^{238}U age of 545 ± 7 Ma (Table 5.4; Fig. 5.7d).

5.6.1.4 Maevarano Suite in the Antananarivo Domain

Sample DA13-004 was collected from the Ambatolampy Quarry approximately 70 km south of Antananarivo (Table 5.1; Fig. 5.2). The granite intrudes into Betsiboka Suite orthogneiss in the Antananarivo Domain basement (D.B. Archibald unpublished ^{207}Pb/^{206}Pb age of 2464 ± 10 Ma) and dykes of the Imorona-Itsindro Suite. The granite is fine-grained, undeformed and is exposed as a series of small intrusions, dykes and lenses (Fig. 5.3d). The sample yielded a ^{206}Pb-^{238}U crystallisation age of 531 ± 6 Ma (Table 5.4; Fig. 5.7e).

Sample DA13-006 was collected from a small quarry approximately 2 km north of Ambositra (Table 5.1; Fig. 5.2). Clear contact relationships with older units were not observed at this outcrop but coeval tourmaline-bearing pegmatite dykes (~10cm wide) and lenses are present. The granodiorite is medium- to coarse grained and undeformed except for discrete zones in the outcrop that show a weakly developed foliation. The sample yielded a ^{206}Pb-^{238}U age of 535 ± 5Ma (Table 5.4; Fig. 5.7f).

5.6.2 Oxygen isotopes

5.6.2.1 Ambalavao Suite

Oxygen isotope data were collected from zircon in ten samples of the Ambalavao Suite. Samples from the Ambalavao Suite intruding into the Antananarivo Domain show a wide range in ^{18}O/^{16}O ratios and δ^{18}O values vary between 5.56 ± 0.71 ‰ and 7.03 ± 0.89 ‰ (Figs. 5.9a, b; Table 5.4). The mean δ^{18}O value for all of the Ambalavao Suite samples is 6.32 ± 1.52 ‰ (n=54). Two samples of the Ambalavao Suite from the Itremo Domain have δ^{18}O values of 7.45 ± 0.68 ‰ and 6.58 ± 0.63 ‰. The average for the two samples in the Itremo Domain is 6.97± 1.09 ‰ (n=11). Ikalamavony Domain samples have lower δ^{18}O values of 5.32 ± 0.58 ‰ and 5.27 ± 0.72 ‰ (mean=5.30 ± 0.64 ‰; n=16). Both samples plot well within the mantle range (Figs. 8a, b).

5.6.2.2 Maevarano Suite

Oxygen isotope data were collected from zircon in two samples of the Maevarano Suite. Twelve analyses on two samples of the Maevarano suite yielded mean δ^{18}O values of 5.58 ± 1.4 (DA13-004; 2σ; n=6) and 7.28 ± 0.76 (DA13-006; 2σ; n=6).

Table 5.3 Summary of U-Pb data and age deductions for the Ambalavao and Maevarano Suites in central Madagascar.

Sample	n	n (≥95%)	Pb_c (%)	Remarks	Age (Ma)
DA13-010 (Ant)	40	18	0.00-1.70	All concordant data yields a weighted-mean $^{206}Pb/^{238}U$ age of 547 ± 9 Ma (MSWD = 3.4; n=18). Omitting the two oldest analyses (interpreted to represent inheritance) and one younger analysis (interpreted as Pb loss) that plot away from the main cluster yields a more precise and reliable $^{206}Pb/^{238}U$ age of 544 ± 5 Ma (MSWD = 0.82; n=15). The spread in data is attributed to common Pb and Pb-loss. One concordant analysis with an age of 775 ± 11 Ma is interpreted to be inherited from the Imorona-Itsindro Suite.	544 ± 5
DA13-018 (Ant)	22	13	0.00-2.02	The data yield a relatively imprecise $^{206}Pb/^{238}U$ age of 579 ± 10 Ma (MSWD = 5.6; n=13). One grain has a concordant $^{206}Pb/^{238}U$ age of 516 ± 8 Ma, but its significance is uncertain. The $^{207}Pb/^{206}Pb$ age for the same data is 662 ± 20 Ma (MSWD = 0.91; n=14). Omitting the two oldest analyses (interpreted to represent inheritance) and two youngest analyses (interpreted as Pb loss domains) that plot away from the main data cluster yields a $^{206}Pb/^{238}U$ age of 580 ± 8 Ma (MSWD = 2.3; n=9) that interpreted as the crystallisation age.	580 ± 8
DA13-037 (Ant)	22	6	0.00-1.12	The spread in concordant data is attributed to post-crystallisation Pb-loss. The weighted-mean $^{206}Pb/^{238}U$ age is 549 ± 9 Ma (MSWD = 1.2; n=6) and is interpreted to best represent the crystallisation age.	549 ± 9
DA13-038 (Ant)	43	19	0.00-0.91	A $^{206}Pb/^{238}U$ age of 545 ± 11 Ma (MSWD = 7.0; n=19) is calculated using only the concordant data. The $^{207}Pb/^{206}Pb$ age for the same data is 614 ± 27 Ma (MSWD = 0.67; n=19). Omitting the two oldest (interpreted as inherited) and youngest ages (Pb loss) to improve age uncertainty and precision gives a $^{206}Pb/^{238}U$ age of 544 ± 7 Ma (MSWD = 2.3; n=15), an age interpreted to best represent the crystallisation age.	544 ± 7
DA13-041 (Ant)	15	5	0.00-0.59	The weighted-mean $^{206}Pb/^{238}U$ age is 550 ± 8 Ma (MSWD = 0.43; n=5), an age interpreted to most accurately represent the crystallisation age.	550 ± 8
DA13-072 (Ant)	29	28	0.00-1.24	The weighted-mean $^{206}Pb/^{238}U$ age is 544 ± 4 Ma (MSWD = 1.6; n=28). The $^{207}Pb/^{206}Pb$ age for the same data yields a less precise age of 546 ± 22 Ma (MSWD = 0.79; n=28).	544 ± 4
DA13-050 (Itremo)	29	18	0.00-0.61	Concordant ages plot as an array along concordia between ~525 Ma and ~620 Ma. The $^{206}Pb/^{238}U$ age weighted-average age is 568 ± 12 Ma (MSWD = 8.6; n=18). The $^{207}Pb/^{206}Pb$ ratios for the same data yield an imprecise age of 583 ± 35 Ma (MSWD = 1.8; n=18). Omitting the oldest and youngest ages that plot away from the main data cluster yields a more precise age with a lower MSWD of $^{206}Pb/^{238}U$ 570 ± 8 Ma (MSWD = 2.5; n=14) that is interpreted best represent the crystallisation age.	570 ± 8
DA13-051 (Itremo)	43	30	0.00-3.58	Tthe $^{206}Pb/^{238}U$ age is 542 ± 5 Ma (MSWD = 2.1; n=30). The $^{207}Pb/^{206}Pb$ age for the same data is 581 ± 33 Ma (MSWD = 0.55; n=30). Although the $^{206}Pb/^{238}U$ age is more precise, the data spread implies the $^{207}Pb/^{206}Pb$ age of 581 ± 33 Ma is more representative of the crystallisation age.	581 ± 33
DA14-126 (Ikal)	28	10 ≥ 90%	0.01-1.54	The ≥ 90% concordance is used because of the lack of ≥ 95% concordant grains. The $^{206}Pb/^{238}U$ age is 556 ± 10 Ma (MSWD = 4.6; n=10). When one analysis is discarded, the remaining nine are within 5% of the concordia and yield a $^{206}Pb/^{238}U$ age of 559 ± 10 Ma (MSWD = 3.6; n=9). The $^{207}Pb/^{206}Pb$ age for the same data yields an older, imprecise age of 629 ± 23 Ma (MSWD = 1.05; n=10). The ^{206}Pb-^{238}U age of 559 ± 10 Ma is considered a better representation of the crystallisation age.	559 ± 10
DA14-128 (Ikal)	22	9 ≥ 90%	0.01-0.71	The $^{206}Pb/^{238}U$ age calculated using the ≥ 90% concordant data yields an imprecise age of 538 ± 17 Ma (MSWD = 4.6; n=9). The $^{206}Pb/^{238}U$ age calculated with the ≥ 95% concordant data is 553 ± 7 Ma (MSWD = 0.63; n=4) but includes only four analyses. By omitting the youngest ≥ 90% concordant analysis that plots away from the main data cluster, a more reliable and more precise $^{206}Pb/^{238}U$ age of 545 ± 7 Ma (MSWD = 1.7; n=8) is obtained. This zircon probably experienced Pb loss and is justifiably omitted from the weighted-mean age calculation.	545 ± 7
DA13-004 Maevarano (Ant)	60	20	0.00-0.32	The weighted mean $^{206}Pb/^{238}U$ crystallisation age is 531 ± 6 Ma (MSWD = 2.9; n=20). Two slightly older concordant grains yield U-Pb ages of 650 ± 8 Ma and 660 ± 8 Ma and are interpreted as inherited from rocks related to the Kiangara magmatic event. Three older grains with Palaeoproterozoic crystallisation ages are also interpreted as inherited but are not shown on Fig. 7e.	531 ± 6
DA13-006 Maevarano (Ant)	57	36	0.00-1.65	The weighted mean $^{206}Pb/^{238}U$ age is 515 ± 8 Ma (MSWD = 7.6; n=36). Using the "unmix" feature in Isoplot, there appears to be two separate age populations with $^{206}Pb/^{238}U$ ages of 535 ± 5 Ma (MSWD = 1.5; n=22) and 495 ± 6 Ma (MSWD = 1.7; n=14). CL images show no significant differences in zoning patterns between the older and younger populations. To visually distinguish between the two groups, the most discordant grains are not plotted on Fig. 7f but are included in Appendix A. Whether this data represents two meaningful ages or whether the spread is explained by a Pb-loss model is unclear. The weighted mean $^{207}Pb/^{206}Pb$ age for all concordant data is 567 ± 23 Ma (MSWD = 0.69; n=36). The imprecision associated with the $^{207}Pb/^{206}Pb$ age and the indication of Pb loss implies that the $^{206}Pb/^{238}U$ age of 535 ± 5 Ma as the most representative crystallisation age.	535 ± 5

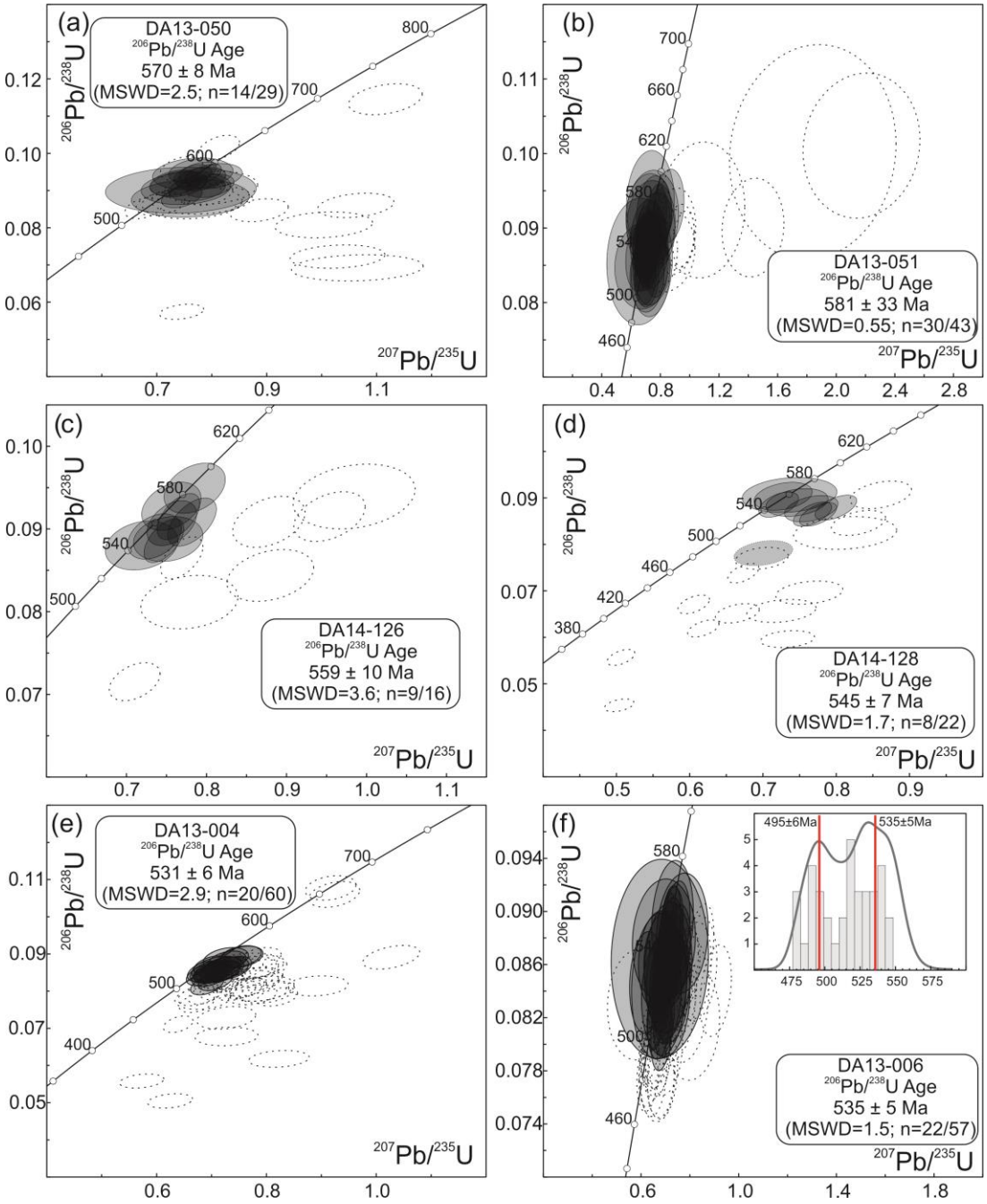

Fig. 5.7 Concordia diagrams showing zircon analyses from the Ambalavao Suite in the Itremo and Ikalamavony Domains and Maevarano Suite in the Antananarivo Domain: (a) DA13-050; (b) DA13-051; (c) DA14-126; (d) DA14-128; (e) DA13-004; and (f) DA13-006. U-Pb data are reported in Appendix 5.2. Data point error ellipses are 2σ. Shaded ellipses were used in the weighted mean age calculation and open ellipses were rejected. The interpreted age of each sample is summarised in Table 5.4.

5.6.3 Hafnium isotopes

5.6.3.1 Ambalavao Suite

Fifty-five analyses from six samples of the Ambalavao Suite intruding the Antananarivo Domain show a wide range in zircon $^{176}Hf/^{177}Hf$ ratios. Age corrected mean $\varepsilon_{Hf}(t)$ values for individual samples vary between -27.8 ± 2.6 and -2.7 ± 6.6 (Table 5.4) with corresponding $T_{DM}c$ model ages between 3.2 ± 0.2 Ga and 1.7 ± 0.4 Ga. Sample DA13-041

had only three zircon analysed for Hf isotopes and the ratios varied (Appendix 5.3). The remaining samples exhibit a narrower range of ε_{Hf} (t) values between -27.8 ± 2.6 and -12.3 ± 1.3 (Figs. 5.8c, d). Twelve analyses of Ediacaran zircon in two samples from the Itremo Domain have mean ε_{Hf}(t) values of -19.7 ± 1.2 and -14.4 ± 2.6 (Table 5.4; Figs. 5.8c, d). Corresponding T_{DM}c model ages are 2.7 ± 0.1 Ga and 2.4 ± 0.2 Ga. Ediacaran zircon from the Ikalamavony Domain have less evolved ε_{Hf}(t)signatures (Table 5.4; Figs. 5.8c, d). Thirteen analyses from two samples have mean ε_{Hf}(t) values of -0.0 ± 3.3 (DA14-126; 2σ; n=7) and +0.2 ± 4.6 (DA14-128; 2σ; n=6). Corresponding T_{DM}c model ages are 1.5 ± 0.2 Ga.

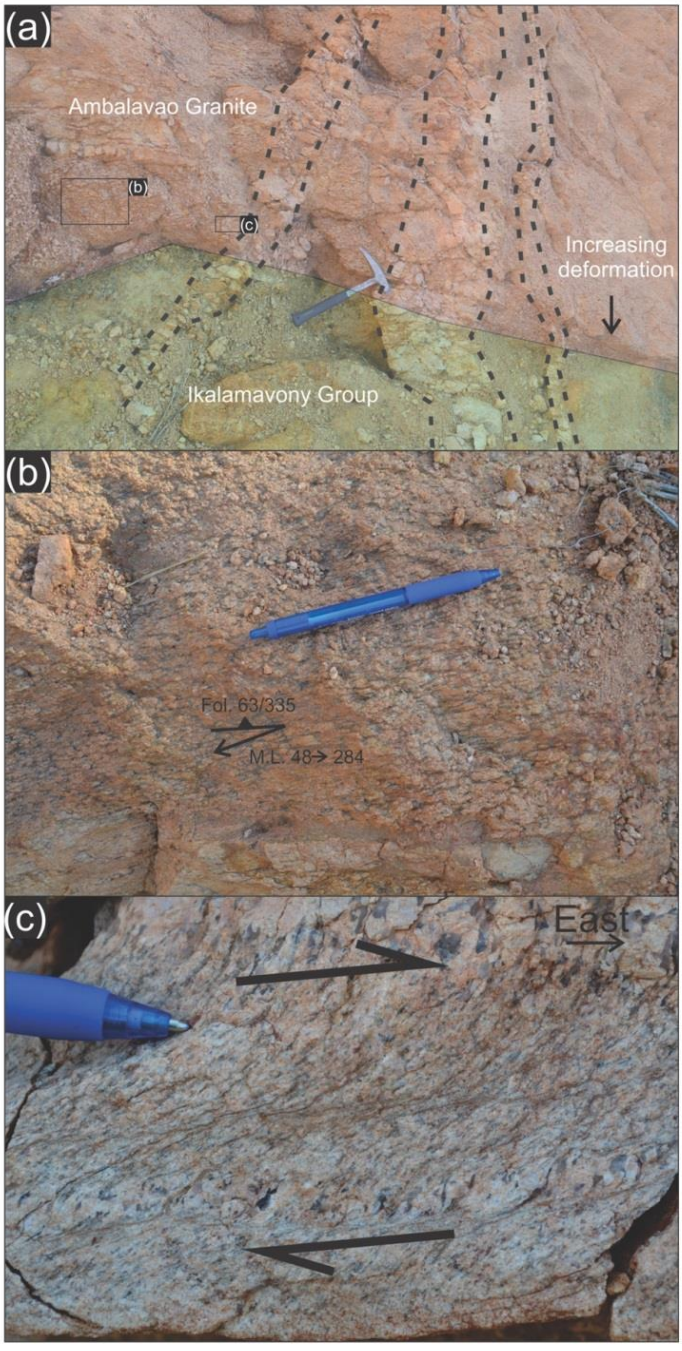

Fig. 5.8 Field photographs of the sampling location of DA14-126. (a) Outcrop photograph showing the contact relationships between the Ambalavao Suite (pink), the Ikalamavony Group (green) and younger pegmatite dykes (outlined by dark broken lines); (b) Strained granite near the contact zone; and (c) S-C fabric near the boundary between the Ikalamavony Group and Ambalavao granite showing top-to-the-west deformation.

5.6.3.2 Maevarano Suite

Thirteen analyses on two samples of the Maevarano Suite yielded age corrected mean zircon $\varepsilon_{Hf}(t)$ values of -22.1 ± 1.3 (DA13-004; 2σ; n=7) and -21.0 ± 1.1 (DA13-006; 2σ; n=6). Corresponding $T_{DM}c$ model ages are ~ 2.8 ± 0.1 Ga.

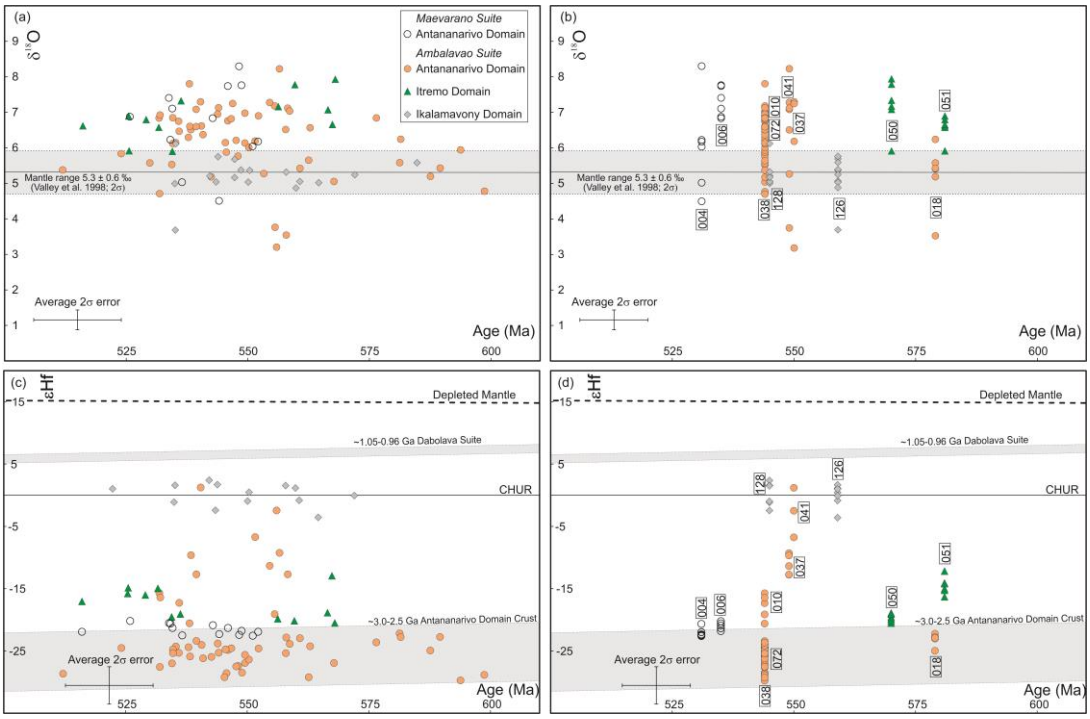

Fig. 5.9 Oxygen and hafnium isotope diagrams for samples of the Ambalavao and Maevarano Suites. $\delta^{18}O$ plotted against (a) zircon crystallisation age and (b) the interpreted sample crystallisation age. $\varepsilon_{Hf}(t)$ plotted against (c) zircon crystallisation age and (d) the interpreted sample crystallisation age. Error bars are 2σ. Range of mantle derived $\delta^{18}O$ (zircon) values are 5.3 ± 0.6 ‰ (Valley et al., 1998). The T_{DM} (crustal) Hf evolution fields are based on a $^{176}Lu/^{177}Hf$ ratio of 0.015 (Griffin et al., 2004). Abbreviations: DM - depleted mantle. CHUR - chondrite uniform reservoir. Note that the DA13- or DA14- prefixes are not included with each sample number for diagram clarity.

Table 5.4 Summary of zircon U-Pb, O, and Hf isotope data collected in this study.

			U-Pb Data (Ma)		Isotope Data		
Sample	Suite	Domain	Inheritance Age (s)	Crystallisation Age	$\delta^{18}O$ (‰; 2σ)	$\varepsilon_{Hf}(t)$ (2σ)	T_{DM} (Ga)
DA13-004	Maevarano	Antananarivo	Palaeoproterozoic and Cryogenian	531 ± 6	5.58 ± 1.40	-22.1 ± 1.3	2.8 ± 0.1
DA13-006	Maevarano	Antananarivo	-	535 ± 5	7.28 ± 0.76	-21.0 ± 1.1	2.8 ± 0.1
DA13-010	Ambalavao	Antananarivo	Tonian	544 ± 5	7.03 ± 0.89	-17.8 ± 3.6	2.6 ± 0.2
DA13-018	Ambalavao	Antananarivo	-	580 ± 8	5.56 ± 0.71	-23.1 ± 1.7	2.9 ± 0.1
DA13-037	Ambalavao	Antananarivo	-	549 ± 9	6.90 ± 1.79	-12.3 ± 1.3	2.2 ± 0.1
DA13-038	Ambalavao	Antananarivo	-	544 ± 7	5.59 ± 0.92	-27.8 ± 2.6	3.2 ± 0.2
DA13-041	Ambalavao	Antananarivo	-	550 ± 8	6.90 ± 1.02	-2.7 ± 6.5	1.7 ± 0.4
DA13-050	Ambalavao	Itremo	-	570 ± 8	7.45 ± 0.68	-19.7 ± 1.2	2.7 ± 0.1
DA13-051	Ambalavao	Itremo	-	581 ± 33	6.58 ± 0.63	-14.4 ± 2.6	2.4 ± 0.2
DA13-072	Ambalavao	Antananarivo	-	544 ± 4	6.56 ± 0.86	-24.8 ± 1.6	3.0 ± 0.1
DA14-126	Ambalavao	Ikalamavony	-	559 ± 10	5.32 ± 0.58	-0.0 ± 3.3	1.5 ± 0.2
DA14-128	Ambalavao	Ikalamavony	-	545 ± 7	5.27 ± 0.72	+0.2 ± 4.6	1.5 ± 0.2

5.6.4 Whole-rock geochemistry

Fourteen samples were selected for whole-rock geochemical analysis including two duplicates (DA14-304 and DA14-372). Major and trace element data are found in Table 5. Most samples are granite and porphyritic granite but published analyses of gabbro, diorite, and charnockite are also included for a more thorough analysis of the geochemical nature of these magmatic suites. New geochemical data are indistinguishable from previously published data. Data for the Ambalavao Suite are from this study, Meert et al. (2001a), BGS-USGS-GLW (2008) and CGS (2009). Maevarano Suite data are from this study, BGS-USGS-GLW (2008), Goodenough et al. (2010) and Zhou et al. (2015a).

5.6.4.1 Ambalavao Suite

Ambalavao Suite samples have SiO_2 compositions varying between 46.98 and 76.45 wt. % (Fig. 5.10). Most samples are low in TiO_2 (<3 wt. %; Fig. 5.10a) and $Fe_2O_3^T$ (FeO $+Fe_2O_3$) contents are variable between 0.94 and 11.85 wt. % (Fig. 5.10b). With the exception of the most mafic samples, MgO contents are also low (< 3 wt. %; Fig. 5.10c) and CaO varies between 0.31 wt. % for the most silica rich sample to 13.49 wt. % for a gabbroic sample (Fig. 5.10d). All four of these major element oxides show a strong negative correlation with increasing SiO_2. K_2O (0.41 - 10.50 wt. %) and Na_2O (1.30 – 5.25 wt. %) contents vary across variable SiO_2 but both elements show a weak positive correlation with SiO_2 (Fig. 5.10e, f). Al_2O_3 contents are variable (12.08 – 18.67 wt. %) and do not correlate with SiO_2 concentrations (Fig. 5.10g). MnO (0.01 – 0.21 wt. %) and P_2O_5 (0.02 – 1.07 wt. %) contents are low and both oxides show a negative correlation with increasing SiO_2 (Fig. 5.10h, i).

Selected trace elements for the Ambalavao Suite display similar patterns on a primitive- mantle normalised spider diagram (Fig. 5.11a). A complete list of all trace elements analysed in this study is found in Table 5. Samples show enrichment in the large-ion-lithophile elements (LILEs) and all samples show Ta-Nb, P, and Ti anomalies but the extent of each anomaly varies among samples (Fig. 5.11a). A chondrite-normalised rare-earth element (REE) diagram shows a moderately steep LREE and a relatively flat HREE profile (Fig. 5.11b). All Ambalavao Suite samples in this study show moderately negative Eu anomalies (0.51 – 0.78; Fig. 5.11b; Table 5.5) implying a significant role for plagioclase fractionation. Some samples from previous studies display strong negative anomalies (as low as 0.28; CGS, 2009) in felsic samples and positive anomalies (up to 3.22; CGS, 2009) in more mafic samples.

5.6.4.2 Maevarano Suite

Maevarano Suite samples show similar major and trace element patterns to the Ambalavao Suite. SiO_2 contents vary between 45.40 to 78.25 wt. % (Fig. 5.10). Most samples are low in TiO_2 (<3 wt. %) and show a negative correlation with increasing SiO_2 (Fig. 5.10a). $Fe_2O_3^T$ contents are slightly higher than the Ambalavao Suite between 1.14 and 13.69 wt. % (Fig. 5.10b). MgO contents are low (< 3 wt. %) but seven samples with the lowest SiO_2 have higher MgO concentrations > 3wt. % (Fig. 5.10c). CaO varies between 0.05 wt. % for the most silica rich sample to 10.68 wt. % for a gabbro sample (Fig. 5.10d). K_2O (0.21 – 6.38 wt. %) and Na_2O (0.05 – 6.77 wt. %) show scatter across various SiO_2 contents but both alkali elements have broad positive correlation with increasing SiO_2 (Fig. 5.10e, f). Al_2O_3 contents are variable (10.13 – 19.58 wt. %) and intermediate rocks have the highest concentrations (Fig. 5.10g). MnO (0.01 – 0.23 wt. %) and P_2O_5 (0.02 – 1.38 wt. %) contents are invariably low and both element oxides show a weak negative correlation with SiO_2, especially at higher SiO_2 concentrations (> 60wt. %; Fig. 5.10h, i).

Table 5.5 Major and trace element geochemical data collected in this study from the Ambalavao and Maevarano Suites. Eu/Eu* (EuN/ [SmN +GdN]) ratios were calculated using chondrite normalising values from Sun and McDonough (1989).

	Maevarano Suite			Ambalavao Suite										
	DA13-004	DA13-006	DA14-304	DA13-018	DA13-031	DA13-037	DA13-038	DA13-041	DA13-050	DA13-051	DA13-072	DA14-126	DA14-128	DA14-372
Lithology	Granite	Grano-diorite	Granite	Monzo-granite	Granite	Granite	Granite	Granite	Granite	Granite	Syeno-granite	Granite	Granite	Syeno-granite
SiO_2 (wt.%)	70.26	64.35	70.16	70.97	73.47	72.71	69.65	68.78	68.37	61.65	62.02	70.50	76.45	62.02
Al_2O_3	14.75	14.52	14.58	14.79	13.93	14.30	14.46	14.58	14.39	14.48	14.99	14.70	12.08	15.18
Fe_2O_3	2.69	5.68	2.73	1.99	0.94	1.38	3.41	2.49	3.75	7.44	5.84	2.21	1.39	5.74
MgO	0.48	1.26	0.48	0.40	0.12	0.30	0.71	0.40	0.76	1.52	1.54	0.31	0.15	1.52
CaO	1.06	3.10	1.03	1.38	0.78	1.38	1.31	1.04	2.05	3.60	3.76	0.65	0.31	3.75
Na_2O	3.63	3.03	3.63	3.47	2.67	3.67	3.31	3.45	2.79	3.47	3.63	4.07	3.06	3.61
K_2O	5.61	5.04	5.58	5.81	6.87	5.05	5.23	8.22	5.84	4.90	4.78	6.06	5.61	4.80
TiO_2	0.36	1.14	0.37	0.26	0.10	0.23	0.61	0.44	0.73	1.35	1.26	0.34	0.24	1.26
P_2O_5	0.11	0.42	0.11	0.07	0.04	0.07	0.17	0.16	0.20	0.65	0.64	0.06	0.03	0.63
MnO	0.01	0.07	0.01	0.02	0.02	0.02	0.05	0.04	0.04	0.11	0.07	0.03	0.01	0.07
LOI	0.6	0.8	0.8	0.6	0.9	0.7	0.7	0.0	0.6	0.2	0.9	0.7	0.5	0.8
Total	99.54	99.45	99.54	99.72	99.82	99.80	99.64	99.60	99.51	99.36	99.41	99.66	99.81	99.39
Ba (ppm)	1805	2031	1869	905	521	710	1049	1517	1610	2571	2535	941	263	2528
Be	<1	2	3	3	8	3	5	1	3	<1	3	<1	<1	1
Co	45	40	42	41	50	22	41	35	27	24	31	29	35	31
Cs	1	2	1	3	8	3	5	2	2	2	0	1	0	0
Ga	17	22	16	19	20	21	21	21	21	23	21	19	16	19
Hf	11	18	11	7	3	6	16	9	16	18	13	14	9	15
Nb	5	35	5	8	36	21	30	61	53	54	29	16	10	29
Rb	181	214	170	270	270	206	257	160	264	174	123	62	62	118
Sn	<1	4	<1	<1	3	1	3	3	3	4	3	1	<1	4
Sr	529	550	518	282	254	288	250	614	298	700	861	83	30	860
Ta	0	2	0	0	5	2	3	6	6	3	2	1	1	2
Th	78	28	76	77	49	46	51	23	61	22	5	13	12	9
U	1	3	1	4	21	7	3	3	6	3	1	4	2	1
V	19	59	18	15	<8	11	35	19	31	57	69	<8	<8	67
W	297	237	309	279	353	150	264	219	185	113	132	205	268	123
Zr	458	831	441	281	79	229	671	343	719	828	560	614	400	658
Y	7	32	7	4	32	12	18	30	40	42	36	30	17	36
La	196.1	148.0	188.6	130.0	37.8	51.6	104.4	112.5	239.0	168.7	126.6	245.1	150.4	133.8
Ce	332.8	288.8	322.9	210.2	64.9	88.1	323.4	239.3	447.7	341.5	250.1	434.6	305.2	261.2
Pr	29.1	30.5	28.9	18.1	7.0	8.8	21.1	25.0	44.7	37.0	27.0	53.6	33.0	28.6
Nd	86.2	104.5	84.5	51.2	22.5	28.1	64.7	79.8	141.4	131.3	96.1	186.0	111.7	102.5
Sm	9.2	15.5	9.5	5.8	4.3	4.2	7.9	12.9	20.8	20.6	16.0	25.9	15.3	16.1
Eu	1.4	2.8	1.4	0.9	0.7	0.9	1.3	2.2	2.7	4.6	3.4	5.2	2.5	3.4
Gd	5.1	11.0	4.8	2.7	4.3	3.0	5.3	8.8	13.3	14.6	11.8	15.3	9.1	11.1
Tb	0.4	1.4	0.4	0.3	0.8	0.4	0.7	1.2	1.8	1.9	1.5	1.8	1.0	1.5
Dy	1.7	6.9	1.5	1.0	4.8	2.3	3.6	5.7	8.3	9.5	7.5	7.9	4.2	7.1
Ho	0.2	1.1	0.2	0.1	1.0	0.4	0.6	1.0	1.4	1.6	1.3	1.2	0.7	1.2
Er	0.6	2.7	0.6	0.4	3.2	1.0	1.7	2.4	3.6	4.0	3.3	2.9	1.6	3.3
Tm	0.1	0.4	0.1	0.1	0.5	0.2	0.2	0.4	0.5	0.6	0.5	0.4	0.2	0.5
Yb	0.5	2.3	0.5	0.4	3.8	1.0	1.4	2.3	3.1	3.6	2.9	2.7	1.5	2.9
Lu	0.1	0.3	0.1	0.1	0.5	0.2	0.2	0.3	0.4	0.5	0.4	0.4	0.3	0.4
Mo	0	1	0	3	<0.1	0	1	1	1	1	1	1	0	1
Cu	21	14	19	2	1	2	10	12	7	8	14	2	4	13
Pb	6	9	6	6	8	7	6	29	7	9	1	9	7	1
Zn	37	98	35	27	7	15	55	10	73	131	58	58	35	58
Ni	2	6	2	1	1	1	3	2	2	1	8	0	1	7
Sc	<1	9	<1	2	3	2	4	3	4	11	9	5	4	9
TOT/C	0.02	0.06	0.02	0.05	<0.02	0.06	0.03	<0.02	0.09	0.02	0.06	0.02	<0.02	0.06
TOT/S	<0.02	0.05	<0.02	<0.02	<0.02	<0.02	<0.02	<0.02	0.04	0.05	0.15	<0.02	<0.02	0.10
Eu/Eu*	0.57	0.61	0.55	0.60	0.51	0.72	0.56	0.60	0.45	0.78	0.73	0.74	0.60	0.73

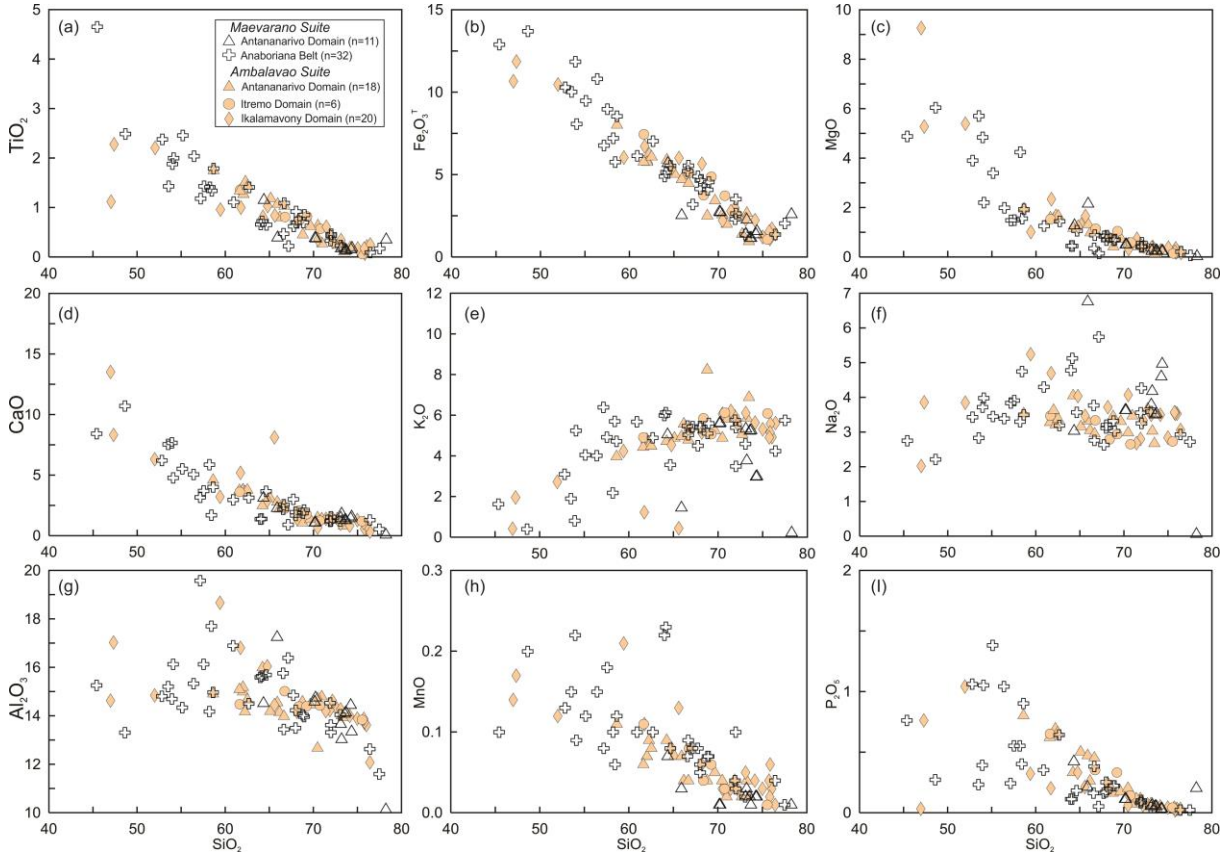

Fig. 5.10 Harker major element variation diagrams for various major element oxides, showing the extent to which Ambalavao and Maevarano Suite samples are fractionated and the degree of compositional overlap between the two suites. Symbols are the same as Fig. 5.4.

Trace elements patterns for the Maevarano Suite mirror those of the Ambalavao Suite when plotted on a primitive mantle normalised spider diagram (Fig. 5.11c). Samples show enrichment in the LILEs and Ta-Nb, P, and Ti anomalies (Fig. 5.11c). A chondrite-normalised rare-earth element (REE) diagram shows a moderately steep LREE profile and a relatively flat HREE profile (Fig. 5.11d). Eu/Eu* ratios for Maevarano Suite granitoid samples analysed in this study are between 0.55 – 0.61 (Fig. 5.11d; Table 5.5), but samples vary between 0.15 – 2.91 for all Maevarano Suite samples (Goodenough et al., 2010).

5.7 Discussion

5.7.1 Age of the Ambalavao and Maevarano Suites

New geochronological data and data from previous studies (see Tucker et al., 2014 and Key et al., 2011 for recent summaries) show that magmatism was essentially continuous in Madagascar between ~650 – 520 Ma with the successive emplacement of the Kiangara, Ambalavao and Maevarano Suites (Fig. 5.12). Geochronologic data indicate that emplacement of the Kiangara Suite was between ~650 – 575 Ma, the Ambalavao Suite between ~575 - 540 Ma and the Maevarano Suite between ~537 - 522 Ma (Paquette et al., 1994; Paquette and Nédélec, 1998; Kröner et al., 1999a; Kröner et al., 2000; Müller, 2000; de Wit et al., 2001; Meert et al., 2001b; Buchwaldt et al., 2003; Tucker et al., 2007; BGS-USGS-

GLW, 2008; GAF-BGR, 2008c, e, d, b, a; CGS, 2009a; Goodenough et al., 2010; JICA, 2012; Zhou et al., 2015a). The Kiangara Suite and the Vohombohitra Subsuite of Ambalavao Suite may be related since some intrusions assigned to the Ambalavao Suite overlap in age with the Kiangara Suite (BGS-USGS-GLW, 2008). Although magmatism was seemingly continuous, pulses occurred at ~630 Ma, ~571 Ma, ~552 Ma, ~541 Ma and ~522 Ma (Fig. 5.12). It is unclear whether these are actual peaks in magmatic activity or are an artefact of data collection.

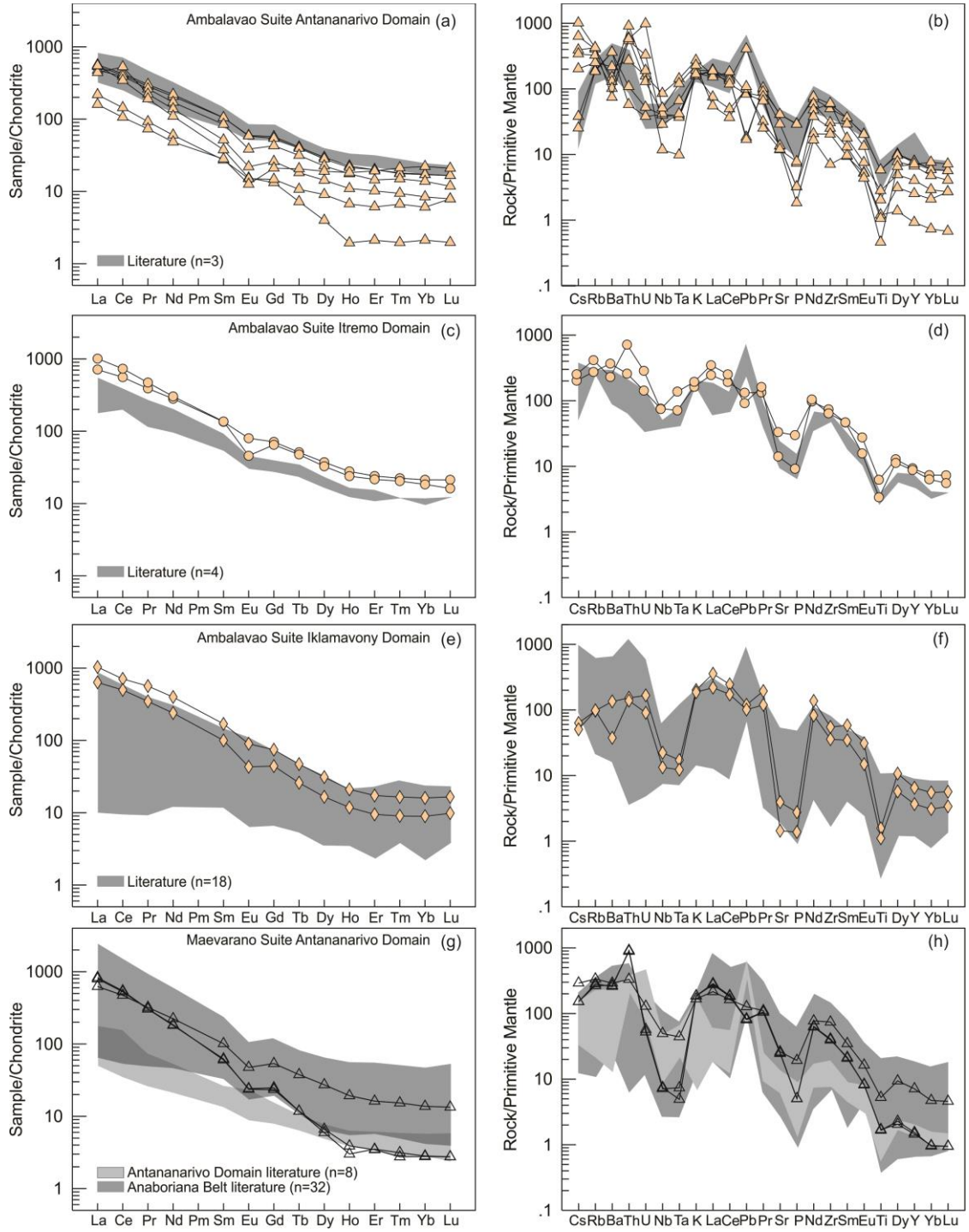

Fig. 5.11 (a) REE diagram and (b) trace-element spider diagram for samples of the Ambalavao Suite intruding into the Antananarivo Domain. (c) REE diagram and (d) trace-element spider diagram for samples of the Ambalavao Suite intruding into the Itremo Domain. (e) REE diagram and (f) trace-element spider diagram for samples of the Ambalavao Suite intruding into the Ikalamavony Domain. (g) REE diagram and (h) trace-element spider

diagram for samples of the Maevarano Suite intruding into the Antananarivo Domain. Shaded fields show the range of REE and trace-element concentrations for literature data from the references listed in Fig. 5.10. Data for this study are from Table 5.5. Chondrite and primitive mantle values are from Sun and McDonough (1989). Symbols are the same as Fig. 5.4.

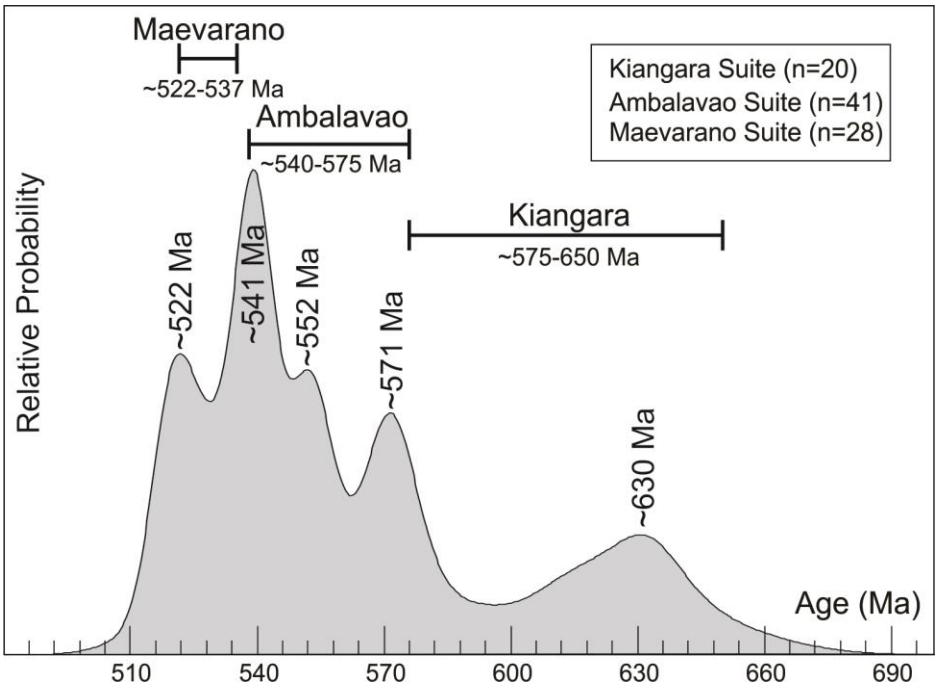

Fig. 5.12 Kernel density plot for all available geochronology data for late Cryogenian to Cambrian magmatism in Madagascar. Included in this are data from this study, BGS-USGS-GLW (2008), Buchwaldt et al. (2003), CGS (2009a), de Wit et al. (2001), GAF-BGR (2008a), GAF-BGR (2008b), GAF-BGR (2008c), Goodenough et al. (2010), JICA (2012), Kröner et al. (2000), Kröner et al. (1999a), Meert et al. (2001b), Müller (2000), Paquette and Nédélec (1998), Paquette et al. (1994), Tucker et al. (2007) and Zhou et al. (2015a). Data was plotted using Density Plotter (Vermeesch, 2012). Approximate periods of magmatism for each suite are after BGS-USGS-GLW (2008).

Spatially, the ~630 Ma magmatism is focussed in an area north of Antananarivo (see Fig. 15 in Tucker et al., 2014). The ~571 Ma, ~552 Ma, and ~541 Ma pulses are widespread across the Antananarivo, Itremo, Ikalamavony and southern Madagascar Domains (see Fig. 15 in Tucker et al., 2014). The ~522 Ma pulse corresponds to the youngest phase of Maevarano Suite magmatism emplaced into the Anaboriana Belt and the northern Antananarivo Domain (Goodenough et al., 2010). These pulses also correspond to regional deformational events in central Madagascar. Previous authors have suggested that the Kiangara Suite was emplaced post-650 Ma after a collisional event (D1; Nédélec et al.,2000; Nédélec et al.,1994) Later emplacement of the Ambalavao Suite coincided with the main phase of the Malagasy Orogeny (D2) between ~560 - 530 Ma (Nédélec et al., 2000; Grégoire et al., 2009). Finally, the Maevarano Suite was emplaced during the waning stages of Gondwana assembly during or post-D2 (Grégoire et al., 2009) or during D3 (Nédélec et al., 2000). Thermochronologic data indicates that the late-Ediacaran to early-Cambrian was also the time of peak metamorphic conditions in Madagascar (Buchwaldt et al., 2003; Jöns et al., 2006; Jöns et al., 2009; Giese et al., 2011). The timing of emplacement of the earliest phase of the Maevarano Suite (Goodenough et al., 2010) coincides with the latter stages of high-grade metamorphism in north Madagascar between ~560 - 530 Ma (Jöns et al., 2006; Jöns et

al., 2009) and south-central Madagascar between ~550 - 520 Ma (Giese et al., 2011). Emplacement of the Ambalavao and Maevarano Suites also coincided with the ~570-530 Ma Kuunga Orogeny (Meert, 2003) located to the south (Fig. 5.1a).

Goodenough et al. (2010) noted that many Maevarano Suite intrusions are associated with ductile shear zones within the Anaboriana-Manampotsy Belt. We support this proposal since many of the Ambalavao and Maevarano Suite samples in this study were collected near major ductile shear zones. All but four samples (DA13-004, DA13-072, DA14-126 and DA14-128) were collected near a major post-650 Ma extensional detachment known as the Betsileo Shear Zone (Collins, 2000; Collins et al., 2003a; Collins, 2006). Samples DA13-004 and DA13-072 were collected near the Angavo Shear Zone (Grégoire et al., 2009; Raharimahefa and Kusky, 2010). The outcrop from which sample DA14-126 was collected in near the edge of an Ediacaran pluton and the intrusion shows evidence for ductile deformation along its margins (Fig. 5.8). Both DA14-126 and DA14-128 were collected near the Dabolava Shear Zone (CGS, 2009a). The association of ductile shear zones, regional metamorphism and post-collisional magmatism is common throughout the rest of the EAO (Jacobs et al., 2008; Viola et al., 2008; Bingen et al., 2009).

5.7.2 Oxygen and Hafnium isotopes

Zircon in equilibrium with mantle-derived melts has a restricted range of $\delta^{18}O$ values (5.3 ± 0.6 ‰; Valley et al., 1998). This range is insensitive to magmatic differentiation since a rise in bulk $\delta^{18}O$ related to fractional crystallisation is compensated for by an increase in zircon/liquid $\delta^{18}O$ fractionation from +0.5 ‰ for mafic to 1.5 ‰ for felsic melts (Valley et al., 2005). Ambalavao and Maevarano Suite samples intruding into the Antananarivo Domain show a wide range in $^{18}O/^{16}O$ ratios, reflective of the diverse crustal sources found within the Antananarivo Domain basement. The Archaean basement contains juvenile magmatic orthogneiss of the Betsiboka Suite, quartzofeldspathic paragneiss, mafic paragneiss and quartzite (BGS-USGS-GLW, 2008; CGS, 2009a; Roig et al., 2012; Tucker et al., 2012). Melting these lithologies would result in a spread of $\delta^{18}O$ values regardless of possible mantle input. A wide range of $\delta^{18}O$ values for the Imorona-Itsindro Suite in the Antananarivo Domain between 9.75 ± 0.24 and 4.21 ± 0.56 was interpreted to represent the diversity of the Antananarivo Domain basement supra-subduction zone mixing of these crustal sources with a depleted mantle component (Archibald et al., 2016). Hafnium isotope systematics are another useful tool for deciphering the source components involved in magma genesis (Kinny and Maas, 2003). $\varepsilon_{Hf}(t)$ values for these same Ediacaran samples are between -27.8 ± 2.6 and -12.3 ± 1.3. This array approximates the range expected for the ~3.0-2.5 Ga Antananarivo Domain crust at ~600-500 Ma (Fig. 9). Previous authors showed the Antananarivo Domain crust originated by mixing between Neoarchaean depleted mantle and Mesoarchaean to Neoarchaean crust based on the juvenile $\varepsilon_{Nd}(t)$ signatures and corresponding Mesoarchaean to Neoarchaean Nd model ages (Tucker et al., 1999b; Kröner et al., 2000; Tucker et al., 2014). Unpublished $\varepsilon_{Hf}(t)$ data for the ~2500 Ma Betsiboka Suite zircon are between +0.7 and +3.8 (D.B. Archibald, unpublished data) and show a minor deflection from the depleted mantle curve at ~2500 Ma. The two samples that plot outside of the Antananarivo Domain evolution field (DA13-037 and DA13-041) are more enriched in ^{176}Hf. These samples likely experienced more depleted mantle input or melted a protolith with a less evolved Hf isotopic signature. Previously published $\varepsilon_{Hf}(t)$ data for Cambrian granites in the Ambatondrazaka Region of the Antananarivo Domain are between -16.4 and -12.9 (Zhou et al., 2015a). These values lie within the range expected for mixing of the Antananarivo Domain basement crustal melts with minor input from a depleted-mantle component.

Samples DA13-050 and DA13-051 are found near the edge of the Itremo Domain along the Betsileo Shear Zone (Fig. 5.2). $\delta^{18}O$ values plot above the range expected for mantle derived zircon (Valley et al., 1998) consistent with their derivation via melting of a Mesoproterozoic supracrustal protolith. $\delta^{18}O$ values collected for the Imorona-Itsindro Suite in the Itremo Domain are dissimilar with more juvenile $\delta^{18}O$ values between 4.60 and 5.43 ‰ (Archibald et al., 2016). Mantle, to slightly below mantle, $\delta^{18}O$ values were interpreted to indicate shallow intrusion and meteoric water involvement during emplacement of Tonian-aged rocks (Archibald et al., 2016). Ediacaran samples in the Itremo Domain have $\varepsilon_{Hf}(t)$ values between -12.9 ± 2.2 and -20.5 ± 3.0, slightly more enriched in ^{176}Hf than the samples from the Antananarivo Domain (Fig. 5.9). The metasedimentary rocks of the Itremo Group are supposedly derived locally from the Antananarivo basement, the Androyen-Anoysen Domain (Tucker et al., 2011b) and possibly from East Africa (Cox et al., 1998; Collins et al., 2003c; Cox et al., 2004; Collins, 2006). The less evolved nature of the rocks intruding the Itremo Group is consistent with the younger Itremo Group being partially assimilated with the magmas and their geochemical variations being largely a consequence of incorporation of different basement lithologies (Fig. 5.9). These two samples along with the two most depleted samples from the Antananarivo Domain are from localities near the Betsileo Shear Zone (Collins et al., 2003c). This extensional detachment may have provided a pathway for depleted-mantle melts to ascend and incorporate crustal material.

Two samples from the Ikalamavony Domain have $\delta^{18}O$ values that plot within the mantle range (Fig. 5.9) demonstrating zircon crystallised from a mantle melt that experienced minor crustal contamination or via melting of a young crustal material derived from a depleted-mantle source. The latter is favoured in which Ediacaran melting of young Dabolava Suite/Ikalamavony Group crust resulted in the less evolved Hf isotopic signatures recorded in Ambalavao Suite samples from the Ikalamavony Domain. $\delta^{18}O$ values for the Imorona-Itsindro Suite in the Ikalamavony Domain show a similar range and were interpreted to be a result of melting of the juvenile Ikalamavony Group/Dabolava Suite crustal material (Archibald et al., 2016). These same Tonian-aged samples have $\varepsilon_{Hf}(t)$ values near CHUR (-0.0 ± 3.3 and +0.2 ± 4.6; Fig. 5.9). Mesoproterozoic volcanic and metasedimentary rocks (Ikalamavony Group) in association with gabbroic and granitoid orthogneiss of the Dabolava Suite comprise the Ikalamavony Domain basement (CGS, 2009a). These rocks are suggested to have formed as a magmatic arc and coeval volcano-sedimentary sequence, respectively, within an oceanic arc tectonic setting (CGS, 2009a; Tucker et al., 2014; Archibald et al., submitted-a). $\varepsilon_{Hf}(t)$ data for the Mesoproterozoic Dabolava Suite shows positive $\varepsilon_{Hf}(t)$ values between +7.5 ± 1.8 and +16.1 ± 1.9 (1σ) indicating a depleted-mantle source with involvement of new, primitive crust for these magmas (Archibald et al., submitted-a). These zircon isotopic values for the Dabolava, Imorona-Itsindro and Ambalavao Suites from the Ikalamavony Domain contrast with values recorded in contemporaneous rocks to the east. The absence of any ages older than the Mesoproterozoic in the Ikalamavony Domain (GAF-BGR, 2008e; CGS, 2009a) suggests that the Dabolava Arc/Ikalamavony Group probably originated as a juvenile Mesoproterozoic oceanic-arc terrane in the Mozambique Ocean before accreting to the Antananarivo Domain by ~900 Ma (Archibald et al., submitted-a). Based on $\delta^{18}O$ values and $\varepsilon_{Hf}(t)$ data, it appears that the components involved in sourcing the Ambalavao and Maevarano Suites were a combination of mostly lithosphere and depleted-mantle derived magmas and the isotopic signatures broadly reflect the protolith components of the lithotectonic domain in which the sample intrudes. In addition, because many of these felsic rocks incorporated crustal material, it is unlikely that samples retained their original mantle isotopic signature if mantle melts were involved. Rather, these rocks represent crustal probes and reflect the isotopic composition of the subcontinental lithosphere and deep crust of central Madagascar during the Ediacaran to Cambrian.

Despite indications of significant crustal involvement as demonstrated by oxygen and hafnium isotopic data, there is little evidence for inheritance of older U-Pb ages (Figs. 5.6, 5.7). Goodenough et al. (2010) also noted the lack of older xenocrystic zircon domains in the Maevarano Suite. This differs from many zircon in the older Imorona-Itsindro Suite that commonly preserve inherited domains, especially in samples intruding the Antananarivo and Itremo Domains (Archibald et al., 2016). U-Pb-Th diffusion rates are sluggish in zircon to temperatures in excess of 1000° C (Cherniak et al., 1997). In south-central Madagascar, peak high-temperature low-pressure metamorphism between ~550-520 Ma was 880 ± 60°C and 8 ± 1 kbar (Markl et al., 2000). In northern Madagascar, P-T estimates are 6.5-8.5 kbar and ~800 - 900 °C (Buchwaldt et al., 2003). In the Ikalamavony Domain between ~560 – 520 Ma, maximum P-T conditions were ~8.3 kbar and ~875°C (CGS, 2009a). The lower crust was presumably much hotter than these preserved metamorphic temperatures in the Ediacaran to Cambrian and was likely hot enough to reset zircon U-Pb age data. The scarcity of inherited ages implies high-temperature magmatism, metamorphism and crustal assimilation above the zircon saturation temperature.

5.7.3 Genesis of the Ambalavao and Maevarano Suites

Late Cryogenian to Cambrian post-collisional magmatism in Madagascar followed the emplacement of four magmatic suites with arc-like geochemical affinities during the preceding ~500 Myr. These older magmatic suites are the ~1080 – 980 Ma Dabolava Suite in the Ikalamavony Domain (Tucker et al., 2007; CGS, 2009a; Archibald et al., submitted-a), the ~850 – 750 Ma Imorona-Itsindro Suite in central Madagascar (see Archibald et al., in review and Tucker et al., 2014 for recent summaries) and the ~760-740 Ma Antsirabe Nord and ~720 – 700 Ma Manambato Suites in North Madagascar (Thomas et al., 2009).

The oldest of the post-collisional magmatic suites is the Kiangara Suite (~635 – 575 Ma). Mainly gneissic, alkaline granitoids and syenite typically exposed as sheet-like intrusions characterise the suite (Guyonnaud, 1951; Nédélec et al., 1995; BGS-USGS-GLW, 2008). Emplacement coincided with extensional deformation (D1) and was correlated with formation of the Betsileo Shear Zone extensional detachment (Collins et al., 2000; Collins, 2006). Previously reported geochemical data for the Kiangara Suite shows two types of intrusions. The first, sub-solvus biotite granitoids have a mildly alkaline composition characterized by strongly fractionated REE patterns and minor Eu anomalies (Nédélec et al., 1995). The other suite is more alkaline and contains pyroxene syenites and amphibole-bearing hypersolvus granites with less fractionated REE patterns and large negative Eu anomalies (Nédélec et al., 1995). These data were said to be consistent with an origin by partial melting of a granodiorite protolith similar to the country rocks of the Antananarivo Domain, but at a deeper level or by an enriched mantle source modified by fractional crystallization towards syenitic and granitic compositions (Nédélec et al., 1995). Nédélec et al. (1995) concluded the petrogenesis of these granites involved mantle derived melts with fractional crystallization and crustal anatexis. Collins and Pisarevsky (2005) posited that the Kiangara Suite formed during post-orogenic extensional collapse following the amalgamation of cratonic Madagascar (as part of 'Azania') with East Africa.

The Ambalavao Suite is more widespread than the Kiangara Suite (CGS, 2009a; Roig et al., 2012). The majority of Ambalavao Suite samples have ages between ~575 - 540 Ma but other, slightly older intrusions (~595 Ma) were assigned to the Vohombohitra Subsuite (BGS-USGS-GLW, 2008). Based on whole-rock geochemistry, Ambalavao Suite granitoids typically have elevated concentrations of total alkalis, Ga/Al ratios, high-field strength elements (HFSE), total REE with lesser amounts of CaO, MgO, Sr, Ni and Cr. These features are attributed to anorogenic or A-type granites (Loiselle and Wones, 1979; Whalen et al.,

1987; Eby, 1990; Frost et al., 2001). Most samples have a moderately negative Eu anomaly suggesting plagioclase fractionation. However, some of the gabbroic and charnockite samples have a positive Eu anomaly suggesting plagioclase accumulation.

Most Ambalavao Suite samples are ferroan, a common feature of A-type granitoids (Fig. 5.13a) and all samples are metaluminous to peraluminous (Fig. 5.13b). Ambalavao Suite samples typically have high Ga/Al ratios and high Zr concentrations (Fig. 5.13c) and plot in the A-type granitoid field (Whalen et al., 1987). Further A-type granitoid classification shows that the majority of samples are A2 type granitoids (Eby, 1992) although most samples plot near the dividing line (Fig. 5.13d). A1 type granites represent differentiates of magmas derived from sources similar to oceanic-island basalts but emplaced in continental rifts or during intraplate magmatism (Eby, 1992). The A2 granites signify magmas derived from continental crust or underplated crust that has been through a cycle of continent-continent collision or island-arc magmatism (Eby, 1992). On tectonic discrimination diagrams (Pearce et al., 1984), samples plot near the boundary between the within-plate granite and volcanic-arc granite fields (Fig. 5.13 e, f). On the Y+Nb versus Rb diagram (Fig. 5.13e), the region where most samples plot is the post-collisional granite field (Pearce, 1996a). This is indicative of intrusion into a post-tectonic setting and reflects the different sources involved during magma genesis (Pearce, 1996a).

Maevarano Suite (~537 – 522 Ma) intrusions are not as extensive as the other two Cryogenian to Cambrian magmatic suites (BGS-USGS-GLW, 2008; Goodenough et al., 2010). Nonetheless, the suite shares many geochemical features that are indistinguishable from both the Kiangara (Nédélec et al., 1995) and the Ambalavao Suites (Figs. 5.10, 5.11). Intrusions show enrichment in LILEs, LREEs and moderately negative Eu anomalies. Samples are predominantly ferroan (Fig. 5.13a) and metaluminous to peraluminous (Fig. 5.13b). The origin of metaluminous to peraluminous ferroan granitoids is attributed to differentiation of a tholeiitic basalt, low pressure melting of the crust and crustal assimilation (Frost and Frost, 2010). Most samples have high Ga/Al ratios and Zr concentrations and plot in the A-type granite field on the Whalen et al. (1987) classification diagram (Fig. 5.13c). The majority of samples have Y/Nb ratios greater than 1.2 and plot in the A2 field (Eby, 1992; Fig. 5.13d) suggesting melt derivation from continental crust or underplated crust that experienced a cycle of continent-continent collision or island-arc magmatism. We note that many samples plot along the boundary between the A1 and A2 fields and the samples collected by Zhou et al. (2015) plot in the A1 field. Although the difference is subtle, Ambalavao Suite samples plot slightly above Maevarano Suite samples closer to the A1 field (Fig. 5.13d). This may reflect progression from primarily intraplate magmatism to magmas derived from underplated crust that experienced continent-continent collision. On granitoid discrimination diagrams (Pearce et al., 1984), Maevarano Suite samples plot in the post-collisional (Fig. 5.13e) and within-plate granite fields (Fig. 5.13f). Therefore, the Ambalavao Suite may correlate with intraplate magmatism associated with D2 related to East-West transpression in the Malagasy Mozambique Belt related to the amalgamated Antananarivo/Masora Domain colliding with the Antongil Domain between ~575-540 Ma and the Maevarano Suite magmatism may represent the manifestation of the post-collisional magmatic underplating (Key et al., 2011).

Sr and Nd isotopic data for Cambrian granites in the Ambatondrazaka Region in Eastern Madagascar (Zhou et al., 2015a) show negative $\varepsilon_{Nd}(t)$ values (-24 and -23), indicating an ancient continental crustal source. Low initial $^{87}Sr/^{86}Sr$ ratios (0.7067 and 0.7069) favour derivation from mafic crustal material with low Rb/Sr ratios (Zhou et al., 2015a). These whole-rock isotope Sr and Nd isotopic data are consistent with Hf isotope data from Cambrian zircon (this study; Zhou et al. 2015).

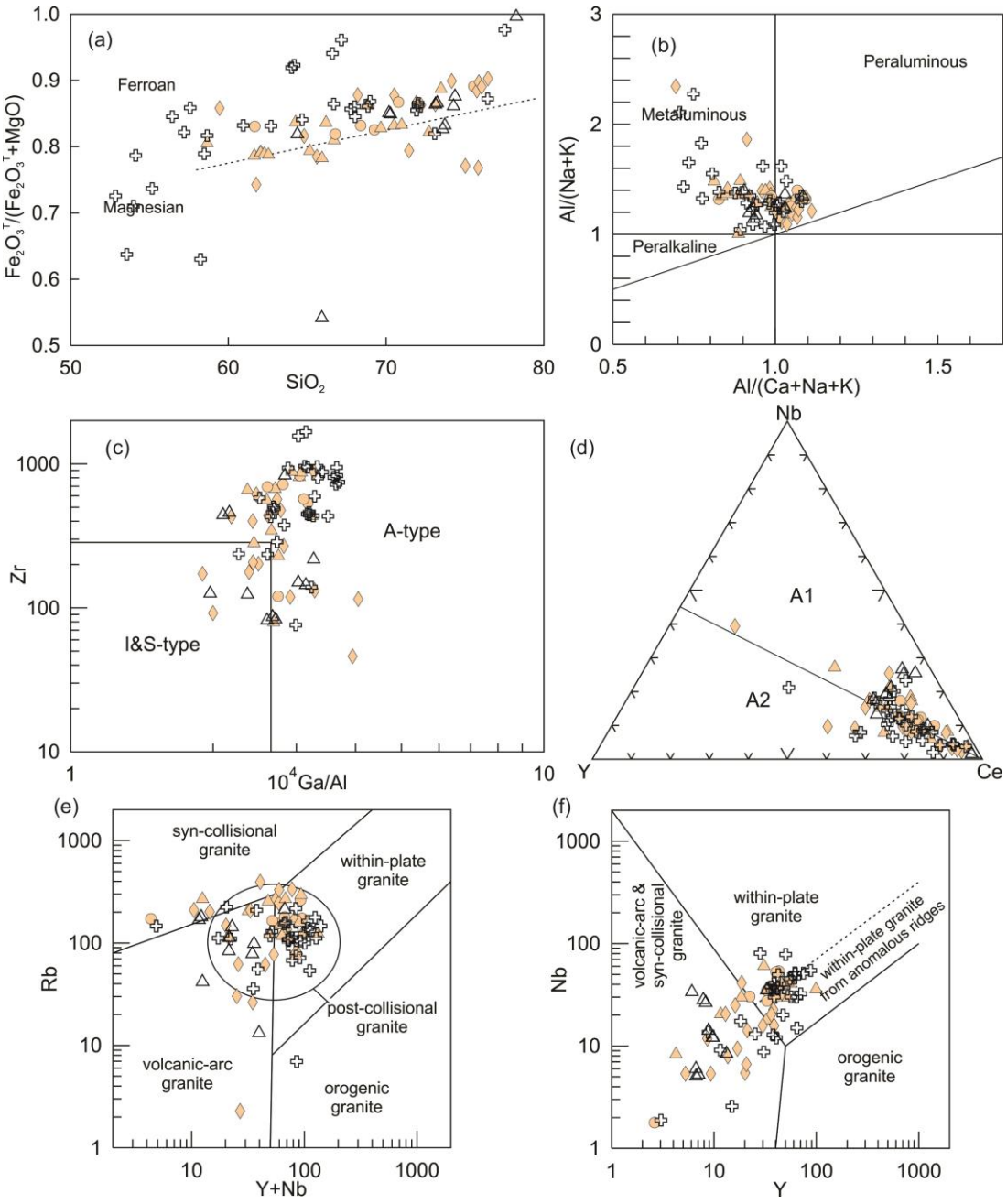

Fig. 5.13 Tectonic setting and classification diagrams for samples of the Ambalavao-Maevarano Suite: (a) Plot of SiO_2 versus $Fe_2O_3^T$ with the ferroan-magnesian dividing line from Frost et al. (2001); (b) Shand index plot. A/NK = molar $Al_2O_3/(Na_2O+K_2O)$; A/CNK = molar $Al_2O_3/(CaO + Na_2O + K_2O)$; (c) Plot of 10^4xGa/Al versus Zr after Whalen et al. (1987) showing the I, S and A-type granite fields; (d) Representation triangular plots for distinguishing A1 and A2 type granitoids. The dividing line for A1 versus A2 granitoids is Y/Nb = 1.2 (Eby, 1992); and (e-f) Tectonic discrimination plots for felsic rocks from Pearce et al. (1984). Post-collisional granite field in (e) is from Pearce (1996a). Data are from Table 5 and the references listed in Fig. 5.4. Symbols are the same as Fig. 5.4.

Though most geochemical features and trends for the Ambalavao Suite are likened to a post-collisional or anorogenic tectonic setting, several other geochemical traits observed are contradictory. Goodenough et al. (2010) also noted many of the geochemical features associated with the Maevarano Suite are inconsistent with an anorogenic setting. For example, some geochemical attributes are often considered arc signatures such as negative Ta-Nb, P,

and Ti anomalies. In addition, anorogenic granites are often anhydrous compared to arc-derived magmas (Winter, 2001). The lithologies present in the Ambalavao Suite vary from anhydrous charnockite to hydrous amphibole and biotite bearing granites and gabbro. Charnockite in central Madagascar are also commonly associated with major shear zones and it has been suggested that charnockite formed during an influx of CO_2 rich fluids related to the Ediacaran to Cambrian deformation events (Nédélec et al., 2014). We suggest that the contradictory "arc-like" geochemical signatures are inherited from the Imorona-Itsindro Suite. The Tonian-aged magmatic suite displays geochemical signatures typical of arc-environments such as negative Nb-Ta, Sr-P and Ti anomalies and enrichment in LREEs and LILEs (Boger et al., 2014, 2015; Archibald et al., submitted-c). Arc-magmatism was widespread throughout Madagascar during Neoproterozoic time (Handke et al., 1997; Handke et al., 1999; Kröner et al., 2000; Boger et al., 2014, 2015; Archibald et al., 2016) and the Ambalavao Suite magmas likely inherited the "arc-like" geochemical signatures. Furthermore, zircon oxygen and hafnium isotopic data dictate incorporation of older crustal material into the Ambalavao and Maevarano Suite granitoids.

These data are important for unravelling the magmatic events related to the final stages of Gondwana amalgamation. Several Ediacaran to Cambrian collisions were suggested by Key et al. (2011) that resulted in the amalgamation of the Masora and Antongil Domains (during separate events) with the Antananarivo Domain. The Ambalavao and Maevarano Suites may embody the magmatic manifestations of syn- or post-amalgamation events or both, thus questioning the Greater Dharwar hypothesis proposed by (Tucker et al., 2014). In the Greater Dharwar model, the Greater Dharwar Craton of India along with its Malagasy extensions (the Antongil, Masora and Antananarivo Domains) was together from nearly 3.0 Ga to continental break-up around 100 Myr. Polyphase Ediacaran-Cambrian deformational events (e.g. Nédélec et al.,2000) and successive magmatic episodes could occur within a stable continent, but, possibly more likely, these deformation and magmatic episodes recorded in rocks from central Madagascar occurred as a result of multiple collisional events during the waning stages of Gondwana assembly. We therefore dispute the Greater Dharwar hypothesis and support the theory that Madagascar was a microcontinent through most of Proterozoic time (Collins and Windley, 2002; Collins, 2006). Eastward directed subduction of oceanic crust beneath central Madagascar during the mid-Tonian closed the Mozambique Ocean (Archibald et al., submitted-c). Later collisions coalesced the Masora and Antananarivo Domains (pre-630 Ma) and the youngest amalgamation occurred ~550 Ma following the collision of the combined Masora/Antananarivo Domain with the Antongil Domain (Key et al., 2011).

5.8 Summary and conclusions

The Ambalavao and Maevarano Suites represent significant, mainly granitoid magmatism in Madagascar throughout the Ediacaran and into the Cambrian Period. This U-Pb, O and Hf isotopic study of zircon and whole-rock geochemistry data provides important information regarding the late Neoproterozoic history of Madagascar during the waning stages of the East African Orogen and the amalgamation of Gondwana leading to the following conclusions:

1) New geochronological data agrees with previously published U-Pb data for the Ambalavao and Maevarano Suites. The compilation of all the available magmatic crystallisation ages in Madagascar shows that magmatism was essentially continuous from the Late Cryogenian to the Cambrian with the successive emplacement of the Kiangara (~ 650 – 575 Ma), Ambalavao (~575 – 540 Ma) and Maevarano (~537 – 522 Ma) Suites. These suites represent the final magmatic manifestations associated with the closure of the Mozambique Ocean and amalgamation of Gondwana in the Malagasy Mozambique Belt. These magmatic suites also

correspond spatially with major late-Neoproterozoic transpressive and transcurrent shear zones and temporally with periods of intense regional deformation.

2) Magmatic zircon oxygen and hafnium isotopic data suggest a significant crustal component during magma genesis, a contrast to previous work which suggested negligible crustal contamination. Curiously, zircon shows little evidence for inheritance of ancient U-Pb ages implying high-temperature magmatism and assimilation above the zircon saturation temperature. Preserved O and Hf isotopic data indicate both suites were derived locally from the crust and some samples show evidence for mixing of crustal and more depleted components. In addition, isotopic data highlight the different basement components present in central Madagascar, in particular, the juvenile nature of the Mesoproterozoic Ikalamavony Domain.

3) Whole-rock geochemical data for the Ambalavao and Maevarano Suites are indistinguishable. Samples are characterised by coherent fractionation trends of major elements, enrichment of HFSEs, LILEs, and REEs (especially the LREEs). Samples of both suites follow similar trends on variation and discrimination diagrams suggesting they had a similar genesis. These geochemical features are consistent with melting in an anorogenic (A-type) post-tectonic setting.

4) The Ambalavao and Maevarano Suites were emplaced during the waning stages of the East African Orogen in the Malagasy Mozambique Belt. Emplacement coincided with peak high-temperature, low pressure metamorphism throughout central Madagascar. Post-tectonic intrusions are often associated with major shear zones and in this study, magmatic intrusions are associated with the Ediacaran to Cambrian Angavo, Betsileo and Dabolava shear zones. Melting occurred during lithospheric underplating and the lithospheric delamination associated with the continent-continent collision and the extensional collapse of the EAO.

5.9 Acknowledgements
The Razafinjoelina family, in particular Auguste and Berthieu are thanked for providing transportation, assistance in the field, and hospitality during fieldwork in Madagascar. Ms. Aoife McFadden and Dr. Benjamin Wade (Adelaide Microscopy) are acknowledged for assistance obtaining CL images and LA-ICP-MS U-Pb data. Anne Nédélec and Kathryn Goodenough provided excellent and constructive criticism on an earlier version of this manuscript. This paper forms TRaX Record ### and is an output of ARC Future Fellowship grant FT120100340. This paper is a contribution to IGCP projects #628 (Gondwana Map) and #648 (Supercontinent Cycles and Global Geodynamics).

Chapter 6

The Dabolava Suite

Prepared for publication:

Archibald, D. B., Collins, A. S., Foden, J. D., Payne, J. L., Holden, P., Razakamanana, T., (prepared for publication). Genesis of the Stenian-Tonian Dabolava Suite of west central Madagascar: Implications for the formation of Rodinia.

Statement of Authorship

Title of Paper	Tectonics and chemistry of late to post tectonic magmatism in the Malagasy Mozambique Belt
Publication Status	__ Published __ Accepted for Publication __ Submitted for Publication X_ Publication Style
Publication Details	Archibald, D.B., Collins, A.S., Foden, J.D., Payne, J.L., Holden, P., Razakamanana, T. prepared for publication. Genesis of the Stenian-Tonian Dabolava Suite of west central Madagascar: Implications for the formation of Rodinia.

Author Contributions

By signing the Statement of Authorship, each author certifies that their stated contribution to the publication is accurate and that permission is granted for the publication to be included in the candidate's thesis.

Name of Principal Author (Candidate) Contribution to the paper Conceptualisation of the work It's realisation Documentation and write-up Development of ideas and conclusions	Donnelly B. Archibald Prepared samples, carried out analyses and interpretation of the data, organised manuscript and data, wrote manuscript, acted as the corresponding author		
Signature		Date	9/7/2016

Name of Co-Author Contribution to the paper	Prof Alan S. Collins (University of Adelaide) Supervised work, assisted with data interpretation and manuscript revision		
Signature		Date	9/7/2016

Name of Co-Author Contribution to the paper	Prof John D. Foden (University of Adelaide) Assisted with manuscript revision		
Signature		Date	11/7/2017

Name of Co-Author Contribution to the paper	Dr. Justin L. Payne (University of South Australia) Assisted with hafnium isotope data collection, manuscript revision		
Signature		Date	7/4/2016

Name of Co-Author Contribution to the paper	Dr. Peter Holden (The Australian National University) Assisted with oxygen isotope data collection and interpretation		
Signature		Date	28/04/2016

Name of Co-Author Contribution to the paper	Dr. Theodore Razakamanana (University of Toliara, Madagascar) Assistance in the field, sample logistics, manuscript editing		
Signature		Date	8/4/2016

Abstract

Madagascar occupies an important location in many Proterozoic plate reconstructions and unravelling its tectonic geography has long been recognised as a key to understanding the amalgamation of central Gondwana. The recent recognition of voluminously extensive, but geographically focussed, Stenian to Tonian magmatism on the island (the Dabolava Suite) demonstrates that it also lay in a tectonically active region during the amalgamation of Rodinia. Dabolava Suite intrusions are only recognised in the Ikalamavony Domain in west-central Madagascar. Gabbroic and granitoid rocks of the suite are subdivided into intermediate to felsic intrusions (Ambatomiefy-type) and predominantly gabbroic intrusions (Vongoa-type). Magmatic rocks show intrusive contact relationships with the Mesoproterozoic Ikalamavony Group which consists of tholeiitic amphibolite, thick paragneiss sequences, calc-silicates, marble and quartzite. New U-Pb (zircon) geochronological data extends the period of magmatism to between ca. 1080-980 Ma. Zircon oxygen isotope ion-probe data illustrate that the parent magmas involved crustal contributions that had been fractionated by a hydrological cycle, whereas hafnium isotopic data yield near depleted mantle signatures with only minor deflection to more evolved values. Together these trends suggest mantle-derived magma intrusion and upper-crustal assimilation of recently intruded pre-existing plutons—a situation commonly found in volcanic island arc settings. Geochemical data show moderate enrichment in large-ion lithophile elements (LILEs) and light rare-earth-elements (REEs) and depletions in Nb, Ta, P, and Ti with relatively flat heavy REE profiles. These magmatic rocks, combined with the interpreted coeval volcanic and metasedimentary rocks of the Ikalamavony Group, are interpreted to represent a magmatic arc and marginal volcano-sedimentary sequence within an oceanic arc tectonic setting that formed within the Mozambique Ocean. The Dabolava Suite formed by westward- or southward-directed subduction that resulted in top-to-the east thrust emplacement over the Antananarivo Domain before the initiation of the Itsindro-Imorona Suite magmatism at ca.850 Ma.

6.1 Introduction

The Archaean shield of Madagascar occupies an important location in many Proterozoic plate reconstructions as it lies within the Gondwana-forming collisional zone that makes up the East African Orogen (Collins and Pisarevsky, 2005; Li et al., 2008; Li et al., 2013; Johansson, 2014; Pisarevsky et al., 2014). In contrast to the dynamic tectonic environment experienced later, late-Palaeoproterozoic to mid-Mesoproterozoic times have been considered tectonically quiet in Madagascar (Key et al., 2011). The Archaean shield of Madagascar is often considered to have been flanked to the south by the Palaeoproterozoic Androyen-Anosyen Domain at this time (Tucker et al., 2014). To the north and west of the stable craton lay an open ocean and continental shelf (Tucker et al., 2014) and to the east was either the Indian Dharwar Craton in the "Greater Dharwar Craton" model for Proterozoic Madagascar (Tucker et al., 2011a), or an open ocean in a hypothesis where central Madagascar formed part of an isolated microcontinent named Azania (Collins and Windley, 2002; Cox et al., 2004; Fitzsimons and Hulscher, 2005; Collins, 2006). In this Azania model, central Madagascar, along with fragments of southern India (the Madurai Block, Plavsa et al., 2014; Collins et al., 2014), East Africa, Yemen and Saudi Arabia (Collins and Windley, 2002), were isolated from both Neoproterozoic India and the Congo-Tanzania-Bangweulu Block by oceanic crust. During Mesoproterozoic time, several sedimentary sequences were deposited in parts of what is now Madagascar. The Andrarona and Sambriano-Sahantaha Groups were deposited along the north and east margins of the craton and have been suggested as correlatives to the Aravalli and Delhi Supergroups of India in the Greater Dharwar model (Tucker et al., 2014). Other metasedimentary sequences namely the Itremo, Ambatolampy, Maha, Tranomaro, Imaloto, and Mangoky Groups were also deposited on the

central, southern and western regions of the Malagasy shield (Key et al., 2011; Tucker et al., 2012; Archibald et al., 2015).

Following, or coeval with, Mesoproterozoic continental basin formation, an active magmatic arc developed to the west of the Antananarivo Domain (Tucker et al., 2014). This arc is represented by the Dabolava Suite (1035-982 Ma; Tucker et al., 2007) in the Ikalamavony Domain and possibly also by the Ankiliabo Suite (930-910 Ma) in the Androyen Domain (Rakotoarimanana, 2001; GAF-BGR, 2008e, a; CGS, 2009a, b; Tucker et al., 2011b). Similar aged arc-magmatism in what eventually became central Gondwana are also recognised in the Irumide Belt of Zambia (Johnson et al., 2005; De Waele et al., 2006a; De Waele et al., 2006b), Kenya (Hauzenberger et al., 2007; Hauzenberger et al., 2014), the Nampula, Unango and Marrupa Complexes of Mozambique (Bingen et al., 2009; Macey et al., 2010), Sri Lanka (Kröner et al., 1987; Kröner et al., 2003; He et al., 2016), Dronning Maud Land (Jacobs et al., 2015), and in the Antarctic Sør Rondane Mountains (Elburg et al., 2015). This arc magmatism was coeval with the amalgamation of Rodinia, a supercontinent that is thought to have formed between 1300 Ma and 900 Ma and is often modelled to have virtually all cratonic blocks existing at that time as part of the continental amalgam (Li et al., 2008; Li et al., 2013). Rodinia may have existed for ~150 Myr before extensional basins opened and widespread continental rifting occurred between ca. 825 Ma and 740 Ma, with episodic plume events at ca. 825 Ma, ca. 780 Ma and ca. 750 Ma (Li et al., 2008; Li et al., 2013). At the same time (~850-750 Ma), central Madagascar was situated in an active continental arc as shown by intrusion of the calc-alkaline Imorona-Itsindro Suite (Handke et al., 1999; Kröner et al., 2000; Archibald et al., 2016; Archibald et al., submitted-c) and the Antsiribe-Nord (~760-750 Ma) and Manambato Suites (~720-700 Ma) in northern Madagascar (Thomas et al., 2009). Some authors have questioned the presence of a widespread Tonian Andean-like arc in Madagascar and favour intracontinental rifting environment to fit the Rodinia model (Tucker et al., 2011a; Yang et al., 2014; Zhou, 2015; Zhou et al., 2015a) but more recent studies demonstrate geochemical and isotopic data for Tonian-aged rocks are more compatible with supra-subduction zone processes (Boger et al., 2014, 2015; Archibald et al., 2016; Archibald et al., submitted-c). The reshuffling of continental blocks throughout the mid-Neoproterozoic eventually culminated in multiple collisions of smaller crustal plates between ~650 Ma and 500 Ma to form Gondwana (Meert, 2003; Collins and Pisarevsky, 2005; Viola et al., 2008; Bingen et al., 2009; Torsvik and Cocks, 2013).

Stenian-Tonian magmatic rocks intruding into the Ikalamavony Domain (Fig. 6.1) form the focus of this paper. The Dabolava Suite has only been recently identified (Rakotoarimanana, 2001; Tucker et al., 2007). It consists of mafic plutons that intrudes into metasedimentary rocks of the Ikalamavony Group, and is restricted to the Ikalamavony Domain (CGS, 2009a; Key et al., 2011; Roig et al., 2012; Tucker et al., 2014). Understanding this magmatic suite is important for grasping the tectonic setting of Madagascar at the beginning of the Neoproterozoic. U-Pb, oxygen and hafnium isotope data from zircon provide new constraints on the age of the suite and magma source components. Complimentary whole-rock geochemical data provide petrogenetic information. These data are used to determine the genesis of the Ikalamavony Domain and resolve the significance of the Dabolava Suite in the tectonic development of Madagascar.

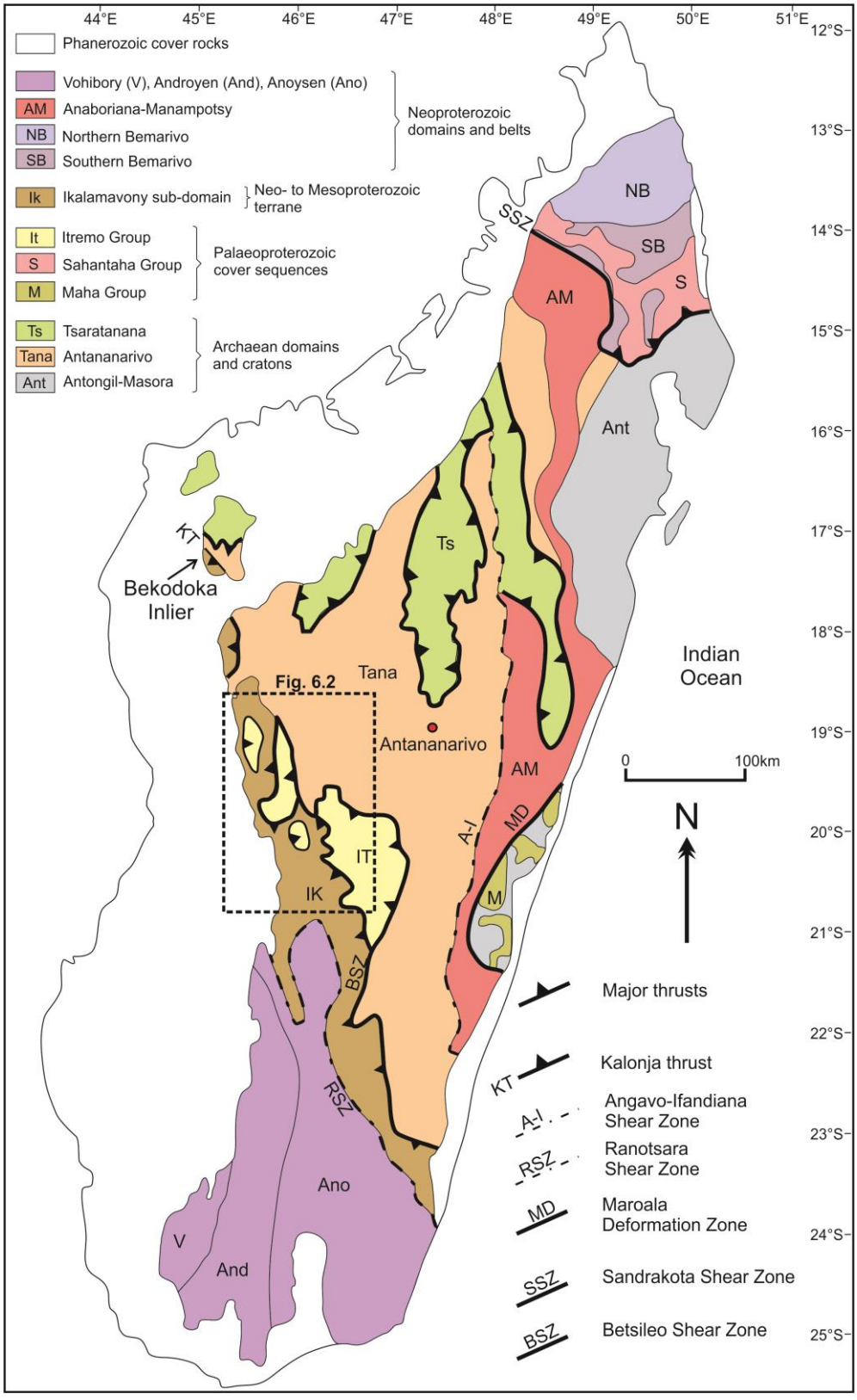

Fig. 6.1 Simplified basement geology of Madagascar showing the major tectonic domains and shear zones (after Collins, 2006 and De Waele et al., 2011).

6.2 Regional geology of Madagascar and Neoproterozoic tectonic development

Madagascar contains several Precambrian to earliest Palaeozoic 'basement' units overlain by Phanerozoic sedimentary and volcanic rocks (Roig et al., 2012). The oldest rocks are located along Madagascar's east coast in the Palaeoarchaean to Palaeoproterozoic Antongil and Masora Domains (Fig. 6.1). These units are considered remnants of the Dharwar Craton of southern India left behind following the Mesozoic break-up of Gondwana (e.g. Schofield et al., 2010). The Antananarivo Domain (including the Tsaratanana Domain) represents the largest Precambrian unit (Fig. 6.1) and underlies much of central Madagascar. Granulite- to upper-amphibolite facies orthogneiss and paragneiss characterise the domain (Kröner et al., 2000; Collins et al., 2003a; Collins, 2006; Roig et al., 2012). The orthogneiss consists of ~2550 – 2500 Ma granitoids (the Betsiboka Suite) that are tectonically interlayered with paragneiss of the Sofia, Ambatolampy and Vondrozo Groups (Besairie, 1968-1971; BGS-USGS-GLW, 2008; Roig et al., 2012).

To the west of the Antananarivo Domain is the metasedimentary Itremo Domain (Fig. 6.2). The Itremo Group consist primarily of quartzite, mica schist and dolomitic marble. Detrital zircon studies show significant U-Pb age populations at ~ 2500 Ma and ~1800 Ma (Cox et al., 2004; Fitzsimons and Hulscher, 2005; De Waele et al., 2011). The precise depositional age of these rocks is poorly constrained to younger than ~1700 Ma based on the youngest detrital zircon (Collins et al., 2003c; Cox et al., 2004; De Waele et al., 2011). The minimum depositional age (~850-750 Ma) is constrained by intrusion of the Imorona-Itsindro Suite (e.g. Handke et al., 1999) or by late Ediacaran to Cambrian metamorphism and intrusion of the Ambalavao and Maevarano Suites (e.g. Key et al., 2011). Some authors (Tucker et al., 2007) have suggested that the lower Ikalamavony Group (discussed in the following paragraph; Fig. 6.2) is a correlative to the Itremo Group which could further constrain the minimum depositional age of these sequences to older than ~1035 Ma, however, these relationships are not fully understood (Tucker et al., 2007). The protolith sediments were deposited on a continental shelf or passive margin sometime after ~1700 Ma (Fernandez et al., 2003; Cox et al., 2004) with their interpreted sediment source in East Africa (Cox et al., 1998; Cox et al., 2004; Fitzsimons and Hulscher, 2005) or locally from the Archaean to Proterozoic basement of Madagascar. However, the precise nature of the relationship of metasedimentary units to the Archaean gneisses of the Antananarivo Domain and the relationship of the Neoproterozoic intrusive rocks in the Itremo Domain is controversial (Tucker et al., 2007). Moine (1967) considered metaigneous rocks to be the crystalline basement to the Itremo Group because many plutons are strongly foliated and have concordant contacts with neighbouring stratified rocks. Cox et al. (1998) suggested the plutons in the Itremo region were relatively undeformed and interpreted the period of pluton emplacement (~833 Ma) as the time of regional metamorphism and deformation. Collins et al. (2000) suggested that Tonian plutons were emplaced into the already intensely folded and translated Itremo Group and hence, the intrusions postdate the isoclinal folds and thrusts of the region. Fernandez et al. (2003) recognized the general concordance between the orthogneiss and the Itremo Group, but they considered the contact to be a thrust that was subsequently folded and metamorphosed during Cambrian time. Tucker et al. (2007) posited that the Neoproterozoic (~1000–720 Ma) plutons were emplaced into the Itremo Group and Archaean basement, and all that all rocks were affected by younger metamorphic events. Itremo Group lithologies generally increase in metamorphic grade from east to west (Tucker et al., 2007) with the lowest-grade rocks (lower greenschist facies) preserved in the hanging-wall of the Betsileo shear zone (Moine, 1974; Collins et al., 2000). Recently, the Itremo Group was correlated with the Maha Group that structurally overlies the Masora Domain in south-east Madagascar (Fig. 6.1), the Sambirano-Sahantaha Group from the southern Bemarivo Domain (De Waele et al., 2011), the Ambatolampy Group (Archibald et al., 2015) and similar-aged metasedimentary rocks in southern India (Plavsa et al., 2014).

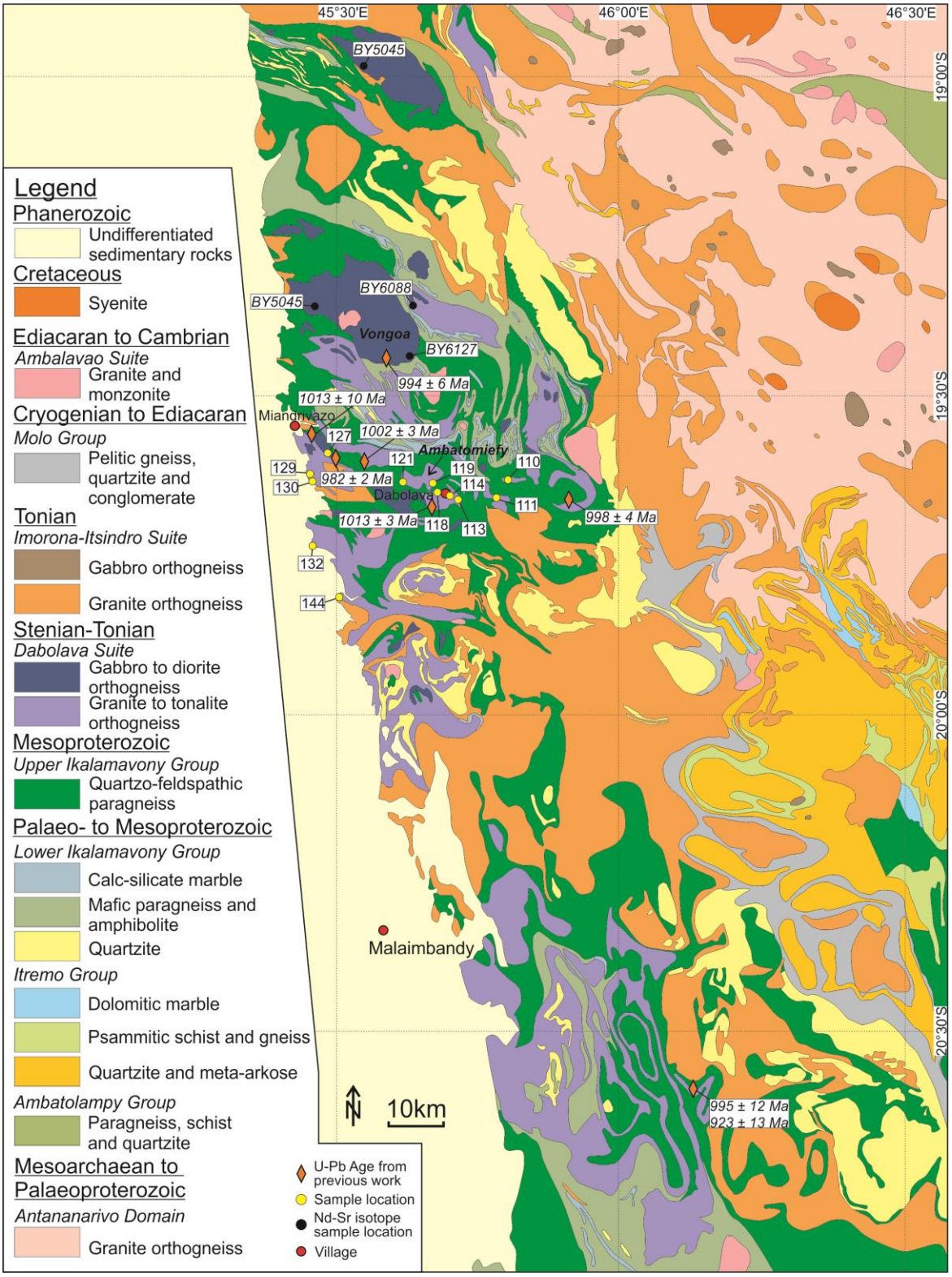

Fig. 6.2 Geologic map of the Ikalamavony Domain and the western margin of the Antananarivo Domain (modified after Roig et al., 2012 and CGS, 2009a) showing the extent of Stenian-Tonian magmatism sampled in this study. Previous geochronologic data are from Tucker et al. (2007), Rakotoarimanana (2001), CGS (2009a), GAF-BGR (2008e), and Tucker et al. (2011b). DA14- prefixes are not included with the sample names to improve map clarity.

The Ikalamavony Domain is more extensive than the Itremo Domain and constitutes a north-northwest trending unit that is traced from southeast to central west Madagascar (Figs. 6.1 and 6.2). In contrast to the Itremo region, the Ikalamavony Domain contains inferred metavolcanic and metasedimentary rocks of mainly intermediate and mafic composition of a probable oceanic origin (GAF-BGR, 2008e; CGS, 2009a). The Ikalamavony Group (formerly known at the Amborompotsy Group; Besairie, 1964; Tucker et al., 2007) consists of ocean floor basalts (now metamorphosed to tholeiitic amphibolite), thick sequences of calcium and magnesium rich paragneiss (now metamorphosed to biotite hornblende gneisses), calc-silicates, and locally marble and quartzite (CGS, 2009a). The precise age of the Ikalamavony Group is unknown but U-Pb zircon crystallisation ages from the Dabolava Suite (Rakotoarimanana, 2001; Tucker et al., 2007; CGS, 2009a; Tucker et al., 2011b) provide the minimum depositional age. Magmatic rocks are mostly calc-alkaline intermediate and felsic orthogneiss emplaced between ~1035 and 982 Ma and are unique to the Ikalamavony Domain. These intrusions are thought to be of similar age to both the tholeiitic amphibolite and the sediments into which they intrude (CGS, 2009a). Regardless of their earlier tectonic history, the Ikalamavony and Itremo Domains amalgamated prior to ~850 Ma and were subsequently intruded by the Imorona-Itsindro Suite (CGS, 2009a). Tonian-aged magmatic rocks are widespread in both domains and primarily show cross-cutting relationships in the Itremo region (Handke et al., 1999; Tucker et al., 2007; Archibald et al., 2016; Archibald et al., submitted-c) and are more orthogneissic showing layer-parallel relationships in the Ikalamavony Domain (Tucker et al., 2007; CGS, 2009a). The poorly understood Molo Group crops out to the west of the Itremo Group (Fig. 6.2) and its depositional age is assumed to be during the late Mesoproterozoic to early Neoproterozoic (Cox et al., 2004; Tucker et al., 2007; André-Mayer et al., 2014).

From the late Mesoproterozoic to the Cambrian, central Madagascar underwent several tectonic disturbances coinciding with magmatic rock emplacement. As stated previously, gabbroic and granitoid rocks of the Stenian-Tonian (~1035-982 Ma; Tucker et al., 2007) Dabolava Suite, in conjunction with coeval volcanic and metasedimentary rocks of the Ikalamavony Group, are thought to represent the volcano-sedimentary and intrusive igneous rocks of a magmatic-arc built (mostly) on oceanic crust that developed during rifting of the Androyen-Anosyen Domain from the Antananarivo Domain prior to ~1000 Ma (CGS, 2009a; Tucker et al., 2014). Tucker et al. (2014) suggested a juvenile origin for the suite based on the absence of Palaeoproterozoic and older detritus in the Ikalamavony Group. The Tonian-aged (~850-750 Ma) Imorona-Itsindro Suite consists of granitoid, syenite and gabbro that intruded, and is interlayered with, most central Madagascar lithotectonic units except for the Ambatolampy Group where definitive contact relationships are inferred but not observed (Archibald et al., 2015). Two opposing views of the tectonic setting of the suite were proposed on the basis of whole-rock and isotope geochemistry: in a supra-subduction zone setting (Handke et al., 1999; Kröner et al., 2000; Key et al., 2011; Boger et al., 2014, 2015; Archibald et al., 2016; Archibald et al., submitted-c) or above a mantle plume (Yang et al., 2014; Zhou et al., 2015b). Younger intrusive rock suites are represented by the ~630 Ma Kiangara Suite A-type granitoids (Nédélec et al., 1994), the post-collisional granitoids of the ~575-540 Ma Ambalavao Suite (Meert et al., 2001a; BGS-USGS-GLW, 2008; Archibald et al., submitted-b) and the post-tectonic granitoids of the ~537-522 Ma Maevarano Suite (Goodenough et al., 2010; Zhou et al., 2015a; Archibald et al., submitted-b).

Southern Madagascar contains three domains divided by high-strain zones that are separated from central Madagascar by the Ranotsara Shear Zone (Fig. 6.1). The westernmost domain is the Vohibory Domain and is composed mainly of mafic and felsic orthogneiss intercalated with paragneiss and marble (GAF-BGR, 2008c; Jöns and Schenk, 2008). The mafic rocks are thought to represent a combination of mid-ocean, back-arc and island arc basalts with inferred extrusion ages between ~850 – 700 Ma (Jöns and Schenk, 2008). Detrital

zircon U-Pb studies of the sedimentary rocks yield a near unimodal population with ages ~900 Ma (Collins et al., 2012). Collectively, rocks from the Vohibory Domain resemble an island-arc and the arc has close geologic affinities to the similarly aged arc terranes in East Africa (GAF-BGR, 2008c). The Androyen Domain contains mostly paragneiss, orthogneiss and ~940-900 Ma anorthosite-leuconorite, olivine gabbro/peridotite and alkali-granites of the Ankiliabo Suite (GAF-BGR, 2008a). Recent work dates the protoliths of this Androyen domain to ~2120–1770 Ma (Tucker et al., 2011b; JICA, 2012). The Anoysen Domain is the most extensive and contains primarily paragneissic rocks of the Iakora Group (~2400–1600 Ma detrital zircon ages) and the inferred Tonian-aged volcano-sedimentary rocks of the Horombe Group (Boger et al., 2014). The inferred felsic volcanic rocks of the Horombe Group are metaluminous and peraluminous, have a similar geochemistry and are the same age as the Imorona–Itsindro Suite (Boger et al., 2014). These metasedimentary packages are suggested to be deposited in the Tonian to Cryogenian based on the inferred absence of the Ankiliabo, Dabolava, and Imorona–Itsindro Suites (GAF-BGR, 2008b; Boger et al., 2014). Deformation and high-temperature metamorphism occurred in two pulses in southern Madagascar. The earliest phase was between 620 – 600 Ma in the Androyen and Vohibory Domains and later at 580 – 520 Ma in the Androyen and Anosyen Domains (Markl et al., 2000; de Wit et al., 2001; Jöns and Schenk, 2011).

6.3 The Dabolava Suite

The Dabolava Suite forms the focus of this paper and derives its name from the town of Dabolava, the main area for gold exploration in the region (CGS, 2009a). The suite is restricted to the Ikalamavony Domain in the region of Miandrivazo and Dabolava (Fig. 6.2) and has yet to be recognised to the east of the boundary between the Ikalamavony and Antananarivo Domains (CGS, 2009a; Roig et al., 2012; Tucker et al., 2014). Plutons and smaller intrusions of Mesoproterozoic rocks are often difficult to distinguish from the more voluminous Tonian-aged Imorona-Itsindro Suite in the absence of geochronological data (CGS, 2009a). Prior to recent U-Pb geochronological work (Rakotoarimanana, 2001; Tucker et al., 2007; CGS, 2009a) rocks of the Dabolava Suite were assigned to the Imorona-Itsindro Suite (Besairie, 1969-1971) and the age of the suite is constrained to ~1035-982 Ma (Tucker et al., 2014).

The magmatic suite is divided into two sub-suites based on whole-rock geochemistry (CGS, 2009a). Ambatomiefy-type intrusions are predominantly granodiorite, diorite, tonalite, and trondjemite orthogneiss. White and grey orthogneiss is medium- to coarse-grained, equigranular and mafic mineral alignment defines the gneissic fabric. These intrusions are sometimes cross-cut by discrete cm-scale bands of mylonitisation and local brecciation (CGS, 2009a). The second sub-suite comprises the mafic and ultramafic rocks and are named Vongoa-type intrusions after the largest intrusion, the Vongoa Pluton (CGS, 2009a). These intrusions are usually small isolated plutons intruding the Ikalamavony Group or are concordant sheets associated with the Ambatomiefy-type orthogneiss (CGS, 2009a). Despite experiencing synchronous deformation, the mafic intrusions are more massive, relatively undeformed and variably metamorphosed compared to their felsic counterparts (CGS, 2009a).

6.4 Analytical methods

A complete description of the methods employed in this study is available in Appendix 6.1. Eleven polished thin-sections were examined under transmitted and reflected light to determine mineralogy and textures including nine samples of Ambatomiefy-type and two samples of Vongoa-type intrusions. Fractions of these same samples were selected for whole-rock geochemical analyses for major, minor and trace elements at ACME Labs in Vancouver, Canada. Five of these Dabolava Suite samples were selected for zircon U-Pb,

oxygen and hafnium isotope analysis. U-Pb analyses were conducted at Adelaide Microscopy in Adelaide, Australia. Zircon standard reference material GJ (Jackson et al., 2004) was used as a primary standard and internal accuracy was monitored using the Plešovice reference material ($^{206}Pb/^{238}U$ age of 337.1 ± 0.37 Ma; 2σ; Sláma et al., 2008). Plešovice analyses yield a weighted average $^{206}Pb/^{238}U$ age of 340.3 ± 3.4 (2σ; MSWD = 3.5; n = 24). Oxygen isotope analyses were conducted at the Australian National University, Canberra, Australia using the SHRIMP II (sensitive high-resolution ion microprobe) instrument following the methods of Ickert et al. (2008). Long term instrument drift was corrected using the Mudtank zircon reference material ($\delta^{18}O$ = 5.03±0.10 ‰; Valley, 2003) and internal accuracy monitored using Temora II zircon ($\delta^{18}O$ = 8.20±0.01 ‰; Valley, 2003). In situ LA-MC-ICP-MS (laser-ablation multi-collector inductively-coupled mass spectroscopy) Hf isotope analyses were conducted at the University of Adelaide Waite Campus facility using a New Wave Research 193 nm Excimer laser attached to a Neptune multi-collector ICP-MS system as per Payne et al. (2013). Analysis locations were in the same cathodoluminescence domains as concordant U–Pb laser spots and in the same site as SHRIMP II oxygen spots. Procedural accuracy was monitored using the Plešovice, Mudtank and Temora II zircon standards. Mean $^{176}Hf/^{177}Hf$ ratios for each standard along with the literature values are presented in the online supplementary Appendix 6.1 (Table A.6.1). $\varepsilon_{Hf}(t)$ and $T_{DM}c$ were calculated using ^{176}Lu decay constant after Scherer et al. (2001). $T_{DM}c$ two stage crustal model ages were calculated using the methods of Griffin et al. (2002) with an average crustal composition of $^{176}Lu/^{177}Hf$ = 0.015.

6.5 Results

6.5.1 Petrography

Ambatomiefy-type

Nine samples analysed in this study have intermediate to felsic compositions of mainly granodiorite and granite (Table 6.1; Fig. 6.3a). Most samples exhibit a strong foliation defined by the alignment of biotite and amphibole and some samples exhibit myrmeckite and/or granophyric textures. Samples are fine- to coarse-grained, inequigranular and individual grains are predominantly subhedral to anhedral.

Alkali-feldspar (10-30%) display tartan and Carlsbad twinning. Grains are predominantly subhedral and most alkali-feldspar grains show varying degrees of sericitisation and commonly display perthitic textures. Plagioclase feldspar (10-40%) exhibits albite and pericline twinning. Grains are mainly subhedral to euhedral and show varying degrees of saussuritisation. Quartz (20-45%) typically displays undulatory extinction and grains are usually larger than alkali-feldspar or plagioclase grains. Biotite (0-5%) exhibits characteristic birds-eye texture. Grains are mainly subhedral to euhedral, pale-yellow to brown, pleochroic and some biotite grains are partially altered to chlorite. Amphiboles (0-5%) are subhedral to euhedral, dark blue/green and pleochroic. Red garnet (0- <1%) was identified in one sample and grains are euhedral. Other accessory minerals identified in felsic samples include zircon (<1%), allanite (<1%), opaque minerals (<1%) and Fe-oxides (<1%).

Vongoa-type

Two samples analysed in this study have gabbroic compositions and belong to the Vongoa-subsuite (Table 6.1; Fig. 6.3b). Samples are weakly foliated highlighted by the alignment of biotite and amphibole. Samples are medium- to coarse-grained, inequigranular and individual grains are predominantly subhedral to anhedral.

Plagioclase feldspar (30-60%) exhibits albite twinning. Grains are mainly subhedral to euhedral and show varying degrees of saussuritisation. Quartz (10-15%) was identified in sample DA14-113 and displays undulatory extinction. Biotite (2-10%) exhibits characteristic birds-eye texture. Grains are mainly subhedral to euhedral, pale-yellow to brown; pleochroic and some grains are partially altered to chlorite. Amphiboles (0-5%) are subhedral to euhedral, dark blue/green and pleochroic. Clinopyroxene (5-30%) grains are mostly altered to green amphibole and sometimes display simple twinning. Other minerals identified in gabbroic samples include twinned orthopyroxene (0-2%), intensely altered olivine (0-5%), opaque minerals (<1%) and Fe-oxides (<1%).

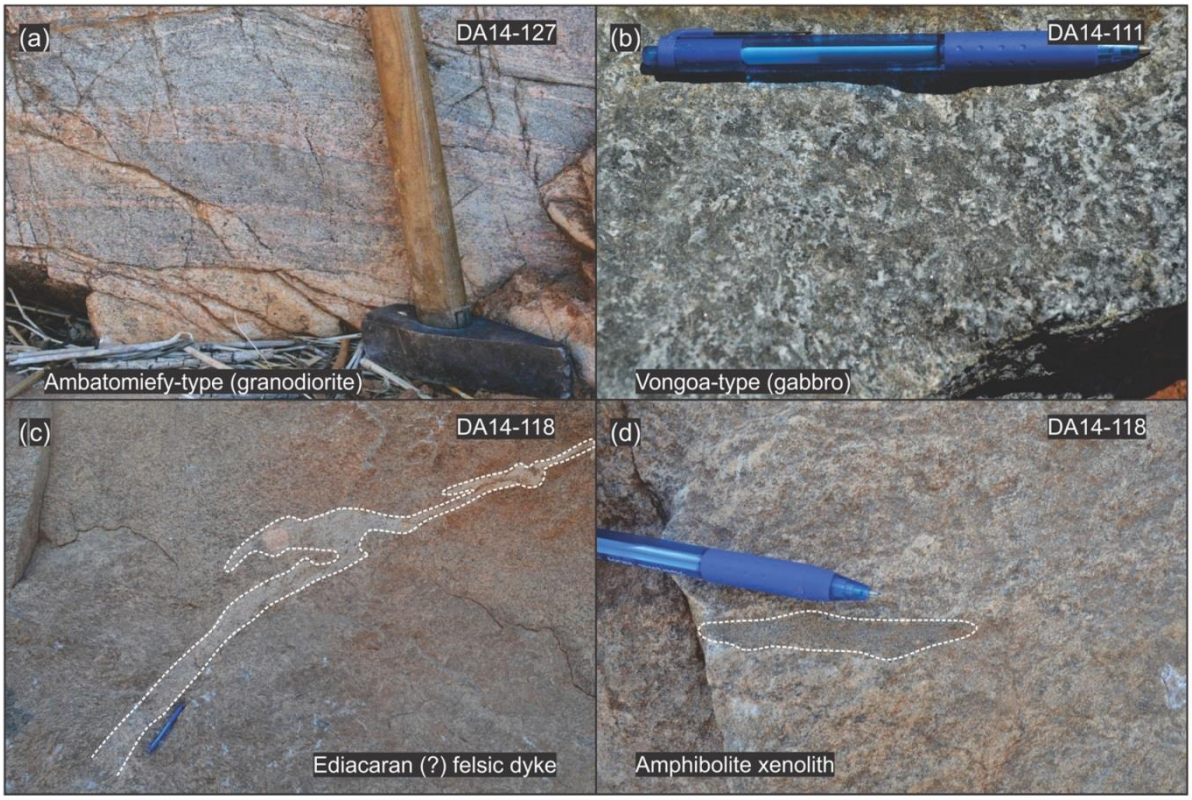

Fig. 6.3 Representative field photographs of the Dabolava Suite: (a)Sample DA14-127 of Ambatomiefy-type granodiorite; (b) Sample DA14-111 of Vongoa-type gabbro; (c) sampling location of DA14-118 showing intrusion of younger granite pegmatite dykes into the granodiorite; and (d) amphibolite xenolith from the Ikalamavony Group in granodiorite at the sampling locality of DA14-118.

6.5.2 U-Pb Geochronology

Five samples of the Dabolava Suite were selected for zircon U-Pb isotope analysis. U-Pb data was collected to confirm the age of each sample and to determine suitable zircon for oxygen and hafnium isotope analyses. Individual zircon grain ages are quoted at the 1σ level and weighted-mean ages are quoted at the 2σ level. Zircon properties are found in Table 6.2 and Fig. 6.4.

Sample DA14-110 was collected from a streambed outcrop ~14km east of Dabolava (Fig. 6.2). The foliated granodiorite is cross-cut by E-W striking pegmatite dykes and quartz veins. Observable field relationships with older lithologies are not recognised at this location.

Forty-five zircon analyses yielded 29 ≥ 90% concordant ages (Fig. 6.5a). Common ^{206}Pb values in concordant grains are low (0.00 - 0.30%) and Th/U ratios are between 0.06 and 0.80 (Appendix 6.2). Data follow a Pb-loss trend with a small cluster of data near ~840 Ma and one concordant rim analysis plots at 539 ± 7 Ma. Concordant data older than 950 Ma yield a weighted-mean $^{207}Pb/^{206}Pb$ age of 1002 ± 17 Ma (MSWD = 0.25; n=22/45). The $^{206}Pb/^{238}U$ age for the same data is 965 ± 14 Ma (MSWD = 6.6; n=22/45). Discordia upper and lower-intercept ages are 1003 ± 29 Ma and 74 ± 690 Ma (MSWD=0.25), a trend that corresponds to Pb-loss. Given the spread of concordant data, the $^{207}Pb/^{206}Pb$ age is interpreted to most accurately represent the crystallisation age. Two concordant grains at 960 ± 13 Ma and 937 ± 12 Ma do not plot along the same concordia and are interpreted to represent Pb loss. The concordant data at ~840 Ma yields a $^{206}Pb/^{238}U$ age of 838 ± 10 Ma (MSWD=0.15; n=4), an age that corresponds with the intrusive age of the Imorona-Itsindro Suite (Archibald et al., 2016). The 539 ± 7 Ma ($^{206}Pb/^{238}U$) rim analysis has the lowest Th/U ratio (0.06) and is interpreted to date Cambrian metamorphism in the Dabolava region.

Table 6.1 Summary of sample names, locations, lithology and mineralogy for samples of the Dabolava Suite.

Sample	Latitude	Longitude	Sub-suite	Lithology	Grain size	Textures	Mineralogy
DA14-110	19° 37' 10.4"	45° 49' 23.9"	Ambatomiefy	Granodiorite	fg-mg	massive	qtz+af+pl+bt+am+op+zrc
DA14-111	19° 38' 30.5"	45° 47' 57.7"	Vongoa	Gabbro	mg-cg	foliated	pl+cpx+opx+ol+am+op
DA14-113	19° 39' 03.8"	45° 44' 31.8"	Vongoa	Gabbro	mg-cg	foliated	pl+am+bt+cpx+qtz+op
DA14-114	19° 39' 03.8"	45° 44' 31.8"	Ambatomiefy	Granite	mg-cg	massive, myrmeckite	pl+afs+qtz+gt+op
DA14-118	19° 37' 45.5"	45° 43' 25.7"	Ambatomiefy	Granite	fg-cg	foliated, myrmeckite	qtz+af+pl+am+bt+op+zrc
DA14-119	19° 37' 45.6"	45° 43' 07.3"	Ambatomiefy	Granodiorite	fg-cg	foliated, myrmeckite	qtz+af+pl+am+bt+op+zrc
DA14-121	19° 37' 18.5"	45° 38' 27.0"	Ambatomiefy	Granite	fg-mg	foliated, granophyric	qtz+af+pl+bt
DA14-127	19° 35' 06.6"	45° 30' 46.2"	Ambatomiefy	Granodiorite	fg-cg	foliated	qtz+pl+af+bt+op+zrc
DA14-129	19° 39' 52.9"	45° 28' 02.2"	Ambatomiefy	Granite	fg-mg	foliated, myrmeckite, granophyric	qtz+af+pl+bt+op
DA14-130	19° 40' 45.5"	45° 28' 01.2"	Ambatomiefy	Granite	fg-mg	foliated, myrmeckite, granophyric	qtz+af+pl+bt+op+zrc
DA14-144	20° 27' 45.6"	45° 45' 53.3"	Ambatomiefy	Granodiorite	fg-mg	massive	qtz+af+pl+bt+op+zrc

Sample DA14-118, a granite sample, was collected from a small roadside quarry where local miners were panning for gold ~1km west of Dabolava (Fig. 6.2). The granite is strongly foliated and cross-cut by undeformed pegmatite dykes and quartz veins (Fig. 6.3c). There are also partially digested xenoliths found within the outcrop (Fig. 6.3d) indicating the intrusive nature of the granite into the Ikalamavony Group.

Twenty-nine zircon analyses yielded 24 ≥ 90% concordant ages (Fig. 6.5b). Common ^{206}Pb values in concordant grains are low (0.00 - 0.81%) and Th/U ratios are between 0.15 and 0.95 (Appendix 6.2). Concordant data follow a Pb-loss trend and yield a weighted-mean $^{207}Pb/^{206}Pb$ age of 1035 ± 20 Ma (MSWD = 0.05; n=24/29). The $^{206}Pb/^{238}U$ age for the same data is 987 ± 10 Ma (MSWD = 2.3; n=24/29). Discordia upper and lower-intercepts are 1030 ± 23 Ma and -122 ± 350 Ma (MSWD=0.05), a trend corresponding to Pb-loss. The $^{207}Pb/^{206}Pb$ age is interpreted to represent the crystallisation age.

Table 6.2 Physical and optical characteristics of zircon from the Dabolava Suite.

Sample	Colour	Size (μm)	Aspect ratio (L:W)	Morphology	Internal zoning
DA14-110	colourless, pale-yellow	50-250	2:1 - 3:1	mostly subhedral	magmatic oscillatory zoning, broad irregular zoning, sector zoning, narrow dark overgrowths
DA14-118	clear, colourless, pale yellow	100-350	2:1 - 4:1	mostly subhedral	narrow to broad magmatic oscillatory zoning, dark inclusions, sector zoning, narrow dark overgrowths
DA14-119	clear, colourless	100-350	2:1 - 3:1	euhedral to mostly subhedral	narrow to broad magmatic oscillatory zoning, unzoned cores, dark inclusions, sector zoning, narrow dark overgrowths
DA14-127	clear, colourless	50-300	2:1 - 4:1	euhedral to mostly subhedral	faint broad zoning, magmatic oscillatory zoning
DA14-130	clear, colourless	50-200	1:1 - 2:1	mostly subhedral	broadly zoned crystal interiors, narrow magmatic oscillatory zoned outer domains, minor sector zoning, dark inclusions

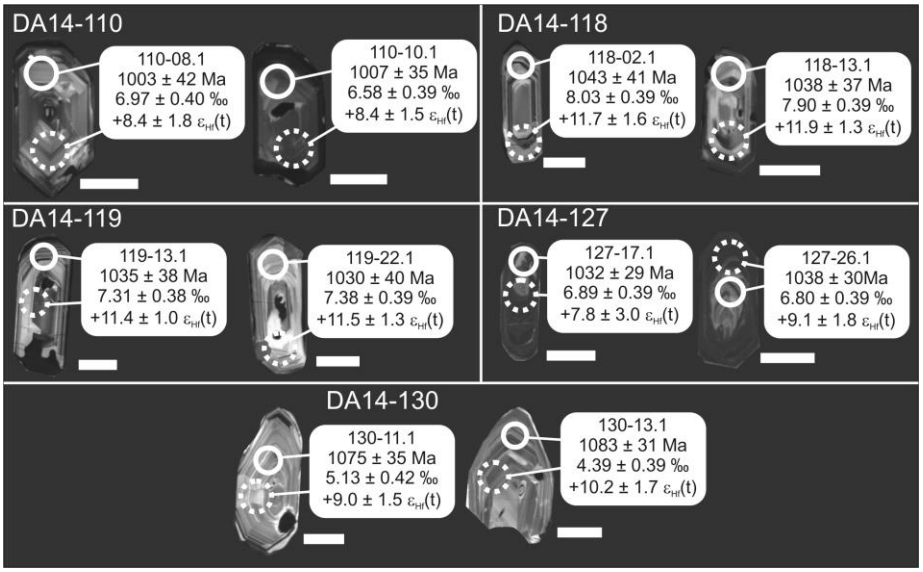

Fig. 6.4 Cathodoluminescence (CL) images for representative zircon from the Dabolava Suite. Analysis names, U-Pb ages with one standard deviation error, $\delta^{18}O$ values with two standard deviation error and $\varepsilon_{Hf}(t)$ values with two standard deviation error are listed beside each image. Solid circles indicate LA-ICP-MS U-Pb analysis spots and broken circles show the location of oxygen and hafnium isotope analyses. Scale bars with each image are ~50 μm.

Sample DA14-119 is coarse-grained granodiorite gneiss that was collected from a streambed outcrop where locals are mining gold near Dabolava (Fig. 6.2). The granodiorite is weakly foliated and cross-cut by narrow (<50cm), undeformed granite dykes and quartz veins.

Twenty-six zircon analyses yielded 23 ≥ 90% concordant ages (Fig. 6.5c). Common 206Pb values in concordant grains are low (0.00 - 0.45%) and Th/U ratios are between 0.12 and 0.59 (Appendix 6.2). Concordant data follow a Pb-loss trend and yield a weighted-mean $^{207}Pb/^{206}Pb$ age of 1028 ± 19 Ma (MSWD = 0.16; n=23/26). The $^{206}Pb/^{238}U$ age for the same data is 1008 ± 10 Ma (MSWD = 2.2; n=23/26). Discordia upper and lower-intercepts are 1025 ± 19 Ma and -234 ±1400 Ma (MSWD=0.16), a trend corresponding to Pb-loss. Given the spread of concordant data, the $^{207}Pb/^{206}Pb$ age is interpreted to most accurately represent the crystallisation age.

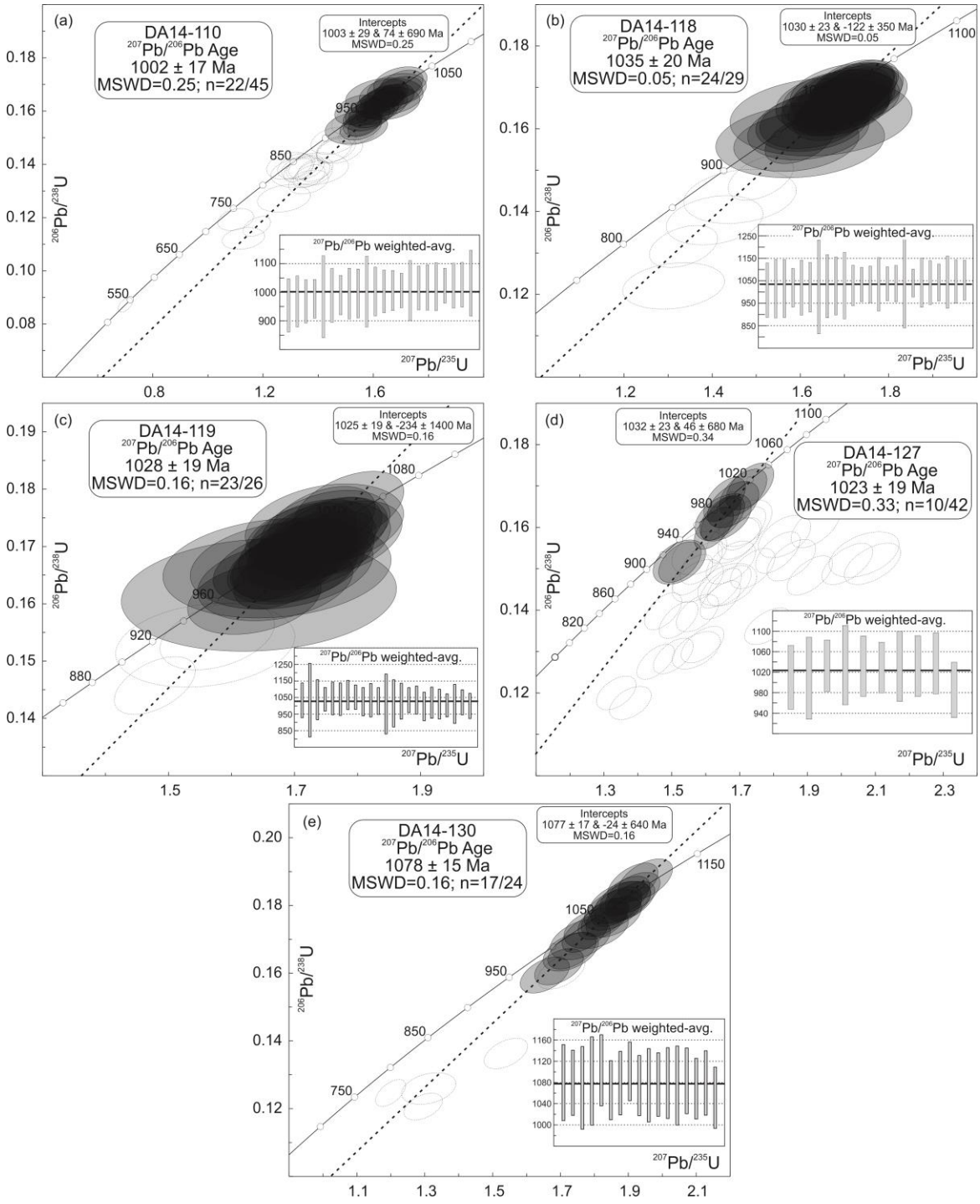

Fig. 6.5 Concordia diagrams showing zircon analyses from the Dabolava Suite: (a) DA14-110; (b) DA14-118; (c) DA14-119; (d) DA14-127; and (e) DA14-130. U-Pb data are reported in Appendix 6.2. Data point error ellipses are 2σ. Shaded ellipses were used in the weighted mean age calculation and open ellipses were rejected.

Sample DA14-127 is a medium-grained granodiorite gneiss sample that was collected from a roadside outcrop ~8km east of Miandrivazo (Fig. 6.2). The homogeneous granodiorite is generally weakly foliated but in some parts of the outcrop the foliation is intense. Small, undeformed pink granite dykes cross-cut the granodiorite. This sampling location is near (~100 m) an exposure of quartz arenite belonging to the Ikalamavony Group (Fig. 6.2).

Forty-two zircon analyses yielded 10 ≥ 90% concordant ages (Fig. 6.5d). Common ^{206}Pb values in concordant grains are low (0.00 - 0.09%) and Th/U ratios are between 0.28 and 0.94 (Appendix 6.2). Concordant data yield a weighted-mean $^{207}Pb/^{206}Pb$ age of 1023 ± 19 Ma (MSWD = 0.33; n=10/42). The $^{206}Pb/^{238}U$ age for the same data is 966 ± 25 Ma (MSWD = 8.5; n=10/42). Discordia upper and lower-intercepts are 1032 ± 46 Ma and 169 ± 680 Ma (MSWD=0.34), a trend corresponding to Pb-loss. Given the spread of concordant data, the $^{207}Pb/^{206}Pb$ age is interpreted to most accurately represent the crystallisation age.

Sample DA14-130 is medium-grained granite gneiss that was collected from a roadside outcrop ~17 km south of Miandrivazo (Fig. 6.2). The granite has a well-developed foliation throughout most of the outcrop but in some areas the rock is relatively undeformed. Parts of the outcrop are cross-cut by granite dykes at a low angle to the foliation. The outcrop shows compositional layering with granodiorite forming "rafts" surrounded by more quartz-rich fine-grained granite transitioning to coarser biotite and alkali-feldspar rich layers. Macroscopically, the biotite-rich layers anastomose around the granodiorite layers that pinch out. To the west, the unconformably overlying Jurassic sediments are exposed (Fig. 6.2).

Twenty-four zircon analyses yielded 17 ≥ 90% concordant ages (Fig. 6.5d). Common ^{206}Pb values in concordant grains are low (0.00 - 0.35%) and Th/U ratios are between 0.40 and 0.84 (Appendix 6.2). Concordant data follow a Pb-loss trend and yield a weighted-mean $^{207}Pb/^{206}Pb$ age of 1078 ± 15 Ma (MSWD = 0.16; n=17/24). The $^{206}Pb/^{238}U$ age for the same data is 1053 ± 18 Ma (MSWD = 7.1; n=17/24). Discordia upper and lower-intercept ages are 1077 ± 17 Ma and -24 ± 640 Ma (MSWD=0.16), a trend corresponding to Pb-loss. Given the spread of concordant data, the $^{207}Pb/^{206}Pb$ age is interpreted to most accurately represent the crystallisation age.

6.5.3 Oxygen and hafnium isotopes

Zircon oxygen and hafnium isotope data were collected from the five samples selected for U-Pb geochronology. Oxygen data were collected for 45 Stenian to Tonian-aged zircon domains (Dabolava Suite) and two middle Tonian-aged domains (Imorona-Itsindro Suite). Overall, Stenian-Tonian zircon has $\delta^{18}O$ values between 4.06 ± 0.39 and 8.21 ± 0.39‰ (Table 6.3). Sample DA14-110 is the youngest sample and has a mean $\delta^{18}O$ value of 6.79 ± 0.56 ‰ (2σ; n=11). Samples DA14-118 and DA14-119 have similar average $\delta^{18}O$ values of 7.85 ± 0.90 ‰ (2σ; n=8) and 7.69 ± 0.55 ‰ (2σ; n=10). Sample DA14-127 has an average $\delta^{18}O$ value of 6.58 ± 0.78 ‰ (2σ; n=8). All four samples have elevated $\delta^{18}O$ values that plot above the range expected for mantle derived zircon (Fig. 6.6a, b). The oldest sample, DA14-130, has an average $\delta^{18}O$ value of 4.62 ± 0.96 ‰ (2σ; n=8), lower than recorded for the younger samples of the Dabolava Suite and plots below the mantle range (Fig. 6.6a, b). Two analyses of middle Tonian-aged zircon give $\delta^{18}O$ values of 6.83 ± 0.37 and 6.39 ± 0.39 ‰. These analyses agree with previously reported $\delta^{18}O$ values for the Imorona-Itsindro Suite intruding into the Ikalamavony Domain that have $\delta^{18}O$ values between 5.16 ± 0.55 and 8.28 ± 0.54 ‰ (Archibald et al., 2016).

Hafnium isotope data were collected from 45 Stenian to Tonian-aged zircon domains (Fig. 6.6c, d) and results show juvenile $\varepsilon_{Hf}(t)$ signatures varying between +7.5 ± 1.8 and +16.1 ± 1.9 (Table 6.4). The youngest samples (DA14-110 and DA14-127) have the most evolved $\varepsilon_{Hf}(t)$ values of +9.0 ± 2.0 (2σ; n=12) and +8.2 ± 1.1 (2σ; n=8). Corresponding $T_{DM}c$ model ages are 1.3 ± 0.1 Ga (2σ; n=12) and 1.3 ± 0.1 Ga (2σ; n=8). Samples DA14-118 and DA14-119 have comparable $\varepsilon_{Hf}(t)$ values of +11.5 ± 0.7 (2σ; n=7) and +11.3 ± 1.1 (2σ; n=10). Corresponding $T_{DM}c$ model ages are 1.1 ± 0.1 Ga (2σ; n=7) and 1.2± 0.1 Ga (2σ; n=10). The oldest sample has more variable $\varepsilon_{Hf}(t)$ values that yield a mean $\varepsilon_{Hf}(t)$ value of +10.5 ± 4.6 (2σ;

n=8). Omitting the highest value, the mean $\varepsilon_{Hf}(t)$ value is 9.7 ± 1.7 (2σ; n=7). Corresponding $T_{DM}c$ model ages are between 1.2 and 1.4 Ga (mean = 1.2 ± 0.3 Ga; 2σ; n=7). Two middle Tonian-aged zircon domains yield $\varepsilon_{Hf}(t)$ values of +6.1 ± 2.0 and +5.6 ± 2.0. $T_{DM}c$ model ages are 1.3 and 1.4 Ga. Similar to the oxygen isotope data, the hafnium data agrees with data collected for the Imorona-Itsindro Suite (+2.8 ± 10.1; 2σ; n=14; Archibald et al., in review).

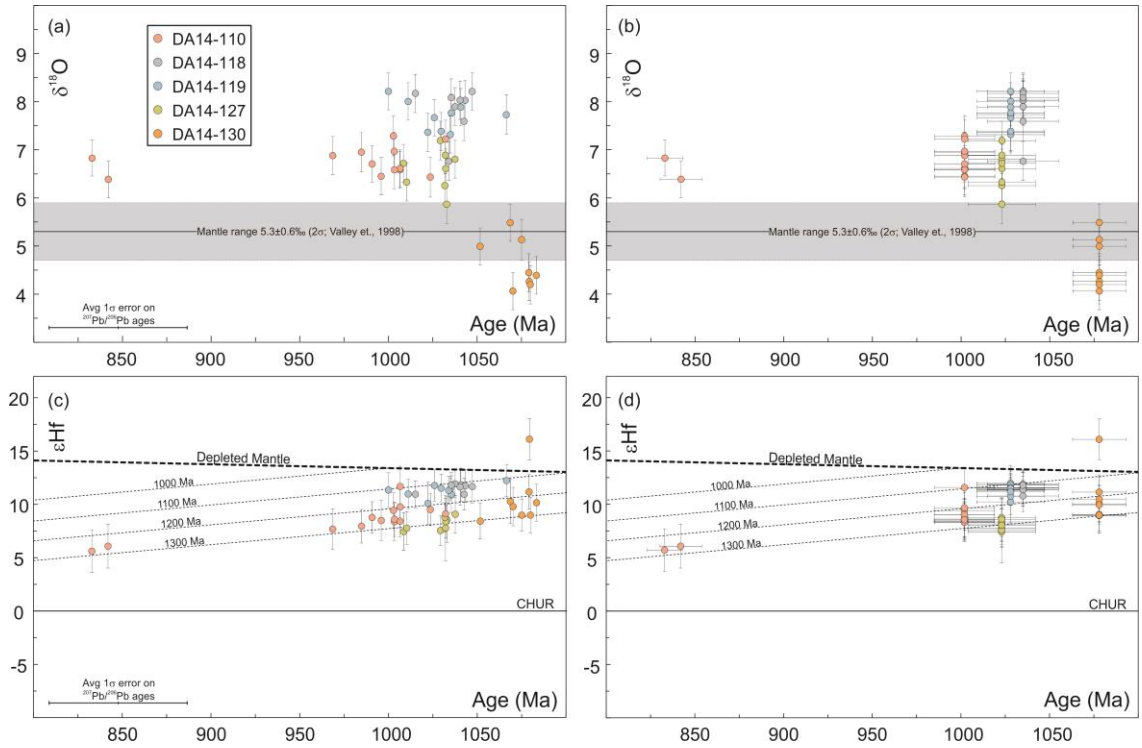

Fig. 6.6 Oxygen and hafnium isotope diagrams for five samples of the Dabolava Suite. $\delta^{18}O$ plotted against (a) zircon crystallisation age and (b) the interpreted sample crystallisation age. $\varepsilon_{Hf}(t)$ plotted against (c) zircon crystallisation age and (d) the interpreted sample crystallisation age. Error bars on $\delta^{18}O$ values and sample ages in (b) and (d) are 2σ. Range of mantle derived $\delta^{18}O$ (zircon) values are 5.3 ± 0.6 ‰ (Valley et al., 1998). The T_{DM} (crustal) Hf evolution fields are based on a $^{176}Lu/^{177}Hf$ ratio of 0.015 (Griffin et al., 2004). Average $\delta^{18}O$ and ε_{Hf} (t) values for each sample are listed in Table 6. Abbreviations: DM - depleted mantle. CHUR - chondrite uniform reservoir.

6.5.4 Whole-rock geochemistry

Eleven samples including the five samples chosen for zircon isotopic analysis were selected for whole-rock geochemical analysis. Of those samples, nine belong to the Ambatomiefy sub-suite and two samples belong to the Vongoa sub-suite. Also included in the foregoing discussion are whole-rock geochemical data collected by CGS (2009a), Rakotoarimanana (2001) and GAF-BGR (2008e). Amphibolite samples from the Ikalamavony Group are also shown but these data are discussed in CGS (2009a) and Rakotoarimanana (2001).

Dabolava Suite samples have SiO_2 concentrations varying between 59.45-79.38 wt. % in Ambatomiefy-type (intermediate to felsic) samples and 45.74-54.5 wt. % in Vongoa-type (mafic) samples (Fig. 6.7; Table 6.5). MgO concentrations for felsic to intermediate samples are between 0.00-3.68 wt. % and $Fe_2O_3^T$ (FeO +Fe_2O_3) contents between 0.22-8.97 wt. %. Both MgO and $Fe_2O_3^T$ demonstrate a negative correlation with increasing SiO_2 concentrations (Fig, 7a, 7b). Al_2O_3 increases then decreases (8.98-18.14 wt. %; Fig. 6.7c) corresponding with

a constant decrease in CaO (0.58-7.43 wt. %; Fig. 6.7d). Na_2O (1.65-7.18 wt. %) and K_2O (0.00-5.84 wt. %) contents vary across variable SiO_2 but both elements illustrate a broad positive correlation with SiO_2 (Fig. 6.7e, f). TiO_2 (0.00-1.08 wt. %), P_2O_5 (0.00-0.31 wt. %), and MnO (0.00-0.14 wt. %) contents are low and exhibit a negative correlation with SiO_2 (Fig. 6.7g-i).

Vongoa-type (mafic) samples have MgO concentrations of 4.10-12.7 wt. % (Fig. 6.7a; Table 6.5). $Fe_2O_3^T$ contents are between 6.97-19.24 wt. % and demonstrate a negative correlation with SiO_2 (Fig. 6.7b). Al_2O_3 increases (10.29-20.51 wt. %; Fig. 6.7c) corresponding with a constant decrease in CaO (0.58-7.43; Fig. 6.7d). Together with the Ambatomiefy-type felsic samples, these trends suggest the removal of clinopyroxene early during fractionation by removing Ca but not Al followed by plagioclase crystallisation removing both Ca and Al (Fig. 6.7). Na_2O (1.54-4.21 wt. %) and K_2O (0.00-4.74 wt. %) contents vary across variable SiO_2 (Fig. 6.7e, f). TiO_2 (0.29-3.17 wt. %), P_2O_5 (0.00-0.66 wt. %), and MnO (0.10-0.42 wt. %) contents are generally higher than Ambatomiefy-type samples and demonstrate a negative correlation with SiO_2 (Fig. 6.7g-i).

Ambatomiefy-type samples have chondrite-normalised rare-earth element diagrams that show moderate to steep enrichment in light rare-earth elements (LREEs) and relatively flat heavy rare-earth element (HREEs) profiles (Fig. 6.8a). La/Sm_N ratios are between 1.79 and 10.45 and Tb/Yb_N ratios are between 0.08 and 0.35 for samples in this study (Table 6.5). Most samples exhibit a negative Eu anomaly and Eu/Eu* ratios between 0.40 and 0.77 (Table 6.5) indicative of plagioclase fractionation. One sample (DA14-114) has a deep Eu anomaly (Eu/Eu*=0.04). This sample is from a mineralised area where locals are gold mining. Primitive mantle normalised multi-element variation diagram exhibits enrichment in large-ion lithophile elements (LILEs) and depletions in Nb, Ta, P, and Ti (Fig. 6.8b). New data are indistinguishable from previously reported trace-element data (Figs. 6.8a, b).

Vongoa-type samples demonstrate flat LREE and HREE profiles (Fig. 6.8c). La/Sm_N ratios for two samples are 0.76 and 1.33 and Tb/Yb_N ratios are 0.23 and 0.22 for samples in this study (Table 6.5). Eu/Eu* ratios are 1.42 and 0.98. Trace-element plots show depletions in Rb, Nb, and enrichment in Cs (Fig. 6.8d). This pattern differs from that of the intermediate to felsic samples. Mafic samples analysed here differ from some previously reported data but it should be noted that only two samples are included in our study. Published data for mafic samples show peaks and troughs are defined by positive Cs, Ba, Th, U, and Pb anomalies and negative Nb-Ta, P, Zr and Ti anomalies (Fig. 6.8d).

6.6 Discussion

6.6.1 U-Pb age and zircon isotopes

The Dabolava Suite represents Stenian-Tonian magmatism in the Ikalamavony Domain in western Madagascar. Four of the analysed samples fall within the time period previously reported (~1035-982 Ma; Tucker et al., 2007) but the fifth sample (DA14-130) yielded a U-Pb zircon age of 1078 ± 15 Ma. Zircon isotopic data varies slightly for this sample compared with the other four samples in that sample DA14-130 has significantly lower $\delta^{18}O$ (Fig. 6; Table 6). These variations are interpreted to represent maturation of the arc, the details of which will be discussed below. Whole-rock geochemical data are indistinguishable from the other dated samples and we suggest that this sample is, in fact, part of the Dabolava Suite, thus extending the period of magmatism back to ~1080 Ma.

Table 6.3 SHRIMP II oxygen isotope results from zircon

		Age (Ma)				$^{18}O/^{16}O$ Data				
Analysis	Suite	Zircon Age (Ma)	± 1σ	Sample Age (Ma)	2σ	$^{18}O/^{16}O$	1σ	$^{18}O/^{16}O$ (‰)	Error T 95%	External error 2σ
DA14-110-01.1	Dabolava	985	71	1002	17	0.0020325	0.0000005	6.95	0.22	0.41
DA14-110-04.1	Dabolava	969	38	1002	17	0.0020323	0.0000004	6.88	0.21	0.40
DA14-110-05.1	Dabolava	996	44	1002	17	0.0020314	0.0000004	6.45	0.19	0.39
DA14-110-08.1	Dabolava	1003	42	1002	17	0.0020325	0.0000004	6.97	0.21	0.40
DA14-110-10.1	Dabolava	1007	35	1002	17	0.0020317	0.0000004	6.58	0.18	0.39
DA14-110-15.2	Dabolava	1003	62	1002	17	0.0020331	0.0000005	7.28	0.23	0.41
DA14-110-20.1	Dabolava	1032	57	1002	17	0.0020330	0.0000004	7.22	0.20	0.39
DA14-110-24.1	Imorona-Itsindro	842	12	842	12	0.0020313	0.0000004	6.39	0.18	0.39
DA14-110-28.1	Dabolava	1007	52	1002	17	0.0020318	0.0000004	6.61	0.19	0.39
DA14-110-29.1	Imorona-Itsindro	833	10	833	10	0.0020322	0.0000003	6.83	0.15	0.37
DA14-110-33.1	Dabolava	991	34	1002	17	0.0020320	0.0000003	6.71	0.17	0.38
DA14-110-39.1	Dabolava	1024	39	1002	17	0.0020314	0.0000005	6.43	0.24	0.41
DA14-110-41.1	Dabolava	1003	37	1002	17	0.0020317	0.0000004	6.58	0.21	0.40
DA14-118-02.1	Dabolava	1043	41	1035	20	0.0020346	0.0000005	8.03	0.22	0.41
DA14-118-13.1	Dabolava	1038	37	1035	20	0.0020344	0.0000004	7.90	0.20	0.39
DA14-118-14.1	Dabolava	1047	48	1035	20	0.0020350	0.0000004	8.21	0.19	0.39
DA14-118-18.1	Dabolava	1043	49	1035	20	0.0020338	0.0000004	7.59	0.22	0.40
DA14-118-20.1	Dabolava	1040	31	1035	20	0.0020347	0.0000004	8.03	0.21	0.40
DA14-118-23.1	Dabolava	1034	38	1035	20	0.0020321	0.0000004	6.76	0.21	0.40
DA14-118-28.1	Dabolava	1015	65	1035	20	0.0020349	0.0000004	8.17	0.21	0.40
DA14-118-29.1	Dabolava	1035	59	1035	20	0.0020348	0.0000004	8.08	0.19	0.39
DA14-119-01.1	Dabolava	1022	38	1028	19	0.0020333	0.0000004	7.36	0.21	0.40
DA14-119-04.1	Dabolava	1067	44	1028	19	0.0020340	0.0000005	7.73	0.22	0.41
DA14-119-09.1	Dabolava	1026	43	1028	19	0.0020339	0.0000003	7.67	0.17	0.38
DA14-119-12.1	Dabolava	1011	45	1028	19	0.0020346	0.0000004	8.00	0.19	0.39
DA14-119-13.1	Dabolava	1035	38	1028	19	0.0020332	0.0000004	7.31	0.18	0.38
DA14-119-18.1	Dabolava	1000	38	1028	19	0.0020350	0.0000004	8.21	0.18	0.38
DA14-119-21.1	Dabolava	1041	49	1028	19	0.0020344	0.0000004	7.89	0.19	0.39
DA14-119-22.1	Dabolava	1030	40	1028	19	0.0020333	0.0000004	7.38	0.19	0.39
DA14-119-25.1	Dabolava	1035	42	1028	19	0.0020341	0.0000004	7.77	0.19	0.39
DA14-119-26.1	Dabolava	1034	52	1028	19	0.0020338	0.0000004	7.60	0.22	0.40
DA14-127-01.1	Dabolava	1029	25	1023	19	0.0020329	0.0000004	7.19	0.22	0.40
DA14-127-04.1	Dabolava	1032	30	1023	19	0.0020318	0.0000005	6.61	0.22	0.41
DA14-127-17.1	Dabolava	1032	29	1023	19	0.0020323	0.0000004	6.89	0.19	0.39
DA14-127-26.1	Dabolava	1038	30	1023	19	0.0020322	0.0000004	6.80	0.20	0.39
DA14-127-27.1	Dabolava	1032	34	1023	19	0.0020311	0.0000004	6.25	0.20	0.40
DA14-127-33.1	Dabolava	1009	40	1023	19	0.0020320	0.0000004	6.72	0.19	0.39
DA14-127-37.1	Dabolava	1033	25	1023	19	0.0020303	0.0000004	5.87	0.22	0.40
DA14-127-42.1	Dabolava	1010	31	1023	19	0.0020312	0.0000004	6.33	0.20	0.39
DA14-130-05.1	Dabolava	1069	29	1078	15	0.0020295	0.0000004	5.49	0.18	0.39
DA14-130-08.1	Dabolava	1079	33	1078	15	0.0020274	0.0000004	4.45	0.20	0.39
DA14-130-09.1	Dabolava	1079	30	1078	15	0.0020270	0.0000004	4.26	0.21	0.40
DA14-130-11.1	Dabolava	1075	35	1078	15	0.0020288	0.0000005	5.13	0.25	0.42
DA14-130-12.1	Dabolava	1080	36	1078	15	0.0020269	0.0000004	4.20	0.21	0.40
DA14-130-13.1	Dabolava	1083	31	1078	15	0.0020273	0.0000004	4.39	0.19	0.39
DA14-130-14.1	Dabolava	1070	39	1078	15	0.0020266	0.0000004	4.06	0.19	0.39
DA14-130-15.1	Dabolava	1052	29	1078	15	0.0020285	0.0000004	4.99	0.18	0.38

Table 6.4 MC-LA-ICP-MS hafnium isotope results from zircon

Age Information					Hf Isotopic Data							
Analysis	Zircon Age (Ma)	1σ	Sample Age (Ma)	2σ	$^{176}Hf/^{177}Hf$	2 S.E.	$^{176}Lu/^{177}Hf$	$^{176}Yb/^{177}Hf$	Hf (i)	$\varepsilon_{Hf}(t)$	2σ	$T_{DM}c$
DA14-110-01.1	985	71	1002	17	0.282418	0.000023	0.001710	0.056853	0.282387	7.95	1.58	1.32
DA14-110-04.1	969	38	1002	17	0.282430	0.000027	0.002210	0.069994	0.282389	7.68	1.90	1.33
DA14-110-05.1	996	44	1002	17	0.282435	0.000027	0.002157	0.067419	0.282395	8.49	1.91	1.30
DA14-110-08.1	1003	42	1002	17	0.282407	0.000025	0.001052	0.031653	0.282387	8.38	1.77	1.31
DA14-110-10.1	1007	35	1002	17	0.282410	0.000021	0.001275	0.040703	0.282386	8.42	1.46	1.31
DA14-110-15.2	1003	62	1002	17	0.282442	0.000024	0.001322	0.040438	0.282417	9.44	1.67	1.24
DA14-110-20.1	1032	57	1002	17	0.282412	0.000021	0.001185	0.035751	0.282389	9.12	1.48	1.29
DA14-110-24.1	842	12	842	12	0.282463	0.000029	0.002430	0.074373	0.282425	6.07	2.04	1.33
DA14-110-28.1	1007	52	1002	17	0.282451	0.000027	0.001415	0.044609	0.282424	9.77	1.92	1.23
DA14-110-29.1	833	10	833	10	0.282451	0.000028	0.002138	0.068562	0.282417	5.61	1.99	1.35
DA14-110-33.1	991	34	1002	17	0.282432	0.000021	0.001391	0.044548	0.282406	8.78	1.47	1.28
DA14-110-35.1	1007	30	1002	17	0.282505	0.000027	0.001448	0.040262	0.282478	11.68	1.90	1.11
DA14-110-39.1	1024	39	1002	17	0.282422	0.000021	0.000853	0.027455	0.282406	9.51	1.47	1.26
DA14-110-41.1	1003	37	1002	17	0.282411	0.000023	0.000971	0.030007	0.282393	8.60	1.61	1.30
DA14-118-02.1	1043	41	1035	20	0.282484	0.000022	0.001432	0.044920	0.282456	11.74	1.55	1.13
DA14-118-13.1	1038	37	1035	20	0.282489	0.000018	0.001223	0.038125	0.282465	11.92	1.27	1.12
DA14-118-14.1	1047	48	1035	20	0.282473	0.000022	0.001069	0.032993	0.282452	11.67	1.55	1.14
DA14-118-18.1	1043	49	1035	20	0.282455	0.000021	0.001076	0.032836	0.282434	10.95	1.49	1.18
DA14-118-20.1	1040	31	1035	20	0.282481	0.000024	0.001317	0.039389	0.282455	11.64	1.70	1.14
DA14-118-28.1	1015	65	1035	20	0.282469	0.000018	0.000908	0.028211	0.282452	10.95	1.26	1.16
DA14-118-29.1	1035	59	1035	20	0.282484	0.000017	0.001078	0.034333	0.282463	11.80	1.22	1.12
DA14-119-01.1	1022	38	1028	19	0.282452	0.000028	0.001511	0.040433	0.282423	10.10	1.96	1.22
DA14-119-04.1	1067	44	1028	19	0.282482	0.000021	0.001312	0.040465	0.282455	12.24	1.50	1.12
DA14-119-09.1	1026	43	1028	19	0.282483	0.000021	0.000774	0.023727	0.282468	11.77	1.47	1.12
DA14-119-12.1	1011	45	1028	19	0.282468	0.000020	0.000680	0.020819	0.282455	10.98	1.38	1.16
DA14-119-13.1	1035	38	1028	19	0.282464	0.000015	0.000602	0.017074	0.282453	11.43	1.02	1.15
DA14-119-18.1	1000	38	1028	19	0.282495	0.000023	0.001195	0.035446	0.282473	11.35	1.64	1.12
DA14-119-21.1	1041	49	1028	19	0.282482	0.000022	0.001089	0.034013	0.282460	11.84	1.56	1.13
DA14-119-22.1	1030	40	1028	19	0.282483	0.000018	0.001238	0.039101	0.282459	11.52	1.29	1.14
DA14-119-25.1	1035	42	1028	19	0.282463	0.000025	0.001293	0.041104	0.282438	10.93	1.75	1.18
DA14-119-26.1	1034	52	1028	19	0.282467	0.000019	0.000867	0.027215	0.282450	11.32	1.30	1.15
DA14-127-01.1	1029	25	1023	19	0.282377	0.000020	0.001561	0.045362	0.282347	7.55	1.39	1.38
DA14-127-04.1	1032	30	1023	19	0.282392	0.000022	0.001236	0.035168	0.282368	8.37	1.53	1.33
DA14-127-17.1	1032	29	1023	19	0.282377	0.000044	0.001317	0.034587	0.282351	7.78	3.06	1.37
DA14-127-26.1	1038	30	1023	19	0.282407	0.000025	0.001136	0.030753	0.282385	9.08	1.78	1.29
DA14-127-27.1	1032	34	1023	19	0.282401	0.000019	0.001075	0.030052	0.282380	8.78	1.34	1.31
DA14-127-33.1	1009	40	1023	19	0.282384	0.000025	0.001417	0.042980	0.282357	7.45	1.78	1.37
DA14-127-37.1	1033	25	1023	19	0.282398	0.000031	0.001274	0.039539	0.282373	8.57	2.15	1.32
DA14-127-42.1	1010	31	1023	19	0.282394	0.000022	0.001500	0.041839	0.282365	7.77	1.54	1.35
DA14-130-05.1	1069	29	1078	15	0.282432	0.000030	0.001653	0.048583	0.282398	10.27	2.07	1.25
DA14-130-08.1	1079	33	1078	15	0.282449	0.000023	0.001563	0.044852	0.282417	11.17	1.62	1.20
DA14-130-09.1	1079	30	1078	15	0.282593	0.000028	0.001805	0.050958	0.282556	16.12	1.93	0.89
DA14-130-11.1	1075	35	1078	15	0.282386	0.000022	0.001385	0.039476	0.282358	8.99	1.52	1.33
DA14-130-12.1	1080	36	1078	15	0.282388	0.000024	0.001633	0.046840	0.282355	9.00	1.66	1.33
DA14-130-13.1	1083	31	1078	15	0.282421	0.000025	0.001715	0.050286	0.282386	10.16	1.74	1.26
DA14-130-14.1	1070	39	1078	15	0.282420	0.000026	0.001798	0.056316	0.282384	9.79	1.80	1.28
DA14-130-15.1	1052	29	1078	15	0.282397	0.000024	0.002025	0.061013	0.282357	8.43	1.68	1.35

Table 6.5 Major and trace element geochemical data collected in this study from the Dabolava Suite. Eu/Eu* (Eu_N/ [Sm_N +Gd_N]), La/Sm_N and Tb/Yb_N ratios were calculated using chondrite normalising values from Sun and McDonough (1989). Abbreviations: A = Ambatomiefy-type; V = Vongoa-type.

Sample	DA14-110	DA14-111	DA14-113	DA14-114	DA14-118	DA14-119	DA14-121	DA14-127	DA14-129	DA14-130	DA14-144
Subsuite	A	V	V	A	A	A	A	A	A	A	A
Lithology	Grano-diorite	Gabbro	Gabbro	Granite	Granite	Grano-diorite	Granite	Grano-diorite	Granite	Granite	Grano-diorite
SiO_2 (%)	74.83	49.21	48.87	74.39	69.77	64.24	74.36	71.38	70.13	77.17	69.26
Al_2O_3	12.17	14.76	16.40	15.44	14.30	15.30	13.76	14.68	15.03	12.49	16.06
Fe_2O_3	3.09	8.03	11.15	0.22	4.37	6.69	1.38	2.40	2.83	1.00	1.19
MgO	0.04	9.72	6.63	<0.01	0.72	1.25	0.22	0.74	1.02	0.15	0.52
CaO	1.00	13.79	10.29	0.73	2.21	3.91	1.03	2.76	2.66	0.67	1.12
Na_2O	4.10	1.72	3.25	7.08	4.48	4.69	3.27	3.89	3.83	3.44	4.39
K_2O	3.53	0.18	0.27	1.67	2.60	1.65	4.99	2.76	2.82	4.63	5.62
TiO_2	0.21	0.68	1.64	<0.01	0.49	0.79	0.12	0.26	0.29	0.11	0.30
P_2O_5	<0.01	<0.01	0.21	0.02	0.11	0.19	0.06	0.09	0.10	0.02	0.11
MnO	0.06	0.14	0.17	0.11	0.08	0.11	0.04	0.05	0.04	<0.01	<0.01
Cr_2O_3	<0.002	0.195	0.029	<0.002	<0.002	<0.002	<0.002	<0.002	<0.002	<0.002	<0.002
LOI	0.7	1.3	0.8	0.3	0.7	1.0	0.6	0.8	0.8	0.1	0.7
Total	99.74	99.72	99.75	99.95	99.81	99.78	99.82	99.79	99.58	99.80	99.31
Ba (ppm)	1201	163	85	11	537	441	968	784	2177	1020	3410
Co	14.0	46.4	48.6	32.6	29.0	26.7	27.3	29.8	38.0	45.8	34.0
Cs	2.0	0.3	0.8	6.5	3.2	1.2	6.2	1.7	0.7	1.9	0.9
Ga	16.5	12.9	17.4	30.7	17.6	21.3	15.5	14.5	15.4	10.7	17.9
Hf	11.3	0.7	2.8	1.6	8.9	12.2	3.2	3.8	4.4	3.1	5.3
Nb	15.8	<0.1	4.6	43.6	9.5	10.5	7.4	9.7	8.7	6.4	12.8
Rb	84.5	2.6	4.4	237.0	70.2	35.0	158.5	83.9	55.8	129.7	111.5
Sr	111.3	388.4	315.3	6.9	136.1	218.4	124.3	427.8	591.3	113.2	1805.7
Ta	1.1	<0.1	0.4	15.3	0.7	0.6	0.6	0.9	0.4	0.3	1.0
Th	15.2	<0.2	0.9	3.8	7.1	4.4	10.1	11.4	20.9	5.6	11.6
U	2.9	<0.1	0.3	3.4	1.8	1.3	2.6	2.1	2.1	2.2	2.1
V	<8	193	264	<8	21	40	<8	30	31	<8	26
Zr	438.3	18.4	118.0	14.7	341.0	536.9	93.2	136.3	187.0	88.3	212.2
Y	81.7	12.0	29.7	27.5	56.7	55.4	16.2	8.6	6.4	28.0	15.5
La	51.7	1.8	9.1	8.7	26.6	25.1	22.3	30.9	72.2	25.2	59.2
Ce	85.8	4.1	23.4	18.0	63.3	60.5	46.4	53.6	124.0	48.1	101.7
Pr	13.28	0.77	3.38	2.20	7.81	7.64	5.27	5.55	11.54	5.44	10.60
Nd	54.1	4.3	16.1	7.9	32.9	34.2	19.8	19.2	34.1	20.5	37.4
Sm	12.11	1.52	4.41	2.84	8.34	9.07	4.48	2.99	4.46	3.80	6.06
Eu	2.41	0.86	1.59	0.04	1.71	2.41	0.57	0.73	1.02	0.60	1.41
Gd	13.65	2.24	5.56	2.76	8.92	9.98	4.03	2.13	2.59	3.71	4.48
Tb	2.28	0.37	0.91	0.56	1.58	1.73	0.62	0.30	0.31	0.65	0.60
Dy	13.61	2.17	5.45	3.63	9.53	9.78	3.14	1.42	1.21	4.08	3.13
Ho	2.86	0.44	1.11	0.71	2.02	2.12	0.54	0.28	0.20	0.96	0.52
Er	8.59	1.33	3.07	2.43	5.99	5.87	1.33	0.81	0.47	2.90	1.51
Tm	1.27	0.18	0.44	0.54	0.87	0.92	0.19	0.11	0.08	0.48	0.21
Yb	7.94	1.11	2.84	5.01	5.77	6.03	1.21	0.73	0.46	3.12	1.49
Lu	1.27	0.17	0.42	0.87	0.91	0.90	0.17	0.12	0.09	0.49	0.21
Cu	5.4	83.3	87.8	0.6	5.8	3.6	5.0	3.6	5.8	8.4	24.2
Pb	3.6	0.3	0.3	6.1	3.2	1.0	2.0	2.3	5.9	0.9	6.7
Zn	71	3	10	<1	67	86	45	46	50	11	17
Ni	0.3	36.2	7.6	0.3	5.2	7.0	1.2	3.3	4.4	0.4	4.1
Au	<0.5	<0.5	6.9	1.2	2.6	2.2	<0.5	<0.5	<0.5	1.4	1.3
Sc	6	50	35	4	8	14	3	4	4	3	<1
Eu/Eu*	0.57	1.42	0.98	0.04	0.60	0.77	0.40	0.84	0.84	0.48	0.79
La/Sm_N	2.76	0.76	1.33	1.98	2.06	1.79	3.21	6.67	10.45	4.28	6.31
Tb/Yb_N	0.20	0.23	0.22	0.08	0.19	0.19	0.35	0.28	0.46	0.14	0.27

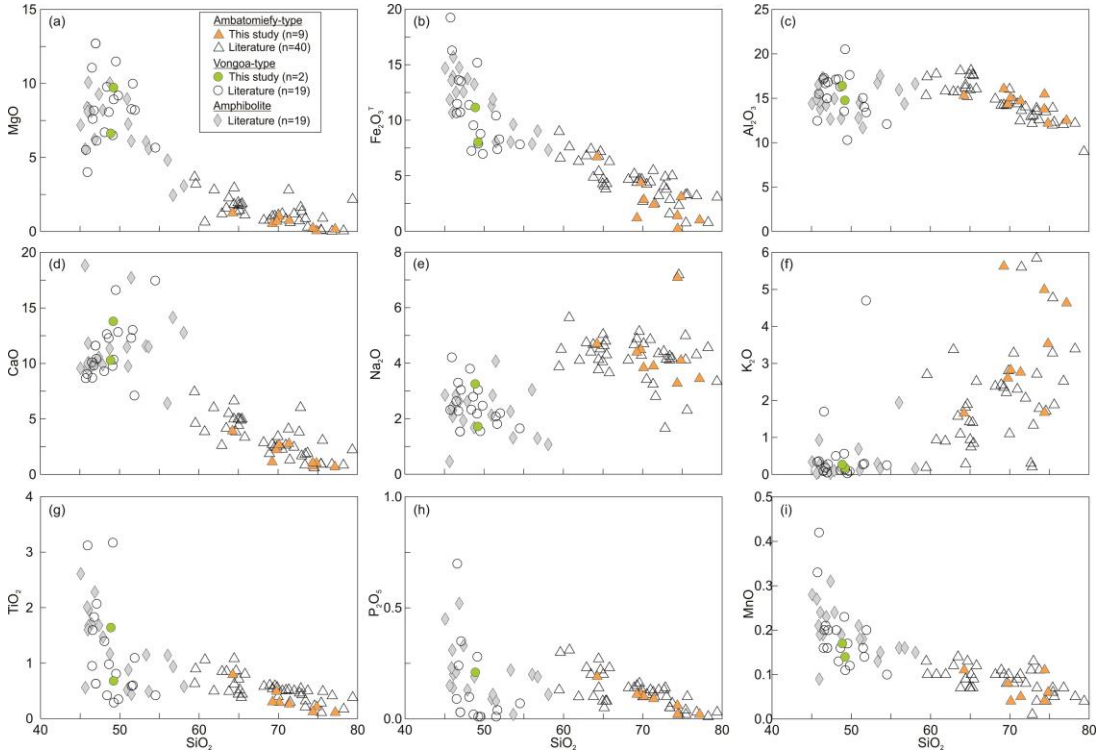

Fig. 6.7 Harker major element variation diagrams for various major element oxides, showing the extent to which Dabolava Suite samples are fractionated and the degree of compositional overlap between the Dabolava Suite and the Ikalamavony Group amphibolite. Data are from this study, Rakotoarimanana (2001), CGS (2009a), and GAF-BGR (2008e).

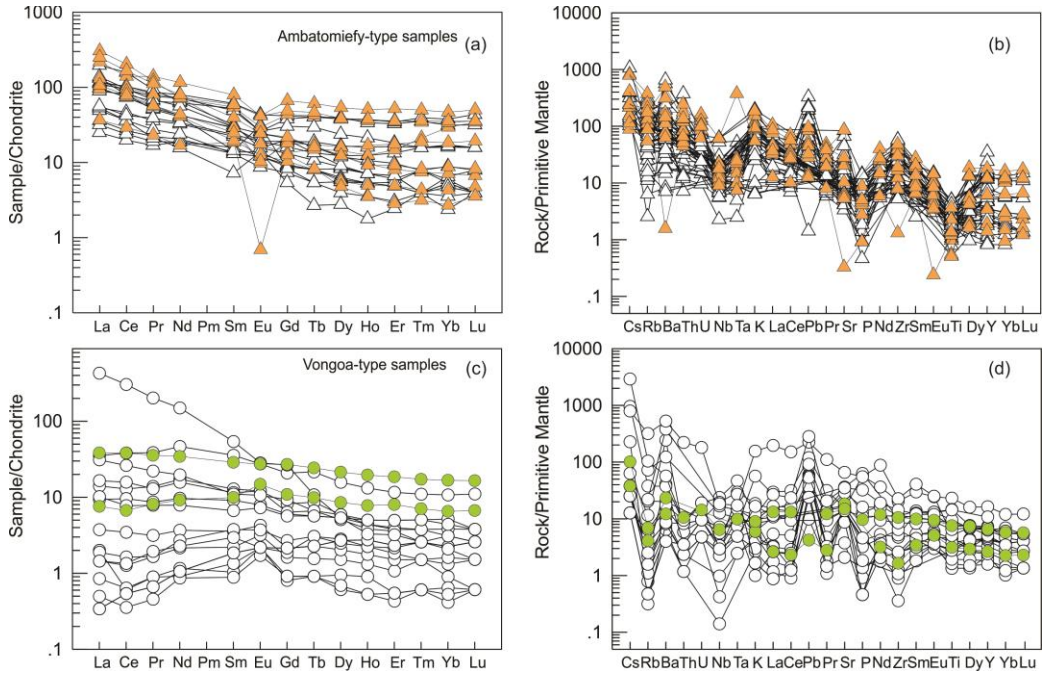

Fig. 6.8 (a) Chondrite-normalized REE diagram and (b) primitive mantle normalised multi-element variation diagram for Ambatomiefy-type intrusions. (c) Chondrite-normalized REE diagram and (d) primitive mantle normalised multi-element variation diagram for Vongoa-type intrusions. White triangles and circles show concentrations for previously collected data from the references listed in Fig. 6.7. Data from this study are listed in Table 6.5. Chondrite and primitive mantle normalizing values are from Sun and McDonough (1989). Symbols are the same as Fig 6.7.

Table 6.6 Summary of zircon U-Pb, oxygen and hafnium results for the Dabolava Suite.

Sample	Sample Age (Ma)	2σ	$^{18}O/^{16}O$ (‰)	2σ	$\varepsilon_{Hf}(t)$	2σ
DA14-110	1002	17	6.79	0.56	9.0	2.0
DA14-118	1035	20	7.85	0.90	11.5	0.7
DA14-119	1028	19	7.69	0.55	11.3	1.1
DA14-127	1023	19	6.58	0.78	8.2	1.1
DA14-130	1078	15	4.62	0.96	9.7	1.7

Zircon isotopic data for Dabolava Suite intrusions also show no evidence of Archaean or Palaeoproterozoic crust. This is noteworthy since many Imorona-Itsindro Suite samples intruding into the Itremo and Antananarivo Domains to the east indicate incorporation of older material (Tucker et al., 1999b; Kröner et al., 2000; Archibald et al., 2016). This implies that the Ikalamavony Domain originated as a juvenile terrane outboard of the older cratonic basement to the east.

Mantle-derived magmas and those sourced by partial melting of crustal rocks are differentiated by O isotopes (Taylor Jr, 1980; Valley et al., 1994). Zircon in equilibrium with mantle-derived melts have a restricted range of $\delta^{18}O$ values (5.3 ± 0.6 ‰; Valley et al., 1998) that is insensitive to magmatic differentiation (Valley et al., 2005). The younger Dabolava Suite samples (DA14-110, DA14-118, DA14-119 and DA14-127) have $\delta^{18}O$ zircon values that plot above the range expected for zircon derived from mantle melting (Table 6.6; Figs. 6.6a, b). The oldest sample has $\delta^{18}O$ values that plot within or slightly below the mantle range (Figs. 6.6a, b). This trend may reflect the evolution of the arc beginning with primitive, mantle-derived magmas progressing to more evolved, crustal assimilating/melting processes within the arc. Stenian-Tonian $\delta^{18}O$ values are broadly similar to those obtained from the Imorona-Itsindro Suite (Fig. 6.6a, b; Archibald et al., in review) and the Ediacaran Ambalavao Suite (Archibald et al., submitted-b). $\delta^{18}O$ values for middle Tonian-aged rocks are highly variable between 5.16 ± 0.55 ‰ to a maximum value of 10.24 ± 0.55 ‰ (Archibald et al., 2016). These values were inferred to indicate partial melting of sedimentary material or crustal assimilation in an extensive ~850-750 Ma subduction zone. Ediacaran zircon from rocks in the Ikalamavony Domain have $\delta^{18}O$ values between 4.87 ± 0.52 ‰ and 6.11 ± 0.52 ‰ (Archibald et al., submitted-b). These $\delta^{18}O$ values plot within the mantle range and were inferred to show zircon crystallised from a mantle melt or via melting of a more depleted source than contemporaneous rocks east in the Antananarivo Domain (Archibald et al., submitted-b).

Hf isotope systematics applied to igneous rocks is an additional tool for determining magmas source components (Belousova et al., 2006; Kemp et al., 2007; Belousova et al., 2010). Dabolava Suite samples have positive $\varepsilon_{Hf}(t)$values that plot below the depleted-mantle line (Figs. 6.6c, d) indicating negligible involvement of ancient (Palaeoproterozoic/Archaean) pre-existing crust. This agrees with the O isotope data discussed above. These $\varepsilon_{Hf}(t)$ data are less evolved than the $\varepsilon_{Hf}(t)$values obtained for the Imorona-Itsindro Suite (Figs. 6.6c, d; Archibald et al., in review) and the Ediacaran Ambalavao Suite (Archibald et al., submitted-b). Mid-Tonian rocks in the Ikalamavony Domain yielded zircon $\varepsilon_{Hf}(t)$values between -4.2 ± 4.2 and +14.0 ± 3.6 while Ediacaran zircon have $\varepsilon_{Hf}(t)$values of -3.6 ± 6.8 and +2.4 ± 6.1. This range of $\varepsilon_{Hf}(t)$values contrasts with $\varepsilon_{Hf}(t)$values obtained for coeval rocks emplaced in the Itremo, Antananarivo and Masora Domains (Archibald et al., 2016). The Imorona-Itsindro Suite magmatic rocks were interpreted to have been derived by crustal melting or assimilation of the less evolved Ikalamavony Group/Dabolava Suite material in an active continental arc (Archibald et al., 2016; Archibald et al., submitted-b).

6.6.2 Petrogenesis of the Dabolava Suite

Negative Nb-Ta-Ti anomalies and moderate LILE enrichment point to a supra-subduction zone origin for the Dabolava Suite (Fig. 6.8). The Nb and Ta depletion recorded in Ambatomiefy-type samples suggest minor crustal contamination, although this can also be explained, along with the negative Ti anomaly, by Fe-Ti oxide fractionation. Modest depletion in P indicates apatite crystallization. Lower Sr may reflect plagioclase fractionation or residual plagioclase in the source region. With the exception of the mobile elements Rb and Ba, gabbroic samples show small variations in trace-element compositions, and display consistent patterns relative to primitive mantle values (Fig. 6.8). Major and trace-element discrimination diagrams are useful tools for classifying plutonic rocks. Samples of Vongoa-type intrusions are mostly tholeiitic while Ambatomiefy-type samples are calc-alkaline (Fig. 6.9a). Felsic rocks are metaluminous to peraluminous and plot predominantly in the I- and S-type field on a granitoid classification diagram (Whalen et al., 1987). Several samples plot in the A-type field but these samples are the most evolved samples with the highest SiO_2 (Table 6.5). Samples are predominantly volcanic-arc and syn-collisional granite (Fig. 6.9b). One anomalous sample (DA14-114) has low Zr and high Ga (Fig. 6.9c) as well as elevated Nb causing it to plot in the within-plate granite field (Fig. 6.9d). This is the same atypical sample with Au mineralisation that was collected near Dabolava village (Fig. 6.2).

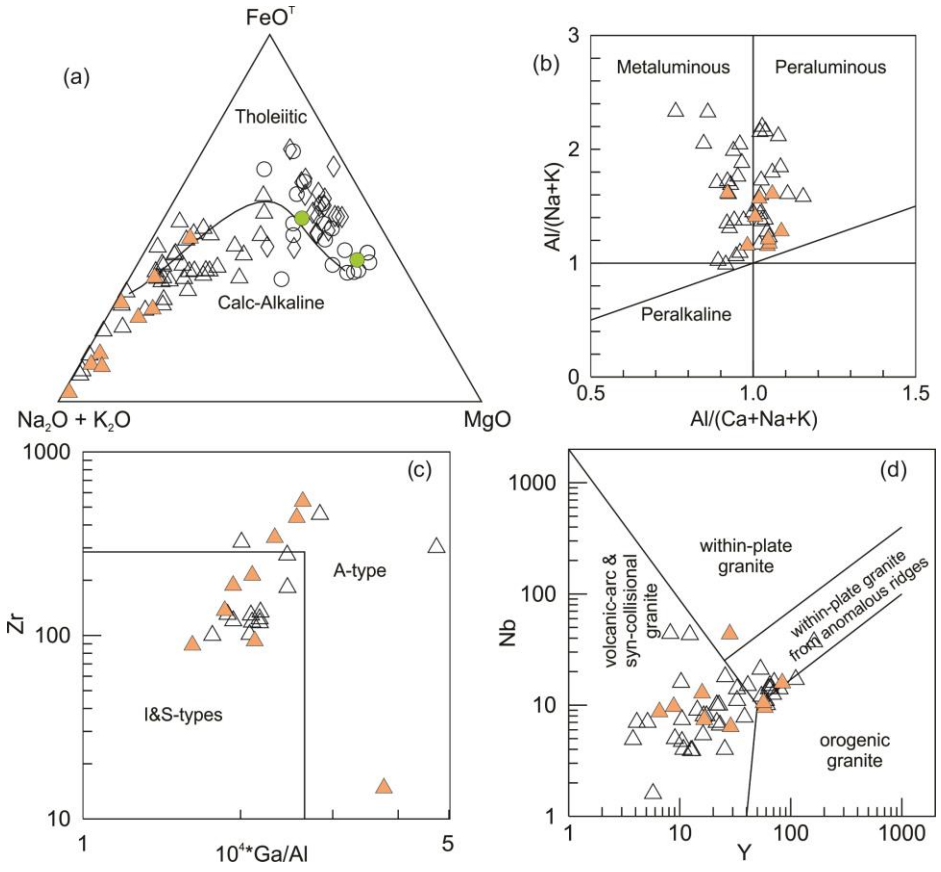

Fig. 6.9 (a) Chondrite-normalized REE diagram and (b) primitive mantle normalised multi-element variation diagram for Ambatomiefy-type intrusions. (c) Chondrite-normalized REE diagram and (d) primitive mantle normalised multi-element variation diagram for Vongoa-type intrusions. White triangles and circles show concentrations for previously collected data from the references listed in Fig. 6.7. Data from list study are listed in Table 6.5. Chondrite and primitive mantle normalizing values are from Sun and McDonough (1989). Symbols are the same as Fig 6.7.

Selected incompatible trace-element ratios for Dabolava Suite samples are plotted against data from the GEOROC database for known tectonic settings, in this case, the Andes and the Aleutian Arc (Fig. 6.10). The Andes are an example of modern subduction of oceanic crust (the Pacific Plate) beneath western South America (Ramos, 1999). The Aleutian Arc is an oceanic island-arc in the North Pacific (Yogodzinski et al., 2010; Cai et al., 2015). Though both tectonic settings involve subduction of oceanic crust, in the Andes, subduction is beneath continental crust and in the Aleutian arc, subduction is beneath oceanic crust (Yogodzinski et al., 2010). The thickness of arc crust and mantle lithosphere contribute significantly to the geochemical features that distinguish island arc lavas from those in Andean-style, continental arcs (Hildreth and Moorbath; Plank and Langmuir, 1988). This difference results in variations in trace element geochemistry in the resulting magmas. There is significant overlap on these diagrams and Dabolava Suite samples possess trace-element characteristics analogous to both arc environments but focusing on the more primitive rocks (Vongoa-type), mafic samples plot mostly within the Aleutian Arc field, especially on the Nb/Y versus La/Yb diagram (Fig. 6.10c). The oceanic arc tectonic environment demonstrated here agrees with the proposals by Rakotoarimanana (2001) and Tucker et al. (2014) for a similar tectonic setting. Based on the trace element geochemistry of the amphibolite lithologies in the Ikalamavony Group, Rakotoarimanana (2001) suggested that the Dabolava Suite intrusions evolved in an active continental margin tectonic setting. Amphibolite interlayered with minor quartzofeldspathic gneiss was suggested to represent coeval extrusive rocks followed shortly after by intrusion of the Dabolava Suite (Rakotoarimanana, 2001). Metamorphosed carbonate and minor quartzite that are interlayered with the lower Ikalamavony Group amphibolite have been suggested as a possible western correlative to the Itremo Group (Roig et al., 2012; Tucker et al., 2012). If these Ikalamavony Group rocks do embody contemporaneous rocks from the Itremo Group, this could constrain the minimum depositional age of both metasedimentary packages to >1080 Ma. However, there is little evidence supporting this correlation and samples so far analysed for detrital zircons in the Ikalamavony Domain do not support this correlation (Cox et al., 2004; GAF-BGR, 2008e; CGS, 2009a).

6.6.3 Implications for Neoproterozoic tectonics in Madagascar

The Dabolava Suite, magmatism in the Vohibory Domain and the Imorona-Itsindro Suite together extend the period of arc magmatism in Madagascar to ~1078–750 Ma or to ~700 Ma if the arc rocks in the Bemarivo Domain (far north of Madagascar) are also included (Boger et al., 2014) although magmatism was not continuous over the entire period. The Ankiliabo Suite (~930-910 Ma) from the Androyen Domain partially bridges the time gap between Dabolava and Imorona-Itsindro magmatism (Rakotoarimanana, 2001; GAF-BGR, 2008e, a; CGS, 2009a, b; Tucker et al., 2011b). The Ankiliabo Suite is a bimodal suite of intrusions consisting of anorthosite-leuconorite, felsic alkali-granite and minor olivine gabbro/peridotite (GAF-BGR, 2008a). These rocks were suggested to have formed via the ponding of a gabbroic magma at the base of the crust related to either a mantle plume or the late stage lithospheric mantle delamination following continental collision (GAF-BGR, 2008a). Unfortunately, the limited spatial extent of the Androyen Domain did not allow the authors to determine in which of these environments was more appropriate for the Ankiliabo Suite but early Neoproterozoic-aged late orogenic or plume magmatism is not recognised elsewhere in Madagascar (GAF-BGR, 2008a). GAF-BGR (2008a) concluded that the Androyen Domain represents a fragment of continental crust that is unrelated to the adjacent Vohibory and Anosyen Domains. Tucker et al. (2014) suggested rifting of the combined Androyen/Anosyen Domain in the Proterozoic and that the Ankiliabo Suite is likely related to this event. Late Mesoproterozoic to early Neoproterozoic subduction polarity in Madagascar must have been westward or southward directed beneath oceanic crust or primitive continental crust

(Ikalamavony Domain). Moreover, the Ikalamavony Domain must have amalgamated to the Antananarivo Domain prior to ~850 Ma when subduction of Mozambique Ocean crust beneath central Madagascar resulted in emplacement of the Imorona-Itsindro Suite across all lithotectonic units except the Antongil Domain.

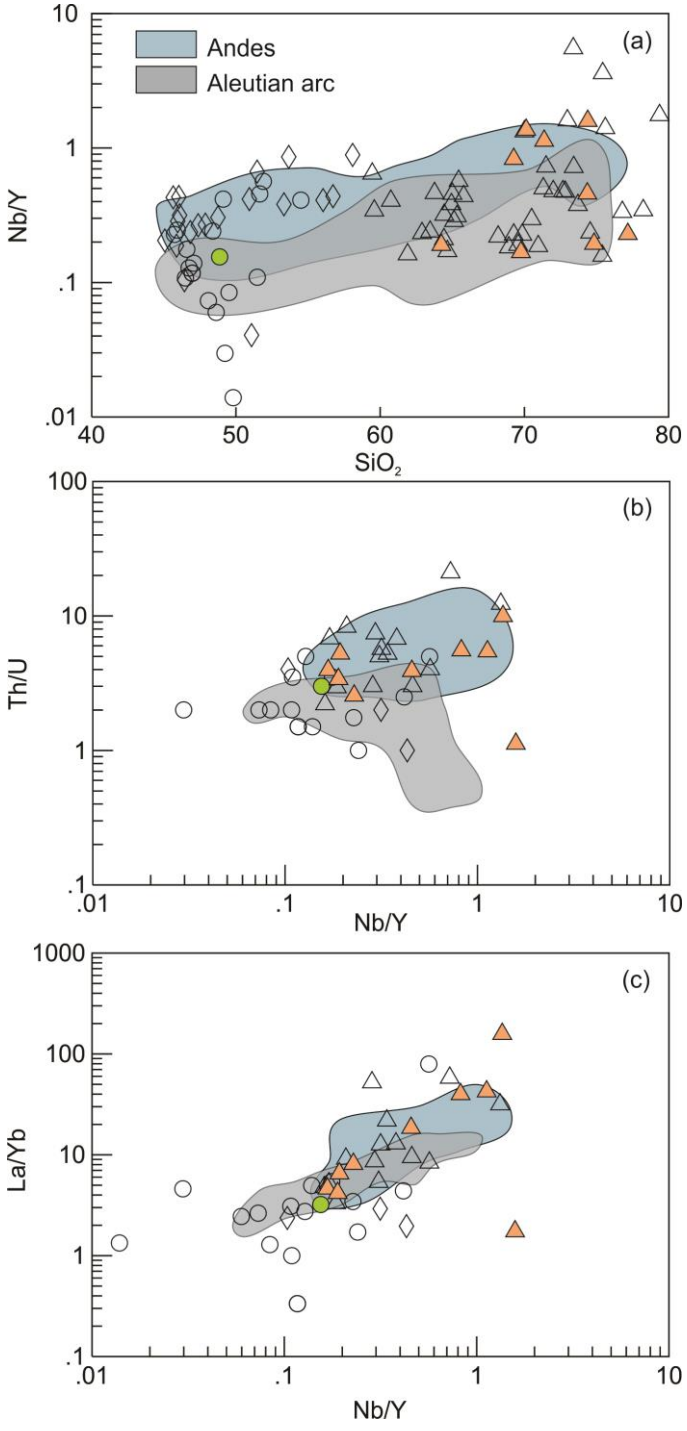

Fig. 6.10 Major and trace-element data for the Dabolava Suite and Ikalamavony Group amphibolite plotted against reference datasets from the GEOROC Database for the Andes continental arc and the Aleutian arc. (a) SiO2 versus Nb/Y; (b) Nb/Y versus Th/U; and (c) Nb/Y versus La/Yb. Reference datasets were initially filtered to include only plutonic rock samples with between 40 and 80 wt. % SiO2. Fields for the Andes (n=168) and Aleutian Arc (n=189) reflect inclusion of > 90% of filtered data. Symbols for Dabolava Suite and Ikalamavony Group samples are the same as in Fig. 6.7.

Given the restricted age range of detrital zircon (GAF-BGR, 2008e; CGS, 2009a) observed in the Ikalamavony Group, the Dabolava arc developed outboard to the western margin of the Antananarivo Domain far enough away to escape sediment input from Madagascar or elsewhere containing Archaean to Palaeoproterozoic rocks (GAF-BGR, 2008e). Most detrital material in the Ikalamavony Group was inferred to be recycled within the arc, thus, replicating the igneous crystallisation ages in the sediments (GAF-BGR, 2008e; CGS, 2009a). During this same time period, the Itremo Group, which does have significant Archaean to Palaeoproterozoic detritus (e.g. Cox et al., 1998; De Waele et al., 2011), was interpreted to be deposited on the western passive margin of the Antananarivo Domain.

Two alternative propositions exist for the Proterozoic tectonic development of central Madagascar. The "Out of Africa" hypothesis suggests that the basement of central Madagascar was originally part of the Congo-Tanzania-Bangweulu Block of East Africa (Fitzsimons and Hulscher, 2005). This idea was largely based on the similarities in detrital zircon age spectra from the Muva Supergroup in Zambia and the Itremo Group (Cox et al., 1998; Collins et al., 2003c; Cox et al., 2004; Fitzsimons and Hulscher, 2005). It was argued that central Madagascar rifted from the Congo-Tanzania-Bangweulu Block in the Palaeoproterozoic to form a microcontinent named Azania (Collins and Windley, 2002) that was later wedged between the African and Indian plates in the Neoproterozoic (Collins and Pisarevsky, 2005). They suggested present-day westward directed subduction of the Mozambique Ocean along the Betsimisaraka Suture resulted in Andean-type arc magmatism across Azania to the west of the Masora and Antongil Domains (Kröner et al., 2000; Collins, 2006). The Neoproterozoic suture between Azania and India (Betsimisaraka Suture) was correlated with the Palghat-Cauvery Shear Zone in southern India (Collins et al., 2007; Plavsa et al., 2014; Plavsa et al., 2015). Key et al. (2011) agreed that central Madagascar was likely an isolated microcontinent during the Neoproterozoic but noted that the Betsimisaraka suture zone as defined by Collins (2006) could not exist given the similar early Neoproterozoic histories of the Antananarivo and Masora Domains on either side of the of the structure. They renamed the Betsimisaraka suture zone as the Anaboriana-Manampotsy Belt (Fig. 6.1) and suggested the Manampotsy Belt (southern Betsimisaraka Domain; Collins, 2006) developed as a pre-terminal Pan-African, pre-Kiangara Suite (>630 Ma) collisional/suture zone between the Antananarivo and Masora Domains (Key et al., 2011). Metamorphic fabrics in the Imorona-Itsindro Suite rocks and metasedimentary rocks are strongly overprinted by terminal Gondwana-amalgamation events in both domains (Key et al., 2011). Near the end of the East African Orogen, the amalgamated Antananarivo-Masora Craton collided with the Antongil Domain (Key et al., 2011) prior to later thrusting of the Bemarivo Belt southwards over the older terranes (Thomas et al., 2009). The Anaboriana Belt (northern Betsimisaraka Domain ; Collins, 2006) represents the suture between the Bemarivo Belt and the Antongil-Antananarivo Craton (Key et al., 2011).

The South Madagascar-India-Wanni-Highland Province (SMIWH) presented an alternative model based on apparent inconsistencies in the "Out of Africa" hypothesis (Tucker et al., 2011b). These discrepancies included the same issues highlighted by Key et al. (2011): (1) the presence of Neoarchaean rocks on both sides of the Betsimisaraka Suture in the Antananarivo, Masora, and Antongil Domains in Madagascar and in the northern Madurai Block and Dharwar craton in India (Schofield et al., 2010; Tucker et al., 2011a), (2) the presence of Tonian plutonic rocks and similar-aged metamorphism on both sides of the suture (Schofield et al., 2010; Tucker et al., 2011a), and (3) similar aged detrital zircon arrays exposed on both sides of the suture (De Waele et al., 2011). Tucker et al. (2011b) proposed that western India and north-central Madagascar were part of a contiguous Proterozoic craton named the Greater Dharwar Craton and that the Androyen-Anosyen Domain together with the Trivandrum Block and the Wanni and Highland Complexes in Sri Lanka represented a

continuous Palaeoproterozoic terrane. This led Tucker et al. (2011a) to propose deep crustal anatexis via crustal dilation and pressure-reduced melting compatible with plume generation or lithospheric mantle delamination during Rodinia break-up as the generator for Tonian-aged Imorona-Itsindro Suite magmatism. However, they were circumspect in acknowledging the ambiguity of geochemical data and proposed that if the Imorona-Itsindro Suite were derived from continental-arc magmatism (Handke et al., 1999; Bybee et al., 2010), the active convergent margin must be located to the west of Madagascar (Tucker et al., 2011a). Boger et al. (2014) agreed that the latter proposition complemented the field and geochemical data better than a plume origin for the Imorona-Itsindro Suite. Their tectonic model included the Greater Dharwar Craton hypothesis and proposed eastward directed subduction beneath central Madagascar and India with the Neoproterozoic suture located to the west in the present-day Mozambique Channel (Boger et al., 2014). Previous studies by Handke et al. (1999) and Bybee et al. (2010) also advocated eastward directed subduction of the eastern edge of the Mozambique Ocean beneath Madagascar, India and the Seychelles. Eastward subduction resulted in continental arc-magmatism throughout all of Madagascar between ~850-700 (including the Bemarivo Domain) and within-plate potassic magmatism manifested in the distal back-arc in the Malani Basin (Boger et al., 2014). Both models require the emplacement of subduction related magmas beginning after collision between the Ikalamavony Domain island arc rocks, the Antananarivo basement and the passive margin sequences (e.g. Itremo Group) of Madagascar prior to ~850 Ma.

Archibald et al. (2016) and Archibald et al. (submitted-c) attempted to resolve the controversy surrounding the subduction polarity associated with Tonian-aged magma emplacement. Archibald et al. (2016) demonstrated that Tonian-aged magmas incorporated significant amounts of continental crust and the corresponding isotopic ratios correlated with the basement rocks but was unable to resolve the issue of Tonian subduction polarity. Archibald et al. (submitted-c) studied the whole-rock geochemistry of the Imorona-Itsindro Suite and showed that rocks have geochemical signatures akin to an Andean-like continental-arc rather than intraplate magmatism as suggested by other studies (e.g. Zhou et al., 2015). They also attempted to resolve the Tonian subduction polarity conundrum and found that spatial geochemical spatial variations favour eastward directed subduction during between ~850-750 Ma. These interpretations support the model of Boger et al. (2014), Bybee et al. (2010) and Handke et al. (1999) in which subduction of the Mozambique Ocean was eastward beneath central Madagascar and the mid-Tonian suture zone is to the west of the Ikalamavony Domain.

Subsequent orogenesis during the Ediacaran to Early Cambrian deformed and metamorphosed all pre-Ediacaran lithological units during the amalgamation of Gondwana (Key et al., 2011; Tucker et al., 2014). Deformation was accompanied by emplacement of the ~630 Ma Kiangara Suite A-type granitoids (Nédélec et al., 1994), the post-tectonic granitoids of the ~575-540 Ma Ambalavao Suite (Meert et al., 2001a; BGS-USGS-GLW, 2008; Archibald et al., submitted-b) and the post-collisional granitoids of the ~537-522 Ma Maevarano Suite (Goodenough et al., 2010; Zhou et al., 2015a; Archibald et al., submitted-b). Magma emplacement accompanied peak high-grade metamorphism across Madagascar. In southern-central Madagascar, peak high-temperature low-pressure metamorphism between ~550-520 Ma was under temperatures of 880 ± 60°C and pressures of 8 ± 1 kbar (Markl et al., 2000). In northern Madagascar, P-T estimates are 6.5-8.5 kbar and 800 - 900 °C (Buchwaldt et al., 2003) and in the Ikalamavony Domain between ~560 – 520 Ma, maximum P-T conditions were ~8.3 kbar and ~875°C (CGS, 2009a). By ~500 Ma, Madagascar was sandwiched between the Congo-Tanzania-Bangweulu Block and India along the East African Orogen in Gondwana (Collins and Pisarevsky, 2005).

6.6.4 Implications for the amalgamation of Rodinia

Stenian to Tonian-aged continental and oceanic arc magmatic rocks are present in the northern Irumide Belt in Tanzania (De Waele et al., 2006a; De Waele et al., 2006b), Kenya (Hauzenberger et al., 2007; Hauzenberger et al., 2014), the Nampula, Unango, and Marrupa Blocks in Mozambique (Bingen et al., 2009; Macey et al., 2010), Sri Lanka (Kröner et al., 1987; Kröner et al., 2003; He et al., 2016), Dronning Maud Land (Jacobs et al., 2015), and in the Sør Rondane Mountains (Elburg et al., 2015). The palaeogeographic positions (Fig. 6.11a) of many of these intrusions are similar to the Dabolava Suite in Rodinia reconstructions (Torsvik, 2003; Li et al., 2008; Li et al., 2013). Many of these magmatic suites have similar emplacement ages, geochemical signatures and the magmatic suites were interpreted to be emplaced in continental or oceanic-arc environments. Kröner et al. (2003) suggested ~1100-880 Ma calc-alkaline granitoid rocks in Sri Lanka originated as magmatic arcs in an active margin setting. In the Antarctic Sør Rondane Mountains, meta-igneous rocks were suggested to represent a juvenile oceanic arc terrane, with subduction-related magmatic activity beginning around 995–975 Ma followed by a period of magmatism from 960–925 Ma that was interpreted to represent the cessation of subduction (Elburg et al., 2015). In Dronning Maud Land, this event was manifest by a major Tonian oceanic arc terrane (Tonian Oceanic Arc Super Terrane, TOAST) that formed from ~1000–900 Ma (Jacobs et al., 2015). In the Zambian Irumide Belt, voluminous syn- to post-kinematic granitoids were emplaced between 1050 and 950 Ma (De Waele et al., 2006a), broadly coeval with continental-arc plutons of the southern Irumide Belt (Johnson et al., 2005) and the Unango and Marrupa Belts of Mozambique (Bingen et al., 2009). Rocks in the Nampula Belt of Mozambique are slightly older (~1130-1075 Ma), but the geochemistry of these rocks suggests that they were generated in a juvenile, island-arc setting (Macey et al., 2010). These examples represent only a few of the Stenian-Tonian magmatic arc systems (Fig. 6.11a). However, as they are configured in this model (Li et al., 2008), all of the active margin suites discussed above are located well within Rodinia, refuting this reconstruction.

These magmatic arc systems are suggested to be related to a long-lived active margin that culminated in the assembly of many continental blocks on the western edge of Rodinia. The Dabolava Arc began to form at ~1080 Ma with oceanic crust-oceanic crust convergence in the Mozambique Ocean outboard of Azania (Fig. 6.11b). This arc developed away from Azania because Archaean and Palaeoproterozoic detritus are absent from the Ikalamavony Group (GAF-BGR, 2008e). Contemporaneous oceanic and continental arc systems developed near the margin of the Congo-Tanzania-Bangweulu (CTB) Block, but the relative position of these arc systems to the Dabolava Arc is uncertain, and the systems are likely to be far separated at this time. From ~1000-950 Ma, these arc systems advanced toward Azania and the CTB Block respectively (Fig. 6.11c). By ~950 Ma, the Southern Irumide Belt and the Nampula, Unango and Marrupa Belts accreted to the CTB Block (De Waele et al., 2006a; Bingen et al., 2009). The timing of accretion of the Dabolava Arc to the Antananarivo Domain is poorly constrained but it must have occurred prior to ~850 Ma when intrusion of the Imorona-Itsindro Suite began, and may be represented by the pre-850 Ma (D1) recumbent folds and nappes that deform the Itremo Group (Collins et al., 2000; Tucker et al., 2007). A rifting event occurred in southern Madagascar between ~930 and 900 Ma coinciding with the emplacement of Ankiliabo Suite. The magmatic suite has geochemical characteristics compatible with a within-plate origin (GAF-BGR, 2008a). Tucker et al. (2014) interpreted the Ikalamavony/Dabolava Arc as volcano-sedimentary and intrusive igneous rocks that originated in a magmatic arc built (mostly) on oceanic crust during a pre-1000 Ma rifting event (Tucker et al., 2014). However, we suggest that this rifting event occurred later in the Tonian, given the presence of the Ankiliabo within-plate suite. Rifting occurred following accretion of the Dabolava Arc to Azania. The Androyen was part of the Antananarivo Domain or at least peripheral to it, possibly part of a Palaeoproterozoic terrane (SMIWH; Tucker et al.,

2011b). A narrow rift developed between the Androyen and the Antananarivo Domain in which the upper Ikalamavony Group may have been deposited. Also at ~900 Ma, the Vohibory Arc originated outboard of Azania (Fig. 6.11d; Jöns and Schenk, 2008). The age of the arc is constrained by a near unimodal U-Pb (zircon) age population in the Vohibory Series dated at ~900 Ma (Collins et al., 2012). The Vohibory Arc may correlate with similar rocks in the Eastern Granulite Terrane (Tenczer et al., 2006) and the Galana Arc (Hauzenberger et al., 2007; Fritz et al., 2013), and possibly south with rocks of the Cabo Delgado Nappe (Mozambique; Bingen et al., 2009) and eastern Dronning Maud Land (the "TOAST" arc; Jacobs et al., 2015) The Vohibory Arc then accreted to the Androyen Domain by ~630 Ma (GAF-BGR, 2008c).

Due to the ambiguity associated with palaeomagnetic data for this time period, the relative positions of the continental blocks discussed above could be reconfigured to form an expansive oceanic/continental arc comparable to the modern Aleutian Arc in the North Pacific. The Aleutian Arc is >3500 km in length (Yogodzinski et al., 2010) and a comparable long-lived magmatic arc system (including the Imorona-Itsindro continental arc) on the Rodinia periphery likely existed from the Stenian to mid-Tonian. This active margin lasted until the Mozambique Ocean closed and Gondwana began to amalgamate.

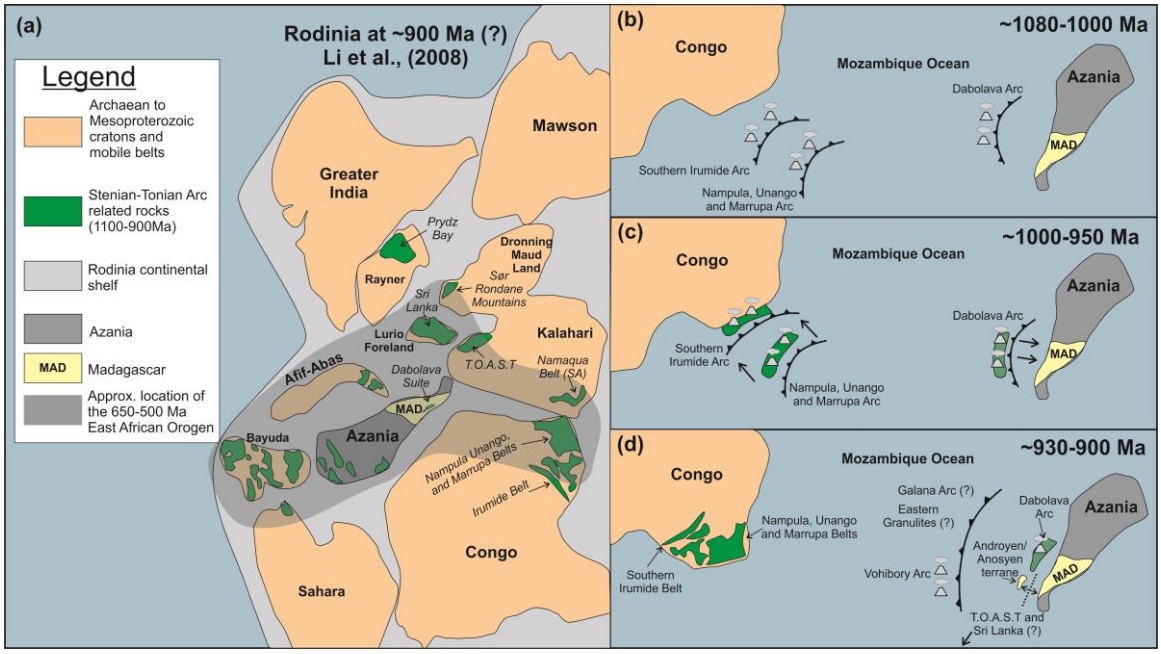

Fig. 6.11 (a) Palaeogeographic reconstruction of the Rodinia Supercontinent at ~900 Ma simplified after Li et al. (2008). The locations of several of the late-Mesoproterozoic to early Neoproterozoic magmatic arc suites discussed in the text are indicated. Also shown is the inferred extent of rocks involved in the ~650-500 Ma East African Orogen. (b-d) Tectonic cartoon illustrating the development of magmatic arcs in the Mozambique Ocean with emphasis on those also involved in the East African Orogen near Madagascar (Azania).

6.7. Summary and conclusions

The Stenian-Tonian Dabolava Suite is a recently recognised suite of magmatic rocks emplaced in west central Madagascar. Prior to identification of the suite, magmatism of this age was not recognised in Madagascar and these intrusions are only found in the Ikalamavony Domain. The Dabolava Suite is divided into two sub-suites consisting of intermediate to felsic lithologies (Ambatomiefy-type) and mafic lithologies (Vongoa-type). New U-Pb (zircon) data extends the period of Dabolava Suite magmatism by ~40 Myr to ~1080-980 Ma. O and Hf

isotopic data indicate that the magmatic arc developed from an arc with initial depleted mantle-like sources to an arc with more evolved signatures, probably due to increased crustal assimilation by ~1000 Ma. The petrography and geochemistry of granodiorite to granite plutons are consistent with calc-alkaline, I-type intrusions. Negative Nb-Ta-Ti anomalies and moderate LILE and LREE enrichment point to a supra-subduction zone origin for the Dabolava Suite. Trace-element ratios show the genesis of the Dabolava Suite is more compatible with an oceanic arc environment rather than a continental arc. In addition, the association of the Dabolava Suite with paragneiss, calc-silicates, marbles and probable ocean floor basalt of a similar age (Ikalamavony Group), suggest that the Ikalamavony Domain collectively may characterise island arc relics that are intercalated with the associated sediments. Contemporaneous Stenian-Tonian magmatic arc rocks elsewhere in similar palaeogeographic positions could indicate the presence of an extensive oceanic/continental-arc system that persisted on the periphery of Rodinia until the Mozambique Ocean closed to form Gondwana.

6.8 Acknowledgements

The Razafinjoelina family, in particular Auguste and Berthieu are thanked for providing transportation, assistance in the field, and hospitality during fieldwork in Madagascar. Ms. Aoife McFadden and Dr. Benjamin Wade (Adelaide Microscopy) are acknowledged for assistance obtaining CL images and LA-ICP-MS zircon U-Pb data. This paper forms TRaX Record ### and is an output of ARC Future Fellowship grant FT120100340. This paper is a contribution to IGCP projects #628 (Gondwana Map) and #648 (Supercontinent Cycles and Global Geodynamics).

Chapter 7

Summary and Conclusions

7.1 The Neoproterozoic tectonic evolution of central Madagascar

This PhD research project of Proterozoic rocks in central Madagascar using zircon isotopic systematics and whole-rock geochemical data leads to the following hypothesis for the tectonic development of the island. The main objective of this project was to collect all of the available isotopic and geochemical data available for Stenian to Cambrian rock units. New isotopic and geochemical data were added and all data were used to test the published hypotheses for the Proterozoic tectonic development of central Madagascar. As new data was collected, the tectonic model evolved to the final model presented below.

Beginning in the Mesoproterozoic, Madagascar was likely an isolated microcontinent in the Mozambique Ocean (Collins, 2006; Key et al., 2011). Central Madagascar contains a number of spatially distinct sedimentary successions that were deposited on the cratonic basement and on the passive margins including the Ambatolampy Group. The youngest concordant detrital zircon age of 1836 ± 25 Ma is interpreted to represent the maximum depositional age for the Ambatolampy Group. This age is considerably older than data previously reported ($^{207}Pb/^{206}Pb$ age of 1001 ± 44 Ma; De Waele et al., 2008) and the distribution of detrital zircon ages is comparable to the Paleoproterozoic Itremo Group. The minimum age of deposition for the Ambatolampy Group is constrained by the timing of high-grade metamorphism obtained from metamorphic overgrowths at 541.0 ± 4.4 Ma and the intrusive age of the Ambalavao Suite (~545 Ma). Many of the metasedimentary units in central Madagascar display remarkably similar detrital zircon arrays (Chapter 2). In particular, the Ambatolampy, the Itremo, the Iakora, the Sambirano-Sahantaha, and the Maha groups are all dominated by Palaeoproterozoic detritus and have late Palaeoproterozoic to Mesoproterozoic maximum depositional ages. Taken together, these units appear to represent an originally contiguous Mesoproterozoic sedimentary basin across central Madagascar. The Ikalamavony Group is dominated by Meso- Neoproterozoic detritus and lacks contributions from older sedimentary sources (CGS, 2009a). The Ikalamavony Group also contains inferred metavolcanic rocks (CGS, 2009a), an important difference compared to the other metasedimentary units. This implies that the Ikalamavony Group was deposited away from Archaean to Palaeoproterozoic cratons, probably outboard of Azania in the Mozambique Ocean.

At ~1080 Ma, the Dabolava Arc began to form in the Mozambique Ocean coeval with the deposition of the volcano-sedimentary rocks of the lower Ikalamavony Group (Chapter 6). The Dabolava Suite is divided into two sub-suites consisting primarily of intermediate to felsic lithologies and mafic lithologies. New U-Pb (zircon) data presented in this thesis extends the period of Dabolava Suite magmatism by ~40 Myr to ~1080-980 Ma (from ~1035-980 Ma; Tucker et al., 2007). Oxygen and hafnium isotopic data indicate that the magmatic arc developed from an arc with initial depleted mantle-like sources to an arc with more evolved isotopic signatures, probably due to increased crustal assimilation by ~1000 Ma. The petrography and geochemistry of granodiorite to granite plutons are consistent with calc-alkaline, I-type intrusions. Negative Nb-Ta-Ti anomalies and moderate LILE and LREE enrichment point to a supra-subduction zone origin for the Dabolava Suite. Trace-element ratios show the genesis of the Dabolava Suite is more compatible with an oceanic arc environment rather than a continental arc. The association of the Dabolava Suite with the Ikalamavony Group suggests that the Ikalamavony Domain collectively may characterise island arc relics that are now intercalated with the associated sediments. The timing of accretion of the Dabolava Arc to the Antananarivo Domain is poorly constrained but it must have occurred prior to ~850 Ma when intrusion of the Imorona-Itsindro Suite began, and may be represented by the pre-850 Ma (D1) recumbent folds and nappes that deformed the Itremo Group (Collins et al., 2000; Tucker et al., 2007). A rifting event occurred in southern Madagascar between ~930 and 900 Ma coinciding with the emplacement of Ankiliabo Suite.

The Ankiliabo Suite has geochemical characteristics compatible with a within-plate origin (GAF-BGR, 2008a). Tucker et al. (2014) interpreted the Ikalamavony Group/Dabolava Arc as volcano-sedimentary and intrusive igneous rocks that originated in a magmatic arc built on oceanic crust during a pre-1000 Ma rifting event (Tucker et al., 2014). This rifting event likely occurred later in the Tonian, given the presence of the Ankiliabo within-plate suite. Rifting occurred after accretion of the Dabolava Arc to Azania. The Androyen Domain was part of the Antananarivo Domain or at least peripheral to it, possibly part of a Palaeoproterozoic terrane (SMIWH; Tucker et al., 2011b). A narrow rift developed between the Androyen and the Antananarivo Domain in which the upper Ikalamavony Group may have been deposited. Also at ~900 Ma, the Vohibory Arc originated outboard of Azania (Fig. 11d; Jöns and Schenk, 2008) and was later accreted to the Androyen Domain by ~630 Ma (GAF-BGR, 2008c).

Voluminous calc-alkaline magmatic rocks intruded into all lithotectonic domains in central Madagascar except the Antongil Domain during the mid-Tonian. Prior to this project, the genesis of this enigmatic magmatic suite focused on two controversies. (1) Were Tonian-aged magmas emplaced in a supra-subduction zone (Handke et al., 1999; Kröner et al., 2000; Key et al., 2011; Boger et al., 2015) or above a mantle plume (Tucker et al., 2011b; Yang et al., 2014; Zhou, 2015; Zhou et al., 2015b), and (2) if these rocks are subduction related, was the subduction polarity eastward (Handke et al., 1999; Bybee et al., 2010; Boger et al., 2014, 2015) or westward directed (Kröner et al., 2000; Collins and Windley, 2002; Collins, 2006)? New U-Pb (zircon) data combined with previously published geochronological data from the Imorona-Itsindro Suite, indicates essentially continuous magmatism over the entire age range (850-750 Ma) with pulses of magmatic activity at ~800 Ma, ~791 Ma, and ~784 Ma (Chapter 3). Isotopic data for Tonian-aged zircon vary in their $\delta^{18}O$ and $\varepsilon_{Hf}(t)$ signatures across all lithotectonic domains. Oxygen and hafnium isotope data have a broad inverse relationship with apparent magmatic cycles occurring on the scale of ~15-40 Ma. These cycles emphasize periods of significant supracrustal assimilation evolving to "mantle-like" (or below) signatures. The spatial distribution of data indicates that the isotopic character of Tonian-aged zircon replicates the basement domain into which the magmas intruded. $\delta^{18}O$ spatial patterns are more apparent than $\varepsilon_{Hf}(t)$ values but both isotope systems display a broadly inverse pattern moving from east to west. To the far west, samples intruding the Ikalamavony Domain exhibit a less evolved $\varepsilon_{Hf}(t)$ signature than any rocks intruding the other tectonic domains, implying melting of a different source material. Spatial plots also highlight a prominent geological feature suggestive of significant mantle input and/or hydrothermal alternation by meteoric fluids at 48° 25' E in the Antananarivo Domain where sub-mantle $\delta^{18}O$ values and the least evolved $\varepsilon_{Hf}(t)$ signatures are recorded. This region was the suggested location of the Betsimisaraka Suture or the intracontinental rift, in which deposition of the Manampotsy Group occurred, but these data alone cannot distinguish between the two models. Altogether, this large zircon isotopic dataset emphasises the large age range and compositional variability of the Tonian lithosphere present in the Ikalamavony, Itremo, Antananarivo, and Masora Domains.

Petrography and whole-rock geochemical data favour Tonian-aged magma generation in an active subduction margin (Chapter 4). Petrological analysis demonstrates a variety of lithologies from ultramafic rocks to granitoid and syenite. Mineralogical data indicates a hydrous mineral assemblage including calcium amphiboles and biotite. Geochemically, Imorona-Itsindro Suite rocks are predominantly calc-alkaline with trace element characteristics consistent with emplacement in a volcanic or continental arc. Radiogenic isotope data show evolved Sr and Nd signatures and indicate crustal assimilation during magma genesis, comparable to the signatures recorded in zircon hafnium isotopic data. Changes in subduction zone dynamics, crustal anatexis and crustal assimilation of the diverse

basement domains contributed to geochemical discrepancies contrasting a continental-arc origin. Prolonged subduction (>100 Myr) provided sufficient time for the arc to mature and a shallow (<100km), metasomatised spinel lherzolite mantle source is preferred. Although some Imorona-Itsindro Suite samples demonstrate within-plate characteristics such as slightly higher Nb/Y ratios and lower Ba/Y ratios, the vast majority of samples exhibit geochemical similarities analogous with Andean –like rocks. Overall, the geochemical characteristics of the diverse suite of lithologies argue for their collective genesis in a supra-subduction zone tectonic setting with the Neoproterozoic suture located to the west of the Ikalamavony Domain. Boger et al. (2014) suggested this subduction system continued until ~700 Ma in northern Madagascar with the emplacement of the Antsirabe Nord and Manambato Suites (Thomas et al., 2009) and contemporaneous rocks in Rajasthan (Malani Suite) represents extension in the back-arc. However, geochemical data for these suites contrasts with the Imorona-Itsindro Suite in that the Antsirabe and Manambato Suites are juvenile Tonian-Cryogenian calc-alkaline metaigneous suites (Thomas et al., 2009). Based on the isotopic character of these rocks (Tucker et al., 1999b), Archaean and Palaeoproterozoic rocks are thought to be absent in this domain. Thomas et al. (2009) proposed that the northern and southern sub-domains formed as coalesced juvenile magmatic arcs, predominantly at ~760 Ma in the south and ~720 Ma in the north.

The Ambalavao and Maevarano Suites represent significant, mainly granitoid magmatism emplaced in Madagascar during the Ediacaran and into the early Cambrian. Magmatism was essentially continuous from the Late Cryogenian to the Cambrian with the successive emplacement of the Kiangara (~ 650 – 575 Ma), Ambalavao (~575 – 540 Ma) and Maevarano (~537 – 522 Ma) Suites. These suites represent the final magmatic manifestations associated with the closure of the Mozambique Ocean and amalgamation of Gondwana in the Malagasy Mozambique Belt. These magmatic suites also correspond spatially with major late-Neoproterozoic transpressive and transcurrent shear zones and temporally with periods of intense regional deformation. Movement along these shear zones has been correlated with collisions of continental blocks during Gondwana assembly (Key et al., 2011). Magmatic zircon oxygen and hafnium isotopic data suggest a significant crustal component during magma genesis, contrasting with previous work which suggested negligible crustal contamination (Goodenough et al., 2010). Oxygen and hafnium isotopic data indicate both suites were derived locally from the crust and some samples show evidence for mixing of crustal and more depleted components. In addition, isotopic data highlight the different basement components present in central Madagascar, in particular, the juvenile nature of the Mesoproterozoic Ikalamavony Domain. Whole-rock geochemical data for the Ambalavao and Maevarano Suites are indistinguishable. Samples are characterised by enrichment of HFSEs, LILES, and REEs (especially the LREEs). Samples of both suites follow similar trends on variation and discrimination diagrams suggesting they had a similar genesis. These geochemical features are consistent with melting in a post-collisional setting. Melting occurred during lithospheric underplating and lithospheric delamination associated with the continent-continent collision and the extensional collapse of the EAO.

The major advances in our understanding of the Proterozoic geology of Madagascar are: (1) the recognition of several contemporaneous, spatially distinct metasedimentary successions across Madagascar, (2) the Imorona-Itsindro Suite represents voluminous continental-arc magmatism, (3) magmatism was essentially continuous between (850-750 Ma) but there were pulses and isotopic data highlights different source components, (4) geochemical data are equivocal but demonstrate subduction polarity was eastward beneath central Madagascar with the suture located west of the Ikalamavony Domain, (5) the Ambalavao and Maevarano Suites correlate spatially with major shear zones and temporally with major deformational events during the final stages of Gondwana assembly and (6) while these Ediacaran-Cambrian deformation events could occur on a continental interior, a more

likely scenario is the polyphase collision of multiple blocks, thus, challenging the Greater Dharwar Craton model (Tucker et al., 2011a). These magmatic systems are suggested to be related to a long-lived active margin on the western edge of the microcontinent Azania that culminated in the collision of many continental blocks along the EAO to form Gondwana by ~500 Ma.

Chapter 8

References

Amarasinghe, U., Chaudhuri, A., Collins, A.S., Deb, G., Patranabis-Deb, S., 2015. Evolving provenance in the Proterozoic Pranhita-Godavari Basin, India. Geoscience Frontiers 6, 453-463.

André-Mayer, A.S., Ramiandrisoa, N., Vanderhaeghe, O., Reisberg, L., Rabeandrasana, S., Zimmermann, C., 2014. Re–Os geochronological constraints on the Dabolava mesothermal gold occurence, Madagascar: Implications for the Ikalamavony sub-domain deposition age. Journal of African Earth Sciences 94, 119-127.

Archibald, D.B., Collins, A.S., Foden, J.D., Payne, J.L., Holden, P., Razakamanana, T., De Waele, B., Thomas, R.J., Pitfield, P.E.J., 2016. Genesis of the Tonian Imorona-Itsindro Magmatic Suite in central Madagascar: Insights from U-Pb, oxygen and hafnium isotopes in zircon. Precambrian Research 281, 312-337.

Archibald, D.B., Collins, A.S., Foden, J.D., Payne, J.L., Macey, P., Holden, P., Razakamanana, T., submitted-a. Genesis of the Stenian-Tonian Dabolava Suite of west central Madagascar: Implications for the formation of Rodinia. Journal of the Geological Society.

Archibald, D.B., Collins, A.S., Foden, J.D., Payne, J.L., Razakamanana, T., Holden, P., submitted-b. Tectonics and chemistry of late to post-tectonic magmatism in the Malagasy Mozambique Belt. Lithos.

Archibald, D.B., Collins, A.S., Foden, J.D., Payne, J.L., Taylor, R., Holden, P., Razakamanana, T., Clark, C., 2015. Towards unravelling the Mozambique Ocean conundrum using a triumvirate of zircon isotopic proxies on the Ambatolampy Group, central Madagascar. Tectonophysics 662, 167-182.

Archibald, D.B., Collins, A.S., Foden, J.D., Razakamanana, T., submitted-c. Petrogenesis of the Tonian Imorona-Itsindro Suite. Journal of Geology.

Be'eri-Shlevin, Y., Katzir, Y., Whitehouse, M., 2009. Post-collisional tectonomagmatic evolution in the northern Arabian–Nubian Shield: time constraints from ion-probe U–Pb dating of zircon. Journal of the Geological Society 166, 71-85.

Belousova, E.A., Griffin, W.L., O'Reilly, S.Y., 2006. Zircon Crystal Morphology, Trace Element Signatures and Hf Isotope Composition as a Tool for Petrogenetic Modelling: Examples From Eastern Australian Granitoids. Journal of Petrology 47, 329-353.

Belousova, E.A., Kostitsyn, Y.A., Griffin, W.L., Begg, G.C., O'Reilly, S.Y., Pearson, N.J., 2010. The growth of the continental crust: Constraints from zircon Hf-isotope data. Lithos 119, 457-466.

Besairie, H., 1964. Madagascar Carte geologique. Service Geographique a Madagascar, Tananarive, pp. Geological map. 1:1,000,000.

Besairie, H., 1968-1971. Description géologique du massif ancien de Madagascar. Document Bureau Géologique Madagascar. no. 177. no. 177a: centre nord et centre nord-est; 177b: région côtière orientale; 177c: région centrale- système de graphite; 177d: région centrale - système du Vohibory; 177e: le sud; 177f: le nord. Bureau Géologique Madagascar, Antananarivo.

Besairie, H., 1969-1971. Carte géologique à 1/500000, de Madagascar, in 8 sheets: 1: Diego Suarez; 2: Antalaha; 3: Majunga; 4: Tamatave; 5: Tananarive; 6: Morondava; 7: Fianarantsoa; 8: Ampanihy. Bureau Géologique Madagascar, Antananarivo.

BGS-USGS-GLW, 2008. Revision de la cartographie geologique et miniere des zones Nord, Centre, et Centre Est de Madagascar. BGS Report CR/08/078. Keyworth, England.

Bingen, B., Jacobs, J., Viola, G., Henderson, I.H.C., Skår, Ø., Boyd, R., Thomas, R.J., Solli, A., Key, R.M., Daudi, E.X.F., 2009. Geochronology of the Precambrian crust in the Mozambique belt in NE Mozambique, and implications for Gondwana assembly. Precambrian Research 170, 231-255.

Black, L.P., Kamo, S.L., Allen, C.M., Davis, D.W., Aleinikoff, J.N., Valley, J.W., Mundil, R., Campbell, I.H., Korsch, R.J., Williams, I.S., Foudoulis, C., 2004. Improved $^{206}Pb/^{238}U$ microprobe geochronology by the monitoring of a trace-element-related matrix effect; SHRIMP, ID–TIMS, ELA–ICP–MS and oxygen isotope documentation for a series of zircon standards. Chemical Geology 205, 115-140.

Blades, M.L., Collins, A.S., Foden, J., Payne, J.L., Xu, X., Alemu, T., Woldetinsae, G., Clark, C., Taylor, R.J.M., 2015. Age and hafnium isotopic evolution of the Didesa and Kemashi Domains, western Ethiopia. Precambrian Research 270, 267-284.

Boger, S.D., Hirdes, W., Ferreira, C.A.M., Schulte, B., Jenett, T., Fanning, C.M., 2014. From passive margin to volcano–sedimentary forearc: The Tonian to Cryogenian evolution of the Anosyen Domain of southeastern Madagascar. Precambrian Research 247, 159-186.

Boger, S.D., Hirdes, W., Ferreira, C.A.M., Schulte, B., Jenett, T., Fanning, C.M., 2015. Reply to comment by J-L Zhou on "From passive margin to volcano-sedimentary forearc: The Tonian to Cryogenian evolution of the Anosyen Domain of southeastern Madagascar" by Boger et al. Precambrian Research, Volume 247, July 2014, Pages 159–186. Precambrian Research 262, 127-130.

Brick, R.A., 2011. Palaeoproterozoic Eclogite Formation in Tanzania: A Structural, Geochronological, Thermochronological, and Metamorphic Study of the Usagaran and Ubende Orogenic Belts. Unpublished PhD Thesis, The University of Adelaide, p. 138.

Buchwaldt, R., Tucker, R.D., Dymek, R.F., 2003. Geothermobarometry and U-Pb Geochronology of metapelitic granulites and pelitic migmatites from the Lokoho region, Northern Madagascar. American Mineralogist 88, 1753-1768.

Bybee, G.M., Ashwal, L.D., Wilson, A.H., 2010. New evidence for a volcanic arc on the western margin of a rifting Rodinia from ultramafic intrusions in the Andriamena region, north-central Madagascar. Earth and Planetary Science Letters 293, 42-53.

Cabanis, B., Lecolle, M., 1989. Le diagramme La/10-Y/15-Nb/8 : unoutil pour la discrimination des series volcaniques et la mise en evidence des processus de melande et/ou de contamination crustale. C. R. Acad. Sci. Ser. II 309, 2023-2029.

Cai, Y., Rioux, M., Kelemen, P.B., Goldstein, S.L., Bolge, L., Kylander-Clark, A.R.C., 2015. Distinctly different parental magmas for calc-alkaline plutons and tholeiitic lavas in the central and eastern Aleutian arc. Earth and Planetary Science Letters 431, 119-126.

CGS, 2009a. Map Explanation of 1:100 000 scale (Zone E) Sheets I46 – Ambararata, J46 – Beopoaka, 47 – Itondy, J47 – Belobaka, K47 – Ambatofotsy, I48 – Miandrivazo, J48 –

Betrondro, K48 – Ambatondradama, I49 – Ankotrofotsy, J49 – Dabolava, K49 – Anjoma-Ramartina, L49 – Vasiana, M49 – Ankazomiriotra, N49 – Antsirabe. . République de Madagascar, Ministère de L'Energie et des Mines – Project de Gouvernance des Ressources Minérales, Antananarivo, Madagascar and Council for Géoscience, Pretoria, South Africa, .

CGS, 2009b. Map Explanation of 1:100 000 scale (Zone F) Sheets G41 – Ambohipaky, H41 – Bevary, G42 – Mangoboky, H42 – Bekodoka, G43 – Andolamasa, H43 – Andrafialava and parts of G40 – Ankasakasa, F40 – Saint-Andre, F41 – Betsalampy, H40 – Maroboaly-Sud, I40 – Soalala-Sud, I41 – Andranomavo, F42 – Marovoay Kely, I42 – Mahabe, F43 – Bebao, F44 – Antranogoaika, G44 – Morafeno, I43 – Ampoza, H44 – Bemolanga and I44 – Makaraingo. Ministère de L'Energie et des Mines – Project de Gouvernance des Ressources Minérales, Antananarivo, Madagascar and Council for Géoscience, Pretoria, South Africa.

Chappell, B.W., Wyborn, D., 2004. Cumulate and Cumulative Granites and Associated Rocks. Resource Geology 54, 227-240.

Cherniak, D.J., Hanchar, J.M., Watson, E.B., 1997. Diffusion of tetravalent cations in zircon. Contributions to Mineralogy and Petrology 127, 383-390.

Cohen, K.M., Finney, S.C., Gibbard, P.L., 2015. The International Chronostratigraphic Chart.

Collins, A.S., 2000. The Tectonic Evolution of Madagascar: Its place in the East African Orogen. Gondwana Research 3, 549-552.

Collins, A.S., 2006. Madagascar and the Amalgamation of Central Gondwana. Gondwana Research (GR Focus) 9, 3-16.

Collins, A.S., Clark, C., Plavsa, D., 2014. Peninsular India in Gondwana: The tectonothermal evolution of the Southern Granulite Terrain and its Gondwanan counterparts. Gondwana Research 25, 190-203.

Collins, A.S., Fitzsimons, I.C.W., Hulscher, B., Razakamanana, T., 2003a. Structure of the eastern margin of the East African Orogen in central Madagascar. Precambrian Research 123, 111-133.

Collins, A.S., Johnson, S., Fitzsimons, I.C.W., Powell, C.M., Hulscher, B., Abello, J., Razakamanana, T., 2003b. Neoproterozoic deformation in central Madagascar: a structural section through part of the East African Orogen, in: Yoshida, M., Windley, B., Dasgupta, S. (Eds.), Proterozoic East Gondwana: Supercontinent Assembly and Breakup. Special Publication of the Geological Society, London, 206, pp. 363-379.

Collins, A.S., Kinny, P.D., Razakamanana, T., 2012. Depositional age, provenance and metamorphic age of metasedimentary rocks from southern Madagascar. Gondwana Research 21, 353-361.

Collins, A.S., Kröner, A., Fitzsimons, I.C.W., Razakamanana, T., 2003c. Detrital Footprint of the Mozambique Ocean: U/Pb SHRIMP and Pb Evaporation Zircon Geochronology of Metasedimentary Gneisses in Eastern Madagascar. Tectonophysics 375, 77-99.

Collins, A.S., Kröner, A., Razakamanana, T., Windley, B.F., 2000. The Tectonic Architecture of the East African Orogen in Central Madagascar - a Structural and Geochronological Perspective. Journal of African Earth Sciences 30, 21.

Collins, A.S., Patranabis-Deb, S., Alexander, E., Bertram, C.N., Falster, G.M., Gore, R.J., Mackintosh, J., Dhang, P.C., Saha, D., Payne, J.L., Jourdan, F., Backé, G., Halverson, G.P.,

Wade, B.P., 2015. Detrital Mineral Age, Radiogenic Isotopic Stratigraphy and Tectonic Significance of the Cuddapah Basin, India. Gondwana Research 28, 1294-1309.

Collins, A.S., Pisarevsky, S.A., 2005. Amalgamating eastern Gondwana: The evolution of the Circum-Indian Orogens. Earth Science Reviews 71, 229-270.

Collins, A.S., Santosh, M., Braun, I., Clark, C., 2007. Age and sedimentary provenance of the Southern Granulites, South India: U-Th-Pb SHRIMP secondary ion mass spectrometry. Precambrian Research 155, 125-138.

Collins, A.S., Windley, B.F., 2002. The Tectonic Evolution of central and northern Madagascar and its place in the Final Assembly of Gondwana. Journal of Geology 110, 325-340.

Compston, W., Williams, I.S., Meyer, C., 1984. U-Pb geochronology of zircons from lunar breccia 73217 using a sensitive high mass-resolution ion microprobe. Journal of Geophysical Research: Solid Earth 89, B525-B534.

Cox, G.M., Lewis, C.J., Collins, A.S., Halverson, G.P., Jourdan, F., Foden, J., Nettle, D., Kattan, F., 2012. Ediacaran terrane accretion within the Arabian–Nubian Shield. Gondwana Research 21, 341-352.

Cox, R., Armstrong, R.A., Ashwal, L.D., 1998. Sedimentology, geochronology and provenance of the Proterozoic Itremo Group, central Madagascar, and implications for pre-Gondwana palaeogeography. Journal of the Geological Society, London 155, 1009-1024.

Cox, R., Coleman, D.S., Chokel, C.B., DeOreo, S.B., Collins, A.S., Kröner, A., De Waele, B., 2004. Proterozoic tectonostratigraphy and paleogeography of central Madagascar derived from detrital zircon U-Pb age populations. Journal of Geology 112, 379-400.

Davies, D.R., Davies, J.H., 2009. Thermally-driven mantle plumes reconcile multiple hot-spot observations. Earth and Planetary Science Letters 278, 50-54.

De Waele, B., Kampunzu, A.B., Mapani, B.S.E., Tembo, F., 2006a. The Mesoproterozoic Irumide belt of Zambia. Journal of African Earth Sciences 46, 36-70.

De Waele, B., Liégeois, J.-P., Nemchin, A.A., Tembo, F., 2006b. Isotopic and geochemical evidence of proterozoic episodic crustal reworking within the Irumide Belt of south-central Africa, the southern metacratonic boundary of an Archaean Bangweulu Craton. Precambrian Research 148, 225-256.

De Waele, B., Thomas, R.J., Horstwood, M., Pitfield, P., Tucker, R.D., Potter, C.J., Key, R., Smith, R., Bauer, W., Randriamananjara, T., Ralison, V., Rafahatelo, J.M., Rabarimana, M.H., 2008. U-Pb detrital zircon geochronological provenance patterns of supracrustal successions in central and northern Madagascar. Geological Society of Africa Projet de Gouvernance des Ressources Minerales (Madagascar), 22nd Colloquium of African Geology, 235-238.

De Waele, B., Thomas, R.J., Macey, P.H., Horstwood, M.S.A., Tucker, R.D., Pitfield, P.E.J., Schofield, D.I., Goodenough, K.M., Bauer, W., Key, R.M., Potter, C.J., Armstrong, R.A., Miller, J.A., Randriamananjara, T., Ralison, V., Rafahatelo, J.M., Rabarimanana, M., Bejoma, M., 2011. Provenance and tectonic significance of the Palaeoproterozoic metasedimentary successions of central and northern Madagascar. Precambrian Research 189, 18-42.

de Wit, M., 2003. Madagascar: Heads it's a Continent, tails it's an Island. Annual Reviews of Earth and Planetary Science 31, 213-248.

de Wit, M.J., Bowring, S.A., Ashwal, L.D., Randrianasolo, L.G., Morel, V.P.I., Rambeloson, R.A., 2001. Age and Tectonic Evolution of Neoproterozoic ductile shear zones in southwestern Madagascar, with implications for Gondwana studies. Tectonics 20, 1-45.

Deer, W.A., Howie, R.A., Zussman, J., 2013. An Introduction to the Rock-Forming Minerals. Mineralogical Society of Great Britain and Ireland.

Doebrich, J.L., Al-Jehani, A.M., Siddiqui, A.A., Hayes, T.S., Wooden, J.L., Johnson, P.R., 2007. Geology and metallogeny of the Ar Rayn terrane, eastern Arabian shield: Evolution of a Neoproterozoic continental-margin arc during assembly of Gondwana within the East African orogen. Precambrian Research 158, 17-50.

Eby, G.N., 1990. The A-type granitoids: A review of their occurrence and chemical characteristics and speculations on their petrogenesis. Lithos 26, 115-134.

Eby, G.N., 1992. Chemical subdivision of the A-type granitoids:Petrogenetic and tectonic implications. Geology 20, 641-644.

Eby, G.N., Woolley, A.R., Din, V., Platt, G., 1998. Geochemistry and Petrogenesis of Nepheline Syenites: Kasungu–Chipala, Ilomba, and Ulindi Nepheline Syenite Intrusions, North Nyasa Alkaline Province, Malawi. Journal of Petrology 39, 1405-1424.

Elburg, M., Jacobs, J., Andersen, T., Clark, C., Läufer, A., Ruppel, A., Krohne, N., Damaske, D., 2015. Early Neoproterozoic metagabbro-tonalite-trondhjemite of Sør Rondane (East Antarctica): Implications for supercontinent assembly. Precambrian Research 259, 189-206.

Elburg, M.A., 2010. Sources and processes in arc magmatism: the crucial role of water. Geologica Belgica 13, 121-136.

Emberger, A., 1958. Les granites stratoïdes du Pays betsileo (Madagascar). Bulletin de la Société géologique de France (6) VIII, 537-554.

Fernandez, A., Schreurs, G., Villa, I.M., Huber, S., Rakotondrazafy, M., 2003. Age constraints on the tectonic evolution of the Itremo region in Central Madagascar. Precambrian Research 123, 87-110.

Fitzsimons, I.C.W., 2016. Pan–African granulites of Madagascar and southern India: Gondwana assembly and parallels with modern Tibet. Journal of Mineralogical and Petrological Sciences 111, 73-88.

Fitzsimons, I.C.W., Hulscher, B., 2005. Out of Africa: detrital zircon provenance of central Madagascar and Neoproterozoic terrane transfer across the Mozambique Ocean. Terra Nova 17, 224-235.

Fritz, H., Abdelsalam, M., Ali, K.A., Bingen, B., Collins, A.S., Fowler, A.R., Ghebreab, W., Hauzenberger, C.A., Johnson, P.R., Kusky, T.M., Macey, P., Muhongo, S., Stern, R.J., Viola, G., 2013. Orogen styles in the East African Orogen: A review of the Neoproterozoic to Cambrian tectonic evolution. Journal of African Earth Sciences 86, 65-106.

Frost, B.R., Barnes, C.G., Collins, W.J., Arculus, R.J., Ellis, D.J., Frost, C.D., 2001. A Geochemical Classification for Granitic Rocks. Journal of Petrology 42, 2033-2048.

Frost, C.D., Frost, B.R., 2010. On Ferroan (A-type) Granitoids: their Compositional Variability and Modes of Origin. Journal of Petrology.

GAF-BGR, 2008a. Final Report. Explanatory notes for the Androyan domain southern Madagascar. Réalisation des travaux de cartographie géologique de Madagascar, révision approfondie de la cartographie géologique et minière aux échelles 1/100,000 et 1/500,000 zone Sud. République de Madagascar, Ministère de l'Energie et des Mines (MEM/SG/DG/UCP/PGRM). 81.

GAF-BGR, 2008b. Final Report. Explanatory notes for the Anosyan domain southeast Madagascar. Réalisation des travaux de cartographie géologique de Madagascar, révision approfondie de la cartographie géologique et minière aux échelles 1/100,000 et 1/500,000 zone Sud. République de Madagascar, Ministère de l'Energie et des Mines (MEM/SG/DG/UCP/PGRM), p. 93.

GAF-BGR, 2008c. Final Report. Explanatory notes for the Vohibory domain southwest Madagascar. Réalisation des travaux de cartographie géologique de Madagascar, révision approfondie de la cartographie géologique et minière aux échelles 1/100,000 et 1/500,000 zone Sud. République de Madagascar, Ministère de l'Energie et des Mines (MEM/SG/DG/UCP/PGRM), p. 85.

GAF-BGR, 2008d. Final Report: Explanatory notes for the Antananarivo domain, Central-east Madagascar. Réalisation des travaux de cartographie géologique de Madagascar, révision approfondie de la cartographie géologique et minière aux échelles 1/100 000 et 1/500 000 zone Sud. République de Madagascar, Ministère de l'Energie et des Mines MEM/SG/DG/UCP/PGRM), p. 41.

GAF-BGR, 2008e. Final Report: Explanatory notes for the Ikalamavony domain, central and western Madagascar. Réalisation des travaux de cartographie géologique de Madagascar, révision approfondie de la cartographie géologique et minière aux échelles 1/100 000 et 1/500 000 zone Sud. République de Madagascar, Ministère de l'Energie et des Mines MEM/SG/DG/UCP/PGRM), p. 79.

Giese, J., Berger, A., Schreurs, G., Gnos, E., 2011. The timing of the tectono-metamorphic evolution at the Neoproterozoic–Phanerozoic boundary in central southern Madagascar. Precambrian Research 185, 131-148.

Glorie, S., De Grave, J., Singh, T., Payne, J.L., Collins, A.S., 2014. Crustal root of the Eastern Dharwar Craton: Zircon U–Pb age and Lu–Hf isotopic evolution of the East Salem Block, southeast India. Precambrian Research 249, 229-246.

Goodenough, K.M., Thomas, R.J., De Waele, B., Key, R.M., Schofield, D.I., Bauer, W., Tucker, R.D., Rafahatelo, J.M., Rabarimanana, M., Ralison, A.V., Randriamananjara, T., 2010. Post-collisional magmatism in the central East African Orogen: The Maevarano Suite of north Madagascar. Lithos 116, 18-34.

Grégoire, V., Nédélec, A., Monié, P., Montel, J.-M., Ganne, J., Ralison, B., 2009. Structural reworking and heat transfer related to the late-Panafrican Angavo shear zone of Madagascar. Tectonophysics 477, 197-216.

Griffin, W.L., Belousova, E.A., Shee, S.R., Pearson, N.J., O'Reilly, S.Y., 2004. Archean crustal evolution in the northern Yilgarn Craton: U–Pb and Hf-isotope evidence from detrital zircons. Precambrian Research 131, 231-282.

Griffin, W.L., Wang, X., Jackson, S.E., Pearson, N.J., O'Reilly, S.Y., Xu, X., Zhou, X., 2002. Zircon chemistry and magma mixing, SE China: In-situ analysis of Hf isotopes, Tonglu and Pingtan igneous complexes. Lithos 61, 237-269.

Grove, T.L., Baker, M.B., Price, R.C., Parman, S.W., Elkins-Tanton, L.T., Chatterjee, N., Müntener, O., 2004. Magnesian andesite and dacite lavas from Mt. Shasta, northern California: products of fractional crystallization of H2O-rich mantle melts. Contributions to Mineralogy and Petrology 148, 542-565.

Guerrot, C., Cocherie, A., Ohnenstetter, N., 1991. West Andriamena ultrabasic complexes (Madagascar): geochronological constraints, BRGM principal Scientific and Technical Results, pp. 100-101.

Guyonnaud, G., 1951. Étude géologique de la feuille Maevatanana. . Haut Commissarat de Madagascar et Dépendances.

Handke, M., Tucker, R.D., Ashwal, L.D., 1999. Neoproterozoic continental arc magmatism in west-central Madagascar. Geology 27, 351-354.

Handke, M.J., Tucker, R.D., Hamilton, M.A., 1997. Age, geochemistry, and petrogenesis of the Early Neoproterozoic (800–790 Ma) intrusive igneous rocks of the Itremo region, central Madagascar. Geological Society of America Abstracts with Programs 29, A-468.

Haschke, M., Günther, A., Melnick, D., Echtler, H., Reutter, K.-J., Scheuber, E., Oncken, O., 2006. Central and Southern Andean Tectonic Evolution Inferred from Arc Magmatism, in: Oncken, O., Chong, G., Franz, G., Giese, P., Götze, H.-J., Ramos, V.A., Strecker, M.R., Wigger, P. (Eds.), The Andes: Active Subduction Orogeny. Springer Berlin Heidelberg, Berlin, Heidelberg, pp. 337-353.

Hauzenberger, C.A., Sommer, H., Fritz, H., Bauernhofer, A., Kröner, A., Hoinkes, G., Wallbrecher, E., Thöni, M., 2007. SHRIMP U–Pb zircon and Sm–Nd garnet ages from the granulite-facies basement of SE Kenya: evidence for Neoproterozoic polycyclic assembly of the Mozambique Belt. Journal of the Geological Society 164, 189-201.

Hauzenberger, C.A., Tenczer, V., Bauernhofer, A., Fritz, H., Klötzli, U., Košler, J., Wallbrecher, E., Muhongo, S., 2014. Termination of the Southern Irumide Belt in Tanzania: Zircon U/Pb geochronology. Precambrian Research 255, Part 1, 144-162.

Hawthorne, F.C., Oberti, R., Harlow, G.E., Maresch, W.V., Martin, R.F., Schumacher, J.C., Welch, M.D., 2012. Nomenclature of the amphibole supergroup. American Mineralogist 97, 2031-2048.

He, X.-F., Santosh, M., Tsunogae, T., Malaviarachchi, S.P.K., 2016. Early to late Neoproterozoic magmatism and magma mixing–mingling in Sri Lanka: Implications for convergent margin processes during Gondwana assembly. Gondwana Research 32, 151-180.

Henderson, B., Collins, A.S., Payne, J., Forbes, C., Saha, D., 2014. Geologically constraining India in Columbia: The age, isotopic provenance and geochemistry of the protoliths of the Ongole Domain, Southern Eastern Ghats, India. Gondwana Research 26, 888-906.

Hildreth, W., Moorbath, S., Crustal contributions to arc magmatism in the Andes of Central Chile. Contributions to Mineralogy and Petrology 98, 455-489.

Hinthorne, J.R., Andersen, C.A., Conrad, R.L., Lovering, J.F., 1979. Single-grain 207Pb206Pb and U/Pb age determinations with a 10-μm spatial resolution using the ion microprobe mass analyzer (IMMA). Chemical Geology 25, 271-303.

Hoskin, P.W.O., Black, L.P., 2000. Metamorphic zircon formation by solid-state recrystallisation of protolith igneous grains. Journal of Metamorphic Geology 18, 423-439.

Hottin, G., 1964. Etude géologique et prospection de la feuille au 1/100.000 Ambatolampy (P.48), Rapport Annuel du Service Géologique pour 1964. Service Géologique de Madagascar, Tananarive, pp. 99-106.

Howard, K.E., Hand, M., Barovich, K.M., Belousova, E., 2011. Provenance of late Paleoproterozoic cover sequences in the central Gawler Craton: exploring stratigraphic correlations in eastern Proterozoic Australia using detrital zircon ages, Hf and Nd isotopic data. Australian Journal of Earth Sciences 58, 475-500.

Ickert, R.B., Hiess, J., Williams, I.S., Holden, P., Ireland, T.R., Lanc, P., Schram, N., Foster, J.J., Clement, S.W., 2008. Determining high precision, in situ, oxygen isotope ratios with a SHRIMP II: Analyses of MPI-DING silicate-glass reference materials and zircon from contrasting granites. Chemical Geology 257, 114-128.

Irvine, T.N., Baragar, W.R.A., 1971. A Guide to the Chemical Classification of the Common Volcanic Rocks. Canadian Journal of Earth Sciences 8, 523-548.

Ishwar-Kumar, C., Santosh, M., Wilde, S.A., Tsunogae, T., Itaya, T., Windley, B.F., Sajeev, K., in press. Mesoproterozoic suturing of Archean crustal blocks in western peninsular India: Implications for India-Madagascar correlations. Lithos.

Jackson, S.E., Pearson, N.J., Griffin, W.L., Belousova, E.A., 2004. The application of laser ablation-inductively coupled plasma-mass spectrometry to in situ U–Pb zircon geochronology. Chemical Geology 211, 47-69.

Jacobs, J., Bingen, B., Thomas, R.J., Bauer, W., Wingate, M.T.D., Feitio, P., 2008. Early Palaeozoic orogenic collapse and voluminous late-tectonic magmatism in Dronning Maud Land and Mozambique: insights into the partially delaminated orogenic root of the East African–Antarctic Orogen? Geological Society, London, Special Publications 308, 69-90.

Jacobs, J., Elburg, M., Läufer, A., Kleinhanns, I.C., Henjes-Kunst, F., Estrada, S., Ruppel, A.S., Damaske, D., Montero, P., Bea, F., 2015. Two distinct Late Mesoproterozoic/Early Neoproterozoic basement provinces in central/eastern Dronning Maud Land, East Antarctica: The missing link, 15–21° E. Precambrian Research 265, 249-272.

JICA, 2012. Results of SHRIMP dating in the Survey Area (Ishizaki, Shunichi), Final Report of U-Pb Geochronology, Project de Gouvernance des Ressources Minerales, Madagascar (PGRM) : Geological Mapping and Mineral Information System Project for the Ministère de l'Energie et des Mines (MEM/SG/DG/UCP/PGRM). Japanese International Cooperation Agency, p. 55.

Johansson, Å., 2014. From Rodinia to Gondwana with the 'SAMBA' model—A distant view from Baltica towards Amazonia and beyond. Precambrian Research 244, 226-235.

Johnson, P.R., Andresen, A., Collins, A.S., Fowler, A.R., Fritz, H., Ghebreab, W., Kusky, T., Stern, R.J., 2011. Late Cryogenian–Ediacaran history of the Arabian–Nubian Shield: A

review of depositional, plutonic, structural, and tectonic events in the closing stages of the northern East African Orogen. Journal of African Earth Sciences 61, 167-232.

Johnson, S.P., Rivers, T., De Waele, B., 2005. A review of the Mesoproterozoic to early Palaeozoic magmatic and tectonothermal history of south–central Africa: implications for Rodinia and Gondwana. Journal of the Geological Society 162, 433-450.

Jöns, N., Emmel, B., Schenk, V., Razakamanana, T., 2009. From orogenesis to passive margin—the cooling history of the Bemarivo Belt (N Madagascar), a multi-thermochronometer approach. Gondwana Research 16, 72-81.

Jöns, N., Schenk, V., 2008. Relics of the Mozambique Ocean in the central East African Orogen: evidence from the Vohibory Block of southern Madagascar. Journal of Metamorphic Geology 26, 17-28.

Jöns, N., Schenk, V., 2011. The ultrahigh temperature granulites of southern Madagascar in a polymetamorphic context: implications for the amalgamation of the Gondwana supercontinent. European Journal of Mineralogy 23, 127-156.

Jöns, N., Schenk, V., Appel, P., Razakamanana, T., 2006. Two-stage metamorphic evolution of the Bemarivo Belt of northern Madagascar: constraints from reaction textures and in situ monazite dating. Journal of Metamorphic Geology 24, 329-347.

Kabete, J., Groves, D., McNaughton, N., Dunphy, J., 2006. The geology, SHRIMP U–Pb geochronology and metallogenic significance of the Ankisatra-Besakay District, Andriamena belt, northern Madagascar. Journal of African Earth Sciences 45, 87-122.

Kemp, A.I.S., Hawkesworth, C.J., Collins, W.J., Gray, C.M., Blevin, P.L., 2009. Isotopic evidence for rapid continental growth in an extensional accretionary orogen: The Tasmanides, eastern Australia. Earth and Planetary Science Letters 284, 455-466.

Kemp, A.I.S., Hawkesworth, C.J., Foster, G.L., Paterson, B.A., Woodhead, J.D., Hergt, J.M., Gray, C.M., Whitehouse, M.J., 2007. Magmatic and Crustal Differentiation History of Granitic Rocks from Hf-O Isotopes in Zircon. Science 315, 980-983.

Kemp, A.I.S., Hawkesworth, C.J., Paterson, B.A., Kinny, P.D., 2006. Episodic growth of the Gondwana supercontinent from hafnium and oxygen isotopes in zircon. Nature 439, 580-583.

Key, R.M., Pitfield, P.E.J., Thomas, R.J., Goodenough, K.M., De Waele, B., Schofield, D.I., Bauer, W., Horstwood, M.S.A., Styles, M.T., Conrad, J., Encarnacion, J., Lidke, D.J., O'Connor, E.A., Potter, C., Smith, R.A., Walsh, G.J., Ralison, A.V., Randriamananjara, T., Rafahatelo, J.-M., Rabarimanana, M., 2011. Polyphase Neoproterozoic orogenesis within the East Africa–Antarctica Orogenic Belt in central and northern Madagascar. Geological Society, London, Special Publications 357, 49-68.

Kinny, P.D., Maas, R., 2003. Lu–Hf and Sm–Nd isotope systems in zircon. Reviews in Mineralogy and Geochemistry 53, 327-341.

Kröner, A., Hegner, E., Collins, A.S., Windley, B.F., Brewer, T.S., Razakamanana, T., Pidgeon, R.T., 2000. Age and magmatic history of the Antananarivo Block, central Madagascar, as derived from zircon geochronology and Nd isotopic systematics. American Journal of Science 300, 251-288.

Kröner, A., Kehelpannala, K.V.W., Hegner, E., 2003. Ca. 750-1100 Ma magmatic events and Grenville-age deformation in Sri Lanka: relevance for Rodinia supercontinent formation and dispersal, and Gondwana amalgamation. Journal of Asian Earth Sciences 22, 279-300.

Kröner, A., Kovach, V.P., Kozakov, I.K., Kirnozova, T., Azimov, P., Wong, J., Geng, H.Y., Zircon ages and Nd–Hf isotopes in UHT granulites of the Ider Complex: A cratonic terrane within the Central Asian Orogenic Belt in NW Mongolia. Gondwana Research.

Kröner, A., Williams, I.S., Compston, W., Baur, N., Vitanage, P.W., Perera, L.R.K., 1987. Zircon Ion Microprobe Dating of High-Grade Rocks in Sri Lanka. The Journal of Geology 95, 775-791.

Kröner, A., Windley, B.F., Jaeckel, P., Brewer, T.S., Razakamanana, T., 1999a. New zircon ages and regional significance for the evolution of the Pan-African orogen in Madagascar. Journal of the Geological Society, London 156, 1125-1135.

Kröner, A., Windley, B.F., Jaeckelt, P., Brewer, T.S., Razakamanana, T., 1999b. New zircon ages and regional significance for the evolution of the Pan-African orogen in Madagascar. Journal of the Geological Society 156, 1125-1135.

Küster, D., Harms, U., 1998. Post-collisional potassic granitoids from the southern and northwestern parts of the Late Neoproterozoic East African Orogen: a review. Lithos 45, 177-195.

Laborde, J., 1928. La nouvelle projection du Service Géographique de Madagascar: Tananarive. Cahiers du Service Géographique de Madagascar 1 70.

Li, X.-H., Li, Z.-X., Ge, W., Zhou, H., Li, W., Liu, Y., Wingate, M.T.D., 2003. Neoproterozoic granitoids in South China: crustal melting above a mantle plume at ca. 825 Ma? Precambrian Research 122, 45-83.

Li, Z.-X., Evans, D.A.D., Halverson, G.P., 2013. Neoproterozoic glaciations in a revised global palaeogeography from the breakup of Rodinia to the assembly of Gondwanaland. Sedimentary Geology 294, 219-232.

Li, Z.X., Bogdanova, S.V., Collins, A.S., Davidson, A., De Waele, B., Ernst, R.E., Fitzsimons, I.C.W., Fuck, R.A., Gladkochub, D.P., Jacobs, J., Karlstrom, K.E., Lu, S., Natapov, L.M., Pease, V., Pisarevsky, S.A., Thrane, K., Vernikovsky, V., 2008. Assembly, configuration, and break-up history of Rodinia: A synthesis. Precambrian Research 160, 179-210.

Loiselle, M., Wones, D., 1979. Characteristics and origin of anorogenic granites, Geological Society of America Abstracts with Programs, p. 468.

Macey, P.H., Thomas, R.J., Grantham, G.H., Ingram, B.A., Jacobs, J., Armstrong, R.A., Roberts, M.P., Bingen, B., Hollick, L., de Kock, G.S., Viola, G., Bauer, W., Gonzales, E., Bjerkgård, T., Henderson, I.H.C., Sandstad, J.S., Cronwright, M.S., Harley, S., Solli, A., Nordgulen, Ø., Motuza, G., Daudi, E., Manhiça, V., 2010. Mesoproterozoic geology of the Nampula Block, northern Mozambique: Tracing fragments of Mesoproterozoic crust in the heart of Gondwana. Precambrian Research 182, 124-148.

Mamani, M., Wörner, G., Sempere, T., 2009. Geochemical variations in igneous rocks of the Central Andean orocline (13°S to 18°S): Tracing crustal thickening and magma generation through time and space. Geological Society of America Bulletin.

Markl, G., Bäuerle, J., Grujic, D., 2000. Metamorphic evolution of Pan-African granulite facies metapelites from Southern Madagascar. Precambrian Research 102, 47-68.

Martelat, J.-E., Lardeaux, J.-M., Nicollet, C., Rakotondrazafy, R., 2000. Strain pattern and late Precambrian deformation history in southern Madagascar. Precambrian Research 102, 1-20.

Martin, L.A.J., Duchêne, S., Deloule, E., Vanderhaeghe, O., 2008. Mobility of trace elements and oxygen in zircon during metamorphism: Consequences for geochemical tracing. Earth and Planetary Science Letters 267, 161-174.

Maxwell, L.A., Fitzsimons, I.C.W., Collins, A.S., Kinny , P.D., Taylor, R.J.M., Clark, C., 2014. Good dates, bad ages – Archean zircon inheritance in Cambrian schist and pegmatite northeast Madagascar. In Abstracts Book, Gondwana 15 North Meets South 15, 109.

McCulloch, M.T., Chappell, B.W., 1982. Nd isotopic characteristics of S- and I-type granites. Earth and Planetary Science Letters 58, 51-64.

McMillan, A., Harris, N.W., Holness, M., Ashwal, L., Kelley, S., Rambeloson, R., 2003. A granite–gabbro complex from Madagascar: constraints on melting of the lower crust. Contributions to Mineralogy and Petrology 145, 585-599.

Meert, J.G., 2003. A synopsis of events related to the assembly of eastern Gondwana. Tectonophysics 362, 1-40.

Meert, J.G., Hall, C., Nédélec, A., Razanatseheno, M.O.M., 2001a. Cooling of a Late-Syn Orogenic Pluton: Evidence from Laser K-feldspar Modelling of the Carion Granite, Madagascar. Gondwana Research 4, 541-550.

Meert, J.G., Nédélec, A., Hall, C., Wingate, M.T.D., Rakotondrazafy, M., 2001b. Paleomagnetism, geochronology and tectonic implications of the Cambrian-age Carion granite, Central Madagascar. Tectonophysics 340, 1-21.

Meert, J.G., Pandit, M.K., Kamenov, G.D., 2013. Further geochronological and paleomagnetic constraints on Malani (and pre-Malani) magmatism in NW India. Tectonophysics 608, 1254-1267.

Meschede, M., 1986. A method of discriminating between different types of mid-ocean ridge basalts and continental tholeiites with the Nb・1bZr・1bY diagram. Chemical Geology 56, 207-218.

Miyashiro, A., 1974. Volcanic rock series in island arcs and active continental margins. American Journal of Science 274, 321-355.

Mohan, M.R., Sarma, D.S., McNaughton, N.J., Fletcher, I.R., Wilde, S.A., Siddiqui, M.A., Rasmussen, B., Krapez, B., Gregory, C.J., Kamo, S.L., 2014. SHRIMP zircon and titanite U-Pb ages, Lu-Hf isotope signatures and geochemical constraints for ~2.56Ga granitic magmatism in Western Dharwar Craton, Southern India: Evidence for short-lived Neoarchean episodic crustal growth? Precambrian Research 243, 197-220.

Moine, B., 1963. Etude géologique et prospection des feuilles Miandravazo-Betrondro-Ambatondradama (I.J.K-48), Rapport Annuel du Service Géologique pour 1963. Service Géologique de Madagascar, Tananarive, pp. 117-146.

Moine, B., 1967. Relations stratigraphiques entre la série < schisto-quartzo-calcaire > et les gneiss environnants (centre ouest de Madagascar). Compte Rendus Semaine Géologique Madagascar, 49-53.

Moine, B., 1968. Carte du Massif Schisto-Quartzo-Dolomitique. 1\200000. Service Géologique de Madagasikara, Antananarivo.

Moine, B., 1974. Caractères de sédimentation et de métamorphisme des séries Précambriennes épizonales á catazonales du centre de Madagascar (Région d'Ambatofinandrahana), Sciences de la Terre, Mémoire, Nancy, France, pp. 293 p., and color Map, scale 291:200 000.

Moine, B., Bosse, V., Paquette, J.-L., Ortega, E., 2014. The occurrence of a Tonian–Cryogenian (~850Ma) regional metamorphic event in Central Madagascar and the geodynamic setting of the Imorona–Itsindro (~800Ma) magmatic suite. Journal of African Earth Sciences 94, 58-73.

Morimoto, N., 1988. Nomenclature of Pyroxenes. Mineralogy and Petrology 39, 55-76.

Müller, B., 2000. The evolution and significance of the Bongolava–Ranotsara shear zone, Madagascar. Rand Afrikaans University, Johannesburg, South Africa, p. 125.

Murphy, J.B., 2006. Igneous Rock Associations 7. Arc Magmatism I: Relationship Between Subduction and Magma Genesis. 2006.

Murphy, J.B., 2007. Igneous Rock Associations 8. Arc Magmatism II: Geochemical and Isotopic Characteristics. 2007.

Nédélec, A., Guillaume, D., Cournède, C., Duran, C., Macouin, M., Rakotondrazafy, M., Giuliani, G., 2014. Incipient charnockitisation due to carbonic fluid transfer related to late Pan-African transcurrent tectonics in Madagascar; implications for mobility of Fe, Ti, REE and other elements. Journal of African Earth Sciences 94, 86-99.

Nedelec, A., Paquette, J.L., Bouchez, J.L., 2015. A-type stratoid granites of Madagascar: evidence of Rodinia rifting at ca. 790 Ma, European Geophysical Union (EGU) General Assembly, Vienna, Austria, p. 349.

Nédélec, A., Paquette, J.L., Bouchez, J.L., Olivier, P., Ralison, B., 1994. Stratoid granites of Madagascar: structure and position in the Panafrican orogeny. Geodinamica Acta (Paris) 7, 48-56.

Nédélec, A., Ralison, B., Bouchez, J.-L., Grégoire, V., 2000. Structure and metamorphism of the granitic basement around Antananarivo: A key to the Pan-African history of central Madagascar and its Gondwana connections. Tectonics 19, 997-1020.

Nédélec, A., Stephens, W.E., Fallick, A.E., 1995. The Panafrican stratoid granites of Madagascar: alkaline magmatism in a post-collisional extensional setting. Journal of Petrology 36, 1367-1391.

Paquette, J.-L., Moine, B., Rakotondrazafy, M.A.F., 2003. ID-TIMS using the step-wise dissolution technique versus ion microprobe U–Pb dating of metamict Archean zircons from NE Madagascar. Precambrian Research 121, 73-84.

Paquette, J.-L., Nédélec, A., 1998. A new insight into Pan-African tectonics in the East–West Gondwana collision zone by U–Pb zircon dating of granites from central Madagascar. Earth and Planetary Science Letters 155, 45-56.

Paquette, J.L., Nédélec, A., Moine, B., Rakotondrazafy, M., 1994. U–Pb, single zircon Pb-evaporation, and Sm–Nd isotopic study of a granulite domain in SE Madagascar. Journal of Geology 102, 523-538.

Payne, J.L., Pearson, N.J., Grant, K.J., Halverson, G.P., 2013. Reassessment of relative oxide formation rates and molecular interferences on in situ lutetium-hafnium analysis with laser ablation MC-ICP-MS. Journal of Analytical Atomic Spectrometry 28, 1068-1079.

Pearce, J.A., 1983. Role of the sub-continental lithosphere in magma genesis at acrive continental margins: p 230-249. in, Hawkesworth, C.J. and Norry, M.J., *eds.,* Continental Basalts and Mantle Xenoliths Shiva Publishing Ltd, Cambridge, Mass. 272p.

Pearce, J.A., 1996a. Sources and settings of granitic rocks. Episodes 19, 120–125.

Pearce, J.A., 1996b. A users guide to basalt discrimination diagrams, in: Wyman, D.A. (Ed.), Trace Element Geochemistry of Volcanic Rocks: Applications for Massive Sulphide Exploration. Geological Association of Canada Short Course Notes 12, pp. 79-113.

Pearce, J.A., Alabaster, T., Shelton, A.W., Searle, M.P., 1981. The Oman ophiolite as a cretaceous arc–basin complex : evidence and implications. Phil. Trans. R. Soc. Lond. A300, 299–317.

Pearce, J.A., Harris, N.B.W., Tindle, A.G., 1984. Trace Element Discrimination Diagrams for the Tectonic Interpretation of Granitic Rocks. Journal of Petrology 25, 956-983.

Peucat, J.-J., Jayananda, M., Chardon, D., Capdevila, R., Fanning, C.M., Paquette, J.-L., 2013. The lower crust of the Dharwar Craton, Southern India: Patchwork of Archean granulitic domains. Precambrian Research 227, 4-28.

Pisarevsky, S.A., Elming, S.-Å., Pesonen, L.J., Li, Z.-X., 2014. Mesoproterozoic paleogeography: Supercontinent and beyond. Precambrian Research 244, 207-225.

Plank, T., Langmuir, C.H., 1988. An evaluation of the global variations in the major element chemistry of arc basalts. Earth and Planetary Science Letters 90, 349-370.

Plavsa, D., Collins, A.S., Foden, J.D., Clark, C., 2015. The evolution of a Gondwanan collisional orogen: A structural and geochronological appraisal from the Southern Granulite Terrane, South India. Tectonics 34, 820-857.

Plavsa, D., Collins, A.S., Foden, J.F., Kropinski, L., Santosh, M., Chetty, T.R.K., Clark, C., 2012. Delineating crustal domains in Peninsular India: Age and chemistry of orthopyroxene-bearing felsic gneisses in the Madurai Block. Precambrian Research 198, 77-93.

Plavsa, D., Collins, A.S., Payne, J.L., Foden, J.D., Clark, C., Santosh, M., 2014. Detrital zircons in basement metasedimentary protoliths unveil the origins of southern India. Geological Society of America Bulletin 126, 791-811.

Preston, J., 2015. GabbroSoft. http://www.gabbrosoft.org/spreadsheets.html.

Raharimahefa, T., Kusky, T.M., 2010. Temporal evolution of the Angavo and related shear zones in Gondwana: Constraints from LA-MC-ICP-MS U–Pb zircon ages of granitoids and gneiss from central Madagascar. Precambrian Research 182, 30-42.

Rakotoarimanana, R.H., 2001. Geology and petrology of the Dabolava Region, west-central Madagascar, with emphasis on granite-hosted gold mineralisation, Faculty of Natural Sciences. Unpublished MSc Thesis, Rand Afrikaans University, p. 89.

Ramos, V., 1999. Plate tectonic setting of the Andean Cordillera. Episodes 22, 183-190.

Raoelison, I.L., 1997. Structure and Metamorphism of the Itremo Group, central Madagascar. Rand Afrikaans University, Johannesburg.

Ratheesh-Kumar, R.T., Ishwar-Kumar, C., Windley, B.F., Razakamanana, T., Nair, R.R., Sajeev, K., 2015. India–Madagascar paleo-fit based on flexural isostasy of their rifted margins. Gondwana Research 28, 581-600.

Razanatseheno, M.O.M., Nédélec, A., Rakotondrazafy, M., Meert, J.G., Ralison, B., 2009. Four-stage building of the Cambrian Carion pluton (Madagascar). Earth and Environmental Science Transactions of the Royal Society of Edinburgh 100, 133-145.

Rekha, S., Bhattacharya, A., Chatterjee, N., 2014. Tectonic restoration of the Precambrian crystalline rocks along the west coast of India: Correlation with eastern Madagascar in East Gondwana. Precambrian Research 252, 191-208.

Rieder, M., Cavazzini, G., D'yakonov, Y.S., Frank-Kamenetskii, V.A., Gottardi, G., Guggenheim, S., Koval', P.V., Mueller, G., Neiva, A.M.R., Radoslovich, E.W., Robert, J.-L., Sassi, F.P., Takeda, H., Weiss, Z., Wones, D.R., 1998. Nomenclature of the micas. The Canadian Mineralogist 36, 905-912.

Robinson, F.A., Foden, J.D., Collins, A.S., 2015a. Geochemical and isotopic constraints on island arc, synorogenic, post-orogenic and anorogenic granitoids in the Arabian Shield, Saudi Arabia. Lithos 220–223, 97-115.

Robinson, F.A., Foden, J.D., Collins, A.S., 2015b. Zircon Geochemical and Geochronological Constraints on Contaminated and Enriched Mantle Sources beneath the Arabian Shield, Saudi Arabia. The Journal of Geology 123, 463-489.

Robinson, F.A., Foden, J.D., Collins, A.S., in press. Geochemical and isotopic constraints on island arc, synorogenic, postorogenic and anorogenic granitoids in the Arabian Shield, Saudi Arabia. Lithos.

Robinson, F.A., Foden, J.D., Collins, A.S., Payne, J.L., 2014. Arabian Shield magmatic cycles and their relationship with Gondwana assembly: Insights from zircon U–Pb and Hf isotopes. Earth and Planetary Science Letters 408, 207-225.

Rogers, N., Macdonald, R., Fitton, J.G., George, R., Smith, M., Barreiro, B., 2000. Two mantle plumes beneath the East African rift system: Sr, Nd and Pb isotope evidence from Kenya Rift basalts. Earth and Planetary Science Letters 176, 387-400.

Roig, J.Y., Tucker, R.D., Peters, S.G., Delor, C., Theveniaut, H., 2012. Carte Géologique de la République de Madagascar à 1/1,000,000, Ministère des Mines, Direction de la Géologie, Programme de Gouvernance des Resources Minérales.

Rubatto, D., 2002. Zircon trace element geochemistry: partitioning with garnet and the link between U–Pb ages and metamorphism. Chemical Geology 184, 123-138.

Saha, D., Patranabis-Deb, S., 2014. Proterozoic evolution of Eastern Dharwar and Bastar cratons, India – An overview of the intracratonic basins, craton margins and mobile belts. Journal of Asian Earth Sciences 91, 230-251.

Santosh, M., Tanaka, K., Yokoyama, K., Collins, A.S., 2005. Late Neoproterozoic-Cambrian Felsic Magmatism Along Transcrustal Shear Zones in Southern India: U-Pb Electron Microprobe Ages and Implications for the Amalgamation of the Gondwana Supercontinent. Gondwana Research 8, 31-42.

Sarkar, T., Schenk, V., Appel, P., Berndt, J., Sengupta, P., in press. Two-stage granulite formation in a Proterozoic magmatic arc (Ongole domain of the Eastern Ghats Belt, India): Part 2. LA-ICP-MS zircon dating and texturally controlled in-situ monazite dating. Precambrian Research.

Sarma, D.S., McNaughton, N.J., Belusova, E., Ram Mohan, M., Fletcher, I.R., 2012. Detrital zircon U–Pb ages and Hf-isotope systematics from the Gadag Greenstone Belt: Archean crustal growth in the western Dharwar Craton, India. Gondwana Research 22, 843-854.

Saunders, A.D., Norry, M.J., Tarney, J., 1988. Origin of MORB and Chemically-Depleted Mantle Reservoirs: Trace Element Constraints. Journal of Petrology Special_Volume, 415-445.

Scherer, E., Münker, C., Mezger, K., 2001. Calibration of the Lutetium-Hafnium Clock. Science 293, 683-687.

Schofield, D.I., Thomas, R.J., Goodenough, K.M., De Waele, B., Pitfield, P.E.J., Key, R.M., Bauer, W., Walsh, G.J., Lidke, D.J., Ralison, A.V., Rabarimanana, M., Rafahatelo, J.M., Randriamananjara, T., 2010. Geological evolution of the Antongil Craton, NE Madagascar. Precambrian Research 182, 187-203.

Shackleton, R.M., 1996. The final collision between East and West Gondwana; where is it? Journal of African Earth Sciences 23, 271-287.

Shibata, T., Nakamura, E., 1997. Across-arc variations of isotope and trace element compositions from Quaternary basaltic volcanic rocks in northeastern Japan: Implications for interaction between subducted oceanic slab and mantle wedge. Journal of Geophysical Research: Solid Earth 102, 8051-8064.

Sláma, J., Košler, J., Condon, D.J., Crowley, J.L., Gerdes, A., Hanchar, J.M., Horstwood, M.S.A., Morris, G.A., Nasdala, L., Norberg, N., Schaltegger, U., Schoene, B., Tubrett, M.N., Whitehouse, M.J., 2008. Plešovice zircon — A new natural reference material for U–Pb and Hf isotopic microanalysis. Chemical Geology 249, 1-35.

Stein, M., Goldstein, S.L., 1996. From plume head to continental lithosphere in the Arabian Nubian shield. Nature 382, 773-778.

Stern, R.A., 2001. A new isotopic and trace element standard for the ion microprobe: preliminary TIMS U–Pb and electron microprobe data, current research. Radiogenic Age and Isotopic Studies. Report 14, Geological Survey of Canada, Ottawa, Canada.

Stern, R.A., 2002. Crustal evolution in the East African Orogen: a neodymian isotopic perspective. Journal Of African Earth Sciences 34, 109-117.

Stern, R.J., 1994. Arc Assembly and continental collision in the Neoproterozoic East African orogeny - implications for the consolidation of Gondwana. Annual Review of Earth and Planetary Sciences 22, 319-351.

Streckeisen, A., 1976. To each plutonic rock its proper name. Earth-Science Reviews 12, 1-33.

Sun, S.S., McDonough, W.F., 1989. Chemical and isotopic systematics of ocean basalts: implications for mantle composition and processes, in: Saunders, A.D.N., M.J. (Ed.), Magmatism in the Ocean Basins. Geological Society of London, pp. 313-345.

Taylor Jr, H.P., 1980. The effects of assimilation of country rocks by magmas on 18O/16O and 87Sr/86Sr systematics in igneous rocks. Earth and Planetary Science Letters 47, 243-254.

Teale, W., Collins, A.S., Foden, J., Payne, J.L., Plavsa, D., Chetty, T.R.K., Santosh, M., Fanning, M., 2011. Cryogenian (~830 Ma) mafic magmatism and metamorphism in the northern Madurai Block, southern India: A magmatic link between Sri Lanka and Madagascar? Journal of Asian Earth Sciences 42, 223-233.

Teklay, M., Kröner, A., Mezger, K., 2002. Enrichment from plume interaction in the generation of Neoproterozoic arc rocks in northern Eritrea: implications for crustal accretion in the southern Arabian–Nubian Shield. Chemical Geology 184, 167-184.

Tenczer, V., Hauzenberger, C.A., Fritz, H., Whitehouse, M.J., Mogessie, A., Wallbrecher, E., Muhongo, S., Hoinkes, G., 2006. Anorthosites in the Eastern Granulites of Tanzania—New SIMS zircon U–Pb age data, petrography and geochemistry. Precambrian Research 148, 85-114.

Thomas, R.J., De Waele, B., Schofield, D.I., Goodenough, K.M., Horstwood, M., Tucker, R., Bauer, W., Annells, R., Howard, K., Walsh, G., Rabarimanana, M., Rafahatelo, J.M., Ralison, A.V., Randriamananjara, T., 2009. Geological evolution of the Neoproterozoic Bemarivo Belt, northern Madagascar. Precambrian Research 172, 279-300.

Tindle, A.G., 2015. Mineral Recalculation Software. http://www.open.ac.uk/earth-research/tindle/AGTWebPages/AGTSoft.html.

Tindle, A.G., Webb, P.C., 1990. Estimation of lithium contents in trioctahedral micas using microprobe data; application to micas from granitic rocks. European Journal of Mineralogy 2, 595-610.

Tomson, J.K., Bhaskar Rao, Y.J., Vijaya Kumar, T., Choudhary, A.K., 2013. Geochemistry and neodymium model ages of Precambrian charnockites, Southern Granulite Terrain, India: Constraints on terrain assembly. Precambrian Research 227, 295-315.

Torsvik, T.H., 2003. The Rodinia Jigsaw Puzzle. Science 300, 1379-1381.

Torsvik, T.H., Ashwal, L.D., Tucker, R.D., Eide, E.A., 2001. Geochronology and paleomagnetism of the Seychelles microcontinent: The India link. Precambrian Research 110, 47-59.

Torsvik, T.H., Cocks, L.R.M., 2013. Gondwana from top to base in space and time. Gondwana Research 24, 999-1030.

Tucker, R.D., Ashwal, L.D., Hamilton, M.A., Torsvik, T.H., Carter, L.M., 1999a. Neoproterozoic silicic magmatism of northern Madagascar, Seychelles, and NW India: clues

to Rodinia's assembly and dispersal. Geological Society of America , Abstracts with Programs 31, 317.

Tucker, R.D., Ashwal, L.D., Handke, M.J., Hamilton, M.A., Le Grange, M., Rambeloson, R.A., 1999b. U–Pb geochronology and isotope geochemistry of the Archean and Proterozoic rocks of north-central Madagascar. Journal of Geology 107, 135-153.

Tucker, R.D., Kusky, T.M., Buchwaldt, R., Handke, M.J., 2007. Neoproterozoic nappes and superposed folding of the Itremo Group, west-central Madagascar. Gondwana Research 12, 356-379.

Tucker, R.D., Peters, S.G., Roig, J.Y., Théveniaut, H., Delor, C., 2012. Notice explicative des cartes géologique et métallogéniques de la République de Madagascar à 1/1,000,000 Ministère des Mines. PGRM, Antananarivo, République de Madagascar.

Tucker, R.D., Roig, J.Y., Delor, C., Amelin, Y., Goncalves, P., Rabarimanana, M.H., Ralison, A.V., Belcher, R.W., 2011a. Neoproterozoic extension in the Greater Dharwar Craton: a reevaluation of the "Betsimisaraka suture" in Madagascar. This article is one of a series of papers published in this Special Issue on the theme of Geochronology in honour of Tom Krogh. Canadian Journal of Earth Sciences 48, 389-417.

Tucker, R.D., Roig, J.Y., Macey, P.H., Delor, C., Amelin, Y., Armstrong, R.A., Rabarimanana, M.H., Ralison, A.V., 2011b. A new geological framework for south-central Madagascar, and its relevance to the "out-of-Africa" hypothesis. Precambrian Research 185, 109-130.

Tucker, R.D., Roig, J.Y., Moine, B., Delor, C., Peters, S.G., 2014. A geological synthesis of the Precambrian shield in Madagascar. Journal of African Earth Sciences 94, 9-30.

Valley, J.W., 2003. Oxygen Isotopes in Zircon. Reviews in Mineralogy and Geochemistry 53, 343-385.

Valley, J.W., Chiarenzelli, J.R., McLelland, J.M., 1994. Oxygen isotope geochemistry of zircon. Earth and Planetary Science Letters 126, 187-206.

Valley, J.W., Kinny, P.D., Schulze, D.J., Spicuzza, M.J., 1998. Zircon megacrysts from kimberlite: oxygen isotope variability among mantle melts. Contributions to Mineralogy and Petrology 133, 1-11.

Valley, J.W., Lackey, J.S., Cavosie, A.J., Clechenko, C.C., Spicuzza, M.J., Basei, M.A.S., Bindeman, I.N., Ferreira, V.P., Sial, A.N., King, E.M., Peck, W.H., Sinha, A.K., Wei, C.S., 2005. 4.4 billion years of crustal maturation: oxygen isotope ratios of magmatic zircon. Contributions to Mineralogy and Petrology 150, 561-580.

Vermeesch, P., 2012. On the visualisation of detrital age distributions. Chemical Geology 312–313, 190-194.

Vervoort, J.D., Patchett, J., Soderlund, U., Baker, M., 2004. Isotopic composition of Yb and the determination of Lu concentration and Lu/Hf ratios by isotope dilution using MC-ICPMS. Geochemistry Geophysics Geosystems 5, Q11002.

Viola, G., Henderson, I.H.C., Bingen, B., Thomas, R.J., Smethurst, M.A., de Azavedo, S., 2008. Growth and collapse of a deeply eroded orogen: Insights from structural, geophysical, and geochronological constraints on the Pan-African evolution of NE Mozambique. Tectonics 27, n/a-n/a.

Whalen, J., Currie, K., Chappell, B., 1987. A-type granites: geochemical characteristics, discrimination and petrogenesis. Contributions to Mineralogy and Petrology 95, 407-419.

Windley, B.F., Razafiniparany, A., Razakamanana, T., Ackermand, D., 1994. Tectonic framework of the Precambrian of Madagascar and its Gondwana connections: a review and reappraisal. Geologische Rundschau 83, 642-659.

Windrim, D.P., McCulloch, M.T., 1986. Nd and Sr isotopic systematics of central Australian granulites: chronology of crustal development and constraints on the evolution of lower continental crust. Contributions to Mineralogy and Petrology 94, 289-303.

Winter, J.D., 2001. An Introduction to Igneous and Metamorphic Petrology. Prentice Hall Publishing, New Jersey.

Woodhead, J., Hergt, J., Shelley, M., Eggins, S., Kemp, R., 2004. Zircon Hf-isotope analysis with an excimer laser, depth profiling, ablation of complex geometries, and concomitant age estimation. Chemical Geology 209, 121-135.

Woodhead, J.D., Hergt, J.M., 2005. A Preliminary Appraisal of Seven Natural Zircon Reference Materials for In Situ Hf Isotope Determination. Geostandards and Geoanalytical Research 29, 183-195.

Yang, X.-A., Chen, Y.-C., Liu, S.-B., Hou, K.-J., Chen, Z.-Y., Liu, J.-J., 2014. U–Pb zircon geochronology and geochemistry of Neoproterozoic granitoids of the Maevatanana area, Madagascar: implications for Neoproterozoic crustal extension of the Imorona–Itsindro Suite and subsequent lithospheric subduction. International Geology Review, 1-17.

Yogodzinski, G.M., Vervoort, J.D., Brown, S.T., Gerseny, M., 2010. Subduction controls of Hf and Nd isotopes in lavas of the Aleutian island arc. Earth and Planetary Science Letters 300, 226-238.

Zhao, J.-x., McCulloch, M.T., Korsch, R.J., 1994. Characterisation of a plume-related ~ 800 Ma magmatic event and its implications for basin formation in central-southern Australia. Earth and Planetary Science Letters 121, 349-367.

Zhou, J.-L., 2015. Nature of Cryogenian felsic igneous rocks in Madagascar reevaluated: A comment on "From passive margin to volcano-sedimentary forearc: The Tonian to Cryogenian evolution of the Anosyen Domain of southeastern Madagascar" by Boger et al. Precambrian Research 262, 123-126.

Zhou, J.-L., Rasoamalala, V., Razoeliarimalala, M., Ralison, B., Luo, Z.-H., 2015a. Age and geochemistry of Early Cambrian post-collisional granites from the Ambatondrazaka area in east-central Madagascar. Journal of African Earth Sciences 106, 75-86.

Zhou, J.-L., Shao, S., Luo, Z.-H., Shao, J.-B., Wu, D.-T., Rasoamalala, V., 2015b. Geochronology and geochemistry of Cryogenian gabbros from the Ambatondrazaka area, east-central Madagascar: Implications for Madagascar-India correlation and Rodinia paleogeography. Precambrian Research 256, 256-270.

Appendix 2.1

SHRIMP II U-Pb (zircon) data for the Ambatolampy Group

DA13-007			Conc (ppm)				Radiogenic Ratios									Ages				
Spot Name	Type	%com ^{206}Pb	U	Th	^{232}Th/^{38}U	± (%)[1]	^{238}U/^{206}Pb*	± (%)[1]	^{207}Pb*/^{206}Pb*	± (%)[1]	^{207}Pb*/^{235}U	± (%)[1]	^{206}Pb*/^{238}U	± (%)[1]	err corr	^{206}Pb/^{238}U	± 1σ	^{207}Pb/^{206}Pb	± 1σ	%Discordant
007-01.1		0.29	252	155	0.64	0.34	3.8	1.36	0.16	1.55	5.6	2.06	0.26	1.36	0.6602	1492	18	2416	26	+43
007-02.1		0.41	738	314	0.44	2.03	6.0	1.31	0.12	1.67	2.7	2.12	0.17	1.31	0.6182	992	12	1889	30	+51
007-03.1		0.00	85	67	0.82	0.57	2.1	1.89	0.19	0.88	12.7	2.09	0.48	1.89	0.9068	2528	40	2755	14	+10
007-04.1	C	0.10	206	85	0.43	0.42	2.2	1.42	0.18	0.60	11.0	1.54	0.45	1.42	0.9196	2403	28	2617	10	+10
007-04.2	R	0.66	2014	86	0.04	0.35	11.5	1.06	0.07	1.26	0.9	1.64	0.09	1.06	0.6438	539	5	973	26	+46
007-05.1		0.20	317	171	0.56	0.32	3.0	1.29	0.16	0.66	7.1	1.45	0.33	1.29	0.8912	1837	21	2410	11	+27
007-06.1		0.03	504	372	0.76	0.23	4.4	1.21	0.15	1.08	4.8	1.62	0.23	1.21	0.7452	1332	15	2375	18	+48
007-07.1		0.12	370	183	0.51	0.73	4.3	1.26	0.14	0.70	4.4	1.44	0.23	1.26	0.8729	1334	15	2211	12	+44
007-09.1		0.28	145	80	0.57	1.52	3.3	1.56	0.15	1.04	6.1	1.88	0.30	1.56	0.8321	1708	23	2304	18	+29
007-10.1		0.00	156	93	0.61	0.45	2.2	1.55	0.16	0.70	10.1	1.70	0.45	1.55	0.9108	2390	31	2494	12	+5
007-11.1		0.32	468	386	0.85	2.69	4.3	1.22	0.14	0.75	4.4	1.43	0.23	1.22	0.8498	1354	15	2168	13	+42
007-12.1		0.06	142	104	0.76	0.45	2.4	1.60	0.16	0.79	9.6	1.78	0.42	1.60	0.8964	2280	31	2501	13	+10
007-14.1		0.27	200	34	0.17	0.98	4.3	1.43	0.16	0.98	5.0	1.73	0.23	1.43	0.8235	1354	17	2418	17	+49
007-15.1		0.94	322	166	0.53	0.91	4.7	2.54	0.17	1.32	4.9	2.87	0.21	2.54	0.8868	1244	29	2521	22	+56
007-16.1	C	0.15	105	68	0.67	0.53	2.0	1.75	0.18	0.84	12.2	1.94	0.49	1.75	0.9010	2582	37	2655	14	+3
007-16.2	R	1.29	3320	80	0.03	0.63	11.9	1.17	0.06	1.57	0.7	1.95	0.08	1.17	0.5971	521	6	648	34	+20
007-17.1		0.12	182	344	1.96	0.33	2.3	1.46	0.17	0.68	10.0	1.62	0.44	1.46	0.9068	2338	29	2516	11	+8
007-18.1		0.05	449	347	0.80	0.45	3.6	1.22	0.15	0.56	5.7	1.34	0.28	1.22	0.9084	1599	17	2319	10	+35
007-19.1		0.15	310	158	0.53	0.31	2.5	1.28	0.16	0.83	9.1	1.53	0.40	1.28	0.8383	2169	24	2503	14	+16
007-20.1		0.12	218	126	0.60	0.36	2.7	1.38	0.16	0.66	7.8	1.53	0.37	1.38	0.9012	2006	24	2405	11	+19
007-21.1		0.07	422	249	0.61	0.26	4.4	1.21	0.14	0.63	4.6	1.37	0.23	1.21	0.8868	1333	15	2278	11	+46
007-22.1		0.10	176	189	1.11	0.36	2.1	1.47	0.18	1.27	12.1	1.95	0.49	1.47	0.7573	2561	31	2654	21	+4
007-23.1		0.90	166	183	1.14	0.35	3.5	1.47	0.19	0.97	7.5	1.76	0.28	1.47	0.8348	1614	21	2749	16	+47
007-24.1		0.08	343	166	0.50	0.31	3.1	1.73	0.16	0.57	7.4	1.82	0.33	1.73	0.9490	1818	27	2494	10	+31
007-25.1		0.11	128	62	0.50	0.50	1.9	1.60	0.19	0.68	13.8	1.74	0.52	1.60	0.9206	2697	35	2767	11	+3
007-26.1		0.22	107	152	1.48	0.45	2.0	1.73	0.18	1.31	12.4	2.17	0.50	1.73	0.7961	2616	37	2654	22	+2
007-27.1		0.08	400	215	0.55	0.28	4.5	1.23	0.14	0.68	4.3	1.40	0.22	1.23	0.8735	1295	14	2216	12	+46
007-28.1		0.05	83	42	0.53	0.62	2.1	3.09	0.17	1.00	10.7	3.25	0.47	3.09	0.9515	2468	63	2519	17	+2
007-29.1		1.11	120	86	0.74	0.47	3.5	1.67	0.15	1.58	5.8	2.30	0.28	1.67	0.7251	1600	24	2348	27	+36
007-30.1		0.06	135	85	0.65	0.46	2.2	1.59	0.18	0.74	11.0	1.76	0.46	1.59	0.9064	2421	32	2611	12	+9
007-31.1		-0.02	199	134	0.70	0.37	2.6	1.42	0.16	0.68	8.5	1.57	0.38	1.42	0.9022	2068	25	2479	11	+19
007-32.1		0.09	79	62	0.81	0.57	1.9	1.89	0.22	0.83	15.8	2.06	0.53	1.89	0.9146	2738	42	2957	13	+9
007-33.1		-0.02	155	52	0.35	0.52	2.0	1.52	0.19	0.65	12.8	1.66	0.50	1.52	0.9202	2606	33	2709	11	+5

DA13-007			Conc (ppm)				Radiogenic Ratios									Ages				
Spot Name	Type	%com ^{206}Pb	U	Th	^{232}Th/^{238}U	± (%)[1]	^{238}U/^{206}Pb*	± (%)[1]	^{207}Pb*/^{206}Pb*	± (%)[1]	^{207}Pb*/^{235}U	± (%)[1]	^{206}Pb*/^{238}U	± (%)[1]	err corr	^{206}Pb/^{238}U	± 1σ	^{207}Pb/^{206}Pb	± 1σ	%Discordant
007-34.1		2.00	76	33	0.45	0.66	2.4	1.92	0.20	1.56	11.7	2.47	0.42	1.92	0.7765	2256	37	2843	25	+24
007-35.1		0.08	371	247	0.69	0.46	3.2	1.30	0.16	0.56	6.8	1.41	0.32	1.30	0.9191	1773	20	2402	9	+30
007-36.1		-0.03	249	137	0.57	0.36	3.5	1.36	0.15	0.71	6.0	1.54	0.29	1.36	0.8871	1624	20	2376	12	+36
007-37.1		0.33	67	31	0.47	0.71	2.1	2.01	0.19	1.08	12.5	2.29	0.48	2.01	0.8810	2549	42	2717	18	+7
007-38.1		0.88	837	446	0.55	0.19	6.2	1.44	0.12	0.95	2.7	1.73	0.16	1.44	0.8361	960	13	1985	17	+55
007-39.1		0.00	249	172	0.71	0.34	2.2	1.44	0.16	0.56	10.3	1.54	0.46	1.44	0.9309	2425	29	2495	9	+3
007-40.1		0.08	91	47	0.53	0.58	2.0	2.66	0.18	0.83	12.4	2.78	0.50	2.66	0.9544	2610	57	2652	14	+2
007-41.1		0.38	303	188	0.64	0.30	3.5	1.76	0.16	0.70	6.4	1.90	0.29	1.76	0.9286	1640	25	2464	12	+38
007-42.1		0.83	56	23	0.43	0.78	2.8	2.14	0.18	1.60	8.9	2.67	0.36	2.14	0.8009	1980	36	2650	26	+29
007-43.1	C	0.02	339	98	0.30	0.36	3.1	1.26	0.16	0.55	7.1	1.37	0.33	1.26	0.9157	1825	20	2420	9	+28
007-43.2	R	0.42	1557	80	0.05	0.33	8.3	1.32	0.09	0.77	1.5	1.53	0.12	1.32	0.8629	730	9	1475	15	+53
007-44.1		0.03	546	300	0.57	0.23	4.0	1.17	0.14	0.53	4.9	1.28	0.25	1.17	0.9107	1427	15	2257	9	+41
007-45.1		0.20	90	61	0.70	0.54	2.2	1.78	0.17	0.94	10.6	2.02	0.46	1.78	0.8838	2448	36	2523	16	+4
007-46.1		0.14	206	137	0.68	0.37	2.1	1.41	0.16	0.69	10.9	1.57	0.48	1.41	0.8983	2524	30	2502	12	-1
007-47.1		0.67	572	632	1.14	0.34	4.5	1.16	0.15	0.75	4.6	1.38	0.22	1.16	0.8406	1286	14	2376	13	+50
007-48.1		0.11	62	34	0.57	0.70	1.9	2.06	0.19	2.15	13.7	2.97	0.51	2.06	0.6918	2672	45	2766	35	+4
007-49.1		0.05	75	64	0.89	0.58	2.0	1.93	0.18	0.92	12.7	2.14	0.50	1.93	0.9030	2633	42	2674	15	+2
007-50.1		0.08	151	172	1.17	0.38	2.3	2.32	0.17	0.73	9.7	2.43	0.43	2.32	0.9535	2288	45	2509	12	+10
007-51.1		0.07	179	88	0.51	0.42	2.1	1.46	0.18	0.62	11.7	1.59	0.47	1.46	0.9202	2491	30	2655	10	+7
007-52.1		0.51	20	28	1.42	1.13	2.3	3.66	0.17	2.66	10.3	4.52	0.44	3.66	0.8092	2345	72	2554	45	+10
007-53.1		0.16	167	161	1.00	0.37	2.2	1.48	0.17	0.69	10.6	1.63	0.46	1.48	0.9059	2460	30	2514	12	+3
007-54.1		0.07	258	123	0.49	0.36	2.2	1.34	0.18	0.54	10.9	1.44	0.44	1.34	0.9265	2372	26	2630	9	+12
007-55.1		-0.03	279	118	0.44	0.36	2.3	1.32	0.18	1.06	10.4	1.69	0.43	1.32	0.7794	2294	25	2612	18	+14
007-56.1		0.13	173	83	0.50	0.44	2.3	2.52	0.16	1.37	9.6	2.86	0.43	2.52	0.8786	2295	49	2491	23	+9
007-57.1		0.41	489	375	0.79	0.73	4.8	1.65	0.14	0.76	4.0	1.82	0.21	1.65	0.9076	1214	18	2219	13	+50
007-58.1		0.14	170	107	0.65	0.42	2.1	1.50	0.18	0.67	11.8	1.64	0.49	1.50	0.9123	2557	32	2609	11	+2
007-59.1		0.05	175	148	0.87	0.38	2.2	1.48	0.17	0.66	10.6	1.62	0.46	1.48	0.9136	2427	30	2533	11	+5
007-60.1		0.02	168	105	0.64	0.42	2.2	1.49	0.18	0.66	11.0	1.63	0.45	1.49	0.9145	2399	30	2622	11	+10
007-62.1		0.51	585	340	0.60	0.22	6.8	1.16	0.12	0.93	2.5	1.48	0.15	1.16	0.7819	885	10	1995	16	+59
007-63.1		0.03	182	165	0.93	0.37	2.5	1.47	0.17	0.69	9.3	1.62	0.39	1.47	0.9062	2139	27	2578	11	+20
007-64.1	C	0.51	66	63	0.99	0.66	2.2	2.18	0.16	1.45	10.0	2.62	0.45	2.18	0.8332	2399	44	2466	24	+3
007-64.2	R	0.60	197	94	0.49	1.12	4.8	3.86	0.15	1.36	4.4	4.10	0.21	3.86	0.9435	1218	43	2373	23	+53
007-65.1		0.59	95	80	0.86	0.52	2.3	1.80	0.18	1.09	10.7	2.10	0.43	1.80	0.8541	2306	35	2659	18	+16

DA13-008			Conc (ppm)				Radiogenic Ratios									Ages				
Spot Name	Type	%com ^{206}Pb	U	Th	$^{232}Th/^{38}U$	± (%)[1]	$^{238}U/^{206}Pb^*$	± (%)[1]	$^{207}Pb^*/^{206}Pb^*$	± (%)[1]	$^{207}Pb^*/^{235}U$	± (%)[1]	$^{206}Pb^*/^{238}U$	± (%)[1]	err corr	$^{206}Pb/^{238}U$	± 1σ	$^{207}Pb/^{206}Pb$	± 1σ	%Discordant
008-01.1		0.93	215	102	0.49	1.88	3.5	2.5	0.172	1.05	6.9	2.7	0.29	2.5	0.92	1638	36	2579	17	+41
008-02.1		0.38	65	65	1.02	0.60	2.3	2.1	0.167	1.27	9.9	2.4	0.43	2.1	0.85	2302	40	2532	21	+11
008-03.1		0.06	266	134	0.52	0.34	2.4	1.3	0.162	0.56	9.2	1.4	0.41	1.3	0.92	2218	25	2479	9	+12
008-04.1		0.08	341	160	0.48	0.31	2.4	1.8	0.180	0.48	10.3	1.9	0.42	1.8	0.97	2240	34	2652	8	+18
008-05.1		0.14	282	162	0.59	0.33	2.6	1.3	0.160	0.61	8.5	1.4	0.39	1.3	0.91	2108	24	2458	10	+17
008-06.1		-0.10	69	42	0.63	0.64	1.8	2.0	0.199	0.91	15.0	2.2	0.55	2.0	0.91	2812	45	2815	15	+0
008-07.1		0.66	369	137	0.38	0.29	5.2	1.2	0.156	0.86	4.2	1.5	0.19	1.2	0.82	1140	13	2414	15	+57
008-08.1		0.10	106	104	1.01	0.47	2.0	1.7	0.180	0.81	12.6	1.9	0.51	1.7	0.90	2650	37	2653	13	+0
008-09.1		0.29	236	140	0.61	0.34	3.7	1.4	0.142	0.86	5.2	1.6	0.27	1.4	0.84	1525	18	2253	15	+36
008-10.1		0.05	104	63	0.62	0.56	2.2	1.8	0.179	0.91	11.4	2.0	0.46	1.8	0.89	2440	36	2645	15	+9
008-11.1	C	0.03	103	92	0.92	0.49	1.9	1.7	0.185	0.77	13.4	1.9	0.53	1.7	0.91	2722	38	2701	13	-1
008-11.2	R	0.14	1379	59	0.04	0.40	7.8	1.5	0.111	0.57	2.0	1.6	0.13	1.5	0.94	780	11	1812	10	+60
008-12.1		0.57	422	498	1.22	0.50	5.4	1.5	0.150	1.19	3.9	1.9	0.19	1.5	0.79	1102	16	2351	20	+58
008-13.1		0.07	272	204	0.78	0.30	2.0	1.3	0.181	0.49	12.2	1.4	0.49	1.3	0.94	2564	28	2661	8	+4
008-14.1		0.09	254	183	0.74	0.32	2.2	1.3	0.166	0.55	10.3	1.4	0.45	1.3	0.92	2389	27	2523	9	+6
008-15.1		0.58	283	167	0.61	0.31	3.8	1.3	0.161	0.82	5.8	1.5	0.26	1.3	0.84	1489	17	2468	14	+44
008-16.1		0.28	318	96	0.31	0.36	4.3	1.3	0.141	0.81	4.5	1.5	0.23	1.3	0.84	1351	15	2244	14	+44
008-17.1		0.07	277	108	0.40	0.36	2.1	1.3	0.192	0.47	12.7	1.4	0.48	1.3	0.94	2516	27	2763	8	+11
008-18.1		0.29	102	41	0.41	0.59	1.9	1.7	0.188	0.82	13.9	1.9	0.54	1.7	0.90	2763	39	2724	13	-2
008-19.1		0.45	393	301	0.79	0.25	3.4	1.2	0.166	0.99	6.8	1.6	0.30	1.2	0.78	1676	18	2519	17	+38
008-20.1	C	0.30	87	61	0.73	0.55	1.9	1.8	0.195	0.87	14.5	2.0	0.54	1.8	0.90	2775	41	2784	14	+0
008-20.2	R	0.38	1565	23	0.02	0.62	12.2	1.7	0.057	1.36	0.6	2.2	0.08	1.7	0.77	506	8	510	30	+1
008-21.1		0.33	49	27	0.57	0.79	2.3	2.5	0.178	3.37	10.9	4.2	0.44	2.5	0.60	2368	50	2635	56	+12
008-22.1		-0.07	106	56	0.55	0.53	2.2	1.7	0.168	0.83	10.7	1.9	0.46	1.7	0.90	2443	35	2537	14	+4
008-23.1		0.22	87	64	0.76	0.54	2.2	1.8	0.169	0.99	10.7	2.1	0.46	1.8	0.88	2442	37	2544	17	+5
008-24.1		-0.02	158	59	0.38	0.48	2.0	1.5	0.183	0.62	12.6	1.6	0.50	1.5	0.92	2606	32	2681	10	+3
008-25.1		0.16	534	267	0.52	0.24	4.3	1.2	0.158	0.56	5.1	1.3	0.23	1.2	0.90	1350	14	2432	10	+49
008-26.1		0.33	174	98	0.58	0.42	2.7	1.5	0.158	0.87	8.1	1.7	0.37	1.5	0.86	2040	26	2436	15	+19
008-27.1		0.08	148	126	0.88	0.42	2.1	1.6	0.184	0.70	12.0	1.7	0.47	1.6	0.91	2489	32	2693	12	+9
008-28.1		0.01	341	195	0.59	0.29	2.3	1.3	0.164	0.47	9.9	1.3	0.44	1.3	0.94	2343	25	2495	8	+7
008-29.1		0.08	299	156	0.54	0.32	2.4	1.3	0.160	0.55	9.1	1.4	0.41	1.3	0.92	2232	24	2458	9	+11
008-30.1		-0.09	108	96	0.92	0.51	2.1	1.8	0.172	0.90	11.1	2.0	0.47	1.8	0.89	2482	36	2573	15	+4
008-31.1		-0.08	172	87	0.52	0.42	3.8	1.5	0.161	0.87	5.9	1.7	0.27	1.5	0.86	1521	20	2463	15	+43

DA13-008			Conc (ppm)				Radiogenic Ratios									Ages				
Spot Name	Type	%com ^{206}Pb	U	Th	$^{232}Th/^{38}U$	± (%)[1]	$^{238}U/^{206}Pb^*$	± (%)[1]	$^{207}Pb^*/^{206}Pb^*$	± (%)[1]	$^{207}Pb^*/^{235}U$	± (%)[1]	$^{206}Pb^*/^{238}U$	± (%)[1]	err corr	$^{206}Pb/^{238}U$	± 1σ	$^{207}Pb/^{206}Pb$	± 1σ	%Discordant
008-32.1		-0.02	196	146	0.77	0.37	2.3	1.4	0.165	0.63	9.8	1.6	0.43	1.4	0.91	2308	28	2504	11	+9
008-33.1		0.21	130	145	1.16	0.41	2.2	1.6	0.165	0.82	10.5	1.8	0.46	1.6	0.89	2448	33	2512	14	+3
008-34.1	C	0.06	120	99	0.85	0.45	2.2	1.6	0.169	0.77	10.7	1.8	0.46	1.6	0.90	2434	33	2547	13	+5
008-34.2	R	0.20	1956	70	0.04	0.76	11.3	1.0	0.058	0.84	0.7	1.3	0.09	1.0	0.78	548	6	529	18	-4
008-35.1	C	0.18	124	59	0.49	0.51	2.1	1.8	0.164	0.82	10.5	1.9	0.47	1.8	0.91	2464	36	2496	14	+2
008-36.1	R	0.18	619	177	0.30	0.26	3.7	1.1	0.145	0.47	5.5	1.2	0.27	1.1	0.92	1555	16	2293	8	+36
008-37.1	C	0.06	285	125	0.45	0.34	2.1	1.3	0.176	0.49	11.4	1.4	0.47	1.3	0.94	2480	27	2620	8	+6
008-37.2	R	0.42	2316	44	0.02	0.45	12.8	1.3	0.060	1.24	0.6	1.8	0.08	1.3	0.72	486	6	608	27	+21
008-38.1		0.21	52	34	0.66	0.73	2.0	2.2	0.195	1.18	13.4	2.5	0.50	2.2	0.88	2613	47	2781	19	+7
008-39.1		0.06	132	62	0.49	0.49	2.1	1.6	0.184	0.70	12.4	1.7	0.49	1.6	0.91	2553	33	2694	11	+6
008-40.1		0.04	157	163	1.07	0.37	2.0	1.5	0.177	0.63	12.0	1.6	0.49	1.5	0.92	2578	32	2628	10	+2
008-41.1		0.15	155	37	0.25	0.60	2.6	1.5	0.200	0.82	10.6	1.7	0.39	1.5	0.88	2108	28	2822	13	+30
008-42.1		0.15	91	69	0.78	0.52	2.0	1.8	0.183	0.85	12.5	2.0	0.50	1.8	0.90	2595	38	2684	14	+4
008-43.1	C	0.24	159	71	0.46	0.44	2.9	1.5	0.160	0.84	7.7	1.7	0.35	1.5	0.87	1916	24	2460	14	+26
008-43.2	R	0.16	2054	14	0.01	8.17	11.7	1.3	0.058	0.89	0.7	1.6	0.09	1.3	0.83	530	7	538	19	+2
008-44.1		0.25	168	133	0.82	0.39	3.1	1.5	0.157	1.98	7.0	2.5	0.32	1.5	0.60	1797	23	2425	34	+30
008-45.1		0.29	601	90	0.15	0.36	5.3	1.8	0.133	0.72	3.5	2.0	0.19	1.8	0.93	1112	19	2138	13	+52
008-46.1		0.41	660	100	0.16	1.83	7.7	1.1	0.109	1.54	2.0	1.9	0.13	1.1	0.60	787	9	1787	28	+59
008-47.1		-0.03	102	81	0.82	0.49	1.9	1.7	0.185	0.75	13.2	1.9	0.52	1.7	0.91	2687	37	2699	12	+1
008-48.1		0.23	194	176	0.93	0.35	2.2	1.4	0.168	0.69	10.4	1.6	0.45	1.4	0.90	2400	29	2537	12	+6
008-49.1		0.05	165	230	1.44	0.35	2.2	1.5	0.180	0.65	11.5	1.6	0.46	1.5	0.92	2443	30	2656	11	+10
008-50.1		0.02	197	139	0.73	0.36	2.2	1.4	0.166	0.60	10.2	1.5	0.45	1.4	0.92	2384	28	2513	10	+6

DA13-014			Conc (ppm)				Radiogenic Ratios									Ages				
Spot Name	Type	%com ^{206}Pb	U	Th	^{232}Th/^{38}U	± (%)[1]	^{238}U/^{206}Pb*	± (%)[1]	^{207}Pb*/^{206}Pb*	± (%)[1]	^{207}Pb*/^{235}U	± (%)[1]	^{206}Pb*/^{238}U	± (%)[1]	err corr	^{206}Pb/^{238}U	± 1σ	^{207}Pb/^{206}Pb	± 1σ	%Discordant
014-01.1		0.06	204	75	0.38	0.63	2.82	1.86	0.16	0.62	7.65	1.96	0.35	1.86	0.9483	1957	31	2417	11	+22
014-02.1		0.37	427	67	0.16	0.35	5.66	1.73	0.11	1.79	2.69	2.49	0.18	1.73	0.6953	1049	17	1805	33	+45
014-03.1		-0.03	197	75	0.39	0.39	2.38	1.86	0.16	0.96	9.56	2.10	0.42	1.86	0.8881	2263	36	2506	16	+11
014-04.1		-0.05	237	74	0.32	0.37	2.36	1.82	0.16	0.50	9.54	1.89	0.42	1.82	0.9641	2277	35	2490	8	+10
014-05.1		0.19	89	75	0.87	0.46	2.67	2.11	0.13	1.02	6.73	2.34	0.37	2.11	0.8994	2049	37	2104	18	+3
014-06.1		0.07	74	73	1.02	0.48	2.01	2.18	0.18	0.76	12.61	2.31	0.50	2.18	0.9439	2606	47	2686	13	+4
014-07.1		-0.04	144	74	0.53	0.41	2.34	1.94	0.16	0.64	9.45	2.04	0.43	1.94	0.9497	2293	37	2459	11	+8
014-08.1	C	-0.02	294	76	0.27	0.36	2.43	1.79	0.15	0.83	8.41	1.97	0.41	1.79	0.9062	2221	34	2328	14	+5
014-08.2	R	0.02	208	76	0.37	0.39	2.39	1.85	0.15	0.57	8.50	1.94	0.42	1.85	0.9563	2252	35	2317	10	+3
014-09.1		0.29	38	74	2.02	0.60	2.28	2.61	0.16	1.33	9.81	2.93	0.44	2.61	0.8915	2343	51	2481	22	+7
014-10.1		0.20	91	72	0.82	1.01	2.82	2.10	0.17	0.94	8.26	2.30	0.35	2.10	0.9134	1956	35	2548	16	+27
014-11.1		-0.04	220	74	0.35	0.38	2.15	1.84	0.17	1.00	10.70	2.09	0.46	1.84	0.8785	2461	38	2528	17	+3
014-12.1		0.06	162	74	0.48	0.40	1.96	1.90	0.19	0.99	13.17	2.15	0.51	1.90	0.8872	2655	41	2721	16	+3
014-13.1		0.00	223	75	0.35	0.75	1.97	1.83	0.19	0.48	13.30	1.89	0.51	1.83	0.9671	2645	40	2743	8	+4
014-14.1		0.30	310	74	0.25	1.21	4.38	1.79	0.13	1.53	4.18	2.36	0.23	1.79	0.7594	1325	21	2138	27	+42
014-15.1		0.00	37	81	2.23	0.65	2.18	2.69	0.20	1.20	12.41	2.95	0.46	2.69	0.9136	2430	55	2798	20	+16
014-17.1		0.20	367	74	0.21	0.84	4.15	1.76	0.14	0.68	4.59	1.89	0.24	1.76	0.9325	1390	22	2205	12	+41
014-18.1		0.22	518	73	0.15	2.36	4.74	1.72	0.15	0.55	4.33	1.80	0.21	1.72	0.9529	1234	19	2333	9	+52
014-19.1		0.14	360	74	0.21	0.58	3.72	1.76	0.12	0.67	4.30	1.88	0.27	1.76	0.9342	1535	24	1895	12	+21
014-21.1		-0.05	169	76	0.46	1.22	2.00	1.97	0.17	0.70	11.55	2.09	0.50	1.97	0.9421	2618	42	2531	12	-4
014-22.1		0.00	148	72	0.50	0.47	2.20	2.71	0.17	0.73	10.34	2.81	0.45	2.71	0.9656	2415	55	2509	12	+4
014-23.1		0.00	108	75	0.72	0.44	1.98	2.04	0.23	0.60	15.82	2.13	0.50	2.04	0.9588	2633	44	3034	10	+16
014-24.1		0.21	179	73	0.42	0.38	3.43	1.86	0.13	0.82	5.13	2.04	0.29	1.86	0.9161	1650	27	2065	14	+23
014-25.1		0.00	79	76	1.00	0.47	2.44	2.15	0.14	0.88	8.16	2.33	0.41	2.15	0.9251	2216	40	2279	15	+3
014-26.1		-0.06	428	73	0.18	0.86	7.19	1.73	0.11	1.20	2.12	2.11	0.14	1.73	0.8211	839	14	1810	22	+57
014-27.1		-0.03	248	74	0.31	0.60	2.66	1.80	0.16	0.49	8.23	1.86	0.38	1.80	0.9644	2054	32	2446	8	+19
014-28.1		-0.03	250	74	0.31	0.59	3.22	2.15	0.12	0.62	5.21	2.24	0.31	2.15	0.9607	1743	33	1982	11	+14
014-29.1		0.02	419	72	0.18	0.75	3.27	1.73	0.15	0.45	6.32	1.79	0.31	1.73	0.9679	1718	26	2347	8	+30
014-30.1		0.04	73	76	1.08	0.48	2.10	2.18	0.17	1.65	11.18	2.74	0.48	2.18	0.7973	2506	45	2564	28	+3
014-31.1		-0.05	197	76	0.40	0.38	2.41	1.85	0.16	0.57	9.20	1.94	0.41	1.85	0.9565	2235	35	2467	10	+11
014-32.1		0.25	899	70	0.08	1.05	8.12	1.76	0.08	0.84	1.37	1.95	0.12	1.76	0.9029	749	12	1220	16	+41
014-33.1		-0.06	261	76	0.30	0.69	2.87	1.79	0.13	0.56	6.38	1.88	0.35	1.79	0.9548	1930	30	2133	10	+11
014-34.1		0.07	225	64	0.30	2.77	2.02	1.97	0.18	1.69	12.18	2.60	0.50	1.97	0.7578	2598	42	2634	28	+2

DA13-014			Conc (ppm)				Radiogenic Ratios									Ages				
Spot Name	Type	%com ^{206}Pb	U	Th	^{232}Th/^{2} ^{38}U	± (%)[1]	^{238}U/ ^{206}Pb*	± (%)[1]	^{207}Pb*/ ^{206}Pb*	± (%)[1]	^{207}Pb*/ ^{235}U	± (%)[1]	^{206}Pb*/ ^{238}U	± (%)[1]	err corr	^{206}Pb/ ^{238}U	± 1σ	^{207}Pb/ ^{206}Pb	± 1σ	%Discordant
014-35.1		0.02	195	77	0.41	0.38	2.23	1.85	0.16	0.53	10.14	1.93	0.45	1.85	0.9610	2389	37	2497	9	+5
014-36.1		0.05	202	58	0.30	0.73	1.97	2.07	0.18	0.90	12.76	2.26	0.51	2.07	0.9176	2642	45	2677	15	+2
014-37.1		0.05	103	76	0.77	0.43	1.99	2.03	0.19	1.04	12.86	2.28	0.50	2.03	0.8900	2626	44	2703	17	+3
014-38.1		-0.03	250	76	0.31	0.71	3.28	1.80	0.15	0.58	6.43	1.89	0.31	1.80	0.9518	1716	27	2379	10	+32
014-39.1		0.11	171	76	0.46	0.38	2.45	1.88	0.16	1.57	9.14	2.45	0.41	1.88	0.7678	2209	35	2479	26	+13
014-40.1		-0.02	345	73	0.22	0.34	3.17	1.75	0.15	0.47	6.63	1.81	0.32	1.75	0.9651	1766	27	2375	8	+29
014-41.1	C	-0.38	27	73	2.76	0.68	2.14	2.88	0.17	1.48	11.06	3.24	0.47	2.88	0.8890	2472	59	2574	25	+5
014-41.2	R	0.15	18	74	4.22	0.81	2.25	3.31	0.17	1.78	10.15	3.76	0.44	3.31	0.8806	2371	66	2514	30	+7
014-42.1		0.22	252	73	0.30	0.35	3.02	2.35	0.16	0.63	7.15	2.43	0.33	2.35	0.9654	1845	38	2417	11	+27
014-43.1		-0.01	186	74	0.41	0.37	2.27	1.85	0.16	0.51	9.98	1.92	0.44	1.85	0.9634	2351	36	2503	9	+7
014-44.1	C	-0.01	193	75	0.40	0.37	2.30	1.84	0.16	0.52	9.80	1.91	0.43	1.84	0.9626	2327	36	2493	9	+8
014-44.2	R	0.02	622	72	0.12	0.55	10.74	1.98	0.07	0.90	0.88	2.18	0.09	1.98	0.9105	574	11	875	19	+36
014-45.1		0.00	233	75	0.33	0.36	2.56	1.80	0.14	0.53	7.37	1.88	0.39	1.80	0.9601	2125	33	2189	9	+3
014-46.1		0.03	1378	73	0.05	0.32	11.52	1.83	0.06	0.75	0.70	1.97	0.09	1.83	0.9245	537	9	538	16	+0
014-47.1		0.01	235	74	0.33	0.88	2.13	1.82	0.19	0.43	12.00	1.87	0.47	1.82	0.9736	2482	38	2701	7	+10
014-48.1		0.04	657	74	0.12	0.91	3.15	2.88	0.12	2.29	5.11	3.68	0.32	2.88	0.7825	1779	45	1904	41	+7
014-49.1		-0.02	136	72	0.54	0.39	2.21	1.91	0.17	0.57	10.40	1.99	0.45	1.91	0.9580	2409	38	2522	10	+5
014-50.1		-0.05	183	74	0.42	0.37	2.63	1.85	0.13	0.61	6.84	1.95	0.38	1.85	0.9490	2075	33	2107	11	+2
014-51.1		0.31	343	70	0.21	0.38	3.71	1.74	0.16	0.55	6.02	1.83	0.27	1.74	0.9541	1538	24	2478	9	+43
014-52.1		0.03	195	74	0.39	0.36	2.18	1.83	0.16	0.49	10.34	1.90	0.46	1.83	0.9657	2432	37	2493	8	+3
014-53.1		0.04	210	74	0.36	0.36	2.16	1.82	0.16	1.03	10.47	2.09	0.46	1.82	0.8711	2451	37	2499	17	+2
014-54.1		0.15	72	74	1.07	0.47	2.26	2.15	0.16	0.89	9.89	2.33	0.44	2.15	0.9247	2364	43	2476	15	+5
014-55.1		0.00	89	73	0.84	0.44	2.18	2.05	0.16	0.71	10.35	2.17	0.46	2.05	0.9445	2432	42	2495	12	+3
014-56.1		0.22	118	79	0.69	0.47	3.06	1.62	0.11	1.23	5.11	2.03	0.33	1.62	0.7960	1825	26	1853	22	+2
014-57.1		0.08	329	145	0.45	0.53	2.39	1.26	0.21	0.45	12.06	1.33	0.42	1.26	0.9425	2255	24	2897	7	+26
014-58.1	C	-0.11	95	102	1.11	0.48	1.92	1.74	0.18	0.81	13.17	1.92	0.52	1.74	0.9066	2707	39	2680	13	-1
014-58.2	R	0.23	93	75	0.83	0.50	2.34	1.70	0.18	0.98	10.39	1.96	0.43	1.70	0.8674	2293	33	2618	16	+15
014-59.1		0.10	316	123	0.40	0.35	2.42	1.29	0.16	0.52	8.99	1.39	0.41	1.29	0.9281	2229	24	2434	9	+10
014-60.1		0.13	1584	102	0.07	0.29	11.52	1.06	0.06	0.90	0.70	1.39	0.09	1.06	0.7632	537	5	563	20	+5
014-61.1		0.11	546	159	0.30	0.27	3.47	1.16	0.16	0.46	6.46	1.25	0.29	1.16	0.9284	1632	17	2483	8	+39
014-62.1		0.15	81	108	1.39	0.50	2.34	1.84	0.15	1.10	8.70	2.14	0.43	1.84	0.8582	2292	35	2320	19	+1
014-63.1		0.12	184	113	0.63	0.38	1.68	1.42	0.22	0.49	18.31	1.50	0.59	1.42	0.9452	3008	34	3005	8	-0

DA13-014			Conc (ppm)				Radiogenic Ratios									Ages				
Spot Name	Type	%com ^{206}Pb	U	Th	$^{232}Th/^{38}U$	± (%)[1]	$^{238}U/^{206}Pb^*$	± (%)[1]	$^{207}Pb^*/^{206}Pb^*$	± (%)[1]	$^{207}Pb^*/^{235}U$	± (%)[1]	$^{206}Pb^*/^{238}U$	± (%)[1]	err corr	$^{206}Pb/^{238}U$	± 1σ	$^{207}Pb/^{206}Pb$	± 1σ	%Discordant
014-64.1	C	0.04	778	222	0.29	0.50	5.85	1.14	0.12	0.56	2.75	1.27	0.17	1.14	0.8975	1017	11	1906	10	+50
014-64.2	R	0.41	444	42	0.10	0.50	6.57	1.28	0.09	2.13	1.85	2.48	0.15	1.28	0.5158	913	11	1389	41	+37
014-65.1		0.00	146	126	0.89	0.39	3.08	1.50	0.11	0.90	5.11	1.75	0.33	1.50	0.8579	1814	24	1865	16	+3
014-66.1		0.04	191	164	0.89	0.34	2.24	2.26	0.17	0.60	10.26	2.34	0.45	2.26	0.9664	2381	45	2523	10	+7
014-67.1	C	0.14	97	44	0.47	0.57	1.94	1.71	0.19	0.80	13.37	1.89	0.51	1.71	0.9061	2677	37	2727	13	+2
014-67.2	R	0.62	1633	148	0.09	0.77	10.91	1.54	0.07	1.36	0.86	2.05	0.09	1.54	0.7493	565	8	865	28	+36
014-68.1		0.27	1619	182	0.12	0.73	10.03	1.18	0.07	1.18	0.94	1.67	0.10	1.18	0.7077	613	7	877	24	+32
014-69.1		0.18	554	235	0.44	0.24	5.79	1.15	0.12	0.73	2.79	1.37	0.17	1.15	0.8432	1027	11	1913	13	+50
014-70.1		0.30	469	424	0.93	4.04	3.19	1.64	0.14	0.57	6.23	1.74	0.31	1.64	0.9448	1758	25	2277	10	+26
014-71.1		0.10	229	160	0.72	0.33	2.39	1.34	0.16	0.59	9.42	1.47	0.42	1.34	0.9160	2253	26	2491	10	+11
014-72.1		0.23	439	151	0.36	0.55	3.37	1.24	0.16	0.57	6.63	1.37	0.30	1.24	0.9091	1674	18	2479	10	+37
014-73.1		0.23	151	74	0.50	0.45	2.04	1.51	0.16	0.72	11.12	1.67	0.49	1.51	0.9014	2570	32	2504	12	-3
014-74.1		0.16	403	126	0.32	0.31	2.93	1.77	0.17	0.52	7.87	1.84	0.34	1.77	0.9595	1893	29	2530	9	+29
014-75.1		0.30	266	127	0.49	0.56	3.42	1.32	0.12	0.89	4.88	1.59	0.29	1.32	0.8285	1655	19	1971	16	+18
014-76.1		0.27	168	218	1.34	0.34	2.41	1.45	0.16	0.77	9.19	1.65	0.41	1.45	0.8825	2238	27	2462	13	+11
014-77.1	C	0.15	139	245	1.82	0.35	2.59	1.51	0.16	0.81	8.35	1.72	0.39	1.51	0.8803	2104	27	2423	14	+15
014-77.2	R	0.42	1434	114	0.08	0.48	11.21	1.08	0.06	1.46	0.72	1.82	0.09	1.08	0.5925	551	6	547	32	-1
014-78.1		0.23	130	71	0.56	0.48	2.27	1.57	0.17	0.86	10.08	1.79	0.44	1.57	0.8783	2353	31	2517	14	+8
014-79.1	C	0.52	90	34	0.39	0.67	2.88	1.85	0.16	1.36	7.88	2.30	0.35	1.85	0.8056	1920	31	2504	23	+27
014-79.2	R	0.50	1420	121	0.09	0.28	11.20	1.07	0.06	1.41	0.73	1.77	0.09	1.07	0.6037	551	6	589	31	+7
014-80.1		0.03	142	86	0.62	0.44	2.43	1.52	0.18	0.72	10.01	1.68	0.41	1.52	0.9049	2222	29	2619	12	+18
014-81.1	C	-0.03	201	161	0.83	0.35	1.87	1.40	0.19	0.53	13.81	1.50	0.53	1.40	0.9343	2756	31	2723	9	-1
014-81.2	R	0.01	1474	14	0.01	0.81	11.15	1.78	0.06	0.80	0.72	1.95	0.09	1.78	0.9128	554	9	547	17	-1
014-82.1		0.18	92	75	0.84	0.52	3.00	1.79	0.11	1.38	5.16	2.26	0.33	1.79	0.7918	1855	29	1836	25	-1
014-83.1		0.29	125	55	0.46	0.52	2.09	1.62	0.16	0.88	10.70	1.85	0.48	1.62	0.8780	2519	34	2480	15	-2
014-85.1		0.14	211	113	0.55	0.38	2.33	1.39	0.16	0.64	9.67	1.53	0.43	1.39	0.9096	2301	27	2491	11	+9

DA13-019			Conc (ppm)				Radiogenic Ratios									Ages				
Spot Name	Type	%com ^{206}Pb	U	Th	$^{232}Th/^{38}U$	± (%)[1]	$^{238}U/^{206}Pb^*$	± (%)[1]	$^{207}Pb^*/^{206}Pb^*$	± (%)[1]	$^{207}Pb^*/^{235}U$	± (%)[1]	$^{206}Pb^*/^{238}U$	± (%)[1]	err corr	$^{206}Pb/^{238}U$	± 1σ	$^{207}Pb/^{206}Pb$	± 1σ	%Discordant
019-01.1		0.06	403	73	0.19	0.30	4.23	2.07	0.13	0.51	4.19	2.13	0.24	2.07	0.9711	1368	26	2076	9	+38
019-02.1		-0.01	311	71	0.24	0.32	2.69	2.31	0.16	0.42	8.02	2.35	0.37	2.31	0.9836	2036	40	2419	7	+18
019-03.1		0.31	286	72	0.26	0.59	2.19	1.74	0.19	0.40	12.08	1.79	0.46	1.74	0.9740	2427	35	2757	7	+14
019-04.1		0.02	472	74	0.16	0.30	4.00	1.70	0.14	0.44	4.72	1.76	0.25	1.70	0.9686	1437	22	2191	8	+38
019-05.1		2.01	326	64	0.20	0.94	3.69	2.17	0.16	1.53	6.07	2.66	0.27	2.17	0.8172	1547	30	2481	26	+42
019-06.1		0.33	199	68	0.35	0.38	3.92	1.80	0.13	1.18	4.65	2.15	0.26	1.80	0.8352	1466	24	2126	21	+35
019-07.1		0.30	257	69	0.28	0.37	2.85	1.76	0.21	0.47	9.94	1.83	0.35	1.76	0.9663	1940	30	2868	8	+37
019-08.1		0.43	217	70	0.33	0.39	3.97	1.84	0.14	0.84	4.86	2.02	0.25	1.84	0.9106	1449	24	2225	14	+39
019-10.1		0.04	314	82	0.27	1.18	3.25	1.83	0.15	1.27	6.22	2.23	0.31	1.83	0.8218	1731	28	2304	22	+28
019-13.1		0.00	856	50	0.06	3.92	3.35	4.47	0.11	4.06	4.68	6.04	0.30	4.47	0.7397	1684	66	1858	73	+11
019-14.1		0.06	198	99	0.51	0.64	2.00	2.23	0.17	1.02	11.46	2.46	0.50	2.23	0.9088	2619	48	2516	17	-5
019-17.1		0.03	297	73	0.25	0.33	2.54	1.76	0.18	0.41	9.94	1.81	0.39	1.76	0.9745	2143	32	2678	7	+23
019-18.1		1.35	796	70	0.09	0.65	8.60	1.98	0.08	1.72	1.25	2.62	0.12	1.98	0.7558	709	13	1153	34	+41
019-19.1		0.24	698	73	0.11	0.65	6.75	1.97	0.09	0.74	1.89	2.11	0.15	1.97	0.9366	891	16	1477	14	+42
019-20.1		1.76	443	65	0.15	0.39	5.15	1.76	0.11	1.61	3.07	2.38	0.19	1.76	0.7379	1144	18	1878	29	+43
019-21.1		0.14	113	74	0.68	0.40	3.31	2.67	0.12	1.00	4.84	2.84	0.30	2.67	0.9368	1702	40	1899	18	+12
019-22.1		0.07	317	73	0.24	0.90	4.71	2.01	0.10	0.70	3.07	2.13	0.21	2.01	0.9443	1241	23	1710	13	+30
019-23.1		0.02	430	72	0.17	1.06	4.81	1.72	0.11	0.55	3.13	1.80	0.21	1.72	0.9517	1218	19	1785	10	+35
019-24.1		0.07	123	73	0.61	0.39	2.84	3.08	0.14	3.55	6.90	4.70	0.35	3.08	0.6552	1946	52	2252	61	+16
019-25.1	C	0.04	287	72	0.26	1.43	5.32	3.22	0.12	0.77	3.09	3.31	0.19	3.22	0.9723	1110	33	1948	14	+47
019-25.2	R	0.18	691	71	0.11	0.97	9.20	1.69	0.07	0.94	1.09	1.93	0.11	1.69	0.8734	665	11	1007	19	+36
019-26.1		2.93	286	72	0.26	1.22	6.69	2.37	0.13	2.66	2.71	3.56	0.15	2.37	0.6656	898	20	2118	47	+62
019-27.1		1.95	431	69	0.17	0.34	5.71	1.90	0.10	1.56	2.53	2.46	0.18	1.90	0.7730	1040	18	1710	29	+42
019-28.1		0.00	143	76	0.55	0.40	3.24	1.93	0.11	0.82	4.86	2.10	0.31	1.93	0.9202	1735	29	1867	15	+8
019-29.1		15.53	487	65	0.14	0.71	8.70	3.02	0.08	6.22	1.32	6.92	0.11	3.02	0.4365	701	20	1274	121	+47
019-30.1		2.12	591	74	0.13	3.27	7.15	2.37	0.09	5.50	1.69	5.99	0.14	2.37	0.3964	843	19	1372	106	+41
019-31.1		0.08	70	77	1.14	0.50	2.11	2.23	0.16	0.91	10.68	2.41	0.47	2.23	0.9257	2504	46	2490	15	-1
019-33.1		3.45	322	68	0.22	0.35	5.25	1.78	0.10	2.28	2.65	2.90	0.19	1.78	0.6149	1124	18	1640	42	+34
019-34.1		-0.01	424	71	0.17	0.60	3.71	1.73	0.14	0.46	5.33	1.79	0.27	1.73	0.9658	1538	24	2268	8	+36
019-35.1		0.00	55	77	1.44	0.54	2.79	2.36	0.14	1.29	6.73	2.69	0.36	2.36	0.8773	1976	40	2177	22	+11
019-36.1		0.16	119	65	0.57	0.41	3.66	2.05	0.15	0.88	5.60	2.23	0.27	2.05	0.9187	1559	28	2327	15	+37
019-38.1		0.18	362	74	0.21	0.34	3.39	1.75	0.15	0.53	5.93	1.83	0.29	1.75	0.9567	1665	26	2298	9	+31
019-39.1		0.23	284	73	0.27	0.82	8.88	1.79	0.09	1.33	1.40	2.23	0.11	1.79	0.8039	688	12	1433	25	+55

DA13-019			Conc (ppm)				Radiogenic Ratios									Ages				
Spot Name	Type	%com ^{206}Pb	U	Th	^{232}Th/^{238}U[2]	± (%)[1]	^{238}U/^{206}Pb*	± (%)[1]	^{207}Pb*/^{206}Pb*	± (%)[1]	^{207}Pb*/^{235}U	± (%)[1]	^{206}Pb*/^{238}U	± (%)[1]	err corr	^{206}Pb/^{238}U	± 1σ	^{207}Pb/^{206}Pb	± 1σ	%Discordant
019-40.1		4.30	786	65	0.09	0.94	11.28	1.73	0.08	4.33	0.95	4.66	0.09	1.73	0.3719	548	9	1149	86	+55
019-41.1		0.45	790	68	0.09	0.72	8.05	1.71	0.07	3.22	1.27	3.65	0.12	1.71	0.4685	755	12	1038	65	+29
019-42.1		0.12	332	71	0.22	0.43	2.69	1.78	0.18	0.48	9.14	1.84	0.37	1.78	0.9656	2038	31	2636	8	+26
019-43.1		1.24	355	74	0.21	0.80	6.43	2.24	0.10	2.32	2.16	3.22	0.16	2.24	0.6951	931	19	1637	43	+46
019-44.1	C	-0.02	305	77	0.26	0.39	2.85	1.81	0.15	0.56	7.32	1.89	0.35	1.81	0.9556	1941	30	2357	10	+20
019-44.2	R	-0.05	78	74	0.98	0.53	2.48	2.25	0.19	1.77	10.51	2.86	0.40	2.25	0.7873	2182	42	2736	29	+24
019-45.1		0.03	163	75	0.48	0.39	1.75	1.90	0.23	0.83	18.37	2.07	0.57	1.90	0.9170	2908	44	3078	13	+7
019-46.1		-0.06	268	69	0.26	0.82	3.45	1.80	0.15	0.55	6.13	1.88	0.29	1.80	0.9563	1640	26	2385	9	+35
019-48.1		0.00	599	163	0.28	1.52	2.12	3.39	0.16	2.37	10.25	4.14	0.47	3.39	0.8203	2489	70	2431	40	-3
019-49.1		0.51	216	68	0.32	0.56	3.38	2.08	0.16	1.03	6.61	2.32	0.30	2.08	0.8958	1672	31	2476	17	+37
019-50.1		0.13	358	79	0.23	0.71	5.98	1.77	0.10	0.95	2.29	2.01	0.17	1.77	0.8799	998	16	1607	18	+41
019-51.1		0.42	978	72	0.08	0.33	9.09	1.67	0.07	1.10	1.07	2.00	0.11	1.67	0.8360	673	11	949	22	+31
019-52.1		3.72	758	69	0.09	2.94	8.59	2.77	0.09	2.51	1.47	3.74	0.12	2.77	0.7409	710	19	1463	48	+54
019-53.1		0.72	308	73	0.25	0.36	4.61	1.78	0.11	1.13	3.34	2.11	0.22	1.78	0.8438	1265	20	1829	21	+34
019-54.1		0.83	523	70	0.14	0.32	5.23	1.99	0.11	1.95	2.81	2.78	0.19	1.99	0.7145	1129	21	1740	36	+38
019-55.1		-0.06	152	74	0.50	0.38	2.79	1.89	0.13	0.69	6.28	2.01	0.36	1.89	0.9391	1977	32	2055	12	+4
019-56.1		0.07	525	72	0.14	0.32	5.36	1.70	0.10	0.62	2.48	1.81	0.19	1.70	0.9397	1103	17	1556	12	+32
019-57.1		0.19	339	74	0.23	0.73	3.06	1.75	0.16	1.08	7.33	2.05	0.33	1.75	0.8516	1823	28	2483	18	+30
019-58.1		0.12	620	71	0.12	1.20	7.68	1.69	0.08	0.79	1.43	1.87	0.13	1.69	0.9053	789	13	1192	16	+36
019-60.1		-0.05	345	73	0.22	1.22	6.83	2.36	0.10	1.52	2.06	2.81	0.15	2.36	0.8410	881	19	1664	28	+50
019-61.1		0.50	765	324	0.44	0.21	5.87	1.12	0.10	0.90	2.31	1.44	0.17	1.12	0.7798	1015	11	1592	17	+39
019-62.1		0.29	1840	126	0.07	0.27	10.30	1.05	0.06	0.92	0.83	1.40	0.10	1.05	0.7516	597	6	677	20	+12
019-63.1		1.88	308	56	0.19	0.80	3.42	1.30	0.12	1.54	4.65	2.01	0.29	1.30	0.6459	1653	19	1885	28	+14
019-64.1		0.61	271	117	0.45	0.36	2.58	1.33	0.16	0.79	8.56	1.54	0.39	1.33	0.8598	2111	24	2457	13	+17
019-65.1		3.04	438	242	0.57	0.60	4.59	2.87	0.16	3.05	4.66	4.19	0.22	2.87	0.6857	1270	33	2406	52	+52
019-66.1		0.05	289	80	0.29	0.39	2.60	1.29	0.17	0.54	8.92	1.40	0.39	1.29	0.9234	2101	23	2537	9	+20
019-67.1		0.34	186	93	0.52	0.40	3.52	1.42	0.11	1.11	4.39	1.81	0.28	1.42	0.7868	1614	20	1830	20	+13
019-68.1		0.56	824	476	0.60	0.18	7.19	1.11	0.10	0.98	1.90	1.48	0.14	1.11	0.7515	840	9	1602	18	+51
019-69.1		0.12	310	77	0.26	0.40	7.31	1.85	0.09	2.13	1.73	2.82	0.14	1.85	0.6565	827	14	1461	40	+46
019-70.1		0.26	862	178	0.21	0.25	6.73	1.11	0.08	1.51	1.71	1.87	0.15	1.11	0.5923	893	9	1285	29	+33
019-71.1		1.43	372	48	0.13	0.49	8.02	2.10	0.18	2.11	3.08	2.97	0.12	2.10	0.7052	757	15	2643	35	+75
019-72.1		0.10	303	149	0.51	0.32	2.88	1.29	0.12	0.65	5.97	1.44	0.35	1.29	0.8929	1924	21	2023	11	+6
019-73.1		1.09	516	215	0.43	0.50	5.93	1.18	0.10	1.51	2.33	1.92	0.17	1.18	0.6163	1005	11	1628	28	+41
019-74.1		0.02	198	203	1.06	0.34	2.35	1.42	0.16	0.65	9.31	1.56	0.43	1.42	0.9096	2289	27	2439	11	+7

DA13-019

Spot Name	Type	%com ^{206}Pb	Conc (ppm) U	Th	$^{232}Th/^{238}U$	± (%)[1]	Radiogenic Ratios $^{238}U/^{206}Pb^*$	± (%)[1]	$^{207}Pb^*/^{206}Pb^*$	± (%)[1]	$^{207}Pb^*/^{235}U$	± (%)[1]	$^{206}Pb^*/^{238}U$	± (%)[1]	err corr	Ages $^{206}Pb/^{238}U$	± 1σ	$^{207}Pb/^{206}Pb$	± 1σ	%Discordant
019-75.1		0.12	1796	100	0.06	0.54	11.13	1.05	0.06	0.81	0.73	1.33	0.09	1.05	0.7920	555	6	565	18	+2
019-76.1		0.00	316	231	0.75	0.32	3.10	1.27	0.15	0.59	6.47	1.40	0.32	1.27	0.9079	1801	20	2294	10	+25
019-77.1		1.62	765	146	0.20	1.02	7.78	1.14	0.11	1.56	1.88	1.93	0.13	1.14	0.5875	779	8	1736	29	+58
019-78.1		2.02	589	242	0.42	0.46	4.96	1.29	0.11	2.95	2.95	3.22	0.20	1.29	0.3999	1184	14	1733	54	+35
019-79.1		3.21	575	162	0.29	0.55	6.28	1.18	0.12	1.83	2.66	2.18	0.16	1.18	0.5424	953	10	1972	33	+55
019-80.1		0.33	1629	207	0.13	0.63	9.64	2.25	0.07	2.59	1.01	3.43	0.10	2.25	0.6557	636	14	954	53	+35
019-81.1		4.07	1121	314	0.29	0.19	8.27	1.13	0.09	2.41	1.54	2.66	0.12	1.13	0.4245	736	8	1471	46	+53
019-82.1		0.81	933	413	0.46	0.22	7.16	1.14	0.10	1.14	1.91	1.61	0.14	1.14	0.7061	842	9	1607	21	+51
019-83.1		0.13	665	347	0.54	0.21	5.18	1.14	0.11	0.67	2.81	1.32	0.19	1.14	0.8606	1138	12	1727	12	+37
019-84.1		0.28	409	206	0.52	0.28	4.07	1.23	0.11	0.89	3.62	1.51	0.25	1.23	0.8105	1416	16	1746	16	+21
019-85.1		0.27	713	160	0.23	0.27	5.84	1.13	0.10	0.81	2.42	1.39	0.17	1.13	0.8116	1019	11	1668	15	+42

C = core; R = rim; * Radiogenic Pb only [1] All errors are 1σ

DA13-087			Conc (ppm)				Radiogenic Ratios									Ages				
Spot Name	Type	%com ^{206}Pb	U	Th	^{232}Th/^{238}U	± (%)[1]	^{238}U/^{206}Pb*	± (%)[1]	^{207}Pb*/^{206}Pb*	± (%)[1]	^{207}Pb*/^{235}U	± (%)[1]	^{206}Pb*/^{238}U	± (%)[1]	err corr	^{206}Pb/^{238}U	± 1σ	^{207}Pb/^{206}Pb	± 1σ	%Discordant
087-01.1		0.000	186	73.7	0.41	0.81	4.25	1.84	0.14	1.68	4.53	2.49	0.24	1.84	0.7398	1361	23	2224	29	+43
087-02.1		0.000	434	71.7	0.17	1.39	8.97	1.87	0.09	0.80	1.36	2.04	0.11	1.87	0.9199	682	12	1392	15	+54
087-03.1		0.000	484	72.3	0.15	0.91	11.66	1.95	0.06	1.05	0.69	2.22	0.09	1.95	0.8804	531	10	549	23	+4
087-06.1		0.018	353	74.2	0.22	0.33	2.68	1.74	0.16	0.73	8.32	1.89	0.37	1.74	0.9230	2043	30	2475	12	+20
087-07.1		-0.071	186	71.1	0.40	0.40	2.88	2.25	0.16	1.24	7.65	2.57	0.35	2.25	0.8764	1920	37	2455	21	+25
087-08.1		0.544	401	73.3	0.19	1.09	11.87	2.01	0.06	2.35	0.65	3.09	0.08	2.01	0.6512	521	10	467	52	-12
087-09.1		0.000	209	73.4	0.36	1.58	5.56	1.82	0.12	1.37	3.09	2.28	0.18	1.82	0.7998	1065	18	2026	24	+51
087-10.1		-0.103	339	72.8	0.22	1.58	9.68	3.20	0.08	2.60	1.14	4.12	0.10	3.20	0.7765	634	19	1202	51	+50
087-11.1		-0.019	228	71.8	0.33	1.40	3.81	2.14	0.15	0.61	5.39	2.23	0.26	2.14	0.9621	1503	29	2331	10	+40
087-12.1		-0.135	310	73.0	0.24	0.79	11.91	1.99	0.06	1.69	0.69	2.61	0.08	1.99	0.7620	520	10	592	37	+13
087-13.1		0.057	350	73.8	0.22	0.38	5.32	1.76	0.13	0.68	3.24	1.88	0.19	1.76	0.9335	1109	18	2029	12	+49
087-14.1		0.063	432	73.1	0.18	0.77	11.30	2.01	0.06	1.28	0.73	2.38	0.09	2.01	0.8445	547	11	598	28	+9
087-16.1		-0.035	393	72.0	0.19	0.78	11.82	1.73	0.06	1.25	0.71	2.13	0.08	1.73	0.8105	524	9	631	27	+18
087-17.1		0.020	352	72.4	0.21	0.33	5.69	1.77	0.12	1.39	3.00	2.25	0.18	1.77	0.7882	1044	17	2013	25	+52
087-18.1		0.064	218	72.8	0.34	0.82	11.95	1.81	0.06	1.88	0.65	2.61	0.08	1.81	0.6948	518	9	469	42	-11
087-19.1		0.106	272	73.8	0.28	1.67	4.43	1.78	0.14	0.70	4.33	1.92	0.23	1.78	0.9308	1313	21	2216	12	+45
087-20.1		-0.036	178	76.3	0.44	0.38	2.28	1.86	0.17	0.58	10.06	1.95	0.44	1.86	0.9553	2341	37	2524	10	+9
087-21.1		0.020	181	72.7	0.42	0.88	3.25	1.88	0.17	0.60	7.14	1.97	0.31	1.88	0.9526	1730	29	2541	10	+36
087-22.1		0.195	299	73.8	0.25	0.65	11.50	2.32	0.06	2.03	0.67	3.08	0.09	2.32	0.7522	538	12	452	45	-20
087-23.1		0.251	268	73.7	0.28	0.34	11.63	1.78	0.06	3.49	0.66	3.91	0.09	1.78	0.4554	532	9	444	78	-21
087-24.1		0.081	614	73.3	0.12	1.41	8.90	2.00	0.09	1.92	1.40	2.78	0.11	2.00	0.7208	686	13	1428	37	+55
087-25.1		-0.048	300	72.0	0.25	0.34	4.28	2.21	0.14	1.84	4.52	2.87	0.23	2.21	0.7683	1354	27	2231	32	+43
087-26.1		-0.017	211	72.8	0.36	0.36	3.02	2.90	0.18	0.54	8.14	2.95	0.33	2.90	0.9829	1842	47	2639	9	+35
087-27.1		-0.130	263	74.0	0.29	0.35	9.30	2.10	0.08	1.32	1.25	2.48	0.11	2.10	0.8470	659	13	1301	26	+52
087-28.1		-0.087	409	71.7	0.18	1.07	11.06	1.72	0.06	1.28	0.73	2.15	0.09	1.72	0.8027	558	9	537	28	-4
087-29.1		-0.291	187	75.0	0.41	0.63	11.74	2.23	0.06	2.51	0.73	3.36	0.09	2.23	0.6641	527	11	668	54	+22
087-30.1	C	0.17	481	158	0.34	0.29	11.46	1.19	0.06	1.76	0.70	2.13	0.09	1.19	0.5619	539	6	538	38	-0
087-30.2	R	0.07	330	80	0.25	0.40	11.39	1.28	0.06	1.88	0.72	2.28	0.09	1.28	0.5632	543	7	581	41	+7
087-31.1		0.00	475	90	0.20	0.36	6.06	1.19	0.12	0.71	2.84	1.39	0.17	1.19	0.8598	985	11	2028	13	+55
087-32.1		0.11	340	155	0.47	0.31	4.28	1.68	0.15	0.71	4.67	1.83	0.23	1.68	0.9211	1352	21	2290	12	+45
087-33.1		0.15	323	53	0.17	0.76	3.83	1.68	0.17	0.67	6.01	1.81	0.26	1.68	0.9291	1495	22	2528	11	+46
087-34.1	C	0.14	593	127	0.22	0.37	8.74	1.22	0.08	1.58	1.24	2.00	0.11	1.22	0.6117	698	8	1167	31	+42
087-34.2	R	0.22	499	67	0.14	0.81	11.36	1.88	0.06	1.98	0.69	2.73	0.09	1.88	0.6886	544	10	490	44	-12
087-35.1		0.82	258	97	0.39	0.38	3.36	1.35	0.18	0.86	7.45	1.60	0.30	1.35	0.8418	1679	20	2669	14	+42
087-36.1	C	-0.10	114	63	0.58	0.53	3.02	1.69	0.16	1.03	7.25	1.98	0.33	1.69	0.8538	1842	27	2446	17	+28

DA13-087			Conc (ppm)				Radiogenic Ratios									Ages				
Spot Name	Type	%com ^{206}Pb	U	Th	^{232}Th/^{238}U	± (%)[1]	^{238}U/^{206}Pb*	± (%)[1]	^{207}Pb*/^{206}Pb*	± (%)[1]	^{207}Pb*/^{235}U	± (%)[1]	^{206}Pb*/^{238}U	± (%)[1]	err corr	^{206}Pb/^{238}U	± 1σ	^{207}Pb/^{206}Pb	± 1σ	%Discordant
087-36.2	R	0.24	443	71	0.17	0.41	11.20	1.22	0.06	2.13	0.70	2.46	0.09	1.22	0.4980	551	6	477	47	-16
087-37.1		0.00	118	95	0.83	0.46	2.79	1.65	0.16	0.89	8.00	1.87	0.36	1.65	0.8802	1976	28	2474	15	+23
087-38.1		0.37	602	120	0.21	0.70	7.30	1.15	0.11	0.95	2.11	1.49	0.14	1.15	0.7727	828	9	1825	17	+58
087-39.1		0.09	129	61	0.49	0.50	3.45	2.47	0.15	1.62	6.10	2.95	0.29	2.47	0.8364	1642	36	2374	28	+35
087-40.1		0.24	321	147	0.47	0.59	5.73	1.28	0.12	0.99	2.89	1.62	0.17	1.28	0.7894	1037	12	1956	18	+51
087-41.1		0.06	314	195	0.64	0.30	3.60	1.28	0.15	0.66	5.66	1.44	0.28	1.28	0.8892	1581	18	2320	11	+36
087-43.1		0.04	22	13	0.63	0.34	2.46	1.35	0.16	0.59	9.06	1.48	0.41	1.35	0.9163	2195	25	2477	10	+13
087-44.1		0.06	24	11	0.46	0.36	2.91	1.34	0.17	0.60	8.21	1.47	0.34	1.34	0.9130	1902	22	2593	10	+31
087-45.1		0.31	23	14	0.63	0.34	3.56	1.36	0.15	0.84	5.63	1.60	0.28	1.36	0.8506	1595	19	2293	14	+34
087-46.1		0.06	42	17	0.42	0.23	11.50	1.47	0.06	1.29	0.70	1.96	0.09	1.47	0.7529	537	8	541	28	+1
087-47.1		0.16	30	7	0.23	0.38	11.19	1.24	0.06	1.95	0.75	2.31	0.09	1.24	0.5380	552	7	628	42	+13
087-48.1		0.33	30	10	0.33	0.30	11.48	1.21	0.06	2.36	0.67	2.65	0.09	1.21	0.4570	538	6	428	53	-27
087-49.1	C	0.07	27	14	0.52	0.35	3.34	1.34	0.17	0.68	6.91	1.50	0.30	1.34	0.8933	1687	20	2532	11	+38
087-49.2	R	0.46	27	8	0.30	0.38	11.23	1.30	0.06	3.09	0.68	3.35	0.09	1.30	0.3869	550	7	436	69	-27
087-50.1		0.31	31	13	0.42	0.29	11.57	1.94	0.06	2.33	0.69	3.03	0.09	1.94	0.6398	535	10	526	51	-2
087-51.1		-0.02	43	15	0.36	0.29	3.92	1.20	0.15	0.54	5.40	1.32	0.25	1.20	0.9106	1464	16	2387	9	+43
087-52.1		0.36	19	5	0.28	0.44	11.75	1.38	0.06	3.46	0.66	3.72	0.09	1.38	0.3712	526	7	454	77	-17
087-54.1		-0.03	46	12	0.28	0.28	8.58	1.50	0.09	0.91	1.40	1.75	0.12	1.50	0.8552	711	10	1368	17	+51
087-55.1		-0.07	22	10	0.46	0.38	2.69	1.36	0.17	1.62	8.66	2.12	0.37	1.36	0.6433	2038	24	2546	27	+23
087-56.1	C	0.02	41	23	0.56	0.27	3.45	1.22	0.17	0.53	6.66	1.33	0.29	1.22	0.9179	1641	18	2523	9	+39
087-56.2	R	-0.06	28	6	0.23	1.05	6.03	1.24	0.13	1.77	3.07	2.16	0.17	1.24	0.5755	990	11	2156	31	+58
087-57.1		0.00	24	7	0.30	0.38	6.38	2.08	0.12	0.92	2.51	2.27	0.16	2.08	0.9137	938	18	1896	17	+54
087-58.1		-0.05	28	11	0.39	0.30	11.47	1.22	0.06	2.61	0.74	2.88	0.09	1.22	0.4237	539	6	650	56	+18
087-59.1		-0.03	43	16	0.38	0.25	11.52	1.15	0.06	1.26	0.69	1.70	0.09	1.15	0.6752	537	6	528	28	-2
087-60.1		0.05	29	10	0.35	0.31	11.26	1.22	0.06	1.53	0.73	1.95	0.09	1.22	0.6235	548	6	604	33	+10
087-61.1		-0.09	32	9	0.27	0.33	11.43	1.21	0.06	1.54	0.76	1.96	0.09	1.21	0.6165	541	6	696	33	+23
087-62.1		0.02	36	12	0.35	0.29	6.51	1.59	0.12	0.77	2.59	1.76	0.15	1.59	0.8990	921	14	1992	14	+58
087-63.1		0.00	37	14	0.38	0.47	11.52	1.17	0.06	1.27	0.68	1.73	0.09	1.17	0.6775	536	6	492	28	-9
087-64.1	C	0.03	40	25	0.63	0.60	4.15	1.22	0.14	0.60	4.76	1.36	0.24	1.22	0.8970	1391	15	2267	10	+43
087-64.2	R	0.19	19	7	0.36	0.36	11.18	1.30	0.06	2.29	0.71	2.63	0.09	1.30	0.4942	552	7	502	50	-10
087-65.1		0.00	47	18	0.40	0.23	11.32	1.14	0.06	1.11	0.71	1.59	0.09	1.14	0.7153	545	6	530	24	-3
087-66.1	C	-0.04	17	14	0.87	0.40	3.17	1.51	0.16	0.85	6.80	1.73	0.31	1.51	0.8726	1765	23	2418	14	+31
087-66.2	R	0.08	22	6	0.30	0.39	11.55	1.86	0.06	2.05	0.70	2.77	0.09	1.86	0.6721	535	10	562	45	+5

DA13-087			Conc (ppm)				Radiogenic Ratios									Ages				
Spot Name	Type	%com ^{206}Pb	U	Th	$^{232}Th/^{238}U$	± (%)[1]	$^{238}U/^{206}Pb^*$	± (%)[1]	$^{207}Pb^*/^{206}Pb^*$	± (%)[1]	$^{207}Pb^*/^{235}U$	± (%)[1]	$^{206}Pb^*/^{238}U$	± (%)[1]	err corr	$^{206}Pb/^{238}U$	± 1σ	$^{207}Pb/^{206}Pb$	± 1σ	%Discordant
087-67.1		-0.05	16	12	0.75	0.42	2.22	1.53	0.17	0.71	10.25	1.69	0.45	1.53	0.9065	2395	31	2510	12	+5
087-68.1		-0.07	25	7	0.29	0.37	11.32	2.22	0.06	1.82	0.74	2.87	0.09	2.22	0.7743	546	12	621	39	+13
087-69.1		0.14	21	6	0.28	0.39	11.29	1.30	0.06	2.07	0.75	2.44	0.09	1.30	0.5306	547	7	658	44	+18
087-70.1		-0.03	20	8	0.42	0.40	3.66	1.38	0.15	0.78	5.48	1.59	0.27	1.38	0.8717	1559	19	2291	13	+36
087-71.1		0.00	36	8	0.22	0.84	5.29	1.20	0.13	1.18	3.35	1.69	0.19	1.20	0.7133	1117	12	2075	21	+50
087-72.1		0.00	18	24	1.35	0.33	2.24	1.43	0.16	0.62	10.07	1.56	0.45	1.43	0.9170	2383	29	2489	11	+5
087-73.1	C	0.07	12	8	0.66	0.45	2.65	1.57	0.16	0.81	8.52	1.77	0.38	1.57	0.8885	2062	28	2498	14	+20
087-73.2	R	-0.04	37	8	0.22	0.35	11.38	1.20	0.06	1.48	0.69	1.91	0.09	1.20	0.6274	543	6	499	33	-9
087-74.1		-0.04	44	6	0.15	0.96	10.75	1.42	0.07	1.19	0.88	1.86	0.09	1.42	0.7660	573	8	887	25	+37
087-75.1		0.08	22	6	0.27	0.44	11.46	1.35	0.06	2.19	0.70	2.58	0.09	1.35	0.5242	540	7	535	48	-1
087-76.1		0.00	50	18	0.36	0.26	5.85	1.18	0.14	1.12	3.28	1.63	0.17	1.18	0.7236	1018	11	2218	19	+58
087-77.1		0.10	28	10	0.39	0.36	5.16	1.32	0.13	0.89	3.52	1.59	0.19	1.32	0.8296	1141	14	2122	16	+50
087-78.1		-0.13	24	9	0.39	0.34	11.76	1.27	0.06	2.02	0.72	2.39	0.09	1.27	0.5324	526	6	644	43	+19
087-79.1		0.15	27	6	0.22	0.43	11.76	1.29	0.06	2.28	0.69	2.62	0.09	1.29	0.4942	526	7	575	50	+9
087-80.1	C	0.19	39	14	0.39	0.28	11.73	1.57	0.06	1.97	0.66	2.52	0.09	1.57	0.6231	528	8	454	44	-17
087-80.2	R	-0.06	35	14	0.41	0.30	11.72	1.85	0.06	1.66	0.69	2.49	0.09	1.85	0.7459	528	9	563	36	+7

C = core; R = rim; * Radiogenic Pb only [1] All errors are 1σ

Appendix 2.2

SHRIMP SI oxygen isotope (zircon) data for the Ambatolampy Group

	Age Information					$^{18}O/^{16}O$ Data				
Spot Name	$^{206}Pb/^{238}U$	± 1σ	$^{207}Pb/^{06}Pb$	± 1σ	%Disc.	$^{18}O/^{16}O$	1σ	$^{18}O/^{16}O$ (‰)	(‰) 1σ	External error 2σ
DA13-007-03.1	2528	40	2755	14	+10	0.00204571	0.00000014	5.84	0.07	0.14
DA13-007-04.1	2403	28	2617	10	+10	0.00204662	0.00000014	6.28	0.07	0.14
DA13-007-10.1	2390	31	2494	12	+5	0.00204648	0.00000022	6.21	0.11	0.21
DA13-007-12.1	2280	31	2501	13	+10	0.00204524	0.00000018	5.60	0.09	0.18
DA13-007-16.1	2582	37	2655	14	+3	0.00204737	0.00000017	6.64	0.08	0.17
DA13-007-17.1	2338	29	2516	11	+8	0.00204497	0.00000013	5.47	0.06	0.13
DA13-007-22.1	2561	31	2654	21	+4	0.00204661	0.00000010	6.27	0.05	0.10
DA13-007-25.1	2697	35	2767	11	+3	0.00204626	0.00000017	6.10	0.08	0.17
DA13-007-26.1	2616	37	2654	22	+2	0.00204981	0.00000017	7.83	0.08	0.17
DA13-007-28.1	2468	63	2519	17	+2	0.00204525	0.00000015	5.61	0.07	0.14
DA13-007-30.1	2421	32	2611	12	+9	0.00204673	0.00000017	6.33	0.08	0.16
DA13-007-32.1	2738	42	2957	13	+9	0.00204667	0.00000015	6.30	0.07	0.14
DA13-007-33.1	2606	33	2709	11	+5	0.00204739	0.00000014	6.65	0.07	0.13
DA13-007-37.1	2549	42	2717	18	+7	0.00204702	0.00000014	6.48	0.07	0.14
DA13-007-39.1	2425	29	2495	9	+3	0.00204675	0.00000013	6.34	0.06	0.13
DA13-007-40.1	2610	57	2652	14	+2	0.00204737	0.00000017	6.65	0.08	0.17
DA13-007-45.1	2448	36	2523	16	+4	0.00204182	0.00000021	3.94	0.10	0.20
DA13-007-46.1	2524	30	2502	12	-1	0.00204510	0.00000014	5.54	0.07	0.14
DA13-007-48.1	2672	45	2766	35	+4	0.00204837	0.00000012	7.13	0.06	0.12
DA13-007-49.1	2633	42	2674	15	+2	0.00205086	0.00000018	8.34	0.09	0.17
DA13-007-50.1	2288	45	2509	12	+10	0.00204272	0.00000012	4.38	0.06	0.11
DA13-007-51.1	2491	30	2655	10	+7	0.00204645	0.00000016	6.20	0.08	0.15
DA13-007-52.1	2345	72	2554	45	+10	0.00204988	0.00000018	7.87	0.09	0.17
DA13-007-53.1	2460	30	2514	12	+3	0.00204507	0.00000019	5.52	0.09	0.18
DA13-007-56.1	2295	49	2491	23	+9	0.00204470	0.00000015	5.34	0.07	0.14
DA13-007-58.1	2557	32	2609	11	+2	0.00204745	0.00000016	6.68	0.08	0.15
DA13-007-59.1	2427	30	2533	11	+5	0.00204349	0.00000018	4.75	0.09	0.18
DA13-007-64.1	2399	44	2466	24	+3	0.00204760	0.00000010	6.75	0.05	0.10
DA13-008-06.1	2812	45	2815	15	+0	0.00204557	0.00000014	5.86	0.07	0.60
DA13-008-08.1	2650	37	2653	13	+0	0.00205067	0.00000015	7.41	0.07	0.15
DA13-008-10.1	2440	36	2645	15	+9	0.00204980	0.00000018	6.98	0.09	0.17
DA13-008-11.1	2722	38	2701	13	-1	0.00204921	0.00000019	6.70	0.09	0.19
DA13-008-13.1	2564	28	2661	8	+4	0.00204877	0.00000014	6.48	0.07	0.14
DA13-008-14.1	2389	27	2523	9	+6	0.00204556	0.00000014	4.91	0.07	0.14
DA13-008-18.1	2763	39	2724	13	-2	0.00204885	0.00000015	6.52	0.07	0.14
DA13-008-20.1	2775	41	2784	14	+0	0.00204913	0.00000015	6.65	0.07	0.15
DA13-008-20.2	506	8	510	30	+1	0.00205048	0.00000016	7.31	0.08	0.15
DA13-008-22.1	2443	35	2537	14	+4	0.00204717	0.00000018	5.70	0.09	0.17
DA13-008-23.1	2442	37	2544	17	+5	0.00204791	0.00000012	6.06	0.06	0.12
DA13-008-24.1	2606	32	2681	10	+3	0.00204734	0.00000018	5.78	0.09	0.18
DA13-008-27.1	2489	32	2693	12	+9	0.00204801	0.00000018	6.11	0.09	0.17
DA13-008-28.1	2343	25	2495	8	+7	0.00204551	0.00000016	4.89	0.08	0.15
DA13-008-30.1	2482	36	2573	15	+4	0.00204542	0.00000014	4.84	0.07	0.13
DA13-008-32.1	2308	28	2504	11	+9	0.00204511	0.00000010	4.70	0.05	0.10
DA13-008-33.1	2448	33	2512	14	+3	0.00204500	0.00000018	4.64	0.09	0.17
DA13-008-34.1	2434	33	2547	13	+5	0.00204383	0.00000020	4.07	0.10	0.19
DA13-008-34.2	548	6	529	18	-4	0.00204951	0.00000015	6.84	0.07	0.15
DA13-008-35.1	2464	36	2496	14	+2	0.00204776	0.00000014	5.99	0.07	0.14
DA13-008-37.1	2480	27	2620	8	+6	0.00204740	0.00000018	5.81	0.09	0.18
DA13-008-38.1	2613	47	2781	19	+7	0.00204547	0.00000013	4.87	0.06	0.12
DA13-008-39.1	2553	33	2694	11	+6	0.00204736	0.00000016	5.80	0.08	0.16
DA13-008-40.1	2578	32	2628	10	+2	0.00204950	0.00000014	6.83	0.07	0.14
DA13-008-42.1	2595	38	2684	14	+4	0.00204802	0.00000014	6.11	0.07	0.14
DA13-008-43.2	530	7	538	19	+2	0.00204518	0.00000017	4.73	0.08	0.16
DA13-008-47.1	2687	37	2699	12	+1	0.00205002	0.00000016	7.09	0.08	0.15
DA13-008-48.1	2400	29	2537	12	+6	0.00204930	0.00000018	6.74	0.09	0.18
DA13-008-49.1	2443	30	2656	11	+10	0.00204841	0.00000019	6.30	0.09	0.19

	Age Information					$^{18}O/^{16}O$ Data				
Spot Name	$^{206}Pb/^{238}U$	± 1σ	$^{207}Pb/^{206}Pb$	± 1σ	%Disc.	$^{18}O/^{16}O$	1σ	$^{18}O/^{16}O$ (‰)	(‰) 1σ	External error 2σ
DA13-008-50.1	2384	28	2513	10	+6	0.00204439	0.00000013	4.35	0.06	0.13
DA13-014-04.1	2277	35	2490	8	+10	0.00204696	0.00000019	6.52	0.09	0.18
DA13-014-05.1	2049	37	2104	18	+3	0.00205045	0.00000003	8.22	0.02	0.03
DA13-014-06.1	2606	47	2686	13	+4	0.00204514	0.00000014	5.63	0.07	0.13
DA13-014-07.1	2293	37	2459	11	+8	0.00204830	0.00000017	7.17	0.09	0.17
DA13-014-08.2	2252	35	2317	10	+3	0.00205283	0.00000010	9.38	0.05	0.10
DA13-014-11.1	2461	38	2528	17	+3	0.00204572	0.00000007	5.91	0.04	0.07
DA13-014-12.1	2655	41	2721	16	+3	0.00204554	0.00000003	5.83	0.02	0.03
DA13-014-13.1	2645	40	2743	8	+4	0.00204488	0.00000014	5.51	0.07	0.13
DA13-014-21.1	2618	42	2531	12	-4	0.00204799	0.00000011	7.02	0.05	0.11
DA13-014-22.1	2415	55	2509	12	+4	0.00204624	0.00000009	6.17	0.04	0.09
DA13-014-25.1	2216	40	2279	15	+3	0.00204602	0.00000010	6.06	0.05	0.10
DA13-014-30.1	2506	45	2564	28	+3	0.00204795	0.00000027	7.00	0.13	0.26
DA13-014-34.1	2598	42	2634	28	+2	0.00204945	0.00000024	7.74	0.12	0.24
DA13-014-35.1	2389	37	2497	9	+5	0.00204628	0.00000005	6.19	0.03	0.05
DA13-014-36.1	2642	45	2677	15	+2	0.00204649	0.00000022	6.29	0.11	0.22
DA13-014-37.1	2626	44	2703	17	+3	0.00204516	0.00000010	5.64	0.05	0.10
DA13-014-41.1	2472	59	2574	25	+5	0.00204513	0.00000023	5.63	0.11	0.22
DA13-014-43.1	2351	36	2503	9	+7	0.00204578	0.00000003	5.94	0.01	0.03
DA13-014-44.1	2327	36	2493	9	+8	0.00204688	0.00000013	6.48	0.06	0.12
DA13-014-45.1	2125	33	2189	9	+3	0.00204169	0.00000016	3.95	0.08	0.15
DA13-014-46.1	537	9	538	16	+0	0.00205638	0.00000020	11.11	0.10	0.19
DA13-014-47.1	2482	38	2701	7	+10	0.00204805	0.00000015	7.05	0.07	0.15
DA13-014-50.1	2075	33	2107	11	+2	0.00205246	0.00000013	9.20	0.06	0.13
DA13-014-52.1	2432	37	2493	8	+3	0.00204532	0.00000009	5.72	0.04	0.09
DA13-014-53.1	2451	37	2499	17	+2	0.00204521	0.00000026	5.66	0.13	0.26
DA13-014-55.1	2432	42	2495	12	+3	0.00204498	0.00000008	5.55	0.04	0.08
DA13-019-14.1	2619	48	2516	17	-5	0.00204654	0.00000010	6.31	0.05	0.10
DA13-019-31.1	2504	46	2490	15	-1	0.00204433	0.00000012	5.24	0.06	0.12
DA13-019-48.1	2489	70	2431	40	-3	0.00204492	0.00000015	5.52	0.07	0.15
DA13-019-55.1	1977	32	2055	12	+4	0.00204671	0.00000012	6.40	0.06	0.11
DA13-087-03.1	531	10	549	23	+4	0.00204916	0.00000009	9.09	0.04	0.08
DA13-087-14.1	547	11	598	28	+9	0.00204975	0.00000011	9.38	0.05	0.11
DA13-087-20.1	2341	37	2524	10	+9	0.00204783	0.00000016	6.74	0.08	0.16
DA13-087-28.1	558	9	537	28	-4	0.00204771	0.00000013	6.68	0.07	0.13

Appendix 2.3

LA-MC-ICP-MS hafnium isotope (zircon) data for the Ambatolampy Group

Spot Number	$^{207}Pb/^{206}Pb$ Age (Ma)	$^{176}Hf/^{177}Hf$	2σ	$^{176}Lu/^{177}Hf$	$^{176}Yb/^{177}Hf$	Hf (i)	$\varepsilon_{Hf}(t)$	1σ	T_{DM}(Ma)
DA13-007-03.1	2755	0.281072	0.000022	0.000511	0.018244	0.281045	1.10	0.79	2997
DA13-007-04.1	2617	0.281250	0.000024	0.000560	0.023515	0.281222	4.19	0.83	2761
DA13-007-10.1	2494	0.281226	0.000032	0.000468	0.013746	0.281203	0.64	1.12	2788
DA13-007-12.1	2501	0.281292	0.000050	0.000693	0.023028	0.281259	2.77	1.75	2715
DA13-007-16.1	2655	0.281218	0.000035	0.000252	0.007998	0.281206	4.50	1.24	2782
DA13-007-17.1	2516	0.281238	0.000041	0.000483	0.016718	0.281215	1.57	1.45	2772
DA13-007-22.1	2654	0.281225	0.000044	0.000420	0.014012	0.281203	4.38	1.55	2786
DA13-007-25.1	2767	0.281114	0.000022	0.000351	0.013683	0.281096	3.21	0.75	2928
DA13-007-26.1	2654	0.281181	0.000022	0.000269	0.010419	0.281168	3.11	0.75	2833
DA13-007-28.1	2519	0.280834	0.000020	0.000560	0.022057	0.280807	-12.86	0.68	3318
DA13-007-30.1	2611	0.281227	0.000035	0.000902	0.031147	0.281182	2.62	1.22	2817
DA13-007-32.1	2957	0.281050	0.000046	0.001316	0.051292	0.280975	3.39	1.60	3091
DA13-007-33.1	2709	0.281303	0.000080	0.001049	0.042448	0.281249	7.27	2.80	2725
DA13-007-37.1	2717	0.281049	0.000028	0.000567	0.019784	0.281020	-0.66	0.99	3031
DA13-007-39.1	2495	0.281273	0.000059	0.000663	0.023616	0.281241	2.02	2.06	2738
DA13-007-40.1	2652	0.281143	0.000025	0.000570	0.021016	0.281114	1.17	0.89	2906
DA13-007-45.1	2523	0.281208	0.000037	0.000895	0.035988	0.281165	-0.04	1.30	2842
DA13-007-46.1	2502	0.280951	0.000040	0.000451	0.018066	0.280930	-8.89	1.41	3153
DA13-007-48.1	2766	0.281146	0.000029	0.000182	0.006829	0.281136	4.63	1.00	2874
DA13-007-49.1	2674	0.281206	0.000036	0.000341	0.012869	0.281189	4.33	1.26	2805
DA13-007-50.1	2509	0.281216	0.000045	0.001316	0.051018	0.281153	-0.78	1.56	2863
DA13-007-51.1	2655	0.281218	0.000033	0.000264	0.008580	0.281204	4.43	1.17	2784
DA13-007-52.1	2554	0.281226	0.000041	0.000754	0.030198	0.281190	1.56	1.44	2808
DA13-007-53.1	2514	0.281224	0.000038	0.000996	0.036819	0.281176	0.13	1.34	2829
DA13-007-56.1	2491	0.280940	0.000039	0.000427	0.016859	0.280920	-9.50	1.35	3166
DA13-007-58.1	2609	0.281229	0.000027	0.000544	0.017173	0.281202	3.31	0.95	2788
DA13-007-59.1	2533	0.281162	0.000034	0.000786	0.027835	0.281124	-1.28	1.17	2897
DA13-007-64.1	2466	0.281235	0.000041	0.000839	0.031329	0.281195	-0.29	1.45	2802
DA13-008-06.1	2815	0.281112	0.000035	0.000533	0.017183	0.281083	3.88	1.21	2945
DA13-008-08.1	2653	0.281223	0.000035	0.001155	0.042881	0.281164	2.97	1.24	2842
DA13-008-10.1	2645	0.281220	0.000037	0.000674	0.025890	0.281185	3.54	1.29	2811
DA13-008-11.1	2701	0.281189	0.000029	0.000840	0.028181	0.281146	3.44	1.01	2864
DA13-008-13.1	2661	0.281148	0.000030	0.000300	0.011078	0.281133	2.05	1.06	2879
DA13-008-14.1	2523	0.281332	0.000072	0.001846	0.073225	0.281243	2.72	2.53	2742
DA13-008-18.1	2724	0.281089	0.000033	0.000555	0.018566	0.281060	0.94	1.15	2977
DA13-008-20.1	2784	0.281120	0.000022	0.000656	0.023272	0.281085	3.24	0.76	2944
DA13-008-20.2	510	0.281407	0.000068	0.001842	0.057192	0.281389	-38.05	2.39	2637
DA13-008-22.1	2537	0.281241	0.000022	0.000400	0.014705	0.281221	2.29	0.77	2763
DA13-008-23.1	2544	0.280825	0.000022	0.000615	0.023392	0.280795	-12.71	0.77	3335
DA13-008-24.1	2681	0.281235	0.000027	0.001480	0.055695	0.281159	3.45	0.95	2849
DA13-008-27.1	2693	0.281149	0.000041	0.000955	0.037521	0.281100	1.62	1.43	2927
DA13-008-28.1	2495	0.281310	0.000035	0.001095	0.044073	0.281257	2.58	1.23	2719
DA13-008-30.1	2573	0.281237	0.000039	0.000968	0.035771	0.281189	1.98	1.37	2809
DA13-008-32.1	2504	0.281256	0.000028	0.000619	0.023412	0.281226	1.70	0.98	2758
DA13-008-33.1	2512	0.281320	0.000038	0.001289	0.046372	0.281258	3.02	1.33	2719
DA13-008-34.1	2547	0.281230	0.000025	0.000520	0.019226	0.281205	1.93	0.89	2786
DA13-008-34.2	529	0.281493	0.000049	0.001439	0.051192	0.281479	-34.45	1.71	2490
DA13-008-35.1	2496	0.281323	0.000020	0.000338	0.013100	0.281307	4.37	0.68	2648
DA13-008-37.1	2620	0.281208	0.000019	0.000490	0.018468	0.281184	2.88	0.66	2813
DA13-008-38.1	2781	0.281070	0.000030	0.000605	0.020761	0.281037	1.46	1.04	3007
DA13-008-39.1	2694	0.281194	0.000037	0.000463	0.016892	0.281170	4.12	1.30	2831
DA13-008-40.1	2628	0.281288	0.000048	0.001579	0.061088	0.281209	3.98	1.69	2783
DA13-008-42.1	2684	0.281178	0.000022	0.000348	0.012996	0.281160	3.56	0.76	2843
DA13-008-43.2	538	0.281442	0.000062	0.001351	0.044166	0.281428	-36.04	2.16	2555
DA13-008-47.1	2699	0.281237	0.000032	0.000719	0.027171	0.281200	5.33	1.12	2790
DA13-008-48.1	2537	0.281188	0.000030	0.000685	0.024559	0.281155	-0.07	1.06	2854
DA13-008-49.1	2656	0.281225	0.000039	0.000757	0.030298	0.281186	3.82	1.36	2810
DA13-008-50.1	2513	0.281015	0.000034	0.000520	0.020723	0.280990	-6.49	1.20	3074

Spot Number	$^{207}Pb/^{206}Pb$ Age (Ma)	$^{176}Hf/^{177}Hf$	2σ	$^{176}Lu/^{177}Hf$	$^{176}Yb/^{177}Hf$	Hf (i)	$\varepsilon_{Hf}(t)$	1σ	T_{DM}(Ma)
DA13-014-04.1	2490	0.281268	0.000029	0.000595	0.022801	0.281240	1.86	1.03	2739
DA13-014-05.1	2104	0.281193	0.000050	0.000639	0.022283	0.281167	-9.71	1.76	2844
DA13-014-06.1	2686	0.280798	0.000028	0.000603	0.024014	0.280767	-10.38	0.98	3370
DA13-014-07.1	2459	0.281127	0.000032	0.000599	0.023356	0.281099	-3.87	1.13	2929
DA13-014-08.1	2328	0.281222	0.000032	0.000813	0.030870	0.281186	-3.87	1.11	2818
DA13-014-11.1	2528	0.281384	0.000041	0.000831	0.031621	0.281344	6.43	1.45	2599
DA13-014-12.1	2721	0.281154	0.000031	0.000545	0.019709	0.281125	3.17	1.08	2890
DA13-014-13.1	2743	0.281141	0.000050	0.001988	0.066711	0.281036	0.54	1.74	3020
DA13-014-21.1	2531	0.281290	0.000041	0.000605	0.023113	0.281261	3.55	1.43	2711
DA13-014-22.1	2509	0.281270	0.000029	0.000704	0.026822	0.281236	2.16	1.01	2745
DA13-014-25.1	2279	0.281350	0.000034	0.000475	0.017895	0.281330	0.12	1.20	2621
DA13-014-30.1	2564	0.281030	0.000043	0.000613	0.024095	0.281000	-4.96	1.51	3062
DA13-014-34.1	2634	0.281154	0.000016	0.001066	0.041117	0.281101	0.27	0.56	2928
DA13-014-35.1	2497	0.281189	0.000016	0.000255	0.009210	0.281177	-0.22	0.56	2821
DA13-014-36.1	2677	0.280927	0.000021	0.000379	0.014843	0.280908	-5.59	0.73	3180
DA13-014-37.1	2703	0.281068	0.000033	0.000579	0.022575	0.281038	-0.35	1.15	3008
DA13-014-41.1	2574	0.281342	0.000034	0.000434	0.015735	0.281320	6.68	1.21	2629
DA13-014-43.1	2503	0.281257	0.000030	0.000591	0.020615	0.281229	1.75	1.05	2755
DA13-014-44.1	2493	0.281346	0.000038	0.001217	0.048222	0.281288	3.63	1.32	2677
DA13-014-45.1	2189	0.281407	0.000030	0.000587	0.020042	0.281383	-0.07	1.05	2552
DA13-014-46.1	538	0.281265	0.000021	0.000805	0.029068	0.281257	-42.11	0.74	2759
DA13-014-49.1	2522	0.281284	0.000031	0.000777	0.030024	0.281246	2.81	1.07	2732
DA13-014-50.1	2107	0.281400	0.000030	0.000784	0.031737	0.281368	-2.48	1.06	2575
DA13-014-52.1	2493	0.281305	0.000031	0.000934	0.035764	0.281261	2.65	1.09	2714
DA13-014-53.1	2499	0.281335	0.000039	0.001017	0.040010	0.281287	3.73	1.38	2679
DA13-014-54.1	2476	0.281239	0.000036	0.000884	0.034450	0.281197	0.00	1.25	2800
DA13-014-55.1	2495	0.281278	0.000045	0.000877	0.033873	0.281237	1.84	1.57	2746
DA13-014-56.1	1853	0.281395	0.000026	0.000460	0.018277	0.281379	-7.97	0.91	2559
DA13-014-58.1	2680	0.281126	0.000034	0.000725	0.026958	0.281089	0.91	1.18	2941
DA13-014-59.1	2434	0.281370	0.000024	0.000242	0.009562	0.281359	4.76	0.83	2579
DA13-014-62.1	2320	0.281279	0.000026	0.000404	0.013900	0.281262	-1.35	0.90	2711
DA13-014-63.1	3005	0.280894	0.000039	0.001242	0.049938	0.280823	-0.92	1.36	3296
DA13-014-65.1	1865	0.281357	0.000030	0.000407	0.016812	0.281342	-9.01	1.07	2608
DA13-014-66.1	2523	0.281292	0.000028	0.000267	0.009464	0.281280	4.04	0.97	2684
DA13-014-67.1	2727	0.280968	0.000032	0.000535	0.020790	0.280940	-3.25	1.12	3137
DA13-014-73.1	2504	0.281255	0.000030	0.000816	0.031403	0.281216	1.33	1.05	2773
DA13-014-77.2	547	0.281386	0.000059	0.000395	0.012692	0.281382	-37.48	2.06	2568
DA13-014-81.1	2723	0.281098	0.000022	0.000349	0.013601	0.281080	1.62	0.76	2949
DA13-014-81.2	547	0.281430	0.000047	0.000489	0.013133	0.281425	-35.95	1.65	2514
DA13-014-82.1	1836	0.281430	0.000024	0.000391	0.015710	0.281416	-7.03	0.86	2508
DA13-014-83.1	2480	0.281319	0.000032	0.001275	0.050154	0.281259	2.29	1.12	2719
DA13-019-14.1	2516	0.281251	0.000037	0.001128	0.043716	0.281197	0.93	1.31	2801
DA13-019-28.1	1867	0.281349	0.000026	0.000208	0.008747	0.281341	-8.97	0.92	2605
DA13-019-31.1	2490	0.281290	0.000025	0.000282	0.010278	0.281277	3.16	0.88	2688
DA13-019-45.1	3078	0.280794	0.000096	0.001225	0.051190	0.280722	-2.79	3.37	3430
DA13-019-48.1	2431	0.280944	0.000085	0.001003	0.039469	0.280898	-11.68	2.96	3208
DA13-019-55.1	2055	0.281323	0.000051	0.000673	0.026512	0.281297	-6.24	1.80	2671
DA13-019-72.1	2023	0.281270	0.000058	0.000723	0.027871	0.281242	-8.91	2.02	2746
DA13-019-74.1	2439	0.281332	0.000067	0.001041	0.036730	0.281283	2.20	2.34	2685
DA13-019-75.1	565	0.281556	0.000074	0.000877	0.030675	0.281547	-31.23	2.60	2367
DA13-087-03.1	549	0.281444	0.000041	0.000765	0.027224	0.281436	-35.52	1.43	2514
DA13-087-14.1	598	0.281588	0.000058	0.000779	0.030289	0.281579	-29.34	2.02	2318
DA13-087-20.1	2524	0.281206	0.000058	0.000499	0.017353	0.281182	0.57	2.05	2817
DA13-087-28.1	537	0.280971	0.000070	0.000595	0.021528	0.280965	-52.47	2.46	3139
DA13-087-30.1	538	0.281623	0.000030	0.000762	0.026962	0.281616	-29.39	1.05	2269
DA13-087-46.1	541	0.281660	0.000075	0.000989	0.037690	0.281650	-28.12	2.62	2232
DA13-087-50.1	526	0.281591	0.000048	0.000744	0.025880	0.281584	-30.79	1.69	2312

Spot Number	$^{207}Pb/^{206}Pb$ Age (Ma)	$^{176}Hf/^{177}Hf$	2σ	$^{176}Lu/^{177}Hf$	$^{176}Yb/^{177}Hf$	Hf (i)	$\varepsilon_{Hf}(t)$	1σ	T_{DM}(Ma)
DA13-087-59.1	528	0.281401	0.000092	0.000564	0.019423	0.281395	-37.43	3.23	2558
DA13-087-65.1	530	0.281614	0.000021	0.000678	0.024206	0.281607	-29.91	0.74	2277
DA13-087-66.2	562	0.281441	0.000057	0.000455	0.014578	0.281436	-35.22	1.99	2497
DA13-087-67.1	2510	0.281221	0.000028	0.000823	0.029730	0.281181	0.22	0.97	2820
DA13-087-72.1	2489	0.281329	0.000065	0.000464	0.017033	0.281307	4.22	2.28	2649
DA13-087-75.1	535	0.281817	0.000061	0.000484	0.017363	0.281813	-22.49	2.14	1989

Appendix 3.1

Analytical Methods for Chapter 3
(Zircon isotopic characteristics of the Imorona-Itsindro Suite)

3.1.1 Sample collection and processing

Twenty-five samples of the Imorona-Itsindro Suite were selected for zircon U-Pb, oxygen and hafnium isotope analysis. Sample collection focused on obtaining a representative sample set including Tonian lithologies from all tectonic domains in central Madagascar (Fig. 3.2). To complement our sample suite, seven Tonian samples collected as part of the World Bank funded mapping program (BGS-USGS-GLW, 2008) were added. The BGS-USGS-GLW (2008) samples are from areas not covered during our 2013 and 2014 field seasons (i.e. Masora Domain and Northern Antananarivo Domain). Approximately 1.5 to 3 kg of each sample was collected for thin sectioning and zircon separation. Zircon was separated by conventional sieving and magnetic separation techniques. Zircon grains were handpicked and mounted in epoxy resin, polished, and imaged under reflected light. To investigate the internal structure of the zircon grains and to select target sites for U-Pb, hafnium, and oxygen isotopic analyses, cathodoluminescence (CL) imaging was carried out using a Philips XL40 or Philips XL20 Scanning Electron Microscope equipped with a tungsten filament electron source and a Gatan CL detector attached for high-resolution imaging at Adelaide Microscopy, University of Adelaide.

3.1.2 U-Pb geochronology

U-Pb zircon analyses were performed by Laser Ablation Inductively Coupled Mass Spectrometry (LA-ICP-MS) at Adelaide Microscopy using an Agilent 7500cs ICPMS unit coupled to a New Wave 213 nm Nd-YAG laser. The 5 or 10 % (based on the number of concordant analyses) concordance level is used to calculate the age because of the presence of common Pb as measured by [(^{204}Pb/ (^{204}Pb+^{206}Pb)] x 100 (Appendix 3.2) and Pb loss. Individual zircon ages are quoted at a 1σ level and weighted-mean ages are at a 2σ level. Individual zircon grains were ablated in a helium atmosphere using a beam diameter of ~30µm, a frequency of 5 Hz and an energy value of 1.4 - 3.5 J/cm^2. U-Pb-Th isotope fractionation was corrected using the GEMOC GJ-1 standard (^{206}Pb/^{238}U age = 600.7 ± 1.1 Ma; Jackson et al., 2004). Internal accuracy was confirmed using Plešovice (^{206}Pb/^{238}U age = 337.1 ± 0.37 Ma; Sláma et al., 2008) as a secondary unknown standard. Analyses of Plešovice yielded a weighted average ^{206}Pb/^{238}U age of 337.1 ± 1.1 (MSWD = 1.6; n = 94), statistically identical to the known value. The results of standard analyses are found in Table A.3.1. Procedural repetition consisted of 2 analyses of the GJ standard, 2 analyses of the Plešovice standard, 1 analysis of the GJ standard, 15 unknown analyses and finally 2 GJ analyses. Data acquisition involved 30 seconds of background measurement, 10 seconds of beam stabilisation and 80 seconds of sample ablation for a total analysis time of 120 seconds. Data were processed using the GLITTER software package (Griffin et al., 2008). Age calculations and Wetherill concordia diagrams were constructed using the Microsoft Excel macro Isoplot 4.15 (Ludwig, 2012).

Zircon U–Pb–Th isotopic data for the seven BGS-USGS-GLW, (2008) samples were collected using the Sensitive High Resolution Ion Microprobe mass spectrometer (SHRIMP II) in the John de Laeter Centre of Mass Spectrometry, Perth, Western Australia. Procedural details and results are found in BGS-USGS-GLW (2008). Analyses of the zircon standard BR266 were interspersed between analyses of unknowns and these results are listed in Appendix 3.2 alongside the U-Pb-Th data. These geochronology data are included here because magmatic crystallisation ages were recalculated following the same process used for the LA-ICP-MS data to ensure consistency.

3.1.3 Oxygen isotopes in zircon

Oxygen isotope analyses were performed using the SHRIMP SI (sensitive high-resolution ion microprobe stable-isotope) or SHRIMP II at The Australian National University in Canberra, Australia. A 10 kV, ~3 nA Cs+ primary ion beam was focused to an ~30 µm diameter spot on an aluminium or gold coated sample. Each analysis consisted of a 2 min pre-burn to allow the secondary ion isotopic composition to stabilise and remove the sample coating prior to the analysis, followed by 14, ~10 second estimates of the ^{18}O/^{16}O ratio. Standards Temora II and Mudtank were analysed first, then again after 5-8 unknown samples. Sample δ^{18}O (zircon) values were determined by difference relative to the mean δ^{18}O (zircon) measured on standards following normalisation for long-term drift in its measured composition. The results of standard analyses are listed in Table A.3.1. CL images were used to analyse as close as possible to the U-Pb (LA-ICP-MS) analysis locations while remaining in the same CL zone. Details of the SHRIMP II method for oxygen isotope analysis are from Ickert et al. (2008).

3.1.4 Zircon Lu-Hf isotope analyses

In situ LA-MC-ICP-MS Hf isotope analyses were carried out at the University of Adelaide Waite Campus facility using a New Wave Research 193 nm Excimer laser attached to a Neptune multi-collector ICP-MS system as per Payne et al. (2013). Only grains with U–Pb ages having ≤ 10% discordance were analysed for Lu–Hf isotope composition. Analysis locations were in the same cathodoluminescence domains as concordant U–Pb laser spots and in the same spot as SHRIMP oxygen spots. The bulk of analyses were carried out using a beam diameter of ~50 µm for large grains and a minimum of ~25 µm for smaller grains. Typical ablation times were 40 –100 seconds using 5 Hz repetition rate, 4 ns pulse rate, and an intensity of ~6-8 J/cm^2. Zircons were ablated in a helium atmosphere, which was then mixed with argon and nitrogen upstream of the ablation cell.

Analyses used a dynamic measurement routine with: ten 0.524 s integrations on ^{171}Yb, ^{173}Yb, ^{175}Lu, ^{176}Hf (+Lu + Yb), ^{177}Hf, ^{178}Hf, ^{179}Hf and ^{180}Hf; one 0.524 s integration on ^{160}Gd, ^{163}Dy, ^{164}Dy, ^{165}Ho, ^{166}Er, ^{167}Er, ^{168}Er, ^{170}Yb and ^{171}Yb, and one 0.524 s integration of Hf oxides with masses ranging from 187 to 196 amu. An idle time of 1.5 s was included between each mass change to allow for magnet settling and to negate any possible effects of signal decay. The measurement cycle was repeated 15 times providing a total maximum measurement time of 3.75 min including an off-peak baseline measurement. Hf oxide formation rates for all analytical sessions in this study were in the range 0.1–0.07%. Hf mass bias was corrected using an exponential fractionation law with a stable ^{179}Hf/^{177}Hf ratio of 0.7325. Yb and Lu isobaric interferences on ^{176}Hf were corrected for following the methods of Woodhead et al. (2004). ^{176}Yb interference on ^{176}Hf was corrected for by direct measurement of Yb fractionation using measured ^{171}Yb/^{173}Yb with the Yb isotopic values of Segal et al. (2003). The applicability of these values were verified by analysing JMC 475 Hf solutions doped with varying levels of Yb with interferences up to ^{176}Yb/^{177}Hf = ~0.5. Lu isobaric interference on ^{176}Hf was corrected using a ^{176}Lu/^{175}Lu ratio of 0.02655 (Vervoort et al., 2004) assuming the same mass bias behaviour as Yb. Confirmation of accuracy of the technique was monitored using the Plešovice, Mudtank and Temora II zircon standards. Mean ^{176}Hf/^{177}Hf values for each standard along with the published values are given in Table A.3.1. $\varepsilon_{Hf}(t)$ and TDMc were calculated using ^{176}Lu decay constant after Scherer et al. (2001). TDMc two stage crustal model ages were calculated using the methods of Griffin et al. (2002) with an average crustal composition of ^{176}Lu/^{177}Hf = 0.015.

Table A.3.1 – Summary of standard data collected for each method in this study.

Standard	Method	n	Measured Value	Reference Value	Reference
U-Pb isotopes (Age)					
Plešovice	LA-ICP-MS	80	337.4 ± 1.3 Ma (MSWD=1.8)	337.1 ± 0.4 Ma	Sláma et al., 2008
Oxygen isotopes (δ^{18}O)					
Temora II	SHRIMP SI	65	8.21 ± 0.25 ‰	8.20 ± 0.01 ‰	Valley, 2003
Mudtank	SHRIMP SI	19	4.79 ± 0.36 ‰	5.03 ± 0.10 ‰	Valley, 2003
Temora II	SHRIMP II	11	8.04 ± 0.43 ‰	8.20 ± 0.01 ‰	Valley, 2003
Mudtank	SHRIMP II	17	5.50 ± 0.24 ‰	5.03 ± 0.10 ‰	Valley, 2003
Hf isotopes (^{177}Hf/^{176}Hf)					
Mudtank	MC-LA-ICP-MS	36	0.282497 ± 0.000010	0.282507 ± 0.000006	Woodhead and Hergt, 2005
Temora II	MC-LA-ICP-MS	6	0.282643 ± 0.000030	0.282686 ± 0.000008	Woodhead and Hergt, 2005
Plešovice	MC-LA-ICP-MS	5	0.282466 ± 0.000015	0.282482 ± 0.000013	Sláma et al., 2008

Abbreviations: LA-ICP-MS = laser ablation inductively coupled mass spectroscopy; SHRIMP SI = sensitive high-resolution ion microprobe stable isotope; MC-LA-ICP-MS = multicollector laser ablation inductively coupled mass spectroscopy.

References

BGS-USGS-GLW, 2008. Revision de la cartographie geologique et miniere des zones Nord, Centre, et Centre Est de Madagascar. BGS Report CR/08/078. Keyworth, England.

Griffin, W.L., Powell, W.J., Pearson, N.J., O'Reilly, S.Y., 2008. “GLITTER: data reduction software for laser ablation ICP-MS”. In Laser ablation ICP-MS in the earth sciences. Mineralogical Association of Canada Short Course Series. Edited by: P., Sylvester. 40, 204–207.

Griffin, W.L., Wang, X., Jackson, S.E., Pearson, N.J., O'Reilly, S.Y., Xu, X., Zhou, X., 2002. Zircon chemistry and magma mixing, SE China: In-situ analysis of Hf isotopes, Tonglu and Pingtan igneous complexes. Lithos 61, 237-269.

Ickert, R.B., Hiess, J., Williams, I.S., Holden, P., Ireland, T.R., Lanc, P., Schram, N., Foster, J.J., Clement, S.W., 2008. Determining high precision, in situ, oxygen isotope ratios with a SHRIMP II: Analyses of MPI-DING silicate-glass reference materials and zircon from contrasting granites. Chemical Geology 257, 114-128.

Jackson, S.E., Pearson, N.J., Griffin, W.L., Belousova, E.A., 2004. The application of laser ablation-inductively coupled plasma-mass spectrometry to in situ U–Pb zircon geochronology. Chemical Geology 211, 47-69.

Ludwig, K.R., 2012. User's Manual for Isoplot 3.75. A Geochronological Toolkit for Microsoft Excel. Berkeley Geochronology Center Special Publication No. 5, 75p.

Payne, J.L., Pearson, N.J., Grant, K.J., Halverson, G.P., 2013. Reassessment of relative oxide formation rates and molecular interferences on in situ lutetium-hafnium analysis with laser ablation MC-ICP-MS. Journal of Analytical Atomic Spectrometry 28, 1068-1079.

Scherer, E., Münker, C., Mezger, K., 2001. Calibration of the Lutetium-Hafnium Clock. Science 293, 683-687.

Segal, I., Halicz, L., Platzner, I.T., 2003. Accurate isotope ratio measurements of ytterbium by multiple collection inductively coupled plasma mass spectrometry applying erbium and hafnium in an improved double external normalization procedure. Journal of Analytical Atomic Spectrometry 18, 1217-1223.

Sláma, J., Košler, J., Condon, D.J., Crowley, J.L., Gerdes, A., Hanchar, J.M., Horstwood, M.S.A., Morris, G.A., Nasdala, L., Norberg, N., Schaltegger, U., Schoene, B., Tubrett, M.N., Whitehouse, M.J., 2008. Plešovice zircon — A new natural reference material for U–Pb and Hf isotopic microanalysis. Chemical Geology 249, 1-35.

Valley, J.W., 2003. Oxygen Isotopes in Zircon. Reviews in Mineralogy and Geochemistry 53, 343-385.

Vervoort, J.D., Patchett, J., Soderlund, U., Baker, M., 2004. Isotopic composition of Yb and the determination of Lu concentration and Lu/Hf ratios by isotope dilution using MC-ICPMS. Geochemistry Geophysics Geosystems 5, Q11002.

Woodhead, J., Hergt, J., Shelley, M., Eggins, S., Kemp, R., 2004. Zircon Hf-isotope analysis with an excimer laser, depth profiling, ablation of complex geometries, and concomitant age estimation. Chemical Geology 209, 121-135.

Appendix 3.2

U-Pb Geochronology Results

Samples with a DA prefix used the LA-ICP-MS Method while samples with a BGS prefix used the SHRIMP II method.

DA14-133	Ikal Domain		Mean cps (background subtracted)							Isotopic Ratios (± 1σ)							Age (Ma ± 1σ)						
Analysis	Core/Rim	$\%Pb_c$	^{204}Pb	^{206}Pb	^{207}Pb	^{208}Pb	^{232}Th	^{238}U	Th/U	$^{207}Pb/^{206}Pb$		$^{207}Pb/^{235}U$		$^{206}Pb/^{238}U$		Rho	$^{207}Pb/^{206}Pb$		$^{206}Pb/^{238}U$		$^{207}Pb/^{235}U$		%Conc
133-01		0.27	330	124070	11899	21081	413573	1908575	0.22	0.0953	0.0012	1.1124	0.0169	0.0847	0.0011	0.5896	1534	24	524	7	759	8	69
133-02		0.65	26	3987	456	1199	49332	68975	0.72	0.1147	0.0021	1.0403	0.0191	0.0658	0.0009	0.3419	1875	33	411	5	724	9	57
133-03		0.02	18	84643	5414	3676	123183	990882	0.12	0.0640	0.0007	0.9320	0.0126	0.1057	0.0013	0.6058	741	24	648	8	669	7	97
133-04		0.06	12	20039	1309	1056	116345	275222	0.42	0.0655	0.0011	0.7896	0.0136	0.0874	0.0011	0.4379	790	34	540	7	591	8	91
133-05		0.01	22	159914	10450	15507	365307	1751939	0.21	0.0655	0.0008	0.9956	0.0132	0.1103	0.0014	0.5896	790	24	674	8	702	7	96
133-06		0.12	98	83466	6101	8121	556641	1157802	0.48	0.0731	0.0009	0.8850	0.0122	0.0878	0.0011	0.5735	1018	24	542	6	644	7	84
133-07		0.19	316	165580	14380	28306	2391995	2589645	0.92	0.0870	0.0013	0.9857	0.0166	0.0822	0.0011	0.5105	1361	29	509	7	697	8	73
133-08		0.03	98	292856	19319	24668	591530	3654854	0.16	0.0658	0.0011	0.9581	0.0175	0.1056	0.0015	0.4862	801	35	647	9	682	9	95
133-09		0.02	250	1065877	71616	95471	2732401	14673889	0.19	0.0666	0.0010	0.8869	0.0154	0.0967	0.0013	0.5263	824	32	595	8	645	8	92
133-10		0.01	7	92310	6073	10393	216054	943567	0.23	0.0657	0.0013	1.1854	0.0247	0.1308	0.0019	0.4309	798	41	793	11	794	11	100
133-11		0.05	23	45500	3014	11783	249513	453395	0.55	0.0660	0.0010	1.1703	0.0198	0.1287	0.0017	0.5021	805	32	781	10	787	9	99
133-12		0.06	262	422148	30807	70341	1571555	4551748	0.35	0.0722	0.0012	1.2170	0.0217	0.1224	0.0017	0.5005	990	33	744	10	808	10	92
133-13		0.02	16	71010	4234	893	47038	917891	0.05	0.0599	0.0008	0.7206	0.0101	0.0873	0.0010	0.4849	599	28	540	6	551	6	98
133-14		0.03	62	241251	15976	24516	595019	3020456	0.20	0.0663	0.0011	0.9629	0.0177	0.1054	0.0015	0.4905	815	35	646	9	685	9	94
133-15		0.37	13	3512	394	1096	13579	47926	0.28	0.1125	0.0024	1.2405	0.0255	0.0800	0.0011	0.2666	1840	38	496	6	819	12	61
133-16		0.01	1	6795	410	210	31378	81379	0.39	0.0606	0.0014	0.7915	0.0182	0.0948	0.0013	0.2679	624	49	584	7	592	10	99
133-17		0.00	45	1282006	84189	27467	636926	12888377	0.05	0.0665	0.0009	1.2090	0.0194	0.1318	0.0018	0.5869	823	28	798	10	805	9	99
133-18		0.01	53	517782	34007	71657	1489260	5176696	0.29	0.0663	0.0015	1.1863	0.0283	0.1299	0.0019	0.3528	816	48	787	11	794	13	99
133-19		0.05	26	53365	3590	7235	152697	498514	0.31	0.0674	0.0009	1.2072	0.0180	0.1299	0.0016	0.5263	851	28	787	9	804	8	98
133-20		0.06	51	84634	6181	14233	250302	849874	0.29	0.0732	0.0011	1.1446	0.0173	0.1134	0.0014	0.4492	1020	29	693	8	775	8	89
133-21		0.09	14	15493	1125	1337	76341	204742	0.37	0.0731	0.0012	0.8947	0.0148	0.0888	0.0011	0.4318	1016	32	549	7	649	8	85
133-22		0.07	96	142282	10401	18343	1211003	2527909	0.48	0.0734	0.0012	0.7349	0.0128	0.0726	0.0010	0.4960	1025	32	452	6	559	8	81
133-23		0.01	17	248912	16587	33530	846955	2693925	0.31	0.0666	0.0013	1.1196	0.0233	0.1220	0.0018	0.4217	825	41	742	10	763	11	97
133-24		0.01	77	644140	43043	57061	1435528	6556670	0.22	0.0668	0.0010	1.1581	0.0187	0.1257	0.0017	0.5380	833	30	763	10	781	9	98
133-25		0.03	7	27326	1800	3015	69344	277491	0.25	0.0664	0.0010	1.1531	0.0199	0.1261	0.0017	0.5012	818	32	765	10	779	9	98

DA14-140	Ikal Domain		Mean cps (background subtracted)							Isotopic Ratios (± 1σ)							Age (Ma ± 1σ)						
Analysis	Core/Rim	$\%Pb_c$	^{204}Pb	^{206}Pb	^{207}Pb	^{208}Pb	^{232}Th	^{238}U	Th/U	$^{207}Pb/^{206}Pb$		$^{207}Pb/^{235}U$		$^{206}Pb/^{238}U$		Rho	$^{207}Pb/^{206}Pb$		$^{206}Pb/^{238}U$		$^{207}Pb/^{235}U$		%Conc
140-01		0.02	22	106824	6311	2058	59345	1399089	0.04	0.0592	0.0007	0.7772	0.0105	0.0952	0.0012	0.6259	576	25	586	7	584	6	100
140-03		0.02	40	252974	14812	5891	168975	3669889	0.05	0.0585	0.0008	0.7380	0.0117	0.0914	0.0012	0.5862	550	29	564	7	561	7	101
140-04		0.00	4	264570	16978	34455	718818	2915034	0.25	0.0641	0.0010	1.0603	0.0181	0.1200	0.0017	0.5347	746	32	730	10	734	9	100
140-06		0.07	12	16089	1053	1018	23751	156927	0.15	0.0659	0.0011	1.0711	0.0189	0.1180	0.0015	0.3807	802	36	719	9	739	9	97
140-07		0.07	210	300839	21856	52797	1282952	3674537	0.35	0.0723	0.0012	1.0827	0.0194	0.1087	0.0015	0.5060	993	33	665	9	745	9	89
140-08		0.07	203	273615	20053	47387	839670	3953692	0.21	0.0733	0.0011	0.9283	0.0158	0.0919	0.0013	0.5422	1021	30	567	8	667	8	85
140-09		0.01	13	90602	5521	4760	127209	1213983	0.10	0.0610	0.0007	0.7678	0.0104	0.0913	0.0011	0.6001	640	25	563	7	579	6	97
140-10		0.02	90	505297	33952	62801	1413066	6535374	0.22	0.0675	0.0014	0.9555	0.0203	0.1026	0.0015	0.4135	854	41	630	9	681	11	92
140-11		0.03	18	70274	4199	3339	93122	912599	0.10	0.0598	0.0007	0.7735	0.0107	0.0938	0.0012	0.5809	595	27	578	7	582	6	99
140-12		0.01	32	240410	15705	23706	563776	2624313	0.21	0.0655	0.0008	1.0680	0.0161	0.1183	0.0016	0.5937	791	27	721	9	738	8	98
140-13		0.17	13	7557	469	290	7060	99954	0.07	0.0621	0.0010	0.7839	0.0134	0.0915	0.0012	0.4474	679	34	564	7	588	8	96
140-14		0.07	7	10673	658	652	21664	135137	0.16	0.0620	0.0011	0.7739	0.0134	0.0906	0.0011	0.3887	673	36	559	7	582	8	96
140-15		0.03	63	186204	11731	15766	642657	2691359	0.24	0.0628	0.0019	0.7703	0.0229	0.0890	0.0014	0.2561	701	63	549	8	580	13	95
140-16		0.03	113	325392	21311	35676	705864	3658664	0.19	0.0652	0.0009	1.0263	0.0164	0.1143	0.0015	0.5393	780	30	698	9	717	8	97
140-17		0.00	1	61344	4042	8598	192568	568374	0.34	0.0660	0.0009	1.2292	0.0186	0.1351	0.0017	0.5458	806	28	817	10	814	8	100
140-18		0.03	57	217097	12991	3643	343812	2871397	0.12	0.0596	0.0008	0.7920	0.0120	0.0964	0.0013	0.5688	590	29	593	7	592	7	100
140-19		0.00	5	613340	38729	55977	1216865	6267057	0.19	0.0633	0.0010	1.1025	0.0189	0.1264	0.0017	0.5112	719	33	767	10	755	9	102
140-20		0.25	215	86383	8107	22955	81473	1166810	0.07	0.0939	0.0012	1.1938	0.0175	0.0922	0.0012	0.5604	1506	24	569	7	798	8	71
140-21		0.01	64	437961	26750	8096	134389	6133051	0.02	0.0608	0.0011	0.7758	0.0154	0.0926	0.0013	0.4305	633	40	571	8	583	9	98
140-22		0.00	0	277357	17506	18949	507826	3728177	0.14	0.0634	0.0009	0.8349	0.0138	0.0955	0.0013	0.5265	723	31	588	8	616	8	95
140-23		0.01	1	14656	917	812	27741	176577	0.16	0.0638	0.0011	0.7936	0.0135	0.0902	0.0011	0.3579	735	36	557	6	593	8	94
140-25		0.00	0	8851	557	505	16245	114605	0.14	0.0638	0.0016	0.7932	0.0197	0.0901	0.0013	0.2560	736	52	556	8	593	11	94
140-28		0.12	29	24880	1551	1263	37546	323822	0.12	0.0622	0.0012	0.8043	0.0162	0.0938	0.0013	0.3762	681	41	578	7	599	9	96
140-29		0.01	14	162931	10322	9140	207784	1736531	0.12	0.0637	0.0009	1.0110	0.0160	0.1150	0.0015	0.5065	733	30	702	8	709	8	99
140-30		0.00	0	383287	24857	30845	716967	3724711	0.19	0.0650	0.0010	1.1383	0.0186	0.1271	0.0016	0.4875	774	31	771	9	772	9	100

DA14-146	Ikal Domain		Mean cps (background subtracted)							Isotopic Ratios (± 1σ)							Age (Ma ± 1σ)						
Analysis	Core/Rim	$\%Pb_c$	^{204}Pb	^{206}Pb	^{207}Pb	^{208}Pb	^{232}Th	^{238}U	Th/U	$^{207}Pb/^{206}Pb$		$^{207}Pb/^{235}U$		$^{206}Pb/^{238}U$		Rho	$^{207}Pb/^{206}Pb$		$^{206}Pb/^{238}U$		$^{207}Pb/^{235}U$		%Conc
146-01		0.03	29	100414	6417	5035	761646	1280861	0.59	0.0641	0.0007	0.8428	0.0111	0.0954	0.0012	0.6017	745	24	587	7	621	6	95
146-03	C	0.02	70	340715	22452	46474	1762160	3770327	0.47	0.0660	0.0008	1.0350	0.0142	0.1138	0.0015	0.6227	805	24	695	8	721	7	96
146-04	R	0.01	17	179210	11587	12687	991913	1824565	0.54	0.0647	0.0007	1.0456	0.0135	0.1172	0.0014	0.6024	765	23	715	8	727	7	98
146-05		0.01	1	18542	1184	1427	42015	182991	0.23	0.0637	0.0018	1.1136	0.0305	0.1268	0.0020	0.2672	732	57	770	11	760	15	101
146-06		0.02	33	162458	10473	10323	1523228	1950500	0.78	0.0645	0.0008	0.9279	0.0129	0.1044	0.0013	0.6102	758	25	640	8	667	7	96
146-07		0.14	18	13209	847	1610	37256	137984	0.27	0.0642	0.0013	1.0942	0.0227	0.1237	0.0018	0.4089	747	41	752	10	751	11	100
146-08		0.04	7	15860	968	730	29503	198613	0.15	0.0608	0.0010	0.7463	0.0122	0.0890	0.0011	0.3867	632	34	550	6	566	7	97
146-09		0.01	38	262557	16876	19741	621400	2958533	0.21	0.0643	0.0008	1.0148	0.0153	0.1146	0.0015	0.5888	750	27	699	9	711	8	98
146-10		0.00	20	434749	27939	41995	876915	5435404	0.16	0.0644	0.0010	0.9301	0.0163	0.1047	0.0014	0.5103	756	33	642	8	668	9	96
146-12		0.02	135	656564	42485	37372	1350890	10146536	0.13	0.0641	0.0017	0.7538	0.0201	0.0853	0.0013	0.3154	746	55	528	8	570	12	92
146-13		0.36	24	6732	420	190	76722	97686	0.79	0.0623	0.0010	0.7166	0.0125	0.0834	0.0011	0.4395	684	35	517	6	549	7	94
146-14	C	0.02	108	470601	30346	24277	829886	5734857	0.14	0.0644	0.0010	0.9525	0.0164	0.1073	0.0015	0.5155	754	32	657	9	679	9	97
146-15	R	0.01	30	264806	17174	21922	1759817	2975495	0.59	0.0644	0.0011	1.0289	0.0185	0.1159	0.0016	0.4885	755	34	707	9	718	9	98
146-16		0.01	30	495168	32500	42900	1417672	5001352	0.28	0.0656	0.0009	1.1524	0.0182	0.1274	0.0017	0.5553	794	29	773	10	778	9	99
146-17		0.00	29	661947	42914	36934	3706745	7103965	0.52	0.0650	0.0011	1.0794	0.0193	0.1205	0.0017	0.4826	773	34	734	9	743	9	99
146-19		0.02	30	130750	8384	12701	377136	1240297	0.30	0.0635	0.0009	1.0566	0.0158	0.1206	0.0014	0.4616	726	30	734	8	732	8	100
146-20		0.03	25	86024	5664	5624	2328568	1084976	2.15	0.0657	0.0008	0.8660	0.0114	0.0956	0.0012	0.5990	797	24	588	7	633	6	93
146-21		0.04	28	76081	4607	1589	380484	1044744	0.36	0.0605	0.0007	0.7431	0.0102	0.0891	0.0011	0.5809	621	26	550	7	564	6	98
146-23		0.02	28	137736	9054	12155	2081611	1471351	1.41	0.0657	0.0008	1.0181	0.0135	0.1124	0.0014	0.5889	798	24	686	8	713	7	96
146-24		0.01	33	377342	24581	46466	1777418	3767834	0.47	0.0656	0.0010	1.1625	0.0191	0.1286	0.0017	0.5248	793	31	780	10	783	9	100
146-25		0.04	29	70714	4254	1824	289554	919108	0.32	0.0600	0.0008	0.7442	0.0108	0.0900	0.0011	0.4951	604	29	555	6	565	6	98
146-26		0.01	39	381642	24865	29257	1715982	4191584	0.41	0.0656	0.0009	1.0439	0.0161	0.1155	0.0015	0.5569	792	28	705	9	726	8	97
146-27		0.05	38	83053	5508	7894	1661058	946569	1.75	0.0665	0.0008	0.9790	0.0139	0.1068	0.0013	0.5573	821	26	654	8	693	7	94
146-28		0.00	0	12777	810	653	38060	169575	0.22	0.0634	0.0011	0.7286	0.0132	0.0834	0.0010	0.3436	721	38	516	6	556	8	93
146-29		0.02	60	333664	21448	23997	4977438	4113041	1.21	0.0649	0.0010	0.9176	0.0158	0.1026	0.0014	0.4849	769	33	630	8	661	8	95
146-30		0.01	35	314675	20700	35916	2856721	3234336	0.88	0.0664	0.0013	1.1277	0.0230	0.1232	0.0017	0.3982	819	41	749	10	767	11	98
146-31		0.00	22	530439	31782	7950	1707670	7279043	0.23	0.0608	0.0009	0.7683	0.0123	0.0917	0.0012	0.5301	631	31	566	7	579	7	98
146-32		0.03	35	107475	6793	3412	265442	1508160	0.18	0.0644	0.0008	0.7485	0.0099	0.0844	0.0010	0.5755	753	24	522	6	567	6	92
146-33		0.02	32	151579	9567	7047	703183	2286227	0.31	0.0641	0.0008	0.7082	0.0097	0.0802	0.0010	0.5844	745	25	497	6	544	6	91
146-34		0.00	0	296167	19330	30875	651727	3060639	0.21	0.0662	0.0010	1.1146	0.0192	0.1222	0.0016	0.4918	812	32	743	9	760	9	98
146-35		0.03	59	215885	12862	4156	1192573	3254884	0.37	0.0603	0.0010	0.6983	0.0122	0.0840	0.0011	0.4911	614	34	520	7	538	7	97

DA14-146	Ikal Domain		Mean cps (background subtracted)							Isotopic Ratios (± 1σ)							Age (Ma ± 1σ)						
Analysis	Core/Rim	$\%Pb_c$	^{204}Pb	^{206}Pb	^{207}Pb	^{208}Pb	^{232}Th	^{238}U	Th/U	$^{207}Pb/^{206}Pb$		$^{207}Pb/^{235}U$		$^{206}Pb/^{238}U$		Rho	$^{207}Pb/^{206}Pb$		$^{206}Pb/^{238}U$		$^{207}Pb/^{235}U$		%Conc
146-36		0.00	7	147588	8789	2221	297071	1913997	0.16	0.0606	0.0007	0.7603	0.0103	0.0911	0.0011	0.5580	624	26	562	6	574	6	98
146-37		0.01	8	100045	5887	1331	118874	1326044	0.09	0.0598	0.0007	0.7379	0.0099	0.0896	0.0011	0.5716	595	26	553	6	561	6	99
146-38		0.02	23	124532	7391	3135	130027	1635856	0.08	0.0602	0.0007	0.7489	0.0101	0.0902	0.0011	0.5690	612	26	557	6	568	6	98
146-39		0.00	9	314580	20606	40391	1416748	3246389	0.44	0.0662	0.0009	1.1076	0.0167	0.1213	0.0016	0.5589	814	28	738	9	757	8	98
146-40		0.01	14	275157	16294	2930	579055	3920025	0.15	0.0600	0.0008	0.7138	0.0105	0.0864	0.0011	0.5560	602	28	534	6	547	6	98
146-41		0.02	48	289787	18889	28147	1980697	3095311	0.64	0.0661	0.0015	1.0673	0.0248	0.1172	0.0017	0.3555	809	47	714	10	737	12	97
146-42		0.03	60	193830	11804	5577	3147049	2741473	1.15	0.0615	0.0009	0.7442	0.0115	0.0878	0.0011	0.5340	657	29	543	7	565	7	96

DA13-055	Itremo Domain		Mean cps (background subtracted)							Isotopic Ratios (± 1σ)							Age (Ma ± 1σ)						
Analysis	Core/Rim	$\%Pb_c$	^{204}Pb	^{206}Pb	^{207}Pb	^{208}Pb	^{232}Th	^{238}U	Th/U	$^{207}Pb/^{206}Pb$		$^{207}Pb/^{235}U$		$^{206}Pb/^{238}U$		Rho	$^{207}Pb/^{206}Pb$		$^{206}Pb/^{238}U$		$^{207}Pb/^{235}U$		%Conc
055_01		0.32	15	4630	340	702	18831	47789	0.39	0.0720	0.0014	1.2594	0.0260	0.1269	0.0018	0.4113	987	39	770	10	828	12	93
055_02		0.00	0	5500	379	575	16618	54682	0.30	0.0672	0.0013	1.2271	0.0254	0.1325	0.0019	0.4191	844	40	802	11	813	12	99
055_03		0.18	11	5982	390	849	23395	56311	0.42	0.0638	0.0012	1.2256	0.0242	0.1393	0.0020	0.4349	736	39	841	11	812	11	104
055_04		0.00	0	5614	361	830	22885	52679	0.43	0.0626	0.0013	1.1939	0.0261	0.1383	0.0020	0.3721	696	44	835	11	798	12	105
055_05		0.03	3	9513	634	1464	41067	93284	0.44	0.0653	0.0011	1.1806	0.0209	0.1313	0.0018	0.4767	783	34	795	10	792	10	100
055_06		0.00	0	3855	251	607	17226	37841	0.46	0.0638	0.0013	1.1528	0.0247	0.1311	0.0019	0.3824	735	43	794	11	779	12	102
055_07		0.73	25	3382	222	455	13503	35697	0.38	0.0639	0.0018	1.1329	0.0320	0.1286	0.0021	0.2909	739	58	780	12	769	15	101
055_08		0.00	0	3301	227	409	11690	37145	0.31	0.0665	0.0032	1.1729	0.0545	0.1281	0.0028	0.1646	822	97	777	16	788	25	99
055_09		0.00	0	4034	266	449	13399	40604	0.33	0.0646	0.0014	1.1307	0.0242	0.1271	0.0018	0.3688	761	43	771	10	768	12	100
055_10		0.01	1	7179	470	1061	31532	70466	0.45	0.0640	0.0012	1.1417	0.0219	0.1294	0.0018	0.4213	743	38	784	10	773	10	101
055_11		0.00	0	5271	362	797	22776	53156	0.43	0.0671	0.0014	1.1652	0.0241	0.1260	0.0018	0.3774	841	41	765	10	784	11	98
055_12		0.00	0	5595	364	800	22975	55167	0.42	0.0638	0.0016	1.1809	0.0301	0.1343	0.0021	0.3090	734	53	813	12	792	14	103
055_13		0.00	0	7091	466	999	28095	68528	0.41	0.0642	0.0013	1.1571	0.0233	0.1308	0.0018	0.3796	749	41	792	10	781	11	101
055_14	C	0.08	4	4711	315	421	12557	44103	0.28	0.0651	0.0029	1.0870	0.0461	0.1212	0.0023	0.0794	776	92	738	13	747	22	99
055_15	R	0.00	0	4104	276	374	9967	40136	0.25	0.0658	0.0015	1.1674	0.0260	0.1288	0.0018	0.3349	799	46	781	10	785	12	99
055_16		0.00	0	6210	407	933	26869	63241	0.42	0.0642	0.0012	1.1248	0.0218	0.1270	0.0018	0.4384	749	38	771	10	765	10	101
055_17		0.28	17	6032	405	886	24608	58448	0.42	0.0659	0.0011	1.1888	0.0217	0.1308	0.0018	0.4511	805	35	792	10	795	10	100
055_18		0.10	5	5032	336	730	21588	52508	0.41	0.0654	0.0015	1.1534	0.0265	0.1279	0.0019	0.3786	788	46	776	11	779	12	100
055_19		0.02	1	4550	296	646	17885	44669	0.40	0.0640	0.0012	1.1344	0.0230	0.1287	0.0018	0.4050	740	41	780	10	770	11	101
055_20		0.19	9	4781	323	701	19631	47462	0.41	0.0662	0.0012	1.1795	0.0233	0.1292	0.0018	0.4263	813	39	784	10	791	11	99
055_21		0.08	7	8561	560	1383	35918	80484	0.45	0.0641	0.0011	1.1973	0.0214	0.1354	0.0018	0.4735	746	35	819	10	799	10	102
055_22		0.15	12	8037	533	786	24028	85501	0.28	0.0644	0.0017	1.1688	0.0320	0.1317	0.0022	0.3396	755	55	797	12	786	15	101
055_23		0.32	17	5225	335	708	20354	52679	0.39	0.0629	0.0017	1.1665	0.0317	0.1346	0.0022	0.3239	704	56	814	12	785	15	104
055_24		0.77	27	3499	235	395	13042	38816	0.34	0.0656	0.0037	1.1587	0.0623	0.1281	0.0031	0.1439	795	112	777	17	781	29	99
055_25		0.00	0	3664	245	406	12182	37664	0.32	0.0653	0.0015	1.1519	0.0269	0.1281	0.0019	0.3722	782	47	777	11	778	13	100
055_26		0.13	8	6351	417	920	26708	63757	0.42	0.0636	0.0014	1.1797	0.0276	0.1346	0.0021	0.3830	728	47	814	12	791	13	103
055_27		0.00	0	7597	502	1220	34165	76558	0.45	0.0643	0.0012	1.1500	0.0228	0.1299	0.0018	0.4451	750	39	787	11	777	11	101
055_28		0.03	1	3958	260	502	14161	40541	0.35	0.0638	0.0018	1.1792	0.0338	0.1341	0.0022	0.3062	734	59	811	13	791	16	103
055_29		0.00	0	2462	167	297	8365	25915	0.32	0.0667	0.0024	1.2013	0.0425	0.1306	0.0024	0.2391	829	73	791	14	801	20	99
055_30		0.29	15	5139	341	744	22377	54525	0.41	0.0651	0.0025	1.2093	0.0456	0.1347	0.0026	0.2411	778	78	814	15	805	21	101
055_31		0.00	0	1637	107	131	3246	15406	0.21	0.0633	0.0020	1.1504	0.0351	0.1319	0.0021	0.2267	717	64	799	12	777	17	103

DA13-055	Itremo Domain		Mean cps (background subtracted)							Isotopic Ratios (± 1σ)							Age (Ma ± 1σ)						
Analysis	Core/Rim	$\%Pb_c$	^{204}Pb	^{206}Pb	^{207}Pb	^{208}Pb	^{232}Th	^{238}U	Th/U	$^{207}Pb/^{206}Pb$		$^{207}Pb/^{235}U$		$^{206}Pb/^{238}U$		Rho	$^{207}Pb/^{206}Pb$		$^{206}Pb/^{238}U$		$^{207}Pb/^{235}U$		%Conc
055_32		0.00	0	3624	239	534	14666	34305	0.43	0.0633	0.0017	1.1550	0.0311	0.1324	0.0020	0.2678	717	57	802	11	780	15	103
055_33		0.21	4	1928	132	228	6122	18367	0.33	0.0659	0.0018	1.1844	0.0324	0.1304	0.0020	0.2655	802	57	790	11	793	15	100
055_34		0.00	0	1541	105	139	3701	15363	0.24	0.0659	0.0021	1.1392	0.0354	0.1254	0.0020	0.2218	804	65	761	11	772	17	99
055_35		0.02	1	4362	281	669	17197	41092	0.42	0.0623	0.0014	1.1327	0.0252	0.1318	0.0019	0.3356	685	46	798	11	769	12	104
055_36		0.00	0	4489	292	673	18351	42790	0.43	0.0632	0.0015	1.1163	0.0266	0.1281	0.0018	0.2952	715	50	777	10	761	13	102
055_37		0.23	8	3474	226	496	13213	33581	0.39	0.0629	0.0015	1.1103	0.0271	0.1280	0.0019	0.2921	705	51	777	11	758	13	102
055_38	C	0.00	1	38173	2587	3266	85719	356596	0.24	0.0654	0.0013	1.1872	0.0233	0.1316	0.0018	0.3666	788	40	797	10	795	11	100
055_39	R	0.00	0	1665	113	174	4762	15781	0.30	0.0662	0.0020	1.1823	0.0356	0.1296	0.0020	0.2229	812	63	785	11	792	17	99
055_40		0.00	0	1608	106	169	4598	15294	0.30	0.0643	0.0020	1.1407	0.0353	0.1287	0.0020	0.2112	751	65	780	11	773	17	101
055_41		0.00	0	7315	474	1198	32087	68820	0.47	0.0630	0.0014	1.1249	0.0257	0.1296	0.0018	0.3023	707	48	785	10	765	12	103
055_42		0.07	2	2837	199	400	11491	27811	0.41	0.0678	0.0028	1.2001	0.0473	0.1283	0.0024	0.1376	863	83	778	14	801	22	97
055_43		0.14	6	4298	306	761	20604	44141	0.47	0.0691	0.0034	1.2078	0.0556	0.1266	0.0026	0.1031	902	97	769	15	804	26	96
055_44		0.04	2	5471	360	681	18828	51594	0.36	0.0642	0.0016	1.1391	0.0282	0.1288	0.0018	0.2557	747	52	781	11	772	13	101
055_45		0.19	8	4304	283	437	11878	40381	0.29	0.0642	0.0017	1.1400	0.0297	0.1289	0.0019	0.2378	747	55	782	11	773	14	101

DA13-056	Itremo Domain		Mean cps (background subtracted)							Isotopic Ratios (± 1σ)							Age (Ma ± 1σ)						
Analysis	Core/Rim	$\%Pb_c$	^{204}Pb	^{206}Pb	^{207}Pb	^{208}Pb	^{232}Th	^{238}U	Th/U	$^{207}Pb/^{206}Pb$		$^{207}Pb/^{235}U$		$^{206}Pb/^{238}U$		Rho	$^{207}Pb/^{206}Pb$		$^{206}Pb/^{238}U$		$^{207}Pb/^{235}U$		%Conc
056_01		0.08	35	42522	3577	6237	103768	400046	0.26	0.0837	0.0014	1.5560	0.0275	0.1348	0.0018	0.4680	1286	32	815	10	953	11	86
056_03		0.04	17	44274	2965	3848	87617	397081	0.22	0.0666	0.0009	1.2103	0.0182	0.1319	0.0016	0.4915	824	29	799	9	805	8	99
056_04		0.06	41	68212	4905	6078	137235	661150	0.21	0.0708	0.0014	1.3028	0.0264	0.1334	0.0019	0.4130	953	39	807	11	847	12	95
056_05		0.01	22	180556	11806	11709	261498	1431552	0.18	0.0644	0.0013	1.2989	0.0266	0.1463	0.0019	0.3166	755	43	880	11	845	12	104
056_06		0.04	11	30652	2370	3939	71664	268013	0.27	0.0752	0.0019	1.2928	0.0314	0.1246	0.0017	0.2261	1074	49	757	10	843	14	90
056_07		0.07	73	106085	7775	15397	338985	961376	0.35	0.0729	0.0013	1.4098	0.0261	0.1404	0.0019	0.4531	1010	35	847	11	893	11	95
056_11		0.29	176	60149	6589	11628	108925	533117	0.20	0.1088	0.0025	1.9335	0.0432	0.1289	0.0017	0.2705	1779	41	782	10	1093	15	72
056_13		0.00	18	1272801	83713	623759	17635626	12226915	1.44	0.0665	0.0016	1.1900	0.0282	0.1299	0.0019	0.3194	821	48	787	11	796	13	99
056_14		1.18	118	9866	2050	4984	35209	135592	0.26	0.2025	0.0044	2.2690	0.0483	0.0813	0.0011	0.2771	2846	35	504	6	1203	15	42
056_16		0.22	79	35542	3242	5830	42976	277267	0.15	0.0911	0.0031	1.8599	0.0605	0.1481	0.0024	0.1817	1448	63	891	14	1067	21	83
056_18		0.66	91	13711	1979	3643	43891	177744	0.25	0.1389	0.0058	1.9325	0.0778	0.1010	0.0021	0.1768	2214	71	620	12	1092	27	57
056_19		0.05	26	47801	3438	4692	102016	455788	0.22	0.0717	0.0013	1.3276	0.0255	0.1343	0.0019	0.4351	977	36	813	11	858	11	95
056_20		0.03	4	13396	882	949	23336	121167	0.19	0.0649	0.0012	1.1317	0.0210	0.1265	0.0016	0.3577	770	38	768	9	769	10	100
056_21		0.15	2	1358	159	278	1924	18051	0.11	0.1168	0.0031	1.4514	0.0375	0.0901	0.0014	0.2425	1908	47	556	8	911	16	61
056_22		0.00	0	115024	7588	10820	260807	1034032	0.25	0.0660	0.0010	1.2405	0.0198	0.1363	0.0017	0.4940	807	30	824	10	819	9	101
056_23		0.06	17	27488	1882	3296	78187	270216	0.29	0.0664	0.0014	1.2075	0.0268	0.1320	0.0019	0.3625	818	45	799	11	804	12	99
056_24		0.03	113	451029	30860	25452	558195	4118465	0.14	0.0681	0.0010	1.2719	0.0206	0.1355	0.0018	0.4896	872	31	819	10	833	9	98
056_26		0.13	109	86973	6854	8738	141295	809385	0.17	0.0787	0.0011	1.3908	0.0213	0.1283	0.0016	0.4875	1164	28	778	9	885	9	88
056_29		0.12	121	100334	8291	9572	145538	862638	0.17	0.0848	0.0029	1.5295	0.0498	0.1310	0.0020	0.1625	1312	64	794	12	942	20	84
056_30		0.39	171	43145	5411	10734	141687	496625	0.29	0.1235	0.0029	1.9157	0.0450	0.1125	0.0017	0.3387	2008	41	687	10	1087	16	63
056_31		0.04	116	257995	18666	20921	408049	2254581	0.18	0.0726	0.0013	1.4132	0.0261	0.1411	0.0019	0.4122	1004	36	851	11	895	11	95
056_32		0.57	282	49123	7064	14268	180585	563551	0.32	0.1395	0.0041	2.2041	0.0639	0.1147	0.0019	0.2655	2221	50	700	11	1182	20	59

DA13-063	Itremo Domain		Mean cps (background subtracted)							Isotopic Ratios (± 1σ)							Age (Ma ± 1σ)						
Analysis	Core/Rim	$\%Pb_c$	^{204}Pb	^{206}Pb	^{207}Pb	^{208}Pb	^{232}Th	^{238}U	Th/U	$^{207}Pb/^{206}Pb$		$^{207}Pb/^{235}U$		$^{206}Pb/^{238}U$		Rho	$^{207}Pb/^{206}Pb$		$^{206}Pb/^{238}U$		$^{207}Pb/^{235}U$		%Conc
063_01	C	0.24	96	40723	3859	7065	531980	661793	0.80	0.0934	0.0013	1.1993	0.0210	0.0932	0.0015	0.6561	1496	26	574	9	800	10	72
063_02	R	0.07	15	23016	1627	1274	75973	305711	0.25	0.0690	0.0009	1.0520	0.0176	0.1106	0.0017	0.6509	899	27	676	10	730	9	93
063_03	C	0.04	25	60182	6396	5074	68859	381129	0.18	0.1042	0.0012	3.4357	0.0546	0.2393	0.0037	0.7285	1700	21	1383	19	1513	13	91
063_04	R	0.06	15	26027	1843	1140	28683	296247	0.10	0.0695	0.0009	1.2694	0.0208	0.1326	0.0020	0.7037	912	25	803	12	832	9	96
063_05		0.15	21	13764	924	877	22032	154146	0.14	0.0659	0.0009	1.2187	0.0211	0.1341	0.0021	0.6563	804	28	811	12	809	10	100
063_06	C	0.04	24	64461	10534	11014	91336	238876	0.38	0.1605	0.0019	9.0216	0.1445	0.4077	0.0062	0.7214	2461	20	2204	29	2340	15	94
063_07	R	0.10	33	34588	2409	5940	144048	373162	0.39	0.0689	0.0017	1.2699	0.0318	0.1338	0.0022	0.3919	895	49	809	12	832	14	97
063_08		0.04	7	18376	1239	2086	49615	220940	0.22	0.0663	0.0016	1.2267	0.0321	0.1342	0.0024	0.4513	816	50	812	14	813	15	100
063_09		0.07	16	22943	1586	2521	77689	273406	0.28	0.0681	0.0010	1.1745	0.0206	0.1251	0.0019	0.6404	871	29	760	11	789	10	96
063_10		0.00	0	18710	1254	1924	64739	220538	0.29	0.0660	0.0009	1.1700	0.0204	0.1287	0.0020	0.6621	806	28	780	11	787	10	99
063_11		0.10	14	13829	968	1608	42738	160273	0.27	0.0689	0.0010	1.2419	0.0220	0.1307	0.0020	0.6424	897	29	792	12	820	10	97
063_12	C	0.01	7	83570	13454	14409	126392	318576	0.40	0.1585	0.0024	8.8861	0.1672	0.4068	0.0065	0.6330	2439	25	2200	30	2326	17	95
063_13	R	0.00	0	14274	956	1228	30761	163774	0.19	0.0660	0.0010	1.1967	0.0216	0.1314	0.0020	0.6274	808	30	796	12	799	10	100
063_14		0.02	6	30010	2023	3474	105230	353660	0.30	0.0664	0.0009	1.1816	0.0206	0.1291	0.0020	0.6681	818	28	783	11	792	10	99
063_15		0.00	0	23217	1551	2998	93215	274340	0.34	0.0655	0.0016	1.1949	0.0314	0.1324	0.0023	0.4363	790	50	801	13	798	15	100

DA13-064	Itremo Domain		Mean cps (background subtracted)							Isotopic Ratios (± 1σ)							Age (Ma ± 1σ)						
Analysis	Core/Rim	$\%Pb_c$	^{204}Pb	^{206}Pb	^{207}Pb	^{208}Pb	^{232}Th	^{238}U	Th/U	$^{207}Pb/^{206}Pb$		$^{207}Pb/^{235}U$		$^{206}Pb/^{238}U$		Rho	$^{207}Pb/^{206}Pb$		$^{206}Pb/^{238}U$		$^{207}Pb/^{235}U$		%Conc
064_01	C	0.07	9	12380	2376	2535	18170	29105	0.62	0.1967	0.0029	13.1388	0.2009	0.4847	0.0059	0.4552	2799	24	2548	26	2690	14	95
064_02	R	0.00	0	5803	388	276	6393	51646	0.12	0.0686	0.0013	1.2152	0.0228	0.1285	0.0016	0.3578	887	38	779	9	808	10	97
064_03	C	0.06	7	12559	1586	4146	37765	39922	0.95	0.1296	0.0020	6.4051	0.1032	0.3588	0.0044	0.4287	2092	27	1976	21	2033	14	97
064_04	R	0.20	26	12738	907	1772	59145	129253	0.46	0.0731	0.0012	1.1233	0.0194	0.1115	0.0014	0.3800	1017	34	682	8	765	9	89
064_05	C	0.01	4	48374	7793	22861	168799	121947	1.38	0.1648	0.0025	10.3806	0.1664	0.4569	0.0056	0.4394	2506	26	2426	25	2469	15	98
064_06	R	0.00	0	6588	441	341	7477	56330	0.13	0.0686	0.0014	1.2722	0.0256	0.1345	0.0017	0.3326	888	41	813	10	833	11	98
064_07		0.00	0	10576	694	1619	36252	89183	0.41	0.0672	0.0012	1.2566	0.0225	0.1356	0.0017	0.3745	845	36	820	10	826	10	99
064_08	C	0.00	0	21177	3558	3894	33534	60200	0.56	0.1748	0.0039	9.2302	0.2030	0.3832	0.0050	0.2714	2604	37	2091	23	2361	20	89
064_09	R	0.00	0	4553	316	247	5981	42519	0.14	0.0701	0.0026	1.1271	0.0403	0.1166	0.0019	0.1478	931	74	711	11	766	19	93
064_10	C	0.00	0	13824	2223	2776	21749	36531	0.60	0.1645	0.0028	9.8014	0.1683	0.4323	0.0054	0.3993	2503	28	2316	24	2416	16	96
064_11	R	0.00	0	6109	399	183	4010	52757	0.08	0.0669	0.0014	1.2181	0.0249	0.1322	0.0017	0.3227	834	42	800	10	809	11	99
064_12		0.24	25	10236	684	1162	29654	95251	0.31	0.0684	0.0014	1.1668	0.0243	0.1238	0.0016	0.3275	880	42	753	9	785	11	96
064_13		0.10	13	12737	957	2205	75824	133458	0.57	0.0777	0.0018	1.1397	0.0255	0.1064	0.0014	0.2809	1140	44	652	8	772	12	84
064_14	C	0.01	2	21978	3478	5950	43520	55765	0.78	0.1611	0.0029	9.9623	0.1834	0.4487	0.0056	0.3678	2467	30	2390	25	2431	17	98
064_15	R	0.11	6	5333	413	384	7004	54372	0.13	0.0796	0.0021	1.2273	0.0320	0.1119	0.0016	0.2404	1186	52	684	9	813	15	84
064_16		0.05	7	14592	944	1747	43010	132820	0.32	0.0660	0.0010	1.1463	0.0186	0.1260	0.0015	0.4241	806	32	765	9	776	9	99
064_17	C	0.00	0	24593	3600	4839	40772	69725	0.58	0.1484	0.0022	8.1467	0.1239	0.3983	0.0048	0.4408	2327	25	2161	22	2247	14	96
064_18	R	0.36	19	5247	379	552	14504	50543	0.29	0.0710	0.0024	1.1077	0.0358	0.1132	0.0018	0.1567	958	67	691	10	757	17	91
064_19		0.11	11	10343	1602	3340	50895	36834	1.38	0.1571	0.0025	6.9751	0.1128	0.3221	0.0040	0.4252	2424	26	1800	20	2108	14	85
064_20		0.03	2	6687	445	344	7042	61512	0.11	0.0681	0.0025	1.2503	0.0441	0.1332	0.0023	0.1941	872	73	806	13	824	20	98
064_21	C	0.00	0	28578	4526	4518	36447	77801	0.47	0.1606	0.0029	9.5771	0.1756	0.4326	0.0056	0.3935	2462	30	2318	25	2395	17	97
064_22	R	0.01	1	10417	693	926	20930	93666	0.22	0.0674	0.0012	1.1957	0.0220	0.1287	0.0016	0.3795	850	37	781	9	799	10	98
064_23	C	0.00	0	5197	493	774	13863	40066	0.35	0.0957	0.0022	1.9060	0.0436	0.1445	0.0020	0.2662	1542	43	870	11	1083	15	80
064_24	R	0.16	10	6226	422	241	5192	55534	0.09	0.0682	0.0013	1.2099	0.0239	0.1287	0.0017	0.3425	875	40	780	9	805	11	97
064_25	C	0.06	12	20165	2256	974	9989	89501	0.11	0.1114	0.0025	3.8126	0.0854	0.2483	0.0033	0.2712	1822	41	1430	17	1595	18	90
064_26	R	0.00	0	8710	574	864	21402	76774	0.28	0.0659	0.0013	1.1718	0.0227	0.1290	0.0016	0.3431	802	40	782	9	788	11	99
064_27	C	0.01	2	26399	4150	4467	39338	78019	0.50	0.1558	0.0039	8.7171	0.2154	0.4060	0.0059	0.2816	2410	42	2197	27	2309	23	95
064_28	R	0.00	0	9001	591	994	33232	87392	0.38	0.0657	0.0013	1.0730	0.0211	0.1185	0.0015	0.3378	796	40	722	9	740	10	98
064_29	C	0.13	13	10216	1675	1367	10167	26577	0.38	0.1632	0.0029	9.9271	0.1819	0.4413	0.0057	0.3737	2489	30	2356	25	2428	17	97
064_30	R	0.13	7	5246	332	282	6655	46100	0.14	0.0632	0.0014	1.1362	0.0249	0.1305	0.0017	0.2956	713	46	791	10	771	12	103
064_31	C	0.00	0	13323	2083	2249	16825	35473	0.47	0.1568	0.0024	9.4694	0.1502	0.4380	0.0055	0.4538	2421	25	2342	25	2385	15	98

DA13-064	Itremo Domain		Mean cps (background subtracted)							Isotopic Ratios (± 1σ)							Age (Ma ± 1σ)						
Analysis	Core/Rim	$\%Pb_c$	^{204}Pb	^{206}Pb	^{207}Pb	^{208}Pb	^{232}Th	^{238}U	Th/U	$^{207}Pb/^{206}Pb$		$^{207}Pb/^{235}U$		$^{206}Pb/^{238}U$		Rho	$^{207}Pb/^{206}Pb$		$^{206}Pb/^{238}U$		$^{207}Pb/^{235}U$		%Conc
064_32	R	0.00	0	6178	426	391	7945	59609	0.13	0.0691	0.0013	1.1467	0.0211	0.1204	0.0015	0.3697	901	37	733	9	776	10	94
064_33	C	0.03	4	13095	1544	1020	9655	49369	0.20	0.1182	0.0026	4.7804	0.1043	0.2934	0.0039	0.2800	1929	39	1658	20	1782	18	93
064_34	R	0.19	27	14378	1293	2798	93692	142720	0.66	0.0888	0.0021	1.4914	0.0356	0.1219	0.0018	0.2943	1399	45	741	10	927	15	80
064_35	C	0.01	5	41950	6657	1639	17587	145879	0.12	0.1594	0.0027	7.1598	0.1247	0.3257	0.0040	0.3774	2450	29	1818	20	2132	16	85
064_36	R	0.15	14	9059	670	780	17088	80829	0.21	0.0737	0.0015	1.3470	0.0282	0.1326	0.0018	0.3318	1033	41	803	10	866	12	93
064_37	C	0.00	0	20699	3306	1997	15972	53927	0.30	0.1584	0.0032	9.8635	0.2028	0.4516	0.0062	0.3482	2439	34	2402	27	2422	19	99
064_38	R	0.16	13	8008	530	913	28974	74659	0.39	0.0667	0.0024	1.2078	0.0415	0.1313	0.0022	0.1923	829	72	795	13	804	19	99
064_39	C	0.00	0	17247	2476	2008	16640	47877	0.35	0.1435	0.0024	8.2666	0.1440	0.4177	0.0053	0.4062	2270	29	2250	24	2261	16	100
064_40	R	0.08	5	6605	437	392	9951	58707	0.17	0.0662	0.0014	1.1968	0.0251	0.1311	0.0017	0.3259	813	43	794	10	799	12	99
064_41		0.06	7	10776	702	1144	28094	100202	0.28	0.0652	0.0012	1.1268	0.0211	0.1253	0.0016	0.3670	782	38	761	9	766	10	99
064_42	C	0.05	6	11939	1625	3033	25163	35555	0.71	0.1362	0.0024	7.3485	0.1325	0.3914	0.0050	0.3931	2179	30	2130	23	2155	16	99
064_43	R	0.06	4	6293	415	264	7338	58839	0.12	0.0660	0.0014	1.1363	0.0238	0.1249	0.0016	0.3257	806	43	759	9	771	11	98
064_44		0.02	4	18150	1383	3276	180355	204260	0.88	0.0755	0.0018	1.1071	0.0266	0.1064	0.0015	0.2981	1082	47	652	9	757	13	86
064_45		0.00	0	11714	766	1353	33581	103300	0.33	0.0655	0.0013	1.1944	0.0238	0.1323	0.0017	0.3528	790	41	801	10	798	11	100
064_46	C	0.01	2	15640	1756	1013	9670	54373	0.18	0.1123	0.0016	5.2044	0.0792	0.3363	0.0042	0.4747	1836	26	1869	20	1853	13	101
064_47	R	0.00	0	8684	582	306	6457	85761	0.08	0.0668	0.0019	1.1343	0.0317	0.1232	0.0019	0.2508	832	58	749	11	770	15	97
064_48		0.15	14	9086	592	1267	29336	82509	0.36	0.0654	0.0011	1.1609	0.0201	0.1289	0.0016	0.4088	786	35	781	9	782	9	100
064_49	C	0.01	4	30900	5343	4584	32009	73888	0.43	0.1734	0.0024	11.7030	0.1745	0.4895	0.0060	0.4863	2591	23	2569	26	2581	14	100
064_50	R	0.00	0	5356	346	252	6310	46887	0.13	0.0649	0.0013	1.1964	0.0234	0.1337	0.0017	0.3529	772	40	809	10	799	11	101
064_51		0.00	0	8063	527	800	18666	73585	0.25	0.0657	0.0012	1.1634	0.0210	0.1285	0.0016	0.3925	796	36	779	9	784	10	99
064_52	C	0.00	0	24418	3859	7767	59461	66650	0.89	0.1590	0.0024	9.3958	0.1469	0.4287	0.0053	0.4620	2445	25	2300	24	2377	14	97
064_53	R	0.17	12	7120	456	529	12282	63772	0.19	0.0645	0.0012	1.1645	0.0219	0.1310	0.0017	0.3701	757	38	794	10	784	10	101
064_54	C	0.03	12	40666	6502	3296	22622	101909	0.22	0.1611	0.0024	10.3770	0.1656	0.4672	0.0058	0.4511	2467	25	2471	25	2469	15	100
064_55	R	0.20	14	7127	484	309	8241	64666	0.13	0.0686	0.0013	1.2041	0.0236	0.1273	0.0016	0.3442	887	40	772	9	803	11	96
064_56		0.26	30	11711	1214	2778	55646	116474	0.48	0.1046	0.0027	1.7653	0.0446	0.1225	0.0018	0.2881	1707	46	745	10	1033	16	72
064_57	C	0.03	11	33524	5433	5980	42205	81464	0.52	0.1643	0.0027	10.8154	0.1816	0.4776	0.0059	0.4211	2500	27	2517	26	2507	16	100
064_58	R	0.00	0	9262	657	991	21595	85701	0.25	0.0720	0.0014	1.2756	0.0260	0.1285	0.0017	0.3557	987	40	779	10	835	12	93
064_59		0.02	1	5983	386	197	5077	57881	0.09	0.0655	0.0020	1.1383	0.0345	0.1260	0.0020	0.2270	792	63	765	11	772	16	99
064_60		0.14	9	6250	392	443	12818	55826	0.23	0.0643	0.0034	1.1093	0.0568	0.1251	0.0026	0.1081	751	108	760	15	758	27	100

DA13-065	Itremo Domain		Mean cps (background subtracted)							Isotopic Ratios (± 1σ)							Age (Ma ± 1σ)						
Analysis	Core/Rim	$\%Pb_c$	^{204}Pb	^{206}Pb	^{207}Pb	^{208}Pb	^{232}Th	^{238}U	Th/U	$^{207}Pb/^{206}Pb$		$^{207}Pb/^{235}U$		$^{206}Pb/^{238}U$		Rho	$^{207}Pb/^{206}Pb$		$^{206}Pb/^{238}U$		$^{207}Pb/^{235}U$		%Conc
065_01		0.12	3	2437	346	934	14424	25233	0.57	0.1384	0.0057	2.6013	0.1013	0.1363	0.0032	0.1966	2207	70	824	18	1301	29	63
065_02		0.00	0	8886	600	1690	42440	82583	0.51	0.0661	0.0011	1.2394	0.0218	0.1360	0.0018	0.4720	810	34	822	10	819	10	100
065_03		0.00	0	13469	943	3305	88718	120795	0.73	0.0689	0.0011	1.2559	0.0202	0.1322	0.0017	0.4551	895	31	801	9	826	9	97
065_04		0.18	28	15180	1138	1284	27416	149176	0.18	0.0736	0.0011	1.3195	0.0222	0.1300	0.0018	0.5038	1031	31	788	10	854	10	92
065_05		0.07	7	10676	702	1721	49302	108211	0.46	0.0647	0.0011	1.1171	0.0199	0.1253	0.0017	0.4682	763	35	761	10	762	10	100
065_06		0.03	6	21406	2802	5764	59593	89294	0.67	0.1294	0.0019	5.0924	0.0787	0.2854	0.0036	0.4783	2090	25	1619	18	1835	13	88
065_07		0.11	22	20836	1745	4284	101392	300258	0.34	0.0796	0.0023	1.0964	0.0321	0.1000	0.0017	0.3249	1186	56	614	10	752	16	82
065_08		0.14	16	11401	1306	3025	34618	61206	0.57	0.1145	0.0027	3.6116	0.0848	0.2289	0.0034	0.3140	1872	42	1329	18	1552	19	86
065_10	C	0.08	301	357163	62872	78196	595420	1221331	0.49	0.1725	0.0020	10.8915	0.1804	0.4580	0.0073	0.7344	2582	20	2431	32	2514	15	97
065_11	R	0.07	29	40917	4875	6023	123078	319567	0.39	0.1185	0.0016	3.1141	0.0533	0.1905	0.0029	0.6580	1934	24	1124	16	1436	13	78
065_12	C	0.01	17	171615	26988	41138	315403	594511	0.53	0.1549	0.0018	9.4508	0.1517	0.4424	0.0068	0.7379	2401	19	2361	31	2383	15	99
065_13	R	0.29	73	25272	1962	979	38284	302862	0.13	0.0764	0.0015	1.4293	0.0320	0.1358	0.0024	0.5496	1105	38	821	13	901	13	91
065_14	C	0.01	6	52770	6072	2646	27484	242521	0.11	0.1133	0.0014	5.2234	0.0857	0.3343	0.0052	0.7233	1853	21	1859	25	1856	14	100
065_15	R	0.47	149	31618	4757	7468	204257	473533	0.43	0.1426	0.0042	2.0575	0.0619	0.1047	0.0020	0.3396	2258	50	642	12	1135	21	57
065_16	C	0.00	0	26045	1769	4165	101973	313766	0.32	0.0670	0.0009	1.1765	0.0202	0.1273	0.0020	0.6838	838	27	773	11	790	9	98
065_17	R	0.17	103	59533	5218	6204	357208	762477	0.47	0.0855	0.0012	1.4518	0.0267	0.1232	0.0020	0.6606	1327	28	749	11	911	11	82
065_18		0.12	75	64097	4996	7996	218593	942855	0.23	0.0764	0.0013	1.1245	0.0232	0.1067	0.0018	0.5735	1106	35	654	10	765	11	85
065_19	C	0.08	19	23774	2861	5227	56009	138893	0.40	0.1187	0.0016	4.2853	0.0733	0.2618	0.0041	0.6855	1937	23	1499	21	1691	14	89
065_20	R	0.08	28	37013	2908	2959	57675	436981	0.13	0.0774	0.0014	1.4153	0.0303	0.1327	0.0022	0.5511	1131	36	803	13	895	13	90
065_21		0.10	37	38519	2861	4571	123045	485523	0.25	0.0726	0.0011	1.2563	0.0238	0.1255	0.0021	0.6404	1003	30	762	12	826	11	92
065_22		0.03	15	53291	5368	5203	136652	591383	0.23	0.0990	0.0017	1.8576	0.0375	0.1362	0.0022	0.5532	1606	32	823	12	1066	13	77
065_23		0.12	58	48970	3796	8549	204893	588011	0.35	0.0756	0.0011	1.3680	0.0257	0.1312	0.0021	0.6436	1085	30	795	12	875	11	91
065_24		0.20	115	57790	5456	9967	234726	750469	0.31	0.0927	0.0014	1.5384	0.0291	0.1204	0.0019	0.6328	1481	29	733	11	946	12	77

DA13-012	C. Ant Domain		Mean cps (background subtracted)							Isotopic Ratios (± 1σ)							Age (Ma ± 1σ)						
Analysis	Core/Rim	$\%Pb_c$	^{204}Pb	^{206}Pb	^{207}Pb	^{208}Pb	^{232}Th	^{238}U	Th/U	$^{207}Pb/^{206}Pb$		$^{207}Pb/^{235}U$		$^{206}Pb/^{238}U$		Rho	$^{207}Pb/^{206}Pb$		$^{206}Pb/^{238}U$		$^{207}Pb/^{235}U$		%Conc
012_01	C	0.07	39	59450	9604	11738	150819	275839	0.55	0.1603	0.0024	5.6831	0.0908	0.2571	0.0032	0.4627	2459	25	1475	17	1929	14	76
012_02	R	0.11	10	8921	608	906	24887	89899	0.28	0.0674	0.0012	1.0854	0.0204	0.1169	0.0015	0.3756	849	38	712	9	746	10	95
012_03	C	0.00	0	13031	2210	1923	15736	36341	0.43	0.1691	0.0038	8.6216	0.1871	0.3697	0.0049	0.2305	2549	37	2028	23	2299	20	88
012_04	R	0.00	0	7516	479	844	26320	83102	0.32	0.0625	0.0032	0.9808	0.0480	0.1138	0.0024	0.1327	693	105	695	14	694	25	100
012_05		0.00	0	10129	646	1061	26908	96526	0.28	0.0641	0.0018	1.0765	0.0294	0.1218	0.0018	0.2329	745	58	741	10	742	14	100
012_06		0.03	8	28724	4663	1023	14838	93360	0.16	0.1597	0.0034	8.2860	0.1794	0.3765	0.0054	0.3408	2452	36	2060	25	2263	20	91
012_07	C	0.01	5	59400	9787	14565	149821	194290	0.77	0.1632	0.0024	7.7368	0.1168	0.3438	0.0041	0.4294	2489	24	1905	20	2201	14	87
012_08	R	0.04	4	10417	701	1020	31916	96558	0.33	0.0668	0.0016	1.0230	0.0240	0.1110	0.0014	0.1965	832	50	679	8	715	12	95
012_09		0.04	4	11122	768	1231	34319	164812	0.21	0.0683	0.0015	0.7166	0.0154	0.0761	0.0010	0.2774	877	44	473	6	549	9	86
012_10	C	0.00	0	20271	3227	2166	18637	55605	0.34	0.1577	0.0034	9.1266	0.1955	0.4197	0.0057	0.3021	2431	36	2259	26	2351	20	96
012_11	R	0.00	0	5579	373	211	4994	76376	0.07	0.0653	0.0018	0.7901	0.0210	0.0878	0.0013	0.2539	783	56	543	8	591	12	92
012_12	C	0.05	34	74349	11738	7993	94378	233373	0.40	0.1567	0.0035	7.0568	0.1513	0.3264	0.0040	0.2069	2421	38	1821	20	2119	19	86
012_13	R	0.00	0	15735	1074	1518	40570	157603	0.26	0.0671	0.0015	1.1045	0.0243	0.1194	0.0016	0.3182	841	45	727	9	756	12	96
012_14	C	0.00	0	11219	1843	2440	21947	32903	0.67	0.1584	0.0034	9.0421	0.1912	0.4142	0.0059	0.3367	2438	35	2234	27	2342	19	95
012_15	R	0.00	0	16178	1083	1584	42429	163473	0.26	0.0660	0.0012	1.0167	0.0187	0.1118	0.0014	0.3407	805	38	683	8	712	9	96
012_16	C	0.00	0	79436	12834	9571	146865	429403	0.34	0.1578	0.0048	5.0276	0.1517	0.2313	0.0038	0.2401	2432	51	1341	20	1824	26	74
012_17	R	0.14	11	7901	517	913	25096	76076	0.33	0.0645	0.0012	1.0778	0.0206	0.1212	0.0016	0.3648	758	39	738	9	743	10	99
012_18	C	0.07	48	67068	11251	8089	886992	510727	1.74	0.1664	0.0035	3.6065	0.0764	0.1573	0.0022	0.3383	2522	35	942	12	1551	17	61
012_19	R	0.17	20	11576	1042	2861	95982	151408	0.63	0.0891	0.0016	1.0868	0.0199	0.0885	0.0011	0.3739	1406	34	547	7	747	10	73
012_20	C	0.09	48	55741	9214	12052	133421	176850	0.75	0.1690	0.0039	7.7532	0.1798	0.3328	0.0043	0.2737	2548	38	1852	21	2203	21	84
012_21	R	0.04	2	5145	371	689	19647	52166	0.38	0.0716	0.0020	1.1884	0.0333	0.1204	0.0019	0.2487	975	57	733	11	795	15	92
012_22	C	0.00	0	110065	18104	16268	142007	312517	0.45	0.1638	0.0030	9.7147	0.1874	0.4304	0.0058	0.4004	2495	31	2308	26	2408	18	96
012_23	R	0.00	0	11493	789	944	24275	112577	0.22	0.0688	0.0013	1.0961	0.0208	0.1156	0.0015	0.3589	892	38	705	8	752	10	94
012_24		0.09	12	13964	1087	4040	142004	181771	0.78	0.0771	0.0014	0.9816	0.0186	0.0924	0.0012	0.3981	1123	36	570	7	694	10	82
012_25	C	0.06	49	86361	16515	4128	81760	558856	0.15	0.1595	0.0059	4.0595	0.1399	0.1860	0.0034	0.1316	2451	61	1099	18	1646	28	67
012_26	R	0.02	2	11966	904	2206	68589	129393	0.53	0.0754	0.0015	1.1651	0.0240	0.1121	0.0015	0.3698	1079	40	685	9	784	11	87
012_27		0.01	8	53406	8321	8510	91092	198721	0.46	0.1563	0.0026	6.8224	0.1178	0.3167	0.0040	0.4389	2416	27	1774	20	2089	15	85
012_28	C	0.09	64	73026	12343	17663	363733	578014	0.63	0.1724	0.0064	3.7203	0.1333	0.1566	0.0027	0.1796	2581	60	938	15	1576	29	60
012_29	R	0.00	0	10161	696	1836	52011	105674	0.49	0.0688	0.0013	1.0852	0.0213	0.1145	0.0015	0.3894	892	39	699	9	746	10	94
012_30		0.09	20	21035	2927	1762	27265	134960	0.20	0.1406	0.0036	3.4142	0.0919	0.1762	0.0025	0.3416	2234	44	1046	14	1508	21	69
012_32	R	0.35	26	7382	509	1043	29682	82555	0.36	0.0693	0.0013	0.9906	0.0181	0.1036	0.0013	0.3683	909	37	636	8	699	9	91

DA13-012	C. Ant Domain		Mean cps (background subtracted)							Isotopic Ratios (± 1σ)							Age (Ma ± 1σ)						
Analysis	Core/Rim	$\%Pb_c$	^{204}Pb	^{206}Pb	^{207}Pb	^{208}Pb	^{232}Th	^{238}U	Th/U	$^{207}Pb/^{206}Pb$		$^{207}Pb/^{235}U$		$^{206}Pb/^{238}U$		Rho	$^{207}Pb/^{206}Pb$		$^{206}Pb/^{238}U$		$^{207}Pb/^{235}U$		%Conc
012_33	C	0.05	27	59062	9535	3329	90432	179767	0.50	0.1656	0.0034	8.1339	0.1626	0.3564	0.0045	0.2546	2514	34	1965	21	2246	18	87
012_34	R	0.00	0	8637	581	1181	33363	83016	0.40	0.0674	0.0012	1.1753	0.0222	0.1265	0.0017	0.3978	851	37	768	10	789	10	97
012_35		0.00	0	14058	1058	3109	106726	156846	0.68	0.0753	0.0013	1.1323	0.0199	0.1091	0.0014	0.4359	1076	33	668	8	769	9	87
012_36	C	0.00	2	53733	8852	9485	80520	149331	0.54	0.1660	0.0023	9.5313	0.1400	0.4165	0.0050	0.4779	2518	23	2244	23	2391	14	94
012_37	R	0.00	0	8746	588	1308	36233	84759	0.43	0.0678	0.0012	1.1322	0.0208	0.1212	0.0016	0.3743	862	37	737	9	769	10	96
012_38	C	0.00	0	47656	7759	7717	74806	146899	0.51	0.1635	0.0025	8.1682	0.1277	0.3623	0.0043	0.3941	2493	26	1993	20	2250	14	89
012_39	R	0.00	0	62658	10329	7272	60744	166915	0.36	0.1651	0.0027	9.6518	0.1577	0.4241	0.0051	0.3796	2509	27	2279	23	2402	15	95
012_40	C	0.28	61	21685	2427	3004	56207	529048	0.11	0.1118	0.0026	0.7075	0.0156	0.0459	0.0006	0.2324	1829	41	289	4	543	9	53
012_41	R	0.00	0	11398	757	1115	31875	117867	0.27	0.0669	0.0013	1.0726	0.0212	0.1163	0.0016	0.3702	835	40	709	9	740	10	96
012_42	C	0.01	3	40562	5843	7164	80800	175020	0.46	0.1454	0.0030	4.9183	0.0961	0.2455	0.0030	0.2151	2292	35	1415	16	1805	16	78
012_43	R	0.05	4	7862	513	1079	27936	71488	0.39	0.0655	0.0012	1.1552	0.0207	0.1279	0.0016	0.3791	790	36	776	9	780	10	100
012_44	C	0.00	0	4597	741	1107	10359	13711	0.76	0.1621	0.0028	8.6862	0.1500	0.3887	0.0051	0.3979	2478	28	2117	24	2306	16	92
012_45	R	0.06	6	10764	707	1888	49491	93944	0.53	0.0661	0.0011	1.2037	0.0210	0.1321	0.0016	0.3834	810	35	800	9	802	10	100
012_46	IC	0.01	3	29879	5122	4697	40283	80438	0.50	0.1708	0.0022	11.3296	0.1693	0.4811	0.0064	0.5990	2566	21	2532	28	2551	14	99
012_47	OC	0.16	21	13241	925	982	25900	116910	0.22	0.0685	0.0019	1.2732	0.0344	0.1350	0.0020	0.2387	884	56	816	11	834	15	98
012_48	R	0.00	0	7528	550	621	18968	93145	0.20	0.0732	0.0016	0.9903	0.0214	0.0982	0.0014	0.3349	1020	43	604	8	699	11	86
012_49	C	0.03	22	66680	10834	5357	69321	249766	0.28	0.1614	0.0024	8.0810	0.1380	0.3632	0.0052	0.5610	2470	25	1998	24	2240	15	89
012_50	R	0.00	0	13890	948	1847	69698	141318	0.49	0.0682	0.0012	1.2376	0.0234	0.1317	0.0019	0.4860	874	35	797	11	818	11	98
012_51	C	0.06	53	94814	15891	20610	309334	596083	0.52	0.1661	0.0033	5.1105	0.1093	0.2233	0.0034	0.4535	2518	33	1299	18	1838	18	71
012_52	R	0.00	0	15954	1111	1200	38691	185973	0.21	0.0696	0.0014	0.9925	0.0196	0.1035	0.0014	0.3667	917	39	635	8	700	10	91
012_53	C	0.06	49	88292	14540	14560	184994	329718	0.56	0.1642	0.0028	8.2150	0.1529	0.3630	0.0052	0.5091	2499	28	1996	25	2255	17	89
012_54	R	0.21	20	9301	624	1254	32654	84050	0.39	0.0673	0.0011	1.3054	0.0233	0.1407	0.0019	0.4754	847	34	849	11	848	10	100
012_55	C	0.00	1	88969	15992	12448	130272	285448	0.46	0.1794	0.0026	10.2182	0.1684	0.4131	0.0057	0.5601	2647	24	2229	26	2455	15	91
012_56	R	0.14	15	10348	996	1722	44623	127044	0.35	0.0963	0.0015	1.3901	0.0236	0.1047	0.0014	0.5037	1554	29	642	8	885	10	73
012_57	C	0.03	33	106749	17375	24053	274548	404090	0.68	0.1648	0.0026	7.6375	0.1310	0.3362	0.0045	0.4963	2505	26	1868	22	2189	15	85
012_58	R	0.07	9	13019	871	1467	40767	129371	0.32	0.0678	0.0013	1.2236	0.0245	0.1310	0.0019	0.4386	861	39	794	11	811	11	98
012_59	C	0.00	0	81172	13310	12261	154733	261127	0.59	0.1658	0.0025	9.1767	0.1531	0.4015	0.0054	0.5286	2515	25	2176	25	2356	15	92
012_60	R	0.04	3	8229	548	1219	35748	73918	0.48	0.0665	0.0015	1.2142	0.0272	0.1325	0.0018	0.3042	822	46	802	10	807	12	99
012_61	C	0.00	1	39766	6502	4499	46035	125981	0.37	0.1647	0.0025	9.5189	0.1615	0.4192	0.0058	0.5509	2505	25	2257	26	2389	16	94
012_62	R	0.00	0	10254	694	1110	29649	100426	0.30	0.0681	0.0012	1.2729	0.0248	0.1356	0.0019	0.4692	872	37	820	11	834	11	98
012_63	C	2.11	28	1298	207	166	1894	5350	0.35	0.1609	0.0049	7.2804	0.2150	0.3282	0.0064	0.2962	2465	50	1830	31	2146	26	85

DA13-012	C. Ant Domain		Mean cps (background subtracted)							Isotopic Ratios (± 1σ)							Age (Ma ± 1σ)						
Analysis	Core/Rim	$\%Pb_c$	^{204}Pb	^{206}Pb	^{207}Pb	^{208}Pb	^{232}Th	^{238}U	Th/U	$^{207}Pb/^{206}Pb$		$^{207}Pb/^{235}U$		$^{206}Pb/^{238}U$		Rho	$^{207}Pb/^{206}Pb$		$^{206}Pb/^{238}U$		$^{207}Pb/^{235}U$		%Conc
012_64	R	0.05	5	9892	671	1000	27615	95920	0.29	0.0677	0.0011	1.2611	0.0228	0.1350	0.0019	0.4902	861	34	817	11	828	10	99
012_65	C	0.00	3	84281	13920	13487	131870	256903	0.51	0.1677	0.0032	9.8421	0.2006	0.4256	0.0060	0.4330	2535	32	2286	27	2420	19	94
012_66	R	0.00	0	12590	828	1742	58190	133267	0.44	0.0654	0.0028	1.1108	0.0465	0.1230	0.0024	0.2003	787	87	748	14	759	22	99
012_67	C	0.06	40	62032	9441	5129	61861	405128	0.15	0.1378	0.0047	4.2492	0.1431	0.2241	0.0042	0.2496	2200	58	1304	22	1684	28	77
012_68	R	0.14	26	17910	1408	4470	153554	223736	0.69	0.0788	0.0015	1.1732	0.0236	0.1080	0.0016	0.4656	1168	36	661	9	788	11	84
012_69	C	0.00	2	58023	9501	15207	135115	166125	0.81	0.1645	0.0026	10.4118	0.1817	0.4591	0.0063	0.5210	2502	26	2436	28	2472	16	99
012_70	R	0.00	0	8925	606	1461	41960	87998	0.48	0.0679	0.0012	1.2314	0.0241	0.1316	0.0018	0.4462	865	38	797	11	815	11	98
012_71	C	0.01	11	92432	15094	10807	101316	296795	0.34	0.1615	0.0025	9.1369	0.1573	0.4105	0.0057	0.5279	2471	26	2217	26	2352	16	94
012_72	R	0.01	1	9496	651	1396	39803	92175	0.43	0.0684	0.0014	1.2493	0.0258	0.1325	0.0019	0.4063	881	40	802	11	823	12	97
012_73	C	0.00	0	22568	3490	3567	39249	86163	0.46	0.1495	0.0039	7.5796	0.2001	0.3680	0.0061	0.3488	2340	44	2020	29	2183	24	93
012_74	R	0.00	0	7152	478	778	21243	67987	0.31	0.0668	0.0018	1.2753	0.0347	0.1385	0.0022	0.3132	831	55	836	12	835	15	100
012_75		0.19	34	18211	1561	5538	213222	316078	0.67	0.0858	0.0023	0.9421	0.0253	0.0796	0.0013	0.3402	1334	50	494	8	674	13	73
012_76	C	0.00	0	1083	188	188	1679	2407	0.70	0.1761	0.0080	9.9636	0.4274	0.4112	0.0088	0.1254	2616	74	2220	40	2431	40	91
012_77	R	0.00	0	898	61	101	2713	6453	0.42	0.0687	0.0030	1.2388	0.0521	0.1309	0.0023	0.0838	889	89	793	13	818	24	97
012_78	C	0.00	0	6842	1811	1037	6734	10885	0.62	0.2617	0.0085	21.7735	0.6768	0.6042	0.0089	0.1373	3257	50	3047	36	3174	30	96
012_79	R	0.00	0	1525	94	103	3432	13147	0.26	0.0624	0.0025	0.9490	0.0364	0.1103	0.0017	0.0862	689	83	675	10	678	19	100
012_80		0.00	0	10511	1633	1457	14845	28645	0.52	0.1525	0.0104	8.0299	0.5247	0.3826	0.0099	0.0844	2374	112	2088	46	2234	59	93
012_81		0.06	1	1811	129	445	11445	13896	0.82	0.0708	0.0032	1.2310	0.0523	0.1262	0.0022	0.0915	953	88	766	13	815	24	94
012_82		0.00	0	1736	198	307	3490	6895	0.51	0.1141	0.0063	3.6511	0.1910	0.2326	0.0051	0.0709	1866	96	1348	26	1561	42	86
012_83		0.09	1	1112	68	64	1926	8113	0.24	0.0632	0.0031	1.1280	0.0532	0.1296	0.0024	0.0777	714	101	786	13	767	25	102
012_84		0.00	0	720	47	87	2475	6538	0.38	0.0686	0.0039	0.9751	0.0533	0.1031	0.0021	0.0597	887	114	633	12	691	27	92
012_85		0.00	0	6418	784	628	12396	25120	0.49	0.1272	0.0068	4.0658	0.2067	0.2318	0.0044	0.0395	2060	92	1344	23	1648	41	82
012_86	C	0.00	0	1283	210	884	6228	2594	2.40	0.1730	0.0085	11.1216	0.5206	0.4664	0.0092	0.0986	2587	79	2468	40	2533	44	97
012_87	R	0.00	0	1339	124	230	8030	18096	0.44	0.1018	0.0113	0.9289	0.0973	0.0662	0.0024	0.0142	1657	192	413	15	667	51	62
012_88		0.00	0	2323	154	584	15925	18375	0.87	0.0683	0.0036	1.1482	0.0588	0.1220	0.0023	0.0756	877	107	742	13	776	28	96
012_89	C	0.00	0	1427	91	42	1376	10755	0.13	0.0685	0.0042	1.1645	0.0684	0.1233	0.0026	0.0399	883	122	750	15	784	32	96
012_90	R	0.59	19	3188	445	1097	31441	52667	0.60	0.1516	0.0083	1.1829	0.0620	0.0566	0.0011	0.0467	2364	91	355	6	793	29	45

DA13-017	C. Ant Domain		Mean cps (background subtracted)							Isotopic Ratios (± 1σ)							Age (Ma ± 1σ)						
Analysis	Core/Rim	$\%Pb_c$	^{204}Pb	^{206}Pb	^{207}Pb	^{208}Pb	^{232}Th	^{238}U	Th/U	$^{207}Pb/^{206}Pb$		$^{207}Pb/^{235}U$		$^{206}Pb/^{238}U$		Rho	$^{207}Pb/^{206}Pb$		$^{206}Pb/^{238}U$		$^{207}Pb/^{235}U$		%Conc
017_01	C	0.01	9	93185	24714	5067	49081	259191	0.19	0.2619	0.0044	18.7348	0.3599	0.5191	0.0079	0.5434	3258	26	2695	34	3028	19	89
017_02	R	0.00	0	9869	704	1370	53798	141055	0.38	0.0706	0.0015	0.9746	0.0219	0.1002	0.0016	0.4433	946	42	615	9	691	11	89
017_03	C	0.06	30	48236	3482	5601	154797	689061	0.22	0.0717	0.0013	0.9883	0.0201	0.1000	0.0015	0.5026	978	37	615	9	698	10	88
017_04	R	0.00	0	7504	534	1812	52947	92086	0.57	0.0705	0.0015	1.1344	0.0261	0.1168	0.0019	0.4255	942	44	712	11	770	12	93
017_05		0.08	9	11190	750	2553	73667	127638	0.58	0.0667	0.0015	1.1136	0.0256	0.1212	0.0019	0.4057	827	45	738	11	760	12	97
017_06		0.29	15	5162	333	929	26465	54353	0.49	0.0641	0.0018	1.0523	0.0293	0.1191	0.0018	0.2600	744	58	725	11	730	14	99
017_07	C	0.02	12	60404	4737	3728	94217	805961	0.12	0.0781	0.0013	1.1275	0.0216	0.1047	0.0016	0.5211	1150	34	642	9	767	10	84
017_08	R	0.00	0	10494	692	1793	53619	118398	0.45	0.0652	0.0011	1.0766	0.0203	0.1198	0.0017	0.4914	780	36	730	10	742	10	98
017_09	C	0.08	2	2433	310	616	11051	18357	0.60	0.1259	0.0033	3.1554	0.0820	0.1818	0.0032	0.3343	2042	45	1077	17	1446	20	74
017_10	R	0.04	3	7787	511	1519	44412	91506	0.49	0.0646	0.0018	0.9699	0.0261	0.1089	0.0017	0.2783	761	56	667	10	688	13	97
017_11		0.00	2	44298	7295	8020	72823	146408	0.50	0.1630	0.0026	9.3443	0.1660	0.4158	0.0060	0.5441	2487	26	2241	27	2372	16	94
017_12		0.04	7	15910	1043	4608	130055	173808	0.75	0.0650	0.0014	1.1328	0.0252	0.1265	0.0019	0.4241	774	43	768	11	769	12	100
017_13		0.01	1	17549	2749	815	8901	65351	0.14	0.1553	0.0039	7.7900	0.2005	0.3638	0.0059	0.3445	2405	42	2000	28	2207	23	91
017_14		0.01	1	8481	668	2498	69234	104846	0.66	0.0777	0.0016	1.1311	0.0244	0.1056	0.0015	0.3856	1140	41	647	9	768	12	84
017_15		0.01	9	65473	10890	2979	66206	294956	0.22	0.1694	0.0037	7.3582	0.1728	0.3156	0.0050	0.4211	2551	36	1768	24	2156	21	82
017_16		0.04	22	54603	9015	4049	47237	195894	0.24	0.1647	0.0023	8.7494	0.1453	0.3855	0.0055	0.6002	2504	23	2102	26	2312	15	91
017_17	C	0.00	0	17627	1084	844	32020	274334	0.12	0.0619	0.0013	0.7676	0.0167	0.0901	0.0014	0.4464	670	43	556	8	578	10	96
017_18	R	0.03	3	11584	724	1166	43317	157025	0.28	0.0613	0.0015	0.8202	0.0205	0.0971	0.0015	0.3270	648	52	597	9	608	11	98
017_19		0.00	0	20518	3780	3592	30959	58382	0.53	0.1830	0.0028	11.9732	0.2042	0.4745	0.0068	0.5521	2681	25	2503	30	2602	16	96
017_20	C	0.01	8	79682	12405	10813	148340	370428	0.40	0.1540	0.0031	6.5312	0.1401	0.3081	0.0048	0.4638	2391	33	1732	24	2050	19	84
017_21	R	0.00	0	12005	764	1053	46377	184402	0.25	0.0634	0.0015	0.7600	0.0189	0.0869	0.0013	0.3418	722	51	537	8	574	11	94
017_22		0.00	0	5386	368	786	23410	55211	0.42	0.0665	0.0021	1.1846	0.0368	0.1291	0.0022	0.2519	823	64	783	13	793	17	99
017_24	R	0.12	20	16275	1369	4075	90726	208531	0.44	0.0837	0.0025	1.2952	0.0390	0.1125	0.0020	0.3044	1284	57	687	11	844	17	81
017_25		0.13	14	10770	746	2370	64406	114410	0.56	0.0693	0.0013	1.1799	0.0238	0.1235	0.0018	0.4306	907	39	751	10	791	11	95
017_26		0.00	0	9401	620	2895	76481	96401	0.79	0.0656	0.0012	1.1730	0.0230	0.1298	0.0019	0.4545	793	38	786	11	788	11	100
017_27	IC	0.02	8	49500	8800	4825	39278	141542	0.28	0.1767	0.0027	11.3177	0.1939	0.4646	0.0065	0.5319	2622	25	2460	28	2550	16	96
017_28	OC	0.09	8	9301	634	2576	76876	99462	0.77	0.0676	0.0012	1.1649	0.0225	0.1251	0.0018	0.4665	855	37	760	10	784	11	97
017_29	R	0.00	0	3020	181	54	2154	45091	0.05	0.0592	0.0019	0.7467	0.0234	0.0916	0.0016	0.2623	574	67	565	9	566	14	100
017_30		0.08	9	11619	1304	1662	46724	131049	0.36	0.1088	0.0048	1.6568	0.0700	0.1104	0.0022	0.1454	1780	78	675	13	992	27	68
017_31	C	0.00	0	7982	533	1435	40048	86409	0.46	0.0662	0.0012	1.1093	0.0210	0.1216	0.0017	0.4690	812	36	740	10	758	10	98
017_32	R	0.01	1	9472	623	1422	41179	103776	0.40	0.0651	0.0012	1.1178	0.0218	0.1246	0.0018	0.4837	778	37	757	10	762	10	99

DA13-017	C. Ant Domain		Mean cps (background subtracted)							Isotopic Ratios (± 1σ)							Age (Ma ± 1σ)						
Analysis	Core/Rim	$\%Pb_c$	^{204}Pb	^{206}Pb	^{207}Pb	^{208}Pb	^{232}Th	^{238}U	Th/U	$^{207}Pb/^{206}Pb$		$^{207}Pb/^{235}U$		$^{206}Pb/^{238}U$		Rho	$^{207}Pb/^{206}Pb$		$^{206}Pb/^{238}U$		$^{207}Pb/^{235}U$		%Conc
017_33	C	0.15	54	35367	4452	4621	247814	399266	0.62	0.1241	0.0031	2.0661	0.0527	0.1210	0.0020	0.3433	2015	44	736	11	1138	17	65
017_34	R	0.12	14	11345	755	2783	81515	129694	0.63	0.0663	0.0014	1.1113	0.0243	0.1216	0.0019	0.4354	817	42	740	11	759	12	97
017_35	C	0.02	11	65631	9807	2718	32101	283498	0.11	0.1482	0.0022	6.3166	0.1064	0.3092	0.0043	0.5532	2325	25	1737	21	2021	15	86
017_36	R	0.18	22	12285	963	2371	90815	165643	0.55	0.0780	0.0017	1.0916	0.0252	0.1016	0.0016	0.3928	1146	43	624	9	749	12	83
017_37	IC	0.00	0	50749	7788	11941	128782	203820	0.63	0.1528	0.0030	7.3565	0.1569	0.3494	0.0054	0.4575	2377	33	1932	26	2156	19	90
017_38	OC	0.05	6	11229	754	4230	123834	119760	1.03	0.0670	0.0011	1.1478	0.0207	0.1244	0.0017	0.4990	836	34	756	10	776	10	97
017_39	R	0.06	4	6167	384	238	11334	98182	0.12	0.0619	0.0014	0.7275	0.0174	0.0852	0.0013	0.3769	672	49	527	8	555	10	95
017_40		0.00	0	11043	1934	1367	11646	31303	0.37	0.1747	0.0027	11.2413	0.1948	0.4667	0.0066	0.5292	2603	26	2469	29	2543	16	97
017_41	C	0.10	18	18259	2558	2700	51459	121683	0.42	0.1402	0.0029	3.7835	0.0809	0.1958	0.0029	0.3980	2229	35	1153	15	1589	17	73
017_42	R	0.22	21	9725	678	2199	62649	101396	0.62	0.0686	0.0022	1.1328	0.0362	0.1199	0.0020	0.2262	885	66	730	11	769	17	95
017_43	C	0.00	0	7130	1154	1783	16683	22083	0.76	0.1621	0.0028	9.5687	0.1800	0.4283	0.0062	0.4831	2477	29	2298	28	2394	17	96
017_44	R	0.14	8	5569	371	944	25953	58028	0.45	0.0667	0.0013	1.1770	0.0247	0.1280	0.0019	0.4256	828	41	776	11	790	12	98
017_45		0.20	18	8778	679	1578	51397	87487	0.59	0.0737	0.0032	1.2680	0.0536	0.1247	0.0025	0.1509	1034	86	758	14	832	24	91
017_46		0.00	0	14307	954	4377	123367	145735	0.85	0.0672	0.0010	1.2177	0.0209	0.1316	0.0018	0.5511	843	31	797	10	809	10	99
017_47	C	0.08	21	26585	4269	5856	56977	96387	0.59	0.1628	0.0034	8.7425	0.1943	0.3895	0.0061	0.4506	2485	34	2121	28	2312	20	92
017_48	R	0.00	1	32870	5219	9340	102760	116614	0.88	0.1596	0.0024	8.2221	0.1408	0.3737	0.0052	0.5353	2452	25	2047	24	2256	16	91
017_49		0.18	18	10169	660	2460	71182	107399	0.66	0.0657	0.0012	1.1540	0.0224	0.1275	0.0018	0.4855	795	37	774	10	779	11	99
017_50	C	0.00	0	61167	9754	11483	116250	211626	0.55	0.1612	0.0025	8.6685	0.1517	0.3902	0.0055	0.5440	2468	26	2124	26	2304	16	92
017_51	R	0.13	13	10077	797	2018	54560	93871	0.58	0.0785	0.0024	1.4592	0.0433	0.1350	0.0022	0.2358	1159	59	817	12	914	18	89
017_52	C	0.06	14	23789	3193	6618	109860	160174	0.69	0.1354	0.0032	3.7460	0.0908	0.2007	0.0031	0.3641	2169	40	1179	17	1581	19	75
017_53	R	0.15	15	9828	644	1381	53709	124317	0.43	0.0663	0.0013	0.9722	0.0207	0.1064	0.0016	0.4331	814	41	652	9	690	11	95
017_54		0.00	0	10198	753	1567	38104	114181	0.33	0.0749	0.0019	1.1941	0.0310	0.1157	0.0018	0.3068	1065	51	706	10	798	14	88
017_55	C	0.02	10	63616	10962	14945	182762	213186	0.86	0.1733	0.0033	9.8481	0.2056	0.4123	0.0062	0.4616	2590	32	2225	28	2421	19	92
017_56	R	0.01	2	26740	4445	1787	24859	100769	0.25	0.1671	0.0048	8.6224	0.2534	0.3743	0.0065	0.3214	2529	48	2050	30	2299	27	89
017_57		0.09	12	12853	936	1542	49563	154349	0.32	0.0733	0.0013	1.1284	0.0218	0.1117	0.0016	0.4761	1021	35	683	9	767	10	89
017_58	C	0.06	22	39392	6666	8918	100958	151205	0.67	0.1704	0.0029	8.2353	0.1550	0.3507	0.0050	0.4962	2561	28	1938	24	2257	17	86
017_59	R	0.33	24	7282	578	2186	124221	112701	1.10	0.0801	0.0022	0.9800	0.0267	0.0888	0.0015	0.3228	1199	52	548	9	694	14	79
017_60		0.00	0	10882	766	1181	41906	115877	0.36	0.0712	0.0020	1.1977	0.0330	0.1221	0.0019	0.2918	963	55	742	11	800	15	93
017_61	C	0.00	0	50808	7943	8079	89510	194359	0.46	0.1582	0.0022	7.5445	0.1215	0.3459	0.0047	0.5782	2437	23	1915	23	2178	14	88
017_62	R	0.37	43	11550	983	2021	146122	195968	0.75	0.0859	0.0016	0.9464	0.0188	0.0799	0.0012	0.4658	1336	35	496	7	676	10	73
017_63	C	0.01	2	20985	3455	3474	30850	66138	0.47	0.1660	0.0029	9.6465	0.1808	0.4216	0.0061	0.4889	2518	29	2268	28	2402	17	94

DA13-017	C. Ant Domain		Mean cps (background subtracted)							Isotopic Ratios (± 1σ)							Age (Ma ± 1σ)						
Analysis	Core/Rim	$\%Pb_c$	^{204}Pb	^{206}Pb	^{207}Pb	^{208}Pb	^{232}Th	^{238}U	Th/U	$^{207}Pb/^{206}Pb$		$^{207}Pb/^{235}U$		$^{206}Pb/^{238}U$		Rho	$^{207}Pb/^{206}Pb$		$^{206}Pb/^{238}U$		$^{207}Pb/^{235}U$		%Conc
017_64	R	0.00	0	11509	753	1478	48589	153534	0.32	0.0661	0.0012	0.9195	0.0182	0.1009	0.0015	0.4673	811	38	619	9	662	10	94
017_65	C	0.00	0	13943	1671	1489	46863	108053	0.43	0.1206	0.0028	2.6975	0.0633	0.1623	0.0024	0.3187	1966	41	970	13	1328	17	73
017_66	R	0.11	13	12310	798	1287	39791	158347	0.25	0.0653	0.0013	0.9487	0.0195	0.1053	0.0015	0.4492	785	40	646	9	677	10	95
017_67	C	0.03	19	69306	10808	5574	68731	287911	0.24	0.1596	0.0037	6.9326	0.1660	0.3153	0.0047	0.3552	2452	39	1767	23	2103	21	84
017_68	R	0.04	4	9614	590	725	25808	140425	0.18	0.0616	0.0013	0.7911	0.0180	0.0932	0.0014	0.4034	662	46	574	8	592	10	97
017_69	C	0.13	11	8620	547	1815	51116	96151	0.53	0.0640	0.0013	1.0591	0.0231	0.1200	0.0018	0.4170	743	43	731	10	733	11	100
017_70	R	0.06	7	12393	735	968	40752	203752	0.20	0.0599	0.0011	0.6557	0.0130	0.0794	0.0011	0.4433	599	40	493	7	512	8	96
017_71	C	0.07	15	20498	2722	1693	47126	170938	0.28	0.1359	0.0029	2.8678	0.0629	0.1531	0.0022	0.3684	2175	37	918	12	1374	17	67
017_72	R	0.00	0	12431	719	577	25329	196224	0.13	0.0584	0.0013	0.6866	0.0159	0.0854	0.0013	0.3913	544	48	528	8	531	10	99
017_73	C	0.00	0	12445	2176	1751	15387	36680	0.42	0.1764	0.0036	11.1349	0.2373	0.4582	0.0069	0.4304	2619	33	2432	31	2535	20	96
017_74	R	0.00	0	9257	597	1703	54386	108787	0.50	0.0651	0.0015	1.0280	0.0249	0.1147	0.0018	0.3683	776	48	700	10	718	12	97
017_75		0.11	15	14146	923	3856	105666	157067	0.67	0.0656	0.0015	1.0971	0.0266	0.1213	0.0019	0.3681	795	49	738	11	752	13	98

DA13-020	C. Ant Domain		Mean cps (background subtracted)							Isotopic Ratios (± 1σ)							Age (Ma ± 1σ)						
Analysis	Core/Rim	$\%Pb_c$	^{204}Pb	^{206}Pb	^{207}Pb	^{208}Pb	^{232}Th	^{238}U	Th/U	$^{207}Pb/^{206}Pb$		$^{207}Pb/^{235}U$		$^{206}Pb/^{238}U$		Rho	$^{207}Pb/^{206}Pb$		$^{206}Pb/^{238}U$		$^{207}Pb/^{235}U$		%Conc
020_01		0.09	12	12838	1175	3861	80413	154183	0.52	0.0920	0.0015	1.3431	0.0238	0.1059	0.0014	0.4751	1467	31	649	8	865	10	75
020_02	C	0.07	13	18869	1291	6401	175290	202512	0.87	0.0691	0.0014	1.2116	0.0255	0.1272	0.0019	0.4440	903	40	772	11	806	12	96
020_03	R	0.05	12	24623	1663	2901	79098	278436	0.28	0.0682	0.0010	1.0757	0.0174	0.1145	0.0015	0.5480	874	29	699	9	742	8	94
020_05	R	0.05	8	14976	969	1140	43622	203768	0.21	0.0656	0.0010	0.8630	0.0149	0.0955	0.0013	0.5124	793	32	588	8	632	8	93
020_06	C	0.10	6	5749	409	1725	48112	63776	0.75	0.0724	0.0014	1.1651	0.0231	0.1168	0.0016	0.4349	997	38	712	9	784	11	91
020_07	R	0.03	9	26671	1744	4676	128090	287171	0.45	0.0664	0.0010	1.0944	0.0186	0.1195	0.0016	0.5091	820	32	728	9	751	9	97
020_08		0.11	18	17096	1218	5235	147375	192906	0.76	0.0724	0.0012	1.1490	0.0202	0.1151	0.0016	0.5066	998	32	702	9	777	10	90
020_09		0.13	43	33244	2420	7642	195138	387873	0.50	0.0727	0.0016	1.1090	0.0251	0.1106	0.0016	0.3472	1007	45	676	9	758	12	89
020_10		0.00	0	18253	1221	3302	88918	189584	0.47	0.0686	0.0012	1.1764	0.0224	0.1244	0.0017	0.4500	886	36	756	10	790	10	96
020_12	C	0.12	23	18394	1384	3965	132154	219909	0.60	0.0772	0.0028	1.2255	0.0444	0.1151	0.0021	0.2321	1127	71	703	12	812	20	86
020_13	R	0.08	14	18467	1285	3650	137653	198024	0.70	0.0716	0.0013	1.1819	0.0229	0.1197	0.0017	0.4328	976	37	729	10	792	11	92
020_14		0.05	20	37754	2655	14089	375167	408228	0.92	0.0722	0.0013	1.1718	0.0221	0.1178	0.0016	0.4391	991	36	718	9	788	10	91
020_16		0.00	0	11136	751	1136	29193	111501	0.26	0.0672	0.0012	1.1606	0.0211	0.1253	0.0017	0.4473	844	35	761	10	782	10	97
020_17	C	0.14	54	37374	2949	8746	205209	449633	0.46	0.0785	0.0019	1.2174	0.0299	0.1125	0.0017	0.3629	1160	47	687	10	809	14	85
020_18	R	0.02	3	18535	1273	1905	51933	247243	0.21	0.0684	0.0011	0.9046	0.0160	0.0960	0.0013	0.4770	879	33	591	8	654	9	90
020_19	C	0.07	18	24465	1844	6110	148494	281302	0.53	0.0760	0.0022	1.2275	0.0356	0.1172	0.0019	0.2944	1094	57	715	11	813	16	88
020_20	R	0.15	19	12862	936	1962	58025	135546	0.43	0.0725	0.0013	1.2295	0.0235	0.1230	0.0017	0.4480	1000	36	748	10	814	11	92
020_21	C	0.01	2	14315	1069	2067	67522	184960	0.37	0.0746	0.0023	1.0844	0.0331	0.1054	0.0018	0.2824	1058	60	646	10	746	16	87
020_22	R	0.16	43	26921	2163	5285	489360	343676	1.42	0.0813	0.0022	1.1835	0.0322	0.1055	0.0017	0.3179	1230	51	647	10	793	15	82
020_24	R	0.20	63	31274	2781	7686	182307	351866	0.52	0.0889	0.0018	1.4037	0.0296	0.1146	0.0016	0.4031	1402	38	699	9	891	13	79
020_25	C	0.02	2	9987	792	1987	43080	113902	0.38	0.0784	0.0022	1.1629	0.0319	0.1076	0.0016	0.2598	1157	54	659	10	783	15	84
020_26	R	0.02	4	24395	1582	7230	184281	259308	0.71	0.0661	0.0018	1.1627	0.0329	0.1276	0.0021	0.3156	810	57	774	12	783	15	99
020_27	C	0.11	31	27574	2097	4390	95607	327538	0.29	0.0761	0.0016	1.1126	0.0247	0.1061	0.0015	0.3665	1097	43	650	9	759	12	86
020_28	R	0.06	9	15624	1255	3204	56401	168121	0.34	0.0809	0.0018	1.3627	0.0314	0.1222	0.0018	0.3830	1219	43	743	10	873	14	85
020_29	C	0.09	64	69781	5364	12663	275114	907569	0.30	0.0789	0.0021	1.1190	0.0302	0.1028	0.0016	0.3371	1171	51	631	9	763	14	83
020_31	C	0.07	5	7061	453	1147	29502	72762	0.41	0.0642	0.0012	1.1117	0.0220	0.1257	0.0018	0.4297	748	39	763	10	759	11	101
020_32	R	0.00	0	15538	1058	2152	57574	163142	0.35	0.0685	0.0011	1.1715	0.0200	0.1240	0.0017	0.5197	884	31	754	10	787	9	96
020_33	C	0.02	4	17709	1247	2805	67556	183561	0.37	0.0709	0.0011	1.2223	0.0204	0.1250	0.0017	0.5361	956	30	759	10	811	9	94
020_35	C	0.00	0	24425	1648	6600	170075	256615	0.66	0.0678	0.0011	1.1568	0.0199	0.1237	0.0017	0.5152	864	32	752	10	780	9	96
020_36	R	0.12	49	39810	3244	7096	161304	471663	0.34	0.0832	0.0017	1.3199	0.0293	0.1151	0.0017	0.4204	1273	40	703	10	855	13	82
020_37	C	0.00	0	3880	259	1044	27938	41412	0.67	0.0675	0.0015	1.1442	0.0259	0.1230	0.0018	0.3816	852	45	748	10	775	12	97

DA13-020	C. Ant Domain		Mean cps (background subtracted)							Isotopic Ratios (± 1σ)							Age (Ma ± 1σ)						
Analysis	Core/Rim	$\%Pb_c$	^{204}Pb	^{206}Pb	^{207}Pb	^{208}Pb	^{232}Th	^{238}U	Th/U	$^{207}Pb/^{206}Pb$		$^{207}Pb/^{235}U$		$^{206}Pb/^{238}U$		Rho	$^{207}Pb/^{206}Pb$		$^{206}Pb/^{238}U$		$^{207}Pb/^{235}U$		%Conc
020_38	R	0.15	27	17861	1294	2333	92515	245159	0.38	0.0718	0.0017	0.9197	0.0224	0.0929	0.0014	0.3223	980	48	573	8	662	12	86
020_39		0.07	16	24399	1965	5188	107907	280274	0.39	0.0826	0.0020	1.3503	0.0335	0.1186	0.0018	0.3707	1259	46	723	11	868	14	83
020_40		0.04	8	19910	1373	3435	92574	215621	0.43	0.0706	0.0014	1.1974	0.0246	0.1230	0.0018	0.4442	946	39	748	10	799	11	94
020_41		0.12	13	10910	757	1930	49183	119712	0.41	0.0715	0.0016	1.2029	0.0278	0.1220	0.0018	0.3907	972	44	742	10	802	13	93
020_42	C	0.27	26	9737	803	5106	126259	104357	1.21	0.0813	0.0020	1.3175	0.0319	0.1175	0.0018	0.3153	1229	46	716	10	853	14	84
020_43	R	0.12	13	11123	724	4439	111329	113937	0.98	0.0659	0.0012	1.1479	0.0227	0.1264	0.0018	0.4406	803	38	767	10	776	11	99
020_44	C	0.00	0	12326	819	1833	46128	124815	0.37	0.0670	0.0013	1.1860	0.0236	0.1284	0.0018	0.4381	837	38	779	10	794	11	98
020_45	R	0.00	0	18285	1348	3411	82991	200870	0.41	0.0749	0.0014	1.2336	0.0250	0.1194	0.0017	0.4406	1067	38	727	10	816	11	89

DA13-029	C. Ant Domain		Mean cps (background subtracted)							Isotopic Ratios (± 1σ)							Age (Ma ± 1σ)						
Analysis	Core/Rim	$\%Pb_c$	^{204}Pb	^{206}Pb	^{207}Pb	^{208}Pb	^{232}Th	^{238}U	Th/U	$^{207}Pb/^{206}Pb$		$^{207}Pb/^{235}U$		$^{206}Pb/^{238}U$		Rho	$^{207}Pb/^{206}Pb$		$^{206}Pb/^{238}U$		$^{207}Pb/^{235}U$		%Conc
029_02	R	0.06	20	34504	2082	558	13423	518334	0.03	0.0603	0.0009	0.7274	0.0123	0.0875	0.0012	0.5390	616	32	541	7	555	7	97
029_03		0.03	14	42336	3076	5947	177853	442716	0.40	0.0731	0.0017	1.2298	0.0293	0.1220	0.0018	0.3275	1017	47	742	10	814	13	91
029_04		0.21	6	2845	193	523	15154	29802	0.51	0.0684	0.0018	1.1371	0.0293	0.1206	0.0018	0.2931	881	52	734	10	771	14	95
029_05		0.56	24	4245	282	529	14957	44937	0.33	0.0664	0.0018	1.1636	0.0324	0.1272	0.0020	0.3037	818	56	772	12	784	15	99
029_06	C	0.01	1	10867	693	7296	303076	105673	2.87	0.0641	0.0013	1.1137	0.0228	0.1260	0.0017	0.3683	745	42	765	10	760	11	101
029_07	R	0.12	13	11079	688	819	27696	136648	0.20	0.0619	0.0013	0.8386	0.0180	0.0983	0.0013	0.3390	671	45	604	8	618	10	98
029_08		0.00	0	21070	1412	2775	83133	231509	0.36	0.0662	0.0019	1.1213	0.0322	0.1228	0.0020	0.2885	814	59	747	12	764	15	98
029_09		0.01	2	29394	1961	4216	117695	291797	0.40	0.0669	0.0012	1.1618	0.0213	0.1259	0.0017	0.4381	836	36	764	10	783	10	98
029_10		0.00	0	15917	1110	2686	62073	149999	0.41	0.0695	0.0020	1.2325	0.0347	0.1287	0.0020	0.2350	912	58	781	11	816	16	96
029_11		0.00	0	16500	1096	2851	78913	164610	0.48	0.0663	0.0012	1.1736	0.0228	0.1284	0.0018	0.4281	816	38	779	10	788	11	99
029_12		0.00	0	6636	443	1017	27727	65455	0.42	0.0667	0.0013	1.1770	0.0244	0.1280	0.0018	0.3807	828	41	777	10	790	11	98
029_13		0.00	0	43511	2869	6544	190875	461626	0.41	0.0644	0.0018	1.1376	0.0321	0.1281	0.0021	0.2967	756	58	777	12	771	15	101
029_14		0.00	0	2599	159	139	5167	31183	0.17	0.0607	0.0031	0.8156	0.0397	0.0975	0.0020	0.1050	628	106	600	12	606	22	99
029_15		0.03	11	39758	2642	4590	143652	428185	0.34	0.0656	0.0016	1.1155	0.0282	0.1233	0.0019	0.3233	794	52	750	11	761	14	99
029_16		0.00	0	6955	464	1107	30405	64701	0.47	0.0667	0.0013	1.1851	0.0234	0.1288	0.0017	0.3658	830	40	781	10	794	11	98
029_17		0.08	7	8487	590	1460	40406	79844	0.51	0.0686	0.0019	1.1575	0.0318	0.1224	0.0018	0.2196	885	57	744	10	781	15	95
029_18		0.00	0	5127	347	862	37535	56178	0.67	0.0689	0.0021	1.0830	0.0321	0.1141	0.0018	0.2422	894	61	696	10	745	16	93
029_19		0.01	2	30706	2004	5529	151754	291949	0.52	0.0657	0.0011	1.1683	0.0199	0.1291	0.0017	0.4592	796	33	783	10	786	9	100
029_20		0.06	16	26167	1703	4684	128120	255927	0.50	0.0662	0.0013	1.1786	0.0246	0.1292	0.0018	0.3961	811	41	783	10	791	11	99
029_21		0.02	8	46073	3020	5505	158496	479259	0.33	0.0658	0.0013	1.1390	0.0239	0.1255	0.0018	0.4141	800	41	762	10	772	11	99
029_22		0.00	0	11905	810	1888	51316	125465	0.41	0.0684	0.0012	1.1134	0.0206	0.1180	0.0016	0.4387	882	36	719	9	760	10	95
029_23	C	0.02	2	10326	689	1750	50020	113749	0.44	0.0672	0.0015	1.0874	0.0243	0.1173	0.0017	0.3792	845	44	715	10	747	12	96
029_24	R	0.07	38	54048	3330	1342	63021	842585	0.07	0.0600	0.0021	0.7381	0.0256	0.0892	0.0016	0.2464	603	74	551	9	561	15	98
029_25		0.00	0	4003	270	691	19274	38273	0.50	0.0680	0.0015	1.2162	0.0272	0.1296	0.0018	0.3458	870	45	786	10	808	12	97
029_26		0.10	6	5817	378	898	25317	56365	0.45	0.0656	0.0014	1.1514	0.0256	0.1272	0.0018	0.3423	795	45	772	10	778	12	99
029_27		0.00	0	7368	519	1320	47121	81400	0.58	0.0682	0.0024	1.1619	0.0411	0.1235	0.0023	0.2423	876	72	751	13	783	19	96
029_28		0.00	0	3179	211	498	14408	32336	0.45	0.0670	0.0018	1.1422	0.0301	0.1237	0.0019	0.2898	837	54	752	11	774	14	97
029_29		0.00	0	6640	478	818	24671	93289	0.26	0.0693	0.0029	0.9326	0.0385	0.0976	0.0019	0.1879	908	85	600	11	669	20	90
029_30		0.00	0	29326	1905	3971	110478	278610	0.40	0.0655	0.0013	1.1858	0.0245	0.1314	0.0018	0.3895	789	41	796	10	794	11	100
029_31		0.00	0	9172	596	1821	48417	85127	0.57	0.0651	0.0011	1.1742	0.0210	0.1309	0.0017	0.4275	776	36	793	10	789	10	101
029_32		0.00	0	2219	143	277	5542	24687	0.22	0.0660	0.0055	0.9174	0.0722	0.1007	0.0031	0.0599	807	164	619	18	661	38	94

DA13-029	C. Ant Domain		Mean cps (background subtracted)							Isotopic Ratios (± 1σ)							Age (Ma ± 1σ)						
Analysis	Core/Rim	$\%Pb_c$	^{204}Pb	^{206}Pb	^{207}Pb	^{208}Pb	^{232}Th	^{238}U	Th/U	$^{207}Pb/^{206}Pb$		$^{207}Pb/^{235}U$		$^{206}Pb/^{238}U$		Rho	$^{207}Pb/^{206}Pb$		$^{206}Pb/^{238}U$		$^{207}Pb/^{235}U$		%Conc
029_33		0.09	21	23237	1528	2596	96408	218367	0.44	0.0660	0.0011	1.1843	0.0207	0.1301	0.0017	0.4423	808	34	788	10	793	10	99
029_34		0.20	48	23766	1748	258691	9068118	264847	34.24	0.0746	0.0022	1.0275	0.0293	0.0999	0.0015	0.2041	1057	58	614	9	718	15	86
029_35	C	0.00	0	8167	538	1194	30014	77102	0.39	0.0662	0.0012	1.1780	0.0220	0.1292	0.0017	0.4128	811	37	783	10	790	10	99
029_36	R	0.13	9	6957	433	810	19256	88617	0.22	0.0632	0.0015	0.8751	0.0213	0.1004	0.0015	0.3242	714	50	617	9	638	12	97
029_37	C	0.00	0	4183	291	870	18999	39583	0.48	0.0700	0.0017	1.2257	0.0289	0.1270	0.0018	0.2984	928	48	771	10	812	13	95
029_38	R	0.30	18	5948	380	637	18663	59657	0.31	0.0639	0.0014	1.1046	0.0247	0.1254	0.0018	0.3507	739	46	761	10	756	12	101
029_39		0.32	20	6235	483	107382	5211888	89918	57.96	0.0786	0.0024	0.9606	0.0292	0.0887	0.0015	0.2420	1161	60	548	9	684	15	80
029_40		0.00	0	4546	290	543	13660	40963	0.33	0.0639	0.0016	1.1573	0.0294	0.1314	0.0019	0.2612	738	53	796	11	781	14	102
029_41		0.00	0	2702	173	792	14976	24174	0.62	0.0639	0.0023	1.1832	0.0413	0.1344	0.0023	0.1833	737	74	813	13	793	19	102
029_42		0.00	0	7879	521	671	61437	93758	0.66	0.0670	0.0015	0.9332	0.0211	0.1010	0.0014	0.3123	839	46	620	8	669	11	93
029_43		0.47	16	3384	221	652	18354	34509	0.53	0.0679	0.0030	1.1704	0.0499	0.1251	0.0024	0.1687	865	88	760	14	787	23	97
029_44		0.15	5	3243	217	568	16233	31875	0.51	0.0681	0.0020	1.1975	0.0344	0.1275	0.0020	0.2494	872	59	774	11	799	16	97
029_45		0.18	8	4327	298	722	27429	47830	0.57	0.0703	0.0025	1.1386	0.0395	0.1175	0.0020	0.2140	937	71	716	12	772	19	93
029_46		0.02	2	11819	792	1432	40175	111926	0.36	0.0676	0.0013	1.1906	0.0234	0.1278	0.0017	0.3958	856	39	775	10	796	11	97
029_47		0.05	4	8349	576	1197	32525	78675	0.41	0.0695	0.0015	1.2037	0.0256	0.1257	0.0017	0.3395	912	42	763	9	802	12	95
029_48		0.00	0	11727	811	1613	43866	111305	0.39	0.0709	0.0018	1.2301	0.0314	0.1259	0.0018	0.2875	955	51	764	10	814	14	94
029_49	C	0.34	13	3798	249	628	17235	37064	0.47	0.0663	0.0016	1.1390	0.0285	0.1247	0.0018	0.2976	815	51	757	10	772	14	98
029_51		0.05	2	3870	263	712	18765	37323	0.50	0.0687	0.0017	1.2148	0.0300	0.1283	0.0018	0.3133	890	49	778	10	807	14	96
029_52		0.08	3	3581	239	462	13481	36151	0.37	0.0673	0.0021	1.1759	0.0359	0.1268	0.0020	0.2641	846	62	770	12	789	17	97
029_53		0.00	0	2899	190	362	9858	28257	0.35	0.0660	0.0017	1.1552	0.0308	0.1269	0.0018	0.2903	807	54	770	10	780	15	99
029_54		0.00	0	4496	299	665	17470	42794	0.41	0.0672	0.0025	1.1529	0.0421	0.1245	0.0021	0.1948	845	75	756	12	779	20	97
029_55		0.00	0	20038	1323	2505	68860	213759	0.32	0.0666	0.0015	1.0583	0.0249	0.1152	0.0016	0.3552	826	47	703	9	733	12	96
029_56		0.18	14	7701	515	819	21621	80647	0.27	0.0673	0.0015	1.1075	0.0261	0.1195	0.0017	0.3514	845	47	727	10	757	13	96
029_57		0.11	4	3729	249	581	16512	36783	0.45	0.0672	0.0017	1.1760	0.0311	0.1269	0.0018	0.3143	845	53	770	11	790	15	98
029_58		0.28	6	2141	144	367	10034	21078	0.48	0.0680	0.0021	1.2031	0.0374	0.1283	0.0020	0.2614	870	63	778	11	802	17	97
029_59		0.00	0	2920	195	367	10762	29532	0.36	0.0675	0.0020	1.1765	0.0358	0.1264	0.0020	0.2792	854	61	767	11	790	17	97
029_60		0.30	5	1651	113	274	7607	16337	0.47	0.0689	0.0023	1.2119	0.0412	0.1277	0.0020	0.2432	894	68	775	12	806	19	96

DA13-049	C. Ant Domain		Mean cps (background subtracted)							Isotopic Ratios (± 1σ)							Age (Ma ± 1σ)						
Analysis	Core/Rim	$\%Pb_c$	^{204}Pb	^{206}Pb	^{207}Pb	^{208}Pb	^{232}Th	^{238}U	Th/U	$^{207}Pb/^{206}Pb$		$^{207}Pb/^{235}U$		$^{206}Pb/^{238}U$		Rho	$^{207}Pb/^{206}Pb$		$^{206}Pb/^{238}U$		$^{207}Pb/^{235}U$		%Conc
049_01		0.02	8	35859	2366	4300	125491	338152	0.37	0.0668	0.0011	1.2093	0.0215	0.1314	0.0017	0.4546	830	34	796	10	805	10	99
049_02		0.00	0	16409	1234	1912	89762	146492	0.61	0.0749	0.0018	1.3302	0.0313	0.1289	0.0018	0.2867	1065	47	782	10	859	14	91
049_03		0.18	53	29907	2653	4914	95521	262338	0.36	0.0886	0.0036	1.6384	0.0643	0.1342	0.0025	0.1350	1395	77	812	14	985	25	82
049_04		0.04	9	20674	1371	1857	56100	206713	0.27	0.0664	0.0015	1.2054	0.0277	0.1316	0.0020	0.3796	820	46	797	11	803	13	99
049_05		0.00	0	19035	1236	1401	35086	170963	0.21	0.0650	0.0010	1.1952	0.0192	0.1334	0.0017	0.4772	774	31	807	10	798	9	101
049_06		0.19	22	11560	788	799	17787	112654	0.16	0.0683	0.0011	1.1579	0.0203	0.1229	0.0016	0.4265	878	34	747	9	781	10	96
049_07		0.06	11	16989	1162	1416	42159	154727	0.27	0.0684	0.0012	1.2254	0.0227	0.1300	0.0017	0.3965	879	36	788	10	812	10	97
049_08		0.09	18	19753	1386	1910	39790	182585	0.22	0.0694	0.0015	1.1920	0.0257	0.1245	0.0017	0.3256	911	43	757	9	797	12	95
049_09		0.05	9	17761	1187	1497	34443	151926	0.23	0.0662	0.0014	1.2236	0.0257	0.1342	0.0018	0.3353	812	43	812	10	811	12	100
049_10		0.00	0	12977	854	1034	25146	120540	0.21	0.0660	0.0012	1.2066	0.0229	0.1325	0.0018	0.4203	808	37	802	10	804	11	100
049_11		0.06	15	27165	1792	2687	103961	257636	0.40	0.0658	0.0010	1.1616	0.0195	0.1280	0.0016	0.4653	801	32	776	9	783	9	99
049_12	C	0.00	0	75577	12470	12431	119553	207107	0.58	0.1632	0.0031	9.5877	0.1907	0.4263	0.0056	0.3768	2489	32	2289	25	2396	18	96
049_13	R	0.00	0	16910	1139	1032	31242	159464	0.20	0.0679	0.0013	1.2315	0.0247	0.1316	0.0018	0.4050	865	39	797	10	815	11	98
049_14		0.00	0	22491	3166	8069	74380	85824	0.87	0.1372	0.0032	5.7707	0.1372	0.3050	0.0043	0.3331	2192	40	1716	21	1942	21	88
049_15	C	0.07	23	34232	2675	3342	54969	339398	0.16	0.0768	0.0017	1.2520	0.0285	0.1183	0.0016	0.3438	1115	44	721	9	824	13	87
049_16	R	0.06	15	23391	1563	1109	27089	218231	0.12	0.0672	0.0010	1.2200	0.0204	0.1318	0.0017	0.4762	843	32	798	10	810	9	99
049_17		0.00	0	16462	1099	1717	46470	161113	0.29	0.0668	0.0011	1.1760	0.0204	0.1277	0.0017	0.4654	832	33	775	10	790	10	98
049_18		0.04	5	13290	884	751	19979	125874	0.16	0.0669	0.0012	1.2003	0.0217	0.1302	0.0017	0.4324	834	35	789	10	801	10	99
049_19		1.81	21	1138	172	1061	22748	10888	2.09	0.1519	0.0049	2.7540	0.0854	0.1315	0.0025	0.2185	2368	54	796	14	1343	23	59
049_20		0.00	0	12372	956	1268	25780	119464	0.22	0.0780	0.0026	1.2718	0.0400	0.1182	0.0019	0.1193	1148	65	720	11	833	18	86
049_21		0.09	17	18501	1473	2652	41555	149378	0.28	0.0785	0.0027	1.4842	0.0479	0.1375	0.0022	0.1308	1159	66	830	12	924	20	90
049_22		0.00	0	48438	3267	3743	85302	528494	0.16	0.0660	0.0008	1.2249	0.0191	0.1346	0.0020	0.7084	808	24	814	11	812	9	100
049_23	C	0.00	0	273689	43502	8548	63368	915683	0.07	0.1555	0.0017	9.5184	0.1468	0.4442	0.0067	0.7294	2407	19	2369	30	2389	14	99
049_24	R	0.00	0	32121	2176	3011	71606	383986	0.19	0.0662	0.0009	1.1465	0.0192	0.1257	0.0019	0.6751	812	27	763	11	776	9	98
049_25		0.00	0	45828	3092	4087	94397	536249	0.18	0.0655	0.0011	1.2200	0.0245	0.1351	0.0022	0.5945	790	35	817	13	810	11	101
049_26	C	0.00	6	147780	24576	52123	395525	469812	0.84	0.1628	0.0019	10.4940	0.1665	0.4678	0.0070	0.7099	2485	20	2474	31	2479	15	100
049_27	R	0.02	9	44475	3030	3155	78464	497793	0.16	0.0667	0.0008	1.2264	0.0202	0.1334	0.0020	0.6873	829	26	807	12	813	9	99

DA13-077	C. Ant Domain		Mean cps (background subtracted)							Isotopic Ratios (± 1σ)							Age (Ma ± 1σ)						
Analysis	Core/Rim	$\%Pb_c$	^{204}Pb	^{206}Pb	^{207}Pb	^{208}Pb	^{232}Th	^{238}U	Th/U	$^{207}Pb/^{206}Pb$		$^{207}Pb/^{235}U$		$^{206}Pb/^{238}U$		Rho	$^{207}Pb/^{206}Pb$		$^{206}Pb/^{238}U$		$^{207}Pb/^{235}U$		%Conc
077_01		0.06	8	13686	799	1845	64953	187548	0.35	0.0586	0.0010	0.7010	0.0125	0.0867	0.0011	0.4146	553	37	536	7	539	7	99
077_02	C	0.00	0	16928	1149	2714	66505	154531	0.43	0.0679	0.0011	1.2121	0.0208	0.1295	0.0016	0.4308	865	34	785	9	806	10	97
077_03	R	0.14	16	11577	756	1030	28415	114689	0.25	0.0650	0.0016	1.1565	0.0283	0.1290	0.0019	0.3242	775	50	782	11	780	13	100
077_04		0.00	0	39539	2638	6299	161179	363744	0.44	0.0667	0.0011	1.1918	0.0200	0.1296	0.0016	0.4547	829	33	785	9	797	9	99
077_05		0.06	9	15467	987	1256	33032	171801	0.19	0.0637	0.0012	0.9733	0.0186	0.1109	0.0015	0.4161	731	38	678	9	690	10	98
077_06		0.00	0	29546	1930	3524	135656	373334	0.36	0.0660	0.0016	0.7834	0.0188	0.0860	0.0011	0.2772	807	49	532	7	587	11	91
077_07		0.00	0	53761	3615	7700	215916	618239	0.35	0.0671	0.0011	0.9786	0.0165	0.1059	0.0014	0.4717	839	32	649	8	693	8	94
077_08		0.14	15	10477	684	1256	34383	115063	0.30	0.0649	0.0017	0.9979	0.0264	0.1116	0.0017	0.2771	770	55	682	10	703	13	97
077_09	C	0.01	2	15094	1005	2087	53097	129767	0.41	0.0675	0.0016	1.2032	0.0290	0.1292	0.0017	0.2854	853	49	783	10	802	13	98
077_10	R	0.09	13	14012	915	990	27779	151820	0.18	0.0656	0.0014	0.9929	0.0212	0.1097	0.0015	0.3502	795	43	671	9	700	11	96
077_11	C	0.00	0	3195	265	528	9893	32118	0.31	0.0827	0.0020	1.4011	0.0334	0.1228	0.0018	0.3164	1263	45	747	10	889	14	84
077_12	R	0.00	0	24157	1640	3195	84627	227541	0.37	0.0677	0.0012	1.2129	0.0226	0.1300	0.0017	0.4309	858	36	788	10	807	10	98
077_13		0.15	13	8770	621	1806	51999	91116	0.57	0.0690	0.0022	1.2021	0.0381	0.1264	0.0021	0.2446	898	65	768	12	802	18	96
077_14		0.08	33	39110	2529	1217	56034	413091	0.14	0.0652	0.0034	0.9316	0.0492	0.1036	0.0022	0.2402	782	106	636	13	669	26	95
077_15		0.00	0	19157	1268	2340	65425	171675	0.38	0.0670	0.0016	1.1913	0.0291	0.1290	0.0018	0.3213	837	49	782	10	797	13	98
077_16	C	0.01	1	12324	805	2357	63924	118530	0.54	0.0652	0.0012	1.0973	0.0210	0.1222	0.0016	0.3593	779	39	743	9	752	10	99
077_17	R	0.02	7	39426	2327	328	11468	571667	0.02	0.0590	0.0009	0.6875	0.0113	0.0846	0.0011	0.4802	567	33	523	6	531	7	98
077_18	C	0.00	0	3764	255	667	17615	35643	0.49	0.0675	0.0015	1.2090	0.0263	0.1299	0.0018	0.3404	854	44	787	10	805	12	98
077_19	R	0.00	0	28815	1820	1238	29244	296291	0.10	0.0633	0.0011	0.9918	0.0180	0.1137	0.0014	0.3744	718	37	694	8	700	9	99
077_20		0.00	0	8306	556	1004	24205	77188	0.31	0.0673	0.0013	1.2061	0.0231	0.1301	0.0017	0.3882	846	38	788	10	803	11	98
077_21		0.00	0	29077	1871	4283	115795	275106	0.42	0.0659	0.0028	1.1989	0.0500	0.1320	0.0025	0.1666	804	87	799	14	800	23	100
077_22		0.01	1	18441	1258	4581	125504	177640	0.71	0.0684	0.0011	1.1863	0.0205	0.1257	0.0016	0.4429	882	34	764	9	794	10	96
077_24	C	0.01	2	15073	1012	1848	50695	145907	0.35	0.0675	0.0012	1.1647	0.0212	0.1251	0.0016	0.4140	854	36	760	9	784	10	97
077_25	R	0.03	8	25682	1632	1439	43249	343842	0.13	0.0640	0.0011	0.7961	0.0143	0.0903	0.0012	0.4155	741	36	557	7	595	8	94
077_26	C	0.10	8	8013	533	1594	44140	78263	0.56	0.0668	0.0014	1.1596	0.0251	0.1259	0.0017	0.3483	832	44	764	10	782	12	98
077_27	R	0.02	5	20486	1250	711	18409	232539	0.08	0.0615	0.0013	0.8738	0.0186	0.1031	0.0014	0.3078	656	45	633	8	638	10	99
077_28		0.17	21	12612	803	1566	32688	104554	0.31	0.0668	0.0029	1.2052	0.0490	0.1308	0.0023	0.0588	832	88	792	13	803	23	99
077_29		0.04	26	65681	4324	10149	274085	645154	0.42	0.0667	0.0017	1.2021	0.0314	0.1308	0.0020	0.2981	827	53	792	11	802	14	99
077_30		0.00	0	32975	2238	4228	121755	334777	0.36	0.0686	0.0017	1.0527	0.0251	0.1113	0.0015	0.2219	887	50	680	9	730	12	93
077_31		0.03	13	44474	3085	7279	221468	467182	0.47	0.0698	0.0011	1.0991	0.0180	0.1143	0.0014	0.4639	921	31	698	8	753	9	93
077_32		0.10	24	24900	1534	1520	38636	268971	0.14	0.0622	0.0015	0.8752	0.0202	0.1021	0.0013	0.2530	681	49	627	8	638	11	98

DA13-077	C. Ant Domain		Mean cps (background subtracted)							Isotopic Ratios (± 1σ)							Age (Ma ± 1σ)						
Analysis	Core/Rim	$\%Pb_c$	^{204}Pb	^{206}Pb	^{207}Pb	^{208}Pb	^{232}Th	^{238}U	Th/U	$^{207}Pb/^{206}Pb$		$^{207}Pb/^{235}U$		$^{206}Pb/^{238}U$		Rho	$^{207}Pb/^{206}Pb$		$^{206}Pb/^{238}U$		$^{207}Pb/^{235}U$		%Conc
077_34		0.06	10	15558	1018	1155	33748	153646	0.22	0.0654	0.0013	1.1319	0.0226	0.1255	0.0017	0.3933	788	40	762	10	769	11	99
077_35	C	0.41	5	1204	86	275	7325	10999	0.67	0.0718	0.0022	1.3068	0.0395	0.1320	0.0021	0.2231	981	61	799	12	849	17	94
077_36	R	0.07	9	12354	719	39	1570	176873	0.01	0.0584	0.0011	0.6734	0.0127	0.0836	0.0011	0.3946	546	39	518	6	523	8	99
077_37		0.00	0	7179	481	1381	37248	64041	0.58	0.0670	0.0013	1.2285	0.0248	0.1329	0.0018	0.3549	839	41	805	10	814	11	99
077_38		1.10	35	3148	274	769	17069	34171	0.50	0.0872	0.0019	1.3239	0.0293	0.1101	0.0015	0.3160	1365	42	673	9	856	13	79
077_39		0.02	2	8460	564	1063	27959	78163	0.36	0.0666	0.0013	1.1785	0.0240	0.1283	0.0017	0.3458	826	41	778	10	791	11	98
077_40		0.06	13	21128	1439	5889	150716	196415	0.77	0.0674	0.0014	1.2329	0.0254	0.1327	0.0018	0.3729	849	41	803	10	816	12	99
077_41		0.40	9	2265	157	505	13912	20558	0.68	0.0692	0.0019	1.2294	0.0336	0.1290	0.0019	0.2376	904	56	782	11	814	15	96
077_43		0.07	7	9875	649	1146	31277	93061	0.34	0.0648	0.0015	1.1738	0.0273	0.1315	0.0019	0.3239	767	48	796	11	788	13	101
077_44		0.00	0	16474	1081	1596	42154	148056	0.28	0.0649	0.0014	1.2130	0.0268	0.1356	0.0019	0.3369	770	45	820	11	807	12	102
077_45		0.00	0	13642	901	1414	39269	127635	0.31	0.0654	0.0014	1.1635	0.0245	0.1291	0.0018	0.3485	786	43	783	10	784	11	100
077_46		0.00	0	21964	1490	4621	112508	212343	0.53	0.0679	0.0014	1.2207	0.0258	0.1304	0.0018	0.3766	865	42	790	10	810	12	98
077_47		0.00	5	14119	924	3570	98891	134903	0.73	0.0658	0.0014	1.2077	0.0259	0.1330	0.0019	0.3828	801	43	805	11	804	12	100
077_48	C	0.01	0	36074	2413	4236	169586	350163	0.48	0.0680	0.0013	1.1198	0.0223	0.1196	0.0015	0.3470	867	40	728	9	763	11	95
077_49	R	0.00	0	27276	1683	631	17946	313949	0.06	0.0617	0.0012	0.8946	0.0182	0.1051	0.0014	0.3679	665	42	644	8	649	10	99
077_50	C	0.00	12	4375	302	553	12860	43618	0.29	0.0696	0.0022	1.2344	0.0377	0.1286	0.0021	0.2462	917	62	780	12	816	17	96
077_51	R	0.03	1	37319	2257	654	8332	509867	0.02	0.0611	0.0014	0.7164	0.0160	0.0852	0.0011	0.3039	641	47	527	7	549	9	96
077_52		0.02	0	4413	306	705	18693	43297	0.43	0.0700	0.0015	1.2005	0.0255	0.1244	0.0017	0.3520	928	42	756	10	801	12	94
077_53	C	0.00	0	7471	512	1468	38457	70970	0.54	0.0692	0.0015	1.1771	0.0262	0.1233	0.0017	0.3036	905	45	750	10	790	12	95
077_54	R	0.00	0	23493	1473	865	24877	292998	0.08	0.0626	0.0015	0.9005	0.0224	0.1044	0.0016	0.3275	693	51	640	9	652	12	98
077_55	C	0.00	0	10566	694	2790	76455	99860	0.77	0.0662	0.0015	1.2238	0.0289	0.1340	0.0019	0.3313	813	48	811	11	812	13	100
077_56	R	0.00	20	18208	1125	812	23569	211388	0.11	0.0624	0.0012	0.8953	0.0172	0.1040	0.0014	0.3849	689	39	638	8	649	9	98
077_57		0.32	0	6215	402	1308	33566	54624	0.61	0.0655	0.0020	1.1978	0.0365	0.1327	0.0020	0.2093	790	64	803	12	800	17	100
077_58		0.00	0	6638	446	1323	39474	65680	0.60	0.0680	0.0018	1.1998	0.0323	0.1281	0.0020	0.2741	867	55	777	11	801	15	97
077_59		0.00	8	3670	253	507	15004	36880	0.41	0.0696	0.0016	1.1599	0.0272	0.1208	0.0017	0.3042	918	47	735	10	782	13	94
077_60		0.15		5205	341	1312	34085	47926	0.71	0.0665	0.0018	1.2350	0.0334	0.1347	0.0020	0.2662	822	56	815	12	817	15	100

DA13-083	C. Ant Domain		Mean cps (background subtracted)							Isotopic Ratios (± 1σ)							Age (Ma ± 1σ)						
Analysis	Core/Rim	$\%Pb_c$	^{204}Pb	^{206}Pb	^{207}Pb	^{208}Pb	^{232}Th	^{238}U	Th/U	$^{207}Pb/^{206}Pb$		$^{207}Pb/^{235}U$		$^{206}Pb/^{238}U$		Rho	$^{207}Pb/^{206}Pb$		$^{206}Pb/^{238}U$		$^{207}Pb/^{235}U$		%Conc
083_01	C	0.52	15	2891	194	925	23695	28311	0.84	0.0676	0.0027	1.1909	0.0468	0.1279	0.0024	0.1673	855	82	776	14	796	22	97
083_02	R	0.06	5	7882	504	2996	85741	79482	1.08	0.0635	0.0014	1.1840	0.0268	0.1353	0.0021	0.4041	724	45	818	12	793	12	103
083_03	IC	0.15	10	6772	427	1599	42567	75069	0.57	0.0618	0.0021	0.9389	0.0316	0.1101	0.0018	0.1859	668	73	674	11	672	17	100
083_04	OC	0.01	1	10887	708	5101	135827	105121	1.29	0.0647	0.0016	1.1648	0.0283	0.1307	0.0019	0.3036	763	50	792	11	784	13	101
083_05	R	0.00	0	7769	493	2100	60148	73691	0.82	0.0632	0.0014	1.1615	0.0266	0.1333	0.0019	0.3320	716	47	807	11	783	12	103
083_06		0.13	9	7013	465	3763	122755	79647	1.54	0.0654	0.0017	1.0884	0.0287	0.1207	0.0019	0.3269	787	54	735	11	748	14	98
083_07	C	0.15	9	5948	391	2612	78463	62446	1.26	0.0655	0.0015	1.1444	0.0261	0.1268	0.0019	0.3718	790	46	769	11	775	12	99
083_08	R	0.08	4	5095	290	467	19267	76765	0.25	0.0567	0.0016	0.6977	0.0192	0.0892	0.0014	0.2962	481	59	551	8	537	11	102
083_09		0.19	10	5138	361	3639	109950	54355	2.02	0.0701	0.0019	1.2163	0.0327	0.1258	0.0020	0.2912	932	54	764	11	808	15	95
083_10	C	0.00	0	4506	298	1829	51196	53656	0.95	0.0650	0.0020	0.9587	0.0288	0.1071	0.0017	0.2097	773	64	656	10	683	15	96
083_11	R	0.00	0	3277	213	1130	33638	34594	0.97	0.0647	0.0016	1.0889	0.0266	0.1222	0.0018	0.3051	764	51	743	10	748	13	99
083_12		0.00	0	10435	821	1600	44886	132125	0.34	0.0773	0.0025	1.0097	0.0314	0.0947	0.0015	0.1511	1129	64	583	9	709	16	82
083_13		0.07	5	7364	496	2666	92628	81234	1.14	0.0671	0.0016	1.0967	0.0266	0.1186	0.0018	0.3087	841	50	722	10	752	13	96
083_14		0.06	5	8501	545	3808	106637	81452	1.31	0.0638	0.0014	1.1753	0.0266	0.1336	0.0019	0.3210	735	47	809	11	789	12	102
083_15		0.09	10	10950	734	5371	156838	120434	1.30	0.0666	0.0018	1.0910	0.0282	0.1187	0.0018	0.2709	827	54	723	10	749	14	97
083_16		0.49	33	6745	461	1923	46114	67282	0.69	0.0679	0.0015	1.1442	0.0253	0.1222	0.0017	0.3307	867	45	743	10	775	12	96
083_17		0.14	17	11771	792	4296	128113	118448	1.08	0.0666	0.0015	1.1262	0.0255	0.1226	0.0017	0.3312	826	46	745	10	766	12	97
083_18		0.05	5	9887	652	3655	101950	100056	1.02	0.0652	0.0010	1.1102	0.0185	0.1235	0.0016	0.4887	781	32	751	9	758	9	99
083_19		0.00	0	5330	351	2651	72499	55018	1.32	0.0651	0.0014	1.1074	0.0237	0.1233	0.0018	0.3801	778	43	750	10	757	11	99
083_20		0.03	2	7552	514	3743	106680	79814	1.34	0.0672	0.0017	1.1497	0.0286	0.1242	0.0019	0.3282	843	50	755	11	777	14	97
083_21		0.00	0	14217	966	2071	52985	180212	0.29	0.0667	0.0011	0.9000	0.0157	0.0979	0.0013	0.4599	828	34	602	8	652	8	92
083_22		0.15	7	4586	394	606	7698	67207	0.11	0.0832	0.0033	1.1107	0.0427	0.0969	0.0020	0.2076	1273	75	596	12	759	21	79
083_23		0.00	0	3455	227	1665	45948	36572	1.26	0.0643	0.0018	1.0122	0.0278	0.1142	0.0017	0.2540	752	58	697	10	710	14	98
083_24	C	0.00	0	5932	392	2266	65580	60929	1.08	0.0647	0.0011	1.1025	0.0205	0.1235	0.0017	0.4449	766	36	751	10	755	10	100
083_25	R	0.22	13	5934	392	2550	78914	60078	1.31	0.0645	0.0013	1.0811	0.0223	0.1217	0.0017	0.3746	756	42	740	10	744	11	99
083_26		0.04	5	13665	912	7173	187842	124864	1.50	0.0651	0.0011	1.2151	0.0214	0.1354	0.0018	0.4489	778	34	818	10	808	10	101
083_27		0.00	0	2371	155	974	27277	23367	1.17	0.0641	0.0016	1.1484	0.0292	0.1300	0.0020	0.3140	744	52	788	11	777	14	101
083_28		0.04	5	11139	726	4601	152518	139799	1.09	0.0634	0.0019	0.9739	0.0288	0.1114	0.0019	0.2985	721	61	681	11	691	15	99
083_29		0.20	7	3567	235	1879	52776	37083	1.42	0.0637	0.0014	1.0898	0.0241	0.1241	0.0018	0.3676	731	45	754	10	748	12	101
083_30		0.02	2	11697	797	5013	137290	110886	1.24	0.0659	0.0013	1.2027	0.0249	0.1324	0.0019	0.3928	802	41	802	11	802	11	100
083_31		0.12	11	9194	634	4606	152205	86776	1.75	0.0676	0.0017	1.1939	0.0299	0.1281	0.0019	0.2824	855	52	777	11	798	14	97

DA13-083	C. Ant Domain		Mean cps (background subtracted)							Isotopic Ratios (± 1σ)							Age (Ma ± 1σ)						
Analysis	Core/Rim	$\%Pb_c$	^{204}Pb	^{206}Pb	^{207}Pb	^{208}Pb	^{232}Th	^{238}U	Th/U	$^{207}Pb/^{206}Pb$		$^{207}Pb/^{235}U$		$^{206}Pb/^{238}U$		Rho	$^{207}Pb/^{206}Pb$		$^{206}Pb/^{238}U$		$^{207}Pb/^{235}U$		%Conc
083_32		0.00	0	9117	603	4132	117529	90912	1.29	0.0650	0.0010	1.1462	0.0193	0.1278	0.0017	0.5022	776	32	775	10	776	9	100
083_33		0.06	6	9723	673	4201	133755	104708	1.28	0.0692	0.0018	1.1877	0.0306	0.1246	0.0020	0.3372	905	51	757	11	795	14	95
083_34		0.08	6	7058	489	2700	79602	71689	1.11	0.0681	0.0011	1.1999	0.0217	0.1278	0.0018	0.4764	872	34	775	10	801	10	97
083_35		0.00	0	5439	347	1942	55780	55932	1.00	0.0638	0.0024	1.1592	0.0427	0.1318	0.0024	0.2174	735	77	798	14	782	20	102
083_36		0.20	14	6875	466	2537	79641	76851	1.04	0.0675	0.0015	1.0857	0.0242	0.1167	0.0017	0.3728	853	44	712	10	746	12	95
083_37		0.07	7	10391	696	3719	145072	116058	1.25	0.0633	0.0025	1.1066	0.0429	0.1269	0.0025	0.2042	718	82	770	14	757	21	102
083_38	R	0.00	0	1539	101	47	1566	24726	0.06	0.0669	0.0033	0.7492	0.0361	0.0813	0.0017	0.1346	835	101	504	10	568	21	89
083_39		0.00	0	7125	462	2924	83534	70963	1.18	0.0645	0.0015	1.2085	0.0292	0.1358	0.0021	0.3686	759	49	821	12	805	13	102
083_40		0.04	5	11266	755	4938	149157	116061	1.29	0.0662	0.0012	1.1105	0.0210	0.1217	0.0017	0.4235	813	37	740	9	758	10	98
083_41		0.03	4	15114	1026	6921	206223	158767	1.30	0.0671	0.0013	1.1137	0.0224	0.1204	0.0017	0.3969	841	40	733	10	760	11	96
083_42		0.00	0	5873	378	1651	44844	55337	0.81	0.0640	0.0014	1.1996	0.0271	0.1359	0.0020	0.3597	743	46	822	11	800	13	103
083_43		0.00	0	7837	558	3811	121502	89713	1.35	0.0708	0.0013	1.1127	0.0223	0.1140	0.0016	0.4303	952	38	696	9	760	11	92
083_44		0.00	0	3834	245	2107	61292	39208	1.56	0.0636	0.0013	1.1048	0.0239	0.1259	0.0018	0.3790	730	44	765	10	756	12	101
083_45		0.18	17	9516	618	4013	132475	115728	1.14	0.0620	0.0028	0.9855	0.0429	0.1155	0.0024	0.1713	673	93	705	14	696	22	101
083_46		0.10	12	11697	896	5580	296604	140377	2.11	0.0772	0.0014	1.0562	0.0199	0.0994	0.0013	0.3844	1126	36	611	8	732	10	83
083_47	C	0.00	0	7756	543	2676	74184	87807	0.84	0.0705	0.0012	1.0723	0.0196	0.1103	0.0015	0.4399	944	35	674	9	740	10	91
083_48	R	0.00	0	10436	673	4206	112442	95740	1.17	0.0649	0.0014	1.1530	0.0249	0.1290	0.0018	0.3274	770	45	782	10	779	12	100
083_49		0.02	2	10290	671	4301	117125	101038	1.16	0.0659	0.0011	1.1662	0.0207	0.1283	0.0017	0.4655	805	34	778	10	785	10	99
083_50		0.00	0	19637	1325	8542	262748	230040	1.14	0.0683	0.0010	1.0075	0.0165	0.1070	0.0014	0.5069	879	31	655	8	708	8	93
083_51		0.17	9	5277	345	3739	107997	53808	2.01	0.0661	0.0012	1.1385	0.0218	0.1250	0.0017	0.4388	809	37	759	10	772	10	98
083_52		0.02	2	9614	634	6125	161797	91109	1.78	0.0668	0.0012	1.1930	0.0228	0.1295	0.0017	0.4131	833	38	785	10	797	11	98
083_53		0.00	0	15690	1026	8678	240995	160268	1.50	0.0664	0.0014	1.1887	0.0263	0.1299	0.0019	0.4091	818	43	787	11	795	12	99
083_54		0.04	4	9852	611	4370	142511	123564	1.15	0.0623	0.0019	0.9808	0.0307	0.1142	0.0020	0.2876	685	65	697	12	694	16	100
083_55		0.11	8	7200	463	5540	158403	73716	2.15	0.0650	0.0012	1.1268	0.0220	0.1257	0.0018	0.4332	775	38	763	10	766	11	100
083_56		0.00	0	13077	845	7282	204797	134259	1.53	0.0654	0.0011	1.1322	0.0211	0.1256	0.0017	0.4650	787	36	763	10	769	10	99
083_57		0.00	0	5559	373	2506	70591	56639	1.25	0.0680	0.0013	1.1819	0.0241	0.1262	0.0018	0.4128	867	40	766	10	792	11	97
083_58		0.32	17	5277	355	2297	61617	61863	1.00	0.0681	0.0018	0.9783	0.0260	0.1041	0.0016	0.2778	873	54	639	9	693	13	92
083_59		0.08	6	7377	486	4604	128150	74450	1.72	0.0668	0.0013	1.1844	0.0247	0.1287	0.0018	0.4172	831	41	780	10	793	12	98
083_60		0.02	2	8090	528	3026	85605	86481	0.99	0.0666	0.0020	1.0201	0.0299	0.1111	0.0017	0.2390	825	61	679	10	714	15	95
083_61		0.46	15	3247	210	1627	43477	30592	1.42	0.0659	0.0014	1.1886	0.0261	0.1309	0.0018	0.3459	803	44	793	10	795	12	100
083_62	C	0.00	0	5096	330	2868	77108	60383	1.28	0.0660	0.0013	0.9580	0.0194	0.1054	0.0015	0.3896	805	40	646	8	682	10	95

DA13-083	C. Ant Domain		Mean cps (background subtracted)							Isotopic Ratios (± 1σ)							Age (Ma ± 1σ)						
Analysis	Core/Rim	$\%Pb_c$	^{204}Pb	^{206}Pb	^{207}Pb	^{208}Pb	^{232}Th	^{238}U	Th/U	$^{207}Pb/^{206}Pb$		$^{207}Pb/^{235}U$		$^{206}Pb/^{238}U$		Rho	$^{207}Pb/^{206}Pb$		$^{206}Pb/^{238}U$		$^{207}Pb/^{235}U$		%Conc
083_63	R	0.00	0	14438	864	649	19152	231496	0.08	0.0610	0.0017	0.7397	0.0206	0.0880	0.0015	0.3429	639	57	544	9	562	12	97
083_64		0.00	0	7762	508	3349	93538	80415	1.16	0.0667	0.0015	1.1923	0.0272	0.1296	0.0019	0.3975	829	45	786	11	797	13	99
083_65		0.00	0	21318	1452	12447	451359	283498	1.59	0.0694	0.0015	0.9826	0.0223	0.1028	0.0016	0.4101	909	44	631	9	695	11	91
083_66		0.14	16	11804	784	5753	161697	115182	1.40	0.0675	0.0012	1.1898	0.0222	0.1279	0.0017	0.4250	852	36	776	10	796	10	97
083_67		0.00	0	20117	1391	16534	586215	216035	2.71	0.0696	0.0015	1.0213	0.0216	0.1063	0.0014	0.2938	917	43	651	8	715	11	91
083_68	C	0.23	8	3521	229	1455	37318	31752	1.18	0.0659	0.0016	1.1884	0.0286	0.1309	0.0018	0.2757	802	50	793	11	795	13	100
083_69	R	0.33	19	5724	361	1911	58091	65351	0.89	0.0639	0.0012	0.9584	0.0188	0.1088	0.0015	0.3957	737	39	666	9	683	10	98
083_70		0.00	0	4111	266	1167	39193	52946	0.74	0.0657	0.0027	1.0051	0.0400	0.1110	0.0022	0.2182	796	82	679	13	706	20	96
083_71		0.00	0	9928	635	3628	108681	113194	0.96	0.0646	0.0012	1.0144	0.0201	0.1139	0.0016	0.4380	761	39	695	9	711	10	98
083_72		0.00	0	7061	470	3522	93631	65416	1.43	0.0670	0.0014	1.1982	0.0258	0.1298	0.0018	0.3293	837	44	787	10	800	12	98
083_73		0.02	3	17970	1184	12723	354423	182736	1.94	0.0668	0.0015	1.1848	0.0274	0.1287	0.0019	0.3640	832	46	780	11	794	13	98
083_74		0.00	0	6678	420	4224	118320	75766	1.56	0.0635	0.0012	0.9774	0.0199	0.1116	0.0016	0.4010	726	41	682	9	692	10	99
083_75		0.09	14	15435	1055	8703	283740	157985	1.80	0.0683	0.0038	0.9973	0.0523	0.1062	0.0023	0.0833	877	110	651	14	702	27	93

DA13-074	E. Ant Domain		Mean cps (background subtracted)							Isotopic Ratios (± 1σ)							Age (Ma ± 1σ)						
Analysis	Core/Rim	$\%Pb_c$	^{204}Pb	^{206}Pb	^{207}Pb	^{208}Pb	^{232}Th	^{238}U	Th/U	$^{207}Pb/^{206}Pb$		$^{207}Pb/^{235}U$		$^{206}Pb/^{238}U$		Rho	$^{207}Pb/^{206}Pb$		$^{206}Pb/^{238}U$		$^{207}Pb/^{235}U$		%Conc
074_01		0.34	16	4651	302	756	20089	43033	0.47	0.0651	0.0015	1.1591	0.0261	0.1291	0.0018	0.3111	778	46	783	10	782	12	100
074_02		0.26	9	3405	227	754	20546	32109	0.64	0.0670	0.0015	1.1890	0.0267	0.1288	0.0018	0.3241	837	46	781	10	796	12	98
074_03		0.18	13	7378	495	720	19737	73325	0.27	0.0671	0.0015	1.2001	0.0270	0.1298	0.0019	0.3714	841	45	787	11	801	12	98
074_04	C	0.05	2	3891	239	645	22524	49681	0.45	0.0611	0.0020	0.8926	0.0288	0.1060	0.0018	0.2516	642	68	650	11	648	15	100
074_05	R	0.15	3	2052	134	327	11011	24270	0.45	0.0655	0.0017	0.9570	0.0246	0.1059	0.0016	0.2907	792	53	649	9	682	13	95
074_06		0.15	9	6082	404	1362	37508	58161	0.64	0.0663	0.0012	1.2009	0.0225	0.1315	0.0018	0.4372	815	37	796	10	801	10	99
074_07		0.00	0	6742	442	970	24454	62323	0.39	0.0661	0.0013	1.1937	0.0237	0.1310	0.0018	0.3742	809	40	794	10	798	11	99
074_08		0.18	11	6086	392	1349	46173	73791	0.63	0.0640	0.0015	0.9557	0.0224	0.1084	0.0016	0.3651	740	47	663	9	681	12	97
074_09		0.00	0	5961	397	863	24119	57521	0.42	0.0669	0.0018	1.2501	0.0339	0.1356	0.0021	0.3035	834	55	820	12	824	15	100
074_10		0.15	8	5170	346	1079	30727	50764	0.61	0.0680	0.0019	1.1703	0.0326	0.1249	0.0019	0.2548	867	57	759	11	787	15	96
074_11		0.00	0	7100	470	1537	45078	70279	0.64	0.0661	0.0017	1.2165	0.0310	0.1335	0.0021	0.3335	810	51	808	12	808	14	100
074_12		0.00	0	5028	337	913	25459	48593	0.52	0.0680	0.0015	1.2123	0.0280	0.1294	0.0019	0.3383	867	46	784	11	806	13	97
074_13		0.00	0	13525	889	1236	36531	174061	0.21	0.0653	0.0018	0.9515	0.0260	0.1057	0.0017	0.3183	783	56	648	10	679	14	95
074_14		0.10	7	6885	454	1732	47406	63540	0.75	0.0672	0.0016	1.2068	0.0281	0.1304	0.0018	0.3137	843	47	790	10	804	13	98
074_15		0.00	1	33651	2177	3600	104709	404950	0.26	0.0653	0.0013	0.9558	0.0195	0.1063	0.0015	0.4094	782	40	651	9	681	10	96
074_16		0.00	0	18520	1203	2061	57061	183545	0.31	0.0647	0.0010	1.1806	0.0208	0.1323	0.0018	0.5075	765	33	801	10	792	10	101
074_17		0.00	0	4818	318	785	21403	45259	0.47	0.0657	0.0013	1.1790	0.0231	0.1302	0.0018	0.3852	796	39	789	10	791	11	100
074_18		0.01	1	8818	516	46	1825	134246	0.01	0.0577	0.0015	0.7169	0.0187	0.0902	0.0014	0.3411	516	55	557	8	549	11	101
074_19		0.10	6	6121	411	1051	29051	57929	0.50	0.0668	0.0012	1.1995	0.0221	0.1303	0.0017	0.4197	832	36	789	10	800	10	99
074_20		0.00	0	6934	459	1019	28066	65483	0.43	0.0655	0.0012	1.2127	0.0227	0.1343	0.0018	0.4348	791	37	812	10	806	10	101
074_21		0.07	10	13832	945	2333	61658	135868	0.45	0.0684	0.0014	1.2558	0.0267	0.1333	0.0019	0.4041	880	42	806	11	826	12	98
074_22		0.00	0	4256	278	624	16950	39531	0.43	0.0653	0.0016	1.1773	0.0290	0.1308	0.0019	0.2910	785	51	792	11	790	14	100
074_23		0.04	3	7711	528	1602	44452	76921	0.58	0.0683	0.0014	1.2211	0.0252	0.1296	0.0018	0.4057	879	40	786	11	810	12	97
074_24		0.02	2	12384	830	1419	40435	123926	0.33	0.0669	0.0013	1.2096	0.0247	0.1312	0.0019	0.4262	834	40	795	11	805	11	99
074_25	C	0.28	10	3562	234	574	15977	35270	0.45	0.0658	0.0019	1.1897	0.0342	0.1313	0.0021	0.2767	798	59	795	12	796	16	100
074_26	R	0.00	0	7237	430	590	23781	102521	0.23	0.0592	0.0012	0.7184	0.0149	0.0880	0.0012	0.3681	575	43	544	7	550	9	99
074_27		0.00	0	7523	510	1305	35717	70677	0.51	0.0676	0.0013	1.2202	0.0245	0.1310	0.0018	0.3688	855	40	794	10	810	11	98
074_28		0.00	0	19319	1258	1951	49951	182826	0.27	0.0647	0.0012	1.2007	0.0229	0.1346	0.0019	0.4317	765	38	814	10	801	11	102
074_29		0.14	12	8631	519	236	7630	119904	0.06	0.0603	0.0015	0.7243	0.0174	0.0871	0.0012	0.2843	616	51	538	7	553	10	97
074_30		0.02	13	61991	3917	18599	483749	644131	0.75	0.0621	0.0015	0.9007	0.0213	0.1053	0.0014	0.1942	677	52	645	8	652	11	99
074_31		0.02	2	8745	572	1944	52261	79196	0.66	0.0652	0.0011	1.1957	0.0219	0.1331	0.0017	0.4162	779	37	806	10	799	10	101

DA13-074	E. Ant Domain		Mean cps (background subtracted)							Isotopic Ratios (± 1σ)							Age (Ma ± 1σ)						
Analysis	Core/Rim	$\%Pb_c$	^{204}Pb	^{206}Pb	^{207}Pb	^{208}Pb	^{232}Th	^{238}U	Th/U	$^{207}Pb/^{206}Pb$		$^{207}Pb/^{235}U$		$^{206}Pb/^{238}U$		Rho	$^{207}Pb/^{206}Pb$		$^{206}Pb/^{238}U$		$^{207}Pb/^{235}U$		%Conc
074_32		0.00	0	9664	647	2332	61150	88870	0.69	0.0668	0.0013	1.2650	0.0256	0.1373	0.0019	0.4003	832	40	829	11	830	11	100
074_33		0.00	0	10357	694	2299	63292	97648	0.65	0.0664	0.0011	1.2058	0.0212	0.1316	0.0017	0.4607	820	34	797	10	803	10	99
074_34		0.00	0	9151	606	2279	62160	86311	0.72	0.0652	0.0014	1.2511	0.0284	0.1392	0.0021	0.3685	781	46	840	12	824	13	102
074_35		0.00	0	13894	931	3001	87653	140268	0.62	0.0655	0.0015	1.1835	0.0274	0.1310	0.0020	0.3689	791	46	794	11	793	13	100
074_36		0.00	0	7281	479	1286	35933	72555	0.50	0.0645	0.0015	1.1672	0.0270	0.1312	0.0020	0.3568	759	47	795	11	785	13	101
074_37		0.21	14	6755	446	1197	32137	61373	0.52	0.0665	0.0017	1.2031	0.0303	0.1312	0.0019	0.2905	823	52	795	11	802	14	99
074_38		0.00	0	4328	287	758	20715	39599	0.52	0.0660	0.0016	1.2467	0.0305	0.1369	0.0020	0.3250	808	50	827	11	822	14	101
074_39		0.00	0	9916	654	2362	64775	93558	0.69	0.0638	0.0014	1.2335	0.0284	0.1402	0.0021	0.3678	736	47	846	12	816	13	104
074_40		0.04	4	10105	668	2045	54953	96043	0.57	0.0654	0.0012	1.1989	0.0238	0.1330	0.0018	0.4218	787	39	805	10	800	11	101
074_41	C	0.10	5	5111	328	840	23233	45825	0.51	0.0650	0.0012	1.1982	0.0231	0.1337	0.0018	0.3792	775	39	809	10	800	11	101
074_42	R	0.26	14	5474	365	762	23254	62544	0.37	0.0678	0.0019	1.0398	0.0289	0.1113	0.0017	0.2754	862	57	681	10	724	14	94
074_43		0.03	2	7785	512	1345	36694	74570	0.49	0.0665	0.0012	1.1677	0.0213	0.1273	0.0017	0.4283	822	36	773	10	786	10	98
074_44		0.16	11	6903	458	855	22710	63009	0.36	0.0669	0.0015	1.2080	0.0269	0.1309	0.0018	0.3222	836	45	793	10	804	12	99
074_45		0.00	0	14051	928	2132	56792	130995	0.43	0.0663	0.0012	1.1360	0.0214	0.1242	0.0016	0.3694	817	38	755	9	771	10	98
074_46		0.00	0	4033	267	595	18332	44135	0.42	0.0667	0.0013	1.0184	0.0203	0.1108	0.0015	0.3787	828	40	677	9	713	10	95
074_47		0.00	0	60059	3929	2296	59573	540821	0.11	0.0655	0.0015	1.1254	0.0254	0.1247	0.0017	0.2806	790	47	757	9	766	12	99
074_48		0.22	8	3653	246	584	16530	37079	0.45	0.0679	0.0014	1.1295	0.0241	0.1207	0.0017	0.3604	865	43	735	10	768	11	96
074_49		0.01	1	6883	453	856	21383	60888	0.35	0.0656	0.0017	1.1768	0.0301	0.1300	0.0019	0.2553	794	53	788	11	790	14	100
074_50		0.34	14	4081	263	605	18733	47220	0.40	0.0649	0.0014	0.9401	0.0201	0.1050	0.0014	0.3519	772	44	644	8	673	11	96
074_51		0.00	0	3348	224	453	12512	31532	0.40	0.0672	0.0017	1.1562	0.0291	0.1248	0.0018	0.2651	844	52	758	10	780	14	97
074_52		0.00	0	10139	659	1805	48442	95941	0.50	0.0651	0.0011	1.1679	0.0212	0.1301	0.0017	0.4351	778	36	788	10	786	10	100
074_53		0.00	0	1911	131	292	7992	18238	0.44	0.0689	0.0017	1.2178	0.0308	0.1283	0.0019	0.2879	895	51	778	11	809	14	96
074_54		0.05	13	24957	1527	1426	39288	309965	0.13	0.0606	0.0015	0.8948	0.0226	0.1071	0.0017	0.3571	624	52	656	10	649	12	101
074_55		0.00	0	92538	6131	3408	86711	871859	0.10	0.0662	0.0010	1.1990	0.0202	0.1314	0.0017	0.4910	813	32	796	10	800	9	99
074_56		0.00	0	13106	876	2351	59897	122652	0.49	0.0672	0.0010	1.2175	0.0197	0.1315	0.0017	0.4948	843	31	796	10	809	9	98
074_57		0.12	5	4307	296	799	21776	40877	0.53	0.0692	0.0013	1.2398	0.0245	0.1299	0.0018	0.3957	906	39	787	10	819	11	96
074_58		0.14	8	5558	372	707	19933	53333	0.37	0.0674	0.0012	1.2080	0.0227	0.1300	0.0018	0.4302	850	37	788	10	804	10	98
074_59		0.00	0	16826	1107	4286	115029	167830	0.69	0.0670	0.0011	1.2096	0.0224	0.1310	0.0018	0.4871	838	35	794	10	805	10	99
074_60		0.00	0	14192	925	1751	47734	146712	0.33	0.0655	0.0011	1.0568	0.0179	0.1170	0.0015	0.4482	791	33	713	9	732	9	97
074_61		0.03	4	13021	858	2643	76900	138572	0.55	0.0669	0.0015	1.1973	0.0280	0.1299	0.0020	0.4076	834	46	787	11	799	13	99
074_62		0.00	0	5160	336	795	20618	48247	0.43	0.0656	0.0012	1.1920	0.0233	0.1317	0.0018	0.3938	795	39	798	10	797	11	100

DA13-074	E. Ant Domain		Mean cps (background subtracted)							Isotopic Ratios (± 1σ)							Age (Ma ± 1σ)						
Analysis	Core/Rim	$\%Pb_c$	^{204}Pb	^{206}Pb	^{207}Pb	^{208}Pb	^{232}Th	^{238}U	Th/U	$^{207}Pb/^{206}Pb$		$^{207}Pb/^{235}U$		$^{206}Pb/^{238}U$		Rho	$^{207}Pb/^{206}Pb$		$^{206}Pb/^{238}U$		$^{207}Pb/^{235}U$		%Conc
074_63		0.04	5	12156	811	2035	54301	118643	0.46	0.0677	0.0012	1.2250	0.0229	0.1313	0.0018	0.4574	859	36	795	10	812	10	98
074_64		0.06	3	4989	320	741	21341	56572	0.38	0.0653	0.0014	1.0179	0.0226	0.1130	0.0016	0.3694	785	45	690	9	713	11	97
074_65		0.19	10	5245	349	872	22645	49386	0.46	0.0670	0.0013	1.1874	0.0243	0.1285	0.0017	0.3631	838	41	780	10	795	11	98
074_66		0.00	0	9479	655	1792	42153	83594	0.50	0.0683	0.0018	1.2239	0.0322	0.1301	0.0019	0.2299	876	55	788	11	812	15	97
074_67		0.03	2	7788	528	1489	54022	93540	0.58	0.0683	0.0015	0.9312	0.0207	0.0989	0.0014	0.3168	878	45	608	8	668	11	91
074_68		0.00	0	25542	1712	5865	179072	274663	0.65	0.0682	0.0017	1.2095	0.0309	0.1286	0.0020	0.3645	875	50	780	12	805	14	97
074_69		0.00	0	18368	1211	5196	140721	181405	0.78	0.0667	0.0011	1.1651	0.0210	0.1268	0.0017	0.4566	827	35	770	10	784	10	98
074_70		0.14	10	7348	490	1909	55878	77101	0.72	0.0683	0.0017	1.2027	0.0314	0.1278	0.0020	0.3404	877	52	775	11	802	14	97

DA13-076	E. Ant Domain		Mean cps (background subtracted)							Isotopic Ratios (± 1σ)							Age (Ma ± 1σ)						
Analysis	Core/Rim	$\%Pb_c$	^{204}Pb	^{206}Pb	^{207}Pb	^{208}Pb	^{232}Th	^{238}U	Th/U	$^{207}Pb/^{206}Pb$		$^{207}Pb/^{235}U$		$^{206}Pb/^{238}U$		Rho	$^{207}Pb/^{206}Pb$		$^{206}Pb/^{238}U$		$^{207}Pb/^{235}U$		%Conc
076_01		0.00	0	6332	433	1382	37211	59932	0.62	0.0674	0.0013	1.2750	0.0257	0.1373	0.0020	0.4205	849	39	829	11	835	11	99
076_02		0.00	0	5196	350	1143	30077	49924	0.60	0.0674	0.0012	1.2155	0.0229	0.1308	0.0018	0.4313	850	37	793	10	808	10	98
076_03		0.00	0	11680	761	1664	42360	105100	0.40	0.0663	0.0013	1.2041	0.0246	0.1318	0.0018	0.3510	815	41	798	10	803	11	99
076_04		0.08	3	3762	244	743	20027	36720	0.55	0.0649	0.0020	1.1768	0.0355	0.1316	0.0021	0.2473	770	63	797	12	790	17	101
076_05	C	0.00	0	5244	347	883	23701	49265	0.48	0.0663	0.0012	1.2150	0.0235	0.1329	0.0018	0.4074	816	38	804	10	808	11	100
076_06	R	0.00	0	13437	855	312	8905	155974	0.06	0.0637	0.0011	0.9499	0.0172	0.1082	0.0015	0.4506	731	36	662	8	678	9	98
076_07	C	0.00	0	15580	1029	2514	67538	148096	0.46	0.0662	0.0011	1.1867	0.0201	0.1299	0.0017	0.4659	814	33	788	10	794	9	99
076_08	R	0.00	0	15647	911	187	6181	225610	0.03	0.0581	0.0009	0.6959	0.0118	0.0868	0.0011	0.4830	534	34	537	7	536	7	100
076_09	C	0.00	0	9947	684	2237	66341	100638	0.66	0.0661	0.0017	1.2148	0.0313	0.1333	0.0021	0.3203	810	53	806	12	807	14	100
076_10	R	0.05	5	9420	552	93	3517	131072	0.03	0.0585	0.0010	0.7266	0.0134	0.0900	0.0012	0.4368	550	38	556	7	555	8	100
076_11	C	0.08	4	4786	315	910	23563	42166	0.56	0.0661	0.0018	1.2755	0.0343	0.1400	0.0021	0.2674	810	56	844	12	835	15	101
076_12	R	0.00	0	6976	463	890	24771	67295	0.37	0.0658	0.0017	1.2170	0.0306	0.1341	0.0020	0.3068	800	52	811	12	808	14	100
076_13		0.00	0	5638	368	1308	34220	50443	0.68	0.0657	0.0014	1.2640	0.0275	0.1396	0.0020	0.3517	795	44	843	11	830	12	102
076_14		0.03	4	13579	876	2400	69027	136133	0.51	0.0644	0.0012	1.1182	0.0214	0.1259	0.0017	0.4238	756	38	764	10	762	10	100
076_15		0.05	6	11040	734	2546	68752	103387	0.66	0.0666	0.0012	1.2208	0.0236	0.1329	0.0018	0.4010	826	38	804	10	810	11	99
076_16		0.00	0	8530	550	1293	35185	77889	0.45	0.0651	0.0011	1.1923	0.0215	0.1328	0.0017	0.4220	779	36	804	10	797	10	101
076_17		0.03	3	8698	572	1968	49837	78806	0.63	0.0657	0.0012	1.2496	0.0243	0.1381	0.0019	0.4133	795	39	834	11	823	11	101
076_18		0.00	0	8339	547	2024	53773	75732	0.71	0.0657	0.0012	1.2372	0.0233	0.1366	0.0018	0.4193	796	37	826	10	818	11	101
076_19		0.00	0	9949	655	1377	34520	89464	0.39	0.0665	0.0013	1.2079	0.0235	0.1318	0.0017	0.3715	822	39	798	10	804	11	99
076_20	C	0.19	8	4273	274	783	19832	38414	0.52	0.0645	0.0014	1.1934	0.0256	0.1342	0.0018	0.3431	759	44	812	10	798	12	102
076_21	R	0.00	0	8324	477	87	3134	114954	0.03	0.0571	0.0011	0.7096	0.0143	0.0902	0.0012	0.3854	493	42	557	7	545	8	102
076_22		0.00	0	9574	629	2014	53076	86535	0.61	0.0655	0.0012	1.2317	0.0232	0.1364	0.0018	0.4142	791	37	824	10	815	11	101
076_23		0.00	0	4225	285	733	19195	38803	0.49	0.0667	0.0014	1.2494	0.0275	0.1359	0.0019	0.3512	829	44	821	11	823	12	100
076_24		0.00	0	7146	492	1498	39286	67497	0.58	0.0663	0.0016	1.2450	0.0299	0.1362	0.0020	0.3249	816	49	823	12	821	14	100
076_25	C	0.12	20	17130	1155	4111	112159	164300	0.68	0.0663	0.0017	1.2401	0.0322	0.1356	0.0021	0.2964	817	53	820	12	819	15	100
076_26	R	0.00	0	9680	638	850	22269	84520	0.26	0.0662	0.0017	1.2167	0.0317	0.1334	0.0019	0.2578	812	54	807	11	808	15	100
076_27		0.00	0	7425	427	74	2680	101386	0.03	0.0571	0.0012	0.6934	0.0149	0.0882	0.0012	0.3332	493	46	545	7	535	9	102
076_28		0.00	0	17497	1181	3489	91789	159278	0.58	0.0660	0.0015	1.2759	0.0301	0.1403	0.0021	0.3281	805	48	846	12	835	13	101
076_29		0.04	8	20597	1414	4376	114457	191480	0.60	0.0662	0.0014	1.2491	0.0271	0.1370	0.0020	0.3561	811	44	828	11	823	12	101
076_30		0.00	0	6614	448	1477	38350	59341	0.65	0.0672	0.0014	1.2470	0.0262	0.1346	0.0018	0.3466	844	43	814	10	822	12	99
076_31		0.00	0	12608	850	3009	79198	112178	0.71	0.0674	0.0010	1.2863	0.0206	0.1386	0.0018	0.5013	849	30	837	10	840	9	100

DA13-076	E. Ant Domain		Mean cps (background subtracted)							Isotopic Ratios (± 1σ)							Age (Ma ± 1σ)						
Analysis	Core/Rim	$\%Pb_c$	^{204}Pb	^{206}Pb	^{207}Pb	^{208}Pb	^{232}Th	^{238}U	Th/U	$^{207}Pb/^{206}Pb$		$^{207}Pb/^{235}U$		$^{206}Pb/^{238}U$		Rho	$^{207}Pb/^{206}Pb$		$^{206}Pb/^{238}U$		$^{207}Pb/^{235}U$		%Conc
076_32		0.07	7	9983	716	2312	54113	101046	0.54	0.0715	0.0012	1.2118	0.0209	0.1229	0.0016	0.4700	973	33	747	9	806	10	93
076_33	C	0.00	0	6535	431	1573	40813	59229	0.69	0.0661	0.0011	1.2173	0.0212	0.1337	0.0017	0.4413	808	34	809	10	809	10	100
076_34	R	0.03	3	9495	603	866	23181	116093	0.20	0.0651	0.0022	0.8072	0.0258	0.0902	0.0014	0.1499	776	69	557	8	601	15	93
076_35		0.03	3	11152	745	2210	56714	103182	0.55	0.0656	0.0013	1.2655	0.0264	0.1399	0.0020	0.4043	795	41	844	11	830	12	102
076_36		0.11	8	7471	483	1456	40673	74828	0.54	0.0643	0.0012	1.1113	0.0221	0.1254	0.0017	0.3998	751	40	762	10	759	11	100
076_37		0.09	13	14685	982	3471	92728	138916	0.67	0.0665	0.0011	1.2040	0.0204	0.1313	0.0017	0.4711	823	33	795	10	802	9	99
076_38		0.02	1	6075	403	1133	30704	55432	0.55	0.0659	0.0013	1.2466	0.0254	0.1374	0.0019	0.3877	802	41	830	11	822	12	101
076_39		0.00	0	5440	356	1215	31699	48986	0.65	0.0654	0.0014	1.2322	0.0265	0.1367	0.0019	0.3507	787	44	826	11	815	12	101
076_40		0.00	0	13753	899	2304	60255	122654	0.49	0.0657	0.0012	1.2051	0.0224	0.1330	0.0017	0.3862	798	38	805	10	803	10	100
076_41	C	0.00	0	7481	498	1553	41721	68842	0.61	0.0667	0.0012	1.2105	0.0223	0.1318	0.0017	0.4112	827	37	798	10	805	10	99
076_42	R	0.11	7	6426	372	32	1460	88482	0.02	0.0579	0.0011	0.6939	0.0132	0.0869	0.0011	0.3798	527	40	537	7	535	8	100
076_43	C	0.00	0	8593	562	1740	45713	76504	0.60	0.0660	0.0012	1.1904	0.0225	0.1309	0.0017	0.3591	805	39	793	10	796	10	100
076_44	R	0.26	29	11285	711	600	21005	174957	0.12	0.0611	0.0019	0.7149	0.0218	0.0850	0.0014	0.2568	641	65	526	8	548	13	96
076_45		0.49	28	5727	386	1308	34249	53656	0.64	0.0671	0.0015	1.2285	0.0278	0.1328	0.0019	0.3358	842	46	804	11	814	13	99
076_46		0.00	0	4641	303	843	22920	43263	0.53	0.0648	0.0012	1.1864	0.0226	0.1328	0.0018	0.4149	767	38	804	10	794	11	101
076_47		0.02	2	11441	761	2507	67925	111966	0.61	0.0657	0.0011	1.1716	0.0203	0.1294	0.0017	0.4743	796	33	784	10	787	10	100
076_48		0.00	0	4917	336	1079	27241	45464	0.60	0.0679	0.0013	1.2332	0.0248	0.1316	0.0018	0.3760	867	40	797	10	816	11	98
076_49		0.11	13	12082	793	1704	45249	114669	0.39	0.0655	0.0012	1.1333	0.0209	0.1255	0.0016	0.3942	791	37	762	9	769	10	99
076_50		0.01	5	42870	2816	10418	268593	384984	0.70	0.0650	0.0010	1.2763	0.0209	0.1424	0.0019	0.5223	774	31	858	11	835	9	103
076_51		0.00	0	10945	723	1345	36444	107918	0.34	0.0654	0.0011	1.1422	0.0204	0.1267	0.0017	0.4481	788	35	769	10	774	10	99
076_52		0.00	0	5028	339	933	24777	47032	0.53	0.0672	0.0013	1.2232	0.0238	0.1321	0.0018	0.3967	843	38	800	10	811	11	99
076_53		0.00	0	9043	587	1163	31425	88593	0.35	0.0645	0.0011	1.1322	0.0208	0.1274	0.0017	0.4390	757	36	773	10	769	10	101
076_54		0.07	7	10725	711	2394	60675	100278	0.61	0.0660	0.0011	1.2052	0.0220	0.1325	0.0018	0.4341	806	36	802	10	803	10	100
076_55		0.00	0	17996	1184	3944	100967	160796	0.63	0.0656	0.0011	1.2551	0.0221	0.1389	0.0018	0.4569	792	34	838	10	826	10	102
076_56		0.10	15	15331	1006	3734	97577	145422	0.67	0.0654	0.0011	1.1810	0.0211	0.1309	0.0017	0.4453	788	35	793	10	792	10	100
076_57		0.00	0	16303	1092	4614	126160	152309	0.83	0.0671	0.0014	1.1704	0.0244	0.1266	0.0017	0.3405	841	42	768	10	787	11	98
076_58		0.19	9	4754	312	835	20272	40786	0.50	0.0659	0.0018	1.2410	0.0334	0.1367	0.0020	0.2468	803	56	826	11	819	15	101
076_59		0.03	3	9762	646	1757	43816	86754	0.51	0.0663	0.0012	1.2954	0.0248	0.1418	0.0019	0.4312	815	37	855	11	844	11	101
076_60		0.00	0	22851	1561	5096	130451	222291	0.59	0.0683	0.0012	1.2367	0.0237	0.1314	0.0018	0.4406	876	37	796	10	817	11	97
076_61		0.00	0	3593	244	724	19825	35539	0.56	0.0682	0.0020	1.2114	0.0358	0.1290	0.0021	0.2499	873	61	782	12	806	16	97
076_62		0.05	8	15772	1057	3819	95277	138854	0.69	0.0676	0.0014	1.1922	0.0237	0.1280	0.0016	0.3132	857	41	776	9	797	11	97

DA13-076	E. Ant Domain		Mean cps (background subtracted)							Isotopic Ratios (± 1σ)							Age (Ma ± 1σ)						
Analysis	Core/Rim	$\%Pb_c$	^{204}Pb	^{206}Pb	^{207}Pb	^{208}Pb	^{232}Th	^{238}U	Th/U	$^{207}Pb/^{206}Pb$		$^{207}Pb/^{235}U$		$^{206}Pb/^{238}U$		Rho	$^{207}Pb/^{206}Pb$		$^{206}Pb/^{238}U$		$^{207}Pb/^{235}U$		%Conc
076_63		0.00	0	5189	345	990	29534	67198	0.44	0.0671	0.0018	0.8637	0.0227	0.0933	0.0014	0.2645	842	54	575	8	632	12	91
076_64		0.00	0	3036	188	423	16573	53074	0.31	0.0609	0.0030	0.7071	0.0341	0.0842	0.0019	0.1722	637	103	521	11	543	20	96
076_65		0.00	0	5877	352	27	1210	93106	0.01	0.0598	0.0015	0.6857	0.0171	0.0832	0.0013	0.3299	597	52	515	8	530	10	97
076_66		0.18	13	7268	451	1233	35579	72877	0.49	0.0629	0.0014	0.9934	0.0214	0.1145	0.0015	0.3017	706	45	699	9	701	11	100
076_67		0.06	7	10875	714	1946	48497	97400	0.50	0.0664	0.0013	1.2023	0.0244	0.1313	0.0017	0.3432	819	41	795	10	802	11	99
076_68		0.05	10	22043	1479	4327	109273	197074	0.55	0.0677	0.0013	1.2135	0.0231	0.1300	0.0017	0.3580	859	39	788	10	807	11	98
076_69		0.00	0	5633	368	1058	27846	51889	0.54	0.0665	0.0013	1.1963	0.0244	0.1304	0.0018	0.3595	823	41	790	10	799	11	99
076_70		0.00	0	11688	789	2696	71774	112573	0.64	0.0685	0.0012	1.2066	0.0226	0.1277	0.0017	0.4127	885	37	775	10	804	10	96
076_71		0.00	0	9689	560	99	4402	154741	0.03	0.0581	0.0016	0.6933	0.0196	0.0865	0.0014	0.3122	534	60	535	8	535	12	100
076_72		0.00	0	6954	459	1545	41348	65058	0.64	0.0669	0.0013	1.2383	0.0256	0.1342	0.0019	0.3830	835	41	812	11	818	12	99
076_73		0.00	0	8868	572	1417	35714	73674	0.48	0.0659	0.0029	1.1949	0.0502	0.1315	0.0024	0.1122	804	89	796	14	798	23	100
076_74		0.07	8	11404	742	1811	47308	104642	0.45	0.0665	0.0013	1.2088	0.0246	0.1319	0.0018	0.3560	821	41	799	10	805	11	99
076_75		0.08	6	7441	489	1478	40090	71388	0.56	0.0670	0.0014	1.1852	0.0246	0.1283	0.0018	0.3641	838	42	778	10	794	11	98

BGS-TK64A	C. Ant Domain	(ppm)			Isotope Ratios									Age (Ma)				
Spot Name	f_{206} (%)	U	Th	Th/U	$^{238}U/^{206}Pb$	±1σ	$^{207}Pb/^{206}Pb$	±1σ	$^{207}Pb/^{235}U$	±1σ (%)	$^{206}Pb/^{238}U$	±1σ (%)	Err Corr	$^{206}Pb/^{238}U$	±1σ	$^{207}Pb/^{206}Pb$	±1σ	%Conc
TK64A-1	0.39	82	125	1.58	8.80010	0.09495	0.05829	0.00162	0.91000	3.00000	0.11360	1.10000	0.36300	694	7	541	61	128
TK64A-2	0.36	85	130	1.58	7.18231	0.07390	0.06478	0.00138	1.24000	2.40000	0.13920	1.00000	0.43600	840	8	767	45	110
TK64A-3	-	85	53	0.65	8.52092	0.08972	0.06772	0.00126	1.10000	2.10000	0.11740	1.10000	0.49300	715	7	860	39	83
TK64A-4	0.11	166	150	0.94	8.30334	0.06258	0.06695	0.00157	1.11000	2.50000	0.12040	0.80000	0.30600	733	5	836	49	88
TK64A-5	0.47	37	60	1.68	7.75907	0.15618	0.06440	0.00298	1.14000	5.00000	0.12890	2.00000	0.39900	781	15	755	98	104
TK64A-6	0.25	810	1366	1.74	8.15011	0.02902	0.06450	0.00068	1.09000	1.10000	0.12270	0.40000	0.31900	746	3	758	22	98
TK64A-7	-	270	391	1.49	8.07955	0.05454	0.06510	0.00092	1.11000	1.60000	0.12380	0.70000	0.43200	752	5	778	30	97
TK64A-8	-	177	289	1.69	8.00640	0.06203	0.06585	0.00111	1.13000	1.90000	0.12490	0.80000	0.41700	759	6	802	35	95
TK64A-9	0.00	148	221	1.54	8.45189	0.12357	0.06534	0.00152	1.07000	2.80000	0.11830	1.50000	0.53100	721	10	785	49	92
TK64A-10	0.34	59	66	1.15	8.23167	0.09427	0.06119	0.00180	1.01000	3.20000	0.12150	1.10000	0.36300	739	8	646	63	114
TK64A-11	0.34	69	90	1.34	9.11910	0.09831	0.06033	0.00170	0.91000	3.00000	0.10970	1.10000	0.35700	671	7	616	61	109
TK64A-12	0.06	440	603	1.42	7.70070	0.03268	0.06439	0.00049	1.15000	0.90000	0.12990	0.40000	0.48600	787	3	754	16	104
TK64A-13	0.00	111	92	0.86	7.80212	0.06474	0.06607	0.00097	1.17000	1.70000	0.12820	0.80000	0.49100	777	6	809	31	96
TK64A-14	0.13	147	122	0.86	7.78263	0.05698	0.06411	0.00088	1.14000	1.60000	0.12850	0.70000	0.47100	779	5	745	29	105
TK64A-15	0.23	161	222	1.43	7.85965	0.05548	0.06461	0.00097	1.13000	1.70000	0.12720	0.70000	0.42400	772	5	762	32	101
TK64A-16	0.08	227	158	0.72	8.02155	0.04939	0.06483	0.00077	1.11000	1.30000	0.12470	0.60000	0.46200	757	4	769	25	99
TK64A-17	0.53	99	140	1.46	7.66444	0.07464	0.06253	0.00152	1.12000	2.60000	0.13050	1.00000	0.37100	791	7	692	52	114
TK64A-18	0.40	116	186	1.66	8.08318	0.09922	0.06444	0.00173	1.10000	3.00000	0.12370	1.20000	0.41600	752	9	756	57	99
TK64A-19	0.18	122	130	1.10	7.86435	0.06258	0.06413	0.00096	1.12000	1.70000	0.12720	0.80000	0.46900	772	6	746	32	103
TK64A-20	0.00	103	78	0.78	8.23644	0.08459	0.06430	0.00119	1.08000	2.10000	0.12140	1.00000	0.48500	739	7	751	39	98
TK64A-21	-	111	169	1.57	8.09571	0.07440	0.06666	0.00133	1.14000	2.20000	0.12350	0.90000	0.41900	751	7	827	42	91

Analyses were conducted during a single session. 7 BR266 standard analyses yielded a 2σ error of the mean of 0.29%. Data were collected using a SHIRMP II instrument as part of BGS-USGS-GLW, 2008.

f_{206} = the proportion of common ^{206}Pb in the total ^{206}Pb; Th/U = $^{232}Th/^{238}U$; All ratios and ages are corrected for common Pb using measured ^{204}Pb and composition appropriate to the age of the zircon (Stacey and Kramers, 1975)

BGS-WB005	C. Ant Domain	(ppm)			Isotope Ratios									Age (Ma)				
Spot Name	f_{206} (%)	U	Th	Th/U	$^{238}U/^{206}Pb$	±1σ	$^{207}Pb/^{206}Pb$	±1σ	$^{207}Pb/^{235}U$	±1σ (%)	$^{206}Pb/^{238}U$	±1σ (%)	Err Corr	$^{206}Pb/^{238}U$	±1σ	$^{207}Pb/^{206}Pb$	±1σ	%Conc
WB005-1	0.06	175	142	0.84	7.71015	0.11253	0.06516	0.00102	1.16534	2.14160	0.12970	1.45947	0.68149	786	11	780	33	101
WB005-2	-	201	172	0.89	7.64806	0.10923	0.06632	0.00069	1.19569	1.76869	0.13075	1.42818	0.80748	792	11	817	22	97
WB005-3	4.34	150	93	0.64	9.94858	0.15959	0.03984	0.00693	0.55217	17.45782	0.10052	1.60416	0.09189	617	9	-361	450	-171
WB005-4	0.06	344	279	0.84	7.58236	0.10413	0.06564	0.00067	1.19361	1.70945	0.13189	1.37333	0.80338	799	10	795	21	100
WB005-5	1.71	2404	511	0.22	10.81249	0.14358	0.05823	0.00207	0.74250	3.78879	0.09249	1.32789	0.35048	570	7	538	78	106
WB005-6	-	92	78	0.88	7.49468	0.11968	0.07148	0.00116	1.31499	2.27788	0.13343	1.59685	0.70102	807	12	971	33	83
WB005-7	0.17	1707	1439	0.87	7.84434	0.10169	0.06467	0.00040	1.13678	1.43748	0.12748	1.29633	0.90181	773	9	764	13	101
WB005-8	0.07	459	428	0.96	7.72021	0.10494	0.06558	0.00046	1.17125	1.52869	0.12953	1.35923	0.88915	785	10	793	15	99
WB005-9	0.52	135	102	0.78	7.62791	0.11594	0.06556	0.00277	1.18504	4.48757	0.13110	1.51989	0.33869	794	11	792	89	100
WB005-10	0.01	1669	1043	0.65	7.13544	0.09314	0.06610	0.00041	1.27727	1.44851	0.14015	1.30538	0.90119	845	10	810	13	104
WB005-11	0.84	106	77	0.75	7.49717	0.11674	0.06002	0.00178	1.10388	3.35603	0.13338	1.55715	0.46399	807	12	604	64	134
WB005-12	0.56	148	118	0.82	8.08644	0.11954	0.06016	0.00182	1.02581	3.37425	0.12366	1.47832	0.43812	752	10	609	66	123
WB005-13	0.06	714	754	1.09	7.48375	0.09868	0.06620	0.00043	1.21967	1.46997	0.13362	1.31856	0.89700	808	10	813	14	99
WB005-14	0.06	589	585	1.03	7.57810	0.10073	0.06606	0.00049	1.20196	1.51863	0.13196	1.32918	0.87525	799	10	808	15	99
WB005-15	0.06	287	225	0.81	8.00277	0.11110	0.06472	0.00095	1.11502	2.02324	0.12496	1.38830	0.68617	759	10	765	31	99
WB005-16	-	536	71	0.14	10.38222	0.13896	0.06017	0.00045	0.79907	1.53274	0.09632	1.33848	0.87326	593	8	610	16	97
WB005-17	0.39	309	232	0.77	7.84661	0.10832	0.06296	0.00110	1.10641	2.22176	0.12744	1.38046	0.62134	773	10	707	37	109
WB005-18	0.06	1537	1254	0.84	7.57822	0.09824	0.06500	0.00030	1.18263	1.37767	0.13196	1.29636	0.94098	799	10	774	10	103
WB005-19	-	110	104	0.98	6.97815	0.12898	0.06802	0.00087	1.34400	2.24942	0.14330	1.84831	0.82168	863	15	869	27	99

Analyses were conducted during on session. 9 BR266 standard analyses yielded a 2σ error of the mean of 0.95%. Data were collected using a SHIRMP II instrument as part of BGS-USGS-GLW, 2008.

f_{206} = the proportion of common ^{206}Pb in the total ^{206}Pb; Th/U = $^{232}Th/^{238}U$; All ratios and ages are corrected for common Pb using measured ^{204}Pb and composition appropriate to the age of the zircon (Stacey and Kramers, 1975)

BGS-WB1451	N. Ant Domain	(ppm)			Isotope Ratios									Age (Ma)				
Spot Name	f_{206} (%)	U	Th	Th/U	$^{238}U/^{206}Pb$	±1σ	$^{207}Pb/^{206}Pb$	±1σ	$^{207}Pb/^{235}U$	±1σ (%)	$^{206}Pb/^{238}U$	±1σ (%)	Err Corr	$^{206}Pb/^{238}U$	±1σ	$^{207}Pb/^{206}Pb$	±1σ	%Conc
WB1451-1	2.23	96	132	1.42	7.88799	0.11558	0.06934	0.00445	1.21211	6.58184	0.12677	1.46528	0.22263	769	11	909	132	85
WB1451-2	4.28	178	234	1.36	8.43220	0.12383	0.03362	0.00759	0.54973	22.63461	0.11859	1.46854	0.06488	722	10	-822	644	-88
WB1451-3	0.09	1563	2090	1.38	8.81514	0.10032	0.06111	0.00029	0.95587	1.23203	0.11344	1.13806	0.92373	693	7	643	10	108
WB1451-4	0.07	140	218	1.60	7.93833	0.10485	0.06521	0.00163	1.13259	2.82622	0.12597	1.32077	0.46733	765	10	781	53	98
WB1451-5	0.10	426	917	2.22	7.46652	0.24891	0.06514	0.00067	1.20291	3.49009	0.13393	3.33362	0.95517	810	25	779	22	104
WB1451-6	0.94	78	100	1.32	7.92323	0.11211	0.05878	0.00270	1.02289	4.81423	0.12621	1.41499	0.29392	766	10	559	100	137
WB1451-7	4.03	237	435	1.90	8.75616	0.11862	0.06320	0.00569	0.99512	9.11142	0.11421	1.35468	0.14868	697	9	715	191	98
WB1451-8	0.22	567	1643	2.99	7.89420	0.09375	0.06331	0.00064	1.10571	1.56362	0.12668	1.18759	0.75951	769	9	719	22	107
WB1451-9	0.00	341	754	2.28	7.75983	0.09515	0.06539	0.00052	1.16189	1.45907	0.12887	1.22618	0.84038	781	9	787	17	99
WB1451-10	-	125	200	1.65	8.20255	0.11073	0.06665	0.00083	1.12041	1.83541	0.12191	1.34997	0.73551	742	9	827	26	90
WB1451-11	-	211	314	1.53	7.80374	0.09875	0.06577	0.00067	1.16213	1.62452	0.12814	1.26540	0.77894	777	9	799	21	97
WB1451-12	0.43	263	435	1.70	8.08383	0.10048	0.06344	0.00133	1.08205	2.44384	0.12370	1.24296	0.50861	752	9	723	45	104
WB1451-13	0.66	260	275	1.09	7.72289	0.10759	0.06500	0.00161	1.16049	2.83714	0.12949	1.39317	0.49105	785	10	774	52	101
WB1451-14	2.04	320	470	1.52	7.86535	0.11211	0.06397	0.00424	1.12133	6.78669	0.12714	1.42531	0.21002	772	10	741	140	104
WB1451-15	0.27	350	538	1.59	7.69019	0.10517	0.06427	0.00092	1.15224	1.97588	0.13004	1.36754	0.69212	788	10	750	30	105
WB1451-16	-	283	298	1.09	8.37939	0.11861	0.06458	0.00078	1.06267	1.85756	0.11934	1.41556	0.76205	727	10	761	25	96
WB1451-17	0.13	1322	1239	0.97	7.92641	0.12133	0.06448	0.00033	1.12156	1.61163	0.12616	1.53070	0.94978	766	11	757	11	101
WB1451-18	0.27	536	1323	2.55	7.61838	0.11361	0.06478	0.00072	1.17236	1.86385	0.13126	1.49121	0.80007	795	11	767	24	104
WB1451-19	-	367	878	2.47	7.54230	0.10291	0.06654	0.00065	1.21642	1.67993	0.13259	1.36444	0.81220	803	10	823	20	97
WB1451-20	1.08	771	438	0.59	9.88693	0.13114	0.05875	0.00162	0.81935	3.06466	0.10114	1.32645	0.43282	621	8	558	60	111
WB1451-21	0.26	1206	1695	1.45	7.36195	0.09600	0.06504	0.00060	1.21820	1.59607	0.13583	1.30397	0.81699	821	10	776	19	106

Analyses were conducted during two sessions. Session 1:16 BR266 standard analyses yielded a 2σ error of the mean of 0.60%.
Session 2: 9 BR266 standard analyses yielded a 2σ error of the mean of 0.95%. Data were collected using a SHIRMP II instrument as part of BGS-USGS-GLW, 2008.

f_{206} = the proportion of common ^{206}Pb in the total ^{206}Pb; Th/U = $^{232}Th/^{238}U$; All ratios and ages are corrected for common Pb using measured ^{204}Pb and composition appropriate to the age of the zircon (Stacey and Kramers, 1975)

BGS-PP 156	**N. Ant Domain**	(ppm)			Isotope Ratios									Age (Ma)				
Spot Name	f_{206} (%)	U	Th	Th/U	$^{238}U/^{206}Pb$	±1σ	$^{207}Pb/^{206}Pb$	±1σ	$^{207}Pb/^{235}U$	±1σ (%)	$^{206}Pb/^{238}U$	±1σ (%)	Err Corr	$^{206}Pb/^{238}U$	±1σ	$^{207}Pb/^{206}Pb$	±1σ	%Conc
PP156-1r	1.73	2903	165	0.06	7.83437	0.09735	0.06834	0.00354	1.2027	5.3224	0.1276	1.2426	0.2335	774.4	9.1	878.8	107.1	88
PP156-2c	1.62	368	106	0.30	3.31514	0.04094	0.15691	0.00246	6.5261	1.9942	0.3016	1.2351	0.6193	1699.5	18.5	2422.7	26.6	70
PP156-3r	0.90	2535	128	0.05	7.20697	0.08404	0.06639	0.00122	1.2702	2.1800	0.1388	1.1661	0.5349	837.6	9.2	818.7	38.5	102
PP156-4r	0.69	4335	288	0.07	7.29801	0.08518	0.06630	0.00084	1.2526	1.7240	0.1370	1.1671	0.6770	827.8	9.1	815.8	26.5	101
PP156-5c	3.44	1327	41	0.03	7.59828	0.09151	0.07319	0.00417	1.3282	5.8229	0.1316	1.2044	0.2068	797.0	9.0	1019.3	115.4	78
PP156-6r	0.35	3293	231	0.07	7.16192	0.08302	0.06599	0.00053	1.2704	1.4068	0.1396	1.1592	0.8240	842.6	9.2	806.1	16.7	105
PP156-7c	-	194	67	0.36	2.10340	0.02784	0.16294	0.00068	10.6807	1.3876	0.4754	1.3234	0.9538	2507.3	27.5	2486.4	7.0	101
PP156-8r	20.89	2436	50	0.02	10.91295	0.20947	0.09381	0.02918	1.1852	31.1637	0.0916	1.9194	0.0616	565.2	10.4	1504.2	587.8	38
PP156-9c	1.60	175	86	0.51	4.72712	0.06337	0.13969	0.00308	4.0744	2.5810	0.2115	1.3405	0.5194	1237.0	15.1	2223.3	38.2	56
PP156-10r	0.79	3234	322	0.10	7.75200	0.08971	0.06740	0.00097	1.1989	1.8510	0.1290	1.1573	0.6252	782.2	8.5	850.2	30.0	92
PP156-11c	0.01	560	168	0.31	2.47059	0.03213	0.15432	0.00137	8.6126	1.5728	0.4048	1.3005	0.8268	2190.9	24.2	2394.4	15.1	92
PP156-12r	1.32	3481	412	0.12	7.53525	0.09734	0.06671	0.00166	1.2206	2.8081	0.1327	1.2918	0.4600	803.3	9.8	828.6	52.0	97
PP156-13c	2.71	316	58	0.19	2.39438	0.04651	0.15961	0.00398	9.1911	3.1603	0.4176	1.9424	0.6146	2249.8	36.9	2451.5	42.2	92
PP156-14c	0.03	201	126	0.65	2.11997	0.03601	0.16031	0.00189	10.4261	2.0672	0.4717	1.6986	0.8217	2491.0	35.1	2458.9	19.9	101
PP156-15r	35.85	1572	836	0.55	17.56142	0.59538	0.10284	0.06091	0.8075	59.3247	0.0569	3.3903	0.0571	357.0	11.8	1676.1	1094.4	21
PP156-16r	2.85	1797	113	0.07	8.20569	0.09762	0.06699	0.00359	1.1256	5.4966	0.1219	1.1897	0.2164	741.3	8.3	837.4	111.8	89
PP156-17c	0.41	218	240	1.14	2.52058	0.03155	0.15749	0.00117	8.6150	1.4566	0.3967	1.2518	0.8594	2154.0	22.9	2428.9	12.6	89
PP156-18r	1.80	2713	144	0.05	7.88023	0.09195	0.06677	0.00213	1.1682	3.3919	0.1269	1.1668	0.3440	770.2	8.5	830.6	66.4	93
PP156-19c	1.07	410	127	0.32	6.04183	0.07445	0.11193	0.00172	2.5544	1.9701	0.1655	1.2322	0.6254	987.3	11.3	1831.0	27.9	54

Analyses were conducted during a single session with standard error on 7 BR266 0.98%. C denotes analysis on core and r on rim. Data were collected using a SHIRMP II instrument as part of BGS-USGS-GLW, 2008.

f_{206} = the proportion of common ^{206}Pb in the total ^{206}Pb; Th/U = $^{232}Th/^{238}U$; All ratios and ages are corrected for common Pb using measured ^{204}Pb and composition appropriate to the age of the zircon (Stacey and Kramers, 1975)

BGS-RT07-032	**N. Ant Domain**	(ppm)			Isotope Ratios									Age (Ma)			
Spot Name	f_{206} (%)	U	Th	Th/U	$^{238}U/^{206}Pb$	±1σ	$^{207}Pb/^{206}Pb$	±1σ	$^{207}Pb/^{235}U$	±1σ (%)	$^{206}Pb/^{238}U$	±1σ (%)	Err Corr	$^{206}Pb/^{238}U$	±1σ	$^{207}Pb/^{206}Pb$	±1σ	%Conc
RT-07-32-1a	0.73	69	171	2.54	8.59121	0.16041	0.05949	0.00363	0.95483	6.38455	0.11640	1.86713	0.29245	710	13	585	133	82
RT-07-32-1b (2)	1.68	71	320	4.67	8.02122	0.15865	0.05531	0.00479	0.95071	8.88269	0.12467	1.97789	0.22267	757	14	425	193	56
RT-07-32-2a	0.96	234	92	0.41	11.87910	0.17918	0.05950	0.00253	0.69064	4.50663	0.08418	1.50837	0.33470	521	8	586	92	112
RT-07-32-2b (2)	1.53	34	45	1.37	8.66793	0.20811	0.05641	0.00577	0.89729	10.50216	0.11537	2.40087	0.22861	704	16	468	226	67
RT-07-32-3a	0.89	132	224	1.75	9.67152	0.15684	0.05561	0.00266	0.79278	5.04499	0.10340	1.62162	0.32143	634	10	437	106	69
RT-07-32-3b (2)	0.15	118	427	3.73	8.03890	0.13980	0.06511	0.00121	1.11680	2.54062	0.12440	1.73904	0.68449	756	12	778	39	103
RT-07-32-4a	1.13	110	173	1.62	9.26636	0.15457	0.05719	0.00350	0.85093	6.33779	0.10792	1.66810	0.26320	661	10	499	135	75
RT-07-32-4b (2)	1.19	146	152	1.08	10.33311	0.18304	0.06312	0.00289	0.84221	4.90304	0.09678	1.77136	0.36128	595	10	712	97	120
RT-07-32-5 (2)	1.09	82	130	1.65	8.99898	0.16999	0.06255	0.00317	0.95844	5.40781	0.11112	1.88896	0.34930	679	12	693	108	102
RT-07-32-6 (2)	0.78	137	178	1.34	9.57963	0.16739	0.05928	0.00220	0.85319	4.10570	0.10439	1.74736	0.42559	640	11	577	81	90
RT-07-32-7 (2)	0.69	74	34	0.47	10.96271	0.21465	0.05801	0.00294	0.72965	5.43783	0.09122	1.95804	0.36008	563	11	530	111	94
RT-07-32-8 (2)	1.25	59	106	1.86	7.58720	0.15678	0.05650	0.00489	1.02668	8.89579	0.13180	2.06634	0.23228	798	16	472	191	59
RT-07-32-9 (2)	0.39	61	180	3.04	7.87363	0.15573	0.06344	0.00182	1.11092	3.47986	0.12701	1.97788	0.56838	771	14	723	61	94
RT-07-32-10 (2)	0.25	110	144	1.36	9.52933	0.16917	0.06256	0.00180	0.90521	3.38083	0.10494	1.77521	0.52508	643	11	693	61	108

Analyses were conducted during two sessions with standard errors 1.13% (S1: 5 BR266) and 1.05% (S2: 9 BR266). Data were collected using a SHIRMP II instrument as part of BGS-USGS-GLW, 2008.

f_{206} = the proportion of common ^{206}Pb in the total ^{206}Pb; Th/U = $^{232}Th/^{238}U$; All ratios and ages are corrected for common Pb using measured ^{204}Pb and composition appropriate to the age of the zircon (Stacey and Kramers, 1975); (#) denotes the session number.

BGS-WB37	**Masora Domain**	(ppm)			Isotope Ratios									Age (Ma)				
Spot Name	f_{206} (%)	U	Th	Th/U	$^{238}U/^{206}Pb$	±1σ	$^{207}Pb/^{206}Pb$	±1σ	$^{207}Pb/^{235}U$	±1σ (%)	$^{206}Pb/^{238}U$	±1σ (%)	Err Corr	$^{206}Pb/^{238}U$	±1σ	$^{207}Pb/^{206}Pb$	±1σ	%Conc
WB37-1	-	269	130	0.50	7.73852	0.09137	0.06771	0.00069	1.20636	1.55560	0.12922	1.18066	0.75897	783	9	860	21	91
WB37-2	1.06	354	223	0.65	7.35191	0.07597	0.06904	0.00229	1.29478	3.47364	0.13602	1.03329	0.29747	822	8	900	68	91
WB37-3	0.28	798	680	0.88	8.02015	0.07565	0.06698	0.00075	1.15157	1.46825	0.12469	0.94322	0.64241	757	7	837	23	90
WB37-4	0.00	193	92	0.49	7.37918	0.08280	0.06686	0.00075	1.24919	1.58689	0.13552	1.12205	0.70707	819	9	833	23	98
WB37-5	0.19	221	63	0.29	7.63514	0.08262	0.06672	0.00077	1.20480	1.57741	0.13097	1.08213	0.68602	793	8	829	24	96
WB37-6	0.14	359	227	0.65	7.83033	0.08020	0.06739	0.00078	1.18667	1.54956	0.12771	1.02421	0.66097	775	7	850	24	91
WB37-7	0.00	347	458	1.36	7.31689	0.07426	0.06795	0.00056	1.28045	1.30669	0.13667	1.01494	0.77672	826	8	867	17	95
WB37-8	0.18	265	141	0.55	7.66327	0.08545	0.06598	0.00074	1.18708	1.57996	0.13049	1.11505	0.70575	791	8	806	23	98
WB37-9	0.08	307	287	0.97	7.53530	0.07856	0.06700	0.00069	1.22588	1.46274	0.13271	1.04252	0.71272	803	8	838	21	96
WB37-10	0.30	132	84	0.66	7.93923	0.09751	0.06621	0.00140	1.14985	2.44614	0.12596	1.22821	0.50210	765	9	813	44	94
WB37-11	0.32	111	65	0.61	7.99394	0.09932	0.06211	0.00119	1.07126	2.28868	0.12509	1.24248	0.54288	760	9	678	41	112

Analyses were conducted during a single session. 10 BR266 standard analyses yielded a 2σ error of the mean of 0.63%. Data were collected using a SHIRMP II instrument as part of BGS-USGS-GLW, 2008.

f_{206} = the proportion of common ^{206}Pb in the total ^{206}Pb; Th/U = $^{232}Th/^{238}U$; All ratios and ages are corrected for common Pb using measured ^{204}Pb and composition appropriate to the age of the zircon (Stacey and Kramers, 1975)

BGS-RK395	Masora Domain	(ppm)				Isotope Ratios									Age (Ma)			
Spot Name	f_{206} (%)	U	Th	Th/U	$^{238}U/^{206}Pb$	±1σ	$^{207}Pb/^{206}Pb$	±1σ	$^{207}Pb/^{235}U$	±1σ (%)	$^{206}Pb/^{238}U$	±1σ (%)	Err Corr	$^{206}Pb/^{238}U$	±1σ	$^{207}Pb/^{206}Pb$	±1σ	%Conc
RK395-1C	1.06	258	311	1.25	9.13792	0.10141	0.06680	0.00224	1.00796	3.53260	0.10943	1.10982	0.31417	669	7	832	70	81
RK395-2R	-	788	7	0.01	12.17191	0.11530	0.05840	0.00047	0.66156	1.23798	0.08216	0.94725	0.76515	509	5	545	17	93
RK395-3R	0.20	1711	48	0.03	12.15744	0.11140	0.05845	0.00052	0.66284	1.27284	0.08225	0.91631	0.71989	510	4	547	19	93
RK395-4C	1.44	127	81	0.66	8.05680	0.10948	0.06903	0.00373	1.18137	5.56624	0.12412	1.35886	0.24413	754	10	900	111	84
RK395-5R	1.67	2069	45	0.02	11.85449	0.10849	0.05777	0.00229	0.67194	4.06694	0.08436	0.91514	0.22502	522	5	521	87	100
RK395-6C	0.32	270	337	1.29	7.53697	0.08079	0.06621	0.00100	1.21126	1.85097	0.13268	1.07195	0.57913	803	8	813	32	99
RK395-7R	0.57	1641	123	0.08	11.92463	0.10998	0.05812	0.00095	0.67197	1.87129	0.08386	0.92231	0.49288	519	5	534	36	97
RK395-8C	0.86	261	379	1.50	7.85844	0.08410	0.06480	0.00182	1.13693	3.00594	0.12725	1.07019	0.35603	772	8	768	59	101
RK395-9R	0.03	1626	31	0.02	12.05478	0.10941	0.05851	0.00033	0.66927	1.06684	0.08295	0.90759	0.85073	514	4	549	12	94
RK395-10C	20.17	418	250	0.62	8.89491	0.25801	0.05068	0.03632	0.78564	71.71699	0.11242	2.90062	0.04045	687	19	226	1656	303
RK395-11R	0.06	2229	58	0.03	12.01635	0.10783	0.05829	0.00031	0.66888	1.04042	0.08322	0.89737	0.86251	515	4	541	12	95
RK395-12C	7.09	246	177	0.74	9.49954	0.12410	0.05515	0.01049	0.80044	19.06638	0.10527	1.30639	0.06852	645	8	418	425	154
RK395-13C	7.00	787	2068	2.71	10.95878	0.13318	0.06346	0.00941	0.79848	14.87990	0.09125	1.21524	0.08167	563	7	724	315	78
RK395-14R	0.10	2233	68	0.03	11.98019	0.10767	0.05772	0.00035	0.66428	1.08085	0.08347	0.89876	0.83153	517	4	519	13	100
RK395-15R	0.01	2468	77	0.03	11.96562	0.10717	0.05815	0.00026	0.67006	0.99958	0.08357	0.89565	0.89603	517	4	535	10	97
RK395-16C	0.21	490	418	0.88	8.34673	0.08086	0.06661	0.00073	1.10032	1.46688	0.11981	0.96872	0.66040	729	7	826	23	88
RK395-17R	0.04	2300	70	0.03	11.96987	0.10857	0.05766	0.00028	0.66420	1.02963	0.08354	0.90702	0.88092	517	5	517	11	100
RK395-18R	0.08	735	8	0.01	12.35641	0.15707	0.05726	0.00057	0.63894	1.61865	0.08093	1.27120	0.78535	502	6	502	22	100
RK395-19C (2)	6.92	189	146	0.79	7.62863	0.11453	0.08292	0.01101	1.49878	13.36619	0.13109	1.50133	0.11232	794	11	1267	259	63
RK395-20C (2)	0.40	211	147	0.72	8.49806	0.10176	0.06598	0.00210	1.07053	3.39727	0.11767	1.19740	0.35246	717	8	806	67	89
RK395-21C (2)	0.68	204	145	0.73	8.36582	0.12378	0.06674	0.00185	1.09993	3.13736	0.11953	1.47958	0.47160	728	10	830	58	88
RK395-22C (2)	0.51	109	141	1.34	7.49573	0.09930	0.06425	0.00171	1.18185	2.97822	0.13341	1.32470	0.44480	807	10	750	56	108

Analyses were conducted during two sessions. (#) denotes session: Session1: 10 BR266 standard analyses yielded a 2σ error of the mean of 0.63%.
Session 2: 19 BR266 standard analyses yielded a 2σ error of the mean of 0.49%. Data were collected using a SHIRMP II instrument as part of BGS-USGS-GLW, 2008.

f_{206} = the proportion of common ^{206}Pb in the total ^{206}Pb; Th/U = $^{232}Th/^{238}U$; All ratios and ages are corrected for common Pb using measured ^{204}Pb and composition appropriate to the age of the zircon (Stacey and Kramers, 1975)

BGS-RK06-349	Masora Domain					Isotope Ratios									Age (Ma)			
Spot Name	f_{206} (%)	U	Th	Th/U	$^{238}U/^{206}Pb$	±1σ	$^{207}Pb/^{206}Pb$	±1σ	$^{207}Pb/^{235}U$	±1σ (%)	$^{206}Pb/^{238}U$	±1σ (%)	Err Corr	$^{206}Pb/^{238}U$	±1σ	$^{207}Pb/^{206}Pb$	±1σ	%Conc
RK06-349-1	18.29	286	157	0.57	8.75490	0.17279	0.12592	0.02709	1.9832	21.6064	0.1142	1.9736	0.0913	697	13	2042	380	34
RK06-349-2	15.19	325	372	1.18	7.47361	0.13171	0.10896	0.02263	2.0101	20.8420	0.1338	1.7623	0.0846	810	13	1782	379	45
RK06-349-3	5.65	147	194	1.36	7.84984	0.10792	0.07750	0.00833	1.3613	10.8414	0.1274	1.3748	0.1268	773	10	1134	214	68
RK06-349-4	0.38	287	243	0.87	7.58332	0.08478	0.06699	0.00093	1.2180	1.7771	0.1319	1.1180	0.6291	799	8	837	29	95
RK06-349-5	0.10	193	146	0.78	7.70726	0.09189	0.06510	0.00114	1.1645	2.1161	0.1297	1.1922	0.5634	786	9	777	37	101
RK06-349-6	0.41	180	102	0.59	7.97420	0.09602	0.06462	0.00091	1.1173	1.8555	0.1254	1.2041	0.6489	762	9	762	30	100
RK06-349-9	0.15	146	92	0.65	7.91613	0.10229	0.06705	0.00167	1.1678	2.8042	0.1263	1.2922	0.4608	767	9	839	52	91
RK06-349-15	1.61	339	223	0.68	8.27305	0.09234	0.06727	0.00273	1.1211	4.2076	0.1209	1.1162	0.2653	736	8	846	84	87
RK06-349-16	1.40	95	65	0.70	7.84063	0.10935	0.06574	0.00359	1.1560	5.6427	0.1275	1.3947	0.2472	774	10	798	115	97
RK06-349-17	8.78	266	170	0.66	8.73305	0.12331	0.08999	0.01188	1.4207	13.2722	0.1145	1.4120	0.1064	699	9	1425	252	49

19 BR266 standard analyses yielded a 2σ error of the mean of 0.49%. Data were collected using a SHIRMP II instrument as part of BGS-USGS-GLW, 2008.

f_{206} = the proportion of common ^{206}Pb in the total ^{206}Pb; Th/U = $^{232}Th/^{238}U$; All ratios and ages are corrected for common Pb using measured ^{204}Pb and composition appropriate to the age of the zircon (Stacey and Kramers, 1975)

Appendix 3.3

SHRIMP SI and SHRIMP II oxygen isotope results for the Imorona-Itisindro Suite

Spot Number	Domain	Age (Ma)	Error	$^{18}O/^{16}O$ Data			
				$^{18}O/^{16}O$	1σ	$^{18}O/^{16}O$ (‰)	External error 2σ
DA14-133-04	Ikal	824	23	0.0020326	0.0000005	6.38	0.54
DA14-133-05	Ikal	824	23	0.0020312	0.0000005	5.67	0.55
DA14-133-11	Ikal	824	23	0.0020319	0.0000005	6.00	0.56
DA14-133-13	Ikal	540	6	0.0020314	0.0000004	5.78	0.52
DA14-133-17	Ikal	824	23	0.0020327	0.0000004	6.41	0.54
DA14-133-19	Ikal	824	23	0.0020310	0.0000005	5.56	0.55
DA14-133-23	Ikal	824	23	0.0020309	0.0000005	5.52	0.54
DA14-133-24	Ikal	824	23	0.0020301	0.0000005	5.16	0.55
DA14-133-25	Ikal	824	23	0.0020322	0.0000005	6.17	0.55
DA14-140-01	Ikal	570	8	0.0020312	0.0000005	5.65	0.55
DA14-140-04	Ikal	770	21	0.0020312	0.0000004	5.70	0.54
DA14-140-06	Ikal	770	21	0.0020342	0.0000004	7.13	0.52
DA14-140-09	Ikal	570	8	0.0020365	0.0000004	8.28	0.54
DA14-140-11	Ikal	570	8	0.0020346	0.0000005	7.35	0.54
DA14-140-12	Ikal	770	21	0.0020331	0.0000005	6.60	0.56
DA14-140-14	Ikal	570	8	0.0020326	0.0000005	6.36	0.55
DA14-140-16	Ikal	770	21	0.0020405	0.0000005	10.24	0.55
DA14-140-17	Ikal	770	21	0.0020354	0.0000004	7.75	0.52
DA14-140-19	Ikal	770	21	0.0020403	0.0000005	10.16	0.54
DA14-140-29	Ikal	770	21	0.0020349	0.0000005	7.52	0.54
DA14-140-30	Ikal	770	21	0.0020341	0.0000005	7.12	0.54
DA14-146-01	Ikal	552	11	0.0020327	0.0000004	6.40	0.53
DA14-146-03	Ikal	774	11	0.0020328	0.0000005	6.45	0.55
DA14-146-04	Ikal	774	11	0.0020328	0.0000006	6.47	0.57
DA14-146-07	Ikal	774	11	0.0020313	0.0000004	5.70	0.53
DA14-146-08	Ikal	552	11	0.0020327	0.0000005	6.40	0.55
DA14-146-10	Ikal	774	11	0.0020346	0.0000005	7.33	0.55
DA14-146-14	Ikal	774	11	0.0020341	0.0000004	7.08	0.52
DA14-146-15	Ikal	774	11	0.0020348	0.0000004	7.45	0.54
DA14-146-24	Ikal	774	11	0.0020326	0.0000005	6.37	0.54
DA14-146-25	Ikal	552	11	0.0020360	0.0000005	8.05	0.54
DA14-146-32	Ikal	552	11	0.0020319	0.0000005	6.00	0.55
DA14-146-36	Ikal	552	11	0.0020311	0.0000005	5.62	0.54
DA14-146-38	Ikal	552	11	0.0020322	0.0000004	6.16	0.53
DA14-146-40	Ikal	552	11	0.0020335	0.0000005	6.81	0.54
DA13-055-31	Itremo	780	7	0.0020310	0.0000003	5.39	0.17
DA13-055-32	Itremo	780	7	0.0020307	0.0000003	5.21	0.16
DA13-055-33	Itremo	780	7	0.0020290	0.0000007	4.38	0.33
DA13-055-35	Itremo	780	7	0.0020316	0.0000003	5.67	0.15
DA13-055-36	Itremo	780	7	0.0020313	0.0000003	5.52	0.13
DA13-055-40	Itremo	780	7	0.0020314	0.0000003	5.54	0.16
DA13-055-41	Itremo	780	7	0.0020320	0.0000003	5.85	0.16
DA13-055-44	Itremo	780	7	0.0020315	0.0000003	5.61	0.15
DA13-055-45	Itremo	780	7	0.0020316	0.0000003	5.66	0.16
DA13-063-05	Itremo	798	8	0.0020310	0.0000004	5.36	0.17
DA13-063-07	Itremo	798	8	0.0020309	0.0000003	5.31	0.17
DA13-063-08	Itremo	798	8	0.0020298	0.0000003	4.80	0.15
DA13-063-11	Itremo	798	8	0.0020322	0.0000003	5.95	0.15
DA13-063-13	Itremo	798	8	0.0020308	0.0000003	5.25	0.13
DA13-063-14	Itremo	798	8	0.0020286	0.0000003	4.20	0.16
DA13-063-15	Itremo	798	8	0.0020240	0.0000004	1.91	0.20
DA13-064-10	Itremo	2500	28	0.0020332	0.0000003	6.45	0.16
DA13-064-11	Itremo	819	19	0.0020303	0.0000003	5.03	0.14
DA13-064-20	Itremo	819	19	0.0020284	0.0000003	4.11	0.17
DA13-064-21	Itremo	2462	30	0.0020335	0.0000003	6.60	0.15
DA13-064-22	Itremo	819	19	0.0020292	0.0000006	4.51	0.31
DA13-064-29	Itremo	2489	30	0.0020318	0.0000004	5.75	0.18

Spot Number	Domain	Age (Ma)	Error	$^{18}O/^{16}O$ Data			
				$^{18}O/^{16}O$	1σ	$^{18}O/^{16}O$ (‰)	External error 2σ
DA13-064-30	Itremo	819	19	0.0020297	0.0000003	4.74	0.16
DA13-064-52	Itremo	2445	30	0.0020353	0.0000003	7.48	0.14
DA13-064-53	Itremo	819	19	0.0020296	0.0000004	4.70	0.20
DA13-064-60	Itremo	819	19	0.0020292	0.0000003	4.50	0.15
DA13-065-13	Itremo	791	17	0.0020294	0.0000003	4.61	0.13
DA13-065-16	Itremo	791	17	0.0020301	0.0000003	4.93	0.15
DA13-065-20	Itremo	791	17	0.0020309	0.0000003	5.33	0.15
DA13-065-21	Itremo	791	17	0.0020296	0.0000004	4.69	0.19
DA13-065-23	Itremo	791	17	0.0020304	0.0000003	5.09	0.16
DA13-012-77	C. Ant	849	17	0.0020319	0.0000006	5.79	0.28
DA13-012-81	C. Ant	849	17	0.0020319	0.0000003	5.79	0.17
DA13-012-83	C. Ant	849	17	0.0020343	0.0000003	6.99	0.13
DA13-012-84	C. Ant	849	17	0.0020328	0.0000003	6.23	0.15
DA13-012-88	C. Ant	849	17	0.0020329	0.0000003	6.31	0.16
DA13-012-89	C. Ant	849	17	0.0020334	0.0000003	6.53	0.16
DA13-017-05	C. Ant	823	17	0.0020490	0.0000001	7.24	0.24
DA13-017-06	C. Ant	823	17	0.0020483	0.0000001	6.92	0.25
DA13-017-10	C. Ant	823	17	0.0020434	0.0000001	4.54	0.25
DA13-017-12	C. Ant	823	17	0.0020512	0.0000001	8.33	0.25
DA13-017-18	C. Ant	620	20	0.0020506	0.0000001	8.03	0.25
DA13-017-19	C. Ant	2681	20	0.0020465	0.0000001	6.02	0.25
DA13-017-22	C. Ant	823	17	0.0020486	0.0000002	7.04	0.25
DA13-017-25	C. Ant	823	17	0.0020450	0.0000001	5.30	0.25
DA13-017-26	C. Ant	823	17	0.0020433	0.0000002	4.46	0.25
DA13-017-27	C. Ant	2622	20	0.0020475	0.0000001	6.54	0.25
DA13-017-28	C. Ant	823	17	0.0020462	0.0000001	5.89	0.25
DA13-017-29	C. Ant	541	20	0.0020354	0.0000003	0.61	0.27
DA13-017-32	C. Ant	823	17	0.0020477	0.0000001	6.63	0.24
DA13-017-34	C. Ant	823	17	0.0020471	0.0000002	6.33	0.25
DA13-017-37	C. Ant	2377	20	0.0020454	0.0000002	5.52	0.25
DA13-017-40	C. Ant	2603	20	0.0020415	0.0000002	3.58	0.25
DA13-017-43	C. Ant	2477	20	0.0020482	0.0000001	6.88	0.25
DA13-017-44	C. Ant	823	17	0.0020464	0.0000001	6.00	0.25
DA13-017-49	C. Ant	823	17	0.0020490	0.0000001	7.24	0.25
DA13-017-50	C. Ant	2468	20	0.0020483	0.0000002	6.91	0.25
DA13-017-63	C. Ant	2518	20	0.0020457	0.0000002	5.65	0.25
DA13-017-68	C. Ant	620	20	0.0020427	0.0000002	4.18	0.25
DA13-017-69	C. Ant	620	20	0.0020466	0.0000002	6.11	0.25
DA13-017-70	C. Ant	541	20	0.0020449	0.0000001	5.26	0.25
DA13-017-72	C. Ant	541	20	0.0020465	0.0000002	6.05	0.25
DA13-017-73	C. Ant	2619	20	0.0020484	0.0000002	6.94	0.25
DA13-017-75	C. Ant	823	17	0.0020473	0.0000001	6.44	0.25
DA13-020-02	C. Ant	758	10	0.0020467	0.0000001	6.12	0.28
DA13-020-03	C. Ant	758	10	0.0020402	0.0000001	2.98	0.28
DA13-020-07	C. Ant	758	10	0.0020446	0.0000001	5.12	0.28
DA13-020-10	C. Ant	758	10	0.0020438	0.0000001	4.71	0.24
DA13-020-16	C. Ant	758	10	0.0020435	0.0000002	4.58	0.25
DA13-020-20	C. Ant	758	10	0.0020459	0.0000001	5.73	0.28
DA13-020-26	C. Ant	758	10	0.0020448	0.0000001	5.19	0.24
DA13-020-31	C. Ant	758	10	0.0020450	0.0000001	5.30	0.25
DA13-020-32	C. Ant	758	10	0.0020402	0.0000002	2.96	0.25
DA13-020-35	C. Ant	758	10	0.0020437	0.0000002	4.67	0.25
DA13-020-37	C. Ant	758	10	0.0020459	0.0000002	6.02	0.31
DA13-020-40	C. Ant	758	10	0.0020446	0.0000001	5.36	0.28
DA13-020-43	C. Ant	758	10	0.0020463	0.0000001	6.22	0.30
DA13-020-44	C. Ant	758	10	0.0020415	0.0000002	3.88	0.30
DA13-029-51	C. Ant	828	14	0.0020347	0.0000003	7.20	0.17

Spot Number	Domain	Age (Ma)	Error	$^{18}O/^{16}O$ Data			
				$^{18}O/^{16}O$	1σ	$^{18}O/^{16}O$ (‰)	External error 2σ
DA13-029-52	C. Ant	828	14	0.0020353	0.0000004	7.48	0.17
DA13-029-53	C. Ant	828	14	0.0020331	0.0000004	6.40	0.21
DA13-029-56	C. Ant	828	14	0.0020342	0.0000003	6.93	0.14
DA13-029-58	C. Ant	828	14	0.0020340	0.0000003	6.84	0.15
DA13-029-60	C. Ant	828	14	0.0020344	0.0000004	7.03	0.19
DA13-049-22	C. Ant	827	16	0.0020324	0.0000003	6.04	0.17
DA13-049-24	C. Ant	827	16	0.0020344	0.0000003	7.02	0.15
DA13-049-25	C. Ant	827	16	0.0020344	0.0000004	7.03	0.18
DA13-049-27	C. Ant	827	16	0.0020352	0.0000003	7.45	0.16
DA13-077-01	C. Ant	527	9	0.0020394	0.0000001	1.47	0.29
DA13-077-04	C. Ant	837	15	0.0020471	0.0000002	5.23	0.30
DA13-077-10	C. Ant	837	15	0.0020451	0.0000000	4.23	0.28
DA13-077-36	C. Ant	527	9	0.0020422	0.0000001	2.81	0.29
DA13-077-39	C. Ant	837	15	0.0020453	0.0000001	4.35	0.29
DA13-077-43	C. Ant	837	15	0.0020450	0.0000002	4.20	0.30
DA13-077-44	C. Ant	837	15	0.0020448	0.0000002	4.10	0.30
DA13-077-45	C. Ant	837	15	0.0020439	0.0000001	3.67	0.29
DA13-077-47	C. Ant	837	15	0.0020430	0.0000002	3.23	0.30
DA13-077-60	C. Ant	837	15	0.0020459	0.0000001	4.64	0.29
DA13-083-48	C. Ant	795	12	0.0020491	0.0000001	6.19	0.29
DA13-083-49	C. Ant	795	12	0.0020496	0.0000001	6.43	0.29
DA13-083-51	C. Ant	795	12	0.0020491	0.0000003	6.22	0.31
DA13-083-52	C. Ant	795	12	0.0020486	0.0000001	5.94	0.29
DA13-083-53	C. Ant	795	12	0.0020474	0.0000002	5.36	0.30
DA13-083-54	C. Ant	677	11	0.0020480	0.0000003	5.63	0.32
DA13-083-55	C. Ant	795	12	0.0020484	0.0000001	5.86	0.29
DA13-083-56	C. Ant	795	12	0.0020493	0.0000002	6.28	0.30
DA13-083-57	C. Ant	795	12	0.0020489	0.0000003	6.12	0.31
DA13-083-59	C. Ant	795	12	0.0020490	0.0000001	6.15	0.29
DA13-083-62	C. Ant	677	11	0.0020474	0.0000004	5.38	0.35
DA13-083-63	C. Ant	547	12	0.0020479	0.0000002	5.62	0.30
DA13-083-66	C. Ant	795	12	0.0020502	0.0000001	6.75	0.29
DA13-083-68	C. Ant	795	12	0.0020497	0.0000001	6.50	0.29
DA13-083-69	C. Ant	677	11	0.0020493	0.0000002	6.29	0.31
DA13-083-70	C. Ant	677	11	0.0020488	0.0000001	6.05	0.29
DA13-083-72	C. Ant	795	12	0.0020475	0.0000003	5.42	0.32
DA13-083-73	C. Ant	795	12	0.0020494	0.0000004	6.34	0.34
DA13-083-74	C. Ant	677	11	0.0020495	0.0000001	6.38	0.29
BGS-TK64A-06	C. Ant	764	16	0.0020282	0.0000004	3.98	0.17
BGS-TK64A-07	C. Ant	764	16	0.0020311	0.0000003	5.40	0.16
BGS-TK64A-12	C. Ant	764	16	0.0020314	0.0000004	5.55	0.17
BGS-TK64A-13	C. Ant	764	16	0.0020303	0.0000003	5.05	0.16
BGS-TK64A-14	C. Ant	764	16	0.0020324	0.0000003	6.04	0.15
BGS-TK64A-16	C. Ant	764	16	0.0020318	0.0000003	5.75	0.17
BGS-TK64A-18	C. Ant	764	16	0.0020302	0.0000003	4.99	0.15
BGS-WB005-01	C. Ant	793	11	0.0020264	0.0000003	3.66	0.14
BGS-WB005-04	C. Ant	793	11	0.0020272	0.0000003	4.04	0.17
BGS-WB005-08	C. Ant	793	11	0.0020264	0.0000006	3.65	0.28
BGS-WB005-09	C. Ant	793	11	0.0020274	0.0000004	4.11	0.22
BGS-WB005-13	C. Ant	793	11	0.0020246	0.0000005	2.75	0.23
BGS-WB005-14	C. Ant	793	11	0.0020264	0.0000004	3.64	0.21
BGS-WB1451-04	N. Ant	774	16	0.0020280	0.0000003	3.90	0.14
BGS-WB1451-09	N. Ant	774	16	0.0020306	0.0000003	5.20	0.14
BGS-WB1451-11	N. Ant	774	16	0.0020294	0.0000003	4.58	0.14
BGS-WB1451-13	N. Ant	774	16	0.0020281	0.0000003	3.95	0.17
BGS-WB1451-17	N. Ant	774	16	0.0020235	0.0000003	1.69	0.13
BGS-WB1451-18	N. Ant	774	16	0.0020279	0.0000003	3.87	0.15

Spot Number	Domain	Age (Ma)	Error	$^{18}O/^{16}O$ Data			
				$^{18}O/^{16}O$	1σ	$^{18}O/^{16}O$ (‰)	External error 2σ
BGS-PP156-03r	N. Ant	819	23	0.0020291	0.0000004	8.00	0.35
BGS-PP156-04r	N. Ant	819	23	0.0020309	0.0000003	8.92	0.34
BGS-PP156-06r	N. Ant	819	23	0.0020254	0.0000003	6.18	0.33
BGS-PP156-12	N. Ant	819	23	0.0020320	0.0000004	9.43	0.36
BGS-PP156-14c	N. Ant	2459	20	0.0020216	0.0000003	4.32	0.35
BGS-PP156-18r	N. Ant	819	23	0.0020285	0.0000003	7.71	0.34
BGS-RT07-32-09	N. Ant	768	8	0.0020258	0.0000005	6.39	0.38
DA13-074-41	E. Ant	821	11	0.0020565	0.0000002	9.79	0.31
DA13-074-43	E. Ant	821	11	0.0020558	0.0000001	9.46	0.29
DA13-074-45	E. Ant	821	11	0.0020562	0.0000002	9.67	0.29
DA13-074-47	E. Ant	821	11	0.0020563	0.0000004	9.71	0.35
DA13-074-48	E. Ant	821	11	0.0020560	0.0000001	9.54	0.29
DA13-074-49	E. Ant	821	11	0.0020561	0.0000001	9.60	0.29
DA13-074-52	E. Ant	821	11	0.0020562	0.0000000	9.67	0.28
DA13-074-53	E. Ant	821	11	0.0020574	0.0000002	10.22	0.31
DA13-074-54	E. Ant	657	11	0.0020587	0.0000001	10.88	0.29
DA13-074-55	E. Ant	821	11	0.0020566	0.0000000	9.84	0.28
DA13-074-56	E. Ant	821	11	0.0020562	0.0000005	9.65	0.36
DA13-074-58	E. Ant	821	11	0.0020563	0.0000000	9.72	0.28
DA13-074-62	E. Ant	821	11	0.0020562	0.0000002	9.65	0.31
DA13-074-63	E. Ant	821	11	0.0020570	0.0000003	10.06	0.31
DA13-074-65	E. Ant	821	11	0.0020574	0.0000002	10.24	0.29
DA13-074-69	E. Ant	821	11	0.0020557	0.0000001	9.41	0.29
DA13-076-46	E. Ant	813	10	0.0020562	0.0000003	9.64	0.31
DA13-076-47	E. Ant	813	10	0.0020552	0.0000004	9.18	0.35
DA13-076-48	E. Ant	813	10	0.0020552	0.0000001	9.17	0.29
DA13-076-49	E. Ant	813	10	0.0020552	0.0000005	9.18	0.36
DA13-076-50	E. Ant	813	10	0.0020559	0.0000006	9.49	0.40
DA13-076-51	E. Ant	813	10	0.0020556	0.0000001	9.35	0.29
DA13-076-52	E. Ant	813	10	0.0020560	0.0000002	9.56	0.30
DA13-076-53	E. Ant	813	10	0.0020536	0.0000002	8.40	0.29
DA13-076-55	E. Ant	813	10	0.0020542	0.0000001	8.67	0.29
DA13-076-56	E. Ant	813	10	0.0020544	0.0000002	8.76	0.30
DA13-076-58	E. Ant	813	10	0.0020558	0.0000002	9.45	0.30
DA13-076-59	E. Ant	813	10	0.0020547	0.0000001	8.94	0.28
DA13-076-60	E. Ant	813	10	0.0020540	0.0000001	8.57	0.29
DA13-076-61	E. Ant	813	10	0.0020557	0.0000003	9.43	0.31
DA13-076-62	E. Ant	813	10	0.0020557	0.0000001	9.42	0.29
DA13-076-64	E. Ant	540	10	0.0020564	0.0000003	9.73	0.32
DA13-076-65	E. Ant	540	10	0.0020553	0.0000002	9.21	0.30
DA13-076-66	E. Ant	650	15	0.0020549	0.0000002	9.03	0.30
DA13-076-67	E. Ant	813	10	0.0020564	0.0000002	9.75	0.30
DA13-076-68	E. Ant	813	10	0.0020547	0.0000002	8.91	0.31
DA13-076-69	E. Ant	813	10	0.0020545	0.0000003	8.81	0.31
DA13-076-70	E. Ant	813	10	0.0020545	0.0000001	8.83	0.29
DA13-076-71	E. Ant	540	10	0.0020554	0.0000003	9.29	0.32
DA13-076-72	E. Ant	813	10	0.0020541	0.0000005	8.64	0.38
DA13-076-73	E. Ant	813	10	0.0020553	0.0000002	9.20	0.30
DA13-076-74	E. Ant	813	10	0.0020560	0.0000003	9.55	0.31
DA13-076-75	E. Ant	813	10	0.0020555	0.0000002	9.33	0.29
BGS-WB37-04	Masora	842	15	0.0020286	0.0000003	4.20	0.14
BGS-WB37-05	Masora	842	15	0.0020240	0.0000003	1.95	0.16
BGS-WB37-06	Masora	842	15	0.0020315	0.0000004	5.61	0.21
BGS-WB37-07	Masora	842	15	0.0020319	0.0000004	5.80	0.20
BGS-WB37-08	Masora	842	15	0.0020316	0.0000003	5.68	0.14
BGS-WB37-09	Masora	842	15	0.0020337	0.0000006	6.69	0.32
BGS-RK395-05	Masora	814	30	0.0020324	0.0000003	6.07	0.16

				$^{18}O/^{16}O$ Data			
Spot Number	Domain	Age (Ma)	Error	$^{18}O/^{16}O$	1σ	$^{18}O/^{16}O$ (‰)	External error 2σ
BGS-RK395-06	Masora	814	30	0.0020344	0.0000009	7.06	0.44
BGS-RK395-08	Masora	814	30	0.0020318	0.0000003	5.76	0.15
BGS-RK395-16	Masora	814	30	0.0020329	0.0000003	6.29	0.15
BGS-RK395-17	Masora	814	30	0.0020345	0.0000004	7.10	0.18
BGS-RK395-20	Masora	814	30	0.0020287	0.0000003	4.23	0.16
BGS-RK395-21	Masora	814	30	0.0020328	0.0000003	6.24	0.14
BGS-RK06-349-04	Masora	796	33	0.0020298	0.0000003	4.79	0.13
BGS-RK06-349-05	Masora	796	33	0.0020310	0.0000003	5.37	0.16
BGS-RK06-349-06	Masora	796	33	0.0020304	0.0000004	5.08	0.17
BGS-RK06-349-09	Masora	796	33	0.0020310	0.0000004	5.37	0.17

Appendix 3.4

LA-MC-ICP-MS hafnium isotope results for the Imorona-Itsindro Suite

Sample	Domain	Age (Ma)	± 2σ	$^{176}Hf/^{177}Hf$	2 S.E.	$^{176}Lu/^{177}Hf$	$^{176}Yb/^{177}Hf$	$^{176}Hf/^{177}Hf$ (intitial)	$\varepsilon_{Hf}(t)$	± 2σ	$T_{DM}c$ (Ga)
DA14-133-10	Ikal	824	23	0.282467	0.000092	0.002000	0.074920	0.282436	6.1	6.4	1.3
DA14-133-11	Ikal	824	23	0.282200	0.000077	0.001808	0.065661	0.282172	-3.3	5.4	1.9
DA14-133-19	Ikal	824	23	0.282508	0.000071	0.002332	0.080539	0.282472	7.4	5.0	1.2
DA14-133-23	Ikal	824	23	0.282701	0.000102	0.002747	0.106268	0.282659	14.0	7.1	0.8
DA14-133-24	Ikal	824	23	0.282244	0.000158	0.004258	0.166682	0.282178	-3.1	11.0	1.9
DA14-133-25	Ikal	824	23	0.282433	0.000064	0.000867	0.031176	0.282419	5.5	4.5	1.4
DA14-140-04	Ikal	770	21	0.282470	0.000153	0.001763	0.075117	0.282444	5.1	10.7	1.3
DA14-140-12	Ikal	770	21	0.282374	0.000074	0.001334	0.047345	0.282355	2.0	5.2	1.5
DA14-140-15	Ikal	770	21	0.282483	0.000140	0.001818	0.068278	0.282456	5.6	9.8	1.3
DA14-140-17	Ikal	770	21	0.282434	0.000145	0.002218	0.091777	0.282401	3.6	10.1	1.4
DA14-140-30	Ikal	770	21	0.282458	0.000056	0.001746	0.058937	0.282433	4.7	3.9	1.4
DA14-146-10	Ikal	774	11	0.282235	0.000127	0.002282	0.099661	0.282202	-3.4	8.9	1.9
DA14-146-16	Ikal	774	11	0.282294	0.000102	0.002829	0.112745	0.282253	-1.5	7.1	1.7
DA14-146-24	Ikal	774	11	0.282211	0.000119	0.002228	0.096106	0.282179	-4.2	8.4	1.9
DA14-146-38	Ikal	552	11	0.282289	0.000053	0.001136	0.040579	0.282272	-0.9	3.7	1.7
DA14-146-39	Ikal	552	11	0.282277	0.000135	0.003522	0.141815	0.282226	-2.5	9.4	1.8
DA14-146-40	Ikal	552	11	0.282252	0.000105	0.003705	0.162535	0.282198	-3.5	7.3	1.9
DA13-055-31	Itremo	780	7	0.281979	0.000023	0.000916	0.031125	0.281966	-11.6	1.6	2.4
DA13-055-32	Itremo	780	7	0.281974	0.000022	0.000782	0.025142	0.281963	-11.7	1.5	2.4
DA13-055-33	Itremo	780	7	0.281991	0.000026	0.001273	0.043007	0.281972	-11.4	1.8	2.4
DA13-055-35	Itremo	780	7	0.282004	0.000029	0.001099	0.036097	0.281988	-10.8	2.0	2.3
DA13-055-37	Itremo	780	7	0.281999	0.000039	0.001330	0.043484	0.281979	-11.1	2.7	2.3
DA13-055-40	Itremo	780	7	0.281971	0.000022	0.000683	0.023562	0.281961	-11.7	1.5	2.4
DA13-055-41	Itremo	780	7	0.281966	0.000036	0.001239	0.042754	0.281948	-12.2	2.5	2.4
DA13-055-44	Itremo	780	7	0.281971	0.000034	0.000876	0.029663	0.281958	-11.9	2.4	2.4
DA13-055-45	Itremo	780	7	0.281982	0.000035	0.001225	0.040601	0.281964	-11.6	2.5	2.4
DA13-063-05	Itremo	798	8	0.281639	0.000021	0.000492	0.013046	0.281631	-23.0	1.5	3.1
DA13-063-07	Itremo	798	8	0.281640	0.000024	0.000717	0.020155	0.281629	-23.1	1.7	3.1
DA13-063-08	Itremo	798	8	0.281650	0.000028	0.000781	0.022110	0.281638	-22.8	1.9	3.1
DA13-063-11	Itremo	798	8	0.281533	0.000035	0.001059	0.034392	0.281517	-27.1	2.4	3.3
DA13-063-13	Itremo	798	8	0.281683	0.000028	0.000555	0.014548	0.281674	-21.5	2.0	3.0
DA13-063-14	Itremo	798	8	0.281714	0.000034	0.001464	0.040448	0.281692	-20.9	2.4	3.0
DA13-063-15	Itremo	798	8	0.281684	0.000025	0.000985	0.026006	0.281670	-21.7	1.8	3.0
DA13-064-10	Itremo	2503	28	0.281320	0.000037	0.000566	0.017841	0.281293	4.0	2.6	2.8
DA13-064-11	Itremo	819	19	0.281503	0.000040	0.000567	0.016256	0.281494	-27.4	2.8	3.4
DA13-064-20	Itremo	819	19	0.281227	0.000053	0.000720	0.023542	0.281216	-37.3	3.7	4.0
DA13-064-21	Itremo	2462	30	0.281594	0.000041	0.000554	0.014949	0.281568	12.9	2.9	2.2
DA13-064-22	Itremo	819	19	0.281727	0.000032	0.000652	0.017402	0.281717	-19.5	2.2	2.9
DA13-064-29	Itremo	2489	30	0.281310	0.000050	0.000769	0.026427	0.281273	3.0	3.5	2.8
DA13-064-30	Itremo	819	19	0.281734	0.000035	0.000405	0.010606	0.281728	-19.1	2.4	2.9
DA13-064-52	Itremo	2445	25	0.281344	0.000050	0.001017	0.040568	0.281296	2.8	3.5	2.8
DA13-064-53	Itremo	819	19	0.281700	0.000036	0.001216	0.035446	0.281681	-20.8	2.6	3.0
DA13-064-60	Itremo	819	19	0.281671	0.000032	0.001046	0.029883	0.281655	-21.7	2.2	3.0
DA13-065-13	Itremo	791	17	0.281676	0.000037	0.000674	0.019082	0.281666	-22.0	2.6	3.0
DA13-065-16	Itremo	791	17	0.281713	0.000048	0.001028	0.028193	0.281698	-20.8	3.4	2.9
DA13-065-20	Itremo	791	17	0.281868	0.000038	0.000680	0.021122	0.281857	-15.2	2.6	2.6
DA13-065-21	Itremo	791	17	0.281703	0.000048	0.001273	0.034705	0.281684	-21.3	3.4	3.0
DA13-065-23	Itremo	791	17	0.281605	0.000056	0.001381	0.041037	0.281584	-24.8	3.9	3.2
DA13-012-77	C. Ant	849	17	0.281559	0.000038	0.000788	0.024091	0.281546	-24.9	2.7	3.2
DA13-012-81	C. Ant	849	17	0.281628	0.000028	0.000957	0.021560	0.281613	-22.5	1.9	3.1
DA13-012-83	C. Ant	849	17	0.281893	0.000028	0.000869	0.028260	0.281880	-13.1	2.0	2.5
DA13-012-84	C. Ant	849	17	0.281715	0.000064	0.004887	0.191042	0.281637	-21.7	4.5	3.0
DA13-012-88	C. Ant	849	17	0.281842	0.000033	0.001181	0.037367	0.281823	-15.1	2.3	2.6
DA13-012-89	C. Ant	849	17	0.282021	0.000034	0.001755	0.052588	0.281993	-9.1	2.3	2.3
DA13-017-05	C. Ant	823	17	0.281691	0.000037	0.001091	0.035094	0.281674	-21.0	2.6	3.0
DA13-017-06	C. Ant	823	17	0.281685	0.000033	0.000954	0.030340	0.281671	-21.1	2.3	3.0
DA13-017-08	C. Ant	823	17	0.281717	0.000036	0.000939	0.023321	0.281702	-20.0	2.5	2.9
DA13-017-10	C. Ant	823	17	0.281724	0.000053	0.001478	0.041404	0.281701	-20.0	3.7	2.9

Sample	Domain	Age (Ma)	± 2σ	$^{176}Hf/^{177}Hf$	2 S.E.	$^{176}Lu/^{177}Hf$	$^{176}Yb/^{177}Hf$	$^{176}Hf/^{177}Hf$ (intitial)	$\varepsilon_{Hf}(t)$	± 2σ	$T_{DM}c$ (Ga)
DA13-017-12	C. Ant	823	17	0.281786	0.000080	0.001996	0.072310	0.281755	-18.1	5.6	2.8
DA13-017-18	C. Ant	541	20	0.281695	0.000050	0.001159	0.032065	0.281683	-27.0	3.5	3.1
DA13-017-19	C. Ant	2681	25	0.281350	0.000030	0.001124	0.043573	0.281292	8.2	2.1	2.7
DA13-017-22	C. Ant	823	17	0.281729	0.000052	0.000801	0.025340	0.281716	-19.5	3.6	2.9
DA13-017-25	C. Ant	823	17	0.281664	0.000042	0.001043	0.031030	0.281648	-21.9	2.9	3.0
DA13-017-26	C. Ant	823	17	0.281698	0.000055	0.001010	0.031120	0.281682	-20.7	3.9	3.0
DA13-017-27	C. Ant	2622	25	0.281334	0.000025	0.000586	0.021185	0.281304	7.2	1.7	2.7
DA13-017-28	C. Ant	823	17	0.281773	0.000071	0.001020	0.028535	0.281757	-18.0	5.0	2.8
DA13-017-29	C. Ant	541	20	0.281761	0.000065	0.000429	0.009745	0.281757	-24.4	4.6	3.0
DA13-017-32	C. Ant	823	17	0.281670	0.000020	0.000616	0.018421	0.281660	-21.4	1.4	3.0
DA13-017-34	C. Ant	823	17	0.281669	0.000058	0.001477	0.033456	0.281646	-21.9	4.1	3.0
DA13-017-37	C. Ant	2377	33	0.281376	0.000052	0.000628	0.020309	0.281347	3.0	3.6	2.7
DA13-017-38	C. Ant	823	17	0.281697	0.000030	0.001034	0.027983	0.281681	-20.7	2.1	3.0
DA13-017-39	C. Ant	541	20	0.281675	0.000098	0.000587	0.015148	0.281670	-27.4	6.8	3.2
DA13-017-40	C. Ant	2603	17	0.281272	0.000032	0.001148	0.046373	0.281215	3.6	2.2	2.9
DA13-017-43	C. Ant	2477	17	0.281399	0.000026	0.000161	0.005963	0.281392	6.9	1.8	2.6
DA13-017-44	C. Ant	823	17	0.281694	0.000020	0.000438	0.012804	0.281687	-20.5	1.4	2.9
DA13-017-49	C. Ant	823	17	0.281704	0.000032	0.001307	0.041080	0.281684	-20.6	2.3	3.0
DA13-017-50	C. Ant	2468	26	0.281297	0.000027	0.000597	0.019861	0.281269	2.4	1.9	2.8
DA13-017-63	C. Ant	2518	29	0.281648	0.000063	0.001096	0.032376	0.281596	15.2	4.4	2.1
DA13-017-69	C. Ant	541	20	0.281723	0.000027	0.001068	0.035823	0.281712	-25.9	1.9	3.1
DA13-017-70	C. Ant	541	20	0.281730	0.000034	0.000640	0.021430	0.281724	-25.5	2.4	3.0
DA13-017-72	C. Ant	541	20	0.281676	0.000113	0.000822	0.019969	0.281668	-27.5	7.9	3.2
DA13-017-75	C. Ant	823	17	0.281658	0.000040	0.000837	0.026274	0.281645	-22.0	2.8	3.0
DA13-020-02	C. Ant	758	10	0.281791	0.000051	0.001891	0.077306	0.281764	-19.2	3.6	2.8
DA13-020-03	C. Ant	758	10	0.281879	0.000088	0.000750	0.024349	0.281868	-15.5	6.1	2.6
DA13-020-07	C. Ant	758	10	0.281834	0.000049	0.001137	0.041977	0.281818	-17.3	3.4	2.7
DA13-020-10	C. Ant	758	10	0.281819	0.000050	0.001005	0.035175	0.281805	-17.8	3.5	2.7
DA13-020-16	C. Ant	758	10	0.281832	0.000042	0.000950	0.035540	0.281819	-17.3	2.9	2.7
DA13-020-20	C. Ant	758	10	0.281963	0.000041	0.000815	0.032191	0.281952	-12.6	2.9	2.4
DA13-020-26	C. Ant	758	10	0.281830	0.000042	0.001104	0.044483	0.281815	-17.4	3.0	2.7
DA13-020-31	C. Ant	758	10	0.281839	0.000046	0.000906	0.034359	0.281826	-17.0	3.2	2.7
DA13-020-32	C. Ant	758	10	0.281912	0.000039	0.000961	0.027489	0.281898	-14.5	2.8	2.5
DA13-020-35	C. Ant	758	10	0.281950	0.000039	0.001702	0.069321	0.281926	-13.5	2.7	2.5
DA13-020-37	C. Ant	758	10	0.281830	0.000054	0.000983	0.036312	0.281816	-17.4	3.8	2.7
DA13-020-40	C. Ant	758	10	0.281796	0.000049	0.001030	0.040549	0.281781	-18.6	3.4	2.8
DA13-020-43	C. Ant	758	10	0.281851	0.000046	0.000991	0.035912	0.281837	-16.6	3.2	2.7
DA13-020-44	C. Ant	758	10	0.281835	0.000022	0.000825	0.032015	0.281824	-17.1	1.6	2.7
DA13-029-51	C. Ant	828	14	0.282099	0.000058	0.001610	0.058015	0.282074	-6.7	4.1	2.1
DA13-029-52	C. Ant	828	14	0.282089	0.000025	0.001077	0.037200	0.282072	-6.7	1.7	2.1
DA13-029-53	C. Ant	828	14	0.282033	0.000031	0.000953	0.035144	0.282019	-8.6	2.2	2.2
DA13-029-56	C. Ant	828	14	0.282063	0.000019	0.000756	0.027080	0.282051	-7.5	1.3	2.2
DA13-029-58	C. Ant	828	14	0.282080	0.000027	0.001195	0.043140	0.282061	-7.1	1.9	2.1
DA13-029-60	C. Ant	828	14	0.282114	0.000031	0.001248	0.039405	0.282094	-5.9	2.2	2.1
DA13-049-22	C. Ant	827	16	0.281805	0.000041	0.001435	0.040498	0.281783	-17.0	2.8	2.7
DA13-049-24	C. Ant	827	16	0.281824	0.000033	0.001624	0.043705	0.281799	-16.4	2.3	2.7
DA13-049-25	C. Ant	827	16	0.281845	0.000027	0.001265	0.033747	0.281825	-15.5	1.9	2.6
DA13-049-27	C. Ant	827	16	0.281867	0.000021	0.001196	0.037064	0.281848	-14.7	1.5	2.6
DA13-077-10	C. Ant	837	16	0.282072	0.000056	0.000513	0.022490	0.282064	-6.8	3.9	2.1
DA13-077-36	C. Ant	527	9	0.282071	0.000037	0.000543	0.022853	0.282065	-13.7	2.6	2.3
DA13-077-39	C. Ant	837	16	0.282012	0.000021	0.000534	0.021550	0.282004	-8.9	1.5	2.3
DA13-077-43	C. Ant	837	16	0.282063	0.000026	0.000684	0.028757	0.282052	-7.2	1.8	2.1
DA13-077-44	C. Ant	837	16	0.282105	0.000121	0.000732	0.030761	0.282094	-5.8	8.5	2.1
DA13-077-47	C. Ant	837	16	0.282125	0.000051	0.000839	0.034908	0.282111	-5.1	3.6	2.0
DA13-077-60	C. Ant	837	16	0.282106	0.000067	0.000727	0.031240	0.282095	-5.7	4.7	2.1
DA13-083-48	C. Ant	795	12	0.281704	0.000043	0.001320	0.050712	0.281684	-21.2	3.0	3.0
DA13-083-49	C. Ant	795	12	0.281713	0.000045	0.001636	0.067997	0.281689	-21.0	3.2	3.0
DA13-083-51	C. Ant	795	12	0.281711	0.000033	0.001431	0.053883	0.281690	-21.0	2.3	3.0

Sample	Domain	Age (Ma)	± 2σ	$^{176}Hf/^{177}Hf$	2 S.E.	$^{176}Lu/^{177}Hf$	$^{176}Yb/^{177}Hf$	$^{176}Hf/^{177}Hf$ (intitial)	$\varepsilon_{Hf}(t)$	± 2σ	$T_{DM}c$ (Ga)
DA13-083-52	C. Ant	795	12	0.281727	0.000044	0.001770	0.062689	0.281700	-20.6	3.1	2.9
DA13-083-53	C. Ant	795	12	0.281731	0.000026	0.000881	0.030138	0.281717	-20.0	1.8	2.9
DA13-083-54	C. Ant	795	11	0.281679	0.000051	0.001378	0.053440	0.281659	-22.1	3.5	3.0
DA13-083-55	C. Ant	795	12	0.281696	0.000043	0.001329	0.051192	0.281676	-21.5	3.0	3.0
DA13-083-56	C. Ant	795	12	0.281723	0.000028	0.001229	0.042956	0.281704	-20.5	2.0	2.9
DA13-083-57	C. Ant	795	12	0.281746	0.000039	0.001948	0.078191	0.281717	-20.1	2.7	2.9
DA13-083-59	C. Ant	795	12	0.281754	0.000057	0.001460	0.051994	0.281732	-19.5	4.0	2.9
DA13-083-62	C. Ant	795	11	0.281769	0.000031	0.001486	0.058685	0.281746	-19.0	2.1	2.8
DA13-083-63	C. Ant	547	12	0.281783	0.000033	0.000779	0.021827	0.281775	-23.6	2.3	2.9
DA13-083-66	C. Ant	795	12	0.281668	0.000034	0.001293	0.051401	0.281649	-22.5	2.4	3.0
DA13-083-67	C. Ant	795	11	0.281786	0.000034	0.001558	0.058241	0.281763	-18.4	2.4	2.8
DA13-083-68	C. Ant	795	12	0.281742	0.000024	0.001067	0.040659	0.281726	-19.7	1.7	2.9
DA13-083-69	C. Ant	795	11	0.281740	0.000027	0.001074	0.040828	0.281724	-19.8	1.9	2.9
DA13-083-70	C. Ant	795	11	0.281740	0.000032	0.001503	0.061032	0.281718	-20.0	2.2	2.9
DA13-083-72	C. Ant	795	12	0.281754	0.000040	0.001648	0.063583	0.281729	-19.6	2.8	2.9
DA13-083-73	C. Ant	795	12	0.281743	0.000049	0.002215	0.087989	0.281710	-20.3	3.4	2.9
BGS-TK64A-06	C. Ant	764	16	0.281849	0.000026	0.001831	0.063802	0.281823	-17.0	1.8	2.7
BGS-TK64A-07	C. Ant	764	16	0.281860	0.000024	0.000954	0.033652	0.281847	-16.2	1.7	2.6
BGS-TK64A-12	C. Ant	764	16	0.281842	0.000030	0.001620	0.056417	0.281818	-17.2	2.1	2.7
BGS-TK64A-13	C. Ant	764	16	0.281804	0.000022	0.000559	0.019316	0.281796	-17.9	1.5	2.8
BGS-TK64A-14	C. Ant	764	16	0.281865	0.000033	0.001224	0.040828	0.281847	-16.1	2.3	2.6
BGS-TK64A-16	C. Ant	764	16	0.281850	0.000022	0.000587	0.020478	0.281842	-16.3	1.6	2.7
BGS-TK64A-18	C. Ant	764	16	0.281826	0.000023	0.001038	0.035666	0.281811	-17.4	1.6	2.7
BGS-WB005-01	C. Ant	793	11	0.281966	0.000035	0.001081	0.038346	0.281950	-11.9	2.5	2.4
BGS-WB005-04	C. Ant	793	11	0.281962	0.000049	0.001532	0.055563	0.281939	-12.2	3.4	2.4
BGS-WB005-08	C. Ant	793	11	0.282039	0.000047	0.001761	0.062401	0.282012	-9.6	3.3	2.3
BGS-WB005-09	C. Ant	793	11	0.281914	0.000044	0.000890	0.032124	0.281901	-13.6	3.1	2.5
BGS-WB005-13	C. Ant	793	11	0.282046	0.000073	0.002816	0.098719	0.282004	-9.9	5.1	2.3
BGS-WB005-14	C. Ant	793	11	0.282023	0.000046	0.001622	0.054546	0.281999	-10.1	3.3	2.3
BGS-WB1451-04	N. Ant	774	16	0.281889	0.000041	0.001482	0.051700	0.281868	-15.2	2.9	2.6
BGS-WB1451-11	N. Ant	774	16	0.281781	0.000067	0.001770	0.066526	0.281755	-19.2	4.7	2.8
BGS-WB1451-11	N. Ant	774	16	0.281867	0.000047	0.001258	0.042998	0.281849	-15.9	3.3	2.6
BGS-WB1451-13	N. Ant	774	16	0.281900	0.000054	0.001833	0.065338	0.281873	-15.0	3.8	2.6
BGS-WB1451-17	N. Ant	774	16	0.281917	0.000079	0.002779	0.100143	0.281876	-14.9	5.5	2.6
BGS-WB1451-18	N. Ant	774	16	0.281957	0.000029	0.001418	0.046309	0.281937	-12.7	2.0	2.4
BGS-PP156-03r	N. Ant	819	23	0.281791	0.000060	0.001746	0.066404	0.281764	-17.9	4.2	2.8
BGS-PP156-04r	N. Ant	819	23	0.281986	0.000071	0.001800	0.069372	0.281958	-11.0	5.0	2.4
BGS-PP156-06r	N. Ant	819	23	0.281974	0.000043	0.001266	0.046230	0.281954	-11.1	3.0	2.4
BGS-PP156-12	N. Ant	819	23	0.282021	0.000043	0.002651	0.087678	0.281980	-10.2	3.0	2.3
BGS-PP156-14c	N. Ant	2459	20	0.281351	0.000024	0.000534	0.021768	0.281326	4.2	1.7	2.7
BGS-PP156-18r	N. Ant	819	23	0.282018	0.000035	0.001219	0.038417	0.281999	-9.5	2.5	2.3
BGS-RT07-32-03b	N. Ant	768	8	0.281772	0.000050	0.003469	0.118676	0.281721	-20.5	3.5	2.9
BGS-RT07-32-05	N. Ant	768	8	0.281841	0.000041	0.001897	0.053088	0.281814	-17.2	2.9	2.7
BGS-RT07-32-09	N. Ant	768	8	0.281781	0.000044	0.002286	0.077106	0.281748	-19.6	3.1	2.9
BGS-RT07-32-10	N. Ant	768	8	0.281660	0.000053	0.002902	0.069268	0.281618	-24.2	3.7	3.1
DA13-074-41	E. Ant	821	11	0.281859	0.000018	0.000321	0.012685	0.281854	-14.6	1.3	2.6
DA13-074-43	E. Ant	821	11	0.281873	0.000018	0.000406	0.016234	0.281867	-14.2	1.2	2.6
DA13-074-45	E. Ant	821	11	0.281855	0.000027	0.000825	0.035952	0.281842	-15.0	1.9	2.6
DA13-074-47	E. Ant	821	11	0.281877	0.000021	0.000412	0.016852	0.281871	-14.0	1.4	2.6
DA13-074-48	E. Ant	821	11	0.281910	0.000020	0.000431	0.016954	0.281904	-12.9	1.4	2.5
DA13-074-52	E. Ant	821	11	0.281822	0.000023	0.000654	0.026849	0.281812	-16.1	1.6	2.7
DA13-074-53	E. Ant	821	11	0.281875	0.000028	0.000382	0.015219	0.281869	-14.1	1.9	2.6
DA13-074-54	E. Ant	657	11	0.281907	0.000020	0.000445	0.017812	0.281902	-16.6	1.4	2.6
DA13-074-55	E. Ant	821	11	0.281882	0.000017	0.000488	0.020734	0.281875	-13.9	1.2	2.5
DA13-074-56	E. Ant	821	11	0.281837	0.000027	0.000655	0.027254	0.281827	-15.6	1.9	2.6
DA13-074-57	E. Ant	821	11	0.281860	0.000014	0.000376	0.015860	0.281854	-14.6	1.0	2.6
DA13-074-62	E. Ant	821	11	0.281845	0.000039	0.000447	0.018596	0.281839	-15.2	2.8	2.6
DA13-074-63	E. Ant	821	11	0.281859	0.000019	0.000593	0.024839	0.281850	-14.8	1.3	2.6

Sample	Domain	Age (Ma)	± 2σ	$^{176}Hf/^{177}Hf$	2 S.E.	$^{176}Lu/^{177}Hf$	$^{176}Yb/^{177}Hf$	$^{176}Hf/^{177}Hf$ (intitial)	$\varepsilon_{Hf}(t)$	± 2σ	$T_{DM}c$ (Ga)
DA13-074-65	E. Ant	821	11	0.281820	0.000025	0.000553	0.022725	0.281812	-16.1	1.8	2.7
DA13-074-69	E. Ant	821	11	0.281873	0.000016	0.000328	0.013940	0.281868	-14.1	1.1	2.6
DA13-076-46	E. Ant	813	10	0.281909	0.000019	0.000478	0.019750	0.281901	-13.1	1.3	2.5
DA13-076-47	E. Ant	813	10	0.281929	0.000011	0.000367	0.015450	0.281923	-12.3	0.8	2.4
DA13-076-48	E. Ant	813	10	0.281887	0.000017	0.000428	0.017249	0.281880	-13.9	1.2	2.5
DA13-076-49	E. Ant	813	10	0.281918	0.000031	0.000451	0.017206	0.281911	-12.8	2.2	2.5
DA13-076-50	E. Ant	813	10	0.281876	0.000024	0.001292	0.058133	0.281857	-14.7	1.7	2.6
DA13-076-51	E. Ant	813	10	0.281864	0.000022	0.000671	0.029788	0.281854	-14.8	1.5	2.6
DA13-076-52	E. Ant	813	10	0.281885	0.000018	0.000507	0.021231	0.281877	-14.0	1.3	2.5
DA13-076-53	E. Ant	813	10	0.281923	0.000018	0.000535	0.022265	0.281914	-12.7	1.3	2.5
DA13-076-55	E. Ant	813	10	0.281910	0.000022	0.000668	0.028784	0.281900	-13.2	1.6	2.5
DA13-076-56	E. Ant	813	10	0.281905	0.000031	0.000511	0.022841	0.281897	-13.3	2.2	2.5
DA13-076-58	E. Ant	813	10	0.281900	0.000041	0.000735	0.030909	0.281889	-13.6	2.9	2.5
DA13-076-59	E. Ant	813	10	0.281906	0.000035	0.001174	0.052971	0.281888	-13.6	2.5	2.5
DA13-076-60	E. Ant	813	10	0.281883	0.000035	0.000709	0.031762	0.281872	-14.2	2.4	2.6
DA13-076-61	E. Ant	813	10	0.281890	0.000026	0.000811	0.034541	0.281877	-14.0	1.8	2.5
DA13-076-62	E. Ant	813	10	0.281886	0.000017	0.000360	0.015032	0.281880	-13.9	1.2	2.5
DA13-076-63	E. Ant	540	10	0.281897	0.000012	0.000533	0.023073	0.281892	-19.6	0.9	2.7
BGS-WB37-04	Masora	842	15	0.281544	0.000063	0.001626	0.050803	0.281518	-26.1	4.4	3.3
BGS-WB37-06	Masora	842	15	0.281677	0.000046	0.001565	0.051829	0.281652	-21.3	3.2	3.0
BGS-WB37-07	Masora	842	15	0.281726	0.000038	0.001170	0.034143	0.281708	-19.3	2.7	2.9
BGS-WB37-08	Masora	842	15	0.281640	0.000046	0.001567	0.049567	0.281615	-22.6	3.2	3.1
BGS-WB37-09	Masora	842	15	0.281702	0.000049	0.003290	0.112566	0.281650	-21.4	3.4	3.0
BGS-RK395-05	Masora	814	30	0.281656	0.000039	0.001510	0.034277	0.281633	-22.6	2.7	3.1
BGS-RK395-06	Masora	814	30	0.281665	0.000031	0.001176	0.033984	0.281647	-22.1	2.1	3.0
BGS-RK395-08	Masora	814	30	0.281663	0.000051	0.001784	0.054140	0.281636	-22.5	3.5	3.1
BGS-RK395-16	Masora	814	30	0.281628	0.000040	0.001233	0.038293	0.281609	-23.4	2.8	3.1
BGS-RK395-17	Masora	814	30	0.281630	0.000044	0.001309	0.035270	0.281610	-23.4	3.1	3.1
BGS-RK395-20	Masora	814	30	0.281548	0.000048	0.001263	0.039274	0.281528	-26.3	3.3	3.3
BGS-RK395-21	Masora	814	30	0.281618	0.000032	0.001019	0.031049	0.281602	-23.7	2.2	3.1
BGS-RK06349-04	Masora	796	33	0.281925	0.000046	0.001867	0.064233	0.281897	-13.7	3.2	2.5
BGS-RK06349-05	Masora	796	33	0.281955	0.000063	0.001346	0.050394	0.281935	-12.3	4.4	2.4
BGS-RK06349-06	Masora	796	33	0.281965	0.000049	0.001133	0.040981	0.281948	-11.8	3.4	2.4
BGS-RK06349-09	Masora	796	33	0.281981	0.000058	0.001222	0.046232	0.281963	-11.3	4.0	2.4

Appendix 4.1

Analytical Methods for Chapter 4
(Petrogenesis of the Imorona-Itsindro Suite)

4.1.1 Sample collection and processing

Approximately 2.5 to 3 kg of each sample was collected in the field for polished thin sectioning and whole-rock geochemical analysis. Samples were cut and 46 x 27 x 10 mm chips were shipped to Continental Instruments in Lucknow, India for the preparation of polished thin sections. The majority of the remaining sample was placed in a jaw crusher. A representative portion of the crushed sample was placed into a tungsten carbide ring mill for ~two minutes to produce a fine, homogeneous powder for whole-rock geochemical analysis.

4.1.2 Petrography and mineral chemistry

Polished thin-sections were analysed under transmitted and reflected light to determine mineralogy, textures and to select sites for mineral analysis. Mineral analyses were obtained at Adelaide Microscopy using a Cameca SX-Five Electron Probe with five wavelength dispersive spectrometers attached. A beam current of 20 nA, an accelerating voltage of 15 kV and a beam size of 5 μm was used for all spot analyses. Unless otherwise stated, mineral analyses were processed using modified Microsoft Excel spreadsheets (Preston, 2015). Feldspar calculations are based on end-member compositions Anorthite (An), Albite (Ab), and Orthoclase (Or). Amphibole formulas were determined based on 23 oxygen atoms and the assumption of 16 cations (i.e. no A site vacancies). Amphiboles are classified as calcium amphiboles as defined by B site occupancy: B(Ca + Σ Mg+Fe^{2+}+Mn)/Σ B site and BCa/ Σ B site ≥ BΣ (Mg+Fe^{2+}+Mn)/Σ B site (Hawthorne et al., 2012). Amphiboles are further classified using the appropriate end-member compositions (Hawthorne et al., 2012). Biotite formulas were calculated based on 11 cations and H_2O calculations after Tindle and Webb (1990). Pyroxenes are classified as sodic-calcic pyroxene based on Na>Fe^{3+} apfu (Morimoto, 1988). Garnet end-member compositions were calculated using a modified Microsoft Excel spreadsheet (Tindle, 2015) based on 12 oxygen atoms and with Fe^{2+}/Fe^{3+} calculated assuming full site occupancy. The six end-members used are Almandine, Andradite, Grossular, Pyrope, Spessartine and Uvarovite. Titanite formula were determined using a modified general recalculation spreadsheet (Tindle, 2015).

4.1.3 Whole-rock geochemistry

Whole-rock geochemical analyses for major, minor and trace elements were collected at ACME Labs in Vancouver, British Columbia, Canada. Table A.1 shows a list of the elements analysed and the appropriate detection limits. Major element oxide data collection procedure involved the crushed rock pulp being mixed with $LiBO_2$/$Li_2B_4O_7$ flux. Graphite crucibles were fused in a muffle furnace for 30 minutes at 980°C. The cooled bead was then dissolved in ACS grade nitric acid and analysed using a SPECTRO AS500 ICP-OES (inductively-coupled plasma optical emission spectroscopy) instrument. LOI (loss on ignition) values were determined by igniting a sample split then measuring the weight lost. For trace element analyses, the crushed rock pulp was digested using a modified Aqua Regia solution of equal parts concentrated HCl, HNO_3 and deionised H_2O for one hour in a heating block or hot water bath. Samples were made up to volume with dilute HCl and analysed using a Perkin-Elmer ELAN 9000 ICP-MS. Quality control protocol involves analysing pulp duplicates to monitor analytical precision and a reagent blank to measure background. In addition, interspersed analyses of reference materials SO-18, OREAS45EA, GS311-1, and GS910-4 monitored the accuracy of results. Total sulphur and carbon values were determined by adding an induction flux to the prepared sample and igniting the sample in a LECO CS230 Carbon/Sulphur Series induction furnace. A carrier gas transports the released carbon and sulphur to be measured by adsorption in an infrared spectrometric cell. Results are total carbon or sulphur.

4.1.4 Sm-Nd and Sr Isotope analysis

Nd, Sm, and Sr isotopes were measured using an Isotopx Phoenix thermal ionization mass spectrometer (TIMS) at the University of Adelaide. Twenty samples of the Imorona-Itsindro suite, 16 of which had previously been dated by U-Pb geochronology and analysed for hafnium isotopes (Archibald et al., in review) were selected for Nd-Sm, and Sr isotopic analysis. Sample powder weight (g) was calculated based on a nominal 2μg of Nd (optimum TIMS accuracy and recovery value). Isotope dilution mass spectrometry was determined by the addition of a nominal 0.4g of $^{150}Nd/^{147}Sm$ enriched spike. This allowed the concentration of Sm/Nd (μgg-1), hence the correction factor for the measured $^{143}Nd/^{144}Nd$ and $^{147}Sm/^{149}Sm$ isotopic ratios to be determined. Samples that contained <0.05g calculated weight were adjusted accordingly, hence also the amount of spike added to the sample. The addition of a strontium spike (~0.12g) allowed $^{87}Sr/^{86}Sr$ to be simultaneously determined. All milled powder and spike weights were accurately recorded (5 decimal places) on a Mettler-Toledo AT201 balance. 0.05-0.2g rock powder was dissolved together with the University of Adelaide mixed spike "H" (concentrations - ^{150}Nd = 283.9797 ng/g; ^{147}Sm = 573.5484 ng/g) in cleaned Teflon bombs with the with an approximate ratio of 2ng sample Nd to 0.4g spike H based on whole-rock Nd values. Samples were then dissolved on a hotplate at 140°C in 2mL of 7M HNO_3 and 4mL of 48% HF to dissolve silicate minerals.

An additional 2 mL of 15M HNO_3 was added prior to complete dryness to prevent the precipitation of insoluble silica fluorides. Next, 2 mL of 7M HNO_3 and 4mL of 48% HF were added to each sample. The capped and sealed bombs were then placed into an oven for 96 hours at 190°C. The Teflon bombs were removed from the oven and allowed to cool before evaporating the samples on a hotplate at 140°C. An additional 2 mL of 15M HNO_3 was added prior to complete evaporation of the sample to prevent the precipitation of fluorides. Samples were then evaporated on a hotplate. 1.5mL of 2M HCl was added to re-dissolve each sample and samples were placed into 2mL centrifuge tubes for centrifuging. Element (Sr, Sm, Nd) purification was achieved by conventional ion chromatography procedures. The first pass to separate Sr from Sm-Nd was completed in 2ml AGW X8 200-400 mesh resin in Polyprep columns. Sm was separated from Nd using 1mL of Eichrom Ln resin SPS in quartz glass columns.
Nd measurement involved multi-dynamic measurements of at least 5 blocks of 20 cycles (>100 ratios). Normalization to $^{146}Nd/^{144}Nd = 0.7219$ was done using exponential mass fractionation correction. Nd concentrations are corrected for 100pg blank. Static Sm isotopic measurements involved 3 blocks of 20 cycles (60 ratios). Sm concentrations corrected for a 50 pg blank. Procedural blanks (n=2), international standards G-2 (n=2) and BCR-2 (n= 1), and internal standards JNdi1 (n=4) and SRM987 (n=4) were analysed prior to and during sample analysis to measure machine accuracy and precision. Procedural blanks registered values of <60 pg Nd, < 5 pg Sm, and < 760 pg Sr indicating negligible contamination or procedural error. International standard G-2 (Weis et al., 2006; Nd µgg-1 = 55±6; Sm µgg-1 = 7.2±0.7; $^{143}Nd/^{144}Nd = 0.512222±6$) yielded values of 53-54 (Nd µgg-1), 7.4-7.5 (Sm µgg-1), and 0.512221-0.512218 ($^{143}Nd/^{144}Nd$). BCR-2 (USGS; Raczek et al., 2003; Nd µgg-1 = 28±2; Sm µgg-1 = 6.7 ± 0.3; $^{143}Nd/^{144}Nd = 0.512641±7$) yielded values of Nd µgg-1 =29; Sm µgg-1 = 6.7 and $^{143}Nd/^{144}Nd = 0.512619$. International Nd reference material JNdi (Tanaka et al., 2000; $^{143}Nd/^{144}Nd = 0.512115±7$) yielded a mean value of 0.512107±3 (n=49) over the period 13/1/2015 to 27/10/2015 based on a 400ng standard loading weight. Based on a 500ng load, internal Sr standard SRM9878 ($^{87}Sr/^{86}Sr = 0.710268±17$; n= >700) yielded a mean value of 0.710245±5 (n=103) over the same time period. G-2 (Weis et al., 2006; $^{87}Sr/^{86}Sr = 0.709770±16$) and BCR-2 (Balcaen et al., 2005; $^{87}Sr/^{86}Sr = 0.705015±13$) yielded $^{87}Sr/^{86}Sr$ ratios of 0.709755±3 (G-2), 0.709732±3 (G-2), and 0.705004±3 (BCR-2). Overall, the analysed standards are within accepted values, hence the Imorona-Itsindro Present day $\varepsilon_{Nd}(t)$ values were obtained using CHUR (chondrite uniform reservoir) values $^{143}Nd/^{144}Nd$ (0.512638) and $^{147}Sm/^{144}Nd$ (0.1966) and depleted mantle values (DM) $^{143}Nd/^{144}Nd$ (0.513150) and $^{147}Sm/^{144}Nd$ (0.2145) ratios taken from Goldstein et al., (1984). Depleted mantle model ages ($T_{DM}c$) are calculated based on these ratios. 14 samples are assigned crystallisation ages directly dated by U-Pb zircon geochronology (Archibald et al., in review). Although not directly dated, the other six samples are considered to be part of the Imorona-Itsindro suite based on field relationships and previous work (e.g. Roig et al., 2012; BGS-USGS-GLW, 2008). These samples are assigned an age of 800 Ma for $\varepsilon_{Nd}(t)$ and $T_{DM}c$ model age calculations.

References

Archibald, D.B., Collins, A.S., Foden, J.D., Payne, J.L., Holden, P., Razakamanana, T., De Waele, B., Pitfield, P.E.J., Thomas, R.J., in review. Genesis of the Tonian Imorona-Itsindro Magmatic Suite in central Madagascar: Insights from U-Pb, oxygen and hafnium isotopes in zircon. Precambrian Research.

Balcaen, L., Schrijver, I.D., Moens, L., Vanhaecke, F., 2005. Determination of the $^{87}Sr/^{86}Sr$ isotope ratio in USGS silicate reference materials by multi-collector ICP–mass spectrometry. International Journal of Mass Spectrometry 242, 251-255.

BGS-USGS-GLW, 2008. Revision de la cartographie geologique et miniere des zones Nord, Centre, et Centre Est de Madagascar. BGS Report CR/08/078. Keyworth, England.

Hawthorne, F.C., Oberti, R., Harlow, G.E., Maresch, W.V., Martin, R.F., Schumacher, J.C., Welch, M.D., 2012. Nomenclature of the amphibole supergroup. American Mineralogist 97, 2031-2048.

Morimoto, N., 1988. Nomenclature of Pyroxenes. Mineralogy and Petrology 39, 55-76.

Preston, J., 2015. GabbroSoft. http://www.gabbrosoft.org/spreadsheets.html.

Raczek, I., Jochum, K.P., Hofmann, A.W., 2003. Neodymium and Strontium Isotope Data for USGS Reference Materials BCR-1, BCR-2, BHVO-1, BHVO-2, AGV-1, AGV-2, GSP-1, GSP-2 and Eight MPI-DING Reference Glasses. Geostandards Newsletter 27, 173-179.

Roig, J.Y., Tucker, R.D., Peters, S.G., Delor, C., Theveniaut, H., 2012. Carte Géologique de la République de Madagascar à 1/1,000,000, Ministère des Mines, Direction de la Géologie, Programme de Gouvernance des Resources Minérales.

Tanaka, T., Togashi, S., Kamioka, H., Amakawa, H., Kagami, H., Hamamoto, T., Yuhara, M., Orihashi, Y., Yoneda, S., Shimizu, H., Kunimaru, T., Takahashi, K., Yanagi, T., Nakano, T., Fujimaki, H., Shinjo, R., Asahara, Y., Tanimizu, M., Dragusanu, C., 2000. JNdi-1: a neodymium isotopic reference in consistency with LaJolla neodymium. Chemical Geology 168, 279-281.

Tindle, A.G., 2015. Mineral Recalculation Software. http://www.open.ac.uk/earth-research/tindle/AGTWebPages/AGTSoft.html.

Tindle, A.G., Webb, P.C., 1990. Estimation of lithium contents in trioctahedral micas using microprobe data; application to micas from granitic rocks. European Journal of Mineralogy 2, 595-610.

Weis, D., Kieffer, B., Maerschalk, C., Barling, J., de Jong, J., Williams, G.A., Hanano, D., Pretorius, W., Mattielli, N., Scoates, J.S., Goolaerts, A., Friedman, R.M., Mahoney, J.B., 2006. High-precision isotopic characterization of USGS reference materials by TIMS and MC-ICP-MS. Geochemistry, Geophysics, Geosystems 7

Table A.4.1: List of major element oxides, minor and trace elements analysed in this study alongside the appropriate detection limits.

Element or Oxide	Detection Limit		Upper Limit		Element or Oxide	Detection Limit		Upper Limit	
SiO_2	0.01	%	100	%	Ho	0.02	ppm	10000	ppm
Al_2O_3	0.01	%	100	%	La	0.1	ppm	50000	ppm
CaO	0.01	%	100	%	Lu	0.01	ppm	10000	ppm
Cr_2O_3	0.002	%	100	%	Mo	0.1	ppm	2000	ppm
Fe_2O_3	0.04	%	100	%	Nb	0.1	ppm	10000	ppm
K_2O	0.01	%	100	%	Nd	0.3	ppm	10000	ppm
MgO	0.01	%	100	%	Ni	0.1	ppm	10000	ppm
MnO	0.01	%	100	%	Pb	0.1	ppm	10000	ppm
Na_2O	0.01	%	100	%	Pr	0.02	ppm	10000	ppm
P_2O_5	0.01	%	100	%	Rb	0.1	ppm	10000	ppm
TiO_2	0.01	%	100	%	Sb	0.1	ppm	2000	ppm
LOI	0.1	%	100	%	Sc	1	ppm	10000	ppm
Sum	0.01	%	100	%	Se	0.5	ppm	100	ppm
Ag	0.1	ppm	100	ppm	Sm	0.05	ppm	10000	ppm
As	0.5	ppm	10000	ppm	Sn	1	ppm	10000	ppm
Au	0.5	ppb	100000	ppb	Sr	0.5	ppm	50000	ppm
Ba	1	ppm	50000	ppm	Ta	0.1	ppm	10000	ppm
Be	1	ppm	10000	ppm	Tb	0.01	ppm	10000	ppm
Bi	0.1	ppm	2000	ppm	Th	0.2	ppm	10000	ppm
Cd	0.1	ppm	2000	ppm	Tl	0.1	ppm	1000	ppm
Ce	0.1	ppm	50000	ppm	Tm	0.01	ppm	10000	ppm
Co	0.2	ppm	10000	ppm	U	0.1	ppm	10000	ppm
Cs	0.1	ppm	10000	ppm	V	8	ppm	10000	ppm
Cu	0.1	ppm	10000	ppm	W	0.5	ppm	10000	ppm
Dy	0.05	ppm	10000	ppm	Yb	0.05	ppm	10000	ppm
Er	0.03	ppm	10000	ppm	Y	0.1	ppm	50000	ppm
Eu	0.02	ppm	10000	ppm	Zn	1	ppm	10000	ppm
Ga	0.5	ppm	10000	ppm	Zr	0.1	ppm	50000	ppm
Gd	0.05	ppm	10000	ppm	TOT/C	0.02	%	100	%
Hf	0.1	ppm	10000	ppm	TOT/S	0.02	%	100	%
Hg	0.01	ppm	50	ppm					

Appendix 4.2

EMPA Mineral Analysis Results
(Petrogenesis of the Imorona-Itsindro Suite)

Appendix 4.2.1: Representative mineral chemistry for alkali-feldspar

	DA13-029-3.1	DA13-029-3.2	DA13-029-3.3	DA13-029-3.4	DA13-029-3.5	DA13-029-3.6	DA13-029-3.7	DA13-029-3.8	DA13-029-3.9	DA13-029-3.10	DA13-029-4.1	DA13-029-4.2	DA13-029-4.3	DA13-029-4.4	DA13-029-4.5	DA13-029-4.6	DA13-029-4.7	DA13-029-4.8	DA13-029-4.9	DA13-029-4.10
SiO_2	64.83	64.63	64.84	64.90	65.08	64.58	64.91	64.65	64.64	64.97	64.49	64.76	64.39	64.92	64.60	64.39	64.18	65.09	64.64	63.74
TiO_2	0.00	0.02	0.00	0.00	0.02	0.00	0.01	0.01	0.01	0.01	0.00	0.00	0.00	0.01	0.02	0.01	0.01	0.02	0.00	0.00
Al_2O_3	17.76	17.77	17.83	17.81	17.92	17.68	17.74	17.72	17.73	17.82	17.79	17.84	17.70	17.77	17.69	17.68	17.75	17.92	17.71	18.63
Cr_2O_3	0.00	0.00	0.00	0.03	0.00	0.01	0.00	0.01	0.01	0.00	0.04	0.00	0.02	0.00	0.00	0.00	0.01	0.01	0.03	0.00
FeOT	0.30	0.00	0.04	0.02	0.20	0.09	0.07	0.27	0.05	0.05	0.02	0.00	0.07	0.04	0.02	0.02	0.03	0.07	0.02	0.02
MnO	0.00	0.00	0.00	0.02	0.00	0.01	0.00	0.00	0.00	0.00	0.00	0.00	0.00	0.01	0.01	0.00	0.01	0.01	0.01	0.00
MgO	0.01	0.00	0.00	0.00	0.00	0.01	0.01	0.03	0.00	0.00	0.01	0.00	0.00	0.02	0.01	0.01	0.00	0.00	0.01	0.00
BaO	0.16	0.14	0.20	0.18	0.23	0.18	0.16	0.20	0.16	0.18	0.19	0.17	0.19	0.15	0.21	0.17	0.18	0.14	0.16	0.14
CaO	0.00	0.00	0.00	0.00	0.00	0.00	0.00	0.00	0.00	0.00	0.01	0.00	0.00	0.00	0.00	0.00	0.00	0.00	0.00	0.00
Na_2O	0.97	0.90	0.82	0.76	0.57	0.76	0.60	0.29	0.51	0.96	0.93	0.83	0.29	0.46	0.40	0.53	0.69	0.50	0.86	0.78
K_2O	14.94	15.39	15.50	15.65	15.76	15.68	15.85	16.14	15.82	15.23	15.34	15.46	16.25	15.89	16.14	15.99	15.70	15.83	15.44	15.15
Total	98.80	98.71	99.04	99.14	99.55	98.79	99.18	99.07	98.76	99.05	98.58	98.89	98.71	99.09	98.86	98.62	98.36	99.44	98.67	98.32
Si	11.85	11.82	11.85	11.87	11.90	11.81	11.87	11.82	11.82	11.88	11.79	11.84	11.77	11.87	11.81	11.77	11.73	11.90	11.82	11.65
Ti	0.00	0.00	0.00	0.00	0.00	0.00	0.00	0.00	0.00	0.00	0.00	0.00	0.00	0.00	0.00	0.00	0.00	0.00	0.00	0.00
Al	3.83	3.83	3.84	3.84	3.86	3.81	3.82	3.82	3.82	3.84	3.83	3.84	3.81	3.83	3.81	3.81	3.82	3.86	3.82	4.01
Fe^{2+}	0.05	0.00	0.01	0.00	0.03	0.01	0.01	0.04	0.01	0.01	0.00	0.00	0.01	0.01	0.00	0.00	0.00	0.01	0.00	0.00
Ca	0.00	0.00	0.00	0.00	0.00	0.00	0.00	0.00	0.00	0.00	0.00	0.00	0.00	0.00	0.00	0.00	0.00	0.00	0.00	0.00
Na	0.34	0.32	0.29	0.27	0.20	0.27	0.21	0.10	0.18	0.34	0.33	0.29	0.10	0.16	0.14	0.19	0.24	0.18	0.31	0.28
K	3.48	3.59	3.61	3.65	3.68	3.66	3.70	3.76	3.69	3.55	3.58	3.61	3.79	3.71	3.76	3.73	3.66	3.69	3.60	3.53
Total	19.55	19.55	19.61	19.62	19.67	19.55	19.61	19.55	19.52	19.62	19.54	19.58	19.49	19.57	19.53	19.50	19.47	19.64	19.54	19.48
An	0.00	0.00	0.02	0.00	0.00	0.00	0.00	0.00	0.00	0.02	0.03	0.00	0.00	0.00	0.00	0.00	0.00	0.00	0.00	0.00
Ab	9.00	8.15	7.46	6.85	5.18	6.87	5.43	2.68	4.68	8.73	8.47	7.53	2.68	4.21	3.64	4.78	6.23	4.55	7.81	7.28
Or	91.00	91.85	92.52	93.15	94.82	93.13	94.57	97.32	95.32	91.25	91.50	92.47	97.32	95.79	96.36	95.22	93.77	95.45	92.19	92.72
Total	100.00	100.00	100.00	100.00	100.00	100.00	100.00	100.00	100.00	100.00	100.00	100.00	100.00	100.00	100.00	100.00	100.00	100.00	100.00	100.00

Appendix 4.2.1: Representative mineral chemistry for alkali-feldspar

	DA13-029-4.11	DA13-040-5.1	DA13-040-5.2	DA13-040-5.3	DA13-040-5.4	DA13-040-5.5	DA13-040-5.6	DA13-040-5.7	DA13-040-5.8	DA13-040-5.9	DA13-040-5.10	DA13-040-7.1	DA13-040-7.2	DA13-040-7.3	DA13-040-7.4	DA13-040-7.5	DA13-040-7.6	DA13-040-7.7	DA13-040-7.8	DA13-040-7.9
SiO_2	64.54	65.04	65.21	65.00	64.49	64.56	64.64	64.80	64.72	64.66	64.28	62.32	62.33	63.07	63.19	63.59	63.49	62.94	62.96	63.45
TiO_2	0.00	0.02	0.02	0.01	0.03	0.18	0.02	0.01	0.01	0.02	0.00	0.07	0.09	0.03	0.04	0.01	0.03	0.01	0.05	0.02
Al_2O_3	17.73	18.23	18.32	18.34	18.14	18.21	18.07	18.17	18.26	18.21	18.12	19.09	19.04	19.18	18.88	19.16	19.19	19.14	19.22	19.07
Cr_2O_3	0.00	0.00	0.00	0.00	0.00	0.01	0.01	0.01	0.01	0.00	0.00	0.00	0.01	0.04	0.01	0.03	0.00	0.03	0.01	0.00
FeOT	0.04	0.28	0.34	0.30	0.28	1.12	0.33	0.25	0.31	0.28	0.27	0.55	0.36	0.11	0.14	0.13	0.10	0.15	0.14	0.15
MnO	0.00	0.01	0.00	0.00	0.00	0.02	0.00	0.02	0.00	0.00	0.01	0.02	0.00	0.00	0.00	0.00	0.00	0.00	0.01	0.00
MgO	0.01	0.00	0.00	0.00	0.01	0.00	0.01	0.00	0.00	0.02	0.00	0.01	0.00	0.02	0.00	0.00	0.00	0.01	0.00	0.00
BaO	0.19	1.53	1.42	1.50	1.47	1.45	1.52	1.43	1.44	1.46	1.41	4.22	4.09	3.76	3.44	3.50	3.57	4.08	4.01	3.50
CaO	0.00	0.00	0.00	0.00	0.00	0.00	0.00	0.00	0.00	0.00	0.00	0.00	0.00	0.00	0.00	0.00	0.00	0.00	0.00	0.00
Na_2O	0.26	1.40	1.72	1.38	0.81	1.48	0.95	1.16	1.29	0.90	0.82	2.24	2.26	1.98	2.00	2.25	2.51	2.43	2.32	2.13
K_2O	16.12	13.92	13.62	14.21	14.79	13.83	14.70	14.35	14.02	14.75	14.68	11.68	11.71	12.21	12.39	12.09	11.73	11.54	11.83	12.09
Total	98.69	98.89	99.21	99.24	98.55	99.37	98.72	98.75	98.60	98.82	98.17	95.95	95.79	96.57	96.64	97.24	97.04	96.21	96.52	96.91
Si	11.80	11.89	11.92	11.88	11.79	11.80	11.82	11.85	11.83	11.82	11.75	11.39	11.40	11.53	11.55	11.63	11.61	11.51	11.51	11.60
Ti	0.00	0.00	0.00	0.00	0.00	0.02	0.00	0.00	0.00	0.00	0.00	0.01	0.01	0.00	0.00	0.00	0.00	0.00	0.01	0.00
Al	3.82	3.93	3.95	3.95	3.91	3.92	3.89	3.92	3.93	3.92	3.90	4.11	4.10	4.13	4.07	4.13	4.14	4.12	4.14	4.11
Fe^{2+}	0.01	0.04	0.05	0.05	0.04	0.17	0.05	0.04	0.05	0.04	0.04	0.08	0.06	0.02	0.02	0.02	0.01	0.02	0.02	0.02
Ca	0.00	0.00	0.00	0.00	0.00	0.00	0.00	0.00	0.00	0.00	0.00	0.00	0.00	0.00	0.00	0.00	0.00	0.00	0.00	0.00
Na	0.09	0.50	0.61	0.49	0.29	0.52	0.34	0.41	0.46	0.32	0.29	0.79	0.80	0.70	0.71	0.80	0.89	0.86	0.82	0.75
K	3.76	3.25	3.18	3.31	3.45	3.22	3.43	3.35	3.27	3.44	3.42	2.72	2.73	2.85	2.89	2.82	2.73	2.69	2.76	2.82
Total	19.48	19.61	19.70	19.69	19.48	19.67	19.53	19.56	19.54	19.55	19.41	19.12	19.10	19.23	19.25	19.39	19.38	19.21	19.26	19.31
An	0.00	0.00	0.00	0.00	0.00	0.00	0.00	0.00	0.00	0.00	0.00	0.00	0.00	0.00	0.00	0.00	0.00	0.00	0.00	0.00
Ab	2.43	13.25	16.07	12.88	7.65	13.97	8.91	10.97	12.27	8.47	7.84	22.54	22.66	19.74	19.74	22.07	24.52	24.23	22.97	21.12
Or	97.57	86.75	83.93	87.12	92.35	86.03	91.09	89.03	87.73	91.53	92.16	77.46	77.34	80.26	80.26	77.93	75.48	75.77	77.03	78.88
Total	100.00	100.00	100.00	100.00	100.00	100.00	100.00	100.00	100.00	100.00	100.00	100.00	100.00	100.00	100.00	100.00	100.00	100.00	100.00	100.00

Appendix 4.2.1: Representative mineral chemistry for alkali-feldspar

	DA13-040-7.10	DA13-049-2.1	DA13-049-2.2	DA13-049-2.3	DA13-049-2.4	DA13-049-2.5	DA13-049-2.6	DA13-049-2.7	DA13-049-2.8	DA13-049-2.9	DA13-049-2.10	DA13-049-7.1	DA13-049-7.2	DA13-049-7.3	DA13-049-7.4	DA13-049-7.5	DA13-049-7.6	DA13-049-7.7	DA13-049-7.8	DA13-049-7.9
SiO_2	62.82	63.93	64.60	64.47	64.45	64.72	64.27	64.51	64.10	64.33	64.58	64.27	63.94	64.14	64.77	64.20	64.58	64.37	64.38	64.34
TiO_2	0.03	0.00	0.00	0.00	0.01	0.01	0.01	0.00	0.01	0.01	0.01	0.01	0.00	0.02	0.01	0.01	0.01	0.01	0.01	0.02
Al_2O_3	19.17	17.79	17.81	17.83	17.71	18.01	17.84	17.86	17.71	17.82	17.85	17.99	17.86	17.88	18.08	18.05	17.95	17.97	18.05	17.90
Cr_2O_3	0.00	0.01	0.03	0.00	0.00	0.02	0.00	0.04	0.03	0.00	0.00	0.00	0.00	0.00	0.00	0.00	0.00	0.01	0.01	0.00
FeOT	0.11	0.02	0.06	0.05	0.03	0.02	0.03	0.01	0.03	0.03	0.07	0.03	0.07	0.03	0.03	0.01	0.05	0.04	0.02	0.04
MnO	0.00	0.03	0.01	0.00	0.00	0.03	0.00	0.00	0.00	0.00	0.00	0.01	0.01	0.00	0.00	0.00	0.03	0.02	0.00	0.03
MgO	0.00	0.03	0.00	0.00	0.01	0.00	0.01	0.00	0.00	0.00	0.00	0.00	0.00	0.01	0.00	0.00	0.00	0.00	0.00	0.00
BaO	4.22	0.44	0.37	0.47	0.50	0.48	0.50	0.50	0.47	0.45	0.49	0.84	0.77	0.82	0.88	0.81	0.90	0.87	0.87	0.86
CaO	0.00	0.00	0.00	0.00	0.00	0.00	0.00	0.00	0.00	0.00	0.00	0.00	0.00	0.00	0.00	0.00	0.00	0.00	0.00	0.00
Na_2O	2.19	0.60	0.86	0.92	0.65	0.84	0.71	0.82	0.61	0.81	0.64	0.65	0.72	0.73	0.82	0.77	0.94	0.60	0.77	0.63
K_2O	11.80	15.44	15.24	15.16	15.49	15.25	15.38	15.36	15.43	15.22	15.49	15.24	15.14	15.29	15.04	15.21	14.88	15.37	15.06	15.35
Total	96.12	97.77	98.57	98.43	98.35	98.85	98.24	98.56	97.88	98.21	98.64	98.18	97.74	98.09	98.75	98.24	98.41	98.36	98.30	98.27
Si	11.49	11.69	11.81	11.79	11.78	11.83	11.75	11.79	11.72	11.76	11.81	11.75	11.69	11.73	11.84	11.74	11.81	11.77	11.77	11.76
Ti	0.00	0.00	0.00	0.00	0.00	0.00	0.00	0.00	0.00	0.00	0.00	0.00	0.00	0.00	0.00	0.00	0.00	0.00	0.00	0.00
Al	4.13	3.83	3.84	3.84	3.82	3.88	3.84	3.85	3.82	3.84	3.85	3.88	3.85	3.85	3.90	3.89	3.87	3.87	3.89	3.86
Fe^{2+}	0.02	0.00	0.01	0.01	0.01	0.00	0.00	0.00	0.00	0.00	0.01	0.00	0.01	0.00	0.00	0.00	0.01	0.01	0.00	0.01
Ca	0.00	0.00	0.00	0.00	0.00	0.00	0.00	0.00	0.00	0.00	0.00	0.00	0.00	0.00	0.00	0.00	0.00	0.00	0.00	0.00
Na	0.78	0.21	0.30	0.33	0.23	0.30	0.25	0.29	0.21	0.29	0.23	0.23	0.26	0.26	0.29	0.27	0.33	0.21	0.27	0.22
K	2.75	3.60	3.55	3.54	3.61	3.56	3.59	3.58	3.60	3.55	3.61	3.55	3.53	3.57	3.51	3.55	3.47	3.58	3.51	3.58
Total	19.16	19.34	19.51	19.50	19.45	19.57	19.44	19.52	19.35	19.44	19.50	19.41	19.34	19.41	19.54	19.45	19.49	19.44	19.45	19.43
An	0.00	0.00	0.00	0.00	0.00	0.00	0.00	0.00	0.00	0.00	0.00	0.00	0.00	0.00	0.00	0.00	0.00	0.00	0.00	0.00
Ab	21.98	5.60	7.88	8.48	6.04	7.76	6.53	7.51	5.63	7.46	5.93	6.07	6.77	6.76	7.68	7.12	8.72	5.59	7.24	5.89
Or	78.02	94.40	92.12	91.52	93.96	92.24	93.47	92.49	94.37	92.54	94.07	93.93	93.23	93.24	92.32	92.88	91.28	94.41	92.76	94.11
Total	100.00	100.00	100.00	100.00	100.00	100.00	100.00	100.00	100.00	100.00	100.00	100.00	100.00	100.00	100.00	100.00	100.00	100.00	100.00	100.00

Appendix 4.2.1: Representative mineral chemistry for alkali-feldspar

	DA13-049-7.10	DA13-055-3.1	DA13-055-3.2	DA13-055-3.3	DA13-055-3.4	DA13-055-3.5	DA13-055-3.6	DA13-055-3.7	DA13-055-3.8	DA13-055-3.9	DA13-055-3.10	DA13-055-4.1	DA13-055-4.2	DA13-055-4.3	DA13-055-4.4	DA13-055-4.5	DA13-055-4.6	DA13-055-4.7	DA13-055-4.8	DA13-055-4.9
SiO_2	64.37	64.58	57.19	64.84	64.83	64.76	64.77	68.72	64.41	65.73	66.42	64.73	64.63	64.99	64.55	65.50	65.76	64.79	64.79	65.45
TiO_2	0.00	0.04	0.02	0.81	0.01	0.00	0.01	0.02	0.01	0.00	0.00	0.01	0.01	0.00	0.02	0.01	0.00	0.00	0.01	0.01
Al_2O_3	17.84	18.34	22.81	19.86	18.37	18.08	18.24	19.94	18.23	18.69	18.82	18.68	18.17	18.28	18.12	18.50	18.47	18.15	18.20	18.52
Cr_2O_3	0.00	0.00	0.30	0.00	0.00	0.01	0.01	0.02	0.06	0.00	0.01	0.07	0.02	0.00	0.02	0.00	0.03	0.02	0.00	0.00
FeOT	0.00	0.05	0.10	1.04	0.03	0.02	0.03	0.02	0.01	0.04	0.02	0.05	0.02	0.02	0.01	0.01	0.01	0.03	0.02	0.01
MnO	0.01	0.02	0.00	0.03	0.00	0.00	0.00	0.01	0.00	0.00	0.00	0.00	0.01	0.03	0.00	0.00	0.00	0.01	0.00	0.03
MgO	0.01	0.01	0.10	0.02	0.01	0.01	0.00	0.01	0.01	0.00	0.00	0.00	0.01	0.00	0.01	0.01	0.01	0.00	0.00	0.00
BaO	0.78	1.47	1.24	0.73	1.28	1.27	1.26	0.68	1.26	1.05	1.17	1.14	1.18	1.04	1.09	1.04	0.72	0.87	0.76	0.95
CaO	0.00	0.00	0.14	1.38	0.00	0.00	0.00	0.58	0.00	0.21	0.10	0.00	0.00	0.00	0.00	0.01	0.00	0.00	0.00	0.08
Na_2O	0.77	1.20	0.74	5.43	1.20	1.02	1.14	6.25	0.98	3.04	3.04	1.47	0.86	1.16	0.84	1.90	2.08	0.98	0.95	2.67
K_2O	15.16	14.53	13.21	7.10	14.62	14.84	14.62	7.06	14.95	11.93	11.87	14.25	15.14	14.50	15.08	13.61	13.47	14.92	15.14	13.06
Total	98.14	98.75	94.21	100.46	99.06	98.71	98.81	102.59	98.58	99.64	100.26	99.18	98.84	98.95	98.63	99.54	99.79	98.87	99.11	99.80
Si	11.77	11.81	10.46	11.85	11.85	11.84	11.84	12.56	11.78	12.02	12.14	11.83	11.82	11.88	11.80	11.97	12.02	11.84	11.85	11.97
Ti	0.00	0.01	0.00	0.11	0.00	0.00	0.00	0.00	0.00	0.00	0.00	0.00	0.00	0.00	0.00	0.00	0.00	0.00	0.00	0.00
Al	3.84	3.95	4.91	4.28	3.96	3.90	3.93	4.30	3.93	4.03	4.05	4.02	3.92	3.94	3.90	3.99	3.98	3.91	3.92	3.99
Fe^{2+}	0.00	0.01	0.01	0.16	0.00	0.00	0.00	0.00	0.00	0.01	0.00	0.01	0.00	0.00	0.00	0.00	0.00	0.00	0.00	0.00
Ca	0.00	0.00	0.03	0.27	0.00	0.00	0.00	0.11	0.00	0.04	0.02	0.00	0.00	0.00	0.00	0.00	0.00	0.00	0.00	0.01
Na	0.27	0.43	0.26	1.92	0.43	0.36	0.40	2.22	0.35	1.08	1.08	0.52	0.30	0.41	0.30	0.67	0.74	0.35	0.34	0.95
K	3.54	3.39	3.08	1.66	3.41	3.46	3.41	1.65	3.49	2.78	2.77	3.32	3.53	3.38	3.52	3.17	3.14	3.48	3.53	3.05
Total	19.42	19.59	18.76	20.25	19.65	19.56	19.59	20.84	19.54	19.95	20.06	19.71	19.57	19.62	19.53	19.81	19.88	19.59	19.64	19.97
An	0.00	0.00	0.84	7.02	0.00	0.00	0.00	2.87	0.00	1.04	0.48	0.00	0.00	0.00	0.00	0.05	0.02	0.00	0.00	0.37
Ab	7.19	11.19	7.74	49.97	11.10	9.43	10.58	55.73	9.02	27.64	27.88	13.54	7.95	10.85	7.82	17.48	19.04	9.06	8.69	23.61
Or	92.81	88.81	91.42	43.00	88.90	90.57	89.42	41.39	90.98	71.32	71.63	86.46	92.05	89.15	92.18	82.47	80.94	90.94	91.31	76.02
Total	100.00	100.00	100.00	100.00	100.00	100.00	100.00	100.00	100.00	100.00	100.00	100.00	100.00	100.00	100.00	100.00	100.00	100.00	100.00	100.00

Appendix 4.2.1: Representative mineral chemistry for alkali-feldspar

	DA13-055-4.10	DA13-064-3.1	DA13-064-3.2	DA13-064-3.3	DA13-064-3.4	DA13-064-3.5	DA13-064-3.6	DA13-064-3.7	DA13-064-3.8	DA13-064-3.9	DA13-064-3.10	DA13-064-4.1	DA13-064-4.2	DA13-064-4.3	DA13-064-4.4	DA13-064-4.5	DA13-064-4.6	DA13-064-4.7	DA13-064-4.8	DA13-064-4.9
SiO_2	62.24	64.61	65.45	64.59	64.34	64.19	65.10	64.93	64.41	64.50	64.64	64.56	64.89	65.37	64.51	64.39	64.36	64.42	64.10	64.46
TiO_2	0.01	0.02	0.03	0.01	0.02	0.00	0.00	0.01	0.04	0.01	0.03	0.00	0.01	0.03	0.00	0.02	0.01	0.01	0.01	0.00
Al_2O_3	19.46	18.10	18.37	18.21	18.19	18.03	18.46	18.42	18.10	18.33	18.27	18.07	18.08	18.53	18.06	17.89	17.87	18.00	17.84	18.03
Cr_2O_3	0.00	0.00	0.00	0.00	0.00	0.01	0.02	0.04	0.00	0.01	0.00	0.00	0.00	0.00	0.00	0.00	0.05	0.00	0.01	0.04
FeOT	0.10	0.03	0.02	0.03	0.02	0.04	0.01	0.03	0.03	0.02	0.01	0.01	0.01	0.04	0.04	0.03	0.02	0.03	0.01	0.05
MnO	0.01	0.00	0.02	0.02	0.03	0.00	0.02	0.00	0.05	0.00	0.00	0.01	0.00	0.00	0.00	0.04	0.01	0.00	0.01	0.03
MgO	0.05	0.00	0.01	0.00	0.00	0.00	0.00	0.02	0.01	0.00	0.00	0.00	0.00	0.00	0.00	0.00	0.01	0.00	0.02	0.01
BaO	1.02	1.01	0.97	1.05	1.07	1.11	1.12	1.17	1.12	1.16	1.19	0.83	0.84	0.73	0.81	0.70	0.80	0.84	0.79	0.84
CaO	0.10	0.00	0.00	0.00	0.00	0.00	0.00	0.00	0.00	0.00	0.00	0.00	0.00	0.00	0.00	0.00	0.00	0.00	0.00	0.00
Na_2O	0.89	1.20	1.80	1.23	0.62	0.84	2.15	1.61	0.96	1.57	1.57	1.00	1.25	0.84	0.96	0.95	0.81	0.75	0.64	0.84
K_2O	13.99	14.66	13.78	14.42	15.25	15.01	13.50	14.22	14.85	13.93	14.04	14.94	14.63	15.11	15.14	15.04	15.16	15.33	15.36	15.18
Total	96.78	98.62	99.45	98.50	98.44	98.11	99.21	99.23	98.39	98.36	98.56	98.57	98.87	99.91	98.71	98.32	98.23	98.54	97.97	98.55
Si	11.38	11.81	11.97	11.81	11.76	11.73	11.90	11.87	11.77	11.79	11.82	11.80	11.86	11.95	11.79	11.77	11.77	11.78	11.72	11.79
Ti	0.00	0.00	0.00	0.00	0.00	0.00	0.00	0.00	0.01	0.00	0.00	0.00	0.00	0.00	0.00	0.00	0.00	0.00	0.00	0.00
Al	4.19	3.90	3.96	3.92	3.92	3.88	3.98	3.97	3.90	3.95	3.94	3.89	3.90	3.99	3.89	3.85	3.85	3.88	3.84	3.88
Fe^{2+}	0.01	0.00	0.00	0.00	0.00	0.01	0.00	0.00	0.01	0.00	0.00	0.00	0.00	0.01	0.01	0.00	0.00	0.01	0.00	0.01
Ca	0.02	0.00	0.00	0.00	0.00	0.00	0.00	0.00	0.00	0.00	0.00	0.00	0.00	0.00	0.00	0.00	0.00	0.00	0.00	0.00
Na	0.32	0.42	0.64	0.44	0.22	0.30	0.76	0.57	0.34	0.55	0.56	0.35	0.44	0.30	0.34	0.34	0.29	0.27	0.23	0.30
K	3.26	3.42	3.21	3.36	3.56	3.50	3.15	3.32	3.46	3.25	3.27	3.48	3.41	3.52	3.53	3.51	3.54	3.57	3.58	3.54
Total	19.19	19.56	19.78	19.54	19.46	19.42	19.79	19.73	19.49	19.55	19.59	19.53	19.62	19.77	19.56	19.48	19.44	19.50	19.38	19.51
An	0.53	0.00	0.00	0.00	0.01	0.00	0.00	0.00	0.00	0.00	0.00	0.00	0.00	0.00	0.00	0.00	0.00	0.00	0.00	0.00
Ab	8.79	11.05	16.53	11.48	5.80	7.86	19.49	14.71	8.92	14.59	14.55	9.20	11.49	7.78	8.79	8.78	7.50	6.96	5.99	7.76
Or	90.68	88.95	83.47	88.52	94.19	92.14	80.51	85.29	91.08	85.41	85.45	90.80	88.51	92.22	91.21	91.22	92.50	93.04	94.01	92.24
Total	100.00	100.00	100.00	100.00	100.00	100.00	100.00	100.00	100.00	100.00	100.00	100.00	100.00	100.00	100.00	100.00	100.00	100.00	100.00	100.00

Appendix 4.2.1: Representative mineral chemistry for alkali-feldspar

	DA13-064-4.10	DA13-069-2.1	DA13-069-2.2	DA13-069-2.3	DA13-069-2.4	DA13-069-2.5	DA13-069-2.6	DA13-069-2.7	DA13-069-2.8	DA13-069-2.9	DA13-069-2.10	DA13-069-4.1	DA13-069-4.2	DA13-069-4.3	DA13-069-4.5	DA13-069-4.6	DA13-069-4.7	DA13-069-4.8	DA13-069-4.9	DA13-069-4.10
SiO_2	65.19	64.45	64.16	63.83	64.46	64.23	64.61	64.11	64.39	64.37	64.41	64.26	63.86	64.01	64.23	64.41	64.29	64.00	64.08	62.99
TiO_2	0.00	0.01	0.03	0.01	0.01	0.00	0.00	0.00	0.01	0.00	0.01	0.01	0.02	0.02	0.01	0.00	0.00	0.02	0.02	0.00
Al_2O_3	18.24	18.13	17.90	17.71	17.90	17.87	18.02	17.84	18.00	18.02	18.07	17.96	18.09	17.96	17.95	17.89	18.00	17.94	18.08	17.68
Cr_2O_3	0.02	0.00	0.00	0.00	0.00	0.00	0.02	0.00	0.00	0.02	0.00	0.00	0.01	0.00	0.00	0.00	0.01	0.00	0.01	0.00
FeOT	0.06	0.01	0.00	0.00	0.03	0.01	0.01	0.00	0.03	0.05	0.03	0.05	0.01	0.03	0.03	0.06	0.05	0.03	0.04	0.04
MnO	0.01	0.00	0.00	0.00	0.00	0.00	0.04	0.04	0.00	0.01	0.00	0.00	0.00	0.00	0.00	0.00	0.00	0.00	0.04	0.02
MgO	0.00	0.01	0.00	0.01	0.00	0.01	0.00	0.01	0.00	0.00	0.00	0.00	0.00	0.00	0.01	0.00	0.00	0.00	0.01	0.04
BaO	0.82	0.90	0.96	0.86	0.87	0.87	0.94	0.82	0.94	1.03	0.98	1.07	1.22	1.04	1.05	0.87	1.19	1.09	1.04	1.12
CaO	0.00	0.00	0.00	0.00	0.00	0.00	0.00	0.00	0.00	0.00	0.00	0.00	0.00	0.00	0.00	0.00	0.00	0.00	0.00	0.01
Na_2O	0.73	1.01	0.90	0.66	0.78	0.93	1.03	0.82	0.89	0.91	0.70	0.88	0.53	0.94	0.93	0.69	0.96	0.73	0.90	0.78
K_2O	15.42	15.09	15.24	15.61	15.27	15.01	14.92	15.30	15.03	15.12	15.46	14.96	15.43	14.84	14.96	15.19	14.86	15.22	15.02	14.83
Total	99.63	98.70	98.23	97.82	98.46	98.05	98.59	98.07	98.34	98.48	98.68	98.12	97.94	97.81	98.10	98.25	98.17	97.95	98.14	96.33
Si	11.92	11.78	11.73	11.67	11.78	11.74	11.81	11.72	11.77	11.77	11.78	11.75	11.68	11.70	11.74	11.77	11.75	11.70	11.72	11.52
Ti	0.00	0.00	0.00	0.00	0.00	0.00	0.00	0.00	0.00	0.00	0.00	0.00	0.00	0.00	0.00	0.00	0.00	0.00	0.00	0.00
Al	3.93	3.91	3.86	3.82	3.86	3.85	3.88	3.84	3.88	3.88	3.89	3.87	3.90	3.87	3.87	3.86	3.88	3.87	3.89	3.81
Fe^{2+}	0.01	0.00	0.00	0.00	0.00	0.00	0.00	0.00	0.00	0.01	0.00	0.01	0.00	0.00	0.00	0.01	0.01	0.00	0.01	0.01
Ca	0.00	0.00	0.00	0.00	0.00	0.00	0.00	0.00	0.00	0.00	0.00	0.00	0.00	0.00	0.00	0.00	0.00	0.00	0.00	0.00
Na	0.26	0.36	0.32	0.23	0.28	0.33	0.37	0.29	0.32	0.32	0.25	0.31	0.19	0.33	0.33	0.25	0.34	0.26	0.32	0.28
K	3.60	3.52	3.55	3.64	3.56	3.50	3.48	3.57	3.51	3.53	3.61	3.49	3.60	3.46	3.49	3.54	3.47	3.55	3.50	3.46
Total	19.71	19.57	19.46	19.36	19.49	19.43	19.54	19.42	19.48	19.51	19.53	19.43	19.36	19.38	19.43	19.43	19.45	19.38	19.44	19.07
An	0.00	0.00	0.00	0.00	0.00	0.00	0.00	0.00	0.00	0.00	0.00	0.00	0.00	0.00	0.00	0.01	0.00	0.00	0.00	0.07
Ab	6.73	9.19	8.27	6.00	7.19	8.64	9.53	7.52	8.26	8.41	6.46	8.20	4.93	8.80	8.61	6.49	8.93	6.81	8.34	7.39
Or	93.27	90.81	91.73	94.00	92.81	91.36	90.47	92.48	91.74	91.59	93.54	91.80	95.07	91.20	91.39	93.50	91.07	93.19	91.66	92.55
Total	100.00	100.00	100.00	100.00	100.00	100.00	100.00	100.00	100.00	100.00	100.00	100.00	100.00	100.00	100.00	100.00	100.00	100.00	100.00	100.00

Appendix 4.2.1: Representative mineral chemistry for alkali-feldspar

	DA13-074-1.1	DA13-074-1.2	DA13-074-1.3	DA13-074-1.4	DA13-074-1.5	DA13-074-1.6	DA13-074-1.7	DA13-074-1.8	DA13-074-1.9	DA13-074-1.10	DA13-074-3.1	DA13-074-3.2	DA13-074-3.3	DA13-074-3.5	DA13-074-3.6	DA13-074-3.7	DA13-074-3.8	DA13-074-3.9	DA13-074-3.10	DA13-076-2.1
SiO_2	64.20	64.39	64.46	64.46	64.51	64.32	64.56	65.05	64.73	64.84	64.71	64.53	64.69	64.55	64.74	64.53	64.44	64.41	64.43	64.59
TiO_2	0.00	0.02	0.01	0.00	0.01	0.00	0.02	0.01	0.01	0.01	0.02	0.02	0.01	0.00	0.02	0.02	0.00	0.01	0.01	0.02
Al_2O_3	17.97	17.97	17.89	17.92	17.98	17.91	17.94	18.04	17.87	17.94	17.98	17.96	17.95	17.88	18.00	17.97	18.05	17.92	18.06	17.95
Cr_2O_3	0.00	0.00	0.03	0.02	0.00	0.00	0.00	0.05	0.00	0.00	0.01	0.00	0.00	0.00	0.03	0.00	0.00	0.00	0.00	0.00
FeOT	0.03	0.03	0.00	0.00	0.00	0.02	0.00	0.04	0.00	0.01	0.03	0.00	0.02	0.01	0.01	0.01	0.03	0.04	0.00	0.01
MnO	0.00	0.03	0.01	0.00	0.04	0.03	0.00	0.00	0.00	0.00	0.00	0.00	0.00	0.01	0.03	0.00	0.00	0.00	0.00	0.00
MgO	0.00	0.02	0.01	0.00	0.00	0.00	0.00	0.00	0.00	0.00	0.00	0.01	0.02	0.00	0.00	0.00	0.00	0.01	0.00	0.01
BaO	0.54	0.60	0.58	0.52	0.60	0.59	0.54	0.47	0.57	0.62	0.55	0.50	0.44	0.47	0.45	0.51	0.61	0.53	0.57	0.61
CaO	0.05	0.05	0.06	0.00	0.04	0.05	0.04	0.10	0.02	0.03	0.05	0.02	0.08	0.02	0.08	0.09	0.05	0.06	0.02	0.08
Na_2O	1.30	1.25	1.13	0.91	1.23	1.14	1.21	1.99	1.49	1.46	1.50	1.23	1.80	1.00	1.85	1.64	1.11	1.17	1.37	1.02
K_2O	14.68	14.75	14.83	15.25	14.66	14.88	14.77	13.64	14.44	14.52	14.35	14.69	13.84	15.01	13.77	14.02	14.74	14.73	14.72	14.92
Total	98.24	98.45	98.37	98.53	98.43	98.33	98.53	98.87	98.55	98.81	98.62	98.45	98.39	98.48	98.47	98.29	98.42	98.34	98.62	98.59
Si	11.74	11.77	11.78	11.78	11.79	11.76	11.80	11.89	11.83	11.85	11.83	11.80	11.83	11.80	11.84	11.80	11.78	11.77	11.78	11.81
Ti	0.00	0.00	0.00	0.00	0.00	0.00	0.00	0.00	0.00	0.00	0.00	0.00	0.00	0.00	0.00	0.00	0.00	0.00	0.00	0.00
Al	3.87	3.87	3.85	3.86	3.87	3.86	3.86	3.89	3.85	3.86	3.87	3.87	3.87	3.85	3.88	3.87	3.89	3.86	3.89	3.87
Fe^{2+}	0.00	0.00	0.00	0.00	0.00	0.00	0.00	0.01	0.00	0.00	0.00	0.00	0.00	0.00	0.00	0.00	0.00	0.01	0.00	0.00
Ca	0.01	0.01	0.01	0.00	0.01	0.01	0.01	0.02	0.00	0.01	0.01	0.00	0.02	0.00	0.02	0.02	0.01	0.01	0.00	0.02
Na	0.46	0.44	0.40	0.32	0.44	0.40	0.43	0.70	0.53	0.52	0.53	0.44	0.64	0.36	0.66	0.58	0.39	0.41	0.49	0.36
K	3.42	3.44	3.46	3.56	3.42	3.47	3.44	3.18	3.37	3.38	3.35	3.43	3.23	3.50	3.21	3.27	3.44	3.43	3.43	3.48
Total	19.51	19.54	19.51	19.52	19.53	19.51	19.55	19.69	19.58	19.63	19.59	19.54	19.58	19.52	19.60	19.54	19.52	19.51	19.60	19.54
An	0.27	0.23	0.28	0.00	0.20	0.24	0.21	0.52	0.09	0.15	0.25	0.11	0.42	0.11	0.42	0.47	0.28	0.33	0.12	0.39
Ab	11.87	11.40	10.35	8.29	11.30	10.41	11.03	18.02	13.52	13.26	13.65	11.31	16.45	9.20	16.92	15.04	10.24	10.71	12.41	9.40
Or	87.87	88.37	89.37	91.71	88.50	89.35	88.76	81.46	86.39	86.59	86.10	88.58	83.13	90.69	82.66	84.49	89.49	88.96	87.47	90.21
Total	100.00	100.00	100.00	100.00	100.00	100.00	100.00	100.00	100.00	100.00	100.00	100.00	100.00	100.00	100.00	100.00	100.00	100.00	100.00	100.00

Appendix 4.2.1: Representative mineral chemistry for alkali-feldspar

	DA13-076-2.2	DA13-076-2.3	DA13-076-2.4	DA13-076-2.5	DA13-076-2.6	DA13-076-2.7	DA13-076-2.8	DA13-076-2.9	DA13-076-2.10	DA13-076-2.11	DA13-076-4.1	DA13-076-4.2	DA13-076-4.3	DA13-076-4.4	DA13-076-4.5	DA13-076-8.1	DA13-076-8.2	DA13-076-8.3	DA13-076-8.4	DA13-076-8.5
SiO_2	65.19	64.22	65.62	67.86	64.98	64.63	65.28	64.47	64.63	64.55	64.46	64.46	64.65	64.28	64.43	64.69	65.72	64.94	64.19	61.12
TiO_2	0.00	0.00	0.01	0.02	0.02	0.00	0.01	0.00	0.01	0.02	0.01	0.00	0.01	0.02	0.01	0.00	0.00	0.01	0.00	0.01
Al_2O_3	18.05	18.14	18.43	19.95	18.27	18.05	18.19	17.97	18.01	17.97	18.01	17.85	17.85	17.71	17.69	18.02	18.89	18.02	18.12	17.26
Cr_2O_3	0.03	0.00	0.03	0.00	0.00	0.01	0.00	0.04	0.03	0.02	0.02	0.00	0.02	0.03	0.00	0.01	0.00	0.01	0.01	0.00
FeOT	0.03	0.01	0.03	0.09	0.02	0.01	0.01	0.02	0.03	0.02	0.04	0.01	0.01	0.02	0.01	0.04	0.05	0.03	0.02	0.06
MnO	0.00	0.01	0.00	0.00	0.00	0.02	0.00	0.00	0.02	0.01	0.00	0.01	0.00	0.02	0.00	0.02	0.00	0.01	0.01	0.00
MgO	0.00	0.01	0.01	0.13	0.00	0.01	0.00	0.00	0.00	0.00	0.02	0.01	0.00	0.00	0.00	0.00	0.02	0.01	0.02	0.01
BaO	0.49	0.52	0.42	0.50	0.43	0.48	0.34	0.55	0.52	0.60	0.55	0.45	0.56	0.56	0.50	0.52	0.42	0.57	0.55	0.49
CaO	0.08	0.08	0.18	0.16	0.18	0.07	0.14	0.06	0.09	0.05	0.04	0.04	0.02	0.03	0.03	0.12	0.43	0.01	0.02	0.21
Na_2O	1.77	1.61	3.44	2.81	2.57	2.53	2.43	1.41	2.08	1.45	1.54	1.22	1.14	1.21	1.46	2.20	3.85	1.08	1.13	1.99
K_2O	14.19	14.13	11.42	11.98	12.51	12.90	13.18	14.42	13.60	14.37	14.35	14.53	14.84	14.70	14.54	13.37	10.77	15.02	14.75	13.41
Total	99.32	98.18	99.14	102.86	98.54	98.18	99.24	98.34	98.44	98.43	98.45	98.12	98.51	97.97	98.16	98.44	99.70	99.10	98.24	94.06
Si	11.92	11.74	12.00	12.41	11.88	11.82	11.93	11.79	11.81	11.80	11.78	11.79	11.82	11.75	11.78	11.83	12.02	11.87	11.74	11.17
Ti	0.00	0.00	0.00	0.00	0.00	0.00	0.00	0.00	0.00	0.00	0.00	0.00	0.00	0.00	0.00	0.00	0.00	0.00	0.00	0.00
Al	3.89	3.91	3.97	4.30	3.94	3.89	3.92	3.87	3.88	3.87	3.88	3.85	3.85	3.82	3.81	3.88	4.07	3.88	3.90	3.72
Fe^{2+}	0.00	0.00	0.01	0.01	0.00	0.00	0.00	0.00	0.00	0.00	0.01	0.00	0.00	0.00	0.00	0.01	0.01	0.00	0.00	0.01
Ca	0.02	0.01	0.04	0.03	0.03	0.01	0.03	0.01	0.02	0.01	0.01	0.01	0.00	0.01	0.01	0.02	0.08	0.00	0.00	0.04
Na	0.63	0.57	1.22	1.00	0.91	0.90	0.86	0.50	0.74	0.51	0.55	0.43	0.40	0.43	0.52	0.78	1.36	0.38	0.40	0.70
K	3.31	3.29	2.66	2.79	2.92	3.01	3.07	3.36	3.17	3.35	3.35	3.39	3.46	3.43	3.39	3.12	2.51	3.50	3.44	3.13
Total	19.77	19.53	19.89	20.54	19.68	19.62	19.82	19.53	19.63	19.55	19.57	19.46	19.53	19.44	19.51	19.64	20.05	19.65	19.49	18.78
An	0.41	0.38	0.90	0.83	0.89	0.34	0.68	0.29	0.45	0.27	0.21	0.22	0.08	0.17	0.16	0.62	2.14	0.03	0.10	1.05
Ab	15.91	14.72	31.11	26.07	23.54	22.88	21.71	12.91	18.80	13.24	13.99	11.27	10.44	11.09	13.22	19.86	34.43	9.81	10.43	18.19
Or	83.68	84.90	67.99	73.09	75.56	76.77	77.61	86.81	80.74	86.49	85.80	88.51	89.48	88.74	86.63	79.52	63.42	90.15	89.47	80.76
Total	100.00	100.00	100.00	100.00	100.00	100.00	100.00	100.00	100.00	100.00	100.00	100.00	100.00	100.00	100.00	100.00	100.00	100.00	100.00	100.00

Appendix 4.2.1: Representative mineral chemistry for alkali-feldspar

	DA13-076-8.6	DA13-076-8.7	DA13-076-8.8	DA13-076-8.9	DA13-076-8.10	DA13-076-8.11	DA13-076-8.12	DA13-077-2.1	DA13-077-2.2	DA13-077-2.3	DA13-077-2.4	DA13-077-2.5	DA13-077-2.6	DA13-077-2.7	DA13-077-2.8	DA13-077-2.9	DA13-077-2.10	DA13-077-2.11	DA13-077-2.12
SiO_2	64.72	66.17	64.59	65.95	65.91	66.44	63.38	65.41	65.38	65.50	64.64	64.87	65.68	64.56	64.86	64.73	64.69	64.69	64.59
TiO_2	0.00	0.02	0.01	0.03	0.00	0.03	0.01	0.00	0.00	0.00	0.01	0.00	0.01	0.01	0.03	0.00	0.01	0.02	0.01
Al_2O_3	18.07	18.89	18.17	18.26	18.42	18.77	17.68	18.39	18.35	18.22	17.96	17.99	18.14	19.07	17.85	18.00	17.83	17.88	17.92
Cr_2O_3	0.00	0.02	0.00	0.00	0.00	0.00	0.00	0.00	0.01	0.00	0.00	0.00	0.00	0.00	0.03	0.00	0.01	0.04	0.04
FeOT	0.02	0.02	0.05	0.02	0.01	0.03	0.03	0.01	0.00	0.00	0.02	0.00	0.00	0.00	0.00	0.01	0.02	0.01	0.02
MnO	0.00	0.00	0.01	0.05	0.00	0.00	0.00	0.01	0.03	0.00	0.00	0.00	0.01	0.00	0.00	0.00	0.02	0.02	0.05
MgO	0.00	0.01	0.00	0.00	0.01	0.01	0.01	0.00	0.01	0.00	0.01	0.00	0.00	0.00	0.01	0.00	0.02	0.01	0.00
BaO	0.49	0.43	0.46	0.49	0.53	0.58	0.48	0.18	0.24	0.25	0.23	0.22	0.17	0.15	0.25	0.18	0.21	0.24	0.27
CaO	0.11	0.45	0.21	0.06	0.05	0.05	0.06	0.05	0.05	0.03	0.03	0.04	0.04	0.02	0.03	0.03	0.04	0.02	0.03
Na_2O	1.91	2.47	2.32	1.85	1.22	1.38	1.67	1.09	1.00	2.00	0.80	0.95	1.70	1.14	1.09	0.90	0.92	0.83	1.04
K_2O	13.86	12.97	13.04	14.10	14.67	14.41	14.02	14.84	15.03	13.65	15.34	15.12	14.14	14.87	14.95	15.35	15.26	15.33	14.90
Total	98.69	100.97	98.40	100.27	100.29	101.10	96.86	99.80	99.81	99.40	98.79	98.98	99.71	99.68	98.81	99.01	98.77	98.77	98.51
Si	11.83	12.10	11.81	12.06	12.05	12.15	11.59	11.96	11.95	11.98	11.82	11.86	12.01	11.80	11.86	11.83	11.83	11.83	11.81
Ti	0.00	0.00	0.00	0.00	0.00	0.00	0.00	0.00	0.00	0.00	0.00	0.00	0.00	0.00	0.00	0.00	0.00	0.00	0.00
Al	3.89	4.07	3.92	3.94	3.97	4.04	3.81	3.96	3.95	3.92	3.87	3.88	3.91	4.11	3.85	3.88	3.84	3.85	3.86
Fe^{2+}	0.00	0.00	0.01	0.00	0.00	0.00	0.00	0.00	0.00	0.00	0.00	0.00	0.00	0.00	0.00	0.00	0.00	0.00	0.00
Ca	0.02	0.09	0.04	0.01	0.01	0.01	0.01	0.01	0.01	0.01	0.01	0.01	0.01	0.00	0.01	0.01	0.01	0.00	0.01
Na	0.68	0.87	0.82	0.66	0.43	0.49	0.59	0.39	0.36	0.71	0.28	0.34	0.60	0.40	0.39	0.32	0.33	0.29	0.37
K	3.23	3.02	3.04	3.29	3.42	3.36	3.27	3.46	3.50	3.18	3.58	3.53	3.30	3.47	3.49	3.58	3.56	3.57	3.48
Total	19.66	20.16	19.64	19.95	19.88	20.06	19.28	19.78	19.78	19.80	19.56	19.61	19.83	19.79	19.59	19.61	19.57	19.55	19.52
An	0.53	2.19	1.07	0.29	0.28	0.24	0.30	0.27	0.24	0.14	0.15	0.21	0.21	0.12	0.15	0.16	0.22	0.08	0.15
Ab	17.21	21.94	21.04	16.56	11.17	12.70	15.29	10.01	9.20	18.15	7.33	8.72	15.40	10.38	10.00	8.15	8.41	7.58	9.54
Or	82.26	75.87	77.89	83.15	88.56	87.05	84.40	89.72	90.56	81.70	92.52	91.07	84.39	89.50	89.85	91.69	91.37	92.34	90.31
Total	100.00	100.00	100.00	100.00	100.00	100.00	100.00	100.00	100.00	100.00	100.00	100.00	100.00	100.00	100.00	100.00	100.00	100.00	100.00

Appendix 4.2.1: Representative mineral chemistry for alkali-feldspar

	DA13-077-2.13	DA13-077-2.14	DA13-077-2.15	DA13-083-1.1	DA13-083-1.2	DA13-083-1.3	DA13-083-1.4	DA13-083-1.5	DA13-083-1.6	DA13-083-1.7	DA13-083-1.8	DA13-083-1.9	DA13-083-1.10	DA13-083-1.11	DA13-083-1.12	DA13-083-5.1	DA13-083-5.2	DA13-083-5.3	DA13-083-5.4
SiO_2	64.98	64.52	64.71	65.24	64.91	57.96	64.88	64.70	59.73	65.45	64.82	65.10	62.66	64.57	65.53	65.11	64.59	64.54	64.25
TiO_2	0.00	0.01	0.00	0.02	0.01	0.02	0.03	0.01	0.02	0.02	0.01	0.01	0.01	0.02	0.01	0.02	0.02	0.01	0.01
Al_2O_3	17.98	17.76	17.94	18.18	17.90	15.85	17.87	17.97	19.78	18.18	17.83	18.49	17.69	17.87	18.19	18.12	17.81	17.82	17.68
Cr_2O_3	0.00	0.00	0.02	0.00	0.00	0.00	0.01	0.00	0.02	0.00	0.00	0.00	0.02	0.00	0.00	0.01	0.02	0.03	0.01
FeOT	0.02	0.03	0.04	0.01	0.04	0.05	0.00	0.06	0.03	0.05	0.00	0.15	0.03	0.02	0.02	0.00	0.06	0.02	0.07
MnO	0.04	0.01	0.00	0.00	0.05	0.00	0.02	0.00	0.00	0.02	0.00	0.00	0.00	0.00	0.00	0.01	0.00	0.00	0.00
MgO	0.00	0.00	0.00	0.00	0.00	0.00	0.00	0.00	0.04	0.00	0.00	0.00	0.01	0.01	0.01	0.01	0.00	0.00	0.00
BaO	0.22	0.17	0.20	0.28	0.28	0.27	0.29	0.29	0.34	0.35	0.30	0.19	0.30	0.36	0.23	0.27	0.30	0.25	0.29
CaO	0.00	0.00	0.01	0.16	0.02	0.01	0.02	0.06	0.10	0.12	0.03	0.51	0.06	0.00	0.09	0.08	0.02	0.01	0.00
Na_2O	0.89	0.72	1.02	2.31	1.51	1.40	1.25	2.35	1.07	2.21	1.23	3.21	1.00	0.71	2.01	1.65	1.40	0.90	1.02
K_2O	15.41	15.53	15.25	13.22	14.50	12.52	14.59	13.03	14.09	13.46	14.58	11.42	14.90	15.29	13.48	14.19	14.63	15.09	15.06
Total	99.27	98.57	98.96	99.15	98.90	87.81	98.65	98.19	94.82	99.50	98.50	98.89	96.36	98.47	99.32	99.18	98.53	98.41	98.08
Si	11.88	11.80	11.83	11.93	11.87	10.60	11.86	11.83	10.92	11.97	11.85	11.90	11.46	11.80	11.98	11.90	11.81	11.80	11.75
Ti	0.00	0.00	0.00	0.00	0.00	0.00	0.00	0.00	0.00	0.00	0.00	0.00	0.00	0.00	0.00	0.00	0.00	0.00	0.00
Al	3.87	3.83	3.87	3.92	3.86	3.41	3.85	3.87	4.26	3.92	3.84	3.98	3.81	3.85	3.92	3.90	3.84	3.84	3.81
Fe^{2+}	0.00	0.01	0.01	0.00	0.01	0.01	0.00	0.01	0.00	0.01	0.00	0.02	0.01	0.00	0.00	0.00	0.01	0.00	0.01
Ca	0.00	0.00	0.00	0.03	0.00	0.00	0.00	0.01	0.02	0.02	0.00	0.10	0.01	0.00	0.02	0.02	0.00	0.00	0.00
Na	0.31	0.25	0.36	0.82	0.54	0.50	0.44	0.83	0.38	0.78	0.44	1.14	0.35	0.25	0.71	0.59	0.50	0.32	0.36
K	3.59	3.62	3.56	3.08	3.38	2.92	3.40	3.04	3.29	3.14	3.40	2.66	3.47	3.57	3.14	3.31	3.41	3.52	3.51
Total	19.66	19.50	19.62	19.78	19.65	17.44	19.57	19.60	18.87	19.84	19.53	19.81	19.11	19.48	19.77	19.72	19.57	19.49	19.44
An	0.00	0.01	0.03	0.81	0.12	0.05	0.12	0.31	0.53	0.59	0.13	2.57	0.31	0.00	0.45	0.41	0.10	0.05	0.01
Ab	8.06	6.55	9.19	20.80	13.66	14.52	11.53	21.45	10.26	19.88	11.35	29.16	9.24	6.56	18.37	14.98	12.68	8.30	9.30
Or	91.94	93.44	90.78	78.39	86.21	85.43	88.34	78.25	89.21	79.52	88.52	68.27	90.45	93.44	81.18	84.61	87.22	91.65	90.69
Total	100.00	100.00	100.00	100.00	100.00	100.00	100.00	100.00	100.00	100.00	100.00	100.00	100.00	100.00	100.00	100.00	100.00	100.00	100.00

Appendix 4.2.1: Representative mineral chemistry for alkali-feldspar

	DA13-083-5.5	DA13-083-5.6	DA13-083-5.7	DA13-083-5.8	DA13-083-5.9	DA13-083-5.10
SiO_2	64.70	64.57	64.70	64.42	64.99	65.00
TiO_2	0.00	0.00	0.00	0.03	0.02	0.01
Al_2O_3	17.78	17.75	17.89	17.81	17.80	18.06
Cr_2O_3	0.03	0.01	0.02	0.04	0.04	0.00
FeOT	0.02	0.02	0.02	0.05	0.01	0.04
MnO	0.00	0.00	0.00	0.01	0.00	0.00
MgO	0.00	0.00	0.01	0.00	0.00	0.00
BaO	0.24	0.30	0.33	0.28	0.26	0.31
CaO	0.00	0.01	0.03	0.00	0.02	0.02
Na_2O	0.94	0.95	1.15	0.95	1.38	1.24
K_2O	15.16	15.30	14.94	15.24	14.61	14.83
Total	98.61	98.60	98.73	98.49	98.83	99.19
Si	11.83	11.80	11.83	11.78	11.88	11.88
Ti	0.00	0.00	0.00	0.00	0.00	0.00
Al	3.83	3.82	3.85	3.84	3.83	3.89
Fe^{2+}	0.00	0.00	0.00	0.01	0.00	0.01
Ca	0.00	0.00	0.01	0.00	0.00	0.00
Na	0.33	0.34	0.41	0.34	0.49	0.44
K	3.53	3.57	3.48	3.55	3.41	3.46
Total	19.53	19.54	19.58	19.52	19.62	19.68
An	0.02	0.05	0.17	0.00	0.11	0.12
Ab	8.60	8.59	10.48	8.66	12.55	11.28
Or	91.38	91.36	89.36	91.34	87.34	88.60
Total	100.00	100.00	100.00	100.00	100.00	100.00

Appendix 4.2.2: Representative mineral chemistry for plagioclase feldspar

	DA13-029-6.1	DA13-029-6.2	DA13-029-6.3	DA13-029-6.4	DA13-029-6.5	DA13-029-6.6	DA13-029-6.7	DA13-029-6.8	DA13-029-6.9	DA13-029-6.10	DA13-029-8.1	DA13-029-8.2	DA13-029-8.3	DA13-029-8.4	DA13-029-8.5	DA13-029-8.6	DA13-029-8.7	DA13-029-8.8	DA13-029-8.9	DA13-029-8.10
SiO_2	67.38	66.59	66.21	66.67	66.86	69.01	66.69	67.49	67.00	64.56	68.66	66.11	66.88	66.25	65.81	67.72	66.35	65.80	66.08	69.03
TiO_2	0.01	0.00	0.01	0.00	0.02	0.00	0.01	0.01	0.00	0.00	0.01	0.00	0.00	0.00	0.00	0.00	0.00	0.00	0.01	0.02
Al_2O_3	21.50	21.08	21.09	21.13	20.67	21.13	21.27	21.25	21.45	20.96	19.75	20.02	20.80	20.85	20.93	20.90	20.48	20.45	20.52	20.49
Cr_2O_3	0.00	0.01	0.03	0.01	0.02	0.00	0.00	0.00	0.00	0.01	0.02	0.00	0.00	0.00	0.00	0.00	0.04	0.02	0.00	0.00
FeOT	0.02	0.04	0.00	0.01	0.00	0.31	0.02	0.03	0.05	1.72	0.10	0.20	0.09	0.03	0.04	0.05	0.12	0.07	0.10	0.57
MnO	0.00	0.00	0.01	0.00	0.01	0.00	0.00	0.00	0.00	0.00	0.01	0.01	0.00	0.00	0.00	0.00	0.04	0.04	0.01	0.01
MgO	0.00	0.00	0.01	0.00	0.00	0.01	0.00	0.00	0.00	0.16	0.02	0.02	0.00	0.00	0.01	0.00	0.00	0.00	0.01	0.02
BaO	0.04	0.02	0.04	0.02	0.00	0.00	0.01	0.00	0.03	0.02	0.04	0.03	0.00	0.02	0.02	0.01	0.05	0.05	0.06	0.00
CaO	2.20	2.02	1.90	1.92	1.64	1.20	2.22	1.88	2.16	2.13	0.56	1.48	1.95	2.10	2.20	1.78	1.83	1.98	1.99	0.95
Na_2O	10.67	10.59	10.47	10.80	10.33	10.96	10.54	10.81	10.66	10.04	11.41	10.87	10.83	10.66	10.59	11.00	10.74	10.78	10.69	11.59
K_2O	0.24	0.24	0.25	0.23	0.18	0.16	0.24	0.20	0.19	0.25	0.08	0.12	0.22	0.15	0.10	0.17	0.21	0.23	0.14	0.06
Total	102.05	100.59	100.00	100.80	99.73	102.79	100.98	101.67	101.55	99.85	100.65	98.87	100.77	100.05	99.69	101.63	99.87	99.42	99.60	102.74
Si	12.32	12.17	12.10	12.19	12.22	12.62	12.19	12.34	12.25	11.80	12.55	12.09	12.23	12.11	12.03	12.38	12.13	12.03	12.08	12.62
Ti	0.00	0.00	0.00	0.00	0.00	0.00	0.00	0.00	0.00	0.00	0.00	0.00	0.00	0.00	0.00	0.00	0.00	0.00	0.00	0.00
Al	4.63	4.54	4.54	4.55	4.45	4.55	4.58	4.58	4.62	4.51	4.26	4.31	4.48	4.49	4.51	4.50	4.41	4.41	4.42	4.42
Fe^{2+}	0.00	0.01	0.00	0.00	0.00	0.05	0.00	0.00	0.01	0.26	0.02	0.03	0.01	0.01	0.01	0.01	0.02	0.01	0.02	0.09
Ca	0.43	0.40	0.37	0.38	0.32	0.24	0.43	0.37	0.42	0.42	0.11	0.29	0.38	0.41	0.43	0.35	0.36	0.39	0.39	0.19
Na	3.78	3.75	3.71	3.83	3.66	3.89	3.73	3.83	3.78	3.56	4.04	3.85	3.84	3.78	3.75	3.90	3.81	3.82	3.79	4.11
K	0.06	0.05	0.06	0.05	0.04	0.04	0.06	0.05	0.05	0.06	0.02	0.03	0.05	0.04	0.02	0.04	0.05	0.05	0.03	0.01
Total	21.22	20.93	20.79	21.00	20.70	21.38	21.00	21.17	21.13	20.61	21.00	20.60	20.99	20.83	20.76	21.18	20.78	20.71	20.73	21.43
An	10.09	9.43	9.00	8.82	8.00	5.65	10.27	8.69	9.94	10.33	2.65	6.95	8.93	9.72	10.26	8.12	8.52	9.09	9.25	4.34
Ab	88.62	89.27	89.62	89.89	90.96	93.44	88.40	90.24	88.99	88.24	96.92	92.38	89.88	89.44	89.17	90.98	90.29	89.67	89.97	95.34
Or	1.29	1.31	1.38	1.29	1.04	0.91	1.32	1.07	1.07	1.43	0.43	0.66	1.19	0.84	0.57	0.90	1.19	1.24	0.78	0.32
Total	100	100	100	100	100	100	100	100	100	100	100	100	100	100	100	100	100	100	100	100

Appendix 4.2.2: Representative mineral chemistry for plagioclase feldspar

	DA13-040-10.1	DA13-040-10.2	DA13-040-10.3	DA13-040-10.4	DA13-040-10.5	DA13-040-10.6	DA13-040-10.7	DA13-040-10.8	DA13-040-10.9	DA13-040-10.10	DA13-040-9.1	DA13-040-9.2	DA13-040-9.3	DA13-040-9.4	DA13-040-9.5	DA13-040-9.6	DA13-040-9.7	DA13-040-9.8	DA13-040-9.9
SiO_2	69.33	68.24	70.24	68.04	68.00	70.37	70.65	69.75	65.28	68.92	65.71	68.85	63.82	69.85	64.91	67.00	71.30	70.45	68.68
TiO_2	0.00	0.01	0.01	0.00	0.01	0.00	0.00	0.01	0.00	0.01	0.01	0.00	0.00	0.00	0.00	0.00	0.00	0.00	0.00
Al_2O_3	20.40	20.31	20.91	20.42	20.43	20.77	20.68	20.81	21.62	20.21	20.00	20.28	21.76	20.95	21.39	19.77	21.02	20.64	20.45
Cr_2O_3	0.03	0.00	0.00	0.00	0.01	0.00	0.00	0.01	0.02	0.00	0.00	0.03	0.01	0.01	0.00	0.00	0.00	0.02	0.00
FeOT	0.20	0.15	0.12	0.25	0.21	0.18	0.24	0.18	0.22	0.25	0.23	0.26	0.28	0.25	0.29	0.29	0.23	0.19	0.15
MnO	0.02	0.00	0.01	0.01	0.00	0.01	0.04	0.00	0.00	0.00	0.01	0.03	0.00	0.00	0.00	0.00	0.00	0.00	0.00
MgO	0.00	0.00	0.02	0.02	0.02	0.01	0.00	0.00	0.07	0.02	0.05	0.00	0.09	0.01	0.06	0.01	0.00	0.00	0.01
BaO	0.00	0.01	0.02	0.00	0.00	0.03	0.00	0.04	0.01	0.00	0.00	0.00	0.00	0.00	0.00	0.01	0.00	0.02	0.02
CaO	0.06	0.10	0.05	0.15	0.10	0.08	0.04	0.05	0.15	0.05	0.10	0.04	0.14	0.03	0.10	0.08	0.04	0.03	0.11
Na_2O	11.66	10.80	11.94	10.88	11.33	11.32	11.66	12.03	9.78	11.17	11.44	11.80	10.79	12.13	11.18	11.68	12.34	11.91	11.76
K_2O	0.21	0.21	0.11	0.13	0.20	0.20	0.16	0.08	0.22	0.19	0.17	0.19	0.27	0.15	0.20	0.21	0.18	0.12	0.15
Total	101.90	99.84	103.42	99.90	100.30	102.96	103.47	102.95	97.37	100.80	97.71	101.47	97.17	103.38	98.12	99.05	105.12	103.38	101.33
Si	13.31	13.10	13.48	13.06	13.05	13.51	13.56	13.39	12.53	13.23	12.61	13.22	12.25	13.41	12.46	12.86	13.69	13.52	13.18
Ti	0.00	0.00	0.00	0.00	0.00	0.00	0.00	0.00	0.00	0.00	0.00	0.00	0.00	0.00	0.00	0.00	0.00	0.00	0.00
Al	4.39	4.38	4.51	4.40	4.40	4.47	4.46	4.48	4.66	4.35	4.31	4.37	4.69	4.51	4.61	4.26	4.53	4.45	4.41
Fe^{2+}	0.03	0.02	0.02	0.04	0.03	0.03	0.04	0.03	0.03	0.04	0.03	0.04	0.04	0.04	0.05	0.04	0.04	0.03	0.02
Ca	0.01	0.02	0.01	0.03	0.02	0.02	0.01	0.01	0.03	0.01	0.02	0.01	0.03	0.01	0.02	0.02	0.01	0.01	0.02
Na	4.13	3.83	4.23	3.86	4.01	4.01	4.13	4.26	3.47	3.96	4.05	4.18	3.82	4.30	3.96	4.14	4.37	4.22	4.17
K	0.05	0.05	0.03	0.03	0.05	0.05	0.04	0.02	0.05	0.04	0.04	0.04	0.06	0.04	0.05	0.05	0.04	0.03	0.04
Total	21.93	21.40	22.27	21.41	21.57	22.08	22.23	22.19	20.77	21.63	21.07	21.86	20.90	22.30	21.14	21.37	22.68	22.25	21.84
An	0.28	0.49	0.22	0.75	0.49	0.37	0.19	0.21	0.81	0.22	0.46	0.17	0.72	0.14	0.46	0.38	0.18	0.14	0.50
Ab	98.57	98.23	99.18	98.48	98.35	98.49	98.92	99.34	97.71	98.68	98.58	98.80	97.69	99.05	98.40	98.47	98.85	99.19	98.65
Or	1.16	1.28	0.59	0.77	1.16	1.14	0.89	0.45	1.48	1.09	0.97	1.03	1.59	0.81	1.14	1.15	0.97	0.68	0.85
Total	100	100	100	100	100	100	100	100	100	100	100	100	100	100	100	100	100	100	100

Appendix 4.2.2: Representative mineral chemistry for plagioclase feldspar

	DA13-040-9.10	DA13-049-1.1	DA13-049-1.2	DA13-049-1.3	DA13-049-1.4	DA13-049-1.5	DA13-049-1.6	DA13-049-1.7	DA13-049-1.8	DA13-049-1.9	DA13-049-1.10	DA13-049-5.1	DA13-049-5.2	DA13-049-5.3	DA13-049-5.4	DA13-049-5.5	DA13-049-5.6	DA13-049-5.7	DA13-049-5.8	DA13-049-5.9
SiO_2	68.50	63.69	64.45	64.52	65.15	65.48	65.30	65.61	65.02	64.70	64.48	64.11	64.58	64.93	64.29	64.40	64.34	65.28	64.37	64.61
TiO_2	0.01	0.00	0.01	0.00	0.00	0.00	0.00	0.00	0.01	0.01	0.00	0.00	0.00	0.01	0.01	0.01	0.00	0.01	0.01	0.00
Al_2O_3	19.94	21.57	21.81	21.70	21.44	21.19	21.14	20.71	21.57	21.99	21.67	21.86	21.83	21.93	21.75	21.95	21.92	21.41	21.88	21.97
Cr_2O_3	0.00	0.00	0.00	0.00	0.00	0.00	0.03	0.00	0.00	0.00	0.00	0.03	0.04	0.02	0.00	0.00	0.03	0.03	0.00	0.01
FeOT	0.14	0.06	0.06	0.05	0.04	0.03	0.06	0.04	0.06	0.06	0.05	0.10	0.12	0.12	0.06	0.10	0.09	0.12	0.14	0.13
MnO	0.00	0.00	0.00	0.01	0.00	0.00	0.01	0.02	0.00	0.00	0.00	0.00	0.01	0.01	0.02	0.00	0.00	0.00	0.00	0.03
MgO	0.00	0.00	0.01	0.00	0.00	0.00	0.00	0.00	0.00	0.01	0.02	0.01	0.00	0.00	0.00	0.00	0.01	0.00	0.00	0.00
BaO	0.00	0.01	0.00	0.06	0.00	0.01	0.00	0.00	0.00	0.00	0.00	0.00	0.02	0.01	0.03	0.01	0.00	0.02	0.00	0.00
CaO	0.07	3.25	3.30	3.18	2.60	2.45	2.65	2.30	2.79	3.18	3.22	3.29	3.31	3.31	3.29	3.32	3.30	2.81	3.36	3.37
Na_2O	11.73	10.16	9.96	9.81	10.32	10.50	10.23	10.47	10.18	10.08	9.96	9.95	9.94	9.86	9.80	10.12	9.81	10.30	9.80	9.81
K_2O	0.15	0.14	0.13	0.18	0.18	0.19	0.15	0.15	0.16	0.11	0.16	0.23	0.24	0.23	0.25	0.23	0.22	0.27	0.22	0.24
Total	100.55	98.88	99.72	99.51	99.73	99.85	99.57	99.29	99.80	100.14	99.55	99.58	100.09	100.43	99.51	100.13	99.72	100.25	99.78	100.17
Si	13.15	11.64	11.78	11.80	11.91	11.97	11.94	11.99	11.89	11.83	11.79	11.72	11.81	11.87	11.75	11.77	11.76	11.94	11.77	11.81
Ti	0.00	0.00	0.00	0.00	0.00	0.00	0.00	0.00	0.00	0.00	0.00	0.00	0.00	0.00	0.00	0.00	0.00	0.00	0.00	0.00
Al	4.30	4.65	4.70	4.67	4.62	4.56	4.56	4.46	4.65	4.74	4.67	4.71	4.70	4.72	4.69	4.73	4.72	4.61	4.71	4.73
Fe^{2+}	0.02	0.01	0.01	0.01	0.01	0.01	0.01	0.01	0.01	0.01	0.01	0.02	0.02	0.02	0.01	0.01	0.01	0.02	0.02	0.02
Ca	0.01	0.64	0.65	0.62	0.51	0.48	0.52	0.45	0.55	0.62	0.63	0.64	0.65	0.65	0.65	0.65	0.65	0.55	0.66	0.66
Na	4.16	3.60	3.53	3.48	3.66	3.72	3.63	3.71	3.61	3.57	3.53	3.53	3.52	3.49	3.47	3.59	3.48	3.65	3.47	3.48
K	0.04	0.03	0.03	0.04	0.04	0.04	0.04	0.03	0.04	0.03	0.04	0.05	0.06	0.05	0.06	0.05	0.05	0.06	0.05	0.06
Total	21.68	20.57	20.70	20.62	20.75	20.79	20.68	20.66	20.74	20.80	20.66	20.67	20.76	20.81	20.63	20.81	20.67	20.83	20.69	20.76
An	0.34	14.90	15.35	15.03	12.12	11.30	12.42	10.73	13.02	14.75	15.04	15.25	15.34	15.47	15.45	15.14	15.47	12.88	15.76	15.75
Ab	98.81	84.32	83.94	83.94	86.89	87.64	86.72	88.45	86.12	84.62	84.06	83.48	83.36	83.24	83.16	83.62	83.28	85.64	83.02	82.91
Or	0.85	0.78	0.71	1.03	0.99	1.06	0.86	0.82	0.87	0.63	0.90	1.27	1.31	1.30	1.39	1.25	1.25	1.48	1.22	1.34
Total	100	100	100	100	100	100	100	100	100	100	100	100	100	100	100	100	100	100	100	100

Appendix 4.2.2: Representative mineral chemistry for plagioclase feldspar

	DA13-049-5.10	DA13-049-5.11	DA13-049-5.12	DA13-049-5.13	DA13-049-5.14	DA13-049-5.15	DA13-055-5.1	DA13-055-5.2	DA13-055-5.3	DA13-055-5.4	DA13-055-5.5	DA13-055-5.6	DA13-055-5.7	DA13-055-5.8	DA13-055-5.9	DA13-055-5.10	DA13-055-7.1	DA13-055-7.2	DA13-055-7.3
SiO_2	64.41	63.31	64.29	64.42	64.33	64.13	61.23	61.63	61.87	62.02	61.56	62.32	59.42	61.06	62.34	61.79	62.98	60.58	60.86
TiO_2	0.00	0.00	0.02	0.00	0.01	0.00	0.01	0.01	0.00	0.02	0.00	0.01	0.02	0.08	0.00	0.01	0.00	0.01	0.00
Al_2O_3	21.83	21.49	21.82	21.87	21.83	21.93	24.25	23.67	24.27	24.30	24.28	24.38	24.68	24.32	24.31	24.10	24.06	24.17	24.47
Cr_2O_3	0.00	0.03	0.00	0.02	0.00	0.00	0.00	0.00	0.03	0.00	0.00	0.00	0.00	0.00	0.00	0.02	0.02	0.00	0.00
FeOT	0.12	0.10	0.11	0.09	0.13	0.06	0.03	0.03	0.01	0.05	0.05	0.08	0.08	0.25	0.04	0.04	0.10	0.00	0.02
MnO	0.01	0.00	0.00	0.00	0.00	0.01	0.02	0.00	0.00	0.00	0.02	0.03	0.03	0.00	0.02	0.01	0.00	0.00	0.00
MgO	0.00	0.01	0.01	0.00	0.01	0.00	0.00	0.01	0.00	0.00	0.00	0.03	0.00	0.00	0.00	0.01	0.00	0.00	0.00
BaO	0.01	0.00	0.02	0.00	0.00	0.02	0.01	0.01	0.02	0.04	0.01	0.03	0.07	0.03	0.07	0.02	0.08	0.02	0.00
CaO	3.37	3.37	3.30	3.31	3.27	3.51	5.98	5.68	5.88	5.92	5.97	5.56	6.99	6.15	5.78	5.91	5.20	6.13	6.39
Na_2O	9.89	9.71	9.72	9.98	9.79	9.85	8.02	8.32	8.47	8.30	8.30	8.48	7.62	8.19	8.36	8.35	8.71	8.14	7.96
K_2O	0.23	0.24	0.22	0.23	0.23	0.24	0.16	0.10	0.15	0.15	0.16	0.08	0.16	0.19	0.14	0.19	0.07	0.12	0.14
Total	99.88	98.27	99.51	99.91	99.60	99.75	99.71	99.46	100.70	100.80	100.36	101.01	99.08	100.27	101.06	100.45	101.23	99.19	99.84
Si	11.78	11.58	11.75	11.78	11.76	11.72	11.19	11.27	11.31	11.34	11.25	11.39	10.86	11.16	11.40	11.30	11.51	11.08	11.13
Ti	0.00	0.00	0.00	0.00	0.00	0.00	0.00	0.00	0.00	0.00	0.00	0.00	0.00	0.01	0.00	0.00	0.00	0.00	0.00
Al	4.70	4.63	4.70	4.71	4.70	4.72	5.22	5.10	5.23	5.23	5.23	5.25	5.32	5.24	5.24	5.19	5.18	5.21	5.27
Fe^{2+}	0.02	0.02	0.02	0.01	0.02	0.01	0.00	0.00	0.00	0.01	0.01	0.01	0.01	0.04	0.01	0.01	0.01	0.00	0.00
Ca	0.66	0.66	0.65	0.65	0.64	0.69	1.17	1.11	1.15	1.16	1.17	1.09	1.37	1.20	1.13	1.16	1.02	1.20	1.25
Na	3.51	3.44	3.45	3.54	3.47	3.49	2.84	2.95	3.00	2.94	2.94	3.01	2.70	2.90	2.96	2.96	3.09	2.88	2.82
K	0.05	0.06	0.05	0.05	0.05	0.06	0.04	0.02	0.03	0.04	0.04	0.02	0.04	0.04	0.03	0.04	0.02	0.03	0.03
Total	20.72	20.38	20.62	20.74	20.65	20.69	20.47	20.46	20.73	20.72	20.64	20.78	20.30	20.60	20.77	20.66	20.84	20.40	20.51
An	15.65	15.87	15.61	15.30	15.38	16.21	28.94	27.25	27.49	28.03	28.19	26.46	33.33	29.00	27.43	27.82	24.71	29.21	30.47
Ab	83.09	82.77	83.13	83.44	83.33	82.45	70.14	72.17	71.68	71.11	70.89	73.07	65.74	69.96	71.77	71.13	74.90	70.11	68.76
Or	1.26	1.37	1.27	1.26	1.29	1.34	0.93	0.58	0.83	0.86	0.92	0.47	0.93	1.04	0.80	1.05	0.39	0.68	0.77
Total	100	100	100	100	100	100	100	100	100	100	100	100	100	100	100	100	100	100	100

Appendix 4.2.2: Representative mineral chemistry for plagioclase feldspar

	DA13-055-7.4	DA13-055-7.5	DA13-064-6.1	DA13-064-6.2	DA13-064-6.3	DA13-064-6.4	DA13-064-6.5	DA13-064-6.6	DA13-064-6.7	DA13-064-6.8	DA13-064-6.9	DA13-064-6.10	DA13-064-6.11	DA13-064-6.12	DA13-064-6.13	DA13-064-6.14	DA13-064-6.15	DA13-069-1.1	DA13-069-1.2	DA13-069-1.3
SiO_2	61.50	61.26	64.45	64.13	64.09	63.96	63.90	64.09	64.43	64.89	64.48	64.06	66.38	64.91	64.75	64.28	64.39	65.51	67.89	100.34
TiO_2	0.04	0.00	0.02	0.00	0.00	0.01	0.00	0.00	0.00	0.00	0.01	0.00	0.00	0.00	0.00	0.00	0.00	0.26	0.09	0.00
Al_2O_3	24.34	23.94	22.21	21.98	22.19	22.08	22.02	22.19	22.40	22.24	22.17	22.16	23.04	22.44	22.29	22.17	22.19	19.35	20.22	0.11
Cr_2O_3	0.01	0.02	0.00	0.00	0.00	0.00	0.05	0.04	0.00	0.01	0.01	0.00	0.01	0.01	0.00	0.02	0.04	0.00	0.01	0.00
FeOT	0.08	0.30	0.09	0.09	0.10	0.07	0.07	0.08	0.08	0.07	0.10	0.05	0.10	0.08	0.10	0.09	0.11	1.85	0.59	0.16
MnO	0.02	0.03	0.03	0.02	0.00	0.01	0.02	0.00	0.00	0.00	0.00	0.00	0.01	0.00	0.00	0.00	0.00	0.00	0.00	0.03
MgO	0.00	0.03	0.00	0.00	0.00	0.01	0.00	0.00	0.01	0.00	0.01	0.00	0.00	0.00	0.01	0.00	0.00	0.03	0.03	0.00
BaO	0.07	0.03	0.01	0.00	0.00	0.03	0.00	0.00	0.00	0.01	0.02	0.00	0.02	0.02	0.04	0.01	0.00	0.00	0.01	0.01
CaO	5.93	5.89	3.51	3.57	3.58	3.57	3.59	3.65	3.52	3.54	3.54	3.55	3.61	3.51	3.60	3.69	3.54	0.86	0.94	0.05
Na_2O	8.24	7.95	9.80	9.58	9.69	9.58	9.59	9.54	9.84	9.73	9.92	9.74	9.42	9.68	9.75	9.50	9.61	10.96	11.39	0.04
K_2O	0.16	0.24	0.23	0.21	0.22	0.25	0.25	0.25	0.20	0.20	0.19	0.23	0.22	0.21	0.24	0.23	0.18	0.13	0.11	0.04
Total	100.40	99.68	100.32	99.57	99.86	99.52	99.42	99.80	100.47	100.67	100.41	99.78	102.77	100.84	100.74	99.98	100.01	98.92	101.24	100.74
Si	11.24	11.20	11.78	11.72	11.72	11.69	11.68	11.72	11.78	11.86	11.79	11.71	12.14	11.87	11.84	11.75	11.77	11.98	12.41	18.34
Ti	0.01	0.00	0.00	0.00	0.00	0.00	0.00	0.00	0.00	0.00	0.00	0.00	0.00	0.00	0.00	0.00	0.00	0.04	0.01	0.00
Al	5.24	5.16	4.79	4.74	4.78	4.76	4.75	4.78	4.83	4.79	4.78	4.77	4.96	4.84	4.80	4.78	4.78	4.17	4.36	0.02
Fe^{2+}	0.01	0.05	0.01	0.01	0.01	0.01	0.01	0.01	0.01	0.01	0.02	0.01	0.01	0.01	0.02	0.01	0.02	0.28	0.09	0.02
Ca	1.16	1.15	0.69	0.70	0.70	0.70	0.70	0.72	0.69	0.69	0.69	0.70	0.71	0.69	0.70	0.72	0.69	0.17	0.18	0.01
Na	2.92	2.82	3.48	3.40	3.43	3.40	3.40	3.38	3.49	3.45	3.52	3.45	3.34	3.43	3.46	3.37	3.40	3.89	4.04	0.01
K	0.04	0.05	0.05	0.05	0.05	0.06	0.06	0.06	0.05	0.05	0.04	0.05	0.05	0.05	0.06	0.05	0.04	0.03	0.03	0.01
Total	20.62	20.43	20.80	20.62	20.70	20.62	20.60	20.67	20.84	20.85	20.84	20.69	21.21	20.88	20.87	20.69	20.71	20.55	21.12	18.43
An	28.18	28.64	16.30	16.88	16.74	16.82	16.88	17.22	16.30	16.55	16.31	16.55	17.26	16.48	16.71	17.44	16.75	4.10	4.32	28.89
Ab	70.88	69.99	82.43	81.93	82.03	81.78	81.74	81.39	82.59	82.31	82.68	82.18	81.48	82.32	81.95	81.25	82.25	95.18	95.05	42.21
Or	0.93	1.37	1.27	1.18	1.23	1.40	1.37	1.39	1.11	1.14	1.02	1.27	1.27	1.20	1.34	1.32	0.99	0.72	0.63	28.90
Total	100	100	100	100	100	100	100	100	100	100	100	100	100	100	100	100	100	100	100	100

Appendix 4.2.2: Representative mineral chemistry for plagioclase feldspar

	DA13-069-1.4	DA13-069-2.1	DA13-069-2.2	DA13-069-2.3	DA13-069-2.4	DA13-069-2.5	DA13-069-2.6	DA13-069-2.7	DA13-069-2.8	DA13-069-2.9	DA13-069-5.1	DA13-069-5.2	DA13-069-5.3	DA13-069-5.4	DA13-069-5.5	DA13-069-5.6	DA13-069-5.7	DA13-069-5.8	DA13-069-5.9	DA13-069-5.10
SiO_2	61.47	66.56	66.55	68.19	67.44	67.95	67.47	67.28	65.76	66.37	66.25	65.95	66.40	66.17	66.01	66.74	65.94	66.33	66.72	66.41
TiO_2	0.02	0.00	0.00	0.01	0.00	0.00	0.00	0.00	0.00	0.01	0.00	0.01	0.00	0.00	0.00	0.00	0.00	0.00	0.00	0.00
Al_2O_3	24.88	20.71	21.07	21.32	21.01	21.20	21.18	20.92	20.58	20.71	21.06	21.55	21.17	21.82	21.36	21.53	21.62	21.59	21.40	21.21
Cr_2O_3	0.00	0.02	0.01	0.02	0.02	0.00	0.00	0.01	0.00	0.00	0.00	0.00	0.03	0.00	0.01	0.02	0.00	0.00	0.02	0.00
FeOT	0.18	0.04	0.08	0.03	0.06	0.02	0.04	0.01	0.04	0.02	0.08	0.03	0.01	0.02	0.04	0.00	0.04	0.01	0.04	0.04
MnO	0.00	0.01	0.00	0.01	0.01	0.00	0.01	0.01	0.04	0.00	0.00	0.00	0.00	0.02	0.00	0.00	0.02	0.00	0.01	0.00
MgO	0.03	0.05	0.00	0.00	0.00	0.01	0.01	0.01	0.00	0.01	0.02	0.01	0.00	0.01	0.00	0.00	0.01	0.00	0.01	0.02
BaO	0.00	0.02	0.03	0.18	0.01	0.00	0.04	0.06	0.00	0.00	0.00	0.00	0.01	0.00	0.03	0.03	0.02	0.01	0.04	0.00
CaO	1.45	1.68	1.87	1.84	1.78	1.79	1.67	1.65	1.64	1.87	1.95	2.20	2.13	2.03	2.28	2.28	2.59	2.44	2.09	1.75
Na_2O	10.01	10.76	10.79	10.65	10.77	10.78	10.99	11.01	10.40	10.56	10.46	10.20	10.48	10.12	10.30	10.54	10.30	10.34	10.48	10.25
K_2O	0.23	0.10	0.12	0.11	0.10	0.10	0.09	0.11	0.14	0.13	0.10	0.12	0.13	0.15	0.16	0.20	0.16	0.18	0.17	0.18
Total	98.24	99.85	100.50	102.15	101.16	101.85	101.43	100.98	98.57	99.67	99.90	100.07	100.33	100.32	100.16	101.30	100.64	100.88	100.88	99.84
Si	11.24	12.17	12.17	12.47	12.33	12.42	12.33	12.30	12.02	12.13	12.11	12.06	12.14	12.10	12.07	12.20	12.05	12.13	12.20	12.14
Ti	0.00	0.00	0.00	0.00	0.00	0.00	0.00	0.00	0.00	0.00	0.00	0.00	0.00	0.00	0.00	0.00	0.00	0.00	0.00	0.00
Al	5.36	4.46	4.54	4.59	4.53	4.57	4.56	4.51	4.43	4.46	4.54	4.64	4.56	4.70	4.60	4.64	4.66	4.65	4.61	4.57
Fe^{2+}	0.03	0.01	0.01	0.00	0.01	0.00	0.01	0.00	0.01	0.00	0.01	0.01	0.00	0.00	0.01	0.00	0.01	0.00	0.01	0.01
Ca	0.28	0.33	0.37	0.36	0.35	0.35	0.33	0.32	0.32	0.37	0.38	0.43	0.42	0.40	0.45	0.45	0.51	0.48	0.41	0.34
Na	3.55	3.81	3.83	3.77	3.82	3.82	3.89	3.90	3.69	3.74	3.71	3.62	3.72	3.59	3.65	3.73	3.65	3.67	3.71	3.63
K	0.05	0.02	0.03	0.03	0.02	0.02	0.02	0.03	0.03	0.03	0.02	0.03	0.03	0.04	0.04	0.05	0.04	0.04	0.04	0.04
Total	20.51	20.80	20.94	21.23	21.05	21.19	21.15	21.06	20.50	20.74	20.77	20.78	20.87	20.82	20.81	21.07	20.91	20.96	20.98	20.73
An	7.30	7.88	8.70	8.66	8.32	8.38	7.69	7.61	7.95	8.84	9.30	10.56	10.00	9.90	10.80	10.58	12.10	11.43	9.82	8.55
Ab	91.34	91.58	90.62	90.72	91.12	91.07	91.81	91.79	91.23	90.43	90.15	88.74	89.25	89.21	88.29	88.30	87.00	87.58	89.25	90.39
Or	1.35	0.54	0.68	0.62	0.56	0.55	0.49	0.59	0.81	0.73	0.55	0.70	0.75	0.89	0.91	1.12	0.90	0.98	0.93	1.06
Total	100	100	100	100	100	100	100	100	100	100	100	100	100	100	100	100	100	100	100	100

Appendix 4.2.2: Representative mineral chemistry for plagioclase feldspar

	DA13-074-5.1	DA13-074-5.2	DA13-074-5.3	DA13-074-5.4	DA13-074-5.5	DA13-074-5.6	DA13-074-5.7	DA13-074-5.8	DA13-074-5.9	DA13-074-5.10	DA13-074-5.11	DA13-074-5.12	DA13-074-5.13	DA13-074-5.14	DA13-074-5.15	DA13-074-6.1	DA13-074-6.2	DA13-074-6.3	DA13-074-6.4	DA13-074-6.5	DA13-074-6.6	DA13-074-6.7
SiO_2	61.87	62.18	61.82	61.96	61.54	61.57	62.24	61.99	62.21	61.71	61.83	61.86	62.00	61.72	62.05	61.88	61.96	61.97	62.36	62.14	62.34	62.26
TiO_2	0.01	0.01	0.00	0.01	0.00	0.00	0.00	0.00	0.00	0.01	0.01	0.00	0.01	0.00	0.01	0.00	0.00	0.00	0.00	0.00	0.00	0.01
Al_2O_3	22.79	22.69	22.88	22.94	22.99	22.95	22.81	22.76	22.69	23.01	23.14	22.78	22.90	23.01	22.72	22.67	22.80	22.75	22.62	22.71	22.72	22.69
Cr_2O_3	0.01	0.02	0.00	0.00	0.00	0.00	0.03	0.02	0.00	0.02	0.00	0.00	0.00	0.01	0.03	0.00	0.00	0.02	0.00	0.00	0.00	0.03
FeOT	0.07	0.07	0.07	0.05	0.09	0.05	0.07	0.10	0.07	0.05	0.09	0.04	0.11	0.07	0.09	0.08	0.05	0.05	0.04	0.07	0.02	0.05
MnO	0.00	0.00	0.01	0.00	0.00	0.00	0.00	0.00	0.00	0.00	0.01	0.00	0.02	0.01	0.00	0.00	0.01	0.02	0.00	0.02	0.00	0.00
MgO	0.00	0.01	0.00	0.00	0.00	0.00	0.01	0.00	0.00	0.01	0.00	0.00	0.00	0.00	0.00	0.01	0.00	0.00	0.01	0.00	0.00	0.01
BaO	0.00	0.04	0.00	0.02	0.00	0.03	0.00	0.01	0.00	0.00	0.00	0.01	0.00	0.00	0.04	0.00	0.00	0.00	0.00	0.00	0.03	0.01
CaO	4.95	5.06	5.07	5.12	5.23	5.33	5.06	5.01	5.04	5.29	5.26	5.07	5.15	5.08	4.85	4.98	4.99	4.91	4.85	4.89	4.86	4.84
Na_2O	8.80	8.79	8.87	8.82	8.58	8.57	8.70	8.70	8.78	8.59	8.69	8.79	8.65	8.73	8.92	8.79	8.81	8.94	8.84	8.74	8.94	8.99
K_2O	0.40	0.43	0.36	0.39	0.38	0.41	0.40	0.43	0.39	0.33	0.33	0.39	0.37	0.37	0.41	0.32	0.35	0.29	0.29	0.34	0.36	0.32
Total	98.91	99.30	99.08	99.30	98.82	98.91	99.33	99.04	99.19	99.01	99.34	98.95	99.22	99.01	99.13	98.73	98.95	98.95	99.00	98.91	99.27	99.22
Si	11.31	11.37	11.30	11.33	11.25	11.26	11.38	11.33	11.37	11.28	11.30	11.31	11.33	11.28	11.34	11.31	11.33	11.33	11.40	11.36	11.40	11.38
Ti	0.00	0.00	0.00	0.00	0.00	0.00	0.00	0.00	0.00	0.00	0.00	0.00	0.00	0.00	0.00	0.00	0.00	0.00	0.00	0.00	0.00	0.00
Al	4.91	4.89	4.93	4.94	4.95	4.95	4.91	4.90	4.89	4.96	4.99	4.91	4.93	4.96	4.90	4.88	4.91	4.90	4.87	4.89	4.90	4.89
Fe^{2+}	0.01	0.01	0.01	0.01	0.01	0.01	0.01	0.02	0.01	0.01	0.01	0.01	0.02	0.01	0.01	0.01	0.01	0.01	0.01	0.01	0.00	0.01
Ca	0.97	0.99	0.99	1.00	1.03	1.04	0.99	0.98	0.99	1.04	1.03	0.99	1.01	1.00	0.95	0.98	0.98	0.96	0.95	0.96	0.95	0.95
Na	3.12	3.12	3.14	3.12	3.04	3.04	3.09	3.08	3.11	3.05	3.08	3.12	3.07	3.09	3.16	3.12	3.12	3.17	3.13	3.10	3.17	3.19
K	0.09	0.10	0.08	0.09	0.09	0.09	0.09	0.10	0.09	0.08	0.08	0.09	0.09	0.09	0.10	0.07	0.08	0.07	0.07	0.08	0.08	0.07
Total	20.42	20.47	20.46	20.50	20.37	20.39	20.47	20.42	20.46	20.41	20.49	20.42	20.45	20.43	20.46	20.38	20.42	20.44	20.43	20.40	20.50	20.49
An	23.18	23.58	23.54	23.76	24.67	25.00	23.76	23.55	23.55	24.90	24.60	23.66	24.25	23.83	22.57	23.41	23.39	22.92	22.88	23.16	22.66	22.51
Ab	74.59	74.06	74.45	74.10	73.20	72.74	73.99	74.04	74.26	73.24	73.57	74.17	73.67	74.09	75.17	74.82	74.69	75.45	75.49	74.92	75.37	75.72
Or	2.23	2.36	2.01	2.14	2.14	2.26	2.25	2.41	2.18	1.85	1.83	2.17	2.08	2.08	2.27	1.77	1.93	1.63	1.63	1.92	1.97	1.77
Total	100	100	100	100	100	100	100	100	100	100	100	100	100	100	100	100	100	100	100	100	100	100

Appendix 4.2.2: Representative mineral chemistry for plagioclase feldspar

	DA13-074-6.8	DA13-074-6.9	DA13-074-6.10	DA13-076-4.1	DA13-076-4.2	DA13-076-4.3	DA13-076-4.4	DA13-076-4.5	DA13-076-4.6	DA13-076-4.7	DA13-076-9.1	DA13-076-9.2	DA13-076-9.3	DA13-076-9.4	DA13-076-9.5	DA13-076-9.6	DA13-076-9.7	DA13-076-9.8	DA13-076-9.9	DA13-076-9.10	DA13-076-9.11	DA13-076-9.12	DA13-076-9.13	DA13-076-9.14
SiO_2	62.21	61.88	62.19	61.91	61.13	62.50	62.01	59.58	61.77	61.93	63.30	57.34	61.27	60.51	62.24	61.14	61.79	61.91	62.00	61.77	62.37	62.35	61.38	62.31
TiO_2	0.00	0.00	0.00	0.00	0.01	0.00	0.00	0.00	0.00	0.02	0.00	0.01	0.00	0.01	0.00	0.01	0.03	0.00	0.01	0.00	0.00	0.01	0.02	0.01
Al_2O_3	22.88	22.70	22.82	22.88	22.56	22.89	22.59	22.28	23.32	22.86	23.23	20.94	22.19	22.03	22.64	22.14	22.45	22.60	22.94	22.68	22.73	22.62	22.39	22.73
Cr_2O_3	0.02	0.01	0.00	0.00	0.00	0.01	0.00	0.02	0.03	0.00	0.02	0.01	0.00	0.18	0.02	0.04	0.00	0.00	0.00	0.00	0.00	0.00	0.05	0.00
FeOT	0.08	0.05	0.04	0.07	0.06	0.06	0.04	0.06	0.06	0.06	0.07	0.08	0.04	0.03	0.07	0.05	0.04	0.07	0.04	0.06	0.13	0.06	0.05	0.04
MnO	0.01	0.00	0.01	0.00	0.00	0.00	0.01	0.02	0.01	0.01	0.03	0.04	0.00	0.00	0.02	0.00	0.00	0.00	0.01	0.00	0.00	0.04	0.01	0.01
MgO	0.00	0.00	0.00	0.00	0.00	0.00	0.02	0.01	0.00	0.00	0.02	0.01	0.00	0.00	0.00	0.00	0.00	0.00	0.00	0.00	0.00	0.00	0.01	0.00
BaO	0.00	0.00	0.00	0.04	0.00	0.00	0.06	0.00	0.00	0.03	0.00	0.04	0.00	0.03	0.02	0.03	0.04	0.00	0.00	0.02	0.02	0.02	0.00	0.03
CaO	4.90	5.04	5.00	5.24	5.11	4.98	4.88	5.43	5.38	4.99	4.79	4.17	4.81	4.57	4.85	4.74	4.72	4.80	4.92	4.91	4.90	4.79	4.65	4.77
Na_2O	8.90	8.83	8.81	8.82	8.46	8.83	8.75	8.15	8.49	8.86	9.09	8.93	8.73	8.32	9.06	8.63	8.73	8.90	8.75	8.61	8.86	8.87	8.70	8.94
K_2O	0.32	0.27	0.30	0.26	0.31	0.32	0.31	0.29	0.26	0.22	0.31	0.34	0.52	0.40	0.32	0.35	0.36	0.32	0.30	0.33	0.31	0.35	0.38	0.34
Total	99.33	98.80	99.17	99.23	97.64	99.59	98.66	95.84	99.32	98.99	100.85	91.89	97.56	96.07	99.21	97.14	98.16	98.60	98.98	98.38	99.33	99.12	97.62	99.17
Si	11.37	11.31	11.37	11.32	11.18	11.43	11.34	10.89	11.29	11.32	11.57	10.48	11.20	11.06	11.38	11.18	11.30	11.32	11.33	11.29	11.40	11.40	11.22	11.39
Ti	0.00	0.00	0.00	0.00	0.00	0.00	0.00	0.00	0.00	0.00	0.00	0.00	0.00	0.00	0.00	0.00	0.00	0.00	0.00	0.00	0.00	0.00	0.00	0.00
Al	4.93	4.89	4.92	4.93	4.86	4.93	4.87	4.80	5.02	4.93	5.00	4.51	4.78	4.75	4.88	4.77	4.84	4.87	4.94	4.89	4.90	4.87	4.82	4.90
Fe^{2+}	0.01	0.01	0.01	0.01	0.01	0.01	0.01	0.01	0.01	0.01	0.01	0.01	0.01	0.00	0.01	0.01	0.01	0.01	0.01	0.01	0.02	0.01	0.01	0.01
Ca	0.96	0.99	0.98	1.03	1.00	0.97	0.96	1.06	1.05	0.98	0.94	0.82	0.94	0.89	0.95	0.93	0.92	0.94	0.96	0.96	0.96	0.94	0.91	0.93
Na	3.15	3.13	3.12	3.12	3.00	3.13	3.10	2.89	3.01	3.14	3.22	3.17	3.09	2.95	3.21	3.06	3.10	3.15	3.10	3.05	3.14	3.14	3.08	3.17
K	0.08	0.06	0.07	0.06	0.07	0.07	0.07	0.07	0.06	0.05	0.07	0.08	0.12	0.09	0.07	0.08	0.08	0.08	0.07	0.08	0.07	0.08	0.09	0.08
Total	20.50	20.40	20.46	20.47	20.12	20.55	20.34	19.72	20.45	20.43	20.82	19.07	20.15	19.75	20.50	20.03	20.25	20.37	20.42	20.28	20.49	20.45	20.14	20.48
An	22.90	23.61	23.49	24.37	24.58	23.32	23.16	26.48	25.56	23.43	22.14	20.09	22.65	22.74	22.42	22.82	22.51	22.53	23.29	23.50	22.98	22.54	22.33	22.33
Ab	75.30	74.85	74.81	74.17	73.63	74.89	75.09	71.85	72.95	75.33	76.15	77.98	74.43	74.92	75.82	75.17	75.43	75.67	75.00	74.63	75.28	75.51	75.52	75.79
Or	1.80	1.53	1.70	1.46	1.80	1.79	1.75	1.67	1.49	1.25	1.71	1.92	2.92	2.35	1.76	2.01	2.06	1.80	1.71	1.87	1.74	1.95	2.14	1.88
Total	100	100	100	100	100	100	100	100	100	100	100	100	100	100	100	100	100	100	100	100	100	100	100	100

Appendix 4.2.2: Representative mineral chemistry for plagioclase feldspar

	DA13-077-5.1	DA13-077-5.2	DA13-077-5.3	DA13-077-5.4	DA13-077-5.5	DA13-077-5.6	DA13-077-5.7	DA13-077-5.8	DA13-077-5.9	DA13-077-5.10	DA13-077-5.11	DA13-077-5.12	DA13-077-5.13	DA13-077-5.14	DA13-077-5.15	DA13-083-2.1	DA13-083-2.2	DA13-083-2.3	DA13-083-2.4	DA13-083-2.5	DA13-083-2.6	DA13-083-2.7	DA13-083-2.8
SiO_2	64.45	64.09	63.91	64.86	65.80	64.31	64.84	65.19	64.29	64.53	65.87	64.91	64.63	65.06	66.72	63.53	63.34	62.97	63.32	63.32	63.97	63.63	63.75
TiO_2	0.00	0.00	0.00	0.00	0.01	0.01	0.00	0.00	0.01	0.00	0.00	0.01	0.00	0.01	0.00	0.01	0.01	0.00	0.00	0.02	0.01	0.00	0.00
Al_2O_3	22.08	21.87	21.67	22.14	22.38	22.05	22.25	22.25	22.14	22.75	22.69	22.11	22.21	22.15	21.32	21.77	21.93	21.86	22.17	22.13	22.41	21.93	22.12
Cr_2O_3	0.00	0.01	0.00	0.03	0.00	0.00	0.00	0.00	0.01	0.01	0.00	0.00	0.01	0.05	0.00	0.00	0.01	0.00	0.01	0.00	0.00	0.03	0.00
FeOT	0.05	0.06	0.07	0.07	0.08	0.06	0.03	0.04	0.05	0.03	0.06	0.06	0.02	0.06	0.07	0.04	0.05	0.05	0.07	0.12	0.07	0.03	0.07
MnO	0.00	0.00	0.01	0.02	0.01	0.02	0.00	0.00	0.01	0.01	0.02	0.00	0.00	0.00	0.00	0.00	0.02	0.00	0.00	0.00	0.01	0.02	0.00
MgO	0.01	0.00	0.01	0.00	0.00	0.00	0.00	0.00	0.01	0.01	0.00	0.00	0.02	0.00	0.00	0.01	0.00	0.00	0.00	0.01	0.02	0.00	0.00
BaO	0.01	0.00	0.00	0.00	0.01	0.01	0.00	0.00	0.00	0.00	0.03	0.00	0.00	0.00	0.00	0.00	0.01	0.00	0.04	0.00	0.01	0.01	0.00
CaO	3.51	3.55	3.50	3.39	3.52	3.58	3.65	3.52	3.56	3.52	3.59	3.58	3.56	3.45	2.31	3.81	3.87	3.95	4.04	4.02	3.91	3.86	3.81
Na_2O	9.62	9.72	9.78	9.90	10.09	9.58	9.52	9.62	9.64	9.79	9.46	9.72	9.68	9.87	10.50	9.60	9.63	9.64	9.37	9.54	9.60	9.39	9.51
K_2O	0.30	0.33	0.30	0.18	0.26	0.26	0.27	0.27	0.30	0.26	0.21	0.26	0.23	0.26	0.15	0.29	0.23	0.19	0.32	0.33	0.38	0.30	0.32
Total	100.03	99.63	99.26	100.61	102.17	99.88	100.56	100.90	100.02	100.91	101.94	100.66	100.36	100.89	101.08	99.06	99.11	98.67	99.35	99.49	100.38	99.19	99.58
Si	11.78	11.72	11.68	11.86	12.03	11.76	11.85	11.92	11.75	11.80	12.04	11.87	11.82	11.89	12.20	11.62	11.58	11.51	11.58	11.58	11.69	11.63	11.65
Ti	0.00	0.00	0.00	0.00	0.00	0.00	0.00	0.00	0.00	0.00	0.00	0.00	0.00	0.00	0.00	0.00	0.00	0.00	0.00	0.00	0.00	0.00	0.00
Al	4.76	4.71	4.67	4.77	4.82	4.75	4.79	4.79	4.77	4.90	4.89	4.76	4.78	4.77	4.59	4.69	4.72	4.71	4.78	4.77	4.83	4.72	4.77
Fe^{2+}	0.01	0.01	0.01	0.01	0.01	0.01	0.00	0.01	0.01	0.00	0.01	0.01	0.00	0.01	0.01	0.01	0.01	0.01	0.01	0.02	0.01	0.00	0.01
Ca	0.69	0.70	0.69	0.66	0.69	0.70	0.72	0.69	0.70	0.69	0.70	0.70	0.70	0.67	0.45	0.75	0.76	0.77	0.79	0.79	0.77	0.76	0.75
Na	3.41	3.45	3.47	3.51	3.58	3.40	3.37	3.41	3.42	3.47	3.35	3.45	3.43	3.50	3.72	3.40	3.41	3.42	3.32	3.38	3.40	3.33	3.37
K	0.07	0.08	0.07	0.04	0.06	0.06	0.06	0.06	0.07	0.06	0.05	0.06	0.05	0.06	0.04	0.07	0.05	0.04	0.07	0.08	0.09	0.07	0.07
Total	20.71	20.66	20.59	20.86	21.19	20.68	20.80	20.88	20.72	20.92	21.05	20.85	20.79	20.91	21.01	20.53	20.54	20.47	20.55	20.61	20.79	20.51	20.62
An	16.50	16.48	16.24	15.75	15.94	16.87	17.22	16.56	16.65	16.34	17.13	16.68	16.69	15.95	10.75	17.69	17.92	18.27	18.91	18.57	17.99	18.19	17.78
Ab	81.82	81.69	82.09	83.23	82.64	81.68	81.25	81.94	81.71	82.22	81.68	81.88	82.03	82.62	88.41	80.70	80.79	80.68	79.30	79.64	79.90	80.13	80.44
Or	1.68	1.83	1.67	1.01	1.42	1.45	1.53	1.50	1.65	1.44	1.19	1.44	1.28	1.43	0.84	1.61	1.29	1.05	1.78	1.79	2.11	1.68	1.79
Total	100	100	100	100	100	100	100	100	100	100	100	100	100	100	100	100	100	100	100	100	100	100	100

Appendix 4.2.2: Representative mineral chemistry for plagioclase feldspar

	DA13-083-2.9	DA13-083-2.10	DA13-083-2.11	DA13-083-2.12	DA13-083-4.1	DA13-083-4.2	DA13-083-4.3	DA13-083-4.4	DA13-083-4.5	DA13-083-4.6	DA13-083-4.7	DA13-083-4.8	DA13-083-4.9	DA13-083-4.10
SiO_2	63.41	63.44	63.75	63.68	63.88	63.77	63.77	63.89	63.88	63.23	63.73	63.86	64.05	64.37
TiO_2	0.04	0.02	0.00	0.00	0.00	0.01	0.01	0.01	0.00	0.02	0.00	0.00	0.00	0.01
Al_2O_3	21.74	21.86	22.04	22.02	22.25	22.15	21.83	22.13	22.10	21.98	22.28	22.30	22.50	22.09
Cr_2O_3	0.01	0.00	0.00	0.02	0.00	0.04	0.00	0.03	0.00	0.00	0.02	0.00	0.01	0.00
FeOT	0.21	0.06	0.05	0.04	0.10	0.01	0.05	0.04	0.05	0.17	0.06	0.06	0.05	0.04
MnO	0.02	0.00	0.00	0.00	0.00	0.00	0.00	0.00	0.01	0.02	0.00	0.02	0.00	0.02
MgO	0.01	0.00	0.01	0.01	0.01	0.00	0.00	0.02	0.00	0.01	0.00	0.00	0.00	0.01
BaO	0.01	0.01	0.00	0.00	0.00	0.03	0.00	0.03	0.01	0.00	0.01	0.02	0.04	0.01
CaO	3.78	3.87	3.85	3.81	3.84	3.82	3.79	3.74	3.81	3.87	3.91	3.93	3.91	3.65
Na_2O	9.49	9.64	9.50	9.42	9.56	9.64	9.75	9.58	9.56	9.63	9.69	9.57	9.56	9.94
K_2O	0.28	0.31	0.26	0.35	0.31	0.31	0.30	0.31	0.32	0.28	0.27	0.28	0.32	0.13
Total	99.01	99.21	99.47	99.35	99.94	99.77	99.50	99.77	99.75	99.20	99.95	100.04	100.45	100.27
Si	11.59	11.60	11.65	11.64	11.68	11.66	11.66	11.68	11.68	11.56	11.65	11.67	11.71	11.77
Ti	0.01	0.00	0.00	0.00	0.00	0.00	0.00	0.00	0.00	0.00	0.00	0.00	0.00	0.00
Al	4.68	4.71	4.75	4.74	4.79	4.77	4.70	4.77	4.76	4.74	4.80	4.80	4.85	4.76
Fe^{2+}	0.03	0.01	0.01	0.01	0.01	0.00	0.01	0.01	0.01	0.03	0.01	0.01	0.01	0.01
Ca	0.74	0.76	0.75	0.75	0.75	0.75	0.74	0.73	0.75	0.76	0.77	0.77	0.77	0.72
Na	3.36	3.42	3.37	3.34	3.39	3.42	3.45	3.40	3.39	3.41	3.43	3.39	3.39	3.52
K	0.07	0.07	0.06	0.08	0.07	0.07	0.07	0.07	0.07	0.07	0.06	0.07	0.07	0.03
Total	20.48	20.57	20.59	20.56	20.70	20.67	20.64	20.66	20.66	20.56	20.72	20.72	20.80	20.80
An	17.76	17.87	18.03	17.92	17.85	17.65	17.39	17.44	17.74	17.88	17.95	18.19	18.10	16.76
Ab	80.66	80.43	80.49	80.14	80.41	80.63	80.98	80.85	80.50	80.58	80.57	80.27	80.13	82.53
Or	1.58	1.71	1.48	1.95	1.74	1.71	1.62	1.71	1.76	1.54	1.48	1.54	1.76	0.71
Total	100	100	100	100	100	100	100	100	100	100	100	100	100	100

Appendix 4.2.3: Representative mineral chemistry for feldspar exsolution lamellae

	DA13-029-4.1	DA13-029-4.2	DA13-029-4.3	DA13-029-4.4	DA13-029-4.5	DA13-029-4.6	DA13-029-4.7	DA13-029-4.8	DA13-029-4.9	DA13-029-4.10	DA13-040-5.1	DA13-040-5.2	DA13-040-5.3	DA13-040-5.4	DA13-040-5.5	DA13-040-5.6	DA13-040-5.7	DA13-040-5.8	DA13-040-5.9	DA13-049-7.1
SiO_2	69.64	70.06	69.88	69.17	70.45	68.47	69.75	68.28	69.20	70.94	70.91	71.34	70.59	70.49	68.22	70.33	70.36	70.39	70.57	69.83
TiO_2	0.00	0.00	0.00	0.00	0.01	0.00	0.00	0.00	0.01	0.00	0.00	0.01	0.00	0.01	0.02	0.00	0.01	0.00	0.00	0.00
Al_2O_3	19.57	19.70	19.70	19.73	20.05	19.93	20.01	20.29	20.66	20.21	19.72	19.80	19.94	20.55	18.91	20.49	20.55	20.05	20.25	20.56
Cr_2O_3	0.01	0.00	0.00	0.00	0.00	0.00	0.00	0.04	0.02	0.03	0.01	0.01	0.01	0.00	0.00	0.00	0.00	0.01	0.00	0.00
FeOT	0.09	0.03	0.01	0.03	0.02	0.04	0.06	0.03	0.03	0.06	0.25	0.25	0.25	0.27	0.24	0.27	0.25	0.22	0.18	0.05
MnO	0.02	0.01	0.00	0.00	0.03	0.02	0.00	0.00	0.00	0.00	0.00	0.00	0.00	0.00	0.00	0.00	0.00	0.03	0.01	0.01
MgO	0.00	0.01	0.01	0.00	0.01	0.02	0.00	0.00	0.00	0.00	0.00	0.00	0.12	0.01	0.00	0.02	0.01	0.01	0.01	0.00
BaO	0.02	0.00	0.00	0.01	0.00	0.03	0.00	0.04	0.00	0.00	0.05	0.02	0.01	0.02	0.02	0.00	0.00	0.01	0.00	0.00
CaO	0.15	0.07	0.09	0.20	0.15	0.48	0.46	0.88	0.76	0.23	0.08	0.02	0.25	0.03	0.07	0.01	0.03	0.04	0.02	0.53
Na_2O	11.70	11.96	12.24	11.71	11.83	11.49	11.66	11.16	11.77	11.89	11.25	11.76	10.78	11.65	11.28	11.87	11.35	10.78	11.58	11.49
K_2O	0.25	0.25	0.15	0.21	0.22	0.15	0.15	0.15	0.14	0.12	0.13	0.13	0.15	0.10	0.11	0.09	0.11	0.10	0.09	0.12
Total	101.40	102.07	102.08	101.05	102.72	100.55	102.08	100.79	102.57	103.45	102.34	103.31	101.96	106.10	98.85	103.07	105.66	103.59	104.70	102.58
Si	12.73	12.81	12.78	12.65	12.88	12.52	12.75	12.48	12.65	12.97	12.96	13.04	12.91	13.44	12.47	13.41	13.41	13.23	13.27	12.77
Ti	0.00	0.00	0.00	0.00	0.00	0.00	0.00	0.00	0.00	0.00	0.00	0.00	0.00	0.00	0.00	0.00	0.00	0.00	0.00	0.00
Al	4.22	4.24	4.24	4.25	4.32	4.29	4.31	4.37	4.45	4.36	4.25	4.27	4.30	4.43	4.07	4.42	4.43	4.32	4.36	4.43
Fe^{2+}	0.01	0.00	0.00	0.00	0.00	0.01	0.01	0.00	0.00	0.01	0.04	0.04	0.04	0.04	0.04	0.04	0.04	0.03	0.03	0.01
Ca	0.03	0.01	0.02	0.04	0.03	0.09	0.09	0.17	0.15	0.05	0.02	0.00	0.05	0.01	0.01	0.00	0.01	0.01	0.00	0.10
Na	4.15	4.24	4.34	4.15	4.19	4.07	4.13	3.96	4.17	4.22	3.99	4.17	3.82	4.13	4.00	4.21	4.02	3.82	4.11	4.07
K	0.06	0.06	0.04	0.05	0.05	0.04	0.03	0.04	0.03	0.03	0.03	0.03	0.03	0.02	0.03	0.02	0.02	0.02	0.02	0.03
Total	21.20	21.37	21.42	21.14	21.48	21.02	21.33	21.02	21.46	21.62	21.28	21.55	21.14	22.06	20.62	22.09	21.93	21.44	21.79	21.41
An	0.70	0.30	0.42	0.93	0.68	2.22	2.11	4.12	3.40	1.05	0.40	0.09	1.27	0.12	0.35	0.05	0.16	0.23	0.12	2.46
Ab	97.93	98.34	98.77	97.91	98.12	96.94	97.09	95.03	95.84	98.30	98.87	99.19	97.84	99.32	99.01	99.48	99.23	99.15	99.40	96.88
Or	1.37	1.36	0.81	1.17	1.20	0.84	0.80	0.85	0.75	0.65	0.72	0.71	0.88	0.56	0.64	0.47	0.61	0.63	0.48	0.66
Total	100	100	100	100	100	100	100	100	100	100	100	100	100	100	100	100	100	100	100	100

Appendix 4.2.3: Representative mineral chemistry for feldspar exsolution lamellae

	DA13-049-7.2	DA13-049-7.3	DA13-049-7.4	DA13-049-7.5	DA13-069-4.1	DA13-069-4.2	DA13-069-4.3	DA13-069-4.4	DA13-069-4.5	DA13-069-4.6	DA13-069-4.7	DA13-069-4.8	DA13-069-4.9	DA13-069-2.1	DA13-069-2.2	DA13-069-2.3	DA13-069-2.4	DA13-069-2.5	DA13-069-2.6	DA13-077-2.1	DA13-077-2.2
SiO_2	69.52	70.73	68.99	69.63	65.50	67.70	68.45	68.93	67.48	67.62	66.64	66.29	65.20	67.75	67.46	68.01	67.97	68.23	67.92	71.23	68.82
TiO_2	0.00	0.00	0.00	0.00	0.00	0.01	0.00	0.00	0.00	0.00	0.00	0.00	0.00	0.00	0.00	0.00	0.02	0.00	0.00	0.02	0.01
Al_2O_3	20.27	20.30	19.90	20.17	21.14	21.22	20.01	21.16	21.45	20.96	21.17	20.15	20.23	20.68	21.15	21.18	21.29	20.97	20.50	20.03	19.00
Cr_2O_3	0.00	0.00	0.01	0.04	0.01	0.00	0.00	0.00	0.00	0.02	0.01	0.00	0.00	0.04	0.00	0.04	0.01	0.02	0.00	0.01	0.00
FeOT	0.06	0.07	0.02	0.04	0.19	0.03	0.04	0.03	0.04	0.00	0.04	0.02	0.11	0.01	0.03	0.01	0.04	0.02	0.04	0.06	0.02
MnO	0.00	0.00	0.00	0.02	0.00	0.00	0.00	0.00	0.01	0.00	0.00	0.00	0.02	0.00	0.00	0.03	0.01	0.00	0.00	0.02	0.00
MgO	0.00	0.00	0.01	0.00	0.04	0.00	0.01	0.01	0.01	0.01	0.00	0.00	0.02	0.00	0.01	0.01	0.01	0.00	0.01	0.00	0.00
BaO	0.04	0.00	0.00	0.02	0.00	0.00	0.00	0.02	0.02	0.03	0.01	0.00	0.00	0.00	0.02	0.05	0.00	0.00	0.00	0.00	0.03
CaO	0.47	0.40	0.38	0.38	1.45	1.70	0.63	1.36	1.94	1.60	1.95	1.50	1.72	1.34	1.77	1.56	1.76	1.39	1.29	0.15	0.13
Na_2O	11.87	11.77	11.64	11.90	10.51	10.76	11.06	11.05	10.42	10.30	10.60	10.98	10.10	11.11	10.79	10.97	10.79	10.97	10.86	12.22	10.29
K_2O	0.10	0.13	0.11	0.10	0.20	0.14	0.15	0.12	0.19	0.75	0.19	0.18	0.66	0.13	0.13	0.10	0.10	0.09	0.12	0.25	3.34
Total	102.29	103.40	101.04	102.23	99.00	101.56	100.35	102.65	101.52	101.23	100.58	99.11	98.02	101.02	101.33	101.84	101.97	101.67	100.72	103.95	101.61
Si	12.71	12.93	12.61	12.73	11.97	12.38	12.51	12.60	12.34	12.36	12.18	12.12	11.92	12.39	12.33	12.43	12.43	12.47	12.42	13.02	12.58
Ti	0.00	0.00	0.00	0.00	0.00	0.00	0.00	0.00	0.00	0.00	0.00	0.00	0.00	0.00	0.00	0.00	0.00	0.00	0.00	0.00	0.00
Al	4.37	4.37	4.29	4.35	4.56	4.57	4.31	4.56	4.62	4.52	4.56	4.34	4.36	4.46	4.56	4.56	4.59	4.52	4.42	4.31	4.09
Fe^{2+}	0.01	0.01	0.00	0.01	0.03	0.00	0.01	0.00	0.01	0.00	0.01	0.00	0.02	0.00	0.01	0.00	0.01	0.00	0.01	0.01	0.00
Ca	0.09	0.08	0.08	0.07	0.28	0.33	0.12	0.27	0.38	0.31	0.38	0.29	0.34	0.26	0.35	0.31	0.34	0.27	0.25	0.03	0.03
Na	4.21	4.17	4.12	4.22	3.73	3.81	3.92	3.92	3.69	3.65	3.76	3.89	3.58	3.94	3.82	3.89	3.83	3.89	3.85	4.33	3.65
K	0.02	0.03	0.03	0.02	0.05	0.03	0.04	0.03	0.04	0.17	0.04	0.04	0.15	0.03	0.03	0.02	0.02	0.02	0.03	0.06	0.78
Total	21.41	21.60	21.13	21.40	20.62	21.14	20.91	21.38	21.08	21.02	20.93	20.69	20.36	21.07	21.09	21.22	21.22	21.18	20.97	21.77	21.13
An	2.11	1.82	1.78	1.73	7.01	7.94	3.03	6.32	9.23	7.59	9.11	6.93	8.27	6.21	8.25	7.27	8.20	6.52	6.13	0.64	0.57
Ab	97.36	97.44	97.59	97.71	91.82	91.25	96.09	93.01	89.72	88.21	89.82	92.08	87.94	93.10	91.02	92.18	91.22	92.96	93.21	98.04	81.93
Or	0.53	0.73	0.63	0.56	1.18	0.80	0.87	0.68	1.05	4.20	1.07	0.99	3.79	0.69	0.73	0.56	0.58	0.52	0.67	1.32	17.50
Total	100	100	100	100	100	100	100	100	100	100	100	100	100	100	100	100	100	100	100	100	100

Appendix 4.2.3: Representative mineral chemistry for feldspar exsolution lamellae

	DA13-077-2.3	DA13-077-2.4	DA13-077-2.5	DA13-077-2.6	DA13-077-2.7	DA13-077-2.8	DA13-077-2.9	DA13-077-2.10	DA13-083-1.1	DA13-083-1.2	DA13-083-1.3	DA13-083-1.4	DA13-083-1.5	DA13-083-1.6	DA13-083-1.7	DA13-083-1.8	DA13-083-1.9	DA13-083-1.10	DA13-083-5.1
SiO_2	71.39	70.56	71.20	71.15	71.36	66.74	71.42	70.55	64.34	64.25	64.09	64.95	64.58	63.92	64.00	64.89	64.00	64.09	64.85
TiO_2	0.00	0.00	0.01	0.01	0.00	0.01	0.00	0.00	0.00	0.00	0.01	0.00	0.01	0.02	0.00	0.01	0.01	0.01	0.01
Al_2O_3	20.16	20.15	20.18	20.10	20.24	22.17	20.19	19.90	21.81	21.78	22.06	22.05	22.18	21.87	21.82	21.85	22.18	22.00	21.85
Cr_2O_3	0.02	0.03	0.01	0.00	0.00	0.03	0.00	0.00	0.00	0.00	0.00	0.00	0.01	0.00	0.02	0.00	0.00	0.01	0.02
FeOT	0.00	0.04	0.04	0.02	0.02	0.04	0.03	0.00	0.02	0.05	0.07	0.05	0.07	0.10	0.07	0.06	0.08	0.05	0.05
MnO	0.03	0.01	0.00	0.02	0.00	0.00	0.01	0.01	0.02	0.00	0.02	0.02	0.02	0.00	0.00	0.01	0.01	0.03	0.03
MgO	0.00	0.01	0.00	0.00	0.00	0.04	0.01	0.00	0.00	0.01	0.00	0.03	0.00	0.02	0.00	0.00	0.02	0.01	0.01
BaO	0.00	0.07	0.03	0.02	0.01	0.03	0.03	0.03	0.00	0.01	0.00	0.02	0.00	0.01	0.02	0.00	0.02	0.04	0.00
CaO	0.14	0.12	0.07	0.13	0.11	0.13	0.09	0.11	3.39	3.41	3.59	3.28	3.44	3.64	3.69	3.17	3.60	3.54	3.16
Na_2O	11.75	11.79	11.98	11.68	11.71	10.64	11.89	11.81	10.03	9.79	9.84	10.04	9.99	9.90	9.76	10.06	9.39	9.97	9.94
K_2O	0.56	0.23	0.21	0.36	0.20	0.24	0.16	0.14	0.09	0.11	0.12	0.14	0.10	0.13	0.11	0.12	0.16	0.10	0.11
Total	104.01	102.89	103.69	103.44	103.64	99.96	103.78	102.52	99.67	99.39	99.78	100.52	100.37	99.58	99.44	100.16	99.44	99.77	99.97
Si	13.05	12.90	13.02	13.01	13.05	12.20	13.06	12.90	11.76	11.75	11.72	11.87	11.81	11.69	11.70	11.86	11.70	11.72	11.86
Ti	0.00	0.00	0.00	0.00	0.00	0.00	0.00	0.00	0.00	0.00	0.00	0.00	0.00	0.00	0.00	0.00	0.00	0.00	0.00
Al	4.34	4.34	4.35	4.33	4.36	4.78	4.35	4.29	4.70	4.69	4.75	4.75	4.78	4.71	4.70	4.71	4.78	4.74	4.71
Fe^{2+}	0.00	0.01	0.01	0.00	0.00	0.01	0.01	0.00	0.00	0.01	0.01	0.01	0.01	0.01	0.01	0.01	0.01	0.01	0.01
Ca	0.03	0.02	0.01	0.03	0.02	0.03	0.02	0.02	0.66	0.67	0.70	0.64	0.67	0.71	0.72	0.62	0.71	0.69	0.62
Na	4.17	4.18	4.25	4.14	4.15	3.77	4.21	4.19	3.55	3.47	3.49	3.56	3.54	3.51	3.46	3.57	3.33	3.53	3.52
K	0.13	0.05	0.05	0.08	0.05	0.06	0.04	0.03	0.02	0.03	0.03	0.03	0.02	0.03	0.02	0.03	0.04	0.02	0.02
Total	21.72	21.50	21.68	21.59	21.63	20.84	21.68	21.43	20.70	20.61	20.70	20.87	20.84	20.67	20.62	20.80	20.57	20.72	20.74
An	0.65	0.54	0.33	0.61	0.49	0.65	0.43	0.49	15.68	16.03	16.67	15.19	15.90	16.77	17.16	14.73	17.33	16.34	14.85
Ab	96.35	98.22	98.52	97.41	98.42	97.92	98.71	98.73	83.83	83.36	82.68	84.05	83.52	82.49	82.25	84.63	81.75	83.12	84.55
Or	3.00	1.24	1.15	1.98	1.09	1.43	0.85	0.78	0.49	0.61	0.65	0.76	0.57	0.74	0.58	0.64	0.92	0.55	0.60
Total	100	100	100	100	100	100	100	100	100	100	100	100	100	100	100	100	100	100	100

Appendix 4.2.3: Representative mineral chemistry for feldspar exsolution lamellae

	DA13-083-5.2	DA13-083-5.3	DA13-083-5.4	DA13-083-5.5	DA13-083-5.6	DA13-083-5.7	DA13-083-5.8	DA13-083-5.9	DA13-083-5.10
SiO_2	65.78	65.03	65.75	66.29	66.13	66.19	65.11	65.51	64.74
TiO_2	0.02	0.01	0.00	0.01	0.01	0.00	0.00	0.00	0.02
Al_2O_3	21.91	22.01	22.00	22.00	21.96	21.82	21.85	22.08	21.71
Cr_2O_3	0.01	0.00	0.02	0.01	0.03	0.00	0.02	0.01	0.01
FeOT	0.03	0.05	0.08	0.07	0.06	0.05	0.08	0.06	0.05
MnO	0.01	0.00	0.00	0.00	0.00	0.00	0.00	0.00	0.03
MgO	0.00	0.01	0.00	0.00	0.00	0.01	0.00	0.02	0.00
BaO	0.01	0.00	0.00	0.01	0.03	0.00	0.02	0.00	0.01
CaO	3.23	3.33	3.15	2.99	2.81	2.62	3.13	3.11	2.97
Na_2O	10.19	10.00	10.28	10.26	10.33	10.71	10.13	10.07	10.07
K_2O	0.12	0.15	0.12	0.12	0.12	0.12	0.13	0.19	0.43
Total	101.27	100.57	101.39	101.74	101.41	101.52	100.44	101.03	99.99
Si	12.03	11.89	12.02	12.12	12.09	12.10	11.90	11.98	11.84
Ti	0.00	0.00	0.00	0.00	0.00	0.00	0.00	0.00	0.00
Al	4.72	4.74	4.74	4.74	4.73	4.70	4.71	4.76	4.68
Fe^{2+}	0.00	0.01	0.01	0.01	0.01	0.01	0.01	0.01	0.01
Ca	0.63	0.65	0.62	0.59	0.55	0.51	0.61	0.61	0.58
Na	3.61	3.54	3.65	3.64	3.66	3.80	3.59	3.57	3.57
K	0.03	0.03	0.03	0.03	0.03	0.03	0.03	0.04	0.10
Total	21.02	20.87	21.06	21.12	21.07	21.15	20.86	20.97	20.77
An	14.81	15.42	14.37	13.77	12.97	11.82	14.49	14.43	13.70
Ab	84.55	83.76	84.99	85.55	86.39	87.55	84.81	84.53	83.94
Or	0.64	0.82	0.65	0.68	0.63	0.63	0.70	1.04	2.35
Total	100	100	100	100	100	100	100	100	100

Appendix 4.2.4: Representative mineral chemistry for biotite

	DA13-029-2.1	DA13-029-2.2	DA13-029-2.3	DA13-029-2.4	DA13-029-2.5	DA13-029-2.6	DA13-029-2.7	DA13-029-7.1	DA13-029-7.2	DA13-029-7.3	DA13-029-7.4	DA13-029-7.5
SiO_2	39.03	38.96	39.10	38.21	39.41	39.14	39.12	39.25	39.10	39.31	40.36	39.09
TiO_2	2.74	2.71	2.70	2.65	2.66	2.70	2.72	2.52	2.49	2.37	2.92	2.89
Al_2O_3	16.02	15.94	16.03	15.74	15.83	15.85	16.22	16.22	15.97	16.37	15.64	16.16
FeOT	16.91	17.13	16.95	17.07	17.13	17.22	17.21	15.91	15.84	16.50	15.96	16.12
MnO	0.61	0.53	0.59	0.54	0.59	0.60	0.41	0.73	0.66	0.70	0.63	0.69
MgO	10.51	10.41	10.61	10.42	10.80	10.67	10.25	11.06	11.40	11.32	10.61	10.96
CaO	0.00	0.00	0.00	0.03	0.01	0.00	0.00	0.01	0.02	0.00	0.00	0.00
Na_2O	0.07	0.12	0.12	0.13	0.15	0.13	0.09	0.15	0.12	0.12	0.09	0.07
K_2O	9.83	9.75	9.89	9.37	9.67	9.67	9.81	9.62	9.65	9.70	9.42	9.85
BaO	0.03	0.03	0.08	0.06	0.06	0.10	0.09	0.06	0.06	0.03	0.02	0.07
ZnO	0.21	0.18	0.17	0.25	0.21	0.15	0.23	0.23	0.15	0.24	0.26	0.23
F	2.41	2.47	2.37	2.24	2.35	2.47	2.20	2.14	2.42	2.33	2.22	2.34
Cl	0.14	0.15	0.16	0.15	0.16	0.16	0.15	0.15	0.17	0.15	0.17	0.17
H_2O*	2.84	2.80	2.86	2.85	2.89	2.81	2.94	2.98	2.83	2.92	2.96	2.88
Subtotal	101.38	101.16	101.63	99.72	101.91	101.70	101.45	101.03	100.90	102.09	101.25	101.54
O=F, Cl	1.05	1.07	1.04	0.98	1.03	1.08	0.96	0.93	1.06	1.02	0.97	1.02
Total	100.33	100.09	100.59	98.74	100.88	100.62	100.49	100.09	99.84	101.08	100.27	100.52
Si	5.83	5.83	5.83	5.80	5.85	5.83	5.83	5.84	5.83	5.81	5.97	5.81
Al iv	2.17	2.17	2.17	2.20	2.15	2.17	2.17	2.16	2.17	2.19	2.03	2.19
Total	8.00	8.00	8.00	8.00	8.00	8.00	8.00	8.00	8.00	8.00	8.00	8.00
Al vi	0.65	0.65	0.64	0.62	0.62	0.62	0.68	0.68	0.64	0.66	0.70	0.64
Ti	0.31	0.30	0.30	0.30	0.30	0.30	0.31	0.28	0.28	0.26	0.32	0.32
Fe^{2+}	2.11	2.14	2.11	2.17	2.13	2.15	2.15	1.98	1.98	2.04	1.97	2.00
Mn	0.08	0.07	0.08	0.07	0.07	0.08	0.05	0.09	0.08	0.09	0.08	0.09
Mg	2.34	2.32	2.36	2.36	2.39	2.37	2.28	2.45	2.53	2.49	2.34	2.43
Zn	0.02	0.02	0.02	0.03	0.02	0.02	0.03	0.03	0.02	0.03	0.03	0.02
Total	5.51	5.51	5.50	5.55	5.53	5.53	5.49	5.52	5.53	5.57	5.44	5.51
Ca	0.00	0.00	0.00	0.00	0.00	0.00	0.00	0.00	0.00	0.00	0.00	0.00
Na	0.02	0.03	0.03	0.04	0.04	0.04	0.03	0.04	0.03	0.03	0.03	0.02
K	1.87	1.86	1.88	1.82	1.83	1.84	1.86	1.83	1.84	1.83	1.78	1.87
Total	1.89	1.90	1.91	1.86	1.88	1.88	1.89	1.87	1.87	1.86	1.80	1.89
OH*	2.83	2.79	2.84	2.88	2.86	2.80	2.92	2.96	2.81	2.87	2.92	2.86
F	1.14	1.17	1.12	1.08	1.10	1.17	1.04	1.01	1.14	1.09	1.04	1.10
Cl	0.03	0.04	0.04	0.04	0.04	0.04	0.04	0.04	0.04	0.04	0.04	0.04
Total	19.40	19.40	19.42	19.41	19.40	19.40	19.38	19.39	19.41	19.43	19.24	19.39
Fe/Fe+Mg	0.47	0.48	0.47	0.48	0.47	0.48	0.48	0.45	0.44	0.45	0.46	0.45

*H_2O calculations after Tindle and Webb (1990).

Appendix 4.2.4: Representative mineral chemistry for biotite

	DA13-029-7.6	DA13-029-7.7	DA13-029-7.8	DA13-029-10.1	DA13-029-10.2	DA13-029-10.3	DA13-029-10.4	DA13-029-10.5	DA13-040-1.1	DA13-040-1.2	DA13-040-1.3
SiO_2	38.61	39.32	38.73	39.08	39.53	38.60	39.57	38.31	43.07	42.70	42.94
TiO_2	2.39	2.64	2.98	2.10	2.12	2.08	2.08	2.06	1.54	1.57	1.59
Al_2O_3	16.30	15.90	15.84	15.65	15.72	15.34	15.80	15.24	11.44	11.33	11.55
FeOT	17.47	16.34	17.60	17.30	17.57	17.38	17.20	17.60	10.80	10.67	10.79
MnO	0.72	0.44	0.35	0.66	0.75	0.69	0.73	0.71	0.16	0.14	0.15
MgO	11.42	11.39	10.79	11.12	11.61	11.08	11.43	10.82	20.64	20.31	20.62
CaO	0.00	0.00	0.00	0.00	0.00	0.02	0.00	0.01	0.01	0.01	0.03
Na_2O	0.14	0.12	0.08	0.14	0.11	0.17	0.13	0.12	0.09	0.10	0.13
K_2O	8.95	9.82	9.67	8.48	8.20	6.58	6.75	9.46	9.65	9.69	9.65
BaO	0.09	0.08	0.04	0.02	0.00	0.03	0.02	0.05	0.21	0.23	0.29
ZnO	0.26	0.26	0.20	0.12	0.11	0.13	0.11	0.10	0.06	0.01	0.05
F	2.18	2.38	2.16	2.54	2.56	2.28	2.24	2.66	2.63	2.66	2.55
Cl	0.15	0.19	0.16	0.12	0.12	0.13	0.10	0.15	0.05	0.06	0.05
H_2O*	2.96	2.87	2.95	2.75	2.79	2.80	2.91	2.63	2.97	2.91	3.01
Subtotal	101.67	101.74	101.56	100.09	101.21	97.30	99.07	99.94	103.41	102.50	103.51
O=F, Cl	0.95	1.04	0.95	1.10	1.11	0.99	0.97	1.16	1.12	1.13	1.08
Total	100.72	100.70	100.62	98.99	100.10	96.32	98.11	98.78	102.29	101.37	102.43
Si	5.74	5.83	5.78	5.88	5.87	5.91	5.93	5.84	6.11	6.11	6.09
Al iv	2.26	2.17	2.22	2.12	2.13	2.09	2.07	2.16	1.89	1.89	1.91
Total	8.00	8.00	8.00	8.00	8.00	8.00	8.00	8.00	8.00	8.00	8.00
Al vi	0.60	0.61	0.56	0.65	0.62	0.69	0.72	0.57	0.02	0.03	0.02
Ti	0.27	0.29	0.33	0.24	0.24	0.24	0.23	0.24	0.16	0.17	0.17
Fe^{2+}	2.17	2.03	2.20	2.18	2.18	2.23	2.16	2.24	1.28	1.28	1.28
Mn	0.09	0.06	0.04	0.08	0.09	0.09	0.09	0.09	0.02	0.02	0.02
Mg	2.53	2.52	2.40	2.49	2.57	2.53	2.55	2.46	4.36	4.34	4.36
Zn	0.03	0.03	0.02	0.01	0.01	0.01	0.01	0.01	0.01	0.00	0.00
Total	5.69	5.53	5.56	5.66	5.72	5.79	5.77	5.61	5.86	5.83	5.85
Ca	0.00	0.00	0.00	0.00	0.00	0.00	0.00	0.00	0.00	0.00	0.00
Na	0.04	0.03	0.02	0.04	0.03	0.05	0.04	0.04	0.02	0.03	0.04
K	1.70	1.86	1.84	1.63	1.55	1.29	1.29	1.84	1.75	1.77	1.75
Total	1.74	1.89	1.86	1.67	1.59	1.34	1.33	1.88	1.77	1.80	1.79
OH*	2.94	2.84	2.94	2.76	2.77	2.86	2.91	2.68	2.81	2.78	2.85
F	1.03	1.12	1.02	1.21	1.20	1.10	1.06	1.28	1.18	1.21	1.14
Cl	0.04	0.05	0.04	0.03	0.03	0.03	0.03	0.04	0.01	0.01	0.01
Total	19.42	19.43	19.42	19.33	19.31	19.13	19.10	19.49	19.63	19.63	19.64
Fe/Fe+Mg	0.46	0.45	0.48	0.47	0.46	0.47	0.46	0.48	0.23	0.23	0.23

*H_2O calculations after Tindle and Webb (1990).

Appendix 4.2.4: Representative mineral chemistry for biotite

	DA13-040-1.4	DA13-040-1.5	DA13-040-2.1	DA13-040-2.2	DA13-040-2.3	DA13-040-2.4	DA13-040-2.5	DA13-040-2.6	DA13-040-2.7	DA13-040-2.8	DA13-040-2.9	DA13-040-2.10
SiO_2	43.19	42.36	42.57	42.08	42.51	42.36	42.22	42.22	42.59	41.38	42.95	41.92
TiO_2	1.55	1.58	1.85	1.82	1.90	1.93	1.89	1.84	1.81	1.84	1.88	1.87
Al_2O_3	11.47	11.31	11.53	11.37	11.40	11.53	11.48	11.54	11.51	11.21	11.56	11.32
FeOT	10.72	10.56	10.69	10.49	10.26	9.94	10.26	10.14	10.23	10.32	10.64	10.87
MnO	0.19	0.16	0.15	0.17	0.17	0.15	0.18	0.13	0.18	0.17	0.14	0.13
MgO	20.53	20.05	20.22	20.19	20.26	20.40	20.45	20.48	20.43	19.74	20.50	20.03
CaO	0.02	0.03	0.00	0.01	0.00	0.04	0.00	0.00	0.00	0.03	0.00	0.00
Na_2O	0.12	0.08	0.10	0.10	0.06	0.09	0.09	0.07	0.06	0.09	0.10	0.07
K_2O	9.69	9.60	9.74	9.80	9.81	9.74	9.94	9.83	9.84	9.82	9.70	9.74
BaO	0.26	0.24	0.53	0.46	0.43	0.40	0.39	0.45	0.42	0.39	0.50	0.53
ZnO	0.09	0.02	0.05	0.12	0.06	0.06	0.03	0.09	0.05	0.10	0.07	0.09
F	2.67	2.75	2.52	2.77	2.71	2.53	2.81	2.68	2.65	2.79	2.64	2.57
Cl	0.06	0.07	0.06	0.04	0.05	0.07	0.06	0.05	0.06	0.06	0.05	0.06
H_2O*	2.95	2.83	2.99	2.84	2.89	2.97	2.84	2.90	2.92	2.76	2.97	2.92
Subtotal	103.65	101.74	103.10	102.31	102.56	102.28	102.68	102.44	102.79	100.79	103.79	102.22
O=F, Cl	1.14	1.17	1.08	1.18	1.15	1.08	1.20	1.14	1.13	1.19	1.12	1.09
Total	102.51	100.56	102.02	101.13	101.40	101.20	101.49	101.30	101.66	99.60	102.67	101.12
Si	6.12	6.11	6.07	6.06	6.09	6.07	6.05	6.06	6.08	6.06	6.08	6.05
Al iv	1.88	1.89	1.93	1.93	1.91	1.93	1.94	1.94	1.92	1.94	1.92	1.93
Total	8.00	8.00	8.00	7.99	8.00	8.00	7.99	8.00	8.00	7.99	8.00	7.98
Al vi	0.03	0.04	0.01	0.00	0.02	0.02	0.00	0.01	0.02	0.00	0.01	0.00
Ti	0.16	0.17	0.20	0.20	0.20	0.21	0.20	0.20	0.19	0.20	0.20	0.20
Fe^{2+}	1.27	1.27	1.28	1.26	1.23	1.19	1.23	1.22	1.22	1.26	1.26	1.31
Mn	0.02	0.02	0.02	0.02	0.02	0.02	0.02	0.02	0.02	0.02	0.02	0.02
Mg	4.33	4.31	4.30	4.34	4.33	4.36	4.37	4.38	4.35	4.31	4.33	4.31
Zn	0.01	0.00	0.00	0.01	0.01	0.01	0.00	0.01	0.01	0.01	0.01	0.01
Total	5.83	5.82	5.81	5.83	5.81	5.80	5.83	5.83	5.82	5.81	5.82	5.85
Ca	0.00	0.01	0.00	0.00	0.00	0.01	0.00	0.00	0.00	0.01	0.00	0.00
Na	0.03	0.02	0.03	0.03	0.02	0.02	0.03	0.02	0.02	0.03	0.03	0.02
K	1.75	1.77	1.77	1.80	1.79	1.78	1.82	1.80	1.79	1.83	1.75	1.79
Total	1.79	1.79	1.80	1.83	1.81	1.81	1.84	1.82	1.81	1.86	1.78	1.81
OH*	2.79	2.73	2.85	2.73	2.76	2.84	2.71	2.77	2.79	2.69	2.80	2.81
F	1.20	1.26	1.14	1.26	1.23	1.15	1.27	1.21	1.20	1.29	1.18	1.17
Cl	0.01	0.02	0.01	0.01	0.01	0.02	0.01	0.01	0.02	0.01	0.01	0.01
Total	19.62	19.62	19.61	19.66	19.62	19.61	19.67	19.65	19.63	19.67	19.60	19.64
Fe/Fe+Mg	0.23	0.23	0.23	0.23	0.22	0.21	0.22	0.22	0.22	0.23	0.23	0.23

*H_2O calculations after Tindle and Webb (1990).

Appendix 4.2.4: Representative mineral chemistry for biotite

	DA13-040-5.1	DA13-040-5.2	DA13-040-5.3	DA13-040-5.4	DA13-040-5.5	DA13-049-3.1	DA13-049-3.2	DA13-049-3.3	DA13-049-3.4	DA13-049-3.5	DA13-049-4.1	DA13-049-4.2
SiO_2	42.79	43.07	42.70	42.65	42.74	39.08	39.52	36.11	39.31	39.70	38.57	39.71
TiO_2	1.47	1.55	1.54	1.58	1.56	0.84	0.87	0.90	0.76	0.74	1.08	1.01
Al_2O_3	11.26	11.22	11.20	11.26	11.20	14.93	15.00	13.13	15.48	16.23	14.83	15.16
FeOT	10.82	10.70	10.77	10.90	10.84	16.74	16.50	16.98	17.11	16.27	16.29	17.22
MnO	0.14	0.15	0.17	0.14	0.18	0.85	0.87	0.76	0.86	0.84	0.82	0.92
MgO	20.45	20.32	20.29	20.26	20.16	12.39	12.75	11.54	12.99	12.86	12.00	12.47
CaO	0.01	0.00	0.01	0.01	0.00	0.03	0.05	0.17	0.18	0.11	0.22	0.19
Na_2O	0.13	0.06	0.14	0.12	0.10	0.05	0.10	0.06	0.11	0.11	0.12	0.13
K_2O	9.63	9.69	9.66	9.53	9.67	9.27	9.34	8.44	7.99	9.25	7.94	8.23
BaO	0.31	0.26	0.28	0.30	0.28	0.00	0.04	0.03	0.02	0.05	0.13	0.10
ZnO	0.04	0.06	0.08	0.07	0.09	0.12	0.13	0.22	0.21	0.18	0.18	0.13
F	2.72	2.69	2.62	2.51	2.76	1.93	2.30	2.28	2.01	1.62	1.61	1.85
Cl	0.04	0.04	0.05	0.06	0.04	0.01	0.00	0.01	0.00	0.02	0.01	0.00
H_2O*	2.90	2.91	2.93	2.98	2.86	3.04	2.90	2.59	3.06	3.29	3.13	3.13
Subtotal	102.77	102.82	102.50	102.44	102.52	99.32	100.37	93.21	100.08	101.28	97.00	100.25
O=F, Cl	1.15	1.14	1.11	1.07	1.17	0.82	0.97	0.96	0.84	0.68	0.68	0.78
Total	101.62	101.68	101.38	101.37	101.35	98.51	99.40	92.25	99.23	100.59	96.31	99.47
Si	6.12	6.15	6.12	6.11	6.13	5.92	5.93	5.90	5.88	5.86	5.94	5.93
Al iv	1.88	1.85	1.88	1.89	1.87	2.08	2.07	2.10	2.12	2.14	2.06	2.07
Total	8.00	8.00	8.00	8.00	8.00	8.00	8.00	8.00	8.00	8.00	8.00	8.00
Al vi	0.02	0.03	0.01	0.02	0.02	0.59	0.58	0.43	0.61	0.69	0.63	0.60
Ti	0.16	0.17	0.17	0.17	0.17	0.10	0.10	0.11	0.09	0.08	0.13	0.11
Fe^{2+}	1.29	1.28	1.29	1.31	1.30	2.12	2.07	2.32	2.14	2.01	2.10	2.15
Mn	0.02	0.02	0.02	0.02	0.02	0.11	0.11	0.11	0.11	0.11	0.11	0.12
Mg	4.36	4.32	4.34	4.33	4.31	2.80	2.85	2.81	2.90	2.83	2.76	2.78
Zn	0.00	0.01	0.01	0.01	0.01	0.01	0.01	0.03	0.02	0.02	0.02	0.01
Total	5.85	5.82	5.84	5.84	5.83	5.73	5.73	5.80	5.86	5.73	5.74	5.78
Ca	0.00	0.00	0.00	0.00	0.00	0.01	0.01	0.03	0.03	0.02	0.04	0.03
Na	0.04	0.02	0.04	0.03	0.03	0.02	0.03	0.02	0.03	0.03	0.04	0.04
K	1.76	1.76	1.77	1.74	1.77	1.79	1.79	1.76	1.52	1.74	1.56	1.57
Total	1.79	1.78	1.81	1.78	1.80	1.81	1.83	1.81	1.58	1.79	1.63	1.64
OH*	2.76	2.77	2.80	2.85	2.74	3.07	2.91	2.82	3.05	3.24	3.21	3.12
F	1.23	1.22	1.19	1.14	1.25	0.93	1.09	1.18	0.95	0.75	0.79	0.88
Cl	0.01	0.01	0.01	0.01	0.01	0.00	0.00	0.00	0.00	0.00	0.00	0.00
Total	19.64	19.61	19.64	19.62	19.63	19.54	19.55	19.61	19.45	19.53	19.37	19.41
Fe/Fe+Mg	0.23	0.23	0.23	0.23	0.23	0.43	0.42	0.45	0.43	0.42	0.43	0.44

*H_2O calculations after Tindle and Webb (1990).

Appendix 4.2.4: Representative mineral chemistry for biotite

	DA13-049-4.3	DA13-049-4.4	DA13-049-4.5	DA13-049-8.1	DA13-049-8.2	DA13-049-8.3	DA13-049-8.4	DA13-049-8.5	DA13-049-8.6	DA13-049-8.7	DA13-049-8.8	DA13-049-8.9
SiO_2	39.12	39.47	39.47	38.75	39.24	38.79	39.73	39.45	39.29	36.70	39.31	38.81
TiO_2	0.95	1.02	1.19	0.95	1.12	1.17	1.22	1.31	1.36	1.25	1.31	1.32
Al_2O_3	14.91	14.92	14.65	14.64	14.55	14.52	14.87	14.38	14.70	13.79	14.95	14.69
FeOT	17.10	16.89	17.27	18.63	19.01	18.98	19.12	18.57	18.73	18.63	18.20	18.82
MnO	0.85	0.99	0.95	0.85	0.86	0.89	0.79	0.79	0.80	0.63	0.68	0.73
MgO	12.18	12.36	12.72	11.56	11.42	11.27	11.52	11.31	11.37	9.79	10.51	10.41
CaO	0.18	0.08	0.11	0.10	0.01	0.02	0.02	0.05	0.07	0.31	0.31	0.21
Na_2O	0.12	0.07	0.07	0.07	0.07	0.09	0.07	0.07	0.07	0.09	0.05	0.09
K_2O	8.34	8.84	8.67	8.71	9.08	8.99	9.01	9.21	8.81	6.51	6.96	7.62
BaO	0.05	0.03	0.08	0.03	0.04	0.05	0.06	0.19	0.09	0.30	0.14	0.14
ZnO	0.15	0.17	0.06	0.14	0.13	0.14	0.11	0.05	0.15	0.07	0.11	0.15
F	2.05	1.98	1.85	1.98	1.86	1.68	1.72	2.04	1.89	1.72	1.95	1.76
Cl	0.01	0.01	0.02	0.00	0.00	0.00	0.01	0.01	0.01	0.01	0.01	0.01
H_2O*	2.98	3.04	3.11	2.99	3.08	3.14	3.20	3.00	3.07	2.87	2.98	3.05
Subtotal	98.99	99.90	100.23	99.41	100.48	99.80	101.46	100.42	100.44	92.67	97.50	97.80
O=F, Cl	0.86	0.84	0.78	0.83	0.79	0.71	0.73	0.86	0.80	0.72	0.82	0.74
Total	98.13	99.06	99.44	98.58	99.69	99.09	100.73	99.56	99.64	91.95	96.67	97.06
Si	5.94	5.94	5.92	5.91	5.93	5.91	5.93	5.97	5.93	5.98	6.03	5.98
Al iv	2.06	2.06	2.08	2.09	2.07	2.09	2.07	2.03	2.07	2.02	1.97	2.02
Total	8.00	8.00	8.00	8.00	8.00	8.00	8.00	8.00	8.00	8.00	8.00	8.00
Al vi	0.60	0.59	0.51	0.54	0.52	0.51	0.55	0.53	0.54	0.62	0.73	0.65
Ti	0.11	0.12	0.13	0.11	0.13	0.13	0.14	0.15	0.15	0.15	0.15	0.15
Fe^{2+}	2.17	2.13	2.17	2.38	2.40	2.42	2.39	2.35	2.36	2.54	2.33	2.42
Mn	0.11	0.13	0.12	0.11	0.11	0.11	0.10	0.10	0.10	0.09	0.09	0.10
Mg	2.76	2.77	2.84	2.63	2.57	2.56	2.56	2.55	2.56	2.37	2.40	2.39
Zn	0.02	0.02	0.01	0.02	0.01	0.02	0.01	0.01	0.02	0.01	0.01	0.02
Total	5.76	5.74	5.78	5.79	5.75	5.75	5.75	5.69	5.73	5.78	5.72	5.73
Ca	0.03	0.01	0.02	0.02	0.00	0.00	0.00	0.01	0.01	0.05	0.05	0.03
Na	0.03	0.02	0.02	0.02	0.02	0.03	0.02	0.02	0.02	0.03	0.02	0.03
K	1.61	1.70	1.66	1.70	1.75	1.75	1.72	1.78	1.70	1.35	1.36	1.50
Total	1.68	1.73	1.70	1.73	1.77	1.78	1.74	1.80	1.73	1.43	1.43	1.56
OH*	3.02	3.06	3.12	3.04	3.11	3.19	3.19	3.02	3.09	3.11	3.05	3.14
F	0.98	0.94	0.88	0.96	0.89	0.81	0.81	0.98	0.90	0.88	0.94	0.86
Cl	0.00	0.00	0.00	0.00	0.00	0.00	0.00	0.00	0.00	0.00	0.00	0.00
Total	19.44	19.48	19.48	19.52	19.53	19.53	19.49	19.49	19.46	19.22	19.15	19.29
Fe/Fe+Mg	0.44	0.43	0.43	0.47	0.48	0.49	0.48	0.48	0.48	0.52	0.49	0.50

*H_2O calculations after Tindle and Webb (1990).

Appendix 4.2.4: Representative mineral chemistry for biotite

	DA13-049-8.10	DA13-055-1.1	DA13-055-1.2	DA13-055-1.3	DA13-055-1.4	DA13-055-1.5	DA13-055-1.6	DA13-055-1.7	DA13-055-1.8	DA13-055-1.9	DA13-055-1.10	DA13-055-8.1
SiO_2	38.21	37.58	37.90	37.11	37.50	37.20	37.42	37.76	38.25	37.72	36.79	37.72
TiO_2	1.32	3.98	4.05	4.02	4.00	4.11	4.01	3.95	3.86	3.93	3.84	3.75
Al_2O_3	13.97	13.91	14.16	13.88	13.95	13.81	13.85	13.93	14.39	13.96	13.59	14.05
FeOT	18.85	22.87	22.90	22.98	23.24	23.35	23.34	23.17	23.30	23.63	23.00	22.56
MnO	0.78	0.30	0.32	0.28	0.31	0.29	0.27	0.32	0.32	0.27	0.31	0.25
MgO	10.74	8.52	8.57	8.39	8.65	8.35	8.51	8.80	8.88	8.72	8.29	8.91
CaO	0.11	0.05	0.03	0.01	0.02	0.02	0.01	0.00	0.01	0.06	0.02	0.03
Na_2O	0.08	0.13	0.12	0.13	0.08	0.08	0.09	0.09	0.06	0.09	0.04	0.13
K_2O	8.68	9.23	9.27	9.16	9.14	9.27	9.32	9.26	9.09	9.06	9.26	9.20
BaO	0.12	0.46	0.43	0.40	0.29	0.33	0.28	0.34	0.29	0.31	0.39	0.40
ZnO	0.15	0.08	0.03	0.09	0.08	0.05	0.10	0.07	0.12	0.09	0.09	0.07
F	2.14	0.07	0.20	0.14	0.13	0.15	0.15	0.17	0.15	0.17	0.14	0.17
Cl	0.00	0.08	0.08	0.06	0.08	0.07	0.06	0.05	0.04	0.09	0.07	0.06
H_2O*	2.84	3.88	3.85	3.81	3.85	3.82	3.84	3.86	3.92	3.85	3.77	3.84
Subtotal	97.98	101.13	101.90	100.47	101.32	100.91	101.28	101.77	102.70	101.95	99.61	101.15
O=F, Cl	0.90	0.05	0.10	0.07	0.07	0.08	0.08	0.08	0.07	0.09	0.08	0.08
Total	97.08	101.08	101.79	100.40	101.25	100.83	101.20	101.69	102.63	101.86	99.54	101.06
Si	5.94	5.74	5.74	5.71	5.71	5.71	5.71	5.73	5.73	5.72	5.72	5.74
Al iv	2.06	2.26	2.26	2.29	2.29	2.29	2.29	2.27	2.27	2.28	2.28	2.26
Total	8.00	8.00	8.00	8.00	8.00	8.00	8.00	8.00	8.00	8.00	8.00	8.00
Al vi	0.51	0.24	0.26	0.23	0.22	0.20	0.21	0.22	0.27	0.21	0.21	0.26
Ti	0.15	0.46	0.46	0.47	0.46	0.47	0.46	0.45	0.43	0.45	0.45	0.43
Fe^{2+}	2.45	2.92	2.90	2.96	2.96	3.00	2.98	2.94	2.92	3.00	2.99	2.87
Mn	0.10	0.04	0.04	0.04	0.04	0.04	0.03	0.04	0.04	0.04	0.04	0.03
Mg	2.49	1.94	1.93	1.93	1.96	1.91	1.94	1.99	1.98	1.97	1.92	2.02
Zn	0.02	0.01	0.00	0.01	0.01	0.01	0.01	0.01	0.01	0.01	0.01	0.01
Total	5.72	5.60	5.60	5.62	5.65	5.63	5.63	5.65	5.66	5.67	5.63	5.63
Ca	0.02	0.01	0.00	0.00	0.00	0.00	0.00	0.00	0.00	0.01	0.00	0.01
Na	0.02	0.04	0.03	0.04	0.02	0.03	0.03	0.03	0.02	0.03	0.01	0.04
K	1.72	1.80	1.79	1.80	1.78	1.81	1.82	1.79	1.74	1.75	1.84	1.79
Total	1.76	1.84	1.83	1.84	1.80	1.84	1.84	1.82	1.75	1.79	1.85	1.83
OH*	2.95	3.95	3.88	3.92	3.92	3.91	3.91	3.91	3.92	3.90	3.91	3.90
F	1.05	0.03	0.10	0.07	0.06	0.07	0.07	0.08	0.07	0.08	0.07	0.08
Cl	0.00	0.02	0.02	0.02	0.02	0.02	0.02	0.01	0.01	0.02	0.02	0.02
Total	19.49	19.45	19.43	19.46	19.46	19.47	19.48	19.46	19.42	19.46	19.48	19.45
Fe/Fe+Mg	0.50	0.60	0.60	0.61	0.60	0.61	0.61	0.60	0.60	0.60	0.61	0.59

*H_2O calculations after Tindle and Webb (1990).

Appendix 4.2.4: Representative mineral chemistry for biotite

	DA13-055-8.2	DA13-055-8.3	DA13-055-8.4	DA13-055-8.5	DA13-064-3.1	DA13-064-3.2	DA13-064-3.3	DA13-064-3.4	DA13-064-3.5	DA13-064-3.6	DA13-064-3.7	DA13-064-3.8
SiO_2	37.28	37.42	37.28	36.89	39.97	41.00	41.26	39.55	39.68	39.81	39.41	39.28
TiO_2	3.78	3.85	3.87	3.84	0.86	0.79	0.87	1.01	1.04	1.02	1.02	1.02
Al_2O_3	13.90	13.89	13.92	13.72	13.88	16.96	17.40	14.33	14.00	14.15	14.22	14.14
FeOT	23.06	22.99	23.09	22.58	15.95	14.75	15.26	16.26	16.48	16.32	16.22	15.99
MnO	0.22	0.26	0.24	0.24	0.97	0.87	0.87	0.91	0.81	0.92	0.93	0.92
MgO	8.73	8.73	8.72	8.53	13.62	12.02	12.43	13.14	13.52	13.62	13.12	13.13
CaO	0.05	0.02	0.03	0.04	0.07	0.09	0.09	0.02	0.04	0.03	0.02	0.01
Na_2O	0.12	0.08	0.08	0.13	0.06	0.05	0.10	0.08	0.06	0.08	0.09	0.07
K_2O	9.22	9.21	9.25	9.29	9.32	7.71	8.09	9.52	9.49	9.44	9.52	9.59
BaO	0.27	0.39	0.39	0.34	0.07	0.08	0.11	0.09	0.03	0.06	0.08	0.06
ZnO	0.10	0.03	0.12	0.08	0.22	0.18	0.18	0.20	0.19	0.20	0.15	0.23
F	0.22	0.15	0.20	0.22	2.13	1.76	1.75	2.16	1.99	2.17	2.03	2.11
Cl	0.07	0.04	0.05	0.06	0.04	0.05	0.03	0.02	0.02	0.01	0.05	0.04
H_2O*	3.79	3.84	3.81	3.75	2.97	3.23	3.31	2.96	3.05	2.98	3.00	2.95
Subtotal	100.80	100.91	101.08	99.70	100.12	99.52	101.78	100.28	100.42	100.81	99.92	99.55
O=F, Cl	0.11	0.07	0.10	0.11	0.90	0.75	0.75	0.92	0.84	0.92	0.87	0.90
Total	100.70	100.84	100.99	99.60	99.21	98.77	101.04	99.36	99.57	99.89	99.05	98.66
Si	5.71	5.72	5.70	5.72	6.00	6.04	5.96	5.95	5.95	5.95	5.95	5.95
Al iv	2.29	2.28	2.30	2.28	2.00	1.96	2.04	2.05	2.05	2.05	2.05	2.05
Total	8.00	8.00	8.00	8.00	8.00	8.00	8.00	8.00	8.00	8.00	8.00	8.00
Al vi	0.22	0.23	0.21	0.23	0.46	0.98	0.93	0.49	0.43	0.44	0.48	0.48
Ti	0.44	0.44	0.45	0.45	0.10	0.09	0.10	0.11	0.12	0.11	0.12	0.12
Fe^{2+}	2.96	2.94	2.95	2.93	2.00	1.82	1.85	2.04	2.07	2.04	2.05	2.03
Mn	0.03	0.03	0.03	0.03	0.12	0.11	0.11	0.12	0.10	0.12	0.12	0.12
Mg	1.99	1.99	1.99	1.97	3.05	2.64	2.68	2.95	3.02	3.03	2.95	2.97
Zn	0.01	0.00	0.01	0.01	0.02	0.02	0.02	0.02	0.02	0.02	0.02	0.03
Total	5.65	5.64	5.65	5.61	5.76	5.65	5.68	5.73	5.76	5.77	5.72	5.73
Ca	0.01	0.00	0.00	0.01	0.01	0.01	0.01	0.00	0.01	0.01	0.00	0.00
Na	0.04	0.02	0.02	0.04	0.02	0.01	0.03	0.02	0.02	0.02	0.03	0.02
K	1.80	1.80	1.81	1.84	1.79	1.45	1.49	1.83	1.82	1.80	1.83	1.85
Total	1.85	1.82	1.83	1.88	1.81	1.48	1.54	1.85	1.84	1.83	1.86	1.88
OH*	3.88	3.92	3.89	3.88	2.98	3.17	3.19	2.97	3.05	2.97	3.02	2.98
F	0.11	0.07	0.10	0.11	1.01	0.82	0.80	1.03	0.95	1.03	0.97	1.01
Cl	0.02	0.01	0.01	0.02	0.01	0.01	0.01	0.01	0.00	0.00	0.01	0.01
Total	19.50	19.47	19.48	19.50	19.57	19.13	19.21	19.58	19.61	19.60	19.59	19.60
Fe/Fe+Mg	0.60	0.60	0.60	0.60	0.40	0.41	0.41	0.41	0.41	0.40	0.41	0.41

*H_2O calculations after Tindle and Webb (1990).

Appendix 4.2.4: Representative mineral chemistry for biotite

	DA13-064-3.9	DA13-064-3.10	DA13-064-3.11	DA13-064-3.12	DA13-064-3.13	DA13-064-3.14	DA13-069-1.1	DA13-069-1.2	DA13-069-1.3	DA13-069-1.4	DA13-069-1.5
SiO_2	40.02	40.42	38.99	43.20	40.63	39.91	39.83	39.89	39.96	40.14	40.11
TiO_2	1.04	1.01	1.05	0.67	0.95	0.89	1.18	1.19	1.19	1.23	1.26
Al_2O_3	14.09	15.53	13.88	23.90	16.45	16.62	13.27	13.13	13.08	13.13	13.10
FeOT	16.26	15.83	17.56	11.78	15.92	16.30	18.22	18.07	18.02	18.21	18.09
MnO	0.95	0.88	0.88	0.41	0.78	0.81	0.24	0.22	0.26	0.27	0.26
MgO	13.86	12.80	12.55	7.38	12.08	10.95	13.72	13.69	13.81	13.85	13.92
CaO	0.05	0.04	0.07	0.09	0.08	0.12	0.02	0.02	0.02	0.03	0.03
Na_2O	0.03	0.06	0.07	0.08	0.08	0.08	0.13	0.09	0.13	0.10	0.13
K_2O	9.38	8.52	8.93	4.82	7.57	7.16	9.48	9.56	9.49	9.51	9.45
BaO	0.04	0.06	0.09	0.04	0.10	0.12	0.08	0.13	0.14	0.18	0.16
ZnO	0.13	0.19	0.11	0.07	0.13	0.14	0.00	0.00	0.09	0.00	0.08
F	2.32	1.79	1.87	0.85	1.59	1.51	2.22	2.21	2.18	2.22	2.18
Cl	0.04	0.04	0.04	0.03	0.03	0.03	0.09	0.11	0.12	0.10	0.10
H_2O*	2.92	3.19	3.03	3.79	3.30	3.26	2.93	2.93	2.94	2.95	2.97
Subtotal	101.14	100.39	99.14	97.14	99.68	97.90	101.43	101.21	101.45	101.95	101.89
O=F, Cl	0.98	0.77	0.80	0.36	0.68	0.64	0.96	0.95	0.95	0.96	0.94
Total	100.15	99.63	98.34	96.78	99.00	97.25	100.48	100.26	100.50	100.99	100.95
Si	5.96	5.98	5.95	6.16	6.00	6.01	5.96	5.98	5.98	5.98	5.97
Al iv	2.04	2.02	2.05	1.84	2.00	1.99	2.04	2.02	2.02	2.02	2.03
Total	8.00	8.00	8.00	8.00	8.00	8.00	8.00	8.00	8.00	8.00	8.00
Al vi	0.43	0.69	0.44	2.18	0.87	0.96	0.30	0.30	0.28	0.28	0.27
Ti	0.12	0.11	0.12	0.07	0.11	0.10	0.13	0.13	0.13	0.14	0.14
Fe^{2+}	2.02	1.96	2.24	1.41	1.97	2.05	2.28	2.27	2.25	2.27	2.25
Mn	0.12	0.11	0.11	0.05	0.10	0.10	0.03	0.03	0.03	0.03	0.03
Mg	3.08	2.82	2.85	1.57	2.66	2.46	3.06	3.06	3.08	3.07	3.09
Zn	0.01	0.02	0.01	0.01	0.01	0.02	0.00	0.00	0.01	0.00	0.01
Total	5.78	5.72	5.79	5.28	5.71	5.69	5.80	5.79	5.80	5.80	5.80
Ca	0.01	0.01	0.01	0.01	0.01	0.02	0.00	0.00	0.00	0.00	0.01
Na	0.01	0.02	0.02	0.02	0.02	0.02	0.04	0.03	0.04	0.03	0.04
K	1.78	1.61	1.74	0.88	1.43	1.37	1.81	1.83	1.81	1.81	1.79
Total	1.80	1.63	1.77	0.91	1.46	1.42	1.85	1.86	1.85	1.84	1.84
OH*	2.90	3.15	3.09	3.61	3.25	3.27	2.93	2.93	2.94	2.93	2.95
F	1.09	0.84	0.90	0.38	0.74	0.72	1.05	1.05	1.03	1.05	1.03
Cl	0.01	0.01	0.01	0.01	0.01	0.01	0.02	0.03	0.03	0.03	0.03
Total	19.58	19.36	19.56	18.20	19.18	19.11	19.65	19.64	19.65	19.63	19.64
Fe/Fe+Mg	0.40	0.41	0.44	0.47	0.42	0.46	0.43	0.43	0.42	0.42	0.42

*H_2O calculations after Tindle and Webb (1990).

Appendix 4.2.4: Representative mineral chemistry for biotite

	DA13-069-2.1	DA13-069-2.2	DA13-069-2.3	DA13-069-2.4	DA13-069-2.5	DA13-069-2.6	DA13-069-2.7	DA13-069-2.8	DA13-069-2.9	DA13-069-2.10	DA13-069-3.1	DA13-069-3.2
SiO_2	39.65	39.82	39.72	39.65	39.47	39.76	39.26	39.39	40.24	40.45	38.76	38.04
TiO_2	1.21	1.21	1.25	1.33	1.28	1.37	1.21	1.21	1.33	1.34	1.17	1.13
Al_2O_3	13.26	13.25	13.14	13.19	13.23	13.35	13.23	12.98	12.99	13.23	13.46	13.44
FeOT	18.51	18.14	18.26	18.17	18.13	18.19	17.45	17.56	17.62	17.64	19.09	19.76
MnO	0.26	0.22	0.23	0.25	0.25	0.27	0.25	0.25	0.28	0.23	0.25	0.24
MgO	13.74	13.57	13.65	13.50	13.60	13.84	13.72	13.67	14.19	14.20	12.48	13.11
CaO	0.00	0.01	0.00	0.00	0.00	0.01	0.00	0.06	0.00	0.00	0.09	0.03
Na_2O	0.09	0.09	0.06	0.02	0.08	0.07	0.08	0.12	0.09	0.11	0.12	0.10
K_2O	9.53	9.64	9.52	9.72	9.60	9.52	9.78	9.53	9.72	9.62	8.60	7.91
BaO	0.17	0.13	0.10	0.09	0.11	0.17	0.11	0.13	0.16	0.12	0.13	0.14
ZnO	0.08	0.12	0.04	0.01	0.00	0.04	0.00	0.02	0.01	0.00	0.00	0.02
F	2.12	2.16	2.11	2.16	2.05	2.16	2.18	2.21	2.33	2.18	1.99	1.86
Cl	0.10	0.12	0.11	0.09	0.10	0.09	0.09	0.10	0.11	0.13	0.13	0.10
H_2O*	2.98	2.95	2.97	2.95	2.99	2.97	2.90	2.89	2.90	2.99	2.94	2.99
Subtotal	101.73	101.44	101.21	101.16	100.93	101.88	100.29	100.19	102.04	102.29	99.20	98.91
O=F, Cl	0.91	0.94	0.91	0.93	0.89	0.93	0.94	0.95	1.01	0.95	0.87	0.81
Total	100.82	100.50	100.29	100.24	100.05	100.95	99.35	99.23	101.03	101.34	98.33	98.10
Si	5.93	5.96	5.96	5.96	5.94	5.93	5.94	5.97	5.98	5.98	5.94	5.85
Al iv	2.07	2.04	2.04	2.04	2.06	2.07	2.06	2.03	2.02	2.02	2.06	2.15
Total	8.00	8.00	8.00	8.00	8.00	8.00	8.00	8.00	8.00	8.00	8.00	8.00
Al vi	0.27	0.30	0.28	0.29	0.29	0.27	0.30	0.28	0.26	0.29	0.37	0.28
Ti	0.14	0.14	0.14	0.15	0.14	0.15	0.14	0.14	0.15	0.15	0.13	0.13
Fe^{2+}	2.32	2.27	2.29	2.28	2.28	2.27	2.21	2.23	2.19	2.18	2.45	2.54
Mn	0.03	0.03	0.03	0.03	0.03	0.03	0.03	0.03	0.04	0.03	0.03	0.03
Mg	3.06	3.03	3.05	3.02	3.05	3.08	3.09	3.09	3.14	3.13	2.85	3.00
Zn	0.01	0.01	0.00	0.00	0.00	0.00	0.00	0.00	0.00	0.00	0.00	0.00
Total	5.83	5.78	5.80	5.78	5.80	5.81	5.77	5.77	5.78	5.78	5.83	5.99
Ca	0.00	0.00	0.00	0.00	0.00	0.00	0.00	0.01	0.00	0.00	0.01	0.01
Na	0.03	0.03	0.02	0.00	0.02	0.02	0.02	0.04	0.03	0.03	0.04	0.03
K	1.82	1.84	1.82	1.86	1.84	1.81	1.89	1.84	1.84	1.81	1.68	1.55
Total	1.84	1.87	1.84	1.87	1.87	1.83	1.91	1.89	1.87	1.85	1.73	1.59
OH*	2.97	2.94	2.97	2.95	3.00	2.96	2.93	2.92	2.88	2.95	3.00	3.07
F	1.00	1.03	1.00	1.02	0.98	1.02	1.05	1.06	1.10	1.02	0.96	0.90
Cl	0.03	0.03	0.03	0.02	0.03	0.02	0.02	0.03	0.03	0.03	0.03	0.03
Total	19.67	19.65	19.64	19.65	19.66	19.64	19.68	19.65	19.65	19.62	19.56	19.58
Fe/Fe+Mg	0.43	0.43	0.43	0.43	0.43	0.42	0.42	0.42	0.41	0.41	0.46	0.46

*H_2O calculations after Tindle and Webb (1990).

Appendix 4.2.4: Representative mineral chemistry for biotite

	DA13-069-3.3	DA13-069-3.4	DA13-069-3.5	DA13-074-2.1	DA13-074-2.2	DA13-074-2.3	DA13-074-2.4	DA13-074-2.5	DA13-074-4.1	DA13-074-4.2	DA13-074-4.3	DA13-074-4.4
SiO_2	39.35	39.88	39.40	37.15	34.70	36.16	37.02	35.76	36.95	35.50	32.64	36.66
TiO_2	1.24	1.22	1.23	3.89	4.07	3.39	3.94	3.90	4.60	4.17	3.09	4.61
Al_2O_3	13.35	13.07	12.83	13.37	13.02	15.68	13.67	13.12	13.30	13.94	15.06	12.87
FeOT	18.99	18.58	18.69	28.60	27.67	27.58	28.81	28.87	29.18	30.63	33.02	29.08
MnO	0.18	0.19	0.21	0.13	0.11	0.27	0.17	0.13	0.20	0.20	0.21	0.19
MgO	12.87	13.23	13.18	4.18	4.04	3.95	4.19	4.00	4.55	4.84	5.16	4.37
CaO	0.00	0.00	0.03	0.06	1.05	0.34	0.04	0.07	0.07	0.11	0.17	0.04
Na_2O	0.09	0.04	0.10	0.16	0.19	0.15	0.13	0.15	0.11	0.09	0.10	0.14
K_2O	9.27	9.46	9.40	8.84	7.01	7.62	9.00	9.09	8.42	6.62	3.82	8.92
BaO	0.09	0.16	0.17	0.29	0.21	0.15	0.34	0.24	0.23	0.16	0.12	0.27
ZnO	0.04	0.06	0.06	0.12	0.08	0.12	0.10	0.08	0.13	0.08	0.17	0.13
F	1.91	2.05	2.11	2.03	1.08	1.89	2.04	2.37	1.68	0.83	0.28	2.16
Cl	0.10	0.13	0.12	0.15	0.14	0.13	0.16	0.15	0.16	0.14	0.11	0.17
H_2O*	3.03	2.98	2.92	2.82	3.10	2.88	2.83	2.57	3.02	3.37	3.52	2.75
Subtotal	100.51	101.06	100.45	101.83	96.47	100.34	102.47	100.51	102.60	100.69	97.47	102.38
O=F, Cl	0.83	0.89	0.92	0.89	0.48	0.83	0.90	1.03	0.74	0.38	0.14	0.95
Total	99.68	100.17	99.53	100.94	95.99	99.52	101.57	99.48	101.86	100.31	97.32	101.43
Si	5.95	6.00	5.98	5.83	5.71	5.69	5.79	5.74	5.75	5.60	5.32	5.76
Al iv	2.05	2.00	2.02	2.17	2.29	2.31	2.21	2.26	2.25	2.40	2.68	2.24
Total	8.00	8.00	8.00	8.00	8.00	8.00	8.00	8.00	8.00	8.00	8.00	8.00
Al vi	0.33	0.31	0.27	0.31	0.23	0.60	0.30	0.23	0.19	0.19	0.22	0.14
Ti	0.14	0.14	0.14	0.46	0.50	0.40	0.46	0.47	0.54	0.49	0.38	0.54
Fe^{2+}	2.40	2.34	2.37	3.75	3.81	3.63	3.77	3.88	3.80	4.04	4.50	3.82
Mn	0.02	0.02	0.03	0.02	0.02	0.04	0.02	0.02	0.03	0.03	0.03	0.03
Mg	2.90	2.97	2.98	0.98	0.99	0.93	0.98	0.96	1.05	1.14	1.25	1.02
Zn	0.00	0.01	0.01	0.01	0.01	0.01	0.01	0.01	0.01	0.01	0.02	0.02
Total	5.81	5.78	5.80	5.53	5.56	5.60	5.54	5.56	5.62	5.90	6.40	5.57
Ca	0.00	0.00	0.00	0.01	0.19	0.06	0.01	0.01	0.01	0.02	0.03	0.01
Na	0.03	0.01	0.03	0.05	0.06	0.05	0.04	0.05	0.03	0.03	0.03	0.04
K	1.79	1.81	1.82	1.77	1.47	1.53	1.79	1.86	1.67	1.33	0.79	1.79
Total	1.81	1.83	1.85	1.83	1.72	1.63	1.84	1.92	1.72	1.38	0.85	1.83
OH*	3.06	2.99	2.96	2.95	3.40	3.03	2.95	2.75	3.13	3.55	3.82	2.88
F	0.92	0.98	1.01	1.01	0.56	0.94	1.01	1.21	0.83	0.42	0.15	1.07
Cl	0.03	0.03	0.03	0.04	0.04	0.04	0.04	0.04	0.04	0.04	0.03	0.05
Total	19.62	19.61	19.65	19.36	19.28	19.23	19.38	19.48	19.33	19.28	19.26	19.40
Fe/Fe+Mg	0.45	0.44	0.44	0.79	0.79	0.80	0.79	0.80	0.78	0.78	0.78	0.79

*H_2O calculations after Tindle and Webb (1990).

Appendix 4.2.4: Representative mineral chemistry for biotite

	DA13-074-4.5	DA13-074-4.6	DA13-074-4.7	DA13-074-4.8	DA13-074-4.9	DA13-074-7.1	DA13-074-7.2	DA13-074-7.3	DA13-074-7.4	DA13-074-7.5	DA13-074-7.6	DA13-074-7.7
SiO_2	36.46	36.49	36.61	36.27	36.69	36.17	37.19	37.45	37.56	37.07	37.56	37.19
TiO_2	4.69	4.76	4.78	4.72	4.70	4.89	4.78	4.73	4.71	4.72	4.66	4.73
Al_2O_3	12.65	13.14	13.08	13.09	13.11	12.96	13.15	13.20	13.30	13.08	13.09	13.06
FeOT	29.20	29.12	29.19	29.19	29.15	29.30	28.48	28.40	28.26	28.64	28.54	28.70
MnO	0.20	0.16	0.21	0.21	0.19	0.18	0.17	0.16	0.14	0.21	0.18	0.16
MgO	4.29	3.99	4.10	4.01	4.09	3.94	4.40	4.38	4.46	4.36	4.46	4.40
CaO	0.06	0.00	0.00	0.00	0.00	0.00	0.00	0.00	0.03	0.01	0.00	0.00
Na_2O	0.12	0.10	0.07	0.09	0.09	0.06	0.09	0.08	0.12	0.11	0.08	0.09
K_2O	9.10	9.06	9.08	8.71	8.99	9.09	9.08	9.16	9.15	9.16	9.12	9.18
BaO	0.28	0.24	0.37	0.35	0.30	0.29	0.35	0.37	0.38	0.41	0.33	0.33
ZnO	0.04	0.04	0.05	0.11	0.13	0.12	0.21	0.11	0.20	0.13	0.11	0.12
F	2.30	2.24	2.40	1.99	2.25	2.27	2.28	2.12	2.06	2.10	2.25	2.24
Cl	0.17	0.15	0.16	0.15	0.15	0.15	0.17	0.15	0.17	0.16	0.17	0.15
H_2O*	2.67	2.71	2.64	2.81	2.72	2.68	2.74	2.82	2.86	2.81	2.76	2.75
Subtotal	102.23	102.21	102.77	101.72	102.55	102.10	103.11	103.14	103.40	102.99	103.32	103.12
O=F, Cl	1.01	0.98	1.05	0.87	0.98	0.99	1.00	0.93	0.90	0.92	0.98	0.98
Total	101.23	101.24	101.73	100.85	101.57	101.11	102.11	102.21	102.49	102.07	102.34	102.14
Si	5.75	5.74	5.74	5.73	5.75	5.72	5.78	5.80	5.80	5.77	5.82	5.78
Al iv	2.25	2.26	2.26	2.27	2.25	2.28	2.22	2.20	2.20	2.23	2.18	2.22
Total	8.00	8.00	8.00	8.00	8.00	8.00	8.00	8.00	8.00	8.00	8.00	8.00
Al vi	0.10	0.18	0.16	0.17	0.18	0.13	0.19	0.22	0.22	0.18	0.21	0.18
Ti	0.56	0.56	0.56	0.56	0.55	0.58	0.56	0.55	0.55	0.55	0.54	0.55
Fe^{2+}	3.85	3.83	3.83	3.86	3.82	3.87	3.70	3.68	3.65	3.73	3.70	3.73
Mn	0.03	0.02	0.03	0.03	0.03	0.02	0.02	0.02	0.02	0.03	0.02	0.02
Mg	1.01	0.94	0.96	0.94	0.96	0.93	1.02	1.01	1.03	1.01	1.03	1.02
Zn	0.00	0.00	0.01	0.01	0.02	0.01	0.02	0.01	0.02	0.01	0.01	0.01
Total	5.55	5.54	5.54	5.57	5.55	5.55	5.52	5.50	5.49	5.52	5.51	5.52
Ca	0.01	0.00	0.00	0.00	0.00	0.00	0.00	0.00	0.00	0.00	0.00	0.00
Na	0.04	0.03	0.02	0.03	0.03	0.02	0.03	0.03	0.04	0.03	0.03	0.03
K	1.83	1.82	1.82	1.75	1.80	1.83	1.80	1.81	1.80	1.82	1.80	1.82
Total	1.88	1.85	1.84	1.78	1.82	1.85	1.83	1.84	1.84	1.86	1.83	1.85
OH*	2.81	2.85	2.77	2.96	2.84	2.83	2.84	2.92	2.95	2.92	2.85	2.86
F	1.15	1.11	1.19	1.00	1.12	1.13	1.12	1.04	1.01	1.04	1.10	1.10
Cl	0.05	0.04	0.04	0.04	0.04	0.04	0.05	0.04	0.04	0.04	0.04	0.04
Total	19.43	19.38	19.38	19.36	19.37	19.40	19.35	19.33	19.33	19.37	19.34	19.37
Fe/Fe+Mg	0.79	0.80	0.80	0.80	0.80	0.81	0.78	0.78	0.78	0.79	0.78	0.79

*H_2O calculations after Tindle and Webb (1990).

Appendix 4.2.4: Representative mineral chemistry for biotite

	DA13-074-7.8	DA13-074-7.9	DA13-074-7.10	DA13-074-7.11	DA13-074-7.12	DA13-074-7.13	DA13-076-1.1	DA13-076-1.2	DA13-076-1.3	DA13-076-7.1	DA13-076-7.2
SiO_2	36.97	36.94	36.36	36.64	36.69	36.17	35.20	35.69	35.57	35.64	33.44
TiO_2	4.44	4.40	4.44	4.39	4.51	4.25	4.37	4.23	4.11	4.14	3.36
Al_2O_3	13.35	13.27	13.19	12.99	13.04	13.06	12.79	12.84	13.17	14.56	13.55
FeOT	28.74	28.89	29.39	28.76	28.80	29.39	29.84	29.52	30.14	30.71	31.29
MnO	0.18	0.16	0.19	0.18	0.20	0.19	0.07	0.09	0.08	0.09	0.07
MgO	4.53	4.54	4.37	4.37	4.34	4.42	3.80	4.02	4.10	4.25	4.78
CaO	0.00	0.01	0.02	0.00	0.00	0.00	0.05	0.04	0.05	0.13	0.10
Na_2O	0.09	0.09	0.09	0.09	0.10	0.13	0.08	0.09	0.09	0.13	0.07
K_2O	8.84	8.80	8.63	8.98	9.00	8.41	8.69	8.91	8.36	6.65	6.14
BaO	0.42	0.29	0.37	0.42	0.43	0.41	0.23	0.28	0.24	0.21	0.14
ZnO	0.12	0.10	0.09	0.02	0.10	0.09	0.20	0.16	0.18	0.22	0.08
F	2.12	2.13	2.04	2.62	2.44	2.14	1.87	1.90	1.99	1.42	1.78
Cl	0.17	0.16	0.17	0.16	0.16	0.14	0.17	0.17	0.17	0.13	0.14
H_2O*	2.80	2.79	2.80	2.52	2.62	2.73	2.78	2.80	2.77	3.11	2.76
Subtotal	102.78	102.58	102.14	102.15	102.45	101.55	100.16	100.72	101.00	101.40	97.69
O=F, Cl	0.93	0.93	0.90	1.14	1.07	0.93	0.82	0.84	0.88	0.63	0.78
Total	101.85	101.65	101.25	101.01	101.38	100.62	99.34	99.89	100.12	100.77	96.91
Si	5.76	5.77	5.72	5.78	5.76	5.73	5.69	5.72	5.68	5.60	5.51
Al iv	2.24	2.23	2.28	2.22	2.24	2.27	2.31	2.28	2.32	2.40	2.49
Total	8.00	8.00	8.00	8.00	8.00	8.00	8.00	8.00	8.00	8.00	8.00
Al vi	0.21	0.21	0.17	0.19	0.18	0.17	0.12	0.15	0.16	0.29	0.15
Ti	0.52	0.52	0.53	0.52	0.53	0.51	0.53	0.51	0.49	0.49	0.42
Fe^{2+}	3.75	3.77	3.87	3.79	3.78	3.89	4.03	3.96	4.03	4.03	4.31
Mn	0.02	0.02	0.02	0.02	0.03	0.03	0.01	0.01	0.01	0.01	0.01
Mg	1.05	1.06	1.03	1.03	1.02	1.04	0.91	0.96	0.98	0.99	1.17
Zn	0.01	0.01	0.01	0.00	0.01	0.01	0.02	0.02	0.02	0.03	0.01
Total	5.57	5.59	5.62	5.55	5.55	5.65	5.63	5.61	5.69	5.85	6.07
Ca	0.00	0.00	0.00	0.00	0.00	0.00	0.01	0.01	0.01	0.02	0.02
Na	0.03	0.03	0.03	0.03	0.03	0.04	0.03	0.03	0.03	0.04	0.02
K	1.76	1.75	1.73	1.81	1.80	1.70	1.79	1.82	1.70	1.33	1.29
Total	1.78	1.78	1.76	1.83	1.83	1.74	1.83	1.86	1.74	1.39	1.33
OH*	2.91	2.90	2.94	2.65	2.74	2.89	3.00	2.99	2.95	3.26	3.04
F	1.04	1.05	1.01	1.31	1.21	1.07	0.95	0.96	1.01	0.70	0.93
Cl	0.04	0.04	0.05	0.04	0.04	0.04	0.05	0.05	0.05	0.03	0.04
Total	19.35	19.37	19.39	19.39	19.38	19.39	19.46	19.46	19.43	19.24	19.40
Fe/Fe+Mg	0.78	0.78	0.79	0.79	0.79	0.79	0.82	0.80	0.80	0.80	0.79

*H_2O calculations after Tindle and Webb (1990).

Appendix 4.2.4: Representative mineral chemistry for biotite

	DA13-076-7.3	DA13-077-1.1	DA13-077-1.2	DA13-077-1.3	DA13-077-1.4	DA13-077-1.5	DA13-077-1.6	DA13-077-1.7	DA13-077-2.1	DA13-077-2.2	DA13-077-2.3	DA13-077-2.4
SiO_2	37.24	35.69	36.31	34.99	36.45	36.32	36.67	36.12	36.10	36.03	36.46	36.42
TiO_2	3.65	3.92	3.91	3.87	4.01	3.87	3.98	3.95	4.25	4.26	4.08	4.11
Al_2O_3	13.61	12.71	12.90	12.34	12.91	12.81	12.94	13.05	12.88	12.89	13.27	13.11
FeOT	29.10	31.22	31.67	31.39	31.87	31.54	31.37	30.61	30.92	30.85	30.21	30.87
MnO	0.05	0.38	0.38	0.43	0.41	0.39	0.41	0.40	0.32	0.32	0.34	0.37
MgO	5.10	2.00	2.05	1.90	2.05	2.05	2.06	1.97	2.02	1.99	2.10	2.08
CaO	0.05	0.02	0.01	0.01	0.01	0.00	0.00	0.03	0.01	0.01	0.02	0.01
Na_2O	0.10	0.10	0.16	0.18	0.16	0.10	0.07	0.26	0.09	0.06	0.06	0.10
K_2O	8.80	8.91	8.91	8.84	8.78	8.92	8.96	8.50	8.99	9.02	9.04	9.00
BaO	0.16	0.18	0.19	0.13	0.17	0.12	0.19	0.13	0.17	0.22	0.18	0.14
ZnO	0.09	0.19	0.20	0.26	0.19	0.26	0.21	0.18	0.23	0.15	0.21	0.21
F	1.96	1.39	1.61	1.89	1.74	1.68	1.15	0.92	1.80	1.71	1.50	1.24
Cl	0.15	0.33	0.35	0.36	0.31	0.32	0.33	0.35	0.34	0.36	0.33	0.32
H_2O*	2.90	2.94	2.89	2.64	2.85	2.85	3.13	3.18	2.78	2.81	2.94	3.08
Subtotal	102.97	99.99	101.54	99.23	101.92	101.25	101.46	99.64	100.90	100.69	100.75	101.07
O=F, Cl	0.86	0.66	0.75	0.87	0.80	0.78	0.56	0.47	0.83	0.80	0.71	0.60
Total	102.11	99.33	100.78	98.35	101.12	100.47	100.90	99.17	100.06	99.89	100.04	100.48
Si	5.77	5.81	5.82	5.78	5.82	5.84	5.85	5.84	5.82	5.81	5.84	5.83
Al iv	2.23	2.19	2.18	2.22	2.18	2.16	2.15	2.16	2.18	2.19	2.16	2.17
Total	8.00	8.00	8.00	8.00	8.00	8.00	8.00	8.00	8.00	8.00	8.00	8.00
Al vi	0.26	0.25	0.26	0.19	0.25	0.26	0.29	0.33	0.26	0.27	0.35	0.30
Ti	0.43	0.48	0.47	0.48	0.48	0.47	0.48	0.48	0.51	0.52	0.49	0.49
Fe^{2+}	3.77	4.25	4.25	4.34	4.26	4.24	4.19	4.14	4.17	4.16	4.05	4.13
Mn	0.01	0.05	0.05	0.06	0.06	0.05	0.05	0.05	0.04	0.04	0.05	0.05
Mg	1.18	0.48	0.49	0.47	0.49	0.49	0.49	0.47	0.49	0.48	0.50	0.49
Zn	0.01	0.02	0.02	0.03	0.02	0.03	0.02	0.02	0.03	0.02	0.03	0.02
Total	5.65	5.54	5.54	5.57	5.55	5.54	5.52	5.50	5.50	5.49	5.46	5.50
Ca	0.01	0.00	0.00	0.00	0.00	0.00	0.00	0.00	0.00	0.00	0.00	0.00
Na	0.03	0.03	0.05	0.06	0.05	0.03	0.02	0.08	0.03	0.02	0.02	0.03
K	1.74	1.85	1.82	1.86	1.79	1.83	1.82	1.75	1.85	1.86	1.85	1.84
Total	1.78	1.89	1.87	1.92	1.84	1.86	1.85	1.84	1.88	1.88	1.87	1.87
OH*	3.00	3.19	3.09	2.91	3.04	3.06	3.33	3.43	2.99	3.03	3.15	3.28
F	0.96	0.72	0.81	0.99	0.88	0.85	0.58	0.47	0.91	0.87	0.76	0.63
Cl	0.04	0.09	0.09	0.10	0.09	0.09	0.09	0.10	0.09	0.10	0.09	0.09
Total	19.43	19.42	19.41	19.49	19.39	19.41	19.37	19.34	19.37	19.37	19.33	19.36
Fe/Fe+Mg	0.76	0.90	0.90	0.90	0.90	0.90	0.90	0.90	0.90	0.90	0.89	0.89

*H_2O calculations after Tindle and Webb (1990).

Appendix 4.2.4: Representative mineral chemistry for biotite

	DA13-077-2.5	DA13-077-2.6	DA13-077-2.7	DA13-077-2.8	DA13-077-2.9	DA13-077-2.10	DA13-077-4.1	DA13-077-4.2	DA13-077-4.3	DA13-077-4.4	DA13-077-4.5	DA13-083-3.1
SiO_2	35.41	35.15	35.19	35.91	35.82	35.91	35.64	35.29	35.97	35.67	36.11	39.91
TiO_2	4.39	4.45	4.49	4.50	4.05	4.29	4.31	4.32	4.25	4.25	4.27	3.68
Al_2O_3	12.46	12.36	12.81	12.61	12.50	12.54	12.44	12.32	12.50	12.40	12.52	13.23
FeOT	31.69	30.74	31.16	31.47	30.75	31.11	31.97	31.75	31.95	31.97	32.09	16.67
MnO	0.34	0.41	0.36	0.38	0.39	0.33	0.36	0.38	0.38	0.39	0.42	0.27
MgO	1.90	1.90	1.83	1.92	2.10	1.99	1.89	1.87	1.97	1.92	1.98	14.03
CaO	0.00	0.01	0.01	0.00	0.00	0.03	0.00	0.01	0.00	0.00	0.00	0.00
Na_2O	0.26	0.26	0.24	0.22	0.08	0.10	0.19	0.21	0.15	0.15	0.13	0.14
K_2O	8.75	8.70	8.80	8.86	8.81	8.81	8.70	8.69	8.88	8.85	8.78	9.46
BaO	0.16	0.24	0.17	0.13	0.15	0.14	0.19	0.24	0.18	0.15	0.17	0.10
ZnO	0.24	0.12	0.19	0.24	0.19	0.22	0.25	0.25	0.16	0.24	0.16	0.09
F	1.51	1.56	1.68	1.61	1.32	1.30	1.64	1.70	1.44	1.49	1.81	1.25
Cl	0.32	0.35	0.33	0.36	0.31	0.31	0.36	0.34	0.33	0.32	0.34	0.10
H_2O*	2.89	2.82	2.80	2.86	2.97	3.00	2.83	2.77	2.95	2.91	2.78	3.48
Subtotal	100.36	99.06	100.07	101.09	99.43	100.06	100.77	100.15	101.13	100.73	101.58	102.42
O=F, Cl	0.71	0.74	0.78	0.76	0.62	0.62	0.77	0.79	0.68	0.70	0.84	0.55
Total	99.66	98.33	99.29	100.33	98.81	99.45	100.00	99.36	100.45	100.03	100.74	101.87
Si	5.76	5.78	5.74	5.79	5.84	5.82	5.78	5.77	5.80	5.79	5.81	5.85
Al iv	2.24	2.22	2.26	2.21	2.16	2.18	2.22	2.23	2.20	2.21	2.19	2.15
Total	8.00	8.00	8.00	8.00	8.00	8.00	8.00	8.00	8.00	8.00	8.00	8.00
Al vi	0.15	0.18	0.20	0.18	0.24	0.22	0.16	0.14	0.18	0.16	0.18	0.13
Ti	0.54	0.55	0.55	0.55	0.50	0.52	0.53	0.53	0.52	0.52	0.52	0.41
Fe^{2+}	4.31	4.23	4.25	4.24	4.19	4.22	4.34	4.34	4.31	4.34	4.31	2.04
Mn	0.05	0.06	0.05	0.05	0.05	0.05	0.05	0.05	0.05	0.05	0.06	0.03
Mg	0.46	0.47	0.44	0.46	0.51	0.48	0.46	0.46	0.47	0.46	0.47	3.07
Zn	0.03	0.01	0.02	0.03	0.02	0.03	0.03	0.03	0.02	0.03	0.02	0.01
Total	5.54	5.50	5.52	5.51	5.52	5.52	5.56	5.56	5.55	5.56	5.56	5.69
Ca	0.00	0.00	0.00	0.00	0.00	0.00	0.00	0.00	0.00	0.00	0.00	0.00
Na	0.08	0.08	0.07	0.07	0.03	0.03	0.06	0.07	0.05	0.05	0.04	0.04
K	1.81	1.83	1.83	1.82	1.83	1.82	1.80	1.81	1.83	1.83	1.80	1.77
Total	1.90	1.91	1.91	1.89	1.86	1.86	1.86	1.88	1.87	1.88	1.84	1.81
OH*	3.14	3.09	3.05	3.08	3.23	3.25	3.06	3.02	3.17	3.14	2.99	3.40
F	0.78	0.81	0.86	0.82	0.68	0.67	0.84	0.88	0.74	0.77	0.92	0.58
Cl	0.09	0.10	0.09	0.10	0.09	0.09	0.10	0.09	0.09	0.09	0.09	0.02
Total	19.44	19.41	19.42	19.40	19.38	19.37	19.42	19.44	19.42	19.44	19.40	19.50
Fe/Fe+Mg	0.90	0.90	0.91	0.90	0.89	0.90	0.90	0.90	0.90	0.90	0.90	0.40

*H_2O calculations after Tindle and Webb (1990).

Appendix 4.2.4: Representative mineral chemistry for biotite

	DA13-083-3.2	DA13-083-3.3	DA13-083-3.4	DA13-083-3.5	DA13-083-3.6	DA13-083-3.7	DA13-083-3.8	DA13-083-3.9	DA13-083-3.10	DA13-083-3.11	DA13-083-3.12
SiO_2	39.58	39.53	39.19	38.72	39.16	39.99	39.34	39.27	39.65	39.23	39.17
TiO_2	3.61	3.41	3.32	2.99	3.56	3.19	3.96	3.98	3.89	3.84	3.72
Al_2O_3	13.00	12.88	12.88	12.91	12.90	13.20	12.87	12.93	12.88	13.03	12.87
FeOT	16.85	16.64	17.25	16.63	16.62	16.49	16.91	16.69	16.53	16.64	16.53
MnO	0.28	0.29	0.28	0.22	0.28	0.28	0.35	0.34	0.32	0.35	0.33
MgO	13.97	14.21	14.12	14.17	13.91	14.55	13.63	13.52	13.89	13.60	13.79
CaO	0.05	0.04	0.05	0.08	0.03	0.05	0.05	0.04	0.05	0.03	0.00
Na_2O	0.10	0.11	0.12	0.14	0.10	0.09	0.12	0.08	0.10	0.12	0.09
K_2O	9.31	9.42	9.02	9.06	9.48	9.38	9.42	9.49	9.42	9.46	9.58
BaO	0.13	0.10	0.11	0.05	0.12	0.13	0.14	0.16	0.10	0.10	0.14
ZnO	0.10	0.10	0.12	0.10	0.09	0.09	0.07	0.11	0.06	0.05	0.10
F	1.12	1.42	1.25	1.37	1.32	1.52	1.47	1.31	1.31	1.29	1.49
Cl	0.09	0.09	0.10	0.09	0.08	0.09	0.08	0.09	0.06	0.13	0.08
H_2O*	3.50	3.35	3.42	3.31	3.38	3.35	3.33	3.39	3.42	3.39	3.30
Subtotal	101.68	101.59	101.22	99.85	101.02	102.42	101.74	101.39	101.68	101.27	101.17
O=F, Cl	0.49	0.62	0.55	0.60	0.57	0.66	0.64	0.57	0.57	0.57	0.64
Total	101.18	100.97	100.67	99.26	100.45	101.75	101.10	100.82	101.11	100.70	100.53
Si	5.85	5.85	5.83	5.83	5.84	5.86	5.83	5.83	5.86	5.83	5.84
Al iv	2.15	2.15	2.17	2.17	2.16	2.14	2.17	2.17	2.14	2.17	2.16
Total	8.00	8.00	8.00	8.00	8.00	8.00	8.00	8.00	8.00	8.00	8.00
Al vi	0.11	0.10	0.09	0.12	0.10	0.14	0.08	0.10	0.10	0.11	0.10
Ti	0.40	0.38	0.37	0.34	0.40	0.35	0.44	0.44	0.43	0.43	0.42
Fe^{2+}	2.08	2.06	2.15	2.09	2.07	2.02	2.10	2.07	2.04	2.07	2.06
Mn	0.03	0.04	0.03	0.03	0.03	0.03	0.04	0.04	0.04	0.04	0.04
Mg	3.08	3.14	3.13	3.18	3.09	3.18	3.01	2.99	3.06	3.01	3.06
Zn	0.01	0.01	0.01	0.01	0.01	0.01	0.01	0.01	0.01	0.01	0.01
Total	5.71	5.73	5.78	5.78	5.71	5.74	5.68	5.66	5.68	5.67	5.69
Ca	0.01	0.01	0.01	0.01	0.01	0.01	0.01	0.01	0.01	0.00	0.00
Na	0.03	0.03	0.03	0.04	0.03	0.03	0.03	0.02	0.03	0.03	0.02
K	1.75	1.78	1.71	1.74	1.80	1.75	1.78	1.80	1.78	1.79	1.82
Total	1.79	1.82	1.75	1.79	1.84	1.79	1.82	1.83	1.81	1.83	1.84
OH*	3.45	3.31	3.39	3.32	3.36	3.27	3.29	3.36	3.37	3.36	3.28
F	0.53	0.67	0.59	0.65	0.62	0.71	0.69	0.61	0.61	0.61	0.70
Cl	0.02	0.02	0.03	0.02	0.02	0.02	0.02	0.02	0.02	0.03	0.02
Total	19.50	19.54	19.54	19.57	19.54	19.52	19.50	19.49	19.49	19.50	19.53
Fe/Fe+Mg	0.40	0.40	0.41	0.40	0.40	0.39	0.41	0.41	0.40	0.41	0.40

*H_2O calculations after Tindle and Webb (1990).

Appendix 4.2.4: Representative mineral chemistry for biotite

	DA13-083-3.13	DA13-083-3.14	DA13-083-3.15	DA13-083-3.16	DA13-083-7.1	DA13-083-7.2	DA13-083-7.3	DA13-083-7.4	DA13-083-7.5
SiO_2	39.22	39.48	39.37	39.19	38.81	40.68	39.77	39.32	39.98
TiO_2	3.87	3.83	3.80	3.63	2.09	2.40	3.12	3.15	3.06
Al_2O_3	13.14	13.05	12.89	12.96	16.12	15.60	14.48	14.32	14.59
FeOT	16.72	16.70	16.93	16.57	10.13	10.90	12.27	12.62	12.61
MnO	0.34	0.33	0.35	0.29	0.26	0.31	0.30	0.33	0.30
MgO	13.72	13.58	13.80	13.78	16.07	16.91	15.86	15.51	15.71
CaO	0.02	0.04	0.02	0.02	0.05	0.02	0.01	0.03	0.03
Na_2O	0.09	0.13	0.07	0.13	0.11	0.06	0.06	0.11	0.11
K_2O	9.53	9.39	9.47	9.62	10.04	9.82	9.90	9.51	9.67
BaO	0.08	0.14	0.11	0.12	0.09	0.08	0.16	0.12	0.13
ZnO	0.01	0.06	0.13	0.06	0.07	0.02	0.10	0.09	0.17
F	1.28	1.34	1.37	1.34	1.53	1.65	1.58	1.42	1.36
Cl	0.08	0.08	0.09	0.11	0.07	0.06	0.07	0.07	0.09
H_2O*	3.42	3.39	3.38	3.37	3.31	3.39	3.34	3.37	3.45
Subtotal	101.51	101.56	101.78	101.17	98.77	101.92	101.04	99.99	101.28
O=F, Cl	0.56	0.58	0.60	0.59	0.66	0.71	0.68	0.62	0.59
Total	100.95	100.98	101.18	100.59	98.11	101.21	100.37	99.37	100.68
Si	5.81	5.85	5.83	5.83	5.75	5.83	5.81	5.81	5.82
Al iv	2.19	2.15	2.17	2.17	2.25	2.17	2.19	2.19	2.18
Total	8.00	8.00	8.00	8.00	8.00	8.00	8.00	8.00	8.00
Al vi	0.11	0.12	0.08	0.11	0.56	0.46	0.31	0.30	0.33
Ti	0.43	0.43	0.42	0.41	0.23	0.26	0.34	0.35	0.34
Fe^{2+}	2.07	2.07	2.10	2.06	1.25	1.31	1.50	1.56	1.54
Mn	0.04	0.04	0.04	0.04	0.03	0.04	0.04	0.04	0.04
Mg	3.03	3.00	3.05	3.06	3.55	3.61	3.46	3.42	3.41
Zn	0.00	0.01	0.01	0.01	0.01	0.00	0.01	0.01	0.02
Total	5.69	5.66	5.71	5.68	5.63	5.68	5.65	5.67	5.66
Ca	0.00	0.01	0.00	0.00	0.01	0.00	0.00	0.00	0.01
Na	0.03	0.04	0.02	0.04	0.03	0.02	0.02	0.03	0.03
K	1.80	1.77	1.79	1.83	1.90	1.80	1.84	1.79	1.80
Total	1.83	1.82	1.81	1.87	1.93	1.82	1.86	1.83	1.83
OH*	3.38	3.35	3.34	3.34	3.27	3.24	3.25	3.32	3.35
F	0.60	0.63	0.64	0.63	0.72	0.75	0.73	0.66	0.63
Cl	0.02	0.02	0.02	0.03	0.02	0.02	0.02	0.02	0.02
Total	19.52	19.48	19.52	19.55	19.57	19.50	19.52	19.50	19.50
Fe/Fe+Mg	0.41	0.41	0.41	0.40	0.26	0.27	0.30	0.31	0.31

*H_2O calculations after Tindle and Webb (1990).

Appendix 4.2.5: Representative mineral chemistry for amphibole

Wt%	DA13-049-3.1	DA13-049-3.2	DA13-049-3.3	DA13-049-3.4	DA13-049-3.5	DA13-049-3.6	DA13-049-3.7	DA13-049-3.8	DA13-049-3.9	DA13-049-3.10	DA13-049-4.1
SiO_2	44.72	44.41	44.72	44.51	44.04	44.24	44.33	44.19	44.38	44.58	44.33
TiO_2	0.51	0.56	0.51	0.54	0.61	0.50	0.54	0.56	0.51	0.52	0.56
Al_2O_3	9.22	9.44	9.17	9.71	9.51	9.55	9.66	9.42	9.41	9.23	9.25
Cr_2O_3	0.01	0.02	0.04	0.00	0.00	0.00	0.00	0.03	0.00	0.00	0.00
FeOT	20.07	20.23	20.01	19.82	20.28	20.33	20.33	20.35	20.28	20.09	20.18
MnO	1.18	1.16	1.12	1.17	1.12	1.21	1.22	1.19	1.22	1.16	1.19
MgO	8.92	8.78	8.79	8.85	8.74	8.75	8.62	8.73	8.67	8.98	8.82
CaO	11.08	11.10	11.02	10.97	11.03	11.04	11.07	11.08	11.05	11.06	11.04
Na_2O	1.58	1.57	1.55	1.60	1.57	1.55	1.61	1.57	1.50	1.57	1.60
K_2O	1.33	1.37	1.34	1.38	1.44	1.35	1.35	1.40	1.38	1.36	1.38
TOTAL	98.61	98.64	98.29	98.54	98.35	98.53	98.73	98.51	98.39	98.55	98.36
Si	6.77	6.74	6.79	6.74	6.71	6.72	6.72	6.72	6.75	6.76	6.75
Al	1.23	1.26	1.21	1.26	1.29	1.28	1.28	1.28	1.25	1.24	1.25
Sum T	8.00	8.00	8.00	8.00	8.00	8.00	8.00	8.00	8.00	8.00	8.00
Al	0.42	0.42	0.43	0.47	0.41	0.43	0.45	0.41	0.44	0.41	0.40
Fe^{3+}	0.00	0.00	0.00	0.00	0.00	0.00	0.00	0.00	0.00	0.00	0.00
Cr	0.06	0.06	0.06	0.06	0.07	0.06	0.06	0.06	0.06	0.06	0.06
Ti	0.00	0.00	0.01	0.00	0.00	0.00	0.00	0.00	0.00	0.00	0.00
Fe^{2+}	2.54	2.57	2.54	2.51	2.58	2.58	2.58	2.59	2.58	2.55	2.57
Mn	0.15	0.15	0.14	0.15	0.14	0.16	0.16	0.15	0.16	0.15	0.15
Mg	1.83	1.80	1.82	1.81	1.79	1.77	1.76	1.78	1.77	1.83	1.81
Sum C	5.00	5.00	5.00	5.00	5.00	5.00	5.00	5.00	5.00	5.00	5.00
Mg^{2+}, Mn^{2+}, Fe^{2+}	0.19	0.19	0.17	0.19	0.20	0.21	0.19	0.20	0.19	0.20	0.19
Ca	1.80	1.80	1.79	1.78	1.80	1.79	1.80	1.80	1.80	1.80	1.80
Na	0.02	0.01	0.03	0.03	0.00	0.00	0.01	0.00	0.01	0.01	0.01
Sum B	2.00	2.00	2.00	2.00	2.00	2.00	2.00	2.00	2.00	2.00	2.00
Ca	0.00	0.00	0.00	0.00	0.00	0.01	0.00	0.00	0.00	0.00	0.00
Na	0.45	0.45	0.42	0.44	0.46	0.46	0.46	0.46	0.44	0.45	0.46
K	0.26	0.27	0.26	0.27	0.28	0.26	0.26	0.27	0.27	0.26	0.27
Sum A	0.70	0.72	0.68	0.70	0.74	0.73	0.72	0.74	0.70	0.72	0.73
TOTAL	15.70	15.72	15.68	15.70	15.74	15.73	15.72	15.74	15.70	15.72	15.73
Classification	Ed	Ed	Ed	Ed	Ed	Ed	Ed	Ed	Ed	Ed	Ed

Abbreviations: Ed=Edenite,Prg=Pargasite (Hawthorne et al. 2012)

Appendix 4.2.5: Representative mineral chemistry for amphibole

Wt%	DA13-049-4.2	DA13-049-4.3	DA13-049-4.4	DA13-049-4.5	DA13-049-4.6	DA13-049-4.7	DA13-049-4.8	DA13-049-4.9	DA13-049-4.10	DA13-049-4.11	DA13-049-4.12
SiO_2	43.97	44.12	44.26	44.24	44.25	44.01	44.25	44.08	44.17	44.07	44.29
TiO_2	0.55	0.57	0.56	0.56	0.59	0.61	0.58	0.57	0.60	0.56	0.63
Al_2O_3	9.44	9.53	9.48	9.41	9.48	9.35	9.55	9.63	9.57	9.46	9.45
Cr_2O_3	0.00	0.00	0.04	0.00	0.02	0.02	0.05	0.00	0.00	0.01	0.03
FeOT	20.38	20.25	20.28	20.03	20.24	20.30	20.24	20.16	20.28	20.49	20.22
MnO	1.09	1.15	1.23	1.27	1.13	1.14	1.13	1.29	1.14	1.20	1.28
MgO	8.75	8.76	8.60	8.72	8.63	8.62	8.79	8.56	8.71	8.68	8.79
CaO	11.01	11.16	11.02	11.01	11.06	11.04	10.98	11.02	11.00	11.00	11.11
Na_2O	1.57	1.59	1.57	1.63	1.52	1.56	1.52	1.47	1.57	1.62	1.57
K_2O	1.40	1.43	1.40	1.41	1.40	1.39	1.38	1.37	1.45	1.40	1.37
TOTAL	98.18	98.56	98.44	98.28	98.31	98.07	98.46	98.15	98.49	98.50	98.73
Si	6.71	6.71	6.73	6.74	6.73	6.72	6.72	6.72	6.71	6.71	6.72
Al	1.29	1.29	1.27	1.26	1.27	1.28	1.28	1.28	1.29	1.29	1.28
Sum T	8.00	8.00	8.00	8.00	8.00	8.00	8.00	8.00	8.00	8.00	8.00
Al	0.41	0.41	0.43	0.43	0.44	0.41	0.43	0.45	0.43	0.41	0.41
Fe^{3+}	0.00	0.00	0.00	0.00	0.00	0.00	0.00	0.00	0.00	0.00	0.00
Cr	0.06	0.06	0.06	0.06	0.07	0.07	0.07	0.07	0.07	0.06	0.07
Ti	0.00	0.00	0.00	0.00	0.00	0.00	0.01	0.00	0.00	0.00	0.00
Fe^{2+}	2.60	2.57	2.58	2.55	2.58	2.59	2.57	2.57	2.58	2.61	2.56
Mn	0.14	0.15	0.16	0.16	0.15	0.15	0.14	0.17	0.15	0.15	0.16
Mg	1.78	1.80	1.76	1.80	1.77	1.78	1.78	1.75	1.78	1.76	1.79
Sum C	5.00	5.00	5.00	5.00	5.00	5.00	5.00	5.00	5.00	5.00	5.00
Mg^{2+}, Mn^{2+}, Fe^{2+}	0.21	0.18	0.19	0.18	0.18	0.19	0.21	0.20	0.20	0.21	0.20
Ca	1.79	1.82	1.80	1.80	1.80	1.81	1.79	1.80	1.79	1.79	1.80
Na	0.00	0.00	0.02	0.02	0.01	0.00	0.00	0.00	0.01	0.00	0.00
Sum B	2.00	2.00	2.00	2.00	2.00	2.00	2.00	2.00	2.00	2.00	2.00
Ca	0.01	0.00	0.00	0.00	0.00	0.00	0.00	0.00	0.00	0.00	0.00
Na	0.46	0.47	0.45	0.46	0.44	0.46	0.44	0.43	0.45	0.48	0.46
K	0.27	0.28	0.27	0.27	0.27	0.27	0.27	0.27	0.28	0.27	0.27
Sum A	0.74	0.75	0.72	0.73	0.71	0.73	0.71	0.70	0.73	0.75	0.73
TOTAL	15.74	15.75	15.72	15.73	15.71	15.73	15.71	15.70	15.73	15.75	15.73
Classification	Ed	Ed	Ed	Ed	Ed	Ed	Ed	Ed	Ed	Ed	Ed

Abbreviations: Ed=Edenite,Prg=Pargasite (Hawthorne et al. 2012)

Appendix 4.2.5: Representative mineral chemistry for amphibole

Wt%	DA13-055-2.1	DA13-055-2.2	DA13-055-2.3	DA13-055-2.4	DA13-055-2.5	DA13-055-2.6	DA13-055-2.7	DA13-055-2.8	DA13-055-2.9	DA13-055-2.10	DA13-055-6.1	DA13-055-6.2
SiO_2	43.77	43.93	43.96	43.92	44.14	44.33	44.11	44.02	43.92	43.91	44.06	43.65
TiO_2	1.27	1.21	1.32	1.33	1.24	1.35	1.27	1.35	1.42	1.28	1.32	1.31
Al_2O_3	10.04	10.12	9.97	9.89	9.85	9.84	10.09	10.11	10.10	10.36	9.94	9.92
Cr_2O_3	0.00	0.03	0.01	0.02	0.00	0.00	0.00	0.00	0.00	0.01	0.04	0.03
FeOT	21.68	21.69	21.60	21.42	21.47	21.46	21.33	21.52	21.23	21.40	21.66	21.66
MnO	0.51	0.53	0.49	0.55	0.50	0.54	0.47	0.53	0.54	0.55	0.53	0.51
MgO	7.38	7.40	7.52	7.47	7.51	7.67	7.54	7.44	7.59	7.45	7.40	7.28
CaO	11.23	11.21	11.11	11.04	11.09	11.10	11.14	11.18	11.21	11.15	11.11	11.18
Na_2O	1.30	1.28	1.32	1.38	1.33	1.35	1.34	1.40	1.37	1.35	1.37	1.34
K_2O	1.30	1.27	1.27	1.28	1.27	1.28	1.28	1.33	1.33	1.35	1.28	1.25
TOTAL	98.50	98.66	98.57	98.31	98.39	98.92	98.59	98.88	98.72	98.80	98.70	98.13
Si	6.67	6.68	6.69	6.70	6.72	6.71	6.70	6.68	6.67	6.66	6.70	6.68
Al	1.33	1.32	1.31	1.30	1.28	1.29	1.30	1.32	1.33	1.34	1.30	1.32
Sum T	8.00	8.00	8.00	8.00	8.00	8.00	8.00	8.00	8.00	8.00	8.00	8.00
Al	0.47	0.49	0.47	0.47	0.49	0.47	0.50	0.48	0.47	0.51	0.48	0.47
Fe^{3+}	0.00	0.00	0.00	0.00	0.00	0.00	0.00	0.00	0.00	0.00	0.00	0.00
Cr	0.15	0.14	0.15	0.15	0.14	0.15	0.15	0.15	0.16	0.15	0.15	0.15
Ti	0.00	0.00	0.00	0.00	0.00	0.00	0.00	0.00	0.00	0.00	0.00	0.00
Fe^{2+}	2.76	2.76	2.75	2.73	2.73	2.72	2.71	2.73	2.69	2.71	2.75	2.77
Mn	0.07	0.07	0.06	0.07	0.06	0.07	0.06	0.07	0.07	0.07	0.07	0.07
Mg	1.55	1.54	1.56	1.57	1.58	1.59	1.58	1.57	1.60	1.56	1.55	1.54
Sum C	5.00	5.00	5.00	5.00	5.00	5.00	5.00	5.00	5.00	5.00	5.00	5.00
Mg^{2+}, Mn^{2+}, Fe^{2+}	0.13	0.14	0.14	0.13	0.13	0.14	0.12	0.12	0.12	0.13	0.13	0.12
Ca	1.83	1.83	1.81	1.80	1.81	1.80	1.81	1.82	1.82	1.81	1.81	1.83
Na	0.04	0.04	0.05	0.07	0.06	0.06	0.07	0.07	0.06	0.06	0.06	0.05
Sum B	2.00	2.00	2.00	2.00	2.00	2.00	2.00	2.00	2.00	2.00	2.00	2.00
Ca	0.00	0.00	0.00	0.00	0.00	0.00	0.00	0.00	0.00	0.00	0.00	0.00
Na	0.35	0.34	0.34	0.34	0.33	0.33	0.33	0.35	0.34	0.33	0.34	0.35
K	0.25	0.25	0.25	0.25	0.25	0.25	0.25	0.26	0.26	0.26	0.25	0.24
Sum A	0.60	0.58	0.59	0.59	0.57	0.58	0.58	0.60	0.60	0.60	0.59	0.59
TOTAL	15.60	15.58	15.59	15.59	15.57	15.58	15.58	15.60	15.60	15.60	15.59	15.59
Classification	Ed	Ed	Ed	Ed	Ed	Ed	Prg	Ed	Ed	Prg	Ed	Ed

Abbreviations: Ed=Edenite,Prg=Pargasite (Hawthorne et al. 2012)

Appendix 4.2.5: Representative mineral chemistry for amphibole

Wt%	DA13-055-6.3	DA13-055-6.4	DA13-055-6.5	DA13-055-6.6	DA13-055-6.7	DA13-055-6.8	DA13-055-6.9	DA13-055-6.10	DA13-064-1.1	DA13-064-1.2	DA13-064-1.3
SiO_2	44.34	43.60	43.96	43.66	44.15	43.88	43.48	43.88	44.21	44.42	43.40
TiO_2	1.26	1.29	1.36	1.39	1.33	1.25	1.26	1.18	0.46	0.42	0.47
Al_2O_3	9.98	10.11	9.97	9.97	10.10	10.02	9.88	10.07	9.83	9.84	10.20
Cr_2O_3	0.02	0.01	0.01	0.00	0.01	0.03	0.02	0.03	0.02	0.00	0.03
FeOT	21.66	21.85	21.83	21.30	21.52	21.78	21.60	21.73	19.96	19.77	20.53
MnO	0.47	0.49	0.57	0.50	0.54	0.52	0.53	0.49	1.14	1.17	1.12
MgO	7.35	7.28	7.29	7.42	7.41	7.33	7.09	7.40	8.96	9.01	8.49
CaO	11.17	11.23	11.21	11.15	11.32	11.24	11.18	11.21	11.22	11.22	11.06
Na_2O	1.34	1.25	1.35	1.28	1.32	1.27	1.27	1.29	1.50	1.31	1.63
K_2O	1.24	1.26	1.27	1.28	1.17	1.26	1.23	1.23	1.38	1.30	1.45
TOTAL	98.84	98.38	98.84	97.97	98.86	98.57	97.54	98.50	98.67	98.46	98.38
Si	6.72	6.66	6.68	6.68	6.69	6.68	6.69	6.68	6.70	6.72	6.62
Al	1.28	1.34	1.32	1.32	1.31	1.32	1.31	1.32	1.30	1.28	1.38
Sum T	8.00	8.00	8.00	8.00	8.00	8.00	8.00	8.00	8.00	8.00	8.00
Al	0.50	0.48	0.47	0.48	0.49	0.48	0.49	0.49	0.45	0.48	0.46
Fe^{3+}	0.00	0.00	0.00	0.00	0.00	0.00	0.00	0.00	0.00	0.00	0.00
Cr	0.14	0.15	0.16	0.16	0.15	0.14	0.15	0.14	0.05	0.05	0.05
Ti	0.00	0.00	0.00	0.00	0.00	0.00	0.00	0.00	0.00	0.00	0.00
Fe^{2+}	2.74	2.79	2.77	2.72	2.73	2.77	2.78	2.77	2.53	2.50	2.62
Mn	0.06	0.06	0.07	0.07	0.07	0.07	0.07	0.06	0.15	0.15	0.14
Mg	1.55	1.52	1.53	1.57	1.56	1.53	1.52	1.54	1.82	1.82	1.72
Sum C	5.00	5.00	5.00	5.00	5.00	5.00	5.00	5.00	5.00	5.00	5.00
Mg^{2+}, Mn^{2+}, Fe^{2+}	0.11	0.14	0.12	0.12	0.11	0.13	0.11	0.14	0.20	0.21	0.21
Ca	1.81	1.84	1.82	1.83	1.84	1.83	1.84	1.83	1.80	1.79	1.79
Na	0.07	0.02	0.05	0.05	0.05	0.04	0.05	0.03	0.00	0.00	0.00
Sum B	2.00	2.00	2.00	2.00	2.00	2.00	2.00	2.00	2.00	2.00	2.00
Ca	0.00	0.00	0.00	0.00	0.00	0.00	0.00	0.00	0.02	0.03	0.02
Na	0.32	0.35	0.35	0.33	0.34	0.34	0.33	0.35	0.44	0.38	0.48
K	0.24	0.24	0.25	0.25	0.23	0.25	0.24	0.24	0.27	0.25	0.28
Sum A	0.56	0.59	0.59	0.58	0.57	0.58	0.57	0.59	0.73	0.67	0.78
TOTAL	15.56	15.59	15.59	15.58	15.57	15.58	15.57	15.59	15.73	15.67	15.78
Classification	Prg	Ed	Ed	Ed	Ed	Ed	Ed	Ed	Ed	Ed	Ed

Abbreviations: Ed=Edenite,Prg=Pargasite (Hawthorne et al. 2012)

Appendix 4.2.5: Representative mineral chemistry for amphibole

Wt%	DA13-064-1.4	DA13-064-1.5	DA13-064-1.6	DA13-064-1.7	DA13-064-1.8	DA13-064-1.9	DA13-064-1.10	DA13-064-3.1	DA13-064-3.2	DA13-064-3.3	DA13-064-3.4	DA13-064-3.5
SiO_2	43.98	43.85	43.84	43.89	43.70	43.75	43.45	44.08	44.11	44.02	44.04	43.04
TiO_2	0.50	0.49	0.50	0.48	0.51	0.40	0.42	0.46	0.43	0.35	0.45	0.52
Al_2O_3	10.02	10.12	10.10	10.14	10.12	10.24	9.92	9.90	10.13	10.05	10.12	10.70
Cr_2O_3	0.00	0.01	0.04	0.00	0.03	0.00	0.00	0.01	0.00	0.00	0.00	0.01
FeOT	20.24	20.29	20.21	20.32	20.36	20.17	19.88	20.17	20.09	20.05	20.21	20.33
MnO	1.11	1.01	1.06	1.09	1.09	1.13	1.09	1.04	1.21	1.15	1.14	1.01
MgO	8.65	8.77	8.62	8.73	8.62	8.77	8.70	8.72	8.63	8.58	8.67	8.42
CaO	11.09	11.02	11.07	11.07	10.99	11.07	11.16	11.09	11.07	11.22	11.15	10.99
Na_2O	1.60	1.58	1.60	1.63	1.70	1.52	1.48	1.62	1.56	1.40	1.53	1.65
K_2O	1.44	1.44	1.42	1.47	1.47	1.44	1.49	1.39	1.39	1.38	1.46	1.52
TOTAL	98.62	98.59	98.46	98.83	98.59	98.49	97.59	98.48	98.63	98.20	98.77	98.20
Si	6.68	6.66	6.66	6.65	6.64	6.65	6.67	6.69	6.69	6.70	6.67	6.58
Al	1.32	1.34	1.34	1.35	1.36	1.35	1.33	1.31	1.31	1.30	1.33	1.42
Sum T	8.00	8.00	8.00	8.00	8.00	8.00	8.00	8.00	8.00	8.00	8.00	8.00
Al	0.47	0.47	0.47	0.46	0.46	0.48	0.46	0.47	0.50	0.50	0.48	0.50
Fe^{3+}	0.00	0.00	0.00	0.00	0.00	0.00	0.00	0.00	0.00	0.00	0.00	0.00
Cr	0.06	0.06	0.06	0.05	0.06	0.05	0.05	0.05	0.05	0.04	0.05	0.06
Ti	0.00	0.00	0.01	0.00	0.00	0.00	0.00	0.00	0.00	0.00	0.00	0.00
Fe^{2+}	2.57	2.58	2.57	2.58	2.59	2.56	2.55	2.56	2.55	2.55	2.56	2.60
Mn	0.14	0.13	0.14	0.14	0.14	0.15	0.14	0.13	0.16	0.15	0.15	0.13
Mg	1.76	1.77	1.76	1.76	1.75	1.76	1.80	1.79	1.75	1.76	1.76	1.71
Sum C	5.00	5.00	5.00	5.00	5.00	5.00	5.00	5.00	5.00	5.00	5.00	5.00
Mg^{2+}, Mn^{2+}, Fe^{2+}	0.19	0.22	0.19	0.21	0.20	0.22	0.19	0.19	0.20	0.19	0.20	0.21
Ca	1.80	1.78	1.80	1.79	1.79	1.78	1.81	1.80	1.80	1.81	1.80	1.79
Na	0.00	0.00	0.00	0.00	0.00	0.00	0.00	0.01	0.00	0.00	0.00	0.00
Sum B	2.00	2.00	2.00	2.00	2.00	2.00	2.00	2.00	2.00	2.00	2.00	2.00
Ca	0.00	0.01	0.00	0.00	0.00	0.03	0.02	0.00	0.00	0.02	0.01	0.01
Na	0.47	0.47	0.47	0.48	0.50	0.45	0.44	0.47	0.45	0.41	0.45	0.49
K	0.28	0.28	0.28	0.29	0.28	0.28	0.29	0.27	0.27	0.27	0.28	0.30
Sum A	0.75	0.75	0.75	0.77	0.78	0.75	0.76	0.74	0.72	0.70	0.74	0.79
TOTAL	15.75	15.75	15.75	15.77	15.78	15.75	15.76	15.74	15.72	15.70	15.74	15.79
Classification	Ed	Ed	Ed	Ed	Ed	Ed	Ed	Ed	Ed	Prg	Ed	Prg

Abbreviations: Ed=Edenite,Prg=Pargasite (Hawthorne et al. 2012)

Appendix 4.2.5: Representative mineral chemistry for amphibole

Wt%	DA13-064-3.6	DA13-064-3.7	DA13-064-3.8	DA13-064-3.9	DA13-064-3.10	DA13-069-1.1	DA13-069-1.2	DA13-069-1.3	DA13-069-1.4	DA13-069-1.5	DA13-069-1.6
SiO_2	43.72	43.71	43.91	43.56	43.21	45.20	44.29	44.77	44.46	45.23	45.05
TiO_2	0.48	0.48	0.55	0.53	0.55	0.54	0.59	0.59	0.61	0.47	0.59
Al_2O_3	10.27	10.26	10.07	10.27	10.39	8.33	9.18	8.98	9.14	8.88	9.07
Cr_2O_3	0.01	0.00	0.01	0.00	0.01	0.01	0.02	0.00	0.02	0.01	0.01
FeOT	20.18	20.59	20.41	20.75	20.49	19.55	20.30	20.23	20.12	19.63	19.96
MnO	1.05	1.09	1.03	1.07	1.13	0.38	0.37	0.36	0.34	0.40	0.35
MgO	8.52	8.57	8.65	8.35	8.38	9.78	9.36	9.60	9.41	9.69	9.57
CaO	11.01	11.10	10.96	10.99	11.12	11.22	10.82	10.96	10.91	11.35	10.83
Na_2O	1.57	1.48	1.69	1.67	1.55	1.45	1.87	1.76	1.83	1.38	1.87
K_2O	1.50	1.52	1.47	1.51	1.56	1.33	1.47	1.43	1.42	1.35	1.46
TOTAL	98.31	98.80	98.75	98.70	98.38	97.79	98.27	98.68	98.26	98.40	98.75
Si	6.66	6.64	6.66	6.63	6.60	6.86	6.73	6.77	6.75	6.82	6.79
Al	1.34	1.36	1.34	1.37	1.40	1.14	1.27	1.23	1.25	1.18	1.21
Sum T	8.00	8.00	8.00	8.00	8.00	8.00	8.00	8.00	8.00	8.00	8.00
Al	0.50	0.47	0.46	0.47	0.47	0.35	0.38	0.36	0.38	0.40	0.40
Fe^{3+}	0.00	0.00	0.00	0.00	0.00	0.00	0.00	0.00	0.00	0.00	0.00
Cr	0.05	0.06	0.06	0.06	0.06	0.06	0.07	0.07	0.07	0.05	0.07
Ti	0.00	0.00	0.00	0.00	0.00	0.00	0.00	0.00	0.00	0.00	0.00
Fe^{2+}	2.57	2.61	2.59	2.64	2.62	2.48	2.58	2.56	2.55	2.48	2.52
Mn	0.14	0.14	0.13	0.14	0.15	0.05	0.05	0.05	0.04	0.05	0.05
Mg	1.74	1.72	1.75	1.69	1.70	2.05	1.92	1.97	1.95	2.01	1.97
Sum C	5.00	5.00	5.00	5.00	5.00	5.00	5.00	5.00	5.00	5.00	5.00
Mg^{2+}, Mn^{2+}, Fe^{2+}	0.19	0.22	0.20	0.20	0.20	0.16	0.20	0.20	0.18	0.17	0.18
Ca	1.80	1.78	1.78	1.79	1.80	1.83	1.76	1.77	1.77	1.83	1.75
Na	0.01	0.00	0.01	0.00	0.00	0.01	0.04	0.03	0.04	0.00	0.07
Sum B	2.00	2.00	2.00	2.00	2.00	2.00	2.00	2.00	2.00	2.00	2.00
Ca	0.00	0.03	0.00	0.00	0.02	0.00	0.00	0.00	0.00	0.00	0.00
Na	0.45	0.44	0.48	0.49	0.46	0.41	0.51	0.49	0.50	0.40	0.47
K	0.29	0.29	0.28	0.29	0.30	0.26	0.28	0.28	0.27	0.26	0.28
Sum A	0.74	0.76	0.77	0.78	0.78	0.67	0.79	0.76	0.77	0.66	0.75
TOTAL	15.74	15.76	15.77	15.78	15.78	15.67	15.79	15.76	15.77	15.66	15.75
Classification	Prg	Ed	Ed	Ed	Ed	Ed	Ed	Ed	Ed	Ed	Ed

Abbreviations: Ed=Edenite,Prg=Pargasite (Hawthorne et al. 2012)

Appendix 4.2.5: Representative mineral chemistry for amphibole

Wt%	DA13-069-1.7	DA13-069-1.8	DA13-069-1.9	DA13-069-1.10	DA13-069-3.1	DA13-069-3.2	DA13-069-3.3	DA13-069-3.4	DA13-069-3.5	DA13-069-3.6	DA13-069-3.7
SiO_2	44.89	44.71	45.15	44.48	46.28	45.59	44.79	44.91	44.15	45.54	45.23
TiO_2	0.59	0.56	0.56	0.58	0.41	0.52	0.52	0.51	0.37	0.48	0.50
Al_2O_3	9.03	9.01	8.90	9.17	8.30	8.63	8.67	8.52	8.70	8.77	8.80
Cr_2O_3	0.04	0.00	0.02	0.04	0.04	0.03	0.00	0.00	0.03	0.02	0.00
FeOT	20.25	20.25	19.94	20.33	20.24	20.29	19.93	20.50	19.32	19.51	19.84
MnO	0.40	0.30	0.34	0.41	0.33	0.34	0.36	0.32	0.30	0.39	0.41
MgO	9.42	9.62	9.67	9.33	9.56	9.48	8.87	9.02	8.96	9.80	9.81
CaO	10.93	10.83	10.92	10.80	11.14	10.84	10.66	10.98	10.63	10.87	10.90
Na_2O	1.79	1.90	1.83	1.90	1.49	1.67	1.75	1.60	1.46	1.77	1.78
K_2O	1.41	1.40	1.38	1.48	1.22	1.31	1.34	1.35	1.21	1.35	1.43
TOTAL	98.74	98.58	98.69	98.53	99.01	98.70	96.88	97.72	95.14	98.50	98.70
Si	6.78	6.76	6.80	6.74	6.93	6.87	6.88	6.85	6.88	6.85	6.81
Al	1.22	1.24	1.20	1.26	1.07	1.13	1.12	1.15	1.12	1.15	1.19
Sum T	8.00	8.00	8.00	8.00	8.00	8.00	8.00	8.00	8.00	8.00	8.00
Al	0.38	0.37	0.38	0.38	0.40	0.40	0.44	0.39	0.48	0.41	0.38
Fe^{3+}	0.00	0.00	0.00	0.00	0.00	0.00	0.00	0.00	0.00	0.00	0.00
Cr	0.07	0.06	0.06	0.07	0.05	0.06	0.06	0.06	0.04	0.05	0.06
Ti	0.00	0.00	0.00	0.00	0.01	0.00	0.00	0.00	0.00	0.00	0.00
Fe^{2+}	2.56	2.56	2.51	2.58	2.54	2.56	2.56	2.62	2.52	2.46	2.50
Mn	0.05	0.04	0.04	0.05	0.04	0.04	0.05	0.04	0.04	0.05	0.05
Mg	1.94	1.97	1.99	1.92	1.97	1.94	1.89	1.90	1.92	2.03	2.01
Sum C	5.00	5.00	5.00	5.00	5.00	5.00	5.00	5.00	5.00	5.00	5.00
Mg^{2+}, Mn^{2+}, Fe^{2+}	0.18	0.20	0.18	0.19	0.16	0.19	0.14	0.16	0.16	0.17	0.19
Ca	1.77	1.75	1.76	1.75	1.79	1.75	1.75	1.80	1.78	1.75	1.76
Na	0.05	0.04	0.06	0.05	0.05	0.06	0.11	0.05	0.06	0.08	0.05
Sum B	2.00	2.00	2.00	2.00	2.00	2.00	2.00	2.00	2.00	2.00	2.00
Ca	0.00	0.00	0.00	0.00	0.00	0.00	0.00	0.00	0.00	0.00	0.00
Na	0.48	0.51	0.48	0.50	0.38	0.42	0.41	0.42	0.38	0.44	0.47
K	0.27	0.27	0.27	0.29	0.23	0.25	0.26	0.26	0.24	0.26	0.28
Sum A	0.75	0.78	0.74	0.79	0.62	0.68	0.67	0.69	0.62	0.70	0.74
TOTAL	15.75	15.78	15.74	15.79	15.62	15.68	15.67	15.69	15.62	15.70	15.74
Classification	Ed	Ed	Ed	Ed	Ed	Ed	Ed	Ed	Ed	Ed	Ed

Abbreviations: Ed=Edenite,Prg=Pargasite (Hawthorne et al. 2012)

Appendix 4.2.5: Representative mineral chemistry for amphibole

Wt%	DA13-069-3.8	DA13-069-3.9	DA13-069-3.10	DA13-069-3.11	DA13-069-3.12	DA13-069-3.13	DA13-069-3.14	DA13-069-3.15	DA13-069-3.16	DA13-069-3.17	DA13-069-3.18
SiO_2	46.78	45.59	44.32	45.68	45.36	45.08	44.57	45.00	45.58	44.77	45.81
TiO_2	0.46	0.51	0.48	0.50	0.54	0.48	0.53	0.61	0.44	0.54	0.46
Al_2O_3	8.02	8.55	8.55	8.95	8.74	8.73	9.03	9.13	7.93	8.76	7.81
Cr_2O_3	0.01	0.00	0.03	0.00	0.00	0.00	0.00	0.04	0.00	0.03	0.02
FeOT	19.28	19.62	19.49	19.50	19.79	19.22	20.15	20.43	18.97	20.61	19.32
MnO	0.37	0.40	0.34	0.35	0.33	0.35	0.34	0.34	0.31	0.41	0.35
MgO	10.11	9.91	9.41	9.62	9.75	9.71	9.23	9.24	9.88	9.08	9.89
CaO	10.76	11.20	10.91	11.17	10.89	11.67	10.91	10.73	11.13	10.83	11.01
Na_2O	1.67	1.46	1.69	1.48	1.80	1.56	1.77	1.91	1.47	1.75	1.39
K_2O	1.21	1.27	1.33	1.34	1.36	1.34	1.42	1.38	1.23	1.46	1.19
TOTAL	98.67	98.49	96.55	98.61	98.57	98.14	97.94	98.81	96.94	98.22	97.25
Si	6.99	6.86	6.83	6.86	6.84	6.82	6.78	6.79	6.95	6.81	6.97
Al	1.01	1.14	1.17	1.14	1.16	1.18	1.22	1.21	1.05	1.19	1.03
Sum T	8.00	8.00	8.00	8.00	8.00	8.00	8.00	8.00	8.00	8.00	8.00
Al	0.41	0.38	0.38	0.44	0.39	0.38	0.40	0.41	0.38	0.38	0.37
Fe^{3+}	0.00	0.00	0.00	0.00	0.00	0.00	0.00	0.00	0.00	0.00	0.00
Cr	0.05	0.06	0.06	0.06	0.06	0.05	0.06	0.07	0.05	0.06	0.05
Ti	0.00	0.00	0.00	0.00	0.00	0.00	0.00	0.00	0.00	0.00	0.00
Fe^{2+}	2.41	2.47	2.51	2.45	2.49	2.43	2.57	2.58	2.42	2.62	2.46
Mn	0.05	0.05	0.04	0.04	0.04	0.04	0.04	0.04	0.04	0.05	0.05
Mg	2.08	2.04	2.01	2.01	2.01	2.09	1.93	1.90	2.11	1.88	2.08
Sum C	5.00	5.00	5.00	5.00	5.00	5.00	5.00	5.00	5.00	5.00	5.00
Mg^{2+}, Mn^{2+}, Fe^{2+}	0.17	0.18	0.16	0.15	0.18	0.10	0.17	0.18	0.13	0.18	0.17
Ca	1.72	1.81	1.80	1.80	1.76	1.89	1.78	1.73	1.82	1.76	1.79
Na	0.11	0.01	0.04	0.05	0.07	0.01	0.05	0.08	0.05	0.06	0.04
Sum B	2.00	2.00	2.00	2.00	2.00	2.00	2.00	2.00	2.00	2.00	2.00
Ca	0.00	0.00	0.00	0.00	0.00	0.00	0.00	0.00	0.00	0.00	0.00
Na	0.38	0.41	0.46	0.38	0.46	0.45	0.47	0.48	0.38	0.46	0.37
K	0.23	0.24	0.26	0.26	0.26	0.26	0.27	0.27	0.24	0.28	0.23
Sum A	0.61	0.66	0.72	0.64	0.72	0.71	0.74	0.74	0.62	0.74	0.60
TOTAL	15.61	15.66	15.72	15.64	15.72	15.71	15.74	15.74	15.62	15.74	15.60
Classification	Ed	Ed	Ed	Ed	Ed	Ed	Ed	Ed	Ed	Ed	Ed

Abbreviations: Ed=Edenite,Prg=Pargasite (Hawthorne et al. 2012)

Appendix 4.2.5: Representative mineral chemistry for amphibole

Wt%	DA13-069-3.19	DA13-069-3.20	DA13-074-3.1	DA13-074-3.2	DA13-074-3.3	DA13-074-3.4	DA13-074-4.1	DA13-074-4.2	DA13-074-4.3	DA13-074-4.4	DA13-074-4.5
SiO_2	45.73	46.36	40.87	40.79	41.11	41.01	41.08	41.00	41.03	37.08	41.72
TiO_2	0.53	0.54	1.88	1.88	1.83	1.73	1.41	1.76	1.79	4.57	1.49
Al_2O_3	8.21	8.46	10.65	10.65	10.56	10.59	10.97	10.96	10.88	13.21	11.06
Cr_2O_3	0.03	0.00	0.00	0.00	0.00	0.00	0.01	0.00	0.00	0.00	0.02
FeOT	19.04	19.86	26.89	26.76	26.85	26.86	27.55	27.13	27.31	29.18	27.27
MnO	0.40	0.33	0.33	0.29	0.31	0.35	0.30	0.32	0.33	0.22	0.31
MgO	9.97	9.89	3.04	3.03	3.06	3.06	2.70	2.84	2.80	4.53	2.91
CaO	11.14	11.10	10.69	10.79	10.81	10.77	10.70	10.59	10.63	0.08	10.68
Na_2O	1.36	1.61	1.70	1.69	1.63	1.65	1.62	1.65	1.68	0.11	1.60
K_2O	1.22	1.26	1.83	1.92	1.88	1.88	1.87	1.89	1.90	8.36	1.85
TOTAL	97.64	99.43	97.87	97.80	98.04	97.90	98.22	98.14	98.35	97.33	98.92
Si	6.92	6.91	6.49	6.48	6.51	6.50	6.51	6.49	6.49	6.03	6.53
Al	1.08	1.09	1.51	1.52	1.49	1.50	1.49	1.51	1.51	1.97	1.47
Sum T	8.00	8.00	8.00	8.00	8.00	8.00	8.00	8.00	8.00	8.00	8.00
Al	0.39	0.39	0.48	0.47	0.48	0.48	0.55	0.53	0.51	0.56	0.58
Fe^{3+}	0.00	0.00	0.00	0.00	0.00	0.00	0.00	0.00	0.00	0.06	0.00
Cr	0.06	0.06	0.22	0.22	0.22	0.21	0.17	0.21	0.21	0.56	0.18
Ti	0.00	0.00	0.00	0.00	0.00	0.00	0.00	0.00	0.00	0.00	0.00
Fe^{2+}	2.41	2.47	3.57	3.55	3.55	3.56	3.65	3.59	3.61	3.91	3.57
Mn	0.05	0.04	0.04	0.04	0.04	0.05	0.04	0.04	0.04	0.03	0.04
Mg	2.09	2.03	0.69	0.71	0.71	0.70	0.59	0.63	0.62	-0.12	0.63
Sum C	5.00	5.00	5.00	5.00	5.00	5.00	5.00	5.00	5.00	5.00	5.00
Mg^{2+}, Mn^{2+}, Fe^{2+}	0.16	0.17	0.03	0.01	0.02	0.02	0.05	0.04	0.04	1.22	0.05
Ca	1.81	1.77	1.82	1.84	1.83	1.83	1.82	1.79	1.80	0.01	1.79
Na	0.03	0.06	0.15	0.16	0.15	0.15	0.14	0.16	0.16	0.77	0.16
Sum B	2.00	2.00	2.00	2.00	2.00	2.00	2.00	2.00	2.00	2.00	2.00
Ca	0.00	0.00	0.00	0.00	0.00	0.00	0.00	0.00	0.00	0.00	0.00
Na	0.37	0.40	0.37	0.37	0.35	0.36	0.36	0.34	0.35	-0.73	0.33
K	0.24	0.24	0.37	0.39	0.38	0.38	0.38	0.38	0.38	1.73	0.37
Sum A	0.60	0.64	0.74	0.75	0.73	0.74	0.74	0.73	0.74	1.00	0.69
TOTAL	15.60	15.64	15.74	15.75	15.73	15.74	15.74	15.73	15.74	16.00	15.69
Classification	Ed	Ed	Ed	Ed	Ed	Ed	Prg	Prg	Prg	Prg	Prg

Abbreviations: Ed=Edenite,Prg=Pargasite (Hawthorne et al. 2012)

Appendix 4.2.5: Representative mineral chemistry for amphibole

Wt%	DA13-074-4.6	DA13-074-7.1	DA13-074-7.2	DA13-074-7.3	DA13-074-7.4	DA13-074-7.5	DA13-074-7.6	DA13-074-7.7	DA13-074-7.8	DA13-074-7.9	DA13-074-7.10
SiO_2	41.62	38.99	38.98	38.92	38.94	38.10	39.23	37.93	39.08	39.33	35.97
TiO_2	1.45	1.81	1.80	1.85	1.86	1.86	1.93	1.86	1.87	1.88	1.74
Al_2O_3	11.04	10.99	10.90	11.04	11.06	11.35	10.98	12.43	11.03	12.03	14.20
Cr_2O_3	0.00	0.00	0.00	0.00	0.01	0.02	0.00	0.07	0.00	0.02	0.59
FeOT	27.49	26.87	26.89	26.95	26.93	26.15	27.11	26.16	27.05	26.57	24.60
MnO	0.33	0.32	0.33	0.34	0.30	0.31	0.31	0.31	0.37	0.33	0.32
MgO	2.84	3.13	3.13	3.11	3.16	3.04	3.15	3.02	3.18	3.12	2.79
CaO	10.79	10.64	10.65	10.60	10.58	10.26	10.67	10.29	10.51	10.40	9.76
Na_2O	1.66	1.72	1.79	1.79	1.79	1.79	1.81	1.84	1.87	1.89	1.72
K_2O	1.84	1.86	1.87	1.86	1.86	1.90	1.84	1.93	1.85	1.93	1.88
TOTAL	99.07	96.34	96.35	96.48	96.48	94.79	97.02	95.86	96.80	97.48	93.57
Si	6.52	6.32	6.33	6.31	6.31	6.27	6.32	6.17	6.31	6.28	5.97
Al	1.48	1.68	1.67	1.69	1.69	1.73	1.68	1.83	1.69	1.72	2.03
Sum T	8.00	8.00	8.00	8.00	8.00	8.00	8.00	8.00	8.00	8.00	8.00
Al	0.56	0.43	0.41	0.42	0.42	0.48	0.41	0.55	0.41	0.54	0.74
Fe^{3+}	0.00	0.00	0.00	0.00	0.00	0.00	0.00	0.00	0.00	0.00	0.00
Cr	0.17	0.22	0.22	0.23	0.23	0.23	0.23	0.23	0.23	0.23	0.22
Ti	0.00	0.00	0.00	0.00	0.00	0.00	0.00	0.01	0.00	0.00	0.08
Fe^{2+}	3.60	3.64	3.65	3.65	3.65	3.60	3.65	3.56	3.65	3.55	3.41
Mn	0.04	0.04	0.05	0.05	0.04	0.04	0.04	0.04	0.05	0.04	0.04
Mg	0.62	0.67	0.67	0.66	0.66	0.65	0.67	0.61	0.66	0.64	0.51
Sum C	5.00	5.00	5.00	5.00	5.00	5.00	5.00	5.00	5.00	5.00	5.00
Mg^{2+}, Mn^{2+}, Fe^{2+}	0.04	0.09	0.08	0.10	0.10	0.10	0.09	0.12	0.11	0.10	0.18
Ca	1.81	1.85	1.85	1.84	1.84	1.81	1.84	1.79	1.82	1.78	1.73
Na	0.15	0.06	0.06	0.06	0.07	0.09	0.07	0.08	0.07	0.12	0.08
Sum B	2.00	2.00	2.00	2.00	2.00	2.00	2.00	2.00	2.00	2.00	2.00
Ca	0.00	0.00	0.00	0.00	0.00	0.00	0.00	0.00	0.00	0.00	0.00
Na	0.36	0.48	0.50	0.50	0.50	0.48	0.50	0.50	0.51	0.46	0.47
K	0.37	0.39	0.39	0.39	0.38	0.40	0.38	0.40	0.38	0.39	0.40
Sum A	0.72	0.87	0.89	0.88	0.88	0.88	0.87	0.90	0.89	0.85	0.87
TOTAL	15.72	15.87	15.89	15.88	15.88	15.88	15.87	15.90	15.89	15.85	15.87
Classification	Prg	Ed	Ed	Ed	Ed	Ed	Ed	Prg	Ed	Prg	Prg

Abbreviations: Ed=Edenite,Prg=Pargasite (Hawthorne et al. 2012)

Appendix 4.2.5: Representative mineral chemistry for amphibole

Wt%	DA13-074-7.11	DA13-074-7.12	DA13-074-7.13	DA13-074-7.14	DA13-074-7.15	DA13-076-1.1	DA13-076-1.2	DA13-076-1.3	DA13-076-1.4	DA13-076-1.5	DA13-076-1.6
SiO_2	38.42	39.14	39.40	39.36	39.38	39.17	40.90	38.61	41.00	41.19	41.16
TiO_2	1.77	1.85	1.87	1.62	1.80	2.04	2.16	1.99	2.17	2.23	2.17
Al_2O_3	11.99	10.93	11.13	11.00	10.88	12.41	11.13	11.84	10.92	10.96	11.05
Cr_2O_3	0.03	0.01	0.00	0.00	0.01	0.00	0.00	0.01	0.00	0.00	0.00
FeOT	26.22	26.83	27.06	27.31	27.03	24.98	27.23	26.24	27.25	27.27	27.32
MnO	0.34	0.33	0.34	0.34	0.33	0.12	0.16	0.13	0.14	0.17	0.18
MgO	3.03	3.04	3.12	3.14	3.19	2.57	2.78	2.68	2.78	2.83	2.92
CaO	10.45	10.59	10.67	10.74	10.83	10.28	10.39	10.38	10.59	10.62	10.58
Na_2O	1.79	1.77	1.84	1.72	1.74	1.55	1.76	1.53	1.74	1.84	1.80
K_2O	1.94	1.85	1.86	1.85	1.84	1.75	1.85	1.80	1.83	1.82	1.82
TOTAL	95.97	96.35	97.30	97.08	97.03	94.88	98.37	95.20	98.41	98.92	98.99
Si	6.24	6.34	6.33	6.34	6.34	6.35	6.45	6.30	6.47	6.46	6.45
Al	1.76	1.66	1.67	1.66	1.66	1.65	1.55	1.70	1.53	1.54	1.55
Sum T	8.00	8.00	8.00	8.00	8.00	8.00	8.00	8.00	8.00	8.00	8.00
Al	0.53	0.43	0.43	0.43	0.41	0.73	0.52	0.58	0.50	0.49	0.50
Fe^{3+}	0.00	0.00	0.00	0.00	0.00	0.00	0.00	0.00	0.00	0.00	0.00
Cr	0.22	0.23	0.23	0.20	0.22	0.25	0.26	0.24	0.26	0.26	0.26
Ti	0.00	0.00	0.00	0.00	0.00	0.00	0.00	0.00	0.00	0.00	0.00
Fe^{2+}	3.56	3.64	3.63	3.68	3.64	3.39	3.59	3.58	3.59	3.58	3.58
Mn	0.05	0.05	0.05	0.05	0.04	0.02	0.02	0.02	0.02	0.02	0.02
Mg	0.64	0.66	0.66	0.65	0.69	0.62	0.61	0.58	0.63	0.65	0.64
Sum C	5.00	5.00	5.00	5.00	5.00	5.00	5.00	5.00	5.00	5.00	5.00
Mg^{2+}, Mn^{2+}, Fe^{2+}	0.10	0.08	0.08	0.11	0.08	0.00	0.05	0.07	0.02	0.01	0.04
Ca	1.82	1.84	1.84	1.85	1.87	1.79	1.76	1.81	1.79	1.78	1.78
Na	0.09	0.08	0.08	0.04	0.05	0.21	0.20	0.11	0.19	0.20	0.18
Sum B	2.00	2.00	2.00	2.00	2.00	2.00	2.00	2.00	2.00	2.00	2.00
Ca	0.00	0.00	0.00	0.00	0.00	0.00	0.00	0.00	0.00	0.00	0.00
Na	0.48	0.47	0.49	0.50	0.49	0.27	0.34	0.37	0.34	0.36	0.36
K	0.40	0.38	0.38	0.38	0.38	0.36	0.37	0.38	0.37	0.36	0.36
Sum A	0.88	0.85	0.87	0.88	0.87	0.64	0.71	0.75	0.71	0.72	0.72
TOTAL	15.88	15.85	15.87	15.88	15.87	15.64	15.71	15.75	15.71	15.72	15.72
Classification	Prg	Ed	Ed	Ed	Ed	Prg	Prg	Prg	Ed	Ed	Ed

Abbreviations: Ed=Edenite,Prg=Pargasite (Hawthorne et al. 2012)

Appendix 4.2.5: Representative mineral chemistry for amphibole

Wt%	DA13-076-1.7	DA13-076-1.8	DA13-076-3.1	DA13-076-3.2	DA13-076-3.3	DA13-076-3.4	DA13-076-5.1	DA13-076-5.2	DA13-076-5.3	DA13-076-5.4	DA13-076-5.5	DA13-076-7.1
SiO_2	41.79	41.00	41.07	40.99	40.81	40.96	41.23	40.82	41.15	40.18	41.18	41.34
TiO_2	2.16	2.21	1.99	1.85	1.91	1.96	2.09	2.05	2.03	2.01	2.05	1.81
Al_2O_3	11.22	11.05	11.06	11.13	10.96	10.92	11.14	10.93	11.11	10.85	11.23	11.02
Cr_2O_3	0.00	0.00	0.00	0.00	0.00	0.00	0.03	0.00	0.00	0.00	0.04	0.00
FeOT	27.00	27.18	27.62	27.06	27.43	27.52	27.13	27.44	27.63	27.23	27.24	27.43
MnO	0.17	0.11	0.12	0.14	0.14	0.15	0.14	0.15	0.14	0.13	0.14	0.10
MgO	3.06	2.84	2.90	2.89	2.80	2.81	2.87	2.89	2.95	2.78	2.85	2.80
CaO	10.48	10.55	10.55	10.57	10.47	10.58	10.57	10.58	10.60	10.67	10.53	10.73
Na_2O	1.87	1.74	1.72	1.72	1.74	1.72	1.76	1.74	1.76	1.61	1.80	1.71
K_2O	1.83	1.84	1.82	1.81	1.82	1.82	1.83	1.79	1.81	1.83	1.85	1.78
TOTAL	99.58	98.52	98.85	98.16	98.09	98.44	98.80	98.39	99.19	97.28	98.91	98.73
Si	6.49	6.46	6.45	6.47	6.47	6.47	6.47	6.45	6.45	6.43	6.46	6.50
Al	1.51	1.54	1.55	1.53	1.53	1.53	1.53	1.55	1.55	1.57	1.54	1.50
Sum T	8.00	8.00	8.00	8.00	8.00	8.00	8.00	8.00	8.00	8.00	8.00	8.00
Al	0.54	0.51	0.50	0.54	0.51	0.50	0.53	0.48	0.50	0.47	0.53	0.54
Fe^{3+}	0.00	0.00	0.00	0.00	0.00	0.00	0.00	0.00	0.00	0.00	0.00	0.00
Cr	0.25	0.26	0.23	0.22	0.23	0.23	0.25	0.24	0.24	0.24	0.24	0.21
Ti	0.00	0.00	0.00	0.00	0.00	0.00	0.00	0.00	0.00	0.00	0.00	0.00
Fe^{2+}	3.50	3.58	3.63	3.57	3.63	3.63	3.56	3.62	3.62	3.64	3.57	3.60
Mn	0.02	0.01	0.02	0.02	0.02	0.02	0.02	0.02	0.02	0.02	0.02	0.01
Mg	0.68	0.64	0.62	0.64	0.61	0.61	0.65	0.63	0.63	0.62	0.63	0.63
Sum C	5.00	5.00	5.00	5.00	5.00	5.00	5.00	5.00	5.00	5.00	5.00	5.00
Mg^{2+}, Mn^{2+}, Fe^{2+}	0.03	0.03	0.06	0.04	0.05	0.05	0.03	0.05	0.06	0.04	0.03	0.02
Ca	1.74	1.78	1.78	1.79	1.78	1.79	1.78	1.79	1.78	1.83	1.77	1.81
Na	0.23	0.19	0.16	0.17	0.17	0.16	0.20	0.16	0.16	0.13	0.20	0.17
Sum B	2.00	2.00	2.00	2.00	2.00	2.00	2.00	2.00	2.00	2.00	2.00	2.00
Ca	0.00	0.00	0.00	0.00	0.00	0.00	0.00	0.00	0.00	0.00	0.00	0.00
Na	0.33	0.34	0.37	0.35	0.37	0.36	0.34	0.38	0.38	0.37	0.35	0.35
K	0.36	0.37	0.37	0.37	0.37	0.37	0.37	0.36	0.36	0.37	0.37	0.36
Sum A	0.70	0.71	0.73	0.72	0.74	0.73	0.70	0.74	0.74	0.74	0.72	0.71
TOTAL	15.70	15.71	15.73	15.72	15.74	15.73	15.70	15.74	15.74	15.74	15.72	15.71
Classification	Prg	Prg	Prg	Prg	Prg	Prg	Prg	Ed	Ed	Ed	Prg	Prg

Abbreviations: Ed=Edenite,Prg=Pargasite (Hawthorne et al. 2012)

Appendix 4.2.5: Representative mineral chemistry for amphibole

Wt%	DA13-076-7.2	DA13-076-7.3	DA13-076-7.4	DA13-076-7.5	DA13-076-7.6	DA13-077-3.1	DA13-077-3.2	DA13-077-3.3	DA13-077-3.4	DA13-077-3.5	DA13-077-3.6
SiO_2	41.27	41.95	41.12	41.14	41.22	40.56	40.40	40.37	40.63	40.34	40.37
TiO_2	1.79	1.83	2.01	2.01	1.95	1.41	1.44	1.42	1.34	1.36	1.37
Al_2O_3	11.32	11.39	11.20	11.22	11.11	10.30	10.33	10.33	10.29	10.35	10.30
Cr_2O_3	0.00	0.00	0.02	0.00	0.00	0.03	0.03	0.00	0.00	0.00	0.00
FeOT	27.62	27.14	27.46	27.58	27.42	30.16	30.07	30.02	30.09	30.47	29.85
MnO	0.12	0.14	0.15	0.16	0.14	0.62	0.68	0.64	0.56	0.62	0.62
MgO	2.83	2.89	2.72	2.71	2.73	1.42	1.38	1.35	1.34	1.36	1.45
CaO	10.75	10.55	10.53	10.48	10.58	10.13	10.17	10.12	10.16	10.23	10.04
Na_2O	1.64	1.81	1.71	1.81	1.67	1.89	1.89	1.89	1.80	1.90	1.97
K_2O	1.78	1.80	1.83	1.89	1.84	1.77	1.81	1.76	1.79	1.78	1.78
TOTAL	99.12	99.50	98.75	99.00	98.65	98.29	98.20	97.89	98.01	98.42	97.76
Si	6.46	6.51	6.46	6.46	6.48	6.52	6.50	6.51	6.54	6.49	6.52
Al	1.54	1.49	1.54	1.54	1.52	1.48	1.50	1.49	1.46	1.51	1.48
Sum T	8.00	8.00	8.00	8.00	8.00	8.00	8.00	8.00	8.00	8.00	8.00
Al	0.55	0.60	0.54	0.53	0.54	0.47	0.46	0.48	0.49	0.45	0.48
Fe^{3+}	0.00	0.00	0.00	0.00	0.00	0.00	0.00	0.00	0.00	0.00	0.00
Cr	0.21	0.21	0.24	0.24	0.23	0.17	0.17	0.17	0.16	0.16	0.17
Ti	0.00	0.00	0.00	0.00	0.00	0.00	0.00	0.00	0.00	0.00	0.00
Fe^{2+}	3.62	3.52	3.61	3.62	3.61	4.05	4.05	4.05	4.05	4.10	4.03
Mn	0.02	0.02	0.02	0.02	0.02	0.08	0.09	0.09	0.08	0.08	0.09
Mg	0.61	0.64	0.59	0.59	0.60	0.22	0.22	0.22	0.22	0.20	0.24
Sum C	5.00	5.00	5.00	5.00	5.00	5.00	5.00	5.00	5.00	5.00	5.00
Mg^{2+}, Mn^{2+}, Fe^{2+}	0.05	0.02	0.04	0.04	0.04	0.12	0.11	0.11	0.10	0.12	0.11
Ca	1.80	1.76	1.77	1.76	1.78	1.74	1.75	1.75	1.75	1.76	1.74
Na	0.14	0.22	0.18	0.19	0.18	0.14	0.14	0.14	0.14	0.11	0.15
Sum B	2.00	2.00	2.00	2.00	2.00	2.00	2.00	2.00	2.00	2.00	2.00
Ca	0.00	0.00	0.00	0.00	0.00	0.00	0.00	0.00	0.00	0.00	0.00
Na	0.35	0.32	0.34	0.35	0.33	0.45	0.45	0.45	0.42	0.48	0.46
K	0.36	0.36	0.37	0.38	0.37	0.36	0.37	0.36	0.37	0.37	0.37
Sum A	0.71	0.68	0.70	0.73	0.70	0.81	0.82	0.81	0.79	0.84	0.83
TOTAL	15.71	15.68	15.70	15.73	15.70	15.81	15.82	15.81	15.79	15.84	15.83
Classification	Prg	Prg	Prg	Prg	Prg	Ed	Ed	Ed	Ed	Ed	Ed

Abbreviations: Ed=Edenite,Prg=Pargasite (Hawthorne et al. 2012)

Appendix 4.2.5: Representative mineral chemistry for amphibole

Wt%	DA13-077-3.7	DA13-077-3.8	DA13-077-3.9	DA13-077-3.10	DA13-077-4.1	DA13-077-4.2	DA13-077-4.3	DA13-077-4.4	DA13-077-4.5	DA13-077-6.1	DA13-077-6.2
SiO_2	40.51	40.61	40.43	39.89	40.73	40.45	40.49	40.49	40.64	40.09	40.28
TiO_2	1.29	1.41	1.11	1.33	1.56	1.56	1.57	1.55	1.56	1.65	1.66
Al_2O_3	10.18	10.30	10.36	10.47	10.34	10.28	10.01	10.06	10.12	9.97	10.28
Cr_2O_3	0.00	0.00	0.03	0.02	0.00	0.02	0.00	0.00	0.00	0.01	0.00
FeOT	29.99	30.02	29.95	29.67	29.76	29.80	29.99	29.97	30.14	29.41	29.57
MnO	0.62	0.61	0.61	0.64	0.59	0.63	0.60	0.63	0.61	0.64	0.63
MgO	1.39	1.48	1.50	1.37	1.41	1.37	1.43	1.40	1.42	1.44	1.37
CaO	10.28	10.22	10.21	10.18	10.41	10.24	10.17	10.25	10.24	10.24	10.12
Na_2O	1.82	1.81	1.87	1.71	1.67	1.55	1.76	1.76	1.71	1.83	1.92
K_2O	1.79	1.79	1.76	1.76	1.79	1.82	1.83	1.79	1.80	1.78	1.78
TOTAL	97.87	98.25	97.83	97.03	98.25	97.73	97.85	97.89	98.24	97.08	97.62
Si	6.54	6.52	6.52	6.49	6.53	6.53	6.53	6.53	6.53	6.52	6.51
Al	1.46	1.48	1.48	1.51	1.47	1.47	1.47	1.47	1.47	1.48	1.49
Sum T	8.00	8.00	8.00	8.00	8.00	8.00	8.00	8.00	8.00	8.00	8.00
Al	0.47	0.47	0.49	0.50	0.48	0.48	0.44	0.44	0.45	0.43	0.46
Fe^{3+}	0.00	0.00	0.00	0.00	0.00	0.00	0.00	0.00	0.00	0.00	0.00
Cr	0.16	0.17	0.13	0.16	0.19	0.19	0.19	0.19	0.19	0.20	0.20
Ti	0.00	0.00	0.00	0.00	0.00	0.00	0.00	0.00	0.00	0.00	0.00
Fe^{2+}	4.05	4.03	4.04	4.04	3.99	4.02	4.05	4.04	4.05	4.00	3.99
Mn	0.08	0.08	0.08	0.09	0.08	0.09	0.08	0.09	0.08	0.09	0.09
Mg	0.24	0.24	0.24	0.21	0.26	0.22	0.24	0.24	0.23	0.28	0.25
Sum C	5.00	5.00	5.00	5.00	5.00	5.00	5.00	5.00	5.00	5.00	5.00
Mg^{2+}, Mn^{2+}, Fe^{2+}	0.09	0.11	0.12	0.12	0.08	0.11	0.10	0.10	0.11	0.07	0.08
Ca	1.78	1.76	1.76	1.77	1.79	1.77	1.76	1.77	1.76	1.78	1.75
Na	0.13	0.13	0.12	0.11	0.14	0.12	0.14	0.13	0.13	0.15	0.17
Sum B	2.00	2.00	2.00	2.00	2.00	2.00	2.00	2.00	2.00	2.00	2.00
Ca	0.00	0.00	0.00	0.00	0.00	0.00	0.00	0.00	0.00	0.00	0.00
Na	0.44	0.43	0.47	0.43	0.38	0.36	0.41	0.42	0.40	0.43	0.43
K	0.37	0.37	0.36	0.37	0.37	0.38	0.38	0.37	0.37	0.37	0.37
Sum A	0.81	0.80	0.83	0.80	0.75	0.74	0.79	0.78	0.77	0.80	0.80
TOTAL	15.81	15.80	15.83	15.80	15.75	15.74	15.79	15.78	15.77	15.80	15.80
Classification	Ed	Ed	Prg	Prg	Ed	Ed	Ed	Ed	Ed	Ed	Ed

Abbreviations: Ed=Edenite,Prg=Pargasite (Hawthorne et al. 2012)

Appendix 4.2.5: Representative mineral chemistry for amphibole

Wt%	DA13-077-6.3	DA13-077-6.4	DA13-077-6.5	DA13-083-2.1	DA13-083-2.2	DA13-083-2.3	DA13-083-2.4	DA13-083-2.5	DA13-083-6.1	DA13-083-6.2	DA13-083-6.3	DA13-083-6.4
SiO_2	40.18	40.40	40.60	46.05	46.29	45.81	46.25	45.76	46.22	45.49	46.20	45.79
TiO_2	1.67	1.70	1.69	1.54	1.58	1.59	1.34	1.76	1.62	1.67	1.61	1.63
Al_2O_3	10.01	10.08	10.13	8.65	8.71	8.65	8.58	8.76	8.63	8.69	8.66	8.60
Cr_2O_3	0.01	0.00	0.00	0.00	0.00	0.02	0.00	0.01	0.01	0.00	0.00	0.00
FeOT	29.88	29.52	29.65	16.08	16.13	16.05	16.40	16.44	16.27	16.35	16.39	16.19
MnO	0.55	0.62	0.58	0.78	0.74	0.73	0.75	0.86	0.85	0.83	0.85	0.88
MgO	1.41	1.44	1.50	11.50	11.61	11.24	11.10	10.97	11.53	11.12	11.33	11.46
CaO	10.17	10.14	10.15	10.92	10.86	10.89	10.89	10.91	10.60	10.60	10.60	10.58
Na_2O	1.85	2.05	1.86	1.74	1.92	1.81	1.84	1.95	1.92	1.95	1.95	1.93
K_2O	1.80	1.79	1.77	1.11	1.11	1.11	1.09	1.10	1.12	1.16	1.16	1.13
TOTAL	97.53	97.73	97.92	98.36	98.95	97.91	98.25	98.52	98.77	97.86	98.75	98.19
Si	6.51	6.52	6.53	6.83	6.83	6.83	6.87	6.80	6.83	6.80	6.84	6.82
Al	1.49	1.48	1.47	1.17	1.17	1.17	1.13	1.20	1.17	1.20	1.16	1.18
Sum T	8.00	8.00	8.00	8.00	8.00	8.00	8.00	8.00	8.00	8.00	8.00	8.00
Al	0.42	0.44	0.45	0.34	0.34	0.35	0.38	0.33	0.34	0.33	0.35	0.32
Fe^{3+}	0.00	0.00	0.00	0.00	0.00	0.00	0.00	0.00	0.00	0.00	0.00	0.00
Cr	0.20	0.21	0.20	0.17	0.18	0.18	0.15	0.20	0.18	0.19	0.18	0.18
Ti	0.00	0.00	0.00	0.00	0.00	0.00	0.00	0.00	0.00	0.00	0.00	0.00
Fe^{2+}	4.05	3.98	3.99	1.99	1.99	2.00	2.04	2.04	2.01	2.04	2.03	2.01
Mn	0.08	0.09	0.08	0.10	0.09	0.09	0.09	0.11	0.11	0.11	0.11	0.11
Mg	0.25	0.29	0.28	2.39	2.40	2.38	2.34	2.32	2.36	2.33	2.34	2.37
Sum C	5.00	5.00	5.00	5.00	5.00	5.00	5.00	5.00	5.00	5.00	5.00	5.00
Mg^{2+}, Mn^{2+}, Fe^{2+}	0.09	0.06	0.08	0.15	0.15	0.12	0.12	0.11	0.18	0.15	0.16	0.18
Ca	1.77	1.75	1.75	1.74	1.72	1.74	1.73	1.74	1.68	1.70	1.68	1.69
Na	0.15	0.19	0.17	0.11	0.14	0.14	0.15	0.15	0.14	0.15	0.16	0.14
Sum B	2.00	2.00	2.00	2.00	2.00	2.00	2.00	2.00	2.00	2.00	2.00	2.00
Ca	0.00	0.00	0.00	0.00	0.00	0.00	0.00	0.00	0.00	0.00	0.00	0.00
Na	0.44	0.45	0.41	0.39	0.41	0.39	0.39	0.41	0.41	0.42	0.40	0.42
K	0.37	0.37	0.36	0.21	0.21	0.21	0.21	0.21	0.21	0.22	0.22	0.21
Sum A	0.81	0.82	0.78	0.60	0.62	0.60	0.59	0.62	0.62	0.64	0.62	0.63
TOTAL	15.81	15.82	15.78	15.60	15.62	15.60	15.59	15.62	15.62	15.64	15.62	15.63
Classification	Ed	Ed	Ed	Ed	Ed	Ed	Ed	Ed	Ed	Ed	Ed	Ed

Abbreviations: Ed=Edenite,Prg=Pargasite (Hawthorne et al. 2012)

Appendix 4.2.5: Representative mineral chemistry for amphibole

Wt%	DA13-083-6.5	DA13-083-6.6	DA13-083-6.7	DA13-083-6.8	DA13-083-6.9	DA13-083-6.10	DA13-083-6.11	DA13-083-6.12	DA13-083-6.13	DA13-083-6.14	DA13-083-6.15
SiO_2	45.82	45.99	46.16	46.14	45.83	45.67	45.32	45.62	46.00	45.66	45.55
TiO_2	1.62	1.60	1.58	1.58	1.63	1.63	1.65	1.64	1.66	1.64	1.52
Al_2O_3	8.61	8.58	8.60	8.48	8.68	8.63	8.65	8.80	8.68	8.72	8.57
Cr_2O_3	0.00	0.00	0.01	0.00	0.01	0.00	0.01	0.00	0.05	0.02	0.00
FeOT	16.16	16.23	16.28	16.08	16.59	16.63	16.56	16.83	16.60	16.67	16.67
MnO	0.89	0.83	0.81	0.81	0.82	0.88	0.87	0.86	0.84	0.87	0.81
MgO	11.39	11.45	11.59	11.55	11.10	11.05	10.74	10.91	11.13	11.04	10.94
CaO	10.60	10.68	10.64	10.71	10.63	10.63	10.55	10.59	10.59	10.61	10.64
Na_2O	1.91	1.93	1.85	1.92	1.99	1.93	1.89	1.90	2.01	2.01	1.95
K_2O	1.16	1.12	1.14	1.13	1.15	1.18	1.13	1.15	1.18	1.16	1.11
TOTAL	98.17	98.42	98.67	98.40	98.43	98.24	97.39	98.30	98.74	98.40	97.77
Si	6.82	6.83	6.83	6.84	6.82	6.81	6.82	6.80	6.82	6.80	6.83
Al	1.18	1.17	1.17	1.16	1.18	1.19	1.18	1.20	1.18	1.20	1.17
Sum T	8.00	8.00	8.00	8.00	8.00	8.00	8.00	8.00	8.00	8.00	8.00
Al	0.33	0.33	0.33	0.33	0.34	0.33	0.35	0.35	0.34	0.33	0.34
Fe^{3+}	0.00	0.00	0.00	0.00	0.00	0.00	0.00	0.00	0.00	0.00	0.00
Cr	0.18	0.18	0.18	0.18	0.18	0.18	0.19	0.18	0.19	0.18	0.17
Ti	0.00	0.00	0.00	0.00	0.00	0.00	0.00	0.00	0.01	0.00	0.00
Fe^{2+}	2.01	2.01	2.02	1.99	2.06	2.07	2.08	2.10	2.06	2.08	2.09
Mn	0.11	0.10	0.10	0.10	0.10	0.11	0.11	0.11	0.11	0.11	0.10
Mg	2.36	2.37	2.38	2.40	2.31	2.30	2.27	2.26	2.31	2.30	2.30
Sum C	5.00	5.00	5.00	5.00	5.00	5.00	5.00	5.00	5.00	5.00	5.00
Mg^{2+}, Mn^{2+}, Fe^{2+}	0.17	0.16	0.18	0.15	0.15	0.16	0.14	0.16	0.15	0.16	0.15
Ca	1.69	1.70	1.69	1.70	1.69	1.70	1.70	1.69	1.68	1.69	1.71
Na	0.14	0.14	0.13	0.14	0.16	0.15	0.16	0.14	0.17	0.15	0.14
Sum B	2.00	2.00	2.00	2.00	2.00	2.00	2.00	2.00	2.00	2.00	2.00
Ca	0.00	0.00	0.00	0.00	0.00	0.00	0.00	0.00	0.00	0.00	0.00
Na	0.41	0.42	0.40	0.41	0.42	0.41	0.39	0.41	0.41	0.43	0.42
K	0.22	0.21	0.21	0.21	0.22	0.23	0.22	0.22	0.22	0.22	0.21
Sum A	0.63	0.63	0.62	0.62	0.64	0.64	0.61	0.63	0.63	0.65	0.63
TOTAL	15.63	15.63	15.62	15.62	15.64	15.64	15.61	15.63	15.63	15.65	15.63
Classification	Ed	Ed	Ed	Ed	Ed	Ed	Ed	Ed	Ed	Ed	Ed

Abbreviations: Ed=Edenite,Prg=Pargasite (Hawthorne et al. 2012)

Appendix 4.2.6: Representative mineral chemistry for clinopyroxene

Sample	DA13-040-1.1	DA13-040-1.2	DA13-040-1.3	DA13-040-1.4	DA13-040-1.5	DA13-040-1.6	DA13-040-1.7	DA13-040-1.8	DA13-040-1.9	DA13-040-1.10	DA13-040-4.1	DA13-040-4.2	DA13-040-4.3	DA13-040-4.4	DA13-040-4.5	DA13-040-8.1	DA13-040-8.2	DA13-040-8.3
SiO_2 (wt%)	52.37	53.70	53.71	53.89	54.03	54.03	53.94	53.49	53.39	53.34	53.86	53.52	53.91	53.69	53.90	53.66	53.56	54.09
TiO_2	0.12	0.12	0.14	0.14	0.17	0.15	0.12	0.12	0.13	0.17	0.15	0.13	0.15	0.15	0.14	0.10	0.12	0.09
Al_2O_3	1.26	0.97	0.75	0.77	0.86	0.84	0.72	0.75	0.79	0.79	0.87	0.75	0.83	0.83	0.82	0.73	0.72	0.71
Cr_2O_3	0.15	0.15	0.12	0.13	0.07	0.18	0.13	0.12	0.06	0.12	0.11	0.14	0.14	0.06	0.12	0.07	0.10	0.10
FeOT	10.12	10.44	10.44	10.33	10.36	10.23	10.44	10.41	10.35	10.34	10.43	10.29	10.40	10.54	10.21	10.37	10.50	10.47
MnO	0.26	0.24	0.30	0.31	0.26	0.26	0.25	0.26	0.27	0.28	0.26	0.31	0.27	0.28	0.29	0.29	0.28	0.30
MgO	11.79	11.87	12.18	12.33	12.32	12.29	12.11	12.16	12.11	12.02	12.23	12.08	12.25	12.21	12.02	12.17	12.13	12.44
CaO	18.09	18.66	18.86	18.84	18.75	18.93	18.77	18.87	18.90	18.84	18.84	18.69	18.75	18.74	18.84	18.57	18.73	18.74
Na_2O	3.08	3.22	3.18	3.16	3.13	3.18	3.20	3.18	3.08	3.16	3.12	3.16	3.20	3.18	3.17	3.09	3.20	3.19
K_2O	0.03	0.02	0.01	0.00	0.01	0.01	0.01	0.00	0.00	0.01	0.00	0.01	0.00	0.01	0.01	0.03	0.00	0.01
Total	97.26	99.39	99.68	99.89	99.96	100.10	99.72	99.36	99.09	99.07	99.86	99.07	99.88	99.69	99.52	99.07	99.33	100.14
Si+Ti	1.99	1.99	1.99	1.99	1.99	1.99	2.00	1.98	1.99	1.99	1.99	1.99	1.99	1.99	2.00	2.00	1.99	1.99
Al (iv)	0.01	0.01	0.01	0.01	0.01	0.01	0.00	0.02	0.01	0.01	0.01	0.01	0.01	0.01	0.00	0.00	0.01	0.01
Al (vi)	0.04	0.04	0.02	0.02	0.03	0.03	0.03	0.02	0.02	0.02	0.03	0.03	0.03	0.02	0.03	0.03	0.02	0.02
Fe^{3+}+Fe^{2+}+Mn	0.33	0.34	0.34	0.33	0.33	0.33	0.33	0.33	0.33	0.33	0.33	0.33	0.33	0.34	0.33	0.33	0.34	0.33
Mg	0.63	0.63	0.64	0.65	0.64	0.65	0.64	0.65	0.65	0.64	0.64	0.64	0.64	0.64	0.64	0.64	0.64	0.65
Mg	0.04	0.03	0.03	0.03	0.04	0.03	0.03	0.02	0.03	0.02	0.03	0.03	0.03	0.03	0.03	0.04	0.03	0.03
Ca	0.73	0.74	0.75	0.74	0.74	0.75	0.74	0.75	0.75	0.75	0.74	0.74	0.74	0.74	0.75	0.74	0.74	0.74
Na	0.23	0.23	0.23	0.23	0.22	0.23	0.23	0.23	0.22	0.23	0.22	0.23	0.23	0.23	0.23	0.22	0.23	0.23
Cations	4.00	4.00	4.00	4.00	4.00	4.00	4.00	4.00	4.00	4.00	4.00	4.00	4.00	4.00	4.00	4.00	4.00	4.00
Wo	48.17	48.69	49.01	48.65	48.08	48.77	48.61	49.28	49.03	49.29	48.48	48.76	48.55	48.72	48.71	48.01	48.92	48.39
En	43.67	43.10	44.06	44.33	43.96	44.05	43.64	44.19	43.70	43.77	43.77	43.84	44.12	44.18	43.24	43.78	44.11	44.69
Fs	8.15	8.21	6.93	7.02	7.96	7.18	7.75	6.54	7.27	6.94	7.75	7.41	7.33	7.10	8.05	8.21	6.97	6.92
Aegerine	20.46	20.43	22.30	21.75	20.41	21.06	21.00	22.83	21.54	22.07	20.94	21.27	21.52	22.44	19.77	20.37	22.54	22.40
Jadeite	3.09	3.36	1.09	1.52	2.79	2.24	2.58	0.52	1.23	1.20	2.12	2.17	2.06	1.07	3.60	2.78	1.05	1.16
Diopside	76.46	76.21	76.61	76.72	76.80	76.70	76.42	76.64	77.22	76.73	76.94	76.56	76.42	76.49	76.64	76.84	76.41	76.44

Appendix 4.2.6: Representative mineral chemistry for clinopyroxene

Sample	DA13-040-8.4	DA13-040-8.5	DA13-040-8.6	DA13-040-8.7	DA13-040-8.8	DA13-040-8.9	DA13-040-8.10
SiO_2 (wt%)	53.73	54.02	53.58	53.70	53.41	52.64	53.07
TiO_2	0.12	0.12	0.13	0.09	0.16	0.12	0.12
Al_2O_3	0.71	0.72	0.78	0.74	1.67	1.38	0.72
Cr_2O_3	0.14	0.10	0.11	0.10	0.08	0.06	0.07
FeOT	10.58	10.45	10.29	10.39	10.19	10.05	10.26
MnO	0.29	0.28	0.31	0.26	0.25	0.28	0.29
MgO	12.13	12.35	12.10	12.09	11.82	11.58	12.17
CaO	18.64	18.71	18.84	18.75	18.33	18.32	18.81
Na_2O	3.14	3.11	3.14	3.15	3.11	2.91	3.02
K_2O	0.00	0.01	0.00	0.00	0.02	0.02	0.01
Total	99.47	99.84	99.28	99.28	99.05	97.37	98.54
Si+Ti	1.99	1.99	1.99	1.99	1.99	2.00	1.99
Al (iv)	0.01	0.01	0.01	0.01	0.01	0.00	0.01
Al (vi)	0.02	0.03	0.02	0.03	0.06	0.06	0.02
Fe^{3+}+Fe^{2+}+Mn	0.34	0.33	0.33	0.33	0.33	0.33	0.33
Mg	0.63	0.64	0.64	0.64	0.61	0.61	0.65
Mg	0.03	0.04	0.03	0.03	0.04	0.04	0.03
Ca	0.74	0.74	0.75	0.75	0.73	0.74	0.75
Na	0.23	0.22	0.23	0.23	0.22	0.21	0.22
Cations	4.00	4.00	4.00	4.00	4.00	4.00	4.00
Wo	48.26	47.96	48.97	48.63	47.66	47.69	48.92
En	43.69	44.04	43.75	43.62	42.79	41.97	44.04
Fs	8.05	8.00	7.29	7.75	9.55	10.34	7.04
Aegerine	21.16	20.70	21.31	20.95	17.87	16.44	21.85
Jadeite	2.21	2.43	1.88	2.39	5.64	5.92	0.66
Diopside	76.63	76.87	76.81	76.66	76.49	77.65	77.49

Appendix 4.2.7: Representative mineral chemistry for titanite

Sample	DA13-040-1.1	DA13-040-1.2	DA13-040-1.3	DA13-040-1.4	DA13-040-1.5	DA13-040-3.1	DA13-040-3.2	DA13-040-3.3	DA13-040-3.4	DA13-040-3.5	DA13-040-3.6	DA13-040-3.7	DA13-040-3.8	DA13-040-3.9	DA13-040-3.10	DA13-049-6.1	DA13-049-6.2	DA13-049-6.3	DA13-049-6.4
SiO_2	30.51	30.90	30.74	31.25	31.81	31.89	32.06	32.14	31.93	31.74	31.86	32.10	31.57	31.81	32.31	31.77	31.53	32.46	31.91
TiO_2	35.05	35.14	35.03	35.15	36.73	37.44	36.88	36.47	37.66	36.36	36.80	36.76	36.18	36.74	37.02	35.29	34.70	34.53	35.03
Al_2O_3	0.50	0.56	0.56	0.56	0.41	0.37	0.40	0.48	0.44	2.02	0.41	0.50	0.45	0.45	0.43	1.52	1.40	2.09	1.76
Cr_2O_3	0.09	0.09	0.12	0.09	0.12	0.06	0.01	0.00	0.05	0.02	0.03	0.01	0.00	0.09	0.03	0.00	0.00	0.02	0.00
Fe_2O_3	0.00	0.00	0.00	0.00	0.00	0.00	0.00	0.00	0.00	0.00	0.00	0.00	0.00	0.00	0.00	0.00	0.00	0.00	0.00
FeOT	2.11	2.16	2.04	2.04	1.51	1.11	1.30	1.49	1.16	1.23	1.49	1.44	1.66	1.43	1.33	1.36	1.41	1.44	1.15
MnO	0.06	0.03	0.07	0.07	0.07	0.04	0.05	0.03	0.12	0.09	0.03	0.06	0.04	0.03	0.04	0.18	0.15	0.24	0.17
MgO	0.00	0.03	0.01	0.02	0.00	0.02	0.00	0.01	0.01	0.05	0.01	0.04	0.00	0.00	0.01	0.02	0.03	0.00	0.01
CaO	25.60	25.53	25.48	25.50	26.94	27.19	27.12	26.89	27.29	26.74	26.83	27.07	26.30	26.71	27.08	26.98	26.71	27.50	26.90
Na_2O	0.14	0.14	0.14	0.16	0.08	0.09	0.08	0.10	0.12	0.17	0.09	0.09	0.10	0.08	0.07	0.03	0.04	0.01	0.07
K_2O	0.00	0.00	0.00	0.01	0.02	0.02	0.01	0.02	0.03	0.05	0.04	0.04	0.03	0.02	0.00	0.00	0.01	0.01	0.01
H_2O	0.00	0.00	0.00	0.00	0.00	0.00	0.00	0.00	0.00	0.00	0.00	0.00	0.00	0.00	0.00	0.00	0.00	0.00	0.00
Totals	94.07	94.57	94.18	94.85	97.70	98.24	97.91	97.63	98.81	98.47	97.59	98.11	96.34	97.35	98.31	97.17	95.98	98.29	97.01
Si	1.06	1.06	1.06	1.07	1.06	1.06	1.06	1.07	1.05	1.05	1.06	1.06	1.07	1.06	1.07	1.06	1.07	1.07	1.07
Ti	0.91	0.91	0.91	0.91	0.92	0.93	0.92	0.91	0.93	0.90	0.92	0.92	0.92	0.92	0.92	0.89	0.88	0.86	0.88
Al	0.02	0.02	0.02	0.02	0.02	0.01	0.02	0.02	0.02	0.08	0.02	0.02	0.02	0.02	0.02	0.06	0.06	0.08	0.07
Cr	0.00	0.00	0.00	0.00	0.00	0.00	0.00	0.00	0.00	0.00	0.00	0.00	0.00	0.00	0.00	0.00	0.00	0.00	0.00
Fe^{+3}	0.00	0.00	0.00	0.00	0.00	0.00	0.00	0.00	0.00	0.00	0.00	0.00	0.00	0.00	0.00	0.00	0.00	0.00	0.00
Fe^{+2}	0.06	0.06	0.06	0.06	0.04	0.03	0.04	0.04	0.03	0.03	0.04	0.04	0.05	0.04	0.04	0.04	0.04	0.04	0.03
Mn	0.00	0.00	0.00	0.00	0.00	0.00	0.00	0.00	0.00	0.00	0.00	0.00	0.00	0.00	0.00	0.01	0.00	0.01	0.00
Mg	0.00	0.00	0.00	0.00	0.00	0.00	0.00	0.00	0.00	0.00	0.00	0.00	0.00	0.00	0.00	0.00	0.00	0.00	0.00
Ca	0.95	0.94	0.94	0.94	0.96	0.96	0.96	0.96	0.96	0.94	0.96	0.96	0.95	0.96	0.96	0.97	0.97	0.97	0.96
Na	0.01	0.01	0.01	0.01	0.01	0.01	0.01	0.01	0.01	0.01	0.01	0.01	0.01	0.00	0.00	0.00	0.00	0.00	0.00
K	0.00	0.00	0.00	0.00	0.00	0.00	0.00	0.00	0.00	0.00	0.00	0.00	0.00	0.00	0.00	0.00	0.00	0.00	0.00
H	0.00	0.00	0.00	0.00	0.00	0.00	0.00	0.00	0.00	0.00	0.00	0.00	0.00	0.00	0.00	0.00	0.00	0.00	0.00
Cations	3.02	3.02	3.03	3.02	3.03	3.03	3.04	3.02	3.02	3.01	3.02	3.02	3.02	3.04	3.03	3.03	3.03	3.03	3.02

Appendix 4.2.7: Representative mineral chemistry for titanite

Sample	DA13-049-6.5	DA13-049-6.6	DA13-049-6.7	DA13-049-6.8	DA13-049-6.9	DA13-049-6.10	DA13-049-6.11	DA13-049-6.12	DA13-049-6.13	DA13-049-6.14	DA13-049-6.15	DA13-049-6.16	DA13-049-6.17	DA13-049-6.18	DA13-069-1.1	DA13-069-1.2	DA13-069-1.3	DA13-069-1.4
SiO_2	32.23	32.26	32.40	32.08	31.88	31.69	31.88	32.21	32.11	31.84	32.35	32.29	31.92	31.95	32.49	32.25	32.07	32.38
TiO_2	34.52	34.23	33.64	36.00	35.17	35.64	34.96	35.84	34.71	33.82	34.47	34.42	34.71	34.93	34.25	34.78	34.54	34.14
Al_2O_3	1.93	2.39	2.02	1.30	1.51	1.22	1.62	1.37	1.90	2.55	2.09	2.12	1.63	1.80	2.14	1.91	1.85	2.17
Cr_2O_3	0.04	0.00	0.02	0.01	0.00	0.00	0.00	0.00	0.03	0.00	0.03	0.03	0.00	0.03	0.01	0.00	0.02	0.00
Fe_2O_3	0.00	0.00	0.00	0.00	0.00	0.00	0.00	0.00	0.00	0.00	0.00	0.00	0.00	0.00	0.00	0.00	0.00	0.00
FeOT	1.35	1.41	2.07	1.18	1.28	1.19	1.35	1.23	1.35	1.43	1.41	1.35	1.49	1.28	1.38	1.33	1.45	1.41
MnO	0.16	0.19	0.18	0.13	0.14	0.15	0.18	0.17	0.18	0.19	0.18	0.19	0.15	0.22	0.04	0.02	0.06	0.03
MgO	0.01	0.01	0.00	0.00	0.00	0.00	0.01	0.00	0.02	0.02	0.00	0.01	0.01	0.02	0.03	0.00	0.02	0.00
CaO	27.37	27.18	27.22	27.20	26.86	26.83	26.88	27.21	26.94	26.87	27.61	27.54	27.11	27.21	27.68	27.46	27.52	27.75
Na_2O	0.07	0.05	0.03	0.03	0.02	0.03	0.02	0.05	0.05	0.07	0.05	0.05	0.06	0.12	0.01	0.01	0.02	0.02
K_2O	0.00	0.02	0.01	0.00	0.01	0.00	0.00	0.00	0.03	0.06	0.01	0.02	0.01	0.03	0.00	0.00	0.00	0.01
H_2O	0.00	0.00	0.00	0.00	0.00	0.00	0.00	0.00	0.00	0.00	0.00	0.00	0.00	0.00	0.00	0.00	0.00	0.00
Totals	97.67	97.74	97.59	97.93	96.86	96.76	96.90	98.07	97.32	96.84	98.19	97.99	97.08	97.59	98.02	97.77	97.55	97.91
Si	1.07	1.07	1.08	1.06	1.07	1.06	1.07	1.07	1.07	1.07	1.07	1.07	1.07	1.06	1.07	1.07	1.07	1.07
Ti	0.86	0.85	0.84	0.90	0.89	0.90	0.88	0.89	0.87	0.85	0.86	0.86	0.87	0.87	0.85	0.87	0.86	0.85
Al	0.08	0.09	0.08	0.05	0.06	0.05	0.06	0.05	0.07	0.10	0.08	0.08	0.06	0.07	0.08	0.07	0.07	0.08
Cr	0.00	0.00	0.00	0.00	0.00	0.00	0.00	0.00	0.00	0.00	0.00	0.00	0.00	0.00	0.00	0.00	0.00	0.00
Fe^{+3}	0.00	0.00	0.00	0.00	0.00	0.00	0.00	0.00	0.00	0.00	0.00	0.00	0.00	0.00	0.00	0.00	0.00	0.00
Fe^{+2}	0.04	0.04	0.06	0.03	0.04	0.03	0.04	0.03	0.04	0.04	0.04	0.04	0.04	0.04	0.04	0.04	0.04	0.04
Mn	0.00	0.01	0.01	0.00	0.00	0.00	0.01	0.00	0.00	0.01	0.00	0.01	0.00	0.01	0.00	0.00	0.00	0.00
Mg	0.00	0.00	0.00	0.00	0.00	0.00	0.00	0.00	0.00	0.00	0.00	0.00	0.00	0.00	0.00	0.00	0.00	0.00
Ca	0.97	0.97	0.97	0.97	0.96	0.96	0.96	0.96	0.96	0.96	0.98	0.98	0.97	0.97	0.98	0.98	0.98	0.99
Na	0.00	0.00	0.00	0.00	0.00	0.00	0.00	0.00	0.00	0.00	0.00	0.00	0.00	0.01	0.00	0.00	0.00	0.00
K	0.00	0.00	0.00	0.00	0.00	0.00	0.00	0.00	0.00	0.00	0.00	0.00	0.00	0.00	0.00	0.00	0.00	0.00
H	0.00	0.00	0.00	0.00	0.00	0.00	0.00	0.00	0.00	0.00	0.00	0.00	0.00	0.00	0.00	0.00	0.00	0.00
Cations	3.02	3.02	3.01	3.01	3.01	3.01	3.01	3.01	3.02	3.01	3.01	3.01	3.01	3.01	3.03	3.03	3.03	3.03

Appendix 4.2.7: Representative mineral chemistry for titanite

Sample	DA13-069-1.5	DA13-069-2.1	DA13-069-2.2	DA13-069-2.3	DA13-069-2.4	DA13-069-2.5	DA13-069-4.1	DA13-069-4.2	DA13-069-4.3	DA13-069-4.4	DA13-069-4.5
SiO_2	32.35	31.54	31.19	31.52	31.99	31.58	31.95	31.92	31.92	32.00	32.24
TiO_2	34.35	35.38	35.10	34.93	35.04	34.79	34.53	34.35	34.48	34.19	34.45
Al_2O_3	2.25	0.98	1.27	1.31	1.48	1.34	1.79	1.79	1.69	1.87	1.82
Cr_2O_3	0.06	0.01	0.02	0.02	0.00	0.00	0.01	0.00	0.00	0.00	0.02
Fe_2O_3	0.00	0.00	0.00	0.00	0.00	0.00	0.00	0.00	0.00	0.00	0.00
FeOT	1.41	1.58	1.52	1.60	1.50	1.40	1.67	1.58	1.63	1.54	1.49
MnO	0.06	0.06	0.06	0.04	0.02	0.04	0.07	0.04	0.06	0.09	0.09
MgO	0.01	0.02	0.01	0.05	0.03	0.05	0.03	0.04	0.05	0.04	0.03
CaO	27.80	26.84	26.77	26.93	27.05	26.27	27.05	27.09	27.04	27.12	27.26
Na_2O	0.01	0.04	0.02	0.03	0.04	0.07	0.04	0.04	0.07	0.08	0.07
K_2O	0.01	0.01	0.00	0.01	0.03	0.02	0.07	0.05	0.06	0.13	0.14
H_2O	0.00	0.00	0.00	0.00	0.00	0.00	0.00	0.00	0.00	0.00	0.00
Totals	98.30	96.46	95.97	96.46	97.16	95.56	97.21	96.91	96.99	97.07	97.60
Si	1.07	1.06	1.06	1.06	1.07	1.07	1.07	1.07	1.07	1.07	1.07
Ti	0.85	0.90	0.90	0.89	0.88	0.89	0.87	0.87	0.87	0.86	0.86
Al	0.09	0.04	0.05	0.05	0.06	0.05	0.07	0.07	0.07	0.07	0.07
Cr	0.00	0.00	0.00	0.00	0.00	0.00	0.00	0.00	0.00	0.00	0.00
Fe^{+3}	0.00	0.00	0.00	0.00	0.00	0.00	0.00	0.00	0.00	0.00	0.00
Fe^{+2}	0.04	0.04	0.04	0.05	0.04	0.04	0.05	0.04	0.05	0.04	0.04
Mn	0.00	0.00	0.00	0.00	0.00	0.00	0.00	0.00	0.00	0.00	0.00
Mg	0.00	0.00	0.00	0.00	0.00	0.00	0.00	0.00	0.00	0.00	0.00
Ca	0.98	0.97	0.97	0.97	0.97	0.95	0.97	0.97	0.97	0.97	0.97
Na	0.00	0.00	0.00	0.00	0.00	0.00	0.00	0.00	0.00	0.00	0.00
K	0.00	0.00	0.00	0.00	0.00	0.00	0.00	0.00	0.00	0.01	0.01
H	0.00	0.00	0.00	0.00	0.00	0.00	0.00	0.00	0.00	0.00	0.00
Cations	3.04	3.02	3.02	3.03	3.02	3.02	3.03	3.03	3.03	3.04	3.03

Appendix 4.2.8: Representative mineral chemistry for garnet

Sample	DA13-074-2.1	DA13-074-2.2	DA13-074-2.3	DA13-074-2.4	DA13-074-2.5	DA13-074-2.6	DA13-074-2.7	DA13-074-2.8	DA13-074-2.9	DA13-074-2.10	DA13-074-2.11
SiO_2	36.86	37.07	37.05	37.05	37.09	37.03	37.12	37.17	37.04	37.15	37.00
TiO_2	0.05	0.05	0.07	0.06	0.05	0.03	0.03	0.06	0.02	0.02	0.04
Al_2O_3	19.81	19.64	19.75	19.73	19.71	19.65	19.83	19.81	19.68	19.66	19.62
FeOT	30.63	30.71	30.95	30.79	30.55	31.06	30.60	30.71	30.90	30.63	30.42
MnO	2.06	1.98	1.96	2.12	2.08	2.34	2.20	2.01	2.23	2.36	2.37
MgO	0.75	0.78	0.83	0.77	0.81	0.78	0.80	0.80	0.75	0.74	0.75
CaO	8.28	8.38	8.43	8.17	8.28	7.97	8.17	8.23	8.15	8.11	8.20
Na_2O	0.03	0.01	0.03	0.01	0.01	0.00	0.01	0.00	0.00	0.02	0.00
K_2O	0.00	0.00	0.00	0.01	0.01	0.01	0.00	0.00	0.00	0.01	0.00
BaO	0.00	0.04	0.00	0.03	0.02	0.00	0.03	0.00	0.02	0.00	0.00
ZnO	0.03	0.07	0.00	0.00	0.00	0.00	0.00	0.08	0.00	0.06	0.00
F	0.00	0.00	0.14	0.17	0.13	0.06	0.12	0.05	0.11	0.06	0.13
Cr_2O_3	0.00	0.00	0.02	0.00	0.00	0.00	0.02	0.03	0.01	0.02	0.01
Total	98.50	98.72	99.24	98.92	98.73	98.92	98.94	98.94	98.91	98.84	98.54
Si	3.02	3.03	3.02	3.03	3.03	3.02	3.03	3.03	3.03	3.03	3.03
Al (iv)	0.00	0.00	0.00	0.00	0.00	0.00	0.00	0.00	0.00	0.00	0.00
Al (vi)	1.92	1.90	1.90	1.90	1.90	1.90	1.91	1.91	1.90	1.90	1.90
Ti	0.00	0.00	0.00	0.00	0.00	0.00	0.00	0.00	0.00	0.00	0.00
Cr	0.00	0.00	0.00	0.00	0.00	0.00	0.00	0.00	0.00	0.00	0.00
Fe^{3+}	0.05	0.06	0.07	0.06	0.06	0.07	0.05	0.05	0.06	0.06	0.06
Fe^{2+}	2.04	2.03	2.04	2.05	2.03	2.05	2.04	2.04	2.05	2.03	2.03
Mn	0.14	0.14	0.14	0.15	0.14	0.16	0.15	0.14	0.15	0.16	0.16
Mg	0.09	0.09	0.10	0.09	0.10	0.10	0.10	0.10	0.09	0.09	0.09
Zn	0.00	0.00	0.00	0.00	0.00	0.00	0.00	0.01	0.00	0.00	0.00
Ca	0.73	0.73	0.74	0.71	0.73	0.70	0.71	0.72	0.71	0.71	0.72
Total	8.00	8.00	8.00	7.99	7.99	8.00	7.99	7.99	8.00	7.99	7.99
Almandine	67.42	67.08	67.01	67.45	66.99	67.53	67.18	67.47	67.35	67.13	66.72
Andradite	2.79	3.26	3.48	2.91	2.83	3.46	2.61	2.67	3.28	2.97	2.99
Grossular	21.83	21.76	21.41	21.45	21.92	20.27	21.63	21.72	20.96	21.19	21.53
Pyrope	3.11	3.22	3.43	3.20	3.36	3.24	3.33	3.32	3.13	3.06	3.12
Spessartine	4.85	4.68	4.60	4.99	4.90	5.50	5.18	4.73	5.25	5.57	5.61
Uvarovite	0.00	0.00	0.07	0.00	0.00	0.00	0.06	0.09	0.03	0.08	0.03
% cations	98.41	97.88	98.28	97.97	97.84	98.05	98.07	97.97	98.07	97.77	97.81

Appendix 4.2.8: Representative mineral chemistry for garnet

Sample	DA13-074-2.12	DA13-074-4.1	DA13-074-4.2	DA13-074-4.3	DA13-074-4.4	DA13-074-8.1	DA13-074-8.2	DA13-074-8.3	DA13-074-8.4	DA13-074-8.5	DA13-074-8.6	DA13-074-8.7
SiO_2	36.72	36.84	36.85	37.20	37.14	37.03	36.99	36.76	37.05	36.88	36.69	36.82
TiO_2	0.04	0.04	0.04	0.07	0.05	0.04	0.04	0.04	0.02	0.03	0.04	0.03
Al_2O_3	19.49	19.77	19.54	19.82	19.84	19.80	19.70	19.61	19.81	19.60	19.70	19.59
FeOT	30.67	30.71	30.81	30.65	30.56	30.26	30.71	29.72	30.58	30.57	30.57	30.34
MnO	2.57	2.58	2.64	2.53	2.73	2.77	2.72	2.76	2.70	2.85	2.98	2.91
MgO	0.72	0.76	0.77	0.75	0.72	0.81	0.76	0.76	0.77	0.78	0.75	0.75
CaO	7.93	7.91	7.87	8.28	7.90	7.72	7.74	7.69	7.80	7.80	7.79	7.80
Na_2O	0.01	0.02	0.01	0.04	0.06	0.04	0.04	0.01	0.02	0.00	0.03	0.04
K_2O	0.01	0.01	0.00	0.00	0.01	0.02	0.02	0.01	0.01	0.00	0.00	0.01
BaO	0.01	0.00	0.03	0.03	0.01	0.00	0.00	0.00	0.01	0.00	0.00	0.05
ZnO	0.09	0.05	0.06	0.06	0.00	0.04	0.00	0.00	0.07	0.02	0.06	0.00
F	0.00	0.00	0.11	0.10	0.05	0.13	0.16	0.09	0.03	0.18	0.13	0.02
Cr_2O_3	0.01	0.00	0.01	0.04	0.00	0.00	0.00	0.02	0.03	0.00	0.01	0.02
Total	98.25	98.71	98.73	99.57	99.09	98.66	98.87	97.48	98.90	98.71	98.76	98.38
Si	3.02	3.02	3.02	3.02	3.03	3.03	3.03	3.04	3.03	3.02	3.01	3.03
Al (iv)	0.00	0.00	0.00	0.00	0.00	0.00	0.00	0.00	0.00	0.00	0.00	0.00
Al (vi)	1.90	1.91	1.89	1.90	1.91	1.91	1.90	1.91	1.91	1.90	1.91	1.90
Ti	0.00	0.00	0.00	0.00	0.00	0.00	0.00	0.00	0.00	0.00	0.00	0.00
Cr	0.00	0.00	0.00	0.00	0.00	0.00	0.00	0.00	0.00	0.00	0.00	0.00
Fe^{3+}	0.07	0.06	0.07	0.06	0.05	0.05	0.06	0.04	0.05	0.07	0.07	0.06
Fe^{2+}	2.04	2.04	2.04	2.02	2.03	2.03	2.04	2.02	2.04	2.03	2.03	2.02
Mn	0.18	0.18	0.18	0.17	0.19	0.19	0.19	0.19	0.19	0.20	0.21	0.20
Mg	0.09	0.09	0.09	0.09	0.09	0.10	0.09	0.09	0.09	0.10	0.09	0.09
Zn	0.01	0.00	0.00	0.00	0.00	0.00	0.00	0.00	0.00	0.00	0.00	0.00
Ca	0.70	0.69	0.69	0.72	0.69	0.68	0.68	0.68	0.68	0.68	0.68	0.69
Total	8.00	8.00	8.00	8.00	7.99	7.99	8.00	7.98	8.00	8.00	8.01	8.00
Almandine	67.16	67.30	67.10	66.54	67.07	67.01	67.31	66.86	67.28	66.75	66.77	66.64
Andradite	3.63	3.11	3.70	3.19	2.60	2.33	2.98	1.83	2.70	3.42	3.49	3.10
Grossular	20.11	20.38	19.74	21.16	20.91	20.74	20.13	21.40	20.38	19.86	19.62	20.20
Pyrope	2.99	3.14	3.18	3.07	2.98	3.38	3.17	3.21	3.19	3.24	3.10	3.11
Spessartine	6.09	6.07	6.24	5.91	6.43	6.55	6.41	6.62	6.35	6.73	6.99	6.89
Uvarovite	0.02	0.00	0.03	0.13	0.00	0.00	0.00	0.08	0.10	0.00	0.02	0.07
% cations	98.13	98.48	98.13	98.19	98.01	97.95	98.03	97.67	98.20	98.10	98.67	98.08

Appendix 4.2.8: Representative mineral chemistry for garnet

Sample	DA13-074-8.8	DA13-074-8.9	DA13-074-8.10	DA13-074-8.11	DA13-074-8.12	DA13-074-8.13	DA13-074-8.14	DA13-074-8.15	DA13-074-8.16	DA13-076-6.1
SiO_2	36.94	36.99	36.98	36.95	36.87	36.84	36.74	37.00	36.85	35.99
TiO_2	0.04	0.04	0.02	0.02	0.03	0.04	0.04	0.03	0.03	0.06
Al_2O_3	19.91	19.79	19.73	19.59	19.70	19.66	19.53	19.58	19.47	19.74
FeOT	30.62	30.03	30.34	30.24	29.82	30.07	30.08	29.67	30.07	31.08
MnO	2.80	2.90	2.82	3.25	3.28	3.38	3.28	3.20	3.23	0.75
MgO	0.77	0.74	0.70	0.57	0.57	0.58	0.59	0.65	0.60	0.88
CaO	7.76	8.09	8.02	7.73	7.76	7.90	7.83	8.07	7.82	9.08
Na_2O	0.01	0.01	0.02	0.06	0.01	0.03	0.04	0.03	0.03	0.03
K_2O	0.00	0.00	0.00	0.00	0.00	0.00	0.00	0.01	0.01	0.00
BaO	0.01	0.04	0.00	0.03	0.03	0.01	0.00	0.05	0.00	0.02
ZnO	0.03	0.00	0.00	0.03	0.06	0.02	0.06	0.00	0.00	0.04
F	0.04	0.09	0.07	0.04	0.15	0.00	0.06	0.16	0.12	0.09
Cr_2O_3	0.05	0.02	0.00	0.00	0.00	0.00	0.04	0.00	0.00	0.01
Total	98.99	98.74	98.69	98.51	98.27	98.53	98.29	98.46	98.23	97.77
Si	3.02	3.03	3.03	3.04	3.03	3.02	3.03	3.04	3.04	2.97
Al (iv)	0.00	0.00	0.00	0.00	0.00	0.00	0.00	0.00	0.00	0.03
Al (vi)	1.92	1.91	1.91	1.90	1.91	1.91	1.90	1.90	1.89	1.90
Ti	0.00	0.00	0.00	0.00	0.00	0.00	0.00	0.00	0.00	0.00
Cr	0.00	0.00	0.00	0.00	0.00	0.00	0.00	0.00	0.00	0.00
Fe^{3+}	0.05	0.05	0.06	0.06	0.04	0.06	0.06	0.05	0.06	0.08
Fe^{2+}	2.04	2.00	2.02	2.02	2.01	2.00	2.01	1.98	2.01	2.07
Mn	0.19	0.20	0.20	0.23	0.23	0.24	0.23	0.22	0.23	0.05
Mg	0.09	0.09	0.08	0.07	0.07	0.07	0.07	0.08	0.07	0.11
Zn	0.00	0.00	0.00	0.00	0.00	0.00	0.00	0.00	0.00	0.00
Ca	0.68	0.71	0.70	0.68	0.68	0.70	0.69	0.71	0.69	0.80
Total	8.00	8.00	8.00	7.99	7.99	8.00	8.00	7.99	7.99	8.03
Almandine	67.32	65.98	66.54	66.67	66.48	65.99	66.27	65.35	66.19	67.53
Andradite	2.63	2.66	2.88	2.85	2.23	3.08	3.13	2.75	3.08	4.08
Grossular	20.18	21.39	21.03	20.38	21.10	20.54	20.24	21.56	20.50	22.93
Pyrope	3.15	3.08	2.89	2.36	2.38	2.41	2.45	2.72	2.53	3.65
Spessartine	6.56	6.83	6.65	7.73	7.80	7.99	7.78	7.62	7.69	1.78
Uvarovite	0.16	0.06	0.00	0.00	0.01	0.00	0.12	0.00	0.00	0.02
% cations	98.60	98.15	98.11	97.76	97.89	98.17	98.06	97.59	97.67	98.92

Appendix 4.2.8: Representative mineral chemistry for garnet

Sample	DA13-076-6.2	DA13-076-6.3	DA13-076-6.4	DA13-076-6.5	DA13-076-6.6	DA13-076-6.7	DA13-076-7.1	DA13-076-7.2	DA13-076-7.3	DA13-076-7.4	DA13-076-7.5
SiO_2	39.89	37.26	37.14	37.37	36.91	37.42	36.95	37.31	37.00	37.08	37.40
TiO_2	0.08	0.03	0.07	0.04	0.04	0.08	0.06	0.06	0.08	0.08	0.05
Al_2O_3	19.67	20.49	20.42	20.42	20.30	20.42	20.37	20.31	20.22	20.32	20.45
FeOT	29.93	31.08	31.10	31.47	31.58	31.27	31.33	31.31	31.22	31.14	31.69
MnO	0.79	0.91	0.80	1.00	1.15	0.77	0.70	0.67	0.67	0.76	0.99
MgO	0.89	0.92	0.94	0.82	0.74	0.91	0.95	0.91	0.92	0.88	0.83
CaO	8.75	8.83	8.95	8.48	8.59	8.92	9.02	8.96	9.05	9.00	8.65
Na_2O	0.01	0.00	0.02	0.01	0.01	0.02	0.02	0.02	0.02	0.00	0.00
K_2O	0.02	0.00	0.01	0.00	0.00	0.00	0.00	0.00	0.01	0.00	0.00
BaO	0.00	0.00	0.00	0.00	0.00	0.00	0.00	0.02	0.02	0.00	0.00
ZnO	0.00	0.03	0.00	0.01	0.00	0.09	0.00	0.00	0.05	0.08	0.03
F	0.00	0.05	0.02	0.08	0.16	0.07	0.07	0.00	0.11	0.01	0.01
Cr_2O_3	0.02	0.00	0.00	0.01	0.00	0.00	0.00	0.00	0.03	0.00	0.01
Total	100.06	99.59	99.46	99.70	99.47	99.96	99.48	99.57	99.40	99.36	100.12
Si	3.16	3.01	3.00	3.02	3.00	3.01	2.99	3.01	3.00	3.00	3.01
Al (iv)	0.00	0.00	0.00	0.00	0.00	0.00	0.01	0.00	0.00	0.00	0.00
Al (vi)	1.84	1.95	1.95	1.95	1.95	1.94	1.94	1.94	1.94	1.94	1.94
Ti	0.00	0.00	0.00	0.00	0.00	0.00	0.00	0.00	0.01	0.00	0.00
Cr	0.00	0.00	0.00	0.00	0.00	0.00	0.00	0.00	0.00	0.00	0.00
Fe^{3+}	0.00	0.03	0.04	0.03	0.05	0.04	0.05	0.04	0.05	0.04	0.04
Fe^{2+}	2.00	2.07	2.06	2.10	2.10	2.07	2.07	2.07	2.07	2.07	2.09
Mn	0.05	0.06	0.05	0.07	0.08	0.05	0.05	0.05	0.05	0.05	0.07
Mg	0.11	0.11	0.11	0.10	0.09	0.11	0.11	0.11	0.11	0.11	0.10
Zn	0.00	0.00	0.00	0.00	0.00	0.01	0.00	0.00	0.00	0.00	0.00
Ca	0.74	0.76	0.78	0.73	0.75	0.77	0.78	0.78	0.79	0.78	0.75
Total	7.91	8.00	8.00	7.99	8.01	8.00	8.01	8.00	8.01	8.00	8.00
Almandine	67.33	68.53	68.30	69.55	69.33	68.59	68.36	68.58	68.30	68.41	69.28
Andradite	0.00	1.62	1.94	1.46	2.34	1.91	2.51	2.09	2.54	2.21	2.01
Grossular	26.87	24.05	24.10	23.31	22.69	24.05	23.67	24.10	23.78	24.05	23.06
Pyrope	3.81	3.71	3.81	3.34	2.99	3.68	3.84	3.69	3.74	3.58	3.34
Spessartine	1.91	2.09	1.84	2.32	2.66	1.77	1.61	1.54	1.54	1.76	2.27
Uvarovite	0.07	0.01	0.00	0.02	0.00	0.00	0.00	0.00	0.10	0.00	0.04
% cations	93.04	99.16	99.23	98.74	99.45	98.80	99.61	98.78	99.19	99.16	99.01

Appendix 5.1

Analytical Methods for Chapter 5
(Ambalavao and Maevarano Suites)

5.1.1 Sample collection and processing

Approximately 1.5 to 3 kg of each sample was collected for thin sectioning and zircon separation. Zircon were separated by conventional sieving and magnetic separation techniques. Zircon grains were handpicked and mounted in epoxy resin, polished, and imaged under reflected light. To investigate the internal structure of the zircon grains and to select target sites for U-Pb, hafnium, and oxygen isotopic analyses, cathodoluminescence (CL) imaging was carried out using a Philips XL40 or Philips XL20 Scanning Electron Microscope equipped with a tungsten filament electron source and a Gatan CL detector at Adelaide Microscopy.

5.1.2 U-Pb geochronology

Ten samples of the Ambalavao and two samples of the Maevarano Suite were selected for U-Pb analysis in zircon. U-Pb zircon analyses were performed by laser ablation inductively coupled mass spectroscopy (LA-ICP-MS) at Adelaide Microscopy using an Agilent 7500cs ICPMS instrument coupled with a New Wave 213 nm Nd-YAG laser. Ten samples of the Ambalavao Suite and two samples of the Maevarano Suite were selected for U-Pb isotope analysis in zircon. U-Pb data was collected to confirm the age of each sample and to determine suitable zircon for oxygen and hafnium isotope analyses. Set-up and procedural information is after Archibald et al. (in review). Instrument and mass calibration were performed before all analytical sessions using the NIST 610 reference glass by maximising the ^{238}U signal and by minimising oxide formation using the ThO+/Th+ ratio (< 1%). (^{204}Pb + ^{204}Hg), ^{206}Pb, ^{207}Pb, ^{208}Pb, ^{232}Th and ^{238}U were measured during analysis. The ^{235}U signal was calculated from ^{238}U on the basis of the ratio $^{238}U/^{235}U$= 137.88. U-Pb-Th isotope fractionation was corrected using the GEMOC GJ-1 standard ($^{206}Pb/^{238}U$ age of 600.7 ± 1.1 Ma; 2σ; Jackson et al., 2004) and accuracy was monitored using the Plešovice standard ($^{206}Pb/^{238}U$ age of 337.1 ± 0.37 Ma; 2σ; Sláma et al., 2008). Plešovice analyses yield a weighted average $^{206}Pb/^{238}U$ age of 338.2 ± 1.8 (2σ; MSWD = 2.6; n = 63). This is within analytical uncertainty of the published value (Table A.5.1). Data were processed using the GLITTER software package (Griffin et al., 2008). Age calculations and Wetherill concordia diagrams were constructed using the Microsoft Excel macro Isoplot 4.15 (Ludwig, 2012). Individual zircon grain ages are quoted at the 1σ level and weighted mean ages are at the 2σ level.Common Pb was not corrected for due to uncertainty associated with the ^{204}Hg interference on the LA-ICP-MS. Monitoring of the ^{204}Pb mass indicated common Pb was present in some samples (Appendix 5.2). Common Pb values are presented as ($^{204}Pb/^{206}Pb$ x 100) in Appendix 5.2. To minimise the influence of common Pb on calculated ages only the ≥ 95 % concordant data and the weighted mean $^{206}Pb/^{238}U$ ratios are used for most samples.

5.1.3 Oxygen isotopes in zircon

Oxygen isotope data was collected using the sensitive high resolution ion mass spectrometer stable isotope (SHRIMP SI) and SHRIMP II instruments at the Australian National University in Canberra, Australia. A 10 kV, ~3 nA Cs+ primary ion beam was focused to a 30 µm diameter spot on an aluminium or gold coated sample. Each analysis consisted of a two minute pre-burn to allow the secondary ion isotopic composition to stabilise and to remove the sample coating prior to the analysis, followed by 14, ~10 second estimates of the $^{18}O/^{16}O$ ratio. Standards Temora II and Mudtank were analysed first, then again after 5-8 unknown samples. Sample $\delta^{18}O$ (zircon) values were determined by difference relative to the mean $\delta^{18}O$ (zircon) measured on standards following normalisation for long-term drift in its measured composition. The SHRIMP II method is after Ickert et al. (2008). CL images were used to analyse within the same CL zone but away from the U-Pb (LA-ICP-MS) analysis pits to avoid potential interference. The results of standard analyses are listed in Table A.5.1.

5.1.4 Zircon Lu-Hf analysis

In situ LA-MC-ICP-MS Hf isotope analyses were carried out at the University of Adelaide Waite Campus facility using a New Wave Research 193 nm Excimer laser attached to a Neptune multi-collector ICP-MS system as per Payne et al. (2013). Only grains with U–Pb ages having ≤ 10% discordance were analysed for Lu–Hf isotope composition. Analysis locations were in the same cathodoluminescence domains as concordant U–Pb laser spots and in the same site as SHRIMP oxygen spots. Full data collection procedures can be found in Archibald et al. (in review) and details on data processing in Payne et al. (2013). Procedural accuracy was monitored using the Plešovice, Mudtank and Temora II zircon standards. Mean $^{176}Hf/^{177}Hf$ ratios for each standard along with the literature values are presented in Table 1. $\varepsilon_{Hf}(t)$ and $T_{DM}c$ were calculated using ^{176}Lu decay constant after Scherer et al. (2001). TDMc two stage crustal model ages were calculated using the methods of Griffin et al. (2002) with an average crustal composition of $^{176}Lu/^{177}Hf$ = 0.015.

5.1.5 Whole-rock geochemistry

Whole-rock geochemical analyses for major, minor and trace elements were collected at ACME Labs in Vancouver, British Columbia, Canada. The major element data collection procedure involved the crushed rock pulp being mixed with $LiBO_2/Li_2B_4O_7$ flux. Graphite crucibles were fused in a muffle furnace for 30 minutes at 980°C. The cooled bead was then dissolved in ACS grade nitric acid and analysed using a SPECTRO AS500 ICP-OES (inductively-coupled plasma optical emission spectroscopy) instrument. LOI (loss on ignition) values were determined by igniting a sample split then measuring the weight lost. For trace element analyses, the crushed rock pulp was digested using a modified Aqua Regia solution of equal parts concentrated HCl, HNO_3 and deionised H_2O for one hour in a heating block or hot water bath. Samples were made up to volume with dilute HCl and analysed using a Perkin-Elmer ELAN 9000 ICP-MS. Quality control protocol involves analysing pulp duplicates to monitor analytical precision and a reagent blank to measure background. In addition, interspersed analyses of reference materials SO-18, OREAS45EA, GS311-1, and GS910-4 monitored the accuracy of results. Total sulphur and carbon values were determined by adding an induction flux to the prepared sample and igniting the sample in a LECO CS230 Carbon/Sulphur Series induction furnace. A carrier gas transports the released carbon and sulphur to be measured by adsorption in an infrared spectrometric cell. Results are total carbon or sulphur.

Table A.5.1 Summary of zircon standard data

Standard	Method	n	Measured Value	Reference Value	Reference
U-Pb isotopes (Age)					
Plešovice	LA-ICP-MS	63	338.2 ± 1.8 Ma (MSWD=2.6)	337.1 ± 0.4 Ma	Sláma et al., 2008
Oxygen isotopes ($\delta^{18}O$)					
Temora II	SHRIMP SI	43	8.20 ± 0.28 ‰	8.20 ± 0.01 ‰	Valley, 2003
Temora II	SHRIMP II	8	7.99 ± 0.53 ‰	8.20 ± 0.01 ‰	Valley, 2003
Mudtank	SHRIMP II	17	5.60 ± 0.54 ‰	5.03 ± 0.10 ‰	Valley, 2003
Hf isotopes ($^{177}Hf/^{176}Hf$)					
Mudtank	MC-LA-ICP-MS	33	0.282496 ± 0.000023	0.282507 ± 0.000006	Woodhead and Hergt, 2005
Temora II	MC-LA-ICP-MS	6	0.282652 ± 0.000051	0.282686 ± 0.000008	Woodhead and Hergt, 2005
Plešovice	MC-LA-ICP-MS	7	0.282468 ± 0.000019	0.282482 ± 0.000013	Sláma et al., 2008

References

Archibald, D.B., Collins, A.S., Foden, J.D., Payne, J.L., Holden, P., Razakamanana, T., De Waele, B., Pitfield, P.E.J., Thomas, R.J., in review. Genesis of the Tonian Imorona-Itsindro Magmatic Suite in central Madagascar: Insights from U-Pb, oxygen and hafnium isotopes in zircon. Precambrian Research.

Griffin, W.L., Powell, W.J., Pearson, N.J., O'Reilly, S.Y., 2008. "GLITTER: data reduction software for laser ablation ICP-MS". In Laser ablation ICP-MS in the earth sciences. Mineralogical Association of Canada Short Course Series. Edited by: P., Sylvester. 40, 204–207.

Griffin, W.L., Wang, X., Jackson, S.E., Pearson, N.J., O'Reilly, S.Y., Xu, X., Zhou, X., 2002. Zircon chemistry and magma mixing, SE China: In-situ analysis of Hf isotopes, Tonglu and Pingtan igneous complexes. Lithos 61, 237-269.

Ickert, R.B., Hiess, J., Williams, I.S., Holden, P., Ireland, T.R., Lanc, P., Schram, N., Foster, J.J., Clement, S.W., 2008. Determining high precision, in situ, oxygen isotope ratios with a SHRIMP II: Analyses of MPI-DING silicate-glass reference materials and zircon from contrasting granites. Chemical Geology 257, 114-128.

Jackson, S.E., Pearson, N.J., Griffin, W.L., Belousova, E.A., 2004. The application of laser ablation-inductively coupled plasma-mass spectrometry to in situ U–Pb zircon geochronology. Chemical Geology 211, 47-69.

Ludwig, K.R., 2012. User's Manual for Isoplot 3.75. A Geochronological Toolkit for Microsoft Excel. Berkeley Geochronology Center Special Publication No. 5, 75p.

Payne, J.L., Pearson, N.J., Grant, K.J., Halverson, G.P., 2013. Reassessment of relative oxide formation rates and molecular interferences on in situ lutetium-hafnium analysis with laser ablation MC-ICP-MS. Journal of Analytical Atomic Spectrometry 28, 1068-1079.

Scherer, E., Münker, C., Mezger, K., 2001. Calibration of the Lutetium-Hafnium Clock. Science 293, 683-687.

Sláma, J., Košler, J., Condon, D.J., Crowley, J.L., Gerdes, A., Hanchar, J.M., Horstwood, M.S.A., Morris, G.A., Nasdala, L., Norberg, N., Schaltegger, U., Schoene, B., Tubrett, M.N., Whitehouse, M.J., 2008. Plešovice zircon — A new natural reference material for U–Pb and Hf isotopic microanalysis. Chemical Geology 249, 1-35.

Table A.5.2: List of major element oxides, minor and trace elements analysed in this study

Element or Oxide	Detection Limit		Upper Limit		Element or Oxide	Detection Limit		Upper Limit	
SiO_2	0.01	%	100	%	Ho	0.02	ppm	10000	ppm
Al_2O_3	0.01	%	100	%	La	0.1	ppm	50000	ppm
CaO	0.01	%	100	%	Lu	0.01	ppm	10000	ppm
Cr_2O_3	0.002	%	100	%	Mo	0.1	ppm	2000	ppm
Fe_2O_3	0.04	%	100	%	Nb	0.1	ppm	10000	ppm
K_2O	0.01	%	100	%	Nd	0.3	ppm	10000	ppm
MgO	0.01	%	100	%	Ni	0.1	ppm	10000	ppm
MnO	0.01	%	100	%	Pb	0.1	ppm	10000	ppm
Na_2O	0.01	%	100	%	Pr	0.02	ppm	10000	ppm
P_2O_5	0.01	%	100	%	Rb	0.1	ppm	10000	ppm
TiO_2	0.01	%	100	%	Sb	0.1	ppm	2000	ppm
LOI	0.1	%	100	%	Sc	1	ppm	10000	ppm
Sum	0.01	%	100	%	Se	0.5	ppm	100	ppm
Ag	0.1	ppm	100	ppm	Sm	0.05	ppm	10000	ppm
As	0.5	ppm	10000	ppm	Sn	1	ppm	10000	ppm
Au	0.5	ppb	100000	ppb	Sr	0.5	ppm	50000	ppm
Ba	1	ppm	50000	ppm	Ta	0.1	ppm	10000	ppm
Be	1	ppm	10000	ppm	Tb	0.01	ppm	10000	ppm
Bi	0.1	ppm	2000	ppm	Th	0.2	ppm	10000	ppm
Cd	0.1	ppm	2000	ppm	Tl	0.1	ppm	1000	ppm
Ce	0.1	ppm	50000	ppm	Tm	0.01	ppm	10000	ppm
Co	0.2	ppm	10000	ppm	U	0.1	ppm	10000	ppm
Cs	0.1	ppm	10000	ppm	V	8	ppm	10000	ppm
Cu	0.1	ppm	10000	ppm	W	0.5	ppm	10000	ppm
Dy	0.05	ppm	10000	ppm	Yb	0.05	ppm	10000	ppm
Er	0.03	ppm	10000	ppm	Y	0.1	ppm	50000	ppm
Eu	0.02	ppm	10000	ppm	Zn	1	ppm	10000	ppm
Ga	0.5	ppm	10000	ppm	Zr	0.1	ppm	50000	ppm
Gd	0.05	ppm	10000	ppm	TOT/C	0.02	%	100	%
Hf	0.1	ppm	10000	ppm	TOT/S	0.02	%	100	%
Hg	0.01	ppm	50	ppm					

Appendix 5.2

LA-ICP-MS U-Pb data
(Ambalavao and Maevarano Suites)

DA13-010 (A)		Mean Counts (background subtracted)								Isotopic Ratios (± 1σ)							Age (Ma ± 1σ)						
Analysis	Core/Rim	^{204}Pb	^{206}Pb	^{207}Pb	^{208}Pb	^{232}Th	^{238}U	(%)^{206} Pb	Th/U	^{207}Pb/^{206}Pb		^{207}Pb/^{235}U		^{206}Pb/^{238}U		Rho	^{207}Pb/^{206}Pb		^{206}Pb/^{238}U		^{207}Pb/^{235}U		%Conc
010-01		0	1404	86	697	27179	19282	0.00	1.41	0.0624	0.0043	0.7731	0.0518	0.0899	0.0021	0.0834	688	141	555	13	582	30	95
010-02		0	722	49	264	9971	9957	0.00	1.00	0.0689	0.0042	0.8416	0.0496	0.0887	0.0018	0.1002	895	120	548	10	620	27	88
010-03		2	7346	436	300	10712	103028	0.03	0.10	0.0601	0.0011	0.7355	0.0145	0.0889	0.0012	0.4140	605	40	549	7	560	8	98
010-04		0	1921	173	1220	70812	29129	0.00	2.43	0.0915	0.0029	1.0432	0.0322	0.0827	0.0014	0.2298	1457	59	512	8	726	16	71
010-06		0	2247	140	448	16629	33020	0.00	0.50	0.0629	0.0018	0.7357	0.0209	0.0848	0.0012	0.2584	706	59	525	7	560	12	94
010-07	Core	13	4573	349	2421	88325	67018	0.28	1.32	0.0779	0.0028	0.9034	0.0315	0.0842	0.0014	0.1936	1144	69	521	9	654	17	80
010-08	Rim	0	19555	1166	532	16679	278529	0.00	0.06	0.0599	0.0010	0.7237	0.0131	0.0877	0.0012	0.4464	600	36	542	7	553	8	98
010-09		0	3467	204	197	13221	49406	0.00	0.27	0.0594	0.0018	0.7125	0.0216	0.0870	0.0013	0.2398	583	65	538	8	546	13	98
010-10		0	332	27	112	4516	4787	0.00	0.94	0.0829	0.0063	0.9933	0.0738	0.0870	0.0020	0.0767	1267	142	538	12	700	38	77
010-11		0	1339	126	1067	46400	19518	0.00	2.38	0.0939	0.0051	1.1010	0.0566	0.0850	0.0019	0.1080	1507	99	526	12	754	27	70
010-12		0	700	41	324	11350	9462	0.00	1.20	0.0595	0.0043	0.7381	0.0527	0.0900	0.0019	0.0772	587	151	556	11	561	31	99
010-14		0	661	39	325	12662	9681	0.00	1.31	0.0599	0.0043	0.7103	0.0499	0.0860	0.0018	0.0857	602	148	532	11	545	30	98
010-15		0	281	16	83	3132	4102	0.00	0.76	0.0584	0.0081	0.6971	0.0954	0.0867	0.0022	0.0369	543	277	536	13	537	57	100
010-17		18	1061	64	359	15013	16402	1.70	0.92	0.0625	0.0071	0.7501	0.0820	0.0871	0.0031	0.0472	692	225	538	19	568	48	95
010-18		10	881	72	522	40881	16232	1.14	2.52	0.0815	0.0035	0.7657	0.0325	0.0682	0.0012	0.1524	1233	83	425	7	577	19	74
010-19		0	3452	220	224	14002	50073	0.00	0.28	0.0637	0.0016	0.7402	0.0181	0.0843	0.0012	0.2974	733	51	522	7	563	11	93
010-20		38	4113	338	1610	124161	59889	0.92	2.07	0.0808	0.0038	0.8894	0.0397	0.0799	0.0016	0.1020	1217	90	495	10	646	21	77
010-21		0	459	30	173	6126	6549	0.00	0.94	0.0657	0.0050	0.7950	0.0597	0.0878	0.0019	0.0801	797	153	543	11	594	34	91
010-22		0	1512	86	879	32679	20704	0.00	1.58	0.0570	0.0020	0.7047	0.0247	0.0897	0.0014	0.1928	491	77	554	8	542	15	102
010-23		28	1397	86	246	8781	18407	2.00	0.48	0.0615	0.0026	0.8172	0.0336	0.0964	0.0016	0.1666	658	87	593	10	607	19	98
010-24		0	350	23	113	4692	4781	0.00	0.98	0.0672	0.0065	0.8404	0.0791	0.0907	0.0023	0.0571	844	188	560	14	619	44	90
010-25		1	959	56	354	12836	13492	0.10	0.95	0.0582	0.0028	0.7029	0.0334	0.0876	0.0015	0.1336	537	103	542	9	541	20	100
010-26		9	9668	630	549	14683	97516	0.09	0.15	0.0652	0.0017	1.1476	0.0300	0.1277	0.0019	0.3037	781	54	775	11	776	14	100
010-27		3	3415	196	724	25343	46578	0.09	0.54	0.0574	0.0018	0.7381	0.0228	0.0932	0.0015	0.2341	507	67	575	9	561	13	102
010-28		5	564	41	264	8719	8239	0.89	1.06	0.0736	0.0048	0.8675	0.0548	0.0855	0.0018	0.0916	1031	125	529	11	634	30	83
010-29		0	1027	63	537	20804	15468	0.00	1.34	0.0616	0.0040	0.7271	0.0458	0.0856	0.0019	0.0931	660	133	530	11	555	27	95
010-30		7	774	47	416	15150	11411	0.90	1.33	0.0607	0.0034	0.6979	0.0389	0.0833	0.0015	0.1115	630	118	516	9	538	23	96
010-31		0	815	53	284	9269	12401	0.00	0.75	0.0665	0.0068	0.7684	0.0756	0.0839	0.0028	0.0523	821	200	519	17	579	43	90
010-33		11	9480	608	3388	148725	126356	0.12	1.18	0.0645	0.0014	0.7887	0.0176	0.0887	0.0012	0.3057	758	46	548	7	590	10	93
010-34		7	973	61	375	13930	13868	0.72	1.00	0.0644	0.0029	0.7571	0.0335	0.0853	0.0015	0.1369	755	92	528	9	572	19	92
010-35		2	1247	73	605	22291	17375	0.16	1.28	0.0597	0.0029	0.7296	0.0350	0.0886	0.0016	0.1293	594	103	547	10	556	21	98

DA13-010 (A)		Mean Counts (background subtracted)								Isotopic Ratios (± 1σ)							Age (Ma ± 1σ)						
Analysis	Core/Rim	^{204}Pb	^{206}Pb	^{207}Pb	^{208}Pb	^{232}Th	^{238}U	(%)^{206} Pb	Th/U	^{207}Pb/^{206}Pb		^{207}Pb/^{235}U		^{206}Pb/^{238}U		Rho	^{207}Pb/^{206}Pb		^{206}Pb/^{238}U		^{207}Pb/^{235}U		%Conc
010-36		5	489	33	214	7299	6800	1.02	1.07	0.0689	0.0049	0.8251	0.0578	0.0869	0.0019	0.0765	896	141	537	11	611	32	88
010-37		5	4067	270	510	50739	60020	0.12	0.85	0.0675	0.0016	0.7483	0.0179	0.0804	0.0011	0.2825	854	49	498	7	567	10	88
010-38		15	2428	157	632	21928	31156	0.62	0.70	0.0658	0.0022	0.8532	0.0274	0.0941	0.0015	0.2013	799	67	580	9	626	15	93
010-39		0	2039	152	852	44110	37746	0.00	1.17	0.0765	0.0031	0.6428	0.0249	0.0610	0.0011	0.1286	1108	78	382	6	504	15	76
010-40		10	1332	79	346	11761	17910	0.75	0.66	0.0612	0.0026	0.7572	0.0310	0.0897	0.0015	0.1481	647	87	554	9	572	18	97
010-41		3	1252	77	290	10310	16647	0.24	0.62	0.0626	0.0032	0.7713	0.0376	0.0893	0.0017	0.1087	696	104	552	10	581	22	95
010-42		0	2431	151	554	20469	34297	0.00	0.60	0.0634	0.0018	0.7399	0.0203	0.0847	0.0012	0.2479	720	58	524	7	562	12	93
010-44		0	3119	196	1727	59431	43951	0.00	1.35	0.0644	0.0019	0.7573	0.0217	0.0854	0.0013	0.2360	753	60	528	7	573	13	92
010-45		8	708	40	375	13932	9682	1.13	1.44	0.0581	0.0035	0.6888	0.0409	0.0860	0.0016	0.0938	532	128	532	9	532	25	100

DA13-018 (A)		Mean Counts (background subtracted)								Isotopic Ratios (± 1σ)							Age (Ma ± 1σ)						
Analysis	Core/Rim	^{204}Pb	^{206}Pb	^{207}Pb	^{208}Pb	^{232}Th	^{238}U	(%)^{206} Pb	Th/U	^{207}Pb/^{206}Pb		^{207}Pb/^{235}U		^{206}Pb/^{238}U		Rho	^{207}Pb/^{206}Pb		^{206}Pb/^{238}U		^{207}Pb/^{235}U		%Conc
018-01		0	59910	3615	22546	672553	680881	0.00	0.99	0.0602	0.0009	0.8225	0.0130	0.0992	0.0012	0.4191	611	33	610	7	610	7	100
018-02		21	42368	2747	29509	980805	551899	0.05	1.78	0.0648	0.0009	0.7935	0.0120	0.0888	0.0011	0.4620	769	30	548	6	593	7	92
018-03		240	64706	7188	50097	1007786	834522	0.37	1.21	0.1083	0.0037	1.4376	0.0476	0.0963	0.0016	0.2012	1771	61	593	10	905	20	66
018-04		44	38450	2637	19156	1048166	548833	0.11	1.91	0.0689	0.0011	0.7578	0.0123	0.0798	0.0010	0.4148	895	32	495	6	573	7	86
018-05		27	75652	4641	45690	1864404	930019	0.04	2.00	0.0611	0.0010	0.8135	0.0143	0.0965	0.0012	0.4143	644	36	594	7	604	8	98
018-06		0	40869	2497	20543	664578	520728	0.00	1.28	0.0612	0.0010	0.7672	0.0127	0.0909	0.0011	0.4192	648	34	561	7	578	7	97
018-07		16	57101	3641	22901	684963	708186	0.03	0.97	0.0642	0.0010	0.8186	0.0131	0.0925	0.0011	0.4235	748	32	570	7	607	7	94
018-08		2	33748	2100	18091	546896	457024	0.01	1.20	0.0627	0.0015	0.7742	0.0189	0.0896	0.0013	0.2898	697	51	553	8	582	11	95
018-09		20	53645	3336	22560	679199	669154	0.04	1.02	0.0628	0.0011	0.7973	0.0136	0.0921	0.0011	0.3902	702	35	568	7	595	8	95
018-10		39	100608	6325	68425	2558153	1290760	0.04	1.98	0.0635	0.0015	0.8223	0.0193	0.0940	0.0013	0.2972	724	49	579	8	609	11	95
018-11		26	27718	1893	6090	167620	344070	0.09	0.49	0.0688	0.0022	0.8413	0.0257	0.0888	0.0013	0.1445	892	65	548	8	620	14	88
018-12		23	32382	2036	16991	479510	402064	0.07	1.19	0.0628	0.0013	0.8164	0.0164	0.0944	0.0012	0.3338	700	42	581	7	606	9	96
018-13		27	28330	1767	11223	459092	342906	0.10	1.34	0.0629	0.0012	0.8278	0.0159	0.0954	0.0012	0.3383	705	40	588	7	612	9	96
018-14		121	15214	2574	10441	192846	249077	0.80	0.77	0.1741	0.0088	1.7813	0.0866	0.0743	0.0016	0.1270	2598	82	462	10	1039	32	45
018-15		11	23662	1681	6789	172711	306752	0.05	0.56	0.0719	0.0014	0.8806	0.0173	0.0889	0.0011	0.3333	983	39	549	7	641	9	86
018-16		15	89213	5378	41341	1265184	1086118	0.02	1.16	0.0619	0.0009	0.8013	0.0122	0.0939	0.0011	0.4570	670	30	579	7	598	7	97
018-17		45	54326	3848	19884	722851	755694	0.08	0.96	0.0724	0.0013	0.8372	0.0155	0.0838	0.0011	0.3823	999	36	519	6	618	9	84
018-18		6	30294	2024	15209	431424	400397	0.02	1.08	0.0681	0.0012	0.8227	0.0144	0.0876	0.0011	0.4018	872	35	541	6	610	8	89
018-19		90	35402	3496	19757	385521	395987	0.25	0.97	0.1008	0.0018	1.3900	0.0253	0.1000	0.0012	0.3442	1640	33	614	7	885	11	69
018-20		0	66108	3934	40093	1278754	815276	0.00	1.57	0.0605	0.0011	0.7873	0.0145	0.0944	0.0012	0.3828	622	38	581	7	590	8	99
018-21		526	109658	14647	162513	1528771	1310220	0.48	1.17	0.1391	0.0048	1.9849	0.0673	0.1035	0.0017	0.1935	2216	59	635	10	1110	23	57
018-22		25	47112	2868	19187	565650	564605	0.05	1.00	0.0622	0.0010	0.8208	0.0140	0.0958	0.0012	0.4069	680	35	590	7	609	8	97
018-23		203	49330	5935	40190	866364	658496	0.41	1.32	0.1252	0.0058	1.6065	0.0722	0.0930	0.0018	0.1321	2032	80	573	11	973	28	59
018-24		29	36197	2708	16186	546177	559538	0.08	0.98	0.0764	0.0013	0.7798	0.0137	0.0741	0.0009	0.3842	1104	34	461	5	585	8	79
018-25		131	45578	5018	33316	1141676	775157	0.29	1.47	0.1126	0.0027	1.0226	0.0238	0.0659	0.0009	0.2517	1841	42	411	5	715	12	58
018-26		365	18106	6577	28732	131263	507634	2.02	0.26	0.3715	0.0090	2.0051	0.0473	0.0392	0.0005	0.2417	3798	36	248	3	1117	16	22
018-27		14	21657	1276	1359	36899	275686	0.06	0.13	0.0603	0.0011	0.7513	0.0141	0.0904	0.0011	0.3603	614	39	558	7	569	8	98
018-28		1029	91055	20605	107583	3018429	1778146	1.13	1.70	0.2366	0.0073	2.0071	0.0609	0.0616	0.0010	0.2243	3097	48	385	6	1118	21	34
018-29		22	85517	4922	730180	32723482	1239696	0.03	26.40	0.0602	0.0019	0.6906	0.0210	0.0833	0.0013	0.2269	609	65	516	8	533	13	97
018-30		0	102100	6095	52963	1599856	1258721	0.00	1.27	0.0619	0.0017	0.8360	0.0234	0.0979	0.0015	0.2588	672	59	602	9	617	13	98

DA13-037 (A)		Mean Counts (background subtracted)								Isotopic Ratios (± 1σ)							Age (Ma ± 1σ)						
Analysis	Core/Rim	^{204}Pb	^{206}Pb	^{207}Pb	^{208}Pb	^{232}Th	^{238}U	(%)^{206} Pb	Th/U	^{207}Pb/^{206}Pb		^{207}Pb/^{235}U		^{206}Pb/^{238}U		Rho	^{207}Pb/^{206}Pb		^{206}Pb/^{238}U		^{207}Pb/^{235}U		%Conc
037-01		12	3395	461	3064	86676	119034	0.35	0.73	0.1357	0.0027	0.7190	0.0150	0.0384	0.0006	0.4132	2173	35	243	4	550	9	44
037-02		0	23123	1412	618	18741	344137	0.00	0.05	0.0608	0.0010	0.7559	0.0134	0.0902	0.0013	0.5295	632	34	557	8	572	8	97
037-03		39	28097	2147	3648	68600	420922	0.14	0.16	0.0761	0.0013	0.9555	0.0181	0.0911	0.0013	0.5057	1098	34	562	8	681	9	82
037-04		1	12444	751	1149	46611	187751	0.01	0.25	0.0603	0.0011	0.7469	0.0144	0.0898	0.0013	0.4841	615	37	555	8	566	8	98
037-05		2	3048	178	1454	61225	45581	0.07	1.34	0.0585	0.0015	0.7228	0.0184	0.0896	0.0014	0.3375	549	54	553	8	552	11	100
037-06		59	10627	1442	3726	38546	201293	0.56	0.19	0.1361	0.0029	1.2813	0.0277	0.0683	0.0010	0.3724	2178	36	426	6	837	12	51
037-07	Core	83	32100	3674	5776	60003	387518	0.26	0.15	0.1141	0.0019	1.7833	0.0334	0.1134	0.0017	0.5121	1865	30	693	10	1039	12	67
037-08	Rim	58	6343	1398	4017	25896	181261	0.91	0.14	0.2211	0.0062	1.4072	0.0386	0.0462	0.0008	0.2713	2988	45	291	5	892	16	33
037-09	Core	40	4180	561	1759	83140	74542	0.96	1.12	0.1345	0.0064	1.5312	0.0704	0.0827	0.0020	0.1884	2158	81	512	12	943	28	54
037-10	Rim	14	13783	967	1247	43498	220103	0.10	0.20	0.0700	0.0012	0.8068	0.0150	0.0836	0.0012	0.4956	929	34	518	7	601	8	86
037-11	Core	7	3857	288	1897	72033	71401	0.18	1.01	0.0729	0.0031	0.7795	0.0320	0.0776	0.0016	0.2014	1010	83	482	10	585	18	82
037-12	Rim	36	15051	1511	2961	141006	232823	0.24	0.61	0.1019	0.0021	1.1464	0.0239	0.0816	0.0012	0.3810	1659	37	506	7	776	11	65
037-13		7	4184	247	1292	54853	64040	0.17	0.86	0.0590	0.0013	0.7092	0.0164	0.0873	0.0013	0.3796	566	48	539	8	544	10	99
037-14		15	2934	203	1944	85101	48618	0.51	1.75	0.0686	0.0021	0.7944	0.0247	0.0840	0.0015	0.2796	887	63	520	9	594	14	88
037-15		18	10644	1030	2250	44492	161799	0.17	0.27	0.0978	0.0020	1.1439	0.0244	0.0849	0.0012	0.3875	1582	38	525	7	774	12	68
037-16		3	4094	268	2347	92177	63703	0.07	1.45	0.0657	0.0014	0.7596	0.0168	0.0839	0.0012	0.3822	795	44	520	7	574	10	91
037-17		24	2683	259	1213	38422	40720	0.89	0.94	0.0979	0.0055	1.1169	0.0588	0.0828	0.0021	0.1053	1584	101	513	12	762	28	67
037-18		23	2048	133	1785	73797	32665	1.12	2.26	0.0648	0.0038	0.7762	0.0441	0.0870	0.0021	0.1185	769	120	538	12	583	25	92
037-19		0	5815	345	932	37532	87086	0.00	0.43	0.0594	0.0012	0.7136	0.0149	0.0871	0.0012	0.4084	583	42	538	7	547	9	98
037-20		39	5902	812	4557	221585	138704	0.66	1.60	0.1371	0.0026	1.0587	0.0209	0.0560	0.0008	0.4321	2190	33	352	5	733	10	48
037-21		5	3998	316	1745	61599	105751	0.13	0.58	0.0787	0.0018	0.5417	0.0126	0.0500	0.0008	0.3596	1163	44	314	5	440	8	71
037-22		6	7451	552	2000	71377	105360	0.08	0.68	0.0744	0.0014	0.9372	0.0183	0.0913	0.0013	0.4284	1053	37	563	8	671	10	84
037-23		17	5620	382	3608	146461	91252	0.30	1.61	0.0679	0.0017	0.7744	0.0200	0.0827	0.0013	0.3326	865	52	512	8	582	11	88
037-24		0	2127	345	1574	34305	51501	0.00	0.67	0.1600	0.0070	1.1510	0.0465	0.0522	0.0012	0.1338	2455	72	328	7	778	22	42
037-25		0	2315	207	436	11469	36871	0.00	0.31	0.0916	0.0036	0.9900	0.0373	0.0784	0.0015	0.1628	1459	73	487	9	699	19	70
037-26		0	3673	231	2037	81801	52070	0.00	1.57	0.0633	0.0014	0.7893	0.0176	0.0905	0.0013	0.3647	718	45	558	8	591	10	94
037-27		41	25843	2377	5369	104889	390225	0.16	0.27	0.0915	0.0020	1.0713	0.0242	0.0850	0.0012	0.3478	1456	42	526	7	739	12	71
037-28		76	10203	1493	3991	30205	195536	0.74	0.15	0.1425	0.0061	1.2138	0.0491	0.0618	0.0012	0.1066	2258	72	387	7	807	23	48
037-29		8	12145	726	2907	117458	175763	0.07	0.67	0.0595	0.0013	0.7380	0.0168	0.0900	0.0013	0.3565	584	47	556	8	561	10	99
037-30		56	6676	602	1418	31801	103066	0.84	0.31	0.0929	0.0026	1.0056	0.0273	0.0785	0.0012	0.2440	1486	52	487	7	707	14	69

DA13-038 (A)		Mean Counts (background subtracted)								Isotopic Ratios (± 1σ)							Age (Ma ± 1σ)						
Analysis	Core/Rim	^{204}Pb	^{206}Pb	^{207}Pb	^{208}Pb	^{232}Th	^{238}U	(%)^{206} Pb	Th/U	^{207}Pb/^{206}Pb		^{207}Pb/^{235}U		^{206}Pb/^{238}U		Rho	^{207}Pb/^{206}Pb		^{206}Pb/^{238}U		^{207}Pb/^{235}U		%Conc
038-01		19	3443	215	1436	55799	51134	0.55	1.09	0.0638	0.0016	0.7437	0.0187	0.0845	0.0012	0.3042	735	52	523	7	565	11	93
038-02		0	5341	338	2241	91338	83083	0.00	1.10	0.0644	0.0013	0.7325	0.0152	0.0825	0.0012	0.4003	755	41	511	7	558	9	92
038-03		0	4830	288	3501	142984	73109	0.00	1.96	0.0609	0.0013	0.7109	0.0160	0.0847	0.0012	0.3602	635	46	524	7	545	9	96
038-04		8	5922	355	1365	56923	85920	0.14	0.66	0.0609	0.0013	0.7458	0.0168	0.0887	0.0013	0.3667	637	46	548	8	566	10	97
038-05		5	2983	234	2482	98231	59129	0.17	1.66	0.0793	0.0022	0.7271	0.0200	0.0665	0.0011	0.2880	1180	54	415	6	555	12	75
038-06		16	2178	138	1548	62115	31381	0.73	1.98	0.0647	0.0017	0.7727	0.0202	0.0866	0.0013	0.2788	765	54	536	8	581	12	92
038-07		0	2598	201	1945	72543	40990	0.00	1.77	0.0788	0.0018	0.8610	0.0196	0.0792	0.0011	0.3369	1168	44	491	7	631	11	78
038-08		11	3294	195	3027	128796	51497	0.33	2.50	0.0603	0.0022	0.7183	0.0255	0.0864	0.0015	0.2264	613	76	534	9	550	15	97
038-09		11	14433	867	531	19154	212189	0.08	0.09	0.0614	0.0011	0.7343	0.0138	0.0868	0.0012	0.4469	652	37	537	7	559	8	96
038-10		6	2863	168	2357	97019	42718	0.21	2.27	0.0601	0.0016	0.6844	0.0177	0.0827	0.0012	0.2783	605	55	512	7	530	11	97
038-11		3	2182	138	1441	60769	33691	0.14	1.80	0.0648	0.0023	0.7618	0.0263	0.0853	0.0015	0.2189	768	72	528	9	575	15	92
038-12		0	3182	192	2476	107613	49599	0.00	2.17	0.0612	0.0022	0.7224	0.0250	0.0857	0.0015	0.2189	645	74	530	9	552	15	96
038-13		0	2385	143	1816	77248	36904	0.00	2.09	0.0611	0.0023	0.7066	0.0265	0.0838	0.0015	0.1930	644	80	519	9	543	16	96
038-14		0	2377	157	1303	56936	37450	0.00	1.52	0.0677	0.0018	0.7407	0.0195	0.0794	0.0012	0.2768	860	54	492	7	563	11	87
038-15		0	3253	226	680	23975	41423	0.00	0.58	0.0715	0.0042	1.0457	0.0578	0.1061	0.0025	0.0941	971	114	650	15	727	29	89
038-16		0	9307	563	395	11661	169401	0.00	0.07	0.0626	0.0024	0.5402	0.0199	0.0626	0.0011	0.1609	694	79	391	6	439	13	89
038-17		6	2194	138	1661	64946	31429	0.27	2.07	0.0639	0.0016	0.7645	0.0192	0.0868	0.0013	0.3033	737	52	537	8	577	11	93
038-18		1	5230	366	1212	28795	76542	0.02	0.38	0.0689	0.0045	0.8079	0.0499	0.0850	0.0022	0.0900	897	128	526	13	601	28	87
038-19		8	2945	188	1829	72560	44086	0.27	1.65	0.0648	0.0021	0.7752	0.0252	0.0867	0.0015	0.2306	769	68	536	9	583	14	92
038-22		14	2059	126	1425	55521	29757	0.68	1.87	0.0620	0.0016	0.7391	0.0191	0.0864	0.0013	0.2917	675	54	534	8	562	11	95
038-23		7	2324	134	803	30893	31406	0.30	0.98	0.0585	0.0019	0.7162	0.0232	0.0889	0.0014	0.2027	547	70	549	8	548	14	100
038-24		10	2456	174	1734	80329	37050	0.41	2.17	0.0720	0.0026	0.7901	0.0272	0.0797	0.0014	0.1866	985	70	494	8	591	15	84
038-25		16	3075	185	957	40686	44053	0.52	0.92	0.0620	0.0035	0.7067	0.0389	0.0825	0.0018	0.1243	676	117	511	11	543	23	94
038-26		5	3127	202	645	21621	44426	0.16	0.49	0.0652	0.0014	0.8042	0.0183	0.0895	0.0013	0.3586	779	46	553	8	599	10	92
038-27		0	2682	175	2246	99421	44434	0.00	2.24	0.0641	0.0033	0.7582	0.0383	0.0858	0.0020	0.1641	745	106	531	12	573	22	93
038-28		0	1807	140	1485	55718	35351	0.00	1.58	0.0777	0.0022	0.7020	0.0198	0.0655	0.0011	0.2692	1139	56	409	6	540	12	76
038-29		14	1541	104	750	28351	20689	0.91	1.37	0.0682	0.0038	0.8637	0.0465	0.0919	0.0021	0.1133	874	112	567	12	632	25	90
038-30		39	17193	1234	1954	51098	418064	0.23	0.12	0.0716	0.0031	0.5008	0.0214	0.0508	0.0010	0.1703	974	87	319	6	412	14	77
038-31		5	2400	141	612	25313	36557	0.21	0.69	0.0591	0.0029	0.7195	0.0347	0.0883	0.0019	0.1447	570	105	546	11	550	20	99
038-32		15	3308	207	735	29387	45405	0.45	0.65	0.0615	0.0023	0.7522	0.0277	0.0890	0.0016	0.1685	655	80	549	9	570	16	96
038-33		4	2300	157	1606	56272	30346	0.17	1.85	0.0679	0.0023	0.8722	0.0289	0.0933	0.0016	0.1936	866	69	575	9	637	16	90

DA13-038 (A)		Mean Counts (background subtracted)								Isotopic Ratios (± 1σ)							Age (Ma ± 1σ)						
Analysis	Core/Rim	^{204}Pb	^{206}Pb	^{207}Pb	^{208}Pb	^{232}Th	^{238}U	(%)^{206} Pb	Th/U	$^{207}Pb/^{206}Pb$		$^{207}Pb/^{235}U$		$^{206}Pb/^{238}U$		Rho	$^{207}Pb/^{206}Pb$		$^{206}Pb/^{238}U$		$^{207}Pb/^{235}U$		%Conc
038-34		6	1652	100	1092	42033	21804	0.36	1.93	0.0608	0.0019	0.8085	0.0245	0.0965	0.0015	0.2472	631	65	594	9	602	14	99
038-35		0	2122	126	1395	55300	29661	0.00	1.86	0.0596	0.0017	0.7490	0.0216	0.0912	0.0014	0.2612	588	62	563	8	568	13	99
038-36		0	3115	183	1356	53213	40192	0.00	1.32	0.0583	0.0018	0.7826	0.0235	0.0973	0.0015	0.2325	541	66	599	9	587	13	102
038-37		0	3031	229	1273	46740	59009	0.00	0.79	0.0749	0.0018	0.6699	0.0162	0.0649	0.0010	0.3112	1065	48	405	6	521	10	78
038-38		0	9294	538	1661	66899	128349	0.00	0.52	0.0576	0.0011	0.7313	0.0147	0.0921	0.0013	0.4117	515	42	568	8	557	9	102
038-39		7	2547	173	1615	62143	38440	0.27	1.62	0.0683	0.0016	0.7925	0.0187	0.0842	0.0012	0.3281	877	47	521	7	593	11	88
038-40		12	2786	169	1309	51586	39985	0.43	1.29	0.0610	0.0016	0.7492	0.0200	0.0891	0.0014	0.2896	639	56	550	8	568	12	97
038-41		10	3738	228	761	27531	52150	0.27	0.53	0.0589	0.0034	0.7149	0.0400	0.0883	0.0021	0.1049	562	122	545	12	548	24	100
038-42		9	2273	139	1733	70989	33027	0.40	2.15	0.0608	0.0021	0.7214	0.0245	0.0860	0.0014	0.1933	633	73	532	9	552	14	96
038-43		4	4129	347	2401	84320	77099	0.10	1.09	0.0839	0.0019	0.7924	0.0181	0.0685	0.0010	0.3419	1289	43	427	6	593	10	72
038-44		14	2969	237	1084	42017	44988	0.47	0.93	0.0777	0.0030	0.8657	0.0322	0.0808	0.0015	0.1591	1140	75	501	9	633	18	79
038-45		1	2342	143	1508	60381	33362	0.04	1.81	0.0608	0.0018	0.7426	0.0213	0.0887	0.0014	0.2512	630	61	548	8	564	12	97

DA13-041 (A)		Mean Counts (background subtracted)								Isotopic Ratios (± 1σ)							Age (Ma ± 1σ)						
Analysis	Core/Rim	^{204}Pb	^{206}Pb	^{207}Pb	^{208}Pb	^{232}Th	^{238}U	(%)^{206} Pb	Th/U	^{207}Pb/^{206}Pb		^{207}Pb/^{235}U		^{206}Pb/^{238}U		Rho	^{207}Pb/^{206}Pb		^{206}Pb/^{238}U		^{207}Pb/^{235}U		%Conc
041-01		0	12483	909	2465	98415	186701	0.00	0.53	0.0740	0.0022	0.8822	0.0256	0.0865	0.0014	0.2683	1040	58	535	8	642	14	83
041-02		0	4383	255	493	18383	65611	0.00	0.28	0.0583	0.0016	0.7211	0.0205	0.0896	0.0014	0.3025	541	61	553	9	551	12	100
041-03		26	4379	272	971	39778	67369	0.59	0.59	0.0641	0.0034	0.7440	0.0378	0.0842	0.0018	0.1250	746	108	521	11	565	22	92
041-04		22	4922	359	1542	72918	77995	0.45	0.93	0.0715	0.0032	0.8797	0.0380	0.0893	0.0019	0.1787	970	88	552	11	641	21	86
041-05		5	2319	165	566	18800	32371	0.22	0.58	0.0727	0.0032	0.9054	0.0389	0.0903	0.0018	0.1529	1006	88	557	11	655	21	85
041-06		18	8568	575	1321	41196	119914	0.21	0.34	0.0676	0.0017	0.8762	0.0228	0.0939	0.0015	0.3189	857	52	579	9	639	12	91
041-07		0	5083	301	2846	113442	75870	0.00	1.50	0.0593	0.0018	0.7365	0.0219	0.0901	0.0015	0.2889	578	63	556	9	560	13	99
041-08		0	1809	112	518	20413	27164	0.00	0.75	0.0622	0.0026	0.7497	0.0308	0.0874	0.0017	0.1734	680	87	540	10	568	18	95
041-09		0	16579	1161	2387	84387	233449	0.00	0.36	0.0710	0.0025	0.9049	0.0314	0.0924	0.0016	0.2321	957	70	570	10	654	17	87
041-10		11	10458	623	1668	68618	157924	0.11	0.43	0.0591	0.0014	0.7277	0.0180	0.0893	0.0014	0.3641	570	51	552	8	555	11	99
041-11		0	2461	154	692	28308	36972	0.00	0.77	0.0628	0.0022	0.7670	0.0267	0.0885	0.0016	0.2304	702	73	547	9	578	15	95
041-12		19	11918	827	3166	108346	149579	0.16	0.72	0.0702	0.0018	0.9603	0.0241	0.0993	0.0015	0.3057	933	50	610	9	683	13	89
041-13		40	12069	971	3157	107123	154494	0.33	0.69	0.0798	0.0030	1.0628	0.0384	0.0967	0.0017	0.1968	1192	71	595	10	735	19	81
041-14		0	519	40	181	8986	8702	0.00	1.03	0.0772	0.0049	0.8406	0.0510	0.0790	0.0021	0.0998	1126	122	490	12	620	28	79
041-15		34	9786	791	1736	68385	126721	0.35	0.54	0.0807	0.0029	1.0679	0.0372	0.0960	0.0017	0.2123	1214	68	591	10	738	18	80

DA13-041 (A)		Mean Counts (background subtracted)								Isotopic Ratios (± 1σ)							Age (Ma ± 1σ)						
Analysis	Core/Rim	^{204}Pb	^{206}Pb	^{207}Pb	^{208}Pb	^{232}Th	^{238}U	(%)^{206} Pb	Th/U	^{207}Pb/^{206}Pb		^{207}Pb/^{235}U		^{206}Pb/^{238}U		Rho	^{207}Pb/^{206}Pb		^{206}Pb/^{238}U		^{207}Pb/^{235}U		%Conc
072-01		15	2607	149	643	24522	36697	0.58	0.67	0.0574	0.0014	0.7075	0.0176	0.0894	0.0013	0.3091	506	54	552	8	543	10	102
072-02		0	3494	212	1259	59154	51501	0.00	1.15	0.0606	0.0015	0.7169	0.0177	0.0858	0.0013	0.3138	625	52	531	7	549	10	97
072-03		6	2479	169	777	44239	46652	0.24	0.95	0.0684	0.0033	0.6109	0.0278	0.0648	0.0013	0.1160	882	95	405	8	484	18	84
072-04	Core	10	1667	98	1088	43271	24471	0.60	1.77	0.0589	0.0016	0.7031	0.0195	0.0866	0.0013	0.2691	564	59	535	8	541	12	99
072-05	Rim	9	5562	322	1390	55092	78765	0.16	0.70	0.0579	0.0011	0.7221	0.0148	0.0904	0.0013	0.4059	527	43	558	7	552	9	101
072-06		6	6515	372	1965	78765	95635	0.09	0.82	0.0571	0.0011	0.6843	0.0137	0.0870	0.0012	0.4148	493	42	538	7	529	8	102
072-07		12	36017	2141	4080	177272	547269	0.03	0.32	0.0594	0.0010	0.7052	0.0129	0.0861	0.0012	0.4808	583	36	532	7	542	8	98
072-08		8	643	37	220	8795	8820	1.24	1.00	0.0587	0.0029	0.7312	0.0351	0.0905	0.0018	0.1289	554	105	559	11	557	21	100
072-09		9	2364	143	611	25710	36779	0.38	0.70	0.0609	0.0024	0.7262	0.0280	0.0865	0.0016	0.1964	637	83	535	10	554	16	96
072-10		0	4191	239	1273	52425	61281	0.00	0.86	0.0570	0.0013	0.6907	0.0160	0.0878	0.0013	0.3528	492	49	543	8	533	10	102
072-12		0	5994	362	2713	119002	93008	0.00	1.28	0.0606	0.0015	0.7109	0.0179	0.0851	0.0013	0.3288	626	52	526	8	545	11	96
072-13	Core	0	1707	102	692	28943	25693	0.00	1.13	0.0602	0.0021	0.7188	0.0241	0.0867	0.0015	0.2188	609	72	536	9	550	14	97
072-14	Rim	7	10719	616	5514	215812	152669	0.07	1.41	0.0572	0.0012	0.7009	0.0148	0.0889	0.0012	0.3741	500	45	549	7	539	9	102
072-15		0	968	57	471	19126	13843	0.00	1.38	0.0594	0.0034	0.7285	0.0401	0.0890	0.0020	0.1085	582	119	549	12	556	24	99
072-16		0	1772	104	425	17927	25596	0.00	0.70	0.0591	0.0017	0.7089	0.0198	0.0871	0.0013	0.2636	570	60	538	8	544	12	99
072-17		0	1009	58	616	24580	14062	0.00	1.75	0.0578	0.0026	0.7011	0.0309	0.0881	0.0017	0.1372	522	97	544	10	540	18	101
072-18		0	2265	126	665	26416	32720	0.00	0.81	0.0558	0.0017	0.6829	0.0202	0.0887	0.0014	0.2573	445	65	548	8	529	12	104
072-19	Core	0	2613	156	737	29201	37982	0.00	0.77	0.0600	0.0016	0.7304	0.0197	0.0884	0.0014	0.2892	602	57	546	8	557	12	98
072-20	Rim	0	608	36	289	11786	8400	0.00	1.40	0.0600	0.0027	0.7546	0.0330	0.0912	0.0017	0.1446	604	94	563	10	571	19	99
072-21		16	2001	115	531	21242	28990	0.80	0.73	0.0573	0.0016	0.6988	0.0191	0.0885	0.0014	0.2848	502	59	547	8	538	11	102
072-22		0	751	43	322	13185	10884	0.00	1.21	0.0570	0.0023	0.6913	0.0276	0.0880	0.0016	0.1758	490	88	544	9	534	17	102
072-23		0	2261	138	527	21028	33790	0.00	0.62	0.0610	0.0019	0.7424	0.0233	0.0883	0.0015	0.2546	639	66	545	9	564	14	97
072-24		0	6020	350	1448	63064	88433	0.00	0.71	0.0578	0.0012	0.6995	0.0149	0.0878	0.0013	0.3933	521	44	543	7	539	9	101
072-25		0	3086	179	1038	41560	45824	0.00	0.91	0.0579	0.0017	0.6990	0.0205	0.0875	0.0014	0.2671	526	63	541	8	538	12	100
072-26		0	860	50	403	16544	12941	0.00	1.28	0.0590	0.0033	0.7112	0.0379	0.0875	0.0019	0.1232	566	116	541	11	546	23	99
072-27		0	2236	133	834	34460	33911	0.00	1.02	0.0596	0.0019	0.7105	0.0221	0.0865	0.0014	0.2560	589	66	535	8	545	13	98
072-28		0	7847	457	2184	86623	112225	0.00	0.77	0.0576	0.0011	0.7181	0.0149	0.0904	0.0013	0.4050	515	43	558	8	550	9	102
072-29		0	2147	127	693	29399	31916	0.00	0.92	0.0594	0.0019	0.7146	0.0226	0.0873	0.0014	0.2405	581	68	539	9	548	13	99
072-30		12	3106	182	1163	44086	41355	0.39	1.07	0.0571	0.0023	0.7352	0.0283	0.0935	0.0017	0.1821	493	85	576	10	560	17	103

DA13-050 (A)		Mean Counts (background subtracted)								Isotopic Ratios (± 1σ)							Age (Ma ± 1σ)						
Analysis	Core/Rim	^{204}Pb	^{206}Pb	^{207}Pb	^{208}Pb	^{232}Th	^{238}U	(%)^{206} Pb	Th/U	^{207}Pb/^{206}Pb		^{207}Pb/^{235}U		^{206}Pb/^{238}U		Rho	^{207}Pb/^{206}Pb		^{206}Pb/^{238}U		^{207}Pb/^{235}U		%Conc
050-01		16	9006	525	2354	88396	110206	0.18	0.80	0.0581	0.0010	0.8134	0.0152	0.1016	0.0014	0.4283	532	39	624	8	604	9	103
050-02		16	2625	165	922	38334	38813	0.61	0.99	0.0638	0.0028	0.7991	0.0345	0.0908	0.0018	0.1714	736	91	560	11	596	19	94
050-03		0	2757	168	1322	50401	35565	0.00	1.42	0.0607	0.0014	0.7804	0.0185	0.0932	0.0013	0.3015	630	50	575	8	586	11	98
050-04		8	3593	228	1154	44089	48311	0.22	0.91	0.0633	0.0014	0.7965	0.0181	0.0913	0.0013	0.3266	717	47	564	8	595	10	95
050-05		0	2048	127	1064	41232	26763	0.00	1.54	0.0620	0.0017	0.8035	0.0213	0.0940	0.0014	0.2675	676	56	579	8	599	12	97
050-06		10	3334	254	918	31697	48626	0.30	0.65	0.0759	0.0019	0.8864	0.0217	0.0848	0.0013	0.2919	1092	49	525	7	645	12	81
050-08		8	2985	282	1412	42077	64052	0.27	0.66	0.0941	0.0021	0.7453	0.0164	0.0575	0.0008	0.3299	1511	41	360	5	566	10	64
050-09		0	4938	285	2026	89163	70703	0.00	1.26	0.0575	0.0012	0.6762	0.0140	0.0853	0.0012	0.3639	511	44	528	7	525	8	101
050-10		6	7794	469	724	27908	96632	0.08	0.29	0.0597	0.0012	0.7790	0.0159	0.0947	0.0012	0.3405	592	43	583	7	585	9	100
050-11		10	1761	109	853	34234	23675	0.57	1.45	0.0619	0.0017	0.7729	0.0212	0.0906	0.0014	0.2513	672	58	559	8	581	12	96
050-12		0	18909	1111	2387	86147	236247	0.00	0.36	0.0583	0.0013	0.7649	0.0177	0.0953	0.0013	0.3099	540	50	587	8	577	10	102
050-13		17	20986	1246	707	26091	262871	0.08	0.10	0.0590	0.0010	0.7649	0.0139	0.0941	0.0012	0.3954	566	38	580	7	577	8	100
050-14		24	8388	477	3343	134611	106902	0.29	1.26	0.0564	0.0012	0.7451	0.0158	0.0960	0.0013	0.3517	466	46	591	8	565	9	104
050-15		4	2079	216	953	23022	34454	0.19	0.67	0.1033	0.0037	1.0291	0.0353	0.0723	0.0013	0.1676	1684	65	450	8	719	18	63
050-16		8	6929	453	1071	36950	99308	0.12	0.37	0.0649	0.0013	0.7974	0.0166	0.0891	0.0012	0.3921	772	42	550	7	595	9	92
050-17		7	9019	530	635	26018	129592	0.08	0.20	0.0578	0.0015	0.7335	0.0191	0.0921	0.0014	0.3181	522	55	568	8	559	11	102
050-18		2	3204	191	1338	55336	47188	0.06	1.17	0.0593	0.0015	0.7068	0.0182	0.0865	0.0013	0.3059	579	54	535	8	543	11	98
050-19		16	5899	546	1296	22155	87232	0.27	0.25	0.0900	0.0034	1.0043	0.0363	0.0808	0.0014	0.1735	1426	70	501	8	706	18	71
050-20		15	12274	759	563	17495	177268	0.12	0.10	0.0612	0.0012	0.7456	0.0151	0.0884	0.0012	0.3999	646	41	546	7	566	9	97
050-21		0	4136	248	594	21029	58393	0.00	0.36	0.0588	0.0024	0.7656	0.0300	0.0946	0.0017	0.1899	559	85	583	10	577	17	101
050-22		0	1689	108	968	40141	26251	0.00	1.53	0.0628	0.0038	0.7611	0.0440	0.0880	0.0021	0.1148	703	123	544	12	575	25	95
050-23		10	2354	214	1630	54401	34845	0.42	1.56	0.0896	0.0024	1.0625	0.0284	0.0861	0.0013	0.2789	1416	51	532	8	735	14	72
050-24		0	3044	181	1029	40821	42330	0.00	0.96	0.0584	0.0017	0.7399	0.0211	0.0919	0.0014	0.2728	546	61	567	8	562	12	101
050-25		0	1617	100	726	25195	21452	0.00	1.17	0.0597	0.0047	0.7438	0.0561	0.0901	0.0025	0.0809	594	161	556	15	565	33	99
050-26		11	3369	207	1405	56482	50380	0.33	1.12	0.0604	0.0028	0.7532	0.0334	0.0907	0.0018	0.1629	617	95	560	11	570	19	98
050-27		0	1142	74	517	20363	17272	0.00	1.18	0.0639	0.0032	0.7642	0.0373	0.0868	0.0018	0.1334	739	103	536	10	576	21	93
050-28		10	23155	1665	1059	14321	262889	0.04	0.05	0.0707	0.0017	1.1165	0.0274	0.1146	0.0017	0.3272	948	49	699	10	761	13	92
050-29		7	3750	435	1508	32074	65124	0.19	0.49	0.1114	0.0053	1.0653	0.0490	0.0693	0.0014	0.1356	1822	84	432	9	736	24	59
050-30		0	803	53	374	12959	11585	0.00	1.12	0.0647	0.0032	0.7820	0.0375	0.0877	0.0016	0.1397	765	100	542	9	587	21	92

DA13-051 (A)		Mean Counts (background subtracted)								Isotopic Ratios (± 1σ)							Age (Ma ± 1σ)						
Analysis	Core/Rim	^{204}Pb	^{206}Pb	^{207}Pb	^{208}Pb	^{232}Th	^{238}U	(%)^{206} Pb	Th/U	^{207}Pb/^{206}Pb		^{207}Pb/^{235}U		^{206}Pb/^{238}U		Rho	^{207}Pb/^{206}Pb		^{206}Pb/^{238}U		^{207}Pb/^{235}U		%Conc
051-01		20	922	52	261	11211	13805	2.17	0.81	0.0578	0.0031	0.6979	0.0365	0.0877	0.0018	0.1269	520	114	542	11	538	22	101
051-02		19	780	45	423	19069	11356	2.44	1.68	0.0590	0.0030	0.7168	0.0351	0.0881	0.0017	0.1344	568	106	544	10	549	21	99
051-05		10	5614	341	691	25867	85001	0.18	0.30	0.0616	0.0020	0.7476	0.0239	0.0880	0.0015	0.2503	661	67	544	9	567	14	96
051-09	Core	21	890	55	473	20872	12880	2.36	1.62	0.0616	0.0040	0.7392	0.0466	0.0871	0.0021	0.0870	660	135	538	13	562	27	96
051-10	Rim	1	656	39	280	11684	8991	0.15	1.30	0.0599	0.0040	0.7578	0.0492	0.0918	0.0022	0.0886	601	139	566	13	573	28	99
051-11		8	629	35	346	15140	9027	1.27	1.68	0.0568	0.0054	0.7316	0.0665	0.0934	0.0029	0.0618	484	196	576	17	558	39	103
051-12		0	1023	57	599	25920	14857	0.00	1.74	0.0563	0.0024	0.6807	0.0278	0.0877	0.0015	0.1665	464	91	542	9	527	17	103
051-13		0	1981	116	439	17520	27567	0.00	0.64	0.0585	0.0017	0.7156	0.0202	0.0888	0.0013	0.2477	549	61	548	8	548	12	100
051-14		45	6435	501	1489	51196	96133	0.70	0.53	0.0785	0.0025	0.9588	0.0301	0.0886	0.0015	0.2482	1160	62	547	9	683	16	80
051-15	Core	0	823	60	303	13545	11895	0.00	1.14	0.0731	0.0048	0.9020	0.0570	0.0896	0.0024	0.0912	1016	129	553	14	653	30	85
051-16	Rim	0	1284	77	816	35727	18590	0.00	1.92	0.0600	0.0025	0.7191	0.0294	0.0870	0.0016	0.1602	604	88	538	9	550	17	98
051-17		19	3810	231	1245	44957	50082	0.50	0.90	0.0609	0.0021	0.7131	0.0239	0.0850	0.0013	0.1252	635	74	526	8	547	14	96
051-18	Core	0	1090	67	642	28130	16774	0.00	1.68	0.0617	0.0029	0.7097	0.0327	0.0834	0.0016	0.1388	665	99	517	10	545	19	95
051-19	Rim	0	848	65	282	11271	12080	0.00	0.93	0.0761	0.0034	0.9317	0.0406	0.0889	0.0018	0.1403	1096	88	549	10	669	21	82
051-21		12	650	41	220	10120	9297	1.85	1.09	0.0625	0.0043	0.7315	0.0484	0.0850	0.0022	0.0698	690	141	526	13	557	28	94
051-22	Rim	0	527	32	243	9966	7836	0.00	1.27	0.0614	0.0043	0.7090	0.0478	0.0838	0.0021	0.0733	653	143	519	12	544	28	95
051-23	Core	4	992	63	267	10815	15929	0.40	0.68	0.0633	0.0049	0.7329	0.0544	0.0840	0.0024	0.0754	718	157	520	14	558	32	93
051-25		0	1373	92	947	40078	20671	0.00	1.94	0.0667	0.0029	0.7783	0.0327	0.0847	0.0016	0.1510	828	88	524	10	585	19	90
051-27		0	4944	289	308	12727	69242	0.00	0.18	0.0573	0.0014	0.6995	0.0169	0.0885	0.0013	0.2966	504	53	547	8	539	10	102
051-28	Core	4	9852	677	462	14933	152865	0.04	0.10	0.0704	0.0028	0.8378	0.0322	0.0864	0.0016	0.2020	941	78	534	10	618	18	86
051-29	Outer Core	13	894	105	477	15387	12697	1.45	1.21	0.1153	0.0075	1.4324	0.0863	0.0901	0.0027	0.0837	1885	113	556	16	903	36	62
051-30	Rim	1	5730	375	468	15642	82369	0.02	0.19	0.0671	0.0034	0.8585	0.0423	0.0930	0.0020	0.1392	839	103	573	12	629	23	91
051-33		8	1852	114	678	27318	25559	0.43	1.07	0.0612	0.0022	0.7762	0.0274	0.0920	0.0016	0.1985	646	76	567	9	583	16	97
051-35		0	2742	167	901	36481	37218	0.00	0.98	0.0602	0.0015	0.7322	0.0178	0.0882	0.0012	0.2812	612	52	545	7	558	10	98
051-37		0	2742	163	1342	54561	39124	0.00	1.39	0.0593	0.0019	0.7225	0.0230	0.0884	0.0014	0.2289	577	69	546	8	552	14	99
051-38		0	1132	68	758	31788	15634	0.00	2.03	0.0602	0.0020	0.7146	0.0231	0.0861	0.0013	0.1954	611	70	532	8	548	14	97
051-39		12	591	35	336	14347	8314	2.03	1.73	0.0590	0.0043	0.7179	0.0506	0.0882	0.0023	0.0765	568	152	545	14	549	30	99
051-40		0	1646	100	459	18560	22212	0.00	0.84	0.0598	0.0026	0.7281	0.0302	0.0882	0.0016	0.1363	598	90	545	10	555	18	98
051-41		14	391	24	185	7072	4972	3.58	1.42	0.0624	0.0044	0.7716	0.0524	0.0896	0.0021	0.0693	689	143	553	12	581	30	95
051-42		0	1509	85	107	3514	19755	0.00	0.18	0.0561	0.0020	0.6917	0.0242	0.0895	0.0014	0.1682	455	77	552	8	534	15	103
051-45		4	2320	144	131	6000	33996	0.17	0.18	0.0624	0.0029	0.7793	0.0357	0.0906	0.0019	0.1626	687	97	559	11	585	20	96

DA13-051 (A)		Mean Counts (background subtracted)								Isotopic Ratios (± 1σ)							Age (Ma ± 1σ)						
Analysis	Core/Rim	^{204}Pb	^{206}Pb	^{207}Pb	^{208}Pb	^{232}Th	^{238}U	(%)^{206} Pb	Th/U	$^{207}Pb/^{206}Pb$		$^{207}Pb/^{235}U$		$^{206}Pb/^{238}U$		Rho	$^{207}Pb/^{206}Pb$		$^{206}Pb/^{238}U$		$^{207}Pb/^{235}U$		%Conc
051-49		5	314	27	139	5410	4610	1.59	1.17	0.0851	0.0099	1.0830	0.1198	0.0925	0.0037	0.0492	1318	210	570	22	745	58	76
051-50		0	953	59	706	28322	14066	0.00	2.01	0.0606	0.0027	0.6960	0.0308	0.0834	0.0015	0.1440	625	95	516	9	536	18	96
051-51		0	258	15	129	5489	3814	0.00	1.44	0.0580	0.0068	0.6792	0.0780	0.0849	0.0024	0.0450	530	238	526	14	526	47	100
051-52		0	329	19	143	5860	5234	0.00	1.12	0.0558	0.0080	0.6578	0.0917	0.0855	0.0035	0.0395	446	291	529	21	513	56	103
051-53		0	211	15	80	3236	3073	0.00	1.05	0.0694	0.0070	0.8336	0.0828	0.0871	0.0023	0.0537	911	196	538	14	616	46	87
051-54		2	1207	73	742	30091	18044	0.17	1.67	0.0587	0.0021	0.6869	0.0244	0.0849	0.0014	0.2018	554	77	526	8	531	15	99
051-55		0	337	20	214	7902	4607	0.00	1.72	0.0590	0.0060	0.7449	0.0737	0.0916	0.0025	0.0530	567	206	565	15	565	43	100
051-56		12	345	21	154	5608	4892	3.48	1.15	0.0590	0.0055	0.7355	0.0675	0.0905	0.0024	0.0613	566	192	558	14	560	39	100
051-57		0	924	53	302	12071	13846	0.00	0.87	0.0553	0.0033	0.6559	0.0381	0.0860	0.0018	0.1054	426	128	532	11	512	23	104
051-58		0	310	18	154	6654	4289	0.00	1.55	0.0570	0.0051	0.7228	0.0635	0.0920	0.0022	0.0644	490	187	567	13	552	37	103
051-59		0	720	121	516	12266	9751	0.00	1.26	0.1560	0.0128	2.1738	0.1630	0.1011	0.0040	0.0841	2413	132	621	23	1173	52	53
051-60		0	1135	164	538	9478	16021	0.00	0.59	0.1335	0.0180	1.8408	0.2323	0.1002	0.0059	0.0755	2144	219	616	35	1060	83	58

DA14-126 (A)		Mean Counts (background subtracted)								Isotopic Ratios (± 1σ)							Age (Ma ± 1σ)						
Analysis	Core/Rim	^{204}Pb	^{206}Pb	^{207}Pb	^{208}Pb	^{232}Th	^{238}U	(%)^{206} Pb	Th/U	^{207}Pb/^{206}Pb		^{207}Pb/^{235}U		^{206}Pb/^{238}U		Rho	^{207}Pb/^{206}Pb		^{206}Pb/^{238}U		^{207}Pb/^{235}U		%Conc
126-01	Core	299	239389	17558	66876	2358015	3139824	0.12	0.75	0.0740	0.0009	0.8896	0.0120	0.0871	0.0010	0.5191	1043	25	539	6	646	6	83
126-02	Rim	56	12753	953	2639	73278	170352	0.44	0.43	0.0756	0.0014	0.9540	0.0182	0.0915	0.0012	0.3944	1085	37	565	7	680	9	83
126-03		116	659781	40372	325235	10232545	9164506	0.02	1.12	0.0624	0.0009	0.7820	0.0125	0.0909	0.0012	0.5425	689	30	561	7	587	7	96
126-04		60	249295	15048	74373	2383471	3379607	0.02	0.71	0.0611	0.0007	0.7468	0.0102	0.0886	0.0011	0.5653	644	26	547	6	566	6	97
126-05		19	6197	365	1552	49432	80383	0.31	0.61	0.0598	0.0011	0.7350	0.0137	0.0891	0.0011	0.3602	597	39	550	7	560	8	98
126-06		71	640797	38282	232727	8159887	8568489	0.01	0.95	0.0606	0.0008	0.7649	0.0109	0.0915	0.0011	0.5677	625	27	565	7	577	6	98
126-07		56	25954	1778	3486	119476	351824	0.22	0.34	0.0701	0.0014	0.8781	0.0185	0.0909	0.0013	0.3647	931	42	561	7	640	10	88
126-08		41	6469	566	2348	81348	117798	0.63	0.69	0.0888	0.0018	0.8066	0.0163	0.0659	0.0009	0.3500	1400	38	411	5	601	9	68
126-09	Core	669	43469	11811	30722	4268106	2105626	1.54	2.03	0.2766	0.0033	0.8810	0.0113	0.0231	0.0003	0.5057	3344	19	147	2	642	6	23
126-10	Rim	32	11218	1018	3216	226180	264201	0.29	0.86	0.0925	0.0020	0.6611	0.0146	0.0519	0.0007	0.3234	1477	41	326	5	515	9	63
126-11		30	14025	832	2061	68269	177936	0.21	0.38	0.0605	0.0010	0.7567	0.0127	0.0907	0.0011	0.4110	621	35	560	7	572	7	98
126-12	Core	408	578763	39094	301336	10739088	8831865	0.07	1.22	0.0693	0.0010	0.7640	0.0124	0.0800	0.0010	0.4859	907	31	496	6	576	7	86
126-13	Rim	25	8103	550	1925	59437	119993	0.31	0.50	0.0696	0.0023	0.7787	0.0248	0.0812	0.0013	0.1914	916	66	503	8	585	14	86
126-15		10	6718	402	784	25136	75486	0.15	0.33	0.0614	0.0015	0.7522	0.0177	0.0888	0.0011	0.1685	654	52	549	7	570	10	96
126-16		472	287681	23173	50413	2859073	4085836	0.16	0.70	0.0807	0.0010	0.8910	0.0118	0.0801	0.0009	0.5163	1214	24	497	6	647	6	77
126-17		11	6901	414	1275	41924	85853	0.16	0.49	0.0600	0.0012	0.7853	0.0157	0.0950	0.0012	0.3480	603	42	585	7	589	9	99
126-18		58	7351	560	1662	65009	98247	0.79	0.66	0.0760	0.0025	0.9848	0.0312	0.0940	0.0016	0.2201	1096	64	579	9	696	16	83
126-19	Core	540	389853	30020	41477	2419981	6407602	0.14	0.38	0.0758	0.0012	0.8045	0.0136	0.0770	0.0010	0.4954	1090	31	478	6	599	8	80
126-20	Rim	19	6155	365	1166	39996	77607	0.31	0.52	0.0592	0.0016	0.7189	0.0186	0.0880	0.0012	0.2150	575	56	544	7	550	11	99
126-21	Core	71	11278	1758	5629	285841	232373	0.63	1.23	0.1561	0.0030	1.1202	0.0209	0.0520	0.0007	0.2861	2414	33	327	4	763	10	43
126-22	Rim	4	12380	941	3438	121152	184790	0.03	0.66	0.0756	0.0019	0.8800	0.0222	0.0844	0.0013	0.2959	1085	50	522	8	641	12	81
126-23	Core	881	676061	51607	265566	11408982	9997106	0.13	1.14	0.0756	0.0012	0.8875	0.0156	0.0852	0.0011	0.4713	1083	32	527	7	645	8	82
126-24	Rim	26	4944	291	1024	31771	61695	0.53	0.51	0.0591	0.0012	0.7561	0.0152	0.0928	0.0012	0.3391	571	43	572	7	572	9	100
126-25		35	8393	666	2087	67742	119446	0.42	0.57	0.0792	0.0034	0.9745	0.0400	0.0892	0.0018	0.1562	1178	82	551	11	691	21	80
126-26		33	12704	911	1394	53637	215343	0.26	0.25	0.0720	0.0013	0.7103	0.0130	0.0716	0.0009	0.4072	986	35	446	6	545	8	82
126-27		166	213941	14591	60322	4766679	3674408	0.08	1.30	0.0685	0.0011	0.6449	0.0109	0.0683	0.0009	0.4307	885	33	426	5	505	7	84
126-28		49	84709	5431	24212	764339	1141527	0.06	0.67	0.0645	0.0008	0.7692	0.0108	0.0866	0.0010	0.5196	757	27	535	6	579	6	92

DA14-128 (A)		Mean Counts (background subtracted)								Isotopic Ratios (± 1σ)							Age (Ma ± 1σ)						
Analysis	Core/Rim	^{204}Pb	^{206}Pb	^{207}Pb	^{208}Pb	^{232}Th	^{238}U	(%)^{206} Pb	Th/U	^{207}Pb/^{206}Pb		^{207}Pb/^{235}U		^{206}Pb/^{238}U		Rho	^{207}Pb/^{206}Pb		^{206}Pb/^{238}U		^{207}Pb/^{235}U		%Conc
128-01		171	365505	23696	111259	4146698	5095863	0.05	0.81	0.0659	0.0009	0.7997	0.0117	0.0880	0.0011	0.5561	804	27	544	7	597	7	91
128-02		212	541746	34731	160623	6582816	7448507	0.04	0.88	0.0650	0.0008	0.7755	0.0104	0.0865	0.0010	0.5686	774	25	535	6	583	6	92
128-03		170	377570	23917	105666	4490192	5282815	0.05	0.85	0.0643	0.0008	0.7679	0.0107	0.0866	0.0011	0.5710	753	26	535	6	579	6	93
128-04		34	7706	496	1158	43412	105371	0.44	0.41	0.0658	0.0014	0.6987	0.0147	0.0771	0.0010	0.2407	799	45	479	6	538	9	89
128-05		550	934079	60176	224157	20853914	20558648	0.06	1.01	0.0659	0.0009	0.5061	0.0077	0.0557	0.0007	0.5230	803	29	350	4	416	5	84
128-06		18	11204	884	2855	166240	284175	0.16	0.58	0.0805	0.0013	0.5037	0.0082	0.0454	0.0006	0.4204	1208	31	286	3	414	6	69
128-07		12	10324	594	2264	71816	140339	0.12	0.51	0.0589	0.0022	0.7365	0.0264	0.0907	0.0015	0.1814	565	78	560	9	560	15	100
128-08		26	12471	974	2820	98577	233117	0.21	0.42	0.0801	0.0022	0.7254	0.0193	0.0657	0.0010	0.2649	1198	52	410	6	554	11	74
128-10		397	365099	25903	93280	7756880	6980408	0.11	1.11	0.0724	0.0009	0.6187	0.0088	0.0620	0.0008	0.5313	998	26	388	5	489	6	79
128-11		0	9423	599	2115	74564	146030	0.00	0.51	0.0650	0.0015	0.7006	0.0164	0.0782	0.0011	0.3035	775	48	485	7	539	10	90
128-12		20	8297	492	1735	56570	109773	0.24	0.52	0.0608	0.0014	0.7465	0.0174	0.0891	0.0012	0.2860	632	49	550	7	566	10	97
128-13		16	32343	1988	4979	181061	445340	0.05	0.41	0.0633	0.0012	0.7662	0.0149	0.0877	0.0012	0.3803	720	40	542	7	578	9	94
128-14		32	23049	1601	3813	204435	324849	0.14	0.63	0.0711	0.0013	0.8305	0.0152	0.0847	0.0011	0.4067	961	36	524	7	614	8	85
128-15		47	14129	952	2723	80455	186090	0.33	0.43	0.0689	0.0014	0.8610	0.0172	0.0907	0.0012	0.3579	894	40	560	7	631	9	89
128-16		35	275798	16200	101570	3475341	3741524	0.01	0.93	0.0591	0.0008	0.7216	0.0111	0.0886	0.0011	0.4969	569	31	547	7	552	7	99
128-17		16	10982	799	2828	147095	201880	0.15	0.73	0.0740	0.0013	0.6651	0.0122	0.0652	0.0009	0.3963	1041	36	407	5	518	7	79
128-19		45	14317	1255	4981	387888	247203	0.31	1.57	0.0892	0.0019	0.7338	0.0151	0.0597	0.0007	0.2287	1408	40	374	5	559	9	67
128-21		108	162078	10545	51544	3386102	2509588	0.07	1.35	0.0661	0.0008	0.6732	0.0087	0.0739	0.0009	0.5515	810	24	459	5	523	5	88
128-22		134	247711	15973	102367	5137810	4354415	0.05	1.18	0.0654	0.0009	0.6055	0.0088	0.0671	0.0008	0.5169	788	28	419	5	481	6	87
128-23		16	7618	437	1471	47518	100604	0.21	0.47	0.0584	0.0013	0.7278	0.0162	0.0904	0.0012	0.3203	544	48	558	7	555	10	100
128-24		31	11939	938	2926	135544	206175	0.26	0.66	0.0795	0.0020	0.7634	0.0187	0.0697	0.0010	0.2706	1185	48	434	6	576	11	75
128-25		63	8865	615	2092	72333	132015	0.71	0.55	0.0714	0.0026	0.8122	0.0288	0.0825	0.0014	0.1727	969	73	511	9	604	16	85

DA13-004 (M)		Mean Counts (background subtracted)								Isotopic Ratios (± 1σ)							Age (Ma ± 1σ)						
Analysis	Core/Rim	^{204}Pb	^{206}Pb	^{207}Pb	^{208}Pb	^{232}Th	^{238}U	(%)^{206} Pb	Th/U	^{207}Pb/^{206}Pb		^{207}Pb/^{235}U		^{206}Pb/^{238}U		Rho	^{207}Pb/^{206}Pb		^{206}Pb/^{238}U		^{207}Pb/^{235}U		%Conc
004-01		15	17163	1018	1638	62108	254943	0.09	0.24	0.0582	0.0010	0.6855	0.0121	0.0854	0.0011	0.4712	538	36	528	7	530	7	100
004-02		11	34781	2237	19083	900649	567147	0.03	1.59	0.0631	0.0011	0.6887	0.0125	0.0792	0.0011	0.4728	712	35	491	6	532	8	92
004-03		110	34094	2097	17855	731631	518693	0.32	1.41	0.0602	0.0011	0.6972	0.0134	0.0841	0.0012	0.4369	609	39	521	7	537	8	97
004-04		0	35461	2189	15619	655426	574892	0.00	1.14	0.0600	0.0016	0.7116	0.0194	0.0860	0.0014	0.3277	605	57	532	8	546	12	97
004-05		17	44821	2716	17667	732896	702891	0.04	1.04	0.0589	0.0010	0.6862	0.0131	0.0845	0.0012	0.4657	564	38	523	7	531	8	99
004-06		2	24401	1545	13190	599500	370612	0.01	1.62	0.0612	0.0010	0.7197	0.0127	0.0853	0.0012	0.4897	647	35	528	7	551	8	96
004-07		0	23183	1411	5040	232177	358875	0.00	0.65	0.0592	0.0011	0.6959	0.0142	0.0852	0.0012	0.4317	576	41	527	7	536	9	98
004-08		39	16141	1232	6233	926724	369795	0.24	2.51	0.0744	0.0021	0.5728	0.0165	0.0559	0.0008	0.2880	1052	56	350	5	460	11	76
004-09		2	27501	1683	7041	305289	415518	0.01	0.73	0.0595	0.0010	0.6992	0.0126	0.0852	0.0012	0.4728	587	36	527	7	538	8	98
004-11		20	10152	650	1842	188034	167359	0.20	1.12	0.0621	0.0013	0.6751	0.0146	0.0789	0.0011	0.3927	678	44	489	7	524	9	93
004-12		14	6954	640	3917	448957	173868	0.20	2.58	0.0899	0.0024	0.6246	0.0167	0.0505	0.0008	0.2798	1422	51	318	5	493	10	64
004-13		0	28744	1922	16078	628108	449134	0.00	1.40	0.0643	0.0011	0.7377	0.0137	0.0833	0.0012	0.4694	750	36	516	7	561	8	92
004-14		28	21489	1377	8035	456399	333060	0.13	1.37	0.0619	0.0011	0.7076	0.0130	0.0830	0.0011	0.4612	671	36	514	7	543	8	95
004-15		0	21263	1331	2924	134934	323573	0.00	0.42	0.0615	0.0010	0.6918	0.0122	0.0817	0.0011	0.4620	655	35	506	6	534	7	95
004-16		0	12702	869	5439	224550	204614	0.00	1.10	0.0672	0.0013	0.7443	0.0149	0.0803	0.0011	0.4183	845	39	498	7	565	9	88
004-17		0	44563	2854	23854	1077792	694914	0.00	1.55	0.0628	0.0010	0.7181	0.0127	0.0829	0.0011	0.4787	703	34	513	7	550	8	93
004-18		0	7184	491	1784	175425	92984	0.00	1.89	0.0680	0.0016	0.7849	0.0184	0.0838	0.0011	0.2321	868	49	519	7	588	10	88
004-19		21	10914	813	4555	230769	204182	0.19	1.13	0.0724	0.0022	0.7269	0.0220	0.0729	0.0012	0.2618	996	61	453	7	555	13	82
004-20		1	20296	1369	14072	646669	288316	0.00	2.24	0.0664	0.0010	0.7865	0.0129	0.0859	0.0011	0.4719	820	32	531	7	589	7	90
004-21		4	8558	550	2154	195429	123862	0.05	1.58	0.0636	0.0020	0.6837	0.0206	0.0780	0.0012	0.1754	729	65	484	7	529	12	92
004-22		5	14579	1150	7442	356006	185147	0.03	1.92	0.0794	0.0022	0.8923	0.0232	0.0815	0.0011	0.1670	1183	53	505	7	648	12	78
004-23		0	17188	1067	3512	99045	170389	0.00	0.58	0.0617	0.0013	0.9172	0.0189	0.1078	0.0013	0.2626	664	45	660	8	661	10	100
004-24		21	16803	1172	8047	339510	245000	0.12	1.39	0.0686	0.0012	0.7668	0.0137	0.0810	0.0010	0.3983	888	36	502	6	578	8	87
004-25		0	16532	1099	5319	591619	279825	0.00	2.11	0.0652	0.0011	0.6393	0.0110	0.0711	0.0009	0.4233	780	34	443	6	502	7	88
004-26		25	21287	1375	9257	577071	342544	0.12	1.68	0.0635	0.0012	0.6729	0.0130	0.0768	0.0010	0.3920	726	39	477	6	523	8	91
004-27		1	9384	719	6860	754810	141135	0.01	5.35	0.0777	0.0026	0.7275	0.0234	0.0679	0.0010	0.1118	1140	66	423	6	555	14	76
004-28		4	8950	546	3653	146038	125900	0.04	1.16	0.0599	0.0012	0.7008	0.0140	0.0849	0.0011	0.3531	599	42	525	7	539	8	97
004-29	Core	1	7046	453	1832	59864	79320	0.01	0.75	0.0632	0.0013	0.9237	0.0190	0.1061	0.0014	0.3351	714	43	650	8	664	10	98
004-30	Rim	12	6742	453	1067	37512	91107	0.18	0.41	0.0657	0.0016	0.7861	0.0184	0.0868	0.0012	0.2721	797	49	536	7	589	10	91
004-31		6	19454	1217	12311	542835	314977	0.03	1.72	0.0630	0.0013	0.7240	0.0154	0.0834	0.0012	0.4370	708	42	517	7	553	9	93
004-32		2	8794	530	2147	126366	135062	0.02	0.94	0.0609	0.0012	0.7159	0.0151	0.0853	0.0012	0.4159	636	43	528	7	548	9	96

DA13-004 (M)		Mean Counts (background subtracted)								Isotopic Ratios (± 1σ)							Age (Ma ± 1σ)						
Analysis	Core/Rim	^{204}Pb	^{206}Pb	^{207}Pb	^{208}Pb	^{232}Th	^{238}U	(%)^{206} Pb	Th/U	^{207}Pb/^{206}Pb		^{207}Pb/^{235}U		^{206}Pb/^{238}U		Rho	^{207}Pb/^{206}Pb		^{206}Pb/^{238}U		^{207}Pb/^{235}U		%Conc
004-33		1	16161	1009	4203	230098	246325	0.01	0.93	0.0627	0.0010	0.7355	0.0127	0.0852	0.0012	0.5108	697	33	527	7	560	7	94
004-34		14	13188	834	5055	299357	211389	0.11	1.42	0.0636	0.0011	0.7234	0.0140	0.0825	0.0012	0.4705	729	37	511	7	553	8	92
004-35		11	8198	570	1781	262266	119387	0.13	2.20	0.0715	0.0019	0.7903	0.0207	0.0802	0.0012	0.2400	970	54	497	7	591	12	84
004-36		26	100917	6191	97545	4444423	1608775	0.03	2.76	0.0618	0.0013	0.7341	0.0160	0.0863	0.0013	0.4439	666	43	534	8	559	9	95
004-37		9	18861	1194	11820	778296	310703	0.05	2.50	0.0643	0.0012	0.7138	0.0142	0.0806	0.0012	0.4546	751	39	500	7	547	8	91
004-38		0	7383	612	2634	115086	109308	0.00	1.05	0.0837	0.0016	1.0278	0.0212	0.0892	0.0013	0.4278	1285	37	551	8	718	11	77
004-39		21	28790	1951	26400	1453194	493661	0.07	2.94	0.0677	0.0019	0.7667	0.0225	0.0822	0.0014	0.3299	858	59	509	8	578	13	88
004-40		24	11085	796	4783	253215	181791	0.22	1.39	0.0729	0.0018	0.8021	0.0201	0.0798	0.0012	0.3376	1012	49	495	7	598	11	83
004-41		1	12703	858	6541	388355	206915	0.01	1.88	0.0681	0.0012	0.7595	0.0149	0.0809	0.0012	0.4585	873	37	501	7	574	9	87
004-42	Core	19	31784	4421	5310	116981	196087	0.06	0.60	0.1405	0.0026	3.9143	0.0749	0.2021	0.0028	0.4209	2233	31	1187	15	1617	15	73
004-43	Rim	20	30890	2191	28507	1548913	541881	0.06	2.86	0.0712	0.0021	0.7922	0.0238	0.0807	0.0014	0.3338	963	59	500	8	592	14	84
004-44		0	14755	880	2077	81377	219223	0.00	0.37	0.0604	0.0012	0.7184	0.0146	0.0863	0.0012	0.4237	617	41	534	7	550	9	97
004-45		0	11602	684	2570	104024	172836	0.00	0.60	0.0601	0.0011	0.7057	0.0135	0.0852	0.0012	0.4397	606	38	527	7	542	8	97
004-46		0	5598	531	3618	135210	101794	0.00	1.33	0.0966	0.0027	0.8231	0.0225	0.0618	0.0009	0.1993	1559	52	387	6	610	13	63
004-46		8	4643	469	963	101879	51394	0.17	1.98	0.1033	0.0060	1.6214	0.0900	0.1143	0.0029	0.1266	1684	103	698	17	979	35	71
004-47	Core	0	7681	1252	1236	42968	24478	0.00	1.76	0.1649	0.0028	8.4131	0.1490	0.3701	0.0049	0.4103	2507	29	2030	23	2277	16	89
004-48	Rim	0	7258	460	1693	53114	99709	0.00	0.53	0.0640	0.0012	0.7585	0.0145	0.0860	0.0011	0.3774	740	39	532	7	573	8	93
004-49		5	8147	477	6838	327289	110860	0.06	2.95	0.0594	0.0014	0.7261	0.0169	0.0888	0.0012	0.3088	581	49	548	7	554	10	99
004-50		4	6075	367	1854	79090	84681	0.07	0.93	0.0611	0.0014	0.7273	0.0166	0.0864	0.0012	0.3183	643	48	534	7	555	10	96
004-51		0	5816	360	1086	53843	75046	0.00	0.72	0.0642	0.0025	0.7681	0.0283	0.0868	0.0014	0.1336	749	79	537	9	579	16	93
004-52		0	8895	665	3798	451660	133669	0.00	3.38	0.0758	0.0014	0.8201	0.0151	0.0785	0.0010	0.3853	1090	35	487	6	608	8	80
004-53		19	7686	466	3263	129196	102704	0.25	1.26	0.0614	0.0013	0.7547	0.0160	0.0892	0.0012	0.3408	652	44	551	7	571	9	96
004-54		5	10013	634	6413	229879	134248	0.05	1.71	0.0643	0.0013	0.7880	0.0159	0.0889	0.0012	0.3607	751	41	549	7	590	9	93
004-55		0	10171	600	5660	227588	135526	0.00	1.68	0.0600	0.0012	0.7278	0.0143	0.0881	0.0011	0.3523	602	41	544	7	555	8	98
004-56		0	9655	557	652	34182	130708	0.00	0.26	0.0587	0.0011	0.7018	0.0139	0.0868	0.0011	0.3517	555	42	537	7	540	8	99
004-57		10	6618	397	2541	92408	86914	0.15	1.06	0.0611	0.0013	0.7528	0.0156	0.0894	0.0012	0.3326	642	43	552	7	570	9	97
004-58		0	10518	664	4288	148434	135923	0.00	1.09	0.0648	0.0018	0.7716	0.0207	0.0864	0.0012	0.2025	767	57	534	7	581	12	92
004-59		0	11499	770	7786	289500	159017	0.00	1.82	0.0673	0.0021	0.7728	0.0229	0.0833	0.0013	0.1950	846	62	516	7	581	13	89
004-60		0	13789	964	9315	389734	210444	0.00	1.85	0.0711	0.0017	0.7751	0.0181	0.0791	0.0011	0.3072	960	47	491	7	583	10	84

DA13-006 (M)		Mean Counts (background subtracted)								Isotopic Ratios (± 1σ)							Age (Ma ± 1σ)						
Analysis	Core/Rim	^{204}Pb	^{206}Pb	^{207}Pb	^{208}Pb	^{232}Th	^{238}U	(%)^{206} Pb	Th/U	$^{207}Pb/^{206}Pb$		$^{207}Pb/^{235}U$		$^{206}Pb/^{238}U$		Rho	$^{207}Pb/^{206}Pb$		$^{206}Pb/^{238}U$		$^{207}Pb/^{235}U$		%Conc
006-01		5	4509	264	556	23196	67783	0.11	0.34	0.0578	0.0013	0.6566	0.0152	0.0824	0.0012	0.3284	522	50	511	7	513	9	100
006-02		0	2122	127	815	35188	32167	0.00	1.09	0.0593	0.0018	0.6701	0.0200	0.0820	0.0013	0.2327	578	64	508	8	521	12	98
006-03		1	2638	157	1239	52073	40615	0.04	1.28	0.0592	0.0017	0.6541	0.0183	0.0801	0.0012	0.2553	576	60	497	7	511	11	97
006-04		0	2212	135	925	40821	34542	0.00	1.18	0.0604	0.0021	0.6464	0.0215	0.0776	0.0013	0.1925	618	72	482	8	506	13	95
006-05		2	1331	85	444	18512	19723	0.15	0.94	0.0630	0.0028	0.6928	0.0294	0.0798	0.0015	0.1292	707	91	495	9	535	18	93
006-06		13	1740	102	513	20901	26583	0.75	0.79	0.0584	0.0016	0.6282	0.0175	0.0780	0.0011	0.2405	545	60	484	7	495	11	98
006-07		0	1390	83	493	21346	20882	0.00	1.02	0.0599	0.0021	0.6587	0.0226	0.0798	0.0013	0.1896	598	74	495	8	514	14	96
006-08		11	2991	171	1691	74737	45911	0.37	1.63	0.0569	0.0015	0.6284	0.0170	0.0801	0.0012	0.2663	486	59	497	7	495	11	100
006-09		3	1132	72	425	17384	17896	0.27	0.97	0.0636	0.0033	0.7278	0.0365	0.0831	0.0018	0.1282	728	106	514	10	555	21	93
006-10		31	1875	119	486	18450	26689	1.65	0.69	0.0636	0.0022	0.6778	0.0228	0.0774	0.0012	0.1516	727	72	480	7	526	14	91
006-11		4	1438	86	662	25474	19074	0.28	1.34	0.0603	0.0019	0.7408	0.0224	0.0891	0.0013	0.2106	616	65	550	8	563	13	98
006-12		19	2521	151	962	38275	34582	0.75	1.11	0.0575	0.0041	0.6686	0.0462	0.0844	0.0023	0.0832	511	151	522	13	520	28	100
006-13		19	7260	421	962	40852	105782	0.26	0.39	0.0576	0.0013	0.6825	0.0159	0.0859	0.0012	0.3355	516	50	531	7	528	10	101
006-14		6	3108	186	799	35953	51213	0.19	0.70	0.0605	0.0022	0.6619	0.0233	0.0794	0.0014	0.2204	620	75	493	8	516	14	96
006-15		3	2266	135	919	40305	34270	0.13	1.18	0.0600	0.0017	0.6575	0.0185	0.0796	0.0012	0.2486	602	60	494	7	513	11	96
006-16		7	1668	91	346	13102	22889	0.42	0.57	0.0530	0.0026	0.6183	0.0289	0.0847	0.0016	0.1084	328	106	524	9	489	18	107
006-17		7	1931	133	688	27462	28731	0.36	0.96	0.0698	0.0029	0.8248	0.0330	0.0857	0.0016	0.1680	922	83	530	10	611	18	87
006-18		0	4727	276	725	29761	65958	0.00	0.45	0.0580	0.0014	0.6816	0.0161	0.0852	0.0012	0.2817	530	52	527	7	528	10	100
006-19		0	2293	136	727	31895	34726	0.00	0.92	0.0587	0.0020	0.6447	0.0209	0.0796	0.0013	0.1951	557	71	494	8	505	13	98
006-20		13	3455	212	1524	64222	53129	0.38	1.21	0.0607	0.0016	0.6784	0.0181	0.0810	0.0012	0.2602	630	57	502	7	526	11	95
006-21		0	5058	330	2203	87985	75045	0.00	1.17	0.0647	0.0014	0.7264	0.0158	0.0814	0.0011	0.3202	764	45	505	7	554	9	91
006-22		0	1674	106	859	35118	25518	0.00	1.38	0.0619	0.0031	0.6658	0.0320	0.0780	0.0016	0.0968	671	104	484	9	518	20	93
006-24		0	3089	198	927	37548	46760	0.00	0.80	0.0643	0.0022	0.7439	0.0243	0.0840	0.0014	0.2040	751	69	520	8	565	14	92
006-25		6	4592	280	1158	45704	67889	0.13	0.67	0.0609	0.0016	0.6884	0.0174	0.0820	0.0012	0.2610	635	54	508	7	532	10	96
006-26		15	4352	475	1012	16721	66120	0.34	0.25	0.1096	0.0050	1.2560	0.0540	0.0831	0.0018	0.1306	1792	80	515	10	826	24	62
006-27		3	1775	104	319	13631	26624	0.17	0.51	0.0580	0.0017	0.6206	0.0176	0.0777	0.0011	0.2081	528	63	482	7	490	11	98
006-28		4	1925	123	549	22234	26981	0.21	0.82	0.0632	0.0022	0.6743	0.0227	0.0774	0.0012	0.1344	714	73	481	7	523	14	92
006-29		0	1038	62	441	18626	15128	0.00	1.23	0.0601	0.0022	0.6550	0.0237	0.0790	0.0013	0.1529	608	79	490	8	512	15	96
006-30		0	1566	96	302	12028	21043	0.00	0.57	0.0603	0.0037	0.6957	0.0406	0.0837	0.0019	0.0646	615	127	518	11	536	24	97
006-31		0	1588	108	720	30325	24397	0.00	1.24	0.0691	0.0024	0.8145	0.0279	0.0855	0.0015	0.2216	901	70	529	9	605	16	87
006-32		0	1745	107	810	32413	26069	0.00	1.24	0.0619	0.0019	0.7427	0.0226	0.0871	0.0014	0.2553	669	64	538	8	564	13	95

DA13-006 (M)		Mean Counts (background subtracted)								Isotopic Ratios (± 1σ)							Age (Ma ± 1σ)						
Analysis	Core/Rim	^{204}Pb	^{206}Pb	^{207}Pb	^{208}Pb	^{232}Th	^{238}U	(%)^{206} Pb	Th/U	^{207}Pb/^{206}Pb		^{207}Pb/^{235}U		^{206}Pb/^{238}U		Rho	^{207}Pb/^{206}Pb		^{206}Pb/^{238}U		^{207}Pb/^{235}U		%Conc
006-33		0	2742	159	712	29395	40606	0.00	0.72	0.0584	0.0014	0.7146	0.0180	0.0887	0.0013	0.3356	546	53	548	8	548	11	100
006-34		12	9343	580	1874	78918	155777	0.13	0.51	0.0628	0.0016	0.7170	0.0186	0.0829	0.0013	0.3555	700	53	513	8	549	11	93
006-35		14	4410	304	1451	56976	66005	0.32	0.86	0.0698	0.0018	0.8408	0.0214	0.0873	0.0013	0.3172	924	51	540	8	620	12	87
006-36		3	1272	84	479	20738	21196	0.24	0.98	0.0670	0.0038	0.7711	0.0415	0.0835	0.0020	0.1258	839	112	517	12	580	24	89
006-37		13	1920	114	942	39833	30498	0.68	1.31	0.0609	0.0021	0.7014	0.0240	0.0836	0.0015	0.2283	635	73	518	9	540	14	96
006-38		0	1758	102	541	21630	26632	0.00	0.81	0.0588	0.0029	0.7235	0.0349	0.0893	0.0019	0.1434	561	105	551	11	553	21	100
006-39		0	1287	79	618	26514	20871	0.00	1.27	0.0617	0.0028	0.7172	0.0321	0.0843	0.0017	0.1662	665	96	522	10	549	19	95
006-40	Core	4	1832	108	390	15403	27582	0.22	0.56	0.0591	0.0018	0.7142	0.0214	0.0876	0.0014	0.2717	572	64	541	8	547	13	99
006-41	Rim	21	2331	179	653	25532	37310	0.90	0.68	0.0778	0.0023	0.9010	0.0263	0.0841	0.0014	0.2853	1141	57	520	8	652	14	80
006-42		5	5095	293	1251	50460	74491	0.10	0.68	0.0578	0.0012	0.7034	0.0148	0.0883	0.0013	0.4017	521	44	546	7	541	9	101
006-43		3	1524	95	480	20394	24134	0.20	0.85	0.0631	0.0022	0.7359	0.0257	0.0846	0.0015	0.2209	711	74	524	9	560	15	94
006-44		4	1555	91	491	22103	25053	0.26	0.88	0.0597	0.0035	0.7056	0.0399	0.0858	0.0020	0.1179	593	122	531	12	542	24	98
006-45		0	1840	111	476	20871	29945	0.00	0.70	0.0606	0.0028	0.7068	0.0314	0.0846	0.0017	0.1655	625	96	524	10	543	19	96
006-46		0	646	35	311	11338	8673	0.00	1.31	0.0563	0.0030	0.6701	0.0353	0.0863	0.0015	0.1002	464	116	534	9	521	21	102
006-47		0	1062	60	255	9332	14688	0.00	0.64	0.0581	0.0023	0.6810	0.0267	0.0850	0.0014	0.1579	534	86	526	8	527	16	100
006-48		5	573	67	282	7882	8038	0.87	0.98	0.1210	0.0081	1.4623	0.0909	0.0876	0.0026	0.0819	1972	114	542	15	915	37	59
006-49		5	690	39	254	9107	9157	0.72	0.99	0.0585	0.0032	0.6960	0.0367	0.0863	0.0015	0.1045	547	114	534	9	536	22	100
006-50		8	518	28	231	8582	6577	1.54	1.30	0.0564	0.0071	0.6714	0.0815	0.0864	0.0031	0.0381	465	256	535	18	522	49	102
006-51		3	593	41	307	11169	8663	0.51	1.29	0.0712	0.0043	0.8012	0.0472	0.0816	0.0018	0.0872	963	120	506	10	598	27	85
006-52		4	2218	127	553	18723	28984	0.18	0.65	0.0588	0.0016	0.7206	0.0192	0.0888	0.0012	0.2462	561	58	549	7	551	11	100
006-53		5	406	20	105	4413	5736	1.23	0.77	0.0506	0.0044	0.5787	0.0499	0.0830	0.0017	0.0580	221	190	514	10	464	32	111
006-54		0	762	48	353	13010	10645	0.00	1.22	0.0641	0.0029	0.7425	0.0327	0.0840	0.0015	0.1268	745	93	520	9	564	19	92
006-55		0	423	23	115	4317	5659	0.00	0.76	0.0568	0.0045	0.6883	0.0529	0.0878	0.0019	0.0693	485	165	543	11	532	32	102
006-56		0	786	48	370	12955	10747	0.00	1.21	0.0627	0.0037	0.7635	0.0433	0.0884	0.0019	0.1005	697	120	546	11	576	25	95
006-57		5	2175	141	108	2521	29516	0.23	0.09	0.0664	0.0018	0.7848	0.0207	0.0858	0.0012	0.2443	817	55	531	7	588	12	90
006-60		7	5923	373	1092	38334	84016	0.12	0.46	0.0649	0.0021	0.7706	0.0239	0.0861	0.0014	0.2216	772	65	533	8	580	14	92

Appendix 5.3

SHRIMP SI and SHRIMP II oxygen isotope data
(Ambalavao and Maevarano Suites)

			Age (Ma)				$^{18}O/^{16}O$ Data			
Analysis	Suite	Domain	$^{206}Pb/^{238}U$	± 2σ	W.A Age	± 2σ	$^{18}O/^{16}O$	1σ	$^{18}O/^{16}O$ (‰)	± 2σ
DA13-004-49	Maevarano	Antananarivo	548	7	531	6	0.0020369	0.0000003	8.29	0.14
DA13-004-50	Maevarano	Antananarivo	534	7	531	6	0.0020327	0.0000003	6.21	0.14
DA13-004-53	Maevarano	Antananarivo	551	7	531	6	0.0020323	0.0000003	6.02	0.17
DA13-004-55	Maevarano	Antananarivo	544	7	531	6	0.0020292	0.0000003	4.49	0.14
DA13-004-56	Maevarano	Antananarivo	537	7	531	6	0.0020303	0.0000002	5.01	0.12
DA13-004-57	Maevarano	Antananarivo	552	7	531	6	0.0020326	0.0000004	6.16	0.19
DA13-006-47	Maevarano	Antananarivo	526	8	535	5	0.0020340	0.0000003	6.86	0.17
DA13-006-49	Maevarano	Antananarivo	534	9	535	5	0.0020351	0.0000003	7.40	0.15
DA13-006-50	Maevarano	Antananarivo	535	18	535	5	0.0020345	0.0000003	7.09	0.13
DA13-006-52	Maevarano	Antananarivo	549	7	535	5	0.0020359	0.0000003	7.75	0.15
DA13-006-55	Maevarano	Antananarivo	543	11	535	5	0.0020340	0.0000003	6.82	0.16
DA13-006-56	Maevarano	Antananarivo	546	11	535	5	0.0020358	0.0000004	7.73	0.19
DA13-010-09	Ambalavao	Antananarivo	538	8	544	5	0.0020359	0.0000004	7.79	0.20
DA13-010-12	Ambalavao	Antananarivo	556	11	544	5	0.0020347	0.0000003	7.17	0.15
DA13-010-14	Ambalavao	Antananarivo	532	11	544	5	0.0020340	0.0000003	6.82	0.13
DA13-010-15	Ambalavao	Antananarivo	536	13	544	5	0.0020332	0.0000003	6.45	0.15
DA13-010-45	Ambalavao	Antananarivo	532	9	544	5	0.0020341	0.0000003	6.91	0.14
DA13-018-06	Ambalavao	Antananarivo	561	7	580	8	0.0020311	0.0000002	5.41	0.12
DA13-018-12	Ambalavao	Antananarivo	581	7	580	8	0.0020314	0.0000003	5.56	0.15
DA13-018-13	Ambalavao	Antananarivo	588	7	580	8	0.0020306	0.0000003	5.18	0.14
DA13-018-20	Ambalavao	Antananarivo	581	7	580	8	0.0020327	0.0000003	6.23	0.13
DA13-018-22	Ambalavao	Antananarivo	590	7	580	8	0.0020311	0.0000003	5.41	0.15
DA13-018-27	Ambalavao	Antananarivo	558	7	580	8	0.0020272	0.0000004	3.52	0.21
DA13-037-02	Ambalavao	Antananarivo	557	8	549	9	0.0020504	0.0000001	8.22	0.28
DA13-037-04	Ambalavao	Antananarivo	555	8	549	9	0.0020485	0.0000001	7.27	0.28
DA13-037-05	Ambalavao	Antananarivo	553	8	549	9	0.0020443	0.0000001	5.25	0.28
DA13-037-13	Ambalavao	Antananarivo	539	8	549	9	0.0020481	0.0000002	7.07	0.28
DA13-037-19	Ambalavao	Antananarivo	538	7	549	9	0.0020469	0.0000002	6.49	0.28
DA13-037-26	Ambalavao	Antananarivo	558	8	549	9	0.0020481	0.0000001	7.11	0.28
DA13-037-29	Ambalavao	Antananarivo	556	8	549	9	0.0020412	0.0000001	3.74	0.28
DA13-038-03	Ambalavao	Antananarivo	524	7	544	7	0.0020455	0.0000002	5.82	0.28
DA13-038-04	Ambalavao	Antananarivo	548	8	544	7	0.0020454	0.0000001	5.75	0.28
DA13-038-08	Ambalavao	Antananarivo	534	9	544	7	0.0020449	0.0000001	5.51	0.28
DA13-038-10	Ambalavao	Antananarivo	512	7	544	7	0.0020446	0.0000002	5.36	0.28
DA13-038-12	Ambalavao	Antananarivo	530	9	544	7	0.0020449	0.0000002	5.55	0.28
DA13-038-31	Ambalavao	Antananarivo	546	11	544	7	0.0020456	0.0000001	5.86	0.28
DA13-038-32	Ambalavao	Antananarivo	549	9	544	7	0.0020461	0.0000002	6.12	0.28
DA13-038-34	Ambalavao	Antananarivo	594	9	544	7	0.0020457	0.0000002	5.92	0.28
DA13-038-35	Ambalavao	Antananarivo	563	8	544	7	0.0020451	0.0000001	5.63	0.28
DA13-038-36	Ambalavao	Antananarivo	599	9	544	7	0.0020433	0.0000001	4.76	0.28
DA13-038-38	Ambalavao	Antananarivo	568	8	544	7	0.0020439	0.0000001	5.03	0.28
DA13-038-40	Ambalavao	Antananarivo	550	8	544	7	0.0020459	0.0000001	5.99	0.28
DA13-038-42	Ambalavao	Antananarivo	532	9	544	7	0.0020432	0.0000001	4.69	0.28
DA13-038-45	Ambalavao	Antananarivo	548	8	544	7	0.0020463	0.0000001	6.19	0.28
DA13-041-07	Ambalavao	Antananarivo	556	9	550	8	0.0020401	0.0000001	3.17	0.27
DA13-041-08	Ambalavao	Antananarivo	540	10	550	8	0.0020485	0.0000001	7.28	0.28
DA13-041-10	Ambalavao	Antananarivo	552	8	550	8	0.0020462	0.0000001	6.17	0.28
DA13-041-11	Ambalavao	Antananarivo	547	9	550	8	0.0020484	0.0000002	7.24	0.28
DA13-072-01	Ambalavao	Antananarivo	552	8	544	4	0.0020477	0.0000002	6.89	0.28
DA13-072-04	Ambalavao	Antananarivo	535	8	544	4	0.0020461	0.0000001	6.13	0.28
DA13-072-06	Ambalavao	Antananarivo	538	7	544	4	0.0020464	0.0000001	6.28	0.28
DA13-072-08	Ambalavao	Antananarivo	559	11	544	4	0.0020480	0.0000002	7.02	0.28
DA13-072-09	Ambalavao	Antananarivo	535	10	544	4	0.0020461	0.0000002	6.10	0.28
DA13-072-13	Ambalavao	Antananarivo	536	9	544	4	0.0020474	0.0000002	6.73	0.28
DA13-072-15	Ambalavao	Antananarivo	549	12	544	4	0.0020478	0.0000001	6.97	0.28
DA13-072-16	Ambalavao	Antananarivo	538	8	544	4	0.0020471	0.0000001	6.59	0.28
DA13-072-17	Ambalavao	Antananarivo	544	10	544	4	0.0020482	0.0000002	7.12	0.28

			Age (Ma)				$^{18}O/^{16}O$ Data			
Analysis	Suite	Domain	$^{206}Pb/^{238}U$	± 2σ	W.A Age	± 2σ	$^{18}O/^{16}O$	1σ	$^{18}O/^{16}O$ (‰)	± 2σ
DA13-072-19	Ambalavao	Antananarivo	546	8	544	4	0.0020474	0.0000001	6.75	0.28
DA13-072-20	Ambalavao	Antananarivo	563	10	544	4	0.0020470	0.0000001	6.55	0.27
DA13-072-21	Ambalavao	Antananarivo	547	8	544	4	0.0020475	0.0000001	6.80	0.28
DA13-072-22	Ambalavao	Antananarivo	544	9	544	4	0.0020478	0.0000001	6.93	0.28
DA13-072-23	Ambalavao	Antananarivo	545	9	544	4	0.0020461	0.0000001	6.13	0.28
DA13-072-24	Ambalavao	Antananarivo	543	7	544	4	0.0020441	0.0000002	5.16	0.28
DA13-072-25	Ambalavao	Antananarivo	541	8	544	4	0.0020466	0.0000002	6.36	0.28
DA13-072-26	Ambalavao	Antananarivo	541	11	544	4	0.0020471	0.0000002	6.60	0.28
DA13-072-27	Ambalavao	Antananarivo	535	8	544	4	0.0020476	0.0000002	6.83	0.28
DA13-072-28	Ambalavao	Antananarivo	558	8	544	4	0.0020469	0.0000001	6.50	0.28
DA13-072-29	Ambalavao	Antananarivo	539	9	544	4	0.0020471	0.0000001	6.58	0.28
DA13-072-30	Ambalavao	Antananarivo	576	10	544	4	0.0020476	0.0000001	6.83	0.28
DA13-050-17	Ambalavao	Itremo	568	8	570	8	0.0020362	0.0000004	7.93	0.19
DA13-050-18	Ambalavao	Itremo	535	8	570	8	0.0020321	0.0000003	5.90	0.16
DA13-050-24	Ambalavao	Itremo	567	8	570	8	0.0020345	0.0000003	7.07	0.14
DA13-050-25	Ambalavao	Itremo	556	15	570	8	0.0020346	0.0000004	7.16	0.18
DA13-050-26	Ambalavao	Itremo	560	11	570	8	0.0020359	0.0000004	7.78	0.21
DA13-050-27	Ambalavao	Itremo	536	10	570	8	0.0020350	0.0000003	7.33	0.15
DA13-051-50	Ambalavao	Itremo	516	9	581	33	0.0020335	0.0000003	6.62	0.16
DA13-051-51	Ambalavao	Itremo	526	14	581	33	0.0020341	0.0000003	6.89	0.16
DA13-051-52	Ambalavao	Itremo	529	21	581	33	0.0020339	0.0000003	6.79	0.14
DA13-051-54	Ambalavao	Itremo	526	8	581	33	0.0020321	0.0000003	5.92	0.15
DA13-051-57	Ambalavao	Itremo	532	11	581	33	0.0020335	0.0000003	6.58	0.14
DA13-051-58	Ambalavao	Itremo	567	13	581	33	0.0020336	0.0000003	6.66	0.14
DA14-126-03	Ambalavao	Ikalamavony	561	7	559	10	0.0020299	0.0000004	5.05	0.53
DA14-126-04	Ambalavao	Ikalamavony	547	6	559	10	0.0020312	0.0000005	5.68	0.56
DA14-126-05	Ambalavao	Ikalamavony	550	7	559	10	0.0020306	0.0000005	5.36	0.54
DA14-126-06	Ambalavao	Ikalamavony	565	7	559	10	0.0020299	0.0000005	5.02	0.56
DA14-126-11	Ambalavao	Ikalamavony	560	7	559	10	0.0020296	0.0000004	4.87	0.52
DA14-126-15	Ambalavao	Ikalamavony	549	7	559	10	0.0020306	0.0000005	5.38	0.54
DA14-126-17	Ambalavao	Ikalamavony	585	7	559	10	0.0020310	0.0000004	5.58	0.54
DA14-126-20	Ambalavao	Ikalamavony	544	7	559	10	0.0020313	0.0000005	5.75	0.56
DA14-126-24	Ambalavao	Ikalamavony	572	7	559	10	0.0020303	0.0000005	5.24	0.54
DA14-126-28	Ambalavao	Ikalamavony	535	6	559	10	0.0020272	0.0000004	3.68	0.53
DA14-128-01	Ambalavao	Ikalamavony	544	7	545	7	0.0020299	0.0000004	5.04	0.53
DA14-128-02	Ambalavao	Ikalamavony	535	6	545	7	0.0020298	0.0000003	4.99	0.51
DA14-128-03	Ambalavao	Ikalamavony	535	6	545	7	0.0020321	0.0000004	6.11	0.52
DA14-128-12	Ambalavao	Ikalamavony	550	7	545	7	0.0020299	0.0000005	5.04	0.56
DA14-128-13	Ambalavao	Ikalamavony	542	7	545	7	0.0020302	0.0000004	5.21	0.53
DA14-128-16	Ambalavao	Ikalamavony	547	7	545	7	0.0020302	0.0000004	5.16	0.54
DA14-128-23	Ambalavao	Ikalamavony	558	7	545	7	0.0020305	0.0000006	5.31	0.56

Appendix 5.4

MC-LA-ICP-MS hafnium isotope data
(Ambalavao and Maevarano Suites)

			Age (Ma)				Hafnium Data							
Sample	Suite	Domain	$^{206}Pb/^{238}U$	± 1σ	W.A. Age	± 2σ	$^{176}Hf/^{177}Hf$	2 S.E.	$^{176}Lu/^{177}Hf$	$^{176}Yb/^{177}Hf$	$^{176}Hf/^{177}Hf$ (intitial)	$\varepsilon_{Hf}(t)$	± 2σ	$T_{DM}c$ (Ga)
DA13-004-49	Maevarano	Antananarivo	548	7	531	6	0.281824	0.000033	0.000717	0.027712	0.281817	-22.44	2.28	2.85
DA13-004-50	Maevarano	Antananarivo	534	7	531	6	0.281874	0.000024	0.000609	0.022339	0.281868	-20.63	1.71	2.74
DA13-004-53	Maevarano	Antananarivo	551	7	531	6	0.281820	0.000053	0.000713	0.023857	0.281813	-22.58	3.70	2.86
DA13-004-55	Maevarano	Antananarivo	544	7	531	6	0.281824	0.000025	0.000369	0.013328	0.281820	-22.31	1.72	2.84
DA13-004-56	Maevarano	Antananarivo	537	7	531	6	0.281818	0.000029	0.000374	0.012517	0.281815	-22.51	2.00	2.86
DA13-004-57	Maevarano	Antananarivo	552	7	531	6	0.281835	0.000028	0.000391	0.014083	0.281831	-21.95	1.95	2.82
DA13-004-59	Maevarano	Antananarivo	516	7	531	6	0.281836	0.000029	0.000516	0.019443	0.281831	-21.94	2.04	2.82
DA13-006-47	Maevarano	Antananarivo	526	8	535	5	0.281882	0.000024	0.000432	0.015819	0.281878	-20.20	1.66	2.72
DA13-006-49	Maevarano	Antananarivo	534	9	535	5	0.281872	0.000026	0.000441	0.017230	0.281868	-20.55	1.79	2.74
DA13-006-50	Maevarano	Antananarivo	535	18	535	5	0.281848	0.000039	0.000234	0.008730	0.281846	-21.33	2.74	2.79
DA13-006-52	Maevarano	Antananarivo	549	7	535	5	0.281839	0.000040	0.000615	0.023039	0.281833	-21.79	2.77	2.82
DA13-006-55	Maevarano	Antananarivo	543	11	535	5	0.281862	0.000039	0.000348	0.012544	0.281858	-20.88	2.74	2.76
DA13-006-56	Maevarano	Antananarivo	546	11	535	5	0.281849	0.000033	0.000329	0.011737	0.281846	-21.33	2.33	2.79
DA13-010-09	Ambalavao	Antananarivo	538	8	544	5	0.281866	0.000033	0.000517	0.016023	0.281861	-20.58	2.32	2.75
DA13-010-12	Ambalavao	Antananarivo	556	11	544	5	0.281913	0.000045	0.000954	0.034631	0.281903	-19.10	3.15	2.66
DA13-010-14	Ambalavao	Antananarivo	532	11	544	5	0.282004	0.000032	0.000541	0.017850	0.281999	-15.71	2.27	2.45
DA13-010-15	Ambalavao	Antananarivo	536	13	544	5	0.281962	0.000045	0.000834	0.030316	0.281954	-17.29	3.14	2.55
DA13-010-45	Ambalavao	Antananarivo	532	9	544	5	0.281986	0.000045	0.000706	0.026849	0.281978	-16.43	3.13	2.49
DA13-018-06	Ambalavao	Antananarivo	561	7	580	8	0.281781	0.000046	0.000940	0.036174	0.281771	-22.99	3.21	2.92
DA13-018-12	Ambalavao	Antananarivo	581	7	580	8	0.281798	0.000039	0.000456	0.015815	0.281793	-22.20	2.76	2.87
DA13-018-13	Ambalavao	Antananarivo	588	7	580	8	0.281722	0.000031	0.000630	0.023884	0.281715	-24.95	2.19	3.04
DA13-018-20	Ambalavao	Antananarivo	581	7	580	8	0.281786	0.000053	0.000863	0.033720	0.281776	-22.80	3.69	2.91
DA13-018-22	Ambalavao	Antananarivo	590	7	580	8	0.281783	0.000033	0.000586	0.020634	0.281777	-22.77	2.30	2.91
DA13-018-27	Ambalavao	Antananarivo	558	7	580	8	0.281780	0.000037	0.000472	0.017692	0.281774	-22.87	2.60	2.91
DA13-037_02	Ambalavao	Antananarivo	557	8	549	9	0.282181	0.000044	0.000311	0.010364	0.282177	-9.27	3.05	2.06
DA13-037_04	Ambalavao	Antananarivo	555	8	549	9	0.282126	0.000054	0.000700	0.024263	0.282119	-11.34	3.75	2.18
DA13-037_13	Ambalavao	Antananarivo	539	8	549	9	0.282085	0.000045	0.000479	0.012888	0.282080	-12.72	3.12	2.27
DA13-037_19	Ambalavao	Antananarivo	538	7	549	9	0.282175	0.000049	0.000817	0.036638	0.282167	-9.64	3.46	2.08
DA13-037_26	Ambalavao	Antananarivo	558	8	549	9	0.282088	0.000095	0.000799	0.034740	0.282080	-12.71	6.63	2.27
DA13-038_03	Ambalavao	Antananarivo	524	7	544	7	0.281755	0.000143	0.000606	0.022775	0.281749	-24.54	9.98	2.99
DA13-038_04	Ambalavao	Antananarivo	548	8	544	7	0.281677	0.000229	0.000942	0.023519	0.281667	-27.44	16.02	3.17

			Age (Ma)				Hafnium Data							
Sample	Suite	Domain	$^{206}Pb/^{238}U$	± 1σ	W.A. Age	± 2σ	$^{176}Hf/^{177}Hf$	2 S.E.	$^{176}Lu/^{177}Hf$	$^{176}Yb/^{177}Hf$	$^{176}Hf/^{177}Hf$ (intitial)	$\varepsilon_{Hf}(t)$	± 2σ	$T_{DM}c$ (Ga)
DA13-038_08	Ambalavao	Antananarivo	534	9	544	7	0.281684	0.000049	0.000418	0.018894	0.281680	-27.01	3.43	3.14
DA13-038_10	Ambalavao	Antananarivo	512	7	544	7	0.281635	0.000033	0.000303	0.010668	0.281632	-28.69	2.28	3.24
DA13-038_23	Ambalavao	Antananarivo	549	8	544	7	0.281642	0.000053	0.000454	0.018908	0.281637	-28.51	3.68	3.23
DA13-038_31	Ambalavao	Antananarivo	546	11	544	7	0.281639	0.000047	0.000379	0.015887	0.281635	-28.59	3.30	3.24
DA13-038_32	Ambalavao	Antananarivo	549	9	544	7	0.281685	0.000046	0.000408	0.015879	0.281681	-26.97	3.24	3.14
DA13-038_34	Ambalavao	Antananarivo	594	9	544	7	0.281605	0.000052	0.000262	0.011263	0.281602	-29.75	3.64	3.31
DA13-038_35	Ambalavao	Antananarivo	563	8	544	7	0.281620	0.000046	0.000359	0.014501	0.281616	-29.24	3.20	3.27
DA13-038_36	Ambalavao	Antananarivo	599	9	544	7	0.281632	0.000133	0.000537	0.025535	0.281627	-28.87	9.30	3.25
DA13-038_38	Ambalavao	Antananarivo	568	8	544	7	0.281685	0.000061	0.000360	0.012746	0.281681	-26.96	4.24	3.14
DA13-038_40	Ambalavao	Antananarivo	550	8	544	7	0.281703	0.000052	0.000595	0.024530	0.281696	-26.41	3.64	3.10
DA13-038_41	Ambalavao	Antananarivo	545	12	544	7	0.281620	0.000048	0.000363	0.012674	0.281616	-29.25	3.36	3.27
DA13-038_42	Ambalavao	Antananarivo	532	9	544	7	0.281667	0.000070	0.000430	0.017521	0.281663	-27.59	4.87	3.17
DA13-038_45	Ambalavao	Antananarivo	548	8	544	7	0.281669	0.000035	0.000352	0.014165	0.281666	-27.50	2.48	3.17
DA13-041_07	Ambalavao	Antananarivo	556	9	550	8	0.282377	0.000074	0.000736	0.027272	0.282369	-2.45	5.16	1.63
DA13-041_08	Ambalavao	Antananarivo	540	10	550	8	0.282479	0.000043	0.000512	0.025957	0.282474	1.24	3.04	1.40
DA13-041_10	Ambalavao	Antananarivo	552	8	550	8	0.282253	0.000057	0.000397	0.013046	0.282248	-6.73	3.99	1.90
DA13-050-17	Ambalavao	Itremo	568	8	570	8	0.281855	0.000043	0.000775	0.025274	0.281847	-20.51	3.04	2.76
DA13-050-18	Ambalavao	Itremo	535	8	570	8	0.281878	0.000034	0.000433	0.014547	0.281874	-19.55	2.35	2.70
DA13-050-24	Ambalavao	Itremo	567	8	570	8	0.281899	0.000037	0.000534	0.019493	0.281893	-18.87	2.62	2.66
DA13-050-25	Ambalavao	Itremo	556	15	570	8	0.281869	0.000042	0.000387	0.013735	0.281865	-19.85	2.91	2.72
DA13-050-26	Ambalavao	Itremo	560	11	570	8	0.281862	0.000045	0.000538	0.017835	0.281856	-20.18	3.13	2.74
DA13-050-27	Ambalavao	Itremo	536	10	570	8	0.281892	0.000069	0.000440	0.014180	0.281887	-19.08	4.83	2.68
DA13-051-50	Ambalavao	Itremo	516	9	581	33	0.281965	0.000039	0.000347	0.010878	0.281962	-16.20	2.8	2.51
DA13-051-51	Ambalavao	Itremo	526	14	581	33	0.282003	0.000049	0.000507	0.018398	0.281998	-14.93	3.4	2.43
DA13-051-52	Ambalavao	Itremo	529	21	581	33	0.281997	0.000045	0.000580	0.020380	0.281991	-15.16	3.2	2.44
DA13-051-54	Ambalavao	Itremo	526	8	581	33	0.282030	0.000036	0.000620	0.022391	0.282023	-14.02	2.5	2.37
DA13-051-57	Ambalavao	Itremo	532	11	581	33	0.282026	0.000037	0.000438	0.015792	0.282021	-14.10	2.6	2.38
DA13-051-58	Ambalavao	Itremo	567	13	581	33	0.282083	0.000032	0.000440	0.015020	0.282078	-12.08	2.2	2.25
DA13-072_01	Ambalavao	Antananarivo	552	8	544	4	0.281752	0.000024	0.000556	0.023117	0.281747	-24.64	1.70	3.00
DA13-072_04	Ambalavao	Antananarivo	535	8	544	4	0.281762	0.000030	0.000599	0.025905	0.281756	-24.31	2.13	2.98

			Age (Ma)				Hafnium Data							
Sample	Suite	Domain	$^{206}Pb/^{238}U$	± 1σ	W.A. Age	± 2σ	$^{176}Hf/^{177}Hf$	2 S.E.	$^{176}Lu/^{177}Hf$	$^{176}Yb/^{177}Hf$	$^{176}Hf/^{177}Hf$ (intitial)	$\varepsilon_{Hf}(t)$	± 2σ	$T_{DM}c$ (Ga)
DA13-072_06	Ambalavao	Antananarivo	538	7	544	4	0.281757	0.000050	0.000492	0.020932	0.281752	-24.43	3.50	2.98
DA13-072_08	Ambalavao	Antananarivo	559	11	544	4	0.281773	0.000031	0.000522	0.021697	0.281768	-23.89	2.14	2.95
DA13-072_09	Ambalavao	Antananarivo	535	10	544	4	0.281746	0.000023	0.000383	0.015077	0.281742	-24.78	1.58	3.00
DA13-072_13	Ambalavao	Antananarivo	536	9	544	4	0.281732	0.000022	0.000491	0.018674	0.281727	-25.34	1.56	3.04
DA13-072_15	Ambalavao	Antananarivo	549	12	544	4	0.281723	0.000031	0.000542	0.022462	0.281718	-25.65	2.14	3.06
DA13-072_16	Ambalavao	Antananarivo	538	8	544	4	0.281715	0.000022	0.000402	0.015729	0.281711	-25.91	1.55	3.07
DA13-072_17	Ambalavao	Antananarivo	544	10	544	4	0.281731	0.000021	0.000372	0.014517	0.281727	-25.32	1.49	3.04
DA13-072_19	Ambalavao	Antananarivo	546	8	544	4	0.281744	0.000024	0.000414	0.016320	0.281740	-24.88	1.70	3.01
DA13-072_20	Ambalavao	Antananarivo	563	10	544	4	0.281759	0.000024	0.000283	0.011613	0.281757	-24.28	1.69	2.97
DA13-072_21	Ambalavao	Antananarivo	547	8	544	4	0.281751	0.000024	0.000387	0.015830	0.281748	-24.60	1.70	2.99
DA13-072_22	Ambalavao	Antananarivo	544	9	544	4	0.281775	0.000029	0.000548	0.022083	0.281769	-23.82	2.03	2.95
DA13-072_23	Ambalavao	Antananarivo	545	9	544	4	0.281748	0.000024	0.000456	0.018270	0.281743	-24.77	1.66	3.00
DA13-072_24	Ambalavao	Antananarivo	543	7	544	4	0.281714	0.000027	0.000553	0.021971	0.281709	-25.98	1.89	3.08
DA13-072_25	Ambalavao	Antananarivo	541	8	544	4	0.281709	0.000050	0.000650	0.027111	0.281702	-26.20	3.49	3.09
DA13-072_26	Ambalavao	Antananarivo	541	11	544	4	0.281768	0.000027	0.000490	0.019519	0.281763	-24.05	1.87	2.96
DA13-072_27	Ambalavao	Antananarivo	535	8	544	4	0.281729	0.000036	0.000360	0.013809	0.281726	-25.37	2.51	3.04
DA13-072_28	Ambalavao	Antananarivo	558	8	544	4	0.281736	0.000033	0.001031	0.040045	0.281726	-25.37	2.28	3.04
DA13-072_29	Ambalavao	Antananarivo	539	9	544	4	0.281788	0.000038	0.000659	0.027224	0.281781	-23.40	2.64	2.92
DA13-072_30	Ambalavao	Antananarivo	576	10	544	4	0.281782	0.000034	0.000701	0.029449	0.281775	-23.64	2.35	2.93
DA14-126_03	Ambalavao	Ikalamavony	561	7	559	10	0.282434	0.000079	0.002308	0.090506	0.282409	-0.83	5.51	1.54
DA14-126_05	Ambalavao	Ikalamavony	550	7	559	10	0.282450	0.000034	0.000438	0.015548	0.282446	0.45	2.40	1.46
DA14-126_06	Ambalavao	Ikalamavony	565	7	559	10	0.282372	0.000098	0.003879	0.155867	0.282332	-3.58	6.86	1.71
DA14-126_11	Ambalavao	Ikalamavony	560	7	559	10	0.282471	0.000038	0.000565	0.021523	0.282465	1.15	2.67	1.42
DA14-126_20	Ambalavao	Ikalamavony	544	7	559	10	0.282486	0.000037	0.000554	0.022006	0.282481	1.69	2.60	1.38
DA14-126_22	Ambalavao	Ikalamavony	522	8	559	10	0.282470	0.000059	0.000785	0.025236	0.282462	1.02	4.10	1.42
DA14-126_24	Ambalavao	Ikalamavony	572	7	559	10	0.282437	0.000037	0.000554	0.020529	0.282431	-0.07	2.62	1.49
DA14-128_01	Ambalavao	Ikalamavony	544	7	545	7	0.282394	0.000133	0.002547	0.098138	0.282368	-2.43	9.29	1.63
DA14-128_02	Ambalavao	Ikalamavony	535	6	545	7	0.282456	0.000123	0.004885	0.192323	0.282405	-1.12	8.64	1.55
DA14-128_03	Ambalavao	Ikalamavony	535	6	545	7	0.282489	0.000060	0.000705	0.024912	0.282481	1.58	4.22	1.38

			Age (Ma)				Hafnium Data							
Sample	Suite	Domain	$^{206}Pb/^{238}U$	± 1σ	W.A. Age	± 2σ	$^{176}Hf/^{177}Hf$	2 S.E.	$^{176}Lu/^{177}Hf$	$^{176}Yb/^{177}Hf$	$^{176}Hf/^{177}Hf$ (intitial)	$\varepsilon_{Hf}(t)$	± 2σ	$T_{DM}c$ (Ga)
DA14-128_12	Ambalavao	Ikalamavony	550	7	545	7	0.282417	0.000063	0.000712	0.027005	0.282410	-0.94	4.41	1.54
DA14-128_13	Ambalavao	Ikalamavony	542	7	545	7	0.282512	0.000088	0.000708	0.028897	0.282504	2.40	6.13	1.33
DA14-128_23	Ambalavao	Ikalamavony	558	7	545	7	0.282488	0.000058	0.000792	0.027190	0.282480	1.54	4.04	1.39

Appendix 6.1

Analytical Methods for Chapter 6
(Dabolava Suite)

6.1.1 Sample collection and processing

Approximately 1.5 to 3 kg of each sample was collected in the field for polished thin sectioning, zircon separation and whole-rock geochemical analysis. Samples were cut and 46 x 27 x 10 mm chips were shipped to Continental Instruments in Lucknow, India for the preparation of polished thin sections. A portion of the remaining sample was placed in a jaw crusher. A representative amount of the crushed sample was placed into a tungsten carbide ring mill for ~two minutes to produce a fine, homogeneous powder for whole-rock geochemical analysis. Polished thin-sections were analysed under transmitted and reflected light to determine mineralogy, textures and to select sites for mineral analysis. Zircons were separated by conventional sieving and magnetic separation techniques. Zircon grains were handpicked and mounted in epoxy resin, polished, and imaged under transmitted and reflected light. To investigate the internal structure of the zircon grains and to select target sites for U-Pb, hafnium, and oxygen isotopic analyses, cathodoluminescence (CL) imaging was conducted using an FEI Quanta 600 Scanning Electron Microscope equipped with a tungsten filament electron source and a Gatan CL detector at Adelaide Microscopy.

6.1.2 U-Pb geochronology

U-Pb zircon analyses were performed by laser ablation inductively coupled mass spectroscopy (LA-ICP-MS) at Adelaide Microscopy using an Agilent 7500cx ICPMS instrument coupled with a New Wave UP-213 laser ablation system. Common Pb was not corrected for due to uncertainty associated with the ^{204}Hg interference when using an LA-ICP-MS system. Monitoring of the ^{204}Pb mass indicated common Pb was present in some samples but concentrations above background are minor (Appendix 6.2). Common Pb values are presented as $\%^{206}$Pbcommon = [^{204}Pb/ (^{204}Pb + ^{206}Pb) x 100]. To minimise the influence of common Pb on calculated ages only the ≥ 90 % concordant data are used. Individual zircon grains were ablated in a helium atmosphere using a ~30µm beam diameter, a frequency of 5 Hz and an energy value of 6.4 – 8.4 J/cm^2. Instrument and mass calibration were performed before all analytical sessions using the NIST 610 reference glass by maximising the ^{238}U signal and by minimising oxide formation using the ThO+/Th+ ratio (< 1%). (^{204}Pb + ^{204}Hg), ^{206}Pb, ^{207}Pb, ^{208}Pb, ^{232}Th and ^{238}U were measured during analysis. The ^{235}U signal was calculated from ^{238}U on the basis of the ratio ^{238}U/^{235}U= 137.88. Procedural repetition consisted of two analyses of the GJ standard, two analyses of the Plešovice standard, one analyse of the GJ standard, 15 unknown analyses and finally two GJ analyses. Data acquisition procedures involved 20 seconds of system washout, 30 seconds of background measurement, 10 seconds of beam stabilisation and 30 seconds of sample ablation for a total analysis time of 90 seconds. U-Pb-Th isotope fractionation was corrected using the GEMOC GJ-1 standard (^{206}Pb/^{238}U age of 600.7 ± 1.1 Ma; 2σ; Jackson et al., 2004) and internal accuracy was monitored using the Plešovice zircon standard (^{206}Pb/^{238}U age of 337.1 ± 0.37 Ma; 2σ; Sláma et al., 2008). Plešovice analyses yield a weighted average ^{206}Pb/^{238}U age of 340.3± 3.4 (Fig. A.5.1; 2σ; MSWD = 3.5; n = 24). Data were processed using the GLITTER software package (Griffin et al., 2008). Individual zircon grain ages are quoted at the 1σ level and weighted-mean ages at the 2σ level. Age calculations and Wetherill concordia diagrams were constructed using the Microsoft Excel macro Isoplot 4.15 (Ludwig, 2012).

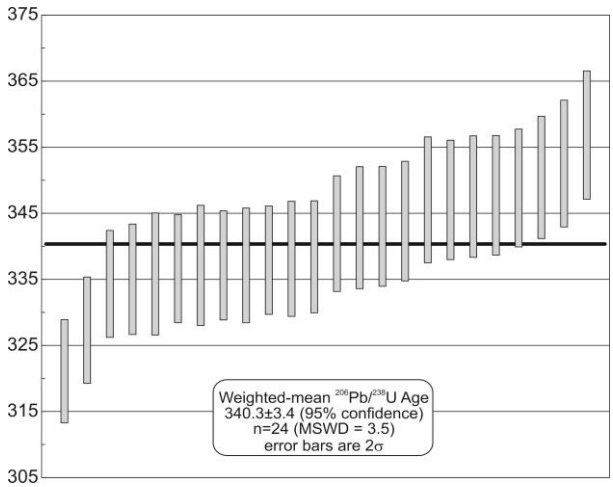

Fig. A.6.1 Results of Plešovice zircon standard analyses (^{206}Pb/^{238}U age of 337.1 ± 0.37 Ma; 2σ; Sláma et al., 2008).

6.1.3 Oxygen isotopes in zircon

Oxygen isotope analyses were conducted at the Australian National University, Canberra, Australia using the SHRIMP II (sensitive high-resolution ion microprobe) instrument following the methods of Ickert et al. (2008). A ~10 kV, ~3 nA Cs+ primary ion beam was focused to a ~30 µm diameter spot on an aluminum coated sample. Each analysis consisted of a 90 second pre-burn to allow the secondary ion isotopic composition to stabilise and to remove the sample coating prior to the analysis, followed by 6, ~20 second estimates of the $^{18}O/^{16}O$ ratio. Long term instrument drift was corrected using the Mudtank zircon reference material ($\delta^{18}O$ = 5.03±0.10 ‰; Valley, 2003) and internal accuracy monitored using Temora II zircon ($\delta^{18}O$ = 8.20 ±0.01 ‰; Valley, 2003).Standards Temora II and Mudtank were analysed first, then again after 5-6 unknown analyses. Sample $\delta^{18}O$ (zircon) values were determined by difference relative to the mean $\delta^{18}O$ (zircon) measured on standards following normalisation for long-term drift in its measured composition. CL images were used to analyse within the same CL zone but away from the U-Pb (LA-ICP-MS) analysis pits to avoid potential interference. The results of standard analyses are listed in Table A.6.1.

6.1.4 Zircon Lu-Hf analysis

In situ LA-MC-ICP-MS Hf isotope analyses were carried out at the University of Adelaide Waite Campus facility using a New Wave Research 193 nm Excimer laser attached to a Neptune multi-collector ICP-MS system as per Payne et al. (2013). Only grains with U–Pb ages having ≤ 10% discordance were analysed for Lu–Hf isotope composition. Analysis locations were in the same cathodoluminescence domains as concordant U–Pb laser spots and in the same spot as SHRIMP oxygen spots. The bulk of analyses were carried out using a beam diameter of ~50 µm for large and a minimum of ~25 µm for smaller grains. Typical ablation times were 40 –100 seconds using 5 Hz repetition rate, 4 ns pulse rate, and an intensity of ~10 J/cm^2. Zircons were ablated in a helium atmosphere, which was then mixed with argon upstream of the ablation cell. Analyses used a dynamic measurement routine with: ten 0.524 s integrations on ^{171}Yb, ^{173}Yb, ^{175}Lu, ^{176}Hf (+Lu + Yb), ^{177}Hf, ^{178}Hf, ^{179}Hf and ^{180}Hf; one 0.524 s integration on ^{160}Gd, ^{163}Dy, ^{164}Dy, ^{165}Ho, ^{166}Er, ^{167}Er, ^{168}Er, ^{170}Yb and ^{171}Yb, and one 0.524 s integration of Hf oxides with masses ranging from 187 to 196 amu. An idle time of 1.5 s was included between each mass change to allow for magnet settling and to negate any possible effects of signal decay. The measurement cycle was repeated 15 times providing a total maximum measurement time of 3.75 min including an off-peak baseline measurement. Hf oxide formation rates for all analytical sessions in this study were in the range 0.1–0.07%. Hf mass bias was corrected using an exponential fractionation law with a stable $^{179}Hf/^{177}Hf$ ratio of 0.7325. Yb and Lu isobaric interferences on ^{176}Hf were corrected for following the methods of Woodhead et al. (2004). ^{176}Yb interference on ^{176}Hf was corrected for by direct measurement of Yb fractionation using measured $^{171}Yb/^{173}Yb$ with the Yb isotopic values of Segal et al. (2003). The applicability of these values were verified by analysing JMC 475 Hf solutions doped with varying levels of Yb with interferences up to $^{176}Yb/^{177}Hf$ = ~0.5. Lu isobaric interference on ^{176}Hf was corrected using a $^{176}Lu/^{175}Lu$ ratio of 0.02655 (Vervoort et al., 2004) assuming the same mass bias behaviour as Yb. Confirmation of accuracy of the technique was monitored using the Plešovice, Mudtank and Temora II zircon standards. Mean $^{176}Hf/^{177}Hf$ values for each standard along with the published values are given in Table A.6.1. $\varepsilon_{Hf}(t)$ and $T_{DM}c$ were calculated using ^{176}Lu decay constant after Scherer et al. (2001). TDM crustal was calculated using the methods of Griffin et al. (2002) with an average crustal composition of $^{176}Lu/^{177}Hf$ = 0.015.

Table A.6.1 Summary of zircon standard data

Standard	Method	n	Measured Value	Reference Value	Reference
U-Pb isotopes (Age)					
Plešovice	LA-ICP-MS	24	340.3 ± 3.4 Ma (MSWD=3.5)	337.1 ± 0.4 Ma	Sláma et al., 2008
Oxygen isotopes ($\delta^{18}O$)					
Temora II	SHRIMP II	9	8.17 ± 0.42 ‰	8.20 ± 0.01 ‰	Valley, 2003
Hf isotopes ($^{177}Hf/^{176}Hf$)					
Mudtank	MC-LA-ICP-MS	12	0.282497 ± 0.000016	0.282507 ± 0.000006	Woodhead and Hergt, 2005
Temora II	MC-LA-ICP-MS	4	0.282631 ± 0.000019	0.282686 ± 0.000008	Woodhead and Hergt, 2005
Plešovice	MC-LA-ICP-MS	5	0.282463 ± 0.000009	0.282482 ± 0.000013	Sláma et al., 2008

6.1.5 Whole-rock geochemistry

Whole-rock geochemical analyses for major, minor and trace elements were collected at ACME Labs in Vancouver, British Columbia, Canada. The major element data collection procedure involved the crushed rock pulp being mixed with $LiBO_2/Li_2B_4O_7$ flux. Graphite crucibles were fused in a muffle furnace for 30 minutes at 980°C. The cooled bead was then dissolved in ACS grade nitric acid and analysed using a SPECTRO AS500 ICP-OES (inductively-coupled plasma optical emission spectroscopy) instrument. LOI (loss on ignition) values were determined by igniting a sample split then measuring the weight lost. For trace element analyses, the crushed rock pulp was digested using a modified Aqua Regia solution of equal parts concentrated HCl, HNO_3 and deionised H_2O for one hour in a heating block or hot water bath. Samples were made up to volume with dilute HCl and analysed using a Perkin-Elmer ELAN 9000 ICP-MS. Quality control protocol involves analysing pulp duplicates to monitor analytical precision and a reagent blank to measure background. In addition, interspersed analyses of reference materials SO-18, OREAS45EA, GS311-1, and GS910-4 monitored the accuracy of results. Total sulphur and carbon values were determined by adding an induction flux to the prepared sample and igniting the sample in a LECO CS230 Carbon/Sulphur Series induction furnace. A carrier gas transports the released carbon and sulphur to be measured by adsorption in an infrared spectrometric cell. Results are total carbon or sulphur.

References

CGS, 2009. Map Explanation of 1:100 000 scale (Zone E) Sheets I46 – Ambararata, J46 – Beopoaka, 47 – Itondy, J47 – Belobaka, K47 – Ambatofotsy, I48 – Miandrivazo, J48 – Betrondro, K48 – Ambatondradama, I49 – Ankotrofotsy, J49 – Dabolava, K49 – Anjoma-Ramartina, L49 – Vasiana, M49 – Ankazomiriotra, N49 – Antsirabe. . République de Madagascar, Ministère de L'Energie et des Mines – Project de Gouvernance des Ressources Minérales, Antananarivo, Madagascar and Council for Géoscience, Pretoria, South Africa, .

Griffin, W.L., Powell, W.J., Pearson, N.J., O'Reilly, S.Y., 2008. "GLITTER: data reduction software for laser ablation ICP-MS". In Laser ablation ICP-MS in the earth sciences. Mineralogical Association of Canada Short Course Series. Edited by: P., Sylvester. 40, 204–207.

Griffin, W.L., Wang, X., Jackson, S.E., Pearson, N.J., O'Reilly, S.Y., Xu, X., Zhou, X., 2002. Zircon chemistry and magma mixing, SE China: In-situ analysis of Hf isotopes, Tonglu and Pingtan igneous complexes. Lithos 61, 237-269.

Ickert, R.B., Hiess, J., Williams, I.S., Holden, P., Ireland, T.R., Lanc, P., Schram, N., Foster, J.J., Clement, S.W., 2008. Determining high precision, in situ, oxygen isotope ratios with a SHRIMP II: Analyses of MPI-DING silicate-glass reference materials and zircon from contrasting granites. Chemical Geology 257, 114-128.

Jackson, S.E., Pearson, N.J., Griffin, W.L., Belousova, E.A., 2004. The application of laser ablation-inductively coupled plasma-mass spectrometry to in situ U–Pb zircon geochronology. Chemical Geology 211, 47-69.

Ludwig, K.R., 2012. User's Manual for Isoplot 3.75. A Geochronological Toolkit for Microsoft Excel. Berkeley Geochronology Center Special Publication No. 5, 75p.

Payne, J.L., Pearson, N.J., Grant, K.J., Halverson, G.P., 2013. Reassessment of relative oxide formation rates and molecular interferences on in situ lutetium-hafnium analysis with laser ablation MC-ICP-MS. Journal of Analytical Atomic Spectrometry 28, 1068-1079.

Scherer, E., Münker, C., Mezger, K., 2001. Calibration of the Lutetium-Hafnium Clock. Science 293, 683-687.

Segal, I., Halicz, L., Platzner, I.T., 2003. Accurate isotope ratio measurements of ytterbium by multiple collection inductively coupled plasma mass spectrometry applying erbium and hafnium in an improved double external normalization procedure. Journal of Analytical Atomic Spectrometry 18, 1217-1223.

Sláma, J., Košler, J., Condon, D.J., Crowley, J.L., Gerdes, A., Hanchar, J.M., Horstwood, M.S.A., Morris, G.A., Nasdala, L., Norberg, N., Schaltegger, U., Schoene, B., Tubrett, M.N., Whitehouse, M.J., 2008. Plešovice zircon — A new natural reference material for U–Pb and Hf isotopic microanalysis. Chemical Geology 249, 1-35.

Valley, J.W., 2003. Oxygen Isotopes in Zircon. Reviews in Mineralogy and Geochemistry 53, 343-385.

Vervoort, J.D., Patchett, J., Soderlund, U., Baker, M., 2004. Isotopic composition of Yb and the determination of Lu concentration and Lu/Hf ratios by isotope dilution using MC-ICPMS. Geochemistry Geophysics Geosystems 5, Q11002.

Woodhead, J., Hergt, J., Shelley, M., Eggins, S., Kemp, R., 2004. Zircon Hf-isotope analysis with an excimer laser, depth profiling, ablation of complex geometries, and concomitant age estimation. Chemical Geology 209, 121-135.

.

Table A.6.2: List of major element oxides, minor and trace elements analysed in this study

Element or Oxide	Detection Limit		Upper Limit		Element or Oxide	Detection Limit		Upper Limit	
SiO_2	0.01	%	100	%	Ho	0.02	ppm	10000	ppm
Al_2O_3	0.01	%	100	%	La	0.1	ppm	50000	ppm
CaO	0.01	%	100	%	Lu	0.01	ppm	10000	ppm
Cr_2O_3	0.002	%	100	%	Mo	0.1	ppm	2000	ppm
Fe_2O_3	0.04	%	100	%	Nb	0.1	ppm	10000	ppm
K_2O	0.01	%	100	%	Nd	0.3	ppm	10000	ppm
MgO	0.01	%	100	%	Ni	0.1	ppm	10000	ppm
MnO	0.01	%	100	%	Pb	0.1	ppm	10000	ppm
Na_2O	0.01	%	100	%	Pr	0.02	ppm	10000	ppm
P_2O_5	0.01	%	100	%	Rb	0.1	ppm	10000	ppm
TiO_2	0.01	%	100	%	Sb	0.1	ppm	2000	ppm
LOI	0.1	%	100	%	Sc	1	ppm	10000	ppm
Sum	0.01	%	100	%	Se	0.5	ppm	100	ppm
Ag	0.1	ppm	100	ppm	Sm	0.05	ppm	10000	ppm
As	0.5	ppm	10000	ppm	Sn	1	ppm	10000	ppm
Au	0.5	ppb	100000	ppb	Sr	0.5	ppm	50000	ppm
Ba	1	ppm	50000	ppm	Ta	0.1	ppm	10000	ppm
Be	1	ppm	10000	ppm	Tb	0.01	ppm	10000	ppm
Bi	0.1	ppm	2000	ppm	Th	0.2	ppm	10000	ppm
Cd	0.1	ppm	2000	ppm	Tl	0.1	ppm	1000	ppm
Ce	0.1	ppm	50000	ppm	Tm	0.01	ppm	10000	ppm
Co	0.2	ppm	10000	ppm	U	0.1	ppm	10000	ppm
Cs	0.1	ppm	10000	ppm	V	8	ppm	10000	ppm
Cu	0.1	ppm	10000	ppm	W	0.5	ppm	10000	ppm
Dy	0.05	ppm	10000	ppm	Yb	0.05	ppm	10000	ppm
Er	0.03	ppm	10000	ppm	Y	0.1	ppm	50000	ppm
Eu	0.02	ppm	10000	ppm	Zn	1	ppm	10000	ppm
Ga	0.5	ppm	10000	ppm	Zr	0.1	ppm	50000	ppm
Gd	0.05	ppm	10000	ppm	TOT/C	0.02	%	100	%
Hf	0.1	ppm	10000	ppm	TOT/S	0.02	%	100	%
Hg	0.01	ppm	50	ppm					

Appendix 6.2

LA-ICP-MS U-Pb zircon data
(Dabolava Suite)

DA14-110			Mean cps (background subtracted)							Isotope Ratios (±1σ)							Age (Ma; ±1σ)						
Analysis	Core/Rim	$\%^{206}Pb_c$	^{204}Pb	^{206}Pb	^{207}Pb	^{208}Pb	^{232}Th	^{238}U	Th/U	$^{207}Pb/^{206}Pb$		$^{207}Pb/^{235}U$		$^{206}Pb/^{238}U$		Rho	$^{207}Pb/^{206}Pb$		$^{207}Pb/^{235}U$		$^{206}Pb/^{238}U$		%Conc
110-01.1	Core	0.09	29	30574	2196	6369	148234	224169	0.66	0.0720	0.0026	1.6412	0.0575	0.1655	0.0029	0.1922	985	71	986	22	987	16	100
110-01.2	Rim	0.00	0	12711	953	1809	42346	100932	0.42	0.0736	0.0013	1.5439	0.0284	0.1522	0.0020	0.4045	1029	36	948	11	913	11	89
110-02.1	Rim	0.00	0	60288	3610	1865	52681	837724	0.06	0.0582	0.0008	0.7004	0.0105	0.0873	0.0011	0.5125	538	30	539	6	539	7	100
110-02.2	Core	0.03	8	24644	1844	1553	31618	218949	0.14	0.0732	0.0012	1.3676	0.0237	0.1356	0.0018	0.4334	1018	33	875	10	820	10	81
110-03.1		0.06	22	34865	2585	5332	149172	342016	0.44	0.0728	0.0023	1.2762	0.0393	0.1273	0.0021	0.2315	1008	62	835	18	772	12	77
110-04.1		0.14	23	16137	1172	3210	77010	122361	0.63	0.0714	0.0013	1.5724	0.0302	0.1598	0.0022	0.3914	969	38	959	12	956	12	99
110-05.1		0.30	23	7682	567	949	23121	58845	0.39	0.0724	0.0016	1.5764	0.0350	0.1580	0.0022	0.3222	996	44	961	14	946	12	95
110-06.1		0.14	23	16163	1167	3328	82507	125671	0.66	0.0703	0.0012	1.5159	0.0273	0.1565	0.0021	0.4149	936	35	937	11	937	12	100
110-07.1		0.00	0	38157	2887	8213	298884	399780	0.75	0.0732	0.0012	1.1778	0.0204	0.1168	0.0015	0.4455	1019	33	790	10	712	9	70
110-08.1		0.14	14	9731	722	1310	32341	74064	0.44	0.0726	0.0015	1.5940	0.0342	0.1592	0.0022	0.3409	1003	42	968	13	952	12	95
110-09.1		0.03	4	13516	1010	2521	61528	102363	0.60	0.0731	0.0014	1.6155	0.0318	0.1604	0.0022	0.3744	1015	38	976	12	959	12	94
110-10.1		0.00	0	22407	1666	4690	114362	175642	0.65	0.0727	0.0013	1.5616	0.0284	0.1557	0.0021	0.4185	1007	35	955	11	933	12	93
110-11.1		0.00	0	13886	1035	2791	76086	115948	0.66	0.0728	0.0014	1.4648	0.0292	0.1459	0.0020	0.3746	1009	39	916	12	878	11	87
110-12.1		0.03	31	97599	7390	28363	791939	823202	0.96	0.0728	0.0012	1.4574	0.0258	0.1452	0.0019	0.4320	1009	34	913	11	874	11	87
110-13.1		0.30	26	8637	618	1151	28983	65774	0.44	0.0697	0.0015	1.5433	0.0338	0.1606	0.0023	0.3370	920	44	948	13	960	13	104
110-14.1		0.19	24	12758	955	2005	49629	97867	0.51	0.0731	0.0015	1.5552	0.0312	0.1543	0.0021	0.3510	1017	39	953	12	925	12	91
110-15.1	Core	0.00	0	77219	5763	19932	462087	583797	0.79	0.0734	0.0011	1.5700	0.0252	0.1553	0.0019	0.4480	1024	30	958	10	930	11	91
110-15.2	Rim	0.00	0	7882	618	1180	24579	62374	0.39	0.0726	0.0023	1.5389	0.0463	0.1538	0.0025	0.2187	1003	62	946	19	922	14	92
110-16.1		0.02	11	68636	5087	11944	255610	580580	0.44	0.0730	0.0013	1.3897	0.0260	0.1381	0.0018	0.3719	1014	37	885	11	834	10	82
110-17.1		0.14	28	19761	1421	2674	62387	167108	0.37	0.0709	0.0014	1.3582	0.0265	0.1390	0.0018	0.3504	954	39	871	11	839	10	88
110-18.1		0.04	85	217442	15895	81906	2068190	2270493	0.91	0.0730	0.0021	1.1287	0.0316	0.1122	0.0017	0.2287	1013	57	767	15	686	10	68
110-18.2		0.08	32	37640	2866	8486	223558	337035	0.66	0.0742	0.0016	1.3653	0.0297	0.1335	0.0018	0.3196	1047	43	874	13	808	10	77
110-19.1		0.04	8	22556	1692	4615	110031	173755	0.63	0.0737	0.0014	1.5535	0.0306	0.1530	0.0020	0.3577	1032	39	952	12	918	11	89
110-20.1		0.00	0	10270	769	1518	33630	73990	0.45	0.0737	0.0021	1.6549	0.0468	0.1630	0.0025	0.2318	1032	57	991	18	973	14	94
110-21.1		0.06	12	20702	1604	3593	94084	185629	0.51	0.0730	0.0027	1.3893	0.0495	0.1384	0.0025	0.1883	1013	73	884	21	835	14	82
110-22.1		0.00	0	39525	2955	3867	93203	343435	0.27	0.0731	0.0013	1.3809	0.0251	0.1371	0.0018	0.3987	1016	35	881	11	828	10	81
110-23.1		0.00	0	56253	4073	11178	275233	454309	0.61	0.0709	0.0016	1.4558	0.0335	0.1489	0.0021	0.3059	955	46	912	14	895	12	94
110-24.1		0.00	0	75535	5359	18028	438894	663817	0.66	0.0674	0.0018	1.2958	0.0339	0.1395	0.0021	0.2684	850	54	844	15	842	12	99
110-25.1		0.00	0	13621	972	2346	56605	117871	0.48	0.0710	0.0025	1.3400	0.0457	0.1370	0.0023	0.1866	957	70	863	20	827	13	87
110-26.1		0.00	0	29335	1999	3560	81983	290920	0.28	0.0669	0.0016	1.1013	0.0266	0.1194	0.0017	0.2795	835	50	754	13	727	10	87
110-27.1		0.01	3	39334	2826	5953	154643	340851	0.45	0.0688	0.0014	1.3206	0.0276	0.1394	0.0019	0.3458	892	42	855	12	841	11	94

DA14-110			Mean cps (background subtracted)							Isotope Ratios (±1σ)							Age (Ma; ±1σ)						
Analysis	Core/Rim	$\%^{206}Pb_c$	^{204}Pb	^{206}Pb	^{207}Pb	^{208}Pb	^{232}Th	^{238}U	Th/U	$^{207}Pb/^{206}Pb$		$^{207}Pb/^{235}U$		$^{206}Pb/^{238}U$		Rho	$^{207}Pb/^{206}Pb$		$^{207}Pb/^{235}U$		$^{206}Pb/^{238}U$		%Conc
110-28.1		0.12	25	20248	1493	3567	80354	143368	0.56	0.0727	0.0019	1.6859	0.0437	0.1681	0.0025	0.2573	1007	52	1003	17	1002	14	100
110-29.1		0.06	15	23157	1656	2917	70168	201926	0.35	0.0699	0.0011	1.3294	0.0220	0.1379	0.0018	0.4498	926	32	859	10	833	10	90
110-30.1		0.06	30	51936	3941	11842	317612	436680	0.73	0.0738	0.0017	1.4786	0.0339	0.1456	0.0021	0.3219	1035	45	922	14	876	12	85
110-31.1		0.00	0	31259	2214	4685	113083	269625	0.42	0.0702	0.0012	1.3440	0.0240	0.1389	0.0018	0.4100	935	35	865	10	838	10	90
110-32.1		0.00	0	25254	1836	5341	126657	185530	0.68	0.0717	0.0012	1.6236	0.0284	0.1643	0.0021	0.4301	978	34	979	11	981	12	100
110-33.1		0.08	18	22964	1680	4851	116058	168452	0.69	0.0722	0.0012	1.6386	0.0292	0.1647	0.0022	0.4253	991	34	985	11	983	12	99
110-34.1		0.00	0	28101	2024	5943	139524	201673	0.69	0.0714	0.0016	1.6386	0.0363	0.1665	0.0023	0.3147	969	44	985	14	993	13	102
110-35.1		0.00	0	61486	4534	13633	323497	450958	0.72	0.0727	0.0011	1.6538	0.0267	0.1649	0.0021	0.4807	1007	30	991	10	984	12	98
110-36.1		0.24	27	11453	854	1554	36613	85624	0.43	0.0735	0.0014	1.6444	0.0329	0.1624	0.0022	0.3693	1027	39	987	13	970	12	94
110-37.1		0.01	5	56756	4207	14571	346386	430855	0.80	0.0724	0.0015	1.6258	0.0355	0.1630	0.0023	0.3617	996	43	980	14	973	13	98
110-38.1		0.13	26	20679	1500	3591	79644	145128	0.55	0.0721	0.0017	1.6986	0.0398	0.1708	0.0024	0.3043	990	47	1008	15	1017	13	103
110-39.1		0.00	0	30682	2262	7440	175598	224001	0.78	0.0734	0.0014	1.6670	0.0335	0.1649	0.0022	0.3685	1024	39	996	13	984	12	96
110-40.1		0.00	0	19237	1414	3002	68974	138439	0.50	0.0732	0.0015	1.6902	0.0359	0.1674	0.0023	0.3470	1020	42	1005	14	998	13	98
110-41.1		0.10	21	20548	1510	3694	84877	147161	0.58	0.0726	0.0014	1.7014	0.0327	0.1699	0.0023	0.3956	1003	37	1009	12	1012	13	101

DA14-118			Mean cps (background subtracted)							Isotope Ratios (±1σ)							Age (Ma; ±1σ)						
Analysis	Core/Rim	$\%^{206}Pb_c$	^{204}Pb	^{206}Pb	^{207}Pb	^{208}Pb	^{232}Th	^{238}U	Th/U	$^{207}Pb/^{206}Pb$		$^{207}Pb/^{235}U$		$^{206}Pb/^{238}U$		Rho	$^{207}Pb/^{206}Pb$		$^{207}Pb/^{235}U$		$^{206}Pb/^{238}U$		%Conc
118-001.1		0.33	12	3607	273	454	11090	33933	0.33	0.0739	0.0027	1.4634	0.0522	0.1437	0.0027	0.2180	1038	72	915	22	866	15	83
118-002.1		0.11	14	13214	1007	2059	49241	108470	0.45	0.0741	0.0015	1.6797	0.0364	0.1645	0.0025	0.4148	1043	41	1001	14	982	14	94
118-003.1		0.00	0	4722	353	613	15364	38125	0.40	0.0735	0.0024	1.6925	0.0544	0.1670	0.0030	0.2531	1028	64	1006	21	996	16	97
118-004.1		0.00	0	4130	309	500	13351	33585	0.40	0.0731	0.0024	1.6757	0.0537	0.1664	0.0029	0.2525	1016	64	999	20	992	16	98
118-005.1		0.00	0	4157	319	739	17255	35215	0.49	0.0735	0.0026	1.6182	0.0563	0.1598	0.0030	0.2250	1027	70	977	22	956	16	93
118-006.1		0.38	11	2857	220	451	10670	23877	0.45	0.0734	0.0039	1.6475	0.0845	0.1629	0.0039	0.1430	1024	104	989	32	973	21	95
118-007.1		0.81	41	4999	381	611	16553	43541	0.38	0.0739	0.0038	1.5999	0.0782	0.1570	0.0036	0.1529	1039	99	970	31	940	20	90
118-008.1		0.00	0	4150	313	516	13201	33395	0.40	0.0733	0.0020	1.6942	0.0471	0.1677	0.0028	0.3013	1022	55	1006	18	999	15	98
118-009.1		0.00	0	11550	860	1677	40773	90505	0.45	0.0732	0.0016	1.7203	0.0384	0.1704	0.0026	0.3955	1020	43	1016	14	1015	14	99
118-010.1		0.00	0	8620	649	1335	32033	68623	0.47	0.0736	0.0017	1.7209	0.0402	0.1697	0.0026	0.3804	1030	45	1016	15	1010	14	98
118-011.1		0.13	7	5577	445	623	19257	60698	0.32	0.0780	0.0029	1.3127	0.0472	0.1221	0.0023	0.2094	1147	72	851	21	743	13	65
118-012.1		0.00	0	4938	370	611	15929	41902	0.38	0.0736	0.0028	1.5911	0.0580	0.1569	0.0029	0.2065	1029	74	967	23	940	16	91
118-013.1		0.00	0	13736	1041	1513	36006	109028	0.33	0.0739	0.0014	1.7283	0.0347	0.1698	0.0025	0.4490	1038	37	1019	13	1011	14	97
118-014.1		0.14	8	5813	447	813	19491	46866	0.42	0.0742	0.0018	1.7119	0.0424	0.1673	0.0026	0.3504	1047	48	1013	16	997	15	95
118-015.1		0.00	0	3156	236	399	9068	25210	0.36	0.0732	0.0022	1.7039	0.0521	0.1688	0.0029	0.2759	1020	61	1010	20	1006	16	99
118-016.1		0.07	7	10362	783	1747	50005	95544	0.52	0.0739	0.0014	1.5105	0.0303	0.1482	0.0022	0.4602	1040	37	935	12	891	12	86
118-017.1		0.10	12	11942	905	649	18267	125024	0.15	0.0736	0.0017	1.3351	0.0316	0.1316	0.0021	0.3834	1030	46	861	14	797	12	77
118-018.1		0.02	1	6619	505	831	19441	53680	0.36	0.0740	0.0018	1.7278	0.0433	0.1693	0.0027	0.3579	1043	49	1019	16	1008	15	97
118-019.1		0.00	0	6347	483	823	21354	53030	0.40	0.0745	0.0017	1.6782	0.0388	0.1635	0.0025	0.3868	1054	44	1000	15	976	14	93
118-020.1		0.02	8	39780	3026	7927	314986	330116	0.95	0.0740	0.0011	1.6814	0.0294	0.1649	0.0024	0.5462	1040	31	1002	11	984	13	95
118-021.1		0.00	0	12263	937	2254	56037	99794	0.56	0.0739	0.0015	1.7169	0.0367	0.1686	0.0026	0.4252	1038	40	1015	14	1004	14	97
118-022.1		0.17	15	8763	662	872	22143	70156	0.32	0.0738	0.0015	1.7317	0.0373	0.1703	0.0026	0.4212	1035	41	1020	14	1014	14	98
118-023.1		0.10	15	14571	1109	2780	72102	126608	0.57	0.0737	0.0014	1.6001	0.0327	0.1574	0.0024	0.4526	1034	38	970	13	942	13	91
118-024.1		0.00	0	6131	462	776	20287	51264	0.40	0.0728	0.0022	1.6282	0.0491	0.1621	0.0028	0.2760	1009	60	981	19	969	16	96
118-025.1		0.42	15	3577	272	434	10489	29549	0.35	0.0740	0.0020	1.6867	0.0469	0.1652	0.0028	0.3129	1043	55	1004	18	986	15	95
118-026.1		0.10	3	3087	237	380	9348	24992	0.37	0.0741	0.0022	1.7198	0.0504	0.1683	0.0029	0.2908	1045	58	1016	19	1003	16	96
118-027.1		0.43	12	2785	213	375	9892	27569	0.36	0.0739	0.0024	1.4058	0.0448	0.1380	0.0024	0.2577	1039	64	891	19	833	14	80
118-028.1		0.18	12	6837	519	794	21346	57112	0.37	0.0731	0.0024	1.6271	0.0523	0.1616	0.0029	0.2448	1015	65	981	20	966	16	95
118-029.1		0.00	0	2961	225	355	8535	24438	0.35	0.0738	0.0022	1.6802	0.0502	0.1652	0.0028	0.2816	1035	59	1001	19	986	16	95

DA14-119			Mean cps (background subtracted)							Isotope Ratios (±1σ)							Age (Ma; ±1σ)						
Analysis	Core/Rim	$\%^{206}Pb_c$	^{204}Pb	^{206}Pb	^{207}Pb	^{208}Pb	^{232}Th	^{238}U	Th/U	$^{207}Pb/^{206}Pb$		$^{207}Pb/^{235}U$		$^{206}Pb/^{238}U$		Rho	$^{207}Pb/^{206}Pb$		$^{207}Pb/^{235}U$		$^{206}Pb/^{238}U$		%Conc
119-001.1		0.23	32	13986	1046	2393	56163	107691	0.52	0.0733	0.0014	1.7855	0.0361	0.1767	0.0026	0.4574	1022	38	1040	13	1049	14	103
119-004.1		0.04	3	8076	619	1123	28366	64154	0.44	0.0749	0.0017	1.7711	0.0408	0.1715	0.0027	0.3934	1067	44	1035	15	1020	15	96
119-005.1		0.00	0	16938	1286	1877	45645	135563	0.34	0.0745	0.0014	1.7453	0.0345	0.1701	0.0025	0.4709	1053	37	1025	13	1012	14	96
119-006.1		0.15	21	13700	1035	2216	54443	112548	0.48	0.0740	0.0013	1.6833	0.0325	0.1651	0.0024	0.4762	1040	36	1002	12	985	13	95
119-007.1		0.41	22	5386	398	666	17772	44429	0.40	0.0731	0.0026	1.6796	0.0593	0.1667	0.0031	0.2348	1016	71	1001	22	994	17	98
119-008.1		0.03	4	11939	935	1970	54879	106870	0.51	0.0740	0.0028	1.5583	0.0581	0.1528	0.0030	0.2065	1041	76	954	23	917	17	88
119-009.1		0.00	0	9461	709	1323	32184	76411	0.42	0.0734	0.0016	1.6906	0.0376	0.1670	0.0025	0.3985	1026	43	1005	14	996	14	97
119-010.1		0.00	0	27083	2007	1053	26456	214354	0.12	0.0726	0.0013	1.7178	0.0324	0.1716	0.0025	0.4943	1004	35	1015	12	1021	14	102
119-011.1		0.00	0	7222	547	963	24607	58673	0.42	0.0741	0.0018	1.7058	0.0430	0.1669	0.0027	0.3482	1045	49	1011	16	995	15	95
119-012.1		0.00	0	9217	685	1177	28261	72770	0.39	0.0729	0.0016	1.7262	0.0403	0.1718	0.0027	0.3850	1011	45	1018	15	1022	15	101
119-013.1		0.00	0	14965	1125	2788	69938	117590	0.59	0.0738	0.0014	1.7524	0.0354	0.1723	0.0025	0.4527	1035	38	1028	13	1025	14	99
119-014.1		0.00	0	10319	766	1478	35176	79690	0.44	0.0730	0.0022	1.7477	0.0514	0.1738	0.0029	0.2750	1013	59	1026	19	1033	16	102
119-016.1		0.08	22	28017	2132	1817	43354	255708	0.17	0.0735	0.0012	1.4781	0.0262	0.1458	0.0021	0.5043	1029	32	922	11	877	12	85
119-017.1		0.16	13	7907	599	788	20023	62288	0.32	0.0738	0.0019	1.7190	0.0441	0.1691	0.0027	0.3287	1035	50	1016	16	1007	15	97
119-018.1		0.00	0	13819	1022	1821	44677	103489	0.43	0.0725	0.0014	1.7430	0.0348	0.1744	0.0025	0.4320	1000	38	1025	13	1036	14	104
119-019.1		0.00	0	9083	684	1311	29439	69701	0.42	0.0732	0.0017	1.7492	0.0420	0.1733	0.0027	0.3548	1020	47	1027	15	1030	15	101
119-020.1		0.08	14	17970	1369	2126	49044	156289	0.31	0.0741	0.0017	1.5775	0.0371	0.1544	0.0024	0.3672	1044	46	961	15	925	13	89
119-021.1		0.00	0	10316	780	1577	34605	80986	0.43	0.0740	0.0018	1.6966	0.0422	0.1663	0.0026	0.3290	1041	49	1007	16	992	14	95
119-022.1		0.00	0	9172	687	1354	34097	71401	0.48	0.0736	0.0015	1.7128	0.0362	0.1688	0.0025	0.4054	1030	40	1013	14	1006	14	98
119-023.1		0.45	24	5363	397	650	16321	43331	0.38	0.0729	0.0033	1.6723	0.0740	0.1663	0.0036	0.1686	1012	90	998	28	991	20	98
119-024.1		0.00	0	8424	633	1040	27968	68685	0.41	0.0739	0.0023	1.6695	0.0504	0.1640	0.0028	0.2690	1038	60	997	19	979	16	94
119-025.1		0.18	20	11198	838	1593	39103	84281	0.46	0.0738	0.0016	1.7540	0.0383	0.1724	0.0025	0.3835	1035	42	1029	14	1026	14	99
119-026.1		0.00	0	6187	463	790	19800	50576	0.39	0.0737	0.0020	1.6364	0.0433	0.1610	0.0026	0.3034	1034	52	984	17	962	14	93
119-027.1		0.00	0	4440	340	793	16709	36077	0.46	0.0738	0.0042	1.6435	0.0893	0.1616	0.0040	0.1152	1035	111	987	34	966	22	93
119-029.1		0.00	0	7831	573	1099	26051	61482	0.42	0.0724	0.0016	1.6608	0.0368	0.1664	0.0025	0.3750	997	43	994	14	992	14	99
119-030.1		0.37	29	7827	581	1074	26622	58968	0.45	0.0736	0.0020	1.7372	0.0472	0.1713	0.0027	0.2902	1029	54	1022	18	1019	15	99

DA14-127			Mean cps (background subtracted)							Isotope Ratios (±1σ)							Age (Ma; ±1σ)						
Analysis	Core/Rim	$\%^{206}Pb_c$	^{204}Pb	^{206}Pb	^{207}Pb	^{208}Pb	^{232}Th	^{238}U	Th/U	$^{207}Pb/^{206}Pb$		$^{207}Pb/^{235}U$		$^{206}Pb/^{238}U$		Rho	$^{207}Pb/^{206}Pb$		$^{207}Pb/^{235}U$		$^{206}Pb/^{238}U$		%Conc
127-001.1		0.02	38	152077	11451	14359	342643	1230926	0.28	0.0736	0.0009	1.6453	0.0243	0.1623	0.0022	0.6106	1029	25	988	9	969	12	94
127-002.1		0.03	18	67125	5234	5866	121959	586253	0.21	0.0761	0.0011	1.5871	0.0254	0.1514	0.0021	0.5678	1097	28	965	10	909	12	83
127-003.1	Core	0.06	22	34563	2992	10498	224735	351722	0.64	0.0846	0.0012	1.5046	0.0240	0.1290	0.0018	0.5579	1306	27	932	10	782	10	60
127-003.2	Rim	0.17	298	173657	17139	33918	468482	1508953	0.31	0.0968	0.0013	2.0179	0.0307	0.1512	0.0020	0.5937	1563	24	1122	10	908	11	58
127-004.1		0.01	14	142300	10684	35320	1058879	1122194	0.94	0.0737	0.0011	1.7105	0.0286	0.1685	0.0023	0.5450	1032	30	1013	11	1004	13	97
127-005.1		0.08	99	117494	10287	17692	546580	1296002	0.42	0.0850	0.0015	1.3780	0.0251	0.1176	0.0016	0.4637	1315	33	880	11	717	9	55
127-006.1		0.11	240	217369	19357	37749	813568	2196063	0.37	0.0876	0.0012	1.5909	0.0258	0.1318	0.0018	0.5650	1374	27	967	10	798	10	58
127-007.1		0.22	138	62732	6217	27734	707922	540171	1.31	0.0977	0.0019	2.0678	0.0421	0.1535	0.0022	0.4269	1581	36	1138	14	921	12	58
127-008.1		0.05	55	109429	9210	19161	528823	1130642	0.47	0.0826	0.0011	1.4526	0.0227	0.1276	0.0017	0.5832	1260	26	911	9	774	10	61
127-009.1		0.05	56	121935	9494	13814	482785	1079688	0.45	0.0762	0.0010	1.5614	0.0242	0.1486	0.0020	0.5827	1101	27	955	10	893	11	81
127-010.1		0.04	63	179886	14215	14237	414991	1636534	0.25	0.0778	0.0014	1.5767	0.0309	0.1471	0.0021	0.4642	1141	36	961	12	885	12	78
127-011.1		0.04	36	102246	8287	14436	337811	896980	0.38	0.0801	0.0013	1.6746	0.0298	0.1516	0.0021	0.5154	1201	31	999	11	910	12	76
127-012.1		0.08	287	358349	30270	90619	3192077	3237011	0.99	0.0830	0.0012	1.6696	0.0265	0.1460	0.0020	0.5679	1268	27	997	10	878	11	69
127-013.1		0.06	90	140579	11158	11254	243515	1202177	0.20	0.0777	0.0014	1.6805	0.0323	0.1569	0.0023	0.4733	1139	35	1001	12	939	13	82
127-014.1		0.10	131	129389	11508	29729	950666	1324531	0.72	0.0875	0.0015	1.5722	0.0291	0.1304	0.0019	0.4904	1371	32	959	11	790	11	58
127-015.1		0.07	121	165028	14051	15273	249213	1509402	0.17	0.0836	0.0010	1.6434	0.0242	0.1425	0.0019	0.6114	1284	24	987	9	859	11	67
127-016.1		0.08	184	226321	18944	19291	444027	2042408	0.22	0.0820	0.0011	1.6446	0.0250	0.1454	0.0020	0.5988	1246	25	988	10	875	11	70
127-017.1		0.03	113	347365	26825	62313	1714513	2794994	0.61	0.0737	0.0011	1.6489	0.0270	0.1624	0.0022	0.5349	1032	29	989	10	970	12	94
127-018.1		0.03	27	94120	7560	12485	285215	774709	0.37	0.0773	0.0014	1.7166	0.0323	0.1611	0.0023	0.4698	1129	34	1015	12	963	13	85
127-019.1		0.06	25	38812	3476	11410	247517	331347	0.75	0.0883	0.0012	1.8530	0.0292	0.1521	0.0021	0.5567	1390	26	1065	10	913	11	66
127-020.1		0.09	195	217962	18902	31619	1102781	1840633	0.60	0.0854	0.0011	1.8129	0.0269	0.1540	0.0021	0.6005	1324	24	1050	10	923	11	70
127-022.1		0.02	21	121133	9502	13427	316190	982621	0.32	0.0777	0.0011	1.7122	0.0266	0.1598	0.0021	0.5700	1139	27	1013	10	956	12	84
127-023.1		0.05	88	170476	13811	41854	999806	1608646	0.62	0.0801	0.0011	1.5202	0.0234	0.1377	0.0018	0.5761	1198	26	939	9	832	10	69
127-024.1		0.10	228	226060	19903	40523	808069	1831281	0.44	0.0870	0.0012	1.9246	0.0296	0.1604	0.0021	0.5776	1361	25	1090	10	959	12	70
127-026.1		0.05	28	51207	3818	8970	217567	391454	0.56	0.0739	0.0011	1.7308	0.0288	0.1700	0.0023	0.5292	1038	30	1020	11	1012	13	98
127-027.1		0.09	26	27706	2046	5852	143575	216302	0.66	0.0737	0.0013	1.6810	0.0310	0.1656	0.0023	0.4679	1032	34	1001	12	988	13	96
127-028.1		0.15	178	114916	11623	31219	737369	986669	0.75	0.1003	0.0015	2.0924	0.0341	0.1513	0.0020	0.5419	1630	27	1146	11	908	11	56
127-029.1		0.03	95	355673	26944	34802	914152	2886727	0.32	0.0737	0.0014	1.6515	0.0339	0.1625	0.0023	0.4258	1034	39	990	13	971	13	94
127-030.1		0.07	183	265163	22004	57738	3997126	2880090	1.39	0.0807	0.0013	1.3365	0.0238	0.1201	0.0017	0.4898	1215	32	862	10	731	10	60
127-031.1		0.16	271	164897	15771	31570	962721	1416242	0.68	0.0932	0.0012	1.9073	0.0274	0.1485	0.0019	0.5985	1491	23	1084	10	892	11	60
127-032.1		0.05	80	160584	13003	22723	466758	1289833	0.36	0.0784	0.0011	1.7003	0.0262	0.1574	0.0021	0.5420	1156	27	1009	10	942	12	82

DA14-127			Mean cps (background subtracted)							Isotope Ratios (±1σ)							Age (Ma; ±1σ)						
Analysis	Core/Rim	$\%^{206}Pb_c$	^{204}Pb	^{206}Pb	^{207}Pb	^{208}Pb	^{232}Th	^{238}U	Th/U	$^{207}Pb/^{206}Pb$		$^{207}Pb/^{235}U$		$^{206}Pb/^{238}U$		Rho	$^{207}Pb/^{206}Pb$		$^{207}Pb/^{235}U$		$^{206}Pb/^{238}U$		%Conc
127-033.1		0.00	0	66815	4985	11584	295248	574052	0.51	0.0728	0.0015	1.5224	0.0317	0.1517	0.0022	0.4077	1009	40	939	13	910	12	90
127-034.1		0.00	0	63781	4702	13976	337456	486644	0.69	0.0720	0.0010	1.6558	0.0251	0.1668	0.0022	0.5550	986	27	992	10	994	12	101
127-035.1		0.16	428	260543	25161	45015	705952	2444438	0.29	0.0950	0.0013	1.7832	0.0280	0.1362	0.0018	0.5483	1527	26	1039	10	823	10	54
127-036.1		0.07	101	135224	11642	24023	617886	1150268	0.54	0.0840	0.0012	1.7388	0.0268	0.1501	0.0020	0.5518	1293	26	1023	10	902	11	70
127-037.1		0.02	63	342357	25870	40488	1030969	2721052	0.38	0.0737	0.0009	1.6245	0.0237	0.1599	0.0021	0.5784	1033	25	980	9	956	12	93
127-038.1		0.02	28	113225	8850	38202	1344641	1028978	1.31	0.0765	0.0010	1.4746	0.0224	0.1398	0.0018	0.5561	1108	26	920	9	844	10	76
127-040.1		0.07	75	102502	8716	21998	519521	901861	0.58	0.0825	0.0017	1.6634	0.0355	0.1462	0.0021	0.3802	1258	40	995	14	880	12	70
127-041.1	Core	0.07	35	47564	3986	10079	281589	432772	0.65	0.0820	0.0012	1.5758	0.0254	0.1394	0.0019	0.5188	1246	28	961	10	841	10	68
127-041.2	Rim	0.02	62	318802	24423	46478	1173571	2593961	0.45	0.0745	0.0015	1.5815	0.0332	0.1539	0.0022	0.3647	1055	41	963	13	923	12	87
127-042.1		0.00	0	169216	12598	17786	422745	1402673	0.30	0.0729	0.0011	1.5240	0.0256	0.1517	0.0020	0.4875	1010	31	940	10	910	11	90
127-043.1		0.11	124	114277	9836	20315	360805	909583	0.40	0.0842	0.0014	1.8329	0.0316	0.1579	0.0021	0.4722	1297	31	1057	11	945	12	73

DA14-130			Mean cps (background subtracted)							Isotope Ratios (±1σ)							Age (Ma; ±1σ)						
Analysis	Core/Rim	$\%^{206}Pb_c$	^{204}Pb	^{206}Pb	^{207}Pb	^{208}Pb	^{232}Th	^{238}U	Th/U	$^{207}Pb/^{206}Pb$		$^{207}Pb/^{235}U$		$^{206}Pb/^{238}U$		Rho	$^{207}Pb/^{206}Pb$		$^{207}Pb/^{235}U$		$^{206}Pb/^{238}U$		%Conc
130-01.1		0.00	0	58594	4500	15173	355385	424950	0.84	0.0754	0.0011	1.8259	0.0302	0.1757	0.0024	0.5155	1079	30	1055	11	1044	13	97
130-02.1		0.00	0	37712	2954	6575	152614	273659	0.56	0.0763	0.0013	1.8574	0.0336	0.1767	0.0024	0.4655	1103	33	1066	12	1049	13	95
130-03.1		0.00	0	54770	3876	4992	114069	553094	0.21	0.0698	0.0009	1.1992	0.0181	0.1247	0.0016	0.5593	922	27	800	8	757	9	82
130-04.1		0.00	0	37458	2849	5475	124406	275013	0.45	0.0749	0.0011	1.7730	0.0276	0.1717	0.0023	0.5336	1066	28	1036	10	1022	12	96
130-05.1		0.01	4	33423	2545	5543	125036	230911	0.54	0.0750	0.0011	1.8905	0.0301	0.1828	0.0024	0.5235	1069	29	1078	11	1082	13	101
130-06.1		0.00	0	52012	4098	7692	231709	536369	0.43	0.0779	0.0013	1.2955	0.0233	0.1207	0.0016	0.4470	1144	33	844	10	734	9	64
130-07.1	Core	0.00	0	26535	2031	4824	111921	187415	0.60	0.0753	0.0011	1.8658	0.0308	0.1797	0.0024	0.5124	1077	30	1069	11	1066	13	99
130-07.2	Rim	0.06	15	25201	1922	3698	84301	201379	0.42	0.0752	0.0013	1.6543	0.0297	0.1595	0.0022	0.4741	1075	33	991	11	954	12	89
130-08.1		0.23	42	18077	1385	2188	50239	126978	0.40	0.0754	0.0013	1.8830	0.0339	0.1811	0.0025	0.4710	1079	33	1075	12	1073	14	99
130-09.1		0.00	0	36674	2812	6214	129434	249007	0.52	0.0754	0.0012	1.9509	0.0327	0.1877	0.0025	0.5090	1079	30	1099	11	1109	14	103
130-10.1		0.00	0	64201	4937	15382	351999	461064	0.76	0.0752	0.0014	1.8758	0.0374	0.1809	0.0026	0.4384	1075	37	1073	13	1072	14	100
130-11.1		0.04	7	17825	1364	2467	56582	127635	0.44	0.0753	0.0013	1.8548	0.0345	0.1788	0.0025	0.4565	1075	35	1065	12	1060	14	99
130-12.1		0.00	0	19855	1530	2832	68396	154332	0.44	0.0754	0.0014	1.7308	0.0333	0.1664	0.0024	0.4505	1080	36	1020	12	992	13	92
130-13.1		0.00	0	37440	2884	6383	140578	262716	0.54	0.0756	0.0012	1.9136	0.0329	0.1837	0.0025	0.5072	1083	31	1086	11	1087	14	100
130-14.1		0.35	47	13484	1028	1595	36096	102164	0.35	0.0751	0.0015	1.7592	0.0362	0.1700	0.0024	0.4169	1070	39	1031	13	1012	13	95
130-15.1		0.00	0	28065	2119	3807	84760	189476	0.45	0.0744	0.0011	1.9136	0.0305	0.1866	0.0025	0.5252	1052	29	1086	11	1103	13	105
130-17.1		0.03	16	49707	3887	8316	216396	389953	0.55	0.0759	0.0012	1.6961	0.0294	0.1620	0.0022	0.4730	1093	32	1007	11	968	12	89
130-18.1		0.12	45	38481	3223	6736	134431	356792	0.38	0.0819	0.0013	1.5395	0.0263	0.1363	0.0018	0.4814	1242	31	946	11	824	10	66
130-19.1		0.00	0	42654	3252	6439	148743	323229	0.46	0.0754	0.0012	1.7345	0.0291	0.1667	0.0022	0.4997	1080	31	1021	11	994	12	92
130-20.1		0.05	19	39346	2991	5484	125624	279483	0.45	0.0752	0.0011	1.8320	0.0289	0.1766	0.0023	0.5269	1075	28	1057	10	1048	13	98
130-21.1		0.01	3	48502	3736	7716	172122	335566	0.51	0.0762	0.0011	1.9065	0.0296	0.1814	0.0024	0.5370	1101	28	1083	10	1074	13	98
130-22.1		0.00	0	30026	2289	5221	187951	303752	0.62	0.0755	0.0019	1.3119	0.0328	0.1260	0.0019	0.3076	1082	49	851	14	765	11	71
130-23.1		0.02	5	25717	1939	3911	90163	185117	0.49	0.0756	0.0016	1.8058	0.0388	0.1733	0.0025	0.3613	1083	42	1048	14	1031	13	95
130-24.1		0.00	0	29477	2289	4259	97502	229693	0.42	0.0769	0.0012	1.7029	0.0286	0.1606	0.0021	0.4813	1119	31	1010	11	960	12	86